SANDIA REPORT
SAND98–2252
Unlimited Release
Printed October 1998

Proceedings of US/Japan Workshop (97FT5-06) on High Heat Flux Components and Plasma Surface Interactions for Next Fusion Devices

Richard Nygren and Diana Kureczko

Prepared by
Sandia National Laboratories
Albuquerque, New Mexico 87185 and Livermore, California 94550

Sandia is a multiprogram laboratory operated by Sandia Corporation, a Lockheed Martin Company, for the United States Department of Energy under Contract DE-AC04-94AL85000.

Approved for public release; further dissemination unlimited.

Sandia National Laboratories

Issued by Sandia National Laboratories, operated for the United States Department of Energy by Sandia Corporation.

Printed in the United States of America. This report has been reproduced directly from the best available copy.

Available to DOE and DOE contractors from
Office of Scientific and Technical Information
P.O. Box 62
Oak Ridge, TN 37831

Prices available from (615) 576-8401, FTS 626-8401

Available to the public from
National Technical Information Service
U.S. Department of Commerce
5285 Port Royal Rd
Springfield, VA 22161

NTIS price codes
Printed copy: A99
Microfiche copy: A01

DISCLAIMER

SAND98-2252
Unlimited Release
Printed October 1998

Proceedings of US/Japan Workshop (97FT5-06) On High Heat Flux Components and Plasma Surface Interactions for Next Fusion Devices

San Francisco, California
December 8 – 11, 1997

Edited by

Richard Nygren
Diana Kureczko

Sandia National Laboratories
P.O. Box 5800
Albuquerque, New Mexico 87185-1129

Abstract

The 1997 US-Japan Workshop on High Heat Flux Components and Plasma Surface Interactions for Next Step Fusion Devices was held at the Warwick Regis Hotel in San Francisco, California, on December 8-11, 1997. There were 53 presentations as well as discussions on technical issues and on planning for future collaborations, and 35 researchers from Japan and the US participated in the workshop.

Over the last few years, with the strong emphasis in the US on technology for ITER, there has been less work done in the US fusion program on basic plasma-materials interactions and this change in emphasis workshops. The program this year emphasized activities that were not carried out under the ITER program and a new element this year in the US program was planning and some analysis on liquid surface concepts for advanced plasma facing components.

The program included a ceremony to honor Professor Yamashina, who was retiring this year and a special presentation on his career.

Page Intentionally Left Blank

Table of Contents

Session I: Activities in Present and Near Term Devices

J-US WORKSHOP
ON HHFC/PSI FOR NEXT FUSION DEVICES
(97 FT5-06)

- WORKSHOP SERIES HAS BEEN PRODUCTIVE AND MUTUALLY BENEFICIAL

  ⇒ USDOE WILL <u>CONTINUE</u> ITS SUPPORT

- <u>CHANGE</u> IN USDOE RESPONSIBILITY FOR HHFC/PSI PROGRAMS

  ⇒ MARVIN COHEN RETIRED IN JAN. 1997

  ⇒ SAM BERK REPLACED MARVIN
  (ALSO RESPONSIBLE FOR FNT PROGRAMS)

- J-US HHFC/PSI COLLABORATION WILL BE <u>STRENGTHENED</u> IN FUTURE

  ⇒ US FUSION PROGRAM BUDGET IS <u>STABLE</u>

  ⇒ FUNDING FOR SUCH COLLABORATIONS WILL <u>INCREASE</u> (US TECHNOLOGY R&D WILL BE LESS FOCUSED ON ITER AFTER FY1998)

  ⇒ HHFC/PSI WORK WILL BE <u>LARGEST</u> ELEMENT OF US TECHNOLOGY R&D

  ⇒ USDOE <u>VALUES</u> COLLABORATION WITH JAPAN AND LOOKS FORWARD TO <u>BUILDING</u> ON PAST SUCCESSES.

US/Japan Workshop on PSI
December 8-11, 1997
Warwick Regis Hotel, San Francisco, USA

Present Status of LHD

LHD

Osamu Motojima

National Institute for Fusion Science
322-6 Oroshicho, Toki 509-52, Japan.

1, Introduction to LHD Project
  Missions in Fusion Physics and Technology
  Specifications of LHD
2, Construction Status/Engineering Achievements
3, Experimental Planning
  Commissioning Tests
  First Plasma Start up Scenario
  Heating System (NBI, Gyrotron, ICRF)
4, Summarizing

OM0299

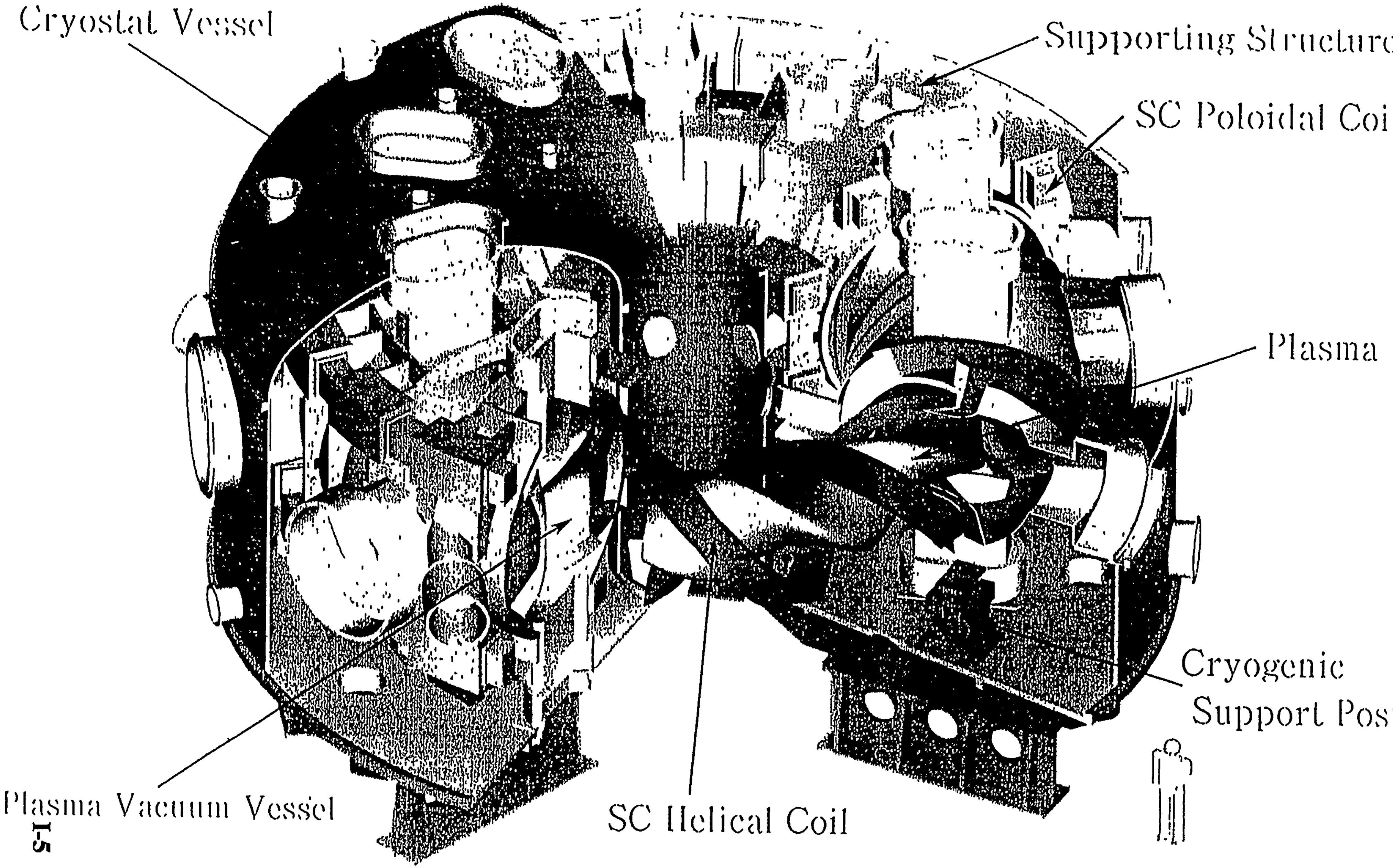

LARGE HELICAL DEVICE

HII S-PI 067

Specifications of LHD

LHD

Major Radius	3.9 m
Coil Minor Radius	0.975 m
Averaged Plasma Radius	0.5~0.65m
ℓ, m	2, 10
Magnetic Field	3(4) T
Helical Coil Current	5.85(7.8) MA
LHe Temperature	4.4(1.8) K
Poloidal Coil Current	
Inner Vertical Coil	5.0 MA
Inner Shaping Coil	-4.5 MA
Outer Vertical Coil	-4.5 MA
LHe Temperature	4.5 K
Plasma Volume	20~30 m^3
Heating Power	40 MW
Coil Energy	0.9(1.6) GJ
Refrigeration Power	9(~15) kW
Total Weight	1,500 ton
LHe Cooled mass	900 ton

OM0289

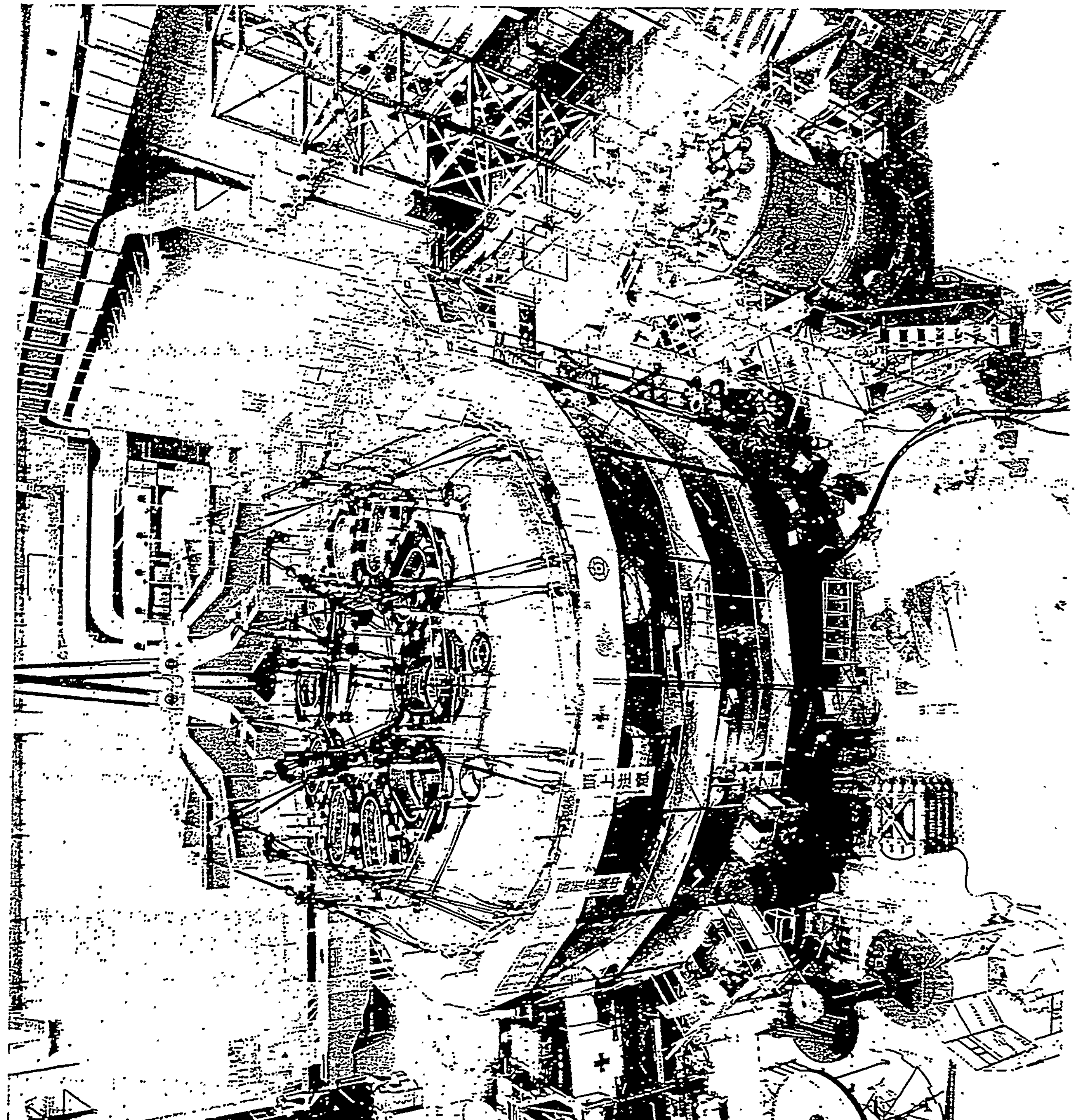

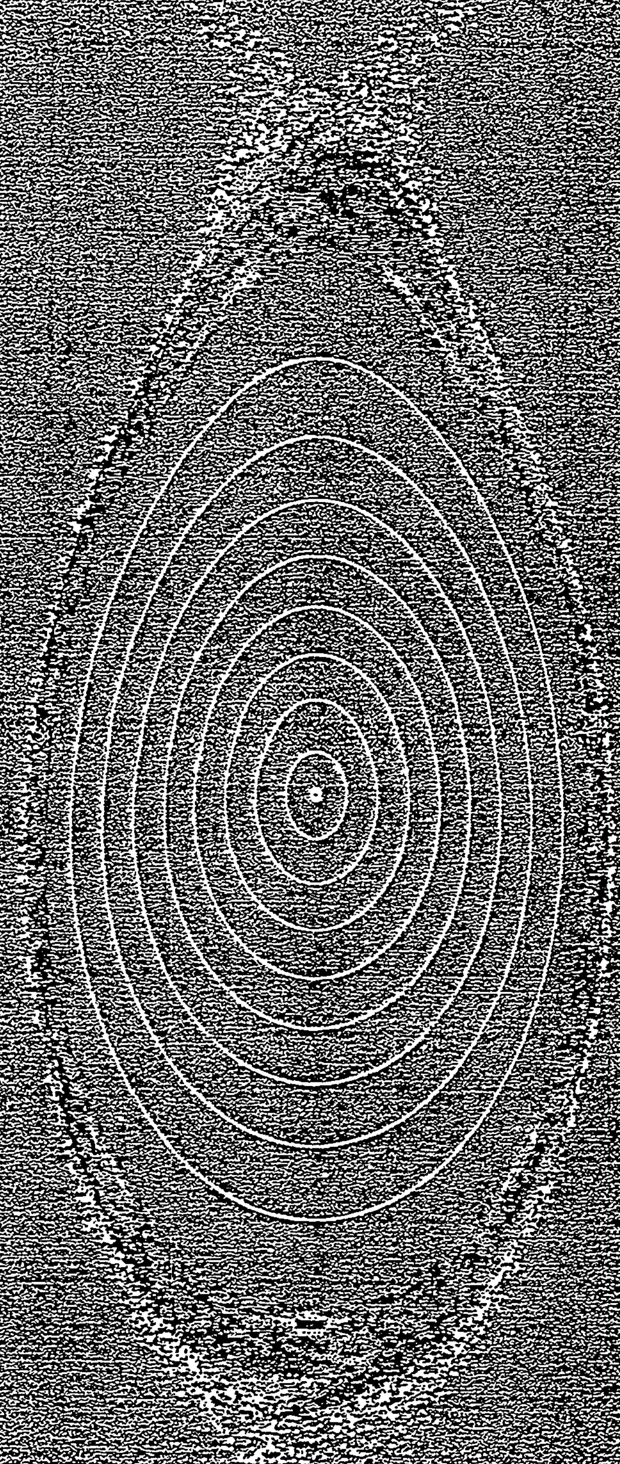

Goal of LHD Project

LHD

1. Physics Experiment Extrapolatable to
   Break Even Condition
   - High $n \tau T$ > 10^{20} $keVm^{-3}s$ ($Q \sim 0.35$)
   - High T > 10 keV
   - High β > 5 %

   Increased Interests on Confinement & Stability
2. Demonstration of Advanced Toroidal Operation
   - Disruption-less
   - Helical Divertor
   - SC Coil System
3. Confinement Improvement
   - Edge Control
   - Flow Shear
   - High Energy (α) Particle
   - Field Optimization
4. Currentless Steady Plasma Production
5. Contribution to Fusion Technology
   - SC, Material, Heating System, Power Control
   - Fusion Mechanics
6. Conjunct to DEMO Relevant Reactor Design
   - Force Free Helical Reactor (FFHR)

OM0289

Platform for experimental study

Device	R(m)	a(m)	ι_0	ι_a
ATF (ORNL)	2.04	0.27	0.26	1.00
CHS (NIFS)	0.94	0.20	0.31	1.10
Heliotron E (Kyoto U.)	2.17	0.21	0.51	2.75
W7-AS (IPP,MPG)	2.00	0.11-0.18	0.33-0.54	0.33-0.54
LHD (NIFS)	3.9	0.6	0.4	1.3

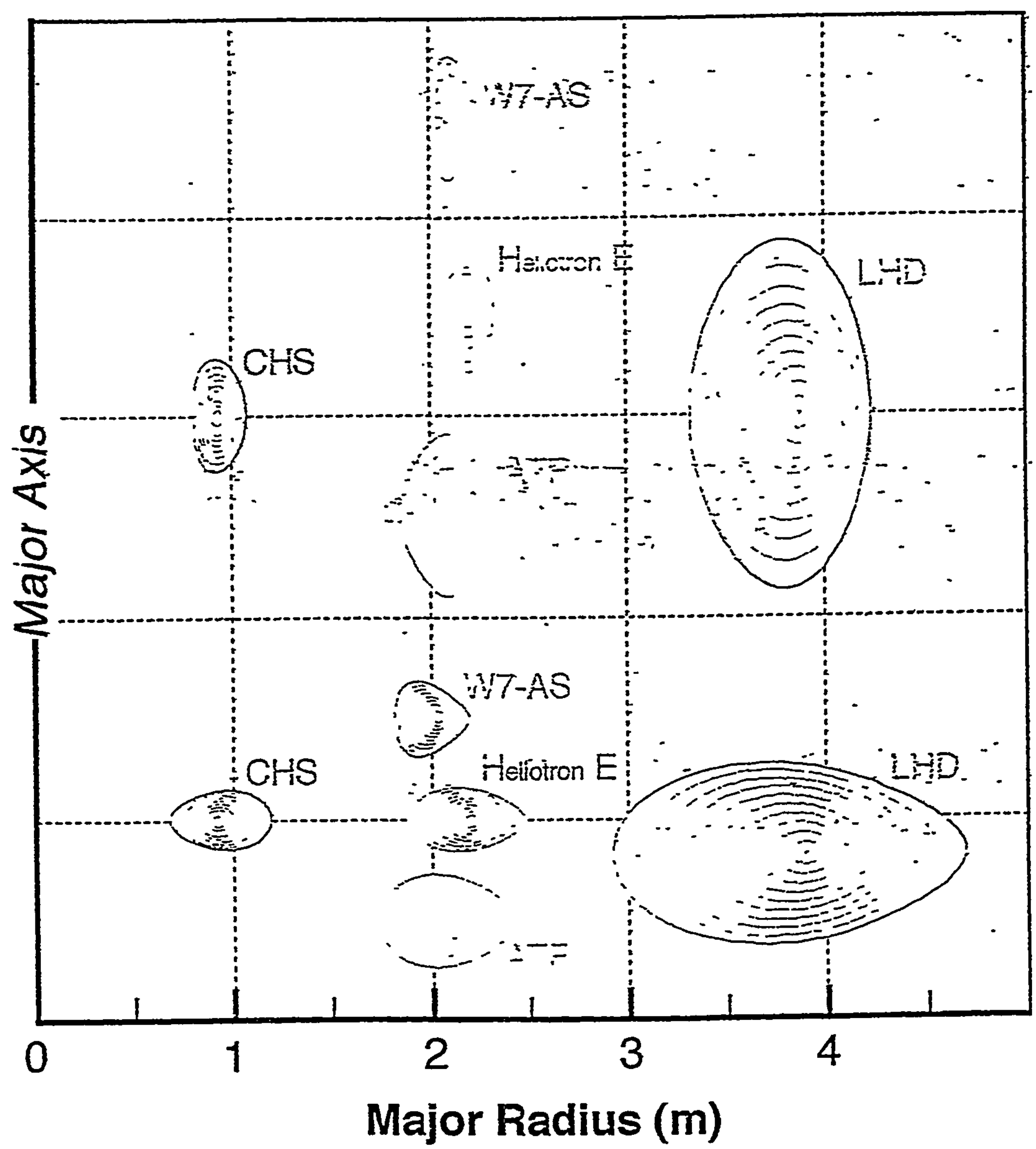

LHD Field Characteristics

LHD

Plasma Currentless System	rot B =0
Large Rotational Transform	$\iota = q^{-1}$ 0.5~1.0
Moderate Shear	θ =3~4 (1/2a)
Finite Well	-10% (hill/vacuum)
	10% (well/β =1.5%)
Double Null Helical Separatrix	
Helical Divertor Configuration	
Local Island Divertor	
Reduced Particle Loss	ΔR=-15 cm
Reduced Bootstrap Current	δ =2 (Ellipticity)

OM0289

International Stellarator Database

NIFS (Japan), IPP (Germany), ORNL(USA), PPLK (Japan)

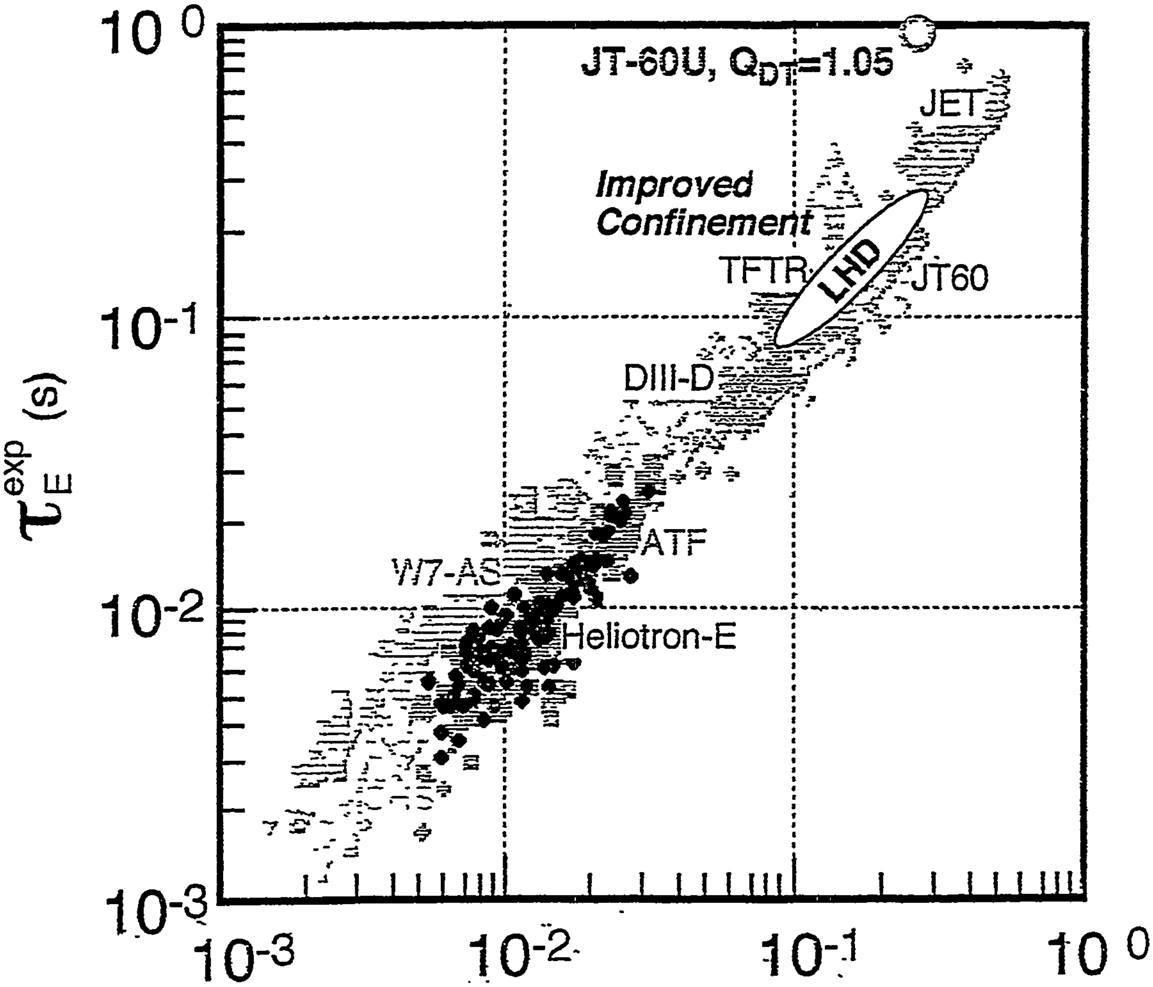

$$\tau_E^{ISS95} = 0.08\, a_p^{\,2.21}\, R_0^{\,0.65}\, P_{abs}^{\,-0.59}\, \bar{n}_e^{\,0.51}\, B_0^{\,0.83}\, ι_{2/3}^{\,0.40}$$

τ_E^{ISS95}(s), a_p (m), R_0 (m), P_{abs}(MW), $\bar{n}_e$(10^{19}m^{-3}), B_0 (T)

Tokamak data from ITER L-mode database.

Magnetic Field Optimization Base

LHD

0. Intensive Theoretical Study → till 1990.
1. Basic Size of Machine → B=3T, R=3.9m, and Plasma Volume $30m^3$

Close Regime to the Break Even

2. Field Configuration → m=10/l=2 Continuous Helix

Reducing the Adoption of Unfavorable Field Harmonies

3. Coil System → Super Conducting Coils

Two Helical Coils and 3 Sets of Poloidal Coils

4. Edge Control → Helical Divertor and Local Island Divertor
5. Heating System → ~30MW with NBI, ICRF and ECRH.

Stead State

OM0298

Basic Prospect of LHD Plasma Confinement

LHD

1. Large Magnetic Rotational Transform and Medium Shear
2. Established Empirical Global Confinement Scaling Law
   in the Vicinity of Plateau Regime

$$\boxed{\tau_E = 0.079 P^{-0.59} B_t^{0.83} \iota_{2/3}^{0.40} n_e^{0.51} R^{0.65} a^{2.21} A_i^{0}}$$

(ISS95-scaling)
– Gyro-Reduce Bohm Type –

3. Neoclassical Type Diffusion Process in Lower-Collision Regime
   Ion Root Condition → Accessible High $n\tau T$ Plasma
   Electron Root Condition → Accessible High T Plasma
   * Radial electric field plays an important role in the combination of plasma rotation and flow shear.
4. MHD Stability optimized
   Satisfying Mercier Criterion and Ballooning Mode Limit
   * Expected average β value is 5%.

Schedule of LHD Machine and Buildings

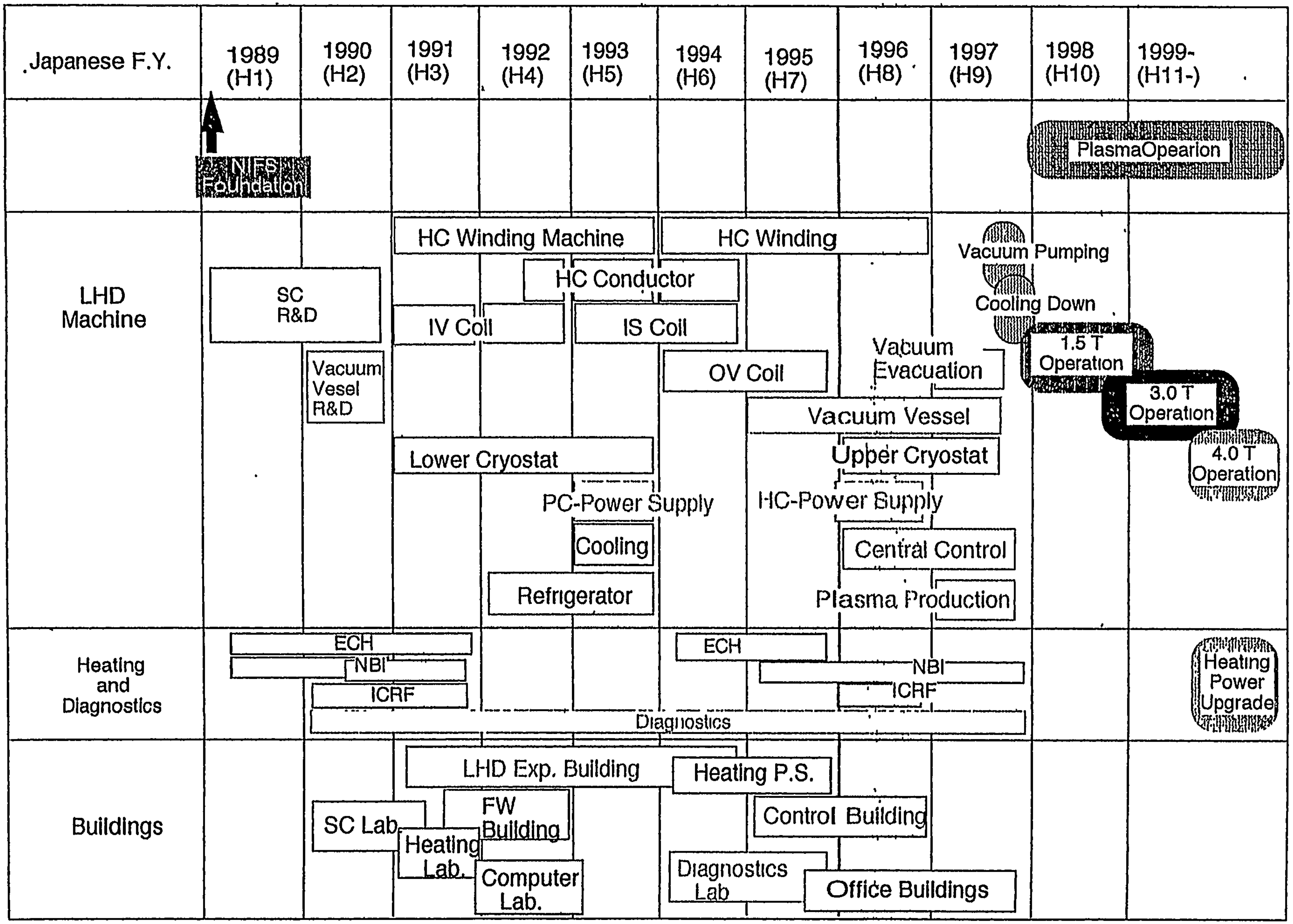

1995/9/20 KY

Progress Summary of LHD Construction

LHD

Complete: 95% of Construction Schedule

1. Coil Fabrication Completed → The Biggest Critical Path
   - Helical Coil: Diameter: 7.8 m、13 kA Nominal; 450 turns x 2; Profile Accuracy ±2 mm
   - Poloidal Coils(OV): Diameter: 11.1 m、–31.3 kA Nominal; 8 Double Pancakes x 2; Profile Accuracy ±2 mm
2. Vacuum Chamber Completed: Profile Accuracy ±10 mm; Up/Down Port 10, Inside 6; Horizontal 10, Tangential 4
3. Helical Divertor Panel Under Construction
   - Divertor R & D Continued: Graphite Tile Heat Load Test (ACT)
4. Power Supply Completed
   - Real Road Test with Fuse Switch: 16 /23 kA Nominal、100 shots
   - Reliability Check: 10^{-6}
5. SC Bus line Completed: 9 lines、32 kA、5 kV、5 Hold T.Tube
6. LHe Liquefier Completed
   - Test Operation: 2,700 ℓ/hr equivalent
7. Control System Under Intensive Construction
   - Center Control System, Timing System (Time Sequence), Experimental LAN, LHe Liquefier Control System, Monitoring System 2,000ch, Interlock System for Safety Operation
8. Utilities Completed
   - Underground Stage、Pressured Air Piping、Wireless System、Safety Sensors、Key Lock System, Gate Valve System, etc.

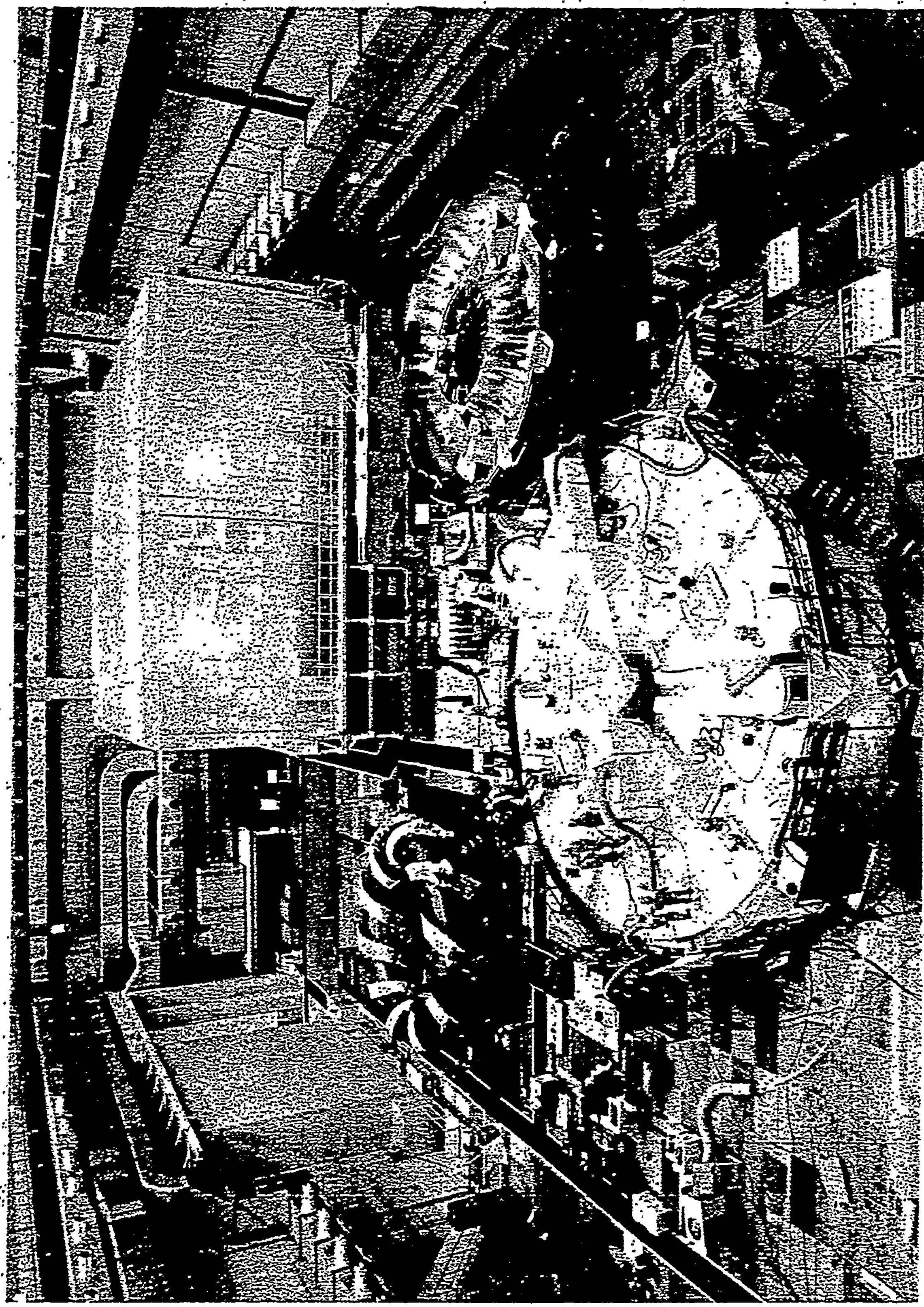

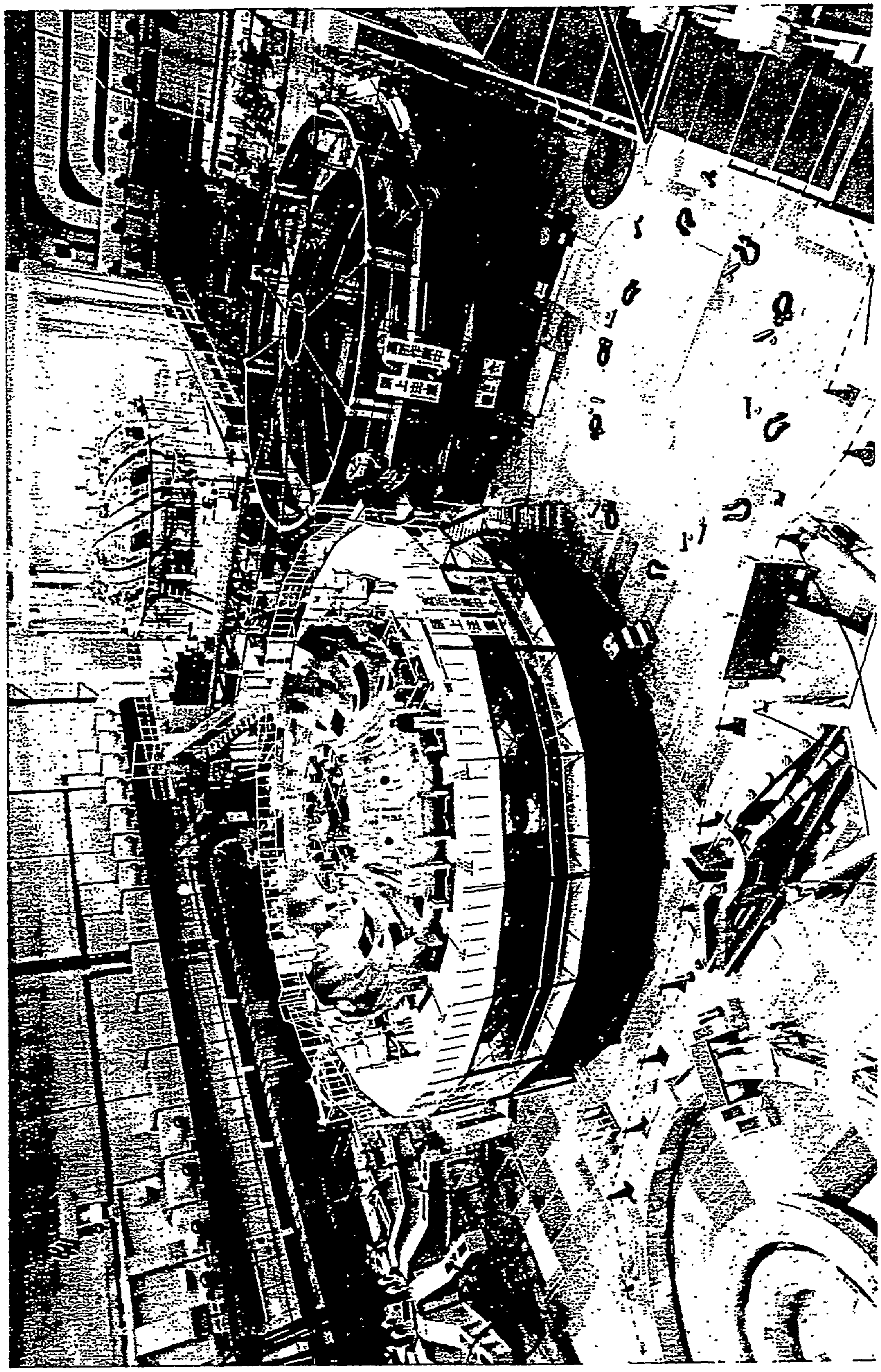

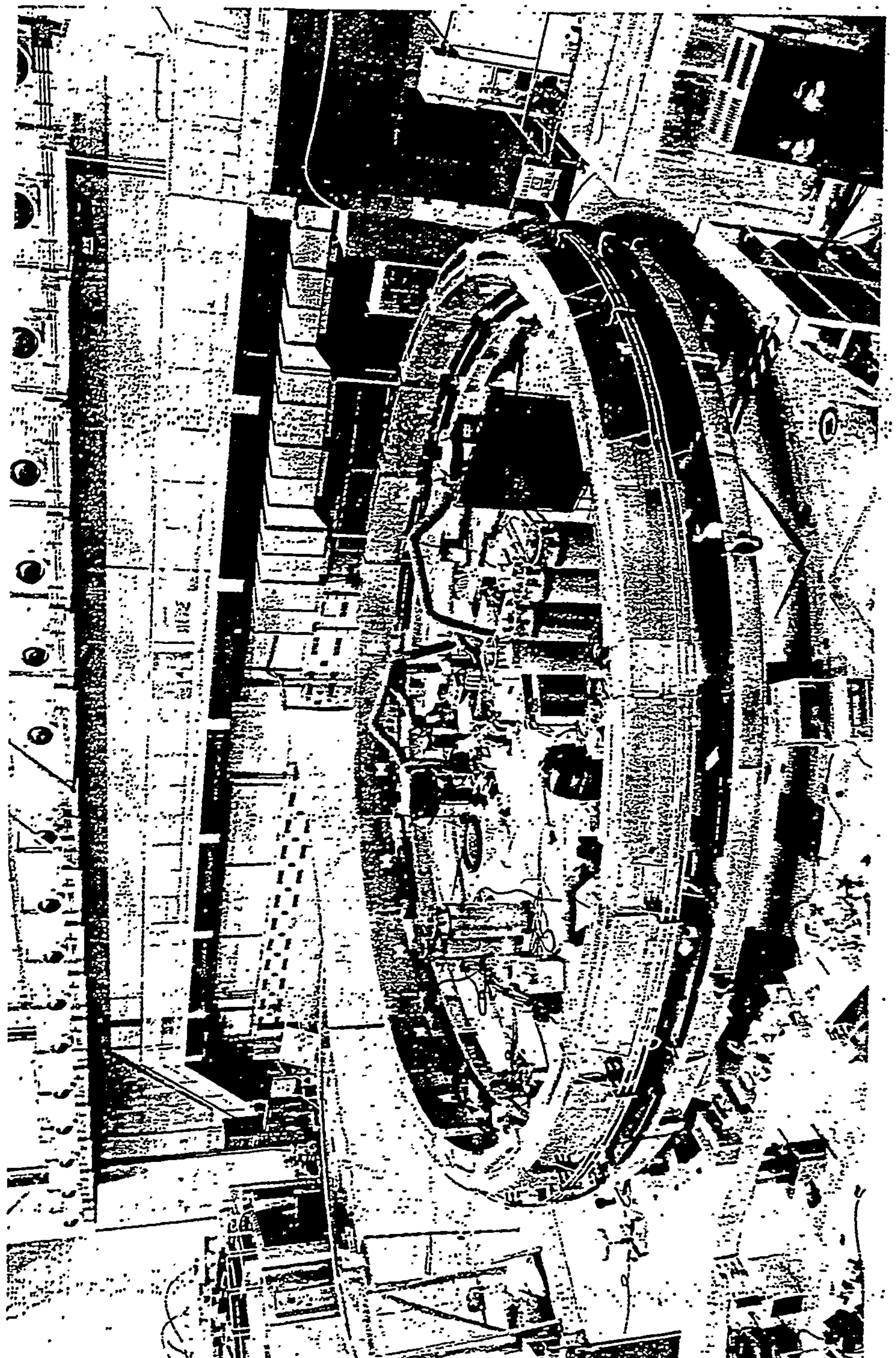

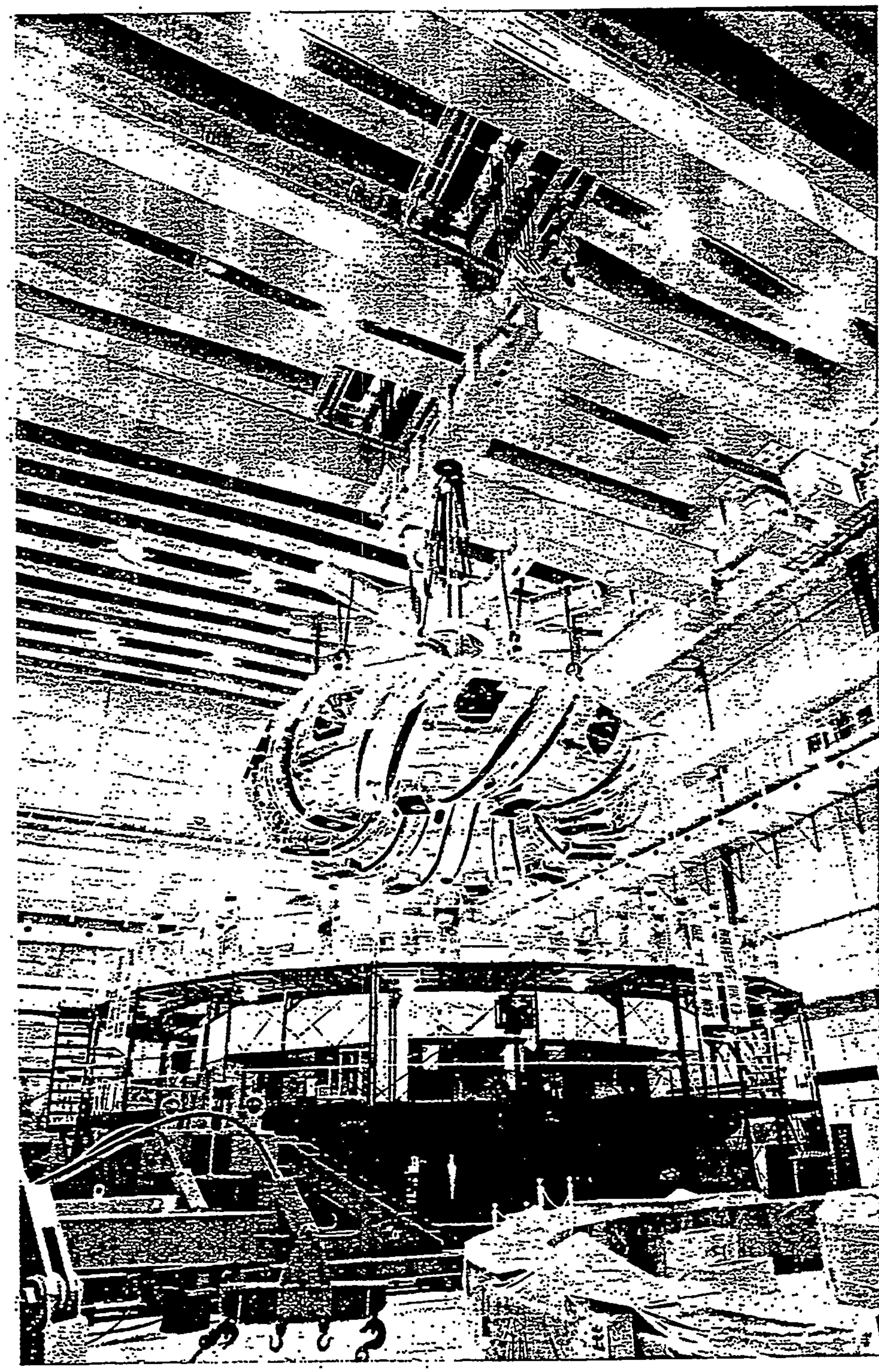

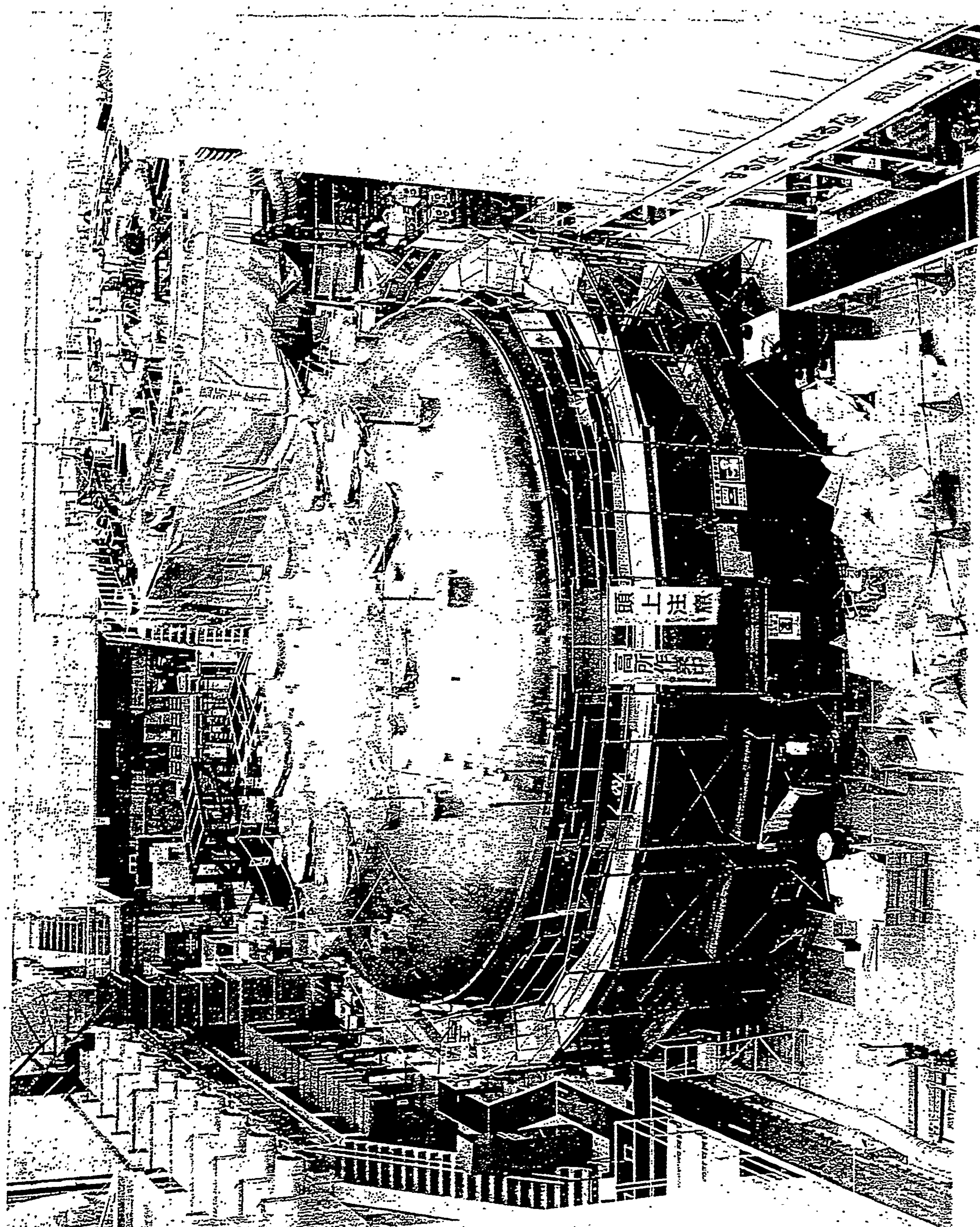

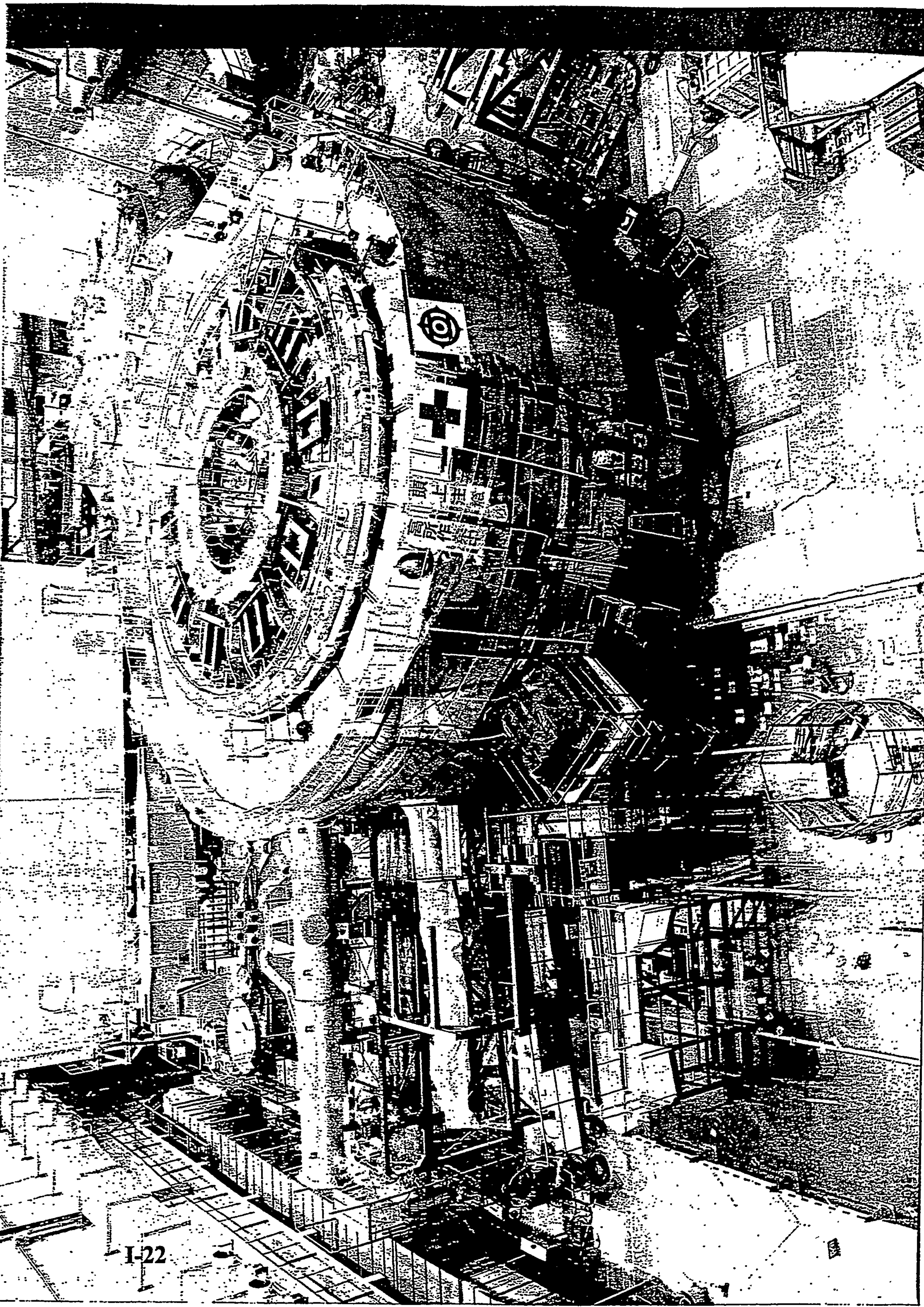

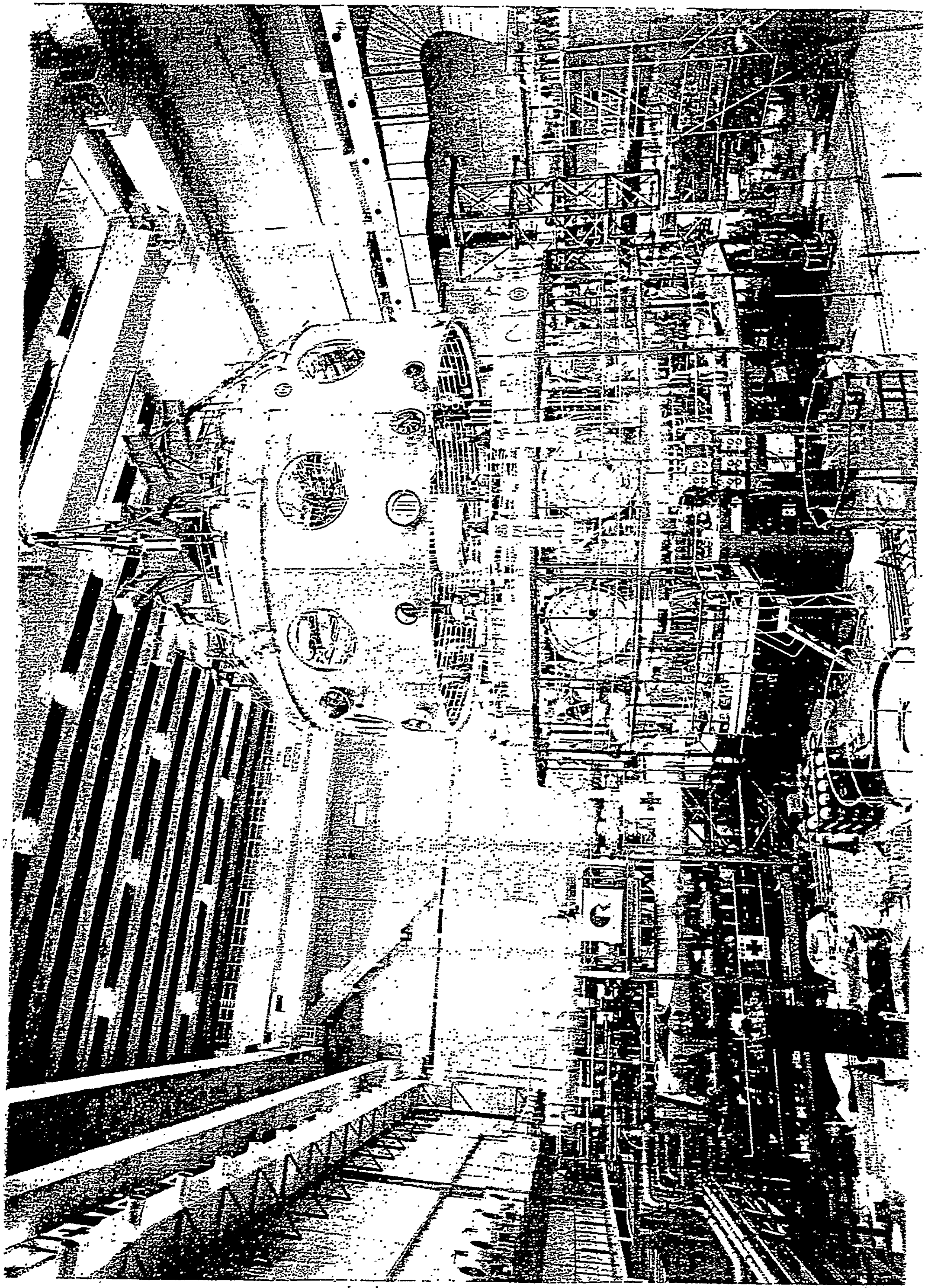

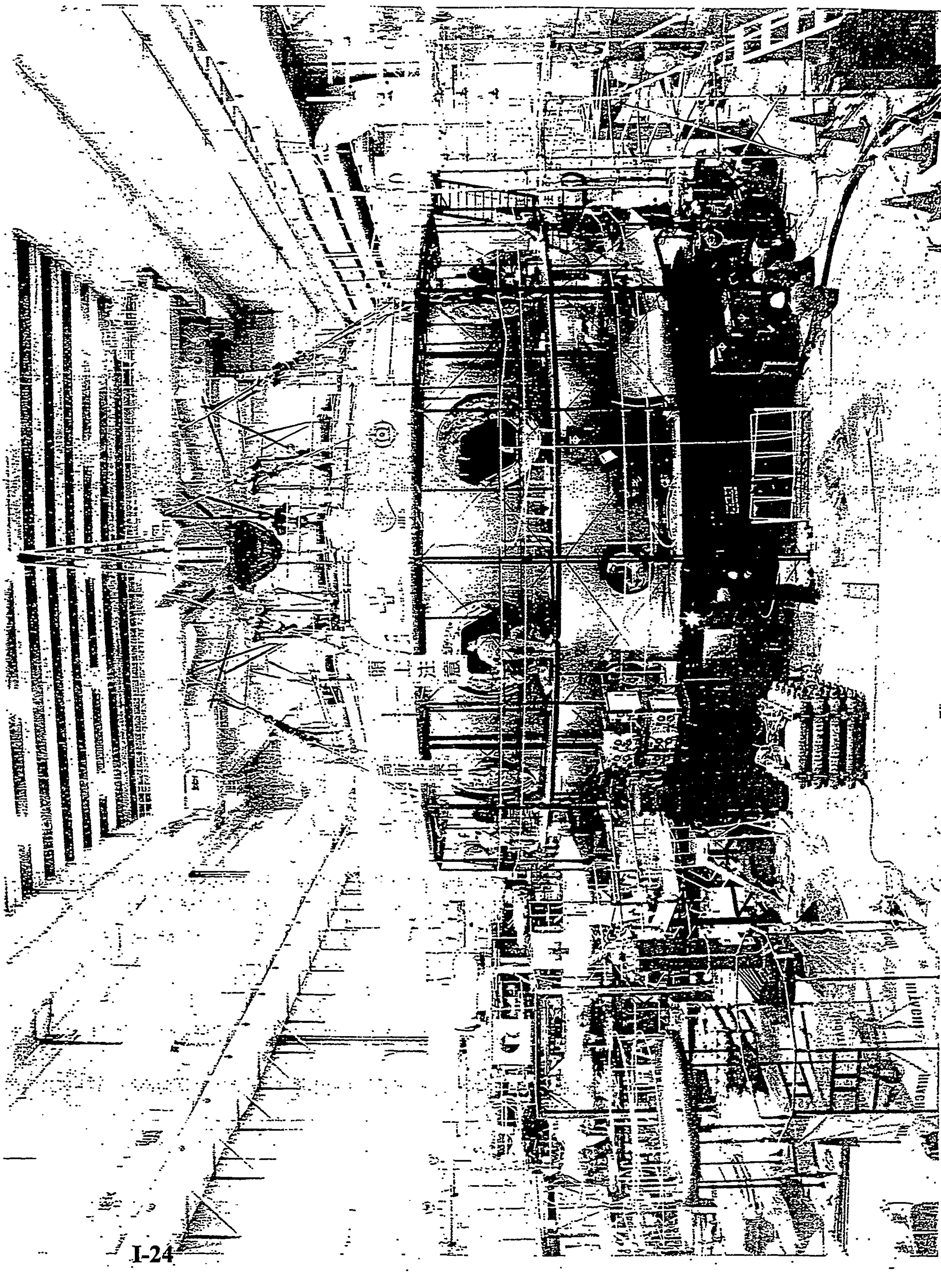

Near-Future Plan of LHD Experiments

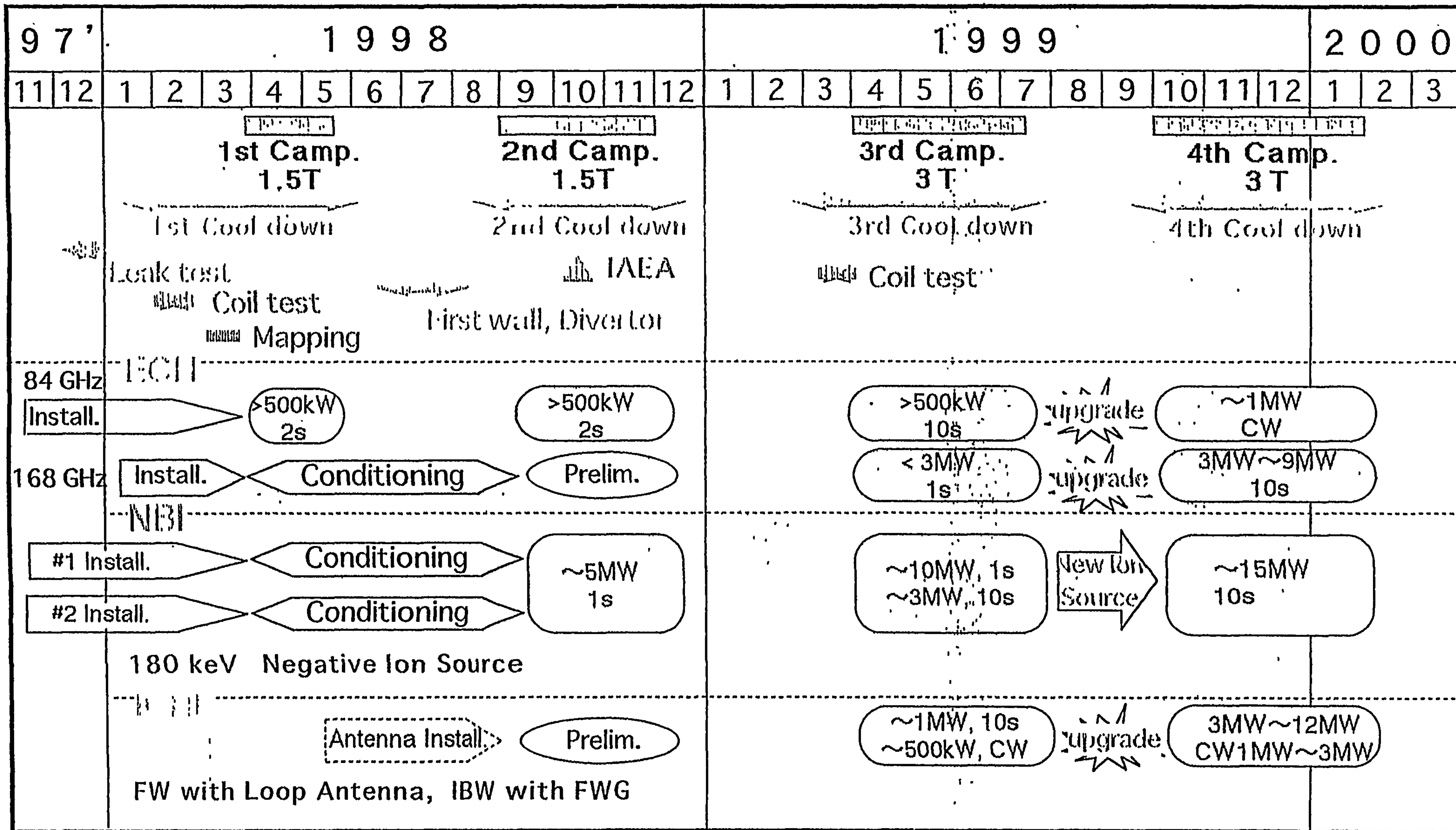

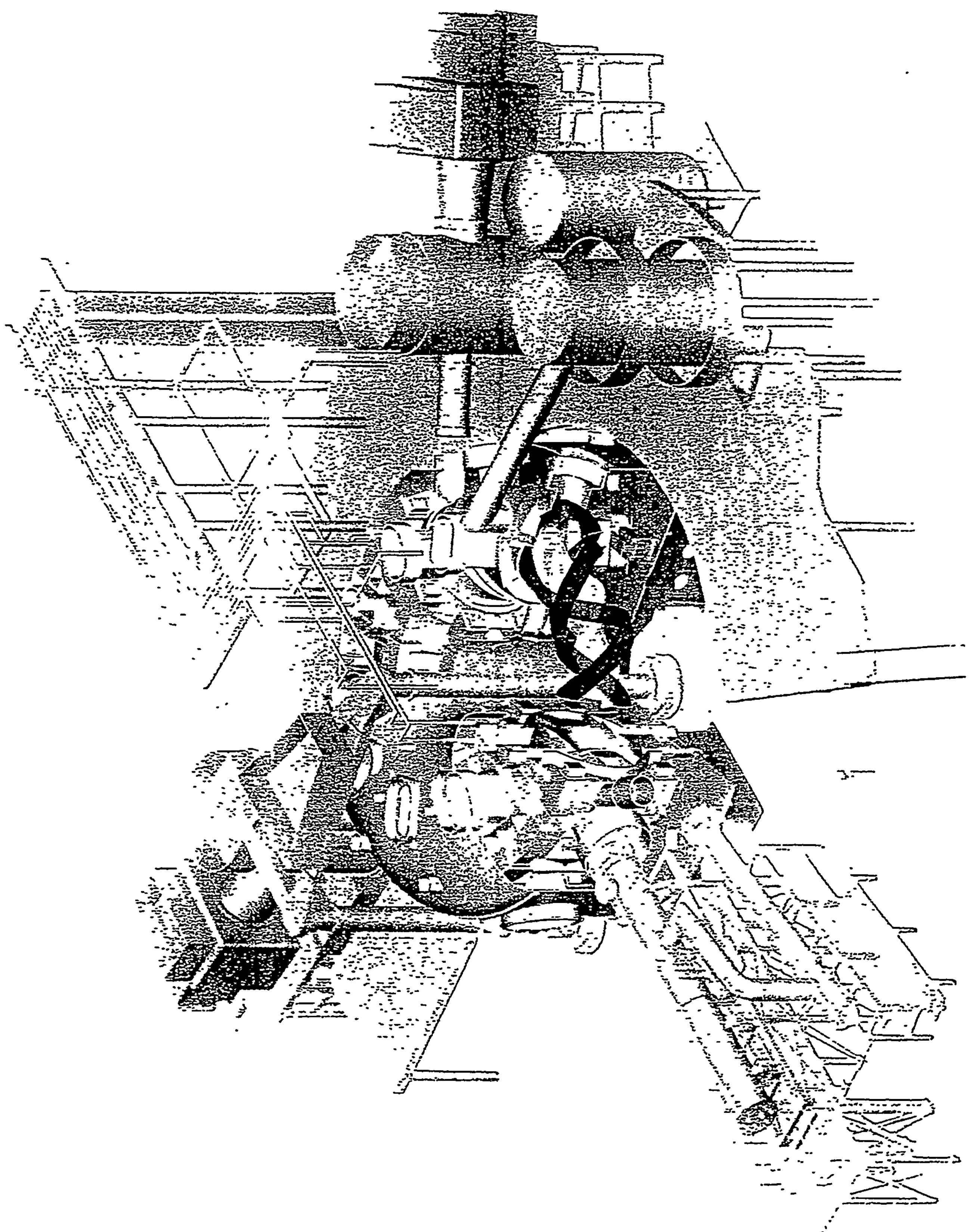

大電力中性粒子入射加熱装置

Neutral Beam Injection Heating System

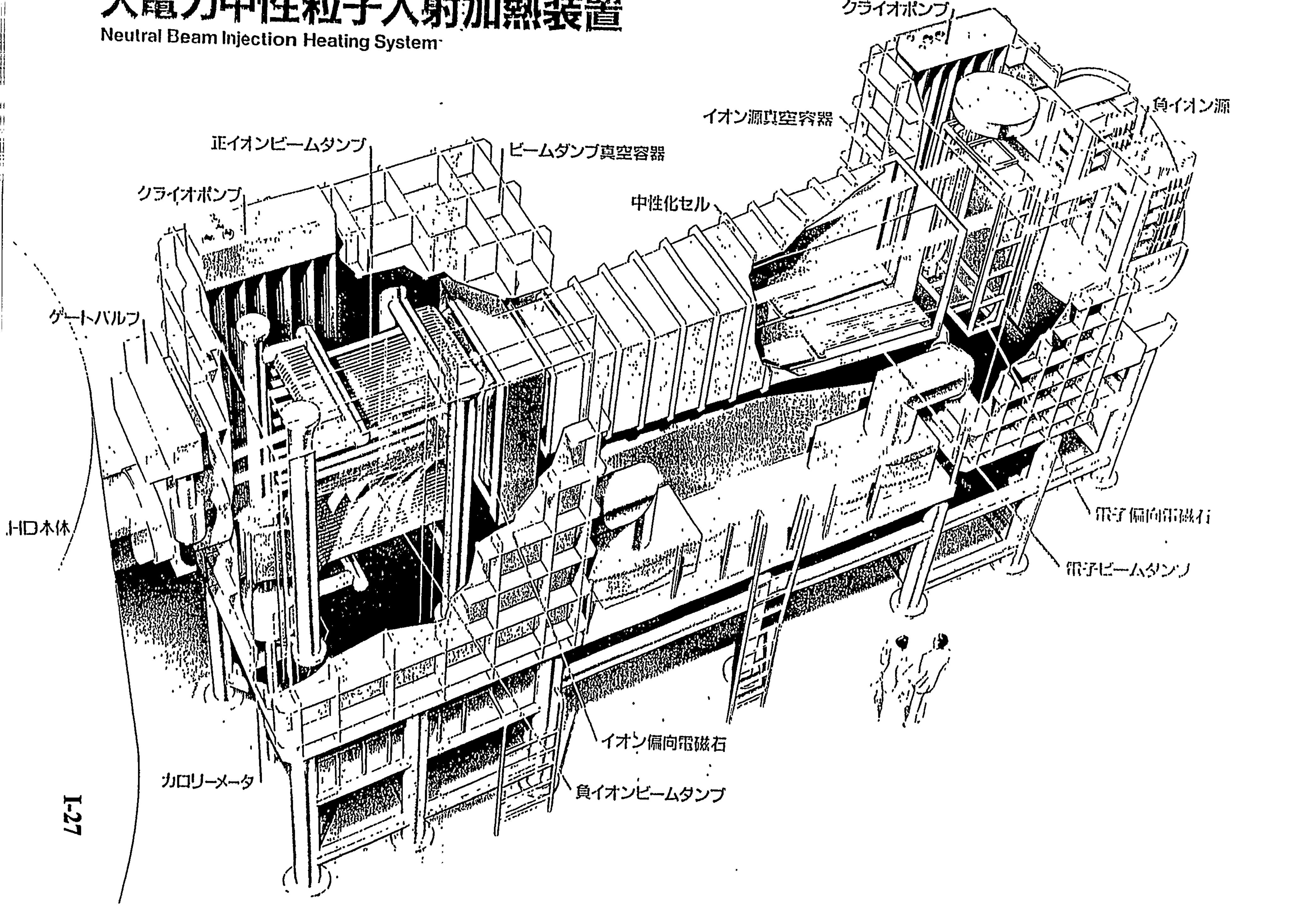

Development of 84GHz High Power CW Gyrotrons

- 400kW 10.5sec., 500kW 2sec., 100kW 30min. oscillation
- The maximum power is limited by window temperature rise.
- The gas pressure increment prevented from obtaining higher duty and CW operations.

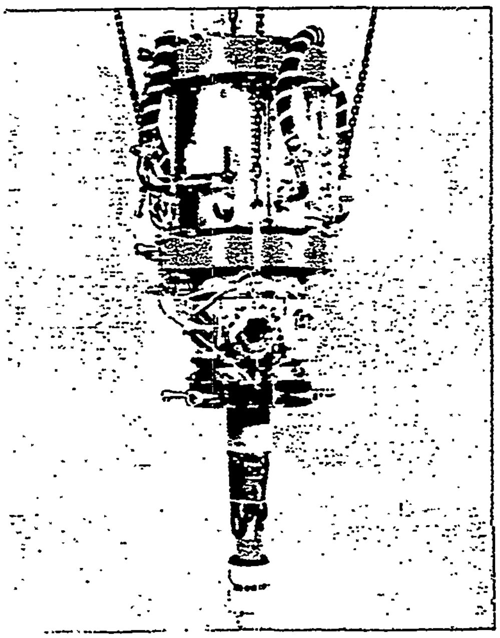

84GHz CW gyrotron

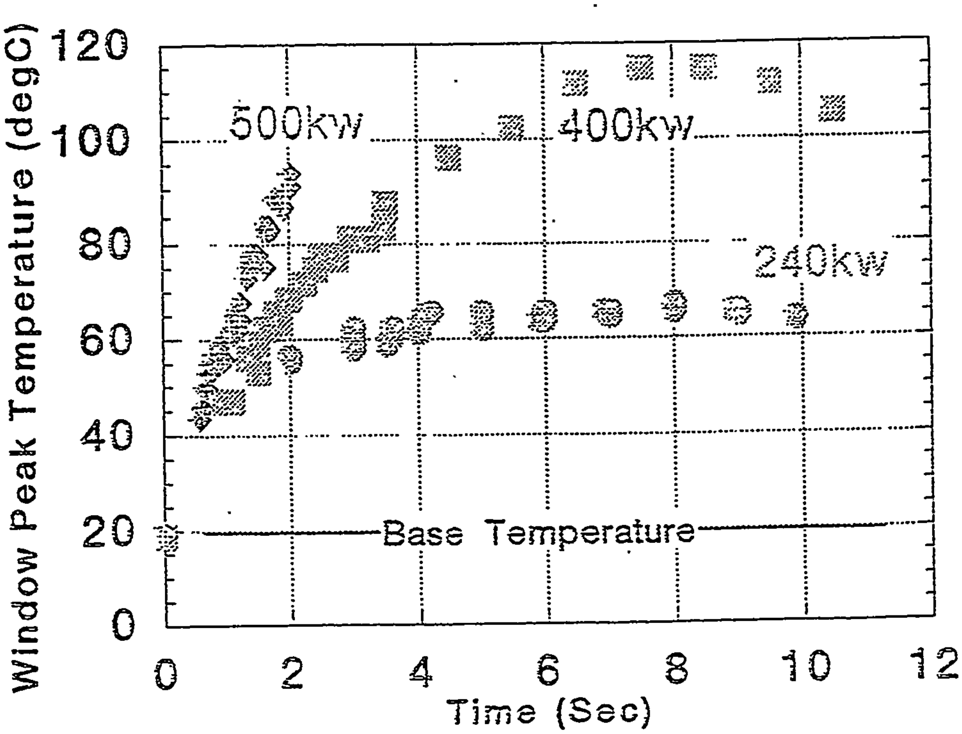

Variation of peak window temperature during RF pulse

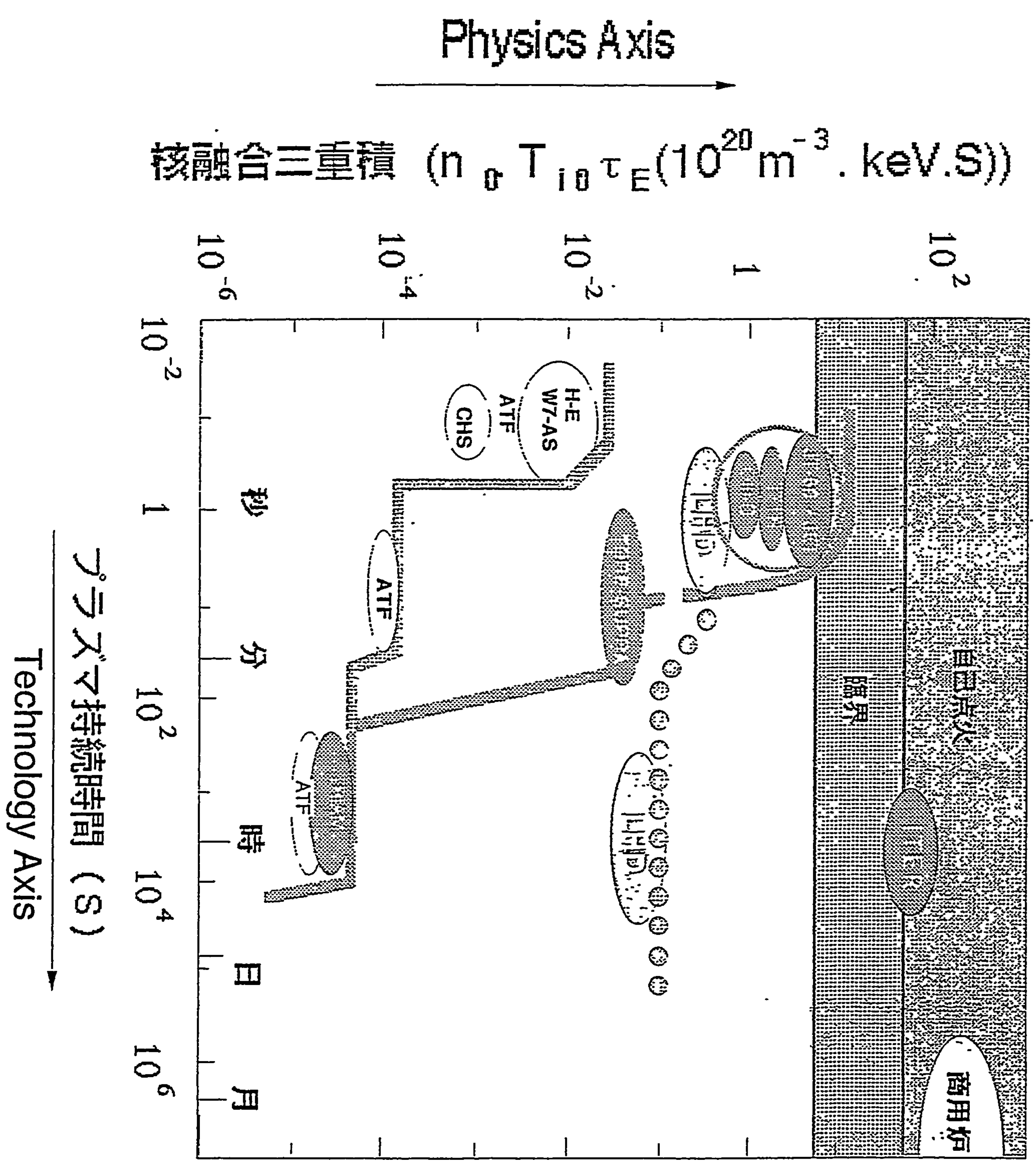
Physics Axis
核融合三重積 (n0 Ti0 τE(10^20 m^-3 . keV.S))
10^-6
10^-4
10^-2
1
10^2
10^-2
1
10^2
10^4
10^6
H-E
W7-AS
ATF
CHS
ATF
ATF
LHD
LHD
臨界
自己点火
商用炉
秒
分
時
日
月
プラズマ持続時間（S）
Technology Axis

Heating Power and Wall Load

LHD

Heating Power	ECRH	10	MW	(10s)
		3	MW	(cw)
	NBI	20	MW	(10s)
	ICRF	9	MW	(10s)
		3	MW	(cw)
Max. Heat load on Divertor Plate				
		5	MW/m^2	(10s, 20MW)
		10	MW/m^2	(5s, >30MW)
		0.75	MW/m^2	(cw, 3MW)
		2.5	MW/m^2	(cw, 10MW)

OM0298

Fueling Plans on LHD

Gas Puff

- H_2, D_2, He : up to 300Pa·m^3/s from 9 inlets
(100Pa·m^3/s from single inlet for the initial operation)
- Ar (>50Pa·m^3) : Plasma shutdown
- High purification control ~10 ppb

Pellet Injectors

Fueler
- 10-barrel single-stage pipe gun
- H_2, D_2 : 1.0 ~ 3.8mmφ
- 500 ~ 1500 m/s

Tracer-encapsulated pellet
- Li and C encapsulated in H_2
- ~ 800m/s

Impurity pellet
- Hydrocarbon, Al, Li, C, Ti etc. : 0.3 ~ 1mmφ
- 300 ~ 500 m/s

NBI

- Negative ion source
- Balanced injection with 2 beam lines
- 180 keV and 90 A in total

Compact Torus Injection (in design)

- Contained particle 1×10^{19}, V_{CT}~300km/s
- Collaboration with Himeji Institute of Technology

Fueling Scenario in LHD Experiment

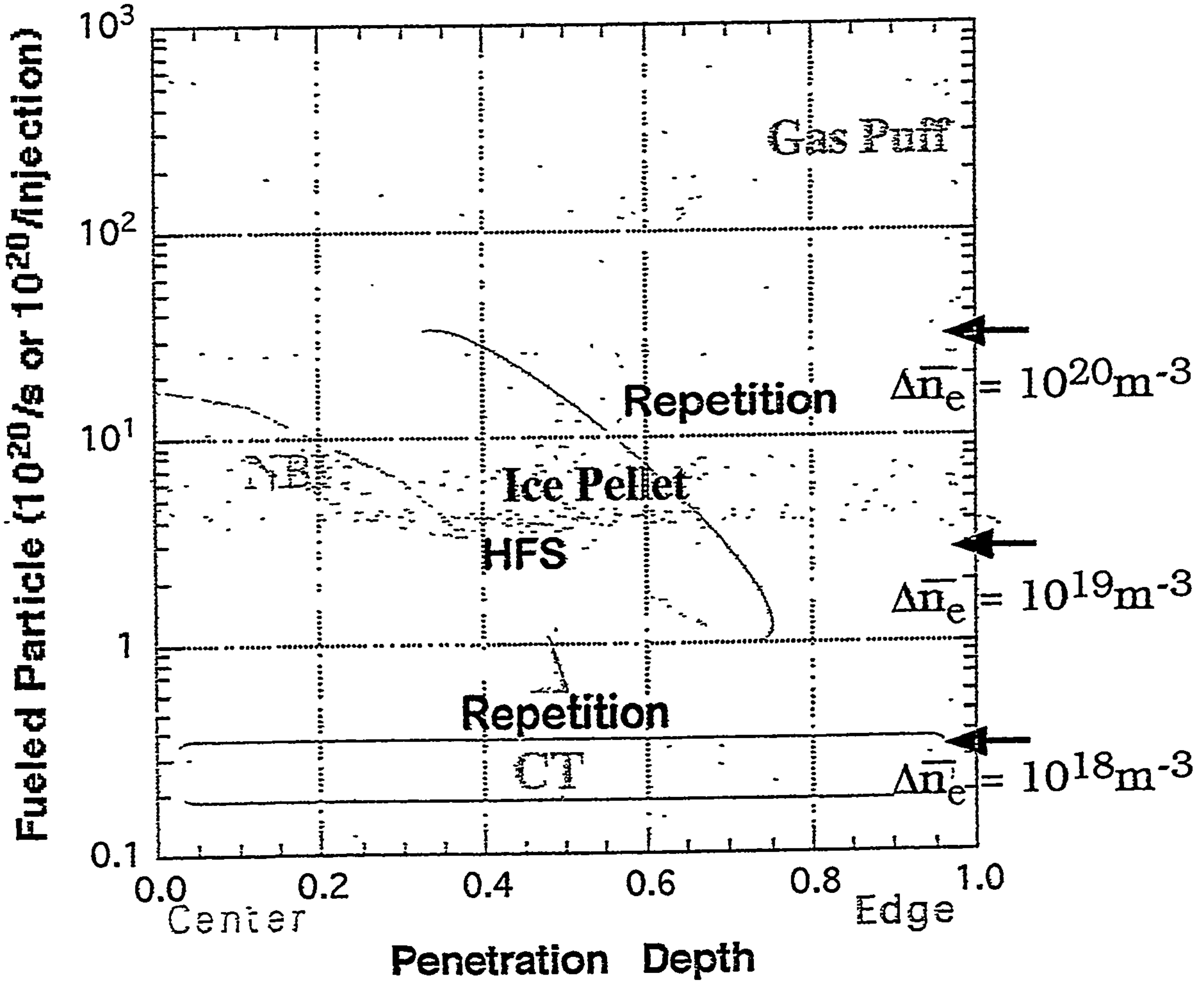

Note :

Fueling efficiency

NBI ~100%, Pellet 20~100%,

CT 15~30%, GasPuff 2~20%

Consistency with capability of pumping systems

Main pumps, LID, Divertor

Specific pellet injectors

Tracer-encapsulated pellet and

Impurity pellets (Li,Al,C, etc)

for transport studies

Divertor concepts for LHD

NIFS

Helical Divertor (HD) ~ Helical divertor geometry ~

* High recycling operation
  - *high density, low temperature* ($n_{div} > 10^{20}$ m^{-3})
  - *edge radiative cooling for safe heat removal*
* Low recycling operation by efficient pumping
  - *low density, high temperature* ($n_{div} < 10^{17}$ m^{-3})
  - *significant improvement of* τ_E *i.e., H-mode*

SHC boundary ~ Helical + Island divertor geometries ~

* Low density, high temperature, steep gradient at LCFS
  - *favorable for H-mode*
* High density, low temperature in ergodic boundary
  - *favorable for radiative cooling*

$m/n = 1/1$ island

Simultaneous achievement of H-mode and radiative Cooling

Local Island Divertor (LID) ~ Island divertor geometry ~

* Closed divertor with high efficient pumping system
  - *low recycling operation for confinement improvement*
* No leading edge problem
* Efficient discharge cleaning

$m/n = 1/1$ island

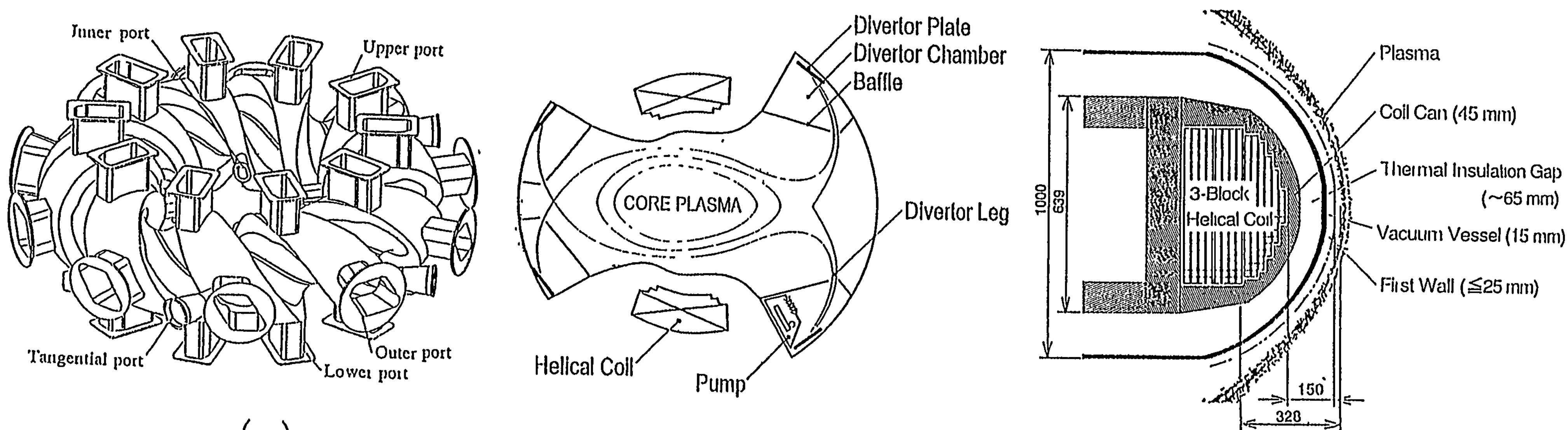
Inner port
Upper port
Tangential port
Outer port
Lower port
Divertor Plate
Divertor Chamber
Baffle
CORE PLASMA
Divertor Leg
Helical Coil
Pump
Plasma
Coil Can (45 mm)
Thermal Insulation Gap
(~65 mm)
Vacuum Vessel (15 mm)
First Wall (≦25 mm)
3-Block
Helical Coil
1000
639
150
328

(a) (b) (c)

SHC boundary configuration

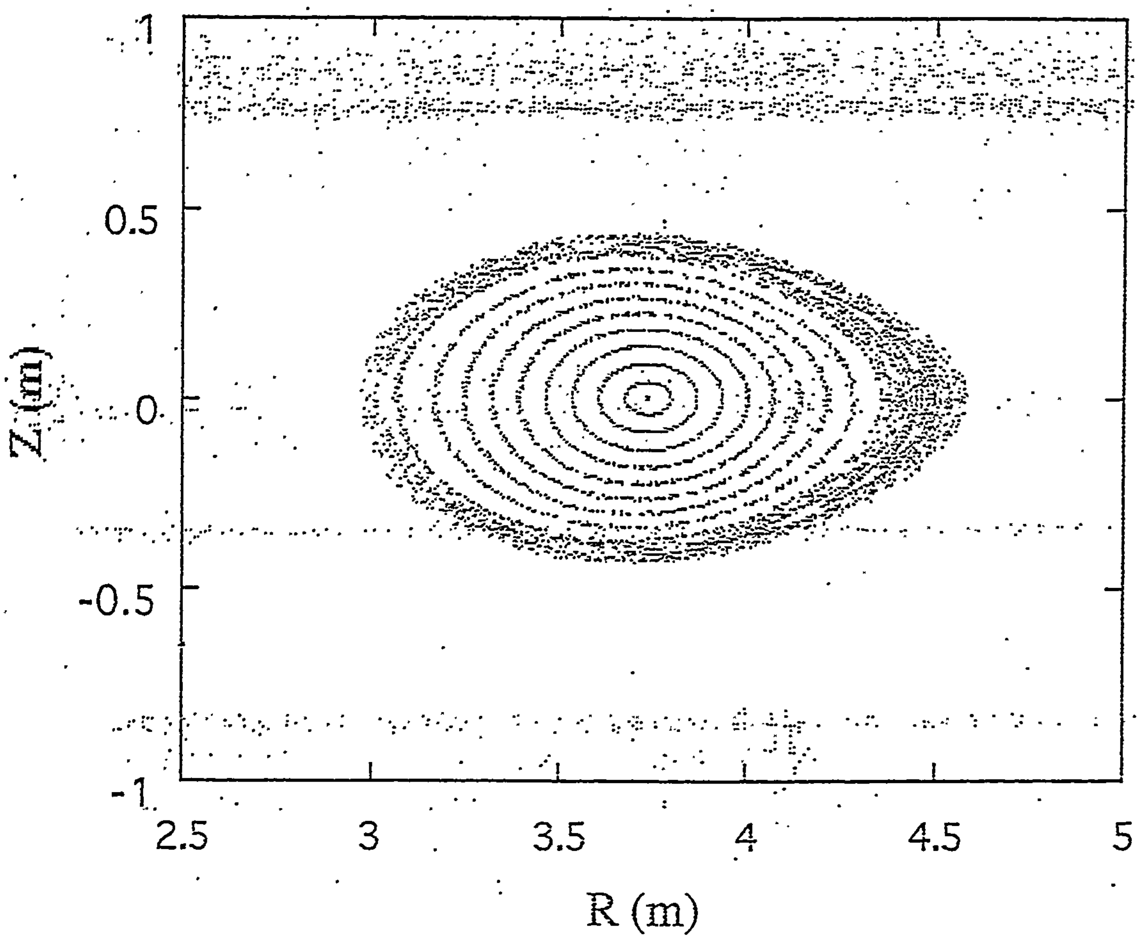

RESEARCH PROGRESS BY HELIOTRON CONCEPT

1980's

PROOF OF PRINCIPLE EXPERIMENT

Heliotron E (KYOTO U.)
CHS (NIFS)

1 keV
$\tau_E > 10$ ms
$\beta = 2\%$

1990's

CONSTRUCTION OF LHD

R&D
ENGINEERING DESIGN
COMPONENT TEST
COMMISSIONING TEST

SC TECHNOLOGY
MATERIAL
HEATING
CONTROL
SYSTEM ENGINEERING
MECHANICS

1998～

LHD EXPERIMENT

FUSION CORE PHYSICS
10 keV
Q > 0.1
CONFINEMENT, STABILITY
STEADY・DIVERTOR

～2025

DEMO REACTOR DESIGN

CONCEPTUAL DESIGN → DETAILED ENGINEERING DESIGN

Force Free Coil
MATERIAL DEVELOPMENT (LOW ACTIVATION)
BLANKET DESIGN (FLiBe)
SAFETY ANALYSIS
COST EVALUATION
R&D
SYSTEM DESIGN

US/Japan Workshop on Advanced Fueling
December 2-3, 1997
Lawrence Livermore National Laboratory, USA

Status of LHD and Fueling Plans

LHD

Osamu Motojima

National Institute for Fusion Science
322-6 Oroshicho, Toki 509-52, Japan

1, Introduction to LHD Project
   Missions in Fusion Physics and Technology
   Specifications of LHD
2, Construction Status
3, Experimental Planning
   Commissioning Tests
   First Plasma Start up Scenario
   Heating System (NBI, Gyrotron, ICRF)
4, Fueling Plans
   Pellet Injection, CT Injection, Gas Puff System
5, Summarizing

OMO298

Divertor, First Wall, and PSI Issues in LHD

Presented by N. Noda (NIFS)

Contents

Present Status of the Divertor Construction

Concept is
Helically Running Discrete Bar Array

Final Goal is
Steady State Removal of > 10 MW/m^2

Stepwise Approach
Mechanically joined C-armor to Cu Heat sink and SS cooling tube

Fabrication of the Divertor is going on

N. Noda

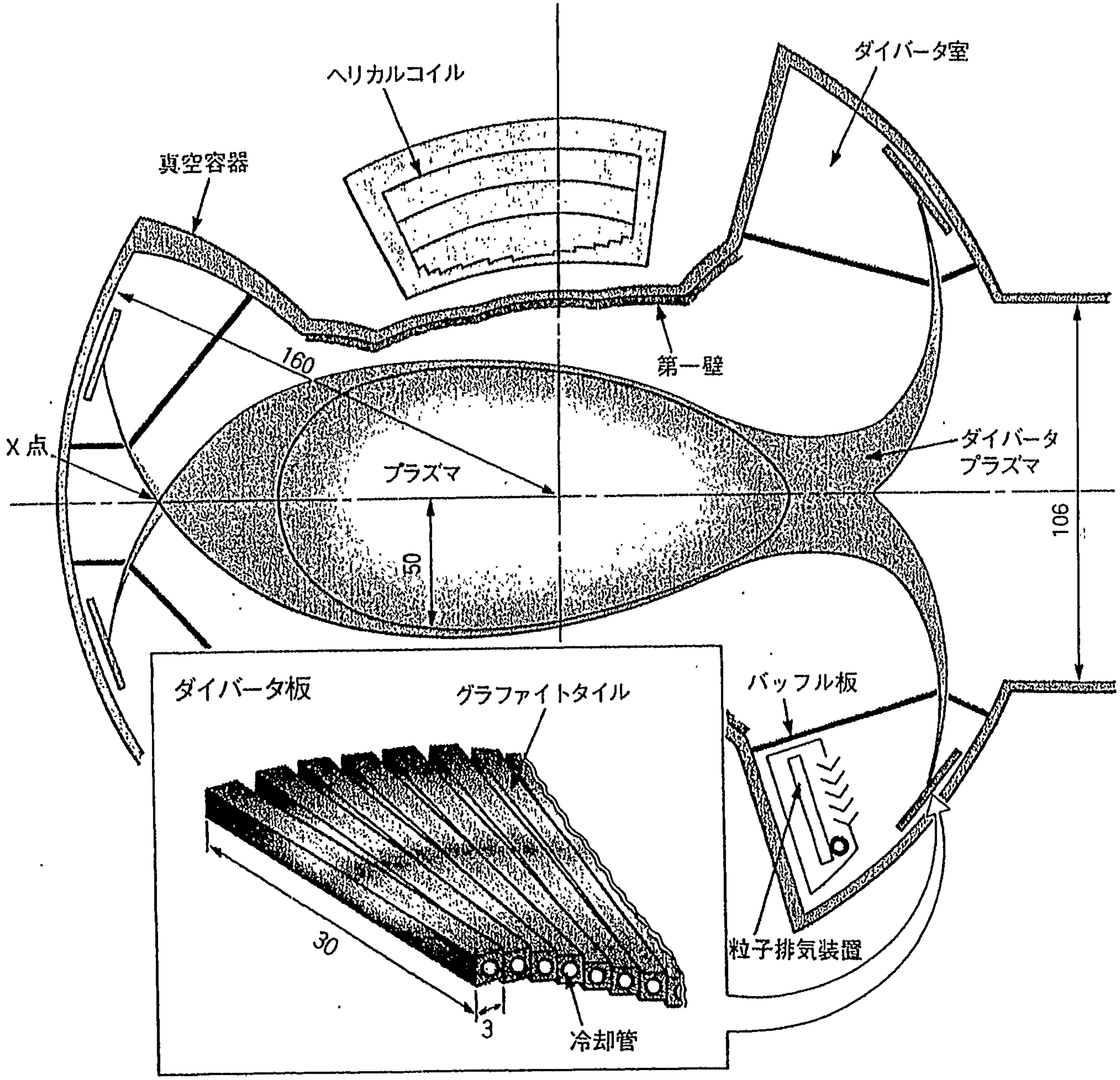

大型ヘリカル装置ポロイダル断面図

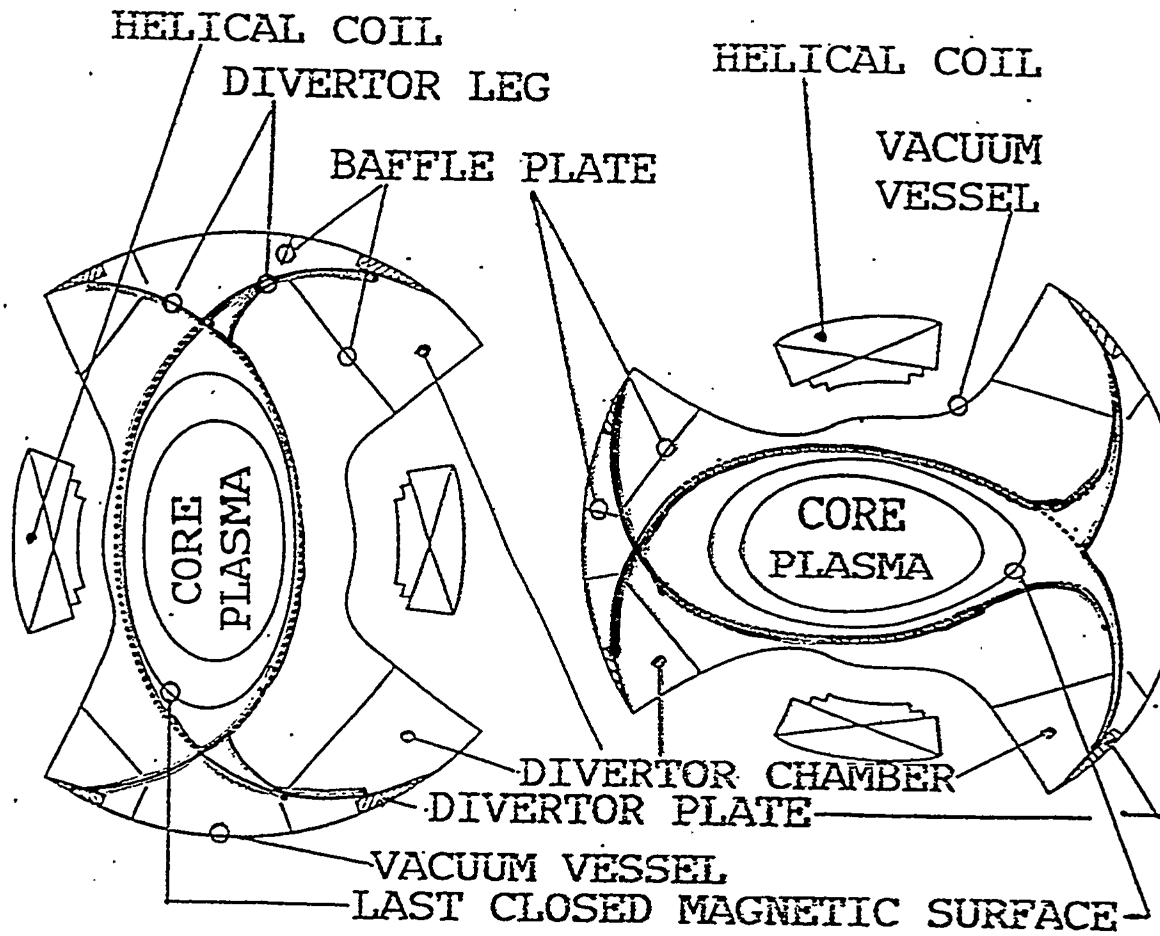

Fig. 1 Cross sectional view of the LHD device
Torus axis is on the left hand side.

Divertor Element and Sub-Unit of LHD

- $B_p \gg B_t$ at the striking points
- Three dimensional structure

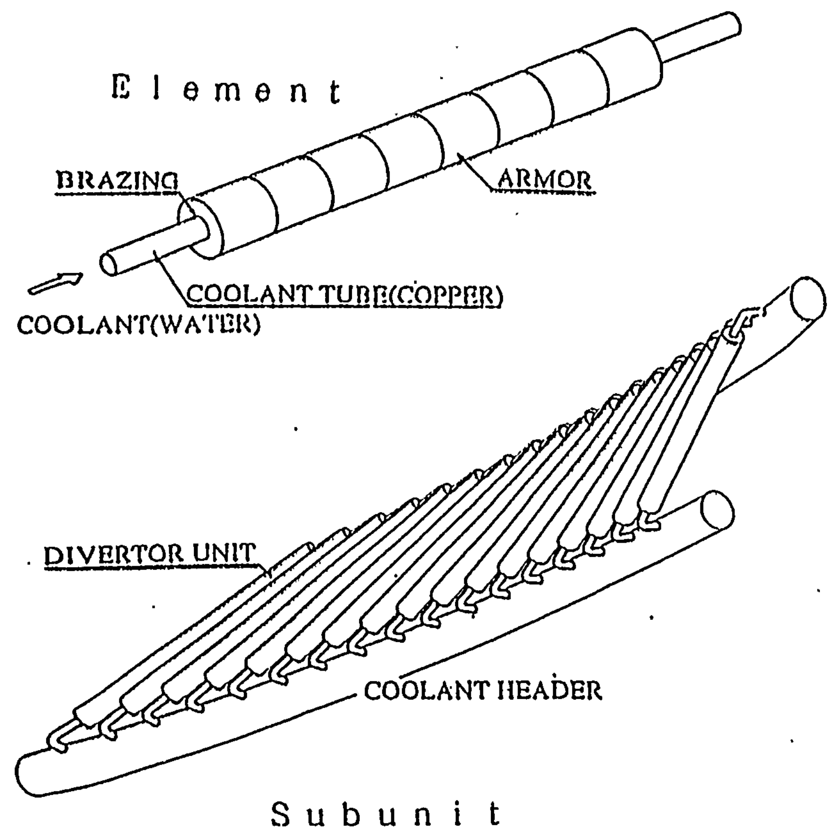

N. Noda

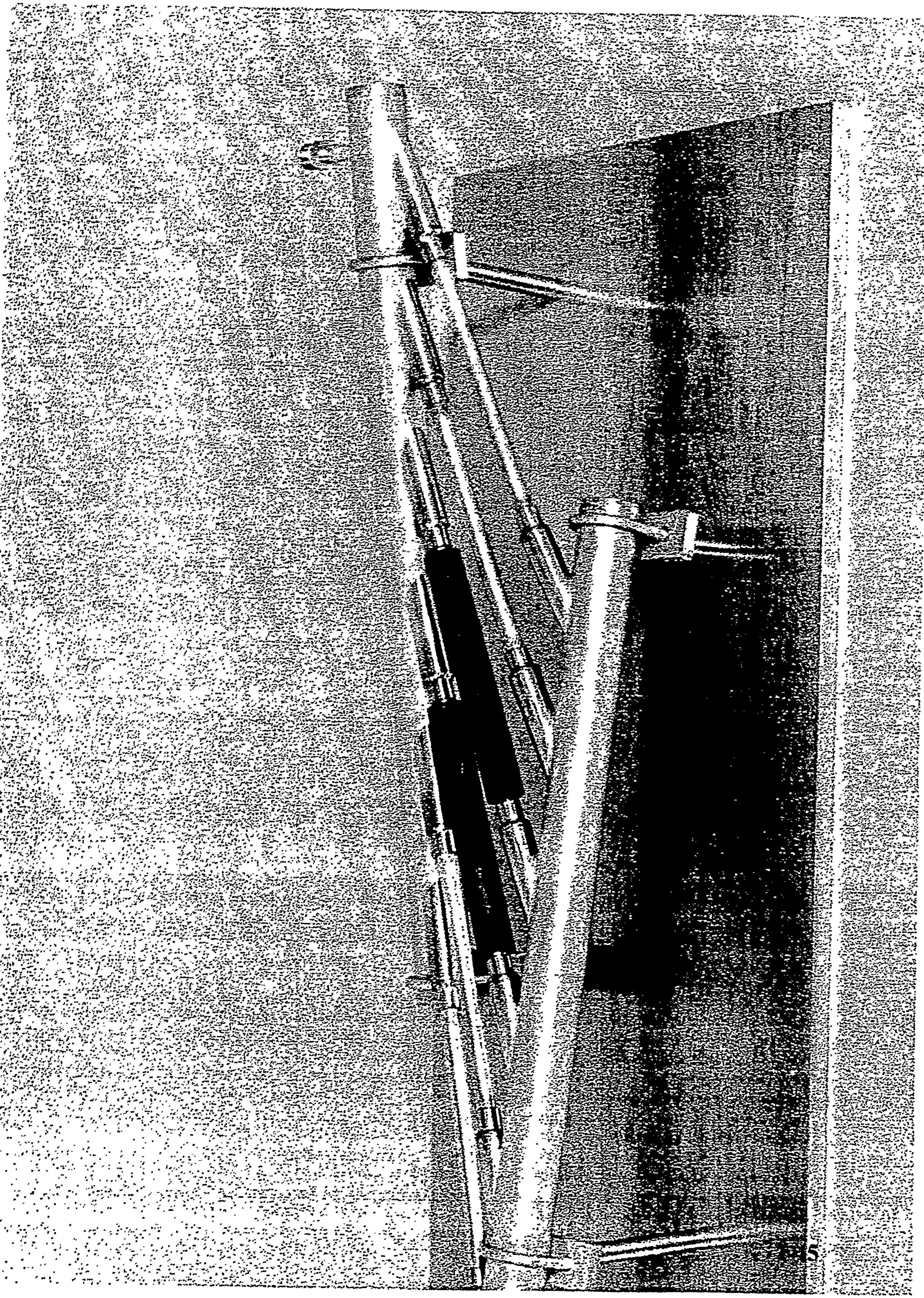

Stepwise approach of Divertor design

- To start with graphite armors mechanically joined to OFHC
  because of limited knowledgeabout the heat distribution
  flexibility of the MJ type configuration
  limitation of budget in the initial phase

- To learn the heat-load distribution during the initial phase experiments

- To replace them to brazed type elements from the highest heat load sectiorts

N. Noda

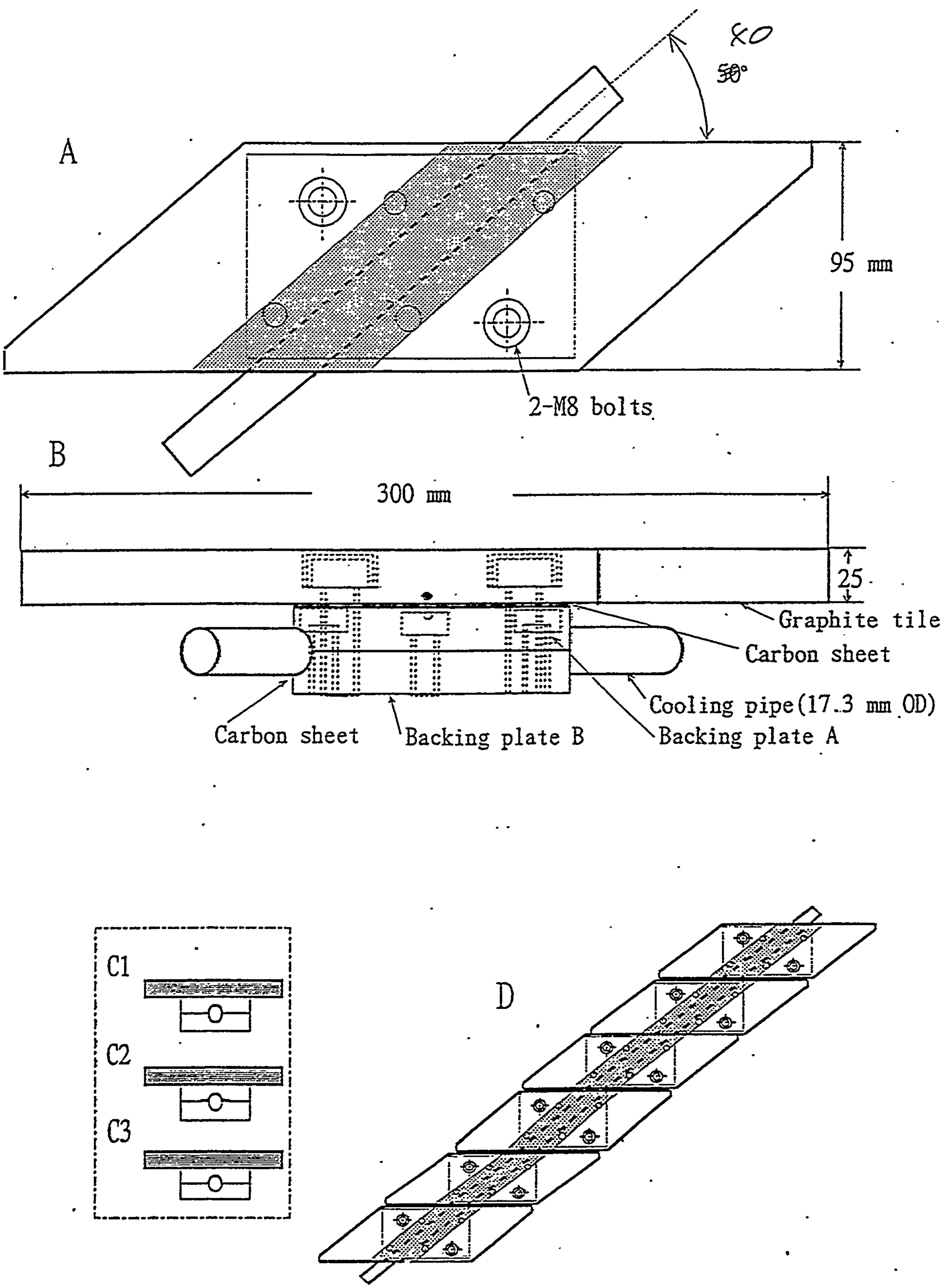

図１　特性評価用実サイズ機械的接合材（タイプ９）

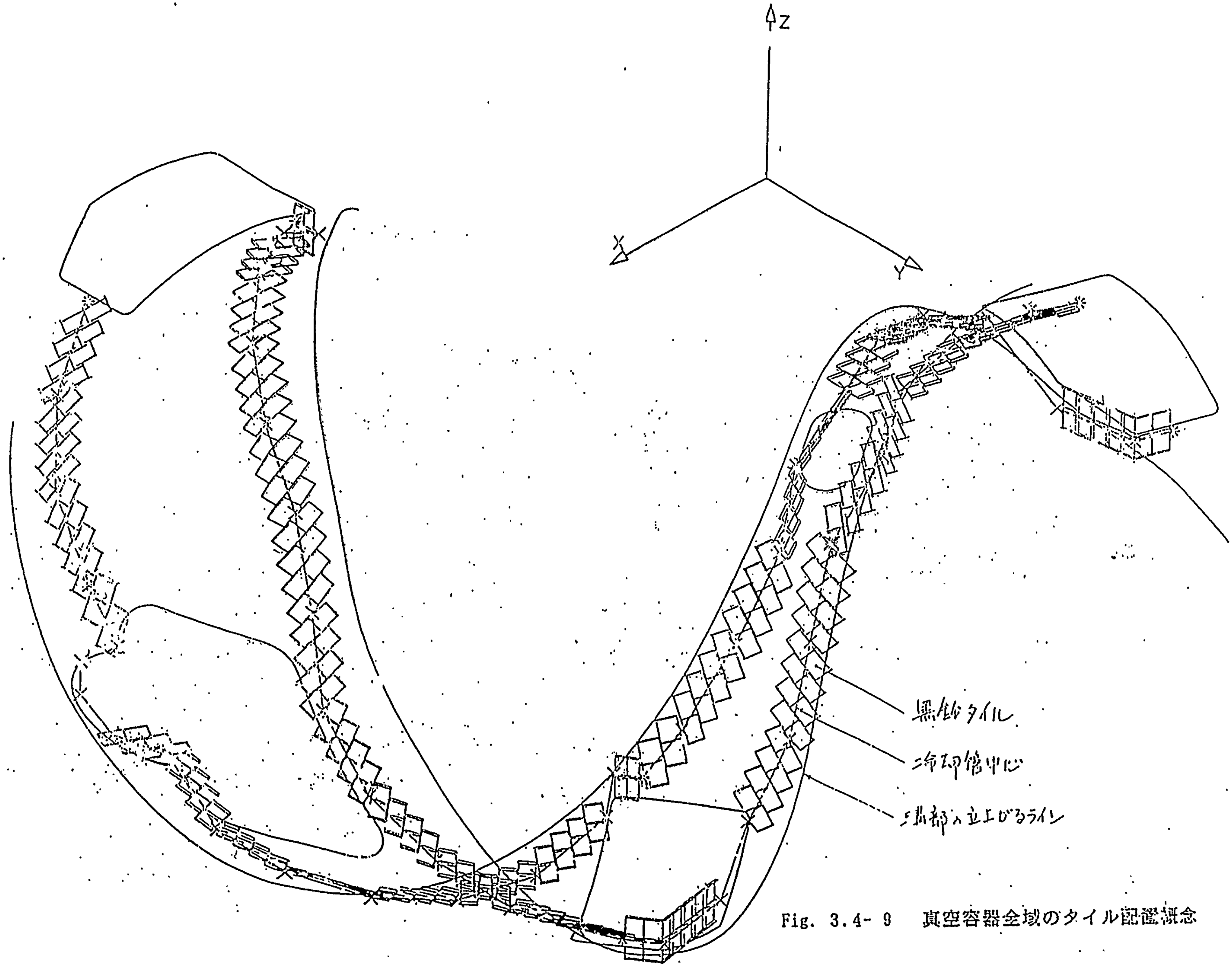

Fig. 3.4- 9　真空容器全域のタイル配置概念

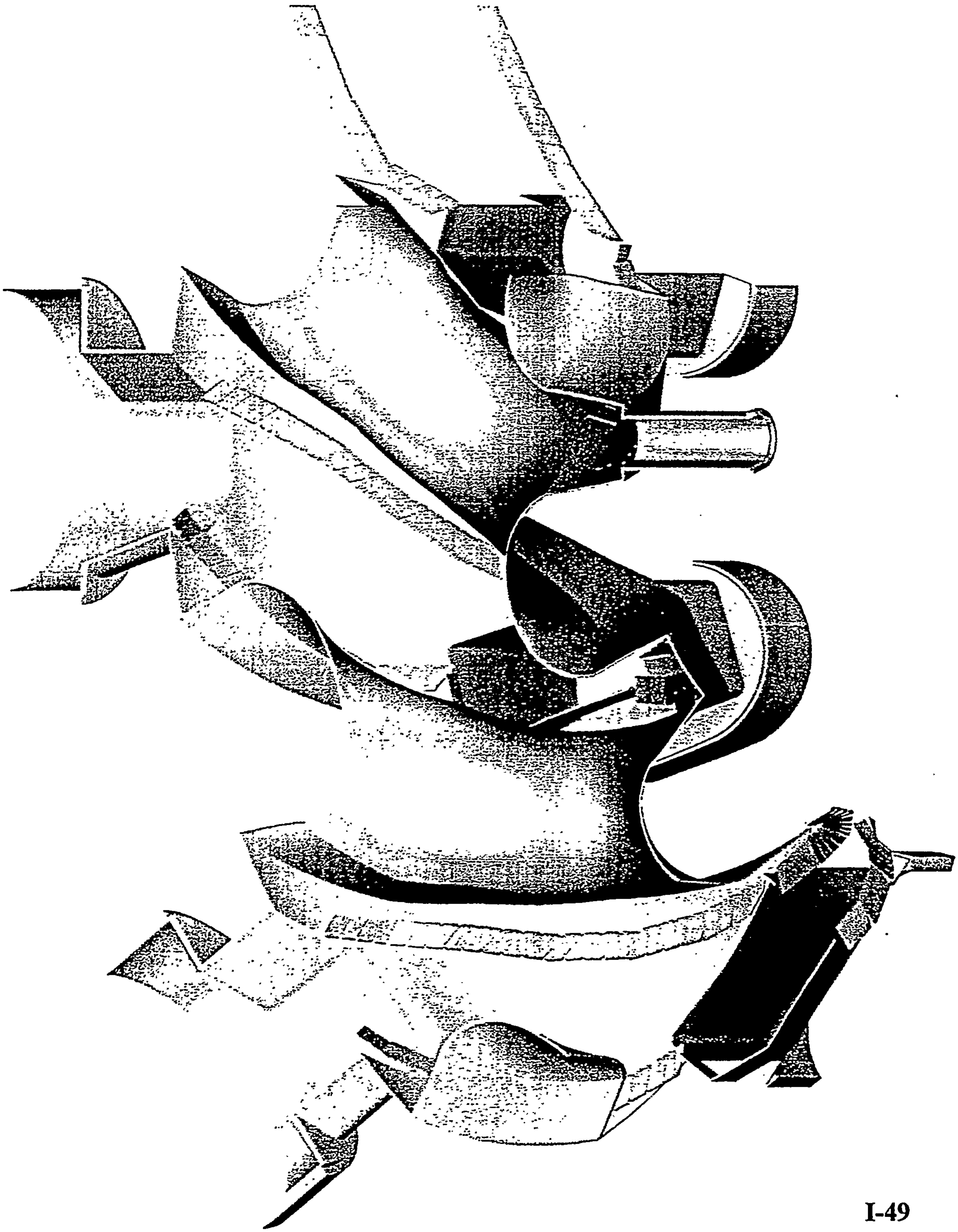

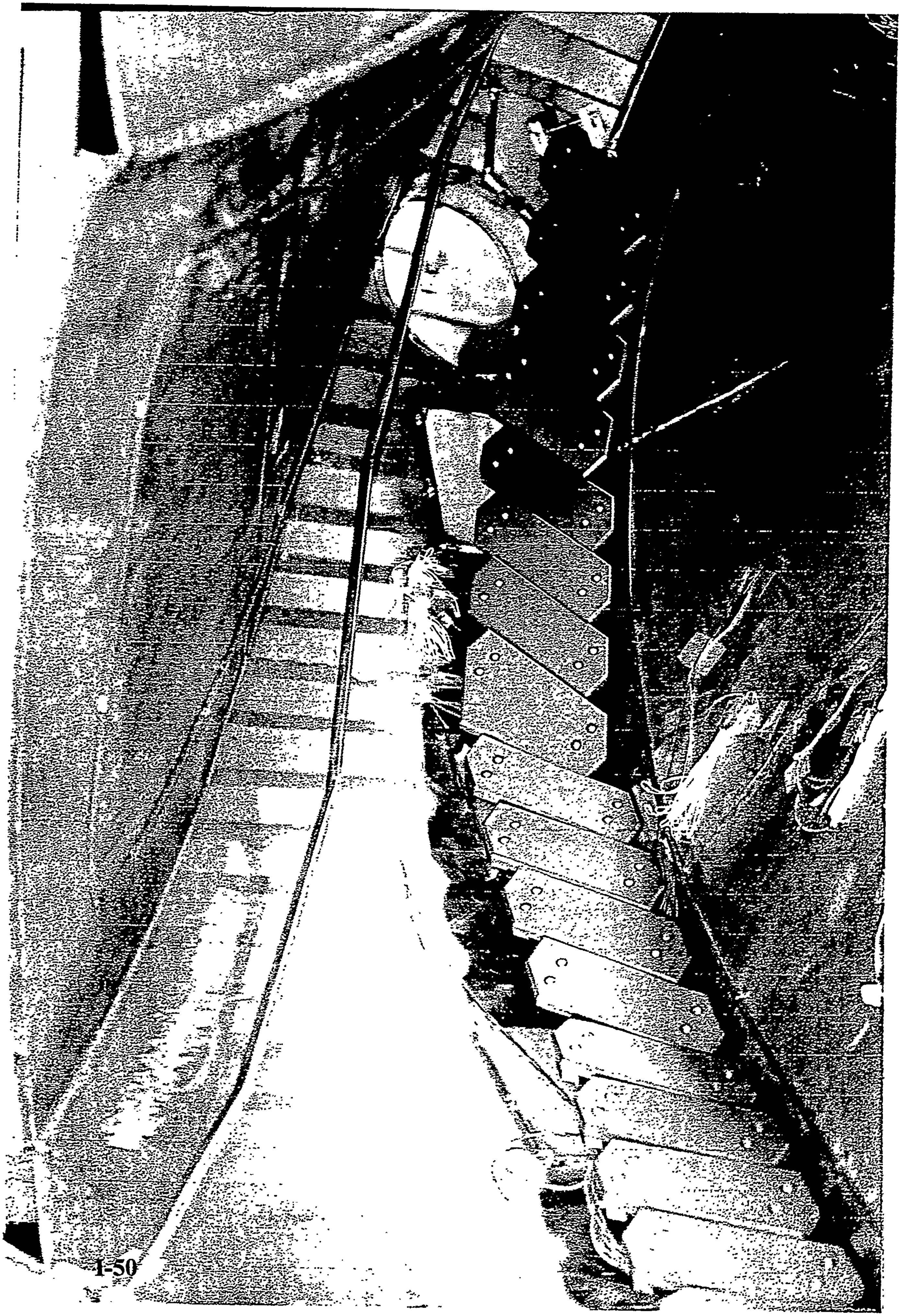

Thermocouple Measurement Hole

Isotropic Graphite Tile:

Hole: 1.1 mm

Thermocouple: 1.0 mm

Cu Heat Sink:

Hole: 1.7 mm

Thermocouple: 1.6 mm

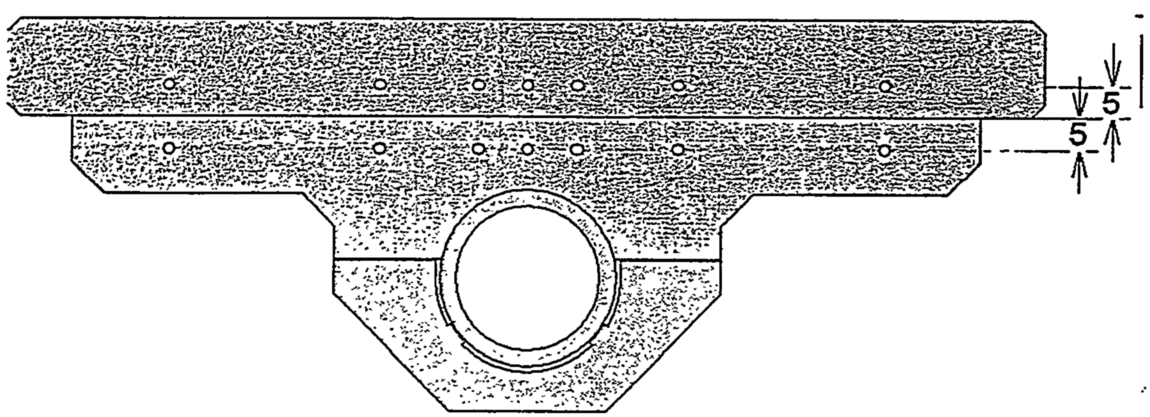

Temperature Profile of Divertor

0.3 MW/m^2, at 1000 s

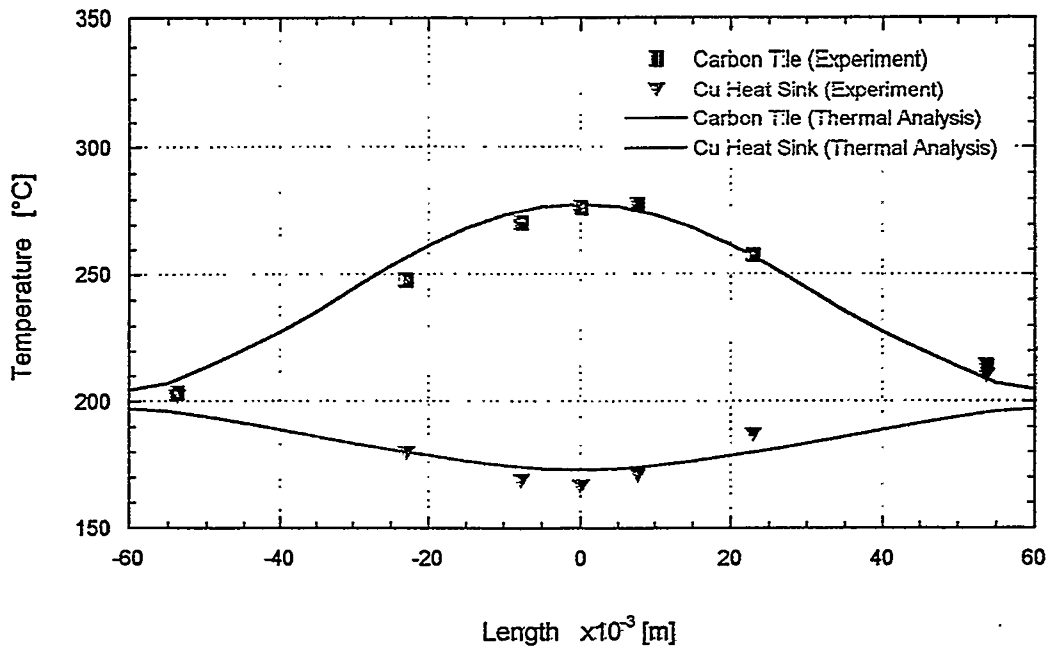

Temperature of
Isotropic Graphite Tile

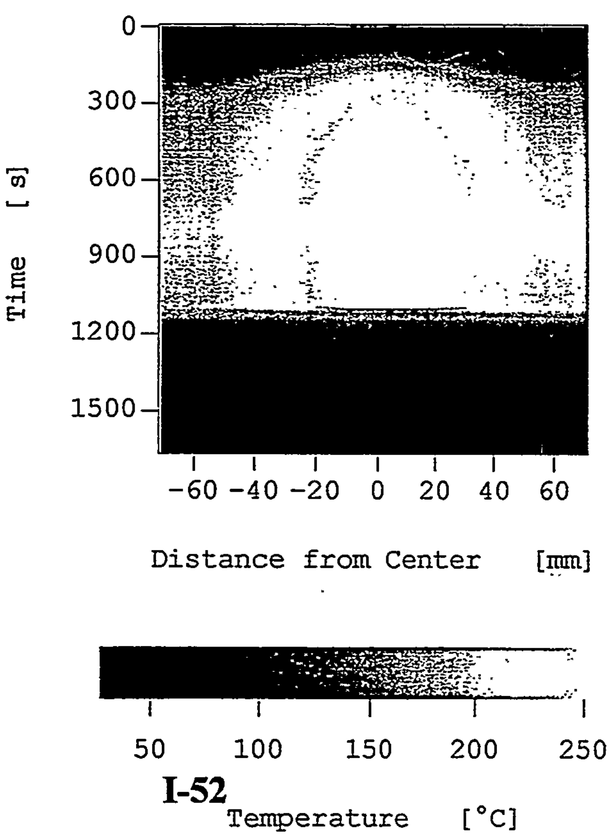

Temperature of
Cu Heat Sink

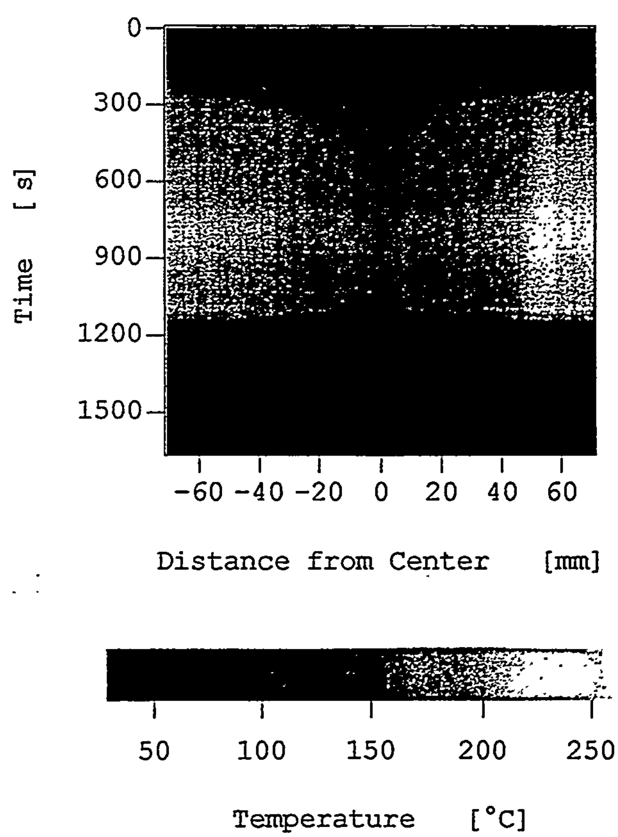

Temperature Change of Divertor Element during Electron Beam Heat Load Test

Cu Heat Sink

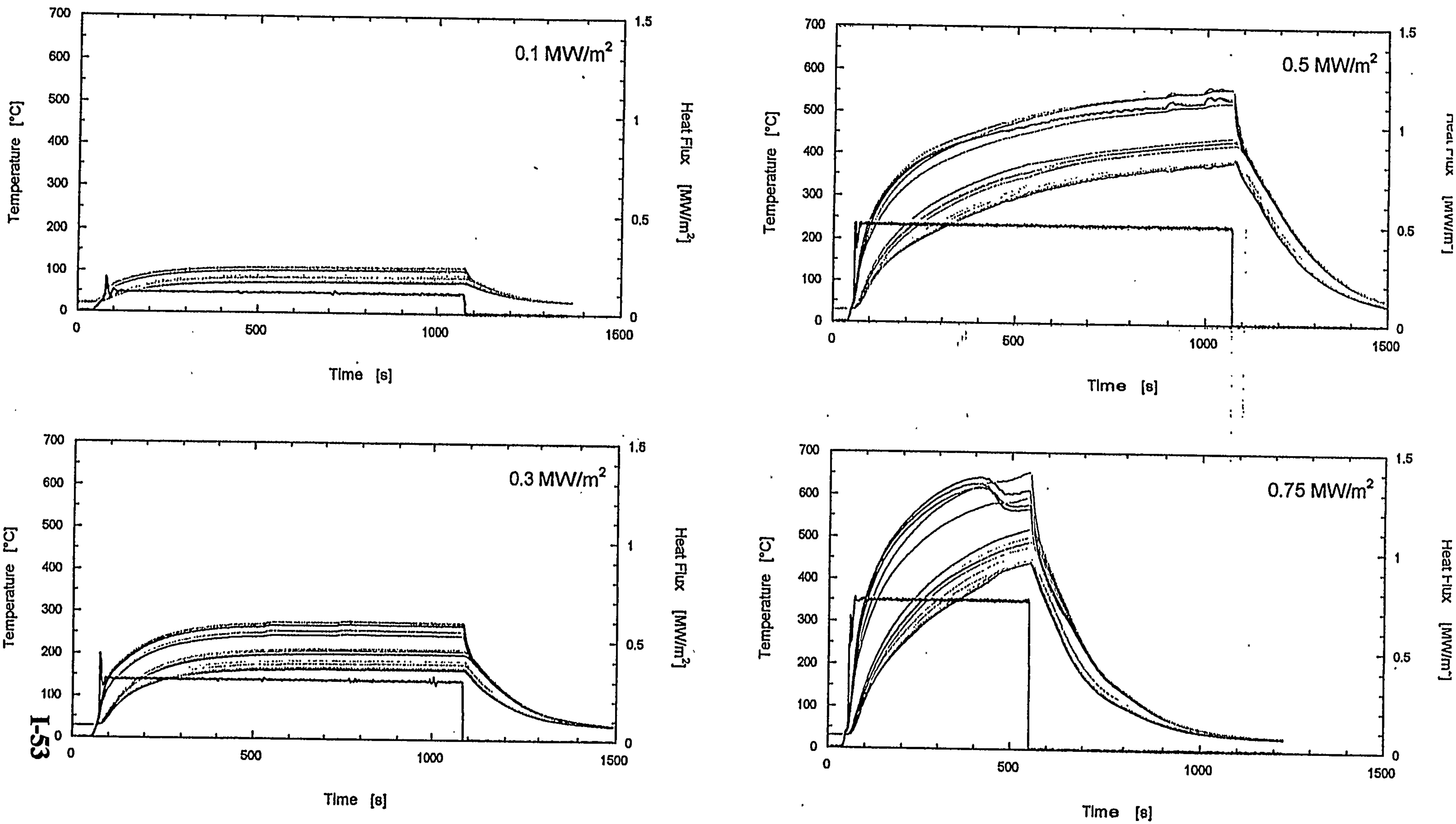

Mo heat sink

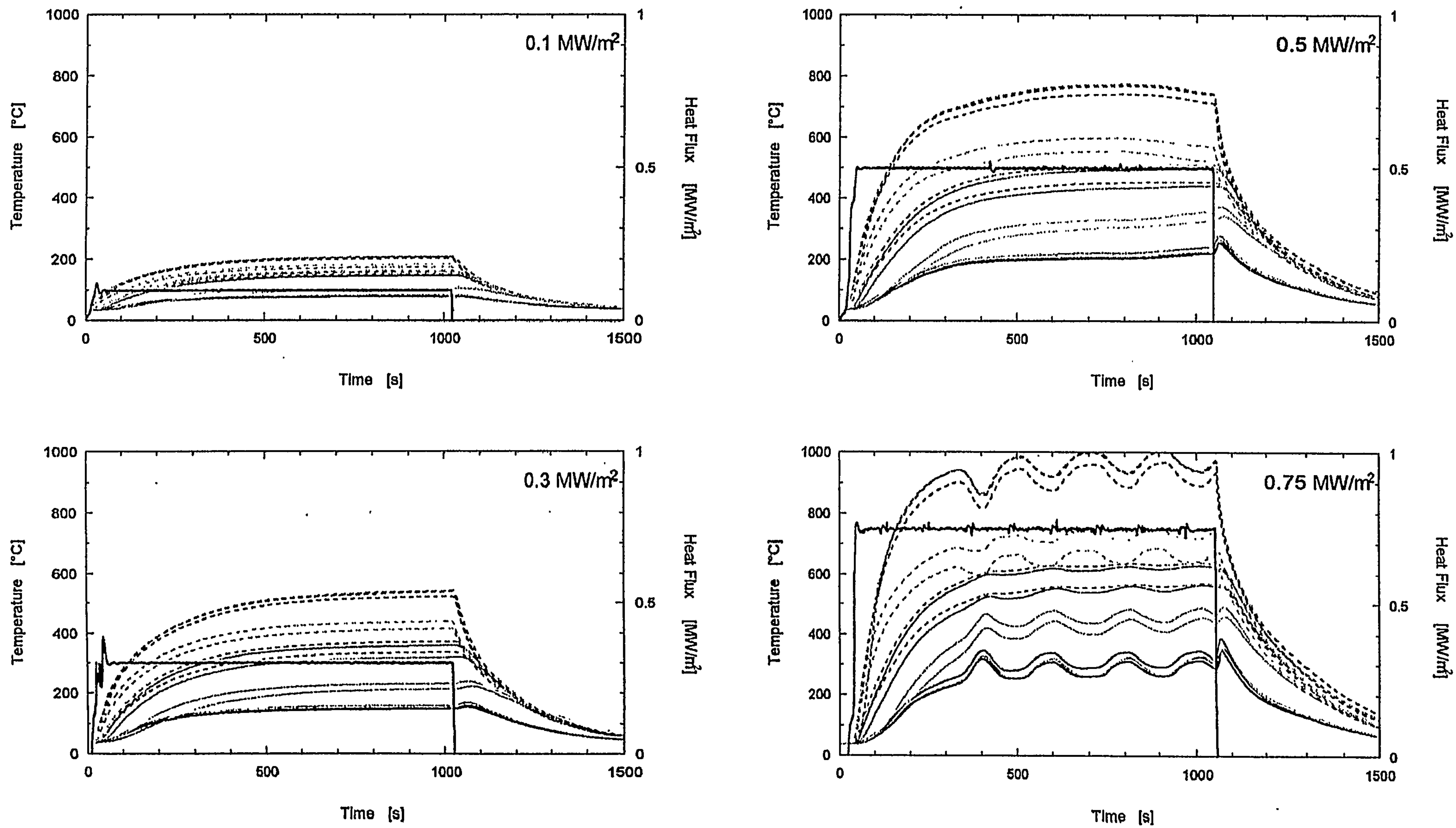

0.1 MW/m2
0.5 MW/m2
0.3 MW/m2
0.75 MW/m2
Temperature [°C]
Heat Flux [MW/m2]
Time [s]
0
500
1000
1500
200
400
600
800
0.5
1

Heat Flux Dependence of Heat Sink Temperature

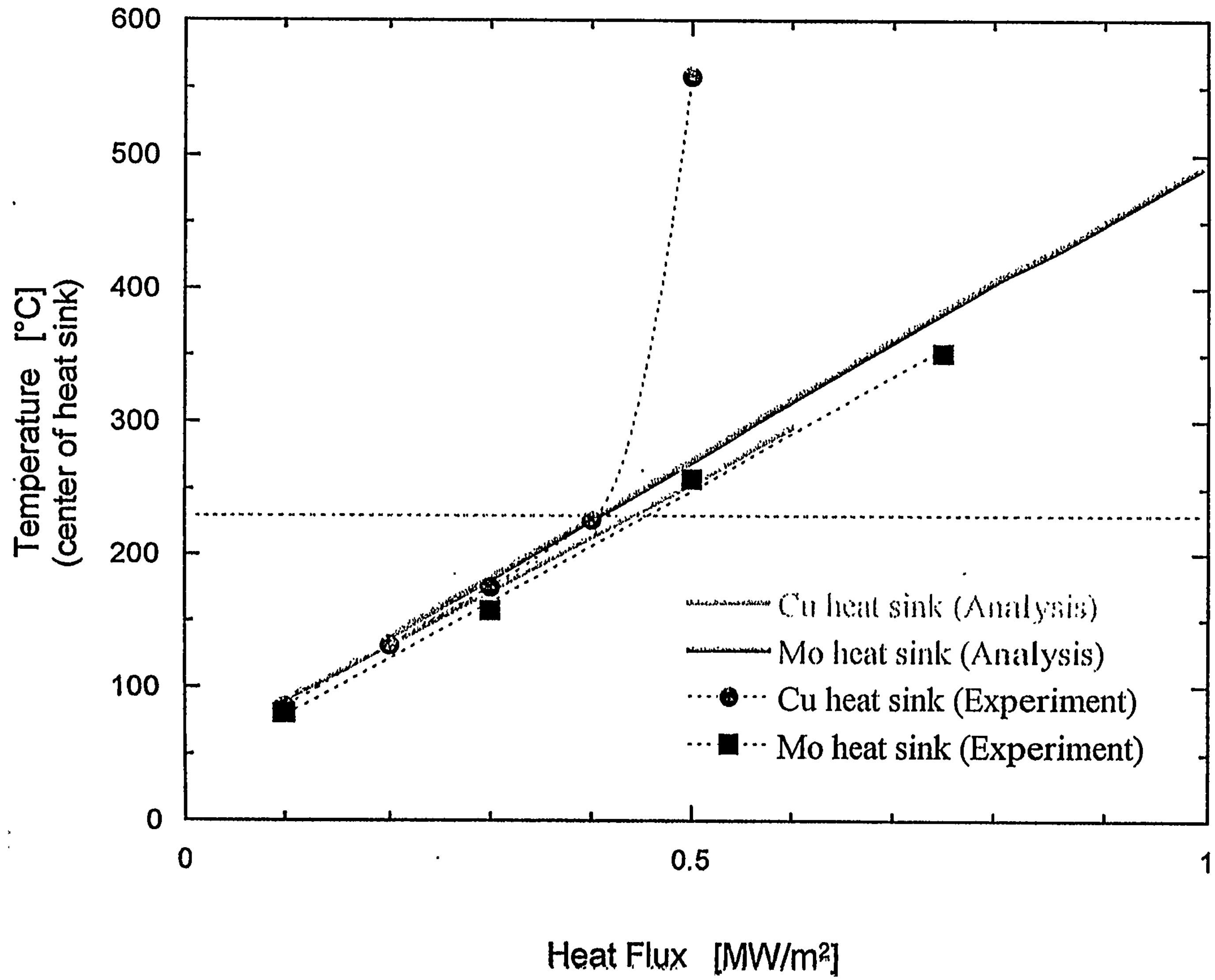

m／n＝１／１のコンポーネント
を加えた磁気面

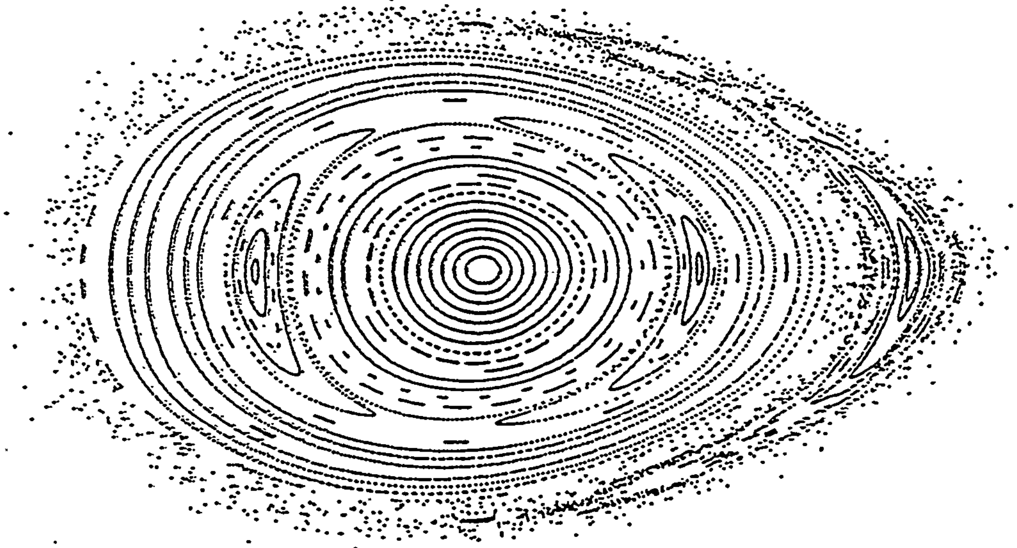

m／n＝２／１を打ち消すコンポ
ーネントを加えた磁気面

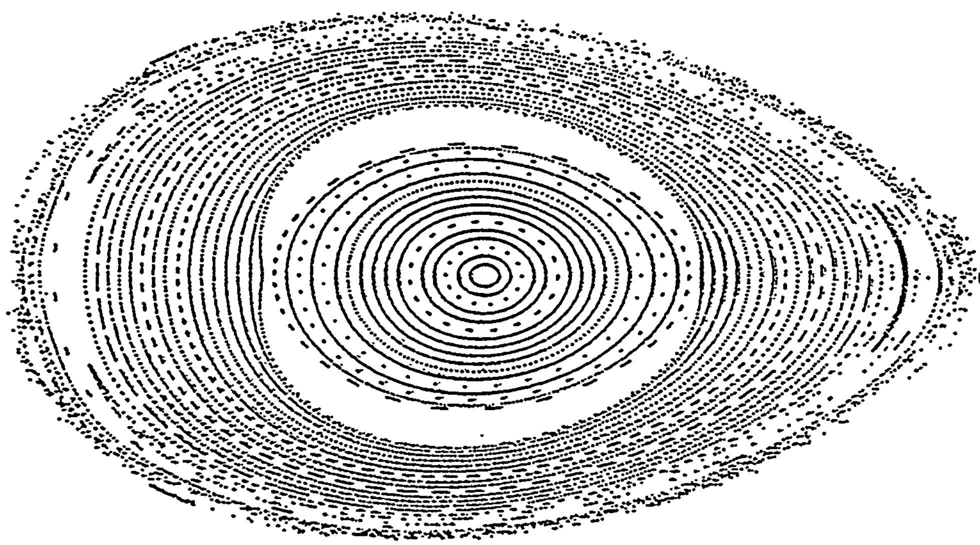

m／n＝１／１のアイランドだけ
が形成された磁気面

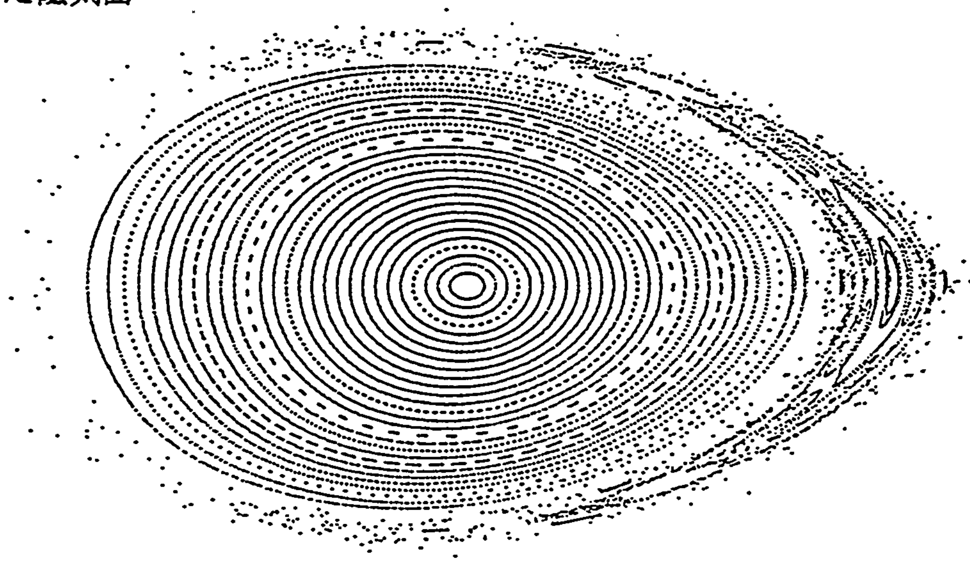

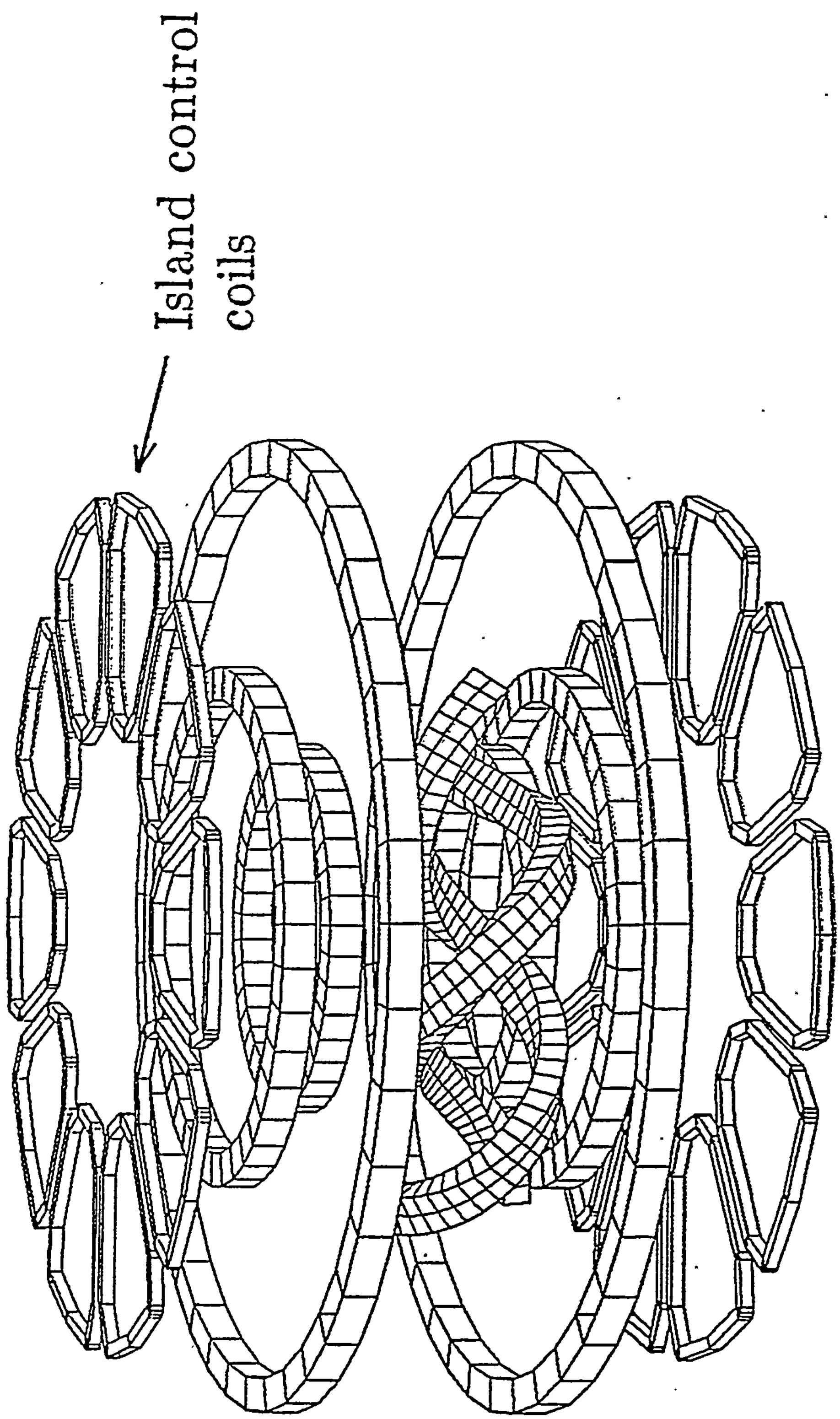
Island control
coils

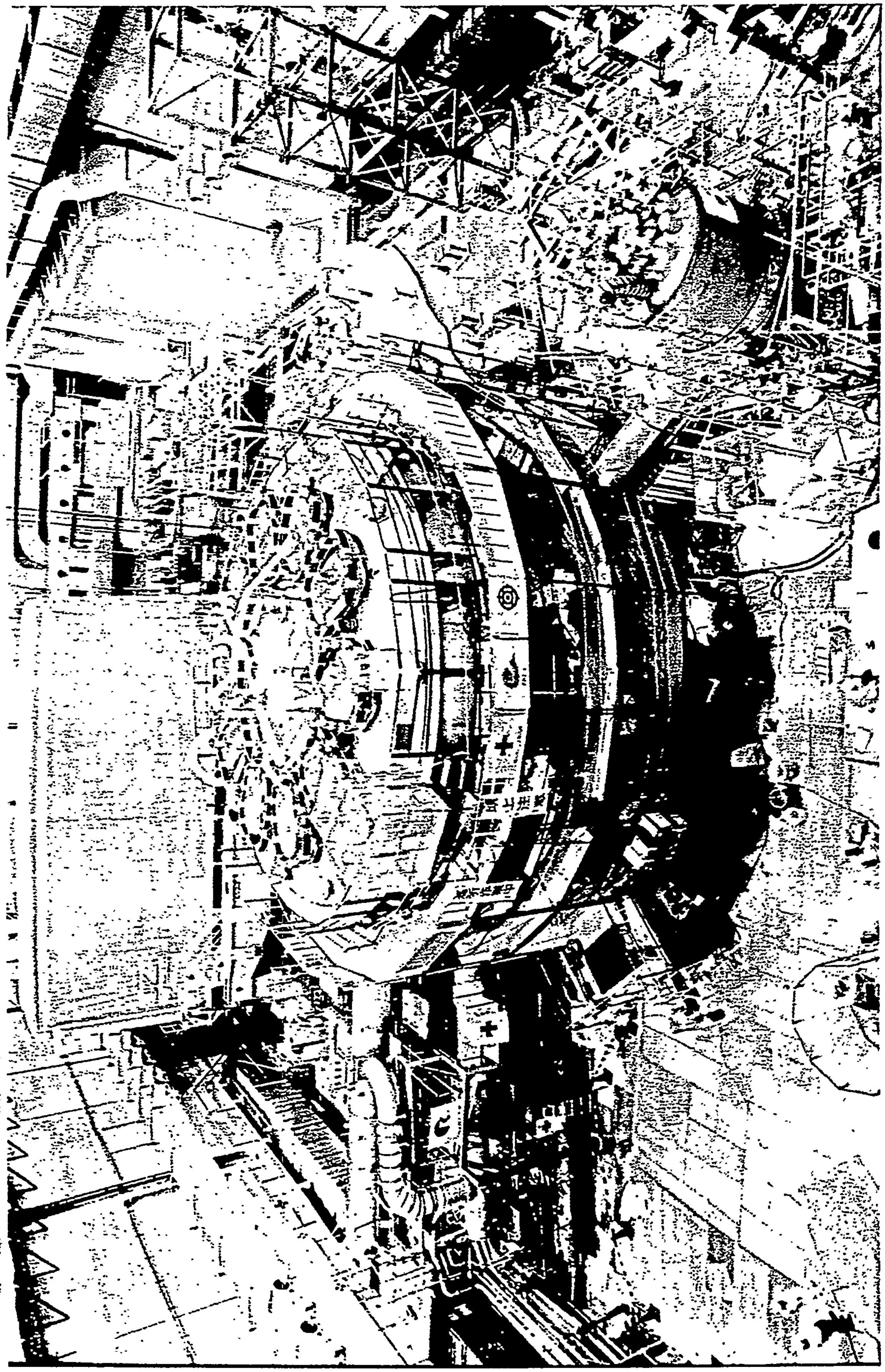

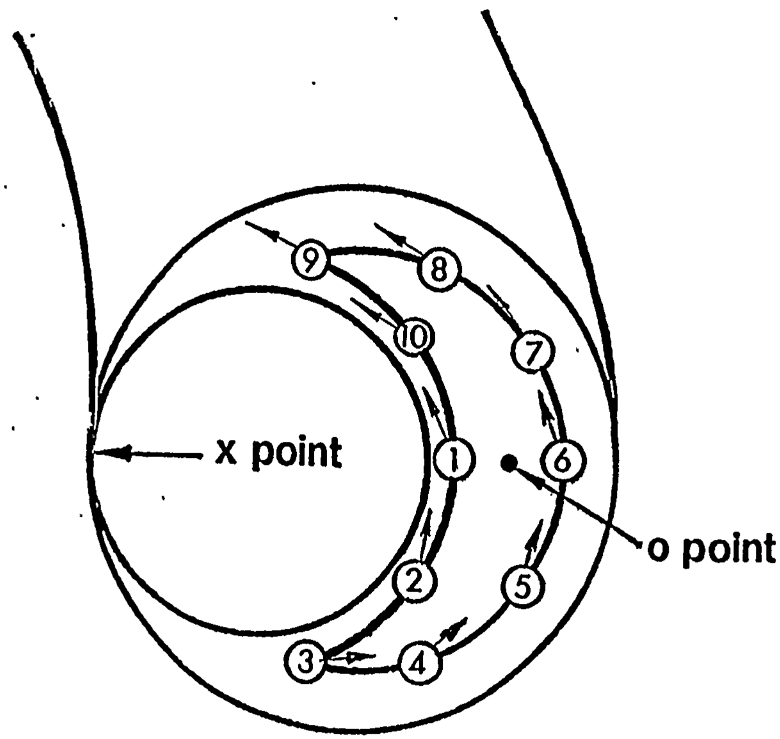

Poloidal cross-section

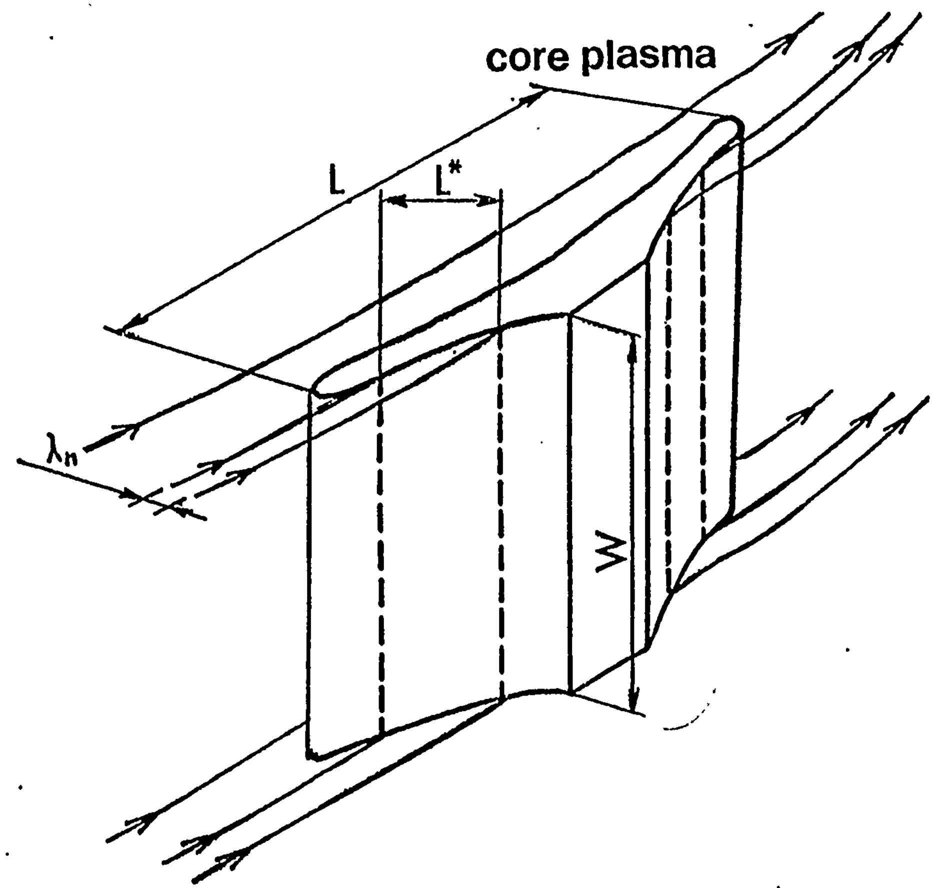

Top view

Local Island Divertor

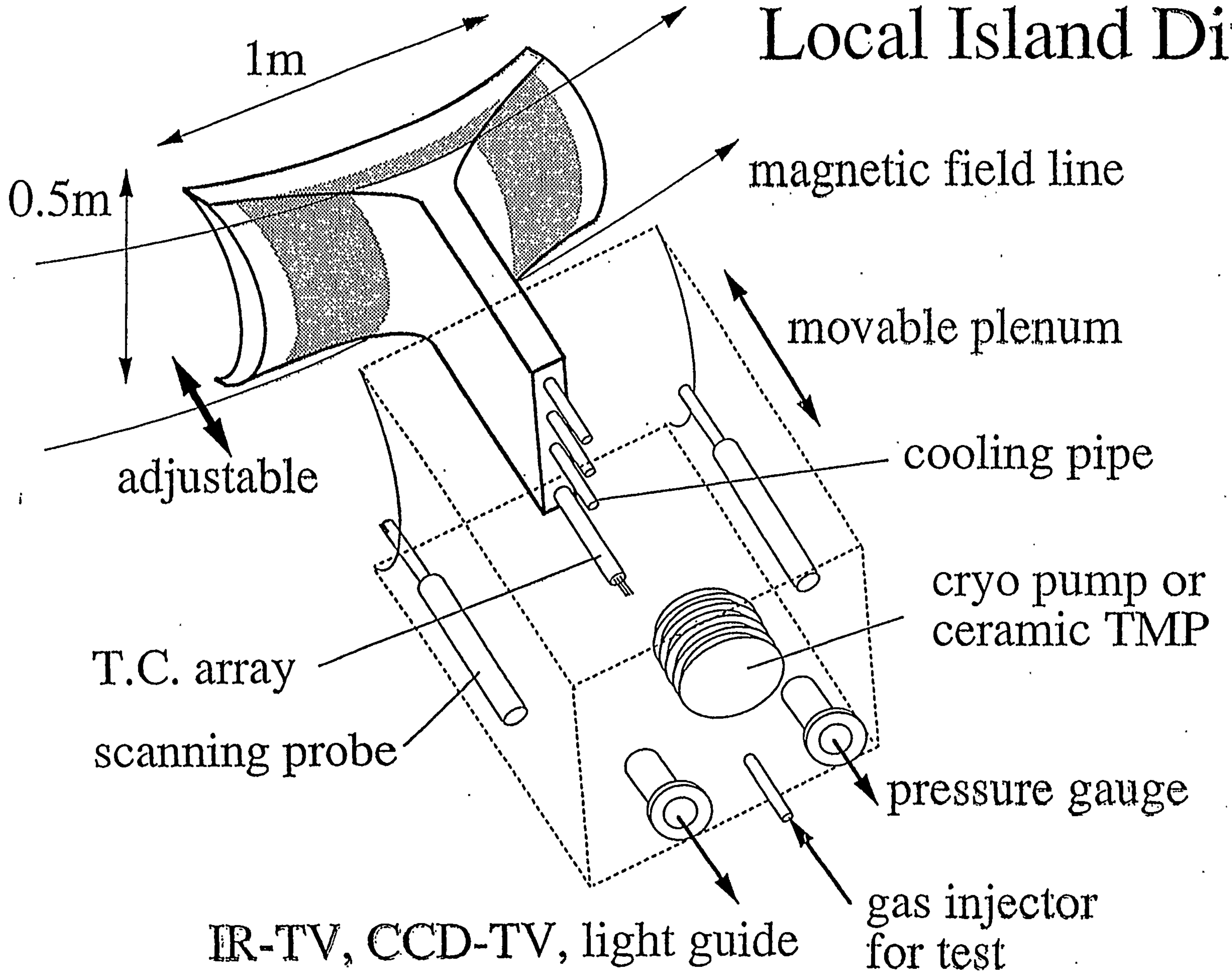

NIFS 930202 A. S

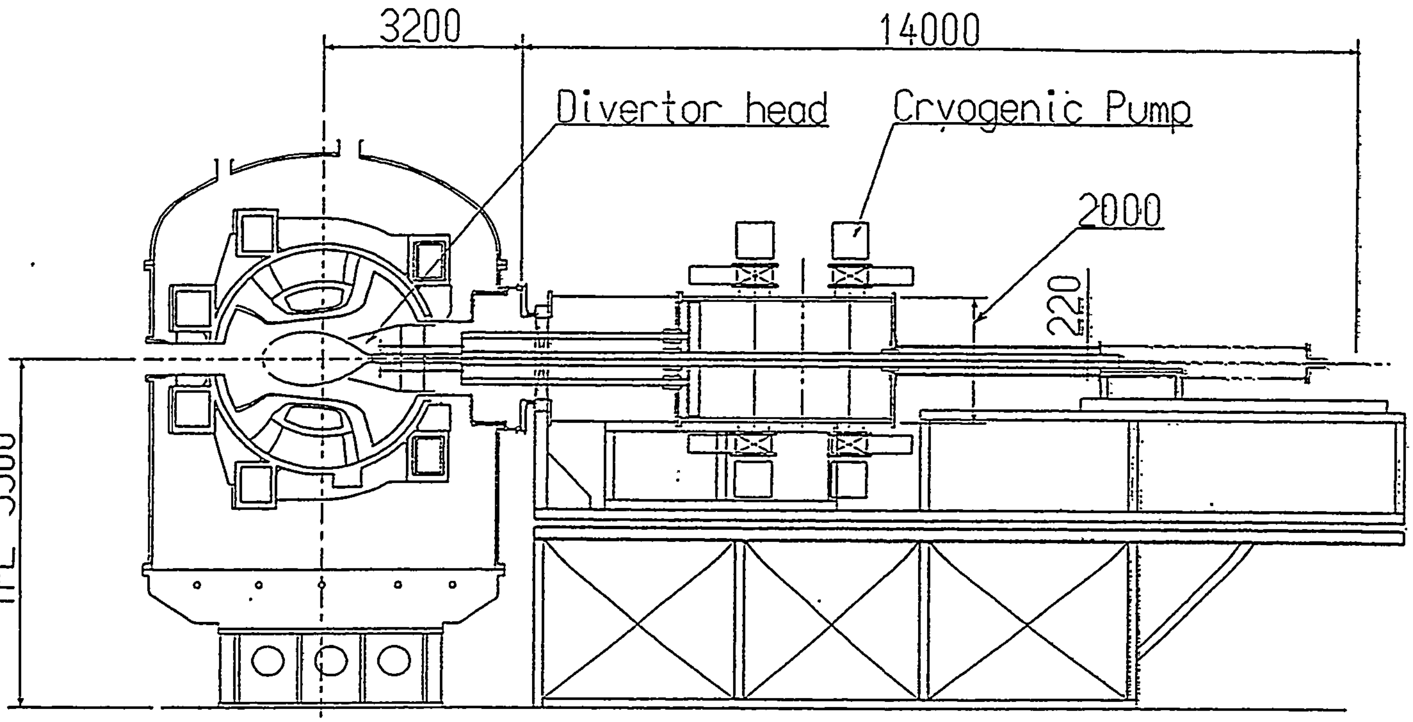

Schematic view of LID

Pumping system : Cryogenic pump

	Pumping speed	~100,000 lit./s
	Pumping capacity	~300,000 torr·lit.
	Maximum pumping flux	~75 torr·lit./s

Steady-state heat load :

	Heat load	~1.5 MW
	Averaged Heat flux	~5 MW/m^2
	Maximum Heat flux	~10 MW/m^2

Cooling system :	Plasma facing material	C/C composite brazed to copper plate cooled by water

Local Island Divertor for the LHD

Calculation Mesh for DEGAS code

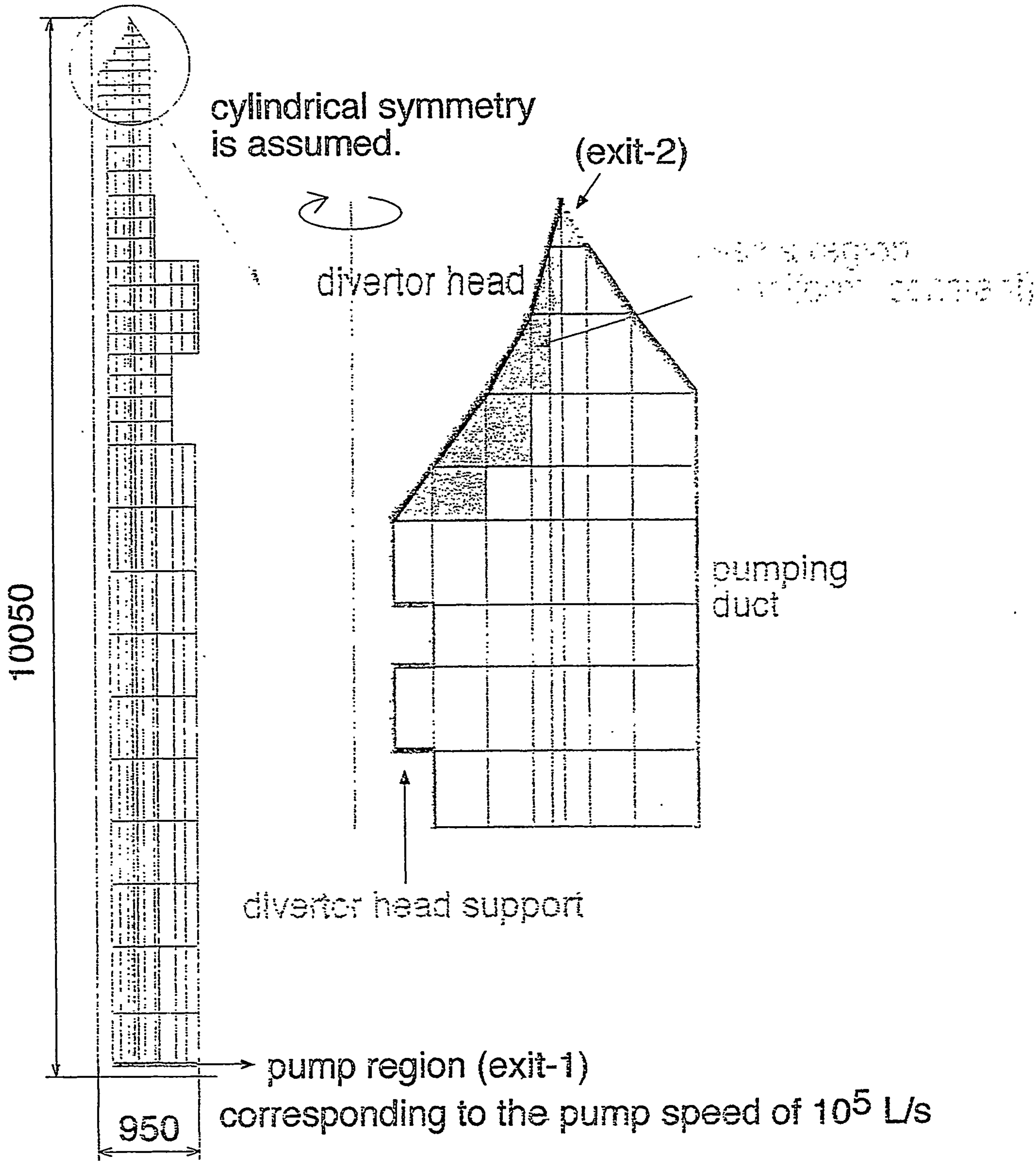

This system has two particle exit.

—> (1) pump, (2) the space between the duct and the head

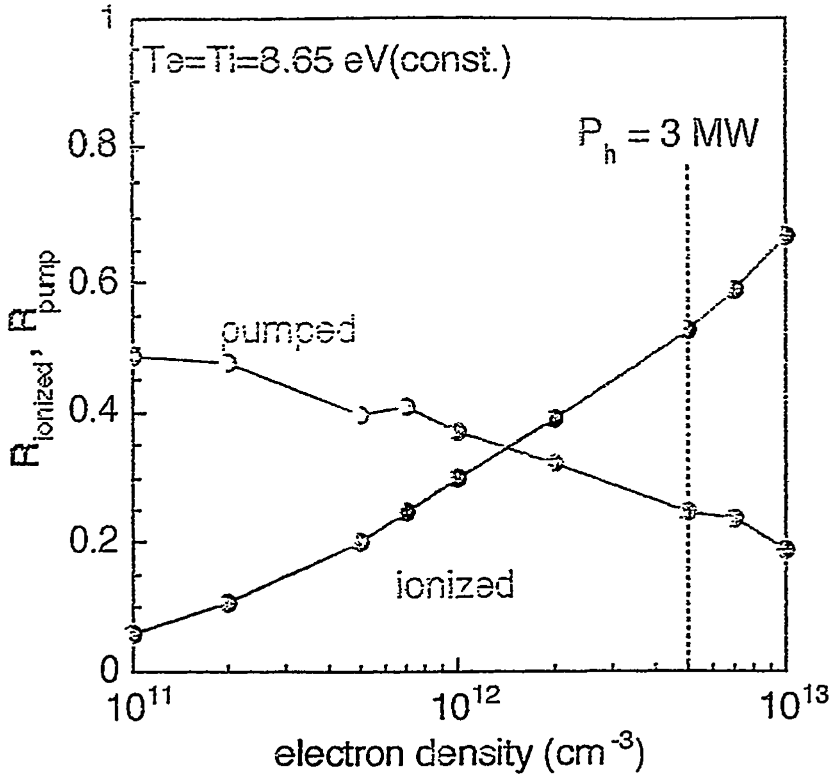

Pumping efficiency as the function of plasma density

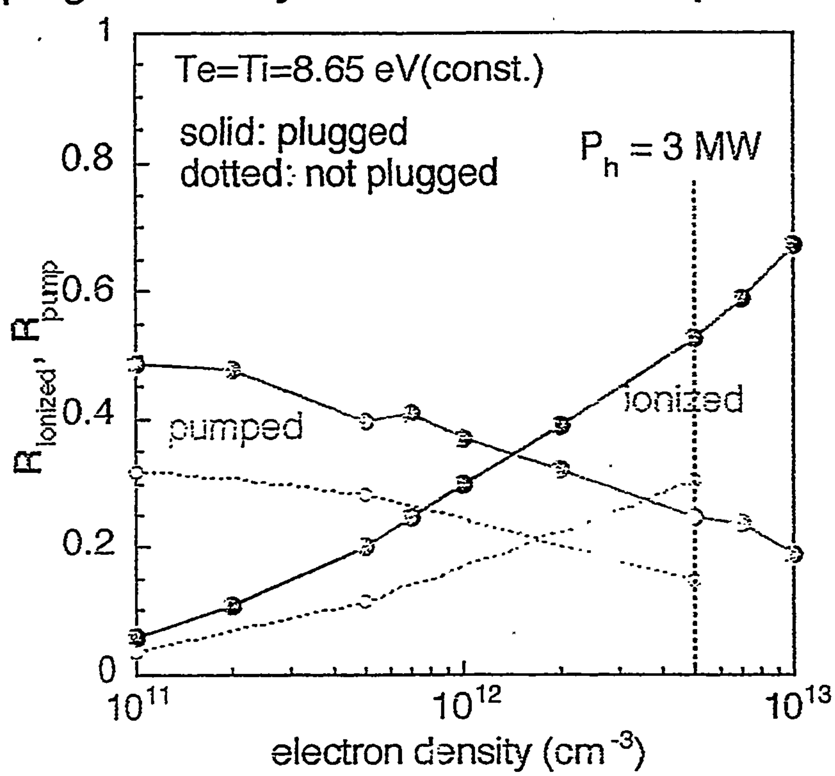

The effect of the plasma plaugging

$$R_{pump} = \frac{N_{pump}}{N_{total}} = \frac{N_{pump}}{N_{ionized}+N_{duct}+N_{pump}}, \quad R_{ionized} = \frac{N_{ionized}}{N_{ionized}+N_{duct}+N_{pump}}$$

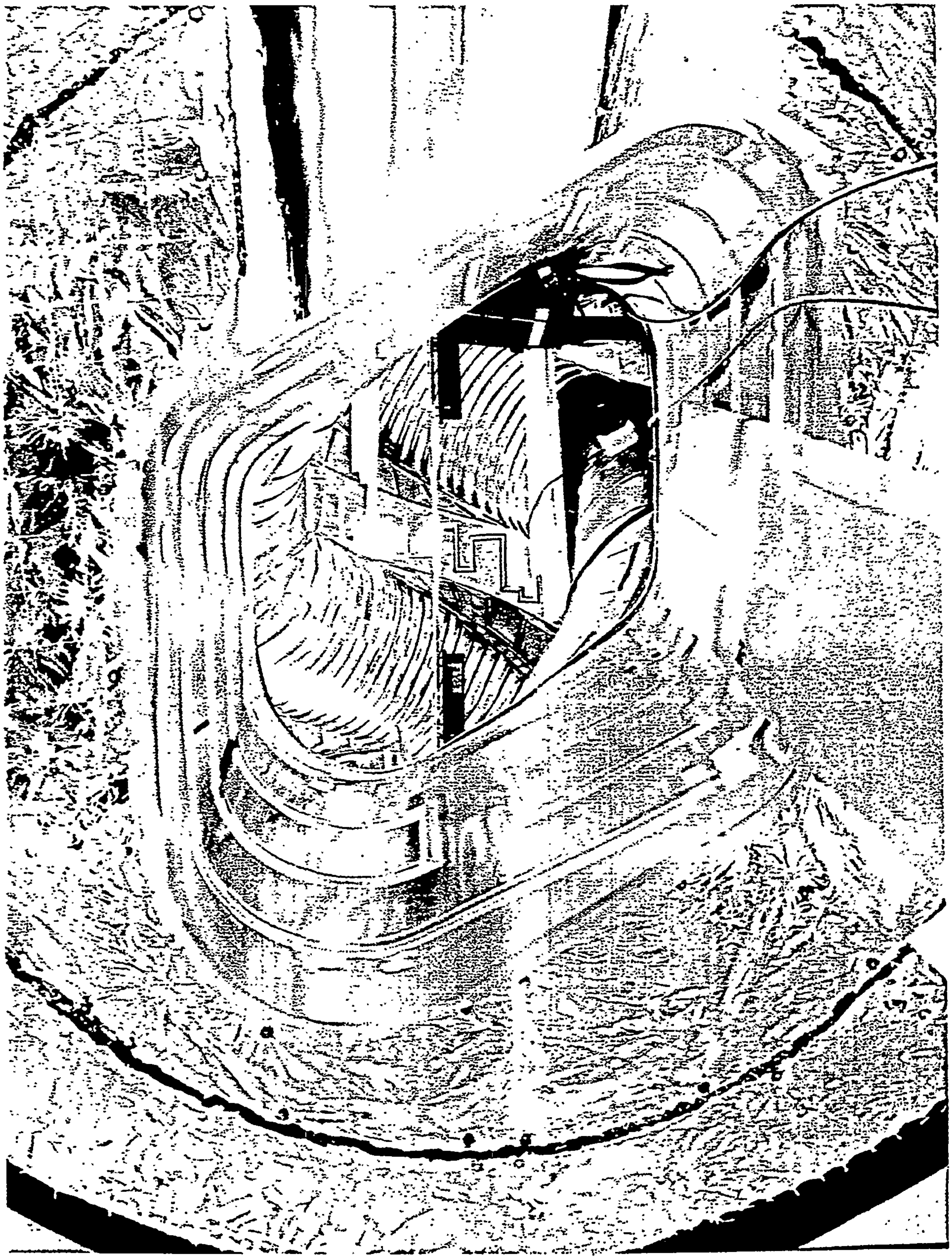

First Wall Concepts

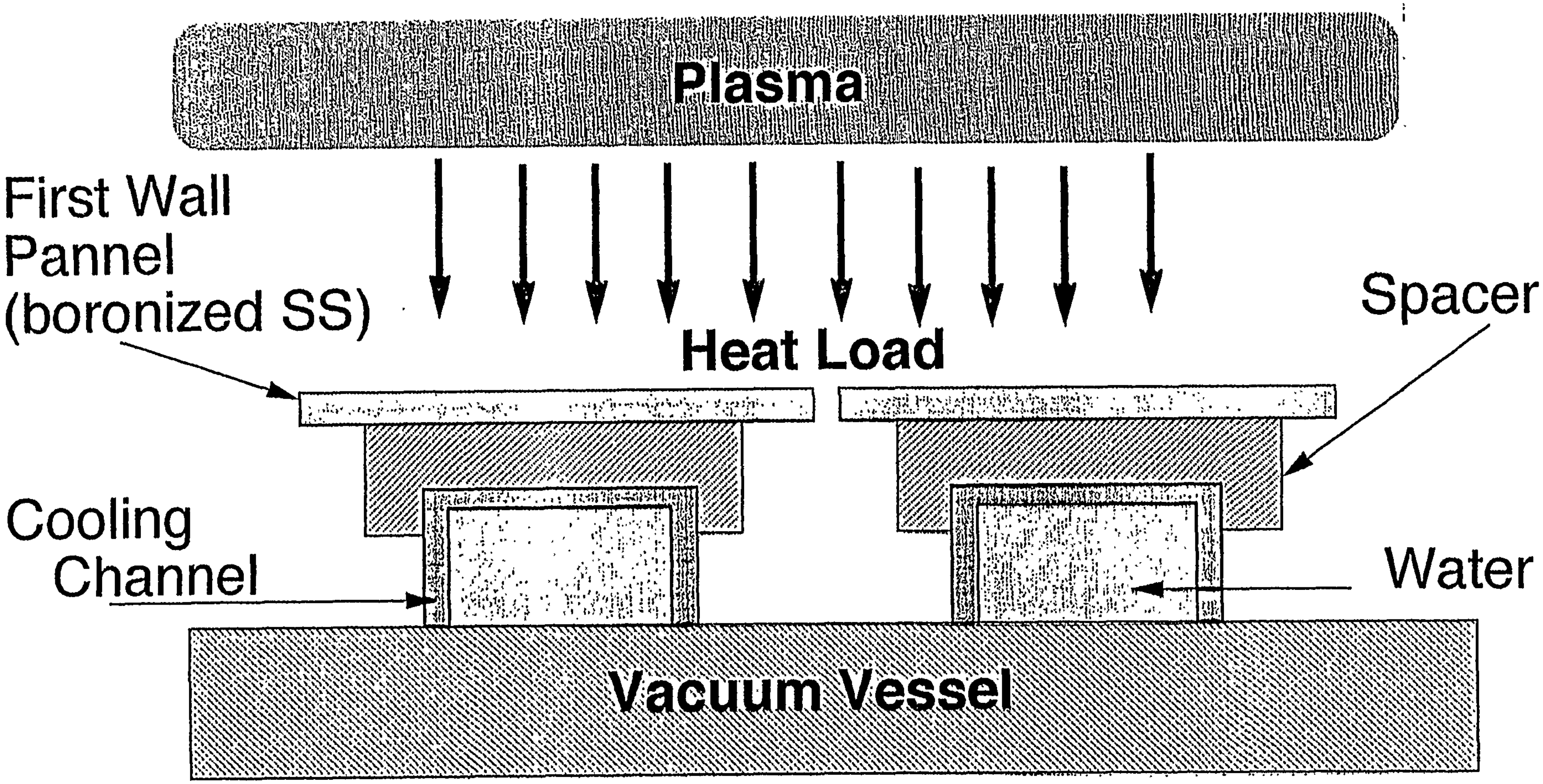

Temperature gradient from 400°C to < 100°C

N. Noda

Summary

- Fabrication of the Divertor is going on

- Heat load limitation is determined by thermal deformation of Cu heat sink
- Heat load of 0.75 MW/m^2 cleared by Mo

- Aux. coils for LID installed
- LID head design completed

- Vacuum vessel completed , cooling channels under welding process

N. Noda

(4)

NSTX

NSTX Status and PSI Issues

Martin Peng
ORNL@PPPL

High Heat Flux Components & Plasma Surface Interactions for Next Fusion Devices
December 8-11, 1997
San Francisco, California, USA

I-69

Spherical Torus Plasma Has Exciting Possibilities of High Performance in Fusion Science

NSTX

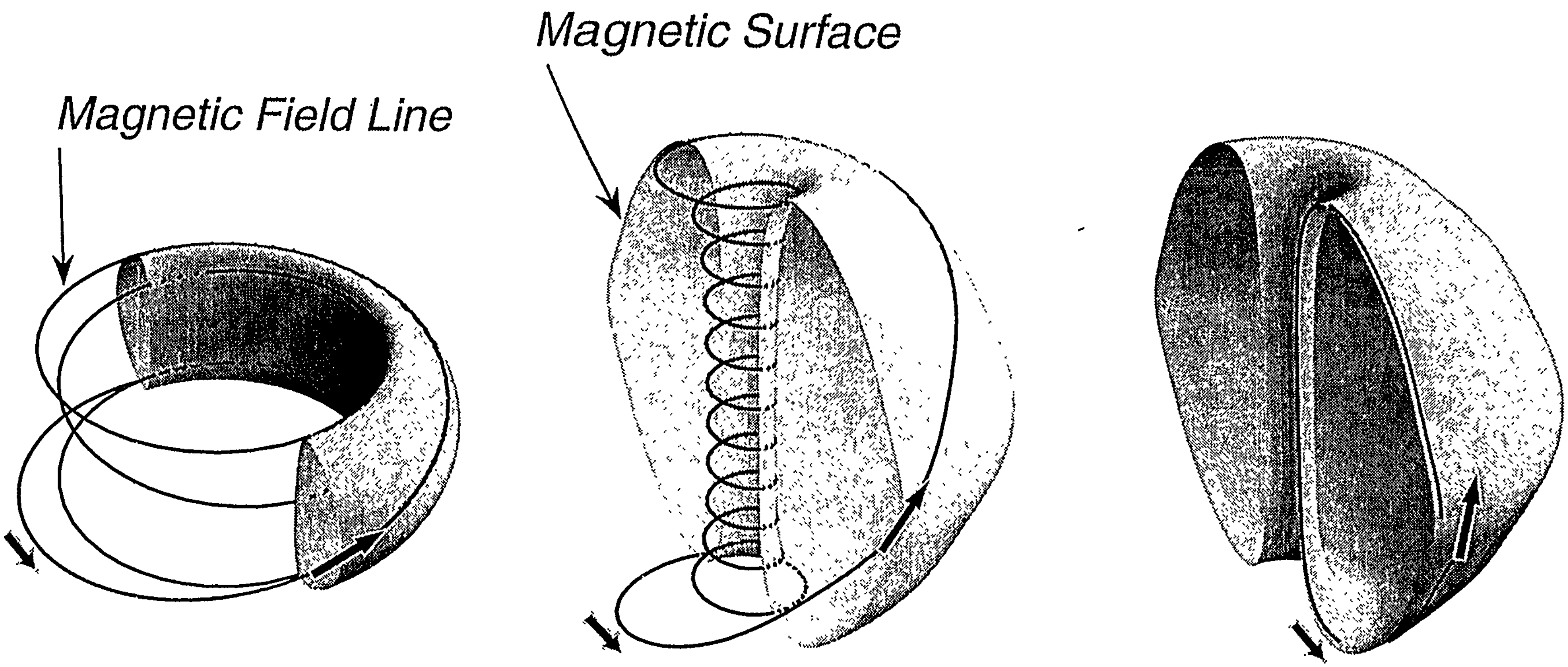

Tokamak Plasma (safety factor q = 4)

Spherical Torus Plasma (safety factor q = 12)

Spheromak Plasma (safety factor q = 0.03)

START Reached ~30% in Average Toroidal β in Well-Confined NBI Plasma (Gates, Sykes et al.)

NSTX

← 1 m →

Plasma current = 0.25 MA

NBI power ≥ 0.4 MW @ 30 kV

ORNL ATF NB system

(courtesy of START Team)

- Central β > 60% and average toroidal β ~ 30%
- Increased operating space and improved plasma
- Recent Upgrades: NBI power ~ 1 MW; field duration ~ 30 ms
- MAST will upgrade the NBI systems from ORNL

NATIONAL SPHERICAL TORUS EXPERIMENT
U.S.A.

NSTX

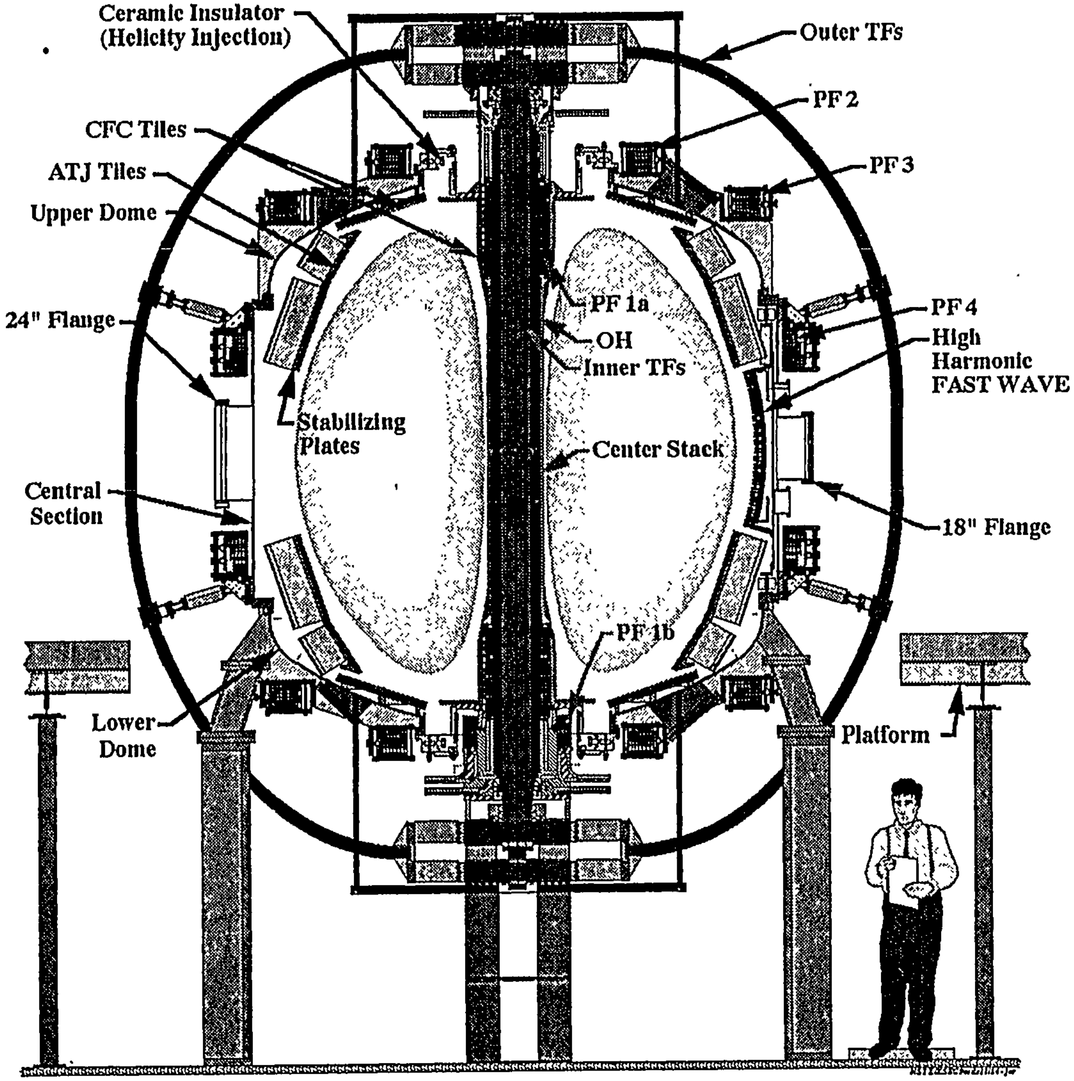

Baseline Parameters

- Major radius
  85 cm
- Minor radius
  68 cm
- Plasma current
  1 MA
- Toroidal field
  0.3 T
- RF heating and current drive
  6 MW
- Flat-top time
  5 s

Project Team: UW Columbia University ornl PPPL PRINCETON PLASMA PHYSICS LABORATORY

The Main Mission of NSTX is to Prove the Physics Principles for Attractive VNS and Power Plant

NSTX

- High beta, high confinement, high bootstrap current fraction simultaneously and near steady state
- Noninductive current startup and maintenance to eliminate Ohmic solenoid and minimize size for next steps
- Feasible power and particle handling to permit practical plasma facing components

Related Research Opportunities

- Further improvements in configuration: $R/a \rightarrow 1$, bridging to CTs (spheromak, FRC, spherical RFP, etc.)
- Excellence in plasma and fusion science

NATIONAL SPHERICAL TORUS EXPERIMENT
U.S.A.

NSTX

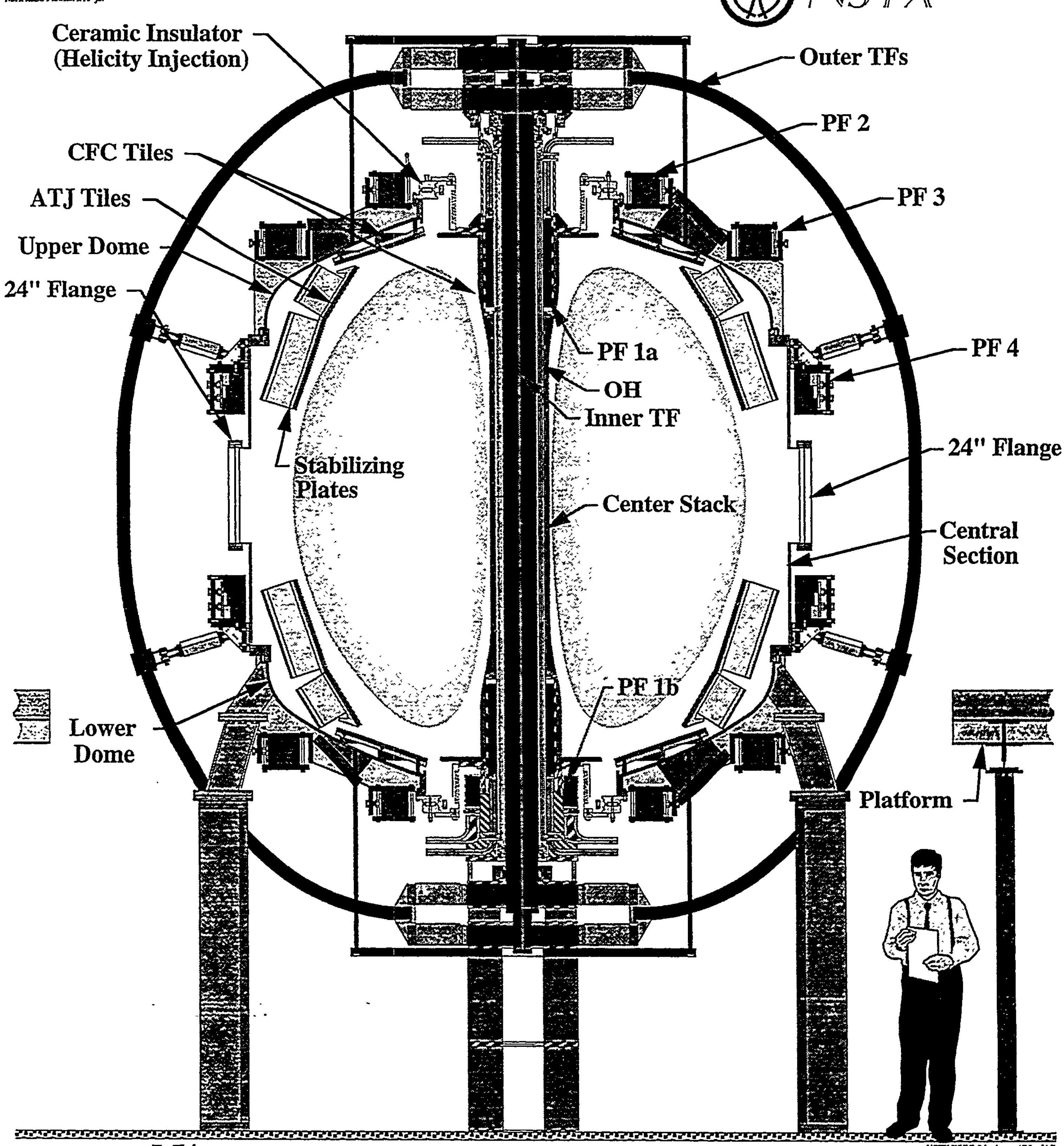

NSTX Test Cell

NSTX

NSTXTestCellFinal NB/RF 9/19/97

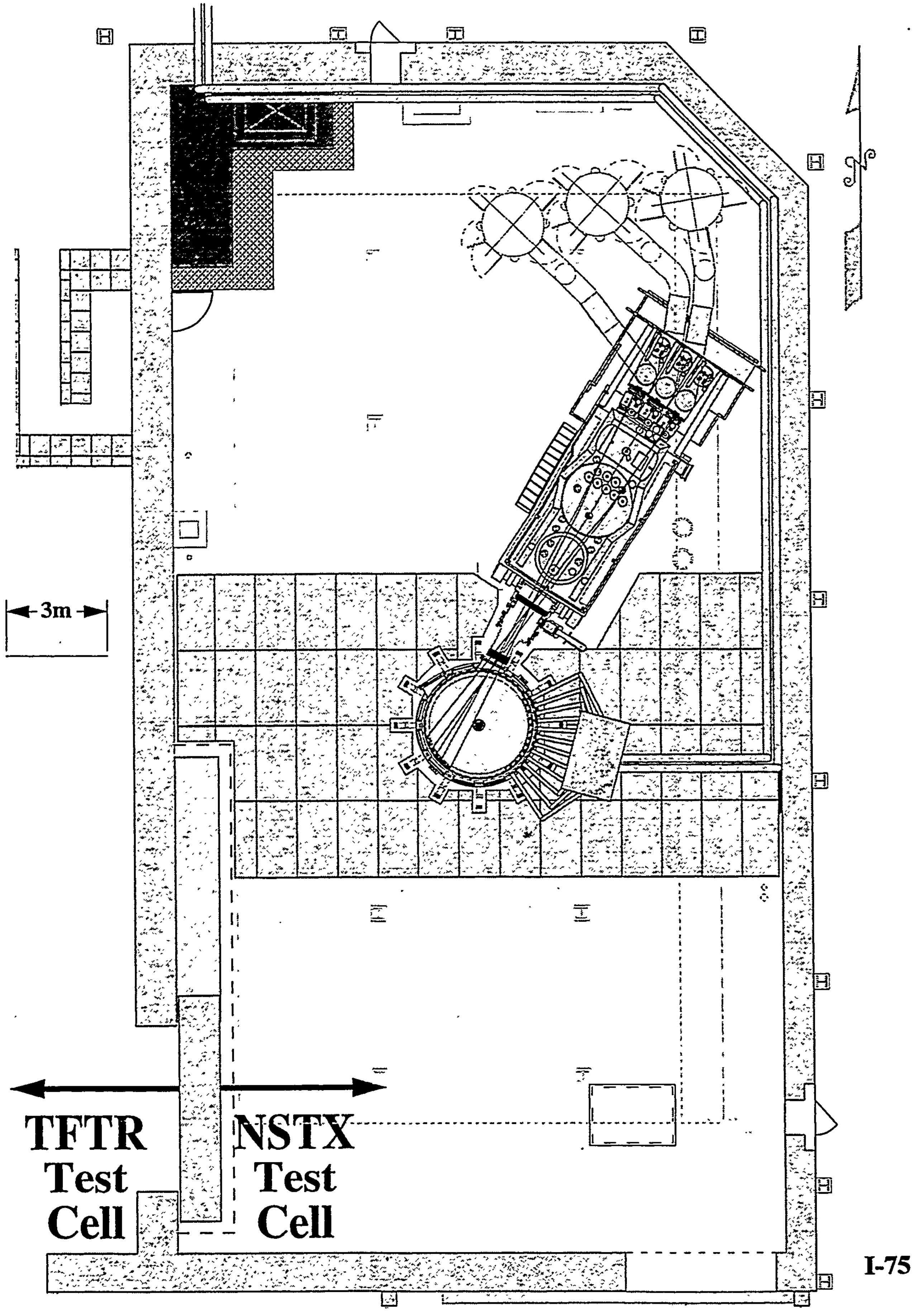

Configurational Flexibility

NSTX

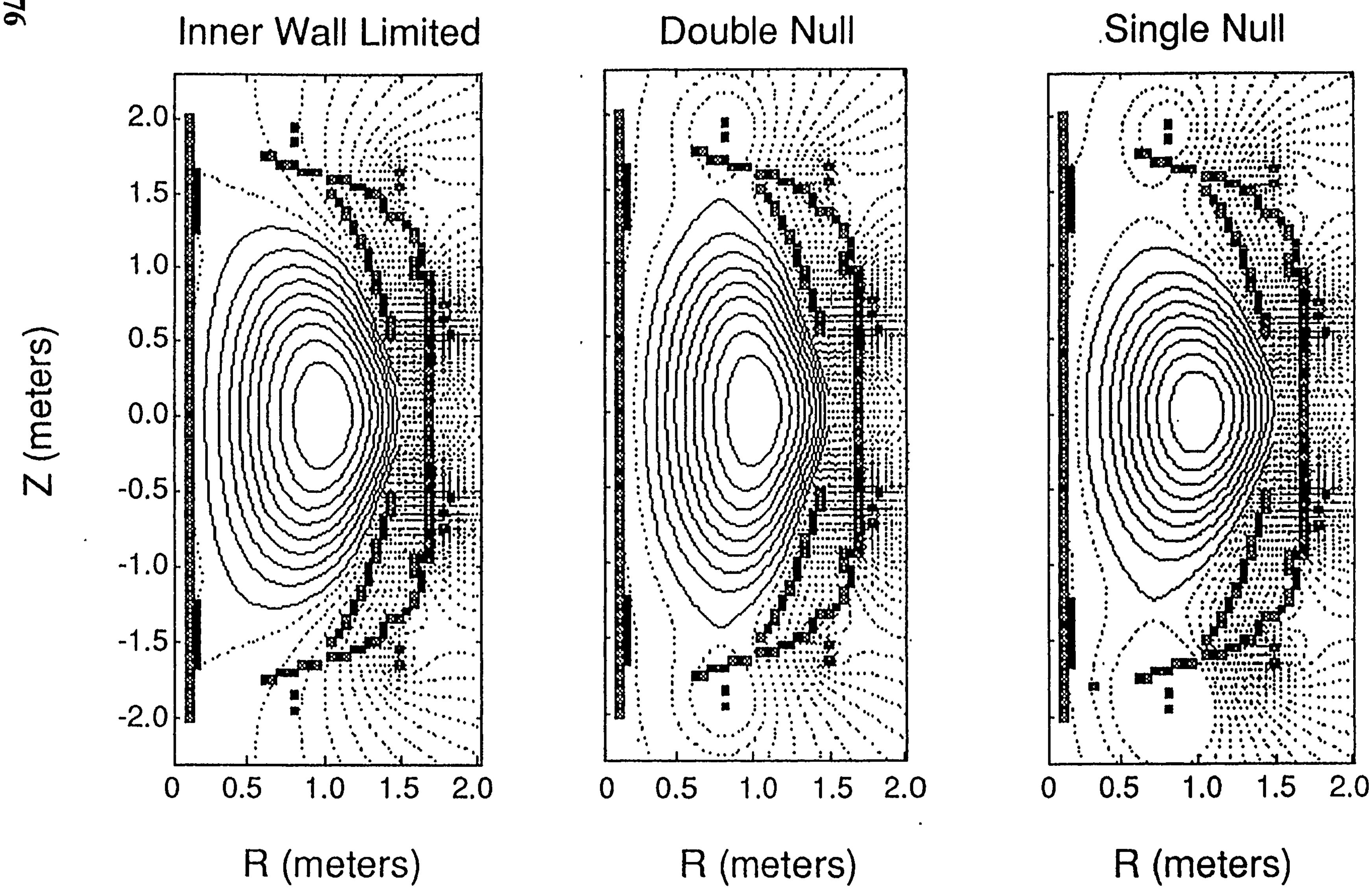

κ=3 Equilibrium
(R/a=0.7/0.5 m)

PF1a = 0.75 kA/turn
PF2 = 8.2
PF3 = -11.9
PF4 = -6.5

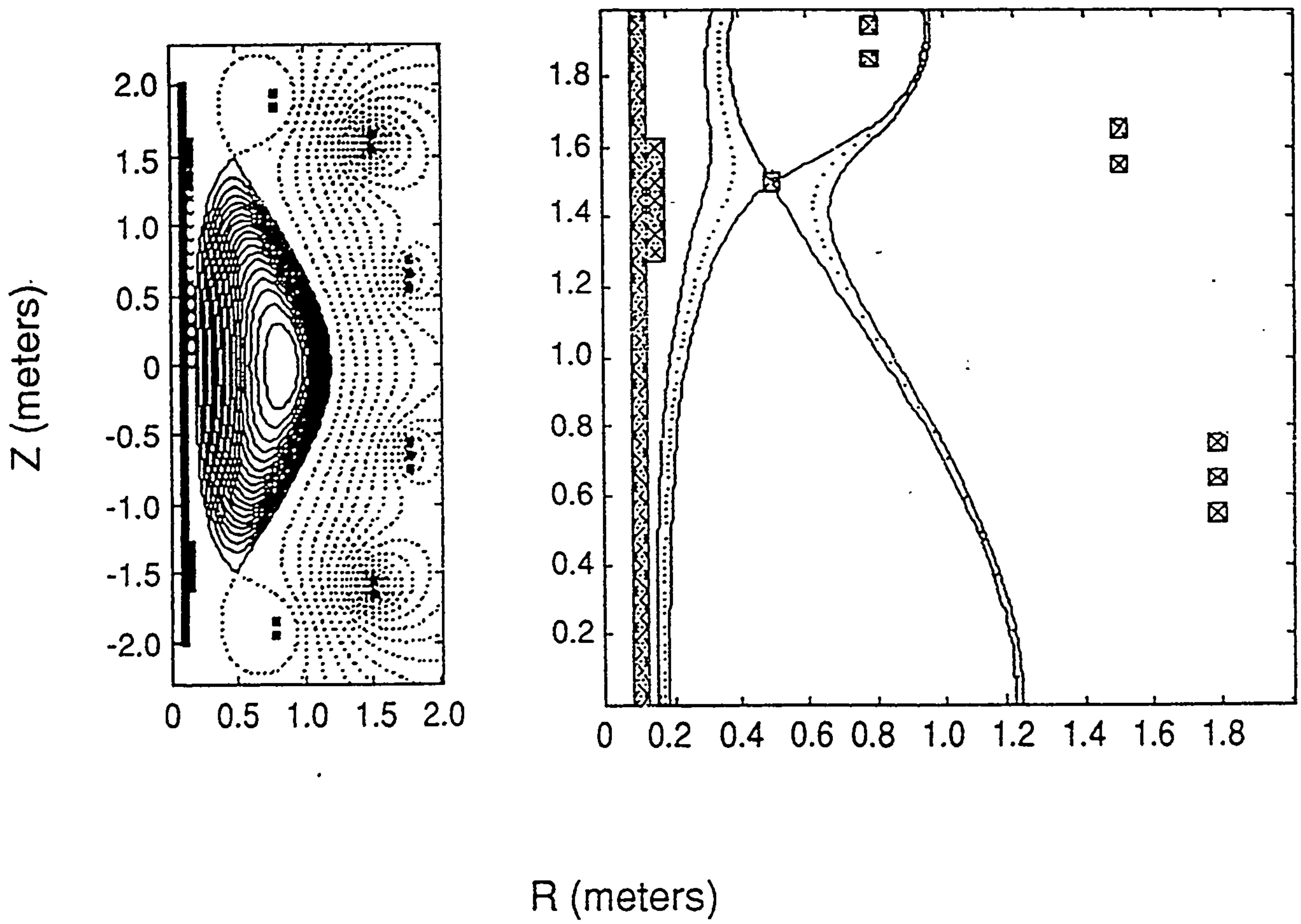

- Ideally unstable to n=0 axisymmetric mode with plates in original position
- Relocation of passive plates farther inboard required for maximizing MHD stability

2-D CALCULATIONS SHOW DIVERTOR PEAK HEAT FLUX DECREASES STRONGLY WITH DIVERTOR RADIATION

- Peak heat flux decreases linearly with divertor radiation until plasma begins to detach from divertor (radiation ~ 60%)

- Peak heat flux dominated by convection for radiation fraction > 65%

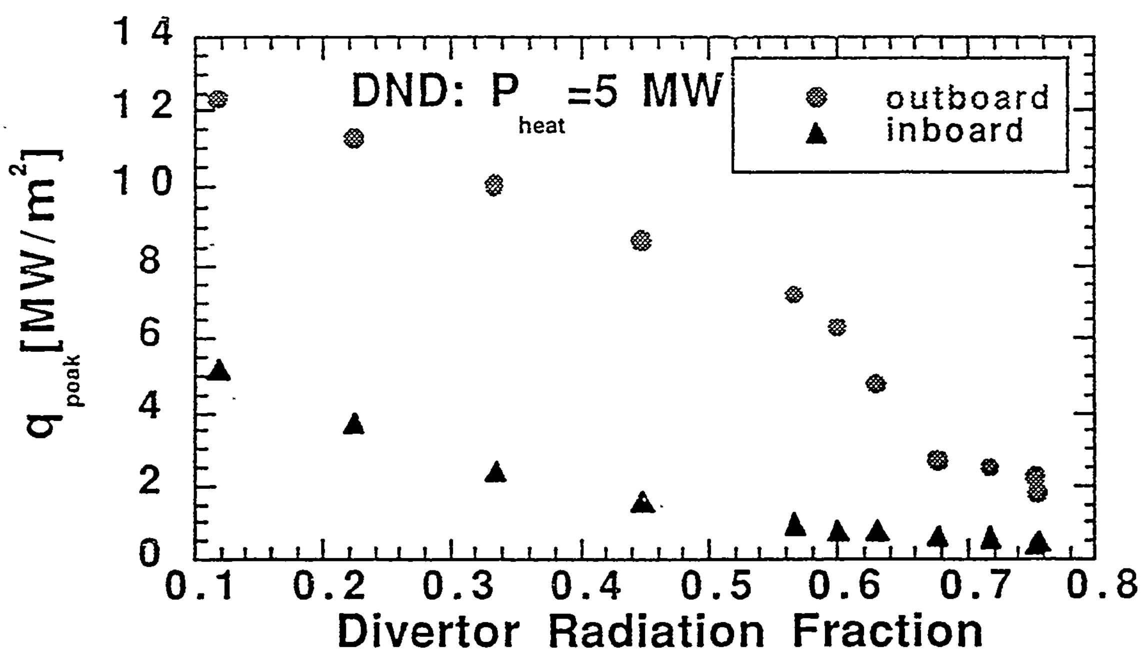

- Divertor radiation increased with multiplier to hydrogenic radiation to simulate impurities

PEAK HEAT FLUX IN LSN CONFIGURATION GOES DOWN SLOWLY AS DIVERTOR RADIATION IS INCREASED

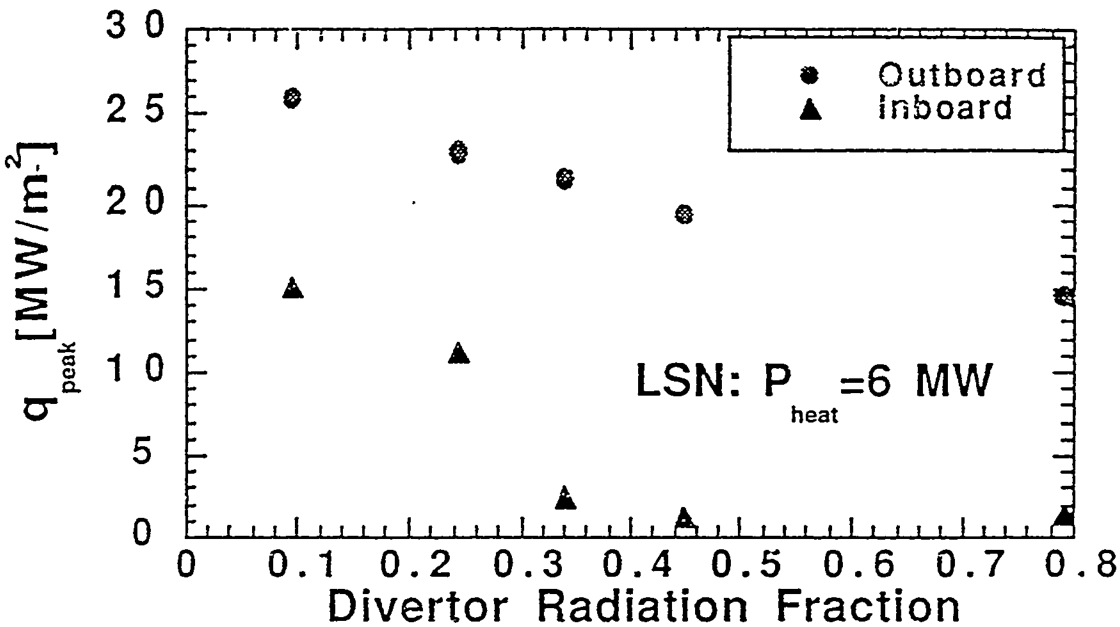

- Most of the increase in divertor radiated power fraction occurs on the inboard leg, driving the inboard heat flux down quickly

- This phenomenon is caused by the in/out geometric size difference in ST's: the inner SOL cross-sectional area and is ~ 1/2-1/3 of the outer SOL area, leading to a similar in/out power split

SOL for Naturally Diverted (ND) Plasma in NSTX Exhibits Unique Magnetic Geometry

NSTX

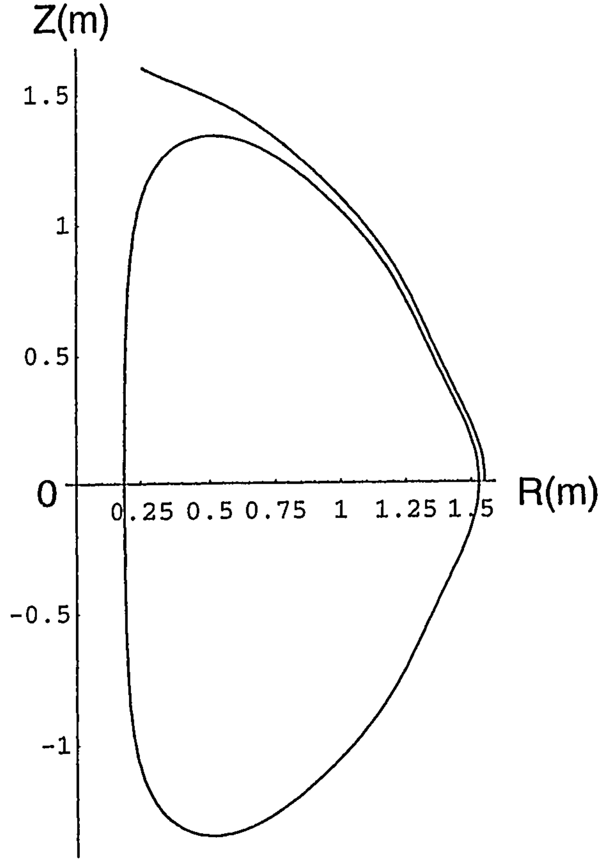

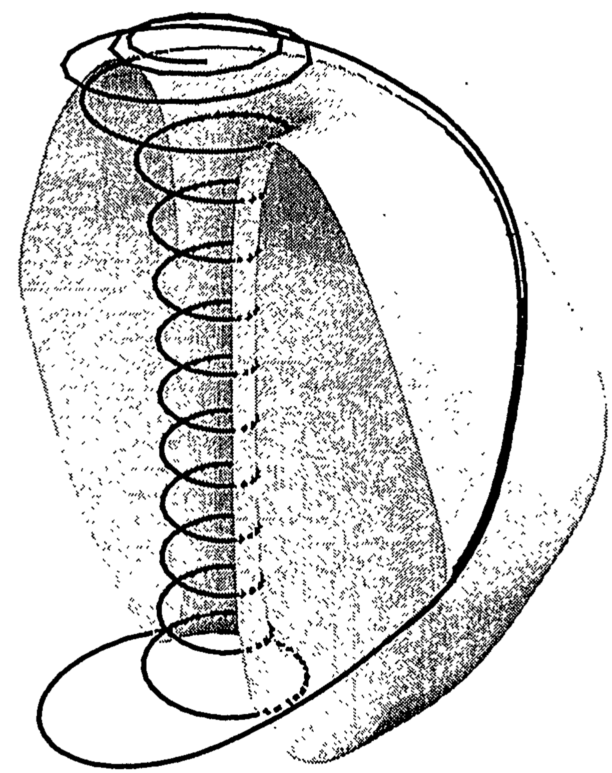

ND Plasma, $A = 1.26$, $\kappa = 2.0$, $\delta = 0.52$, $q_a = 13+$, $\beta_t = 25\%$

Naturally Diverted SOL Contains Large Magnetic Field Mirror (NSTX, A = 1.26, D = 2 cm) (Strickler)

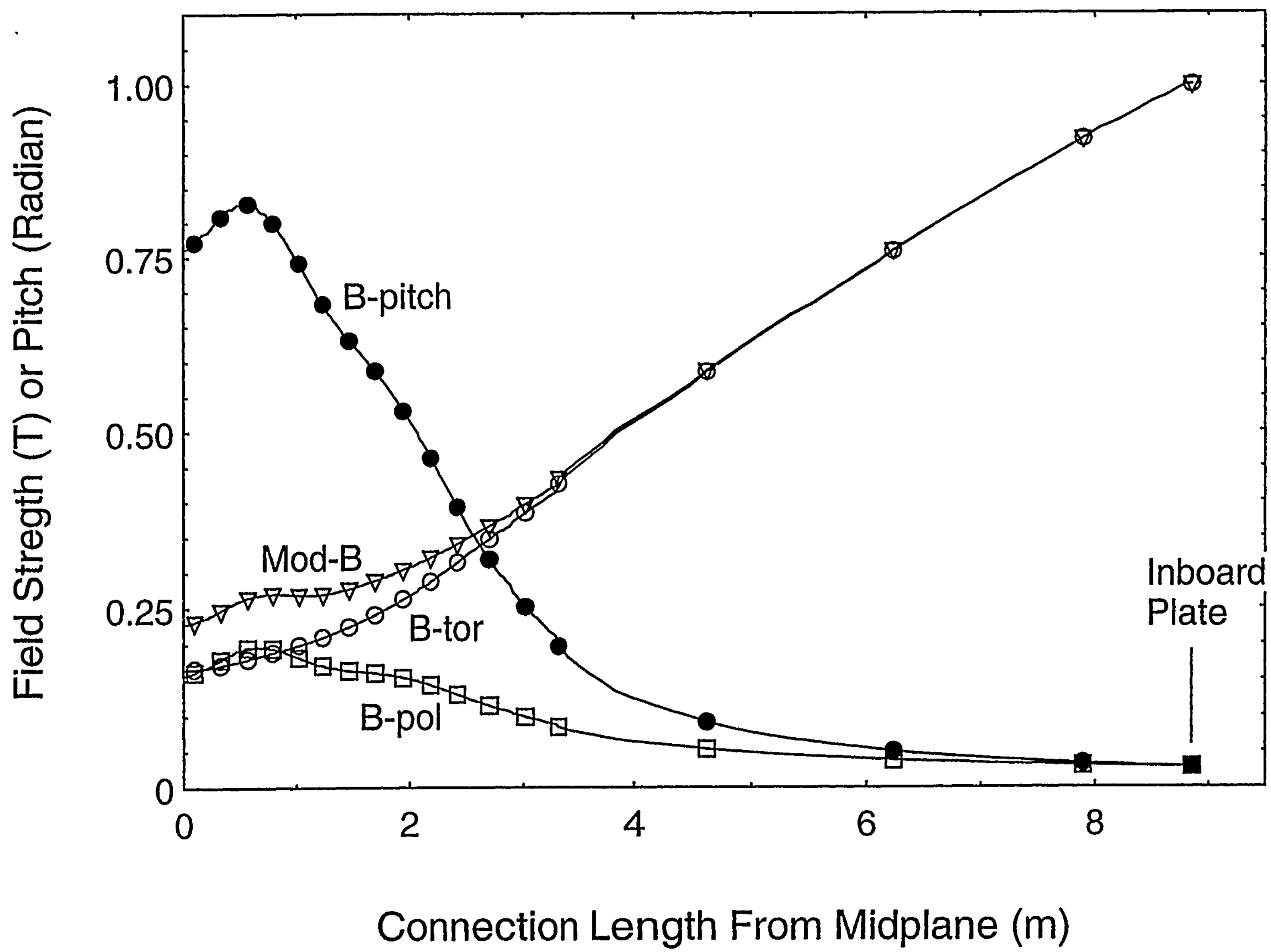

Natural Divertor Increases SOL Flux Tube Expansion and Connection Length (Strickler)

NSTX

($A = 1.26$, $\kappa = 2.0$, $\delta = 0.52$, $q = 13+$)

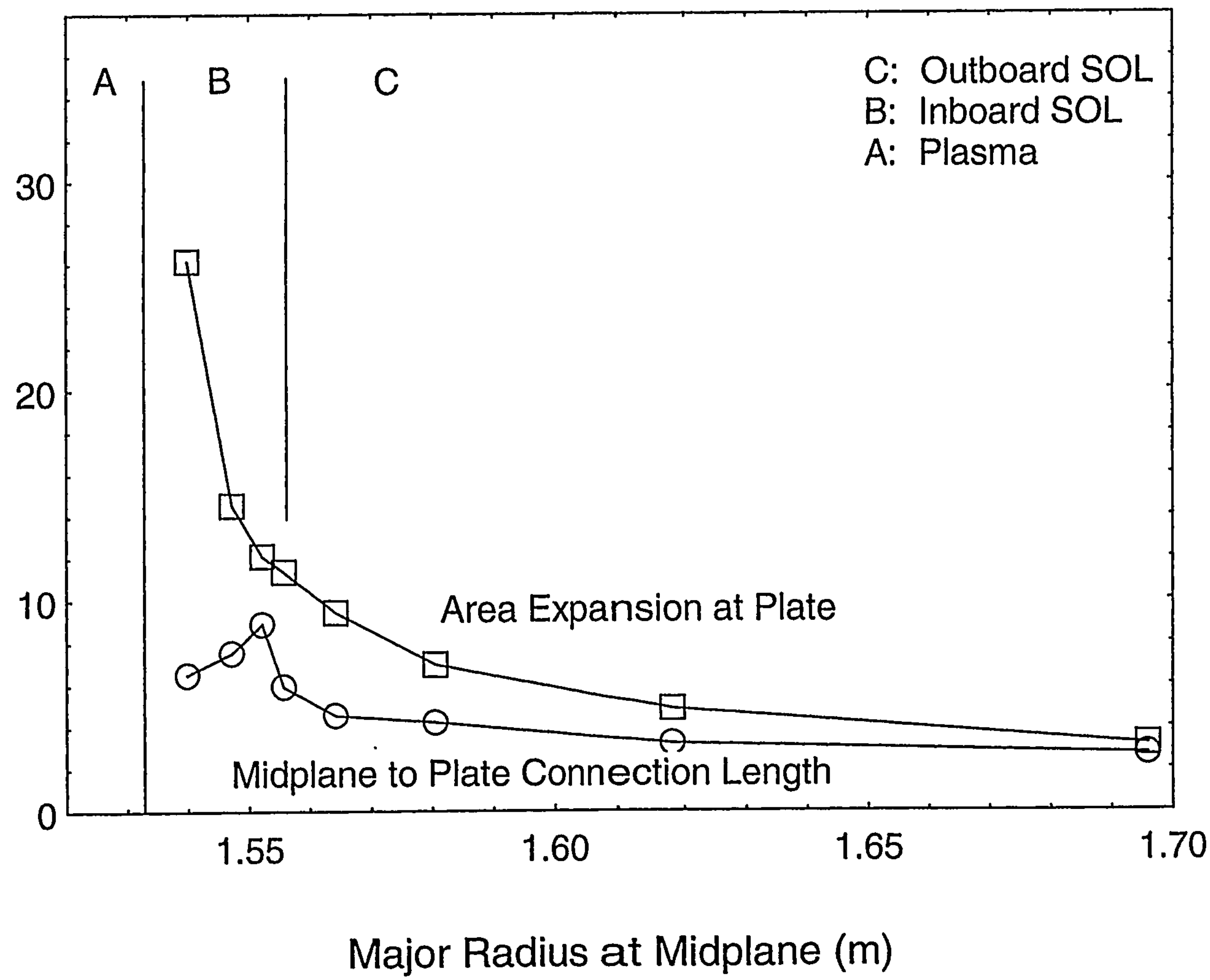

Requirements/Design Criteria - Thermal loads

- Normal Operation, peak surface flux

- Center stack ~ 200 W/cm^2 peak

- Inboard divertor
  ~ 700 W/cm^2 for single null

- OB divertor
  ~ 1100 W/cm^2 for $\lambda = 3$ cm
  ~ 1700 W/cm^2 for $\lambda = 1.5$ cm
  (peak from calc = 1400 W/cm^2)

- Passive plates ~10 W/cm^2

- Disruption
  - Peak surface flux: TBD

- NBI shine (upgrade only)
  - Peak surface flux: TBD

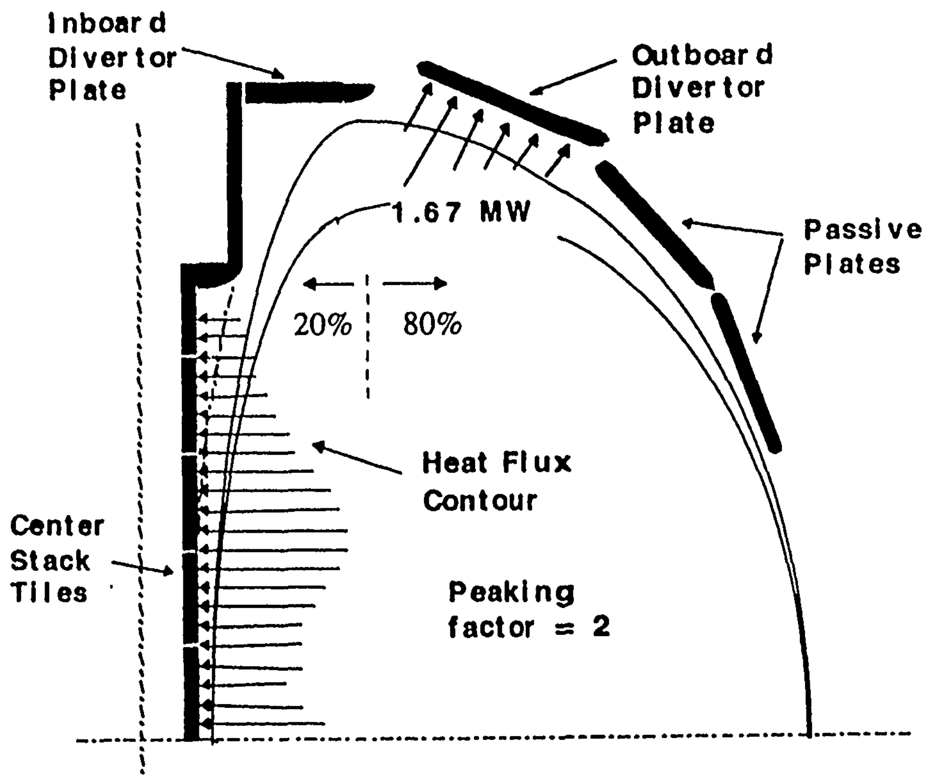

I-83

1-84

Outboard Divertor Plate Cooling/thermal analysis

- Copper plate is cooled at 50 to 100 C and baked out to 350C by Dowtherm
- Analysis shows feasibility for divertor tile operating at about 1500 W/cm^2 ($\lambda \sim 2$ cm)
- Divertor tile can be returned to 150C after pulse in 3 minutes

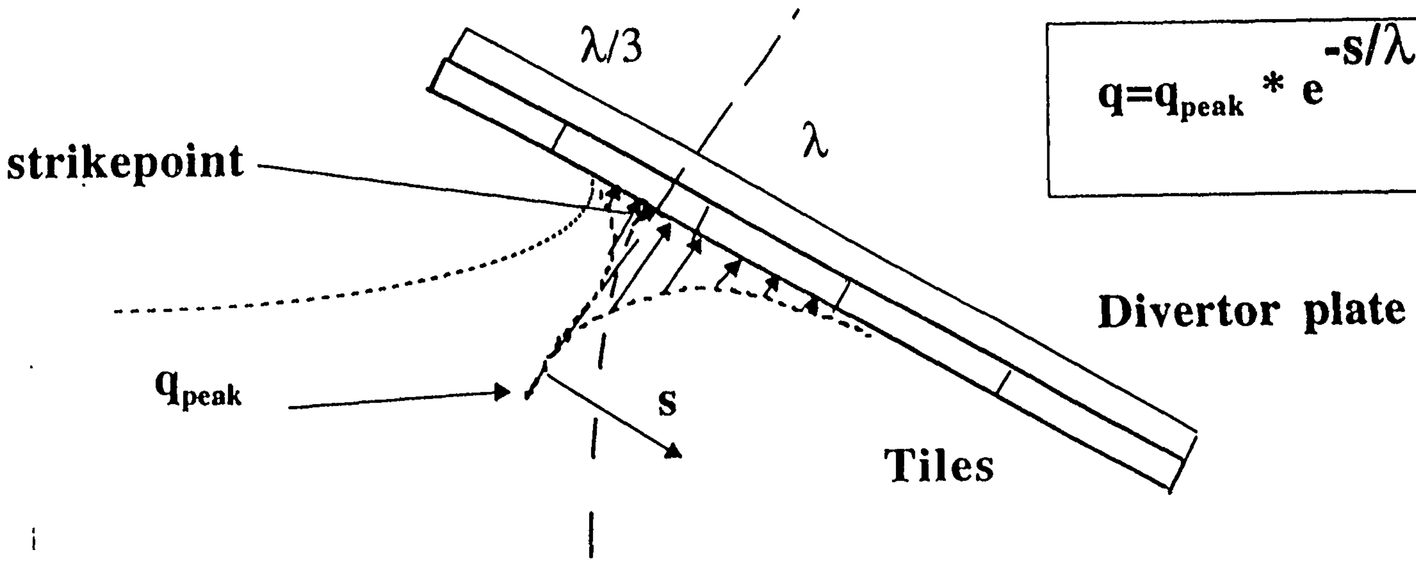

$$q = q_{peak} * e^{-s/\lambda}$$

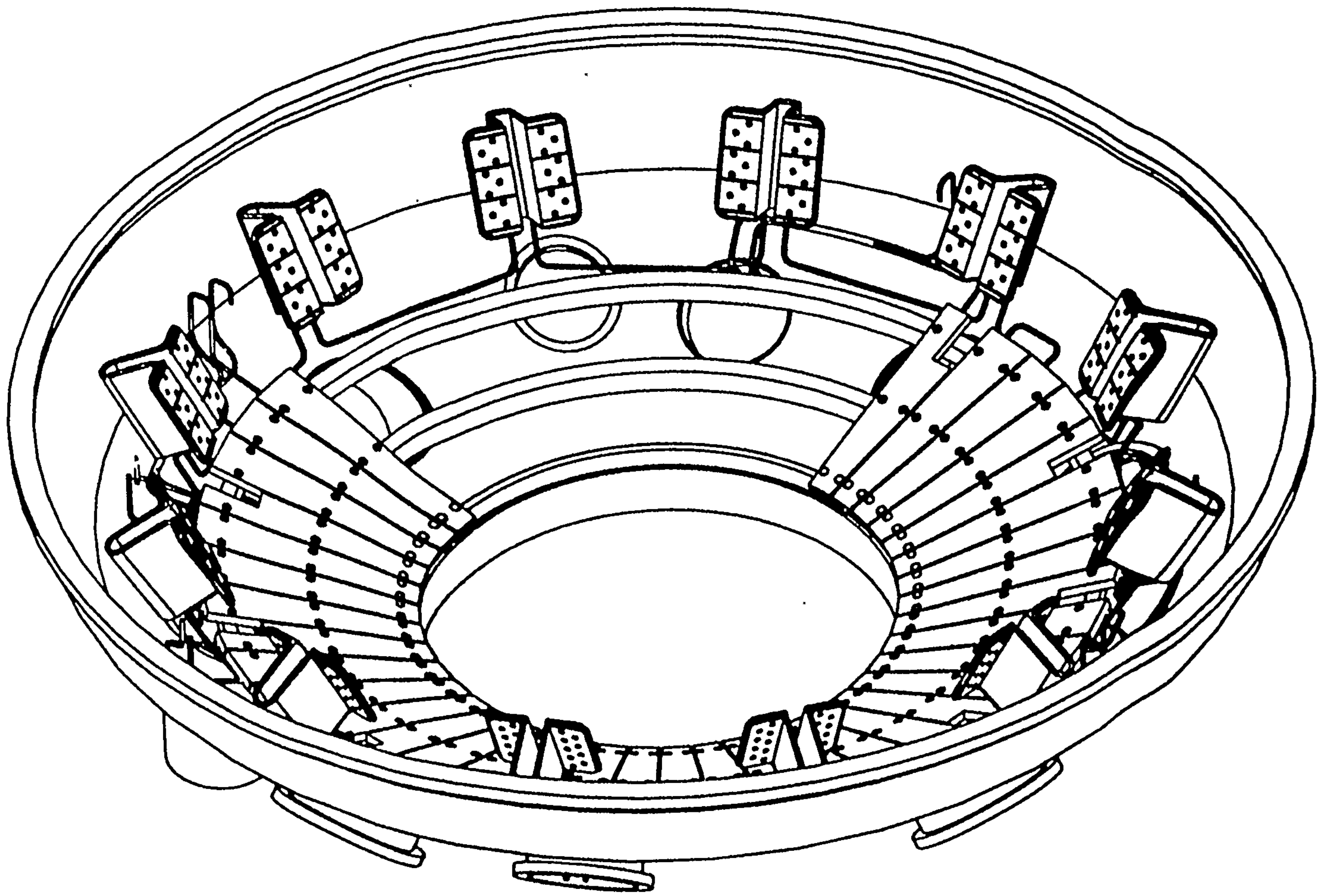

SIMPLFD REP:SHELL

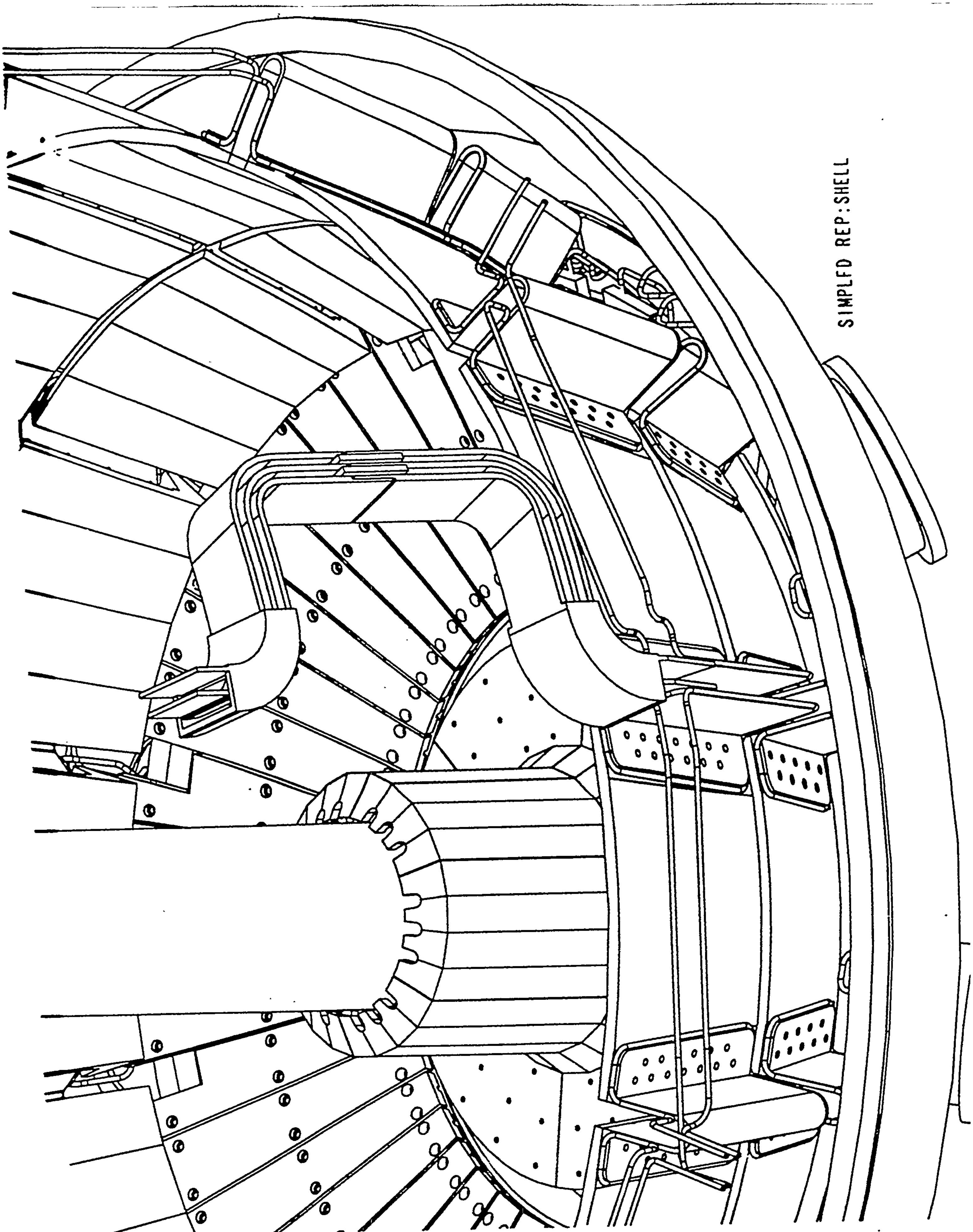
SIMPLFD REP:SHELL

Center Stack Tile Design - Vertical Bolted Rail

TZM rails with carbon covers clamp vertical rows of tiles

- Robust, all metal retainers
- Graphite tiles, FMI-4D carbon-carbon covers
- Good thermal expansion capability
- Fair, controlled thermal isolation
- Multiple fasteners per tile
- Relatively simple parts

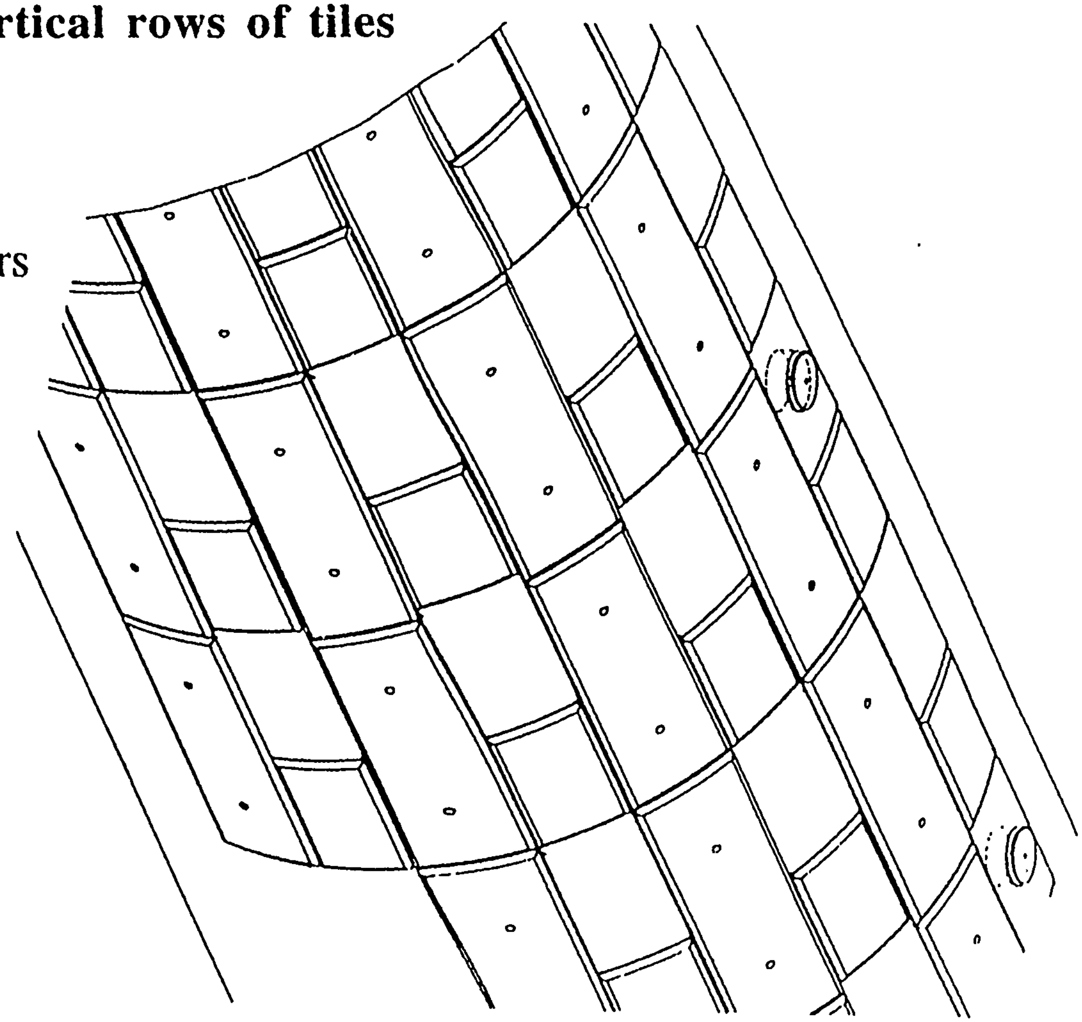

I-87

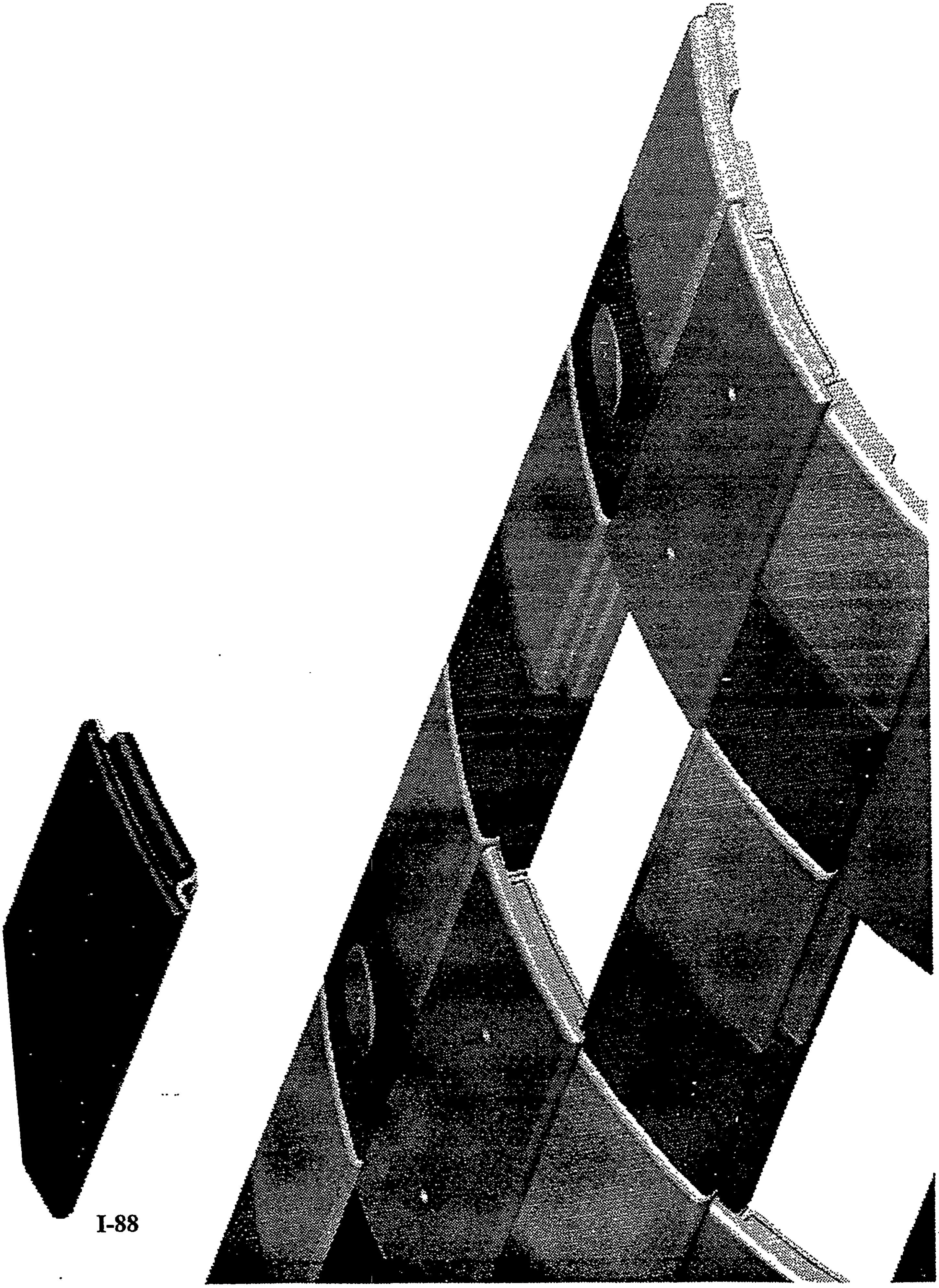

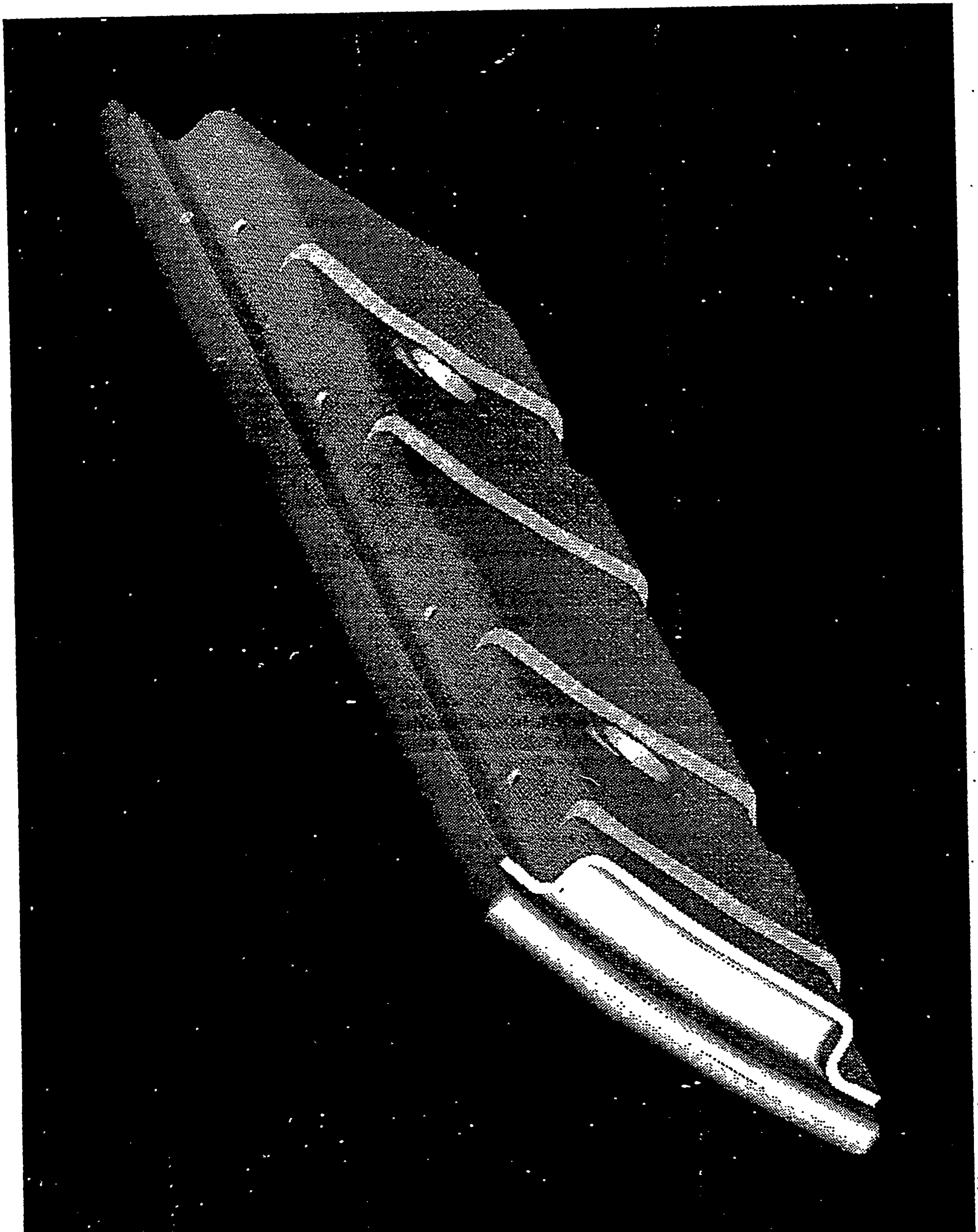

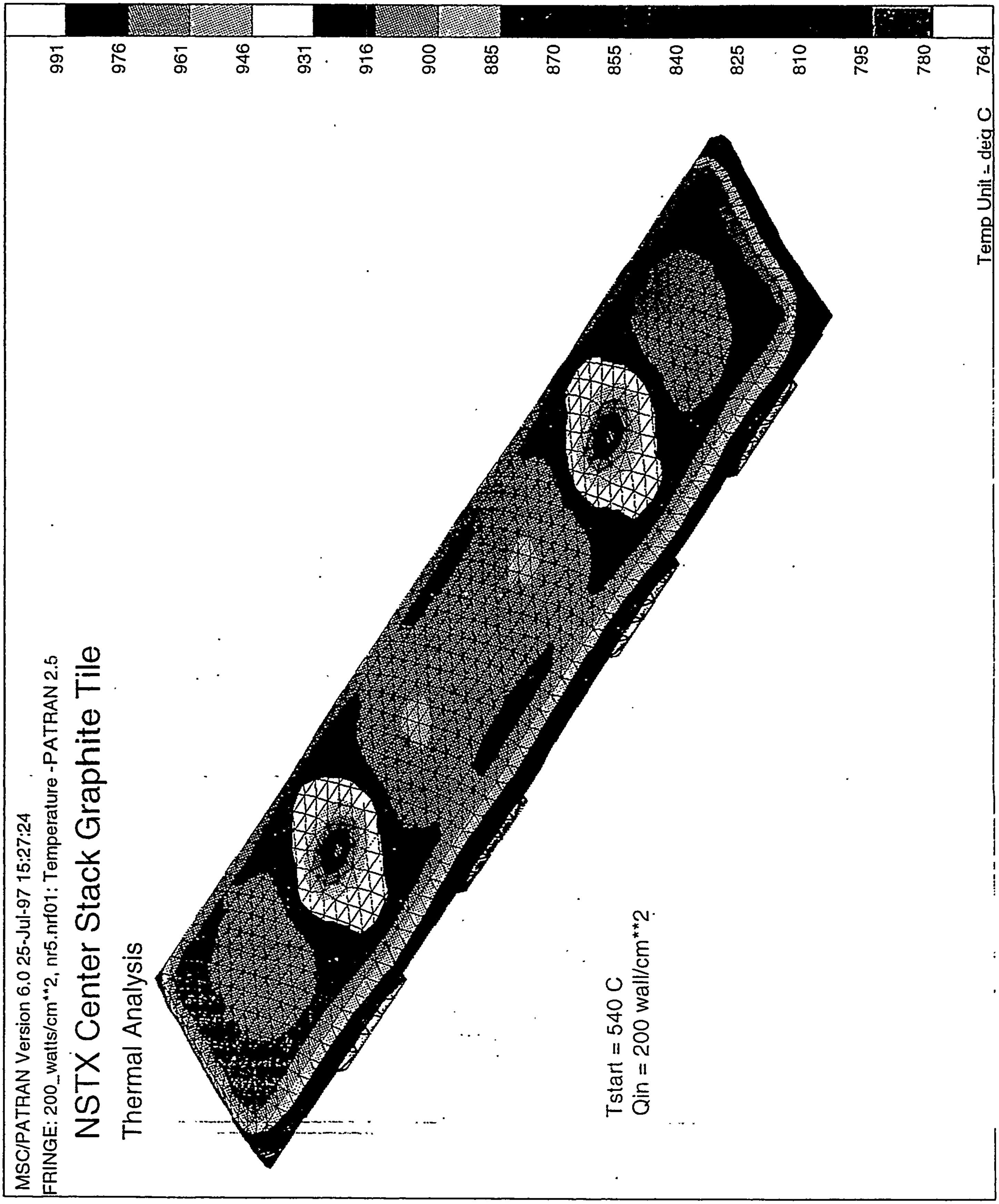
MSC/PATRAN Version 6.0 25-Jul-97 15:27:24
FRINGE: 200_watts/cm**2, nr5.nrf01: Temperature -PATRAN 2.5
NSTX Center Stack Graphite Tile
Thermal Analysis
Tstart = 540 C
Qin = 200 wall/cm**2
991
976
961
946
931
916
900
885
870
855
840
825
810
795
780
764
Temp Unit - deg C

NSTX Research Will Cover a Wide Range of Topics and Provide Ample Opportunities for Collaboration

NSTX

NSTX Working Group Topics • Subtopics	FY 1999	FY 2000	FY 2001
WG1) Slow (MHD) Mechanisms for Current Formation and Sustainment			
• Inductive mechanisms (w & w/o electron-cyclotron preionization)	√		
• Plasma operational space	√	√	
• Coaxial helicity injection, CHI	√	√	√
• Noninductive RF techniques		√	√
WG2) Fast Mechanisms for Heating and Current Drive			
• HHFW heating and current drive physics	√	√*	√*
• NBI heating and current drive physics		√*	√*
• Large and well-aligned bootstrap current physics			√*
WG3) Magnetics and Stability Limits			
• Beta limiting processes	√	√*	√*
• Fast-ion driven instabilities (e.g., Alfven modes)		√*	√*
• Control of plasma and unstable modes		√*	√*
WG4) Plasma Transport and Fluctuations			
• Global confinement	√	√*	√*
• Local transport		√*	√*
• Microinstabilities and turbulence		√*	√*
• Turbulence suppression and transport barrier formation			√*
WG5) Divertor, Scrape-Off Layer, Power and Particle Handling			
• Vessel and tile conditioning	√	√	
• SOL properties of diverted and inboard wall limited plasmas	√	√	√*
• Maintenance of edge transport barriers		√	√*
• Effects of large mirror ratios (e.g., velocity-space instabilities)		√	√*

* NBI and NBI-based diagnostics assumed

NSTX and MAST Will Prove the Physics Principles for Volume Neutron Source and Power Plant

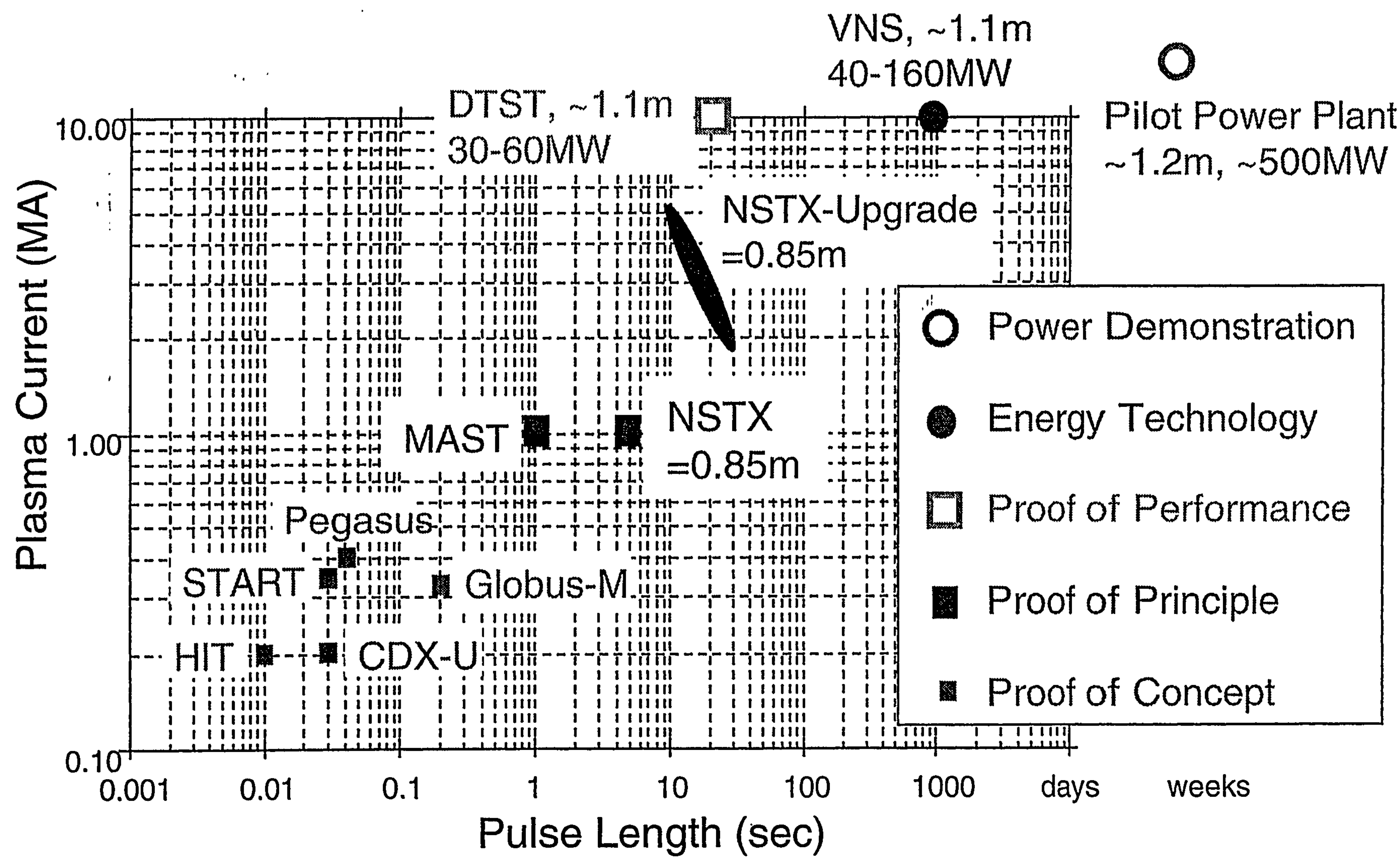

ST Development Pathway Provides a Good Example of Potential Benefits from Innovation

Pathway

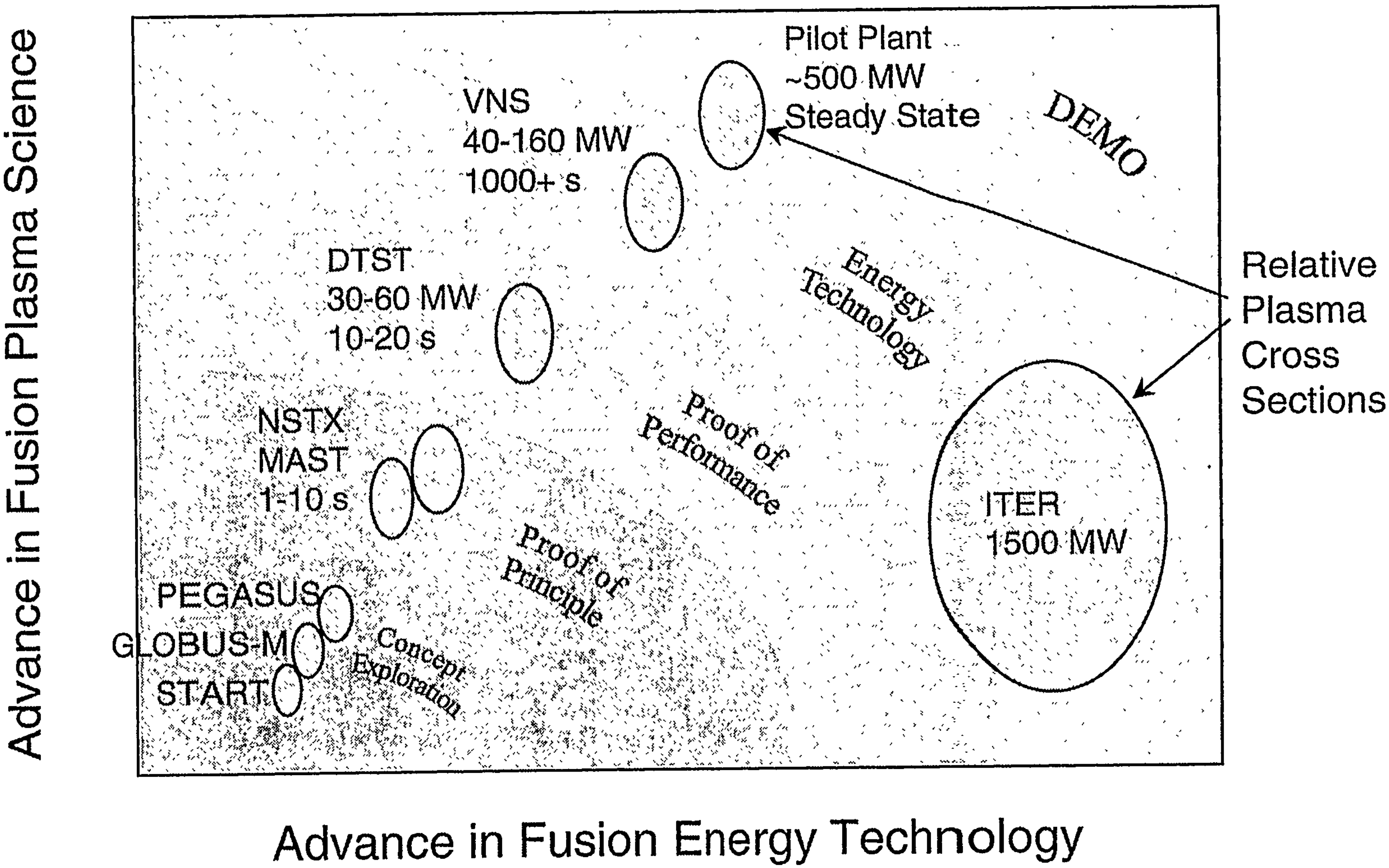

An ST VNS Design Can Take Advantage of a Smaller and Simpler Fusion Core

ST-VNS

(Dimensions in Meter)

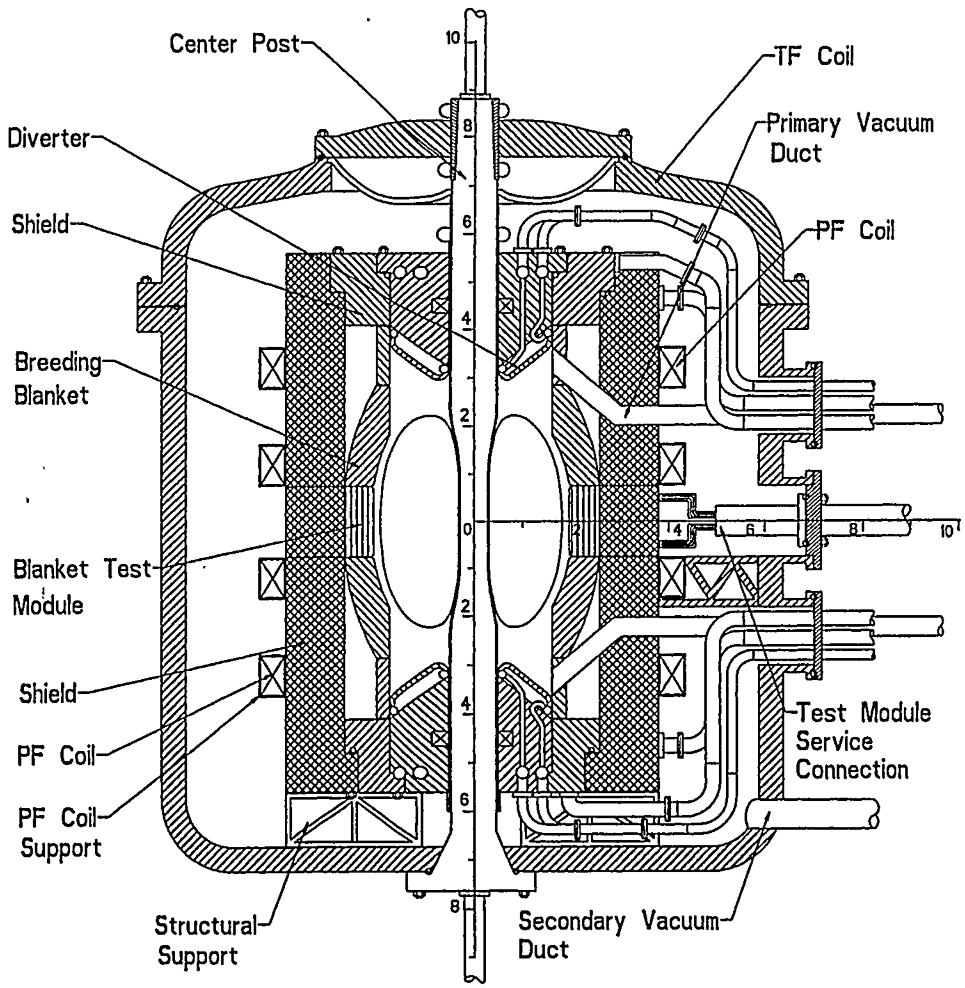

Features

- Modular design
- H_2O cooled N/C TFC
- Demountable, low-load center leg
- Combine VV with TFC return leg
- Simplified load path
- Full remote maintenance for activated components
- Hands-on maintenance for the rest after shutdown
- Full access to test modules

Naturally Diverted Plasma in ST-VNS Show Mostly Diverted SOL

ST-VNS

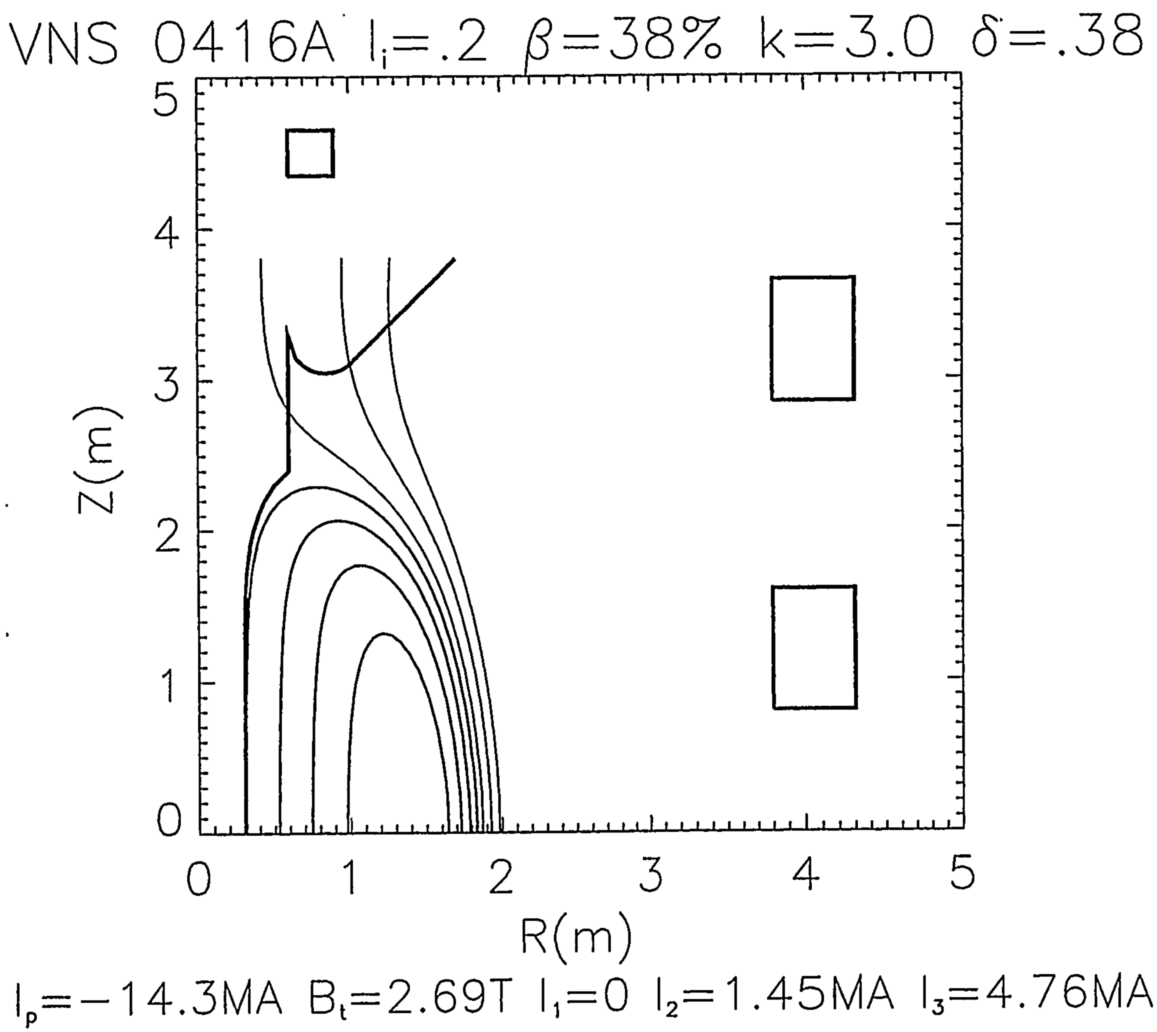

I-95

Naturally Diverted Plasma in ST-VNS Show Large SOL Flux Expansion

ST-VNS

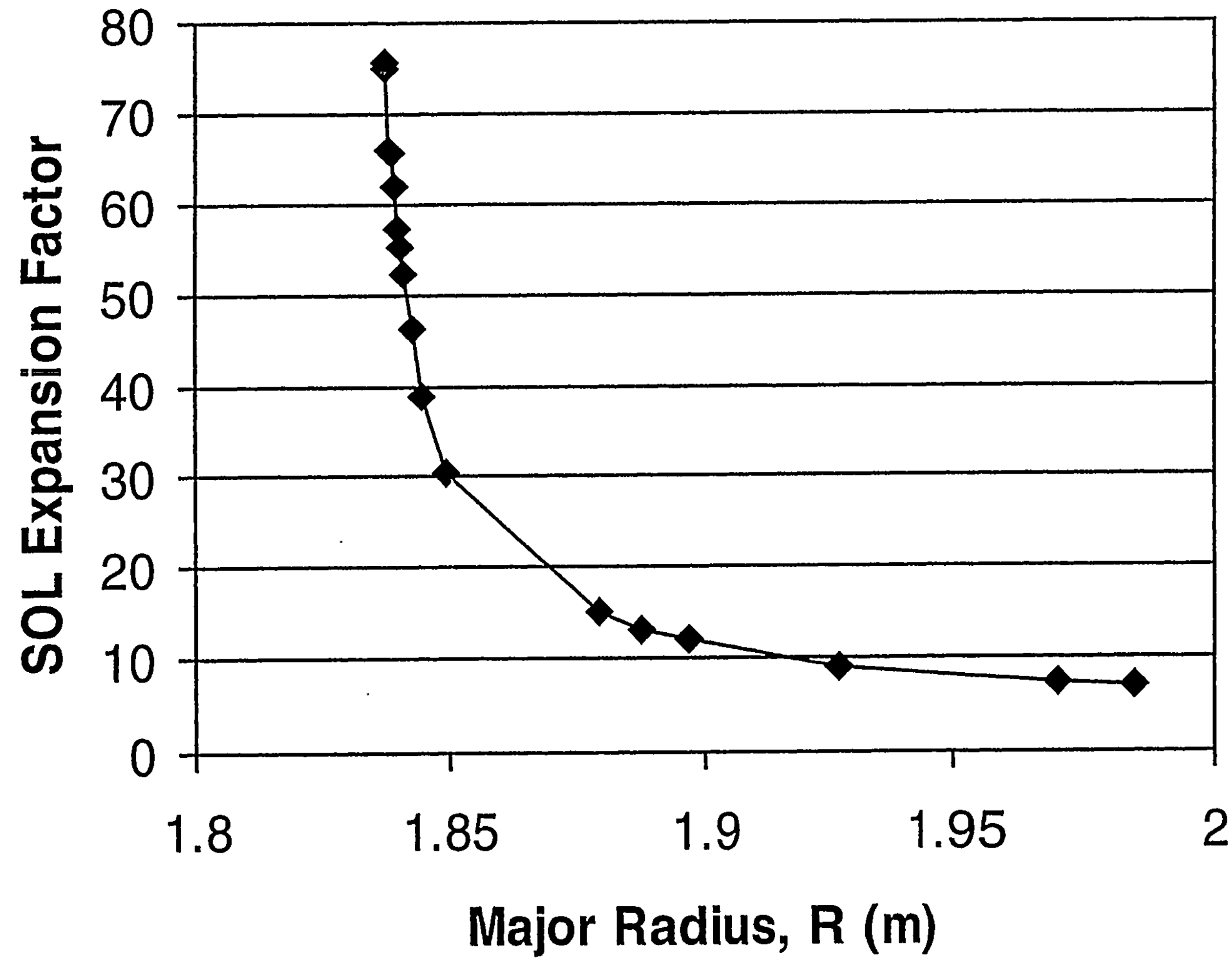

Summary

NSTX

- Spherical Torus plasma has exciting possibilities for high performance in fusion plasma science
- NSTX will prove the physics principles for attractive VNS and power plants, which may have high demands on HHFC & PSI performances
- NSTX Research will cover a wide range of topics and provide ample opportunities for collaboration, including HHFC & PSI enabling technology
- NSTX Research Program is being prepared for start of operation in May 1999.
- HHFC & PSI researchers are encouraged to collaborate and utilize the NSTX device and facility

Please view NSTX Research Program Webpage:

http://fileroom.pppl.gov/nstxhome/index.html, Research_Program folder

5

Design and initial operation of W-shaped divertor in JT-60U

K. Masaki (JAERI)

Design of W-shaped divertor

Structure: target plates, dome, baffle plates, first wall tiles and gas seels

Initial operation

Recent result and investigation of the inside structures and the first wall tiles

JAERI

Modification from open divertor to W-shaped divertor

The work of this modification started end of February in 1997, and was completed in May.

Objective

to realize radiative divertor plasma and good H-mode confinement simultaneously.

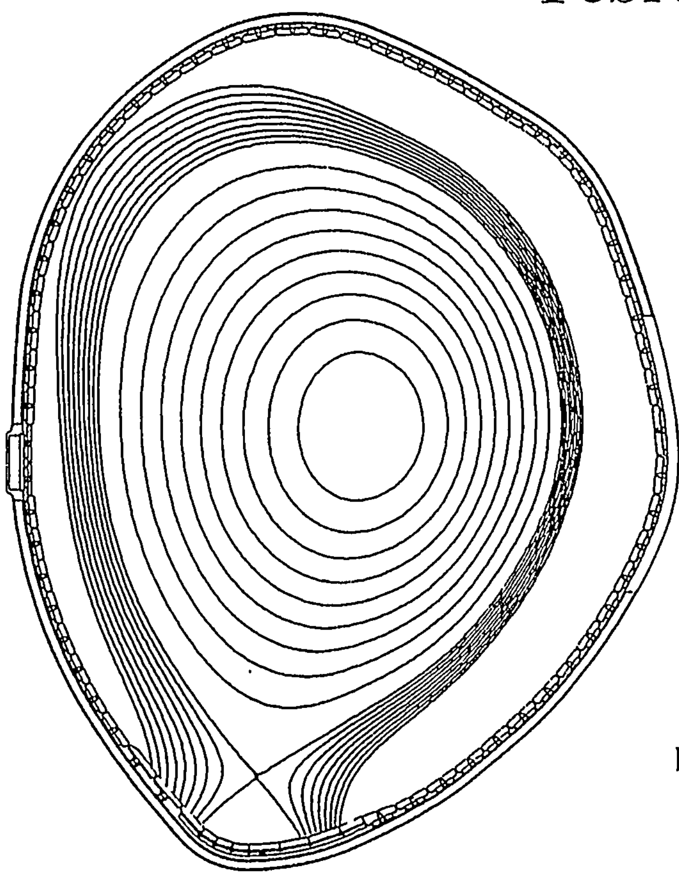

Open divertor

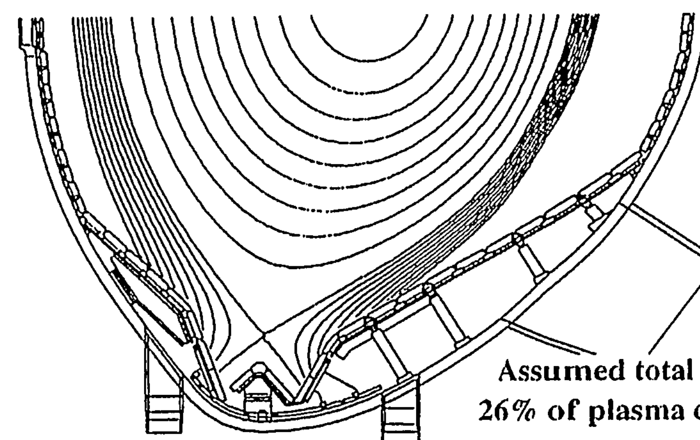

Designed value
3MA, 4T
30MW(net heaing power)

Assumed total halo current
26% of plasma current (3MA)
toroidal peaking factor of 2.5

W-shaped divertor

JAERI

Structure of W-shaped divertor

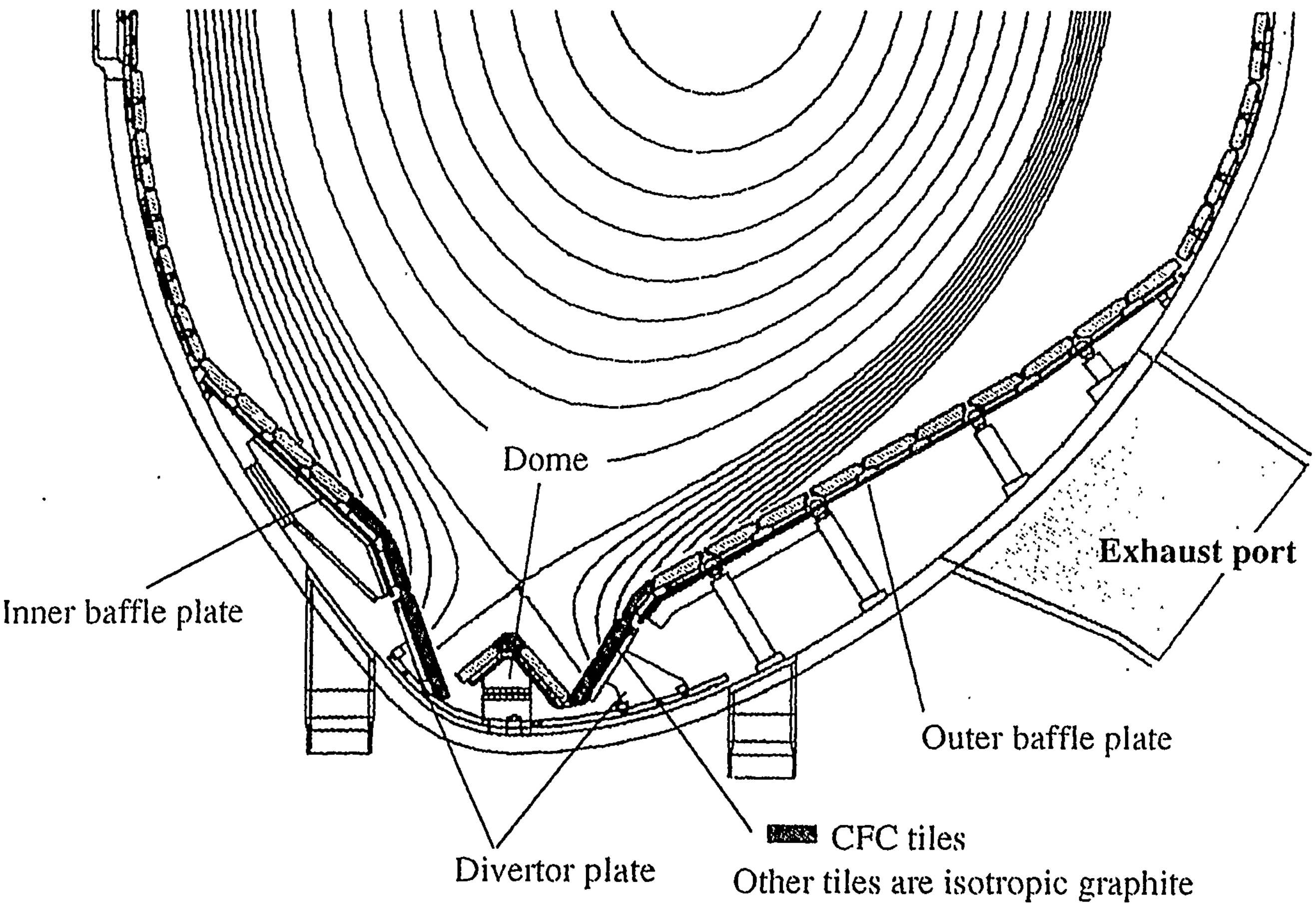

<Inclined target>

High recycling, dense and cold divertor

<Baffle>

to suppress back flow of neutral particles

<Dome>

to reduce generation of carbon impurity

<Pumping>

(only inner divertor)

Particle control

JAERI

Location of gas injection port , exhaust port and NBI port

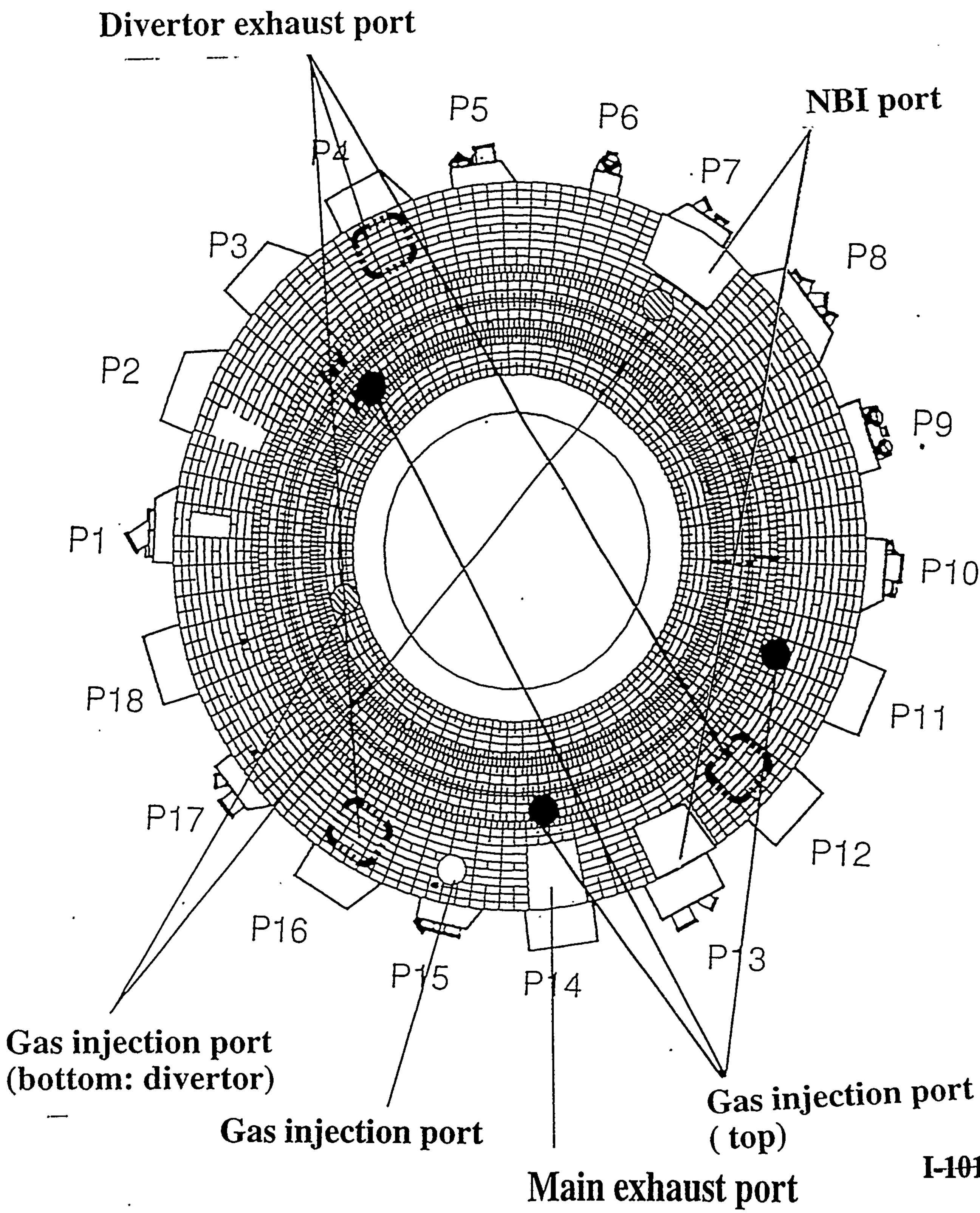

W-shaped divertor

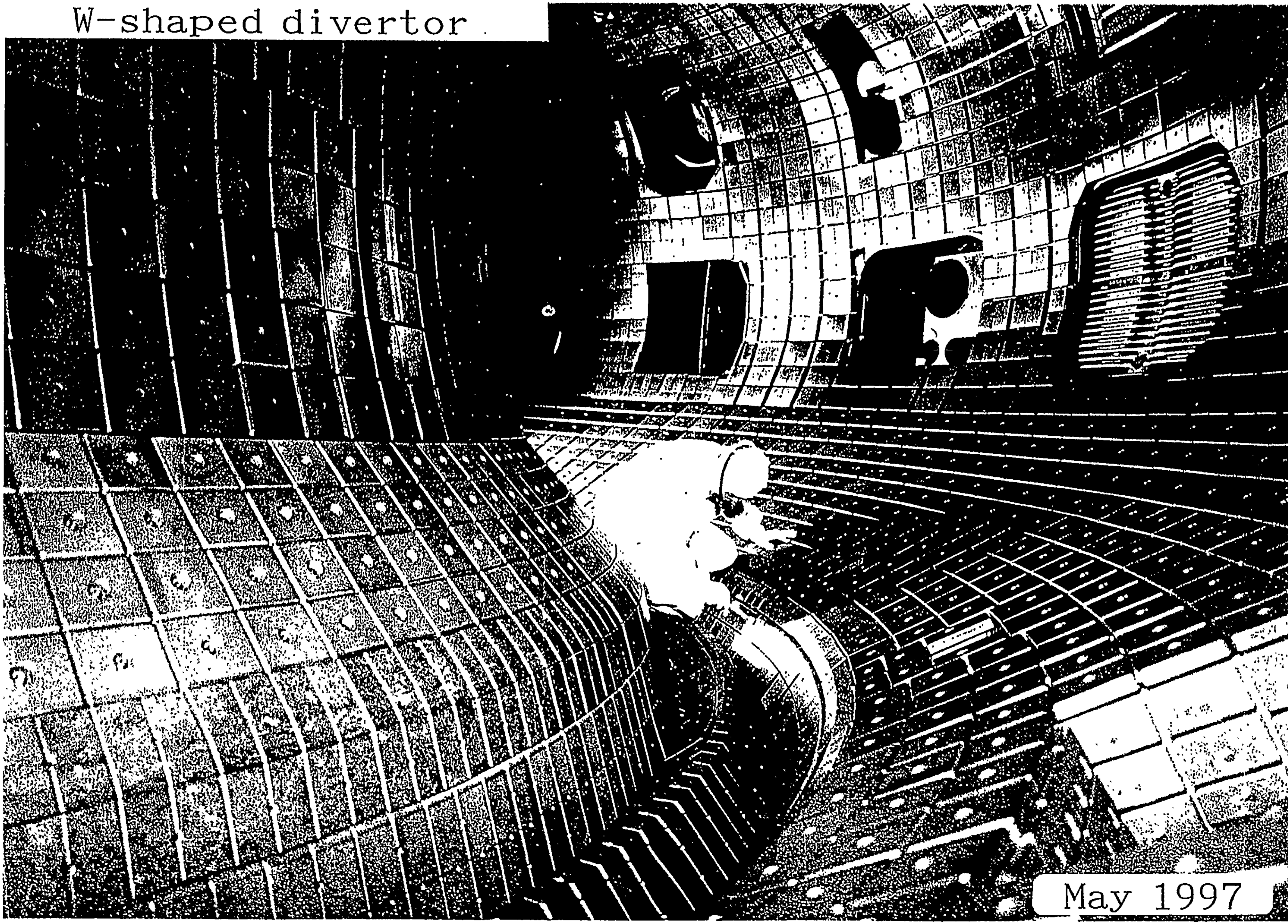

Inner divertor (1 unit)

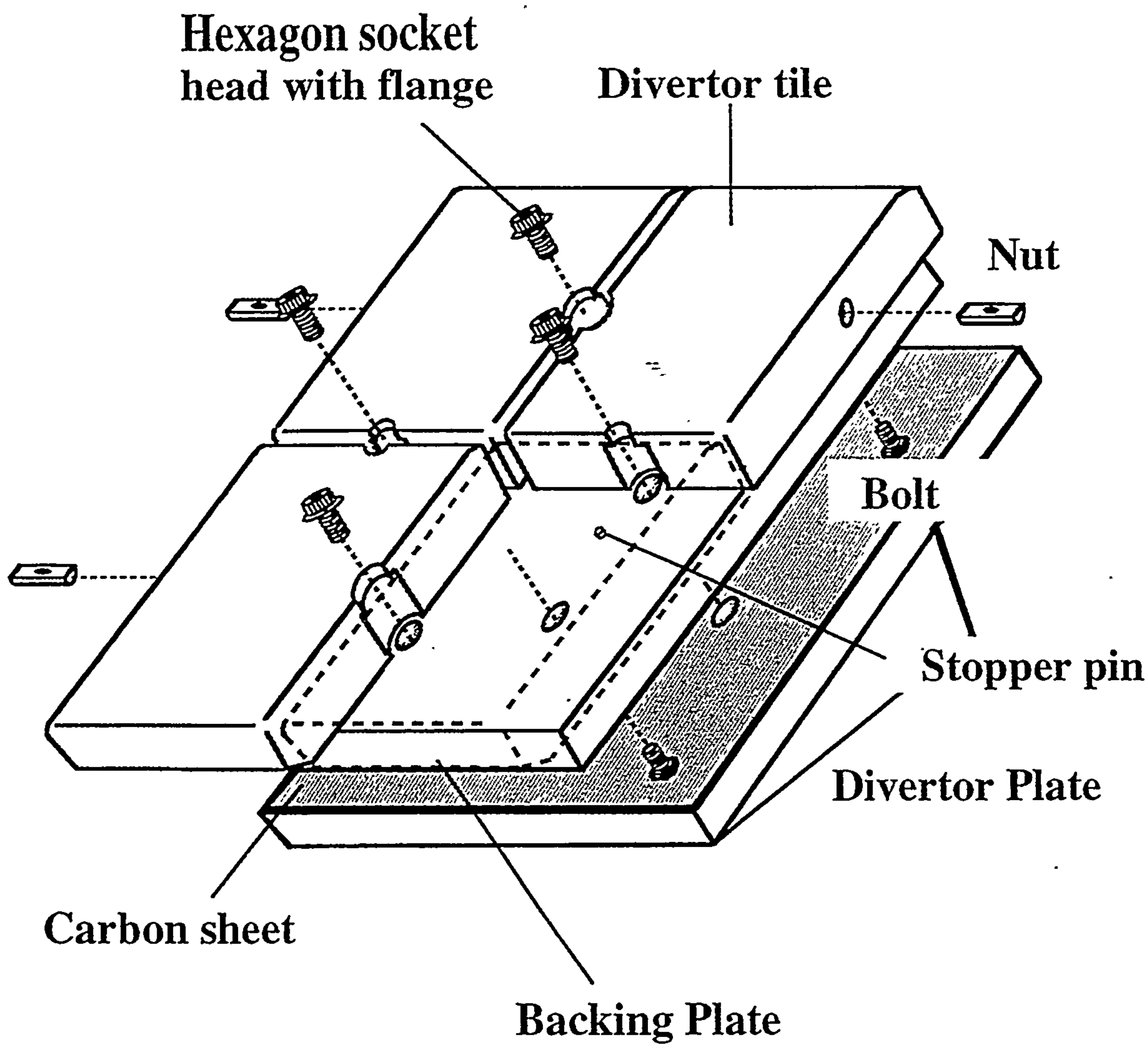

Inner divertor : 125 units
outer divertor : 125 units   Total 250 units

These divertor tiles were designed as the surface is circumscribed (inner divertor) and inscribed (outer divertor) **in each circles of inner and outer divertor plates.**

These tiles were tapered to avoid the heat concentration to the tile edge.

Schematic view of tile alignment

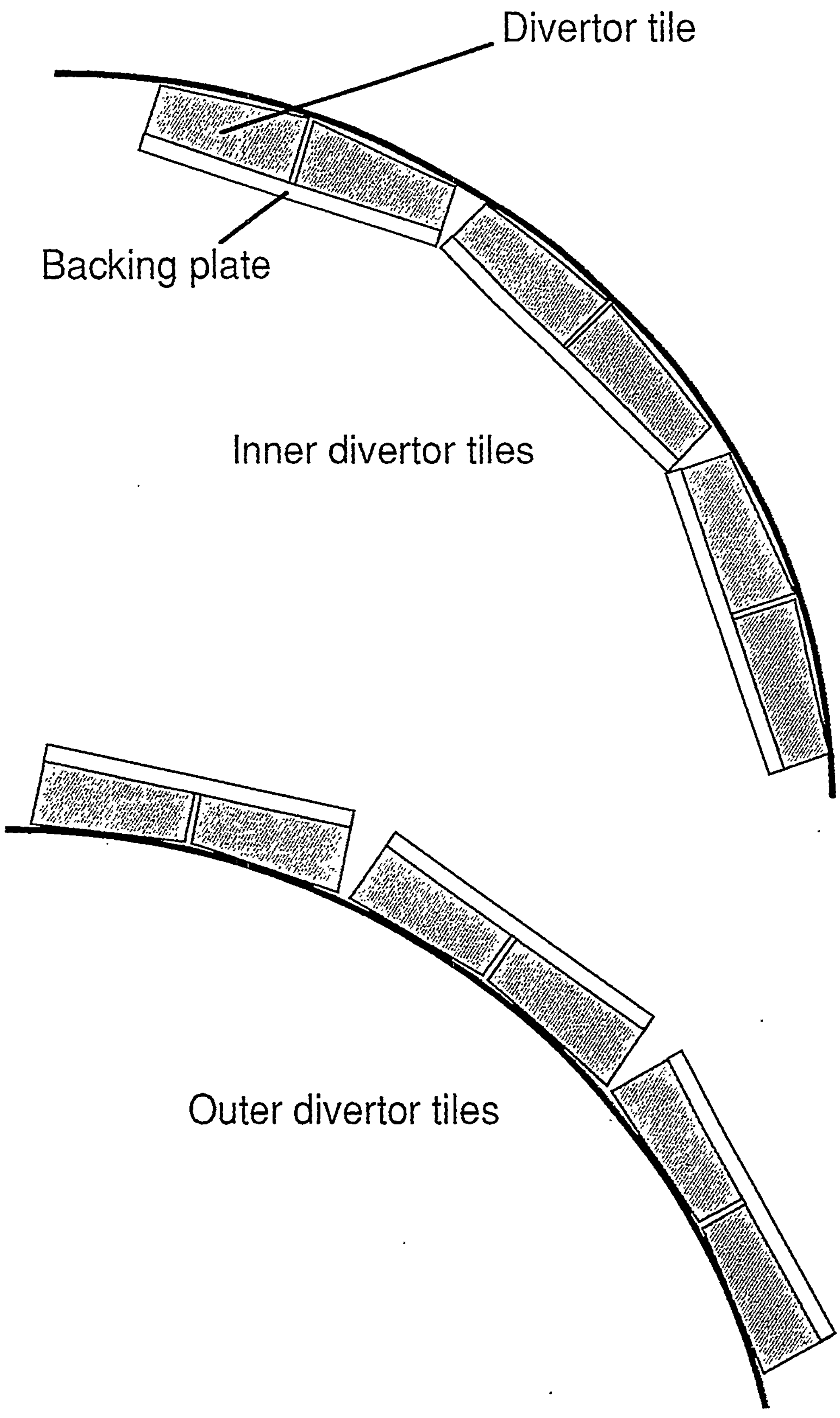

Taper of divertor tile
(Inner divertor)

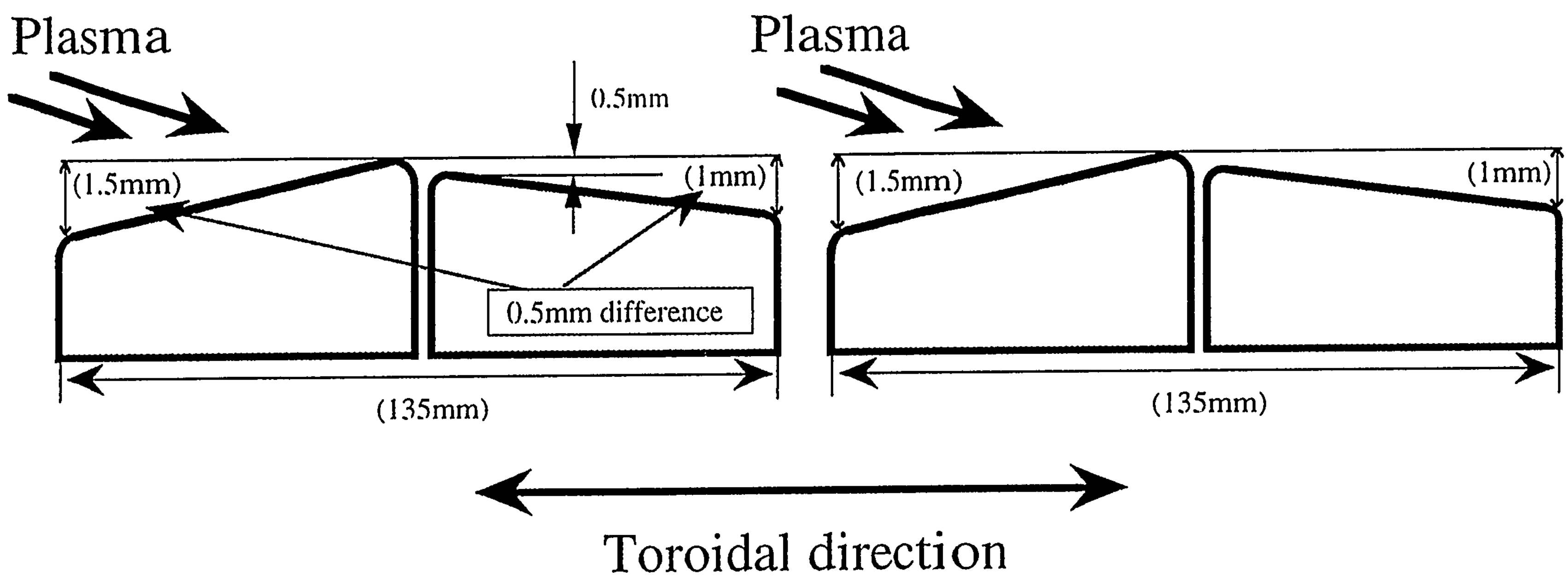

JAERI

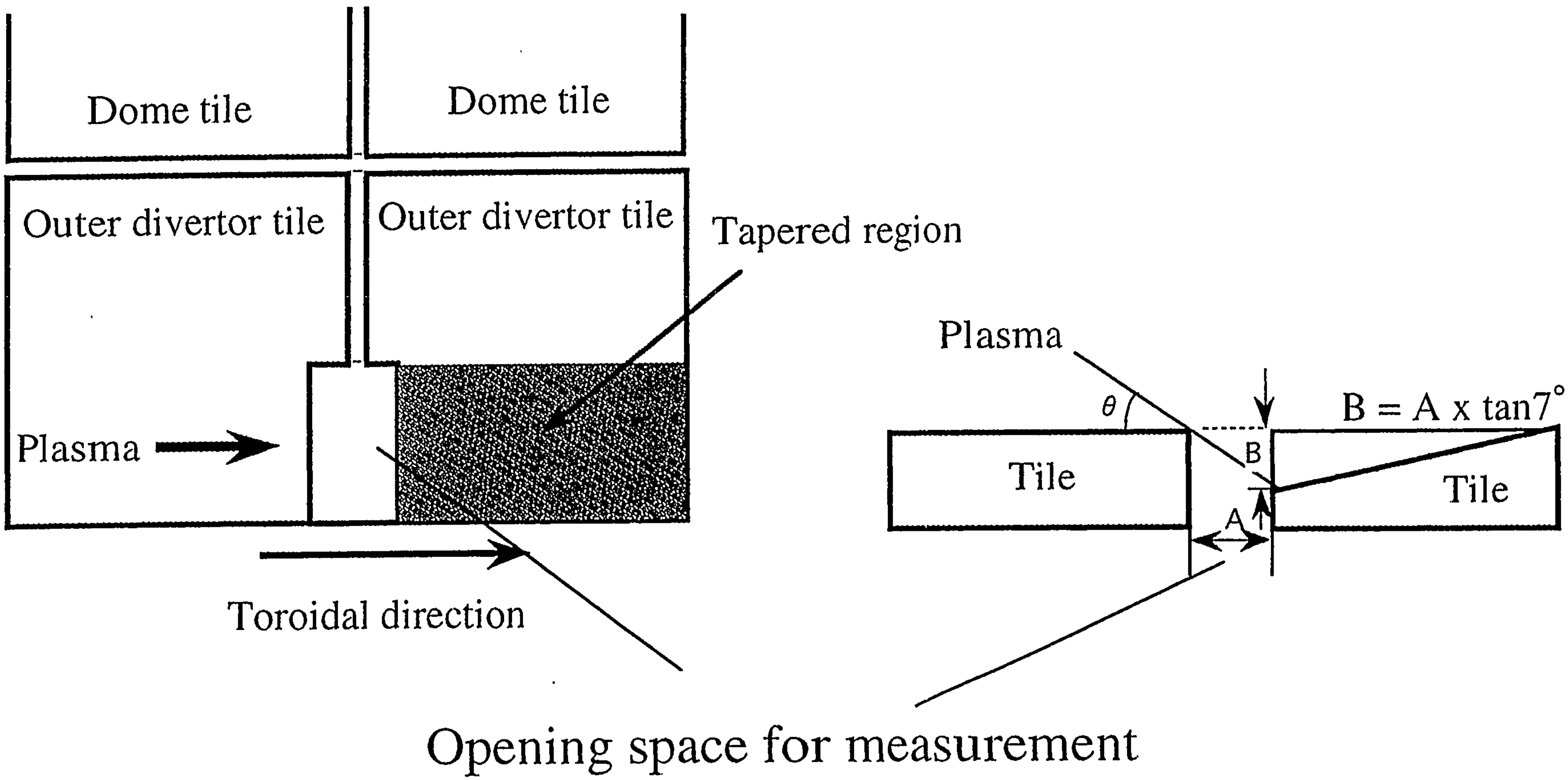
Dome tile
Dome tile
Outer divertor tile
Outer divertor tile
Tapered region
Plasma
Toroidal direction
Plasma
θ
B = A x tan7°
B
A
Tile
Tile
Opening space for measurement

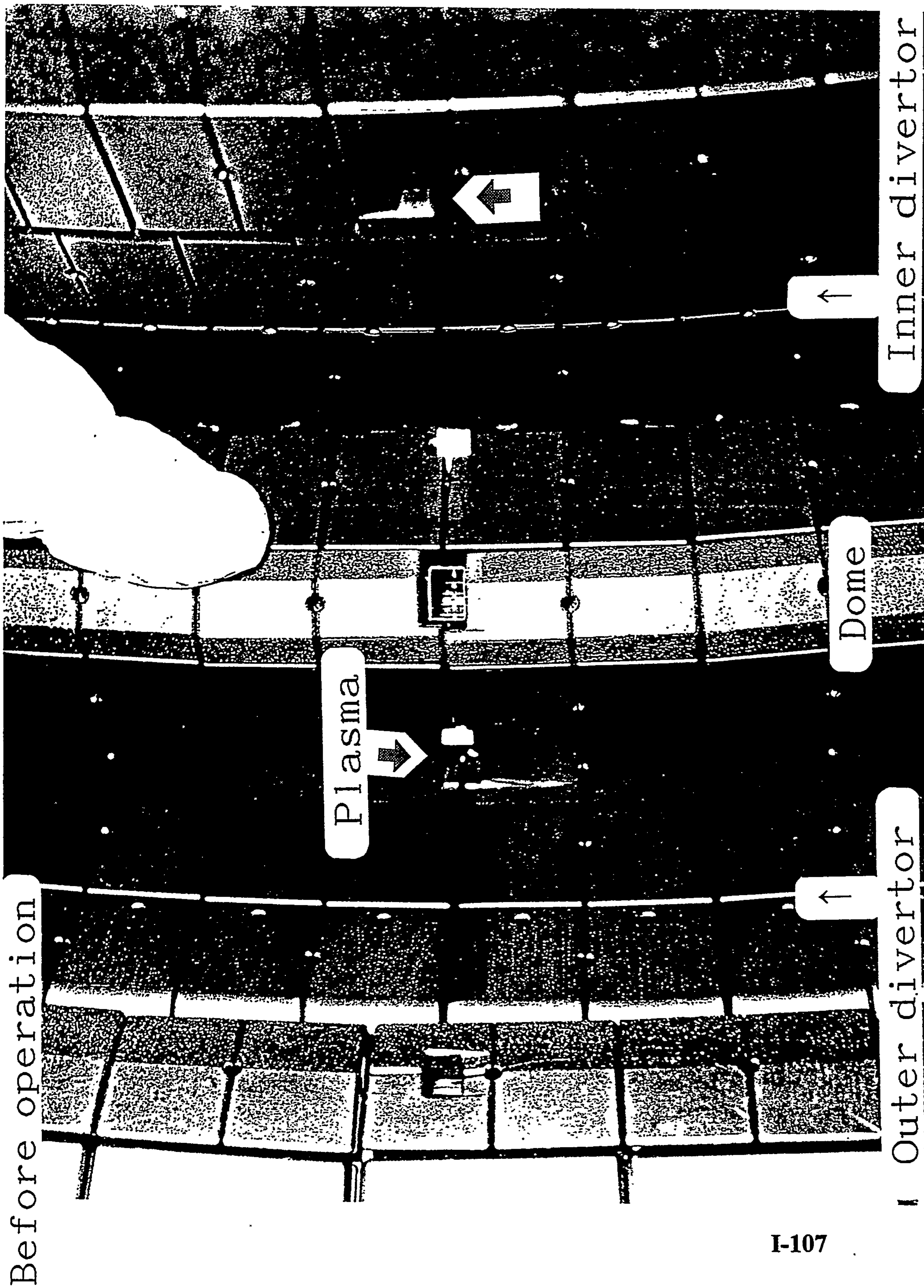
Before operation
Plasma
Dome
Inner divertor
Outer divertor

Dome (1 unit)

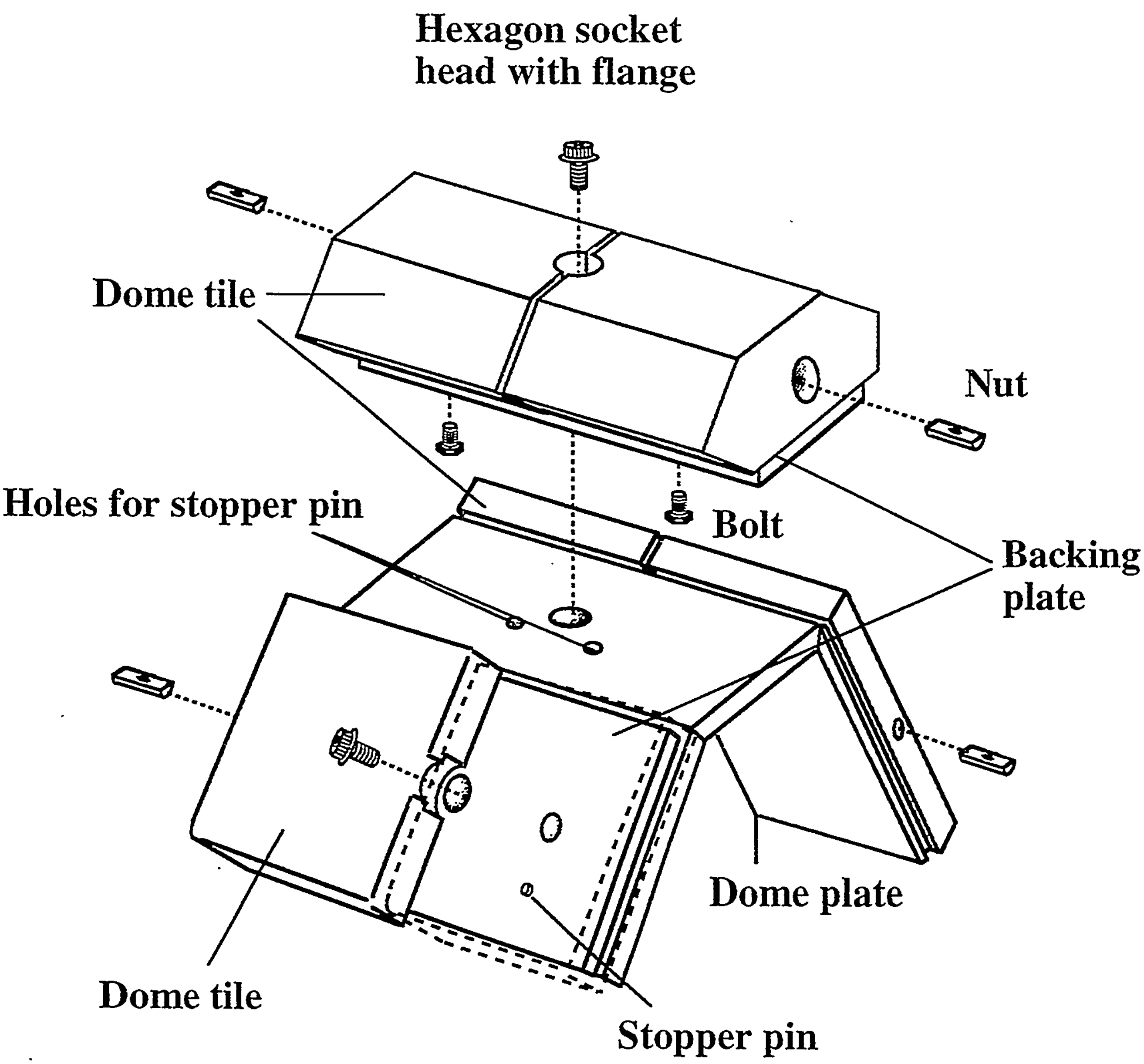

Total : 125 units

Inner and outer baffle plates

Inner baffle plate

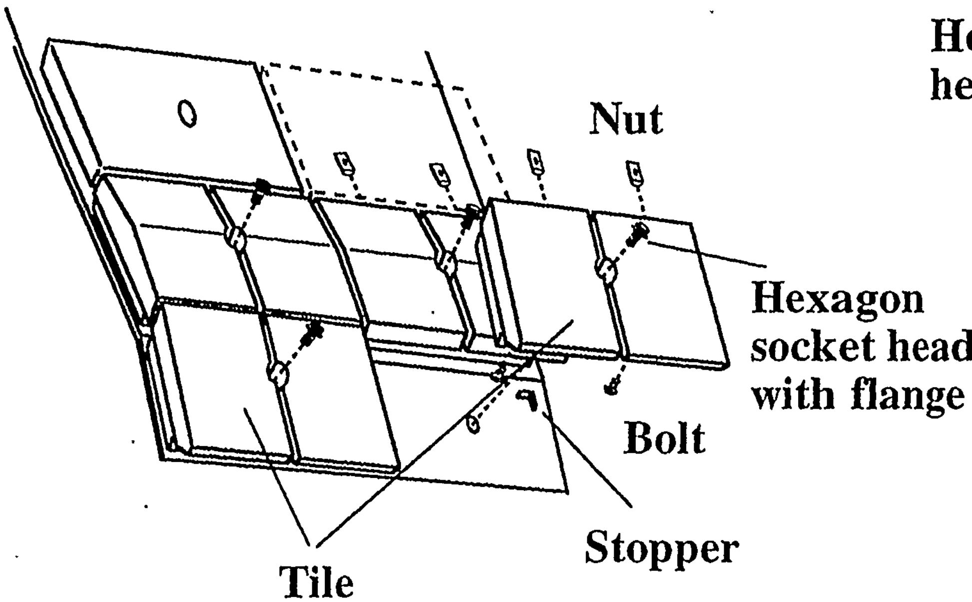

Inner baffle plate : 72 plates

Outer baffle plate

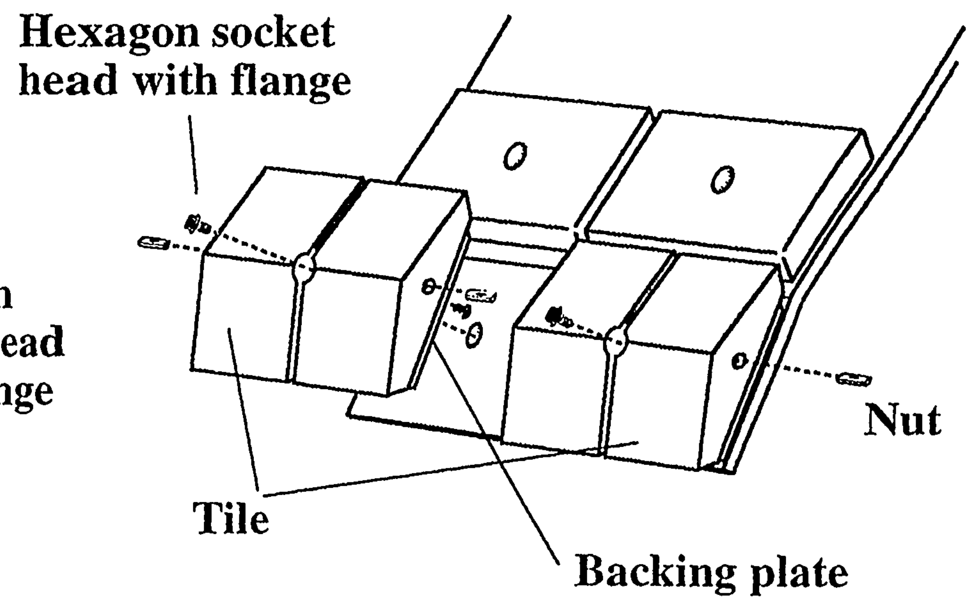

Outer baffle plate : 72 plates

These baffle tiles were designed as the surface is circumscribed (inner baffle) and inscribed (outer baffle) in each circles of inner and outer divertor plates.

These tiles were tapered to avoid the heat concentration to the tile edge.

JAERI

Baffle plate tile

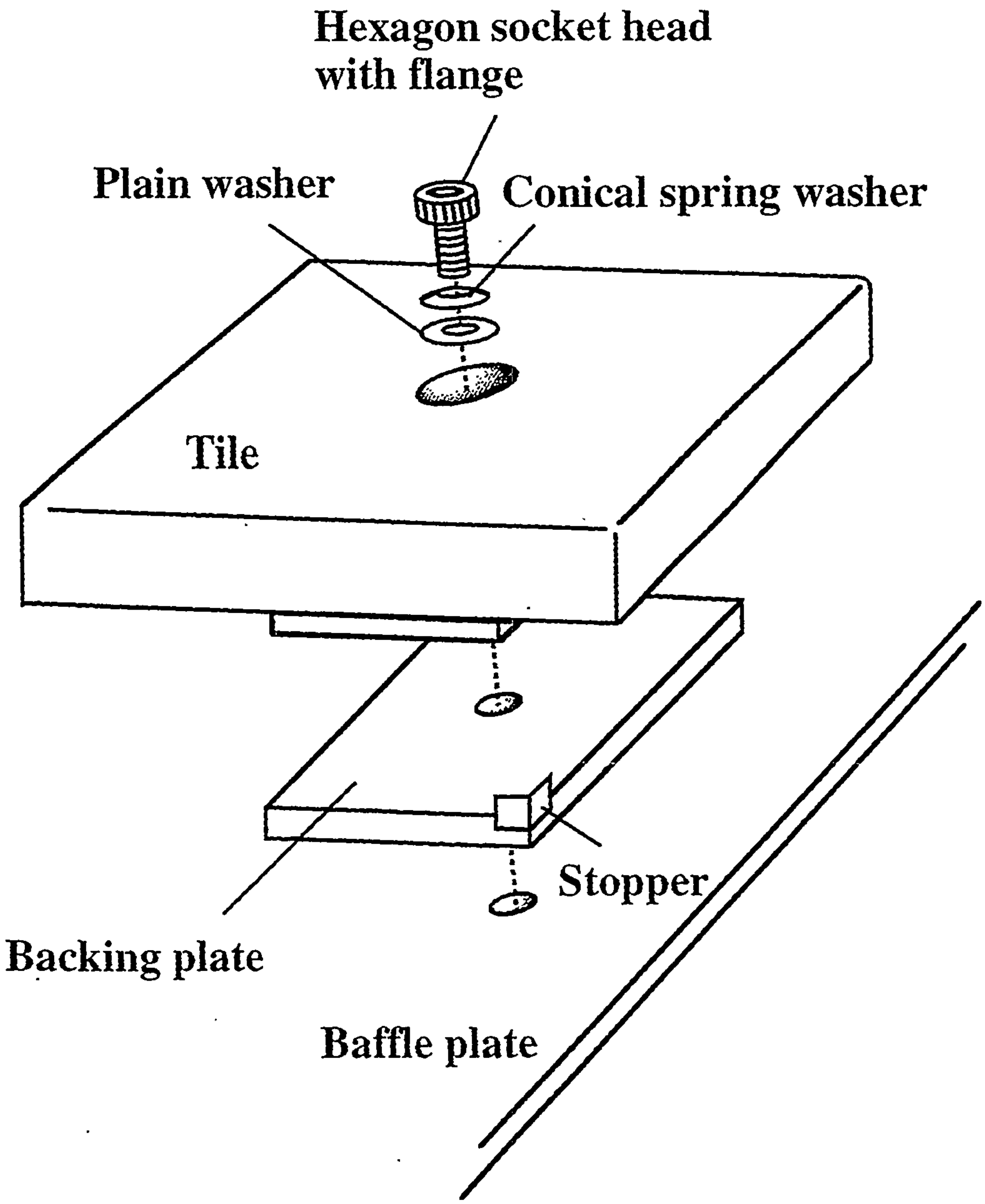

Gap and level difference between each tile

section	gap	level diff.
inner baffle (T)	>1.5	-1~0*,2~0
in. baffle/div. (P)	3.5~4.5	
inner divertor (T)	>1.0	-1.5~0
dome (T)	0.5~2.0	-2~0
outer divertor (T)	>1.5	-1.5~0
out. baffle/div. (P)	3.5~4.5	
outer baffle (T)	1.5~2	-1~0*,±2

(T) : Toroidal direction

(P) : Poloidal direction

-1~0* : Near the Divertor region

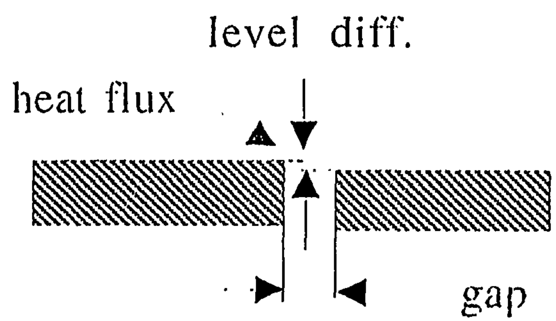

JAERI

Thermal analysis

Expected heat flux

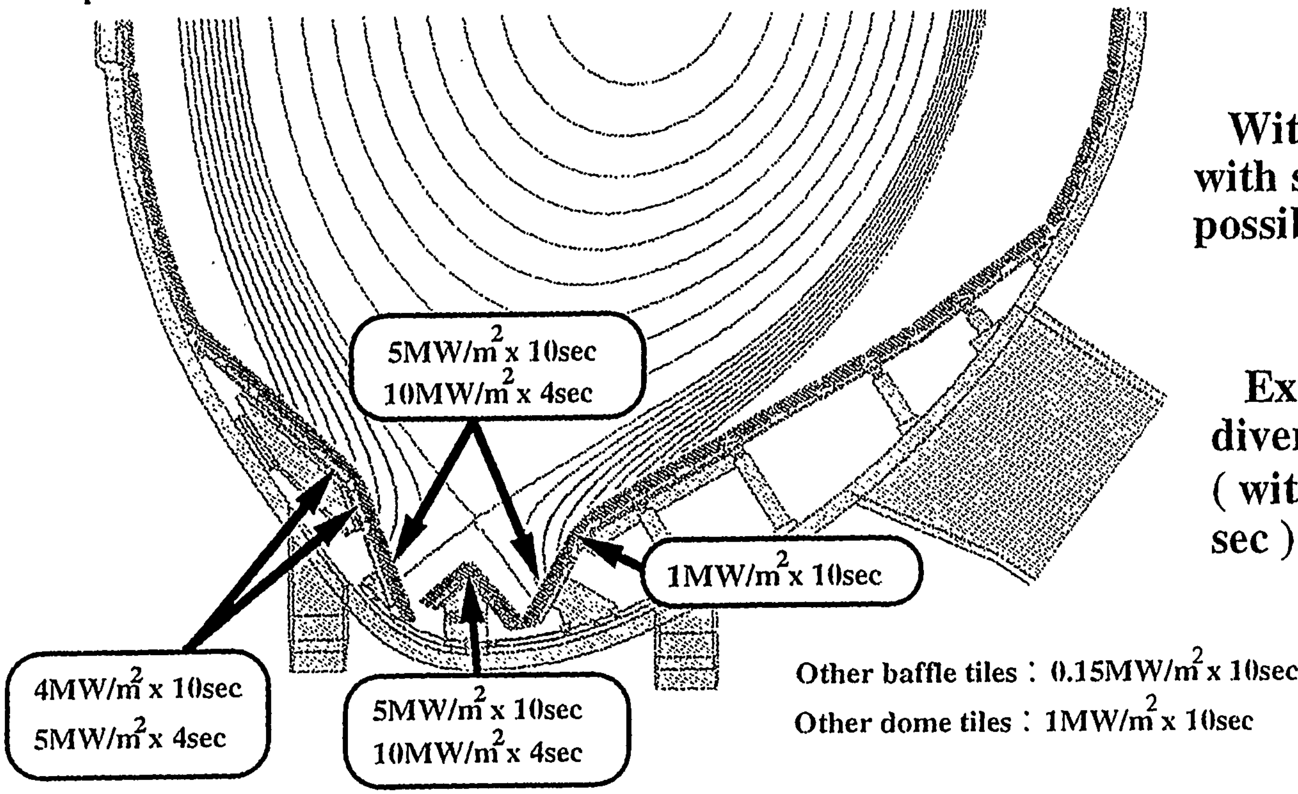

Without water cooling, operations with shot intervals of 20 min. are possible.

Expected surface temperature of divertor tile is approximately 1200℃ (with water cooling - 10MW/m^2 x 4 sec).

Structure of gas seal (baffle palte)

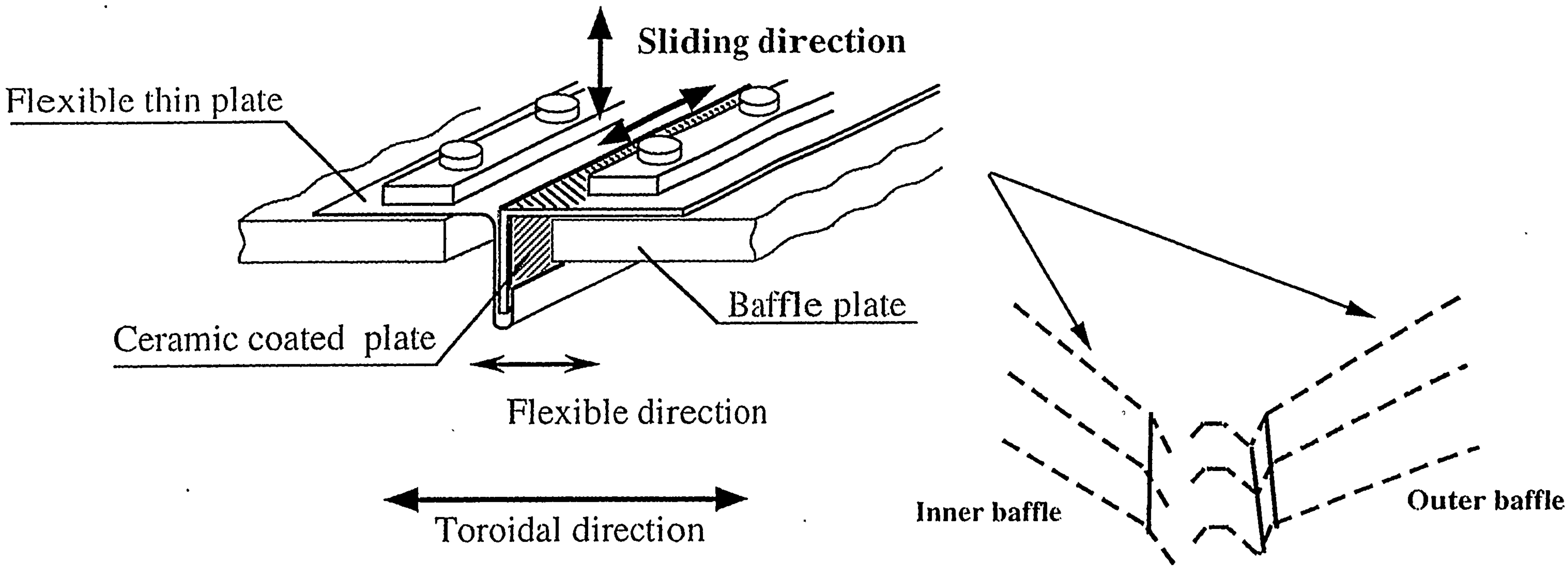

Poloidal gaps between the segmented baffle sturctures are sealed by inserted-sliding mechanizm.

Sliding parts are insulated by sprayed ceramic coating to avoid arcing across the gaps.

JAERI

Structure of gas seal
(divertor palte and dome plate)

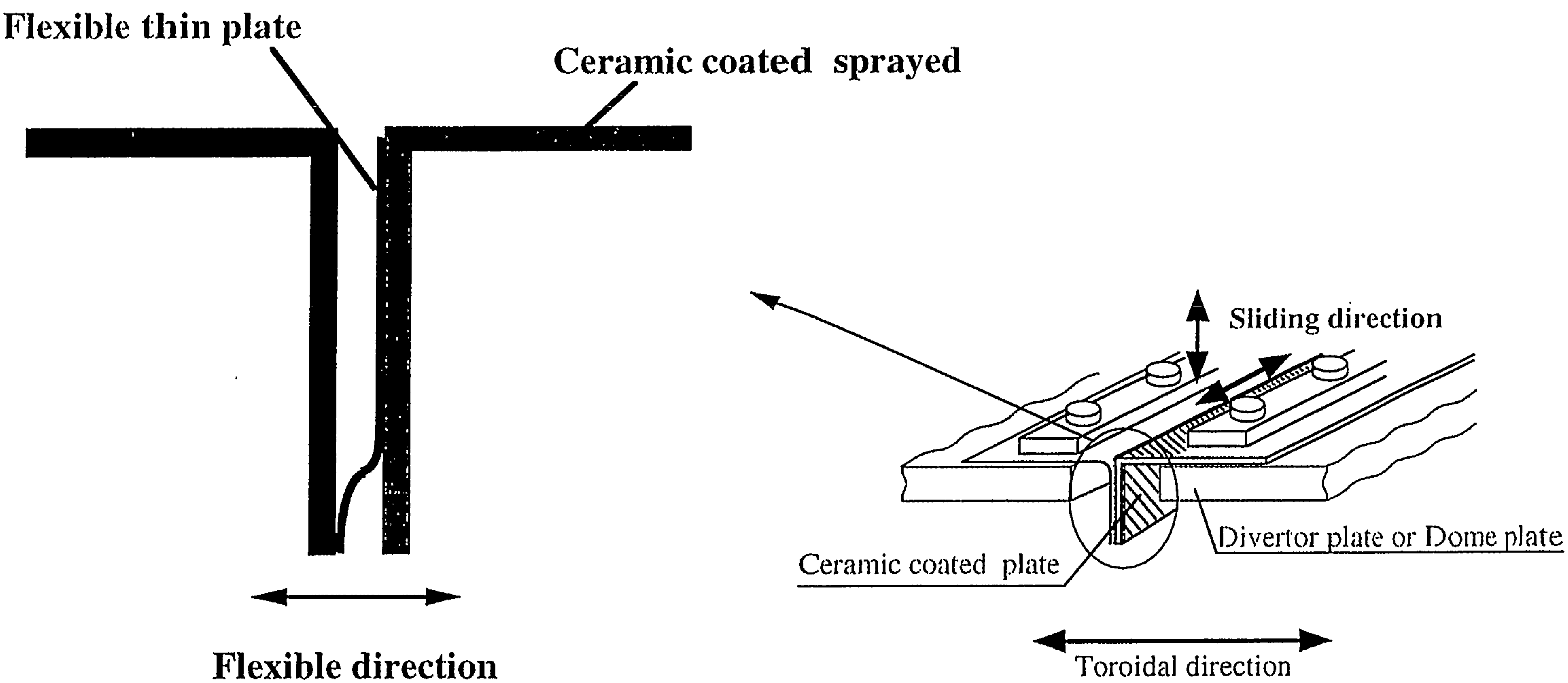

JAERI

W-shaped divertor measurement systems

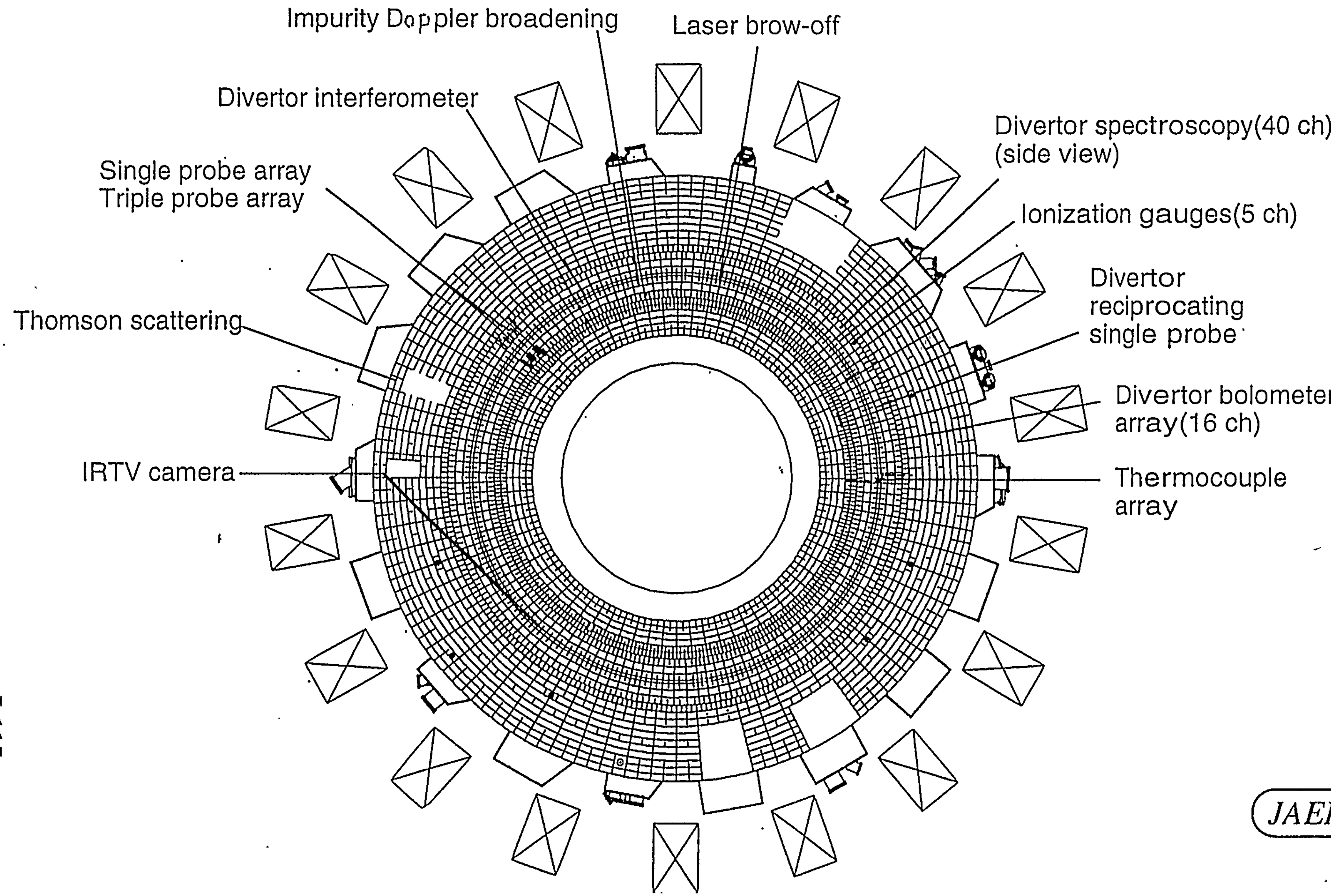

JAERI

Initial operation of W-shaped divertor

< Recent results >

Halo current

Helium exhaust

Steady-state high performance

< Investigation of the inside structures and the first wall tiles >

JT-60 was vented in November for maintenance.
(after 5 months operation)

JAERI

Halo current in W-shaped divertor

to simulate VDE

move plasma downward actively .

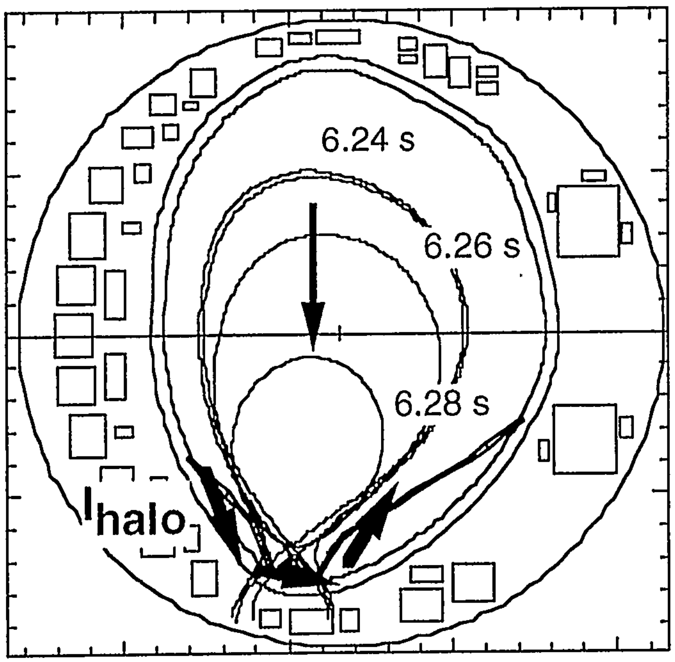

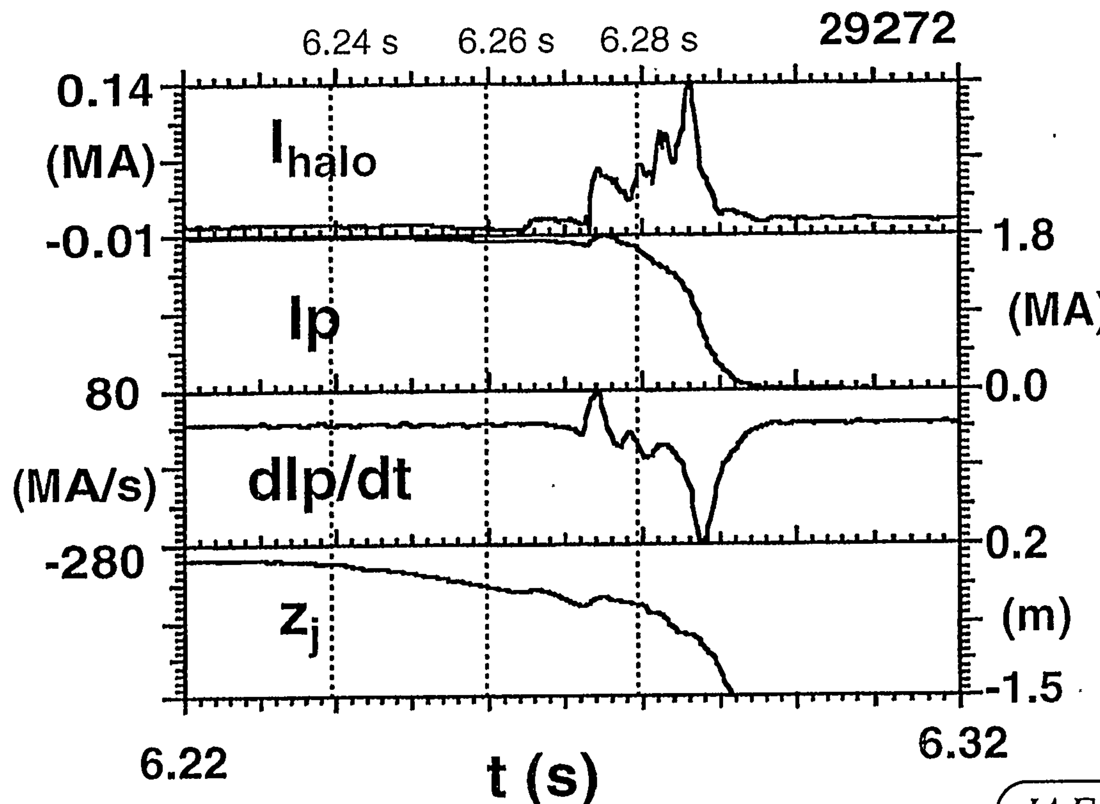

JAERI

Rogowski coil for halo current

[Specification]

- Material of coiling wire : MI (Mineral Insulation)cable (1mm Φ)
- Sheath : Inconel
- Working temperature : < 500 °C
- Cross section : 0.6 m^2/m
- Frequency Responce : < 5 kHz

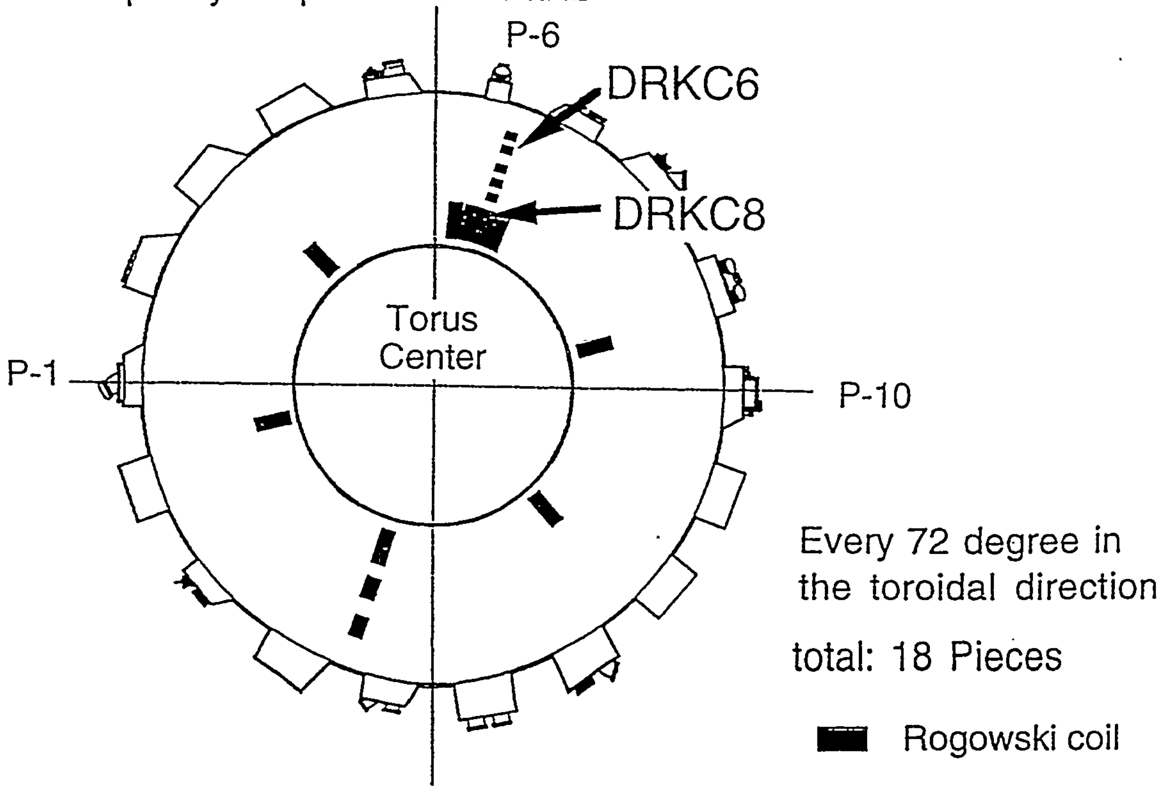

Top View of Vacuum Vessel

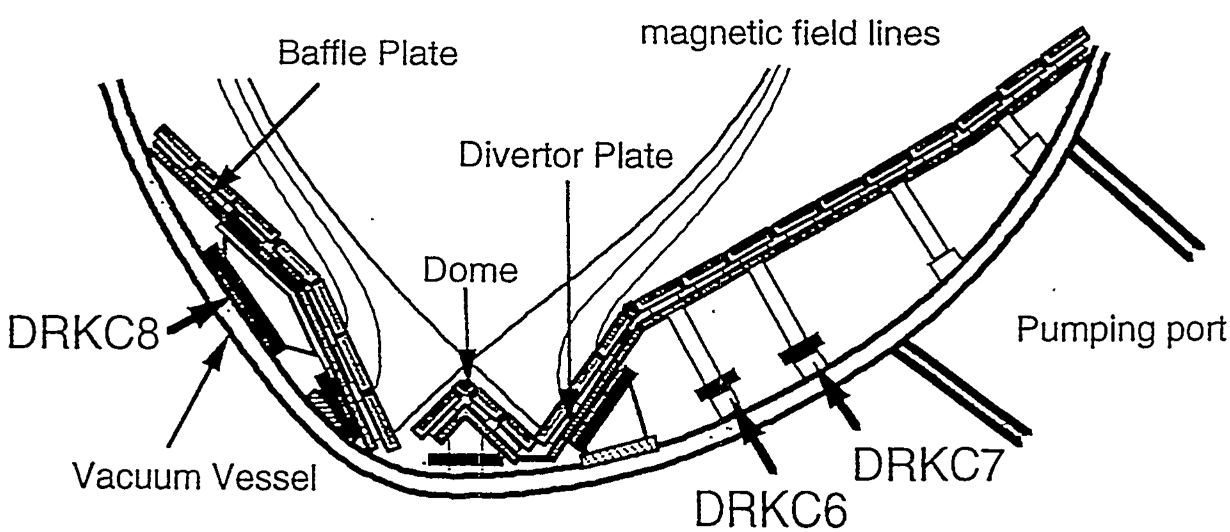

Side View of Vacuum Vessel
(P-6 section)

Rogowski coil

Halo current in W-shaped divertor

Ih/Ip = 0.05~0.25

TPF(Toroidal peaking factor) = 1.4~3.6

Ih/Ip x TPF < 0.52
(lower than the previous data of medium size tokamaks (0.75))

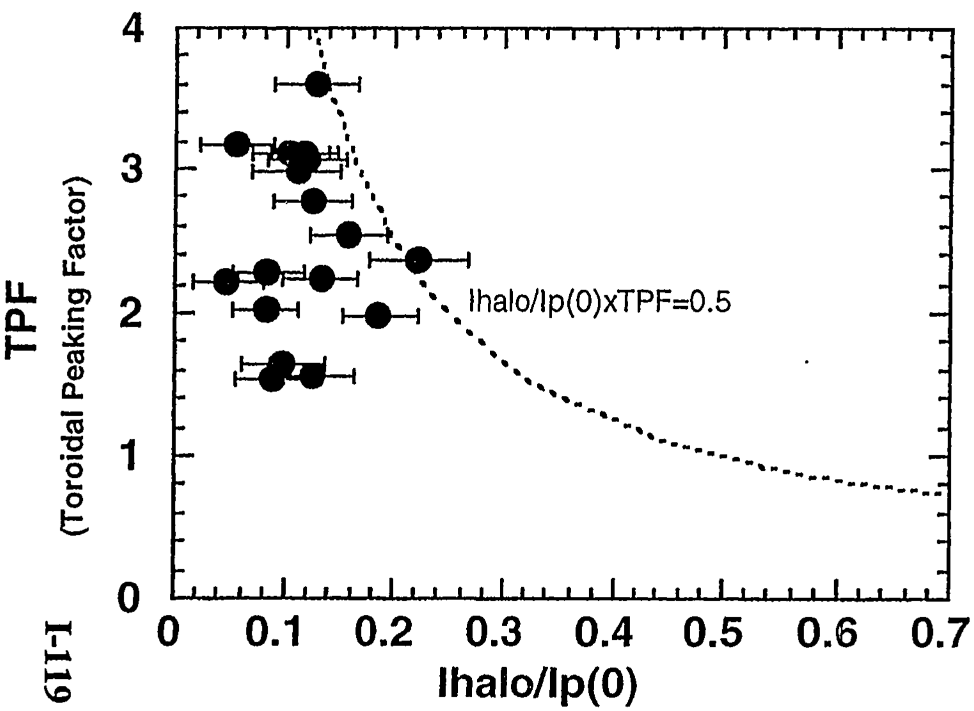

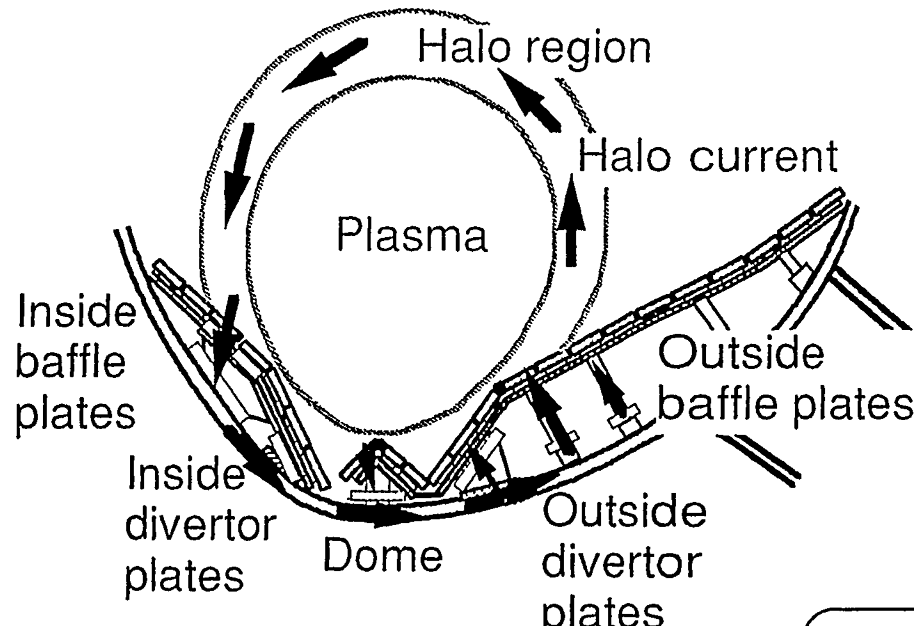

JAERI

Steady-state high performance with W-shaped divertor

Steady-state ELMy H-mode for 9sec

No serious increase in recycling and carbon impurity

~22MW (NBI) x 9sec : ~200MJ

Surface temperature of divertor tile exceeded 1000℃

1.5MA／3.5T

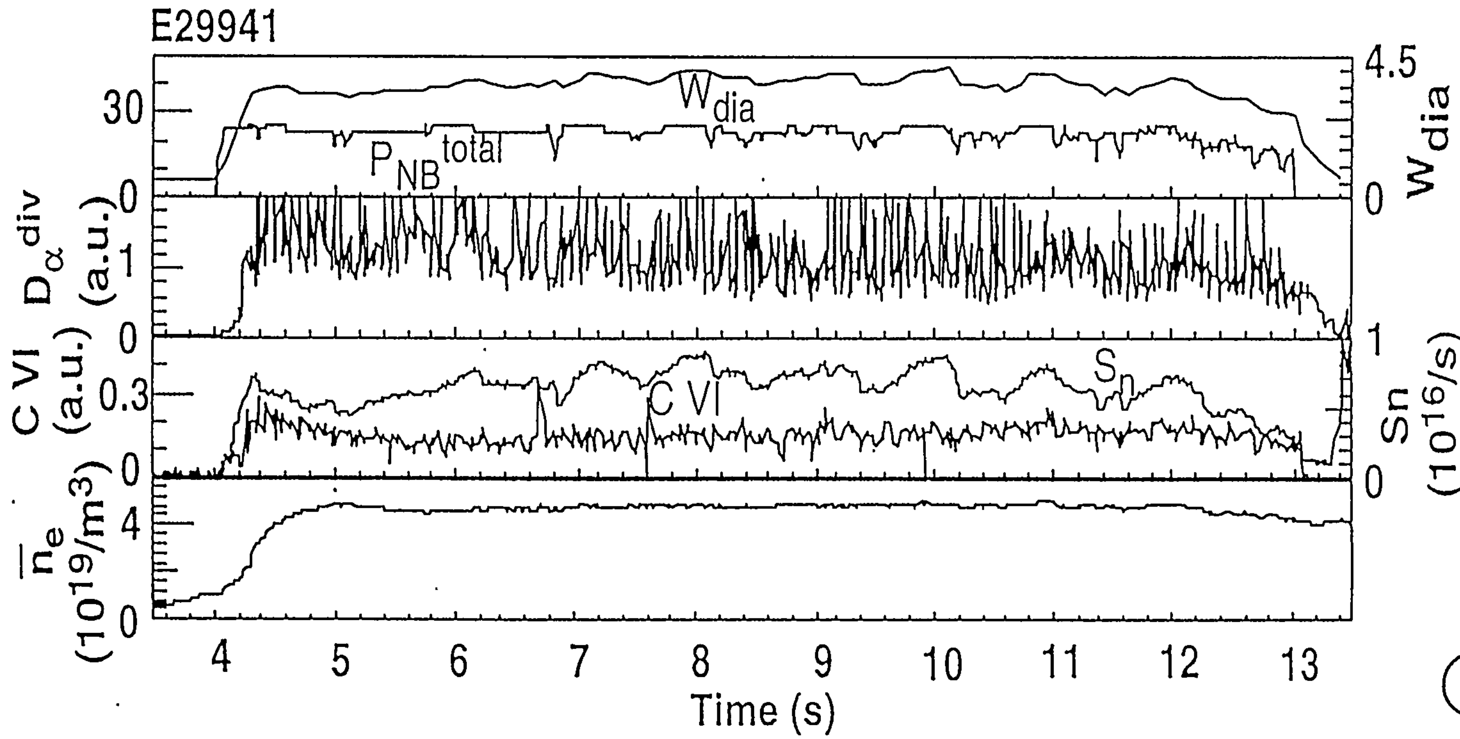

JAERI

Helium exhaust

○Helium beam injection into ELMy H-mode.

○1.4MA／3.5T

Helium exhaust was demonstrated with divertor pump (argon frost cryopumps for He exhaust).

$\tau_{He}^{*} / \tau_E = 4$

(In ITER ELMy H-mode, < 8~15)

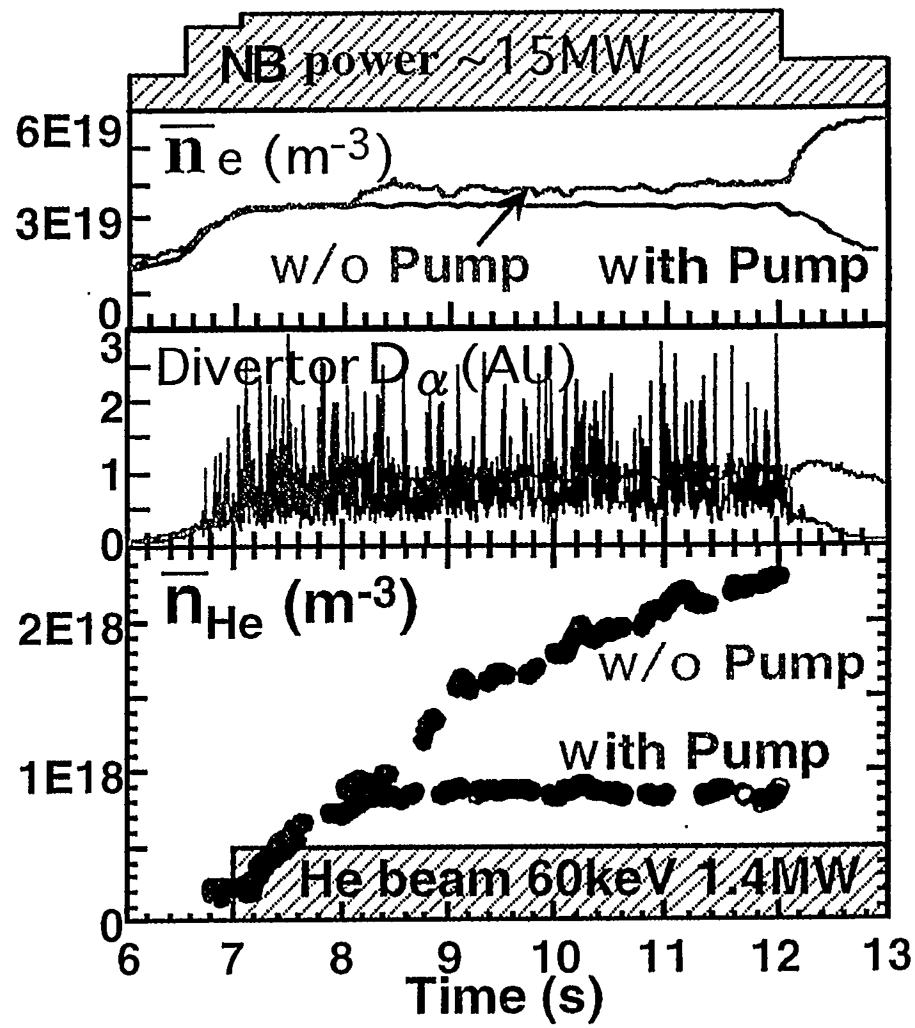

JAERI

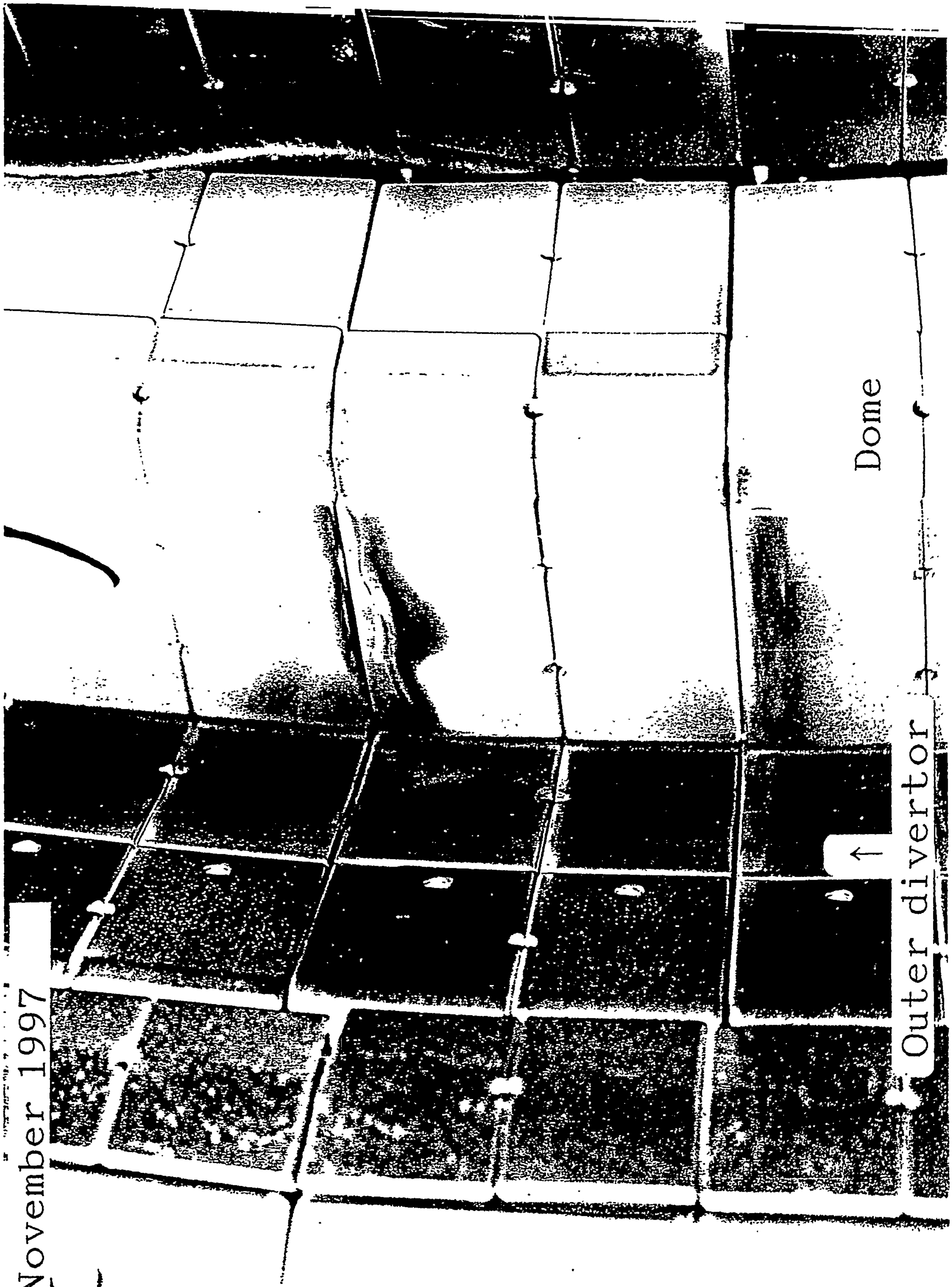
November 1997
Dome
Outer divertor

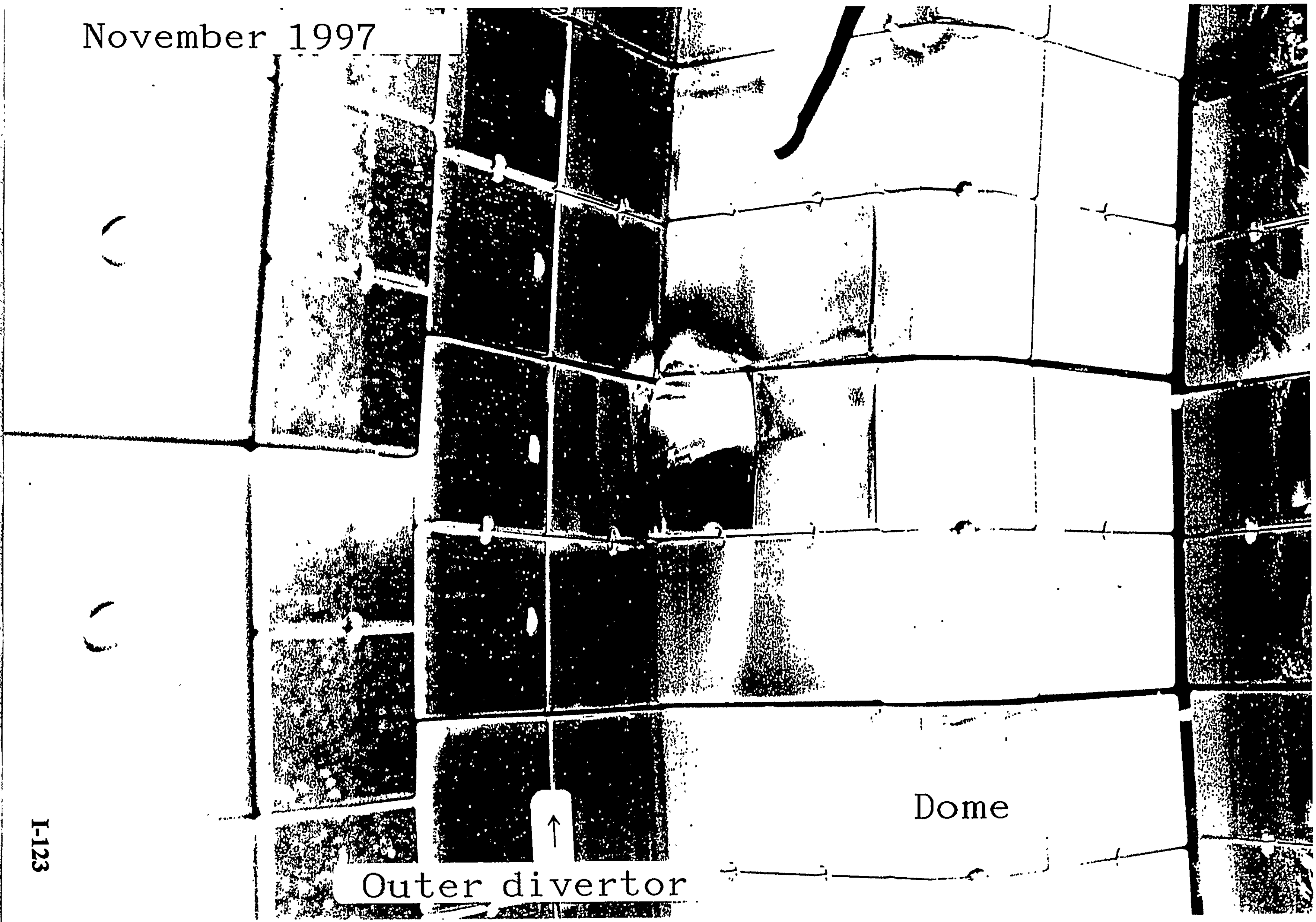
November 1997
Dome
Outer divertor

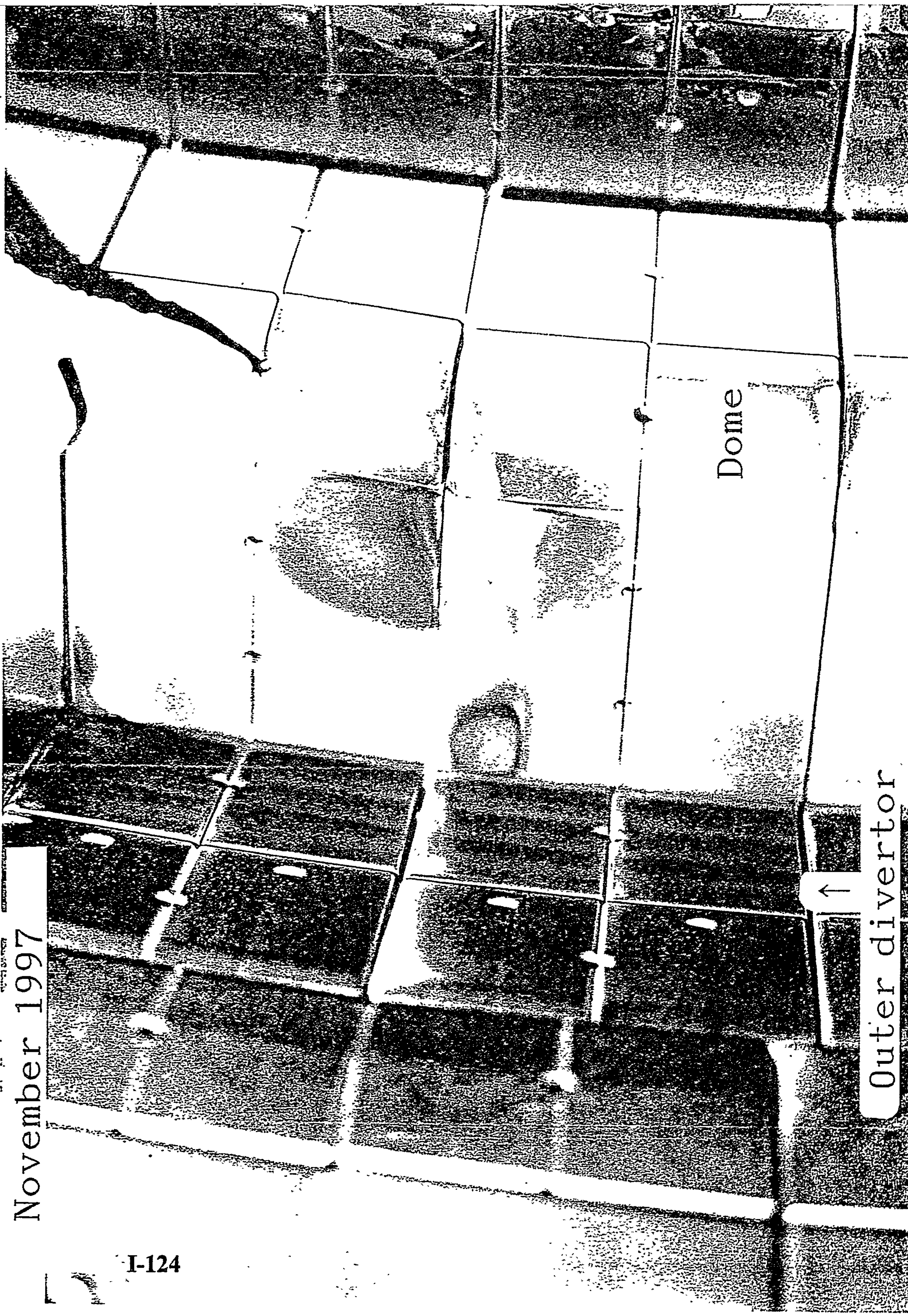
November 1997
Dome
Outer divertor
↑

Summary

○ JT-60U divertor was modified to W-shaped divertor

CFC tiles were used for divertor target tile.

Operations with intervals of 20 minutes are possible.

Insulated structure was adopted for gas seal.

○ Halo current   Ih/Ip = 0.05~0.25 , TPF = 1.4~3.6 , Ih/Ip x TPF < 0.52

○ Helium exhaust was successfully demonstrated with divertor pump.

○ Steady-state ELMy H-mode for 9s was observed.

○ Dome tile severely eroded.

Two tiles were broken due to thermal shock.

Thick deposition layer was observed on the inner divertor tiles

JAERI

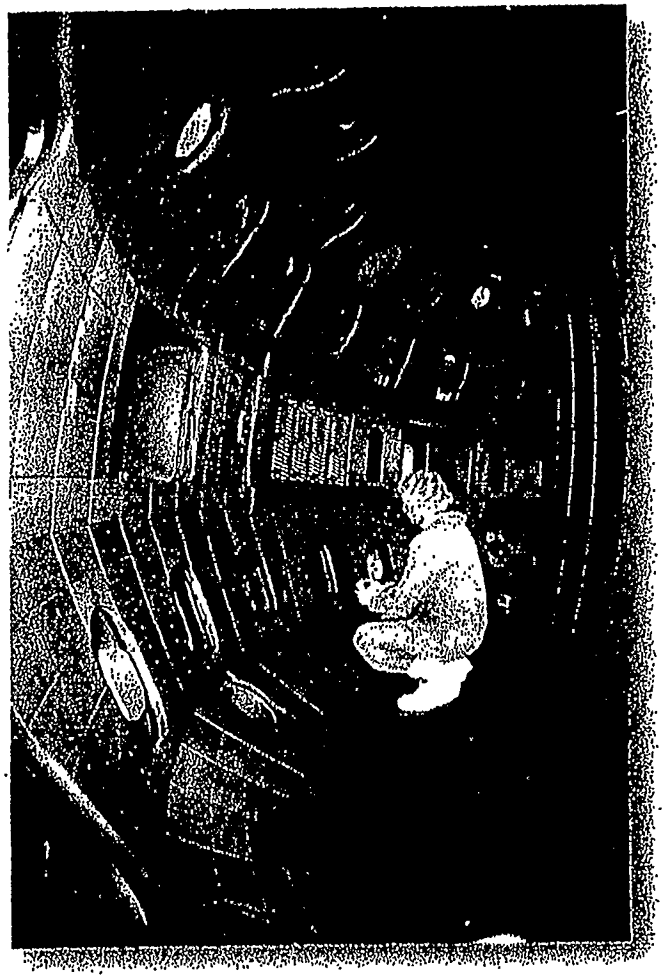

(6)

E-126

PROGRESS IN DIII-D

by

Clement Wong

Presented at

U.S./Japan Workshop on High Heat Flux Components and Plasma Surface Interactions for Next Generation Fusion Devices

San Francisco, California

December 8–11, 1997

Sandia National Laboratories ornl PPPL UCSD UCLA GENERAL ATOMICS

290-97

DIII–D IS LINKED TO THE INTERNATIONALLY INTEGRATED ITER PHYSICS R&D PROGRAM

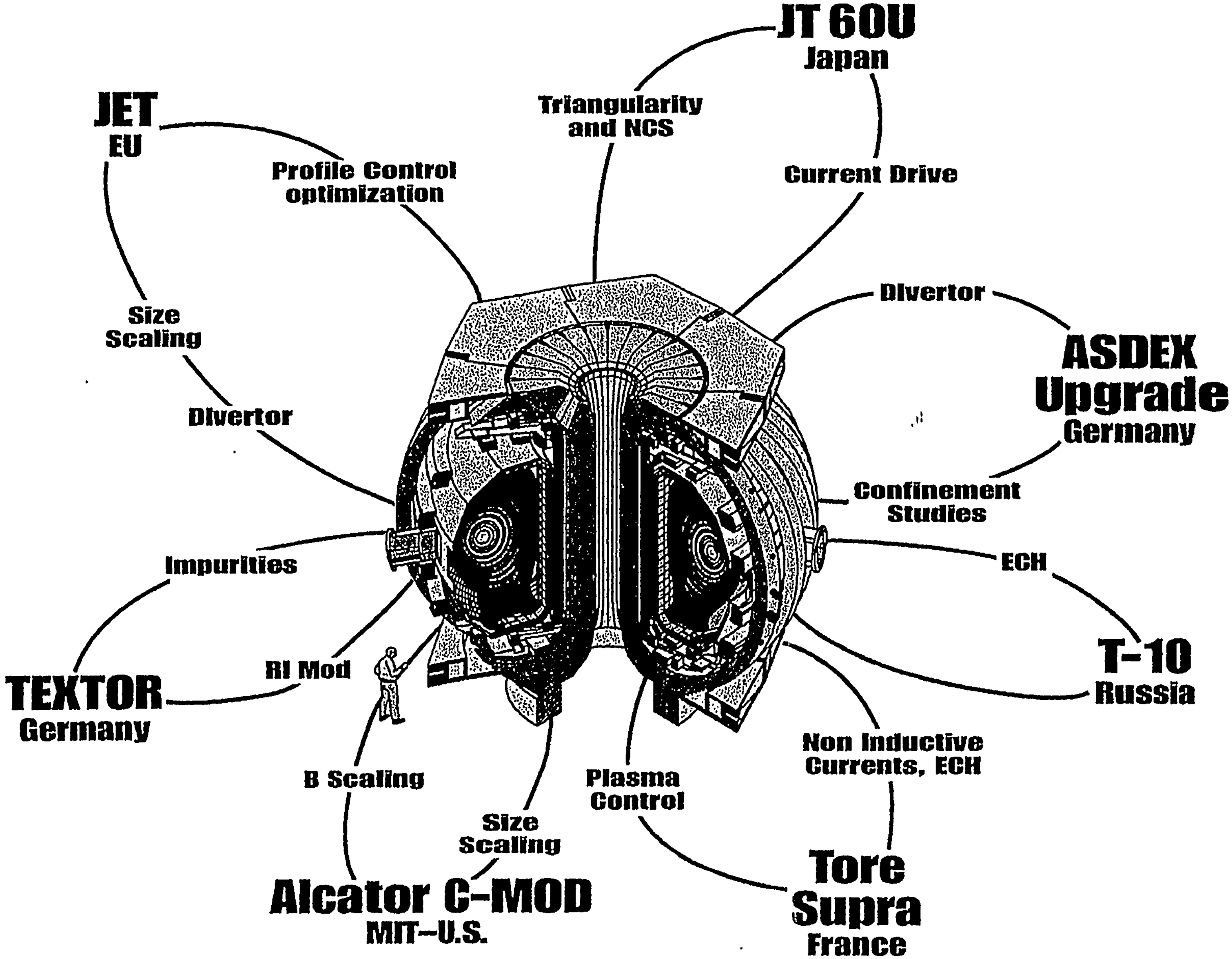

258–97

GENERAL ATOMICS

DIII–D TOKAMAK CAPABILITIES

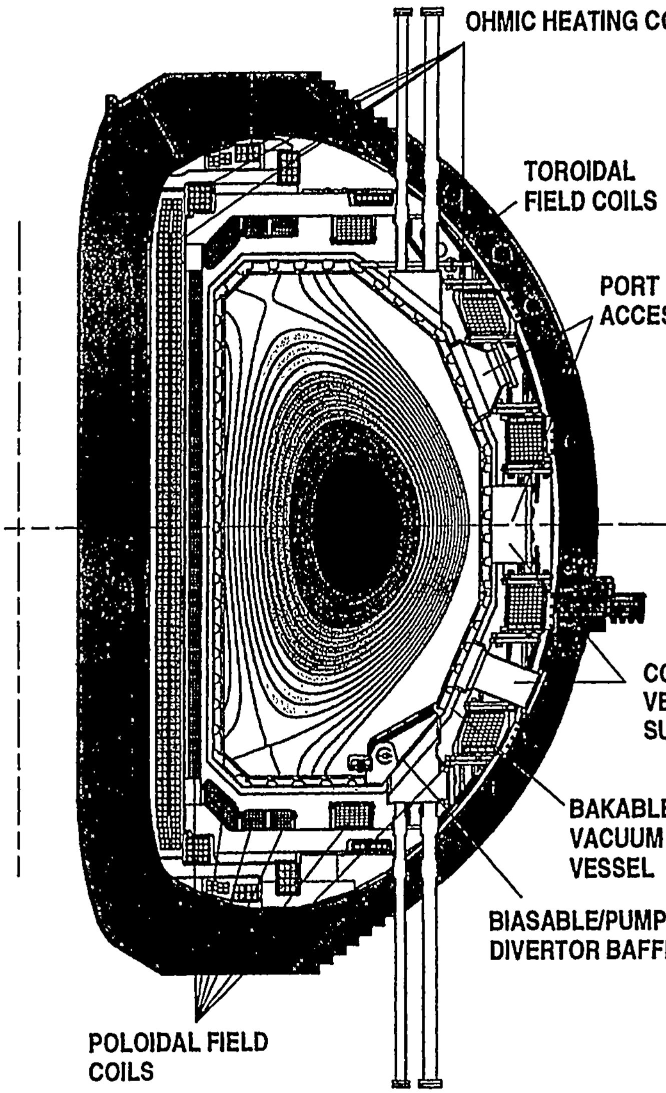

	PRESENT	PROPOSED
Major radius	1.67 m	
Minor radius	0.67 m	
Maximum toroidal field	2.2 T	
Available OH flux	5.0 V–s	7.5 V–s
Maximum plasma current	3.0 MA	3.5 MA
Neutral beam power (80 keV)	20 MW	
ECH power (110 GHz)	2 MW	10 MW
ICH power (30–120 MHz)	6 MW	
Current flattop (divertor at 2 MA)	5 s	10 s

GENERAL ATOMICS

232-97

OVER FIFTY DIAGNOSTICS PROBE DIII–D PLASMAS

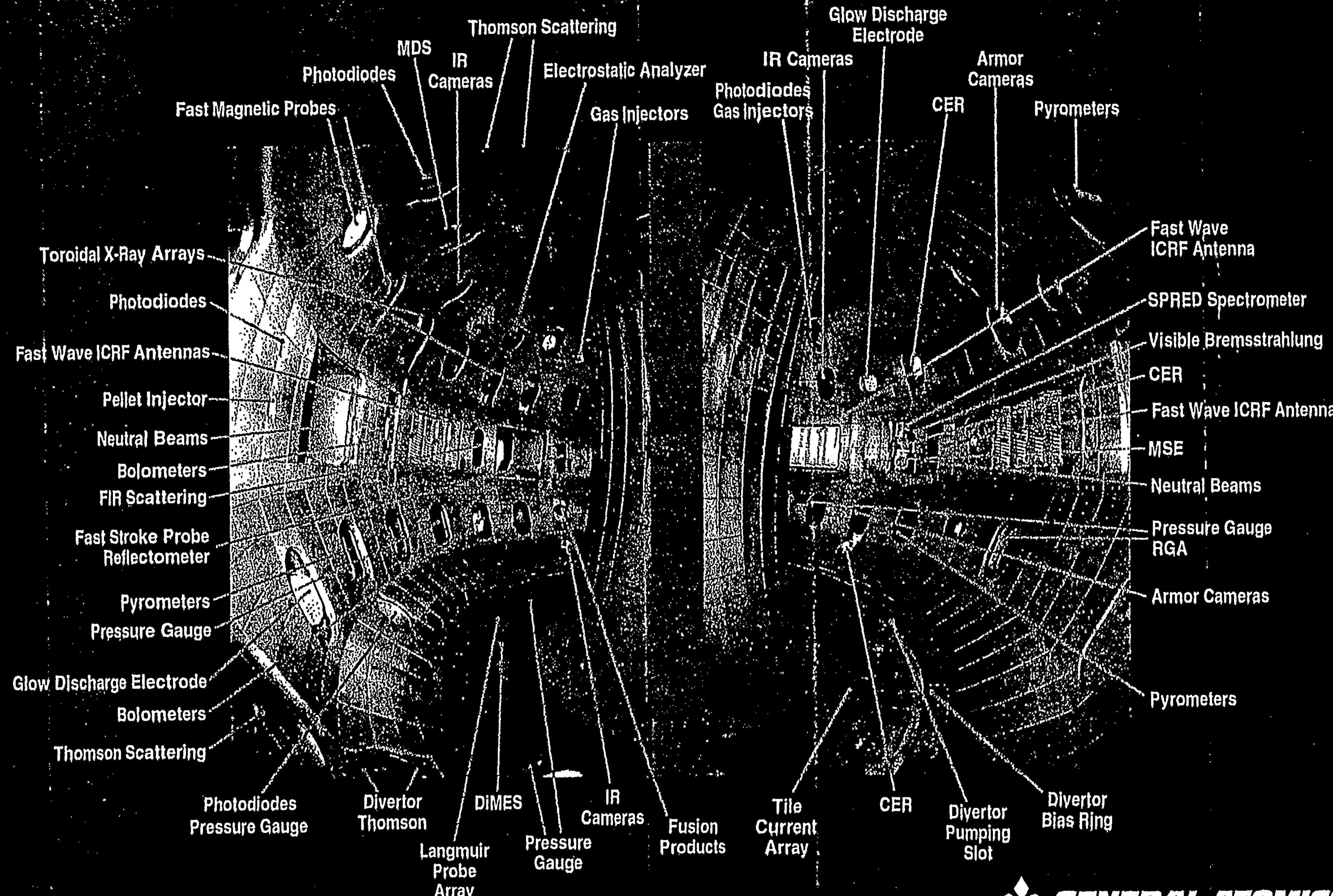

GENERAL ATOMICS

HIGHLIGHTS OF 1997 DIII–D EXPERIMENTS

- Transport
  - Developed H–mode edge pedestal scaling
  - Triggered core transport barrier expansion and contraction
- MHD stability and descriptions
  - Demonstrated disruption halo current dependence on vertical instability growth rate and mitigation with killer pellet injection
  - Increased neoclassical tearing mode beta limit with $q(r)$ and δ
  - Studied wall stabilization and resistive wall modes
- Divertor and boundary
  - Developed understanding of parallel energy transport and dissipation (convection and recombination)
  - Achieved density control with pumped closed divertor
- Wave-particle
  - Utilizing steerable ECH to test transport theories
  - Demonstrated on-axis current drive

258–97

GENERAL ATOMICS

H-mode Pedestal and Plasma Performance

- In stiff ITG-mode turbulent transport models, the core transport coefficients depend strongly on the plasma edge parameters which enter as a boundary condition.
  - o ITER H and Q increase with T_i^{PED}
    (Results at right from IFS/PPPL model, taken from "Memorandum on Confinement Projections," FESAC ITER Confinement Reviews, M.Kotschenreuther and W. Dorland.)

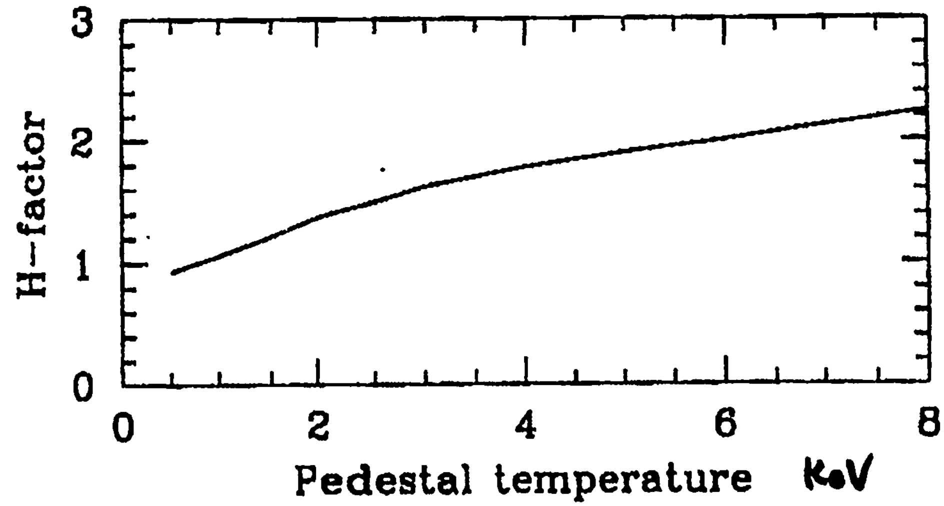

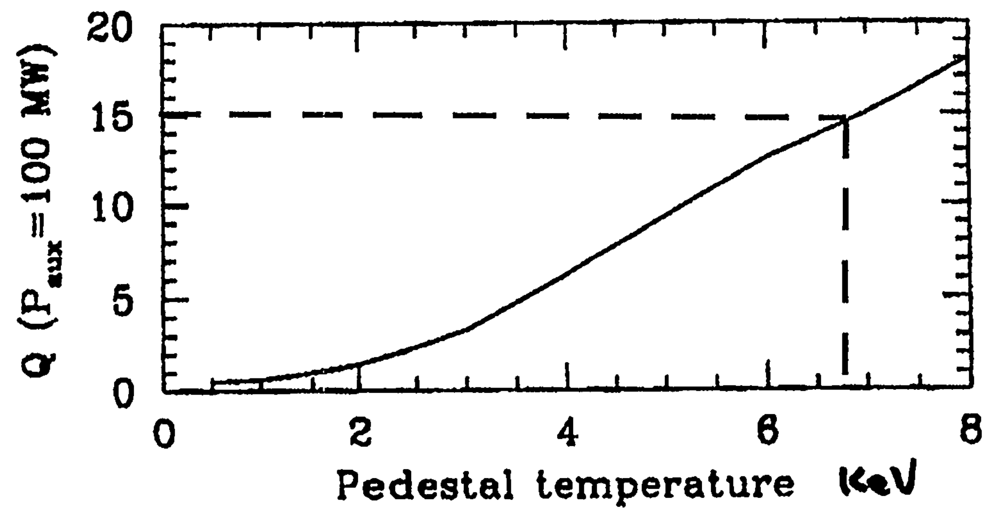

T. Osborne, HMWS, 1997

GENERAL ATOMICS

DIII–D H–MODE EDGE PEDESTAL STUDIES

- 6,328 pedestal database created
- Suggests 5 keV ITER pedestal ⇒ ignition

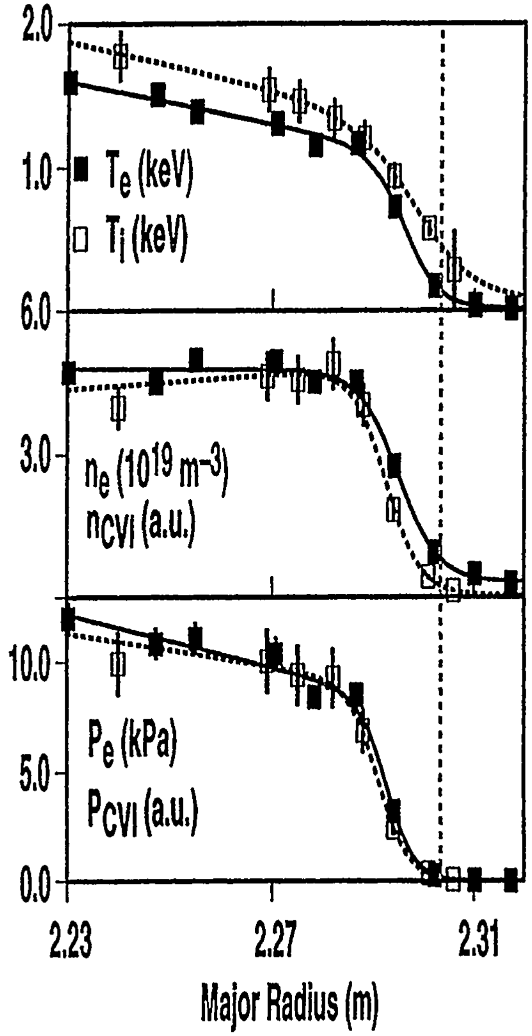

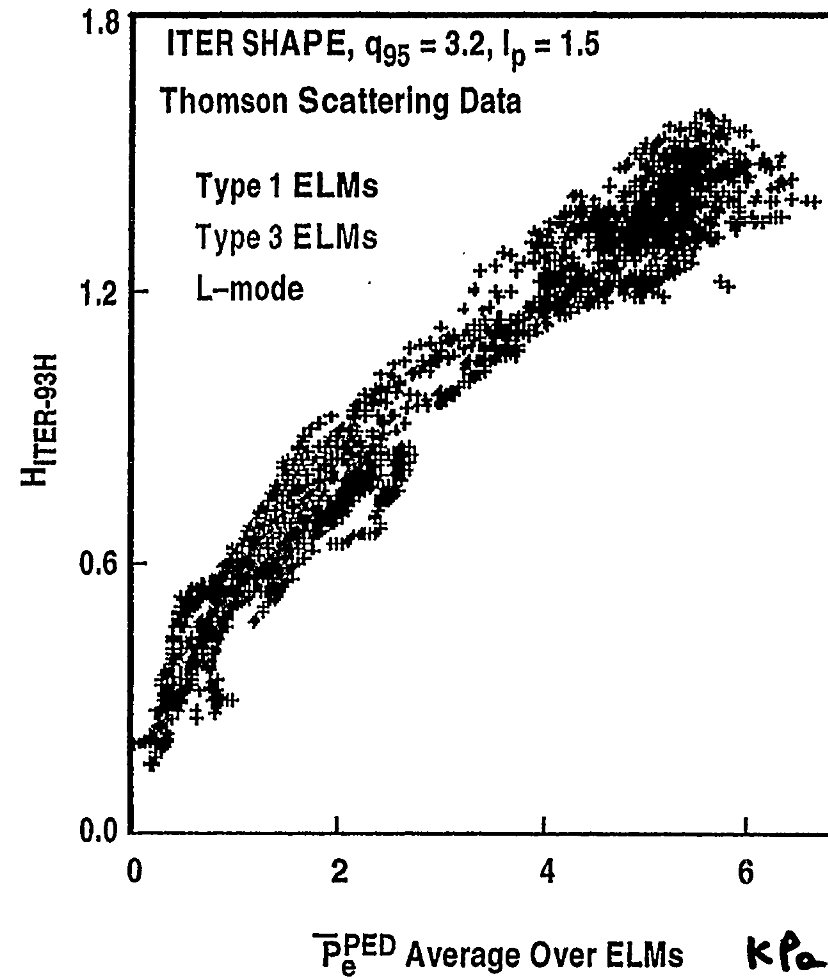

258–97

GENERAL ATOMICS

Halo Current and Toroidal Peaking Factor Reduced by Neon and Argon "Killer" Pellet Injection into VDE Disruption

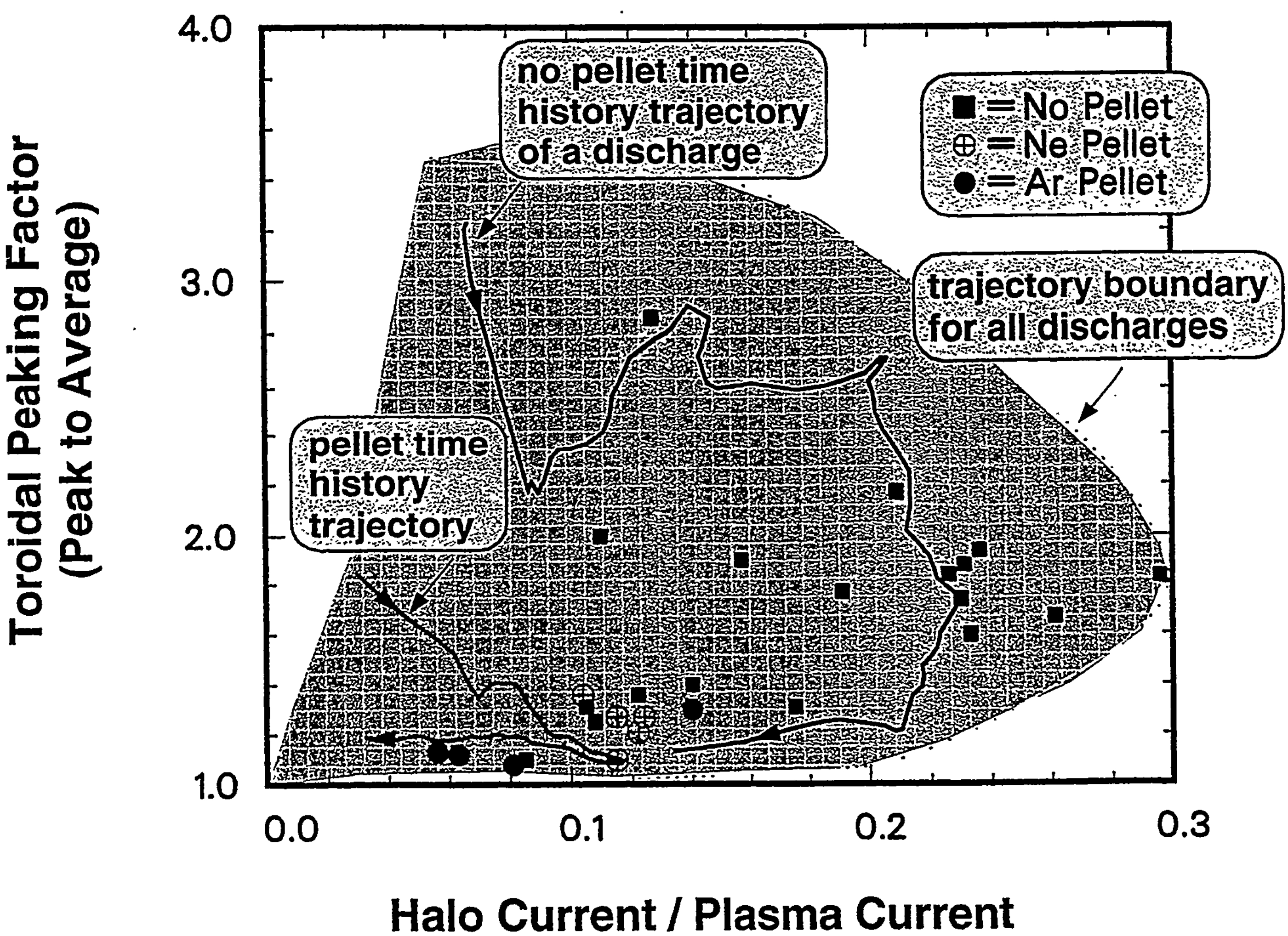

Pure neon pellets reduce the vessel loading by a factor of 4-5

Pure argon pellets reduce the vessel loading by a factor of 8-10

GENERAL ATOMICS

tee-dws97-7 1996 EVANS APS 7F10

DIII-D Divertors

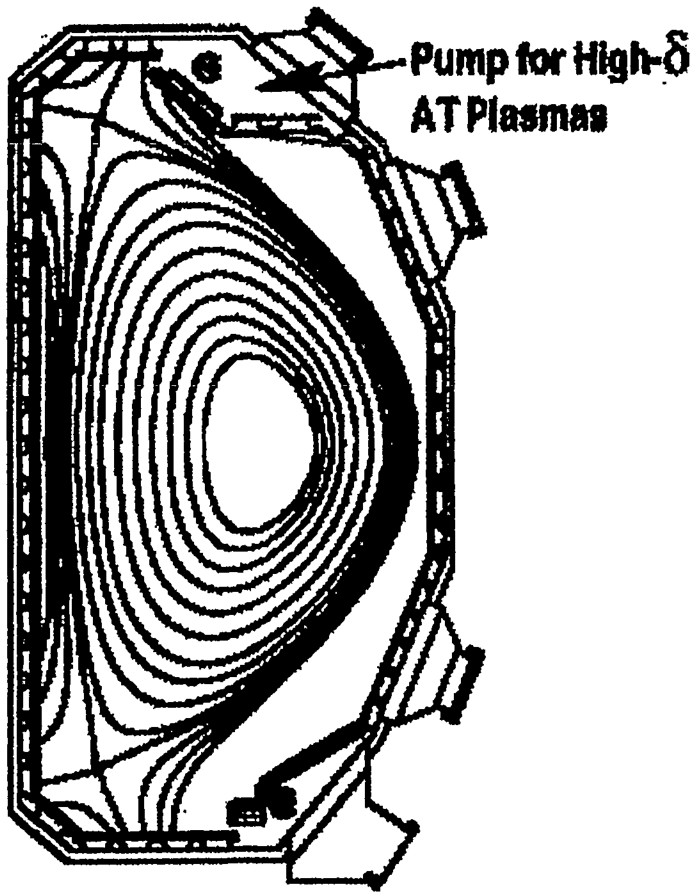

Open Low-δ Divertor

- Upper Divertor pump high-δ plasmas
- Lower Divertor pump low -δ plasmas
- Pumping speed ~40,000 l/s

GENERAL ATOMICS

DIII–D DIVERTOR PLAN FOR PARTICLE CONTROL

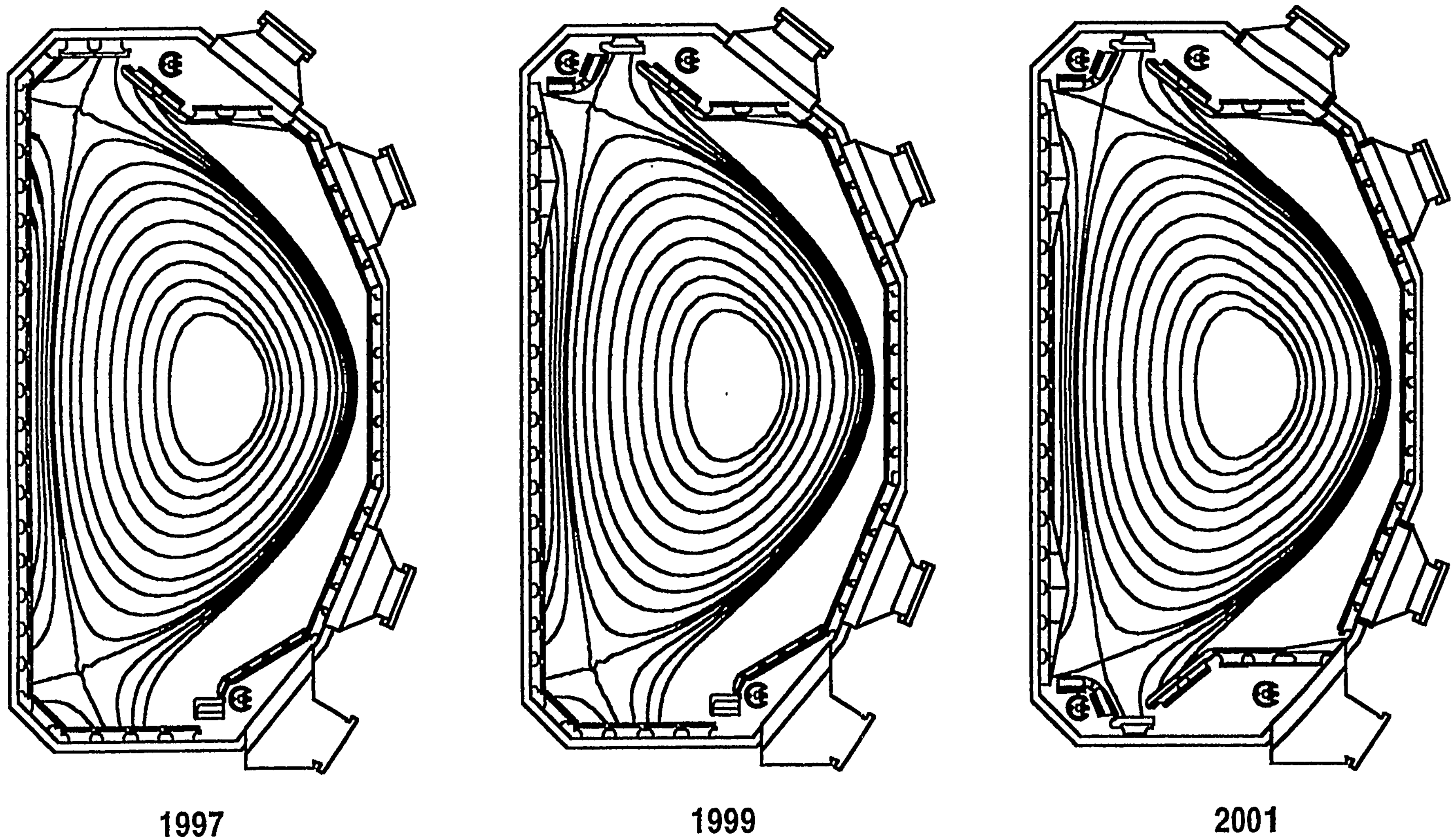

258–97

GENERAL ATOMICS

Results from the New High-δ Upper Pump and Baffle on DIII–D

Presented for the AT+D Campaign on DIII–D *by S. L. Allen*

Lawrence Livermore National Laboratory

- n_e control achieved in high-δ Plasmas
  - $\Rightarrow$ $n_e / I_p \sim 2.5$ (ELMing H-mode), similar to low-δ
  - $\Rightarrow$ Impurity density similar in low-δ, high-δ, and pumped
- Open vs. Closed divertor comparisons have shown:
  - $\Rightarrow$ Reduction in core ionization and midplane Hα
  - $\Rightarrow$ Exp. results are similar to UEDGE+DEGAS predictions
  - $\Rightarrow$ τ_e similar
- Experiments with high-δ DN plasmas in progress
  - $\Rightarrow$ Design shape obtained, similar VH-mode, Jan. 1998 pumping

I-133

ornl UCLA Fusion Energy Research Program UCSD Sandia National Laboratories PPPL PRINCETON PLASMA PHYSICS LABORATORY Dickinson GENERAL ATOMICS

Density Control in a High-δ Plasma

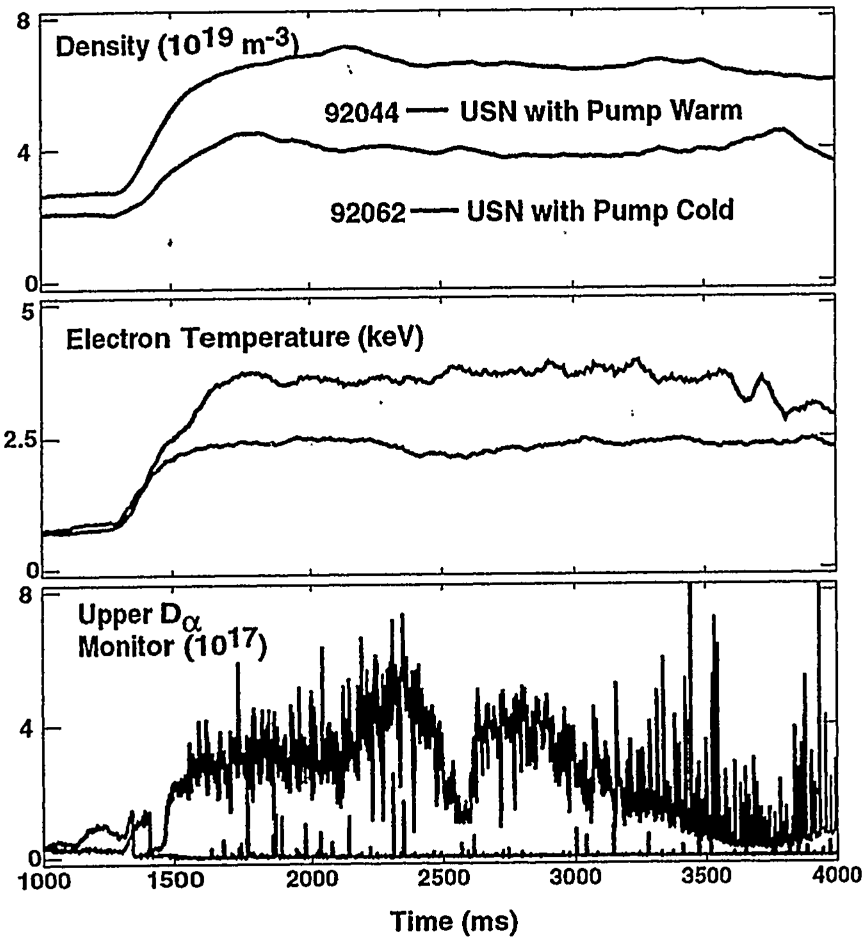

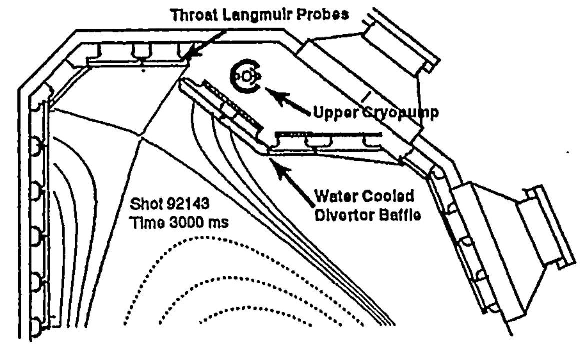

Shot	92143
Time	3000
Elongation	1.832
Upper δ	0.677
Lower δ	0.377
q95	4.585
Wdia(MJ)	1.452
Ipmeas(MA)	1.489
BT(0)(T)	-2.064

Low T_e, High n_e in Radiative Divertor

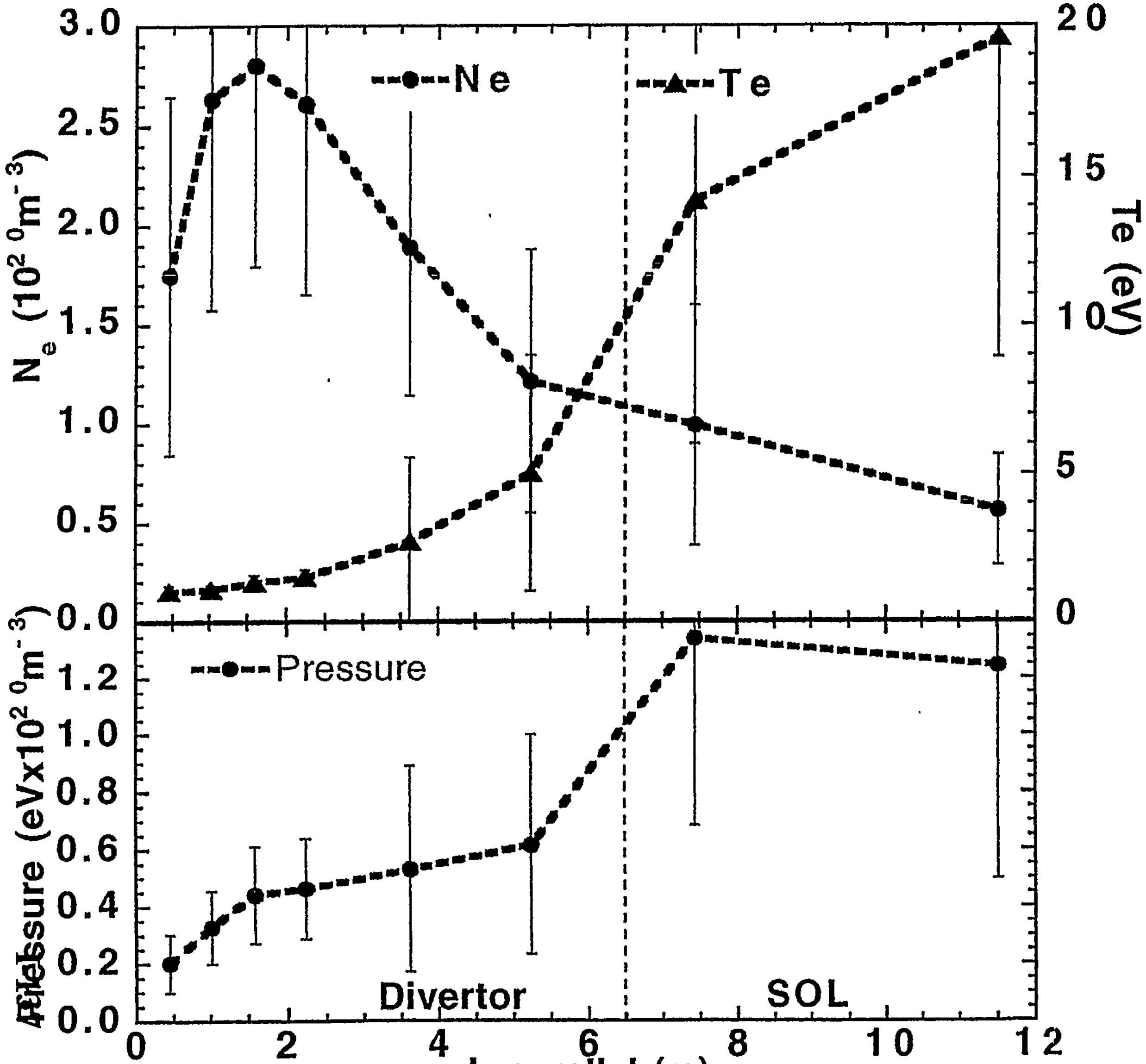

Shot 87506-7

- Very low T_e, 1-3 eV through much of divertor.
- Very high density, ~$3x10^{20}m^{-3}$.
- Large pressure drop near X-point, gradual decline to divertor plate.

Summary of Results

I-138

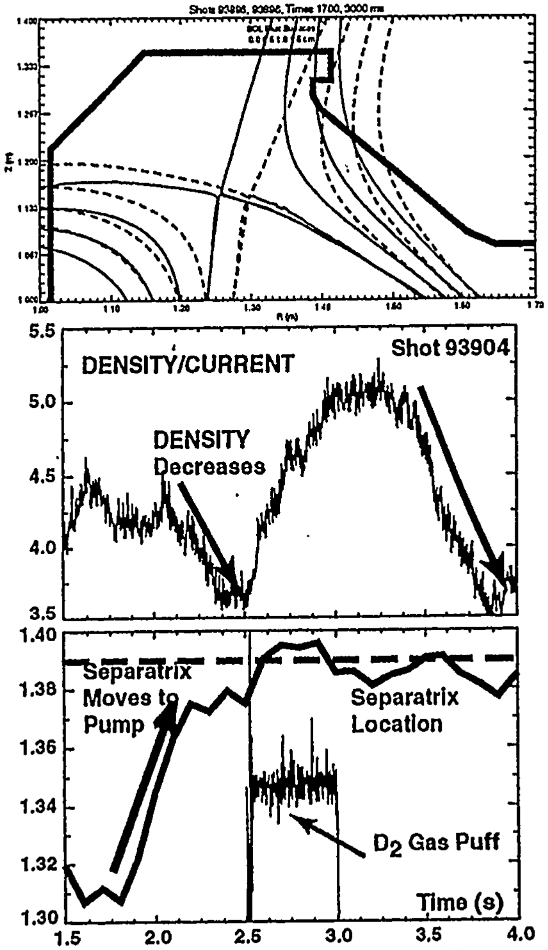

High - δ Plasma with pumping

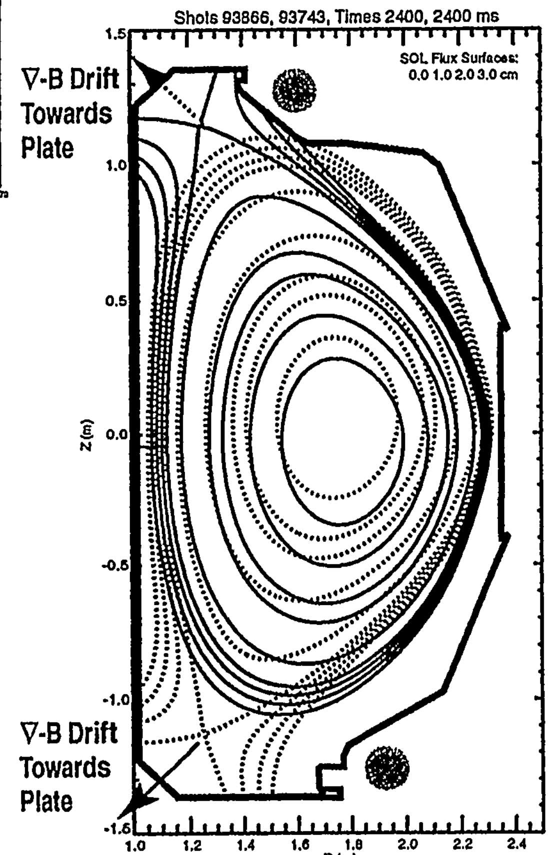

Open/Closed Comparison

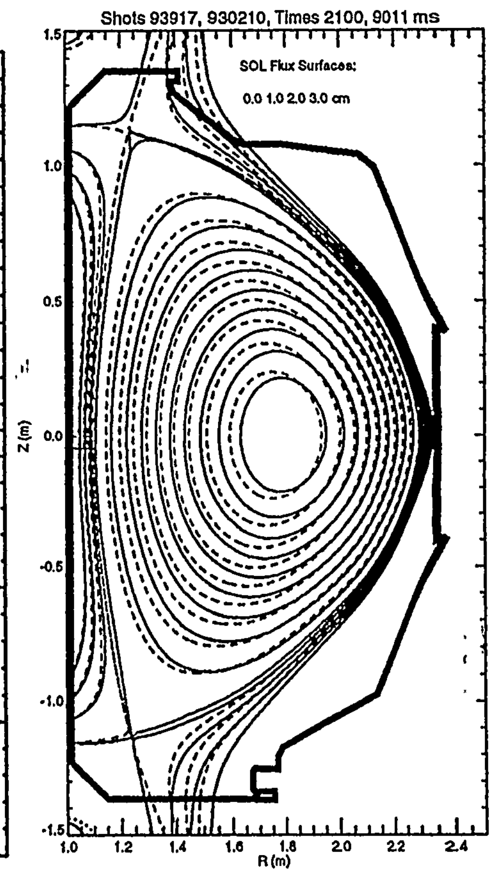

Double Null

Current Focus on Dissipation of Energy and Particle Flux

- <u>Goal</u>: Dissipate as much Energy through Radiation and Particle Flux through Recombination as Possible.

- Parallel Energy Transport given by:

$$q_{\|} = \underbrace{\kappa T_e^{5/2} \frac{dT_e}{ds}}_{\text{Classical Electron Thermal Conduction}} + \underbrace{n v_{\|} \left[\frac{5}{2}(T_e + T_i) + \frac{1}{2} m v_{\|}^2 + I_o \right]}_{\text{Plasma Convection}}$$

DIII-D Achieves Heat Flux Reduction without Highly Localized Divertor Radiation

I-1140

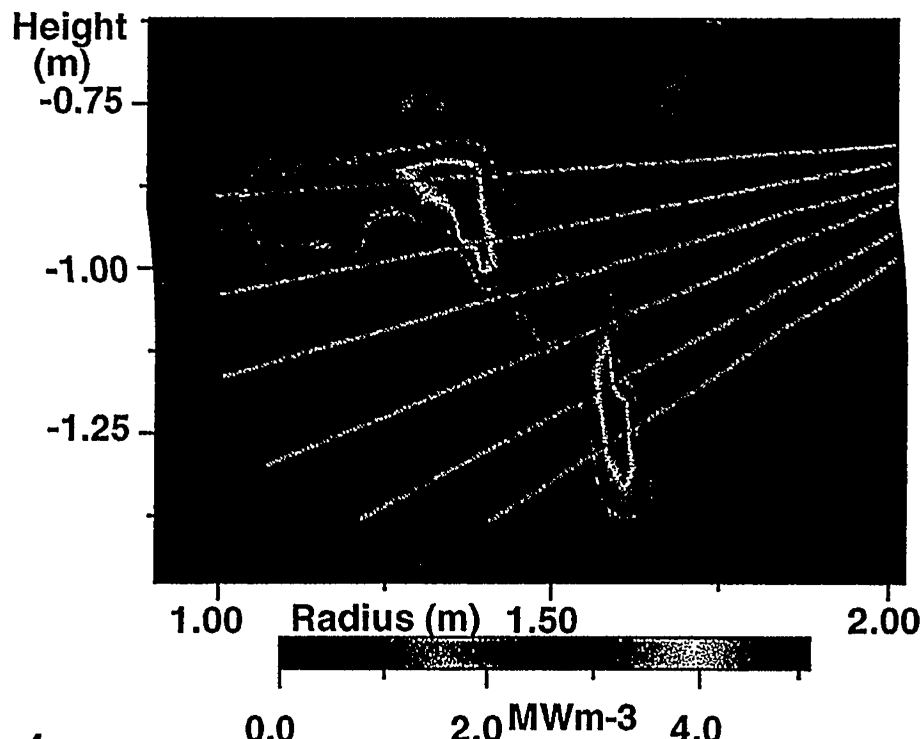

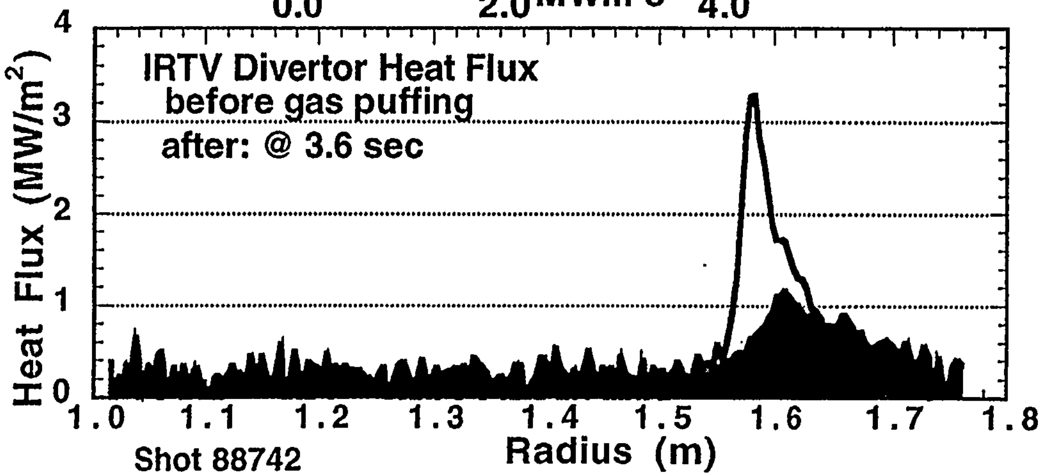

- 6 bolometer chords from X-point to divertor target; less than 2:1 variation in divertor radiation.
- Factor of 3 peak heat flux reduction.
- Carbon the dominant impurity.

A. Leonard APS 11/18/97

GENERAL ATOMICS

Carbon and Deuterium Radiation Spread through Divertor

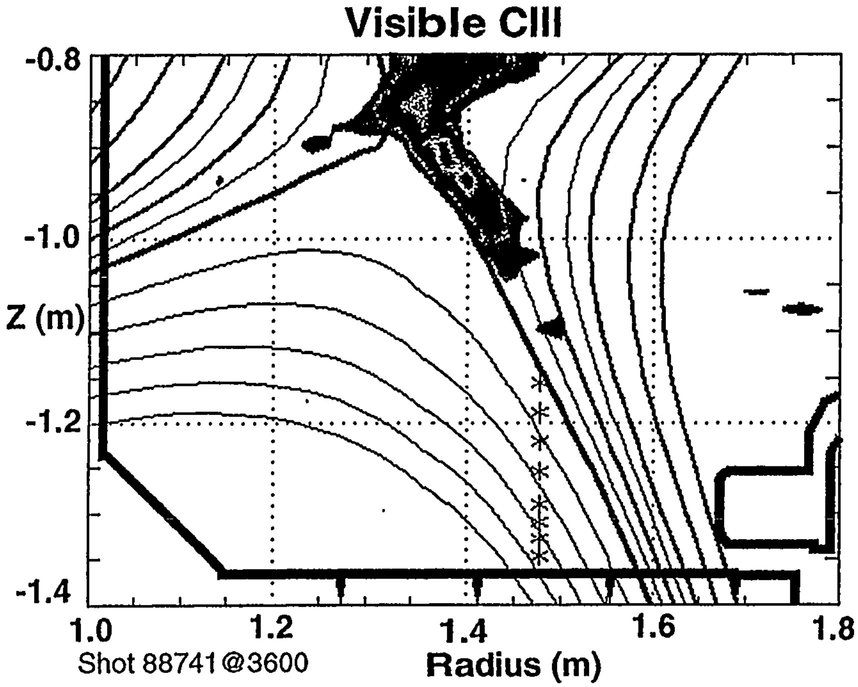

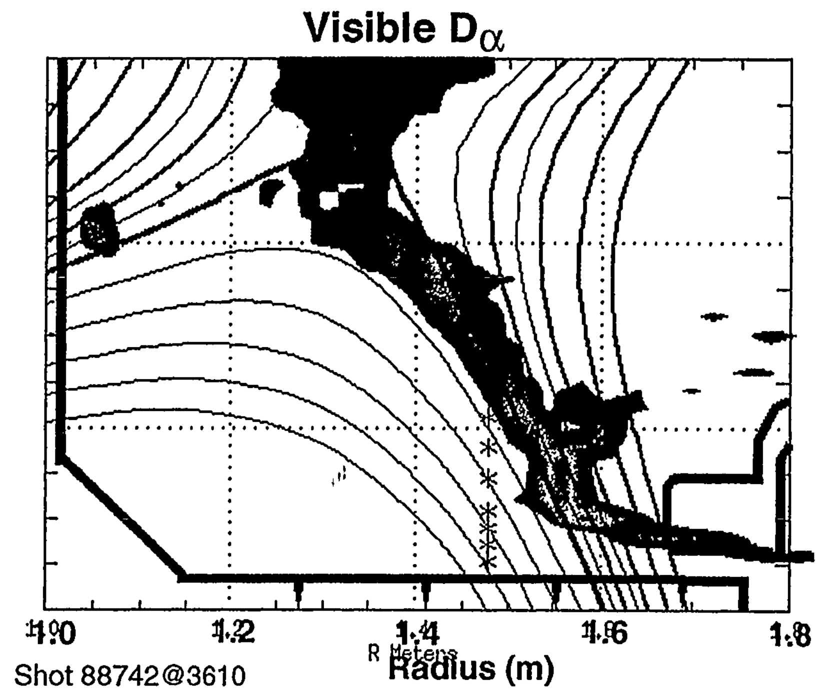

- VUV spectroscopy indicates CIII peaks where T_e~10 ev.
- Both Carbon and Deuterium radiation spread over larger region than conduction model would indicate.

I-141

T_e in Radiative Divertor cannot Support Observed Energy Flux through Conduction

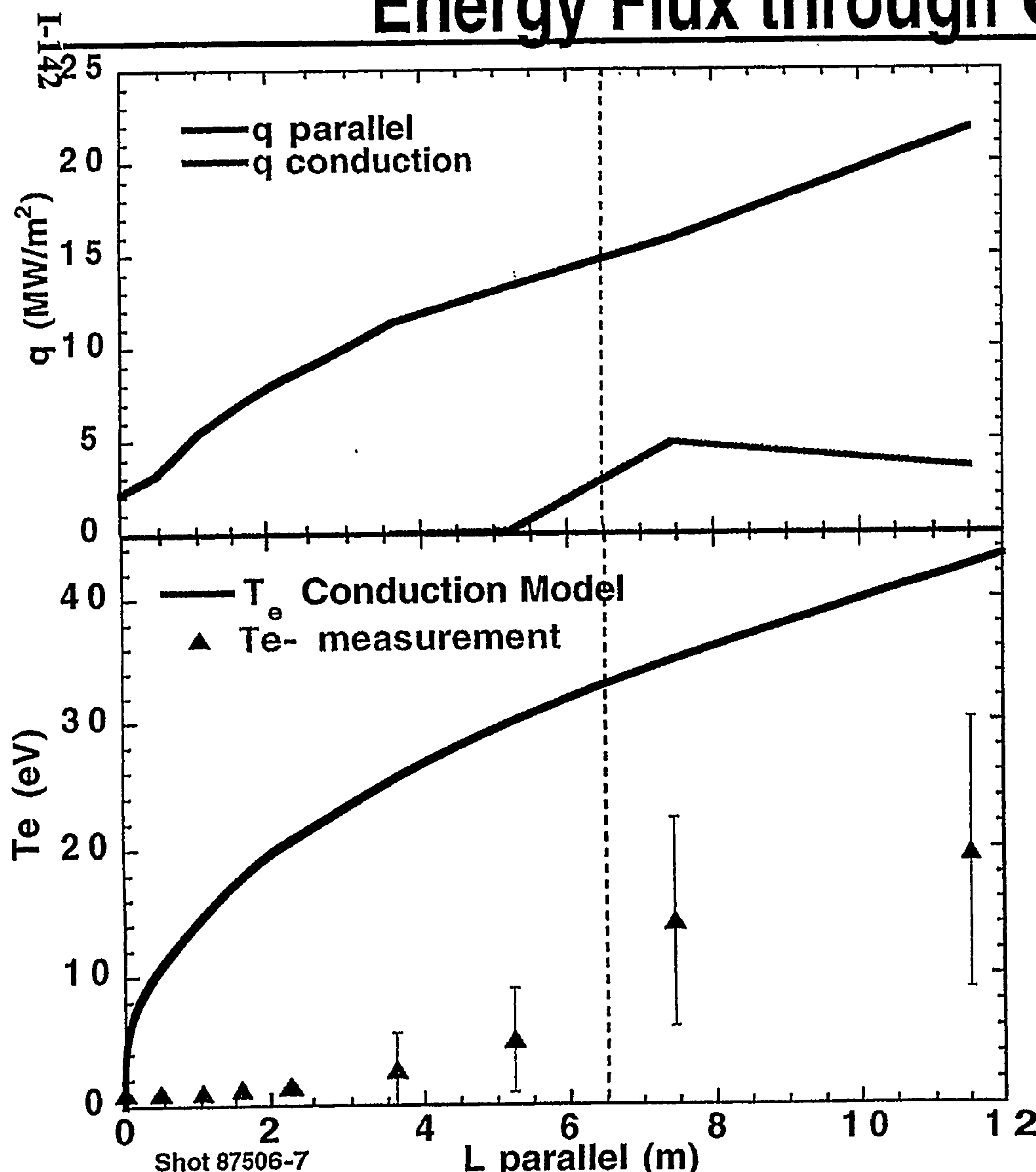

- About 90% of power flowing into divertor is radiated.
- Measured T_e can support very little energy flux.
- Region of 8-12 eV, ΔL~1-2 m, larger than implied by conduction. Volume consistent with total Carbon Radiation.
- Large volume of cold plasma, T_e< 2eV.

A. Leonard APS 11/18/97

GENERAL ATOMICS

Conclusions

- Power balance coupled with n_e and T_e profile measurements allow study of parallel energy transport processes in the divertor and SOL.
- Plasma flow can greatly expand the plasma volume at high density and low temperature for efficient low Z impurity radiation and plasma recombination.
- It is possible to exceed limits on radiation and recombination predicted by conductive transport models.
- New 2D diagnostics are begining to measure the plasma flow and recombination profiles in the divertor.

I-143

I-144

Divertor Detachment in DIII-D Helium Plasmas

D.N. Hill, *Lawrence Livermore National Laboratory*

and the DIII-D Divertor Group

- Motivation
  - Partially Detached Divertor Operation (PDD) is the reference scenario for power handling in ITER
  - All divertor experiments show peak heat flux reduction with gas puffing.
  - Scaling to ITER or other future high power density tokamaks requires understanding the underlying physics

Helium Operation Helps Identify Relevant Atomic Processes Associated with Divertor Detachment

Likely steps to detachment	How helium should be different
1. Gas puffing drives radiation ⇑	No chemical sputtering: carbon radiation ⇓
2. Increased radiation drives $T_{e,div}$ ⇓	Higher density to produce same radiation
3. Ionization moves upstream	Longer λ_{mfp} yields detachment at higher T_e
4. Convection carries remaining energy in divertor	
5. High n_e, low T_e allow volume recombination	No molecules
6. Recombination reduces plate ion current	Less recombination ⇒ less drop in I_{plate}

I-145

GENERAL ATOMICS

DNH Nov 1997 APS

Heat Flux Profiles are Similar to PDD Plasmas in Deuterium

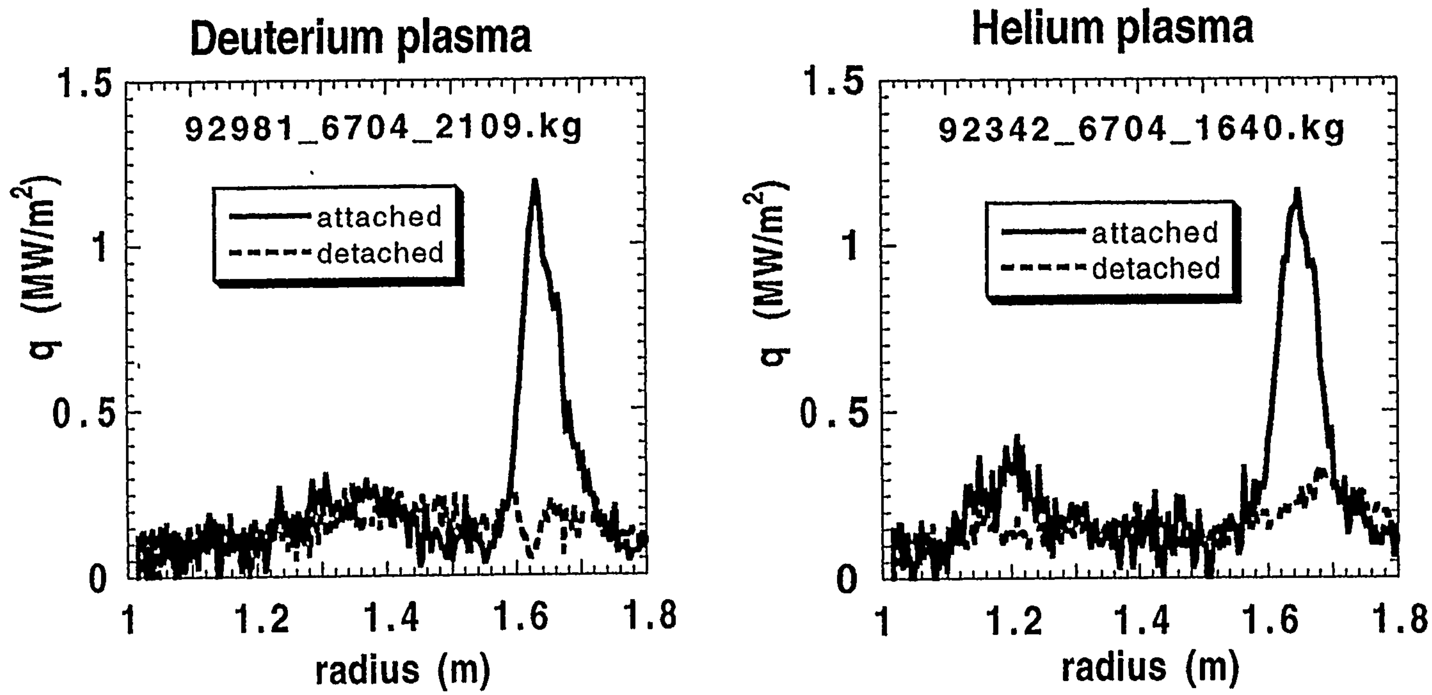

- Lower single-null, P_{beam}=2MW, H-mode in deuterium, L-mode in helium
- Peak heat flux reduced by a factor of four
- ELMs and radiation produce most of residual.

GENERAL ATOMICS

Radiation Profiles in Helium Show A Maximum Near X-point, as in Detached Deuterium Plasmas

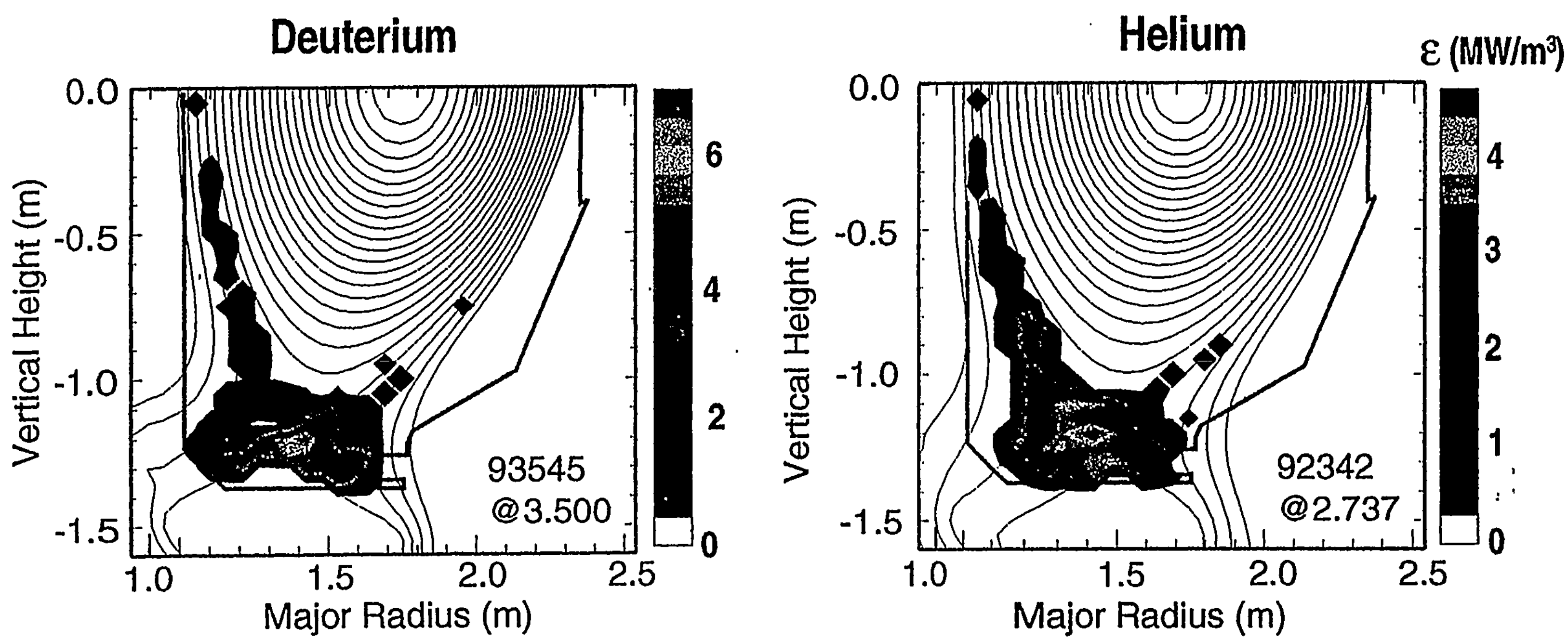

- Both plasmas at similar density, but D^+ plasma has 2x more input power.
- Both plasmas have emissivity peaked near x-point after detachment.
- Helium plasma has more distributed radiation.

I-147

I-148

CIII emission is reduced by a factor of at least 5 in helium detached plasmas.

- Distribution of C III is different in helium plasma.
- C III 465nm filter FWHM = 3nm may pick up He II emission at 468.6nm
  - Reduction in carbon emission is larger than infered from these images.

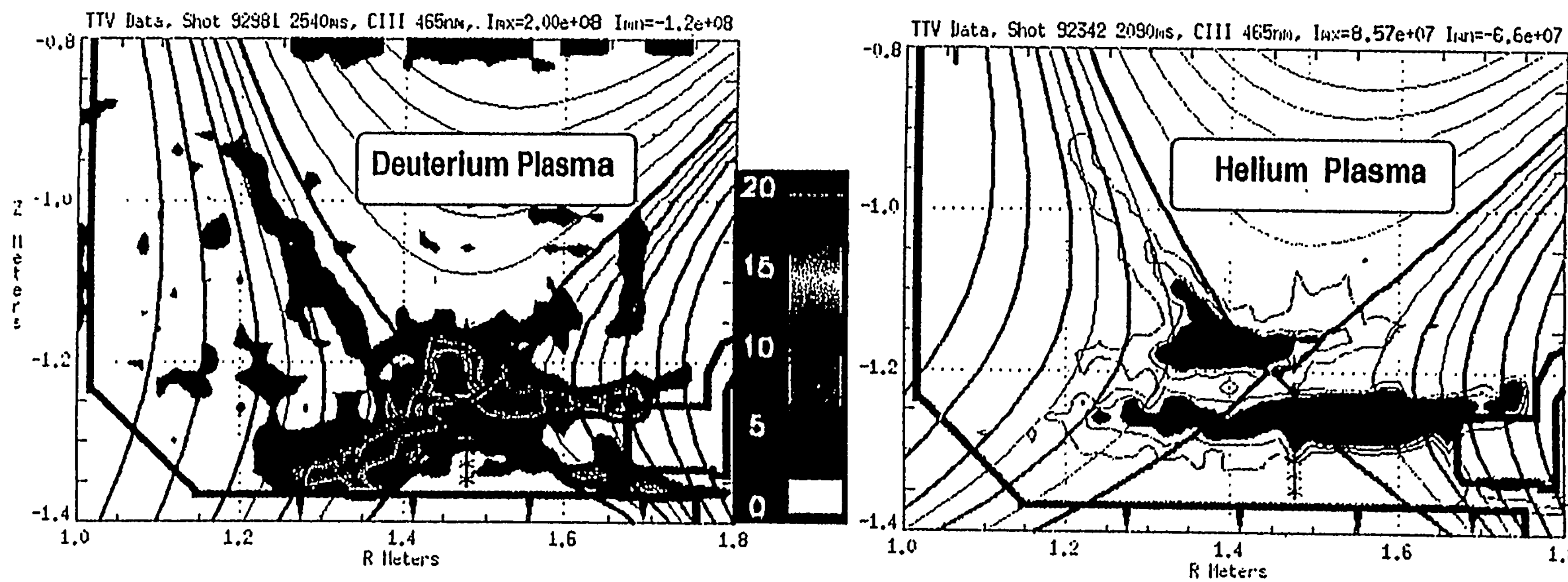

C III images reconstructed from a tangentially viewing filtered TV system.

Summary

- Helium operation lowers carbon concentration by a factor of four or more
  - core and divertor content both reduced, especially during helium puffing
  - suggestive of chemical sputtering effect, but may be due to different confinement times in the core or different screening effects
- A radiative divertor with significant heat flux reduction can be obtained in helium plasmas: helium replaces carbon as the main radiator
- The behavior of the divertor plasma is similar to that of deuterium plasmas
  - similar threshold density
  - similar radiation distribution
  - similar heat flux reduction and profiles, but no drop in ion flux
  - similar divertor density and temperature in the detached state.

I-149

PROGRESS IN DIII-D
KEY RESULTS PRESENTED

- H-mode edge pedestal determined and results suggested the ignition of ITER
- Killer pellet injection can reduce VDE disruption vessel loading by a factor 4-10
- n_e control achieved in the new high-δ upper pump and baffled divertor
- Radiative divertor experiments indicate the importance of plasma convection including the effects of recombination
- Comparison of D and He gas puffing shows helium can replace carbon as main radiator and chemical sputtering as the main source for carbon

SCIENTIFIC PROGRESS: DIII–D FUSION PERFORMANCE HAS DOUBLED EVERY TWO YEARS

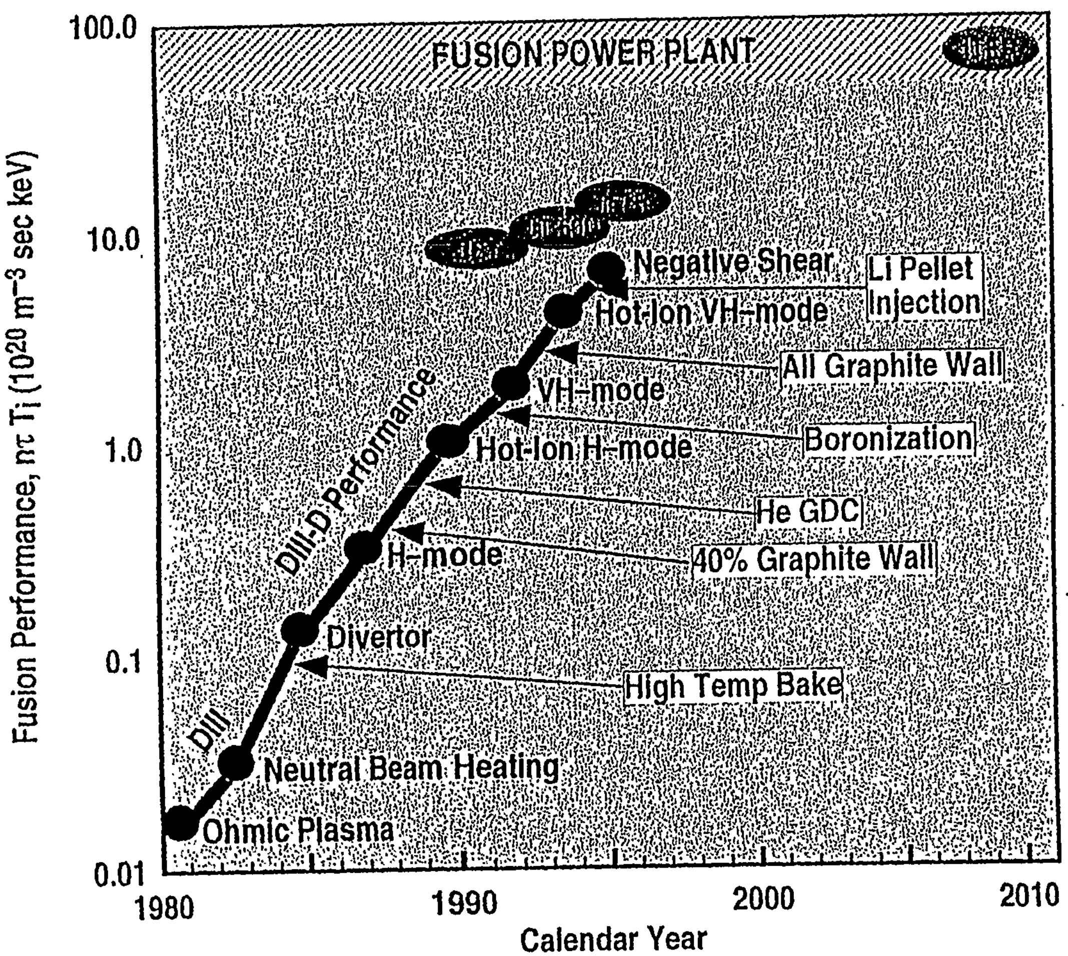

GENERAL ATOMICS

051-96

A NEW 5-YEAR DIII–D RESEARCH PLAN HAS BEEN FORMULATED

- July 9–11, 1997 National Tokamak Workshop

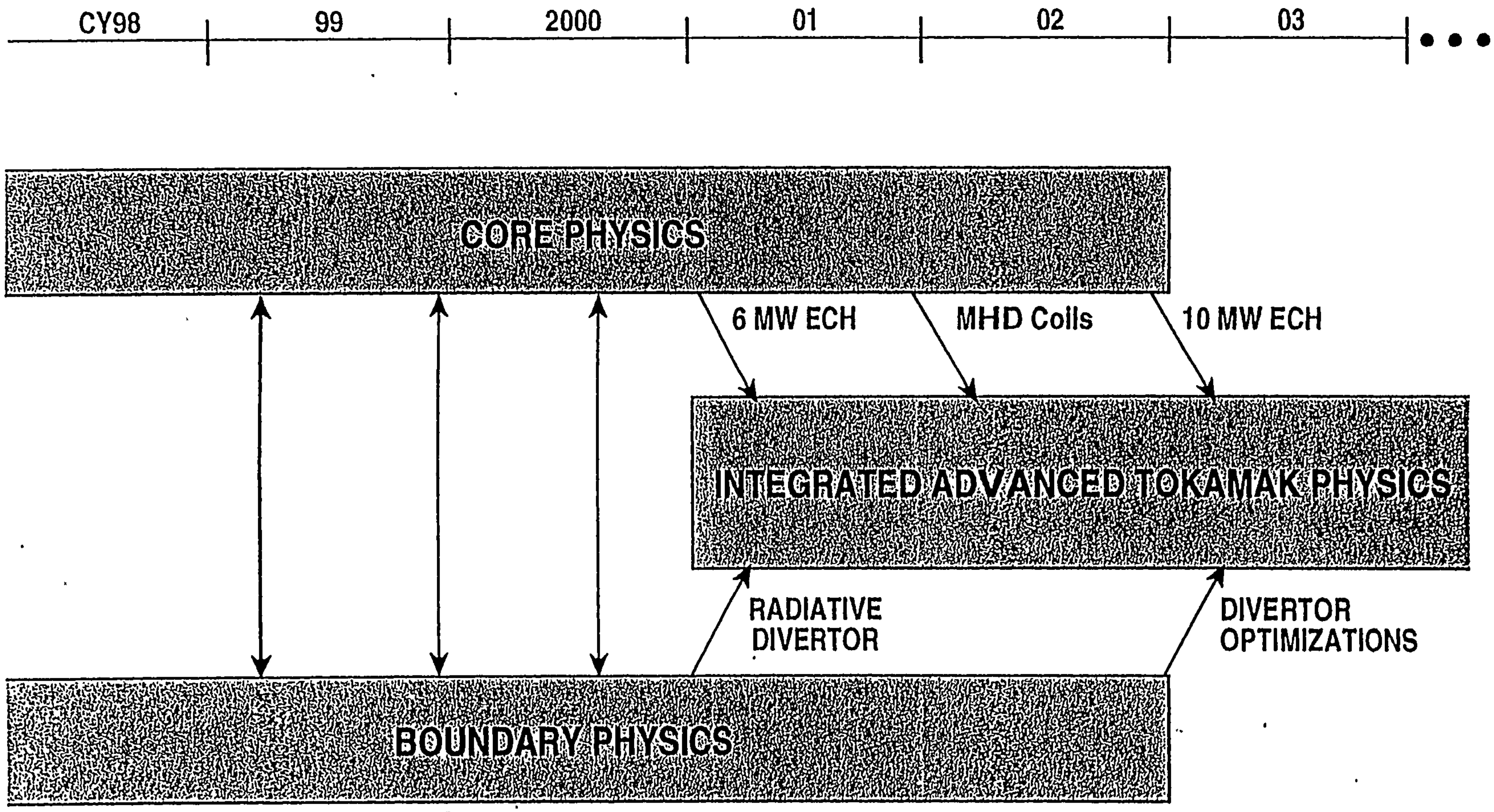

258–97

GENERAL ATOMICS

Session II: PFC Development for Near Term Devices

CIRSE
Nagoya University
Center for Integrated Research in Science and Engineering

On the Utilization of High Z Materials as Plasma Facing Component

T. Tanabe, CIRSE, Nagoya University
M. Akiba, JAERI
Y. Ueda, Osaka University
K. Ohya, Tokusima University
M. Wada, Doshisha University
V. Philipps, Julich Research Center

Contents

1. Introduction

◎ Various concerns for application of high Z to ITER
Influence on plasma
Influence from plasma

◎ For fundamental understanding of PMI
from low Z to high Z
PFM will modify plasma character

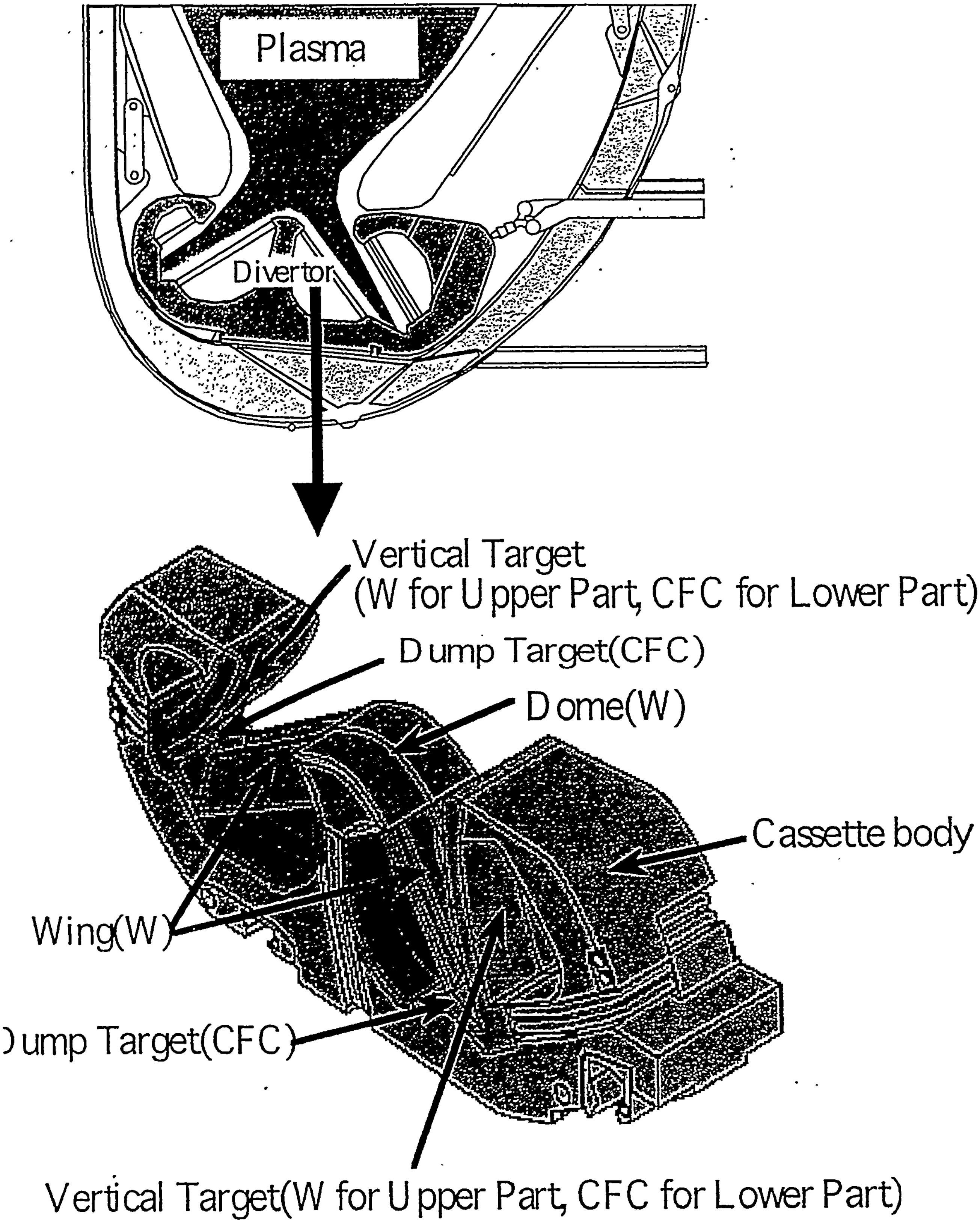

Divertor Cassette of ITER
(Vertical Target Option)

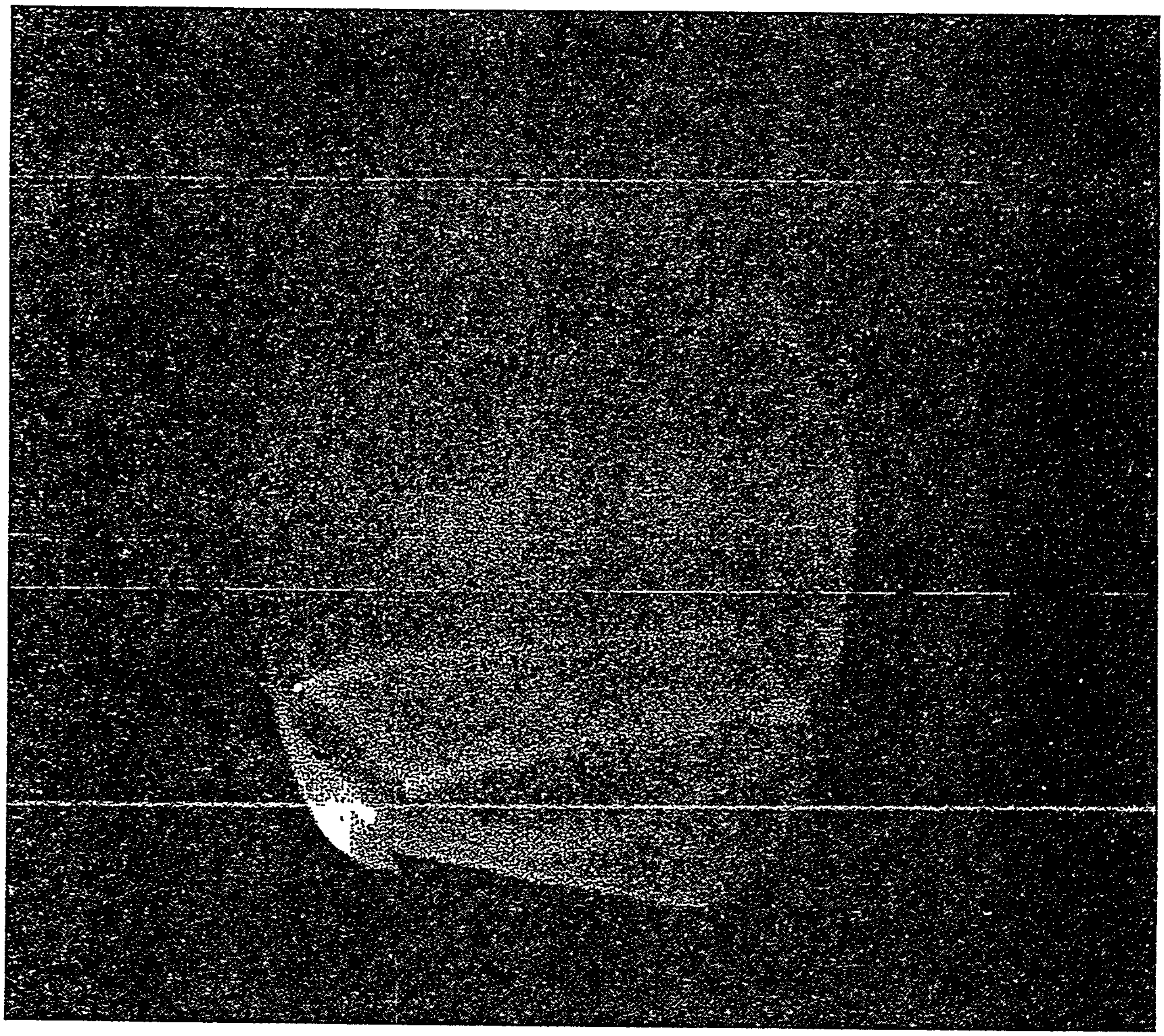

TEXTORプラズマとALT-Ⅱトロイダル
ポンプリミター（接線方向の窓より撮影）
詳細はP 1参照

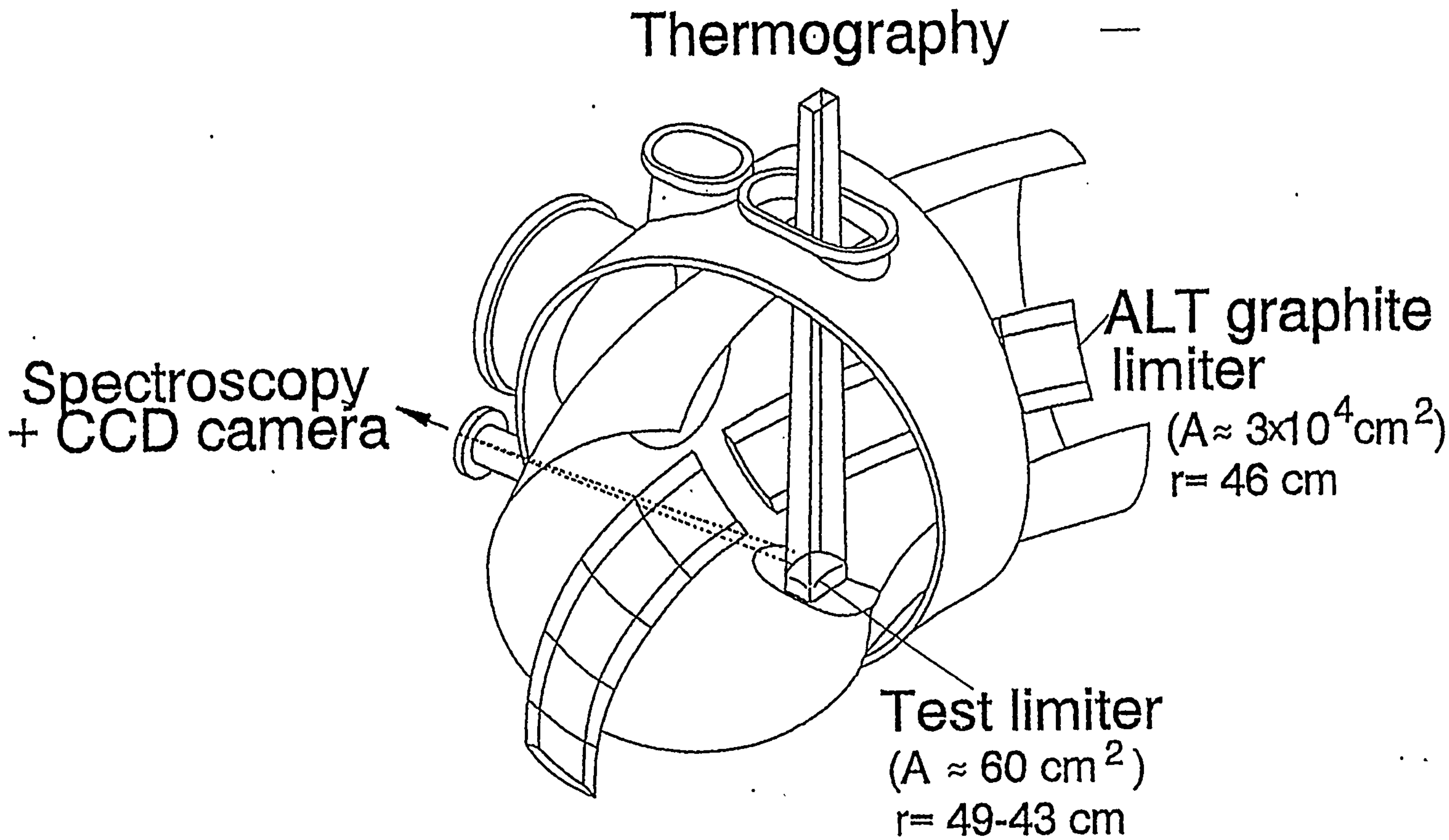
Thermography
ALT graphite limiter
(A ≈ 3x10⁴cm²)
r= 46 cm
Spectroscopy + CCD camera
Test limiter
(A ≈ 60 cm²)
r= 49-43 cm

Fig. 1

Core Plasma Diagnostics.

- T_e, n_e, I_p, etc.
- Prad (Bolometer array).
- X-ray (VUV W-band).

Edge Plasma Diagnostics.

- Tel, nel (He-beam, Li-beam).

IR-Thermography of the limiter surface.

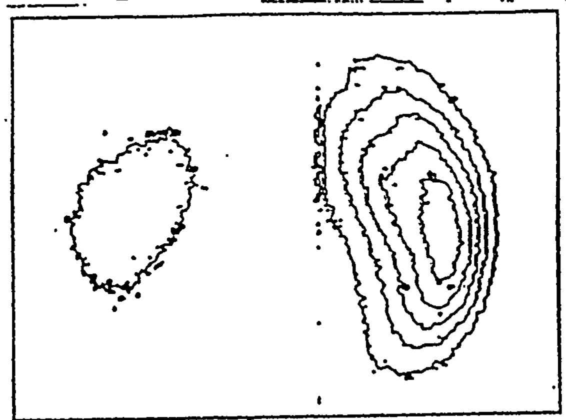

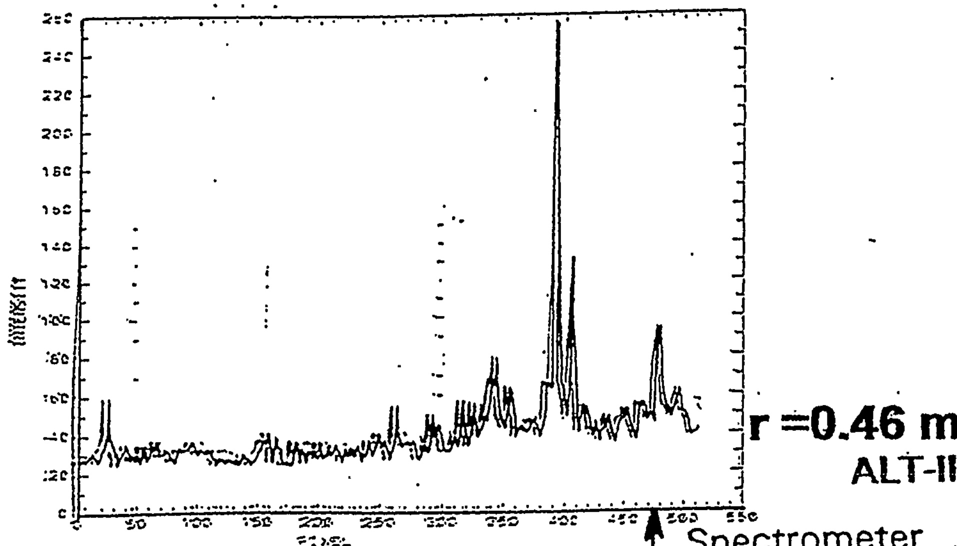

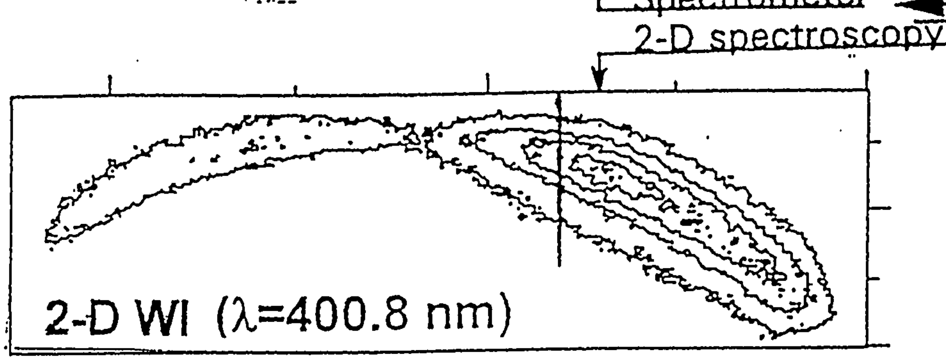

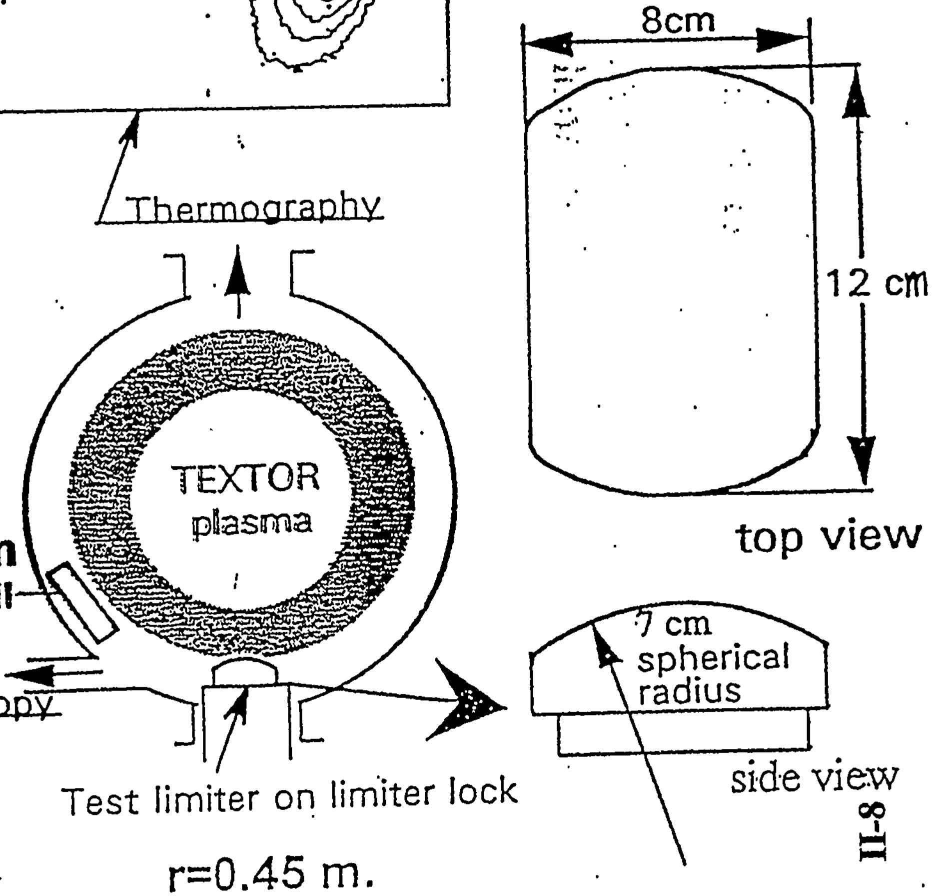

Experimental setup in TEXTOR

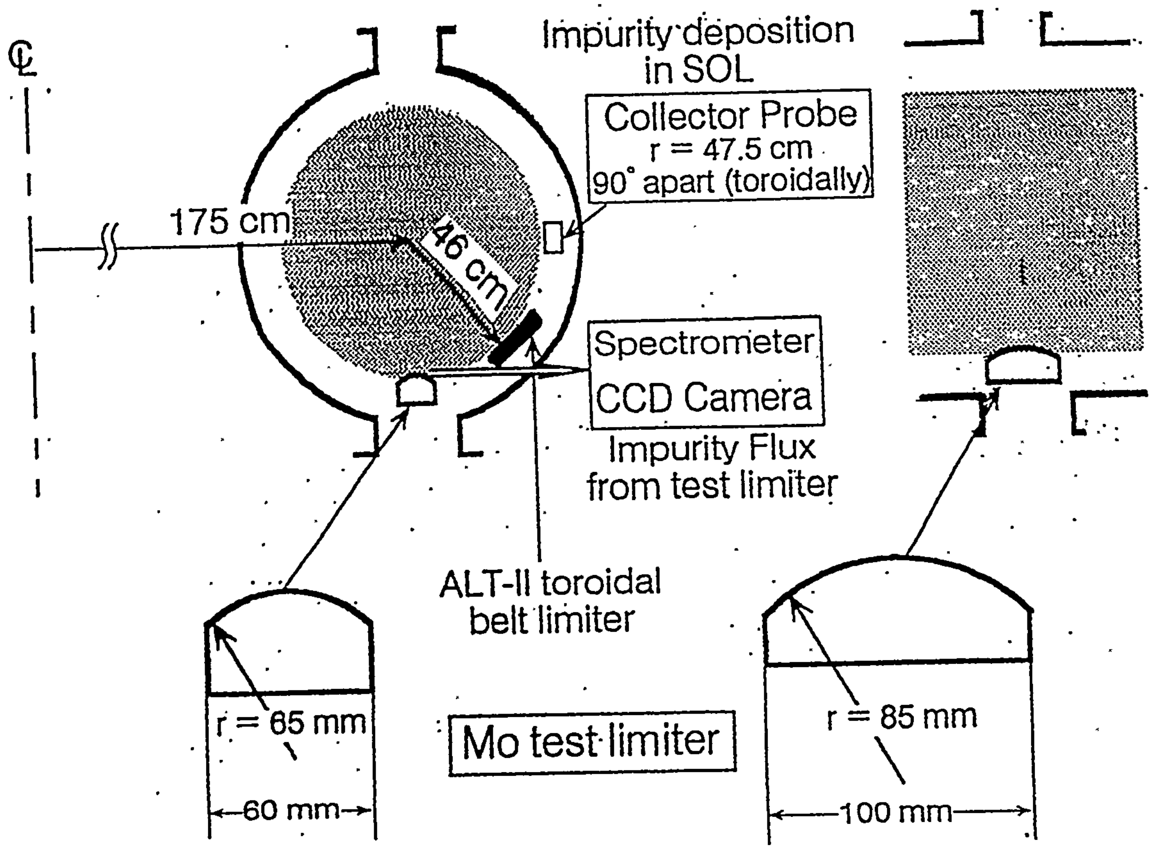

$$\frac{E_{lim}}{E_{conv}} \lesssim 5\% \text{(in this presentation)}$$

$\longrightarrow$ Most of E_{conv} flows into ALT-II

E_{lim} : Deposition energy to the test limiter

E_{conv}: Total convective energy

$$E_{conv} = \int (P_{heat} - P_{rad})\, dt$$

2. Influence on plasma performance

☆ No accumulation in ASDEX-Upgrade, Alcator C-Mod and FTU tokamak.

☆ Plasma instability in high density ohmic heated plasmas in TEXTOR but not in auxiliary heated (NBI and ICRH) ones (Auxiliary heating enhanced the saw tooth activity and hence the W accumulation was weakened).

☆ Accumulation of high Z impurities in TEXTOR is not directly related to the released amount of high Z impurities from the limiter but is very likely controlled by impurity transport properties of the plasma.

☆ High Z release from the PFM is mostly due to sputtering by low Z impurities of C and O except for the anomalous release upon the melting of limiter surface in TEXTOR.

☆ Inhomogeneous temperature profiles with local surface melting. (Artificial hot spot experiments are in preparation)

☆ If the central accumulation of high Z impurities can be avoided by suitable transport control, the high radiation property of high Z may be useful for edge cooling instead of Ne and Ar puffing which are being studied in the present large tokamaks.

Evolution of T_e, $\bar{n}_e$ and P_{rad}
for OH and NBI plasmas

OH Plasma (r_{lim} = 44.5 cm)

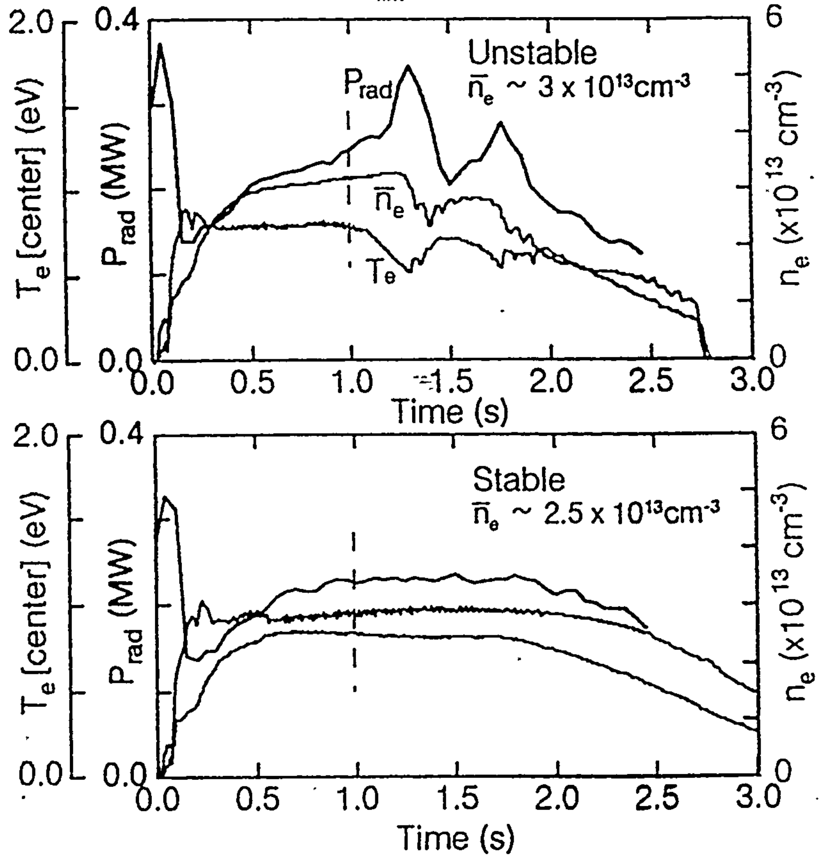

NBI Plasma (r_{lim} = 45 cm)

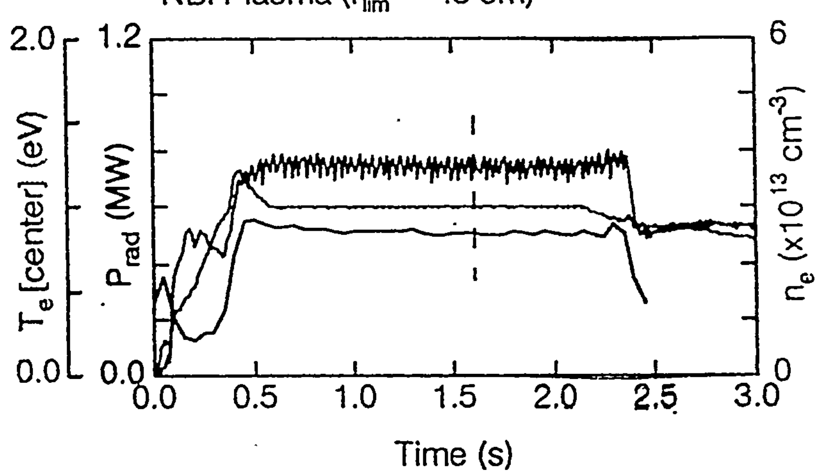

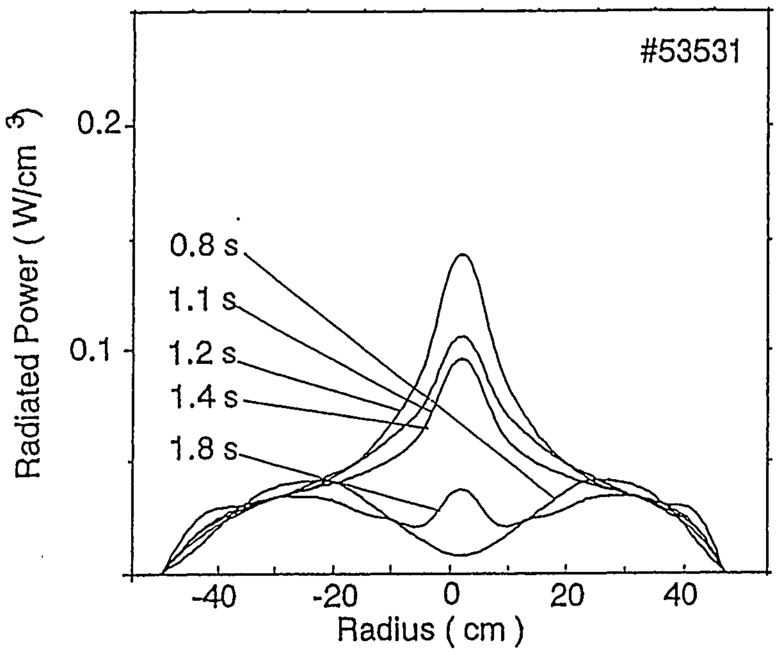

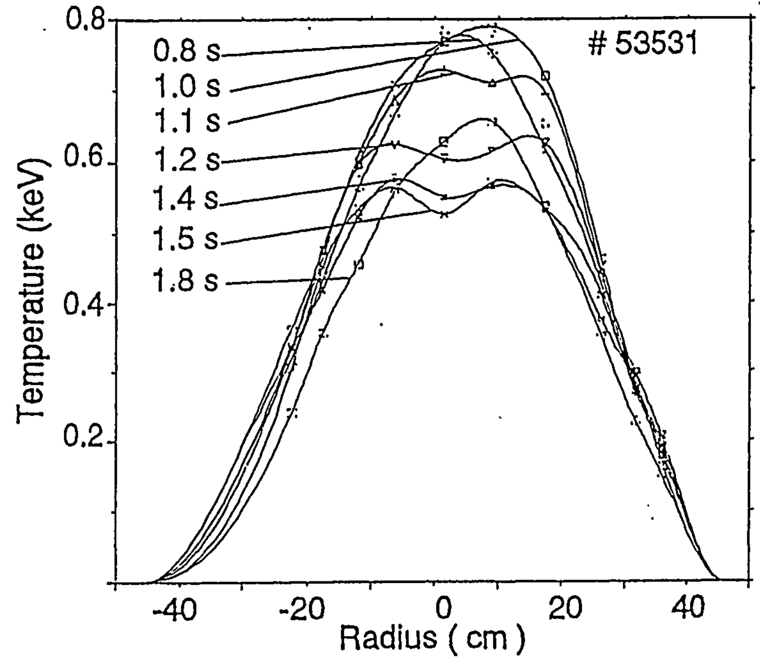

Evolution of profiles of radiated power (left) and temperature (right) during discharge (53531) with Mo accumulation in the plasma center. Strong central radiation results in hollow temperature profiles. Similar behaviour is observed for W limiter under high density ohmic conditions.

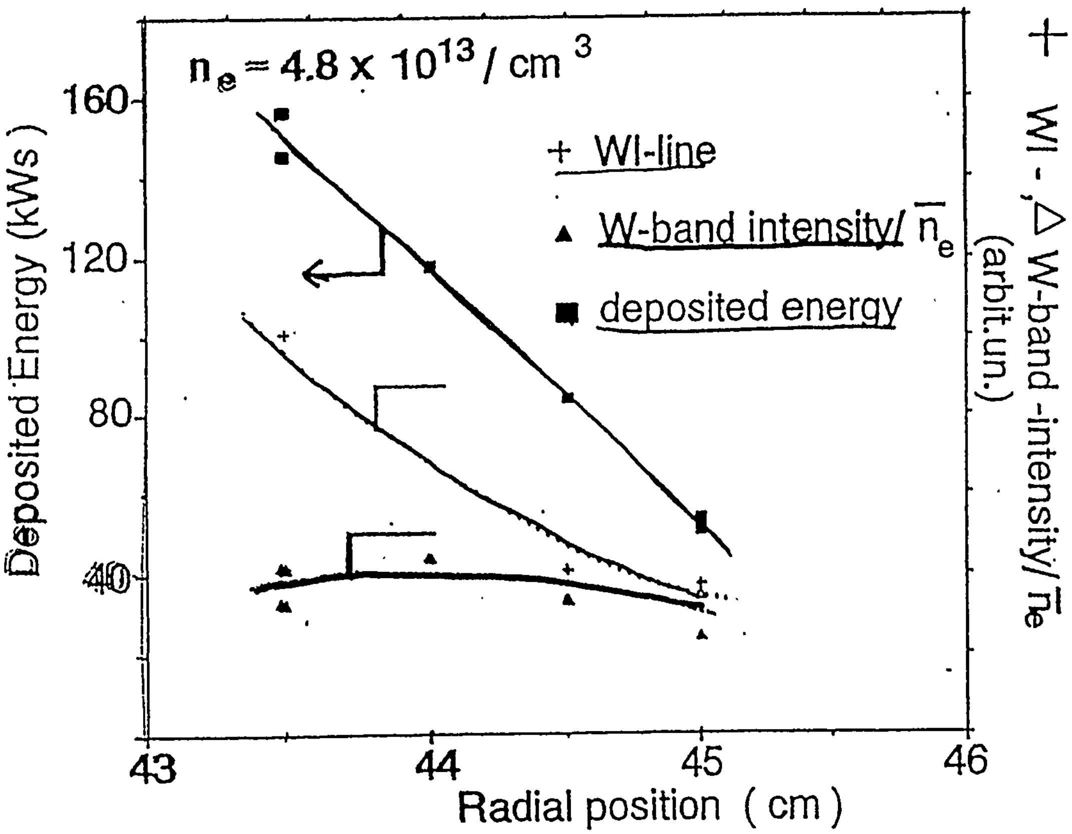

Demonstration of local screening of released W from W limiter at high dense NBI heating conditions:
the deposited energy (squares) and the local W release (cross) increase by about a factor of two by inserting the W limiter from r= 45cm to r= 43.5 cm.
W-spectroscopy (open triangles) and bolometrie (not shown) show no increase of W-concentration in the plasma.

Accumulation of high Z impurities is not directly related to the released amount of high Z impurities from the limiter

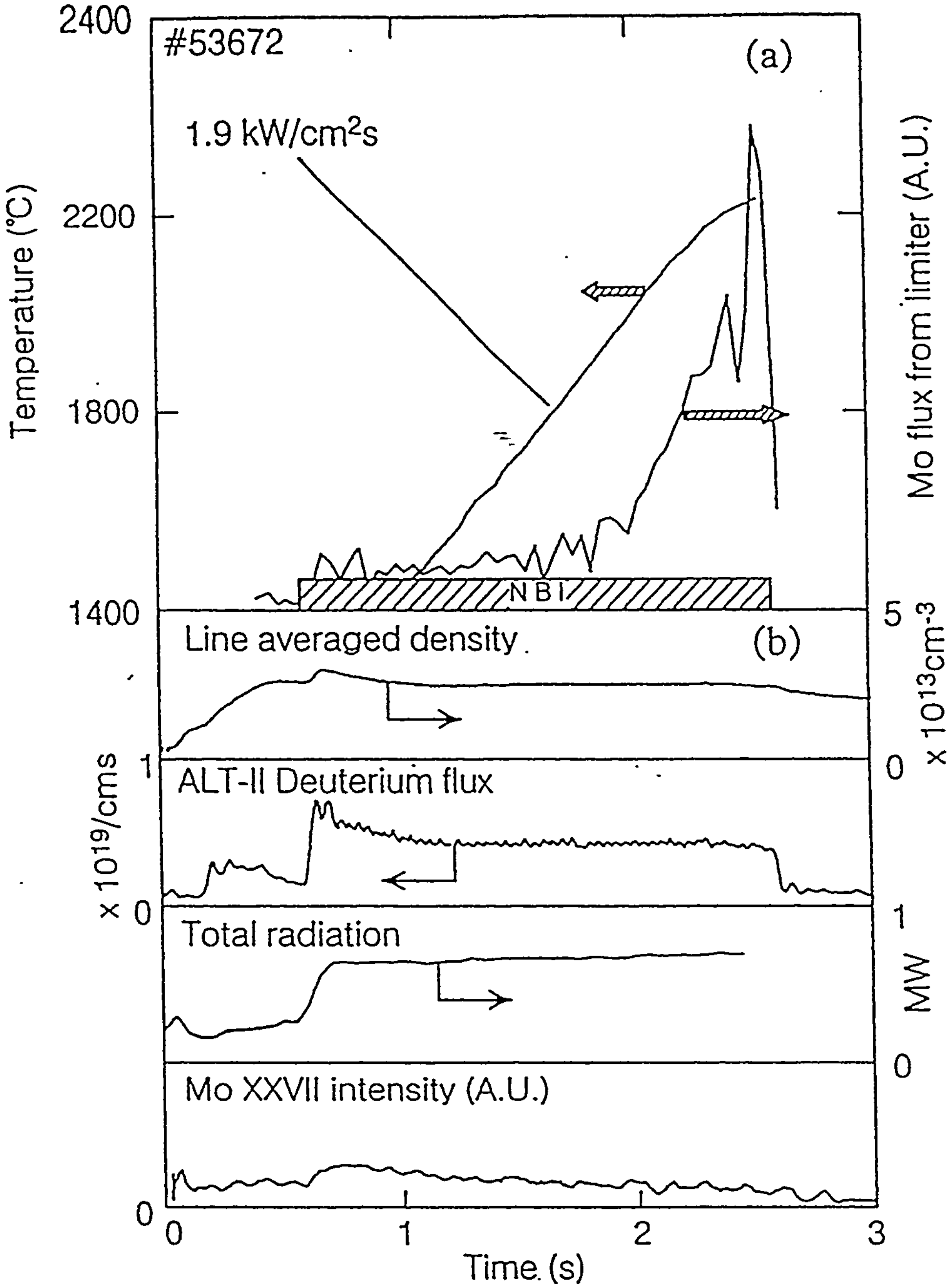

Prompt redepsotion of within the first gyromotion of W^+ ion

Important parameter : $\dfrac{\textbf{Gyororadius(rg)}}{\textbf{Ioniztion length (s)}}$

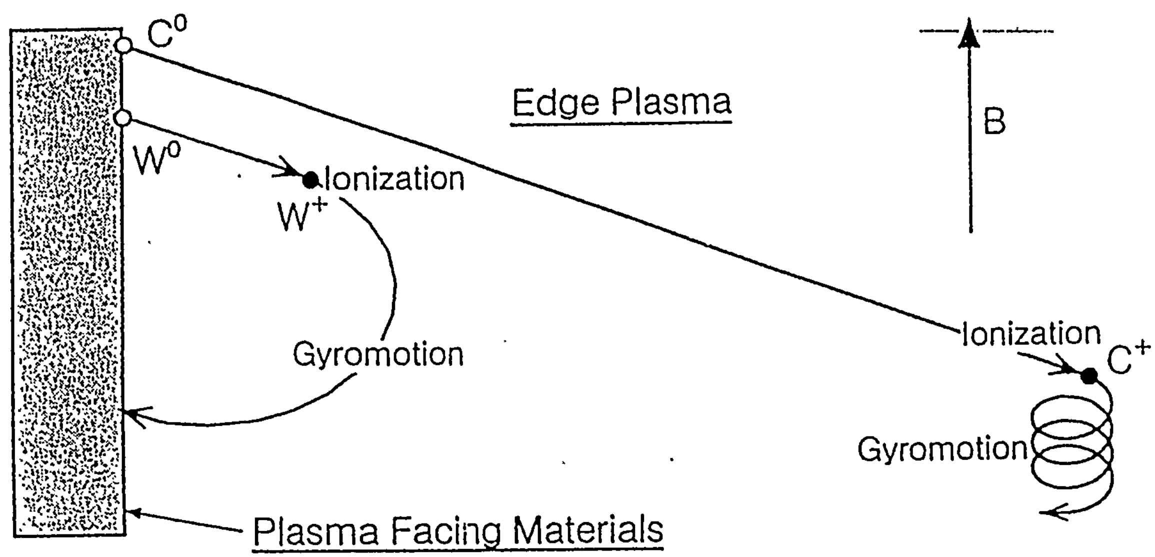

HT-2

Ionization Length of Mo Neutral

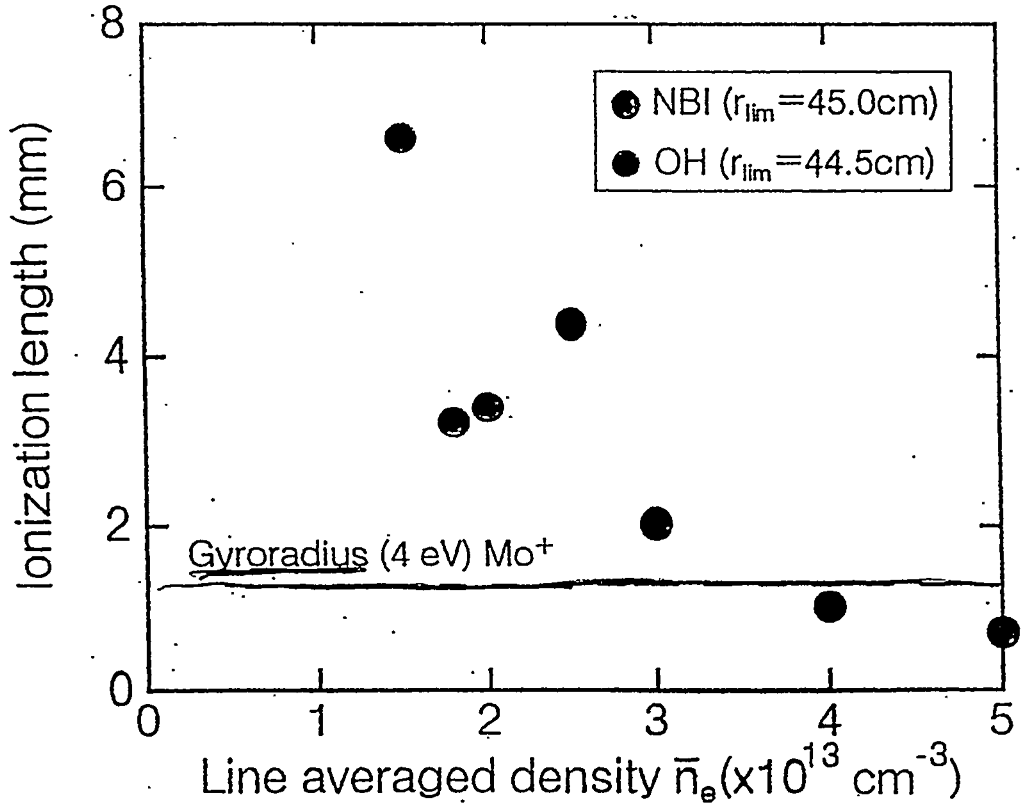

In high density NBI plasma ($\bar{n}_e \geq 4 \times 10^{13}$ cm^{-3},
n_e [limiter surface] $\gtrsim 1 \times 10^{13}$ cm^{-3}),
Ionization length of Mo is less than gyroradius of Mo^+
and probability of prompt deposition is much high.

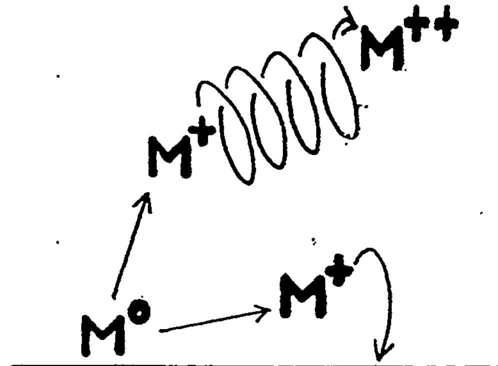

3. Erosion and Redeposition

★High Z release by low Z impurity sputtering.

★Prompt redeposition would reduce erosion and plasma contamination.

★Vapor shielding may be very helpful to reduce the erosion but no clear evidence.

★Chemical erosion by oxygen does not dominate the erosion.

★Carbon readily reacts with Mo and W to form carbides at high temperatures and deposited carbon may have important role on erosion.

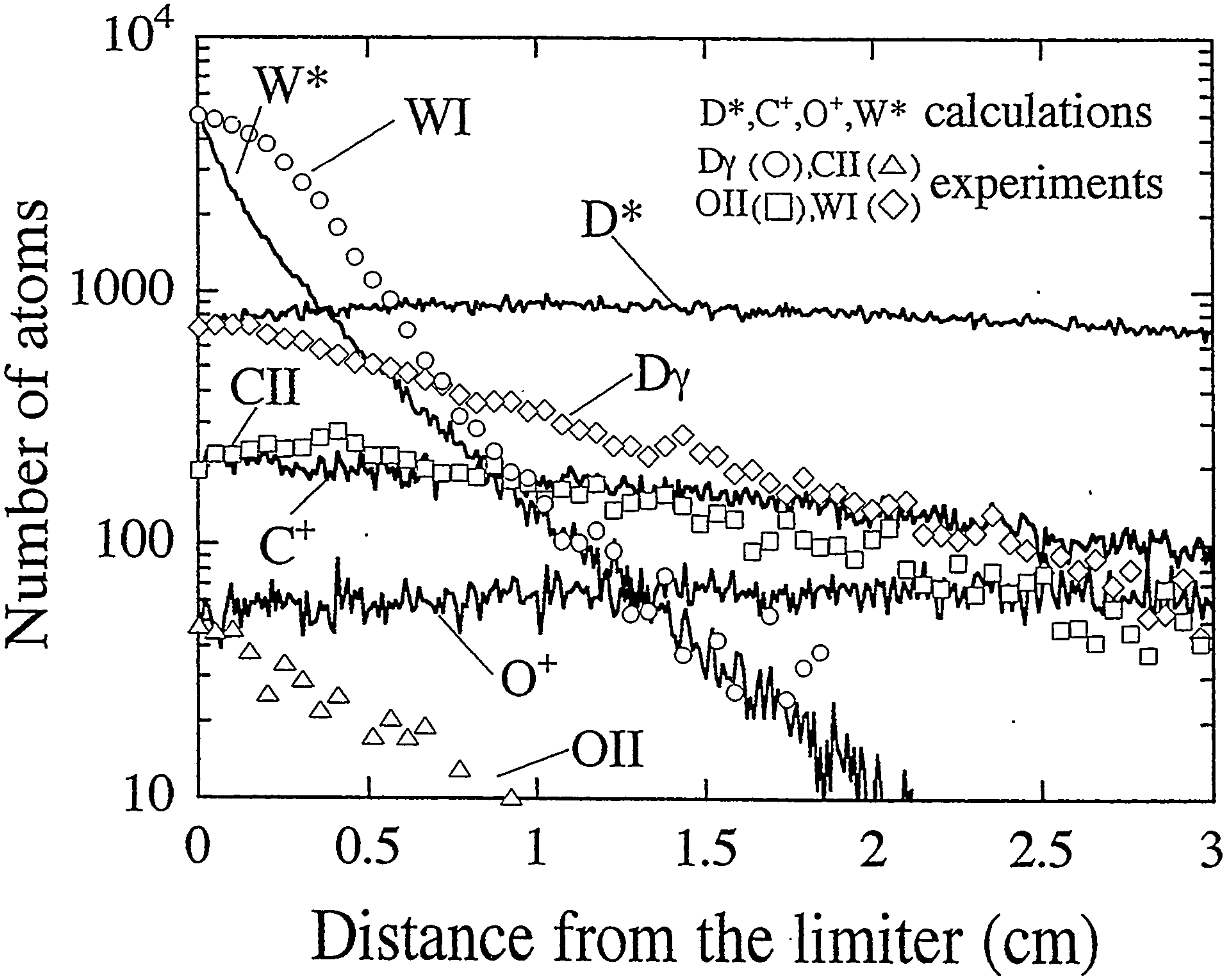

W*
WI
D*,C+,O+,W* calculations
Dγ (○),CII (△)
OII(□),WI (◇)
experiments
D*
Dγ
CII
C+
O+
OII
10^4
1000
100
10
0
0.5
1
1.5
2
2.5
3
Number of atoms
Distance from the limiter (cm)

DEPOSITION RATES (FLUXES) OF HIGH - Z METALS ON THE COLLECTOR PROBES EXPOSED TO NBI HEATED PULSES

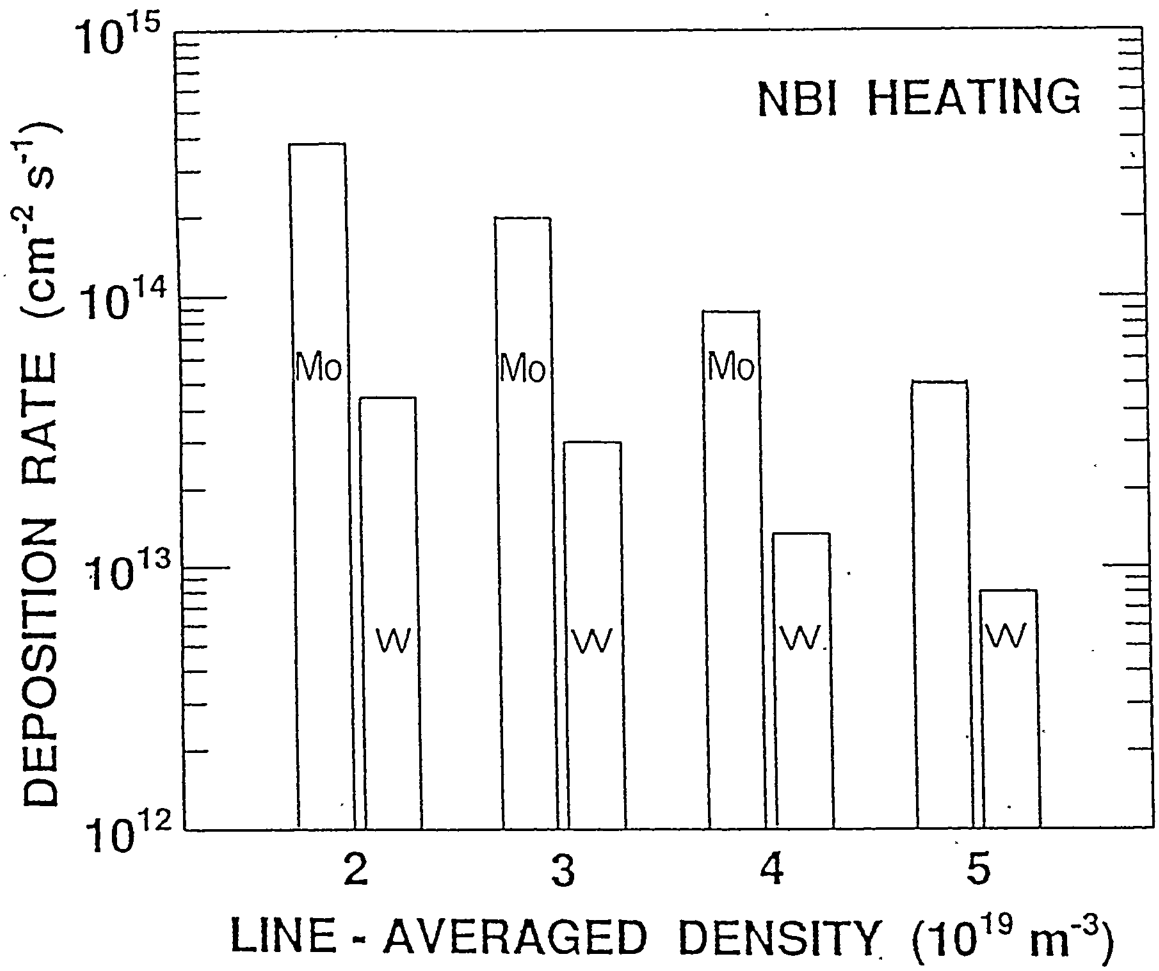

RESULTS:

1. $\Phi_{Mo} : \Phi_W = 7 : 1$

2. THE DECREASE OF HIGH - Z FLUXES (EROSION) WITH THE INCREASE OF ELECTRON DENSITY.

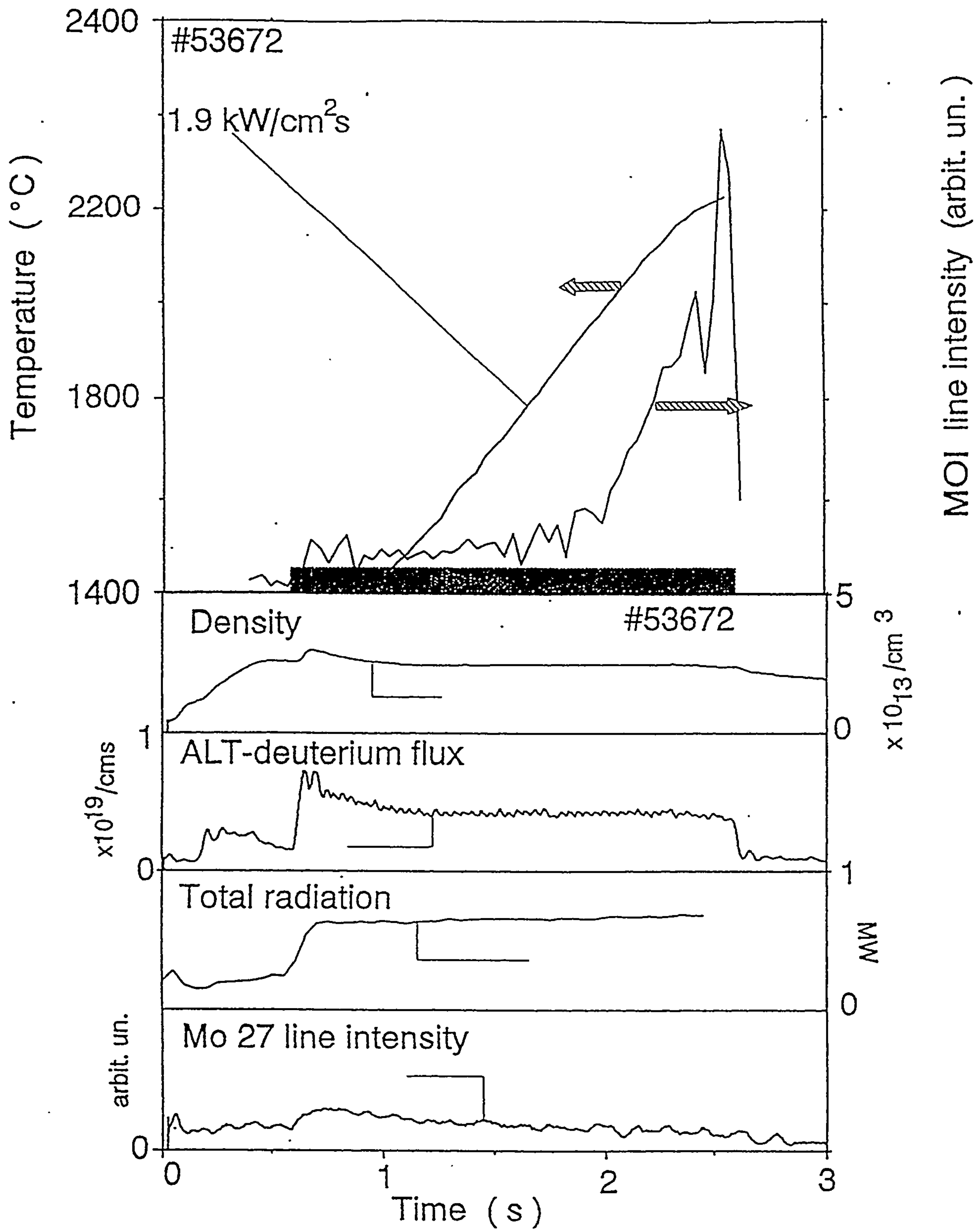

Fig.5. Time sequences of various plasma parameters for the particular shot where the Mo-limiter subjected to surface melting as seen in the increase of the MoI line in the figure.

CIRSE
Nagoya University
Center for Integrated Research in Science and Engineering

4. Energy deposition and reflection

- ◇ Particle and energy reflection coefficients are higher for higher Z.
- ◇ The deposited energy on the W limiter is a little smaller than that of the Mo limiter under the similar plasma condition.

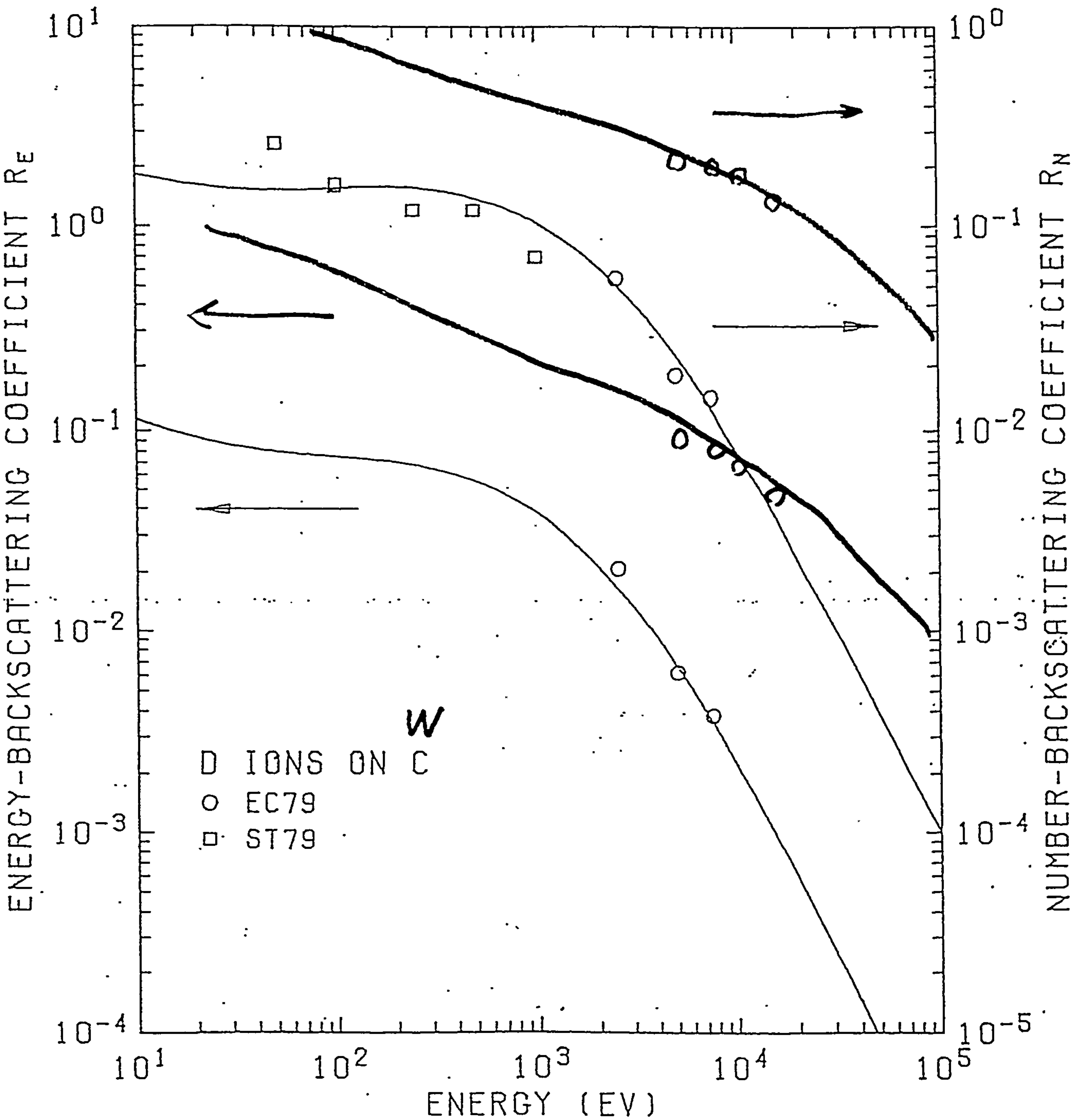

Fig. 16. R_N and R_E of D ions on $_6C$.

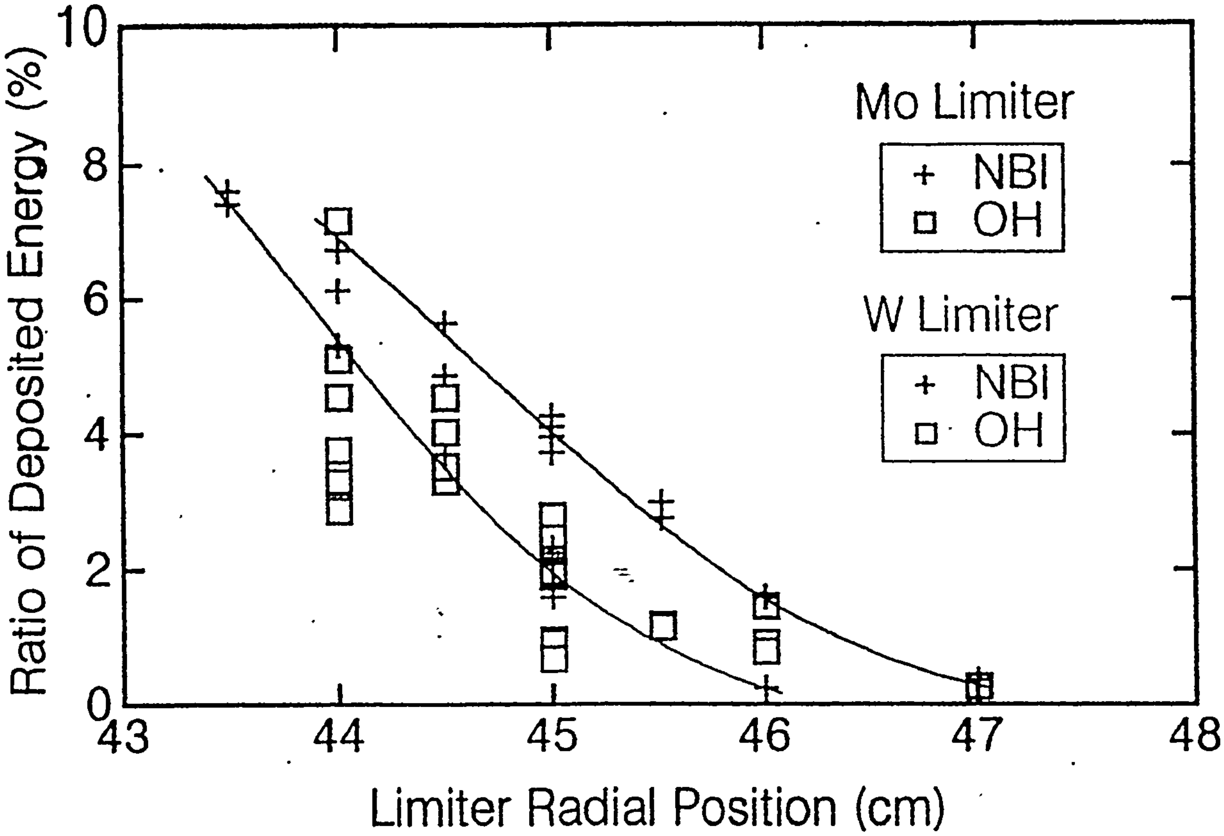

Ratio of Deposited Energy : E_{Lim}/E_{con}

Convective loss Energy : E_{con}

$$E_{con} = \int (P_{OH} + P_{NBI} - P_{rad})dt$$

Ratio of Deposited Energy to Limiter vs Limiter Radial Position

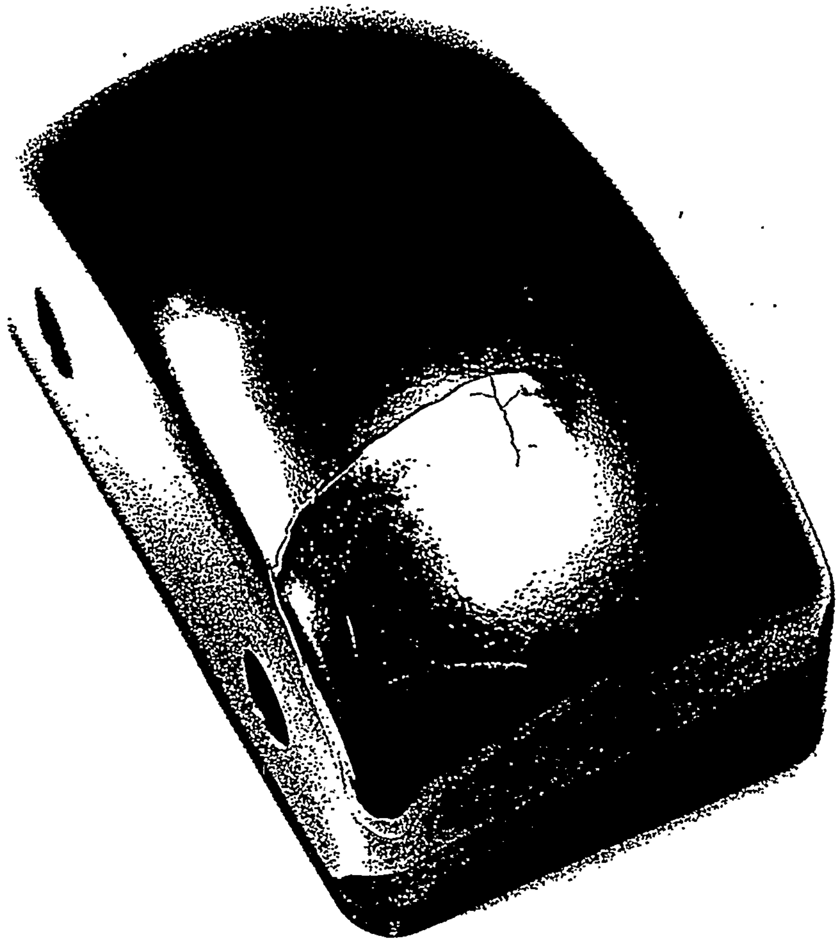

Molded edges will be completely removed.

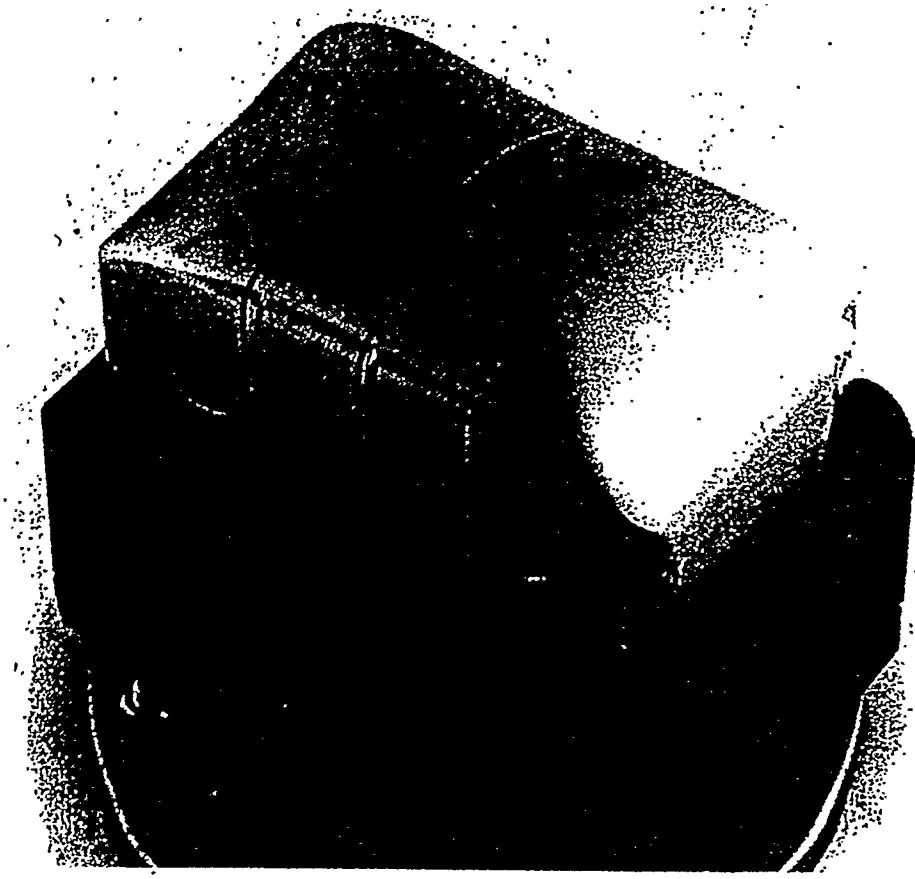

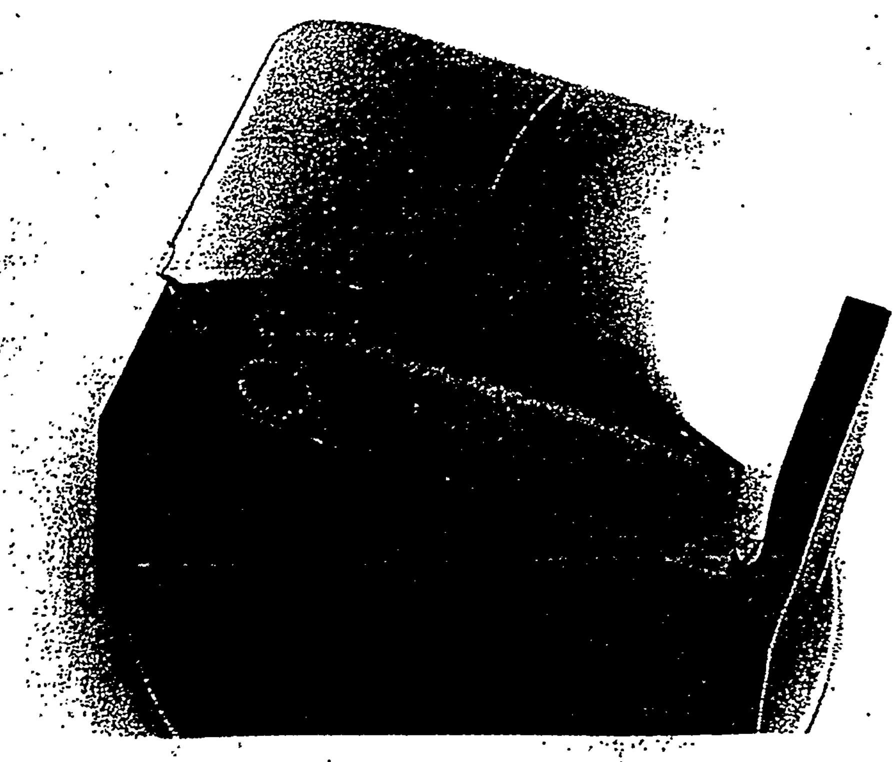

T921t360_asc

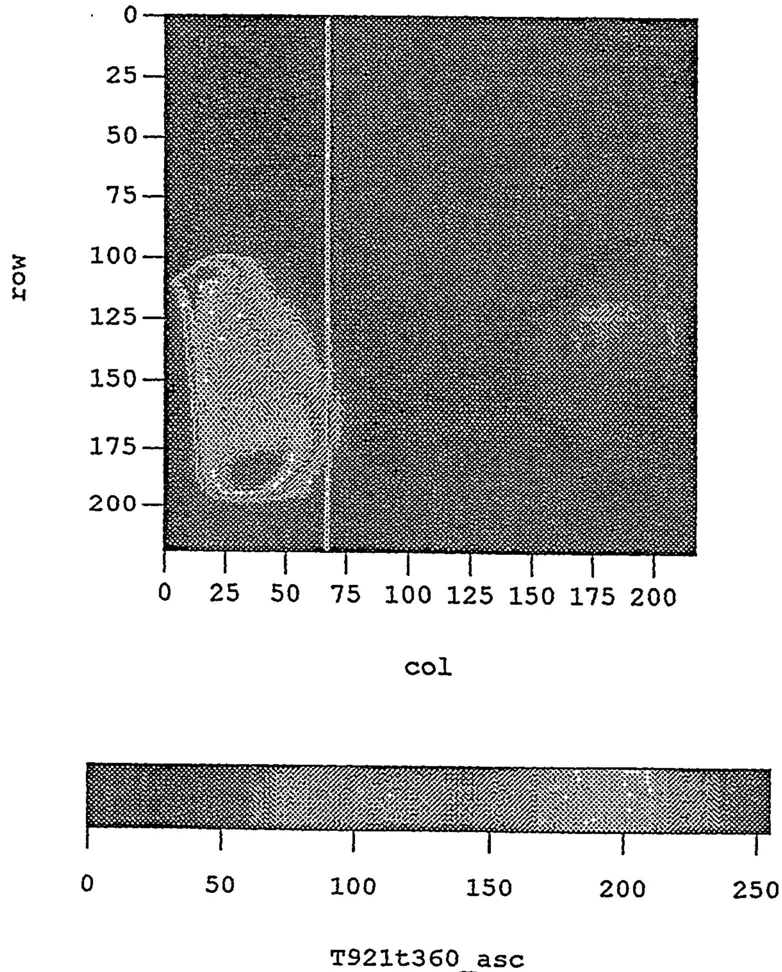

5. Material responce to high heat load

- Maximum power fluxes of about 20 MW/cm^2 for 4 s could be loaded on the W limiter preheated at about 500 °C.
- W limiter showed significant cracking when operated below DBTT. The cracks were initiated by the residual stress introduced by the manufacturing process.
- Intergranular cracking originated from recrystallization and grain growth are unavoidable for high temperature use of bulk materials manufactured by power metallurgy.
- Improvement of brittle nature of Mo and W by alloying is advancing. Effect of alloying element on plasma exposure or under high temperature operation should be studied.

Recrystallization to columnar grains and intergranular cracking are unavoidable at high temperature operation

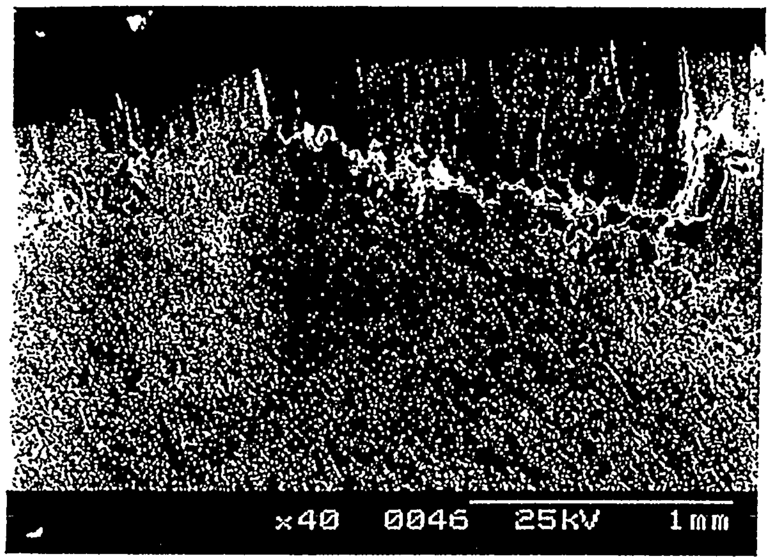

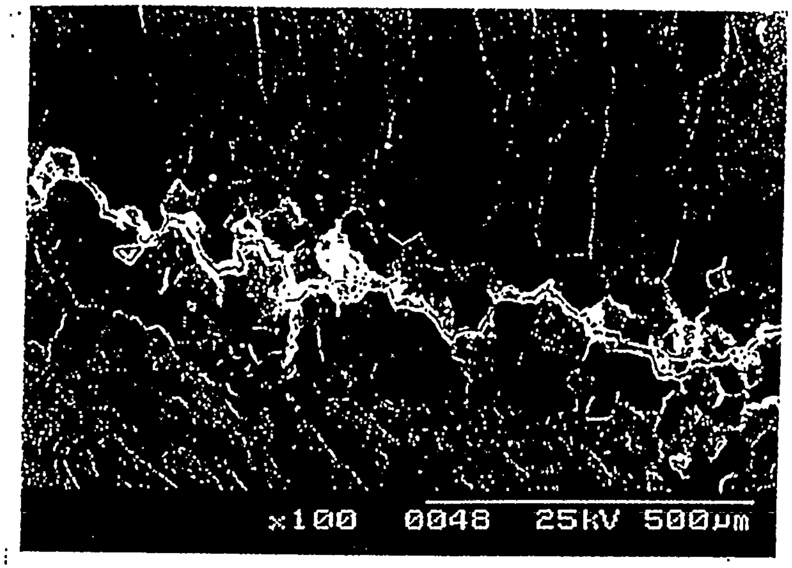

Journal of Nuclear Materials 233–237 (1996) 645–649

Manufacturing and high heat flux loading of tungsten coatings on fine grain graphite for the ASDEX-Upgrade divertor

S. Deschka [a,*], C. García-Rosales [a], W. Hohenauer [b], R. Duwe [b], E. Gauthier [c], J. Linke [b], M. Lochter [d], W. Malléner [b], L. Plöchl [e], P. Rödhammer [e], A. Salito [f]

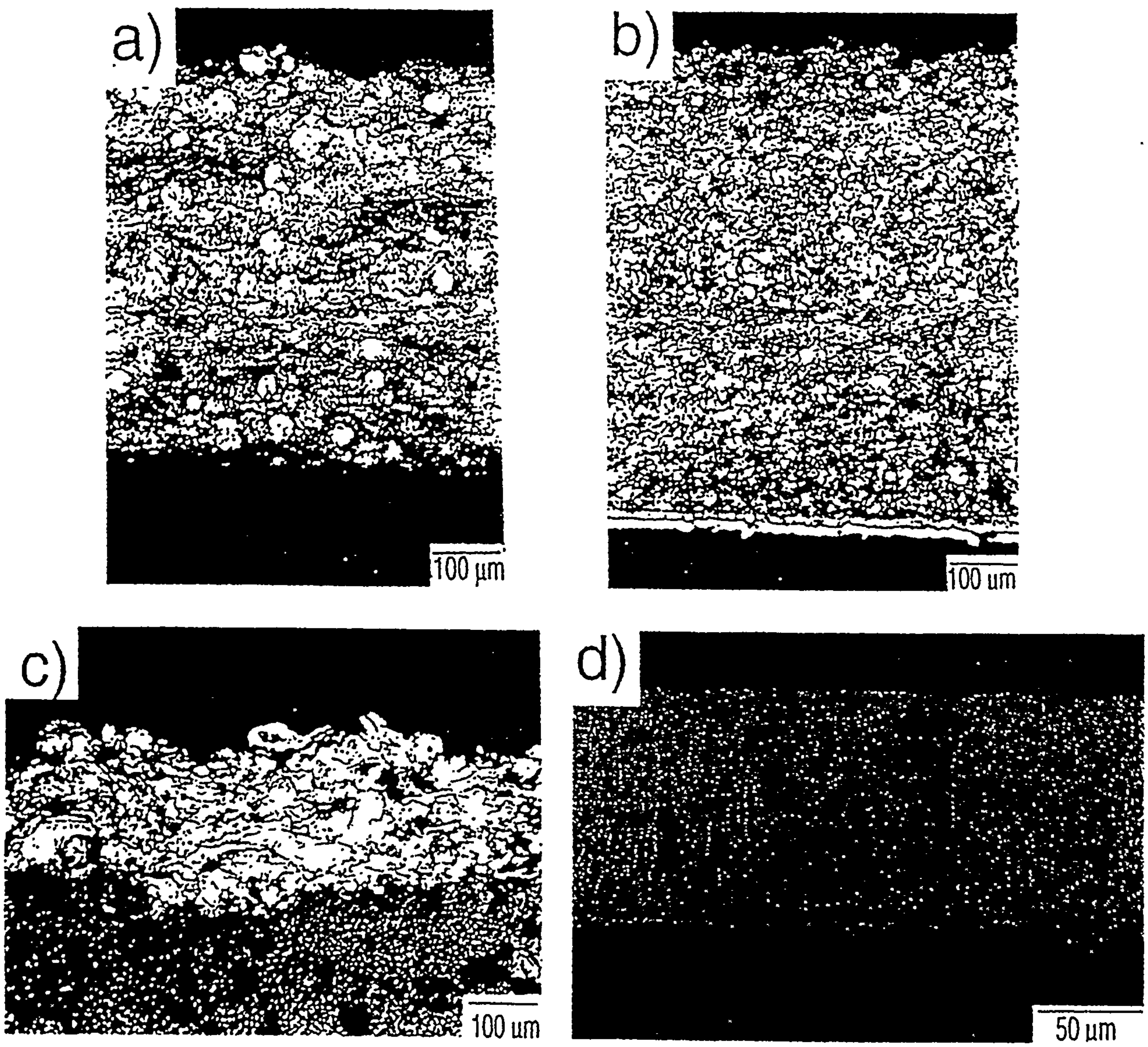

Fig. 1. Metallographic sections of the four different types of coatings: (a) VPS-coating, KFA Jülich, (b) VPS-coating with Re-containing intermediate layer, P/SM AG, (c) IPS-coating, CEN Cadarache, (d) PVD-coating from Plansee with Re-containing intermediate layer

II.29

- Pure W must change to W-Re alloy by neutron irradiation. Even neutron irradiation is known to increase the DBTT significantly.
- W cannot be a structure material but be used as a thin tile or deposited film and CVD coating with columnar grain structure seems promising. → $\bar{F}$W-P2 (Nagamura et al.)
- Large difference in thermal expansion coefficient makes brazing of W to substance difficult.
- We need some optimization in operating temperatures of W to avoid brittlement (higher is better) and recrystallization (lower is better), and depending on the utilization (operation) temperature the microstructure of W might be changed to suitable form and much effort is needed in future.

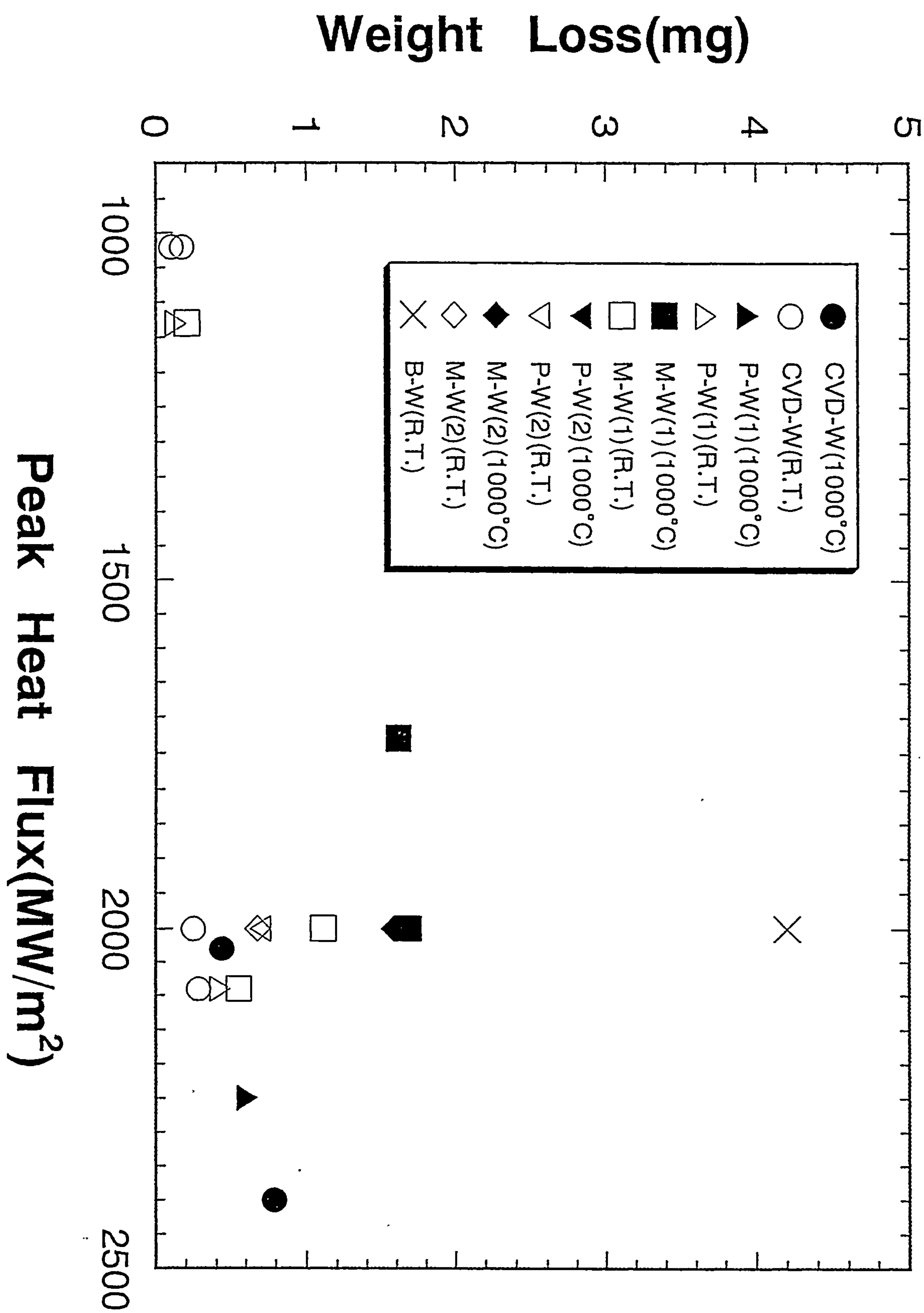
Weight Loss(mg)
0
1
2
3
4
5
CVD-W(1000°C)
CVD-W(R.T.)
P-W(1)(1000°C)
P-W(1)(R.T.)
M-W(1)(1000°C)
M-W(1)(R.T.)
P-W(2)(1000°C)
P-W(2)(R.T.)
M-W(2)(1000°C)
M-W(2)(R.T.)
B-W(R.T.)
1000
1500
2000
2500
Peak Heat Flux(MW/m2)

Journal of Nuclear Materials 233–237 (1996) 638–644

High heat load test on tungsten and tungsten containing alloys

M. Fujitsuka [a,*], I. Mutoh [a], T. Tanabe [a], T. Shikama [b]

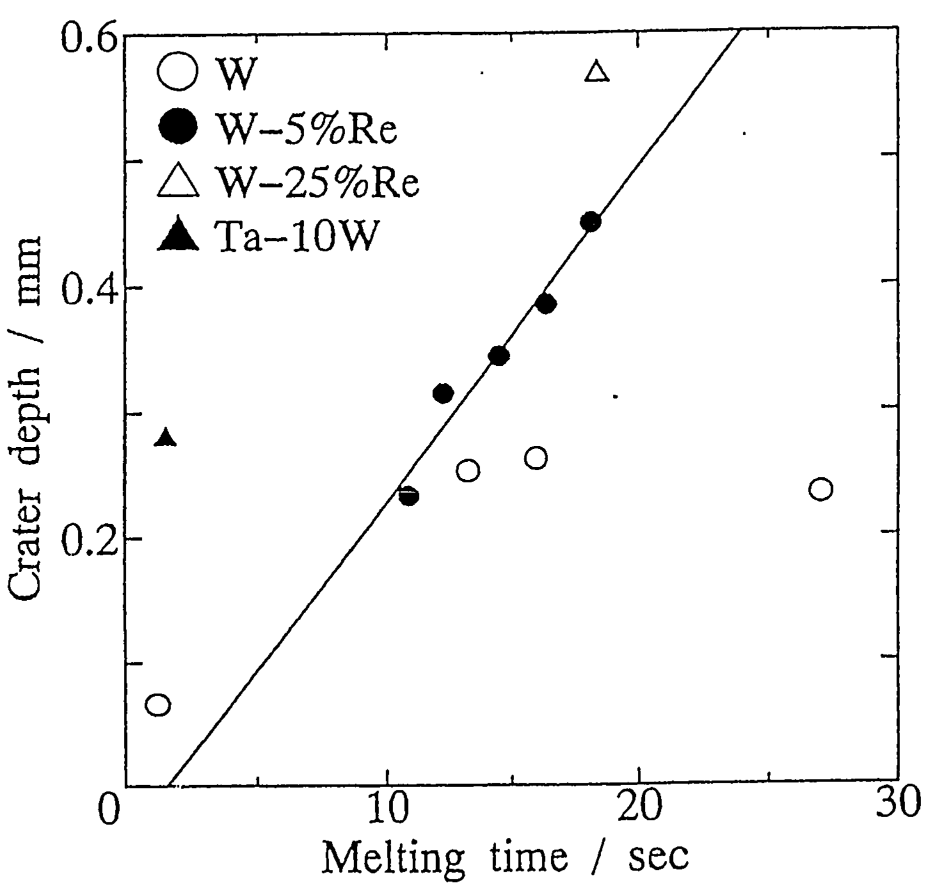

Fig. 5. Crater depth as a function of melting time.

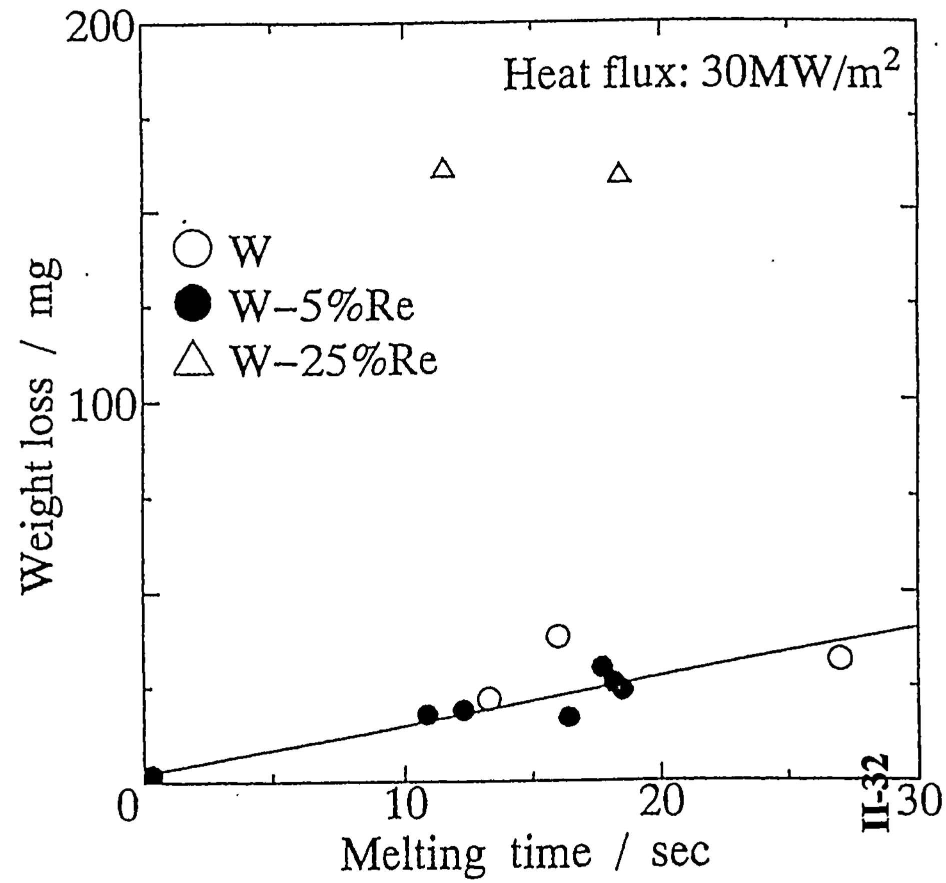

Fig. 7. Weight loss as a function of melting time.

CIRSE
Nagoya University
Center for Integrated Research in Science and Engineering

6. Hydrogen effect

- Tritium retentionin Mo and W at high temperatures is generally not concerned and hydrogen embrittlement too.
- Below 500 K hydrogen retention in plasma sprayed W coating on graphite for ASDEX is reported to be similar level to graphite.
- Materials performance like crack formation under high flux of energetic hydrogen loading should be studied further.

7. SUMMARY AND CONCLUSIONS

Influence to plasma

1. The accumulation of high Z impurity in plasma center has hardly appeared except for plasma instability observed in high density ohmic heated plasmas in TEXTOR.
2. The accumulation is not directly connected to the released amount of high Z from PFM but is very likely controlled by impurity transport in the plasma.
3. If the central accunulation of high Z impurities can be avoided by suitable transport control, the high radiation property of high Z may be useful for edge cooling.
4. The appearance of prompt redeposition of high Z atoms is very promising for the utilization of high Z materials.

(continued)

7. SUMMARY AND CONCLUSIONS (part 2)

Influence from plasma

5. Heat deposition is likely reduced for higher Z materials owing to its higher reflection coefficient.
6. Although tritium retention at high temperature might be small, materials performance under high flux of energetic hydrogen loading should be studied further.
7. Mo and W bulk limiters are approved to be utilized above their DBTT without severe damage even with surface melting.
8. Intergranular cracking originated from recrystallization and grain growth are unavoidable for high temperature use of bulk materials manufactured by power metallurgy.
9. Some optimization in operation temperatures to avoid brittlement (higher is better) and recrystallization (lower is better) and control of grain structures are needed.
10. Bulk tungsten is too heavy to handle and CVD coating with columnar grain structure seems promising.

General message for ITER

◇ There should be some operational window compatible with high Z wall.

◇ Large radiation from evaporated or sputtered high Z impurities may be helpful for edge cooling!

◇ Thin layer (tiles) is only realistic solution for utilization of high Z.

Tungsten Brush Development
ITER Divertor Task T221

US-Japan Workshop on Fusion Technology

San Francisco, CA
8 - 9 December 1997

G.W. Wille
The Boeing Company

CONTRIBUTORS

U.S. Home Team

- **SANDIA NATIONAL LABS - NEW MEXICO**
  - R. Watson, M. Ulrickson
- **SANDIA NATIONAL LABS - LIVERMORE**
  - C. Cadden, B. Odegard
- **BOEING - ST. LOUIS**
  - J. Davis, D. Deuser, D. Driemeyer, R. Lederich, K. Slattery, J. Wille
- **PLASMA PROCESSES**
  - T. McKechnie, S. O'Dell
- **SURMET CORPORATION**
  - R. Cooke, N. Gunda, S. Sastri

Tungsten Brush Fabrication - 3 Methods

U.S. Home Team

PLASMA SPRAY METHOD

1) Fixture Pointed W Rods in Honeycomb
2) Plasma Spray Cu to Tips of Rods
3) HIP Diffusion Bond to CuCrZr Heat Sink at 450°C-550°C/200MPa/180min

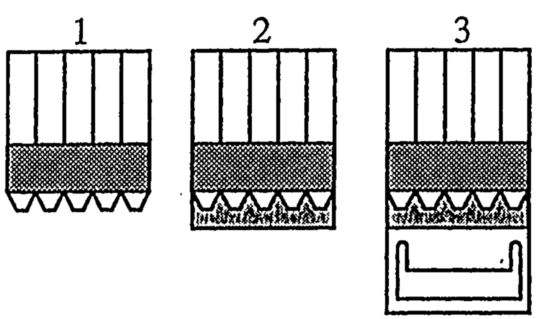

CAST METHOD

1) Fixture Tapered W Rods in Honeycomb
2) Cast Cu to Tips of Rods
3) HIP Diffusion Bond to CuCrZr Heat Sink at 450°C/200MPa/180min

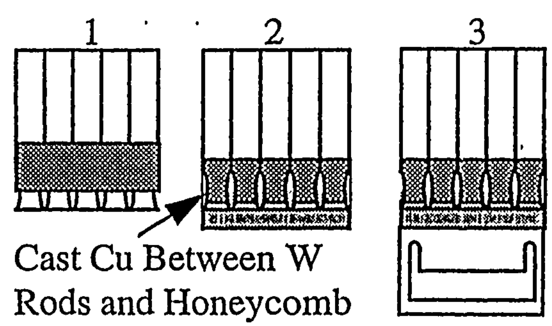

DIRECT DIFFUSION BOND METHOD

1) Fixture Pointed W Rods in Honeycomb & PVD Coat Rod Tips with Diffusion Aid
2) HIP Diffusion Bond to CuCrZr Heat Sink (a) at 450°C/200MPa/180min, Driving Rods into OFHC Cladding (b)

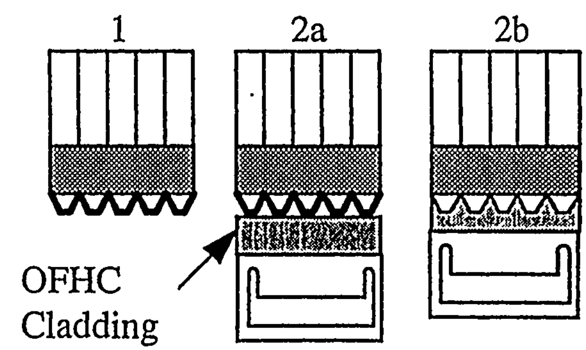

Tungsten Brush Mechanical Testing

U.S. Home Team

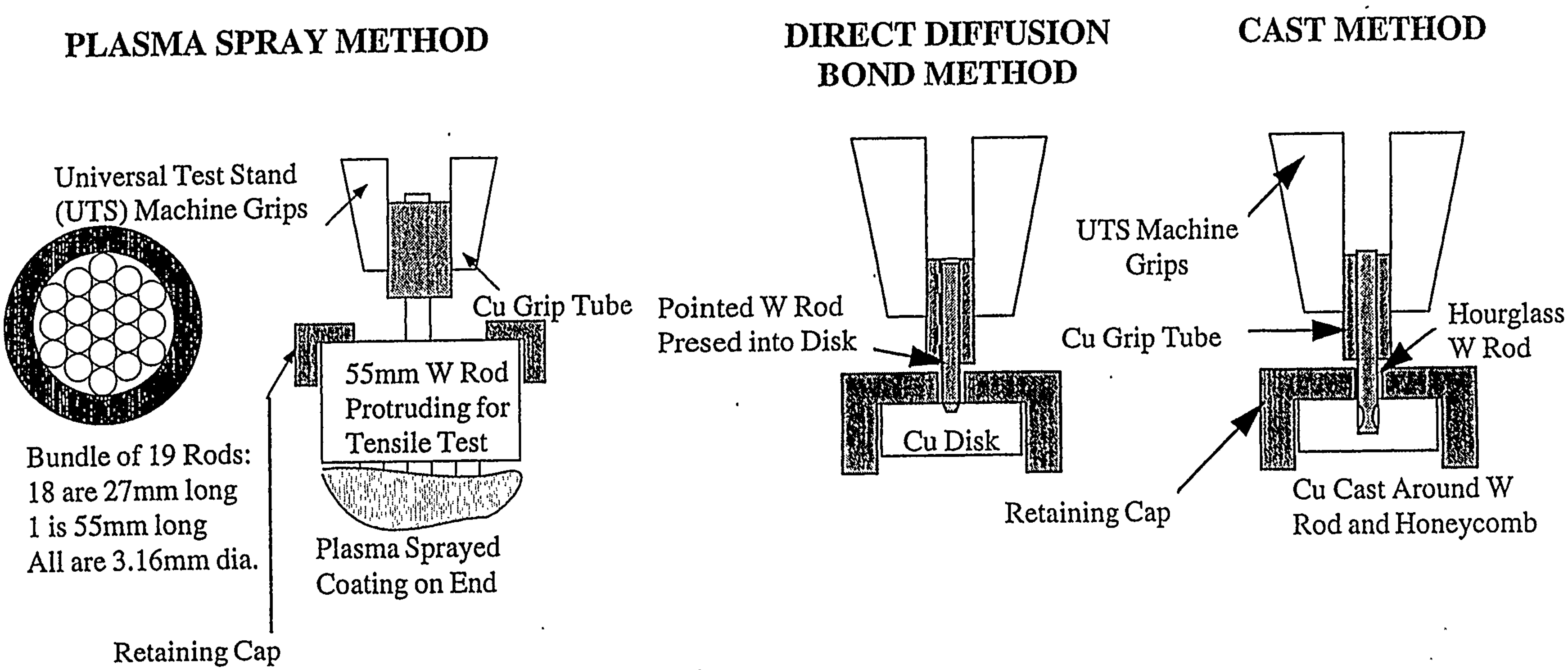

Mechanical Testing Results

U.S. Home Team

PLASMA SPRAY METHOD - ALL TESTS @ 280°C

PLASMA SPRAYED COATING	THERMAL TREATMENT CYCLES	FAILURE STRESS (MPa)
Cu	Vacuum Anneal 900°C & HIP	139
Cu	HIP	136
Fine Ni	Vacuum Anneal 900°C	110
Fine Ni	Vacuum Anneal 600°C & HIP	118
Fine Ni	Vacuum Anneal 900°C & HIP	108
Fine Ni	HIP	101
Coarse Ni	Vacuum Anneal 600°C	119
Coarse Ni	Vacuum Anneal 900°C & HIP	109
Coarse Ni	HIP	107
PPI-1	Vacuum Anneal 600°C	141
PPI-1	HIP	97

CAST METHOD - ALL TESTS @ 280°C
Grip Tube Slipped and Test Discontinued
370MPa for Cu cast on 5mm of rod
425MPa for Cu cast on 6mm rod

Failure Stress Refers to Axial Stress in W Rod When Bond Failed

Mechanical Testing Results

U.S. Home Team

DIRECT DIFFUSION BOND METHOD

SPECIMEN IDENTIFICATION & Cu ALLOY BASE IF NOT OFHC	COATING	TIP	THERMAL TREATMENTS	TEST TEMP (°C)	FAILURE STRESS (MPa)
316	PVD Nb	45° 1/2 taper	none	300	112
317	PVD Cu	45° 1/2 taper	none	300	67
319R	PVD Ni	45° 1/2 taper	none	280	94
320, 323, 340, 346, 349	PVD Nb & Ni	45° 1/2 taper	none	300	133, 106, 101, 120, 110
341	PVD Nb & Ni	45° 1/2 taper	none	RT	310
353	PVD Nb & Ni	45° 1/2 taper 2mm deep	none	280	179
354	PVD Nb & Ni	45° 1/2 taper 3mm deep	none	280	156
355	PVD Nb & Ni	45° full taper 4mm deep	none	280	123
356	PVD Nb & Ni	flat	none	280	0
359 (CuCrZr Cn A)	PVD Nb & Ni	45° 1/2 taper 2mm deep	none	280	2
360 (CuCrZr Cn HT)	PVD Nb & Ni	45° 1/2 taper 2mm deep	none	280	5
361 (CuCrZr Cn A)	PVD Nb & Ni	45° full taper 4mm deep	none	280	0
357	PVD Nb, Nb & Ni	45° 1/2 taper	1800°C, 30min	280	47
321	PVD Cu & Ni	45° 1/2 taper	none	300	75
324	PVD Cu & Ni	45° 1/2 taper	none	307	66
326	PVD Ni & Ni	45° 1/2 taper	800ºC, 60min	300	64
327	PVD Cu, Ni & Ni	45° 1/2 taper	1000ºC, 60min	320	32

*353, 354, 355, 361 bent during pressing

Failure Stress Refers to Axial Stress in W Rod When Bond Failed

Rod Tips

U.S. Home Team

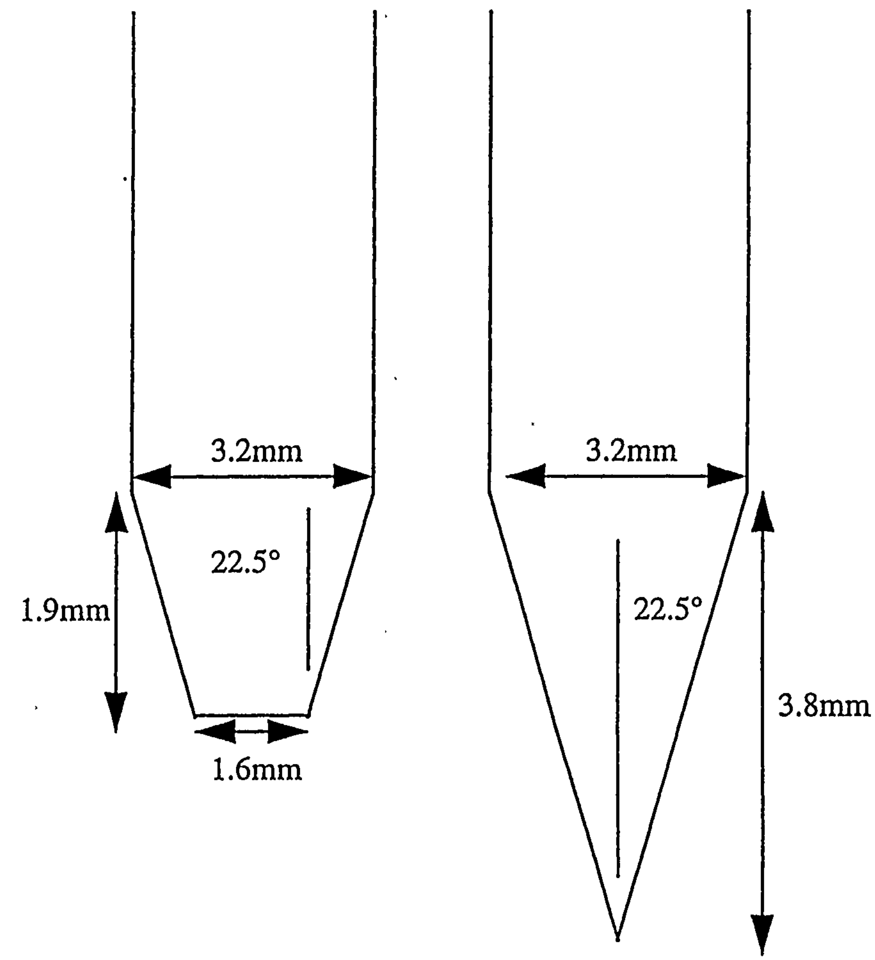

Mechanical Testing Results

U.S. Home Team

DIRECT DIFFUSION BOND METHOD

SPECIMEN IDENTIFICATION & Cu ALLOY BASE IF NOT OFHC	COATING	TIP	THERMAL TREATMENTS	TEST TEMP (°C)	FAILURE STRESS (MPa)
328	PS PPI-1 PVD Ni & Ni	45° 1/2 taper	1000ºC, 60min	280	129
329	PS PPI-2 PVD Ni & Ni	45° 1/2 taper	1000ºC, 60min	280	44
330, 358	PS fn Ni PVD Ni & Ni	45° 1/2 taper	1000ºC, 60min	280	175, 131
331	PS cs Ni PVD Ni & Ni	45° 1/2 taper	1000ºC, 60min	280	73
332	PS Cu PVD Ni & Ni	45° 1/2 taper	1000ºC, 60min	280	20
334	SUR-1	45° 1/2 taper	none	280	130
335	SUR-2	45° 1/2 taper	none	280	66
337	SUR-4	45° 1/2 taper	none	280	33
338	SUR-5	45° 1/2 taper	none	280	73
339	SUR-6	45° 1/2 taper	none	280	106
347	SUR-7	45° 1/2 taper	none	280	21
348	SUR-8	45° 1/2 taper	none	280	121
350	Cast Cu & PVD Ni	45° 1/2 taper	none	280	12
351	Cast Cu & PVD Ni	flat	none	280	151

Failure Stress Refers to Axial Stress in W Rod When Bond Failed

W/Cu Interfaces - Plasma Sprayed

U.S. Home Team

Interface Between W and Plasma Sprayed Cu with Ni Bond Coat

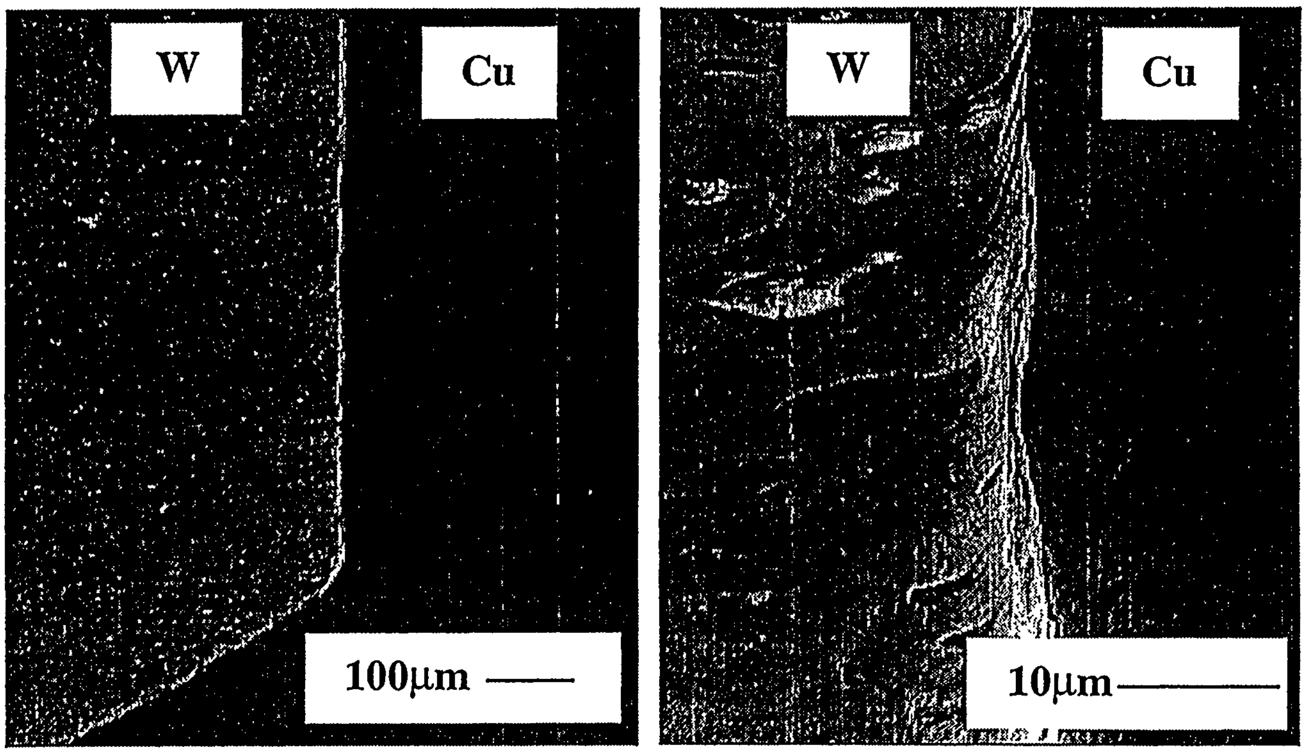

W/Cu Interfaces - Cast Method

U.S. Home Team

Reaction zones in
Cu at interface

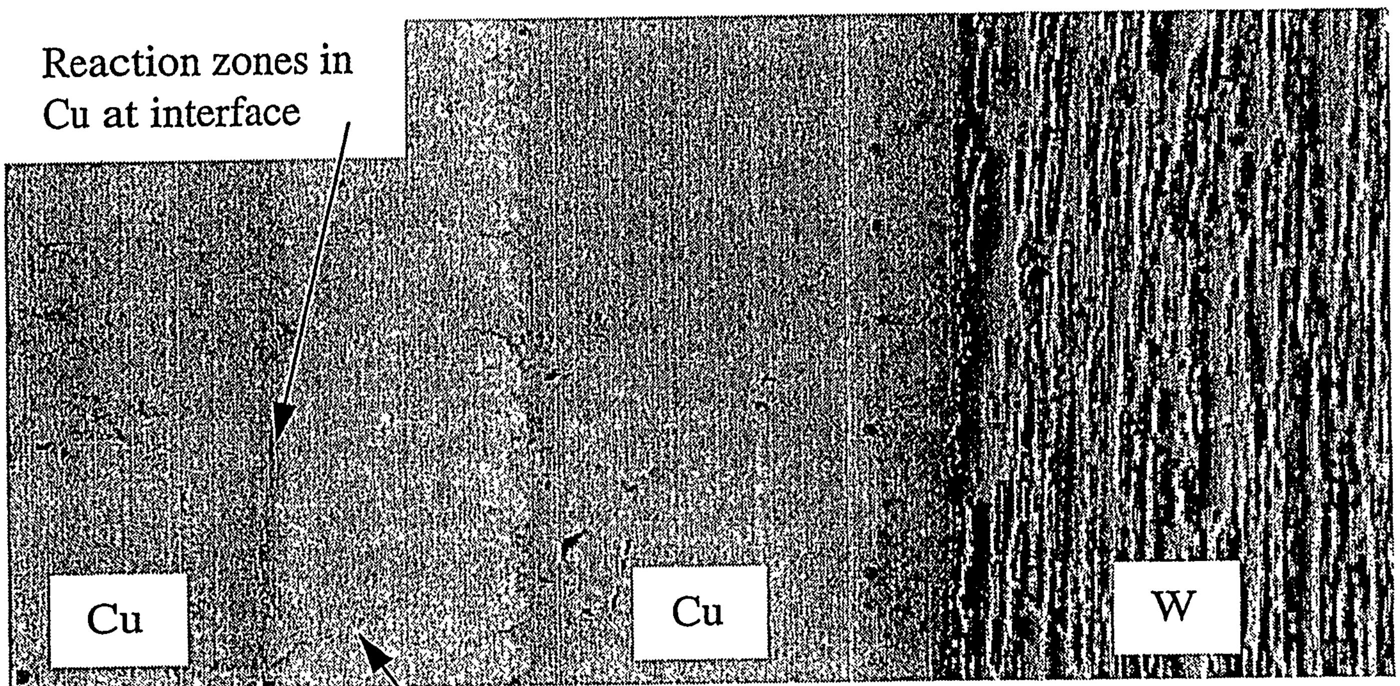

100μm thick Inconel 600 foil honeycomb cell wall

Cast Cu Around W Rod

U.S. Home Team

Specimen 393 - Grip Tube Slipped at 370MPa

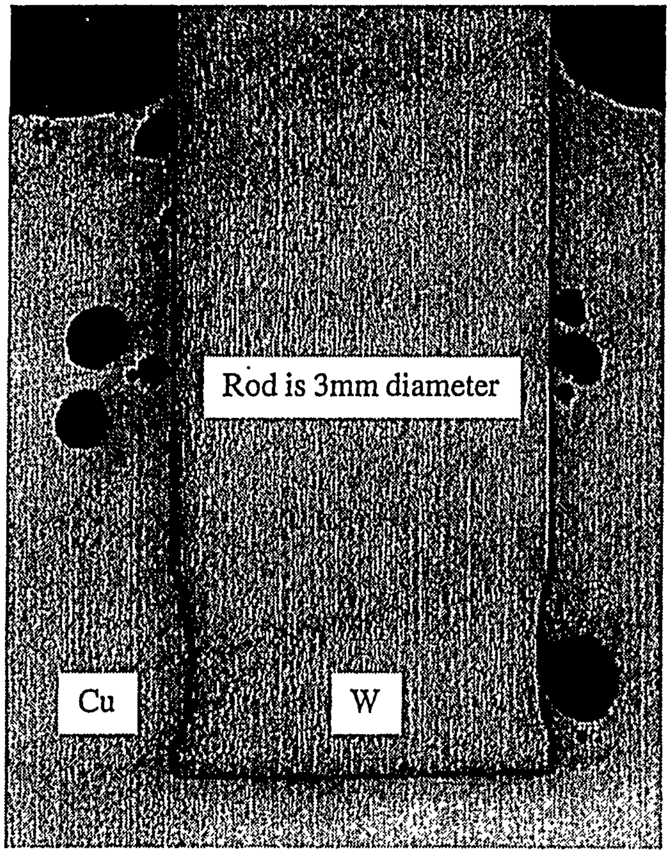

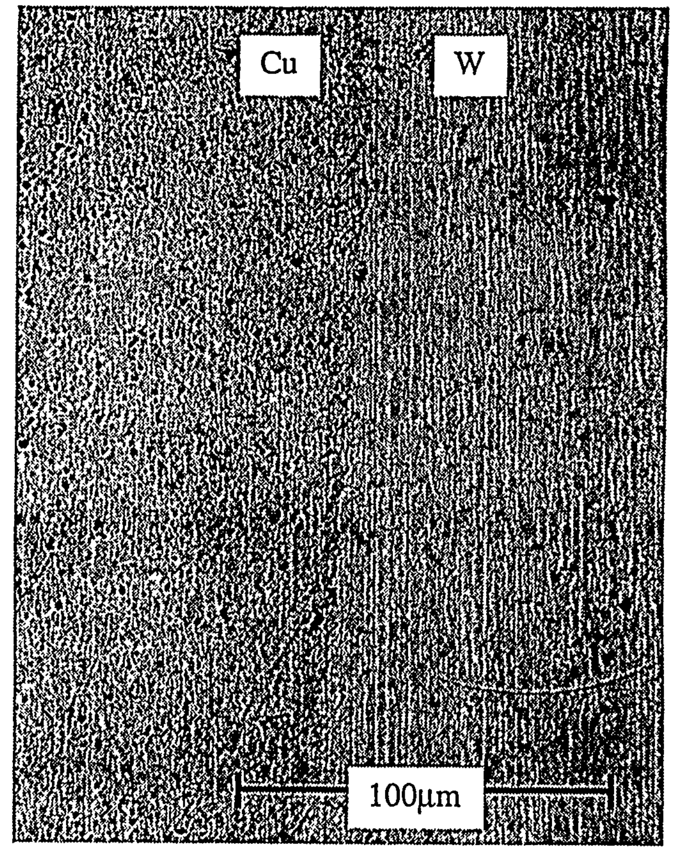

Direct Diffusion Bonded Joint

U.S. Home Team

Fractured W Rod from Crosshead Impact

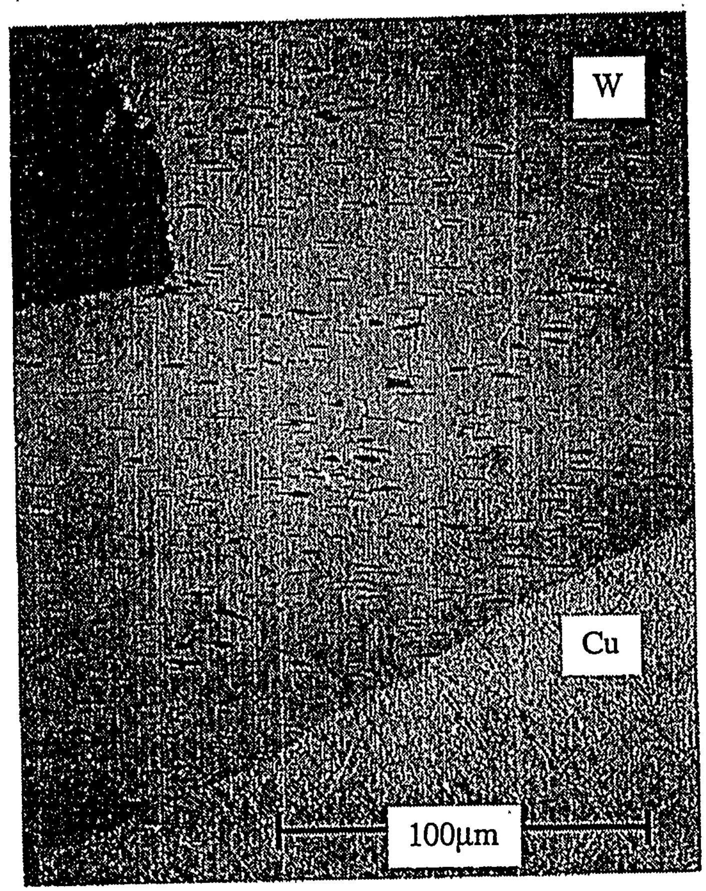

Tungsten Brush Mock-ups PW-9 and PW-4

U.S. Home Team

Mock-up PW-4
Plasma Spray
1.6mm dia Rods

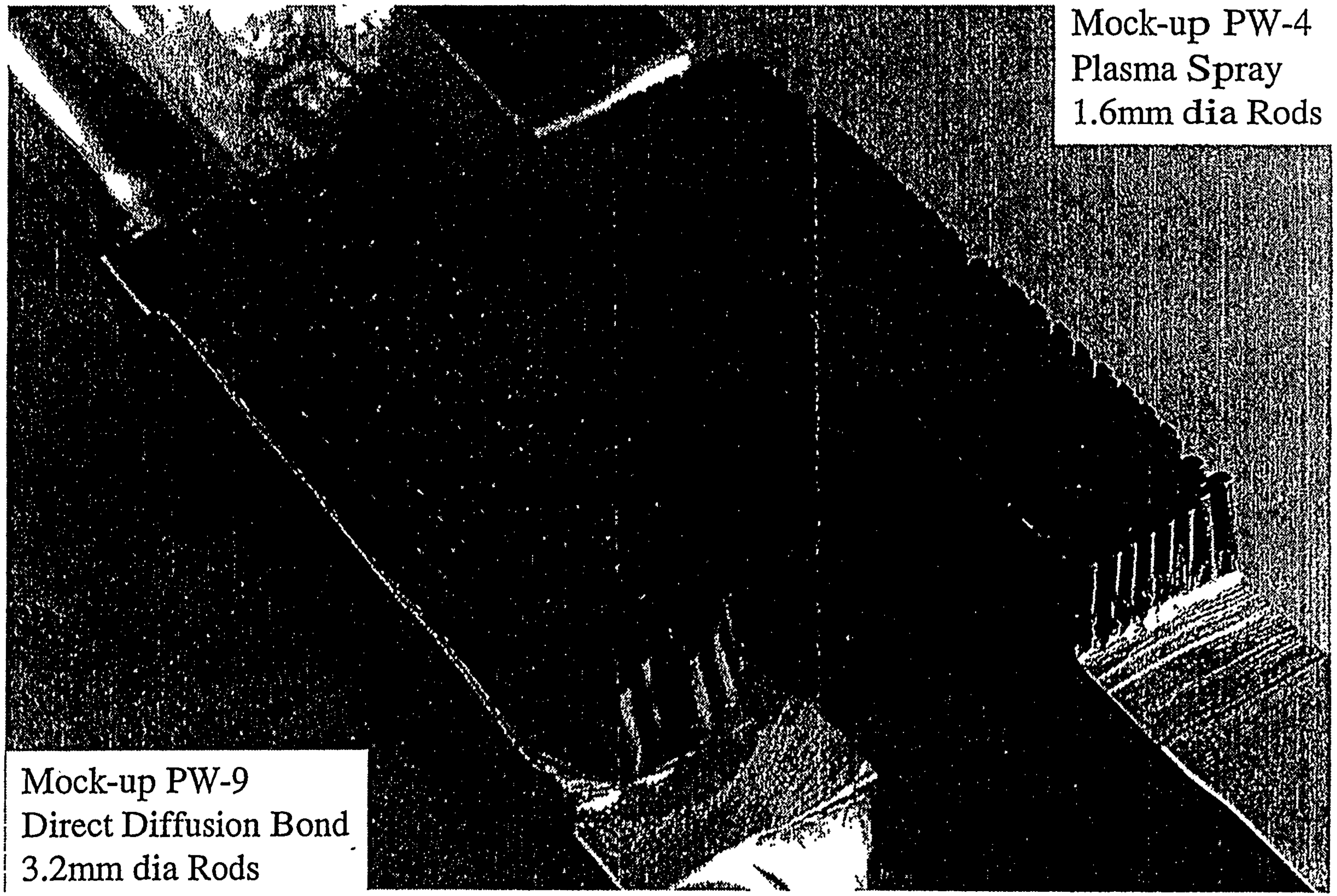

Mock-up PW-9
Direct Diffusion Bond
3.2mm dia Rods

Tungsten Brush Mock-ups PW-9 and PW-4

U.S. Home Team

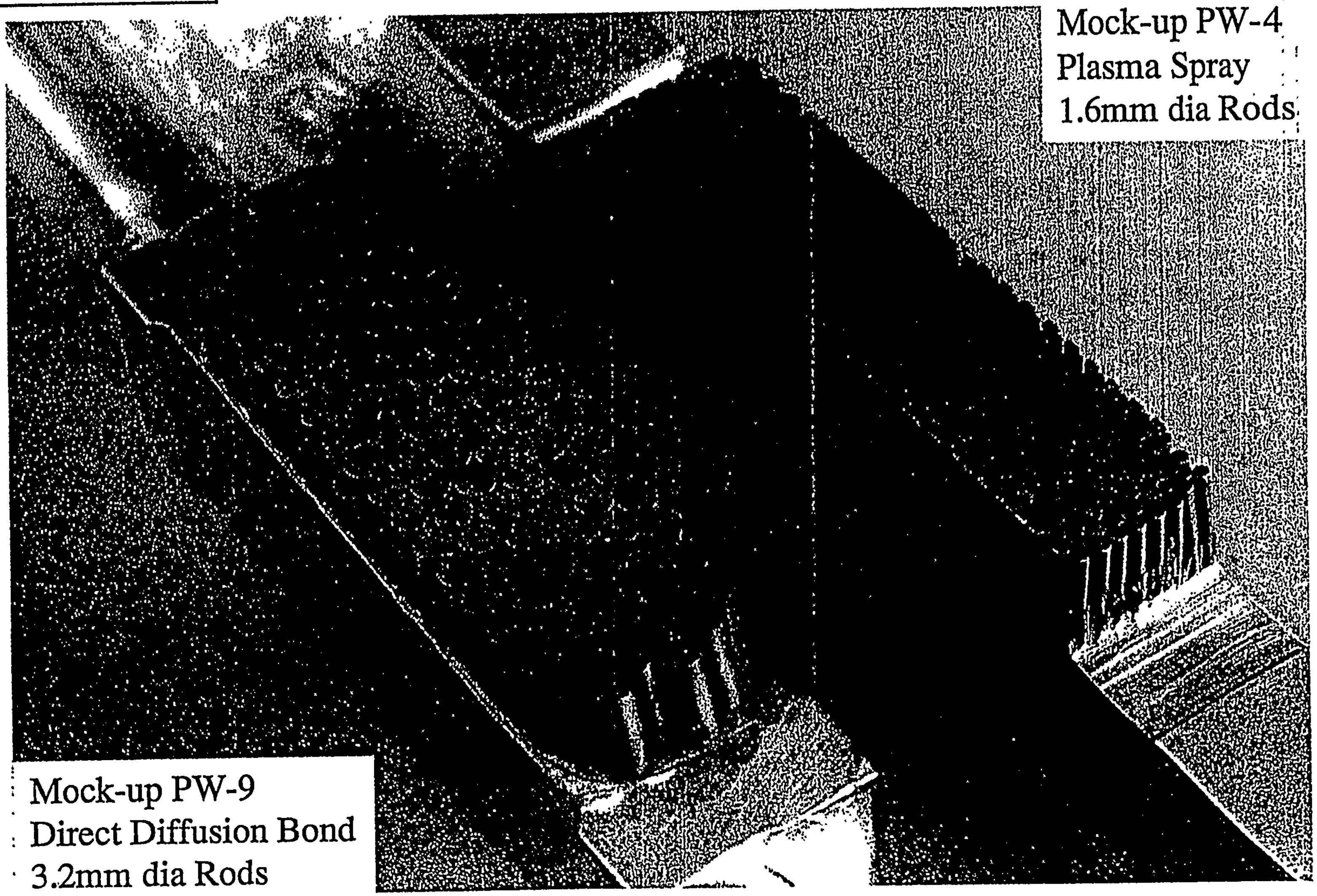

Mock-up PW-4
Plasma Spray
1.6mm dia Rods

Mock-up PW-9
Direct Diffusion Bond
3.2mm dia Rods

US-Japan Workshop on Plasma Material
Interaction and High Heat Flux Components,
December 8-11, 1997,
Sandia National Lab., San Francisco, US

Development of High Heat Flux Components at JAERI

K. Nakamura
JAERI

1. Overview
2. R&Ds on Divertor Component Development
3. Summary

Progress in 1997

- 1D/3D hybrid CFC was newly developed, and withstood up to a heat load of 20 MW/m^2, 15 s.
- 5 mm thick CVD-W was successfully coated on both OFHC Cu and W/Cu heat sink. Small divertor mock-ups meet the ITER steady-state heat load condition; 5 MW/m^2, 15 s for 1000 cycles.
- Full-scale length Vertical Target with W, CFC armors were successfully fabricated.
- SiC doped 1D CFC with high thermal conductivity and high thermal shock resistance has been developed.
- Neutron irradiation of Be, CFCs and CVD-W was finished at JMTR, and post-irradiated tests will be started soon.

ITER Divertor

Cross-section of ITER

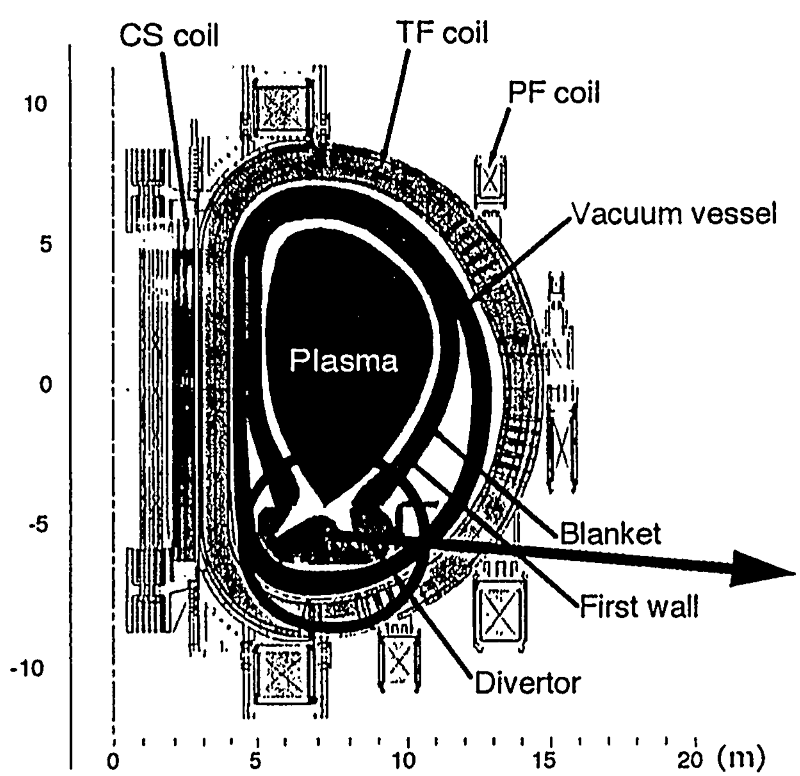

ITER Divertor Cassette

Dimension: 5mL x 2mH x 1mW

Weight: ~ 25 ton

60 Cassettes are toroidally mounted in the Vacuum Vessel.

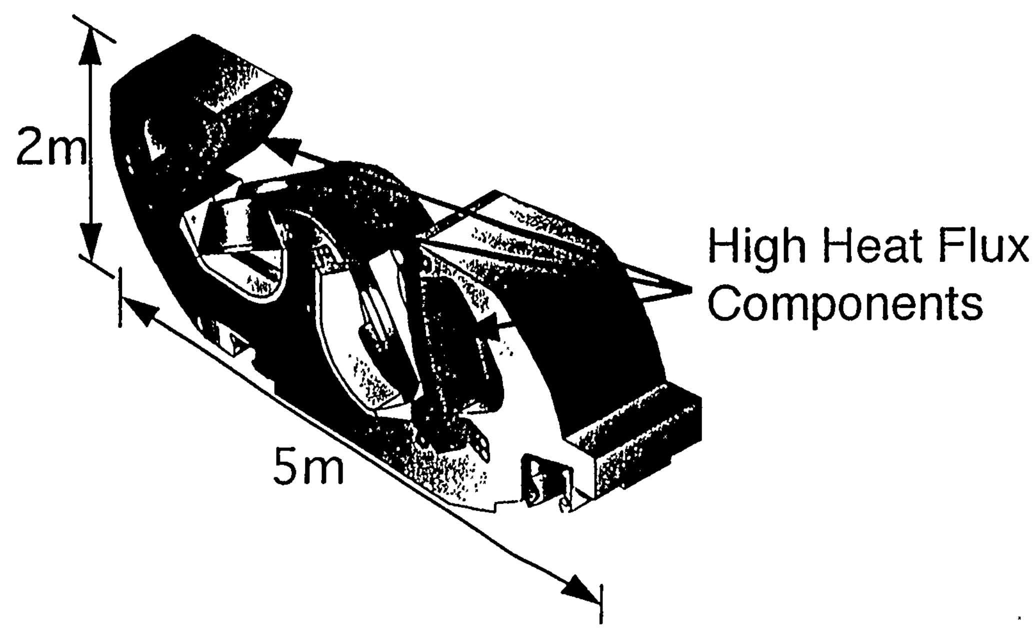

Divertor Cassette

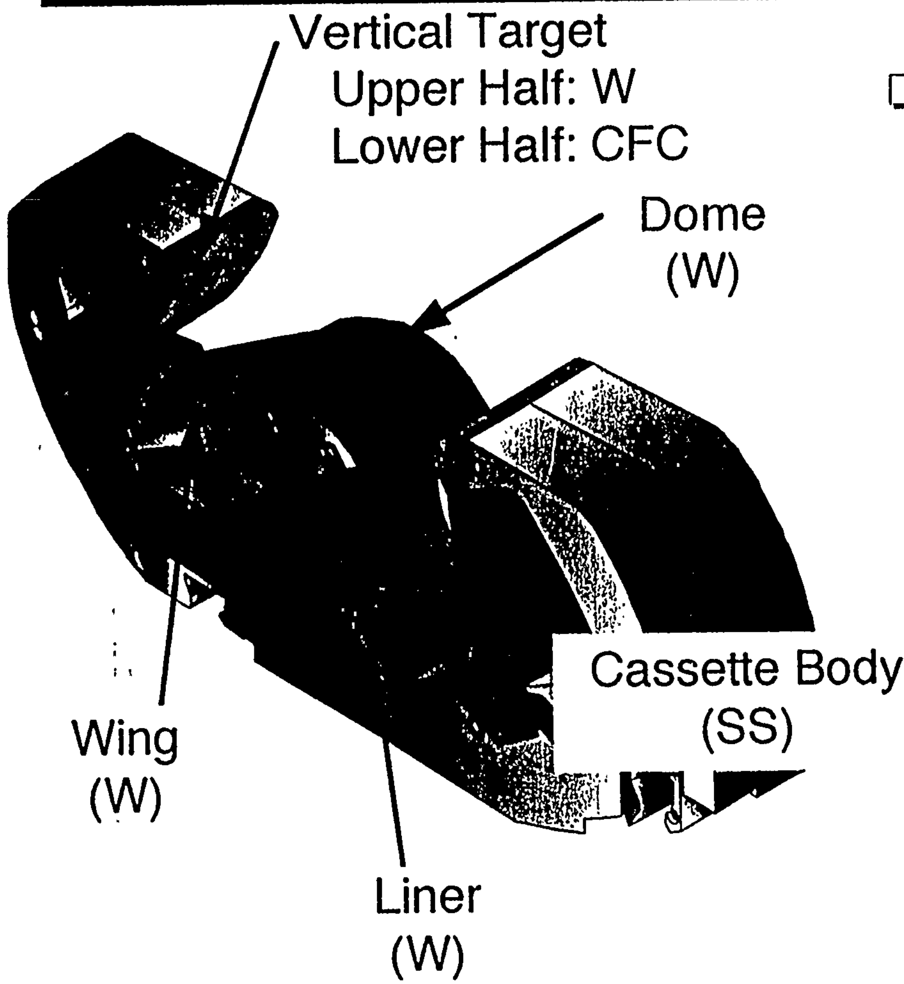

- Divertor Design
  - Surface Heat Load
    - —Steady State 5 MW/m^2
    - —Transient 20 MW/m^2 (less than 10 s)
  - Plasma Facing Materials
    - —CFC
    - —Tungsten (W)
    - —(Beryllium)
  - Structural Materials
    - —SS
    - —Cu alloy (for Cooling Tube)
  - Coolant Water

Major Design Parameters of ITER Divertor

Component	[redacted]	First Wall	
		Nominal	Limiter/Baffle
Normal Operation			
Steady-State Heat Load (MW/m^2)	0.2 - 5 (10)	0.25 - 0.5	3 - 5
Transient Heat Load (MW/m^2)	20	-	-
Incident Ion Flux($ions/m^2/s$)	$< 10^{24}$	$< 10^{20}$	$< 10^{20}$
Incident Ion Energy(eV)	< 100	100 - 500	100 - 500
Neutron Load (MW/m^2)	0.1 - 1	1	1
Plasma Disruption (Thermal Quench)			
Disruption Heat Load (MJ/m^2)	< 100	TBD	TBD
Duration (ms)	0.1 - 3	0.1 - 3	0.1 - 3
Cooling Conditions			
Coolant	Water	Water	Water
Inlet Pressure (MPa)	4	< 4	< 4
Inlet Temperature (°C)	140	TBD	TBD
Materials			
Plasma Facing Material	CFC, W	CFC, W, Be	CFC, W, Be
Structural Material	Cu alloy, SS	Cu alloy, SS	Cu alloy, SS

-1996 R&D-
3D-CFC Armored Divertor Mock-ups with Silver-free Braze

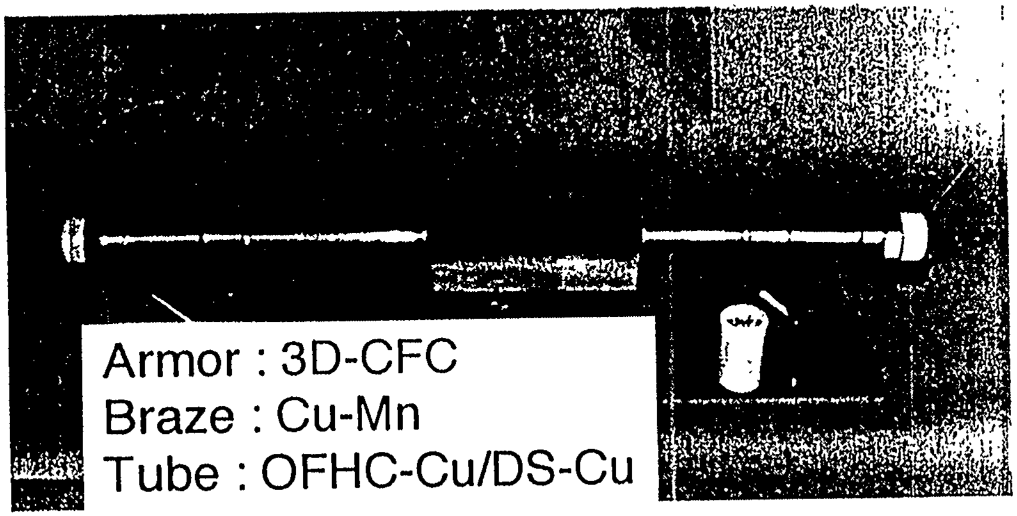

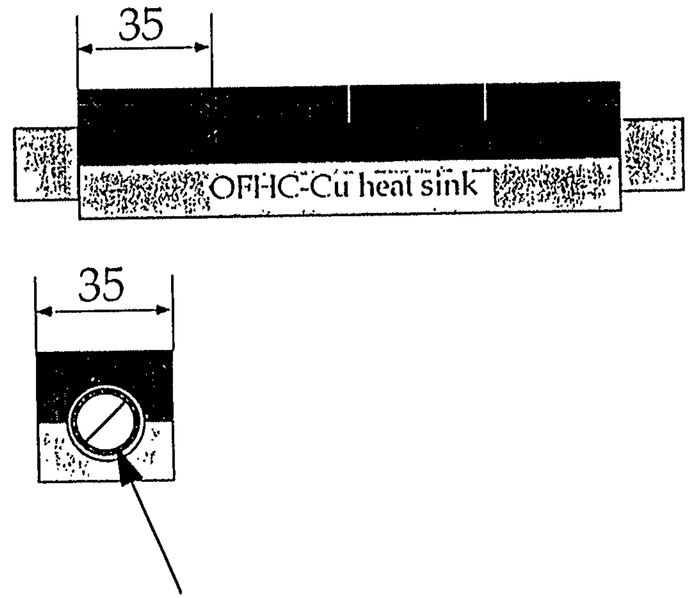

OFHC-Cu cladded DS-Cu tube
- outer skin : OFHC-Cu
- inner core : DS-Cu
- O.D./I.D. = 20/15

High Heat Flux Experiment on 3D-CFC Divertor Mock-up

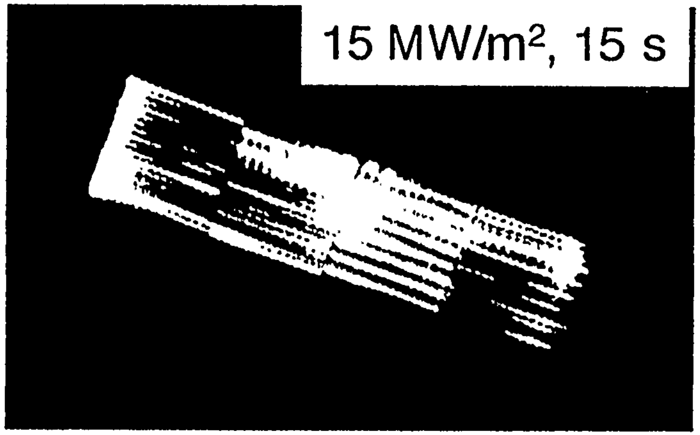

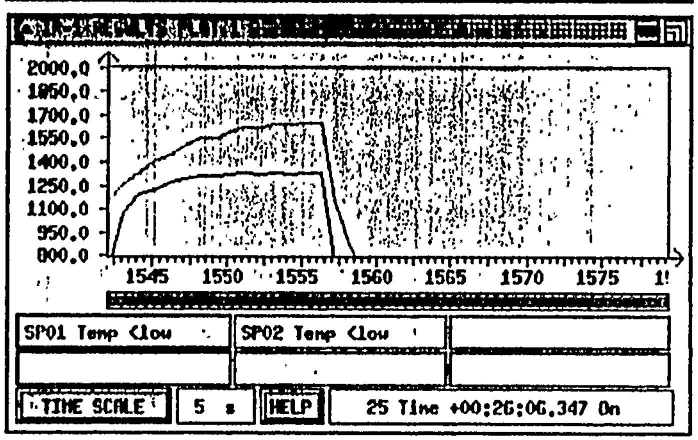

- 3D-CFC armor tiles silver-free-brazed on DSCu cooling tube endured a heat load of up to 15 MW/m^2, 15 s without failure.
- Fibers brazed onto the cooling tube and the heat sink were well cooled, while thermal conduction was not sufficient for fibers in other directions.
- To achieve higher thermal conduction between fibers, modification of fabrication method of 3D-CFC is on going.

1D/3D Hybrid CFC

1D/3D Hybrid CFC

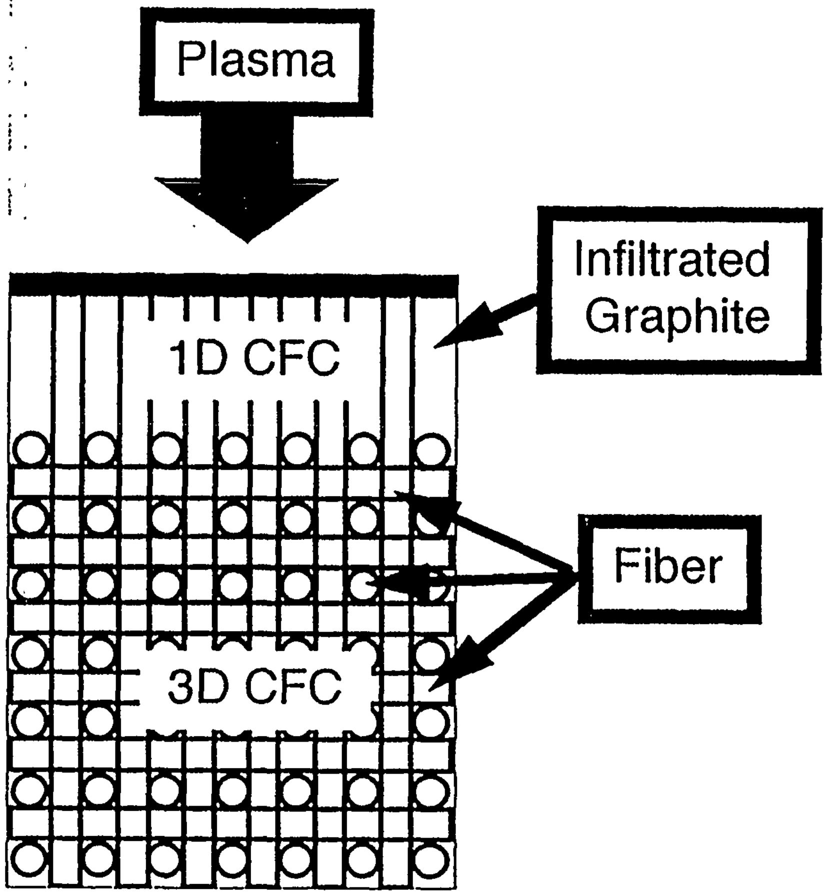

Cross-section of Hybrid CFC

- Full weaved CFC
- Graphite powder is infiltrated in the 1D part.
- Infiltrated graphite is highly graphitized to achieve high thermal conductivity.
- Thermal Conductivity;
  - in 1D = ~550 W/m/K
  - in 3D = ~450 W/m/K (at room temperature)

1D/3D Hybrid CFC withstands the ITER heat load requirement.

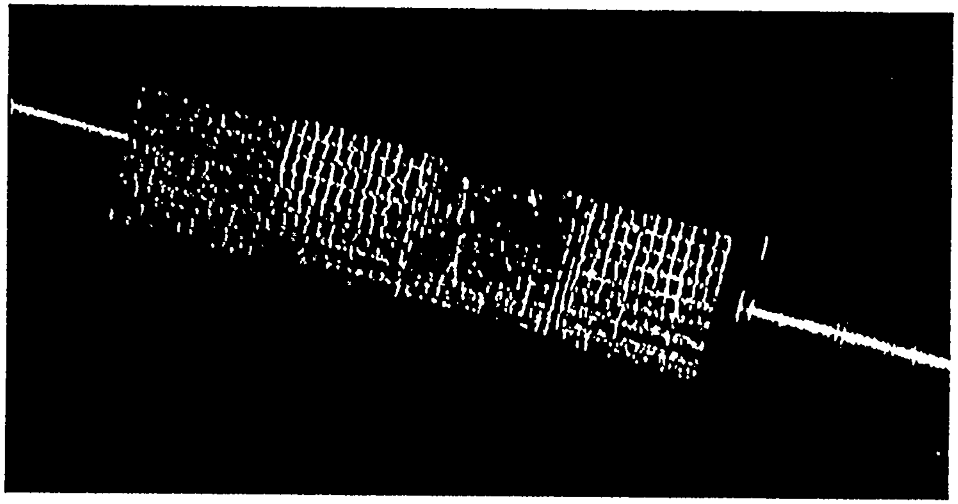

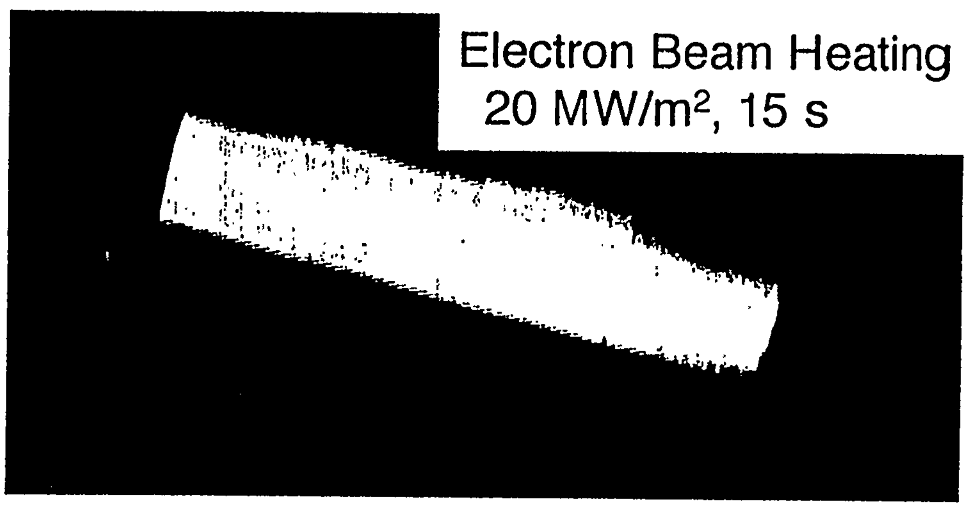

Electron Beam Heating
20 MW/m^2, 15 s

- The mock-up endured a heat load of 20 MW/m^2, 15 s.
- The armor surface is uniformly heated.
- The surface temperature is reduced, and local erosion of fibers are also reduced.

5 mm thick CVD-W layer was successfully coated on OFHC Cu and on W/Cu heat sinks.

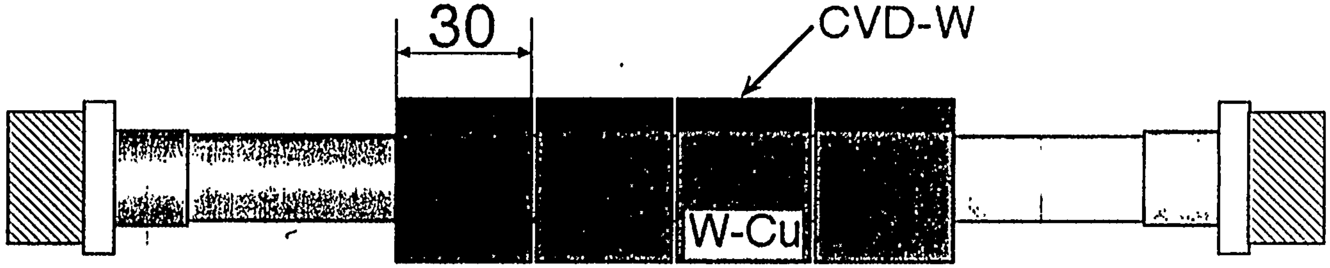

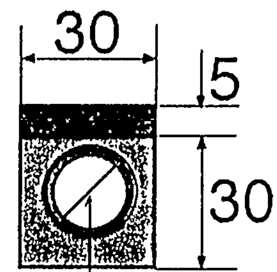

Inner core:DSCu
Outer layer:OFHC-Cu
Tape twist ratio:3

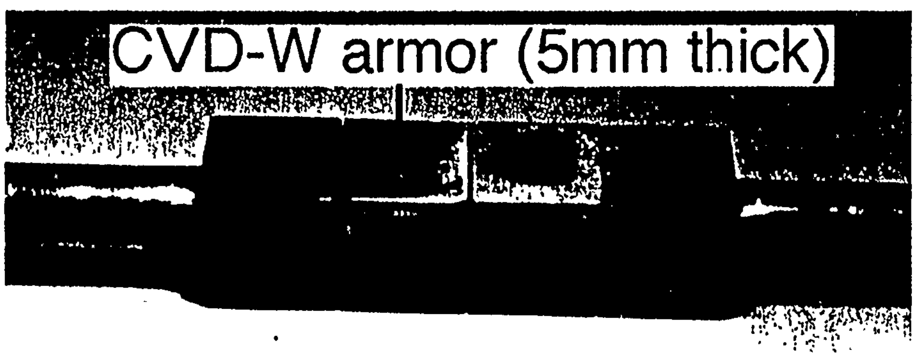

CVD process

Working gas : WF_6

$T_{env.}$: 700 -750 °C

Coating rate : $0.2mm^t/h$

Heating Tests on 5mm thick CVD-W coated on the W/Cu heat sink

Thermal cycling experiment
at 5 MW/m², 15s

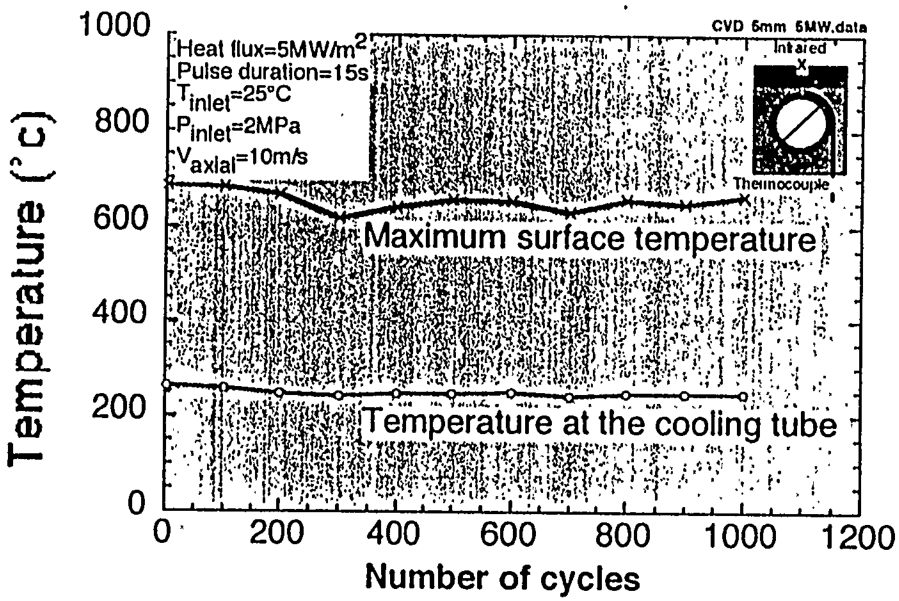

No degradation of bonding interface was found at the ITER steady-state heat load.

Screening experiment
at 20 MW/m², 15s

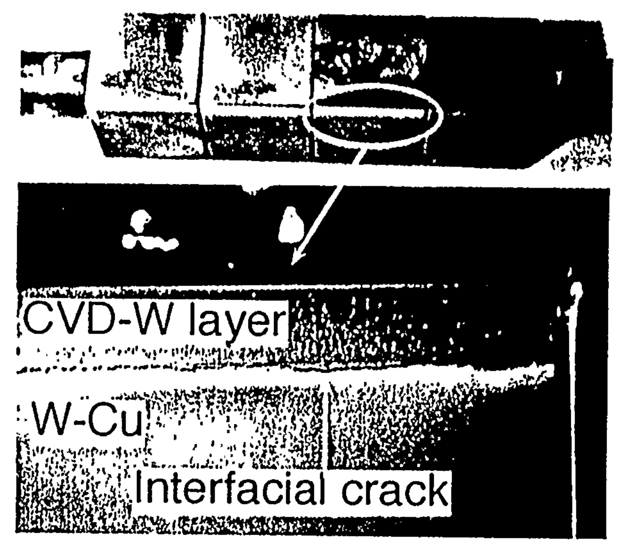

The mock-up survived up to 18 MW/m², though the surface was melted at 20 MW/m².

Further R&D's are necessary for coating on the OFHC-Cu heat sink.

- 5 mm thick CVD-W was coated on the OFHC-Cu heat sink.

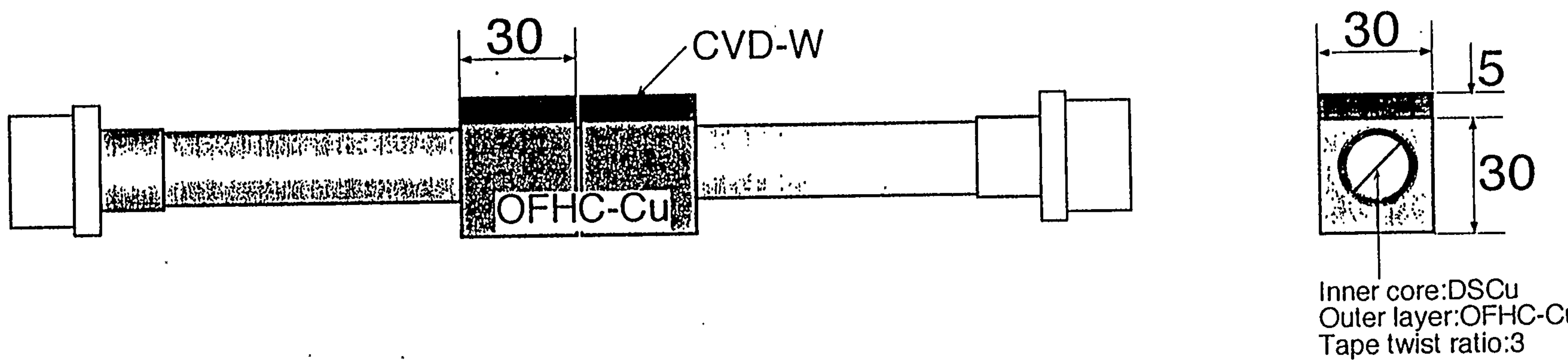

- Thermal cycling experiment at 5 MW/m^2, 15 s

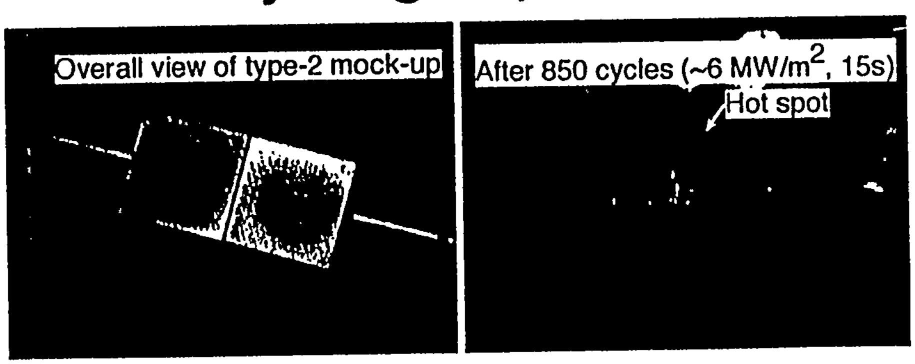

One tile survived more than 2,000 thermal cycles, but the other tile was detached after 850 cycles.

3 mm thick CVD-W was successfully coated on the cylindrical W/Cu heat sink.

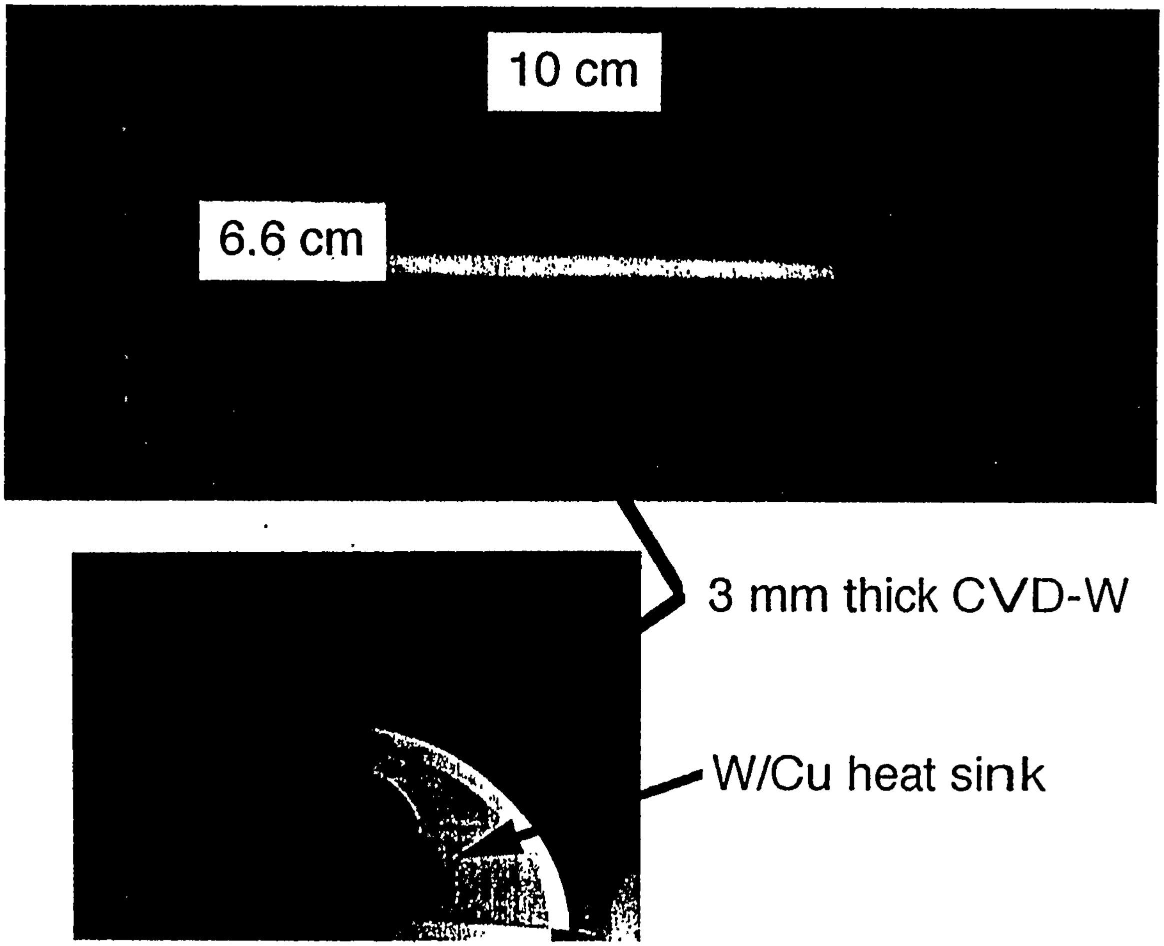

- The wing edge needs coating technique on a rounded surface.
- 3 mm thick CVD-W was coated on the cylindrical surface of W/Cu.

- 1996 R&D -
Full-scale Length Vertical Target Mock-ups

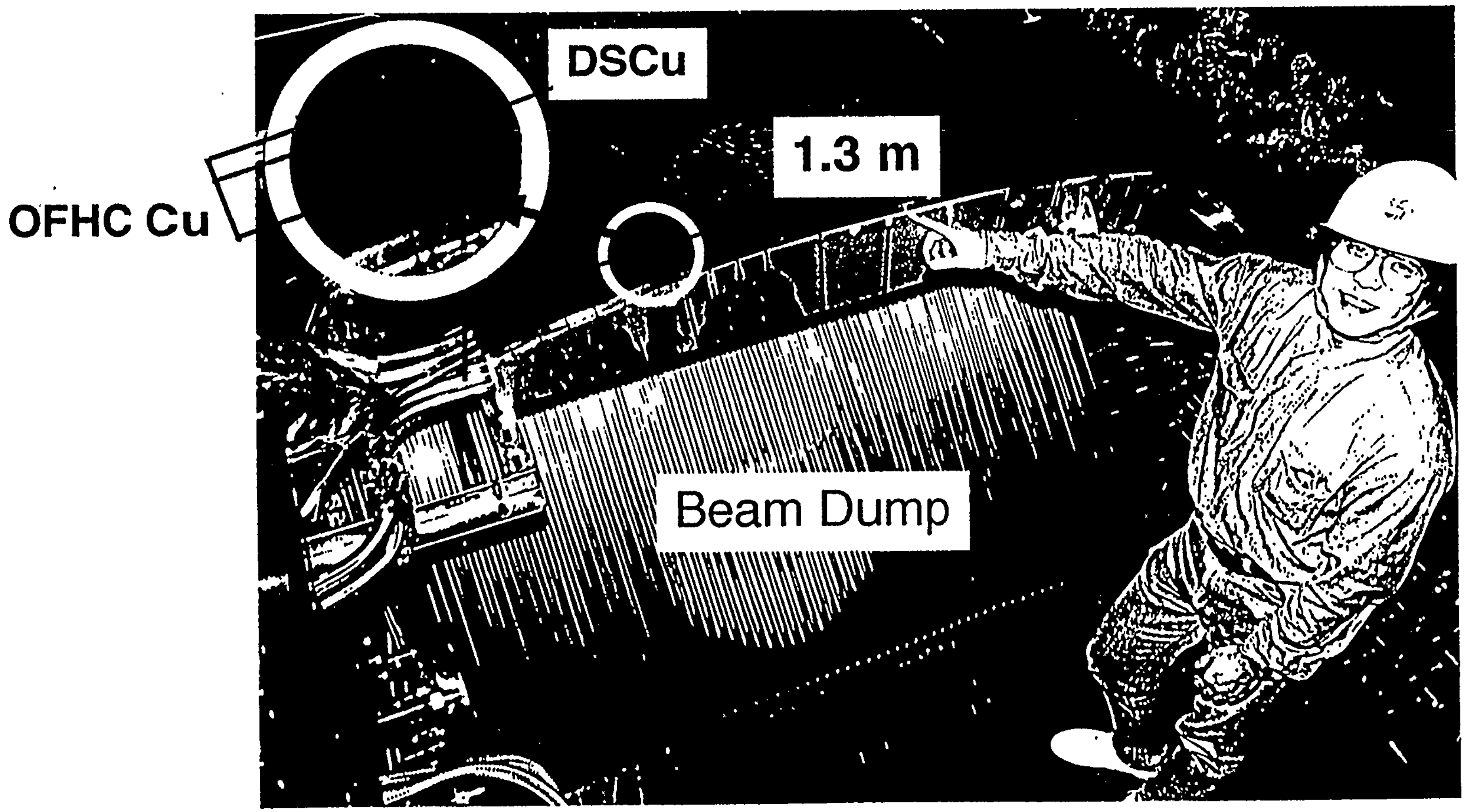

- 1996 R&D -
Heating Tests on Vertical Target Mock-ups

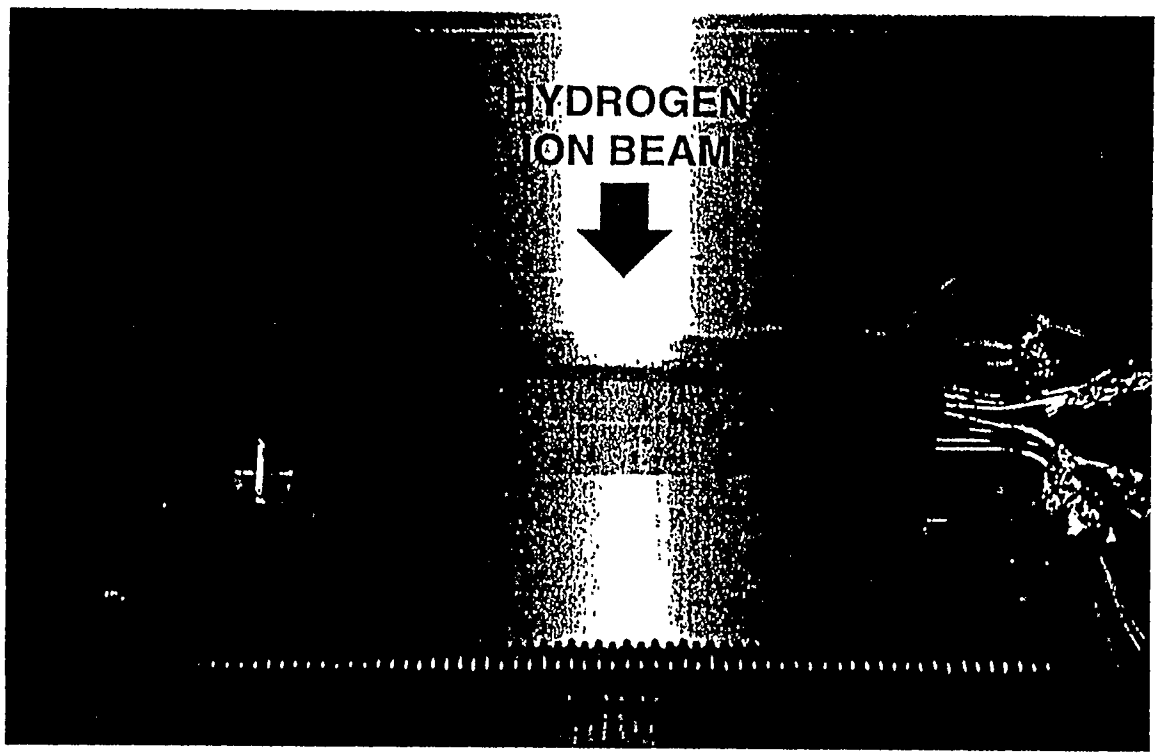

- The mock-up with the DSCu swirl tube withstood 20 MW/m^2, 15 s for 1,000 cycles.

Almost Full-scale Vertical Target was fabricated.

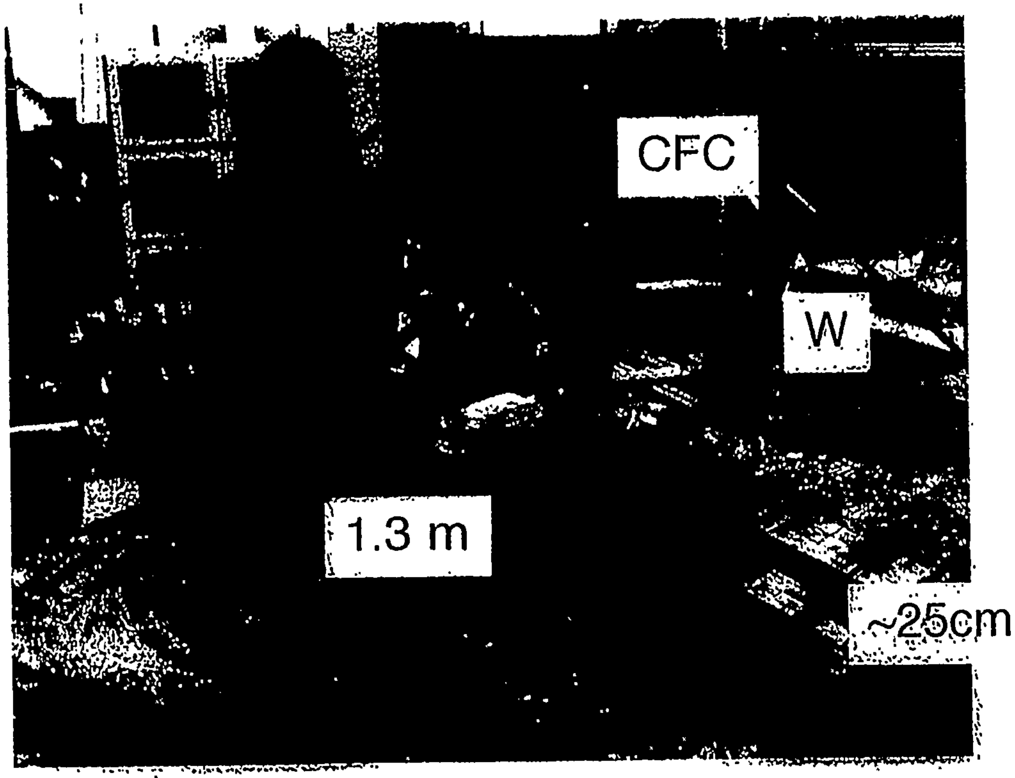

- (Almost) Full-scale Vertical Target (Inboard) was successfully fabricated, which consists of 8 elements. (The full-scale mock-up consists of 9 elements.)
- The upper half of the mock-up has W-armors, and the lower half has CFC-armors.
- 5 mm thick CVD-W armors are used for one element. 10 mm thick pure tungsten is used for one element, and 5 mm thick pure tungsten is used for 6 elements.
- Heating tests will start soon.

Weight Loss of Doped CFCs and Non-doped CFC with Electron Beam Irradiation

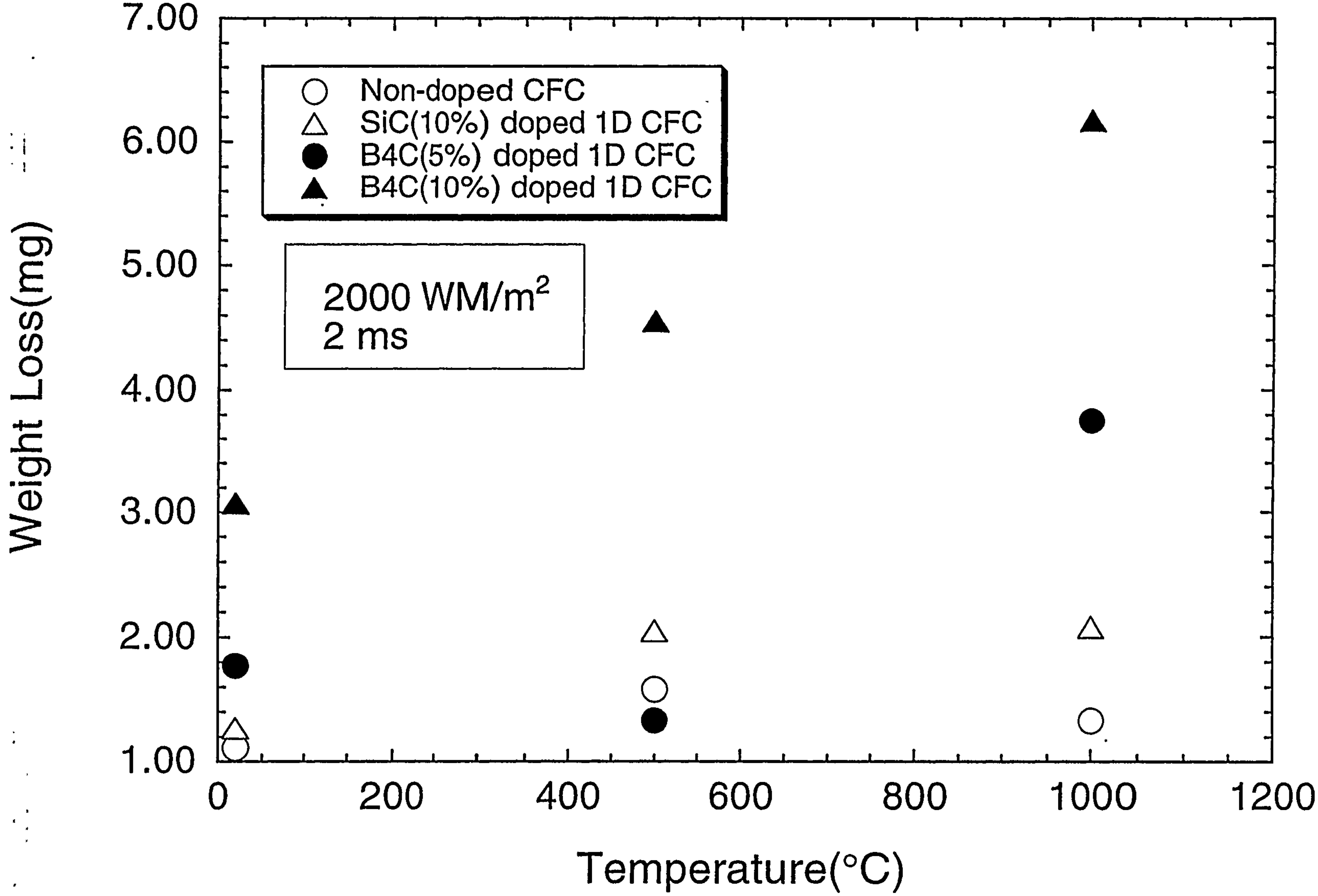

Non-doped CFC

SiC(10%) doped CFC

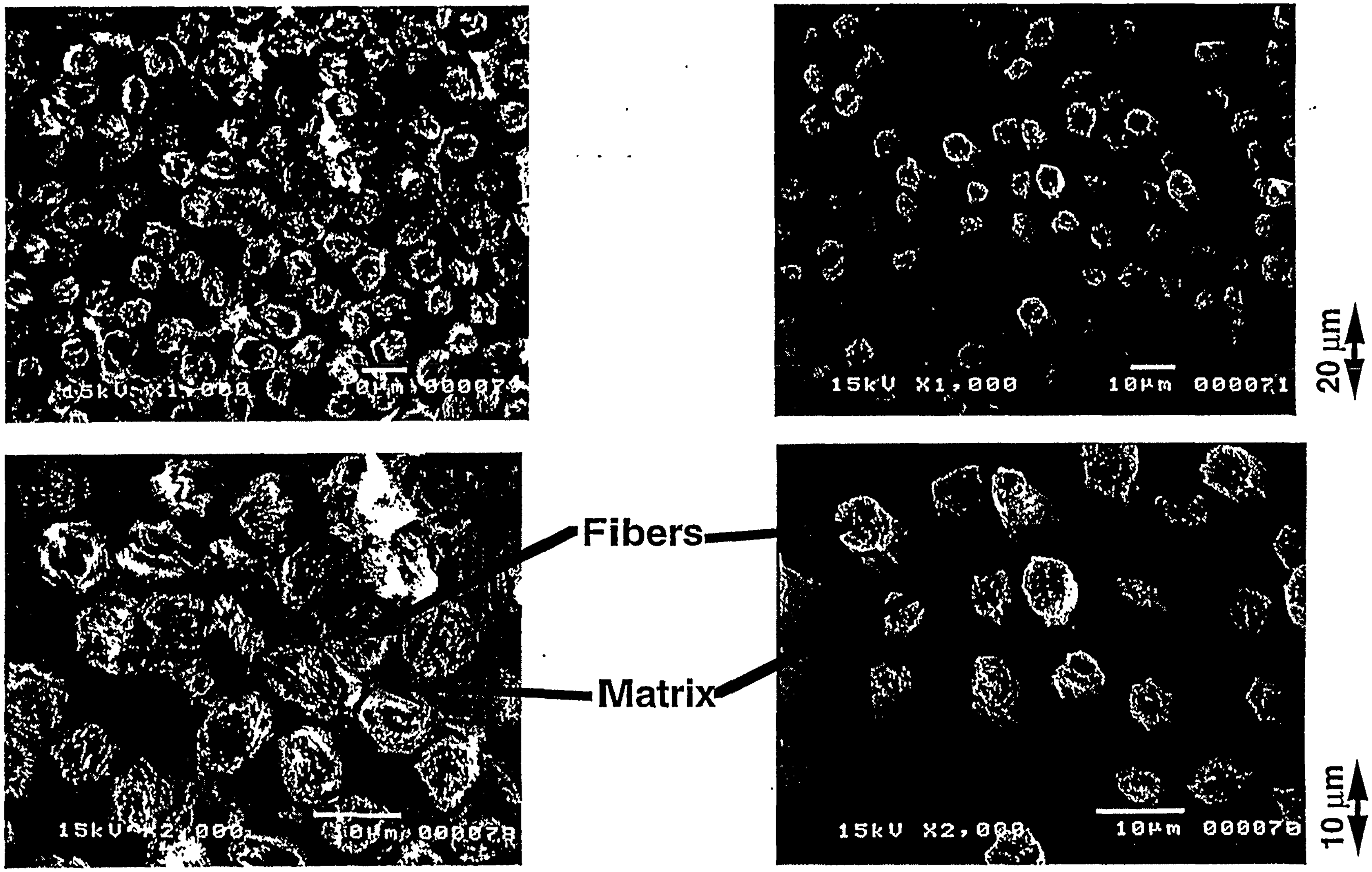

Photographs of electron irradiated SiC(10%) doped CFC and non-doped CFC with a heat flux of 1000MW/m^2 for 4ms at RT. The matrix part of SiC doped CFC was largely eroded comparing with that of non-doped CFC.

Non-doped CFC SiC(10%) doped CFC

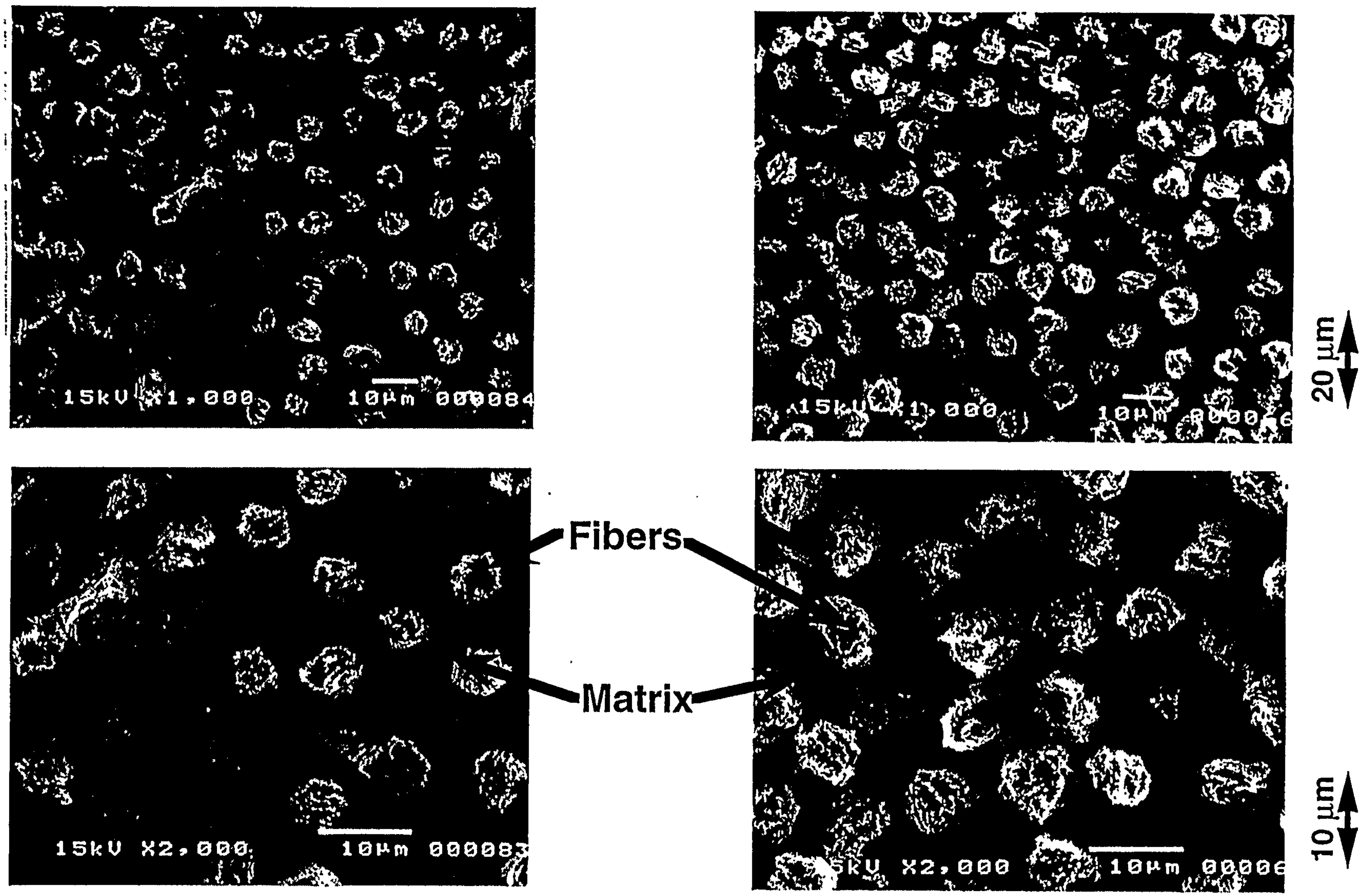

Photographs of electron irradiated SiC(10%) doped CFC and non-doped CFC with a heat flux of 1000MW/m^2 for 4ms at 500°C. The both matrix part of SiC doped and non-doped CFC were not so much eroded.

Non-doped CFC | SiC(10%) doped CFC

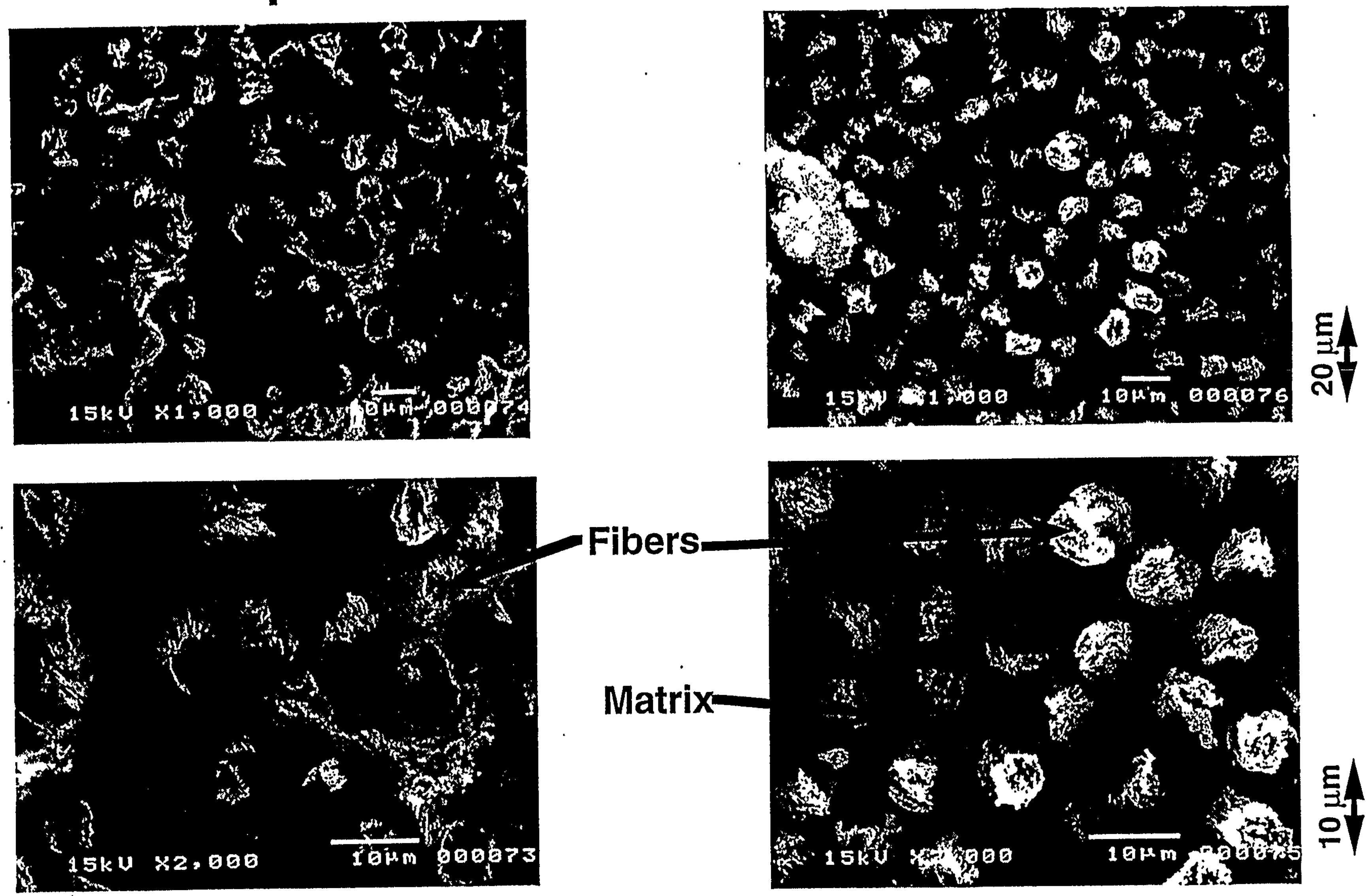

Photographs of electron irradiated SiC(10%) doped CFC and non-doped CFC with a heat flux of 2000MW/m^2 for 2ms at 1000°C. The both matrix part of SiC doped and non-doped CFC were largely eroded.

Schedules of Neutron Irradiation and Post-irradiated Tests

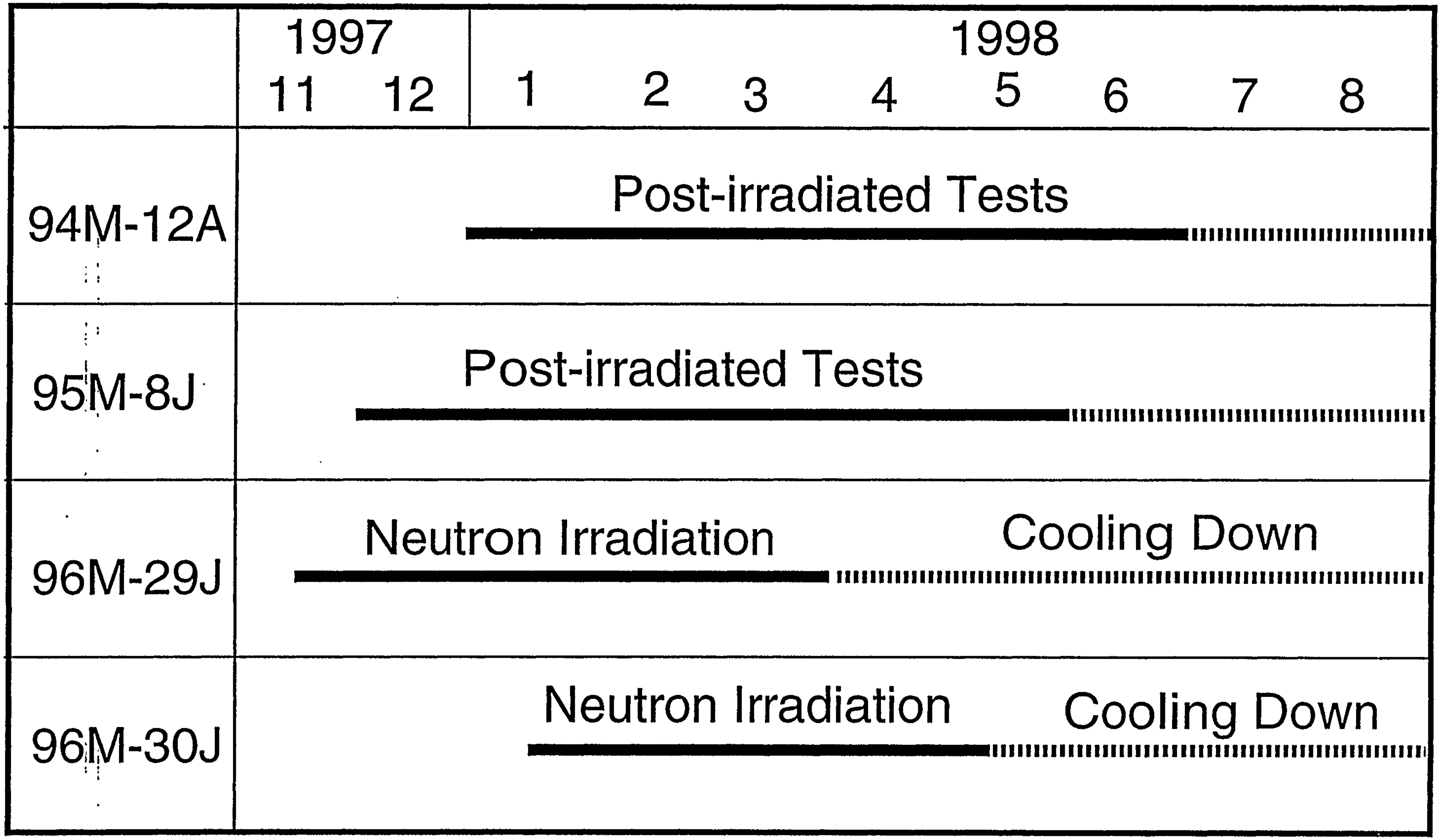

Neutron Irradiated Samples in JMTR

94M-12A(0.925 dpa, 400~500 °C, already irradiated):

- Thermal conductivity test

  MFC-1(2), CX-2002U(2), PCC-2S(2), Be(2), OFCu(2), DSCu(2), MFC-1/OFCu(2), MFC-1/DSCu(2)

- Tensile strength test

  MFC-1/OFCu(4), Be/OFCu(4), MFC-1/DSCu(4), Be/DSCu(4)

- Bending test

  CX-2002U(1), Be(1), OFCu(1), DSCu(1), MFC-1/OFCu(3), Be/OFCu(3), MFC-1/DSCu(3), Be/DSCu(3)

95M-8J(0.3~0.7 dpa, 300~400 °C, already irradiated):

- Thermal fatigue test

  MFC-1/OHCu(2), CVD-W/OHCu(4), Be/OHCu(6)

- Disruption erosion test

  MFC-1(4), CX-2002U(4), NIC-01(4), CVD-W(10), Be(15)

96M-29J(8.3×10^{19} n/cm^2, ~200°C, under irradiation):

- Thermal conductivity test

  DSCu(3), CuCrZr(2)

- Tensile strength test

  OFCu(2), DSCu(2), CuCrZr(2)

- Bending test

  OFCu(1), DSCu(2), CuCrZr(1),

- Thermal fatigue test

  CVD-W/OFCu(2), MFC-1/OFCu(2), CX-2002U/OFCu(2), NIC-01/OFCu(2)

- Disruption erosion test

  MFC-1(2), CX-2002U(2), NIC-01(2), CVD-W(4), P-W(4), Be(4)

96M-30J(6.5×10^{19} n/cm^2, 300~500°C, to be irradiated soon):

- Thermal conductivity test

  CVD-W(2), P-W(2), 1D CFC(MFC-1 grade)(2), NIC-01(2)

- Tensile strength test

  P-W(4), MFC-1(1), 1D CFC(MFC-1 grade)(2), CX-2002U(1), NIC-01(2), PCC-2S(1)

- Bending test

  P-W(4), MFC-1(1), 1D CFC(MFC-1 grade)(2), NIC-01(2), PCC-2S(1)

- Disruption erosion test

  P-W(12), 1D CFC(MFC-1 grade)(3), NIC-01(3)

SUMMARY

- 1D/3D hybrid CFCs are promising as an armor material.
- A divertor with 5 mm thick CVD-W armors can meet ITER requirement.
- Full-scale Vertical Target with W, CFC armors were successfully fabricated. Heating tests will start soon. Full-scale length Wing with CFC armors are also going to be ready soon.
- SiC doped 1D CFC is also promising as an armor material.
- Post-irradiation tests will give us very useful information for evaluation of armor material.

II-76

Be-Cu Joining Technologies for Plasma Facing Components in the ITER Fusion Reactor

B.C. Odegard Jr, C.H. Cadden, R.D. Watson

Sandia National Laboratories

and

K.T. Slattery

The Boeing Co.

Topics

- Introduction
- Beryllium-Copper Joining Technology
    - I. Plasma Spraying
    - II. Brazing
    - III. Diffusion Bonding
- Summary
- Future Studies

II-78

Challenges to Beryllium-Copper Joining

- Be is chemically reactive with most elements in forming brittle intermetallics. Exceptions are:

  Ge, Si, Al, Ag

- Be has limited room temperature tensile ductility (~5%)

- Coefficient of Thermal Expansion (μm/m-K)

Be -	11.6
Cu -	16.8
Al -	23.6
AlBeMet-150 -	17.6

Aluminum seemed the most promising both as a filler metal and a compliant layer.

Beryllium Reacts with the Copper Alloy at Bonding Temperatures

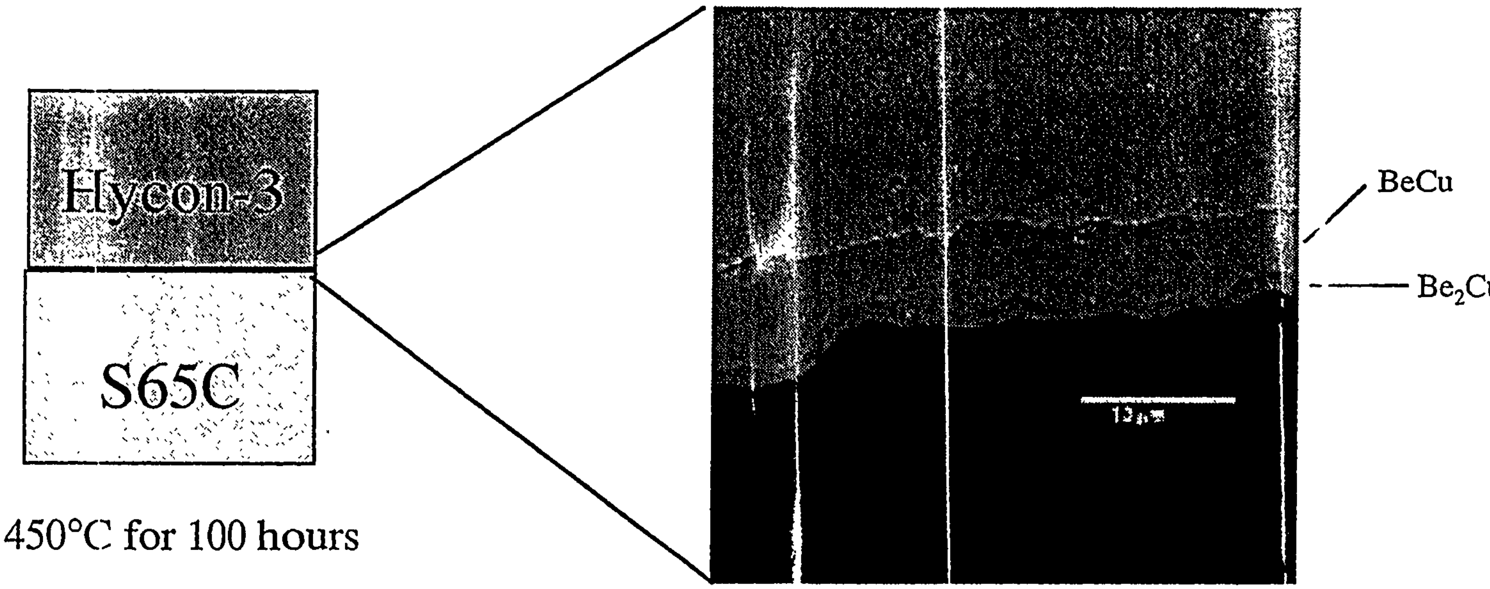

450°C for 100 hours

Beryllium reacts with copper to form two intermetallic phases BeCu and Be_2Cu. A better bonding solution would be to use a diffusion barrier to eliminate this strong, brittle phase.

(Kawamura and Kato, US-Japan Workshop, Jackson Lake, 1995)
(Odegard et al, Proc. Nuclear Fusion Tech., Tokyo, 1997)

Beryllium-Aluminum Phase Diagram Predicts no Intermetallics and Low Solubility

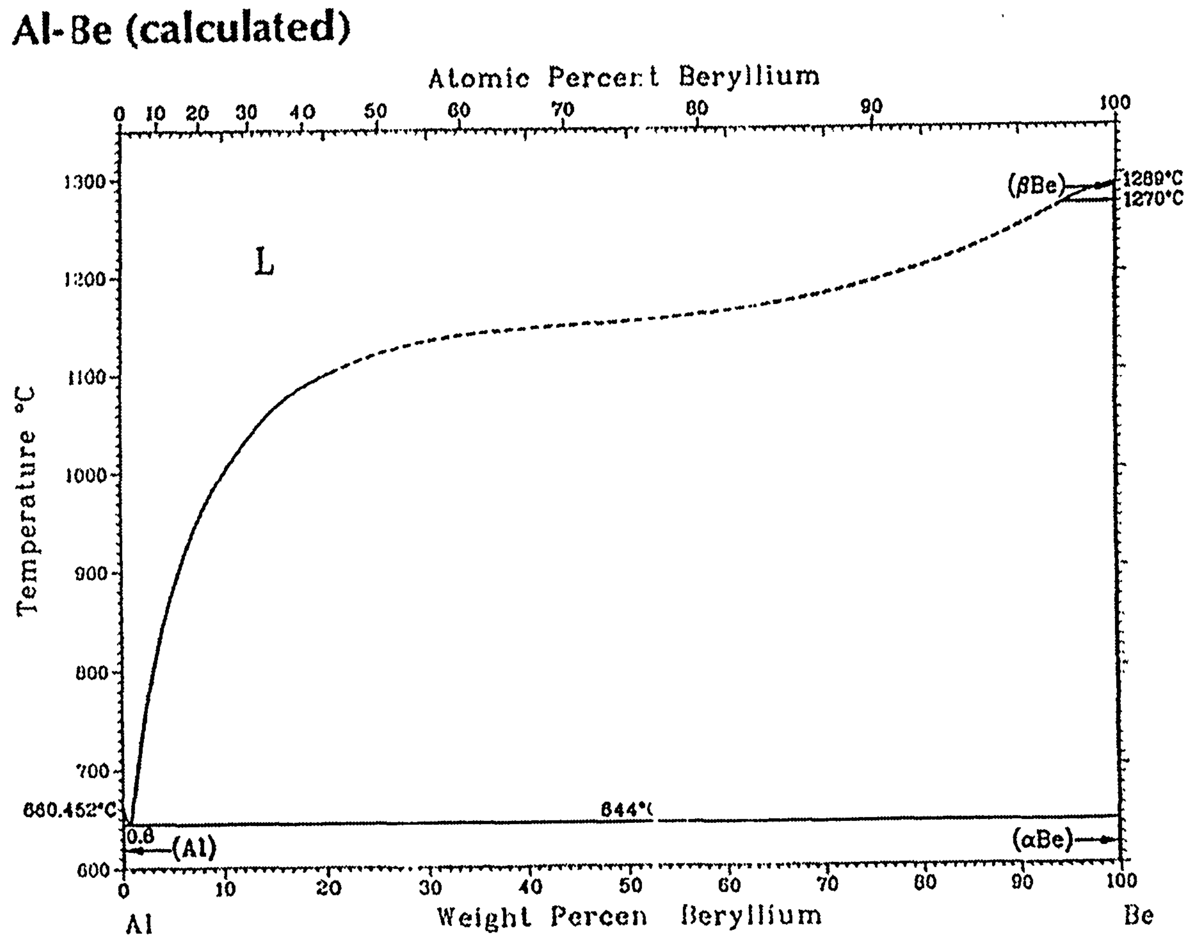

Aluminum-Copper Phase Diagram

- Phase diagram predicts several intermetallics, 10% Cu solubility in Al with no intermetallics.

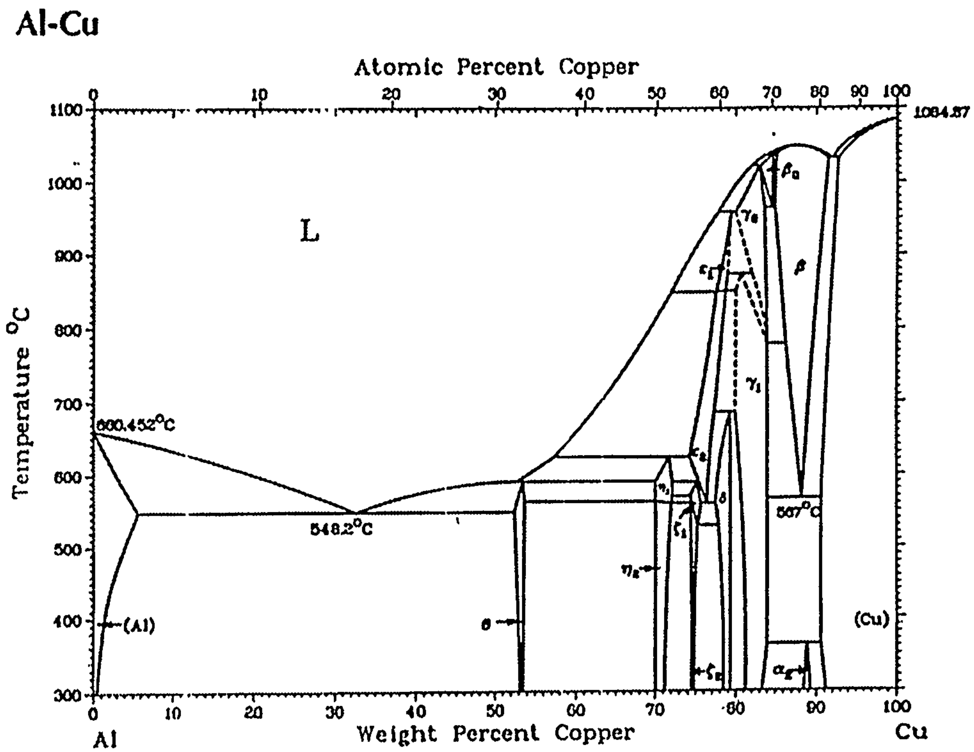

Joining aluminum to copper without a diffusion barrier was a problem.

II-81

Explosive bonding is an effective method of bonding 1100-Al or AlBeMet-150 to copper alloys.

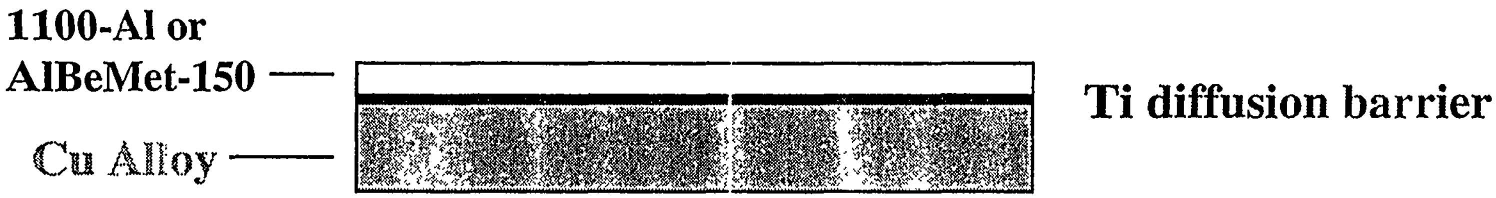

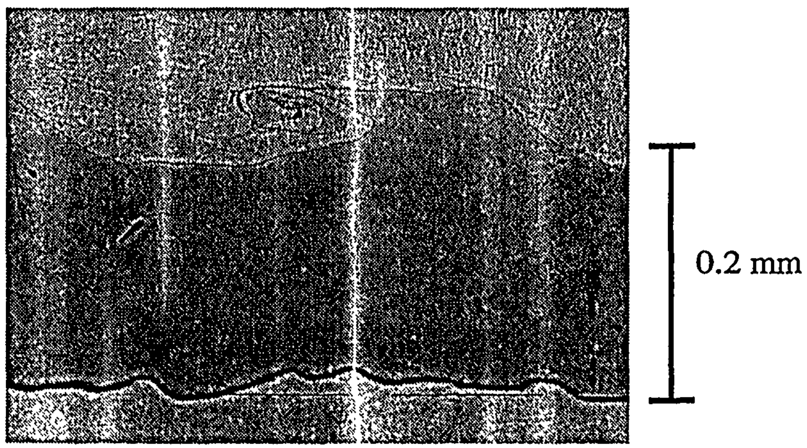

Beryllium to Copper Joining Technology

- I. Beryllium Plasma Spraying:
  1. directly on copper heat sink
  2. directly on an aluminum compliant layer
  3. as an *in situ* repair of beryllium tiles
- II. Brazing:
  1. directly onto an aluminum compliant layer
  2. directly onto an aluminum composite (AlBeMet-150)
- III. Diffusion Bonding:
  1. directly onto an aluminum compliant layer
  2. directly onto an aluminum composite (AlBeMet-150)

Plasma Sprayed Beryllium on Copper

- LANL Vacuum Plasma Spray Facility developed process which produces high density Be deposits.
- Negative transferred arc (cathodic) cleaning of substrate removes surface oxides prior to spray deposition
- Process could be utilized for both initial fabrication and *in-situ* repair

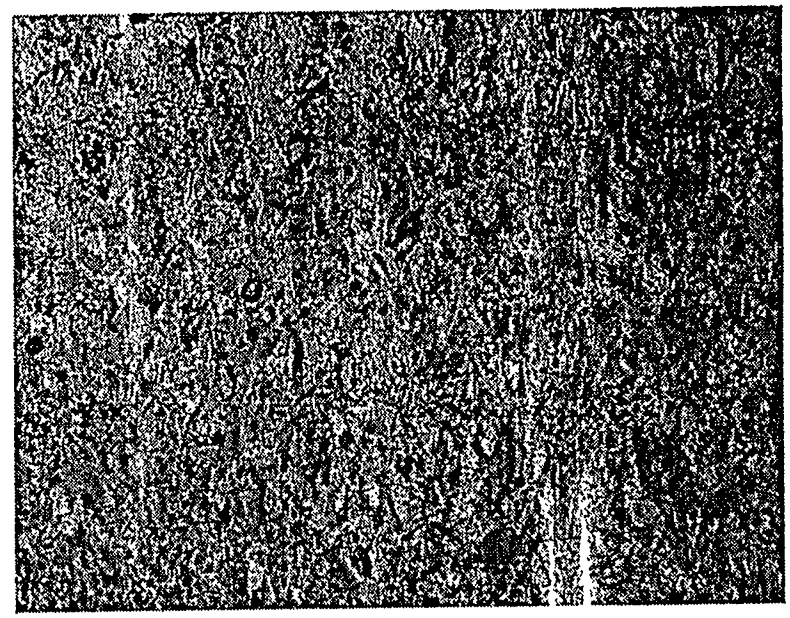

Micrograph of as-plasma sprayed Be

Vacuum plasma sprayed Be can produce Be/Be, Be/Cu and Be /Al specimens possessing good strength.

Bond Strength

VPS Be / HP Be: **110 - 220 MPa**

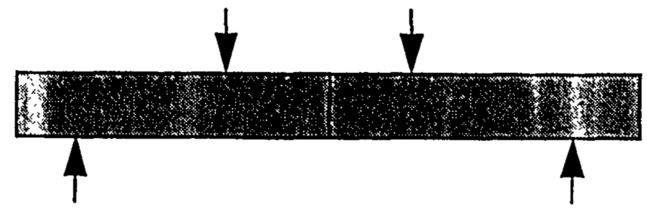

VPS Be / Cu: **~70 MPa**

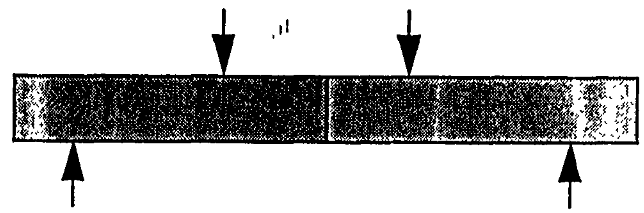

VPS Be / Al: **~120 MPa**

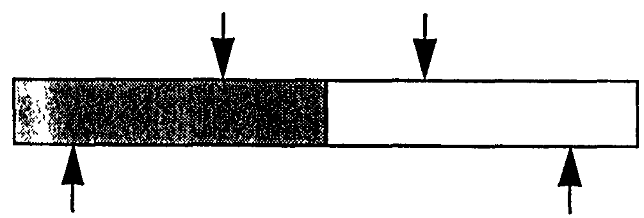

Vacuum Plasma Sprayed Be/Cu EBTS Specimens

- Be on CuNiBe

  Cu cooled during spraying to minimize Be/Cu intermetallic formation

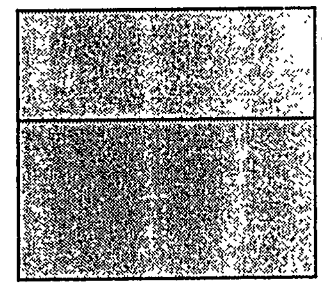

- Be on Al-coated CuCrZ

  Cu cooled during spraying to prevent melting of Al

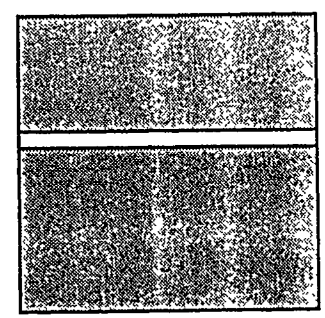

High Heat Flux Test (EBTS) Specimen

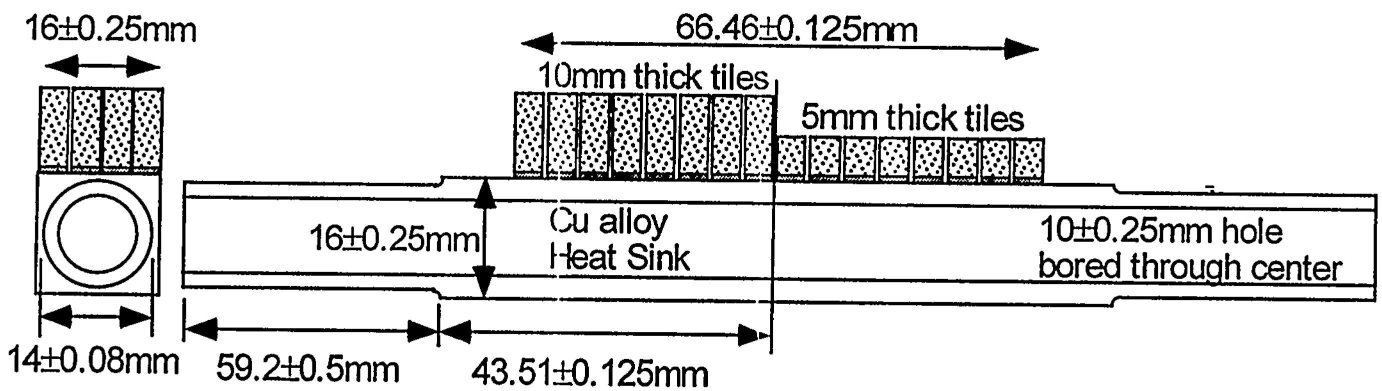

Actively cooled high heat flux sample geometry used at the EBTS facility at Sandia National Laboratories-New Mexico

Vacuum Plasma Sprayed Beryllium-Copper EBTS Specimens

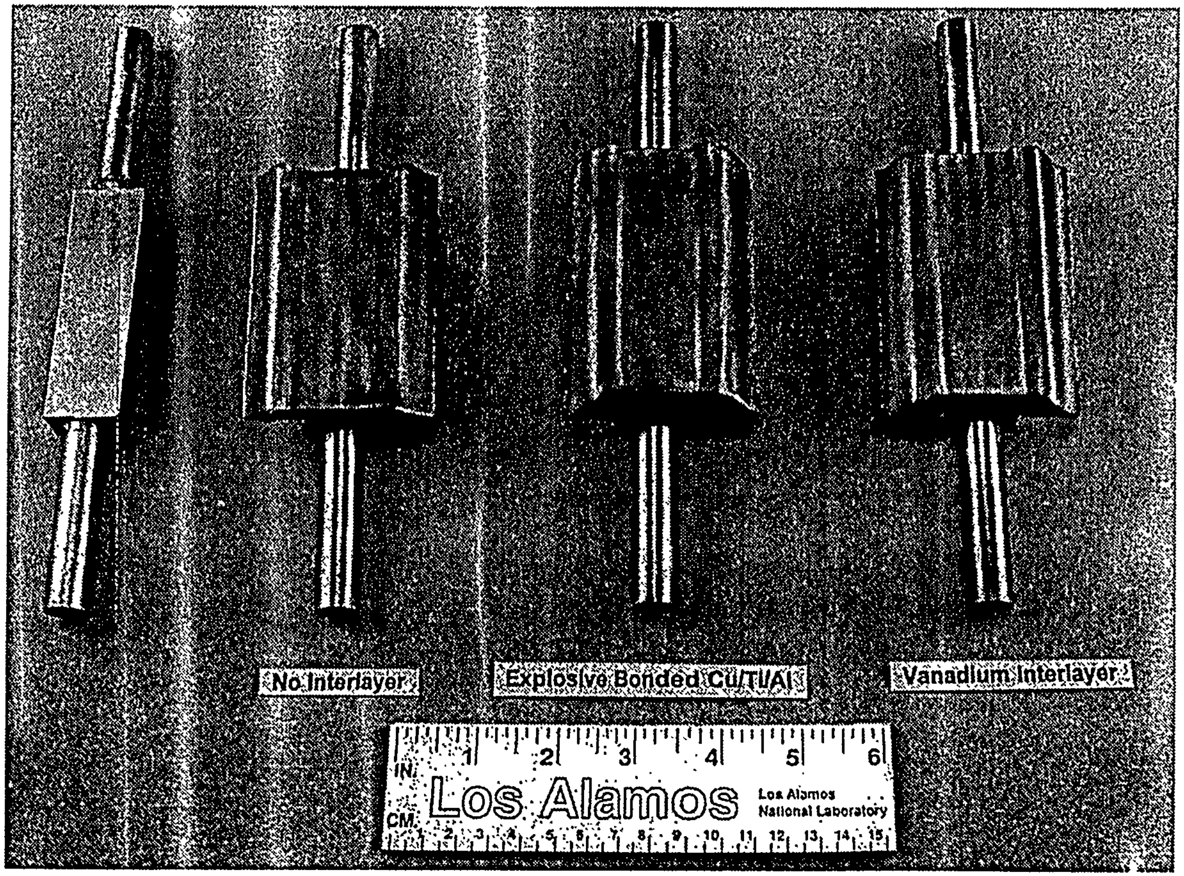

EBTS Results for VPS Beryllium on Copper

H_2O - 180°C, 4 MPa, 1 m/s
Pulse - 3 cycles/m

	1 MW/m^2	3 MW/m^2
VPS Be on CuNiBe (knurled surface)	3000 cycles (No damage)	10 cycles (lateral cracking of Be no damage at Be/Cu bond)
VPS Be on CuCrZr w/aluminum cladding (knurled surface)	1400 cycles (No damage)	40 cycles (lateral cracking of Be no damage at Be/Cu bond)

II. Brazing of Beryllium to Copper

- Explosion bond Ti, Al to Cu
  - Ti acts as diffusion barrier between the Cu/Al
  - Al is compatible with Be and adds compliancy to the interface
  - Al has good thermal conductivity
- Coat Be with Al by VPS or PVD
  - to prevent oxidation of the Be surface
- Braze with layer of PVD Si or Al-12Si foil
- Best results using HIP 625°C / 60 min / 200 MPa

- Al-12Si
  or
- 1 µm Si

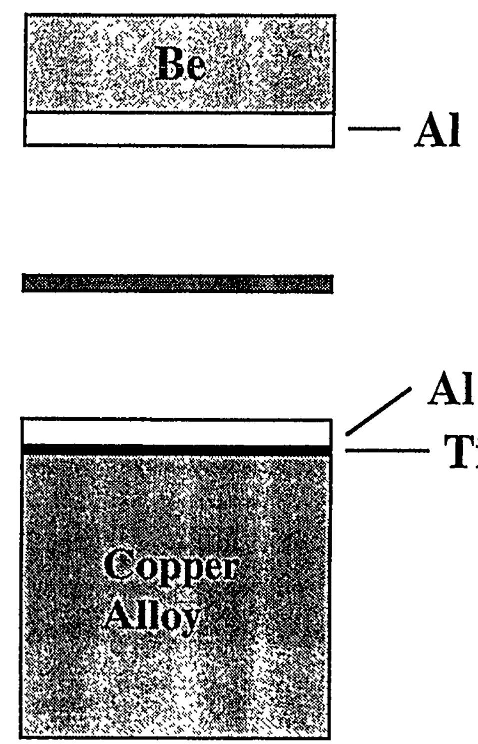

Brazing techniques can produce Be/Al/Cu specimens possessing good strength and ductility.

	Fracture Strength MPa	Elongation %
Be/Al/Cu + Al-12Si	115	~15
Be/Al/Cu + 1 μm Si	100	~3
1100 Al	90	~35

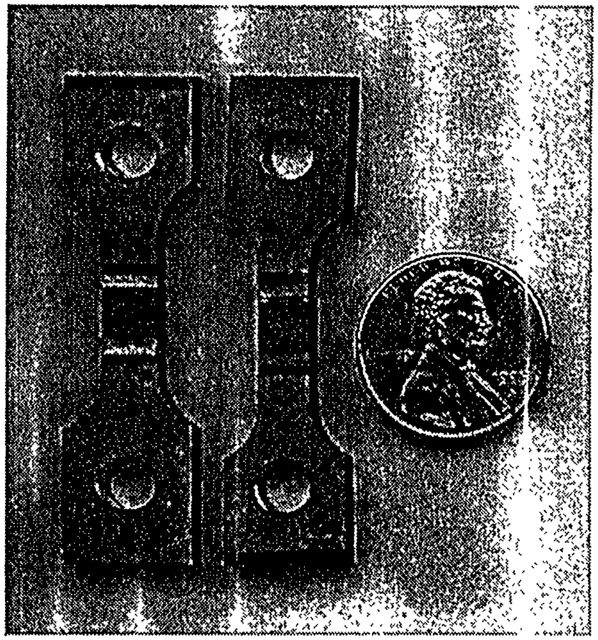

Strain measurement was not accurate.
Failure occurred in the aluminum compliant layer.

III. Diffusion Bonding of Beryllium to Copper

- **Explosion bond:**
  - Ti, Al
  - Ti, Al-50%Be
- **Ti diffusion barrier** (250 μm)
- **Al compatible with Be and adds compliancy**
- **AlBeMet-150 is stronger than 1100-Al**
  (350 MPa vs. 80 MPa - ultimate tensile strength)
- **AlBeMet-150 has a better CTE match with beryllium and copper**
  Be - 11.6, Cu - 16.8, Al - 23.6, AlBeMet-150 - 17.6 (μm/m-K)
- **Be etched or Al-coated**
- **HIP Parameters**
  600-650°C / 60 min / 100 MPa

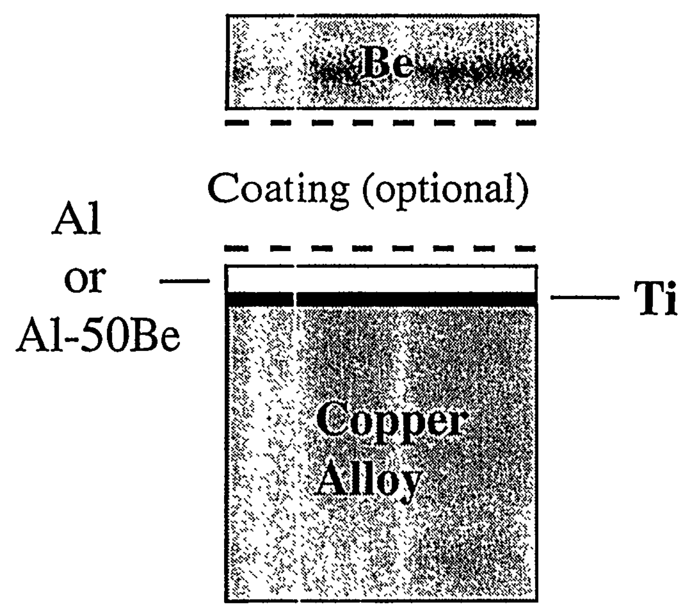

Diffusion bonding techniques can produce Be/Al/Cu specimens which exhibit good strength and ductility.

	Fracture Strength (MPa) 25°C	Fracture Strength (MPa) 300°C
1. Cu /Ti/AlBeMet-150 (Cu film) Be + PVD Al (Cu film)	195	98
2. Cu /Ti/1100-Al (Cu film) Be + VPS Al (Cu film)	115	not tested
3. Cu / Ti/AlBeMet-150 (NaOH) Be (HNO$_3$ + HF)	92	not tested

EBTS Specimen

Braze

Be + VPS Al

Al-12Si (filler metal)

Cu / Ti /1100-Al

(HIP Parameters - 625°C/60 m/105 MPa)

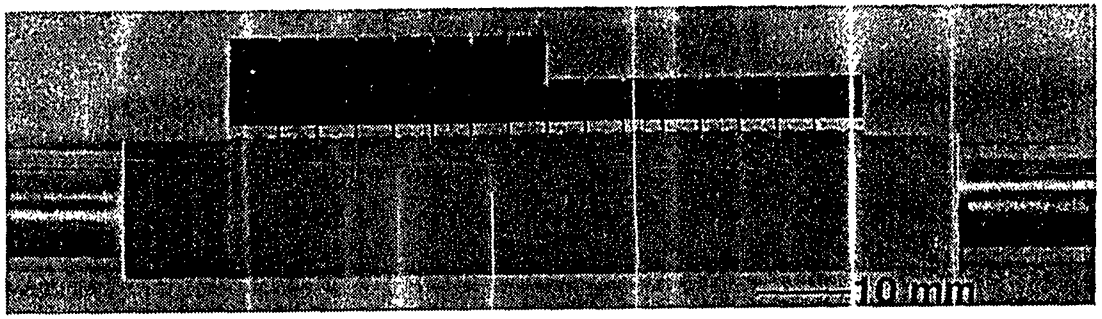

Diffusion Bond

Be + PVD Al (Cu film)

Cu / Ti / AlBeMet-150 (Cu film)

(HIP Parameters - 625°C/60 m/105 MPa)

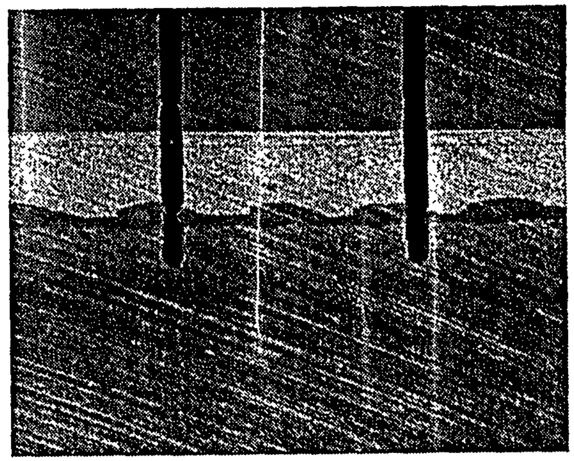

EBTS Results for Brazed and Diffusion Bonded Be on Cu

H_2O - 20°C, 1 MPa, 15 m/s
Pulse - 3 cycles/m

	1 MW/m^2	3 MW/m^2	10 MW/m^2
Braze	1000 cycles No damage	1000 cycles No damage	1000 cycles No damage
Diffusion Bond	1000 cycles No damage	1000 cycles No damage	1000 cycles No damage

The mock-ups were subjected to several heat loads to 250 MJ/m^2 (0.5 s) in which the beryllium tiles melted. No beryllium tile de-bonding was noted.

Summary

Several joining techniques have been studied as a methodology to join beryllium to a copper alloy heat sink:

1. Aluminum brazing of beryllium to copper with an aluminum or AlBeMet-150 compliant layer;

2. Diffusion bonding of beryllium to copper with an aluminum or AlBeMet-150 compliant layer;

3. Plasma spraying beryllium directly on copper or an aluminum compliant layer

The results of high heat flux testing suggest that these bonding technologies can be used successfully for PFC applications.

Future Work - Diffusion Bonding

- Replace explosive bond with sputtered coatings
  - enables thinner coatings
  - compatible with curved geometries

- Reduce bonding temperature
  - prevent degradation of CuCrZr mechanical properties
  - focus on Al - Al bond using diffusion enhancing coatings - Ge, Si, Cu

Problems and Evaluation of Plasma Facing Materials

Naoaki YOSHIDA
RIAM, Kyushu University

US-Japan Workshop(97FT5-06) on High Heat Flux Components & Plasma Surface Interactions for Next Fusion Devices

(December 8-11, 1997, San Francisco)

High Heat Load Properties of Tungsten Coated Carbon Materials

K. Tokunaga, N. Yoshida (RIAM / Kyushu University)

N. Noda (NIFS)

T. Sogabe (Toyo Tanso Co., LTD)

T. Kato (Nippon Plansee K.K)

Objective

W as Armor Plate of PFC

W and W alloys seem promising candidate materials for plasma facing components in next fusion experimental devices.

Advantages

low sputtering yield, good thermal properties

Disadvantages

difficulty of machining and welding, very heavy

For technical realization of a W material:

W coatings on *light* CFC by plasma spray or physical vapor deposition (PVD)

→good thermal conductivity & mechanical strength, light weight

PRESENT WORK

- **Thick W coatings on CFC as well as isotropic fine graphite was successfully produced.**
- **High heat flux experiments were performed on the coated samples in order to prove the suitability and load limit of such coating.**

Samples

- **W Coating:**

  Vacuum plasma spraying technique (VPS) **<Plansee>**

  thickness ··· 0.5 mm & 1.0 mm.

  density ······ 92.5% of theoretical density

- **Substrate Materials:**

  C/C composite CX-2002U & Isotropic fine graphite IG-430U

  <Toyo Tanso Co.>

  size······20mm x 20mm x 10mm

- **Diffusion barrier of Re between W and substrate to suppress the formation of brittle carbide.**

- **Heat treatment was performed to stabilize microstructure of the sample.**

Thermal Conductivity of Carbon and Tungsten

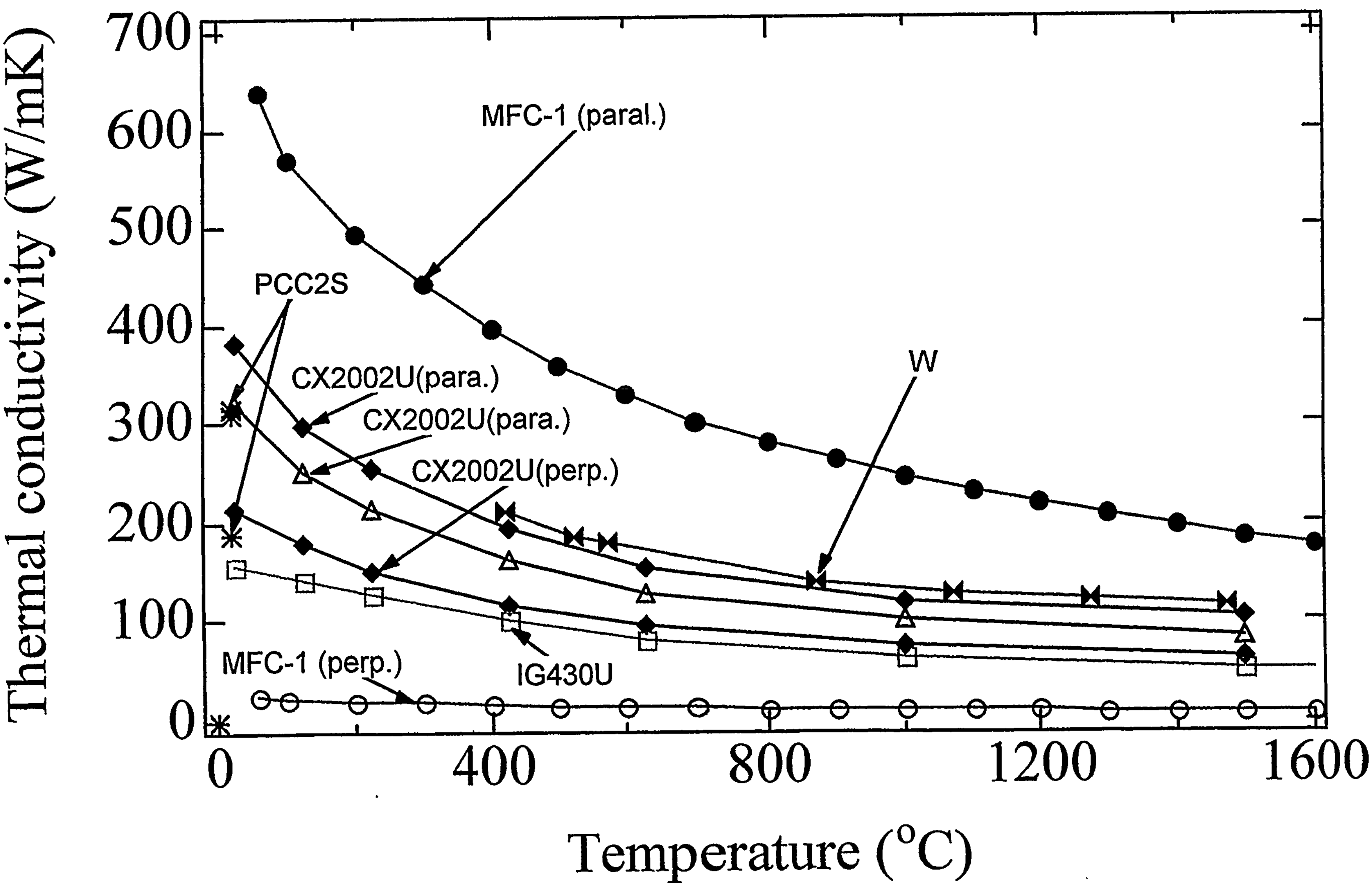

SEM Image of Cross Section

VPS-W(1mm thick) coated CX-2002U(#6)

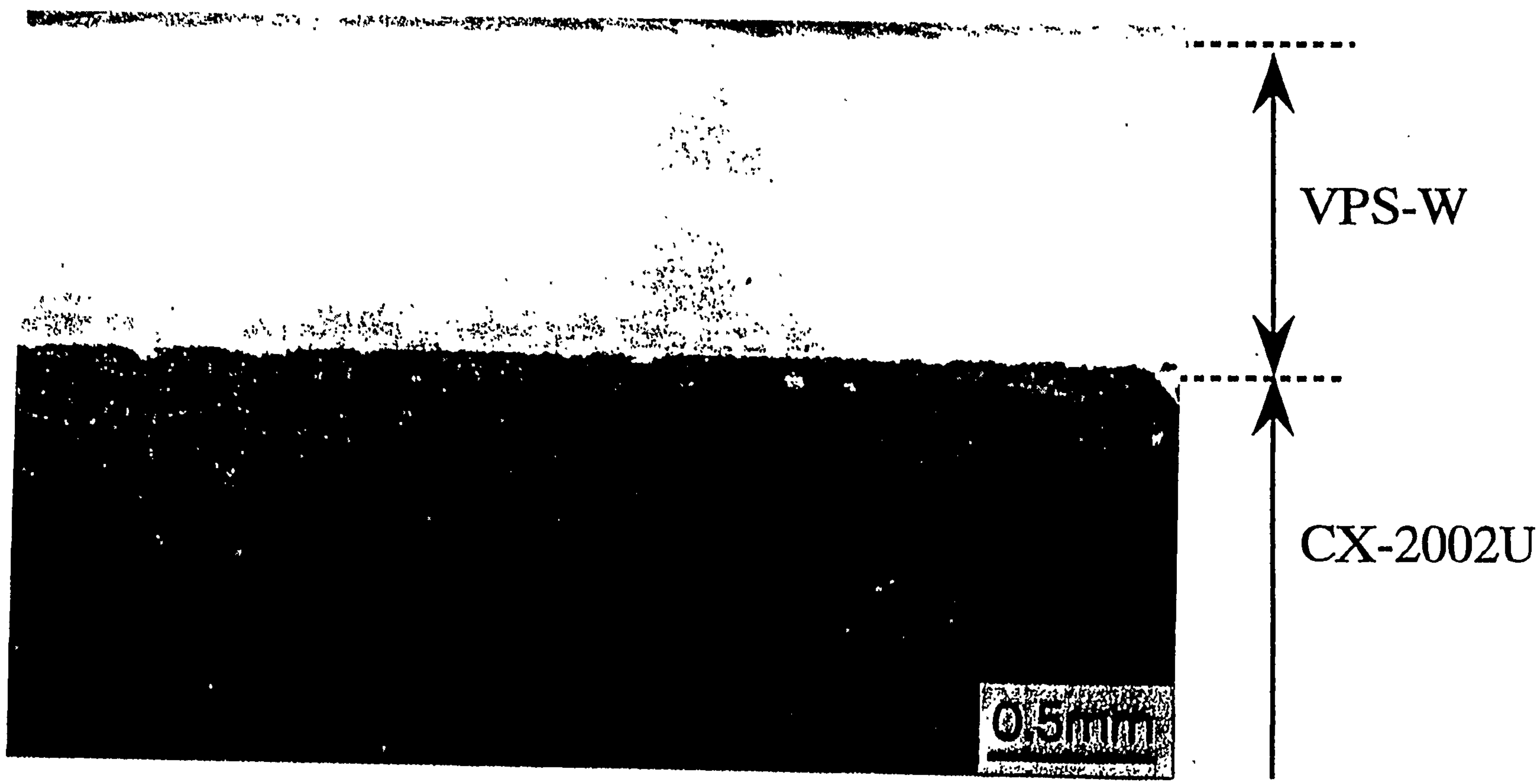

Heat Load Test (1)

Electron Beam Heat Load Simulator (HLS) at RIAM:

- Electron beam energy : 20 keV
- Beam diameter : 8 mm ϕ
- Duration of heat load: 10 sec.

Fixing of samples:

- Mechanical fixing on a copper block actively cooled with water.
- Carbon sheet (0.38 mm thick) between sample and copper block

Surface temperature:

- two-color optical pyrometers(400-1100℃, 1000-3100℃).
- scanning optical pyrometer (two-dimensional distribution)

Emitted gases:

- quadrupole mass spectrometer(QMS)

Heat Load Test (2)

Estimation of heat flux:

- Heat flux was estimated from the beam diameter and net electron beam current, which was measured by applying a bias voltage to the sample to suppress the secondary electrons.

Estimation of heat removable capavility:

- Temperature difference between inlet and outlet water of cooled copper block was measured by *Δ T system* to evaluate heat removable capability of the sample. Water flow rate was also measured.

Observation of Surface Morphology:

- Before and after the irradiation, the sample surface was observed with SEM(scanning electron microscope)

Electron Beam Heat Load Simulater (HLS)

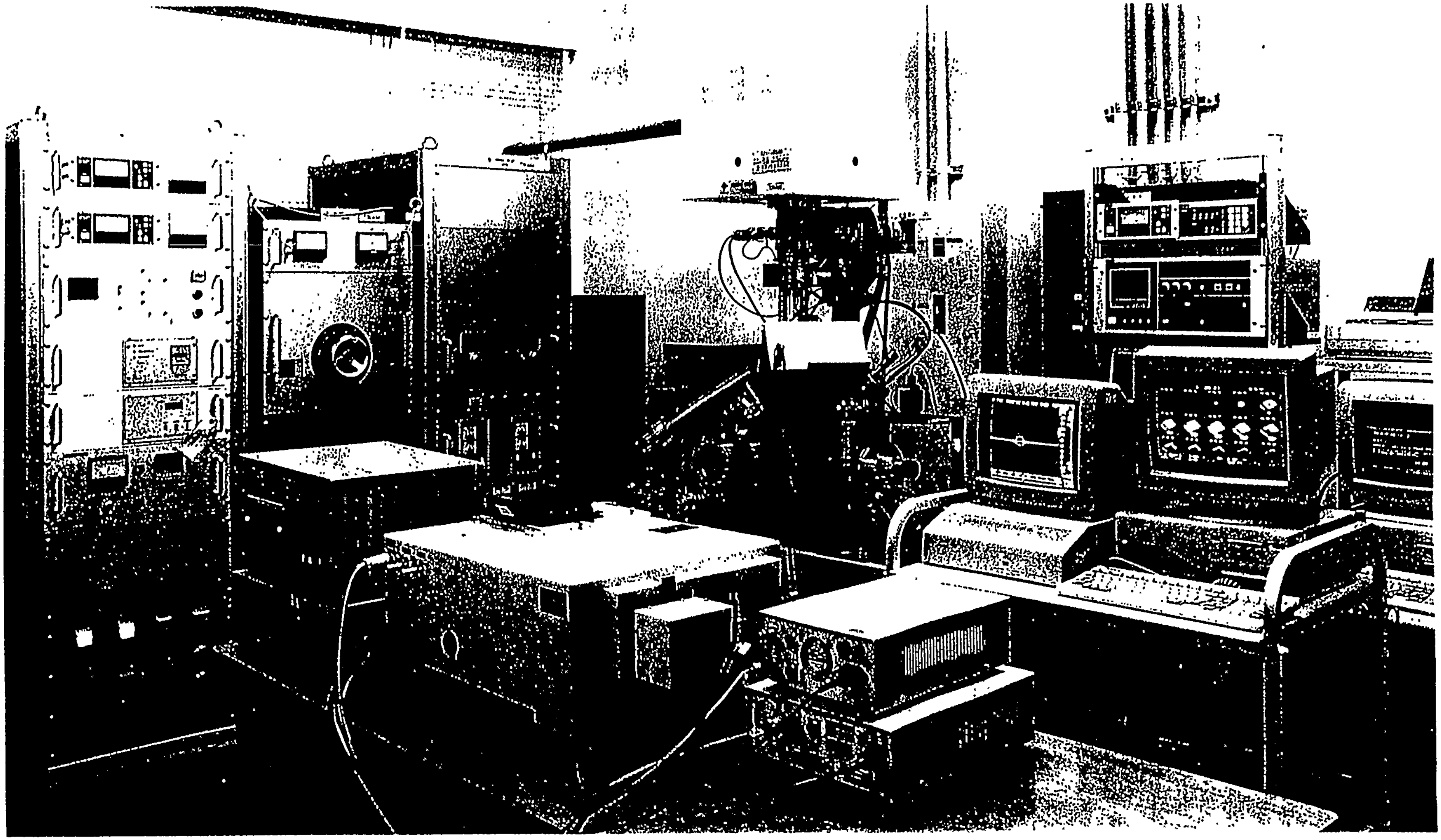

Time Evolution

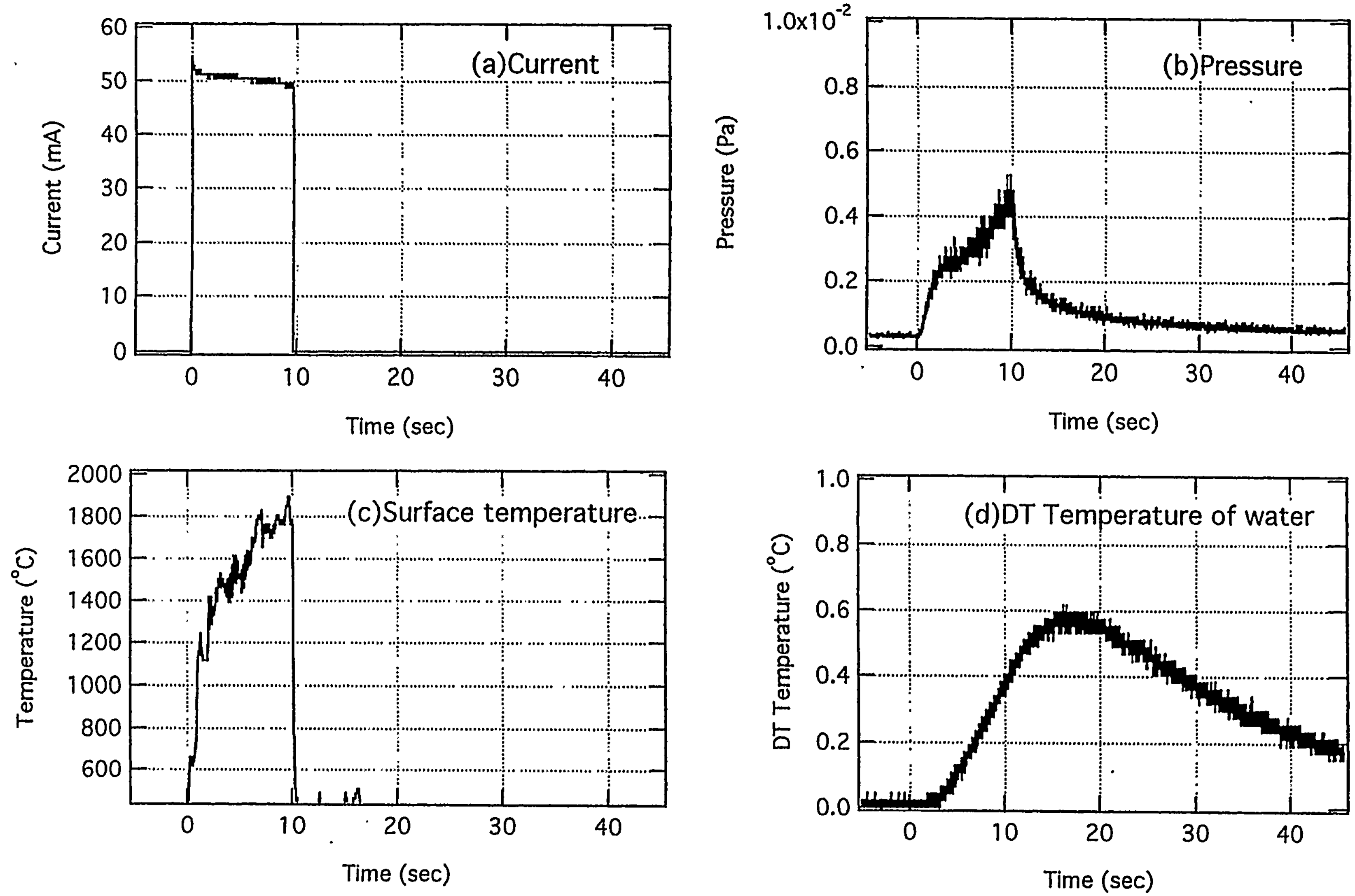

Increasing of Surface Temperature

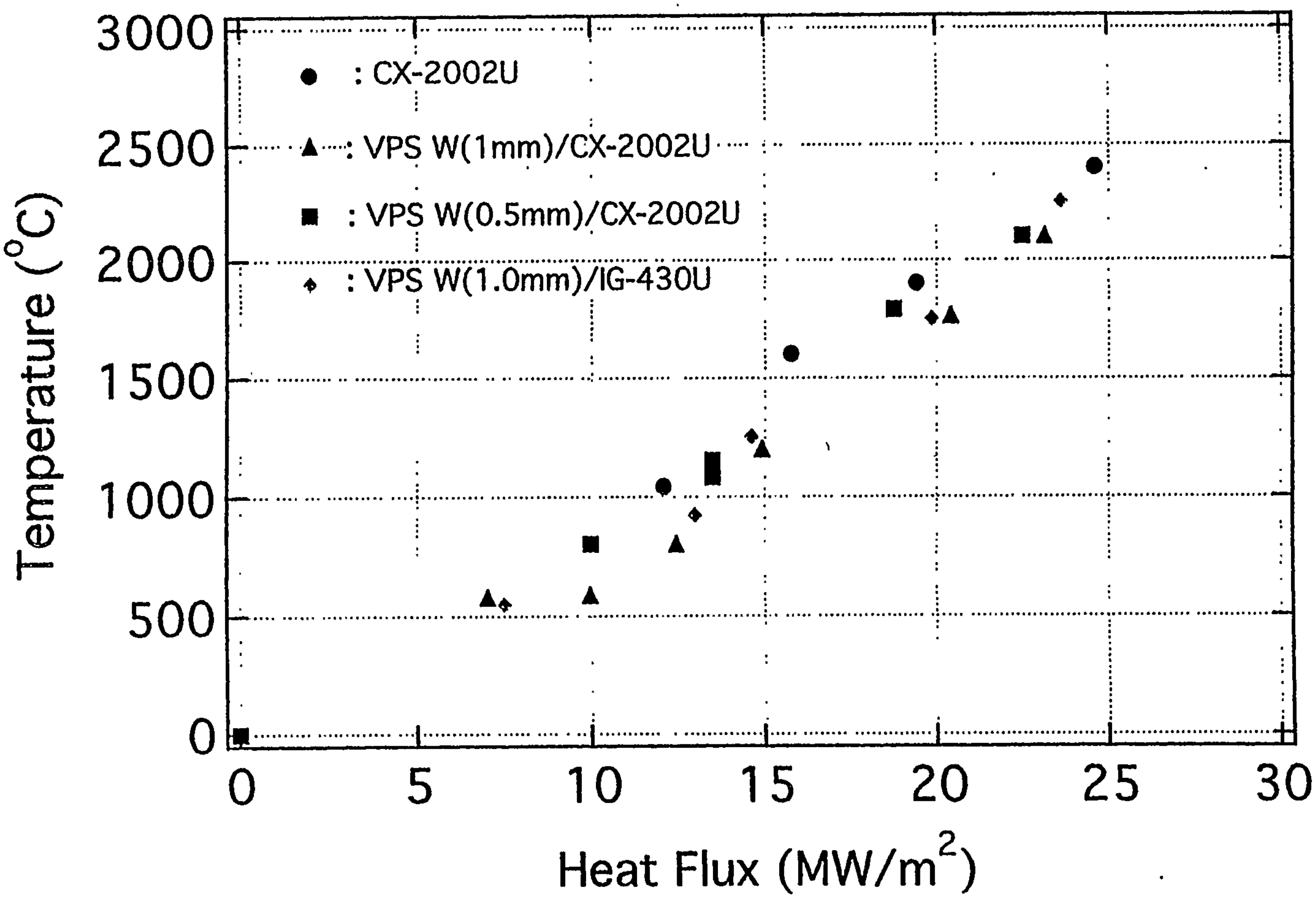

QMS Signal before and during Heat Load Test

QMS VPS-W(0.5mm)/CX-200U, 6s/10s, 18.6MW/m^2

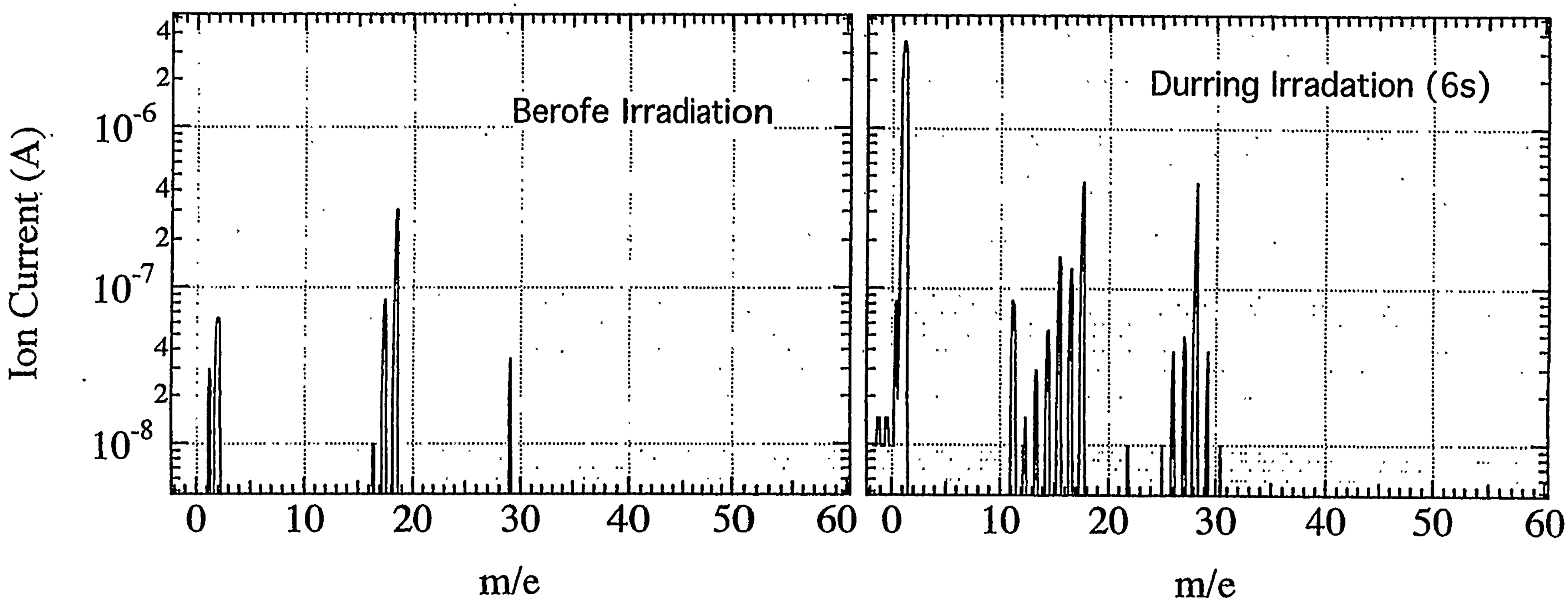

SEM Images of Heat Loaded Surface

(a) VPS-W(1.0mm)/CX-2002U(#14)
(b) VPS-W(0.5mm)/CX-2002U(#10)
(c) VPS-W(1.0mm)/IG-430U(#17)

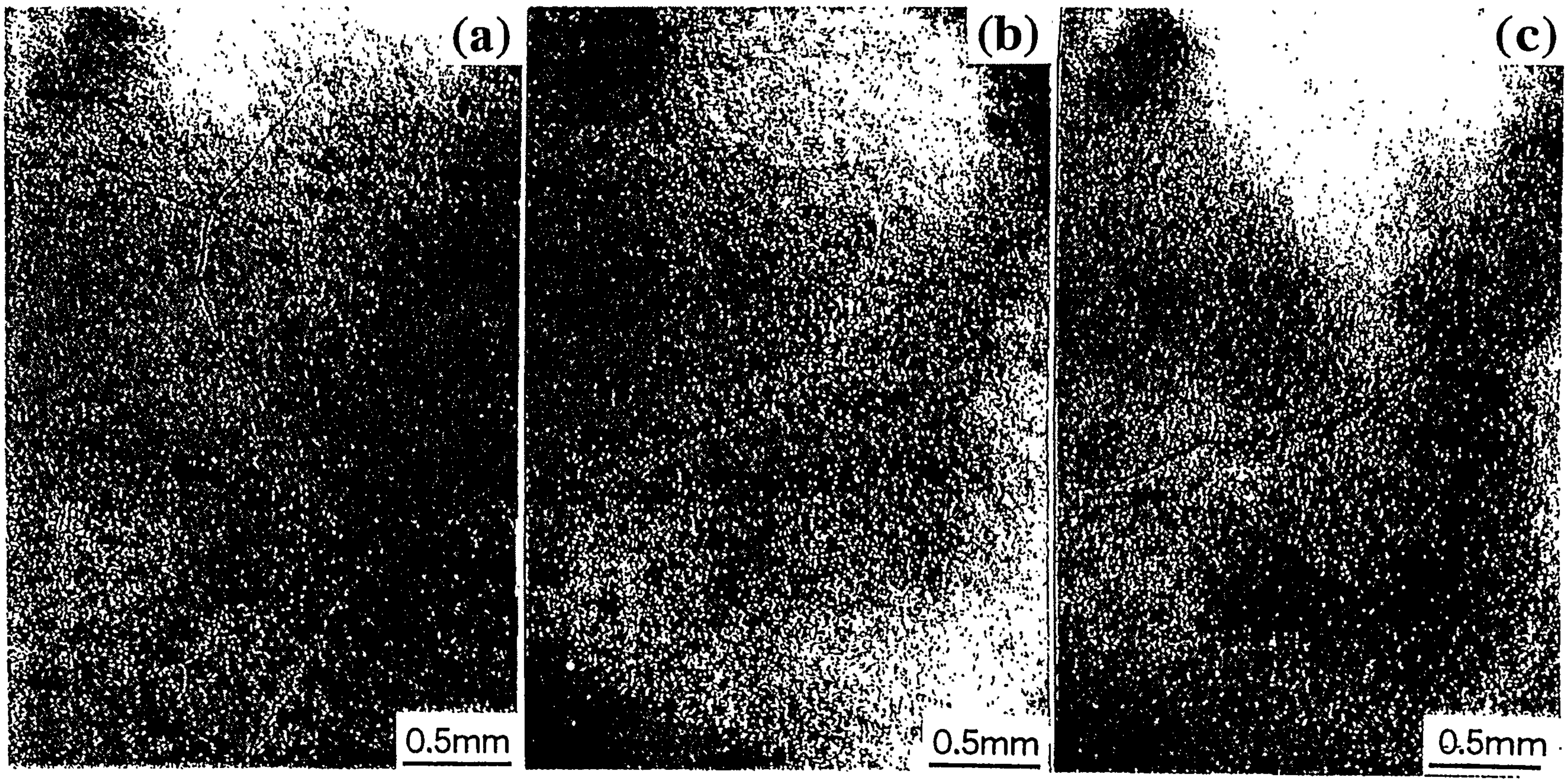

SEM Images of Heat Loaded Surface

(High Magnification)

VPS-W(0.5mm)/CX-2002U(#10)

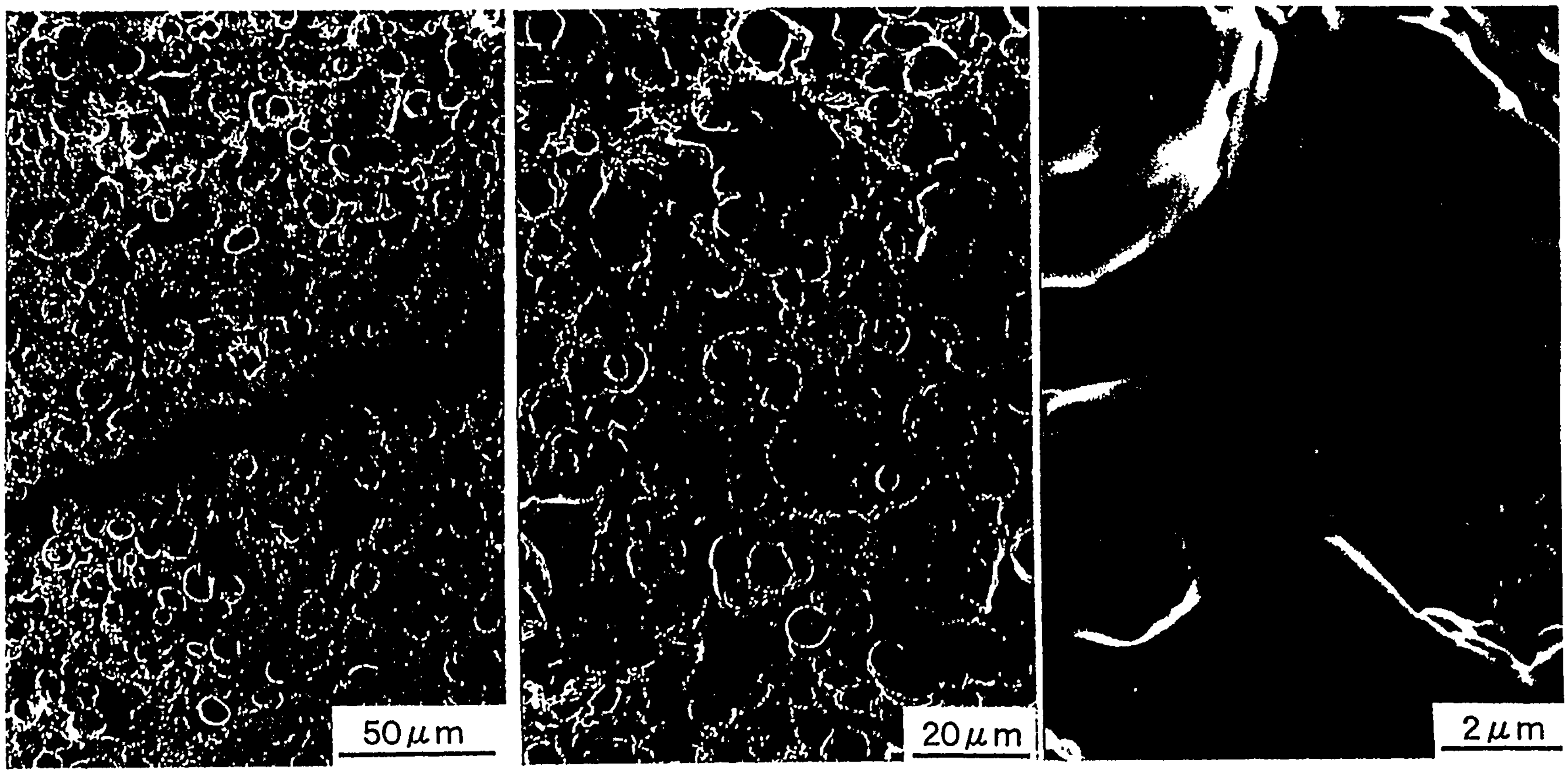

SEM Image of W Surface (before heat load)

VPS-W(0.5mm thick) coated CX-2002U(#10)

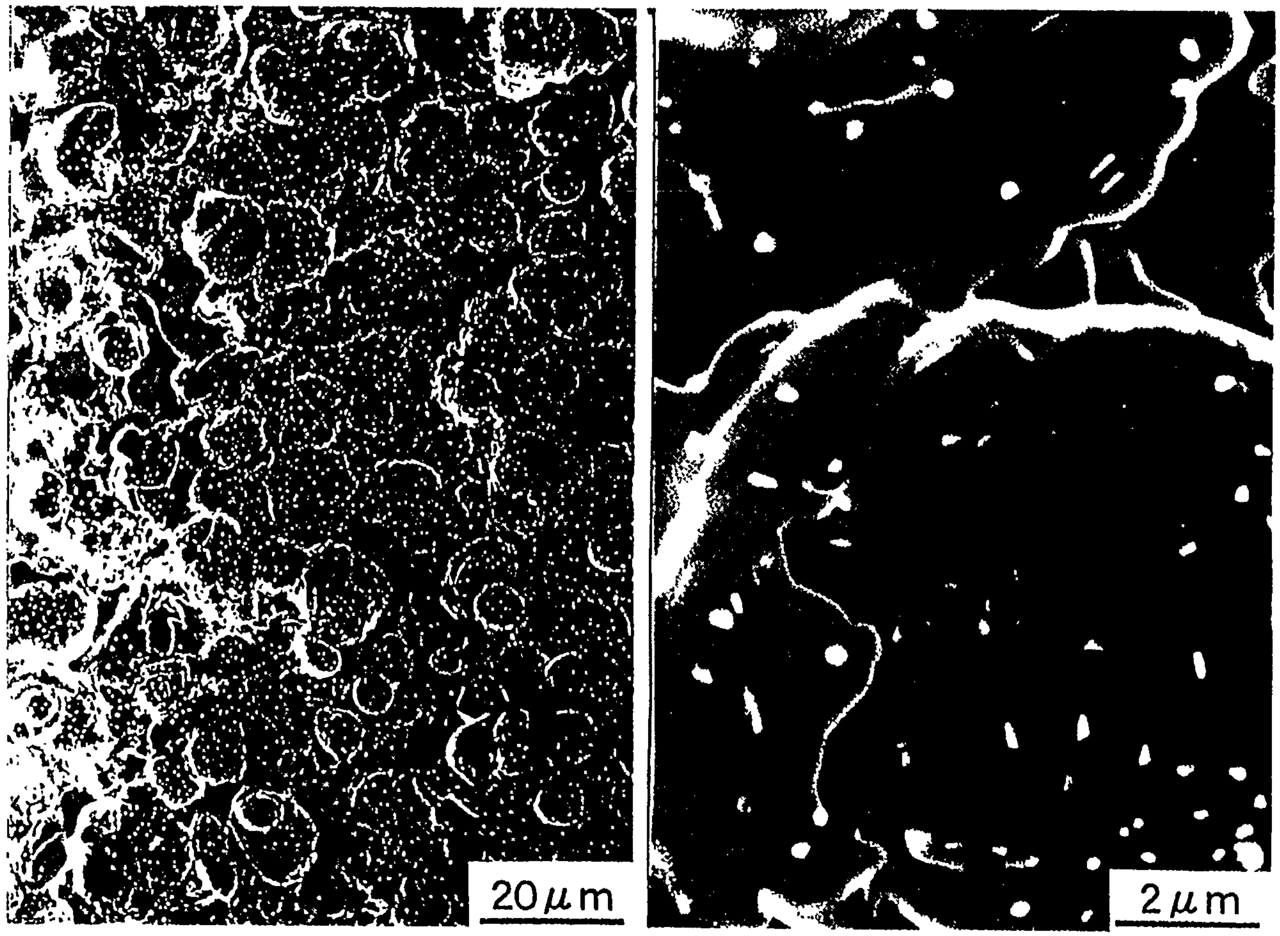

Summary

- W coatings of 0.5mm and 1.0mm thick were successfully deposited by Vacuum Plasma Spraying Technique on carbon-carbon fiber composite, CX-2002U, and isotropic fine grain graphite, IG-430U.

- High heat flux experiments were performed on the coated and non-coated samples in order to prove the stability and load limit of such coating materials.

- There was little difference in temperature increase among CX-2002U and the coated materials up to 2200℃. This result indicated that thermal and adhesion properties of the W coated materials were good under high heat flux (~25MW/m^2)

- A few large cracks were formed in W coating, but plastic deformation and micro-cracks due to grain growth by re-crystallization were not observed below 2200℃. The cracks may be formed by local thermal stress due to spot-like electron beam.

Future Planes

- **Investigation of microscopic change of VPS-W/CFC interface**
  phase change (WC formation), compositional change, Re-crystallization, mechanical properties, etc.
- **Thermal fatigue test··· estimation of life time**
- **Heat loading test of actively water-cooled mockups**
  (~Jan. 1998)

Thermal Response of CFC/OFHC Cooling Pipe Mock-up for LHD/LID

T. Tokunaga, N. Yoshida
RIAM / Kyushu University

Y. Kubota, S. Inagaki, R. Sakamoto, A. Sagra,
A. Komori, A. Noda, N. Ohyabu, O. Motojima
National Institute for Fusion Science

Y. Soman
Mitsubishi Heavy Industry Co.

Objective

LHD / NIFS

- Helical Divertor:
  $10MW/m^2$ for 10s & $0.75W/m^2$ in steady state
  $\Longrightarrow$ C tiles bolted to SS cooling tube

- Local Island Divitor(LID):
  $6\text{-}8MW/m^2$ in steady state $\Longrightarrow$ C tiles brazed to Copper

R&D Issues of LID divertor plate

- Armor material and brazing layer with high thermal conductivity and strong mechanical properties
- High heat transfer of cooling pipe/water
  (optimum conditions for pressure, flow rate and temperature)

PRESENT WORK

Evaluation of thermal response and thermal fatigue for the newly developed two CFC/Cu armor mock-ups

Mock-up Samples

Armor material: MFC-1 (one-dimensional CFC, Mitsubishi Chem.)
CX-2002U (two-dimensional CFC, Toyo Tanso)

Heat sink material: OFHC with cooling pipe

Brazing filler: 63%Ag-35.25%Cu-1.75%Ti (Mitsubicshi H.I)

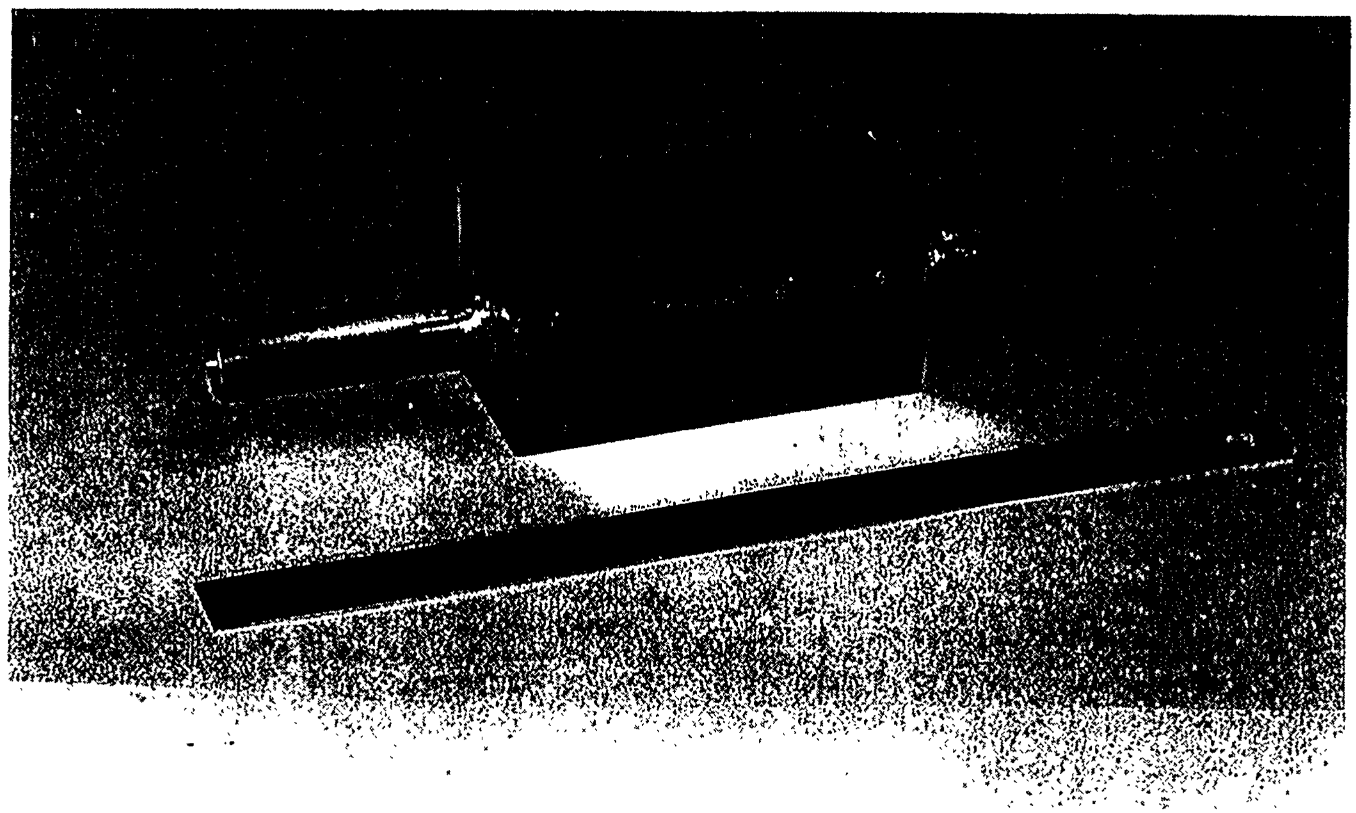

Thermal Conductivity of Carbon Materials

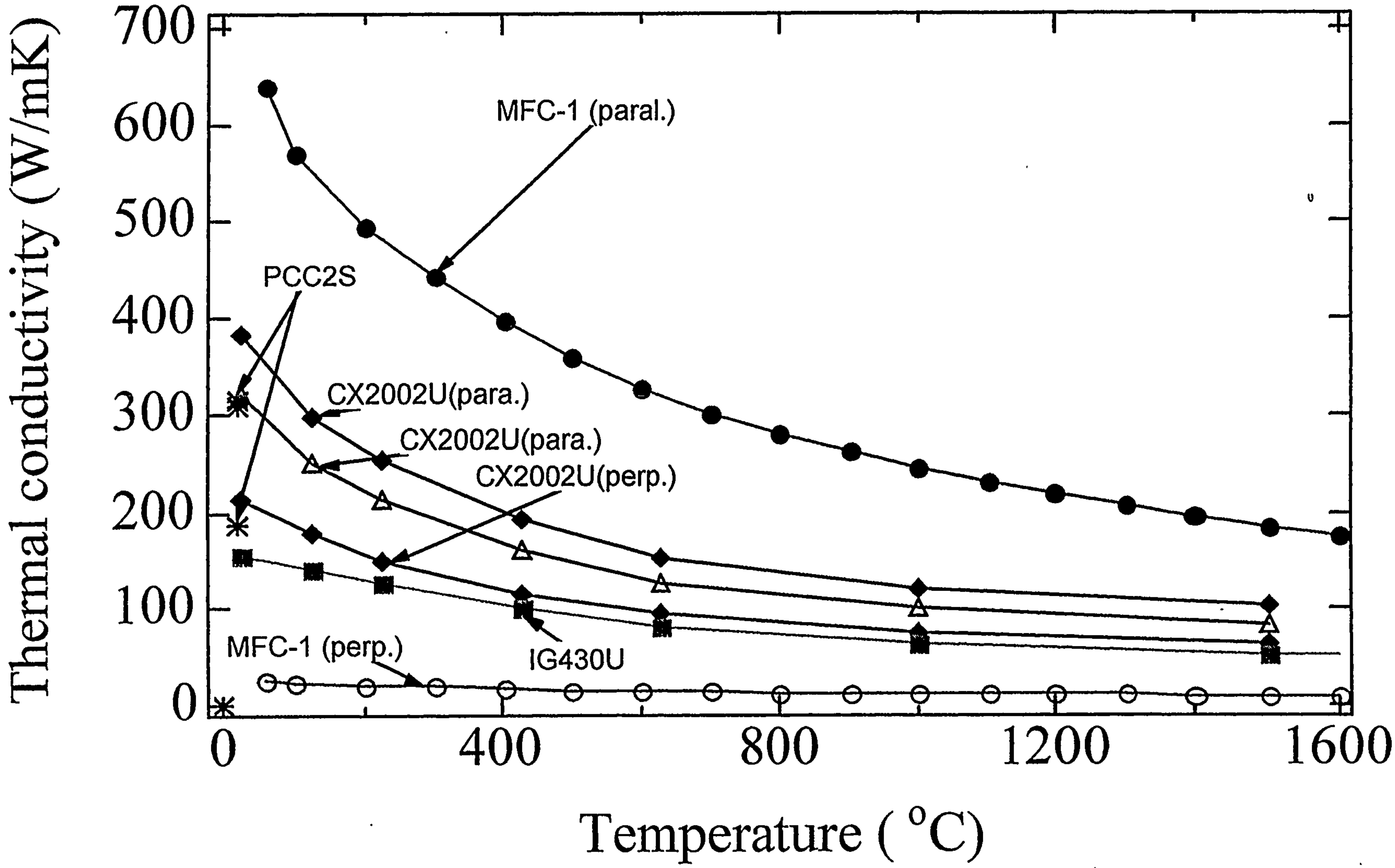

Experimental Procedure

- **Heat Load Testing Device: ACT at NIFS**

- **Operation Conditions**

  electron beam: 30keV, 60s, beam size 30mmx30mm
  heat flux: 1-16MW/m^2
  water cooling : pressure 0.5 MPa
  temperature 20-30℃(inlet)
  flow rate 7.5 m/s

- **Diagnostic**

surface temperature	pyrometers
bulk temperatures	thermocouples (top and bottom of I.F.)
heat removal capability	water calorimetry
gas analysis	QMA

CFC/Armor Mock-up

Figure 1
(a-1)

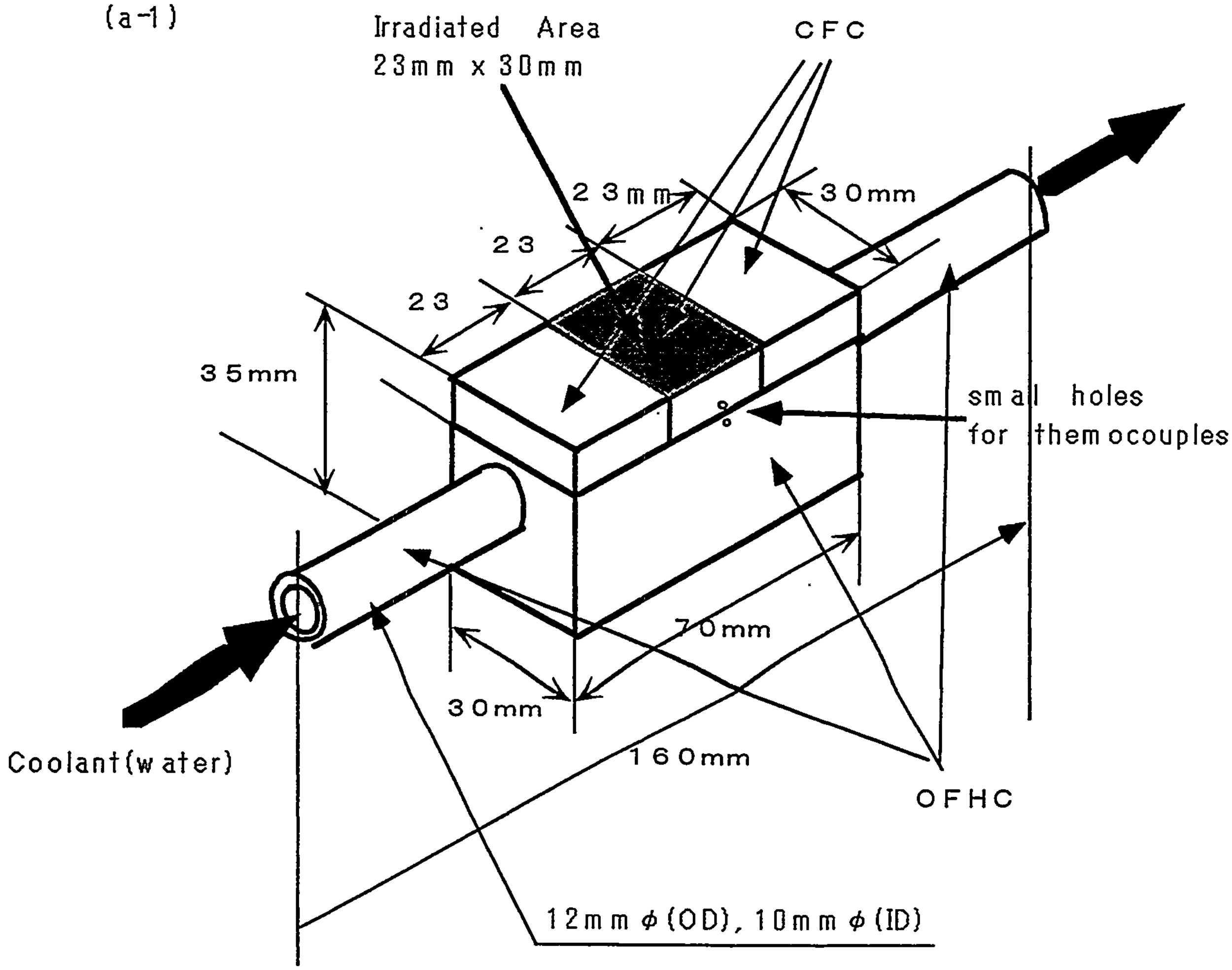

(a-2)

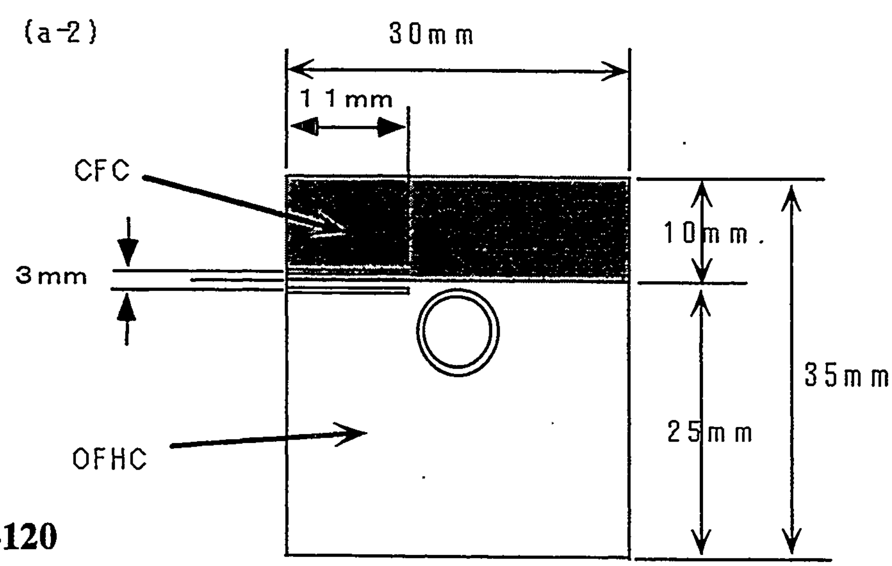

Time Evolution under Beam Irradiation

CX-2002U/OFHC, 10MW/m^2

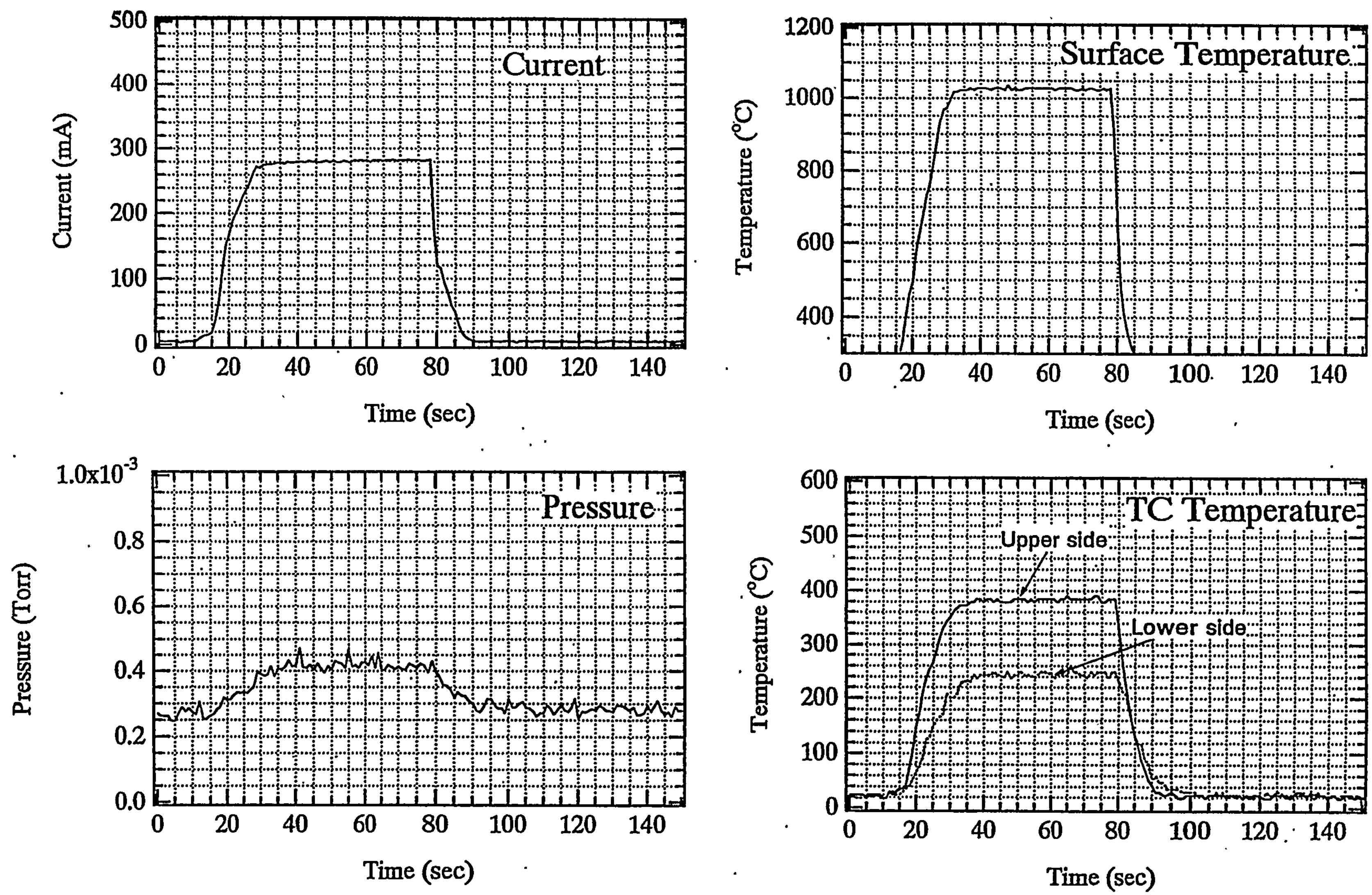

Time Evolution under Beam Irradiation

MFC-1/OFHC, 10MW/m^2

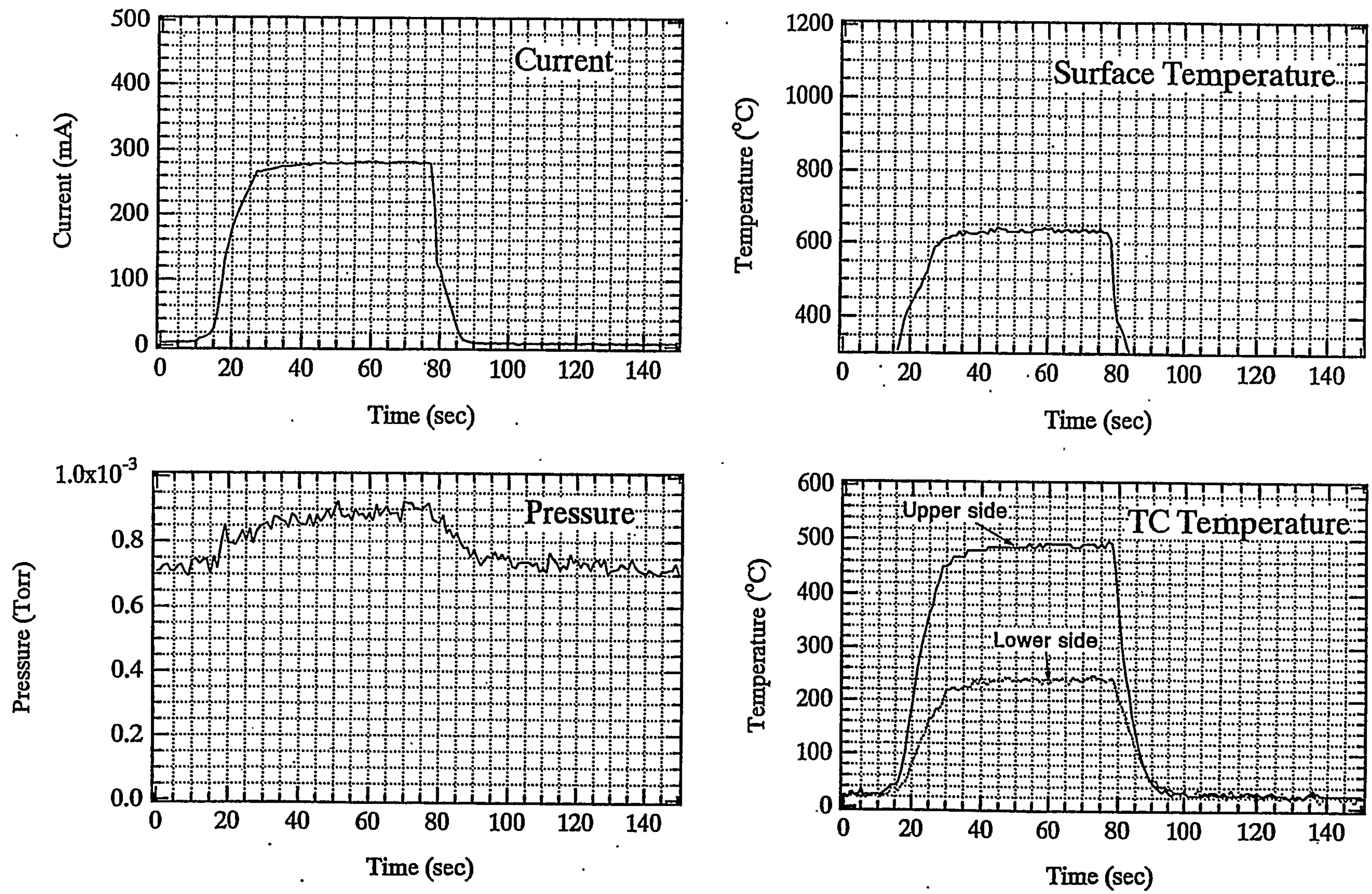

Surface Temp. / Heat Flux

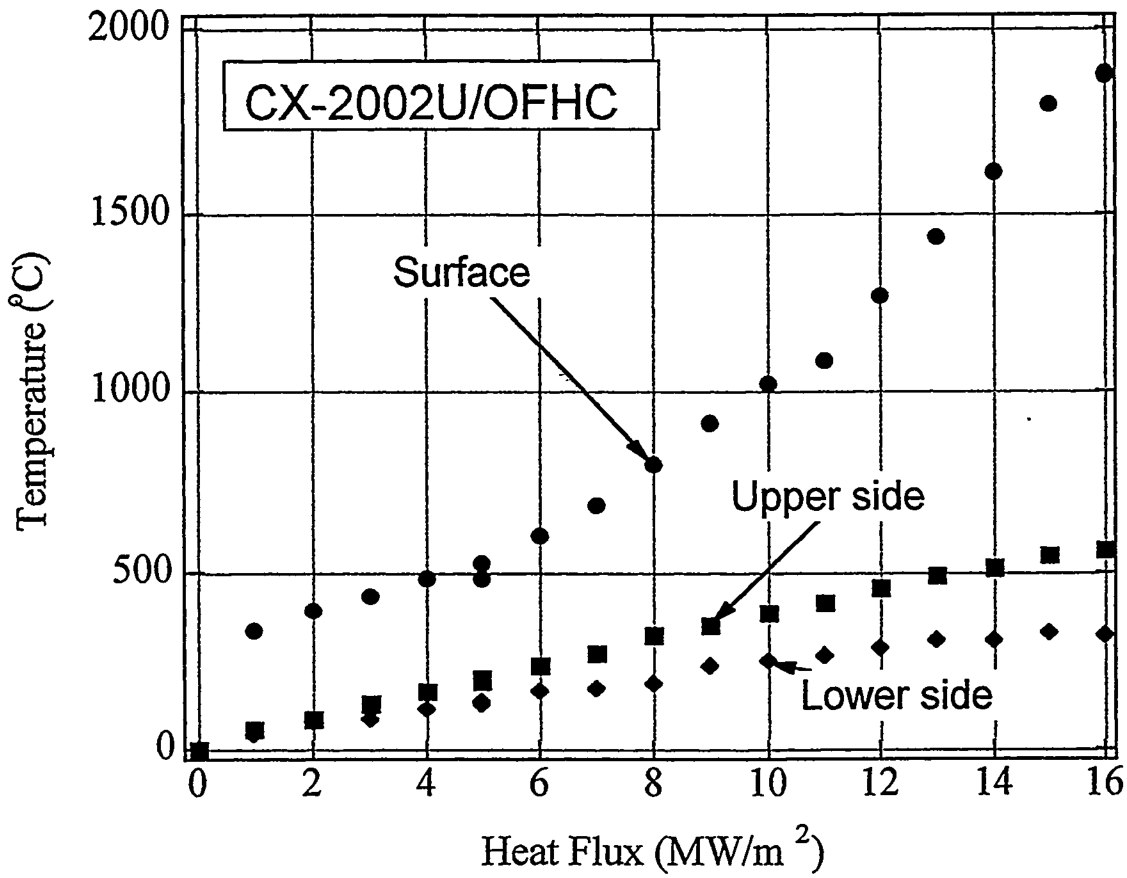

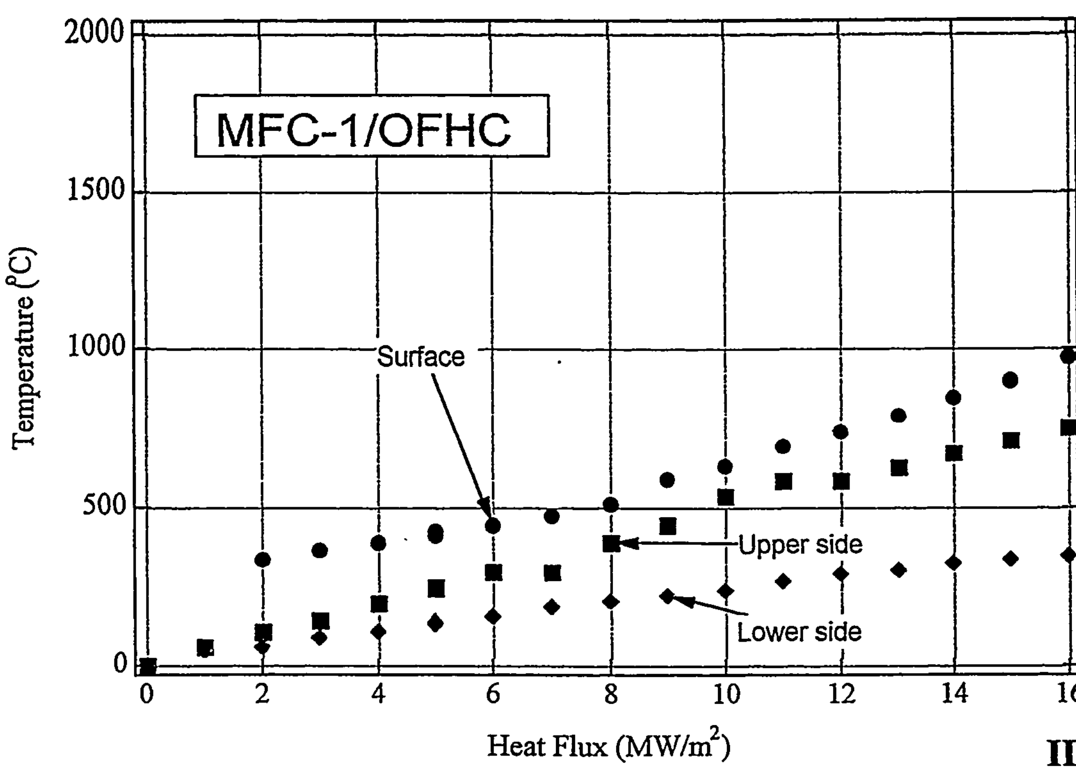

Gas Emission

CX2002U/OFHC, 15MW/m^2

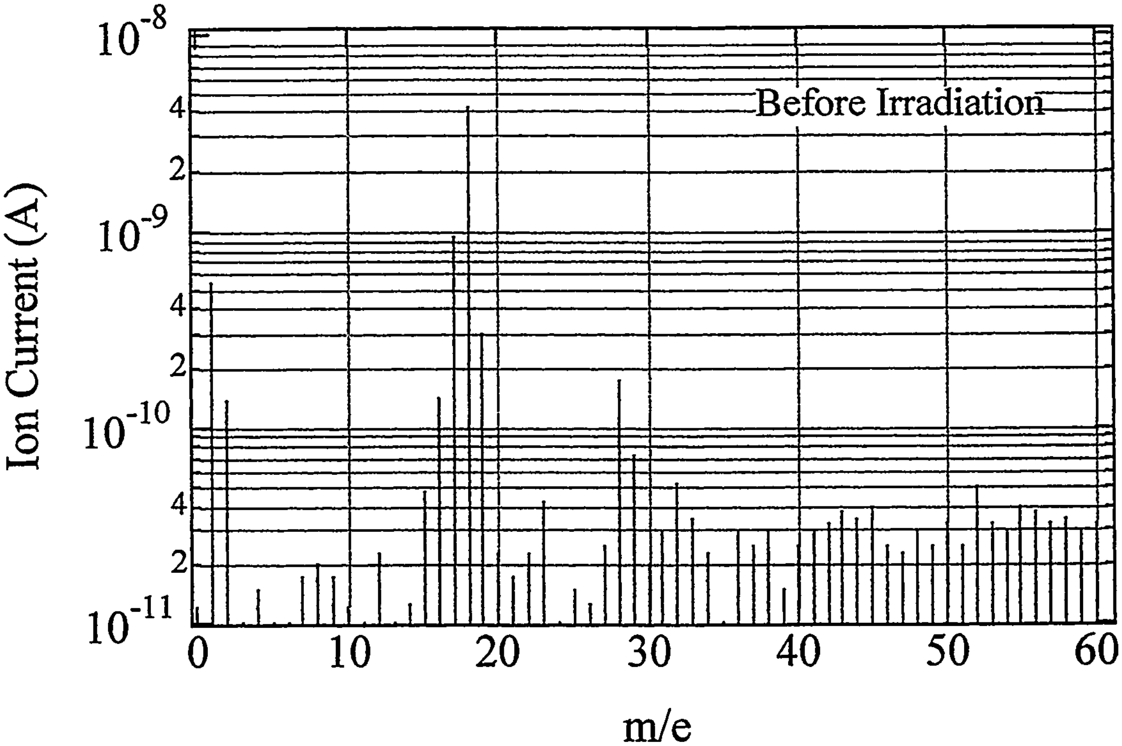

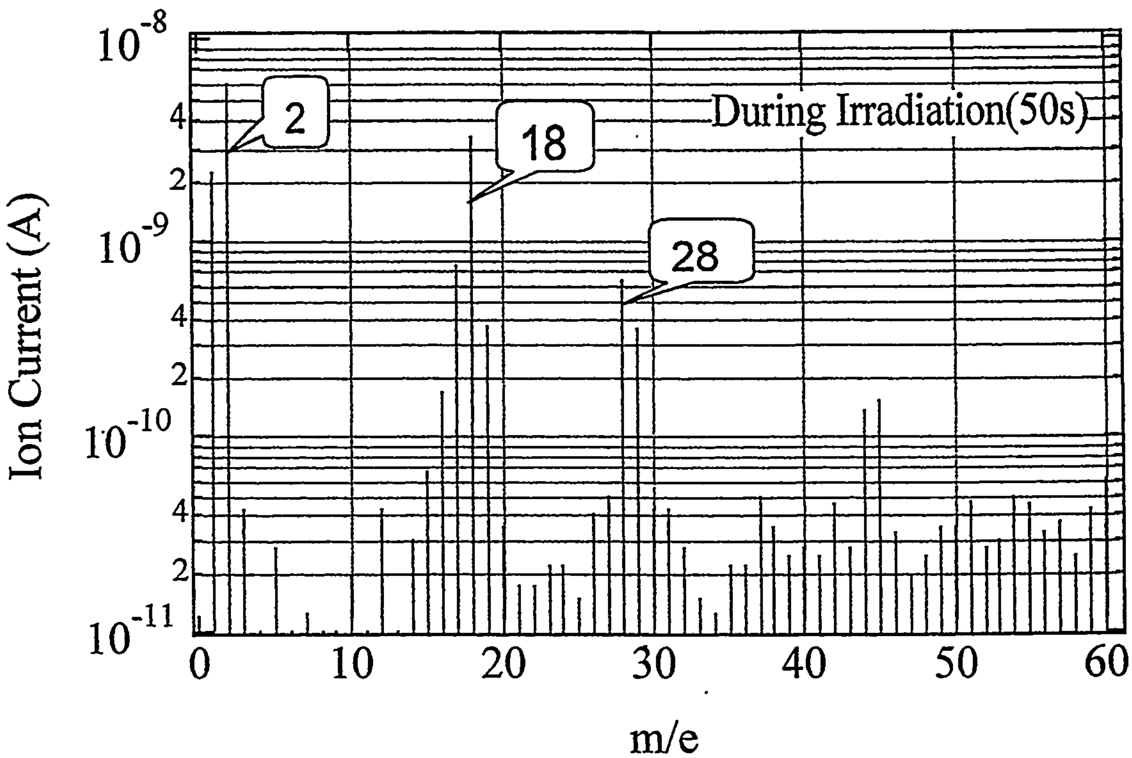

QMS Signal during Heat Loading

CX-2002U/OFHC, 15MW/m^2

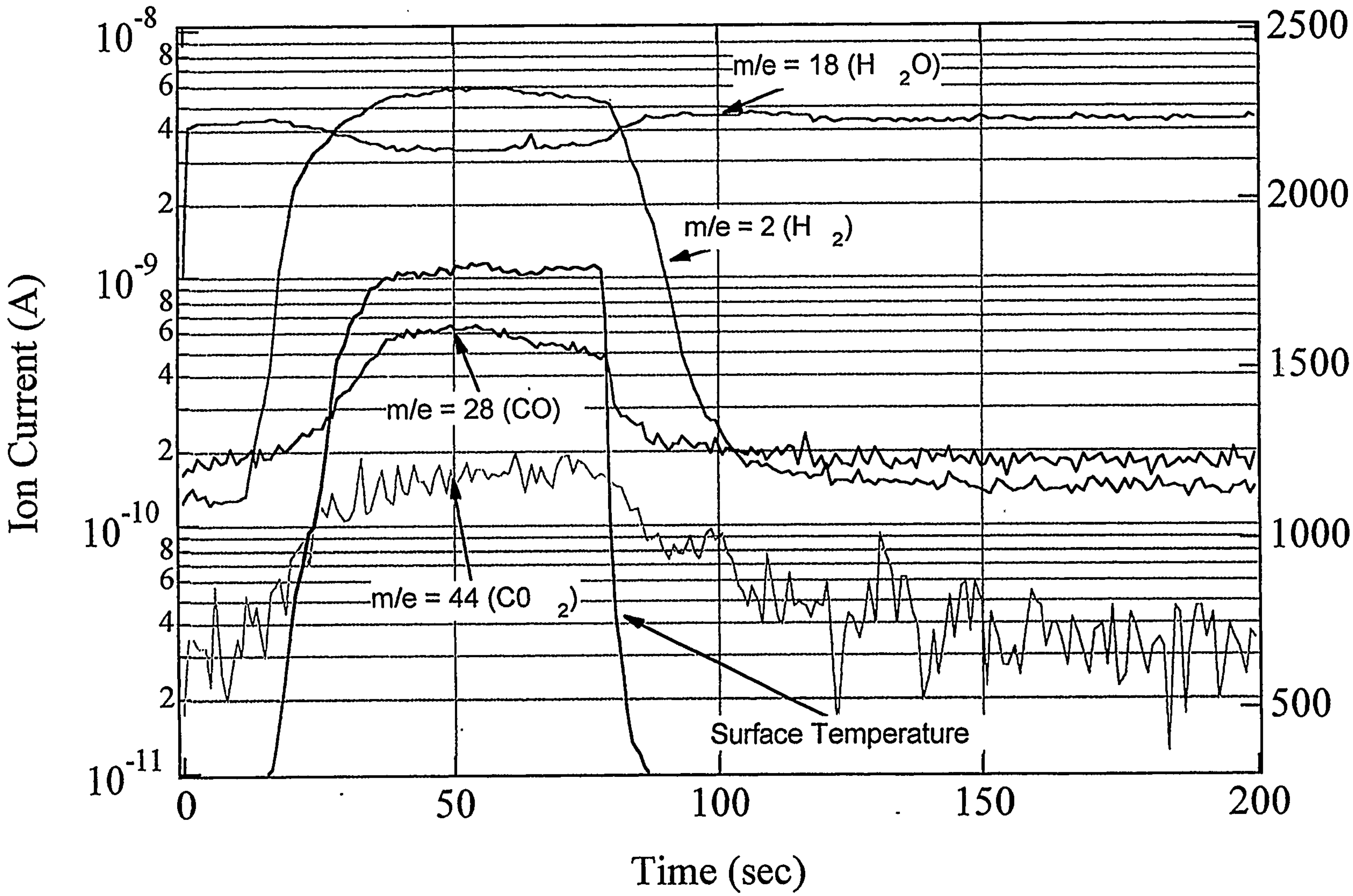

Result of Thermal Fatigue Test

MFC-1, 10MW/m^2, 20 ℃, 1.0 MPa, 10 m/s, 20 sec

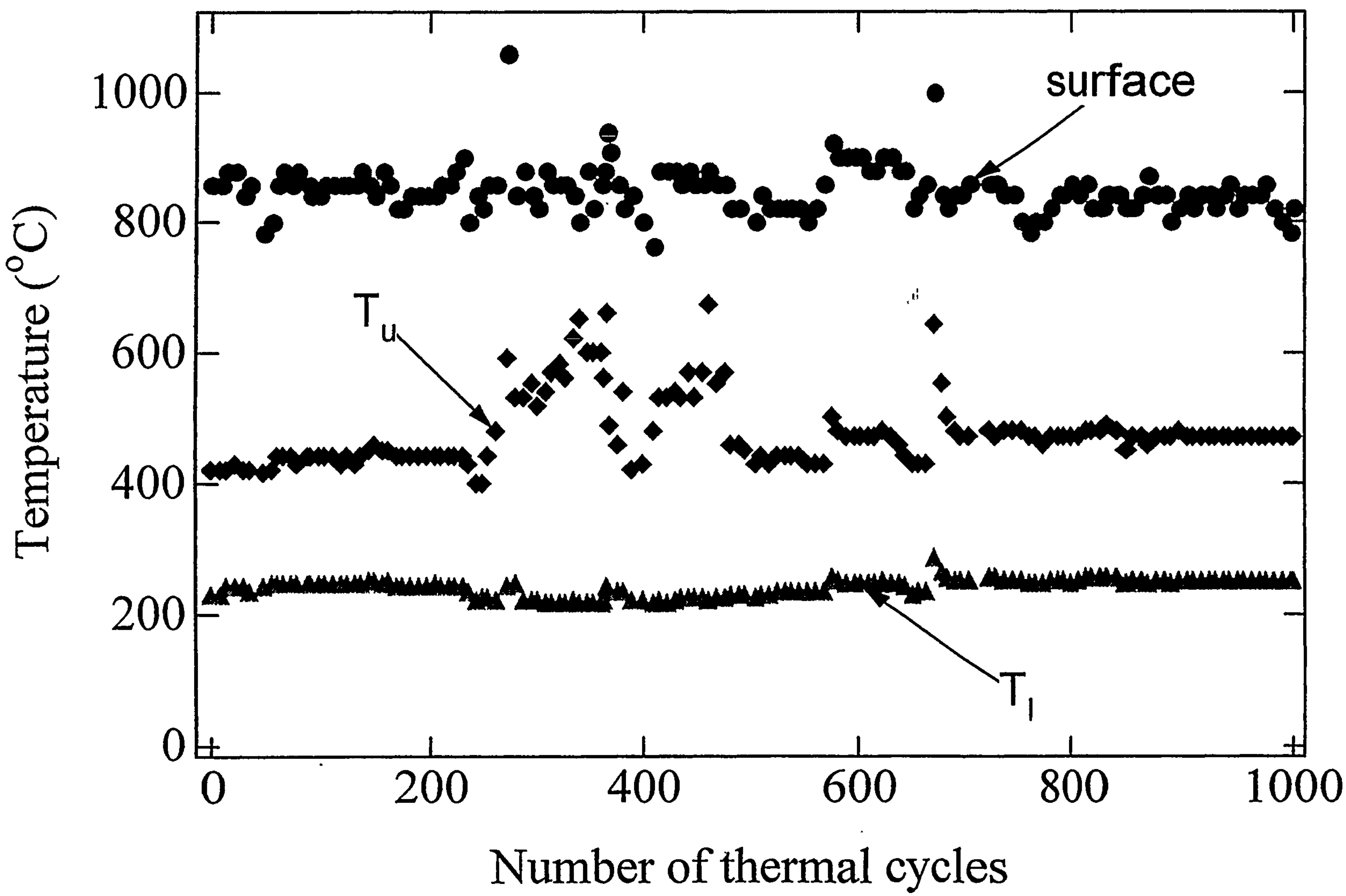

Summary (1)

- Two mockups of CFC brazed to OFHC for the LID divertor plate were fabricated.
  CX2002U/OFHC (two-dimensional CFC)
  MFC-1/OFHC(one-dimensional CFC)

- Their thermal response, material damage (and thermal fatigue lifetime tests) by high flux heat loading were examined by using electron beam facilities ACT and HHF.

- The MFC-1 mockup showed excellent heat removal performance due to its high thermal conductivity.

- In the case of CX-2002U mockup, surface temperature is about 1000°C at 10 MW/m^2. This satisfies requirement for armor materials of LID/LHD.

Summary (2)

- Thermal fatigue test of the MFC-1 mockup was performed (HHF). Though anomalous increase of temperature was not observed until 1000 cycles, strange fluctuation of temperature indicates the possibility of bonding degradation.

- Analysis of residual gas indicates that H_2O gas reacts with C at the high temperature CFC surface. Influence to erosion?

In Future:

- Improvement of brazing for MFC-1/OFHC mockup.

- Thermal fatigue tests for CX2002U/OFHC and MFC-1/OFHC mockups

Special Session III: Historical Progress in PSI Studies

A SMALL PERSONAL HISTORY

T. YAMASHINA

SURFACE STUDY TO FUSION STUDY 1956 ~ 1985

CORROSION 1956~1960
WET AND DRY CORROSION

CATALYSIS 1960~1970
CLEAN SURFACES, LEED, HIGH VACUUM

VACUUM ENGINEERING 1969~1980
THIN SOLID FILMS, EXTREME-ULTRA-HIGH VACUUM
CHARACTERIZATION OF SOLID SURFACES

NUCLEAR FUSION 1978~
PLASMA SURFACE INTERACTIONS
IMPURITY ANALYSIS IN PLASMA MACHINES
PLASMA FACING MATERIALS

SURFACE-CHARACTERIZATION-TECHNIQUES 1958~1983

1958	QUARZ SPIRAL MICROBALANCE X-RAY DIFFRACTION	DRY CORROSION
1959	HIGH ENERGY ELECTRON DIFFRACTION	SURFACE OF METAL OXIDES
1960	ULTRA-HIGH VACUUM WITH OMEGATRON MASS SPECTROMETER (FIRST JAPANESE MADE)	CATALYSIS BY CLEAN SURACES LOW PRESSURE CHEMICAL REACTIONS
1963	TORTION TYPE MICROBALANCE	SURFACE OXIDATION AND REDDUCTION
1965	QUADRUPOLE MASS SPECTROMETER (FIRST JAPANESE MADE)	LOW PRESSURE GAS REACTIONS
1967	ULTRA-HIGH VACUUM SYSTEM SPUTTERING APPARATUS	THIN SOLID FILMS REACTIVE SPUTTERING PROCESS

1970	SURFACE ROUGHNESS FACTOR	SURFACE AREA WITH ATOMICAL SCALE
1970	(JOINED TO NUCLEAR FUSION STUDY)	
1971	AUGER EELECTRON SPECTROSCOPY (FIRST AES IN JAPANESE UNIVERSITY)	SURFACE SEGREGATION OF BINARY ALLOYS
1973	AES-SIMS COMBINED SYSTEM	SURFACE CHARACTERIZATION OF FIRST WALL
1978	ION-MASS-MICRO-ANALYSIS(IMMA)	ENERGY DISTRIBUTION OF SPUTTERED IONS
1981	XPS-AES COMBINED SYSTEM PROBE-MEASUREMENTS IN JIPPT-II (FIRST EXPERIMENTS WITH REAL PLASMA MACHINE)	PLASMA SURFACE INTERACTIONS IMPURITY DISTRIBUTION OF WALL SURFACES
1983	PROBE-MEASUREMENTS IN HELIOTRON E	IMPURITTY DISTRIBUTION OF WALL SURFACES

SURFACE ANALYSIS STUDY IN PLASMA WALL INTERACTIONS

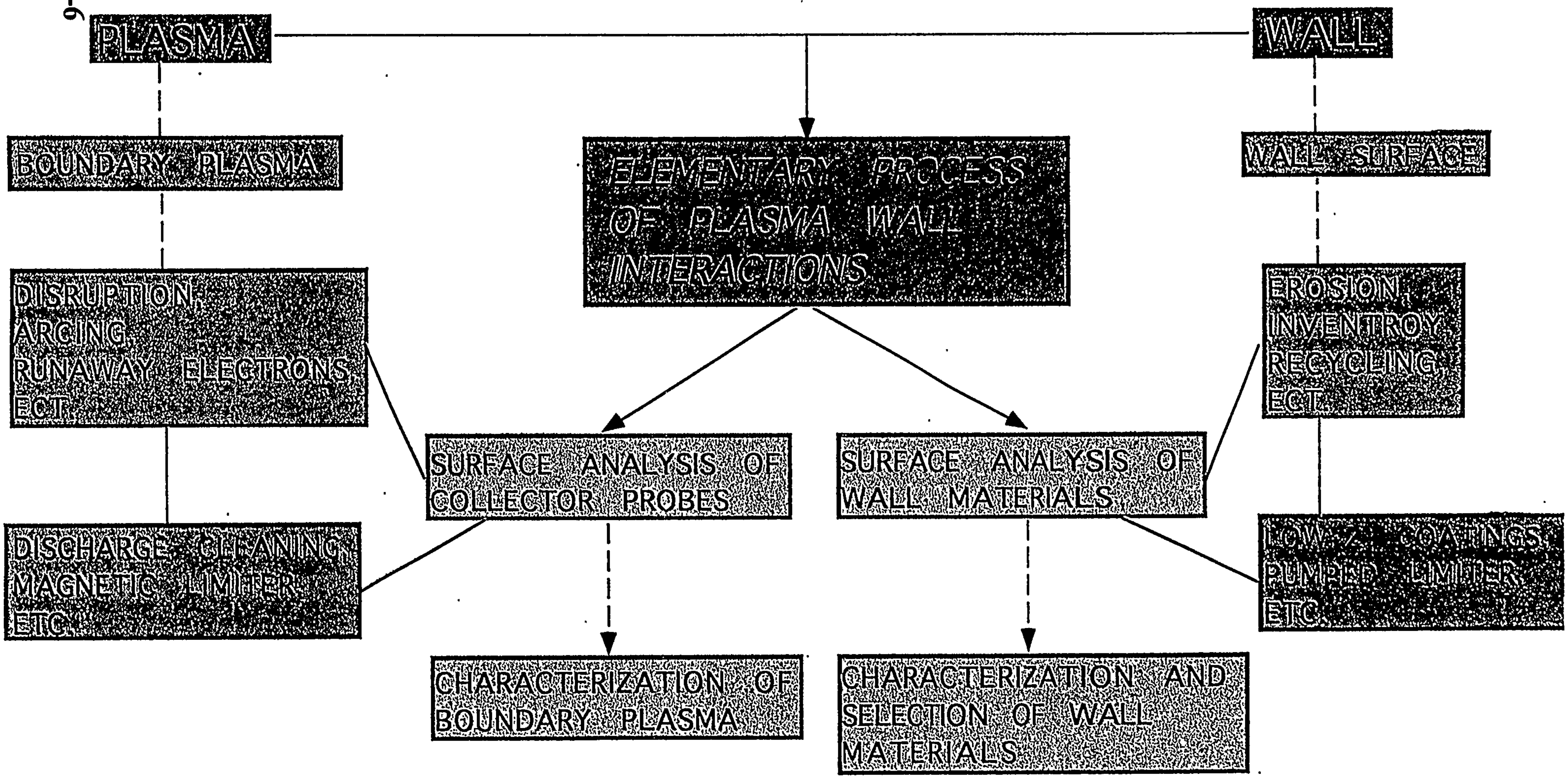

SURFACE ANALYSIS STUDY FOR PLASMA WALL INTERACTIONS

OUR VIEW

1. Plasma Wall Interactions ⟷ Surface Analysis Techniques
2. Torus Machine Experiments ⟷ Simulation Experiments
3. Surface Collector Probes ⟷ Long Term Exposed Materials

OUR RESULTS

Torus Machine Experiments by Heliotron E
JIPPT-IIU
Doublet III

1. Impurity	WHAT?	species	PIXE
	WHERE?	source	AES, XPS, SIMS
	HOW?	flux, energy	RBS, AES
	WHEN?	time	AES
2. Hydrogen Deuterium	HOW?	flux, energy	NRA, TDS
3. Wall Materials			
	WHAT?	erosion & sputtering yield	RBS, XPS, AES

III-8

OUR FIRST CONTRIBUTION
TO PLASMA·SURFACE·INTERACTIONS
CONFERENCE CULHAM 1977

Journal of Nuclear Materials 75 (1978) 7–13

SPUTTERING PROCESS OF A SILICON CARBIDE SURFACE WITH ENERGETIC IONS BY MEANS OF AN AES–SIMS–FDS COMBINED SYSTEM

Mamoru MOHRI, Kuniaki WATANABE and Toshiro YAMASHINA
Department of Nuclear Engineering, Faculty of Engineering, Hokkaido University, Sapporo, Japan 060

Received 20 February 1978

Surface phenomena on silicon carbide following interaction with energetic hydrogen ions and argon ions have been studied by means of simultaneous, in situ measurements with a combined system of AES–SIMS–FDS (Flash Desorption Spectroscopy). Bombardment by 0.7 and 1.5 keV argon ions was observed to sputter the surface atoms, both silicon and carbon, with the same sputtering yields. In the case of bombardment by hydrogen ions, on the other hand, silicon atoms were sputtered out preferentially through chemical sputtering to form silicon hydrides at room temperature. In-depth composition profiles of silicon carbide irradiated by 100-keV D^+ ions were also examined by the combined system.

IMA (Ion Microprobe Mass Analysis) 1977

Ion beam (Duoplasmatron)
0 ~ 30 KeV, 0.1 mmφ (scanning)
several tens μA ($H^+, D^+ \ldots$)

Mass analyzer (Stigmatic second order double focussing mass spectrometer)

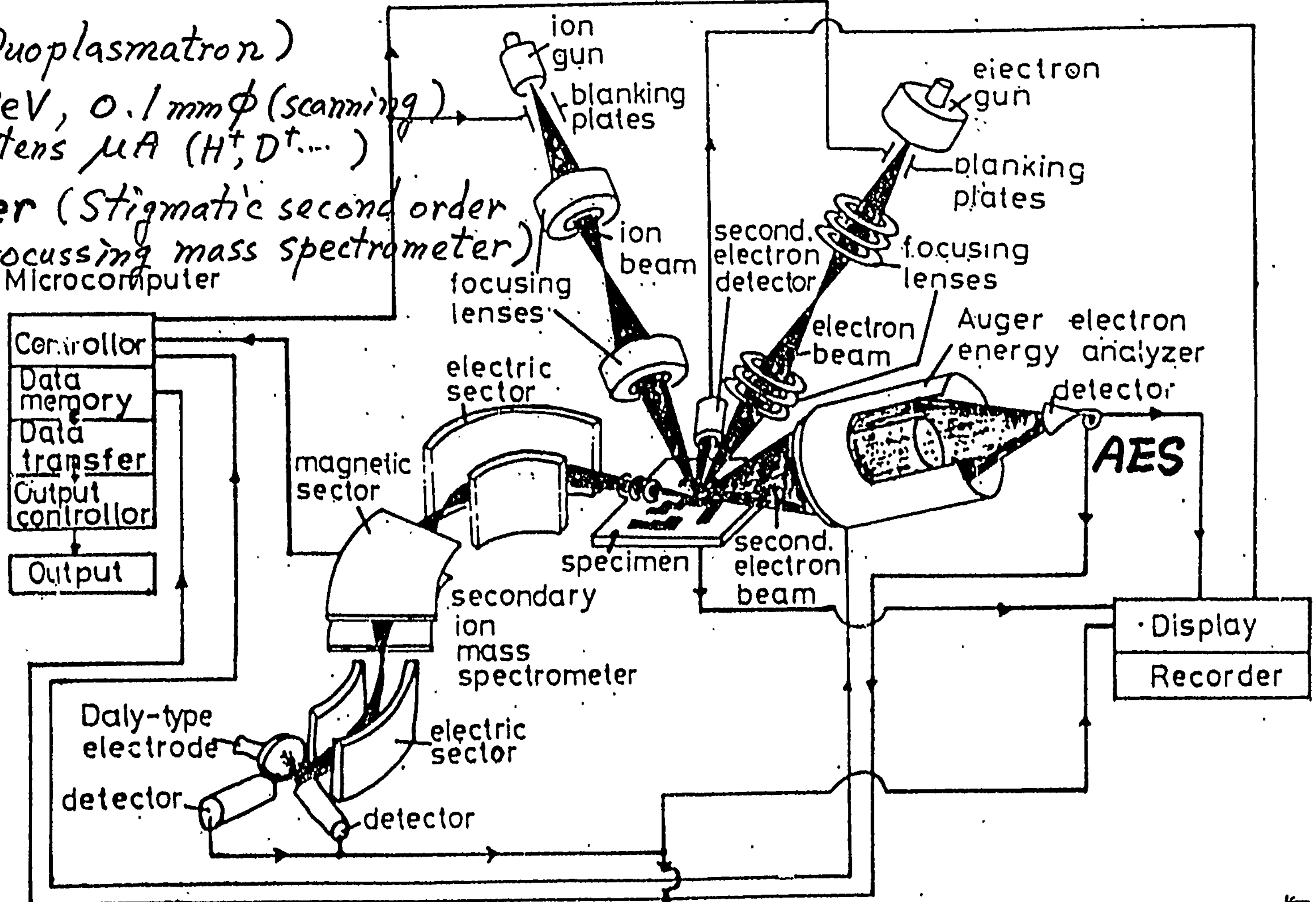

Fig. 1. Schematic construction of the AES-IMA combined system.

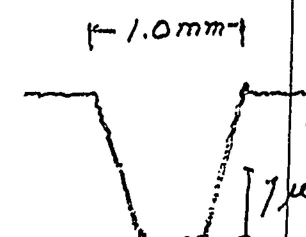

The beam could be scanned with sawtooth waves, and the surfaces were evenly etched

1. Sputtering yield measurement by volumetric method
2. Chemical and physical sputtering processes
3. Energy distribution analysis of sputtered species

1977

Physical and Chemical Sputtering Processes of SiC by Energetic Hydrogen Ions

SiC clean surface

after simultaneous treatments with Ar^+-etching and heating at 600 °C.

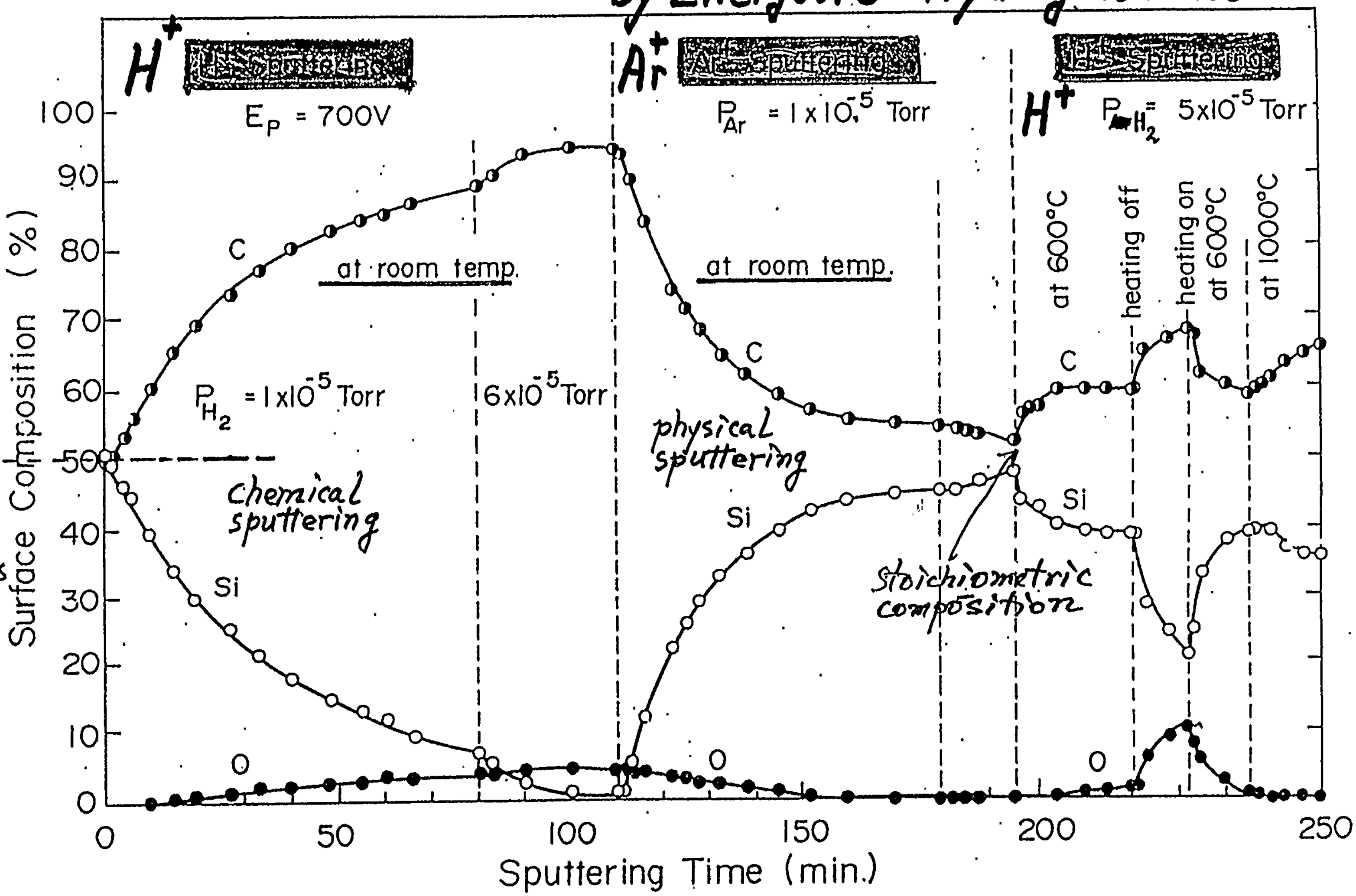

Fig. 5. Variation of surface composition during borbardment with H^+ and Ar^+ ions at various temperatu

SIMS measurement revealed that H^+ or D^+ bomb. produced silicon hydrides and hydrocarbons.
AES measurement showed a decrease in the concentration of Si and an increase of C.
Subsequent bomb. by H_0^+ or Ar^+ ions brought about a stoichiometric composition 50:50

COLLABORATION WITH VARIOUS MACHINES

1980 ~

JIPPT-II (NAGOYA UNIV.)
HELIOTORN-E (KYOTO UNIV.)
STORAGE RINGS (CERN)
TEXTOR (KFA)
DOUBLET III (GA)
JT-60, JT-60U (JAERI)
LHD (NIFS)

ARGONNE NL
SANDIA NL (LIVERMORE AND ALBUQUERQUE)
OAKRIDGE NL

SURFACE PROBE STUDIES IN TORUS DEVICES

JIPP T-IIU 1981～
HELIOTRON E 1983～

1. EFFECTIVE UTILIZATION OF SURFACE ANALYSIS TECHNIQUES

2. TRANSPORT PROCESSES OF IMPURITIES

   a) DETECTION OF IMPURITIY SPECIES
   b) AREAL DISTRIBUTION OF IMPURITIES
   c) ENERGY ESTIMATION OF IMPURITIES

3. TRANSPORT PROCESSES OF PLASMA PARTICLES

   a) FLUX OF HYDROGEN IN SCRAPED-OFF LAYER
   b) TIME RESOLVED ANALYSIS
   c) ENERGY ESTIMATION OF PLASMA PARTICLES

1981 ~

JIPP T-II U

MOHRI · NODA

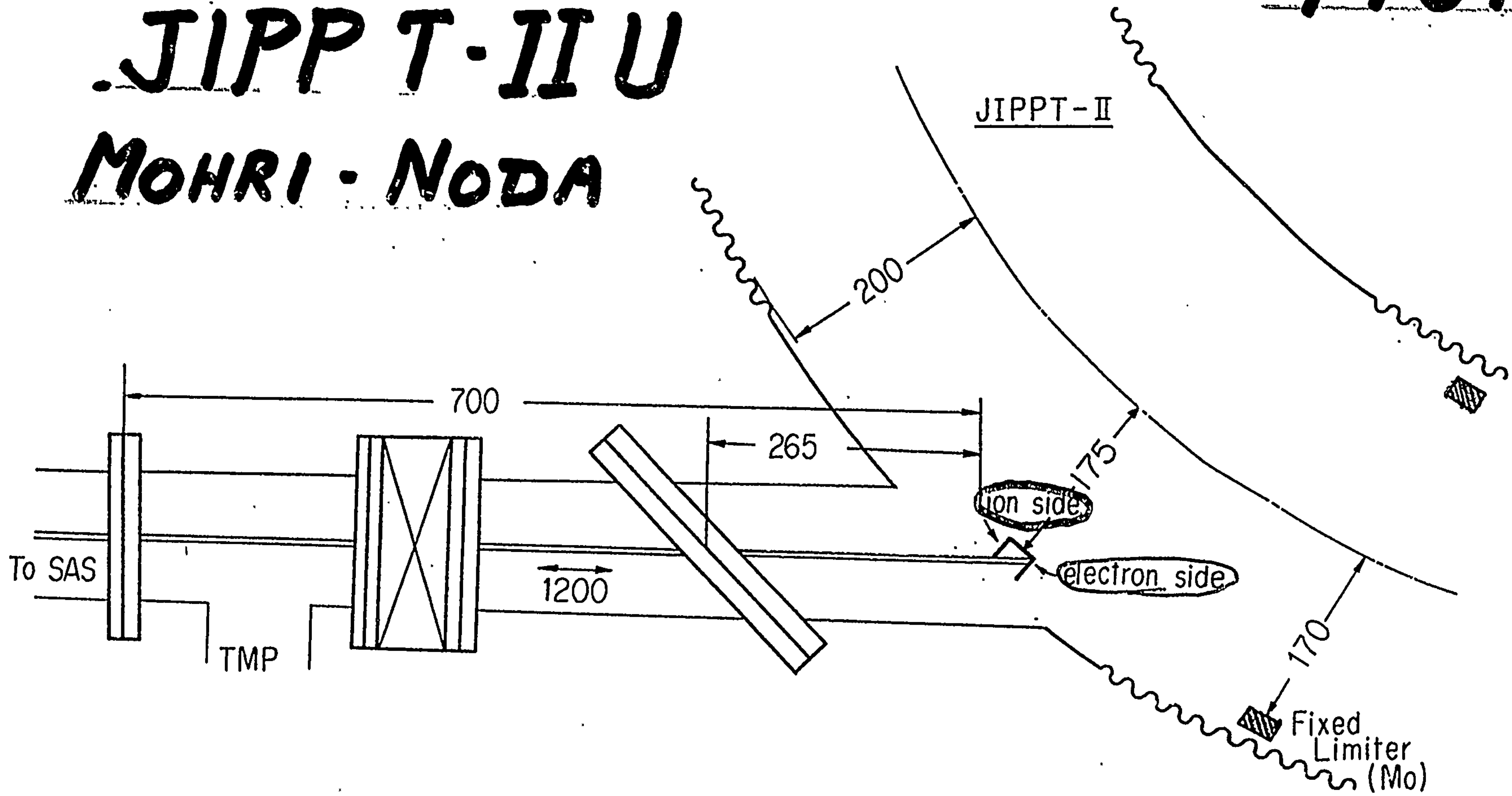

GEOMETRY OF THE SAMPLE PROBE INTRODUCED INTO JIPP T-II

1983 ~

Surface Analysis Station

HELIOTRON E

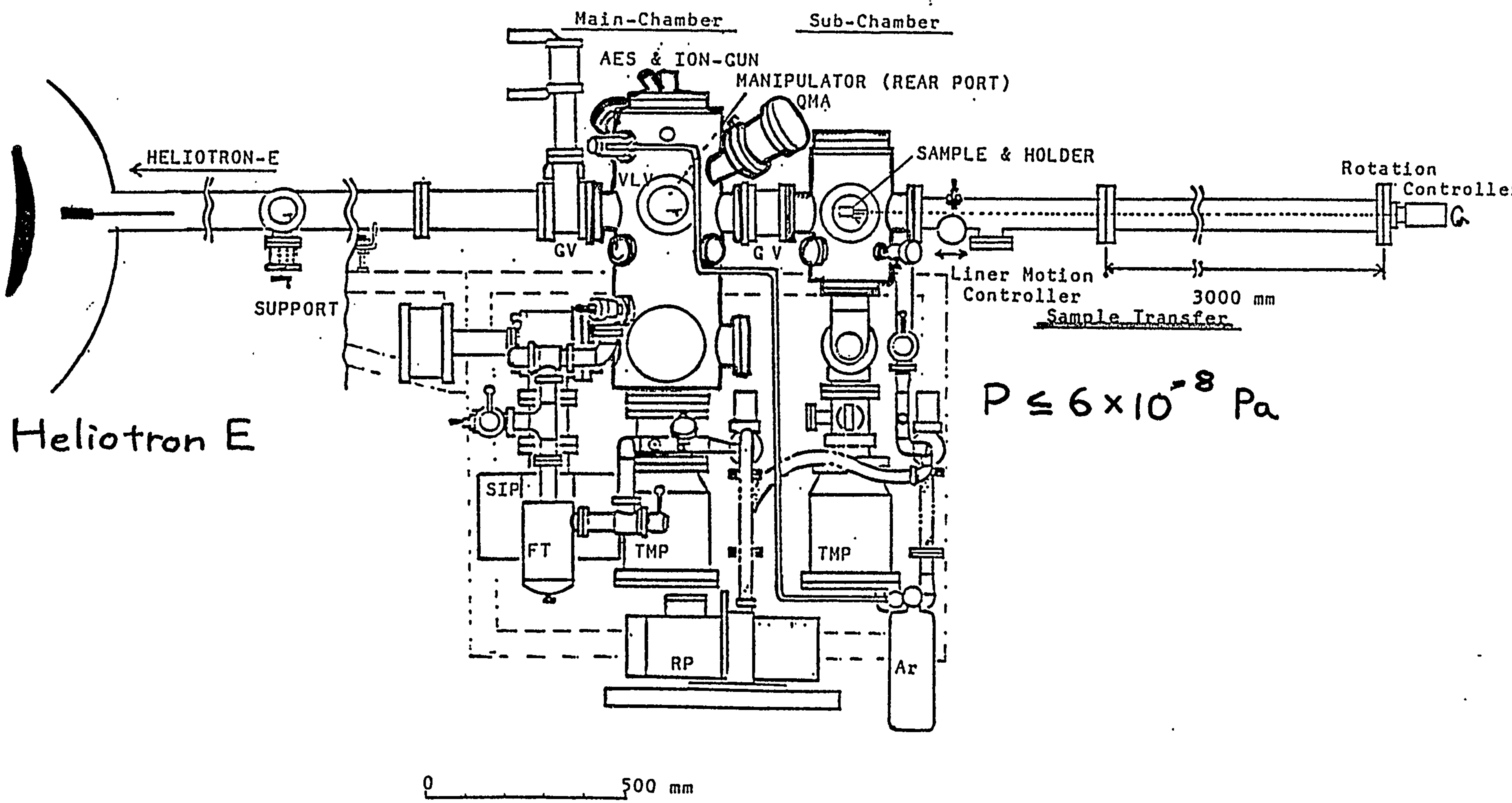

1984
HELIOTRON E
MOHRI · MOTOJIMA

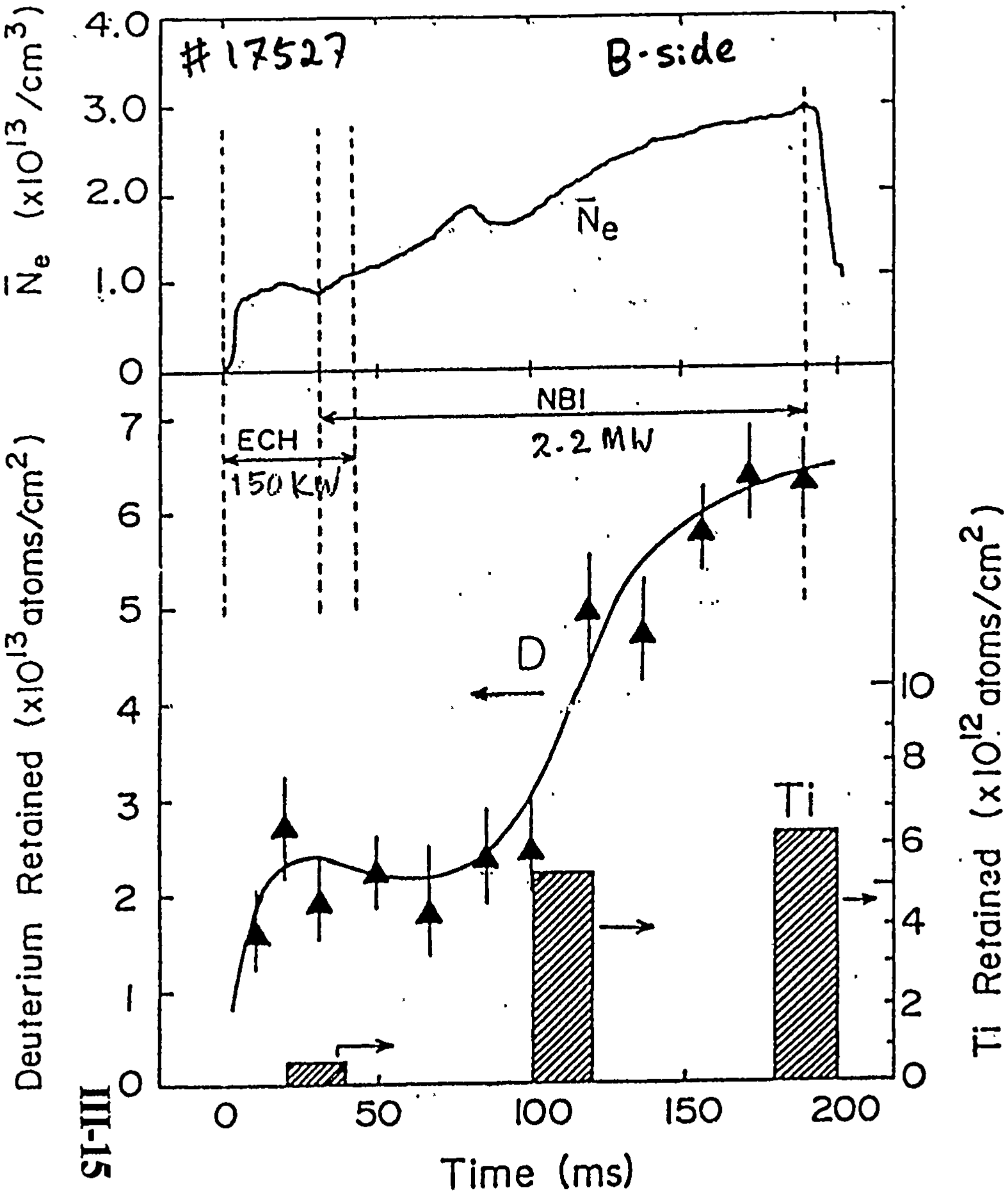

Fig. 16 Time resolved analysis of deuterium and titanium retained on the rotatable surface probe and averaged electron density during currentless plasma discharge.

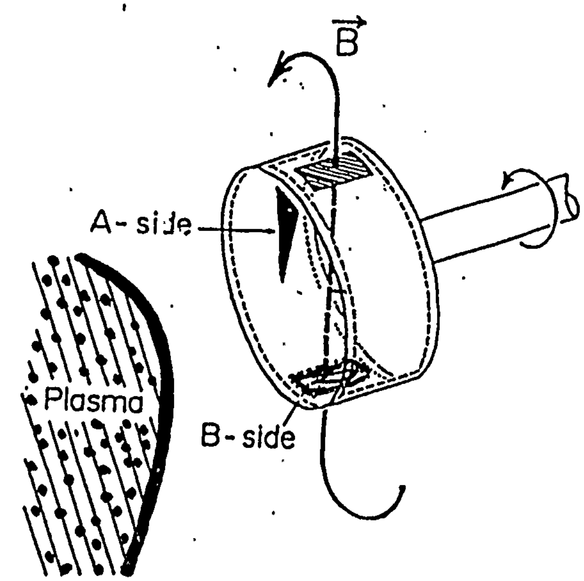

Fig. 2. A schematic view of the rotatable surface collector probe.

DAMAGE ANALYSIS OF ARMOR / LIMITER TILE OF PLSMA MACHINES

JIPP-TII (TiC LIMITER)
1982~

D-III (SiC LIMITER)
1982~

TEXTOR (GRAPHITE ALT-II)
1984~

JT-60 (GRAPHITE ARMOR)
1990~

DOUBLET III

1982 ~

TRESTER
HOPKINS

NEUTRAL BEAM ARMOR/LIMITER PANEL DOUBLET III

SiC COATINGS

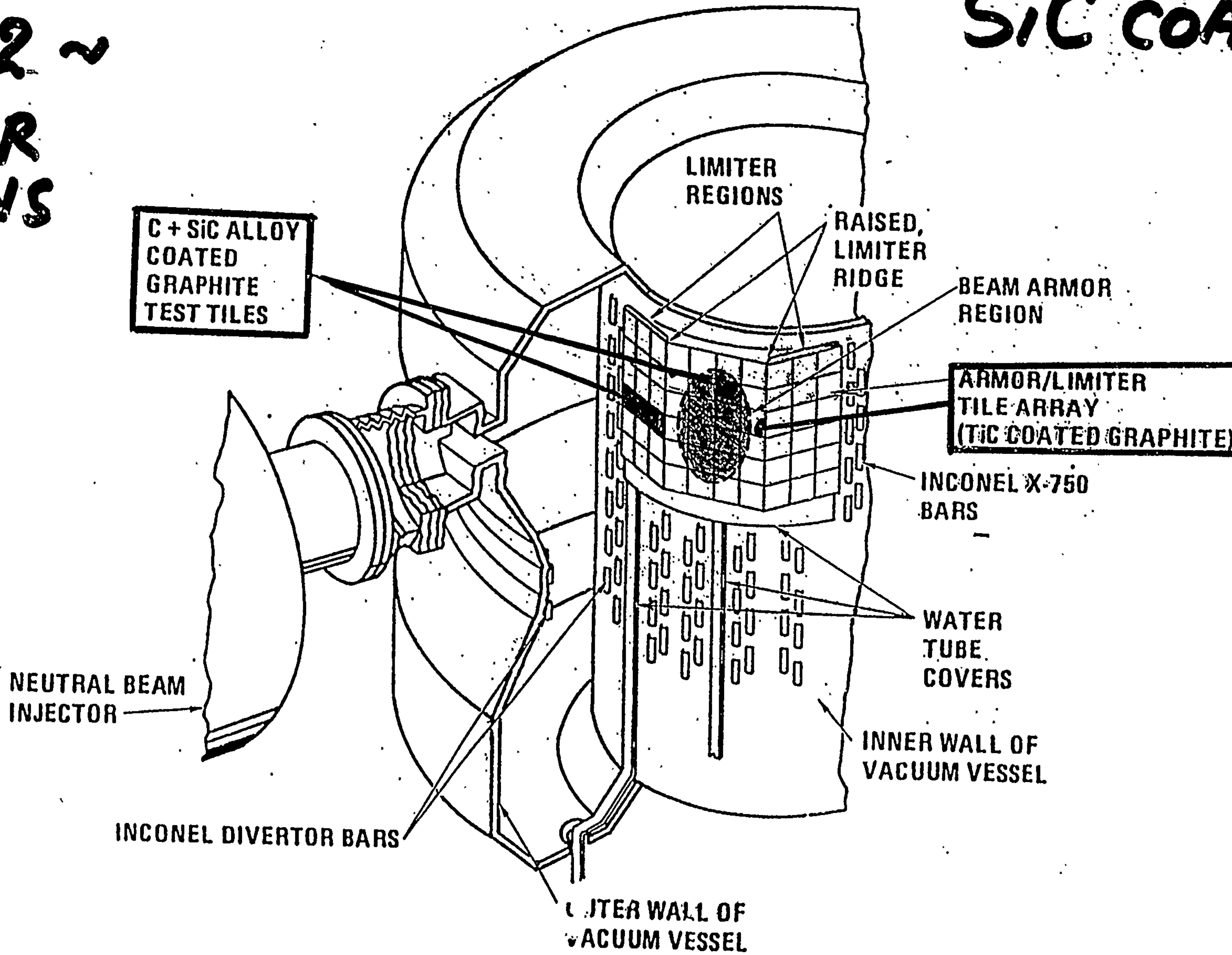

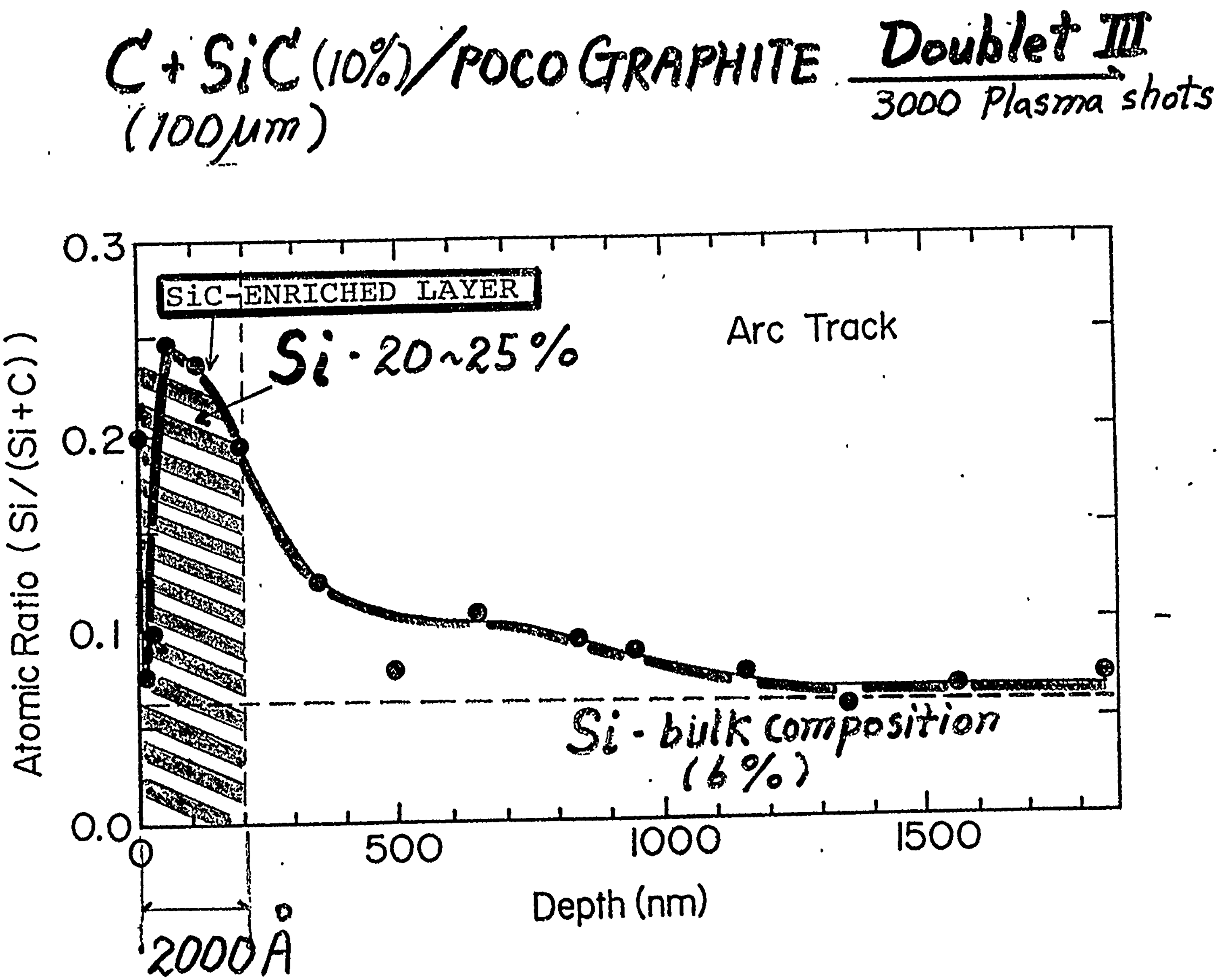

DEPTH PROFILE OF C+SiC(10%)/C SURFACE AFTER
LONG TERM PLASMA EXPOSURE IN DOUBLET III.

JT-60 1990~

AKIBA
ANDO

GRAPHITE COMMUNTY

1986 ~ 1990

OVERALL CHARACTERIZATIONS OF GRAPHITES AS FUSION FIRST WALL MATERIAL AND EVALUATION OF THE STABILITY AGAINST PLASMAS

INTERIM REPORT

by
Fusion First Wall Material Research Group,
Nuclear Fusion Research Project,
The Ministry of Education,
Science and Culture, Japan

January 1989

Edited by Toshiro Yamashina, Project Leader
Hokkaido University, Sapporo, Japan

JAPANESE COMPANIES

Table 1 Product names of graphite materials and the companies. ISOTROPIC GRAPHITES {High Density, Low Density}

Company name	Product name of graphite
Ibiden Co.	T−6P, T−4MP, ETP−10
Nippon Steel Chemical Co.	#880, #781
Tokai Carbon Co.	G1950, G347S
Toyo Carbon Co.	AX650, KMT200K, AX280K, YPD−K
Toyo Tanso Co.	ISO−880U, ISO−630U, IG−110U
Hitachi Chemical Co.	PDX−80S, PDX−60S
Nippon Carbon Co.	EFG262, EFG301

1991 ~

RESEARCH NETWORK OF FUSION ENGINEERING IN JAPAN

TOSHIRO YAMASHINA
HOKKAIDO UNIVERSITY

PRESENT STATUS OF FUSION ENGINEERING STUDIES

RESEARCH NETWORK PLAN OF ENGINEERING FUSION

~~JAPAN — THE HOST COUNTRY FOR ITER~~

NETWORK PLAN ~ FUSION REACTO ENGINEERING

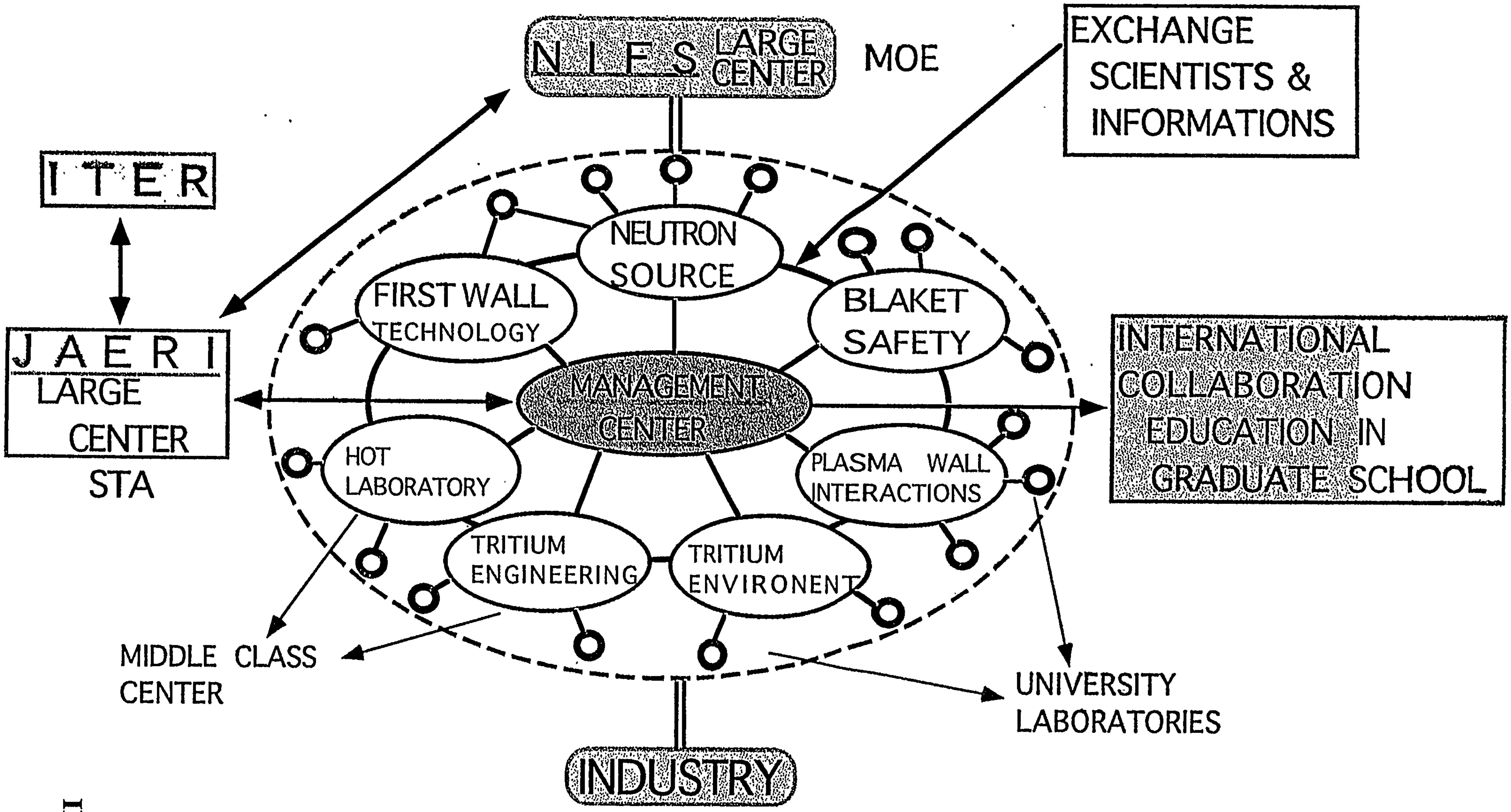

1981~1990

EFFECTIVE UTILIZATION OF SURFACE ANALYSIS TECHNIQUES TO ENVIRONMENTS

OUR SIDELINES

MICROANALYTICAL STUDIES OF ENVIRONMENTS AND AIR POLLUTION CAUSED BY STUDDED TIRES OF AUTOMOBILES

MAMORU MOHRI
SUSUMU AMEMIYA
SHIGERU MAEDA
SHIN FUKUDA
SHIGEKI KATO
MASAO HASHIBA
TOSHIRO YAMASHINA

北海道大学工学部研究報告
第114号（昭和58年）

Bulletin of the Faculty of Engineering,
Hokkaido University, No. 114 (1983)

1982～

スパイクタイヤ車粉塵の精密分析（第二報）

毛利　衛　雨宮　進*　前田　滋
福田　伸　加藤茂樹　佐竹　徹
橋場正男　山科俊郎

（昭和57年12月27日受理）

Microanalysis of Dust Particles from Road Surface Scraped off by Studded Tires of Automobiles —— Part 2

Mamoru MOHRI, Susumu AMEMIYA, Shigeru MAEDA,
Shin FUKUDA, Shigeki KATO, Tohru SATAKE,
Masao HASHIBA and Toshiro YAMASHINA

(Received December. 27, 1982)

Abstract

Investigations of particulate substances originating from the use of studded tires of automobiles were performed. The amount of floating dust particles was measured by particle induced X-ray emission spectroscopy (PIXE) as a function of the horizontal distance from a road-edge and the vertical distance from the ground in the city of Sapporo. The results were compared with those of the city of Nagoya. It was found that the amount of floating dust particles in Sapporo was four to five times larger in November and April, while it was much less in February than that in Nagoya. The chemical composition of studs of studded tires and paint of road marking were analyzed by Auger electron spectroscopy (AES) and atomic absorption spectroscopy, respectively. Based upon these measurements the particulate substances collected from a road surface were examined and identified by use of scanning electron microscopy (SEM) and X-ray microanalyzer (XMA). They could be attributed to mainly pieces of studs, paint from road markings and paving materials. Alveoli of the lungs of dogs and mice which inhaled such dust particles were also examined by SEM and XMA. Ferruginous components were found to segregate on the wall surface of the alveoli.

車粉じん分析に用いた各種分析機器

SEM (Scanning Electron Microscopy)
走査型電子顕微鏡

AES (Auger Electron Spectroscopy)
オージェ電子分光器

XMA (X-ray Microprobe Analyzer)
X線マイクロアナライザー

TEM (Transmission Electron Microscopy)
透過型電子顕微鏡

IMA (Ion Micro Probe Mass Analyzer)
イオンマイクロアナライザー

PIXE (Particle Induced X-ray Emission)
粒子励起X線放出分光

IR (Infrared Spectroscopy)
赤外線分光

XPS (X-ray Photoelectron Spectroscopy)
X線光電子分光

Comparison of Dust Particle Amount

(Sapporo and Nagoya)

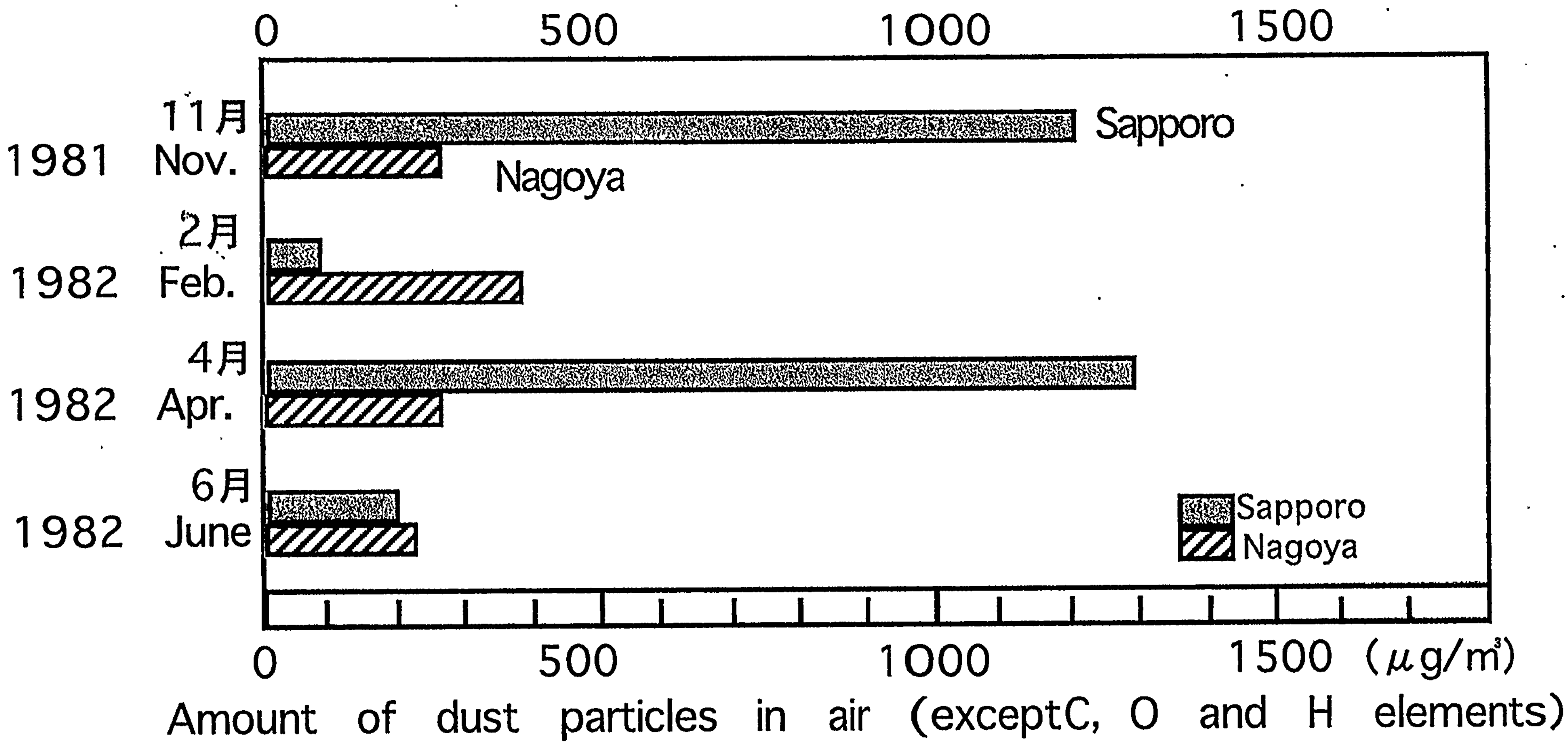

Amount of dust particles in air of Sapporo and Nagoya measured in defferent seasons. (by PIXE)

1989~

INVITING PROJECT FOR ITER SITE OF CONSTRUCTION

EAST AREA OF TOMAKOMAI HOKKAIDO (BIG) TOMATOH

- *HUGE FLAT AREA (1000 ha)*
- *EASY ACCESS TO INTERNATIONAL AIRPORT (SAPPORO) 15 km*
- *REQUIED COOLANT AVAILABLE FACING TO SEASIDE*
- *ELECTRIC POWER ABAILABLE 635 MWe*
- *MILD WEATHER AND BEAUTIFUL RESORTS*

Session IV: Wall Conditioning, Sputter, Erosion

Wall Conditioning at the Start up Phase of LHD

Akio Sagara

National Institute for Fusion Science, Toki 509-52, Japan

The first cycle of the LHD plasma operation is scheduled to set off from the end of March, 1998. At this first stage the magnetic flux density at the plasma axis B_0 is 1.5T, and the plasma heating with 84GHz ECH of the total input power over 0.5MW is arranged, which is operated using the second harmonics with the cut-off plasma density of $8.8 \times 10^{19} m^{-3}$.

According to the estimate of radiation loss using the 1-D time-dependent transport code under the first operation condition [1], it is required for the oxygen concentration in the hydrogen plasma to be less than 1.8%, that is, the Z_{eff} lower than 2 in order to obtain the line averaged plasma density $<n_e>$ of about $2 \times 10^{19} m^{-3}$ with the plasma temperature $T_e(0)$ higher than 1.5keV.

On the other hand, according to the results observed in the wall conditioning procedure performed in the start up phase of CHS [2], ECR discharge cleaning using hydrogen was effective to reduce down partial pressures of H_2O, CO and CH_4, resulting in suppression of uncontrollable density rise under ECH discharges by mainly reducing down oxygen impurities.

Reduction of oxygen impurities is therefore the main purpose of the wall conditioning at the start up phase of LHD. Suppression of hydrogen recycling is also necessary after conditioning with H_2. Standing on this guide line, the main scenario of wall conditioning in LHD has been decided including arrangement of hardware required.

The 300kW hot water utility is arranged for baking the vacuum vessel which is made of 316 stainless steel with the total surface area of $777 m^2$ and the total mass of 77.7ton including ports and bellows. However, this baking procedure is not sufficient, because the temperature is limited at the max. 100°C and there is only one week for baking scheduled before starting the SC coils cooling down.

The main wall conditioning method is the 20kW ECR(2.45GHz)-DC with H_2. It is expected to take about a half day to evacuate adsorbed H2O molecules, and to take at least a few days to reduce oxide layers [2, 3]. After this procedure, the main discharge is set off with 84GHz ECH, which is also considered as an effective conditioning of the wall surfaces, especially with repeated short pulse and high power operations of 10-20Hz and 10-20% duty.

Titanium-gettering is arranged as one of backup methods, which covers the 30% area of V/V and suppresses both of oxygen impurities and hydrogen recycling [4]. The film thickness of only 30 monolayers is sufficient [5], and the total operation time is limited to avoid peeling off of Ti films thicker than 10 μm.

Glow discharge with He is also arranged as the other backup method to reduce oxide layers and to suppress hydrogen recycling after ECR-DC with H_2. Based on intensive R&D results, boronization using glow discharge is scheduled to be put into operation from the 2'nd cycle in 1998.

References :
[1] H. Yamada, 13th meeting of J. Plasma and Fusion Research (1996) 22aD2, p187.
[2] N. Noda, Annual Review of IPP Nagoya University (April, 1988 - May, 1989) p9.
[3] E. Jotaki and S. Itoh, Fusion Eng. Design, 36 (1997) 447.
[4] A. Sagara, J. Nucl. Mater., 93&94(1980) 847.
[5] S. Besshou and O. Motojima, Annual Review of PPL Kyoto Univ., (1981) p64.

Wall Conditioning at the Start up Phase of LHD

Akio Sagara

National Institute for Fusion Science, Japan

The first cycle of the LHD plasma starts from the end of March, 1998

At the operation condition with

- ♦ the magnetic flux density $B_0 < 1.5T$
- ♦ the plasma heating with 84GHz ECH
- ♦ the total input power > 0.5MW

This condition requires the oxygen concentration less than1.8%, that is, Zeff < 2

- ♦ to obtain $\langle n_e \rangle \sim 2x1019m-3$
- ♦ with $T_e(0) > 1.5keV$

Wall Conditioning at the Start up Phase of LHD

1998	Jan. / Feb. / March	27 Fri / 28 Sat / 29 Sun	30 Mon / 31 Tue / April / May / 13 Wed
Preparation ECRDC (20kW) Ti-getter x 3 (20kW) GDC (20kW) Baking (300kW) interlock gass-inlet	Cooling of SCM: 9 → - - - Pumping of V/V: 20 → - - -	Discharge Cleaning	First Cycle Operation of LHD
Pumping	60,000 L/s (CP) + 10,000 L/s (TMP)	3,600 L/s (TMP)	60,000 L/s (CP) + 10,000 L/s (TMP)
Magnetic Field	- - -	875G	1.5T (<--> 875G)
Wall Temp.	baking 1W 100°C ↔ - - - -	r.t. (water)	- - - - → baking + ECRDC ?
Conditioning Procedure **Operation**	- - - Test	ECRDC/H_2	ECH (84GHz) —— ECH - - - → ◇ Long pulse > 500 kW Short pulse(10-20Hz) @ duty 10 -20% @ <P> = 20 -30kW @ P = 150 -250kW ↓ ◇ GDC/He, Ti-getter, ECRDC ↓ ◇ GDC/He, Ti-getter, ECRDC
Evaluation	Evacuation of H_2O, CO - - - Q-mass,	Spectroscopy	Oxygen < 2 % Visible x 2, VUV Reduction of H recycling Ne(cut-off) = 8.8e19/m3

1997.12.3 A.S

Estimate of Radiation Loss with Transport

- *Several times larger than estimate from Corona Equilibrium*

Fixed parameters

R/a = 3.9/0.6 m

Bt = 3 T

Pech = 0.5 MW

Impurity : Oxygen

1 %concentration ⇒ Zeff=1.6

Zeff=2 ⇒ 1 . 8 %concentration

Zeff=3 ⇒ 3 . 6 %concentration

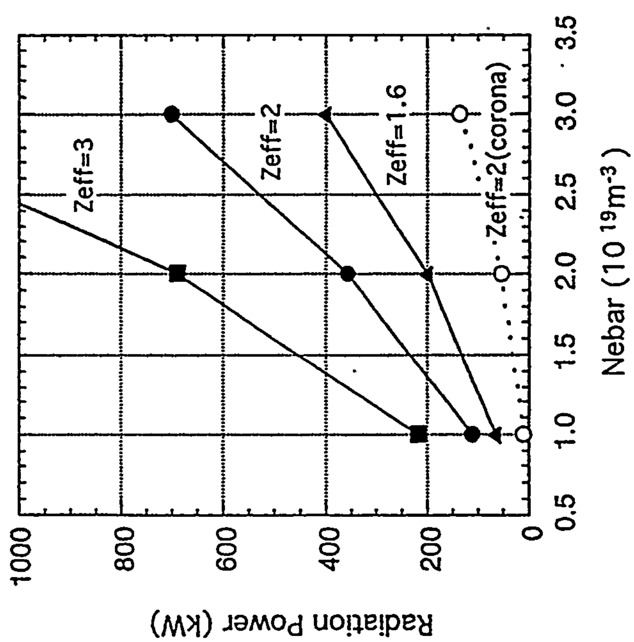

H. Yamada

Reduction of oxygen impurities is the main purpose of the wall conditioning at the start up phase of LHD

After pumped down to the range of 10^{-8} Torr,
the 300kW hot water is used for baking the V/V

- ♦ made of 316 stainless steel
- ♦ the total surface area of $777 m^2$
- ♦ the total mass of 77.7ton

However, this baking procedure is not sufficient,
because the temperature is limited at the max.100°C
and there is not enough time before the first cycle.

The main wall conditioning method is ECR-DC with H_2.

- ♦ 2.45GHz ECR
- ♦ input power of 20kW ($\sim 50 W/m^2$)
- ♦ Remote control
- ♦ Water-cooled window

It takes <u>about 10~20h</u>
to evacuate adsorbed H_2O.

It takes <u>at least a few days</u>
to reduce oxide layers.
(cf. CHS, JIPP T-IIU, TRIAM-IM)

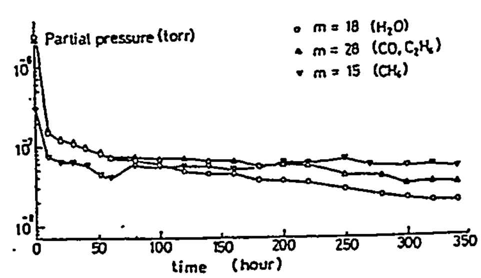

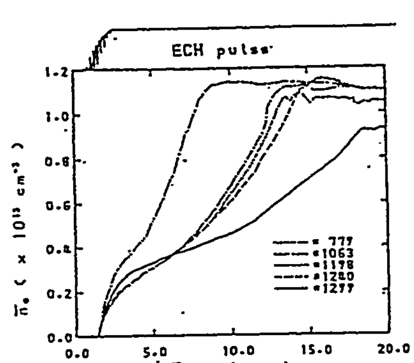

ECR-DC in CHS, 1988, N.Noda

JIPP T-IIU. by Y. Hori

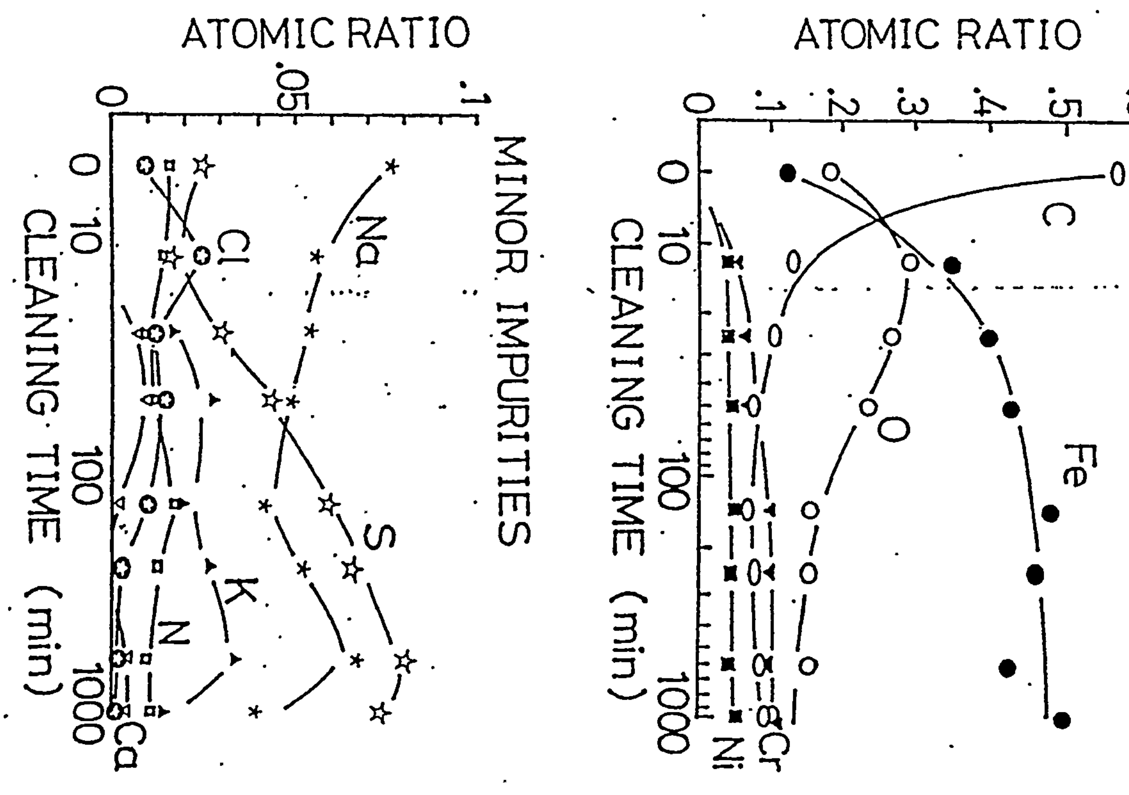

Fig. 3-7 Surface composition ratios of stainless steel sample as a function of discharge cleaning time.

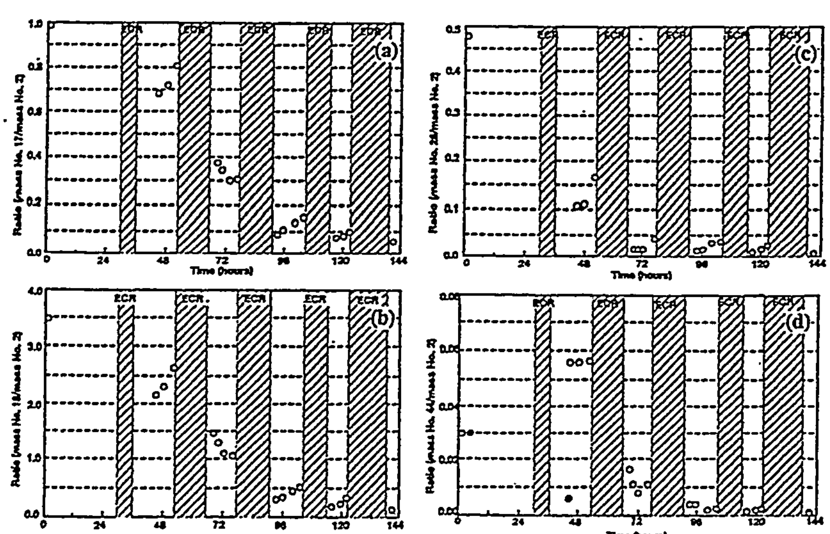

Fig. 2. Dependencies of impurity components on duration of ECR–DC. (a) OH; (b) H_2O; (c) CO and (d) CO_2. Shaded intervals indicate the periods of ECR–DC. The three impurities a, b and c exhibit a similar trend in reduction. However, the tendency for d (CO_2) differed slightly in that the quantity increased with initial ECR–DC, and thereafter declined in a manner similar to the other impurities. In these graphs, the open circles indicate data after rebuilding, and the closed circles show data from ordinary experimental terms before rebuilding.

IV-7

The main 84GHz ECH discharges will be effective for reducing oxide layers.

Especially with repeated short pulse and high power operations

- ♦ 10 - 20Hz
- ♦ duty 10 -20%
- ♦ <P> = 20 - 30 kW
- ♦ P = 150 - 250 kW

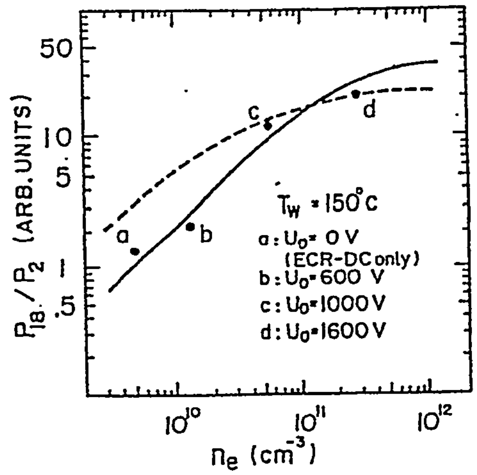

図5-7. 放電洗浄中の水蒸気分圧 P_{18} と水素分圧 P_2 の比のプラズマ密度依存[13].

P_{18}/P_2 vs. n_e under DC, '90, N. Noda

Titanium-gettering is arranged as backup to suppress O impurities

- ♦ with 3 sets in every 120°, and movable in 50cm
- ♦ max.1 h flashing at B=0
- ♦ ~ 30% coverage of V/V
- ♦ Ti films > 30 monolayers

In order to avoid peeling off of Ti films thicker than 10 μm,

- ♦ Total operation < 30 hrs

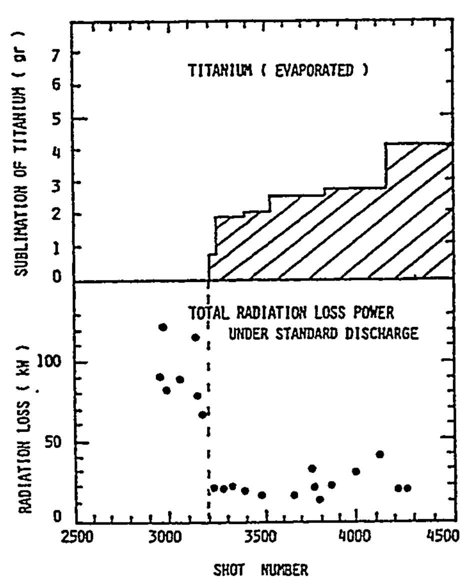

(Heliotron-E, '81) ~1g, 30%, 30layers

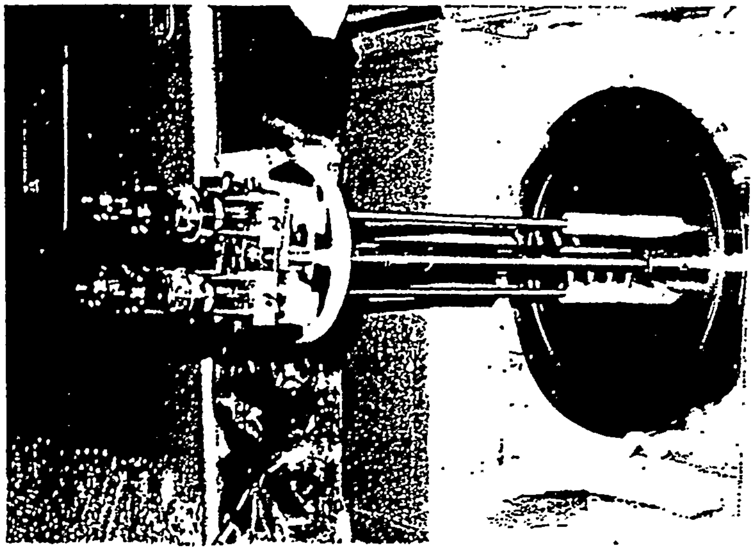

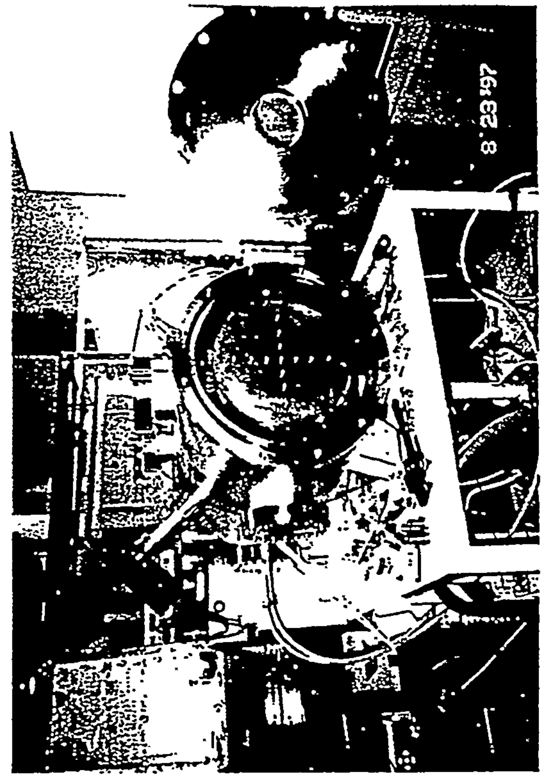
8 23 '97

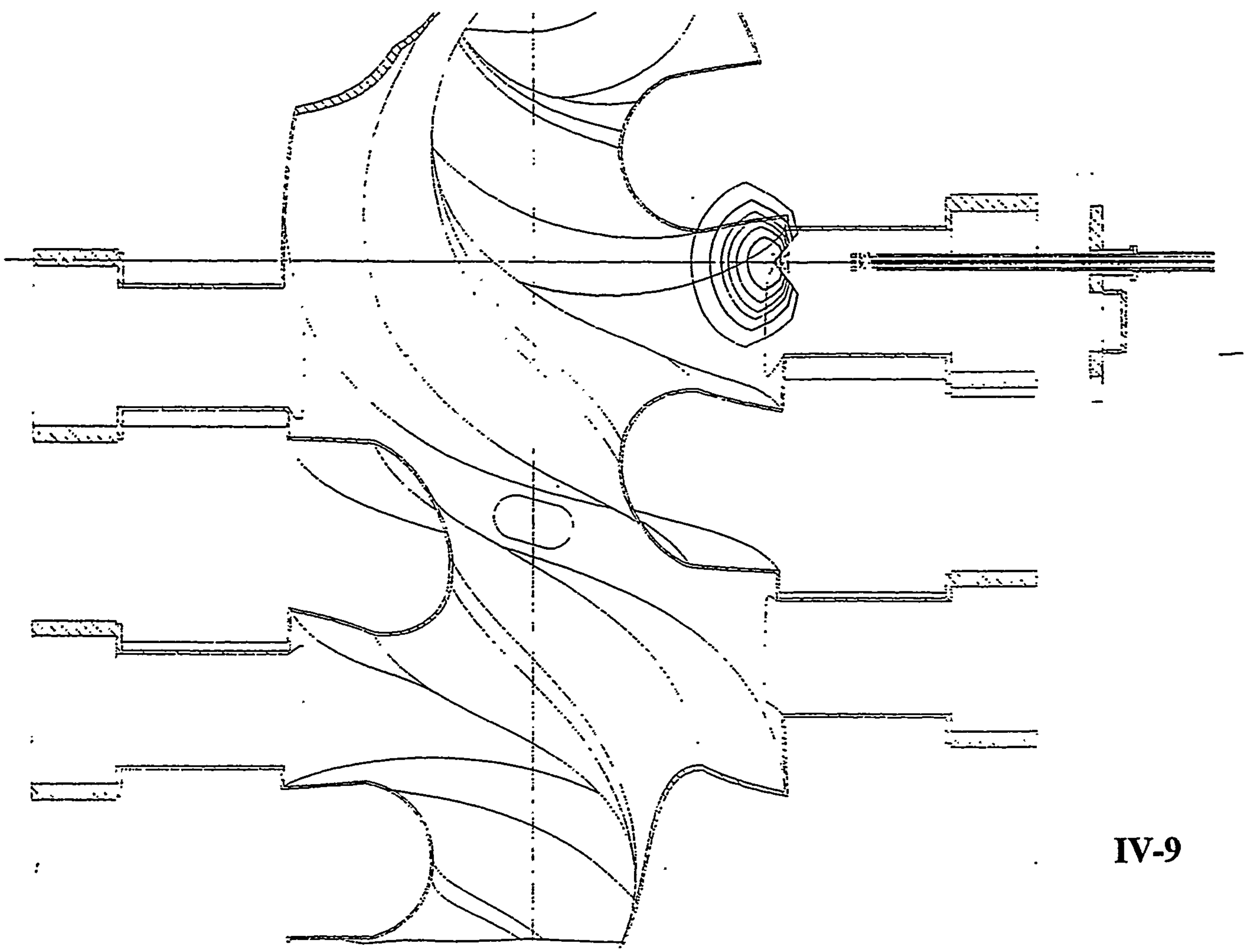

Glow discharge with He is arranged as the other backup method to reduce H recycling after ECR-DC

- ♦ One electrode for the 1'st cycle
  (3 electrodes from the 2'nd cycle)
- ♦ Graphite head under inertia cooling
- ♦ Boronization using glow discharge is scheduled to be put into operation after the 2'nd cycle in 1998.

Conclusion

(1) Reduction of O impurities is the main purpose.

(2) Baking at 100°C with 300kW hot water is arranged.

(3) ECR-DC with H_2 is mainly used to evacuate H_2O in a half day, and to reduce oxide in a few days.

(4) The main 84GHz ECH is also effective.

(5) Ti-gettering and G-DC/He are arranged as backup.

(6) Boronization is scheduled after the 2'nd cycle.

Plasma Conditioning for Magnetic Confinement Fusion Systems

Don Cowgill

- Why condition
- Current techniques
- Our work on removing H-C codeposits
- The optimum discharge parameters
- Conditioning with energetic neutrals

/Sandia National Laboratories

Why is Conditioning Needed?

DFC032693b

- To reduce plasma contamination by minimizing impurity influx from walls and plasma-facing components.
  - Surfaces contain hundreds of monolayers of volatile gases (Graphite tiles have huge surface areas: $1 m^2/gm$)
  - Particularly important: O-bearing contaminants (water)
- To reduce H-recycling during plasma startup, needed for reliable density control.
  - Particularly important for systems with graphite tiles (Hydrogen codeposits with sputtered carbon at 0.4 H/C)
- To control in-vessel tritium inventory.
  - Particularly important for systems with graphite tiles

Co-Deposition is Expected to be a Major Source of In-Vessel Tritium Inventory

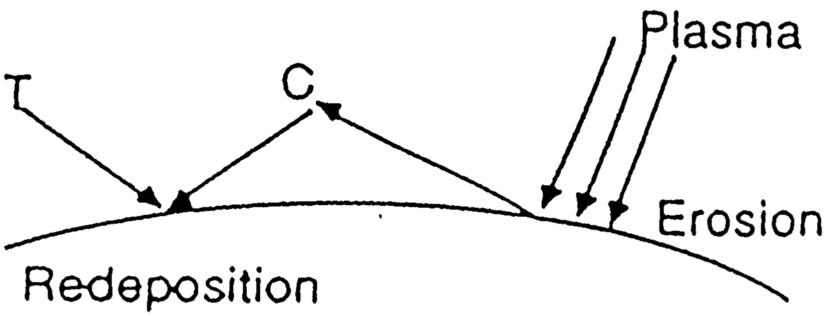

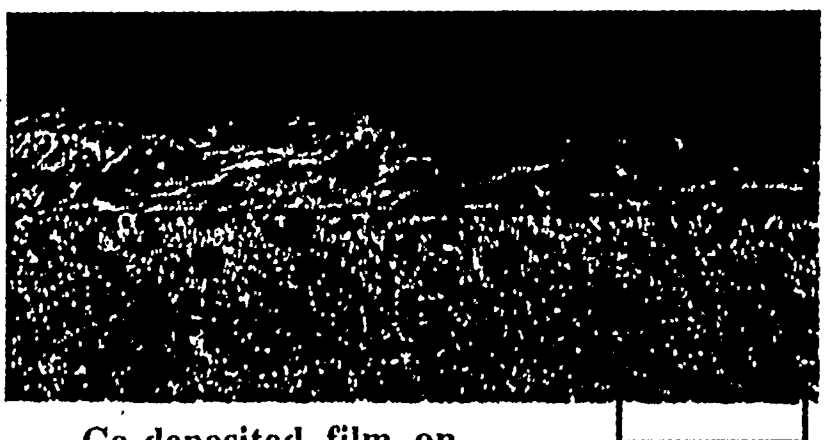

Co-deposited film on TFTR bumper limiter

50 μm

- Carbon erosion from high flux areas results in redeposition of carbon along with tritium
- Tritium concentration ~ 0.4 T/C expected in a DT device
- The thickness of the co-deposited layer increases monotonically with discharge time

KLW:080890D

Current Techniques Used to Condition Tokamaks:

DFC940110m

- Prebaking of invessel materials
- Vacuum bakeout (Outgassing of graphite requires T>1000°C)
- Operation at elevated temperatures
- Active contaminant gettering with B, Be, Li, Si, etc.
- Discharge conditioning: GDC, TDC, PDC, DDC (H, He)

Machine	Op. Temp.	Conditioning Discharges
JET	300°C	GDC, He PDC
Tore-Supra	190°C	
TFTR	RT	GDC, TDC, He PDC, DDC
DIII-D	RT	GDC
JT-60	250-300°C	GDC, He PDC
ASDEX-U	RT	GDC, He TDC

Needs for Future / Current Machines

DFC940110y

- Tore-Supra: Long pulse, steady-state B-field
  - Improved conditioning for impurity control
  - New field-on techniques

- LHD: Not bakeable, steady-state B-field
  - New field-on techniques
  - International Cooperation

- NSTX: Graphite, low bakeout temperature, inertial cooling
  - Improved conditioning for impurity and density control
  - Have started discussions with PPPL

- JET: High near-surface D and T inventories
  - Long conditioning treatments required to keep neutron radiation at acceptible levels
  - More rapid/frequent conditioning methods needed

Glow discharges are used to remove surface impurities

- H(D) volatilizes hydrocarbons to methane ($C_xH_y + H \Rightarrow CH_4$) and weakly-bound oxides to water ($M_xO_y + H \Rightarrow M + H_2O$)
- He desorbs surface and near-surface H (300eV He range ≈ 3.6nm in C, 4.5nm in Be)
- O agressively removes hydrocarbons, volatilizing C to CO
- He-O rapidly removes thick a-C:H codeposits

We studied the He-O erosion process

- To optimize discharge parameters for rapid, efficient conditioning, while minimizing resultant O-contamination
- To identify the best method for use in ITER (steady-state, high B-field)

Our investigations showed He-O GDC removes C-H codeposits

DFC032692

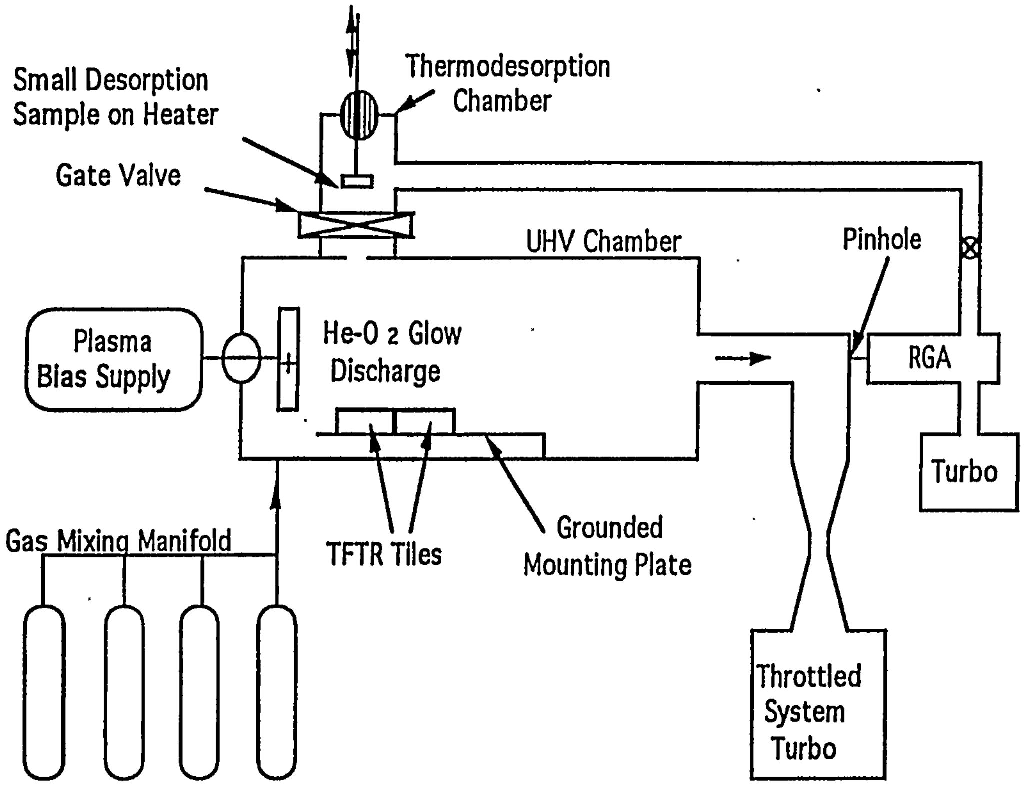

DPE(LAMPE) System

- Codeposit erosion rate ~ 0.3μ/hr
- Efficient removal from gap between tiles
- Surfaces roughened
- O-contamination of tiles

He-Oxygen Glow Discharges Removed Codeposits from TFTR Tiles

DFC970509.5

Cross-section of Codeposit

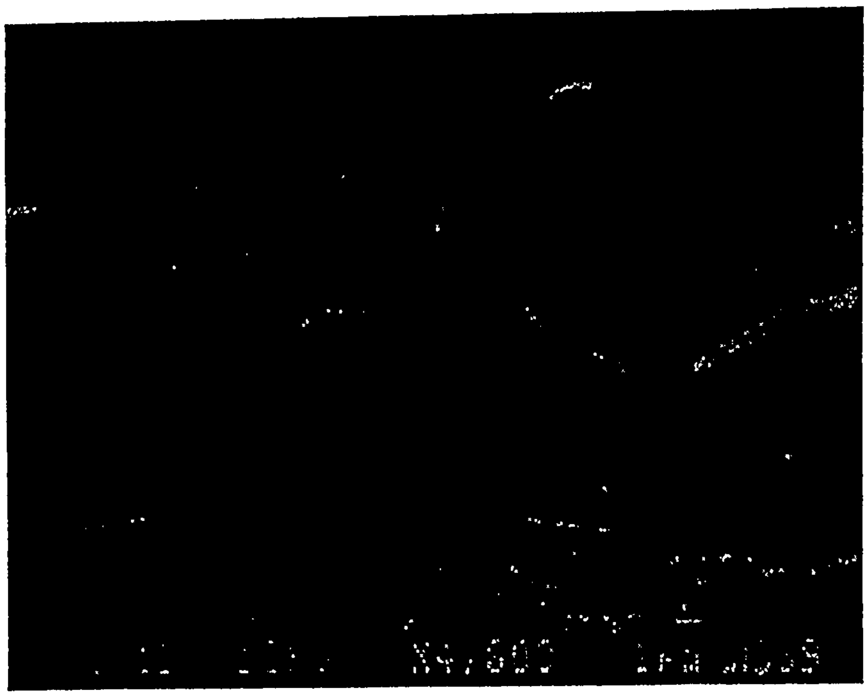

- Erosion is ion-induced:
  - Occurs normal to plasma sheath
- Surfaces become highly textured
- Average codeposit erosion rate:
  - $\approx$ .07 μm/hr from tiles
  - $\approx$ .25 μm/hr from lab. codeposits

We investigated the mechanisms of codeposit erosion by He-O GDC

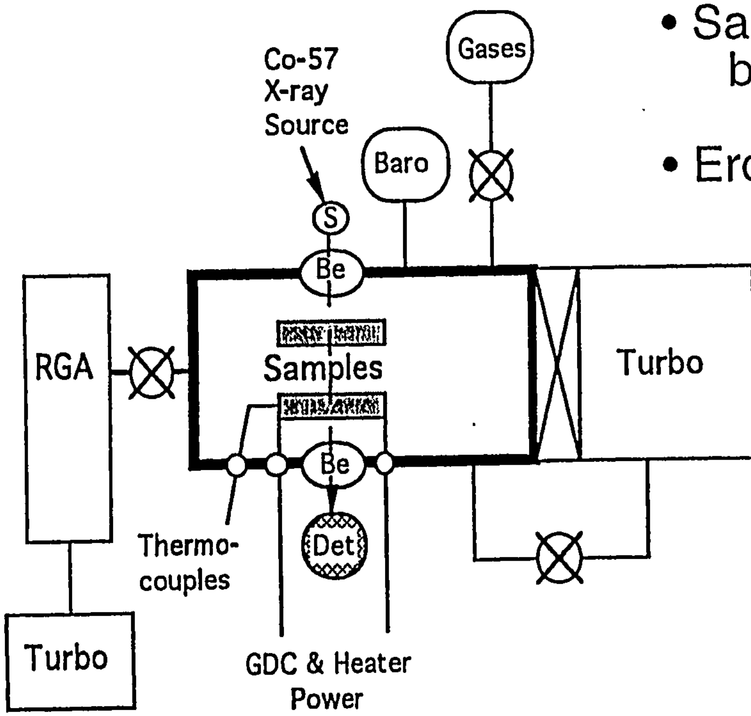

ACX Apparatus

- Sample erosion/oxidation was measured by differential soft x-ray attenuation
- Erosion is correlated with COx production

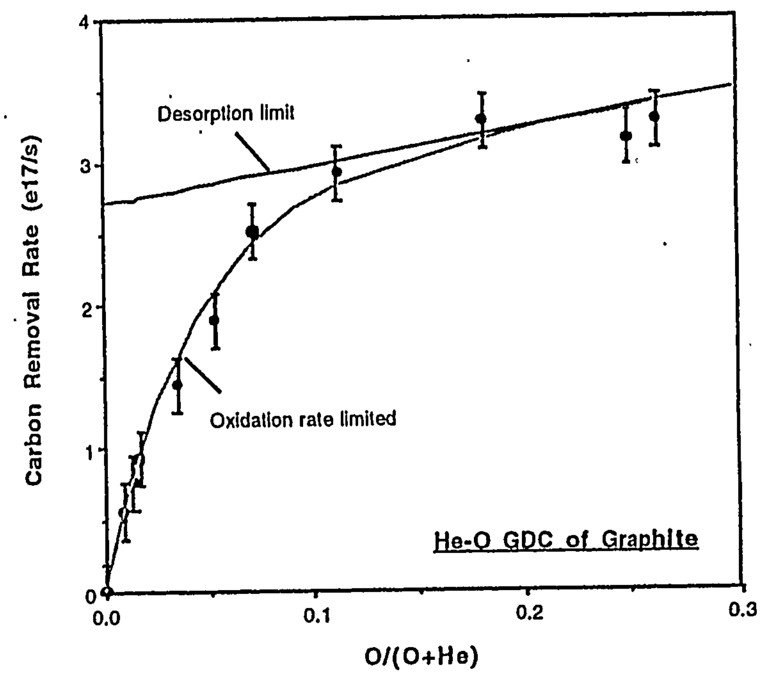

The experiments also showed how bulk O-Contamination can be reduced

DFC940110p

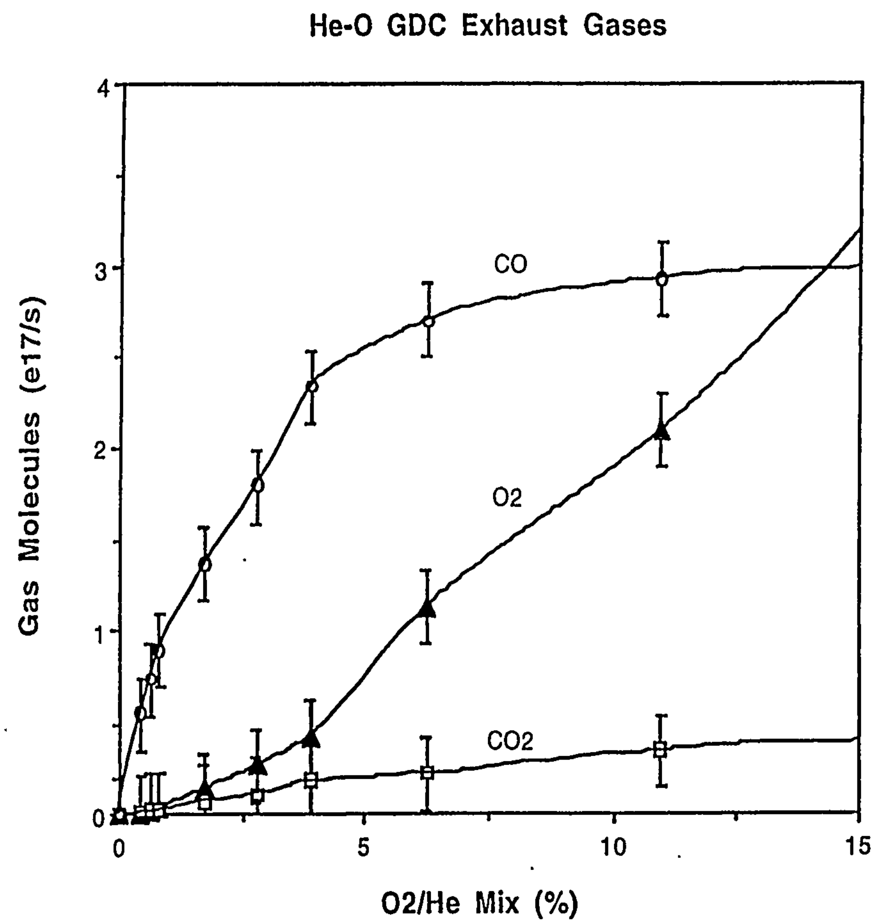

- Input oxygen is rapidly converted to CO and CO_2
- Conversion is even more efficient for Ar-O GDC
- *For low oxygen concentration, little molecular O_2 remains to permeate into graphite pores.*

Summary of RG-O GDC observations:

- Slow pumping (long CO residence time) causes C redeposition and O reuse.
- In desorption limit, a-C:H codeposits are eroded ~3x more rapidly than C.
  (HCO can be used for discrimination)
- Desorption of CO increases with impact energy up to few kV.
  At 400 eV He, desorption yield ≈ 20 CO/He.
- Erosion is normal to plasma sheath: Shielded surfaces are not conditioned.
  Graphite surface becomes textured.
- Observed erosion rates at 2 mA/cm^2, and > 90% oxygen-use efficiency:

	4% O/He GDC	12% O/Ar GDC
Total carbon etch rate -	5.2×10^{15} C/cm^2-s	9.5×10^{15} C/cm^2-s
Graphite surface erosion -	1.4Å/s	2.6Å/s

If texturing is eliminated, overnight conditioning at these rates will remove 6-10 microns of codeposit.

Optimum characteristics for efficient discharge conditioning were determined

DFC940110q

- Particle impact energies of few hundred eV
  - for large desorption yield.
- Particle impact at random angles
  - for large yield, good depth, and no texturing.
- Low electron energies (< 10 eV)
  - for minimal ionization or dissociation of desorbed impurity gases.
- Low background gas pressure ($<10^{-5}$ torr),
  - for rapid evacuation and low gas throughput.

He discharges can produce large energetic He° fluxes by charge exchange

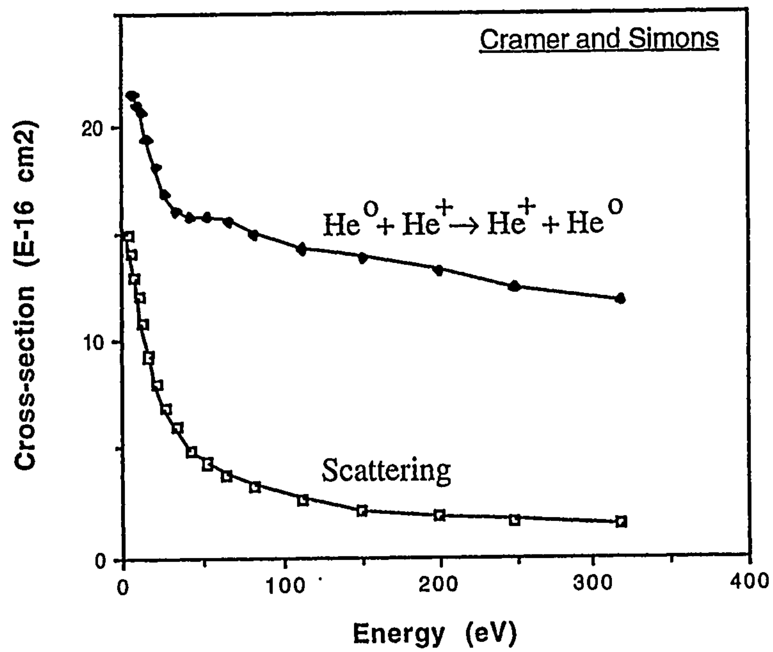

Only He has *high* charge-exchange, but *low* scattering, cross-sections
He can be directly energized by a transverse RF_{ICR} field
Electrons are *slowly* heated by ion scattering
He° energy is determined by the mean-free path to charge exchange

ICR conditioning can produce wall impact energies and fluxes similar to He GDC

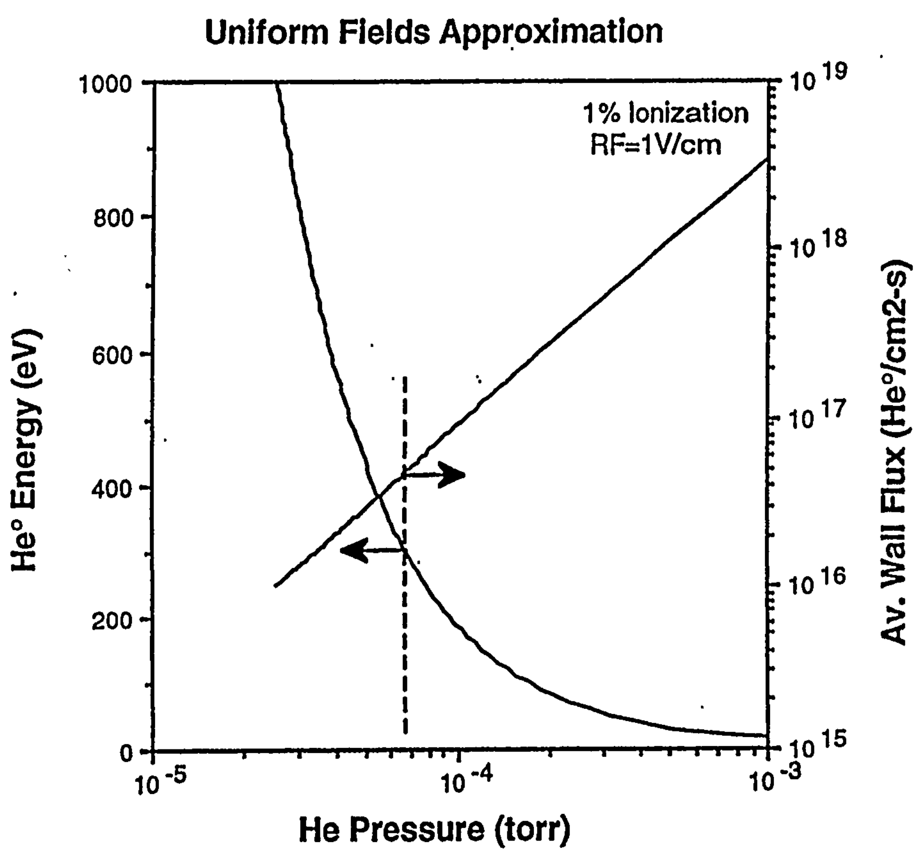

- In uniform fields, He° energy is determined by mean-free-path to charge exchange.

Low gas pressure is required to produce energetic neutrals.

- Discharge is sustained by increase in σ_{ioniz} for He at higher energies.
- The typical He GDC conditions

  300eV, 10^{13}-10^{14} He^{+}/cm^{2} s

  are exceeded by ICR in uniform fields.

We propose that in high B-fields, He ICR can produce optimum conditioning via energetic He°

DFC940110w

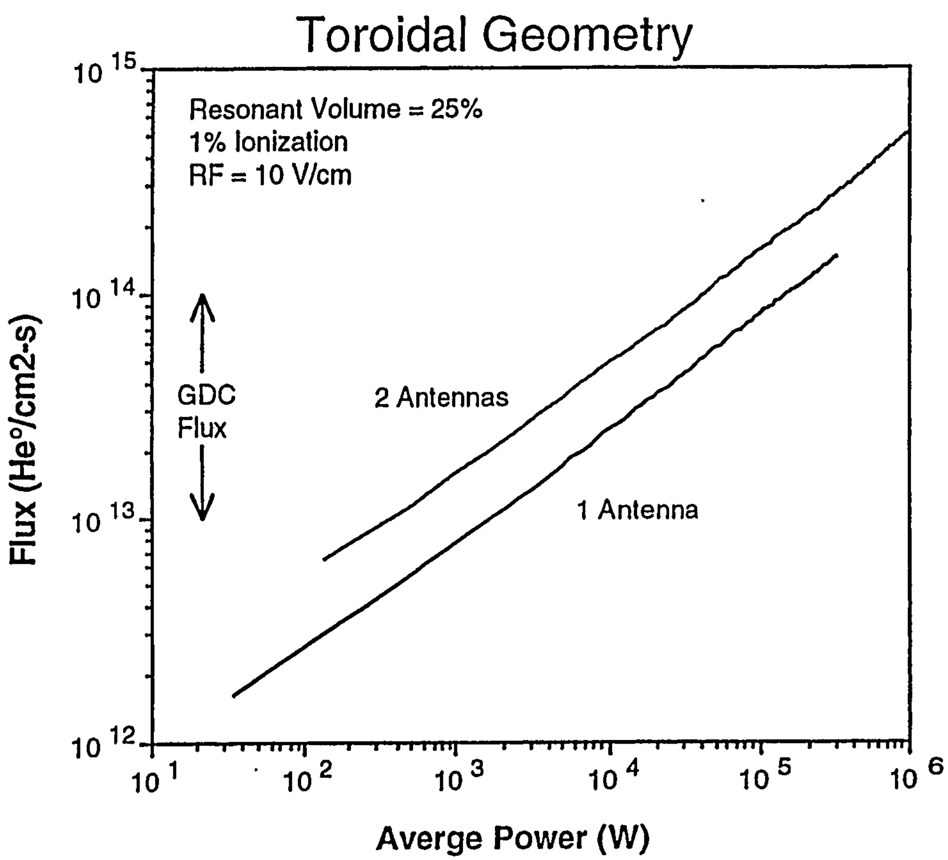

- Charge-exchange wall flux is similar to GDC ion flux
- More efficient than GDC due to
  - lower pressure
  - random impact angle
  - better penetration into gaps between tiles
- C-H codeposit removal using He-O mixture
- Uniform or spot treatment

We are investigating C-H codeposit removal by plasma discharges in high B-fields

DFC971116.1

- Using a 3 Tesla Penning-style trap configuration
  - DC and RF excitation
- Determining removal rates for O-containing discharges (He-O) from rate of carbon oxidation
- Separating erosion rates due to ionized and neutral species
- Exploring penetration into shadowed/confined regions
- Varying plasma power, gas flow/mix
  - maximize removal rate
  - minimize residual O-contamination

We have preliminary data on erosion due to neutrals: atomic-O and He°.

High-field Probe Configuration
11/6/97

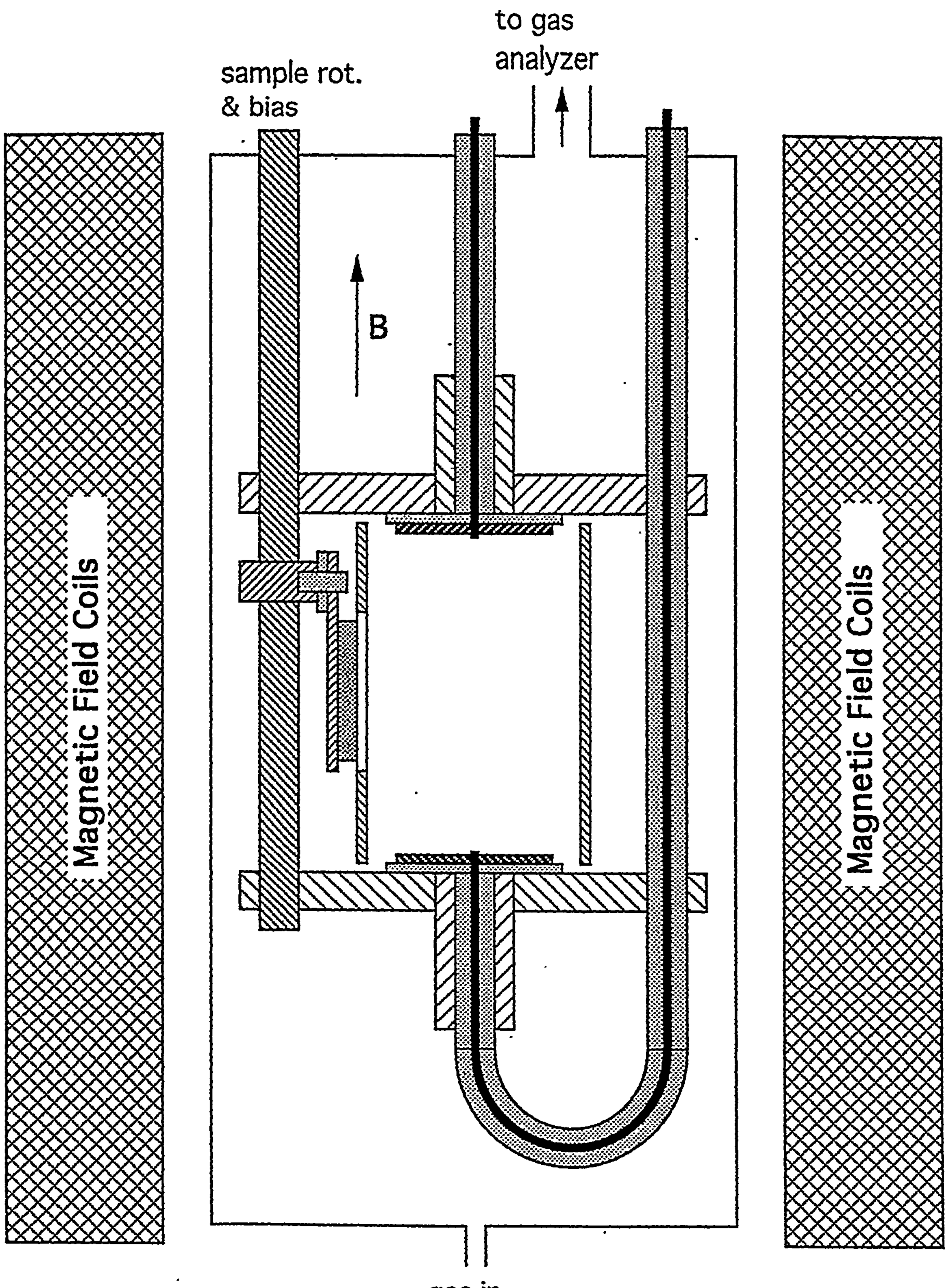

Input O_2 is consumed during the production of volatile CO and CO_2

DFC971116.4

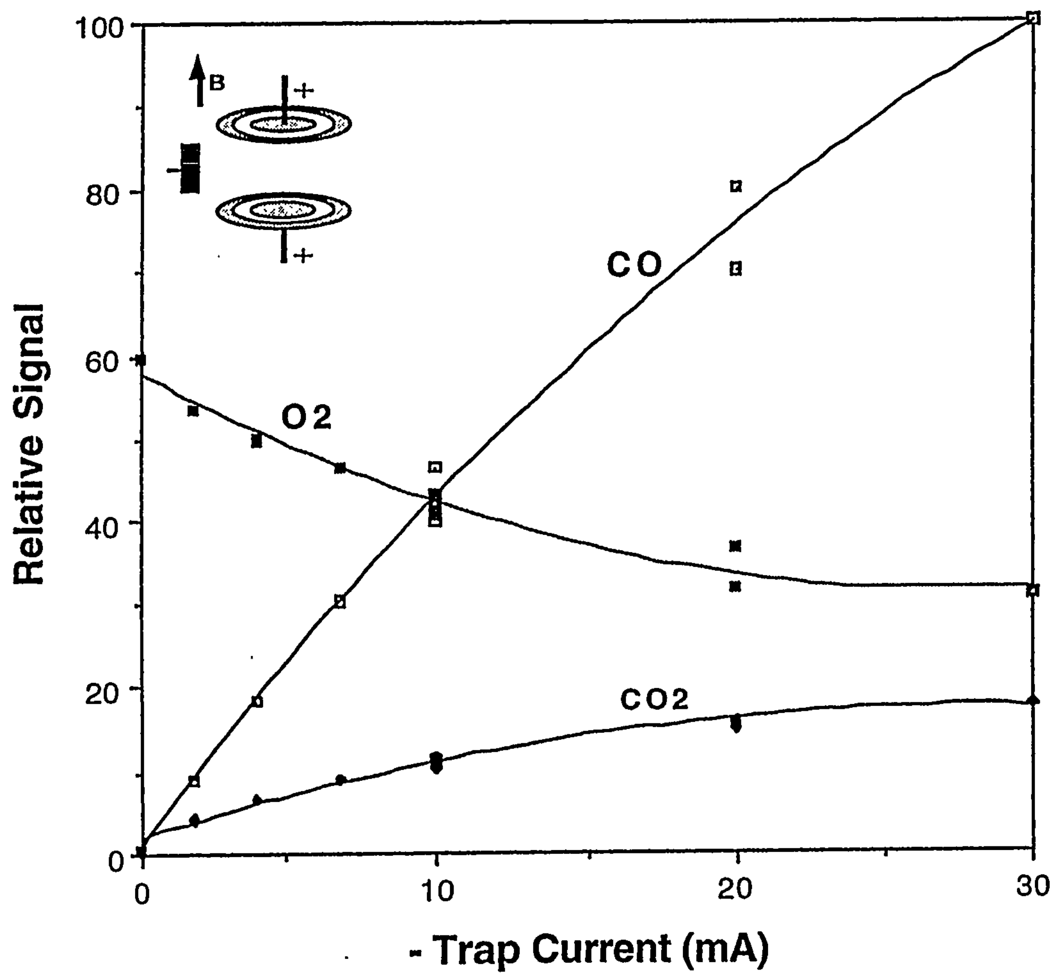

- Ion and neutral effects are sorted by varying trap polarity and sample bias
  - inverted trap produced much smaller signals
- Outgassing background is determined from pure He discharge
  - eliminated by reducing discharge current

Erosion by neutral species was observed using low power discharges

DFC971116.5

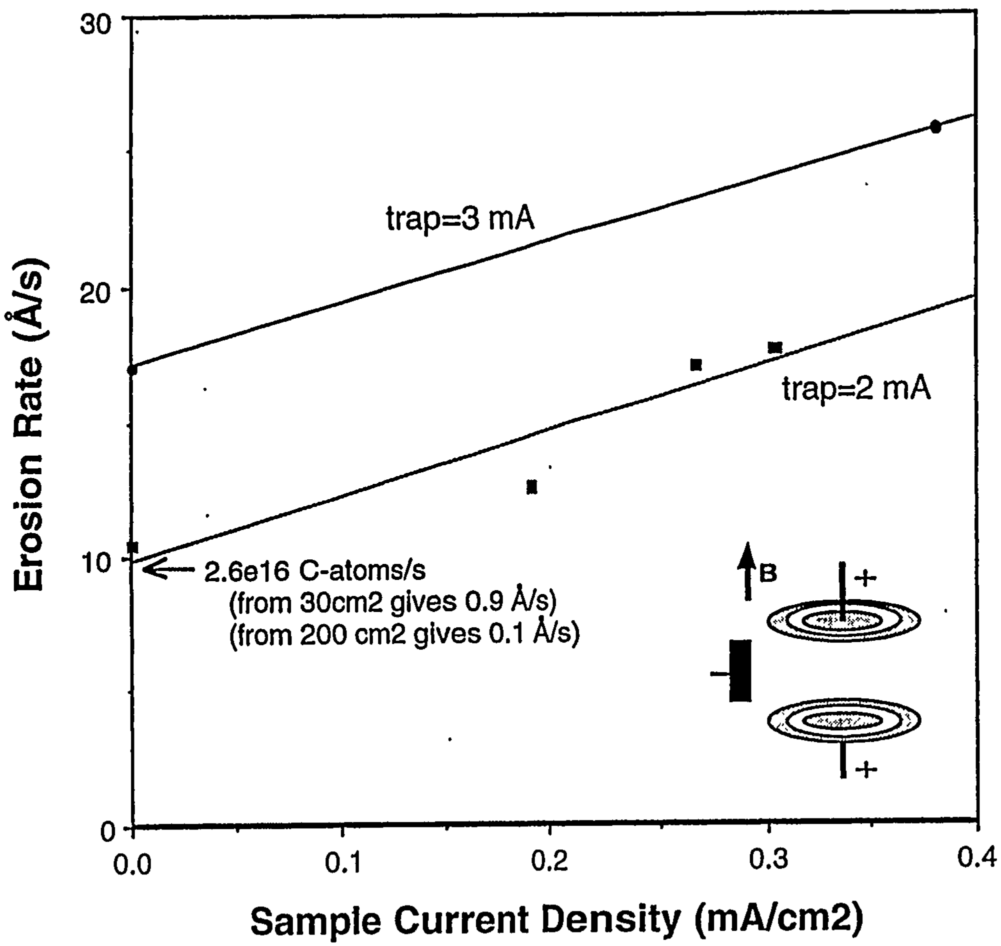

- Erosion by ions increases with sample bias (-) and current
- Erosion by ions is eliminated by zero (or +) sample bias
- Erosion by neutral increases with trap (plasma) current
- Area eroded by neutrals is larger than sample area
  - Carbon is also removed from deposits on walls

Summary:

DFC971116.6

- We have a simple, versatile test probe for studying codeposit erosion in high magnetic fields.

- Initial studies using Penning discharges show erosion due to neutral species can be separated from erosion due to ions.

- Preliminary measurements indicate atomic-O from a weak He-O plasma will cross magnetic field lines and erode carbon materials at 0.1-.3 μm/hr.

- Larger erosion rates are expected for C-H codeposits (~3x) using optimized discharges, and elevated sample temperatures.

- The initial studies also indicate atomic-O can reflect off surfaces, allowing it to reach around corners and penetrate into confined regions.

US-Japan PMI/HHF Workshop in San Francisco
December 8-11th, 1997

Erosion and Redeposition of High-Z Materials in Linear Divertor Simulator

N. Ohno, M. Kojima, Y. Ido, N. Ezumi, and S. Takamura

Department of Energy Engineering and Science,
Graduate School of Engineering,
Nagoya University
Furo-cho, Chikusa-ku, Nagoya 464-01, Japan

Outline

- Introduction
- Erosion and Redepositon Process of Mo with Oblique Incidence of Magnetic Field
- Modification of W Surface by the Low Energy and High Flux Plasma Irradiation
- Introduction of New Divertor Plasma Simulator, NAGDIS-II
- Conclusions

Introduction

High Z materials are recently focused for the material of future divertor target plate, because of

(1) good thermal properties,

(2)high threshold value of physical sputtering,

(3) low hydrogen retention.

Systematic investigation on high Z materials is required including the atomic and transport processes.

-- Linear plasma device with high particle /heat flux plasma and a simple magnetic structure is a suitable one for investigating underlying individual physics in a series of atomic and transport processes.

In this presentation,

(1) Erosion and redeposition processes of a high Z material (Mo) with oblique Incidence of Magnetic Field

(2) Modification of W surface by the low energy and high flux He and H plasma irradiation

(Enhancementof heat load due to thermoelectron emission)

Experimental Set-up in TPD-I

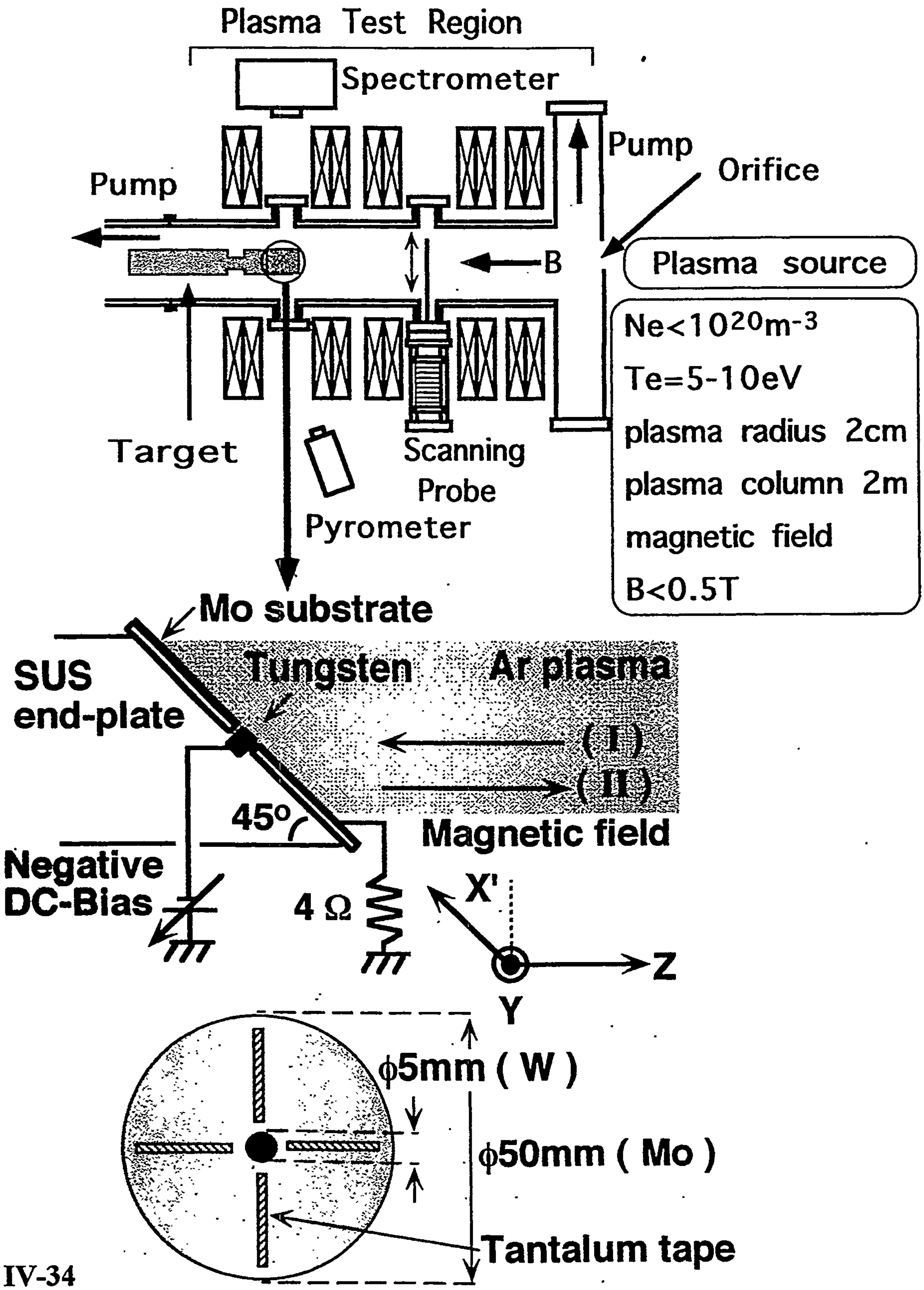

IV-34

Contour plot of a Mo substrate after Ar plasma exposure

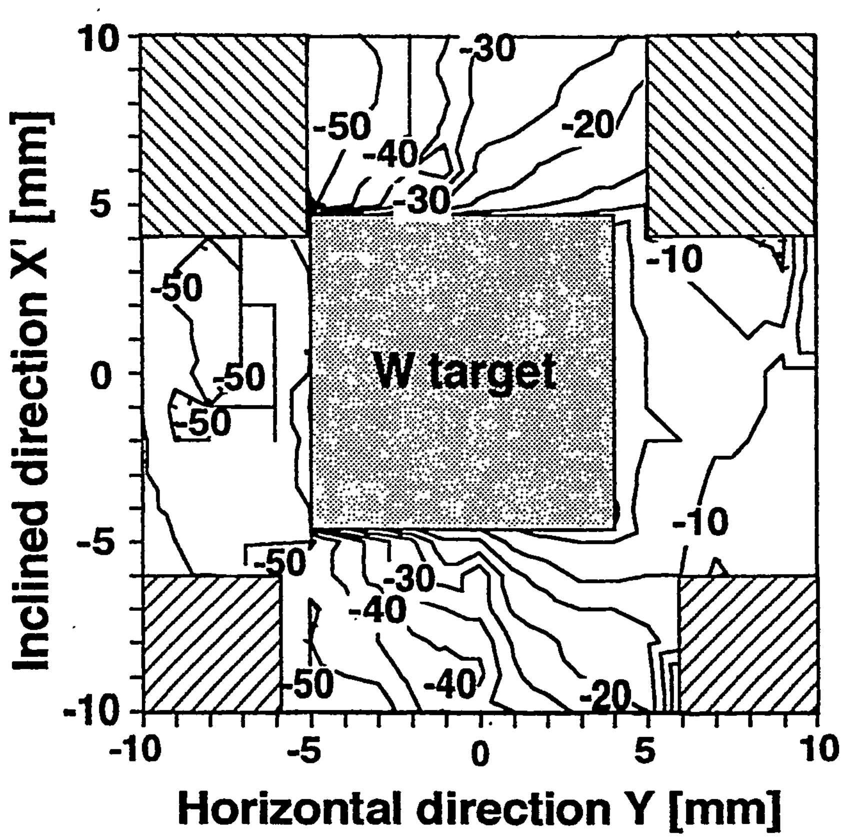

- Exposure time: 90 minutes
- Surface temperature: 1100℃
- The levels correspond to the erosion depth in μm units.

Mo surface was characterized by Electron Probe Micro Analysis (EPMA).

----- Mo, Ta and carbon are only obsered

W is not found (< 100 p.p.m.)

Asymmetric erosion profiles for the different directions of magnetic field

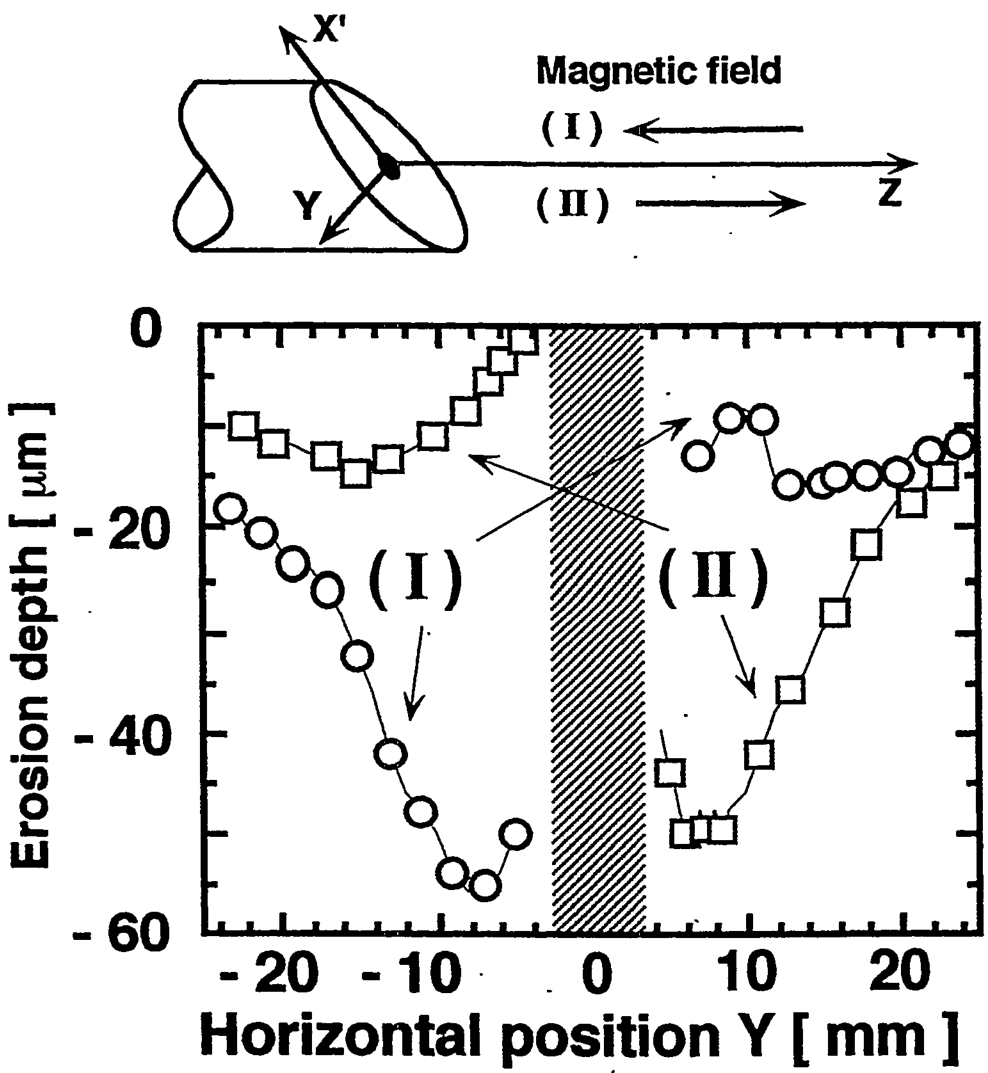

Experimentally observed asymmetric erosion profiles along horizontal direction Y with the different directions of magnetic field. The hatched area shows the position of W target.

Radial profiles of plasma paramters for Ar plasma in TPD-I

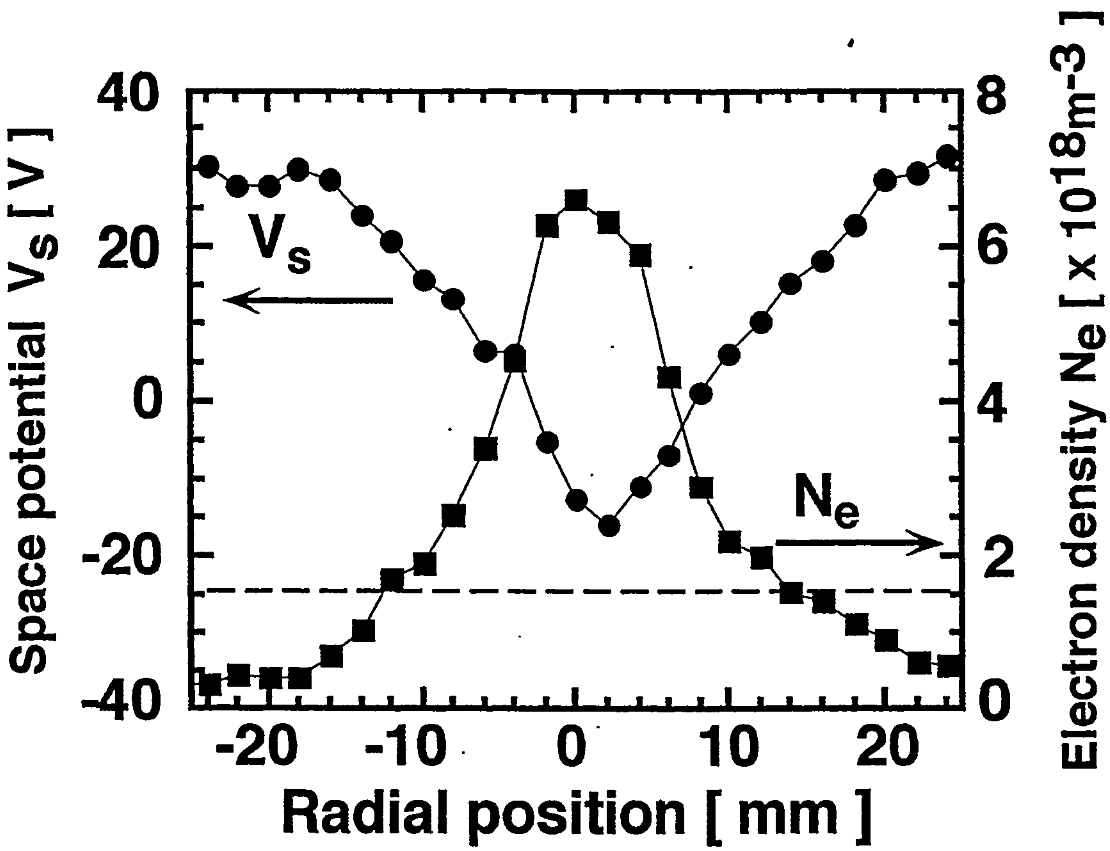

Radial profile of space potential and electron density for argon plasma. The dotted line shows the potential of Mo substrate.

-These parameters are measured using a fast-scanning Langmuir probe located at 30 cm away from the substrate.

- Electron temperature is almost uniform around 7 eV.

3-D Monte Carlo simulation code

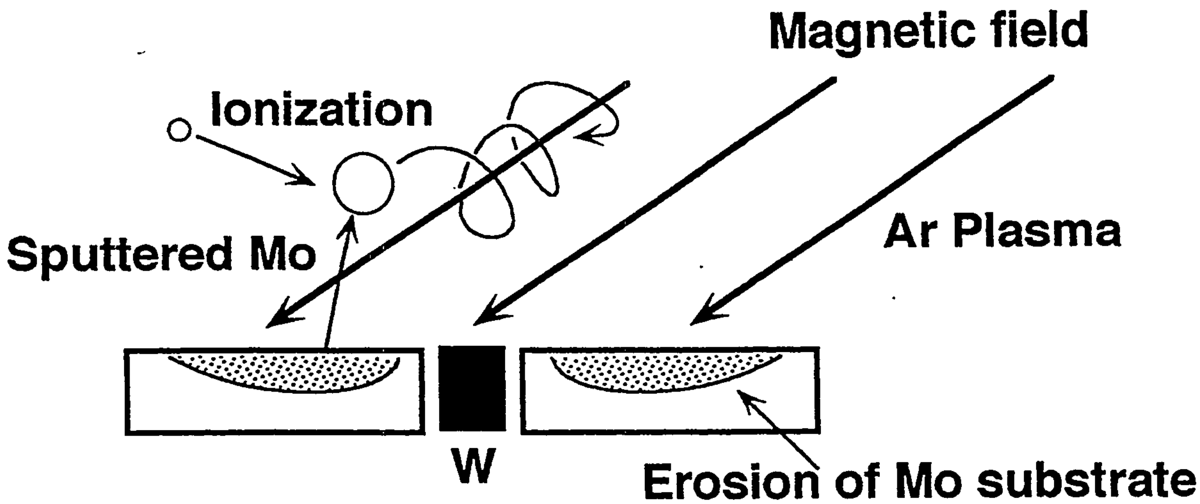

Collision processes in a plasma

- o Elastic collisions (rigid sphere collision)
- o Coulomb collisions
- o Electron impact ionization
- o Charge exchange

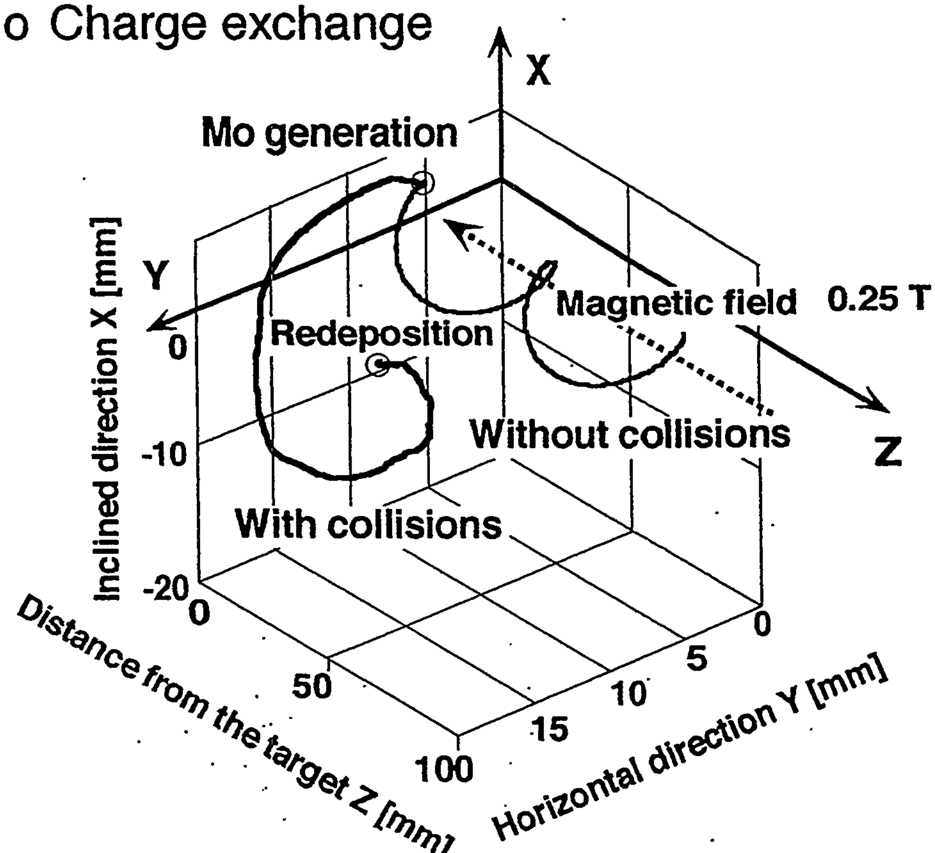

Erosion-redeposition model on a plasma-facing material

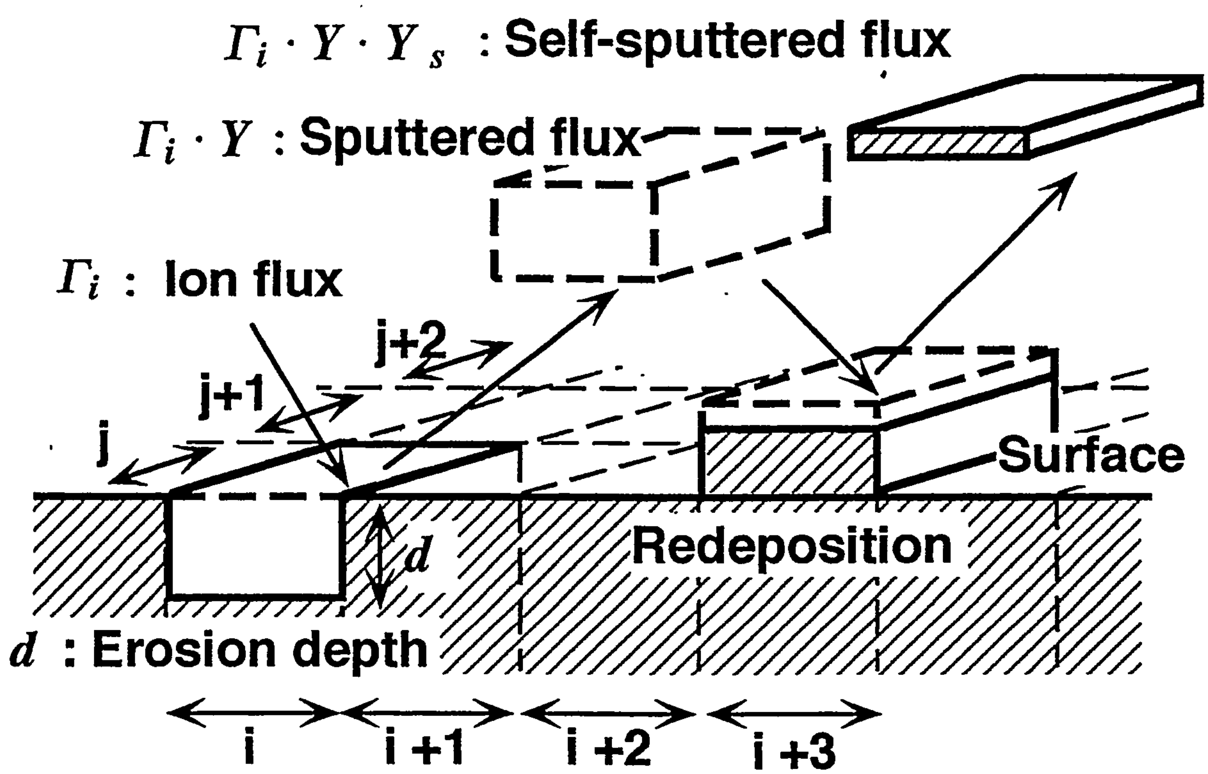

(a) Erosion process

Local erosion depth d (i, j) [m] is given by

$$d(i,j) = \Gamma_i(i,j) \times Y(i,j) \times M \times T/\rho .$$

Γ_i (i, j) [m^{-2}. s^{-1}]	: the average flux of plasma ions
Y (i, j) [atoms / ion]	: sputtering yield at that zone
M [kg]	: atomic mass of the substrate
ρ [kg. m^{-3}]	: mass density of the bulk
	(Mo is 1.02×10^4 kg. m^{-3})
T [s]	: plasma exposure time

(b) Redeposition process process

Redeposition depth at (i+3, j)

$$d(i+3,j) = \Gamma_i \times Y \times \{1 - Y_s^1(i+3,j)\} \times M \times T/\rho$$

Y_s^1 (i+3, j) : the self sputtering yield at the zone (i+3, j)

2-D erosion distributions caluculated by Monter Carlo code

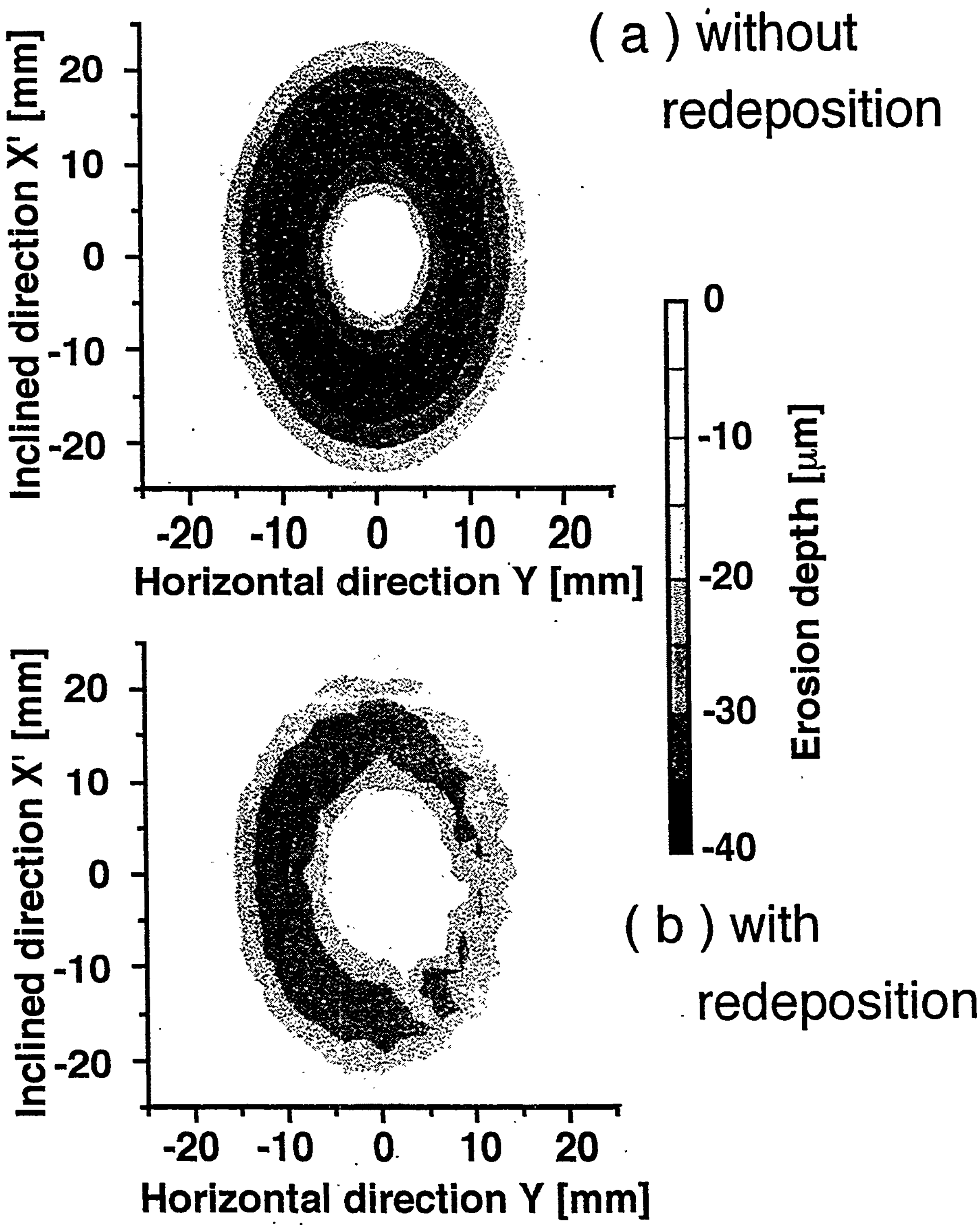

Sliced erosion profiles in horizontal direction (X'=0)

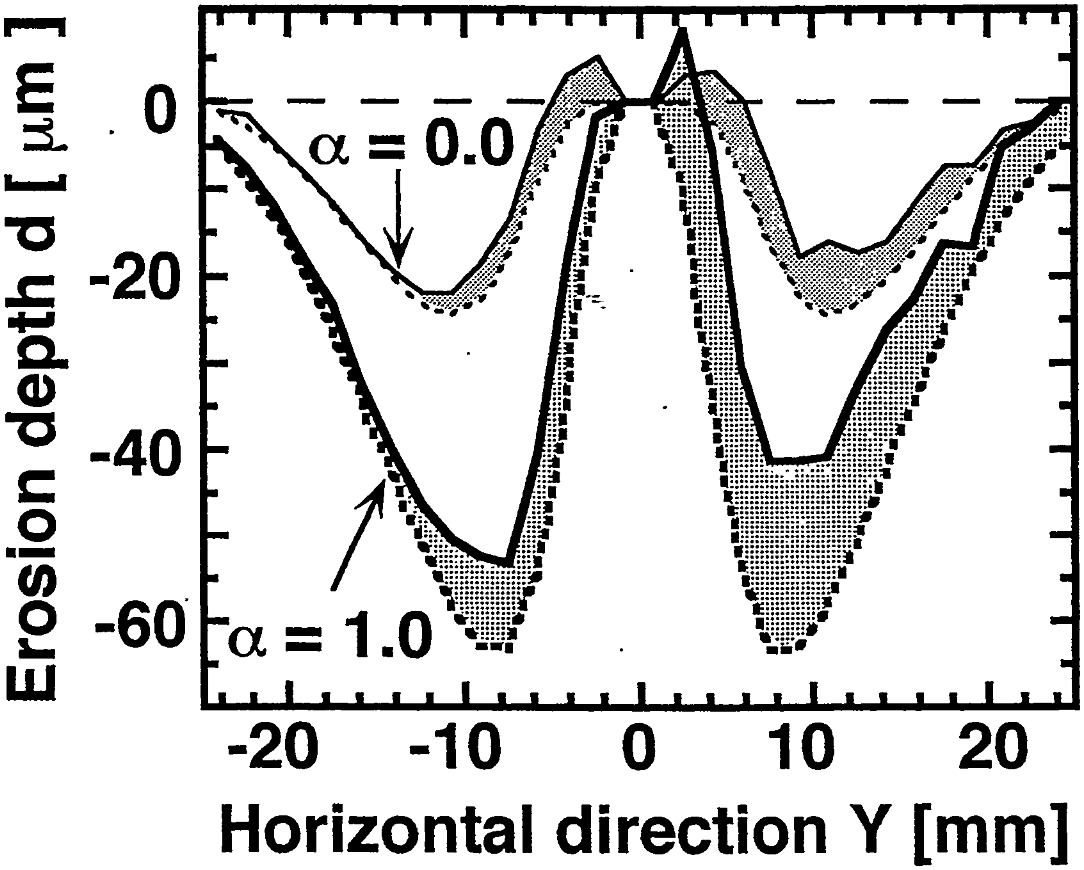

- α : the ratio of Ar^{2+} density to Ar^{1+}
- Solid and dotted lines show the profiles with and without redeposition process.
- Shadow regions correspond to the redeposited depth of sputtered Mo.

--> Asymmetric redeposition profile

Takamura Lab. Nagoya University

Redeposition of Mo

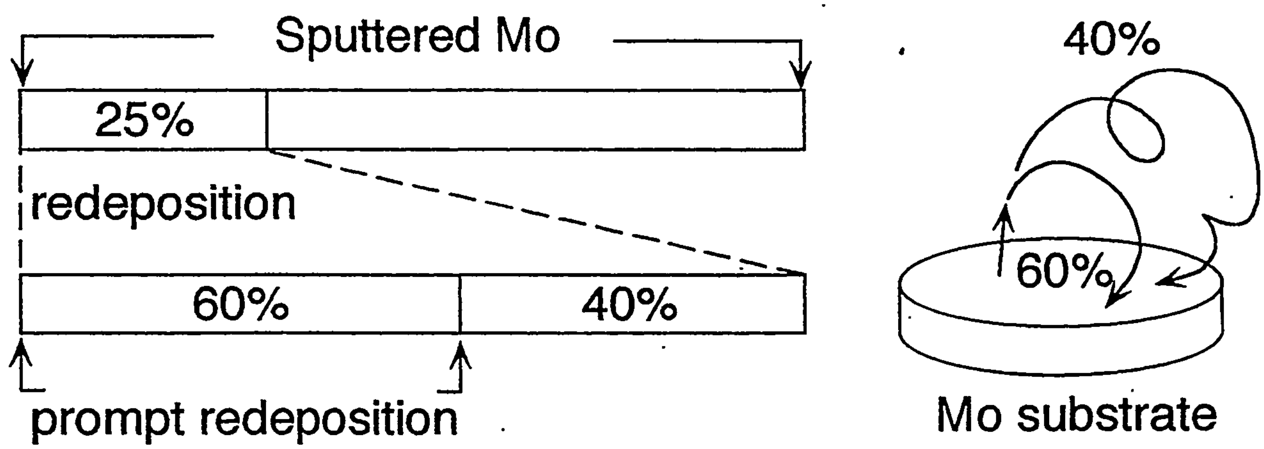

About 25 % of sputtered Mo return back to the substrate as mainly an ionized Mo, and redeposited. About 60 % of their returned particles redeposit within their first gyrations

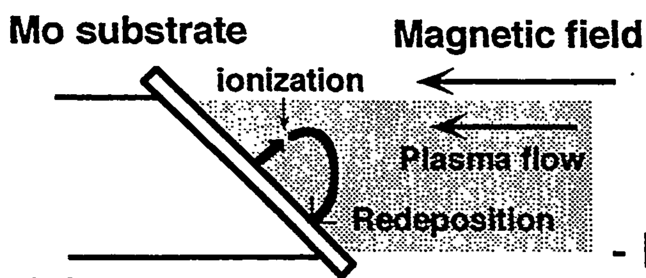

(a) $\lambda_i < r_t$

- Ionization mean free path ~16 mm ($n_e \sim 2.0\times10^{18}\ m^{-3}$, Te ~ 7 eV)
- Gyro radius~ 8 mm (B ~ 0.25T, average energy of sputtered Mo is 2 eV)

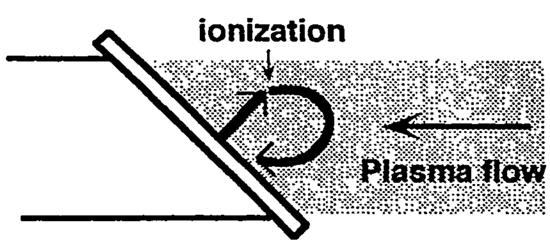

(b) $\lambda_i > r_t$ with collisions

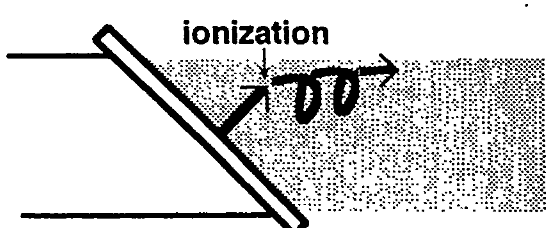

(c) $\lambda_i > r_t$ without collisions

Erosion of Mo

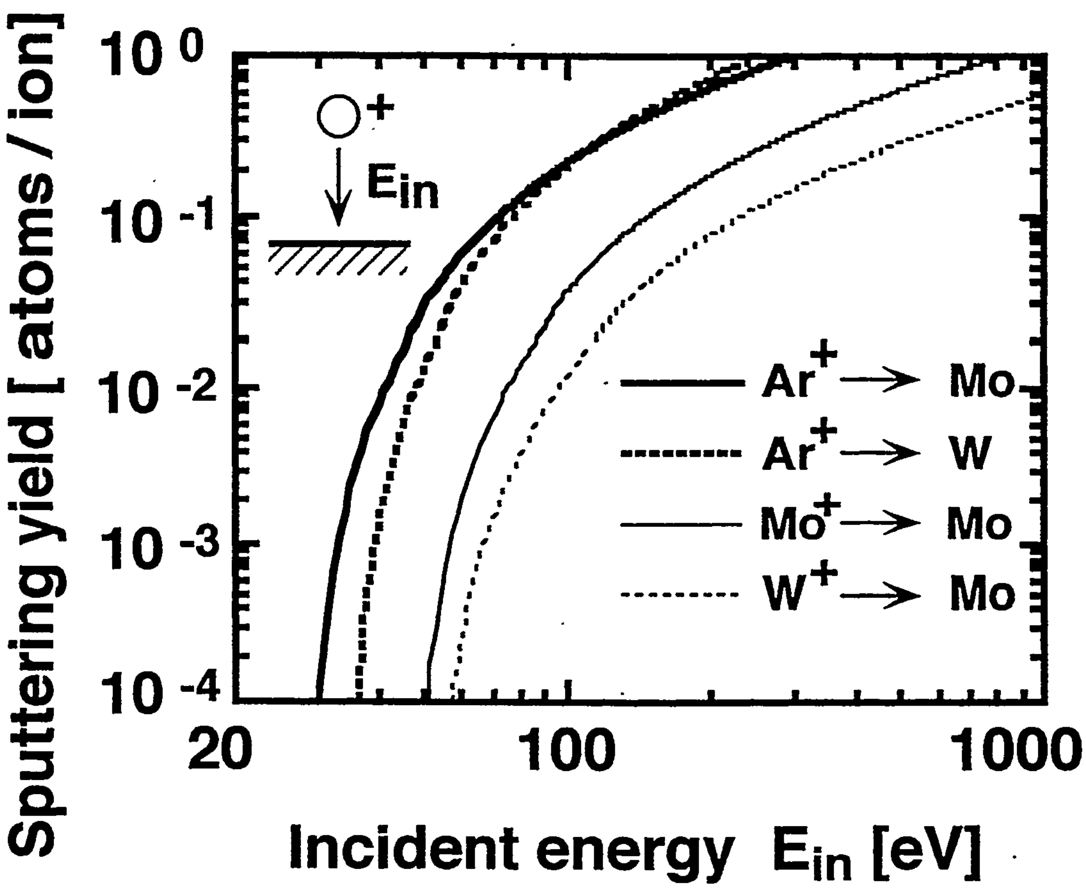

Sputtering yields of various ion-material components at normal incidence, calculated from an empirical formula [*].

* Y. Yamamura and H. Tawara, Atomic Data and Nucl. Data Tables **62**, 149 (1996).

Summary(1)

1) Experiments:

The effect of prompt redeposition of Mo is clearly demonstrated in a linear plasma device. Mo ions which are returned back to the substrate locally redeposit on it depending on the direction of magnetic field due to the effects of prompt redeposition.

2) Numerical analysis:

To analyze the transport of sputtered particles in a plasma and the subsequent redeposition on a plasma-facing material, a particle simulation (Monte Calro) code has been developed. We have a qualitative agreement for the erosion profiles with the results of numerical code predictions with the effect of prompt redeposition for high Z material. However, we have quantitative differences for their erosion rates.

Experimental set-up for plasma irradiation to W in NAGDIS-I

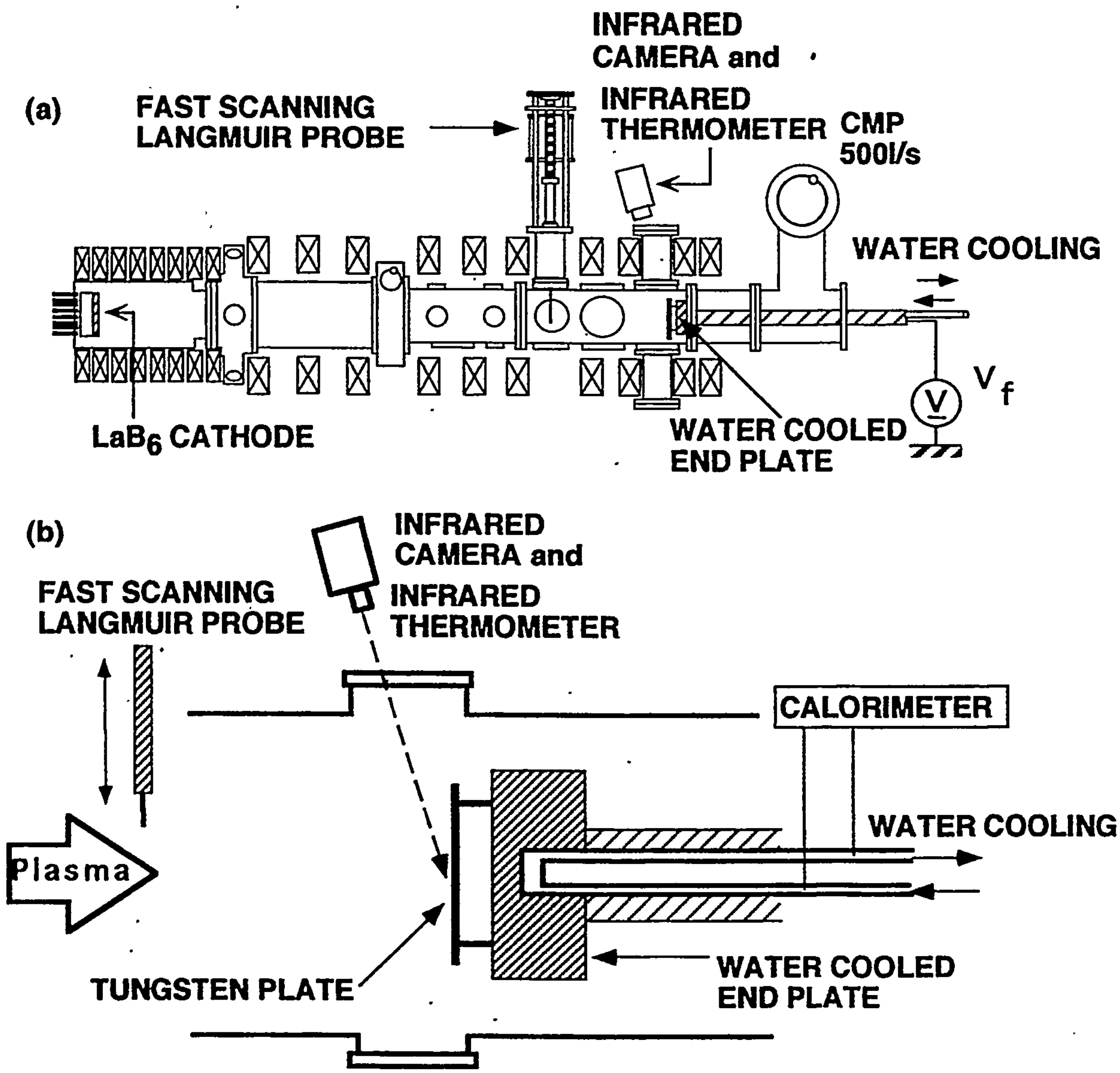

Tungsten can be irradiated by the helium and hydrogen plasmas with the diameter of about 6 cm and Te = 5-10eV, n_e = 0.5-4.0 X 10^{18} m^{-3}, corresponding to the flux of (0.27-3.1)X $10^{22}$$He^{+}$ ions $m^{-2}s^{-1}$ and a tungsten plate temperature of up to about 3200 K.

3. Experimental results

A. Tungsten irradiated by the helium plasma

SEM micrographs of tungsten surface show clearly that the microstructure of the tungsten surface is changed due to the helium plasma irradiation.

1) No obvious the change of microstructure of tungsten surface irradiated by helium plasma with the flux of 4.4 X 10^{21} He^{+} ions $m^{-2}s^{-1}$ corresponding to a tungsten plate temperature of 1144 K.

before irradiation

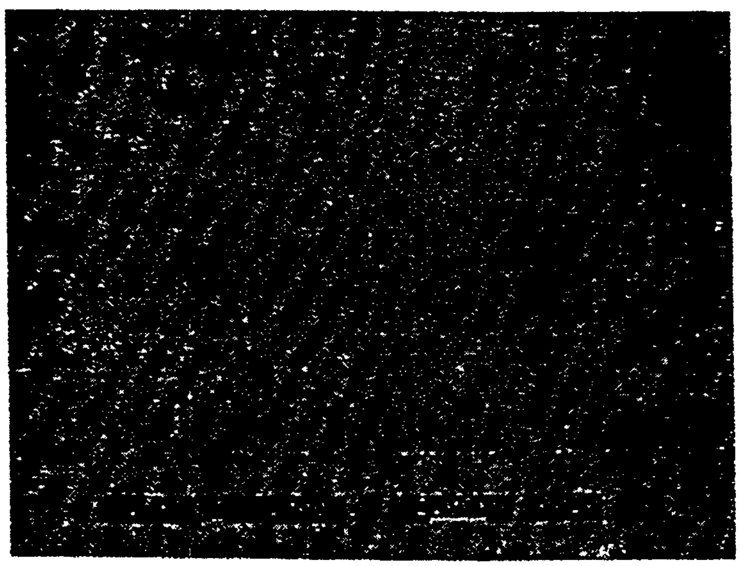

after irradiation
flux: 4.4×10^{21} He^{+} ions/m^2s

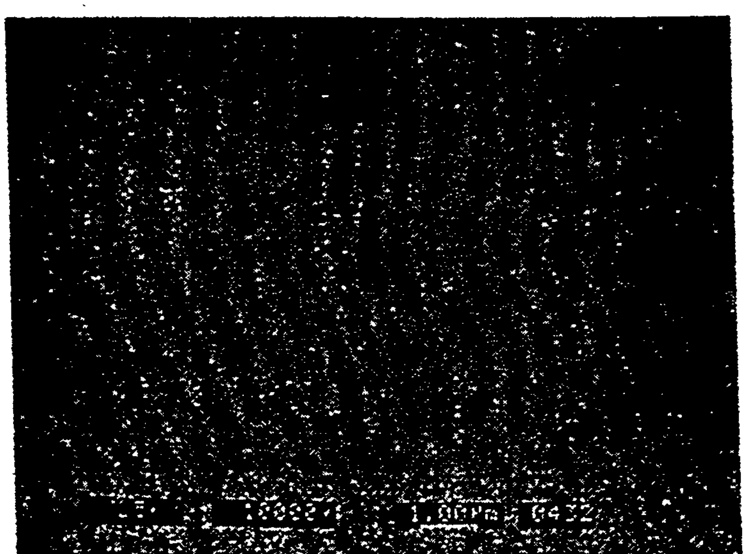

2) Many holes of 0.1-0.5μm in diameter which appear in the tungsten surface irradiated by helium plasma with the higher flux corresponding to a higher tungsten plate temperature

T=1496K
Flux ~ 4.5×10^{21} He^+ ions/m^2s
Energy ~ 31 eV

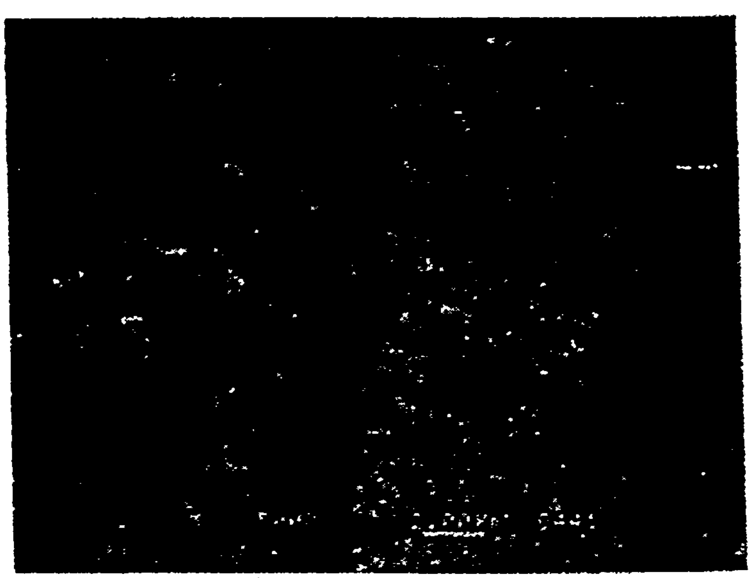

T=1580K
Flux ~ 5.2×10^{21} He ions/m^2s
Energy ~ 30 eV

3) When tungsten was irradiated by the helium plasma with the more higher flux of 2.4 X $10^{22}He^+$ ions $m^{-2}s^{-1}$ corresponding to a tungsten plate temperature of up to near 3200 K.

i) The size of holes becomes large with the diameter of about 1-4μm

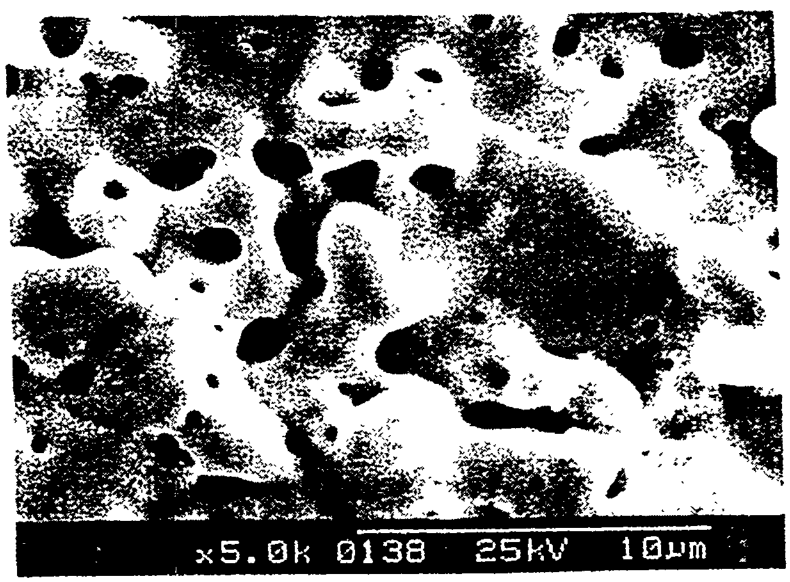

3200 K, 2.4 X 10^{22} He^+ ions/m^2s

ii) A large undulation appear in tungsten surface

iii) The redeposited layers of W are formed at the periphery of the irradiation region on tungsten surface.

B. Tungsten irradiated by the hydrogen plasma

To obtain a comparison with different ion-species, the tungsten plate was irradiated by the hydrogen plasma with 3.3×10^{22} H^+ ions m^{-2} s^{-1}, corresponding to a tungsten plate temperature of near 2800 K. Surface morphology of tungsten irradiated by the hydrogen plasma is found to be quite different from the helium case.

A large crystal structure appears in the tungsten surface without any holes appearing.

There is no redeposition of W observation in the case of the hydrogen plasma irradiation.

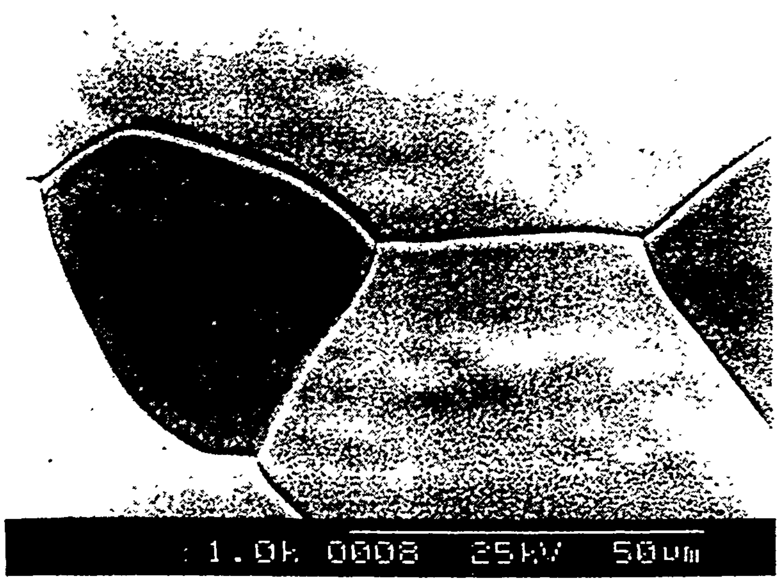

2800K
3.3×10^{22} H^+
ions/m^2s

Summary(2)

For a high temperature tungsten plate irradiated by a low energy and high flux plasma, surface modification is observed in experiments.

A surface undulation are formed and many holes of 0.1- 5 μm in diameter appear in the tungsten surface after the helium plasma irradiation.

The redeposition of W are observed due to the helium plasma irradiation at high plate temperature.

Microsructure changes of the tungsten irradiated by the hydrogen plasma is found to be quite different from the helium plasma case.

The size and the density of holes has an obvious relation to the incident ion energy, flux as well as the surface temperature distribution on the tungsten surface. But we can't get a quantitative relation in our experiments.

In the experiments we can't controll the ions flux, energy and target plate temperature, separately because tungsten plate is only heated by plasma.

Now a further experiments are considered for getting quantitative relation through some improvement of experimental setup.

1. A controll of plate temperature by external heating power
2. A controll of incident ions energy by bias voltage on plate
3. A controll of incident ions flux by plasma density

Erosion and Impurity Effects on PFC Materials in PISCES-B

presented by
R. Doerner

A summary of work performed by the PISCES-B materials research team.
R. Doerner, A. Grossman, S. Luckhardt, R. Seraydarian, F.C. Sze and D. Whyte

Fusion Energy Research Program,

University of California - San Diego, La Jolla, CA. 92093-0417

UC San Diego

work supported under DOE grant # DE-FG03-95ER-54301.

Outline:

- Interaction of beryllium with a 'clean' plasma
  - erosion
  - surface modifications
  - deuterium retention
- PISCES-B mixed-material experiments
  - Beryllium & Carbon
  - Tungsten & Carbon
- Conclusions and future directions

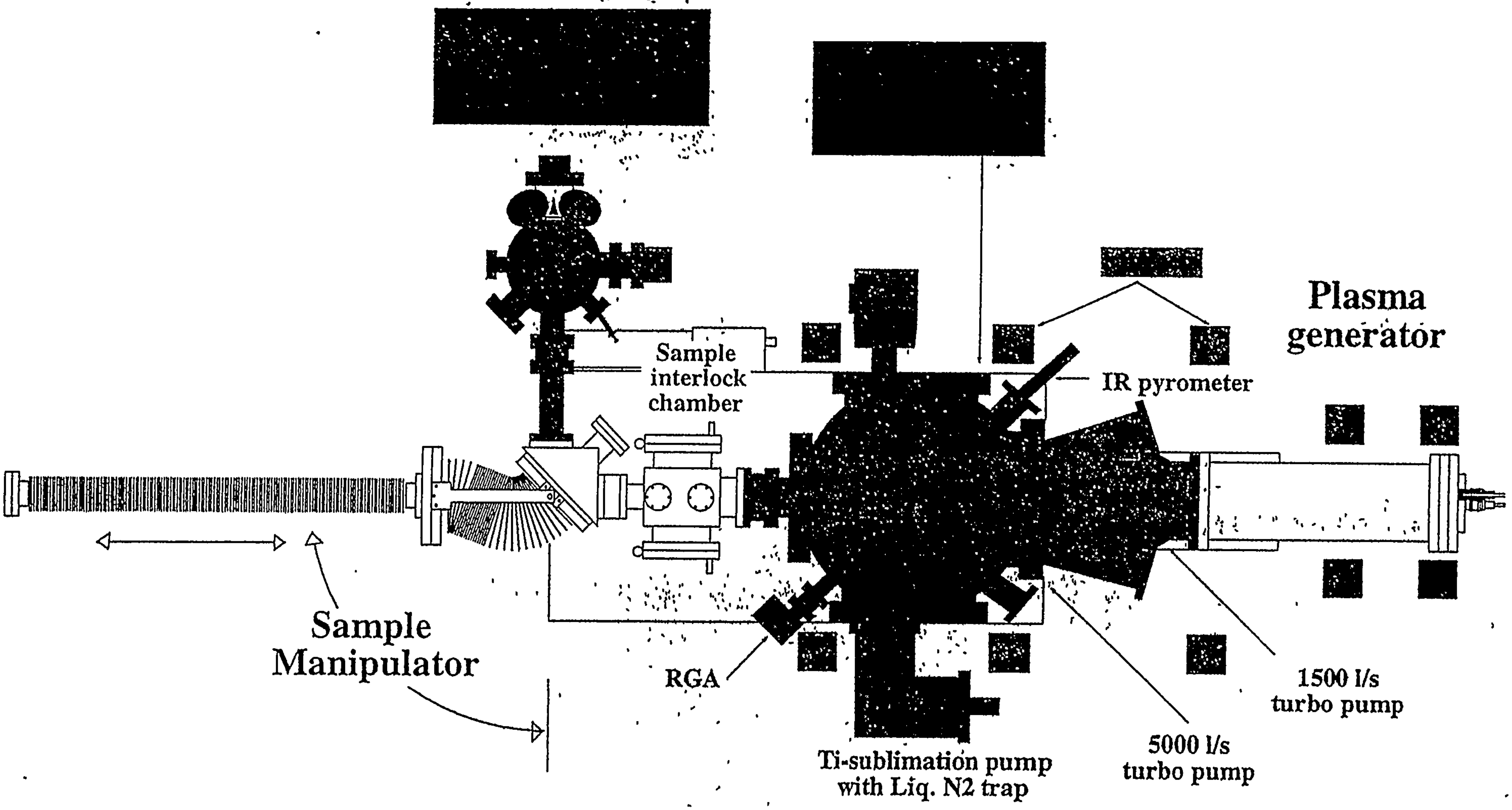

THE PISCES-B FACILITY

Sputtering Yield Measurements in a 'Clean' (<0.2% Carbon & <0.1% Oxygen) Plasma Agree with the Computed Sputtering Yield of Beryllium-Oxide

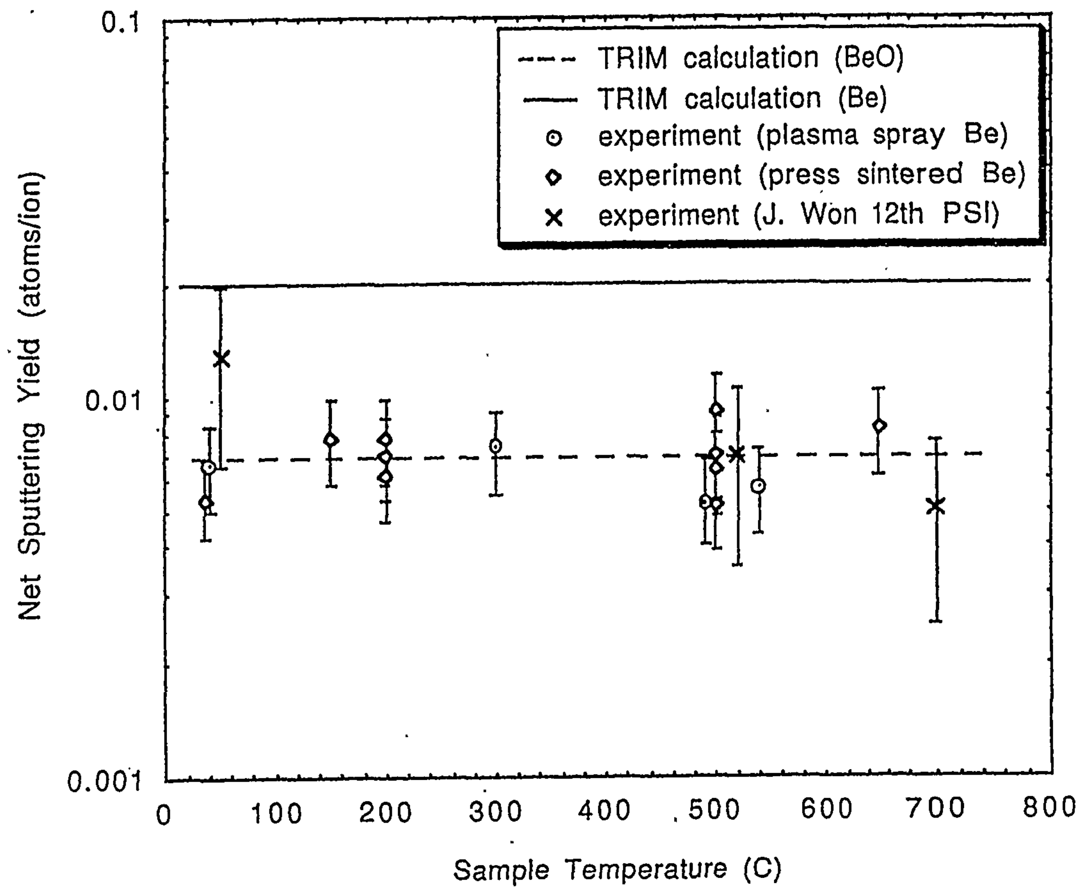

Beryllium samples exposed to plasma bombardment at high temperature exhibit surface damage

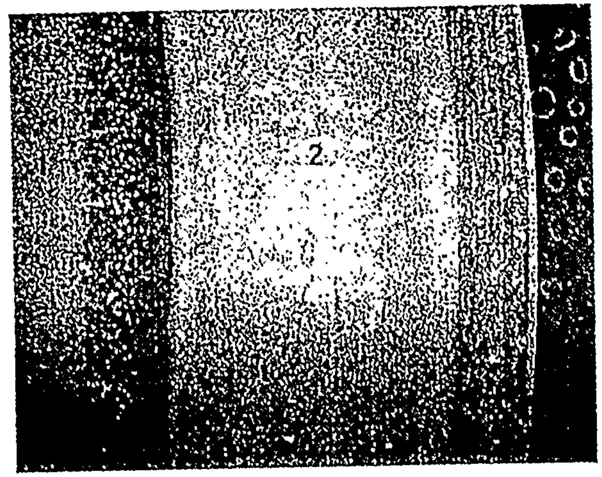

Area 1 - High-temperature exposure (500°C)

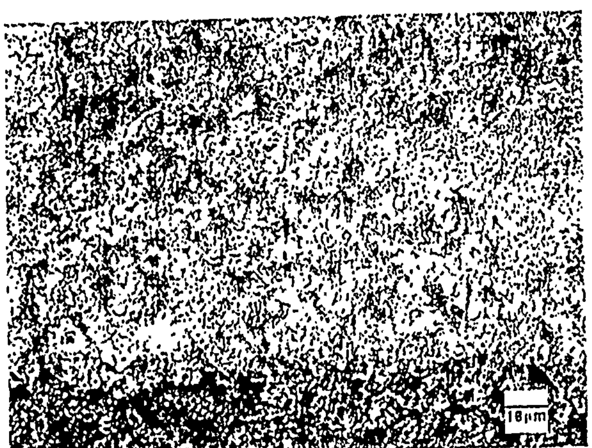

Area 2 - Low-temperature exposure (200°C)

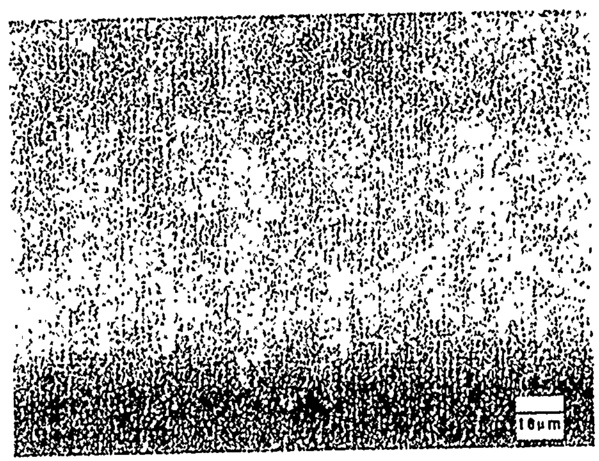

Area 3 - Surface hidden from plasma exposure

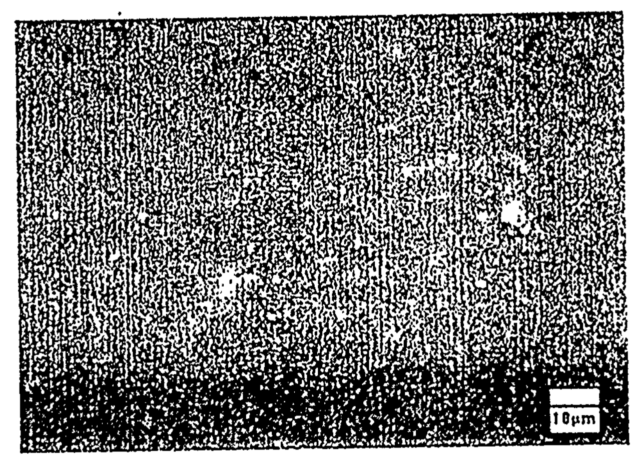

Profilometry indicates increasing surface roughness during higher temperature sample exposures

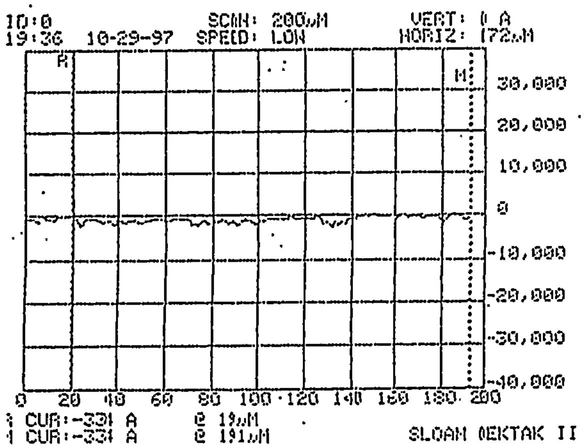

Pre-exposure surface

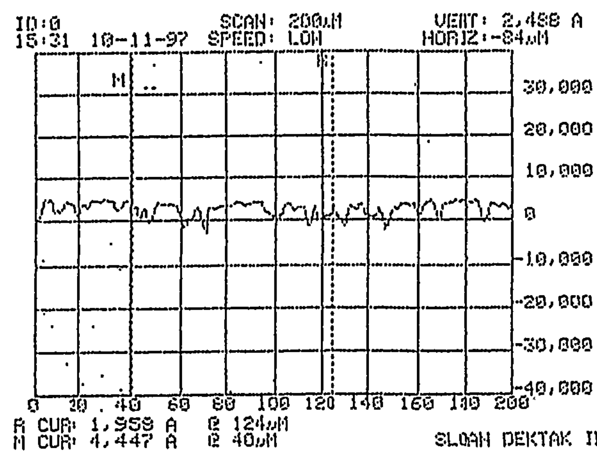

ion flux = 1.7 x 10^{21} m^{-2} s^{-1}
ion energy = 100 eV
exposure time = 60 min.
sample temp. = 40°C

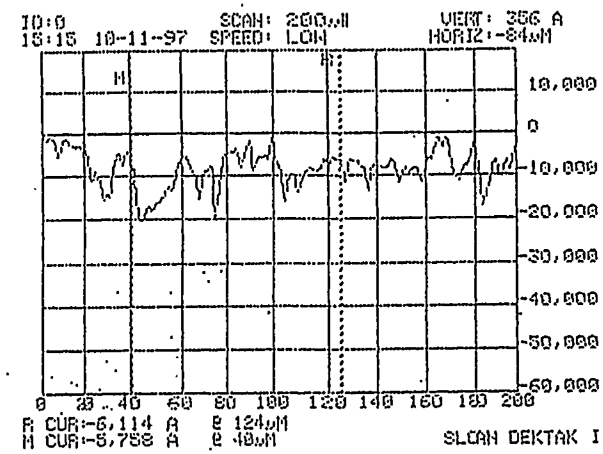

ion flux = 1.5 x 10^{22} m^{-2} s^{-1}
ion energy = 100 eV
exposure time = 30 min.
sample temp. = 500°C

Surface damage increases with increasing fluence during high temperature sample exposure to plasma.

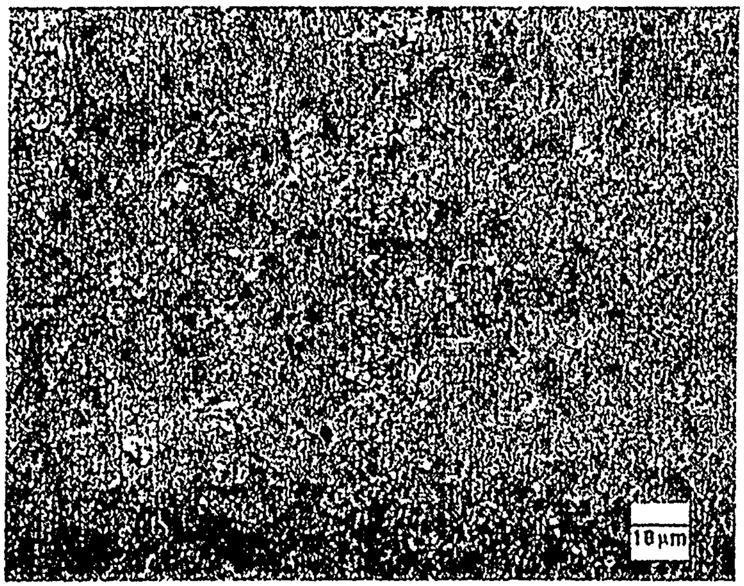

ion flux = $1.5 \times 10^{22}\ m^{-2}\ s^{-1}$
ion energy = 100 eV
exposure time = 30 min.

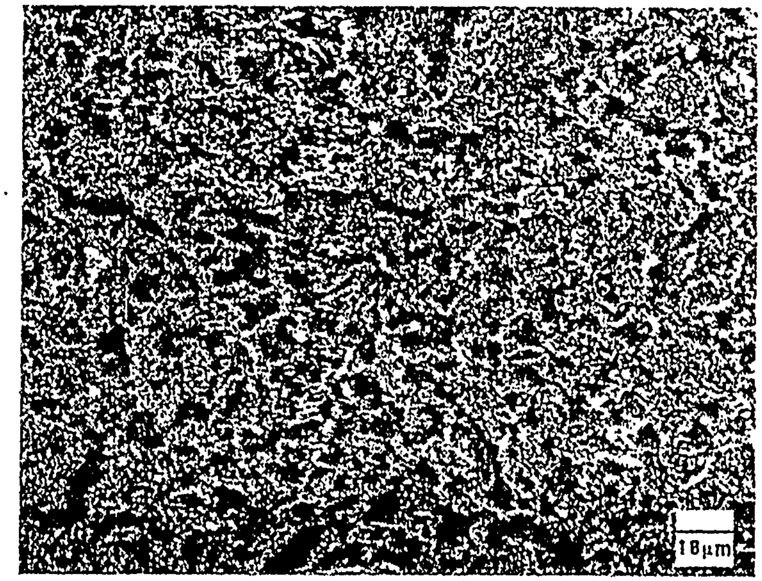

ion flux = $1.5 \times 10^{22}\ m^{-2}\ s^{-1}$
ion energy = 100 eV
exposure time = 6 hrs.

Profilometer quantifies increasing surface roughness with increasing plasma fluence during high temperature sample exposure to plasma

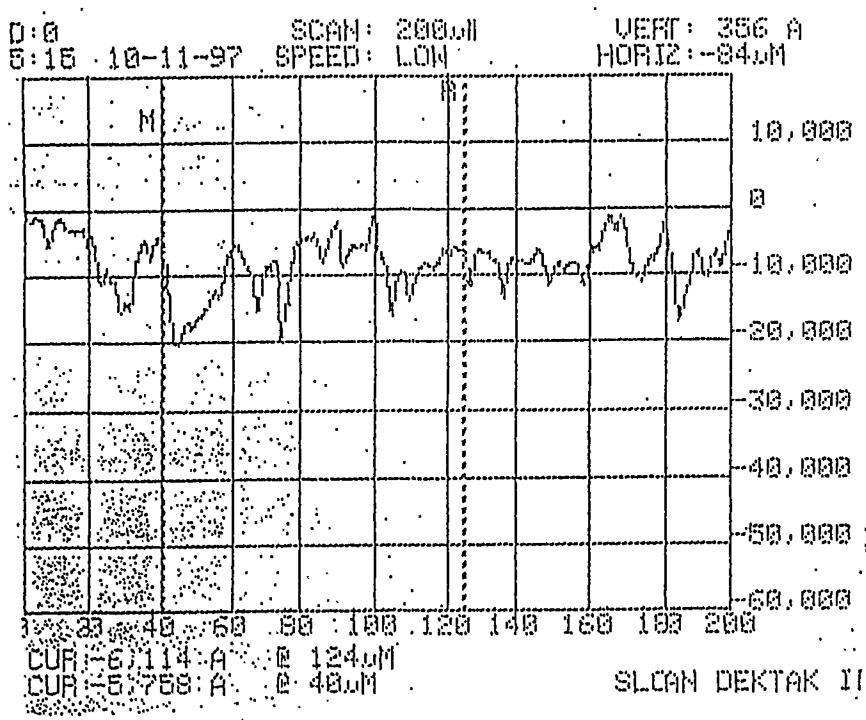

ion flux = 1.5 x 10^{22} m^{-2} s^{-1}
ion energy = 100 eV
exposure time = 30 min.

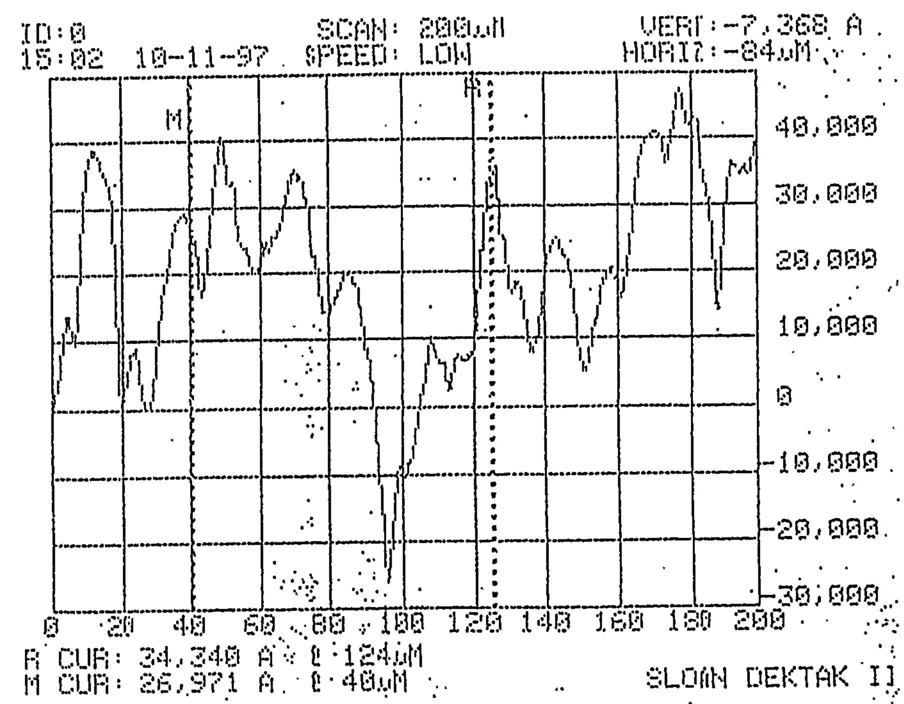

ion flux = 1.5 x 10^{22} m^{-2} s^{-1}
ion energy = 100 eV
exposure time = 6 hrs.

Deuterium Retention in Beryllium Saturates at During Extended Plasma Exposures

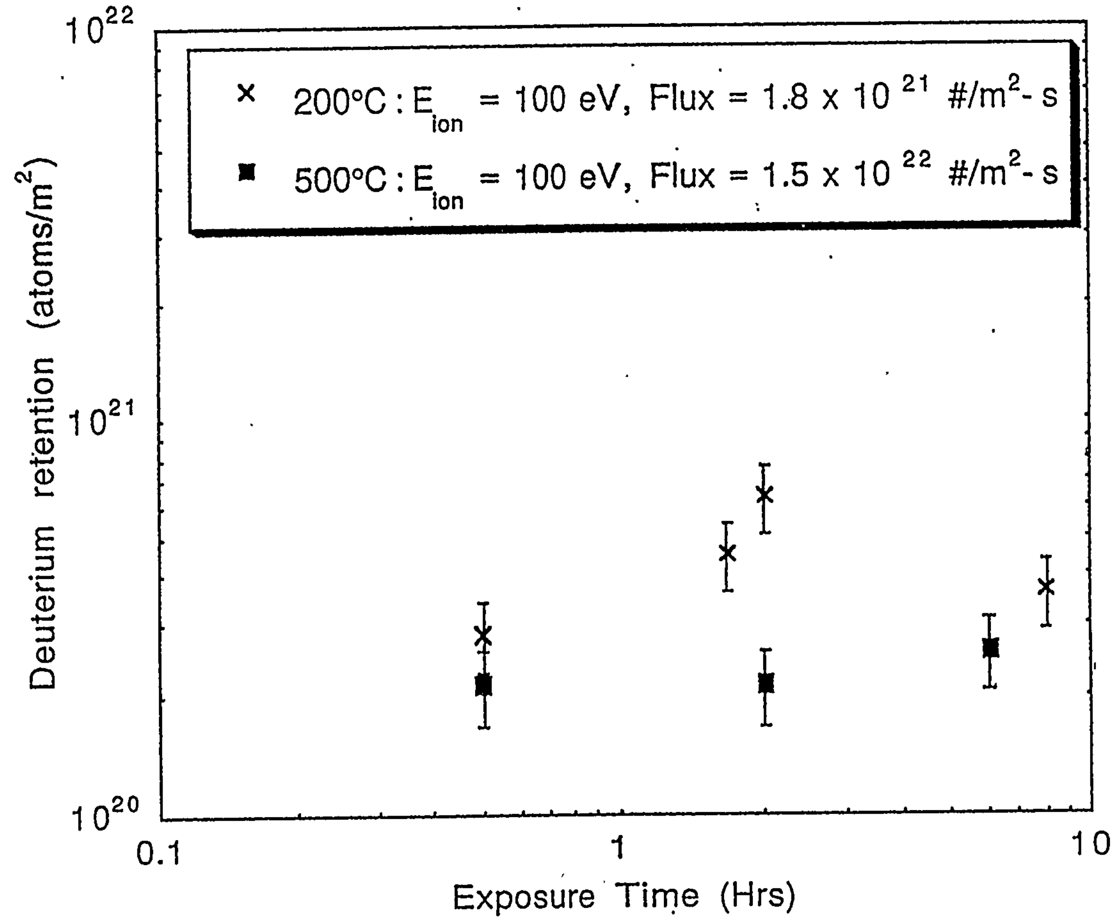

UC San Diego

PISCES-B Mixed-Materials Experimental Configuration

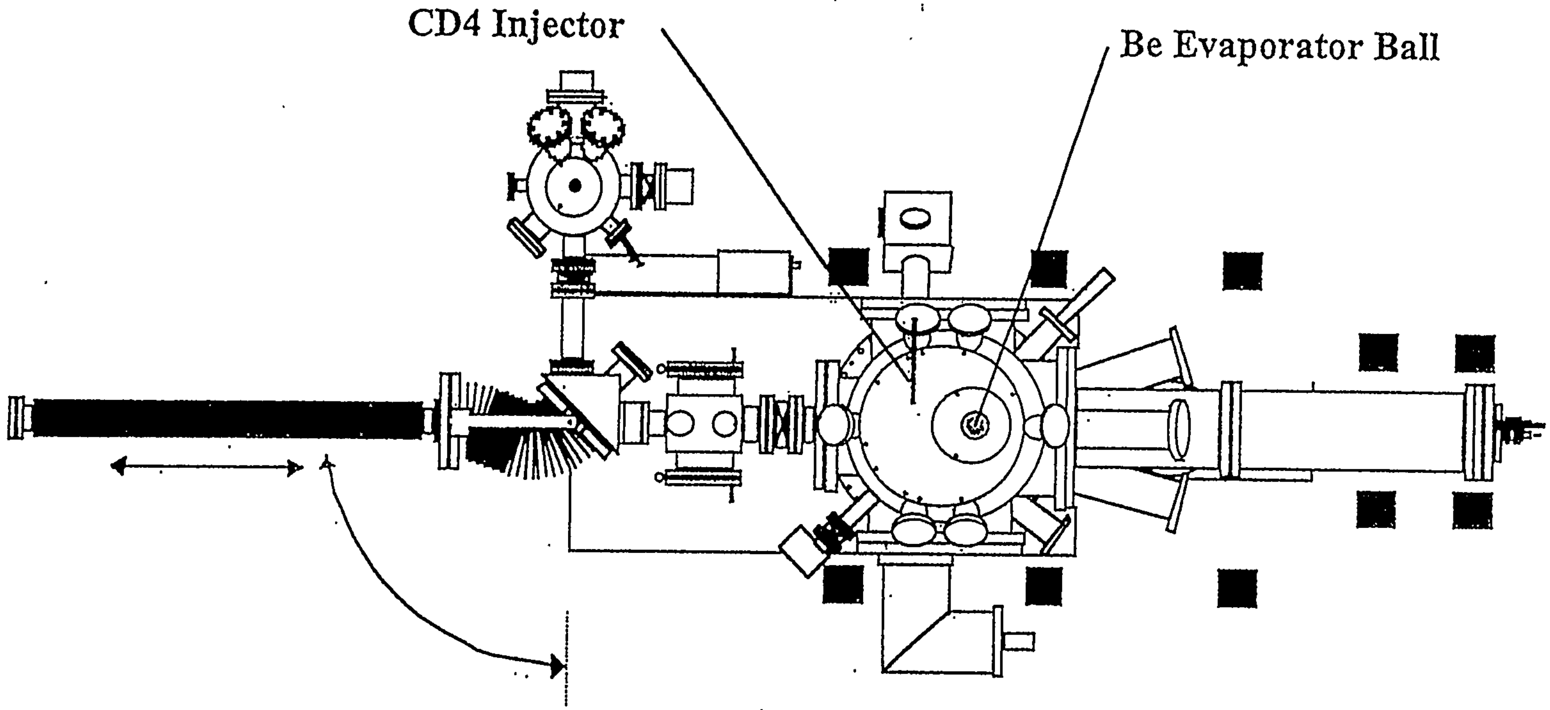

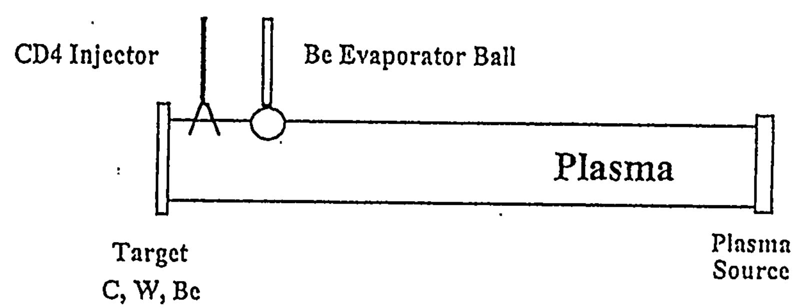

UCSanDiego

Carbon-containing mixed-material layer formation conditions for beryllium exposed to deuterium plasma in PISCES-B

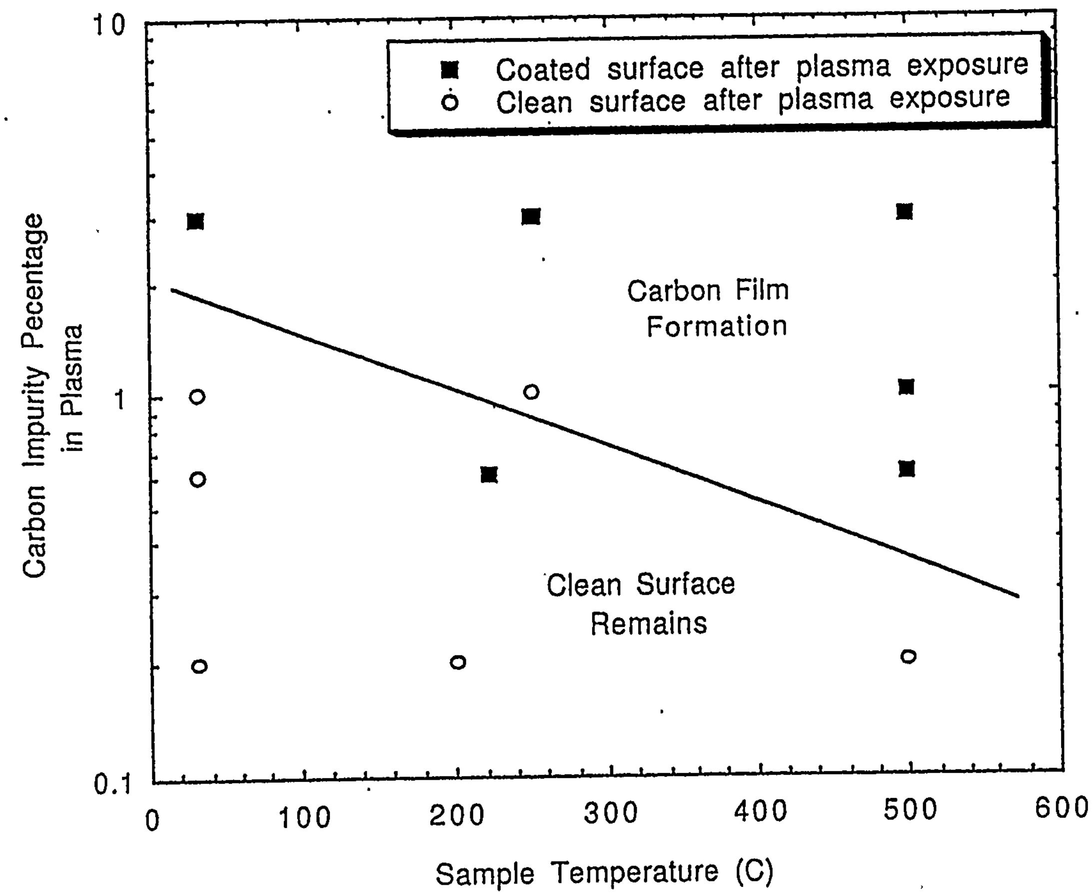

Preliminary Data From PISCES-B

UC San Diego

Plasma-Sprayed Beryllium Exposed to Plasma in PISCES-B Retains Less Deuterium than S65-C Beryllium. However, if Carbon-Containing Mixed-Material Layers Form*, the Total Retention Tends to Increase.

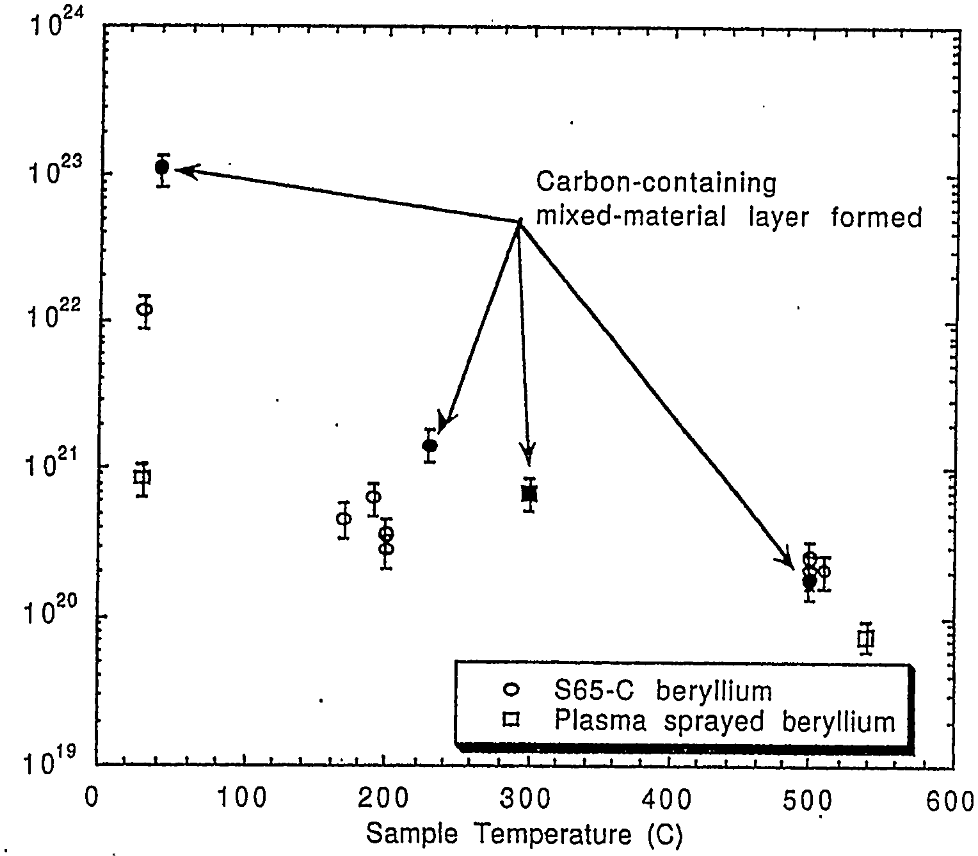

* C containing layers form on Be when the C impurity fraction in the plasma reaches ≈0.5%

Preliminary Data From PISCES-B

UC San Diego

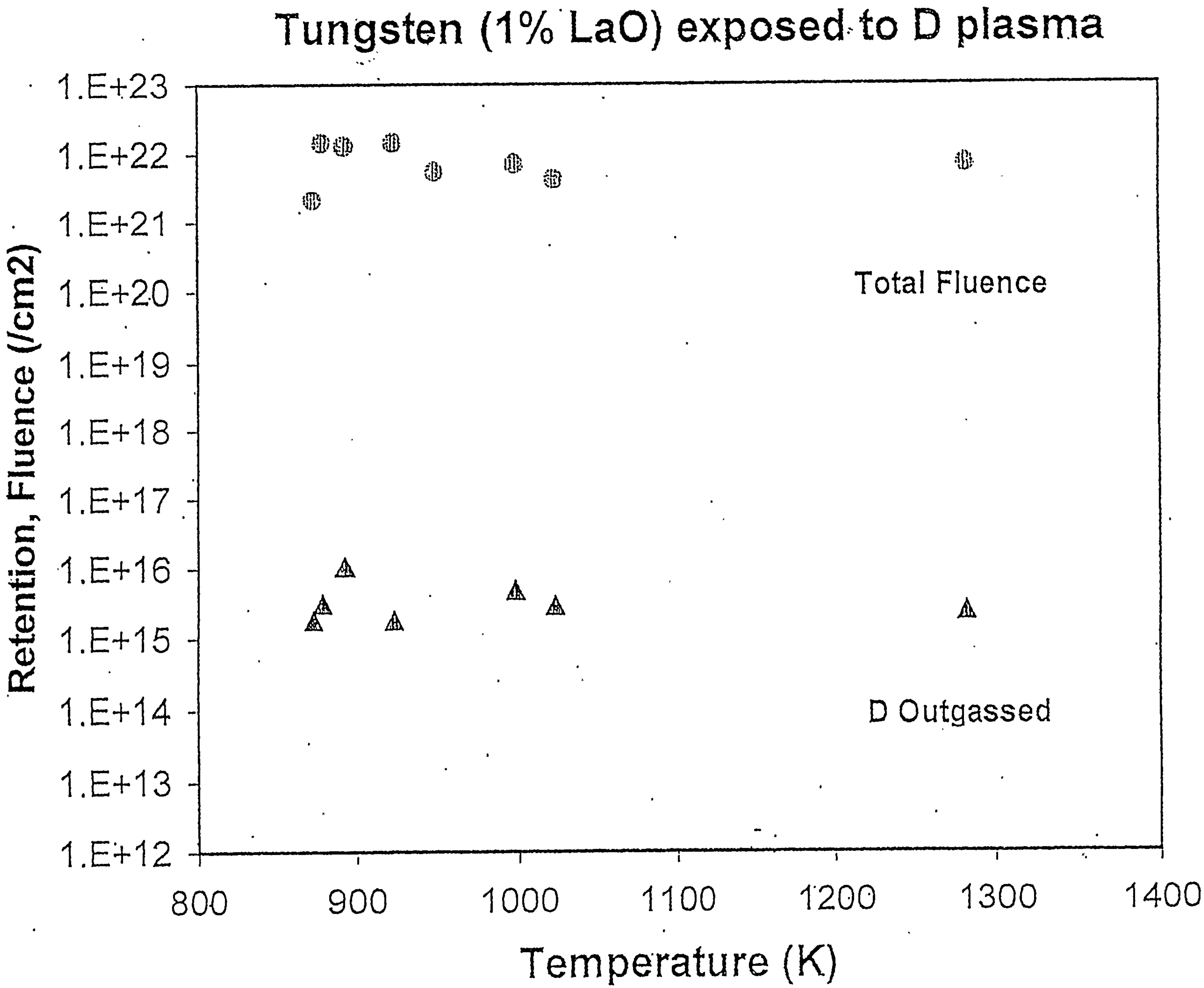

Tungsten (1% LaO) exposed to D plasma
Retention, Fluence (/cm2)
1.E+23
1.E+22
1.E+21
1.E+20
1.E+19
1.E+18
1.E+17
1.E+16
1.E+15
1.E+14
1.E+13
1.E+12
Total Fluence
D Outgassed
800
900
1000
1100
1200
1300
1400
Temperature (K)

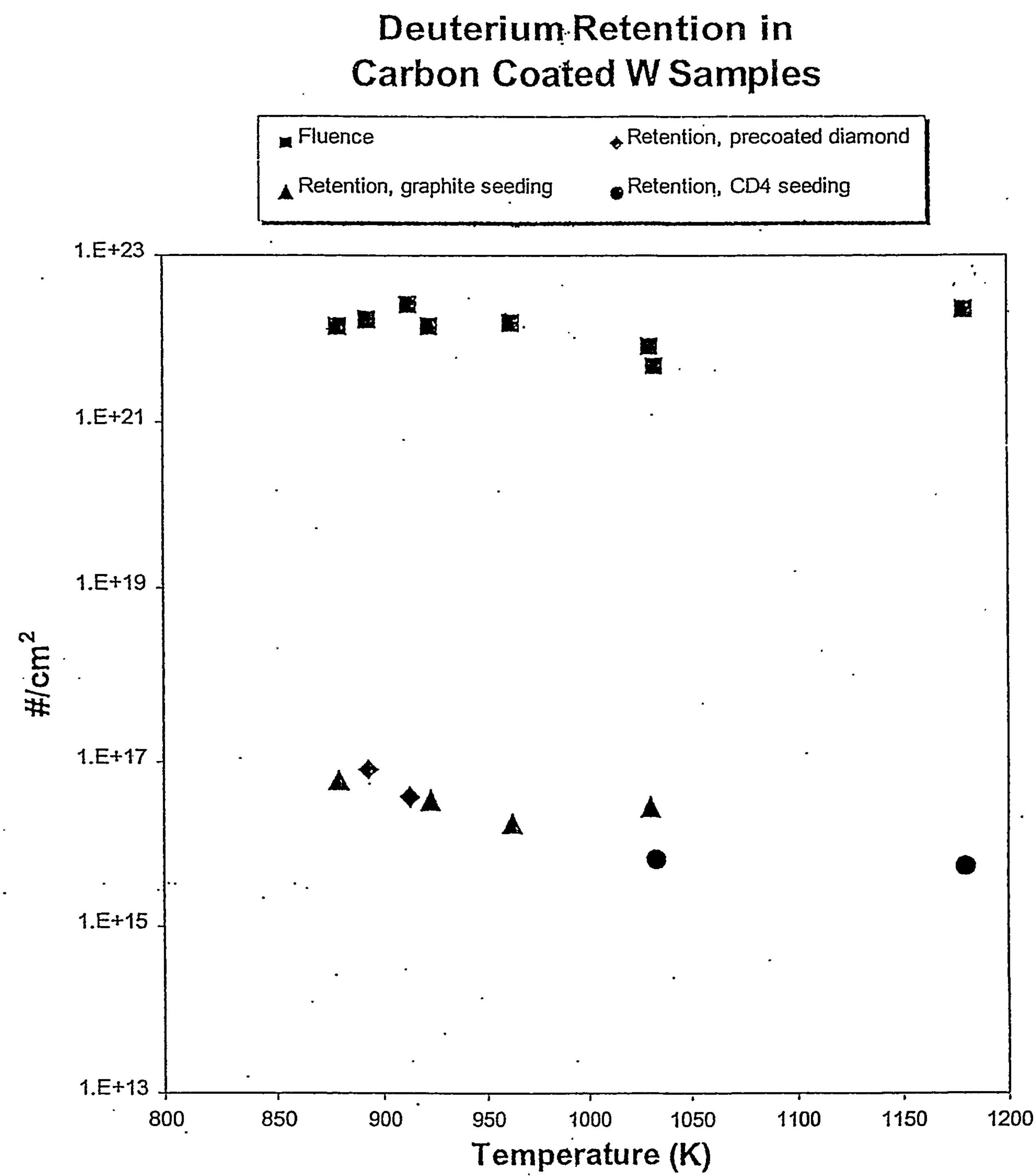

Deuterium Retention in
Carbon Coated W Samples
Fluence
Retention, precoated diamond
Retention, graphite seeding
Retention, CD4 seeding
1.E+23
1.E+21
1.E+19
1.E+17
1.E+15
1.E+13
#/cm2
800
850
900
950
1000
1050
1100
1150
1200
Temperature (K)

Deuterium Retention in Tungsten

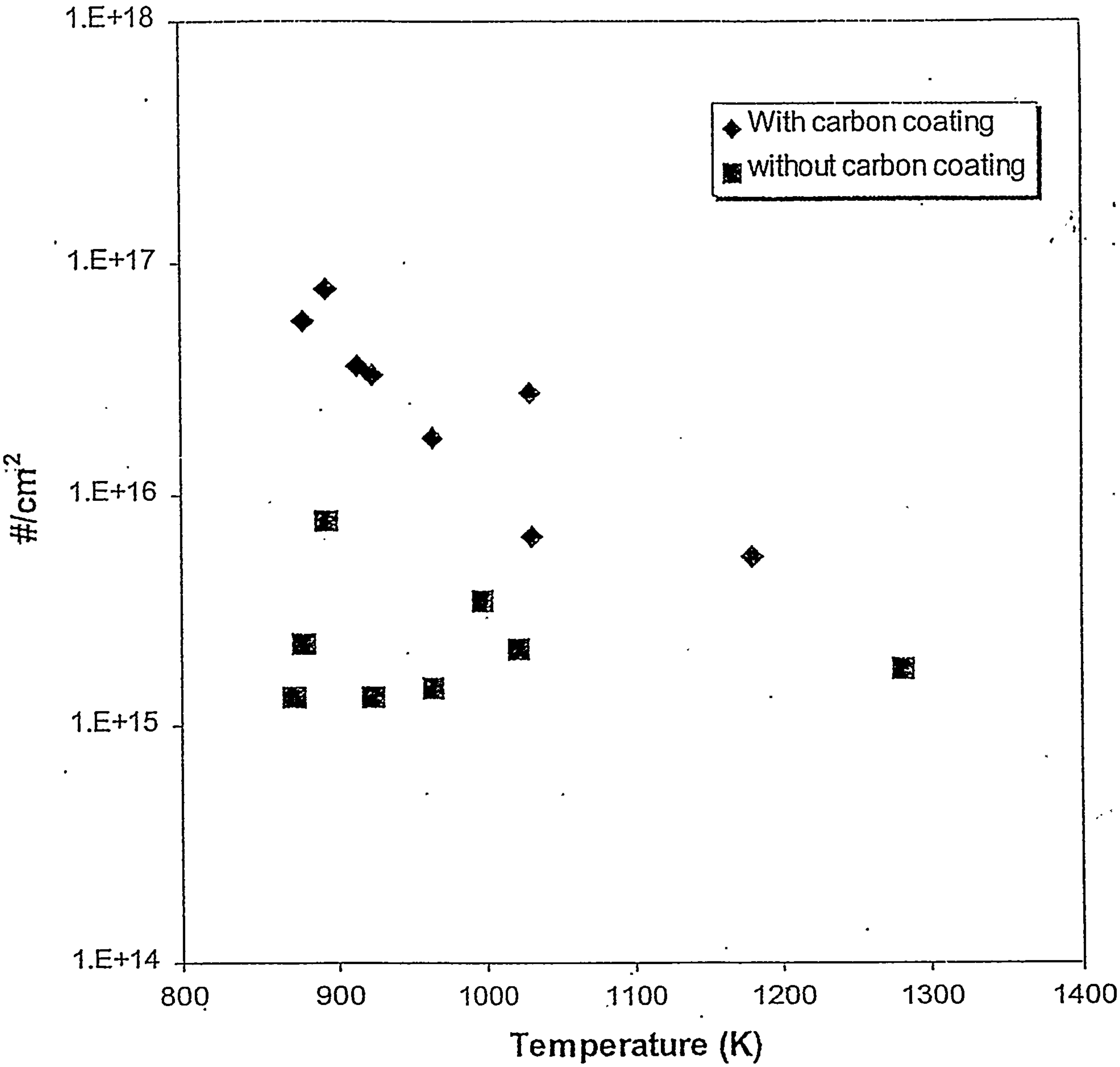

Exposed Tungsten with carbon seeding

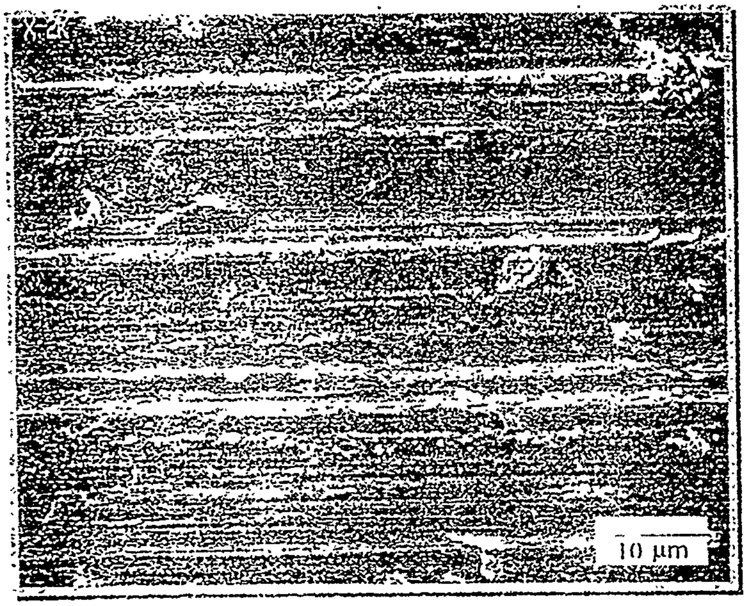

Pre-exposed Tungsten surface

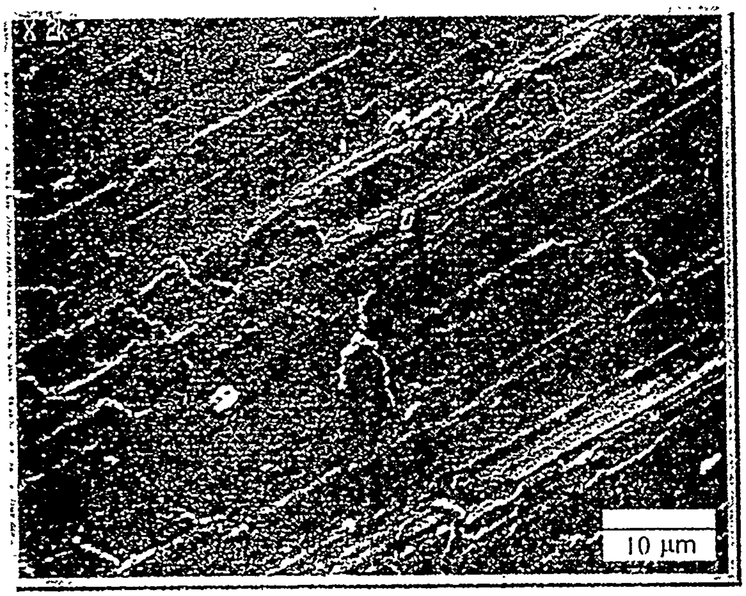

Exposed tungsten surface with carbon seeding at 907 K.

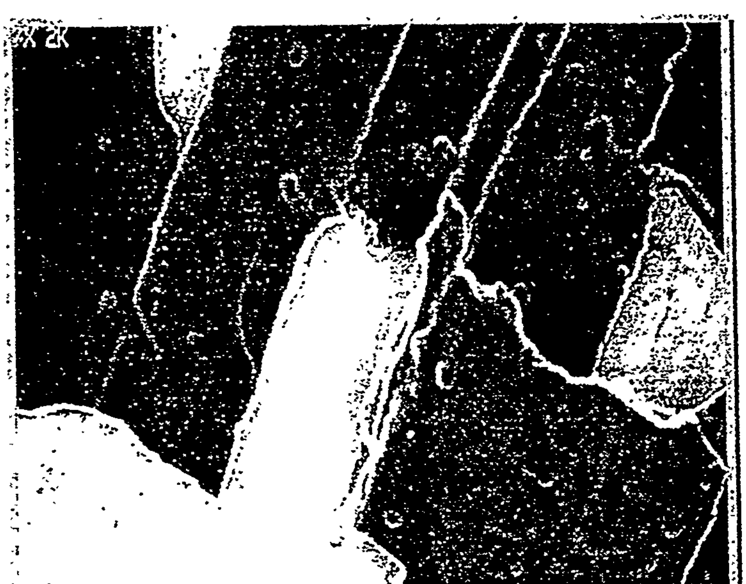

Exposed tungsten surface with carbon seeding at 1031 K.

Exposed Tungsten with CD_4 seeding in Deuterium Plasma

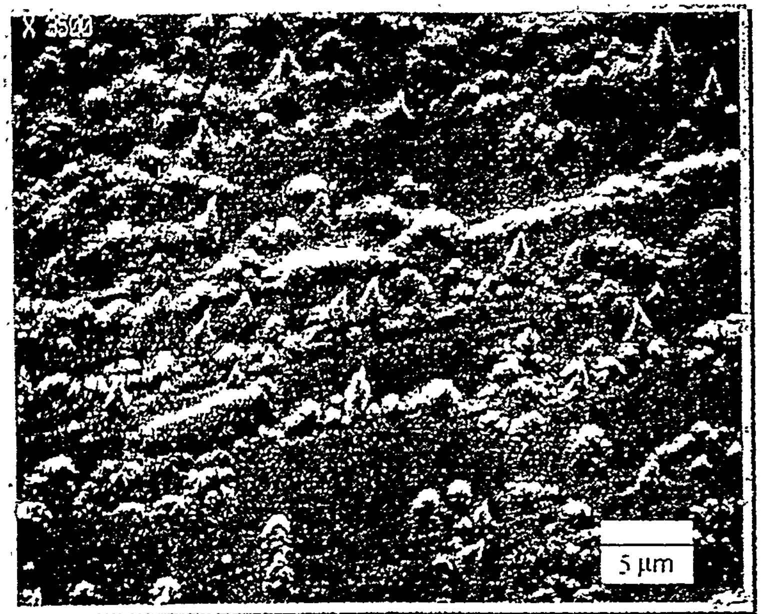

Sample temperature at 1033 K with 0.8 % CD_4

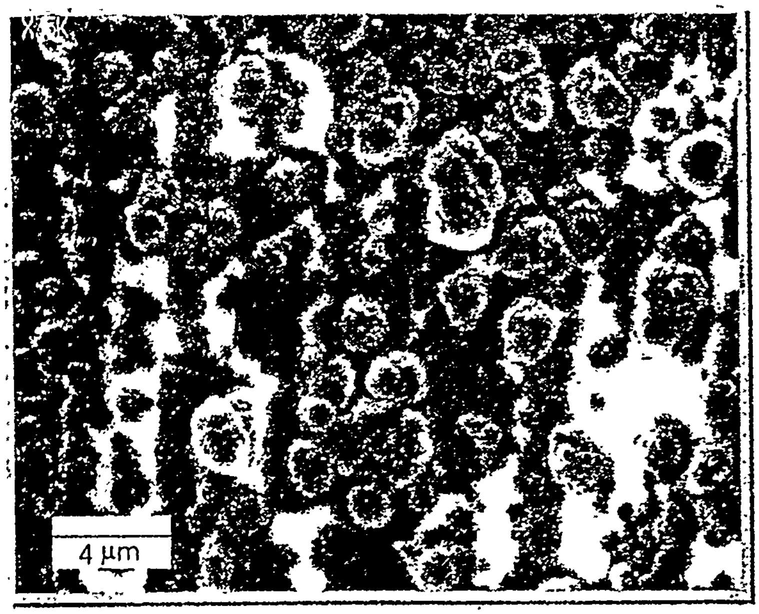

Exposed tungsten at 1033K with 1% CD_4

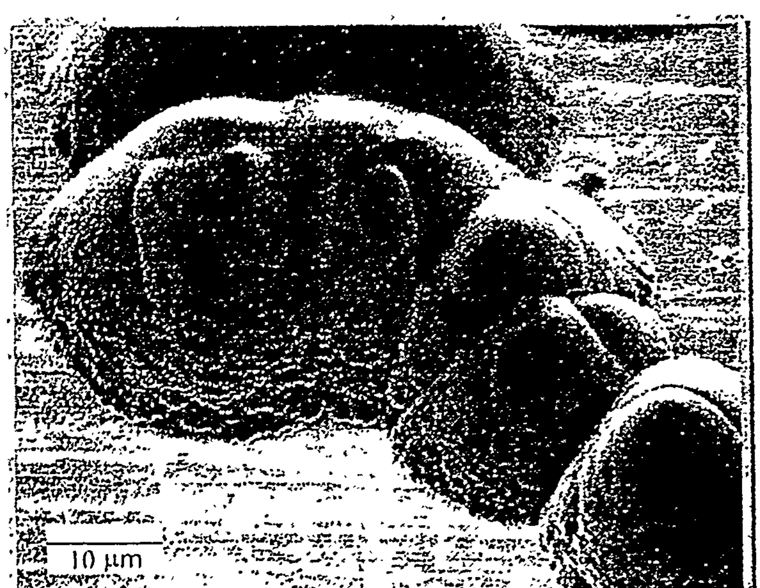

Exposed tungsten at 1180 K with 1.4% CD_4

Conclusions & Future Directions:

- Net sputtering yield of 'clean' beryllium agrees with the expected sputtering yield of beryllium-oxide

- Near surface damage of beryllium results from 100 eV D+ plasma bombardment
  - damage extends well beyond implantation depth
  - surface temperature effects damage formation

- Deuterium retention in plasma-sprayed beryllium is less than press-sintered beryllium
  - temperature dependent reduction

Impurity injection experiments are underway in PISCES-B to study mixed-material layers

- Determine formation conditions and growth rates for mixed-material layers on different substrate materials

- Carbon-containing layers can have a drastic impact on deuterium retention

- Investigate the role of metallic impurities incorporated in mixed-material layers

"Recent Erosion/Redeposition Analysis"

J. N. Brooks/D. K. Sze
Argonne National Laboratory
Argonne IL, USA

US-Japan Workshop on
High Heat Flux Components & Plasma Surface Interactions for Next Fusion Devices, San Francisco,
December 8-11, 1997

EROSION/REDEPOSITION ANALYSIS

PERSONNEL: J.N. Brooks, A. Hassanein

COLLABORATIONS: D. Ruzic et al. (UIUC), F. Federici et al. (ITER/JCT), D Whyte et al. (GA), R. Bastasz, R. Causey et al. (SNL), Y. Hirooka et al (PISCES).

GOAL: use, develop, and validate models/codes to predict:

1) Sputtering-erosion-limited plasma facing component lifetime

2) Impurity transport and plasma contamination

3) Tritium co-deposition

4) Heat deposition and related sheath phenomena

CURRENT ACTIVITIES:

1) ITER Vertical Divertor and First Wall erosion/ codeposition analysis

2) DIII-D/DiMES modeling and code validation

3) ALPS (just starting), JET modeling (just starting)

4) Theory and code development; maintenance of ANL Integrated Erosion Code Center capability.

DIII-D/DiMES Code Validation; D79
Brooks/Whyte

- DiMES 79 experiment - ELM'ing H mode attached plasma

- Carbon divertor analyzed with REDEP/WBC codes

- Code output compared with data:

  1) predicted carbon net erosion rate compared with probe erosion/redeposition data.
  2) predicted core plasma contamination compared with core measurement data.
  3) predicted gross carbon erosion rate compared with photon data.

- **Code/data comparison is good.**

REDEP/WBC Code Matches the Features of Carbon Net Erosion at the DIII-D Divertor as Measured by DiMES

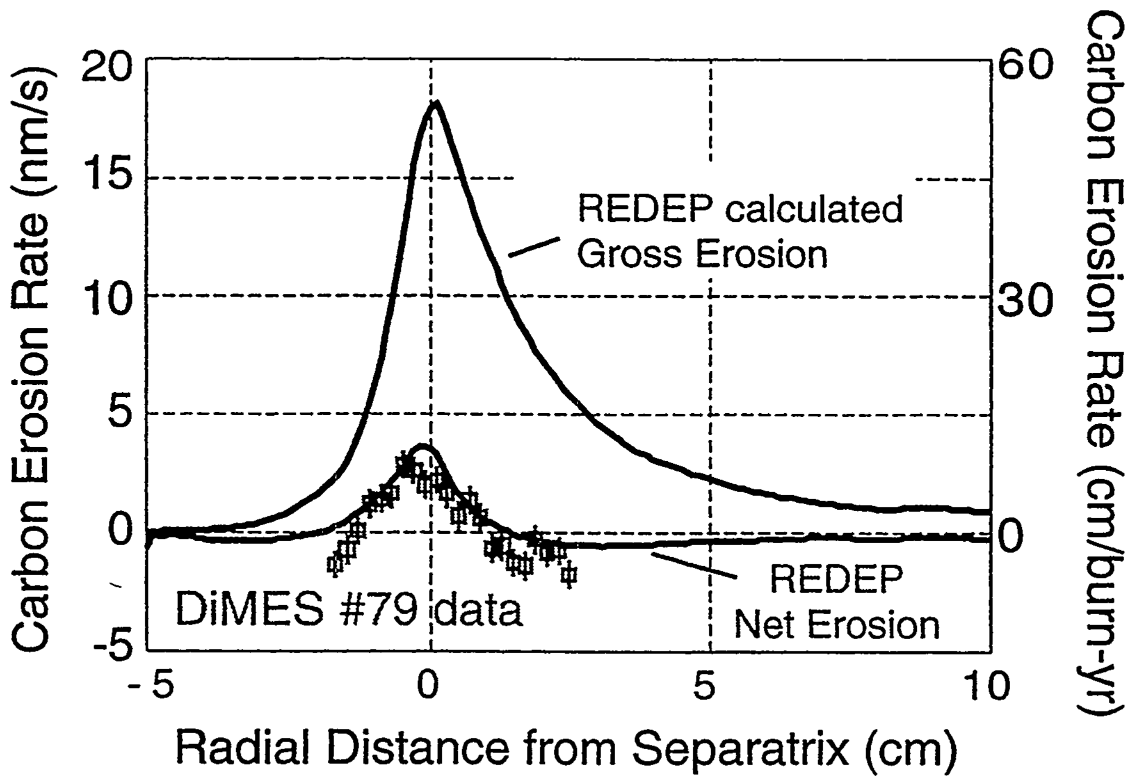

Exposure Conditions

Attached ELMing H-mode
$0.7\ MW/m^2$
$T_{e,OSP} = 70\ eV$

Sandia National Laboratories · Argonne National Laboratory · UCSD · GENERAL ATOMICS

Erosion/Redeposition Analysis of ITER

- REDEP/WBC/DEGAS+/VFTRIM codes used to compute physical and chemical sputtering of carbon divertor plate and beryllium first wall for "semi-detached" plasma solution (Kukushkin et al.)

- Tritium codeposition is computed using surface temperature dependent H/C, H/Be trapping ratios.

- Methane-only chemical sputtering analyzed, due to lack of data/models for higher hydrocarbon atomic and molecular cross sections. (Future work will examine higher hydrocarbon transport).

- Dominating process for net chemical erosion and codeposition is formation of carbon atom from complex molecular transport, and subsequent non-local redeposition due to low electron temperature in semi-detached plasma region.

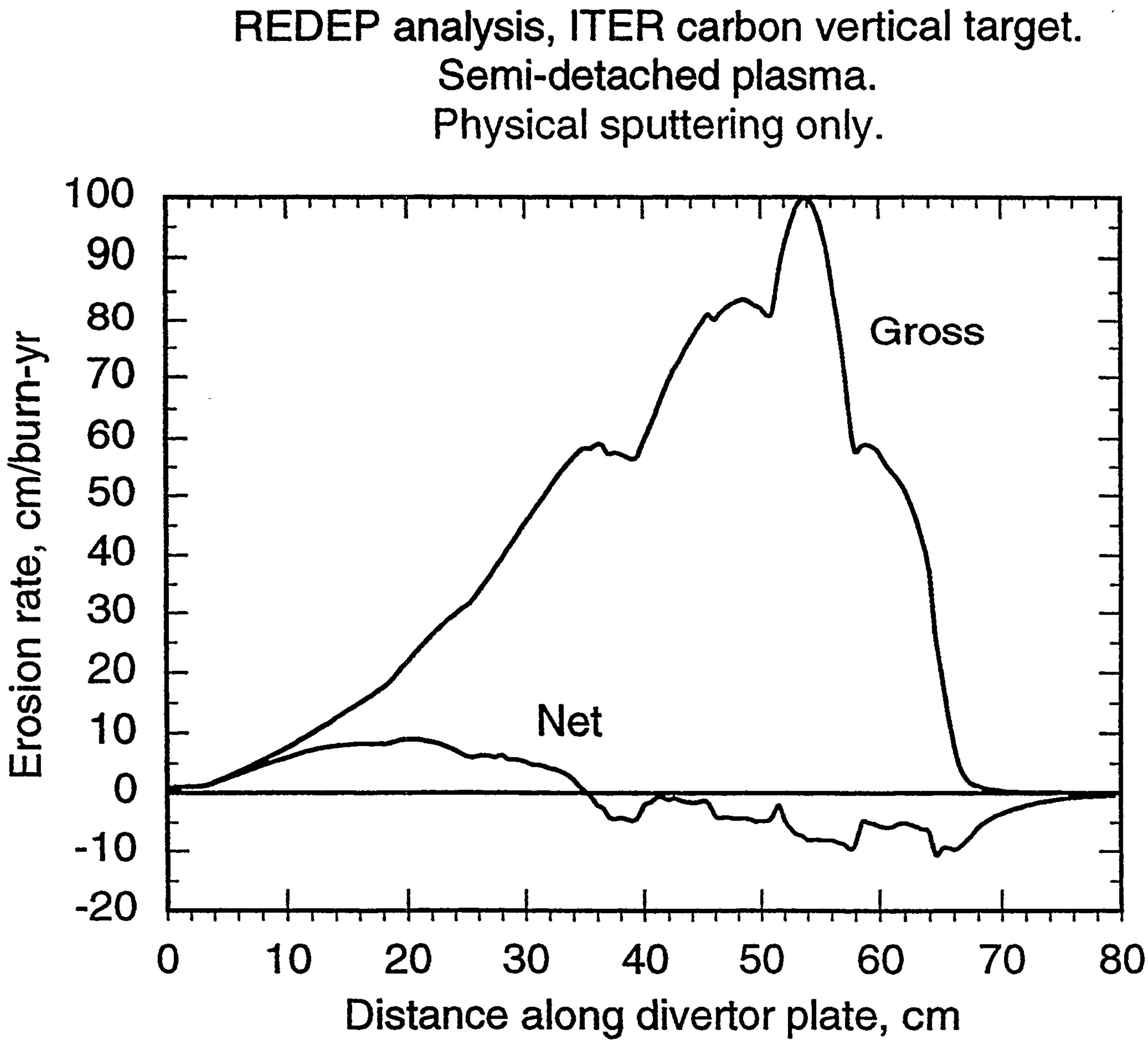
REDEP analysis, ITER carbon vertical target.
Semi-detached plasma.
Physical sputtering only.
Erosion rate, cm/burn-yr
100
90
80
70
60
50
40
30
20
10
0
-10
-20
Gross
Net
0
10
20
30
40
50
60
70
80
Distance along divertor plate, cm

WBC analysis, ITER carbon vertical target.
Semi-detached plasma.
Chemical sputtering only.

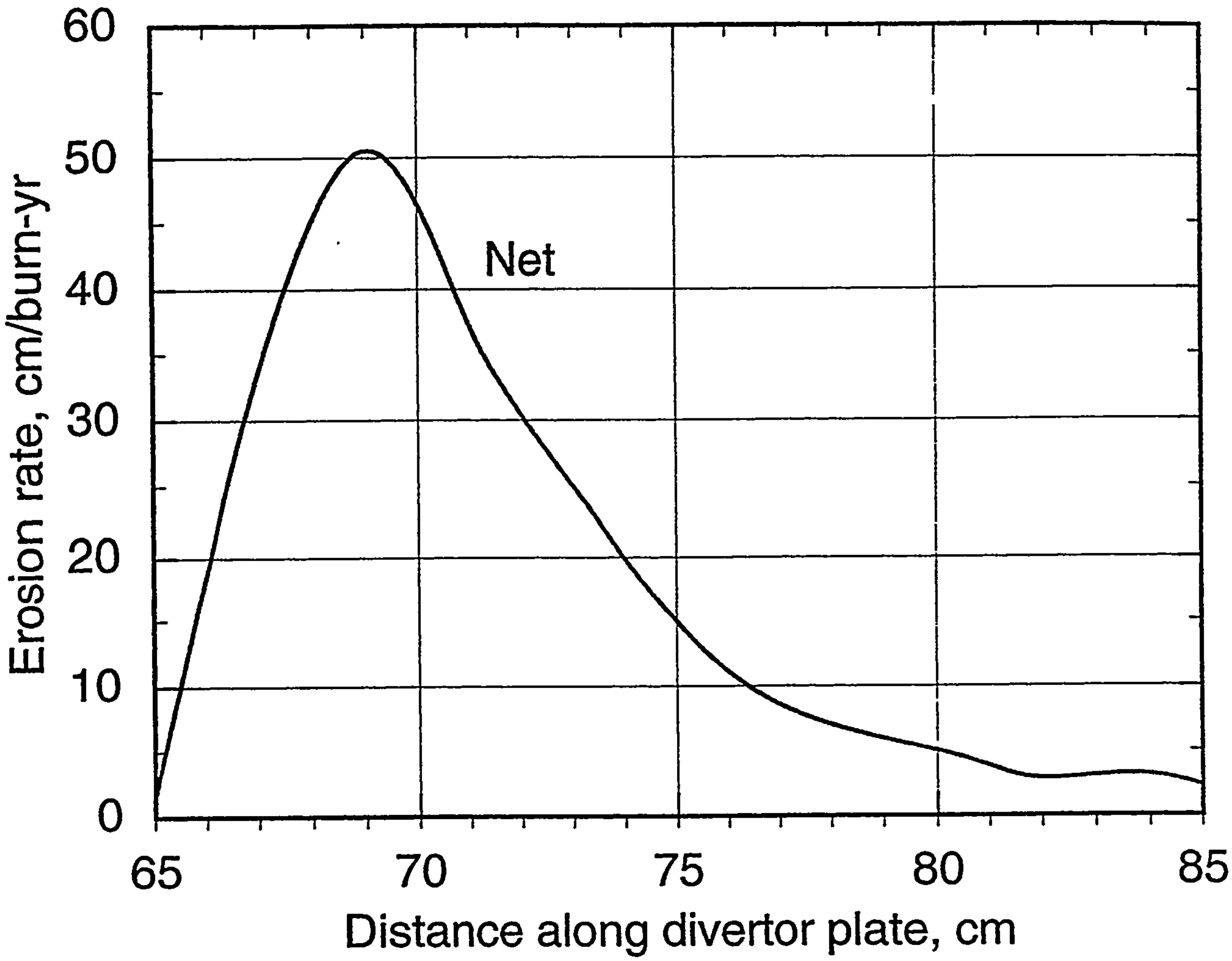

Peak net erosion rate is high in detached plasma zone.

ITER Erosion/Redeposition Analysis- Results for semi-detached edge plasma regime ("Case 98" , ~1% Neon). (Preliminary results— numerous models to be upgraded).

- Peak net erosion rate, (pure) carbon coated divertor: 50 cm/burn-yr

- Average net erosion rate, beryllium coated first wall: 0.05 cm/burn-yr

- Peak net erosion rate, beryllium, due to gas-puffing: very high-implies need for more spread out gas puffing

- Tritium codeposition rate in redeposited carbon: 10.1 g/1000 s pulse

- Tritium codeposition rate in redeposited beryllium: ~0.1 g/1000 s

- Conclusions: Semi-detached regime is better than fully detached regime, net carbon erosion and tritium codeposition is probably acceptable for ITER low duty-factor operation

Dependence of graphite erosion yield on irradiation flux close to actual edge plasma condition

Y. Ueda, Y. Ohtsuka, M. Isobe, M. Nishikawa
Osaka University, Japan
(Presented by Y. Ueda)

December 8-11, 1997 at Warwick Regis Hotel

US-Japan workshop on High Heat Flux Components and Plasma Surface Interactions for Next Fusion Devices

Outline

1. Background of this work
2. Experimental setup
   - high flux irradition test stand
   - temperature control
3. Experimental results of RES of graphite
4. Discussion on RES in high flux regime
5. Summary and future plan

Background 1

Erosion Process Unique to Graphite

- Radiation Enhanced Sublimation (RES)

  Enhanced erosion of graphite over 1200 K by any energetic particle impact

- Chemical Sputtering

  Enhanced erosion of graphite around 800 K by energetic hydrogen and oxygen impact

Erosion of Graphite under High Heat Flux Condition in Tokamak Devices

- RES

  TEXTOR : not observed [1]
  JET : not observed clearly [2]
  TFTR : slightly observed over 1900 K [3]

- Chemical

  JET : not observed clearly [4]
  JT-60 : not observed clearly [5]

[1] V. Philipps et al., Nucl. Fusion 33 (1993) 953.
[2] R. Reichle et al., J. Nucl. Mater. 176&177 (1990) 375.
[3] A. Ramsey et al., Nucl Fusion 31 (1991) 1811.
[4] K. H. Behringer, J. Nucl. Mater. 145-147 (1987) 574.
[5] H. Kubo et al., J. Nucl. Mater. 196-198 (1992) 71.

Background 2

Complex Situation for PFC

- High (Heat - Particle) Flux
- Many Species of Ions

  Proton, Deuteron, Triton

  Helium ash

  Low Z materials (Be, B, C)

  High Z (W)
- Redeposition
- Energy Distribution

  Maxwellian plasma ions

  Fast Neutral

  Ripple Loss Ion
- Angular Distribution
- High Fluence Irradiation

Aims of This Work

Detailed Database of Graphite Erosion by High Flux Beam Irradiation

- Dependence on irradiation flux
- Dependence on angle of incidence
- Dependence on graphite types (isotropic, pyrolytic etc.)

Models for Graphite Erosion Applicable to Actual PFM Conditions

- Lifetime estimation of graphite PFC
- Proposal of favorable edge plasma conditions

High Flux Irradiation Test Stand

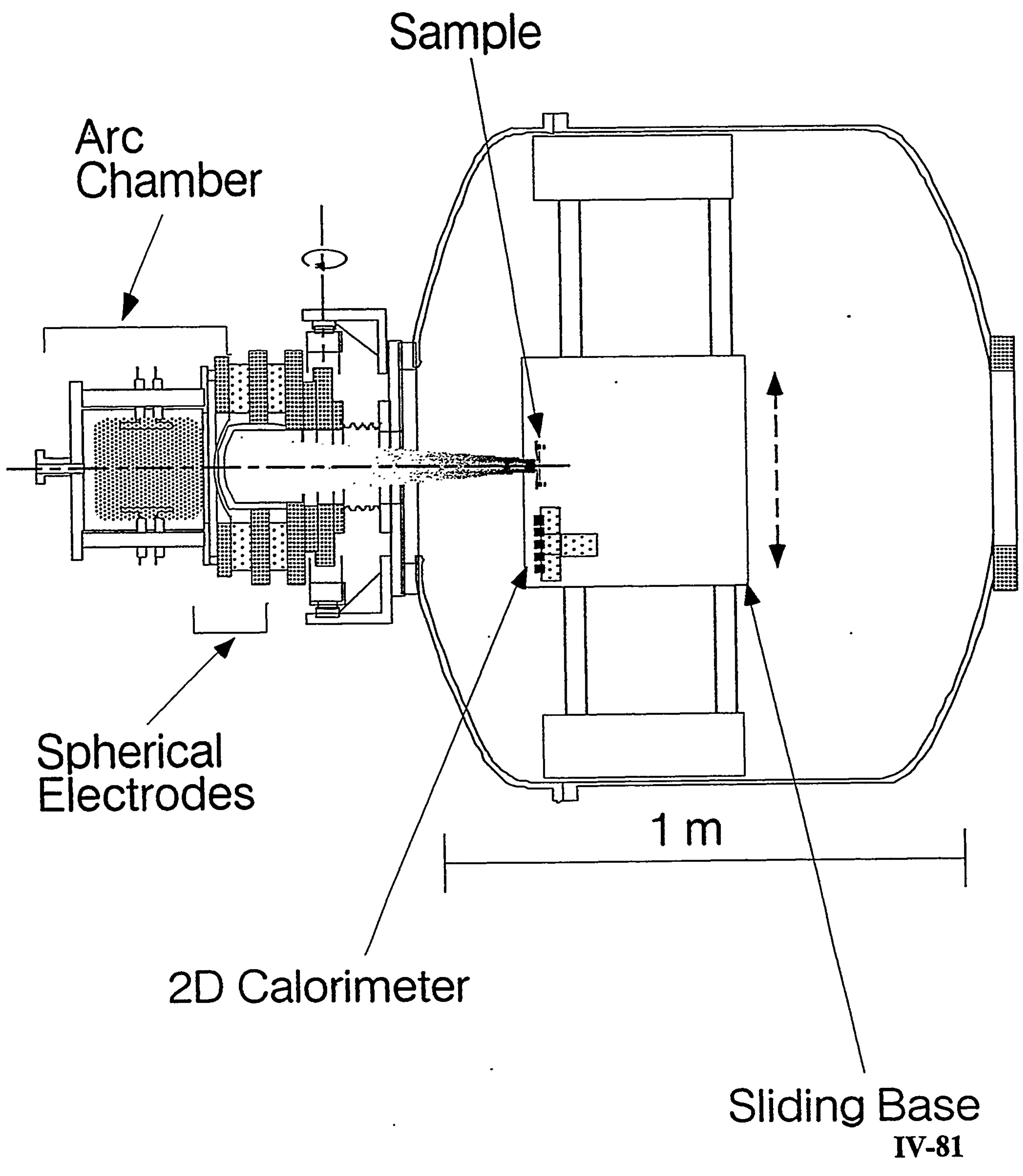

Advantages of Our Device
(compared with Plasma Simulator)

Control of irradiation angle

- Angular Dependence

Multi-beam irradiation

- Multi-species Irradiation (D+C, D+He, and so on)
- Irradiation with Different Energy

Detailed diagnostics of sputtered particle

- Separation of Beam Source and Samples
- Direct Measurements of Sputtered Particles

Disadvantages

- Difficulty in producing very low energy ($\leq$ 100 eV) and high flux ($> 10^{21}$ $m^{-2}s^{-1}$).

Beam Specification

Ion Source

- Bucket source

  Arc discharge with thermionic cathodes

- Electrodes

  Spherical electrode

  Effective diameter : 14 cm

  Radius of curvature : 50 cm

- Gas : D_2 : 5 - 10 mTorr

  Ar : 5 mTorr

Beam Characteristics

- Energy : ~ 5 keV
- Power density : 3.5 MW/m^2 (D)

  1.2 MW/m^2 (Ar)

- Flux : 1.0×10^{22} D/m^2s

  1.5×10^{21} Ar/m^2s

- Pulse length : 4 sec

Sample Holder

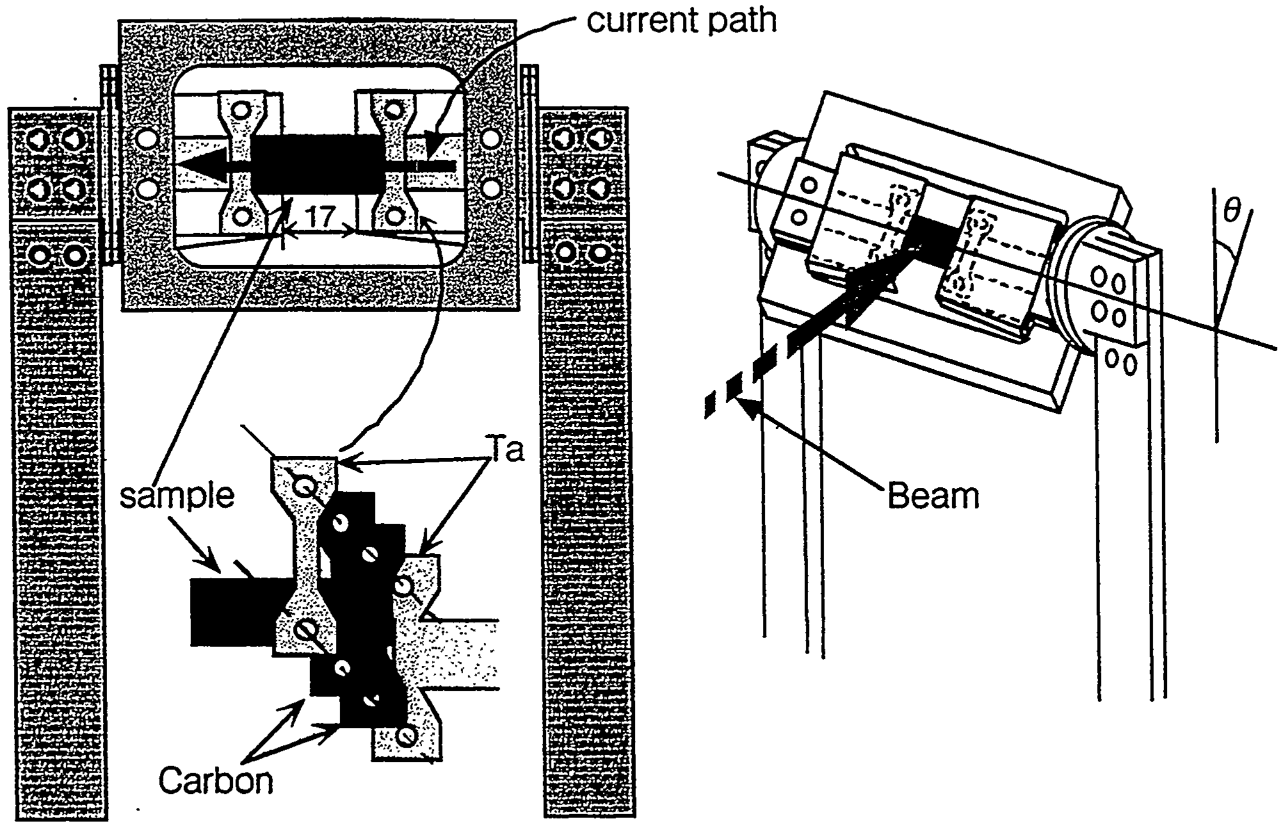

Sample

Isotropic graphite (IG-430, ISO-630 [Toyo Tanso])
Pyrolytic graphite [Union Carbide]
Doped Graphite (RG-Ti [NIIGrafit])

Sample Size

$(8\sim10) \times 40 \times (0.1\sim0.2)^t$ mm^3

Irradiation Angle

IV-84 0 deg ~ 75 deg

Temperature Control

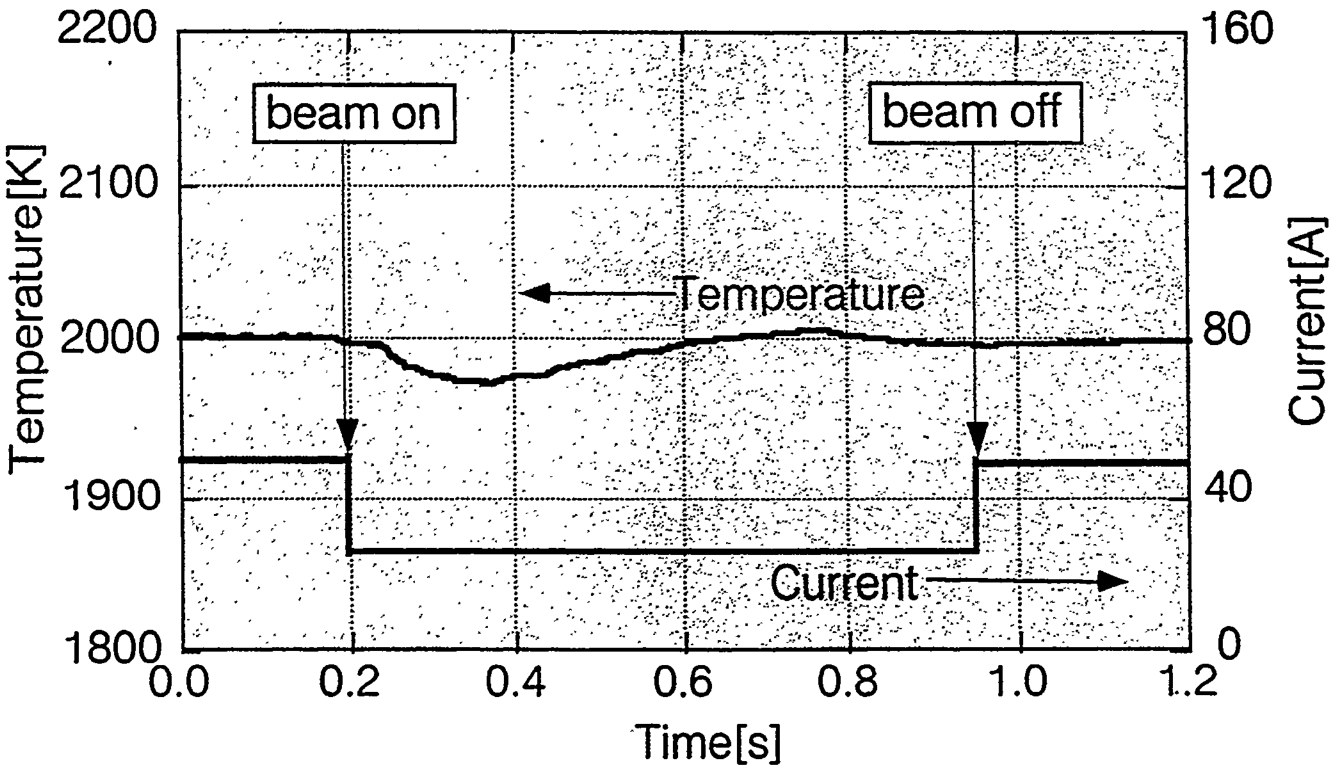

Beam Power : 0.96 MW/m^2、 5 keV Ar

Sample : Isotropic Graphite (ISO-630)
40 x 10 x 0.2 mm^3

Surface temperature of samples was controlled by changing heating current during beam irradiation.

Temperature dependence

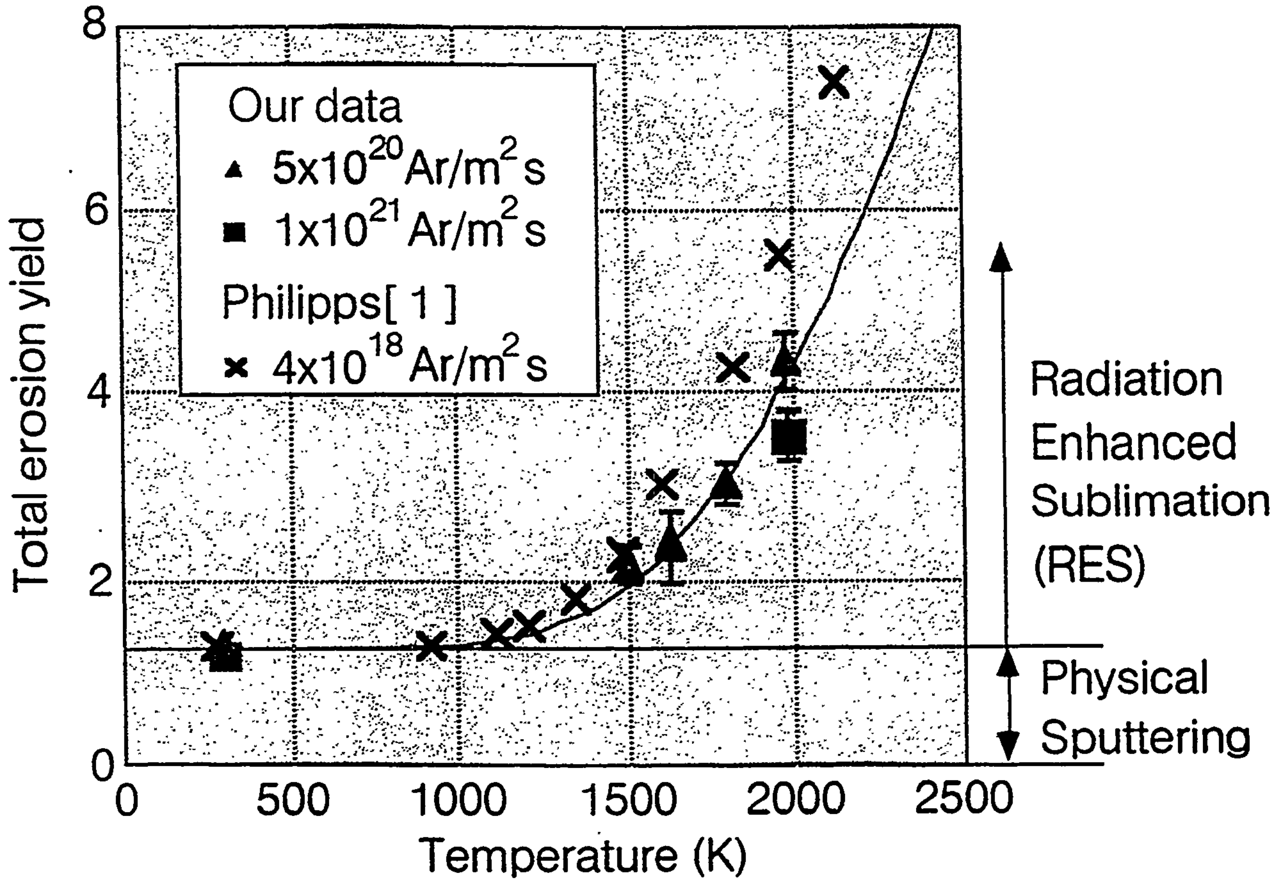

Beam : 5 keV Ar

Sample : Isotropic Graphite (ISO-630)

Irradiation Angle : 0 deg

[1] Philipps et al., J. Nucl. Mater. 155-157 (1988) 319.

Flux Dependence

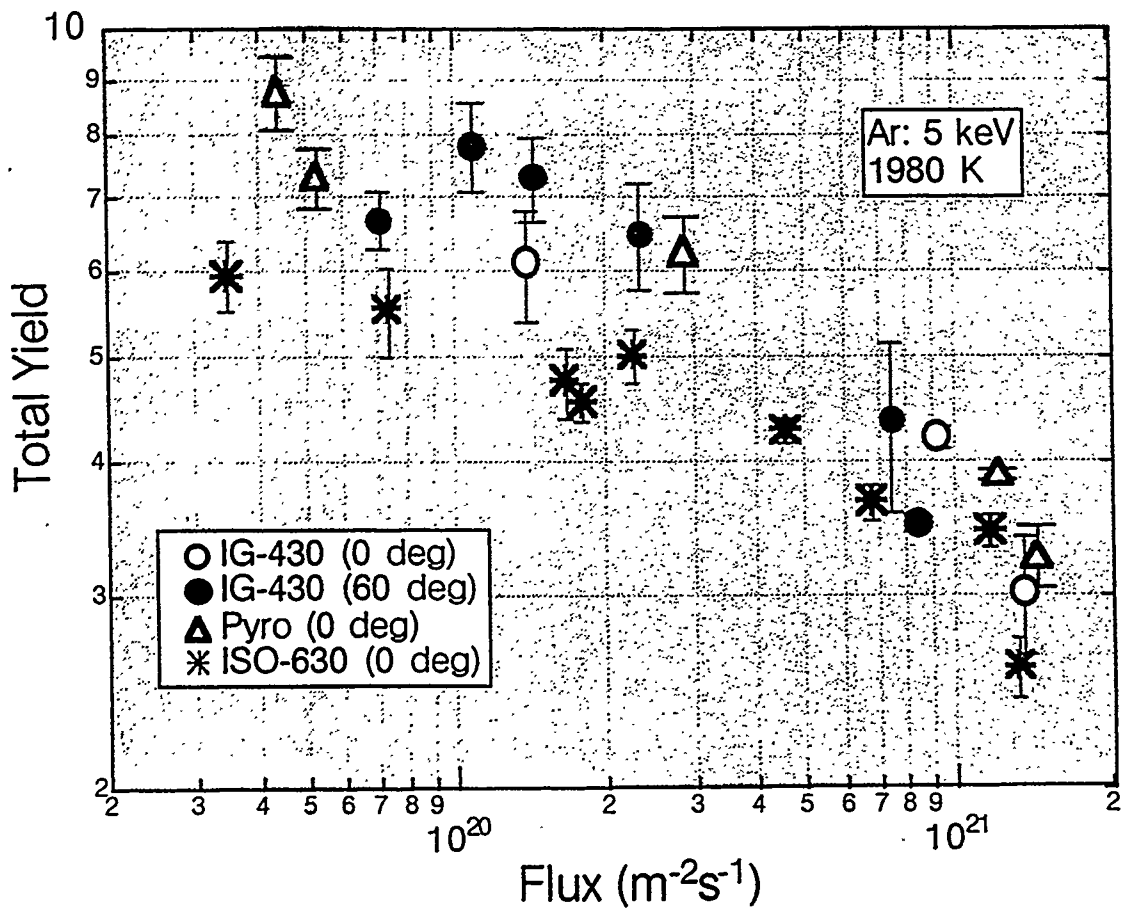

Flux dependence of total yield at 1980 K

Total yield at 1980 K shows clear reduction with flux for IG-430 (0 deg and 60 deg) and ISO-630 (isotropic graphite), and pyrolytic graphite.

The dependence is similar for these materials.

Surface Morphology of RG-Ti

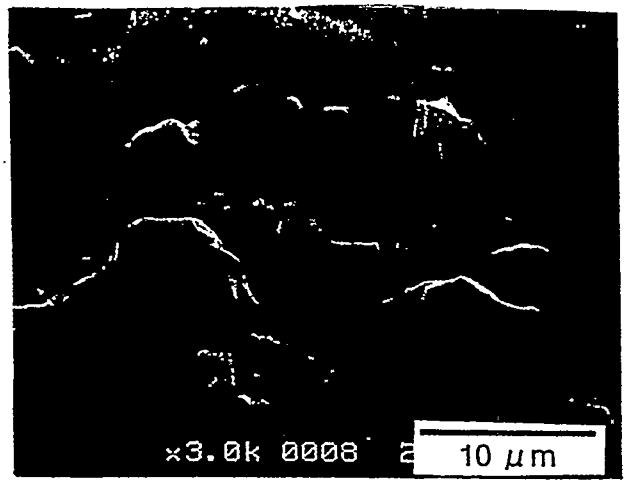

Low Flux
1.2 x 10^{20} Ar/m^{2}s
(1.9 x 10^{23} Ar/m^2)

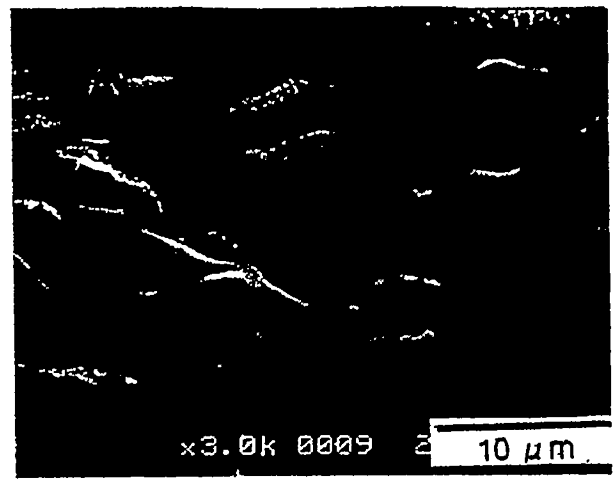

High Flux
8.0 x 10^{20} Ar/m^{2}s
(4.2 x 10^{23} Ar/m^2)

Samples : RG-Ti (1.7at% Ti included)

Irradiation Beam : 5 keV Ar

Temperature : 1780 K

TiC grains are eroded by physical sputtering, while graphite parts are eroded mainly by RES.

Erosion rate of graphite at elavated temperature is dependent on flux, which causes higher protuberances of TiC grains in the lower flux case.

Angular dependence

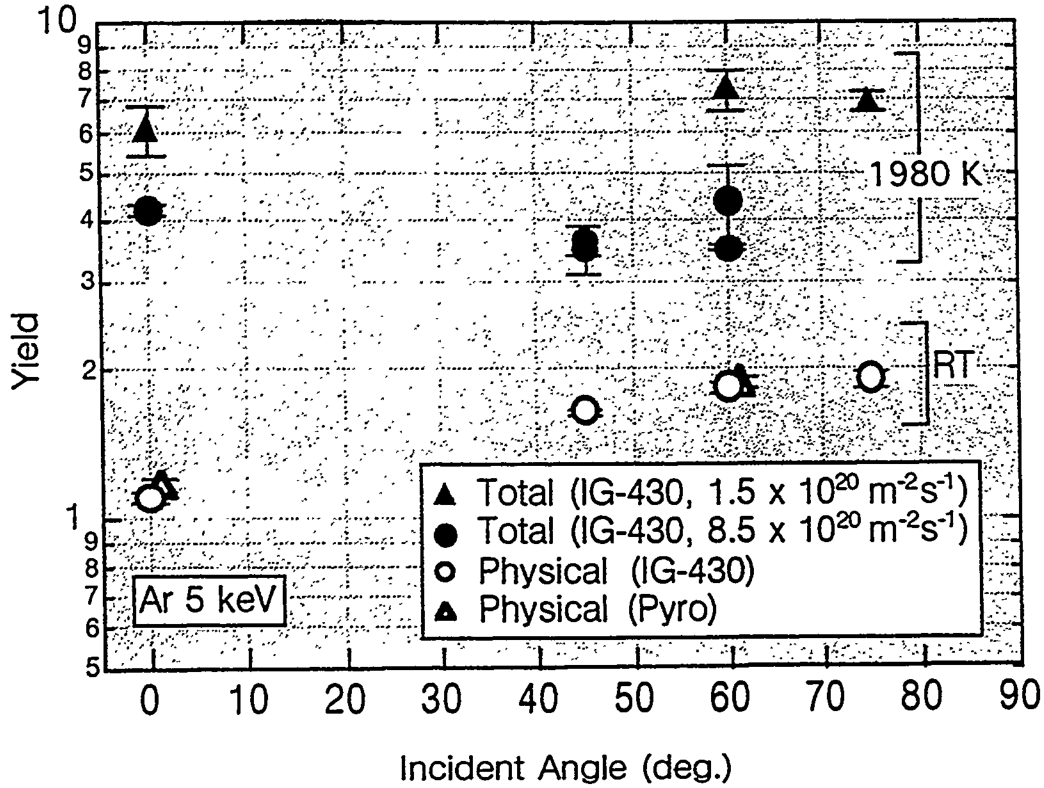

Angular dependence of total yield for various condition

Physical sputtering (RT)

- Increase with angle
- No difference between IG-430 and Pyro

RES + Physical (1980 K)

- No clear dependence on angle
- (clear flux dependence,

Illustration of Model

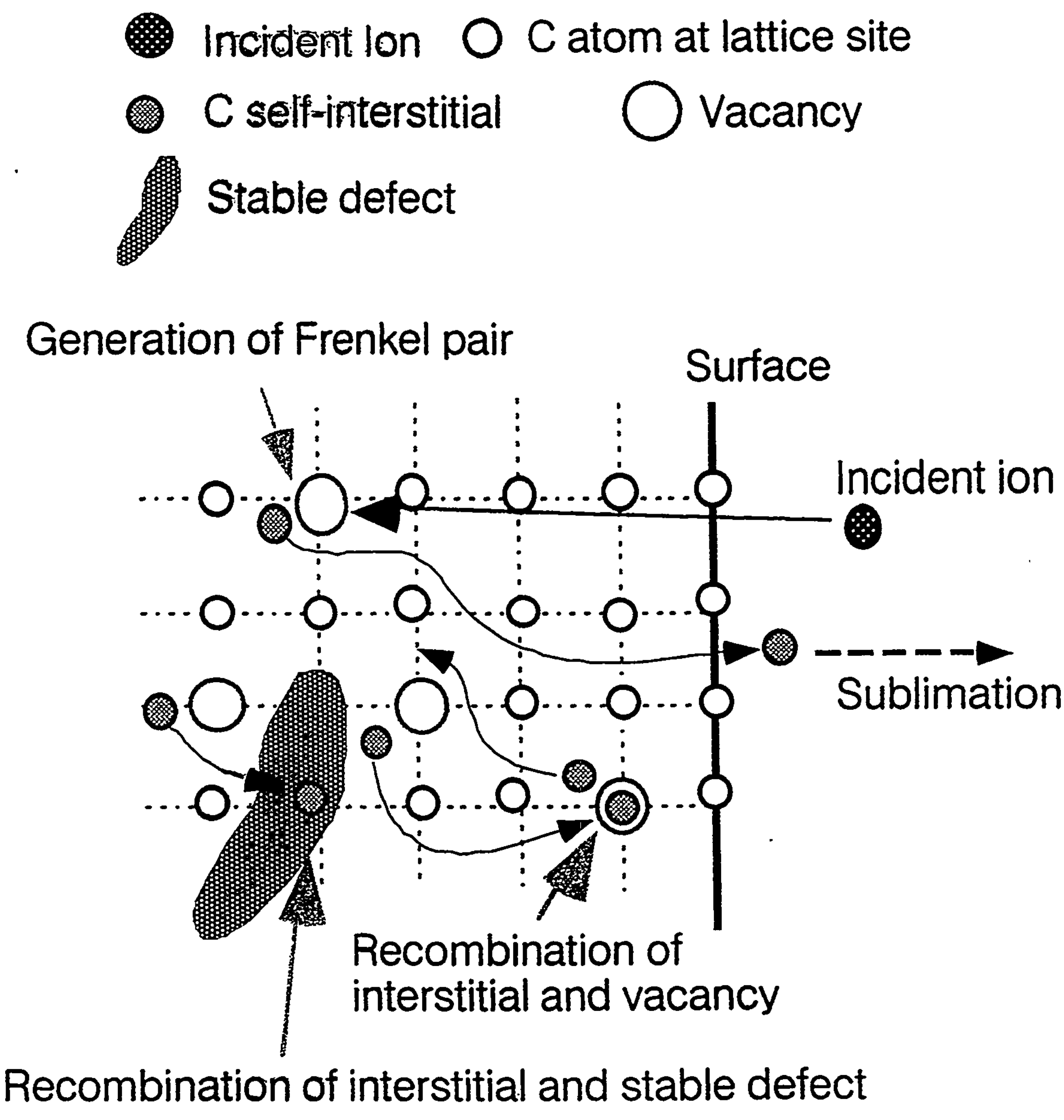

Model Calculation and Exp.

Sinks for Interstitial

- Low flux regime → Stable defects

  RES Yield → Flux independent
- High flux regime → Vacancy

  RES Yield → Flux dependent ($\sim \phi^{-0.25}$)

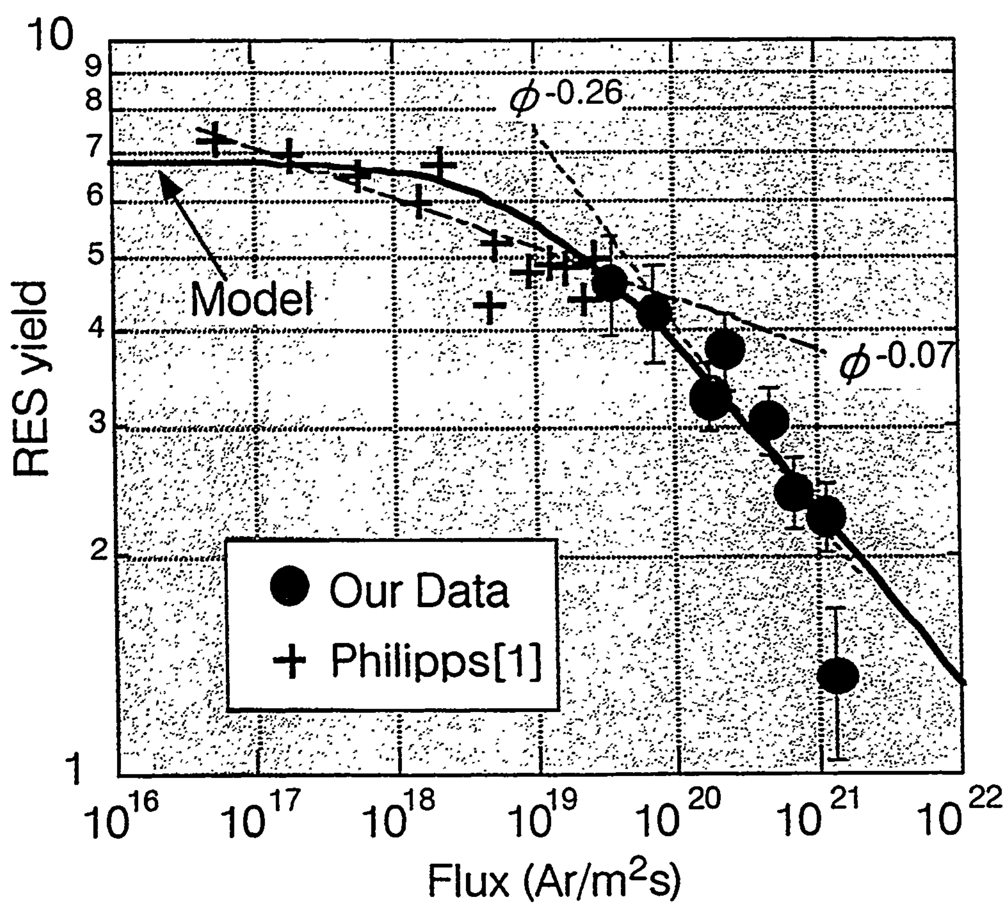

Model assumption

- Steady state
- Stable defect density : $5 \times 10^{-3}\ n_c$

n_c : carbon density

Erosion under PFM conditions

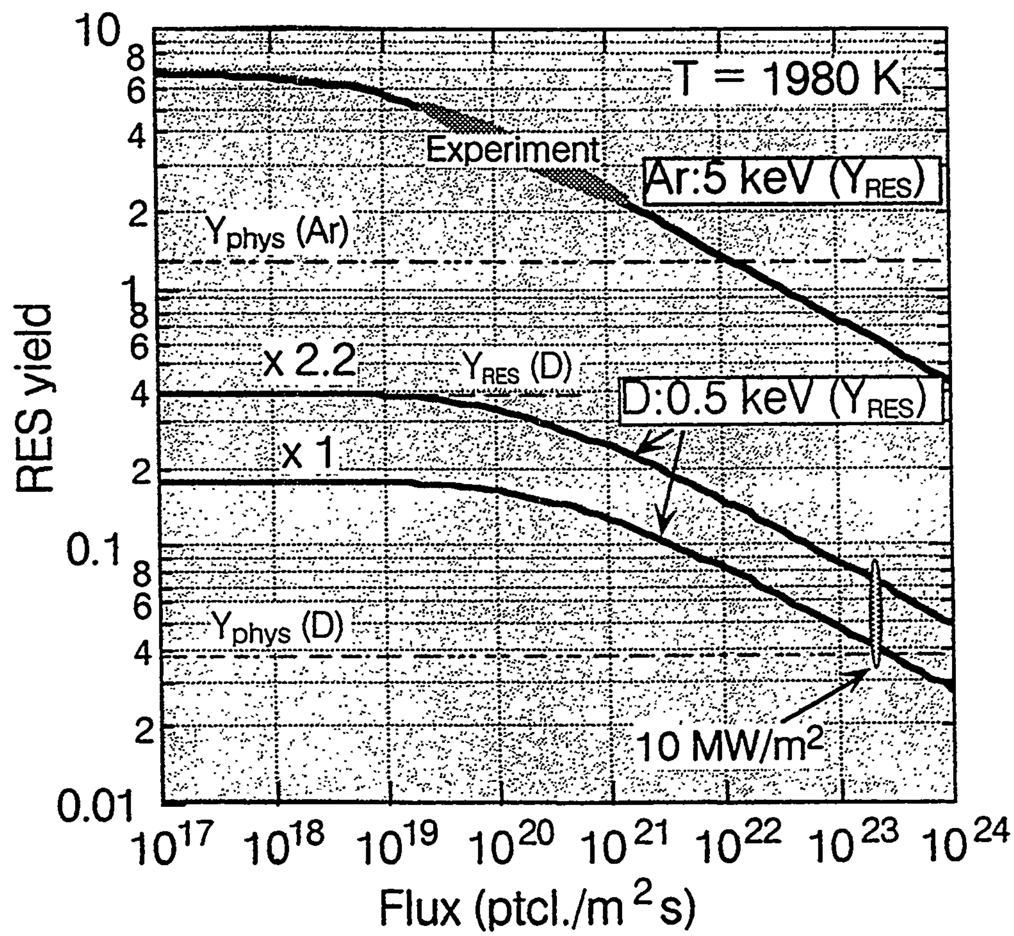

Under high heat flux edge plasma condition
(Ion heat flux : 10 MW/m^2)

- RES yield is less than 1/5 of previous low flux data
- Total erosion yield (RES+Phys.) is less than 1/4 of previous low flux data (T = 1980 K)

Particle Measurement

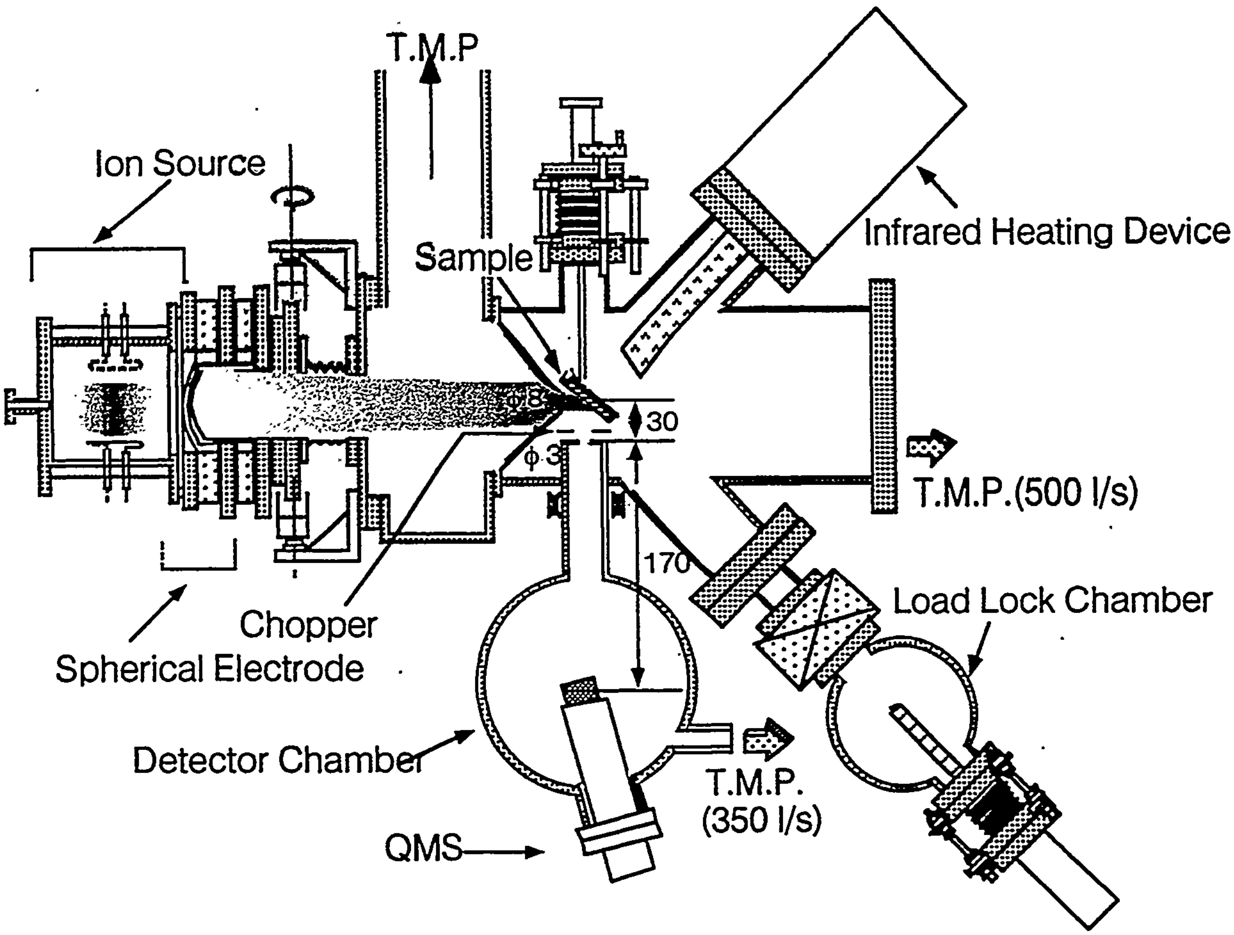

Arrangement of Sputtered Particle Measurement

Summary and Future Plan

1. Erosion yield of radiation enhanced sublimation (RES) of various graphite (IG-430, ISO-630, PG) in high flux regime (5 keV Ar, ~10^{17} Ar/m^2s) significantly decreases with flux. Observation of surface structure of RG-Ti (Ti doped graphite) supports these results. No clear angular dependence of RES yield was observed.

2. The above result is consistent with RES model based on diffusion and annihilation of C self-interstitial, in which dominant sinks are vacancies in high flux regime (strong flux dependence).

3. Under tokamak edge plasma condition (0.5 keV D, 10MW/m^2), RES yield can be reduced by more than a factor of 5 compared with that of low flux irradiation experiments.

Future Plan

- Direct measurements of sputtered particle
- New CW ion source for high fluenece and multi-beam irradiation

DiMES Erosion and Dust Experiments on DIII-D

presented by
D.G. Whyte, UCSD

at the US-Japan Workshop on High Heat Flux Components & Plasma Surface Interactions for Next Fusion Devices
December 8-11, 1997
San Francisco

for the DiMES Team

R.B. Bastasz, W.R. Wampler,
Sandia National Laboratory

J.N. Brooks,
Argonne National Laboratory

C.P.C. Wong, W.P. West
General Atomics

and I. Opimach
Triniti Lab

Sandia National Laboratories   UCSD   GENERAL ATOMICS

Erosion Validation: Agreement

1. Current understanding of erosion production and transport are sufficient to predict net erosion rates in attached regions of divertor plasmas for a single species PFC tokamak. This is validated by comparisons of models and experiment.

2. Short duration, dedicated erosion measurements accurately represent long term erosion rates.

3. Net erosion rate of the DIII-D carbon divertor, under attached conditions, will be ~ 10's cm/burn-yr and is peaked near the outer strike point. This is correctly predicted by REDEP/WBC.

4. In DIII-D the hydrogenic inventory build-up rate is determined by the attached outer divertor's net erosion rate and subsequent redeposition at the detached inner leg.

UCSD

GENERAL ATOMICS

Divertor Material Evaluation Studies (DiMES)

OBJECTIVES

- Measure erosion rates and redeposition mechanisms under tokamak divertor conditions.
- Validate and improve erosion codes.
- Determine the implications for fusion power plant plasma facing components.

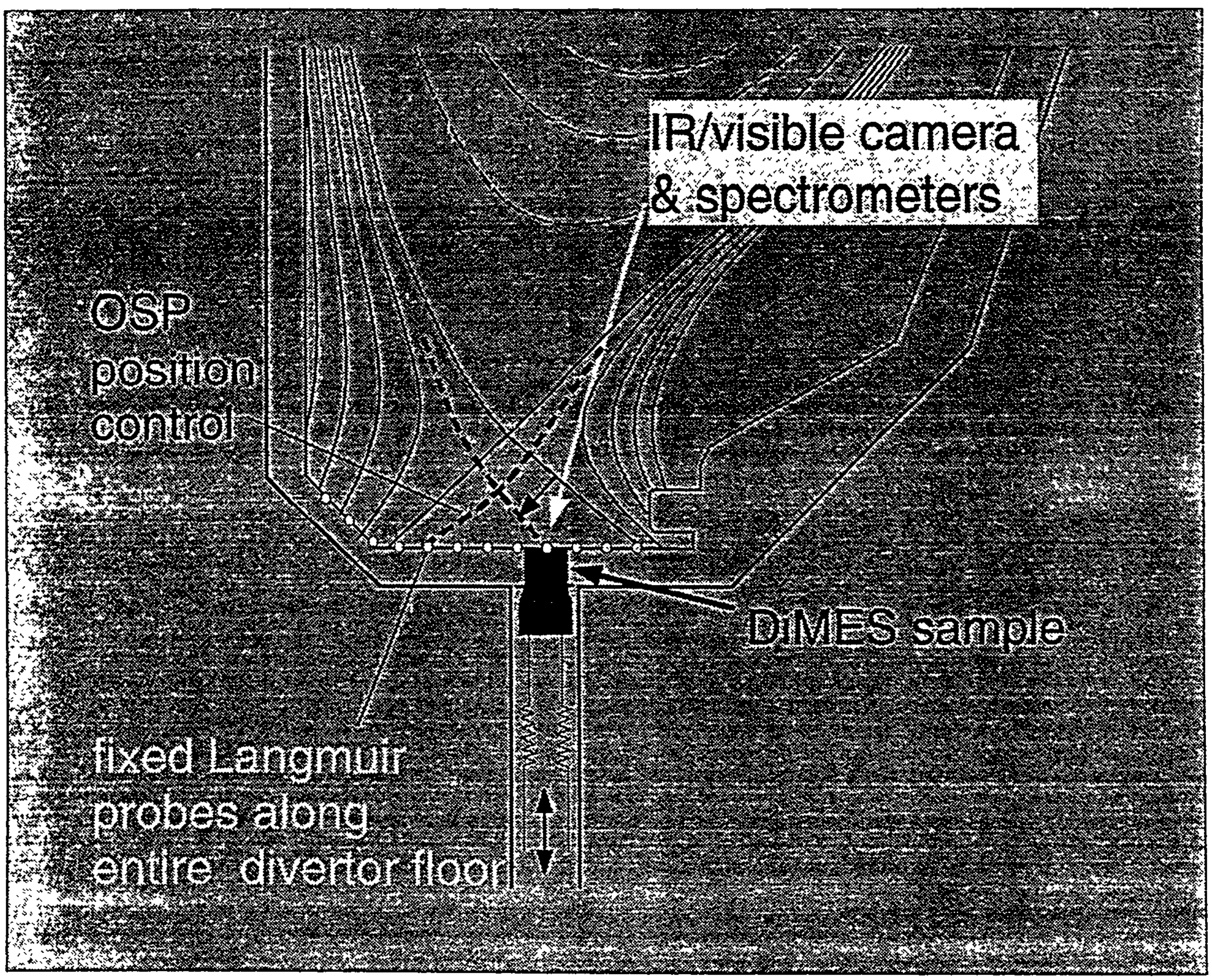

DiMES, DIII-D Divertor & Diagnostics Provide Controlled, Characterized Exposure Conditions for Candidate Materials

Sample and Exposure Geometry

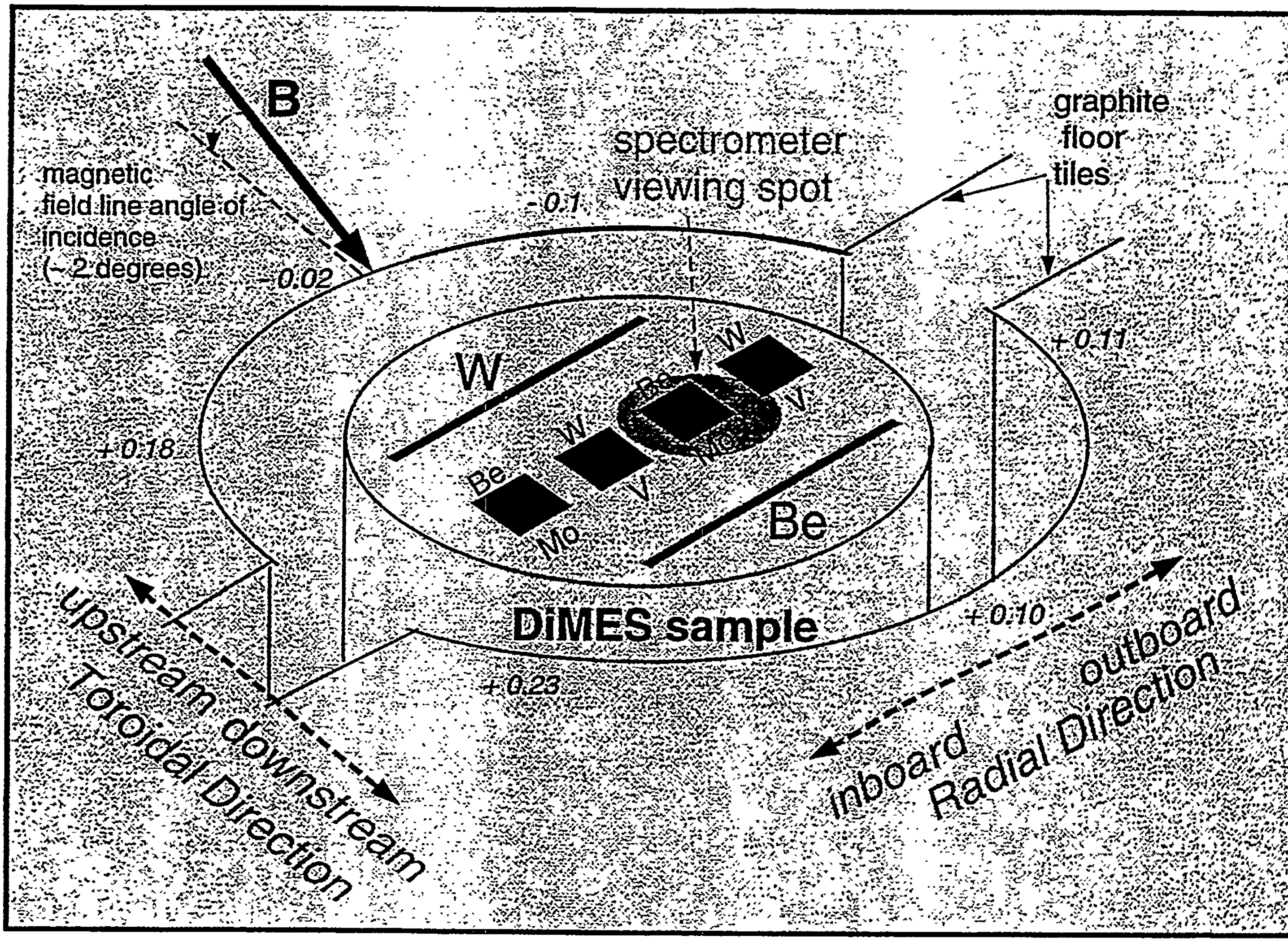

DiMES Rooftop Alignment to Surrounding Tiles Allows for High Power Exposures with Uniform Heat Flux to DiMES and No Leading Edges

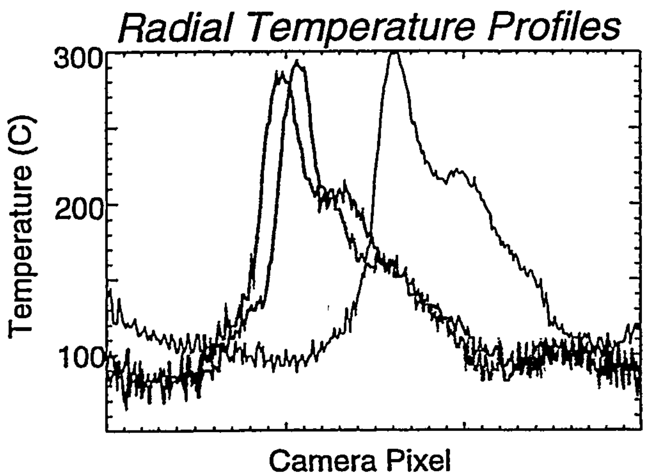

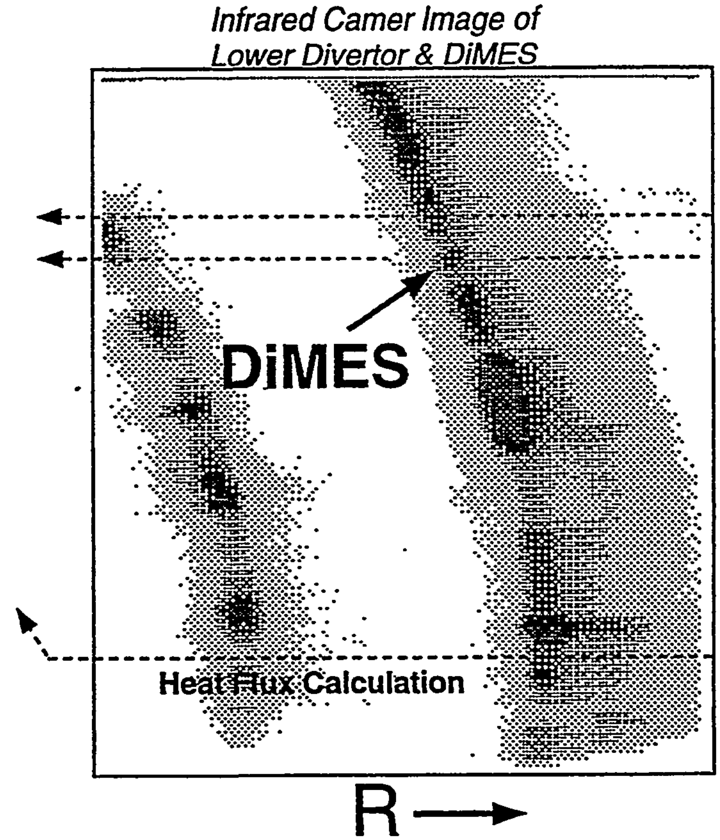

- No sign of previous "hot spot" which caused enhanced erosion and redeposition on DiMES sample.
- Good repeatability.
- DiMES #72 (Be/W stripes) now being analyzed.

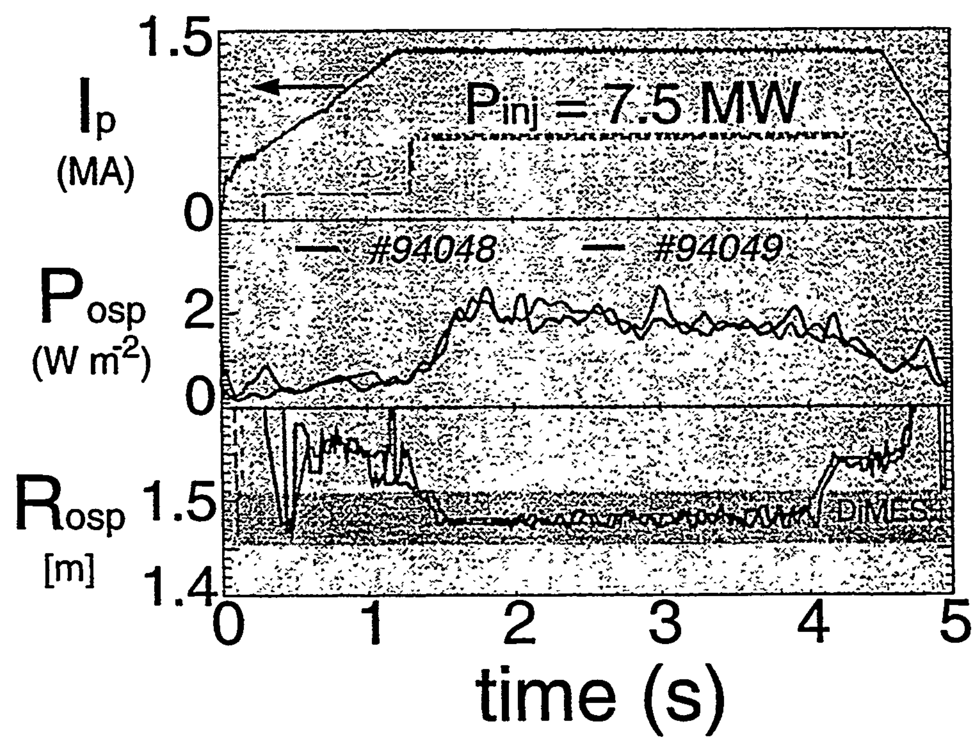

DIII-D Diagnostics & SNL Materials Evaluation Provide Complete Divertor Plasma Erosion Characterization to REDEP/WBC Erosion Models

Plasma

- High spatial resolution radial profiles of outer strike point are obtained from non-exposure, characterization discharges with a slow radial sweep:
  - electron density (*probe array, Thomson*)
  - electron temperature (*probe array, Thomson*)
  - incident ion flux (*probe array*)
- Magnetic geometry, including field line angle of incidence, from EFIT reconstructions.
- Impurity spectroscopy, including core plasma carbon and oxygen contamination.
- Strike point position control ensures that samples are exposed to steady-state divertor conditions.

Sample

- ATJ graphite samples contain implanted Si depth-marker. RBS measures net carbon of Si measures erosion/redepostion to +/- 10 nm.
- Pre and post-mortem sample analysis provides net carbon erosion and metallic redeposition patterns.

Sandia National Laboratories

UCSD

GENERAL ATOMIC

Near-Surface Transport of Sputtered Material is Well Characterized by REDEP/WBC Code

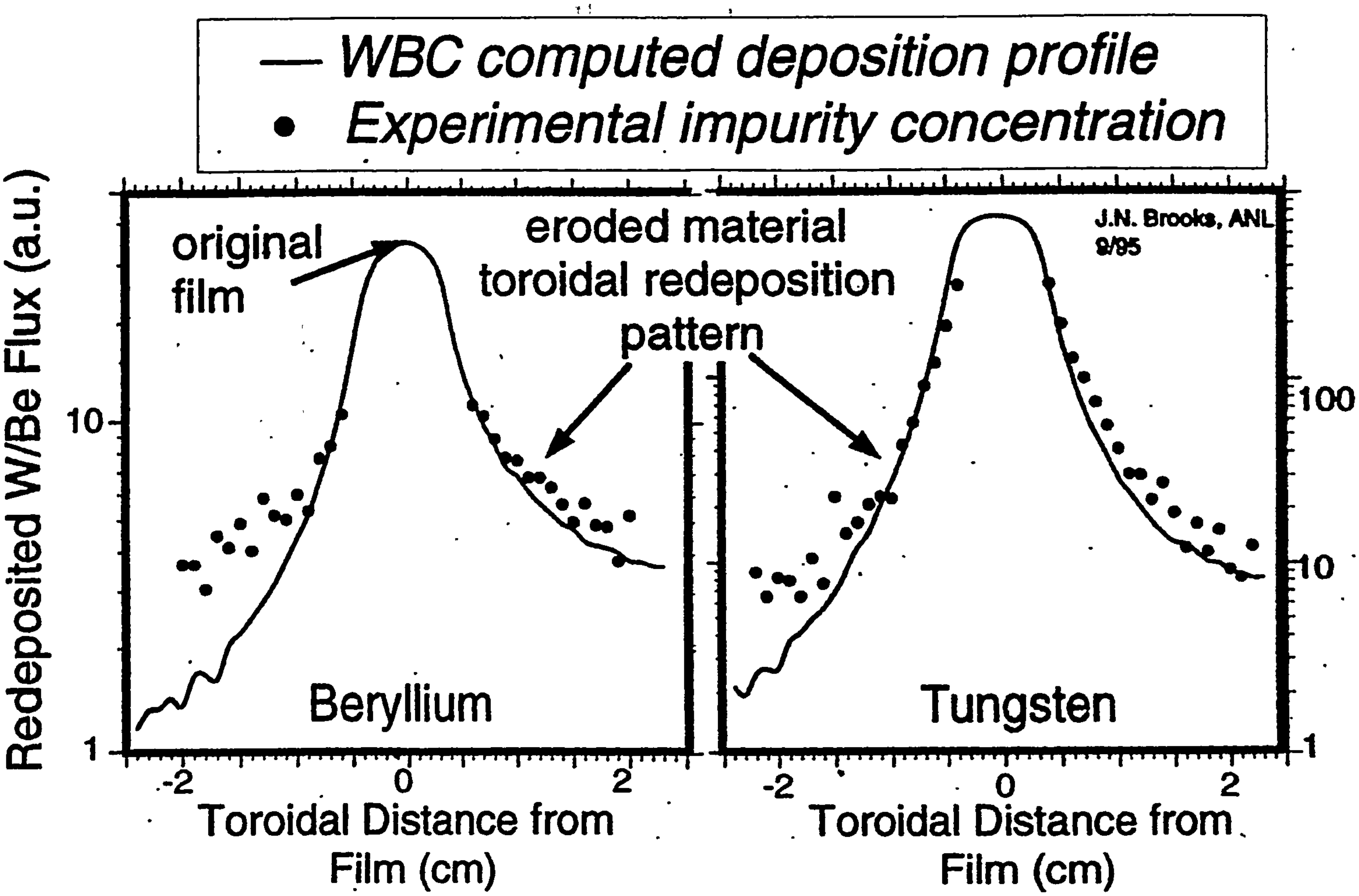

- WBC Monte Carlo impurity transport code computes the sputtering, in-plasma transport and redeposition of impurity atoms/ions. Code treats Lorentz motion and plasma-impurity collisions in detail and uses measured plasma and magnetic field parameters.
- Code/data comparison of Be II (467.3 nm) intensity predict an erosion rate of 2 nm/s, agreeing well with the surface analysis techniques.

Sandia National Laboratories

GENERAL ATOMICS

REDEP Code Agrees with Spectroscopic Measurements of Gross Carbon Flux. Experimental Redeposition Fraction ≈ 88%

- CCD camera with CII filter and vertical view of lower divertor.
- Carbon outflux from CII emission × S/XB (ionization/photon ration from CR model).
- This method achieves best results when ionization length is short (i.e. near strike point).

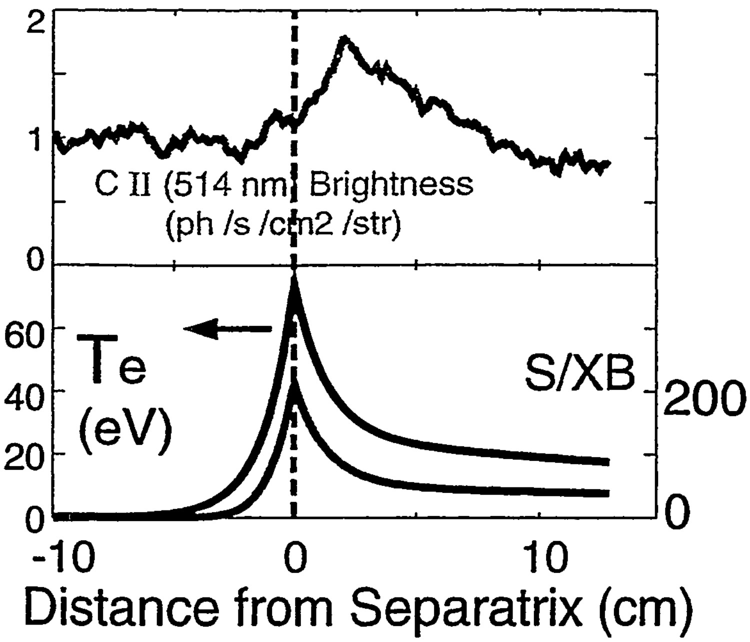

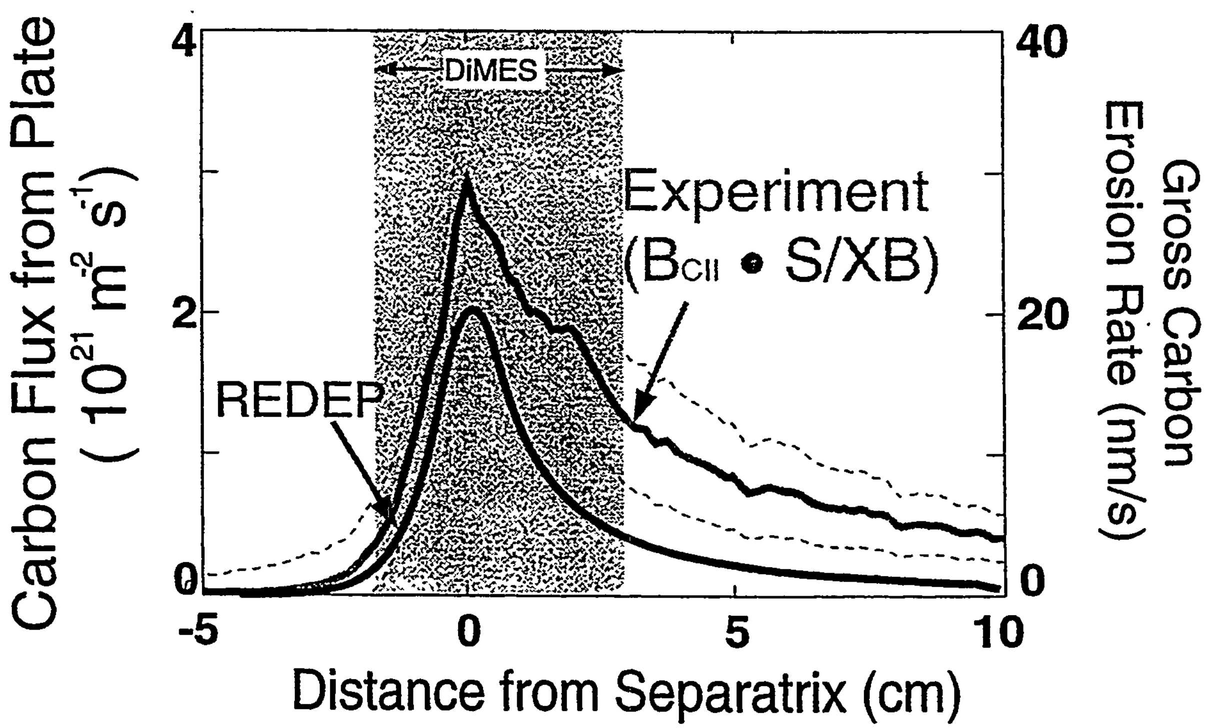

ARGONNE NATIONAL LABORATORY • UNIVERSITY OF CHICAGO •
UCSD
GENERAL ATOMICS

REDEP/WBC Code Matches the Features of Carbon Net Erosion at the DIII-D Divertor as Measured by DiMES

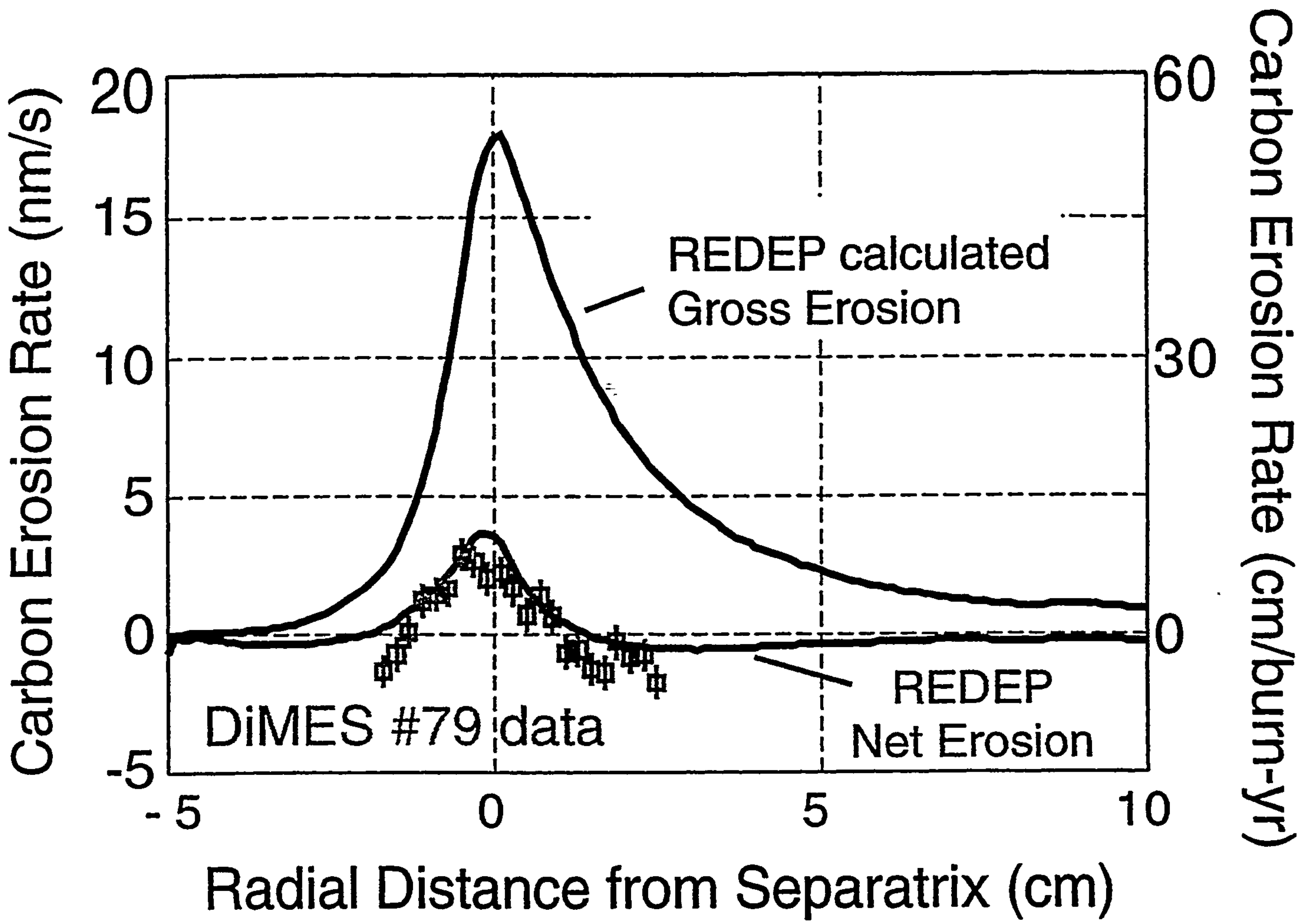

Exposure Conditions

Attached ELMing H-mode
0.7 MW/m²
$T_{e,OSP}$ = 70 eV

Sandia National Laboratories · Argonne National Laboratory, University of Chicago · UCSD · GENERAL ATOMICS

Effective Carbon Sputtering Yield is > 10% for Attached Plasmas

- Effective sputtering yield (Carbon outflux / ion influx) includes effects of carbon self-sputtering.

- Model and experiment agree near separatrix.

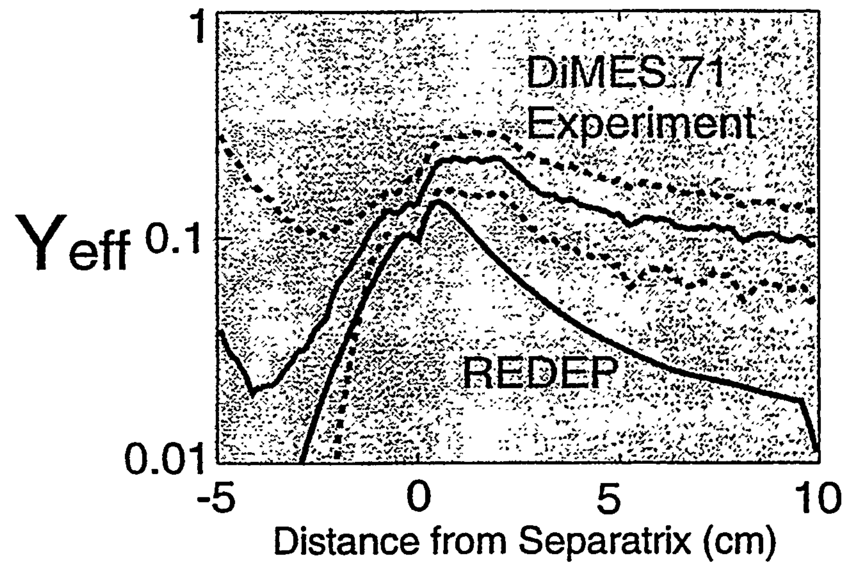

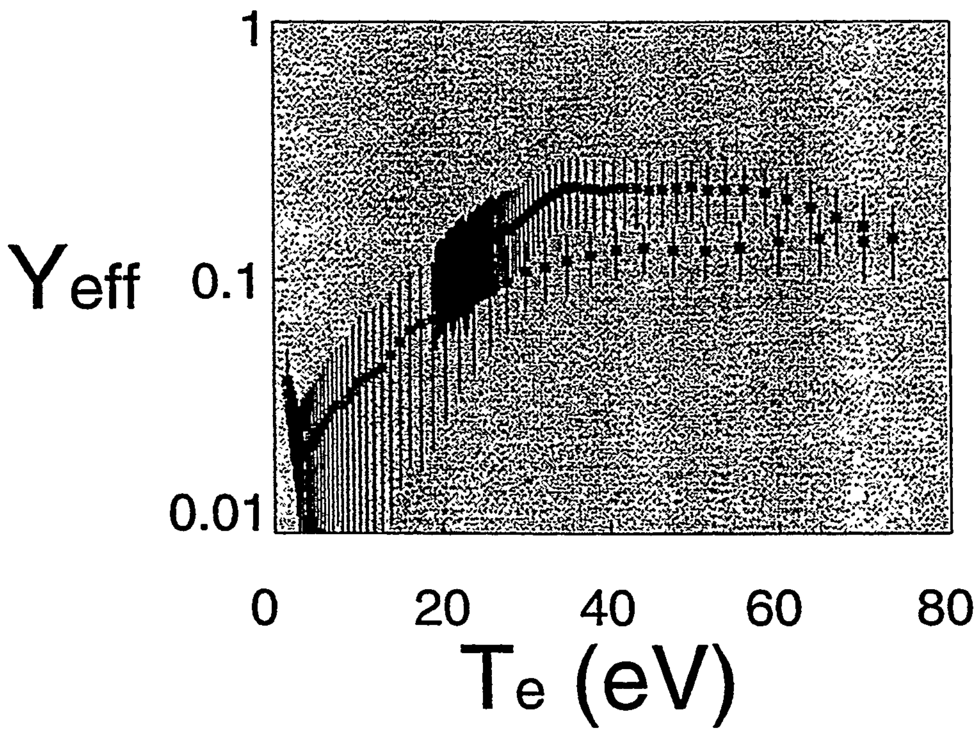

The Peak Net Erosion Rate of the DIII-D Outer Divertor Graphite Plates Increases with Incident Heat Flux for Attached Plasmas

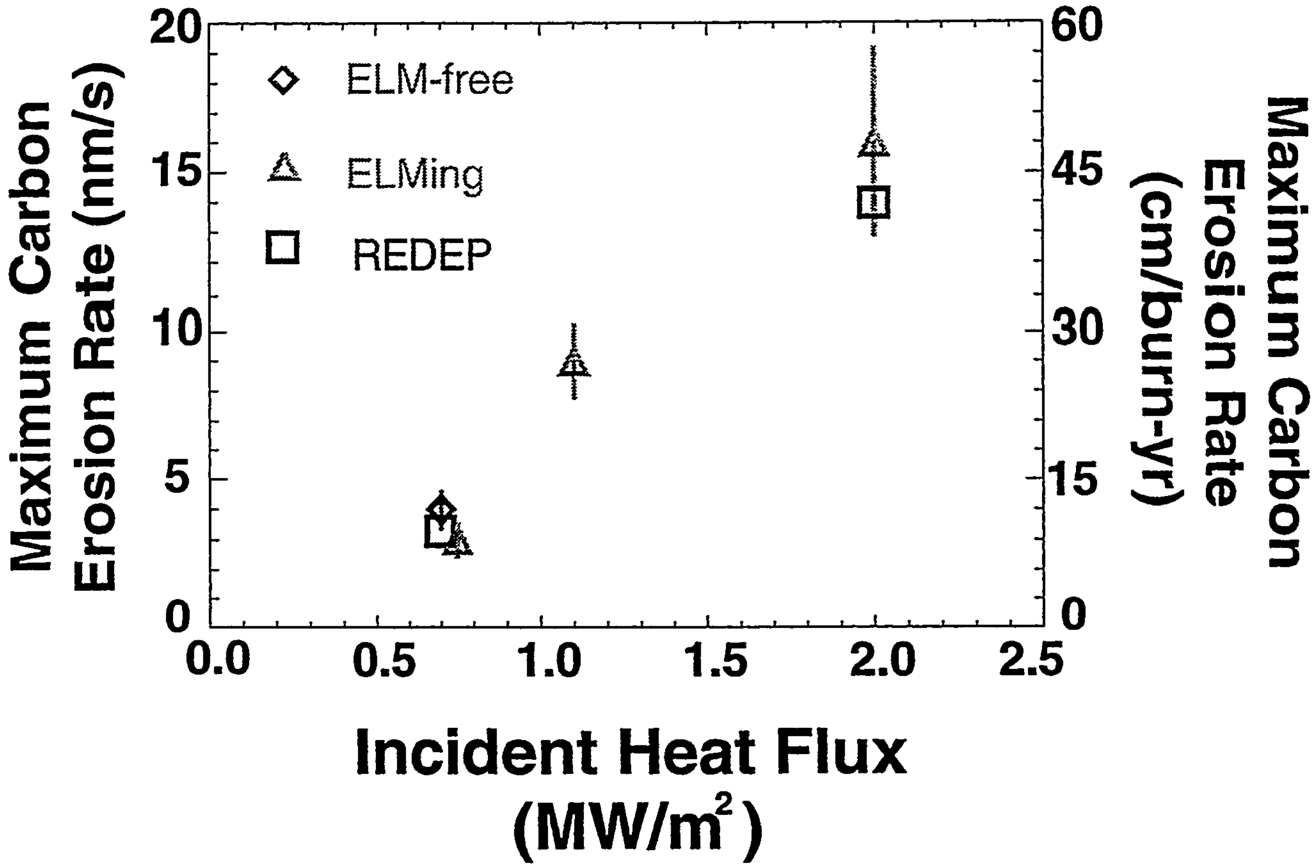

OSP parameters at 2 MW/m^2 :
$\theta_B = 2°$, $\theta_{inc.} \approx 50°$, $T_{plate} \approx 500$ °K,
$T_e = 45$ eV, $n_e = 1.0 \times 10^{20}$ m^{-3}

Simple models that neglect oblique inicidence and self-sputtering can underestimate the net erosion rate by a factor of 10!

Sandia National Laboratories   UCSD   GENERAL ATOMICS

Long term study of divertor tiles show that co-deposited inventory increases with erosion rate.

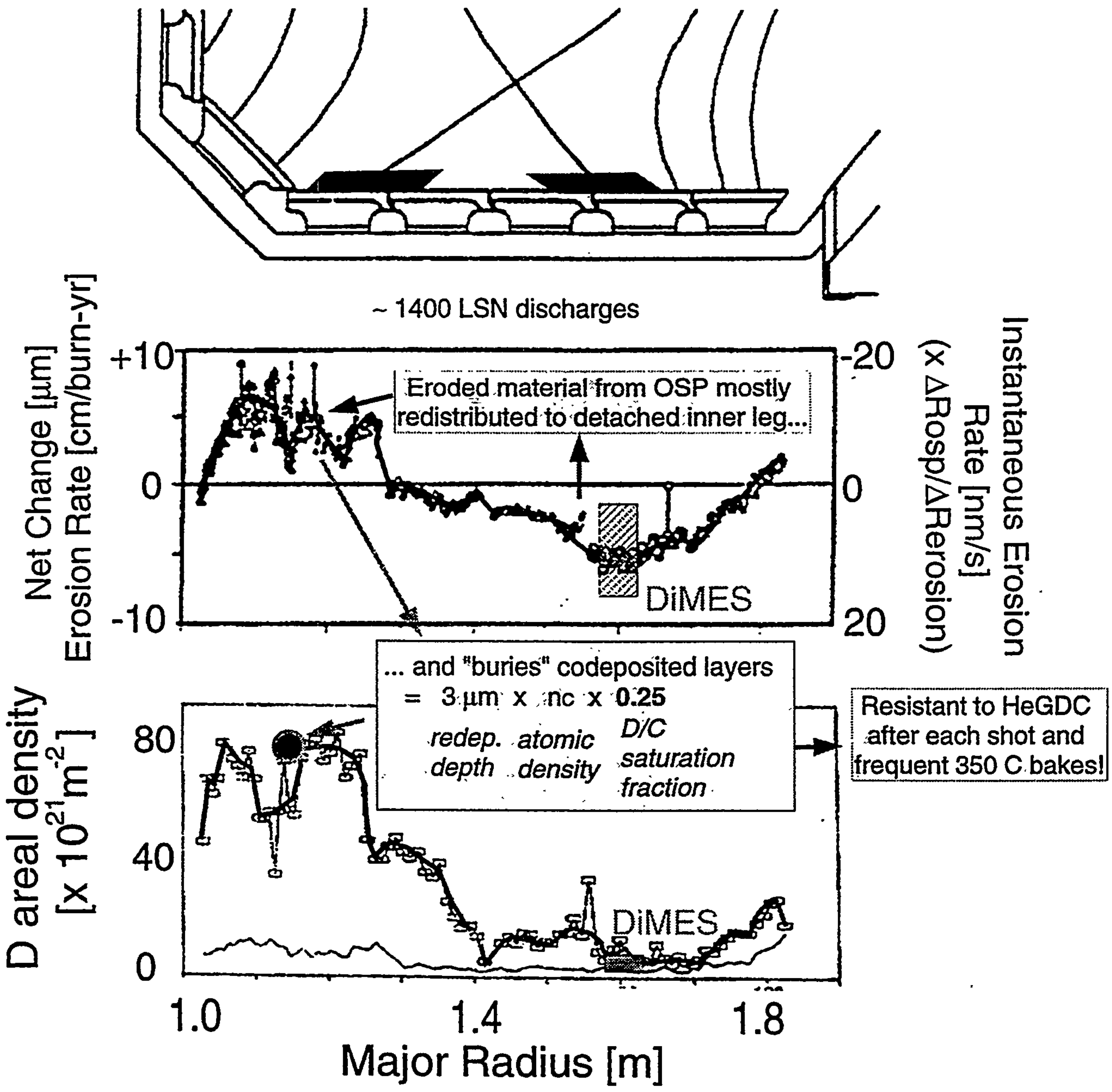

- The presence of large hydrogenic inventories in codeposited layers affects recycling and performance. This inventory is principally determined by the net erosion rates in the divertor.

With Peak Heat Flux < 1 MW/m^2, Outer Divertor Erosion Accounts for Observed Core Plasma Carbon Accumulation and Lack of Density Control in ELM-free H-mode

- Strike point is moved to DiMES probe (#71) during ELM-free H-mode.

- Net carbon erosion of 3.6 nm/s and width 2 cm, corresponds to 7 x 10^{19} atoms/s net loss rate from outer divertor.

- Initial increase in electron density due to better particle confinement.

- After 2 s linear electron increase is accounted for by carbon accumulation and ionization, with the major source of carbon being outer strike point erosion.

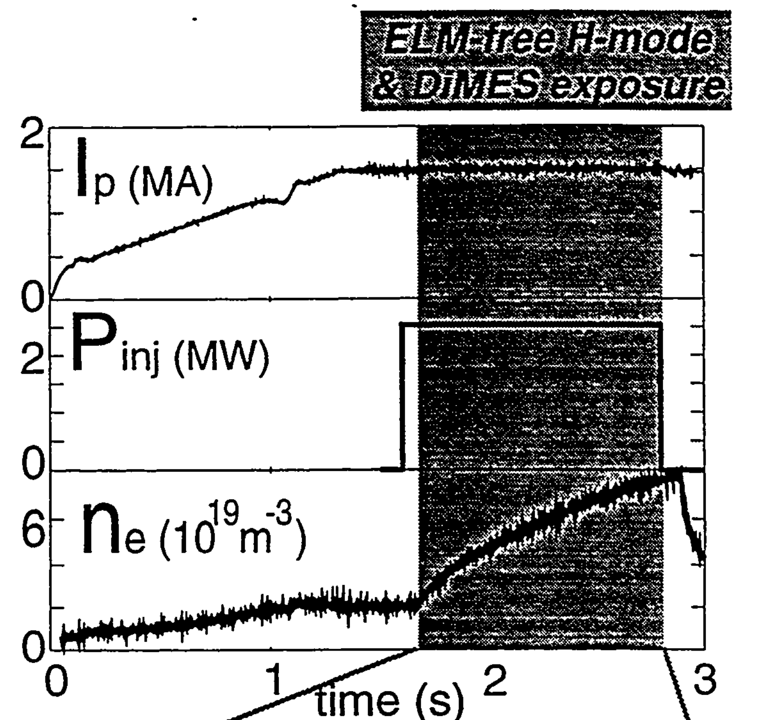

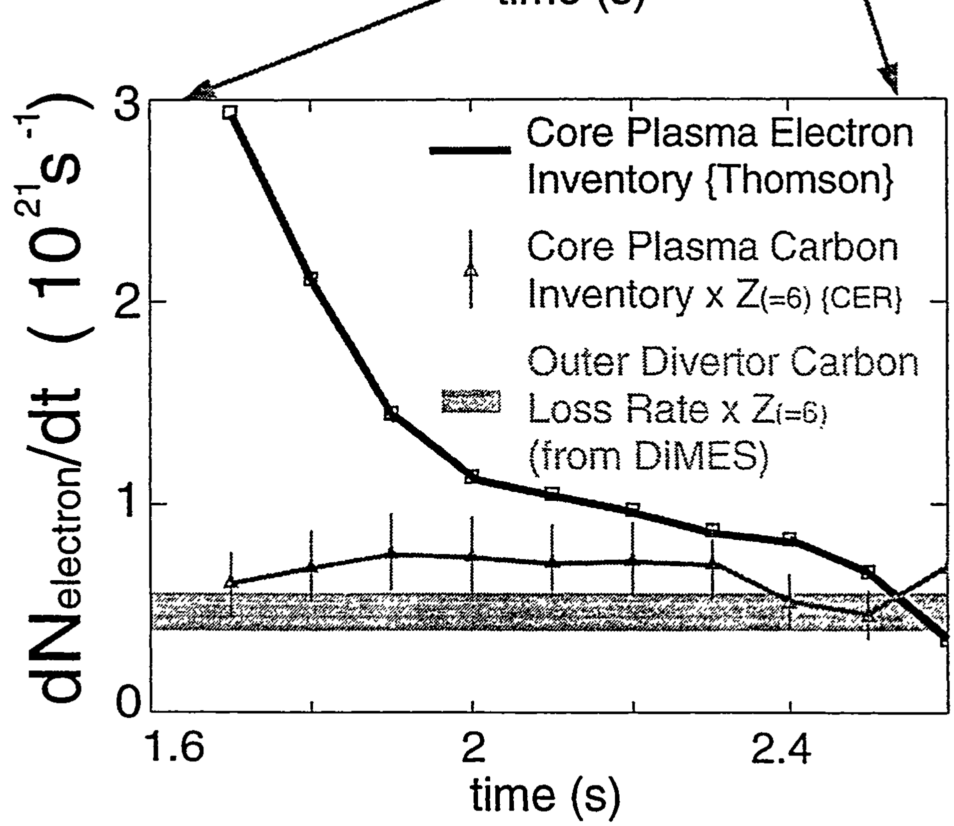

Sandia National Laboratories

UCSD

GENERAL ATOMICS

Preliminary Results from DiMES Dust Production Experiments

- Sample cap with 0.7 mm raised lip was exposed to 500 ms of 3 source ELMing H-mode plasma. Estimated parallel heat flux to lip ~ 50 MW/m^2.

- SEM shows 5-10 μm globules forming adjacent to lip in area of intense redeposition.

- Silicon dust collector wafer has a 0.5 μm carbonaceous film and carbon dust particles of 1-10 μm size.

- Deuterium/Carbon fraction ~ 0.1 for film on Si wafer. Note that film is not direclty exposed to ion flux.f

- Preliminary calculation shows that this results in:
  - Codeposited build-up rate of 0.2 g in 1,000 seconds for every square centimeter of misalignment (does not include dust formation).
  - Dust formation: 10 mg in 1,000 s / square cm.

- Quantitative analysis of dust particles is ongoing.

DiMES Dust Collection Experiment

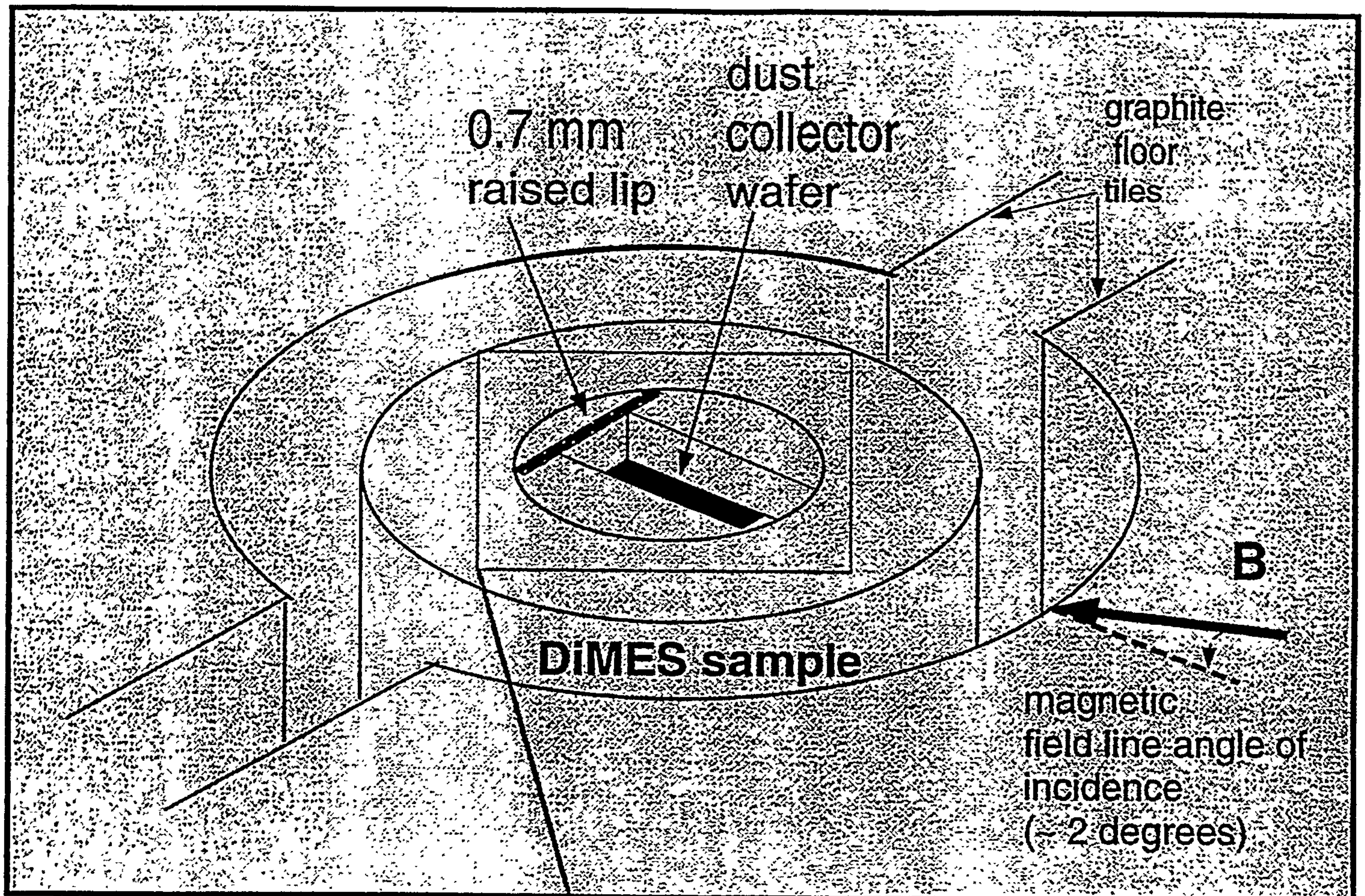

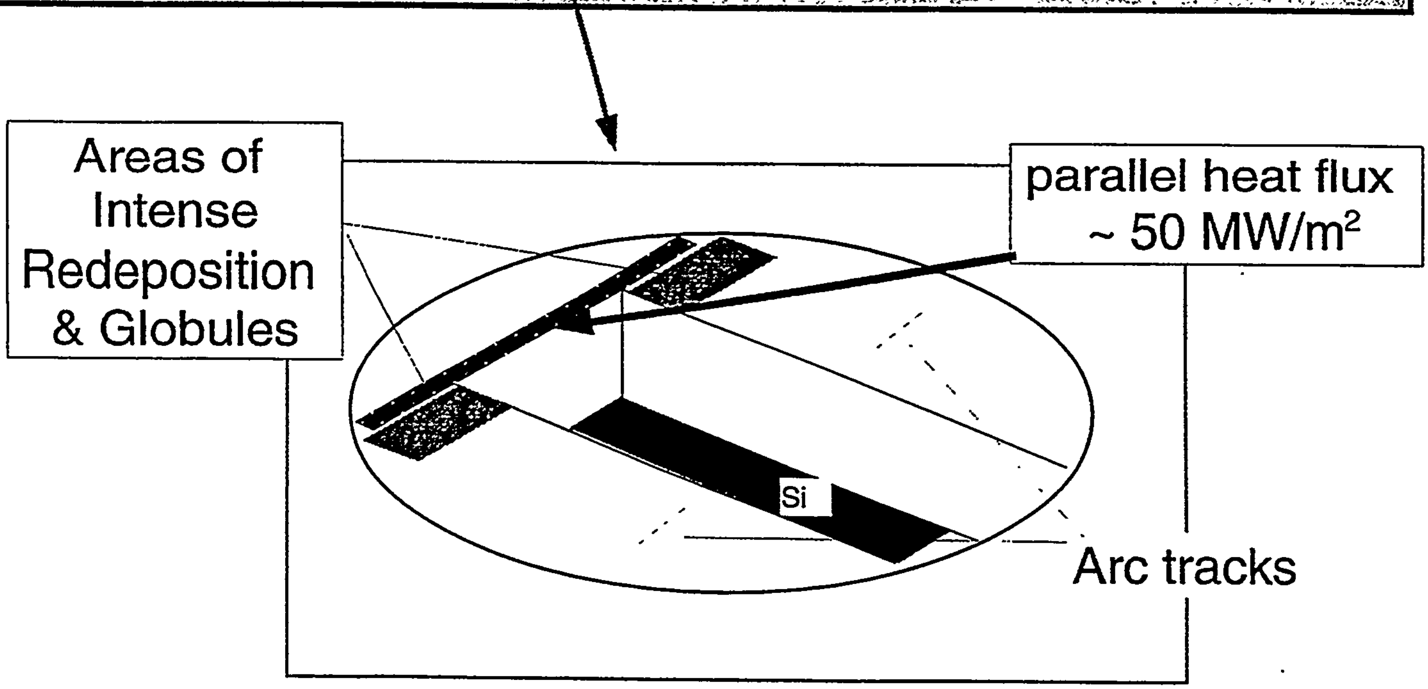

Sandia National Laboratories ARGONNE NATIONAL LABORATORY UNIVERSITY OF CHICAGO UCSD GENERAL ATOMICS

Area of Intense Redeposition Shows Foramtion of 5-10 micron "Globules"

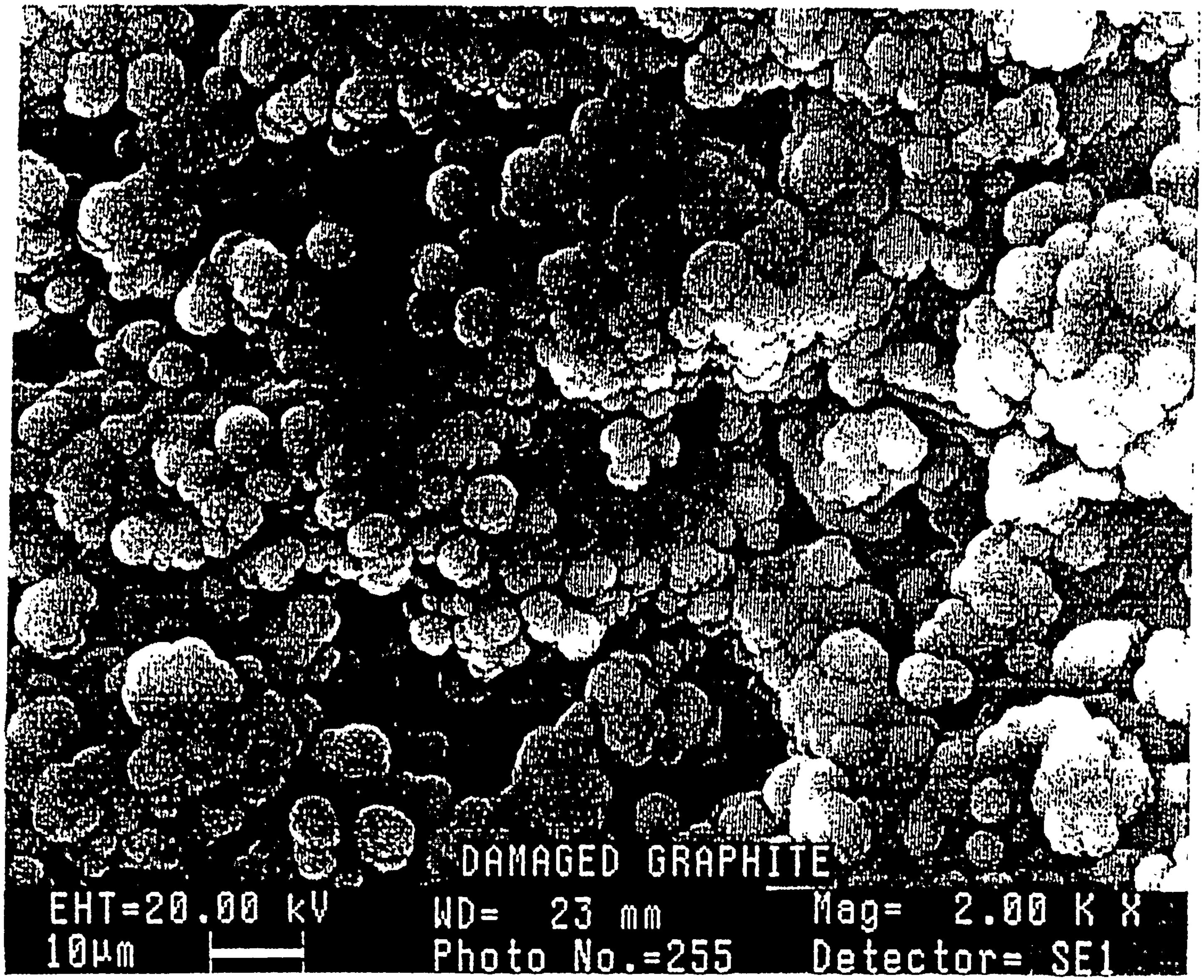

Si collection wafer has an adhered, uniform carbonaceous film (0.5 micron thickness) & 5-10 micron carbon dust flakes

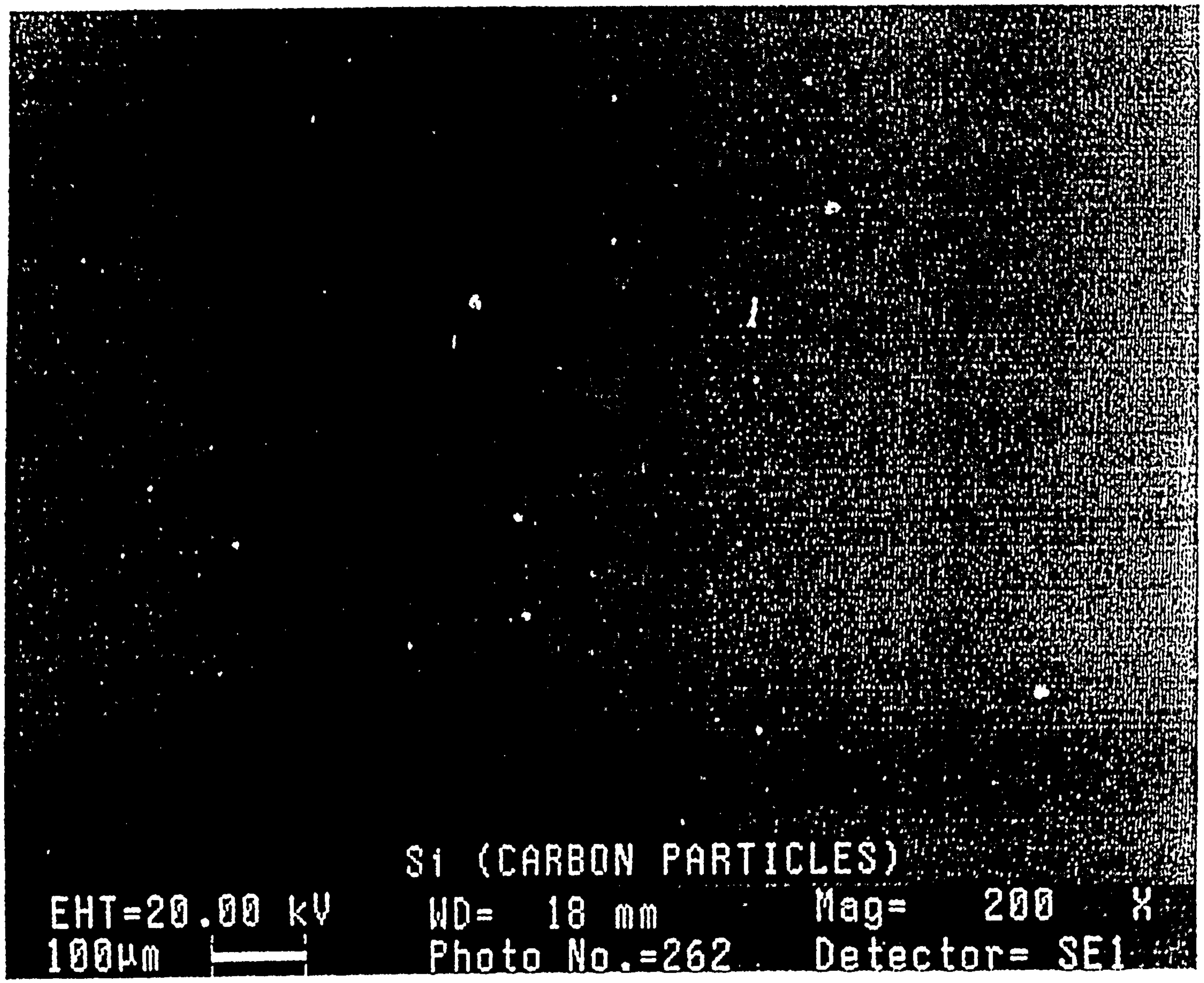

Reflected Neutral Particle Spectrum on MAI

S. Ohtsu, K. Kobayashi and S. Tanaka

Faculty of Engineering, University of Tokyo

US-JAPAN PMI/HHF Workshop
December 8-11th, San Francisco

Particle Reflection Process

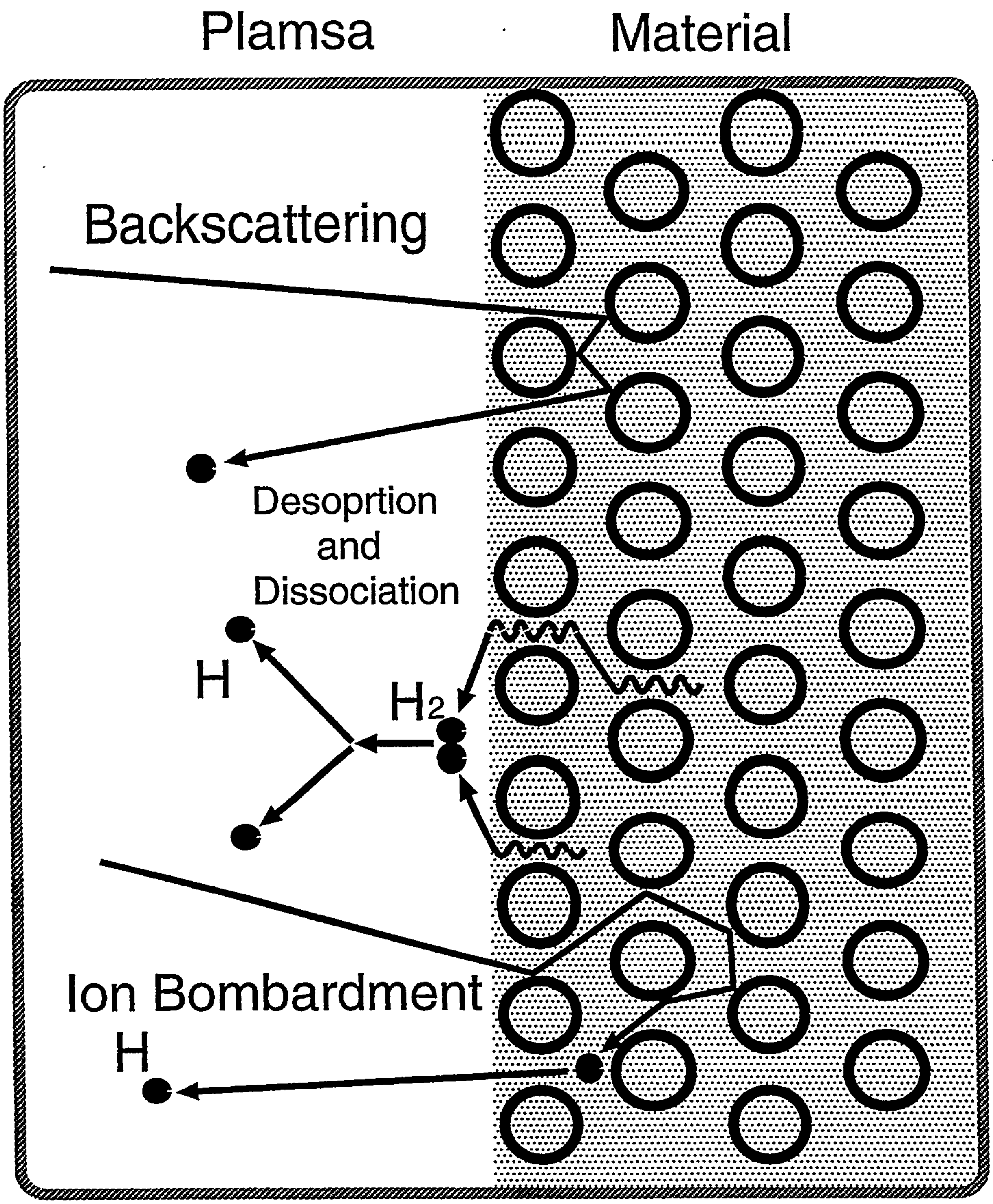

Particle reflection processes on the material serfa
in the low energy region (~100eV) should be investigated.

- Energy distribution
- Anglar distribution
- Excited states

Contents

Spectroscopic measurements of the neutral particles near the solid target in linear steady plasma facility MAP

H alpha spectrum profiles at different incident angles to the target.

Time dependant mesurement of Halpha intensity profile

Monte-Carlo Simulation of neutral particle transports

↓

Investigation of the energy and angler distribution of backscattered neutral particles and their excited states.

Linear Steady Plasma Facility
MAP(Material and Plasma)

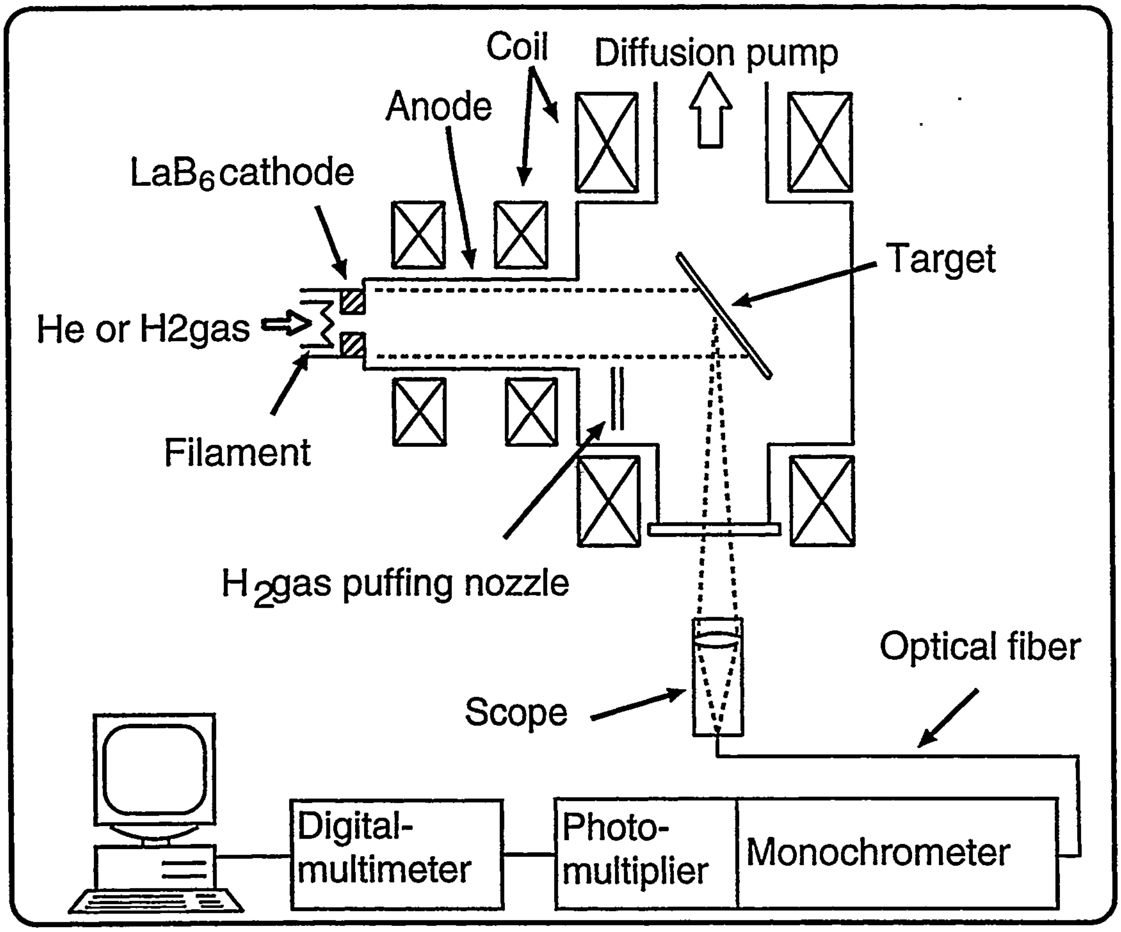

● Experimental conditions

Temperature : ~10eV, Density :1.0×10E18~ 1/m^3.
Diameter of the plasma column : 3cm.
Plasma column length : 20cm.

- Target : Copper (100mm×100mm × 2mm).
- Magnetic field : 0.03T.
- Gas pressure : 5.0×10^{-5} Torr.

- Wave length resolution of the monochrometer : 0.011nm.

- Target angle (Insident angle) : 0 , 30 , 45 , 60 .

Spetrum Mesurement

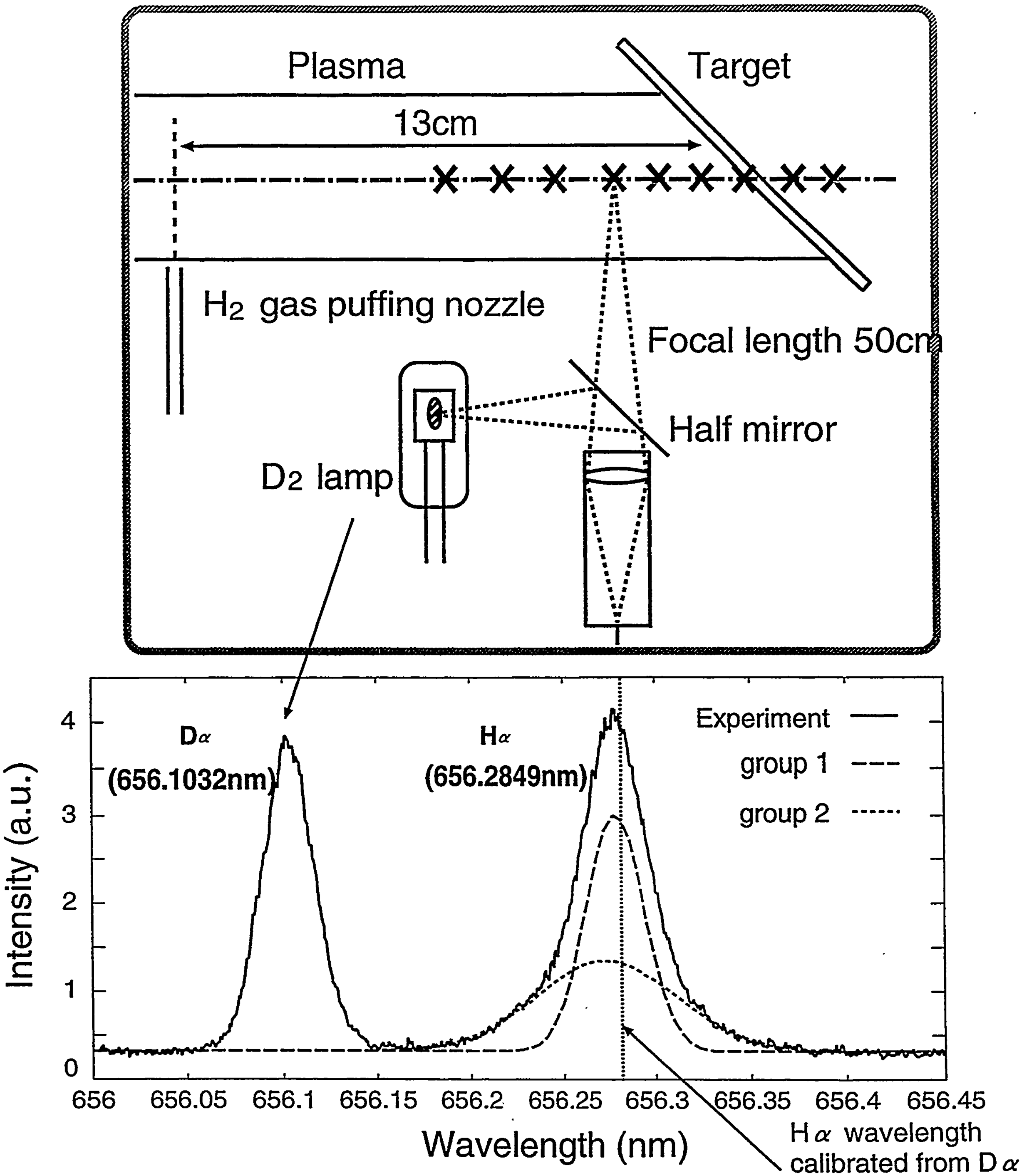

$H\alpha$ spectrum at 3mm from the target
um into two gaussian curves

- $H\alpha$ spectrum is broader than $D\alpha$ spectrum.
  Doppler-broadening
- $H\alpha$ is not symmetric.
  (wide at shorter wavelength)
- The peak of the group 2 spectrum slightly shifts to lower wavenumber.
  Doppler-shift

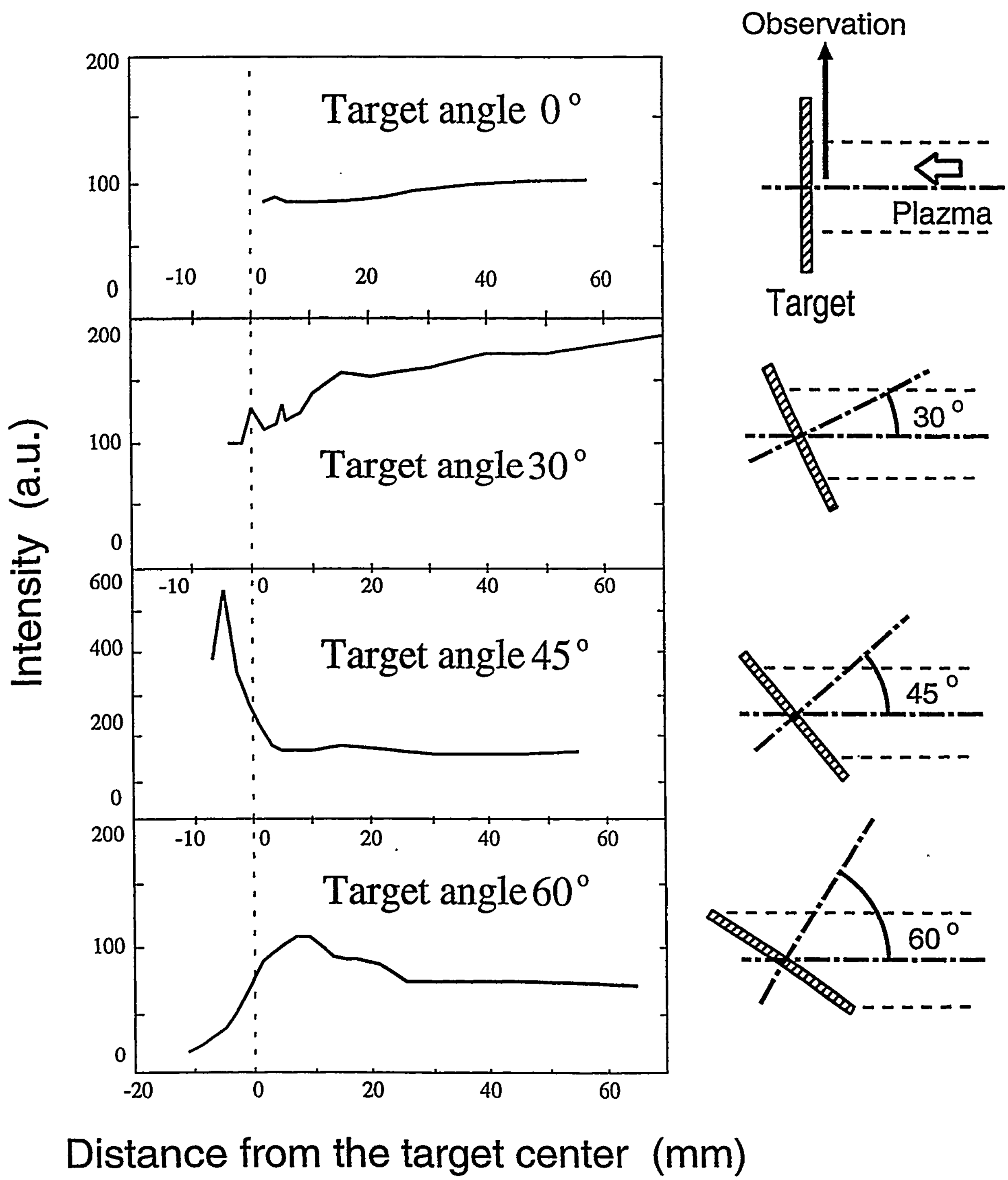

Axial distribution of the Hα intensity

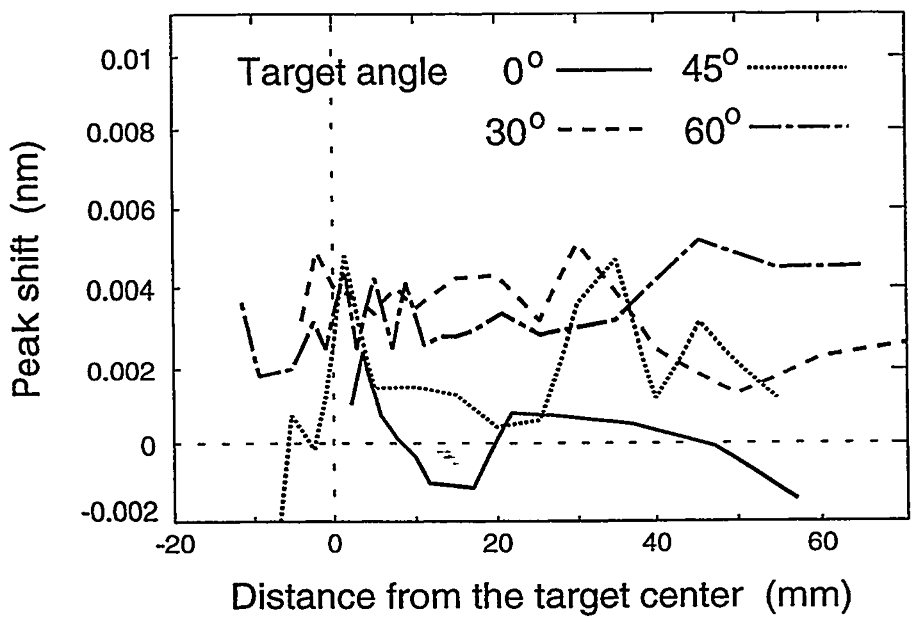

Peak shift to the shorter wavelength of the group 1 spectrum

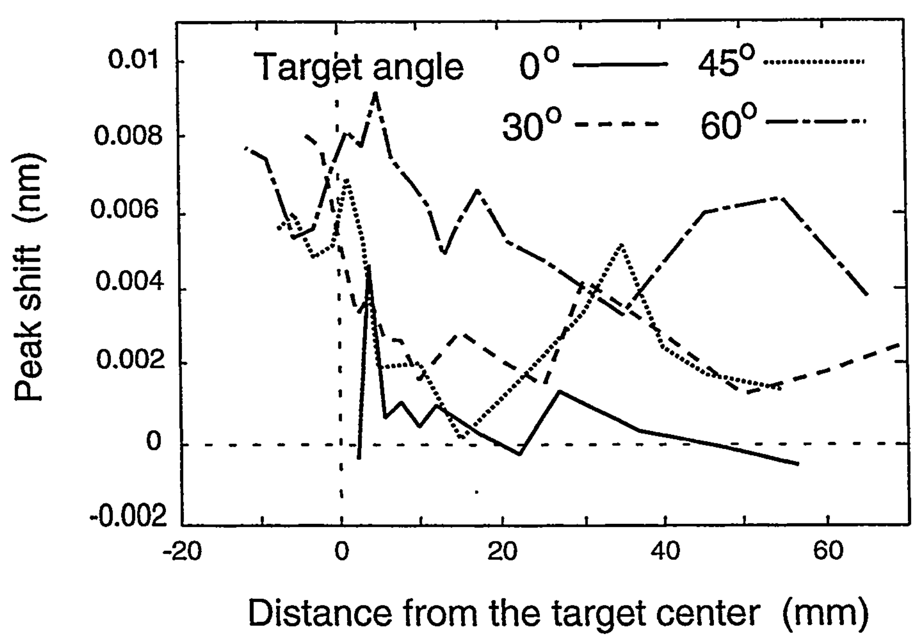

Peak shift to the shorter wavelength of the group 2 spectrum

Time Dependant Intensity Profile

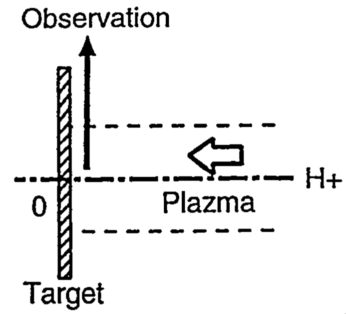

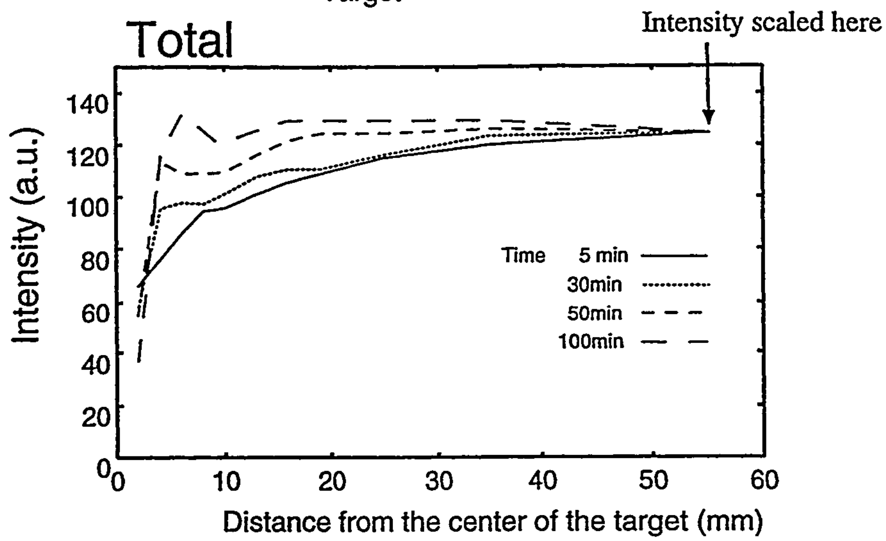

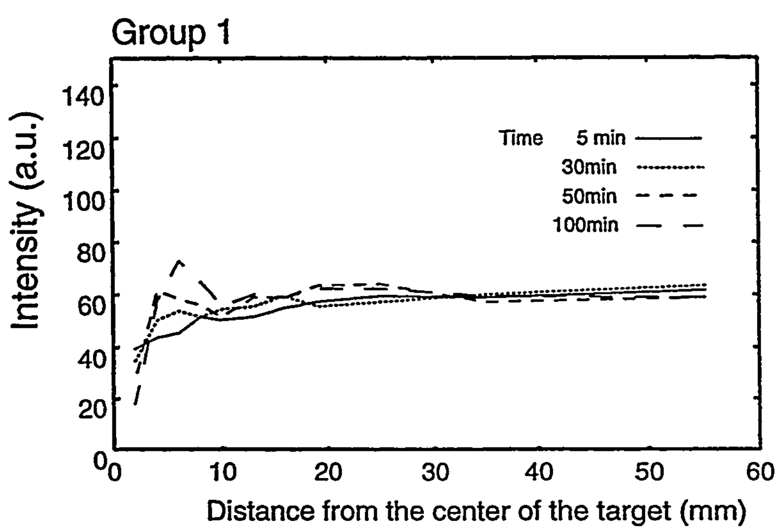

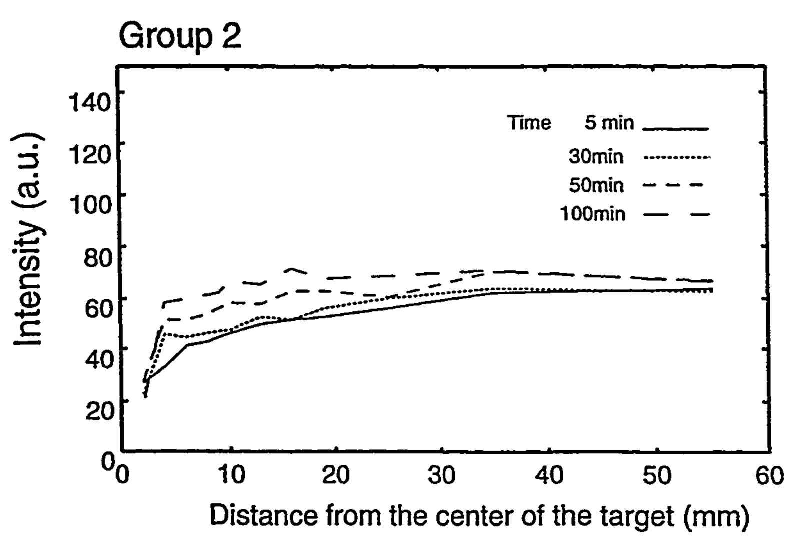

• Calculation of the Hα spectrum

We calculated Hα spectrum emitted from reflected hydrogen atoms by following two processes.

(1)Simulation of the reflecting process by the TRIM code.

+

(2)Simulation of the excitation process by Monte Carlo method.

(1)Simulation of the reflecting process by the SRIM97 (aka TRIM) code.

Incident angle (target angle) : 0°、30°、45°、60°
Incident particle : 10,000 hydrogen ions,
Incident energy : 30eV,

· Nuclear stopping

$$\theta = \pi - 2\int_{r_{min}}^{\infty} \frac{p}{\sqrt{1-\frac{p^2}{r^2}-\frac{U(r)}{Er}}}\frac{dr}{r^2} \qquad U(R) = \frac{z_1 z_2 e^2}{aR}\Phi(R)$$

p : Impact parameter $\Phi(R)$: universal-screening-function

· Electronic stopping

$$\Delta E_e = LNS_e(E) \qquad S_e(E) = S_L(E) = kE^p$$

$$k = k_L = \frac{1.212 z_1^{\frac{7}{6}} z_2}{(z_1^{\frac{2}{3}} + z_2^{\frac{2}{3}})^{\frac{3}{2}} M_1^{\frac{1}{2}}}, \quad p = \frac{1}{2}$$

ΔE_e : Electronic energy loss

(2)Simulation of the excitation process by Monte Carlo method.

Target surface is divided into rectanglular meshes and particles are supposed to be reflected at the center of each meshes.

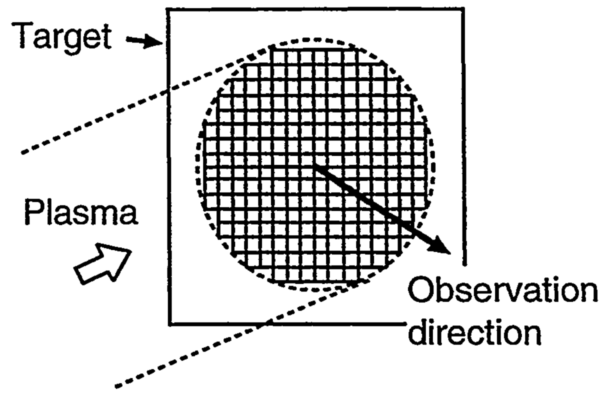

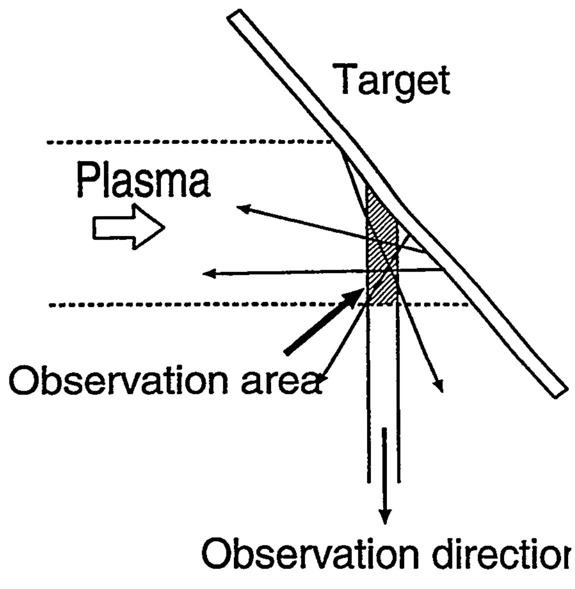

Then we calculate the coordinates of each particle until it emits Hα spectrum, and from the amount of the emission in the observation area, we obtain the intensity distribution of the Hα spectrum emitted by the reflected particles.

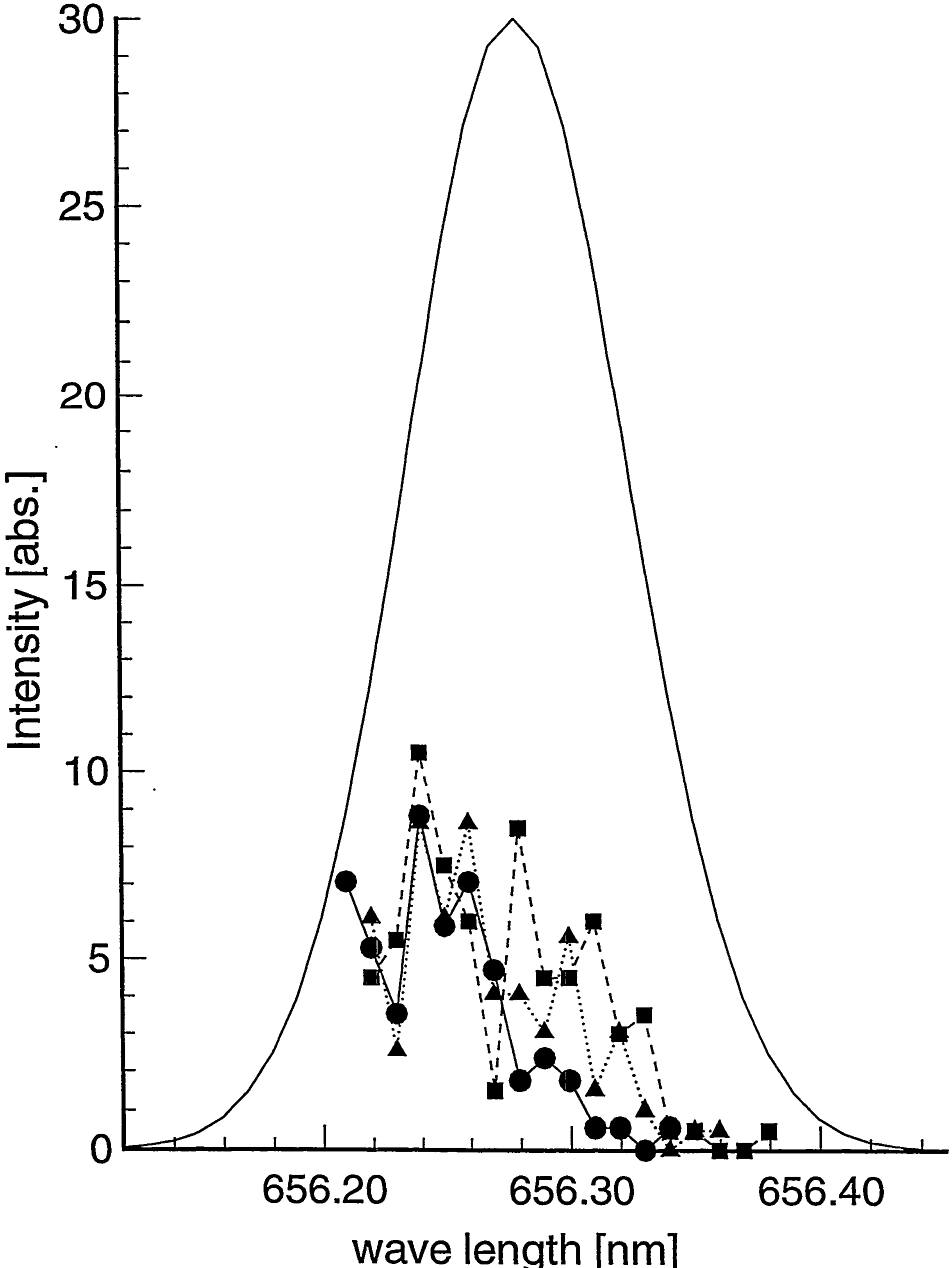
Intensity [abs.]
30
25
20
15
10
5
0
656.20
656.30
656.40
wave length [nm]

Summary

The H α spectrum of the reflected hydrogen atoms were observed by spectroscopic analysis.
Spectrum of the backscattered particles were identified by the decomposition of the H α spectrum. They were included in the high energy spectrum componet (group2).

After long time discharge, increase of H α intensity in group1 (low energy group) was observed near the target. It is because low energy desorped particles are increased.

Session V: Plasma Studies

Ion Heating and Plasma Fluctuations in the UC San Diego PISCES Experiments

S.C. Luckhardt, J. Cuthbertson*, R. Doerner, D. Whyte,
and the UCSD PISCES Group

US-Japan Workshop (97FT5-06)
High Heat Flux Components & Plasma Surface Interactions for Next Fusion Devices
December 8-11, 1997

San Francisco, CA

* Presently at San Diego Econometrics

PISCES and Collaboration Experimental Program Staff

16 Scientists and Engineers, 4 Graduate Students

Scientific and Research Personnel:

J. Boedo (DIII-D and TEXTOR Collaborations)
Prof. R. W. Conn (Dean of engineering)
R. Doerner (PISCES-B Materials group leader)
D. Gray (DIII-D Collaborations)
A. Grossman (Plasma Materials Modeling)
Y. Hirooka (PISCES/TFTR Materials)
R. Lehmer (DIII-D Collaboration)
S. Luckhardt (Experimental Division, PISCES-A)
R. Moyer (DIII-D Collaborations)
R. Saraydarian (PISCES Materials, spectroscopy)
D. Sze (PISCES Materials surface science)
D. Whyte (joining in 2/97, PISCES Materials, boundary)

Engineering Staff:

L. Chousal (Mechanical Engineer, Design, Beryllium Operations)
G. Gunner (Control Systems, Beryllium Operations)
P. Luong (Electronics, Vacuum Systems, Beryllium Ops.)
A. Viray (Safety Engineer, Beryllium Safety)

Graduate Students:

L. Blush
Y. Duan
A. Liebscher
J. Zhang

Visiting Scientists:

Prof. H.Y. Chang (KAIST)
Dr. S. Zweben (PPPL)

Admin. Staff:

J. Hylton (Personnel, Payroll)

M. Garcia (Accounting)
T. Garcia (Clerical)

FACILITIES: UCSD Fusion Program Laboratories

PISCES-B Mod Plasma Beryllium and Mixed Materials Interaction Facility

Surface Analysis Module Scanning Etching Ion Beam, Auger Electron Spectroscopy (AES), X-ray Photoelectron Spectroscopy (XPS), Thermal Desorption Spectroscopy (TDS).

PISCES-A Plasma Boundary Science Facility: Divertor and Edge Plasma Simulator

PISCES Surface Science Laboratory (Scanning Electron Microscope, Back Scattered Electron Spectroscopy, Profilometer)

UC SAN DIEGO PISCES A+B

"FLUX TUBE" DIVERTOR SIMULATOR

ION BEHAVIOR, MAIN H, D, He, IMPURITY C, O
IS IMPORTANT FOR

- ENERGY SPECTRUM OF CX FLUX
- DIVERTOR ION HEAT FLUX

$$q_{\parallel i} = n V_i \left[\frac{5}{2} T_i + \frac{1}{2} m_i V_{\parallel i}^2 + I_0 \right]$$

- ION GYRO-RADIUS EFFECTS: GYRO SHEATH, etc
- MIXED MATERIALS EFFECTS
  IMPURITY ION FLUXES, ENERGY RANGE, IMPURITY DENSITY, ...

PAST YEAR
PISCES GROUP EXPERIMENTAL CAMPAIGN
TO CHARACTERIZE MAIN / IMPURITY IONS

- MAIN ION TEMPERATURES $T_{\parallel}, T_{\perp}$
- IMPURITY ION DENSITY AND TEMPERATURE
- IMPURITY DENSITY CONTROL: CD_4 PUFFING

WHAT DO YOU EXPECT?

$T_i = ?$
a) 2eV, b) 5eV, c) 15eV,
d) none of the above?

? DISSOCIATION ENERGIES: 2-3eV

? $T_i \ll T_e$

→ RESULTS ~5 – 20eV RANGE!!

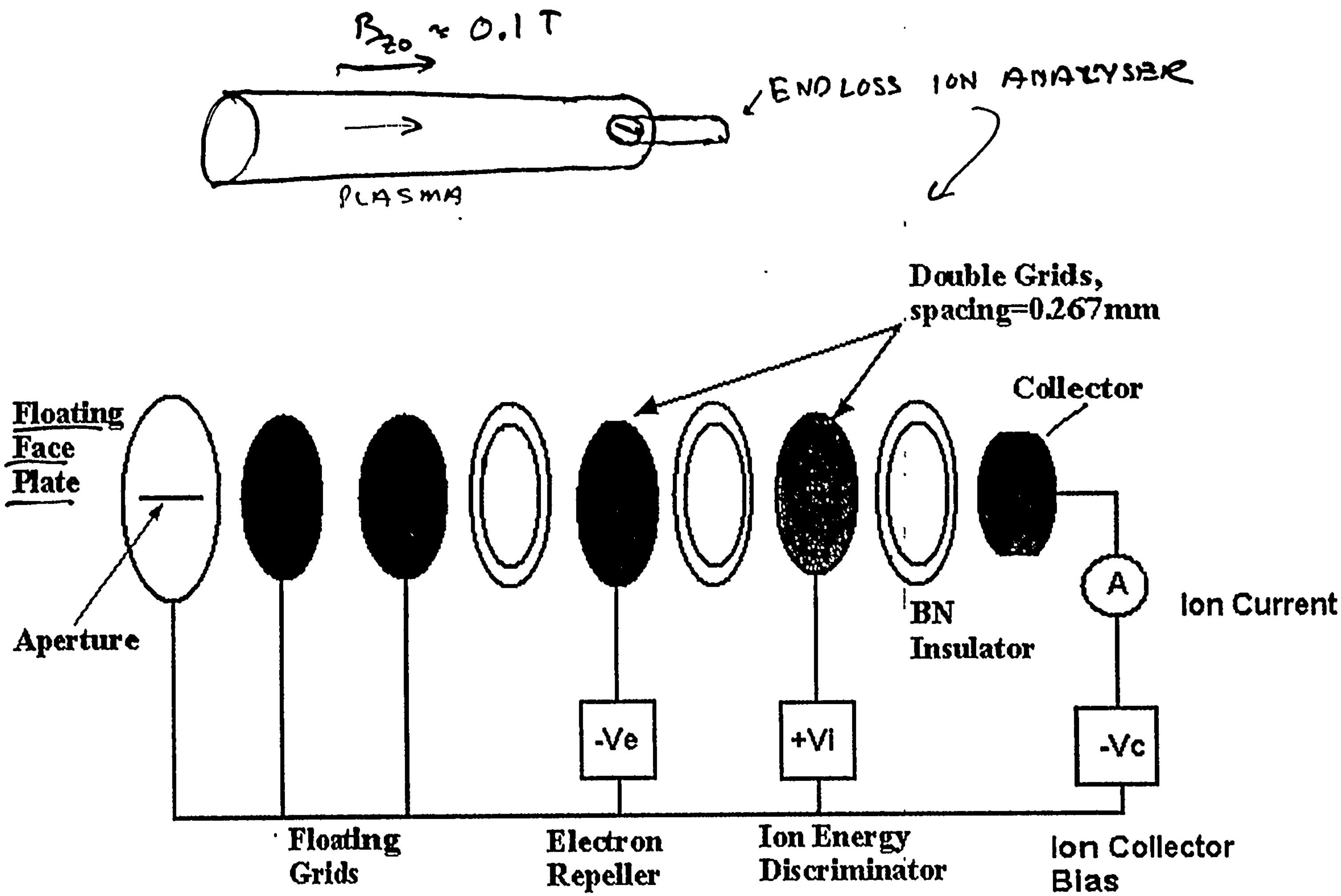

Schematic of components of the gridded energy analyzer (GEA) and the internal electric potential.

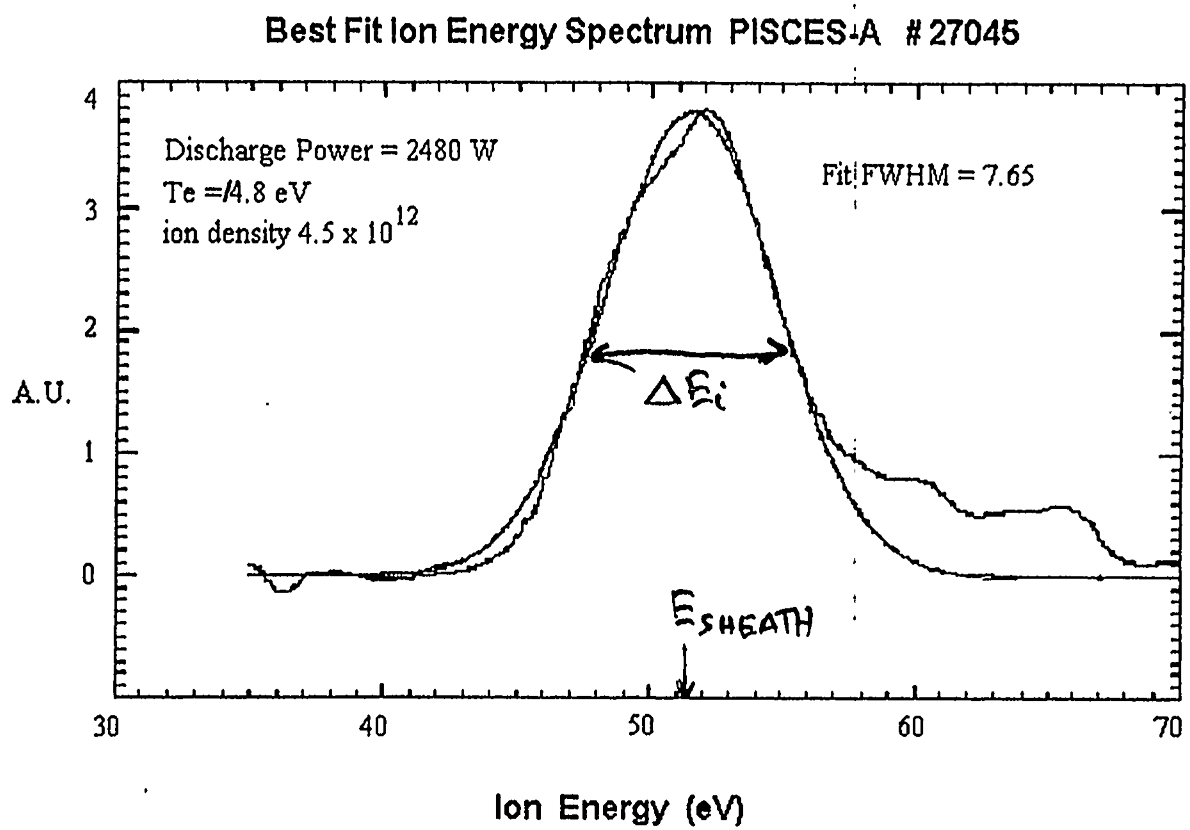

$\Delta E_{i_{\parallel}} = 7.6 \text{ eV}$

$T_e = 14.8 \text{ eV}$

$n_i = 4.5 \times 10^{18} \text{ m}^{-3}$

$C_s = \left(\frac{Z_i T_e + T_i}{m_i} \right)^{1/2}$

$V_{SHEATH} = ?$

$\frac{T_e}{2} \ln \left[\frac{m_i}{2 m_e (1 + T_i/T_e)} \right]$

Kinetic energy distribution of ions exiting the end of the PISCES-A plasma column as measured by the GEA.

FLOATING POTENTIAL AUTO-POWER SPECTRUM
CHARACTERISTIC FREQUENCY RANGE 100kHz
PISCES-A

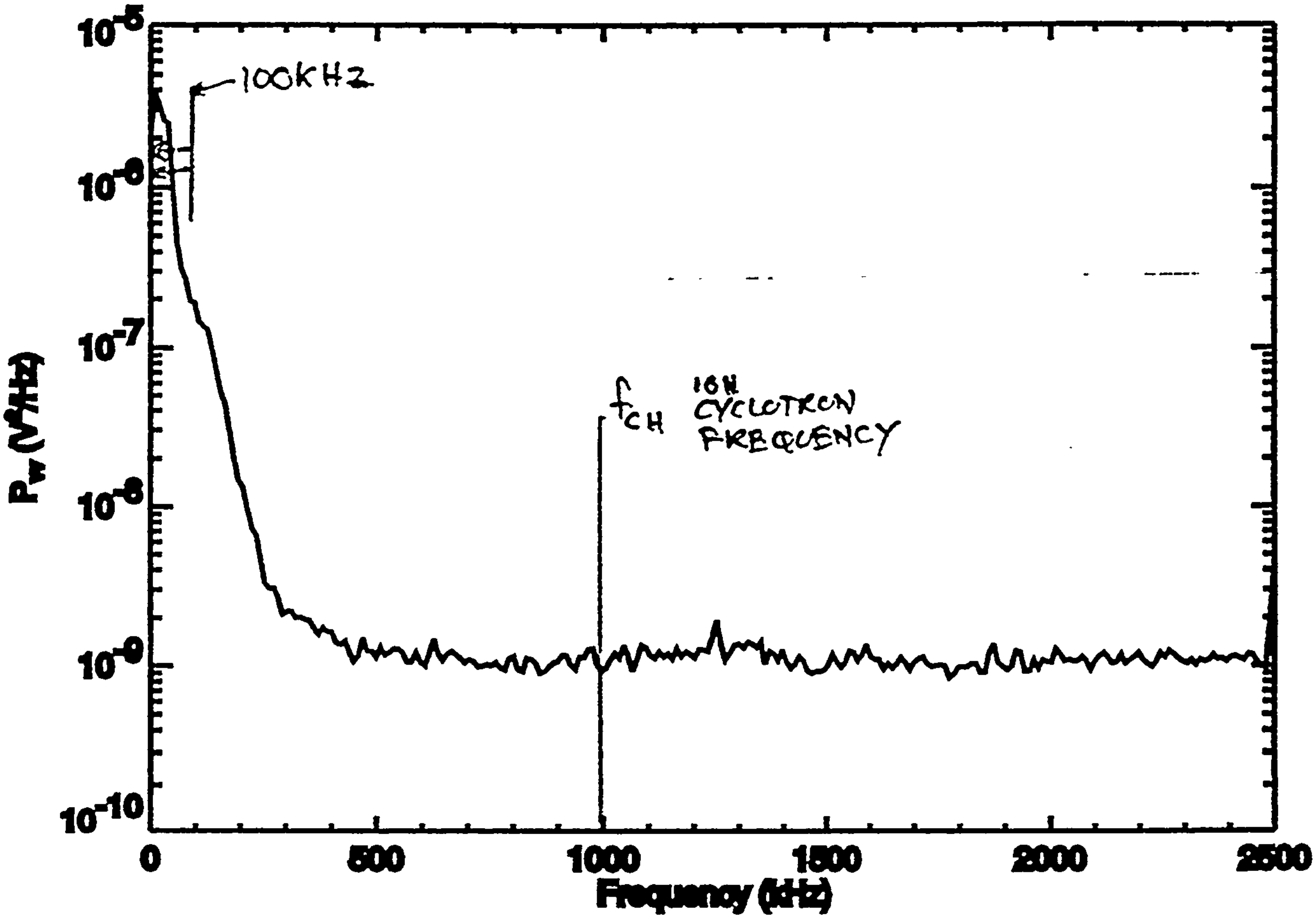

ION ENERGY SPECTRUM WIDTH CORRELATED WITH PLASMA TURBULENCE: UCSD-PISCES-A DATA

Correlation of energy distribution width and potential fluctuation amplitude

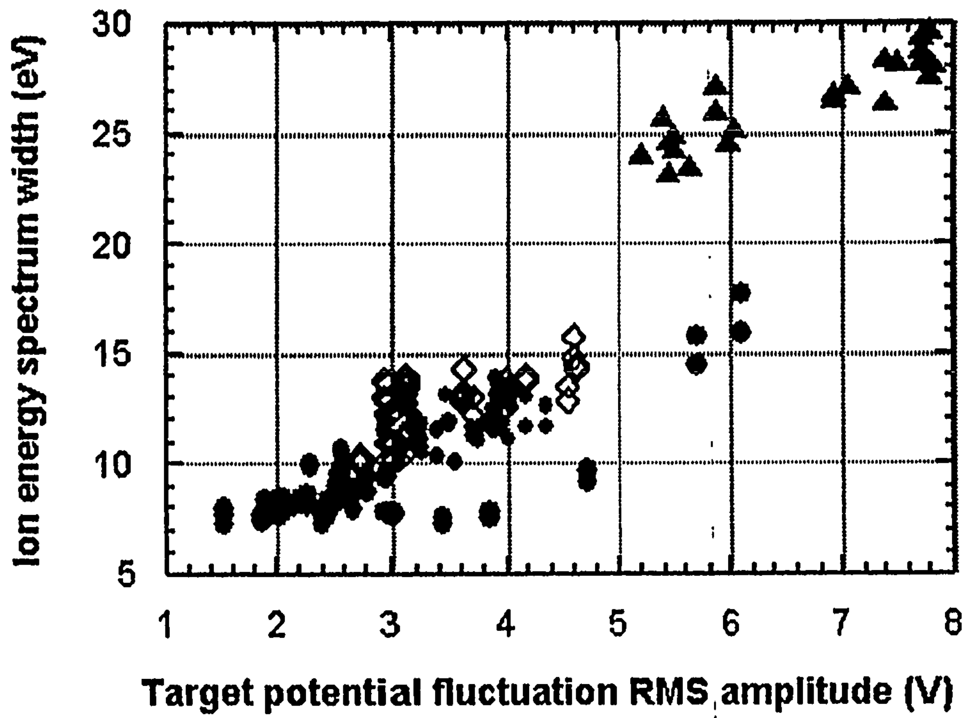

$$\Delta E_{i_{\parallel}} \sim 3\text{-}4 \left\langle \delta\phi^2_{FLUCT} \right\rangle^{1/2}$$

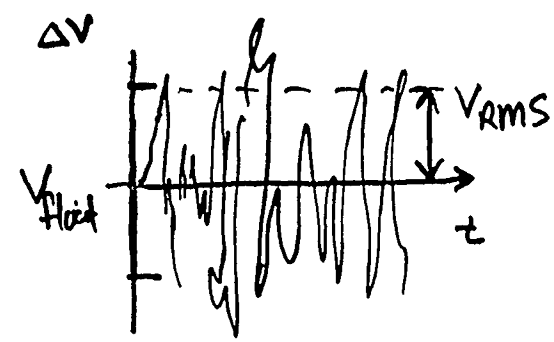

PISCES-B Impurity Experiments

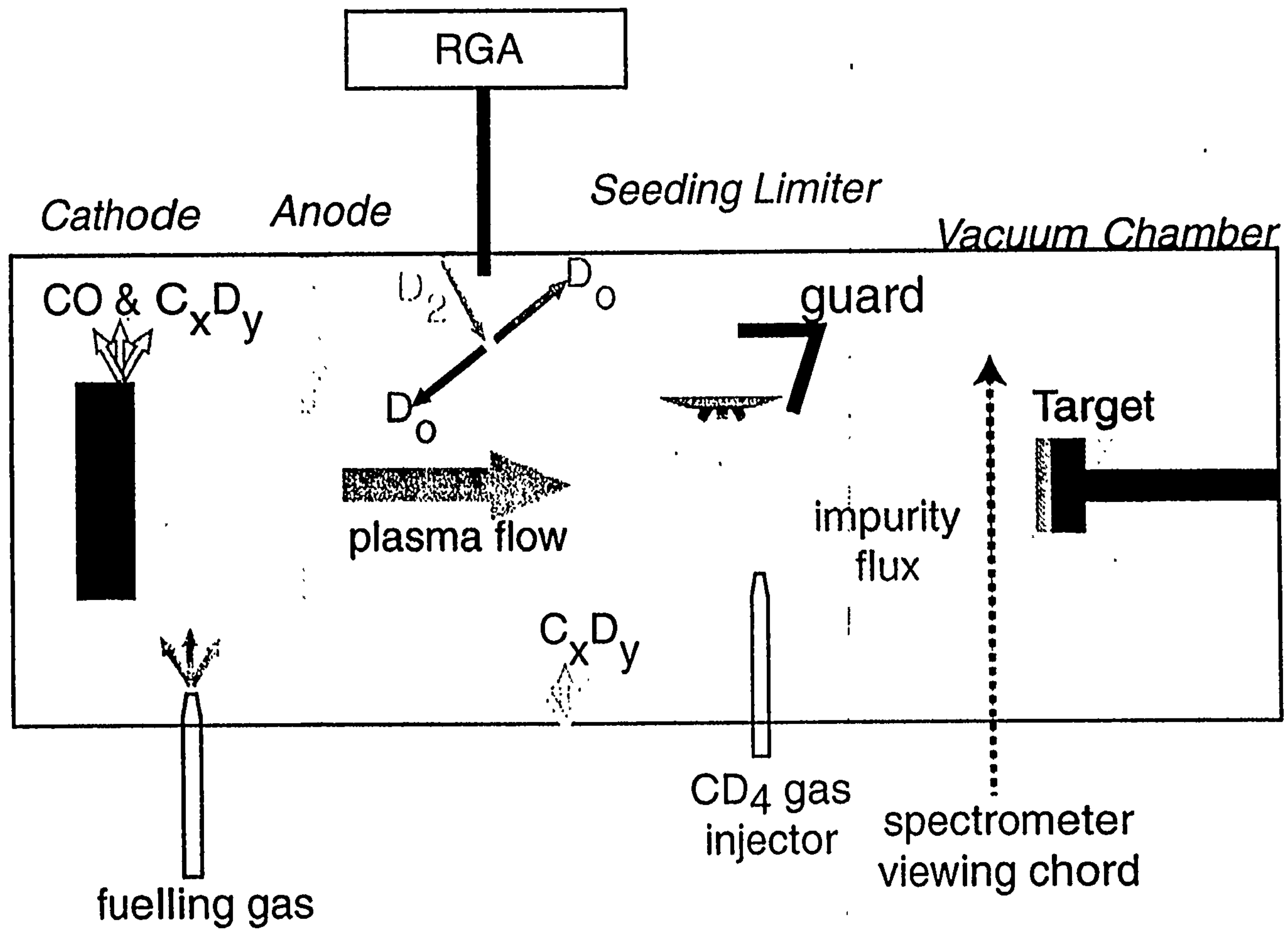

Sputtered Carhon
should he in ~1eV energy range

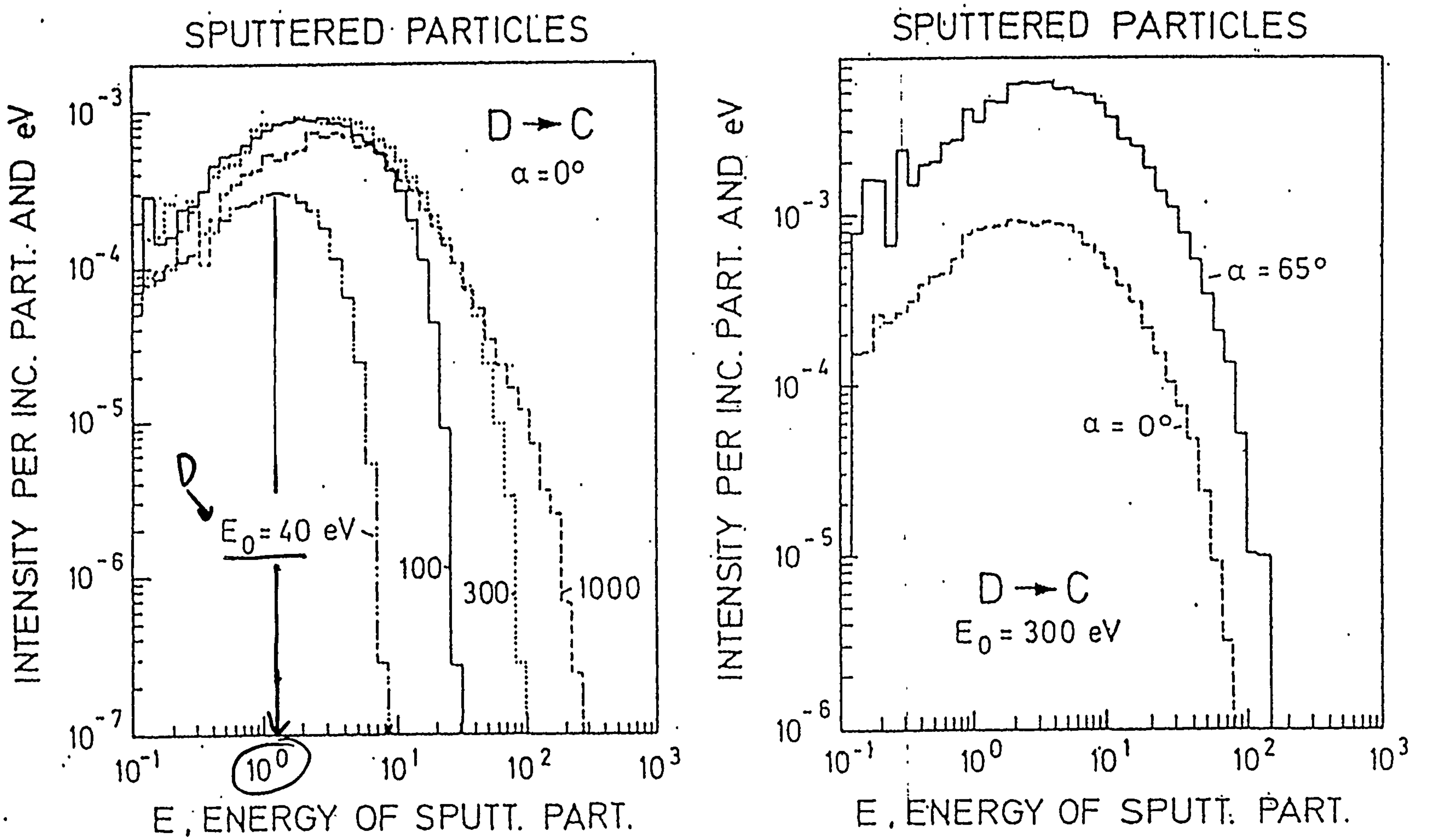

FIGURE 9. Energy distributions (integrated over all emission directions) of sputtered atoms. Carbon is bombarded with deuterium at normal incidence, $\alpha = 0°$, and several energies. Data are calculated with the Monte Carlo program TRSPV1CN.

Sample Spectra from Deuterium Plasma Operations

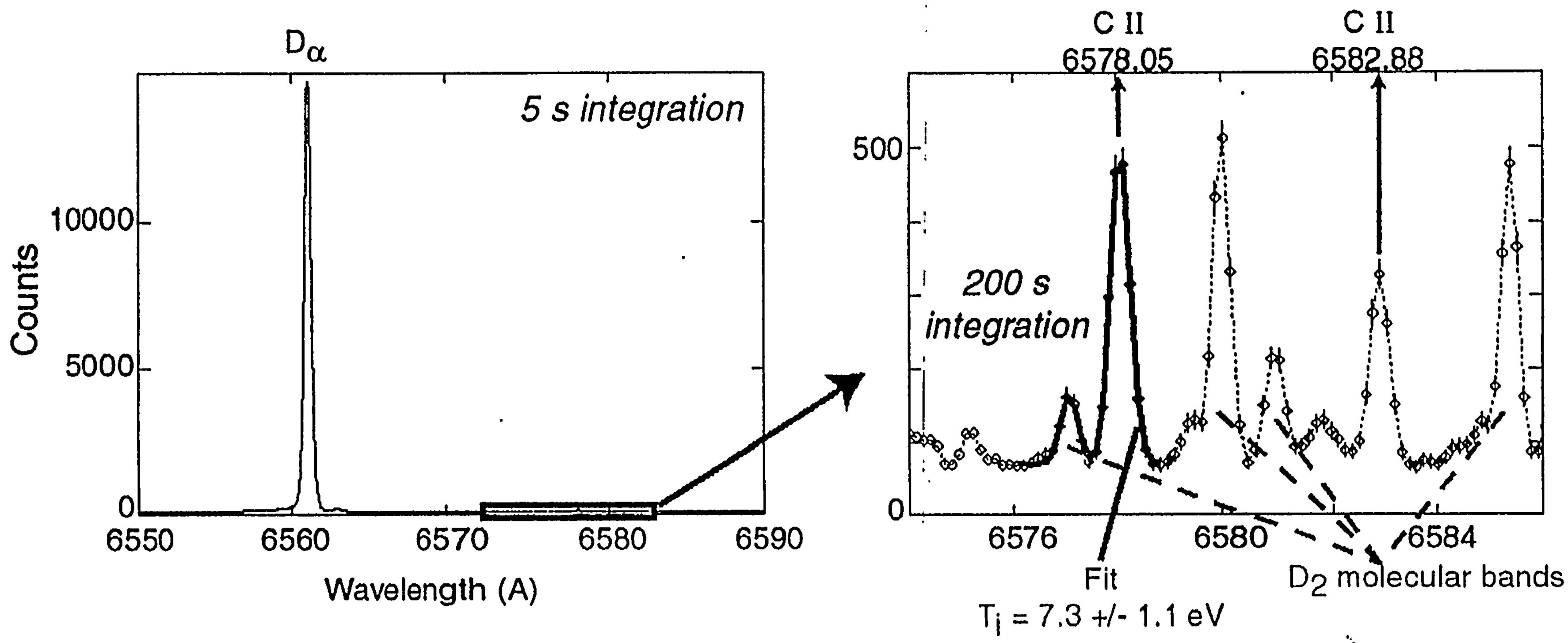

Baseline Ion Temperatures

Deuterium $T_e = 40$ eV $n_e = 0.7 \times 10^{12}\ cm^{-3}$

$T_{i,Carbon}$ = **7-9** eV (Doppler broadening)

$T_{i,D}$ ~ **20-40** eV (CX component of D_α from spectroscopy)

Helium $T_e = 30$ eV $n_e = 10^{12}\ cm^{-3}$

$T_{i,Carbon}$ = **7-9** eV (Doppler broadening)

$T_{i,He}$ ~ **10-15** eV (Doppler broadening of He II)

$T_{i,He}$ ~ **10-20** eV (Energy grid analyzer [Cuthbertson, et al.])

Plasma Carbon Concentrations

The CII doublet at 6578 and 6583 Å ($2s^2(^1S)3p$ - $2s^22p3s$) can be measured simultaneously with D_α (6561 Å) or He I (6678 Å) to provide carbon ion concentrations.

$$f_C = \frac{B_{CII}}{B_{D_\alpha(HeI_{6678})}} \frac{\langle \sigma v \rangle_{D_\alpha(HeI_{6678})}}{\langle \sigma v \rangle_{CII}} \frac{n_{D_0(He_0)}}{n_e}$$

"Baseline" Impurity Contamination (Spring 1997)

Deuterium

$f_{Carbon} = 0.2\%$

$P_{Cx} / P_{D2} = 0.3\%$

$f_{Oxygen} \leq 0.1\%$

$n_e = 9 \times 10^{11}\ cm^{-3}$, $T_e = 40\ eV$

Helium

$f_{Carbon} = 0.015\%$

$f_{(D+H)} = 0.1\%$

$f_{Oxygen} \leq 0.05\%$

$n_e = 10^{12}\ cm^{-3}$, $T_e = 30\ eV$

- Dominant source of carbon in hydrogenic plasmas appears to be hydrocarbon release from walls.
- Upper bound on oxygen content given from spectroscopy detection limit.

Plasma Carbon Concentration Increases with Gaseous Concentration

- Several weeks of active injection increased the baseline impurity a factor of three.
- CD4 replaced CO as main gas impurity.
- Typical range of tokamak carbon concentrations now available for sample exposures.

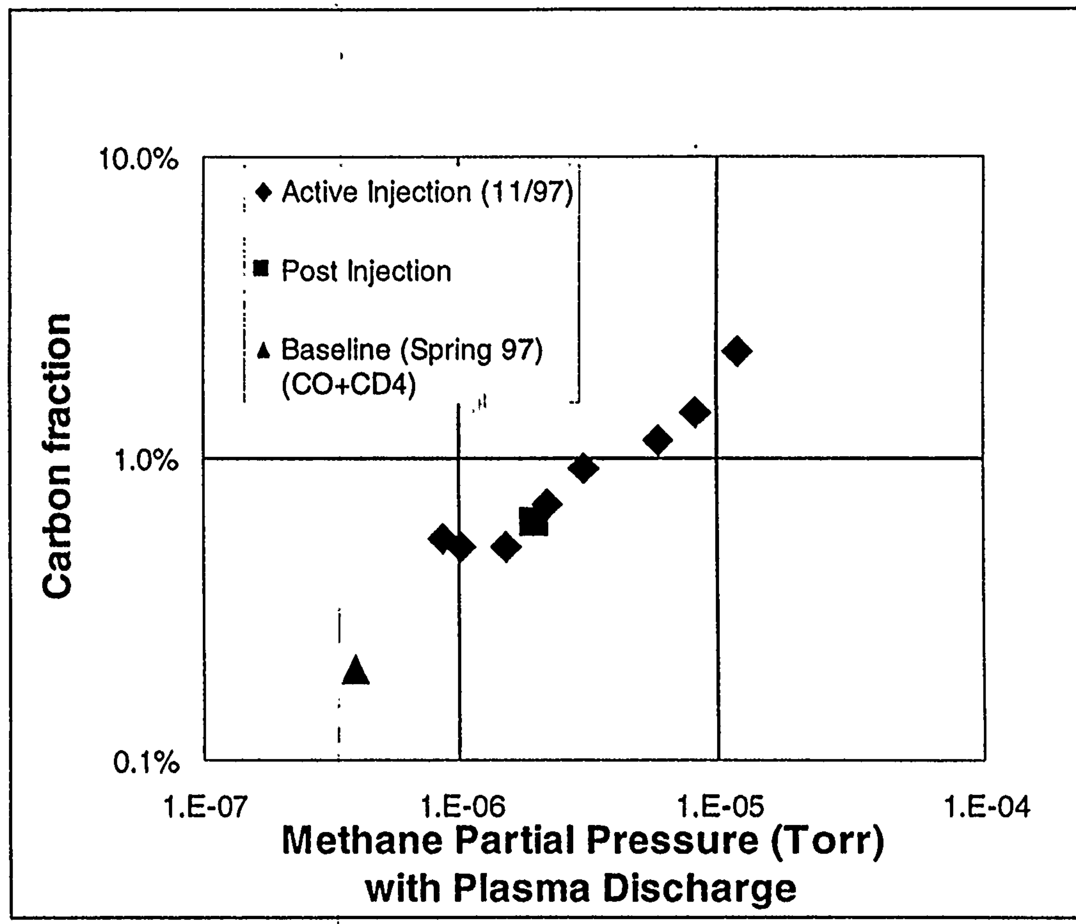

Deuterium Plasma

DOLLOP : Improved Plasma Performance using a New Concept for Mitigating the Plasma-Wall Interaction in Fusion Devices

PPPL

C.H. Skinner, D.K. Mansfield
&
the TFTR Group

Motivation:
To Improve Performance by Modifying the Plasma - Wall Interaction with Minimal Perturbation to the Core

Experimental Technique: Lithium Introduced onto Limiter by Injection of Pellets

PPPL

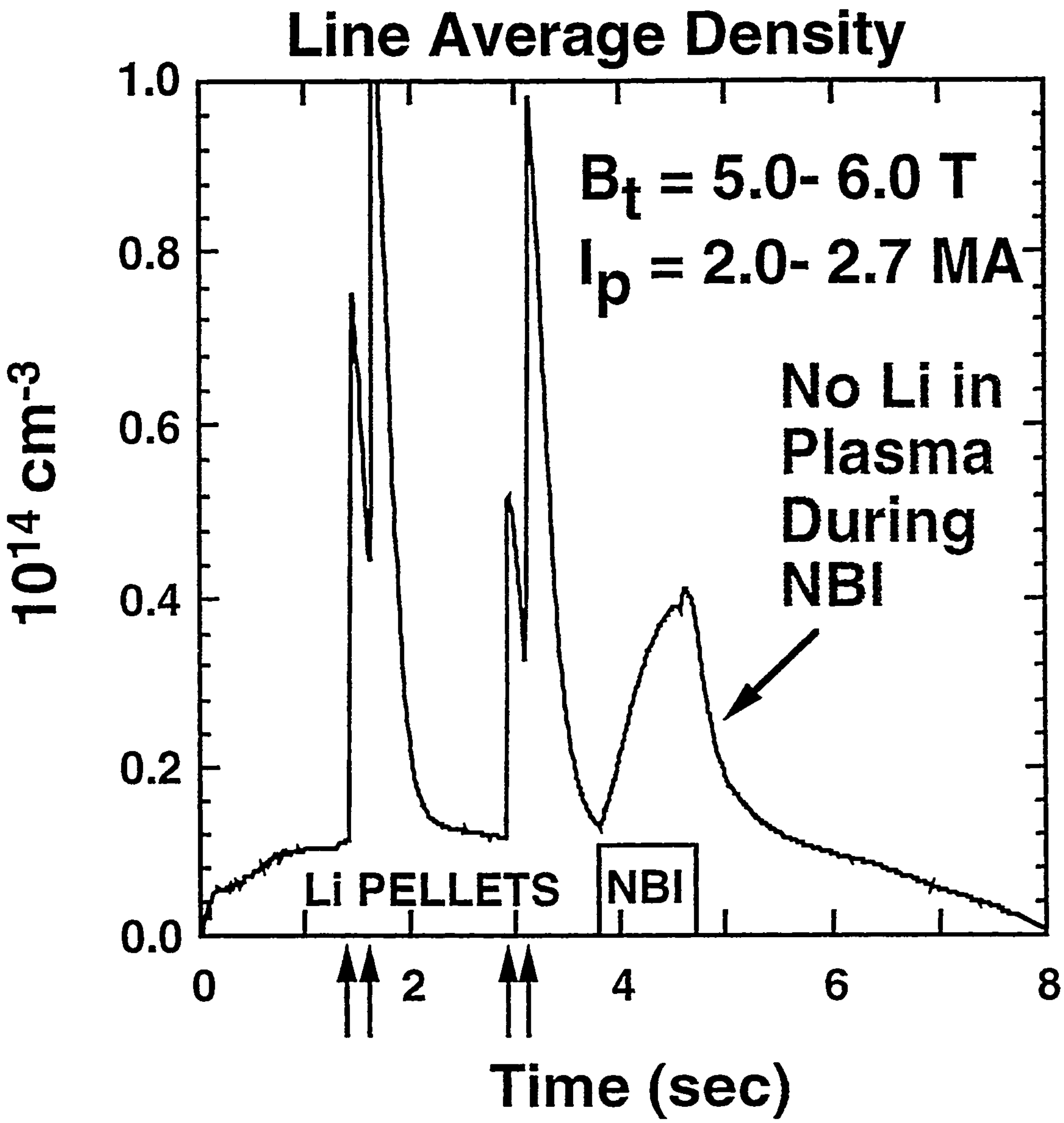

- Extended Clean-up Campaign Necessary
- Li Accumulated by Pre-conditioning
- Minimizing Limiter Contact is Helpful

High $n_e(0)$, τ_E, $T_i(0)$ } Record Lawson Product

$n_H \tau_E^* T_i = 8.5 \times 10^{20}$ m^{-3} s keV

PPPL

- Tritium-only Supershot 4 Pellets + Painting

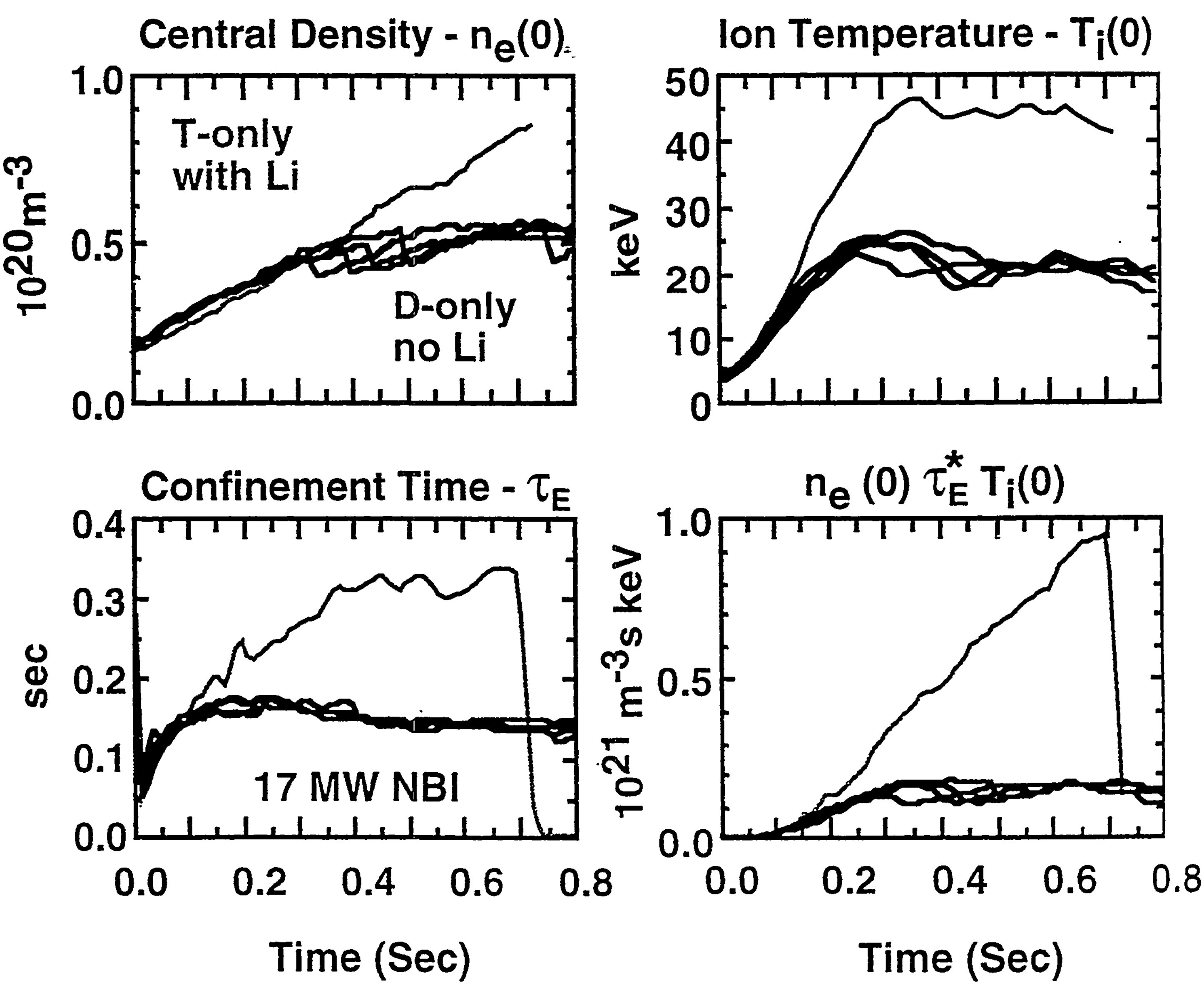

DOLLOP: Li Aerosol Controls Influxes and Increases Performance - Nonperturbing and Controllable

PPPL

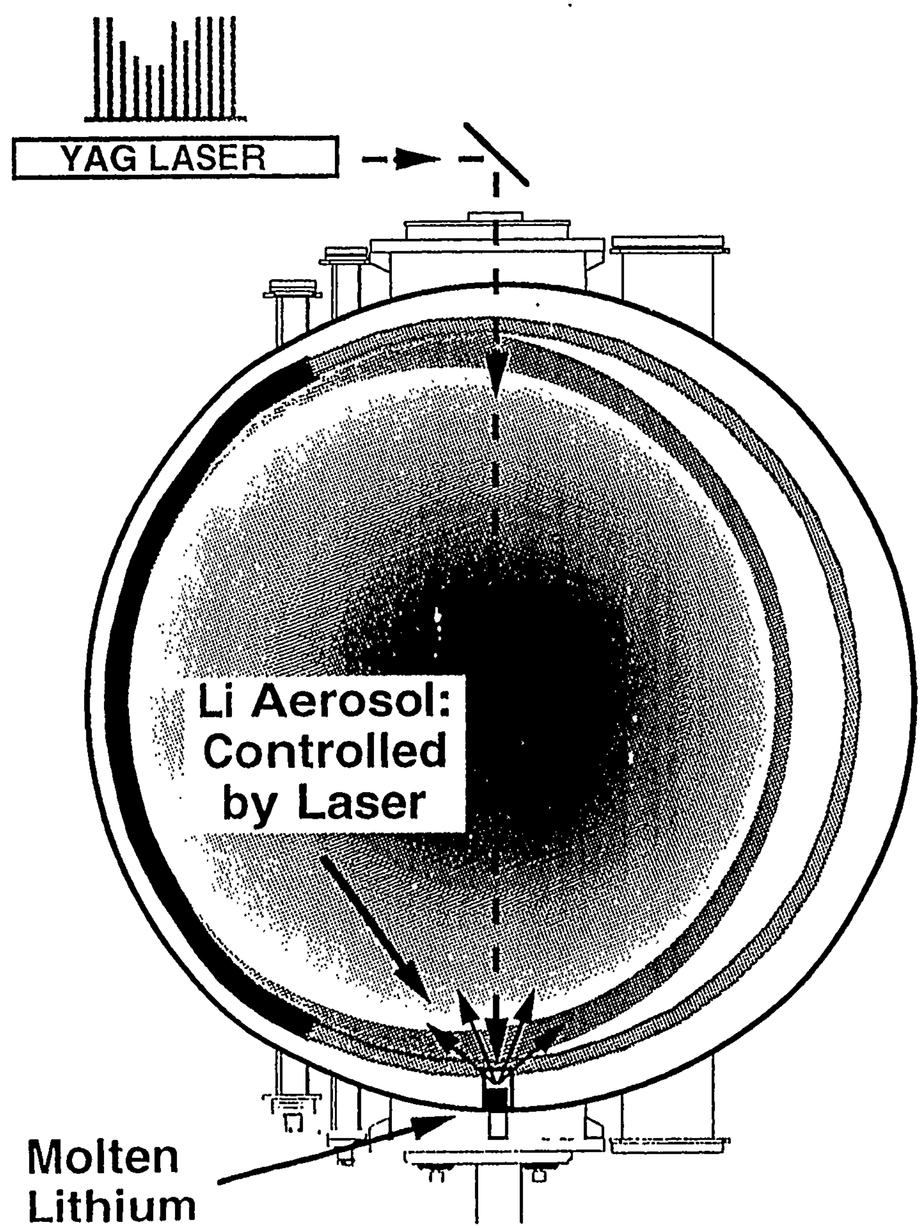

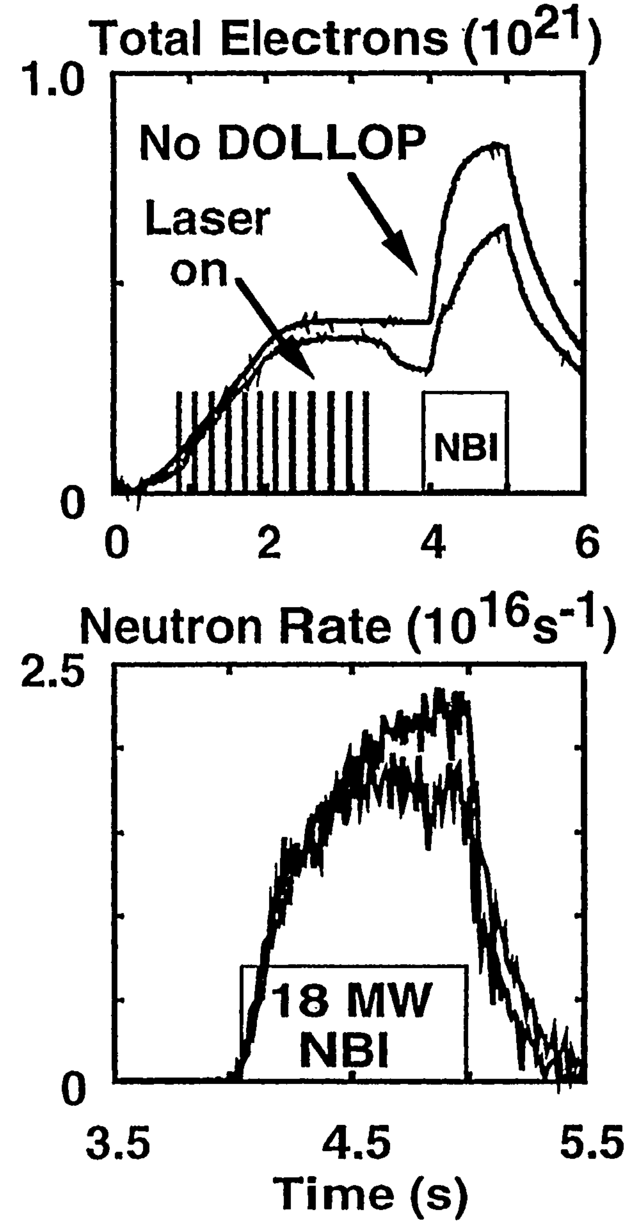

DOLLOP : Initial Effects of Laser-induced Li Aerosol on Ohmic Discharges

PPPL

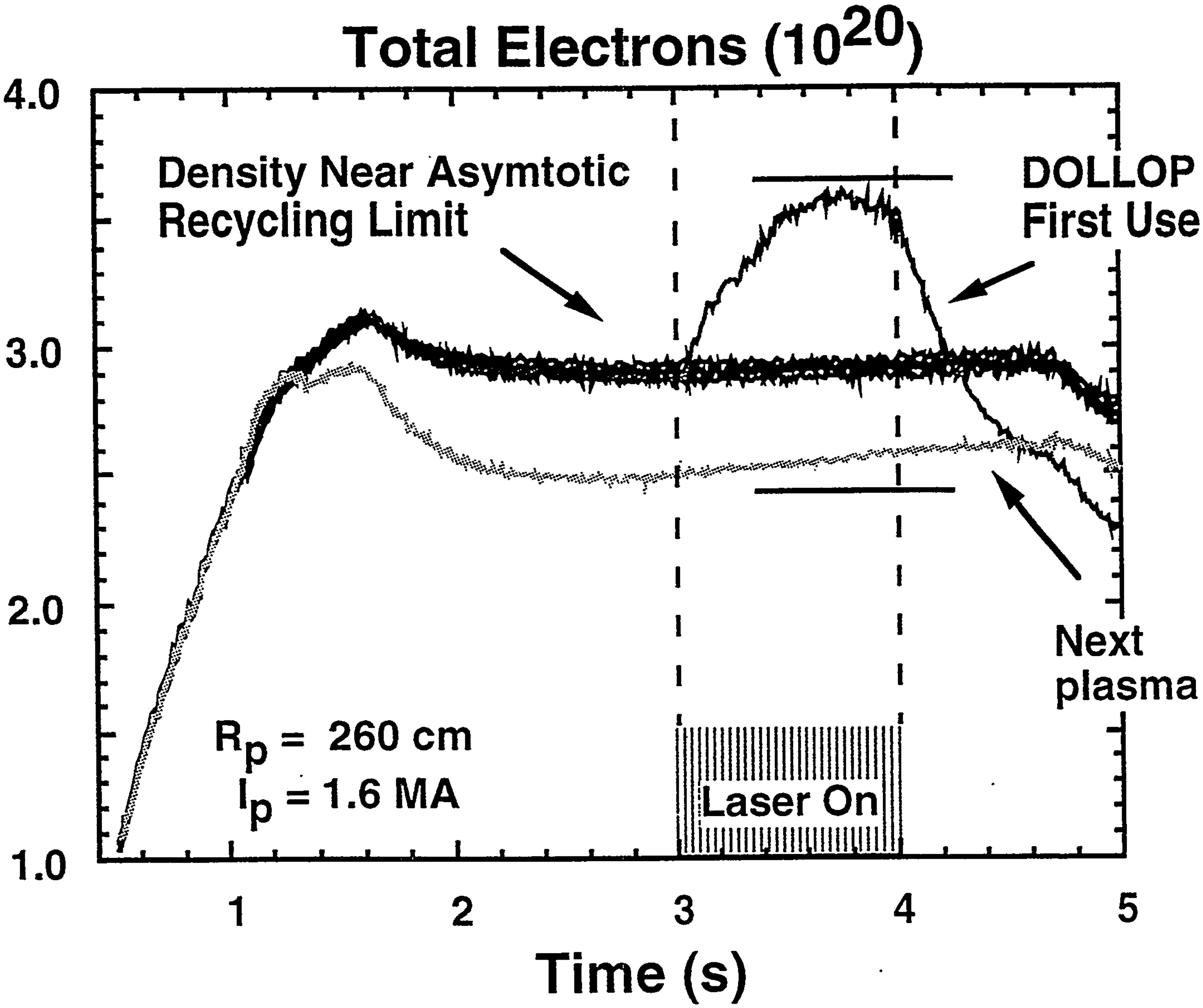

- Residual conditioning is clear
- Both a source and a sink of particles
- Several time constants at work

103979,80,82,83,104002,03

DOLLOP : Initial Effects of Laser-induced Li Aerosol on Ohmic Discharges

PPPL

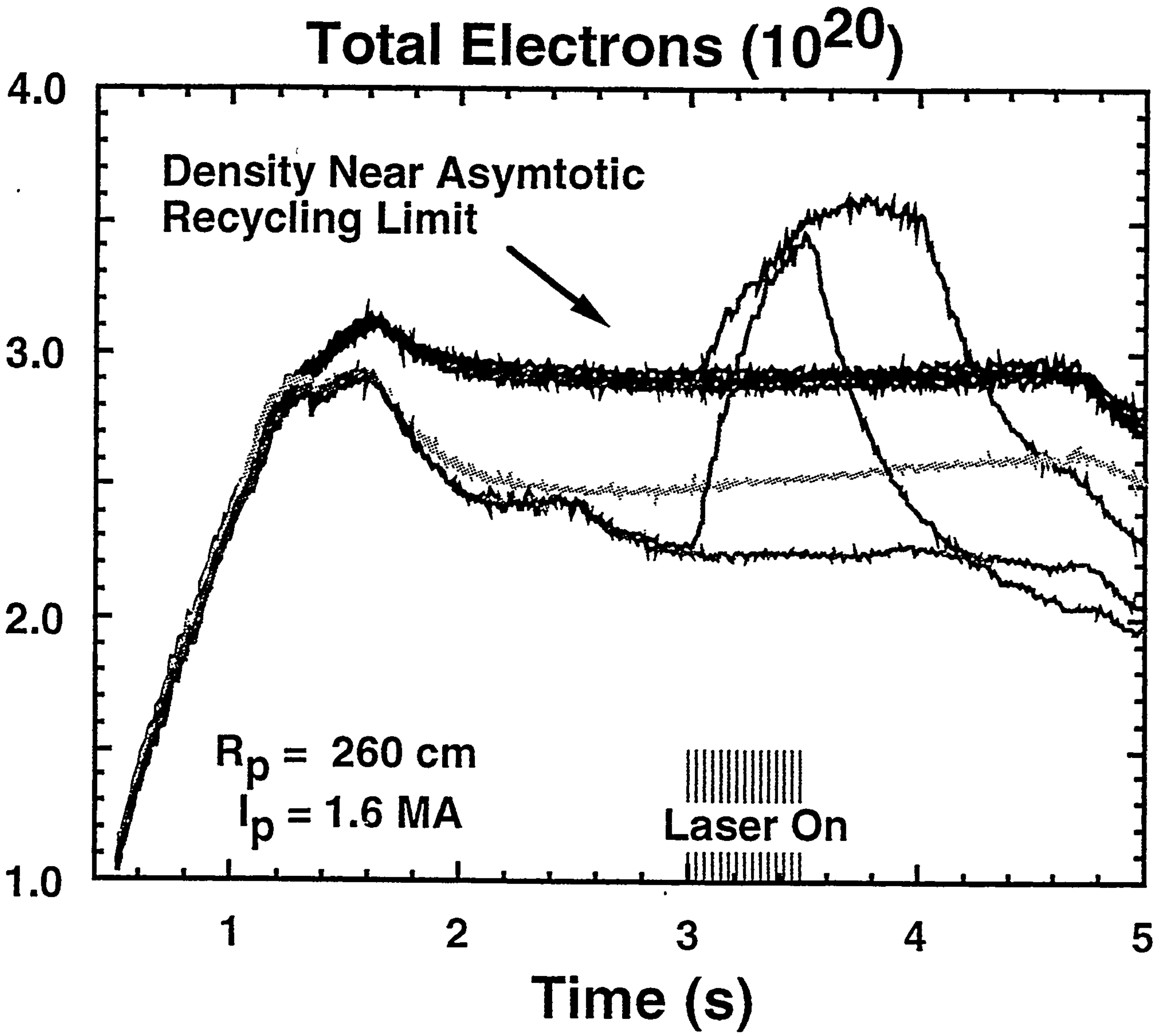

- Deposition controlled optically
- 5 % of Li to Plasma - 95 % to SOL
- Plasma reaction benign

103979,80,82,83,104002,03

DOLLOP Deposits Li Preferentially into the Scrape-off Layer - the Li then Migrates to the Contact Point(s)

PPPL

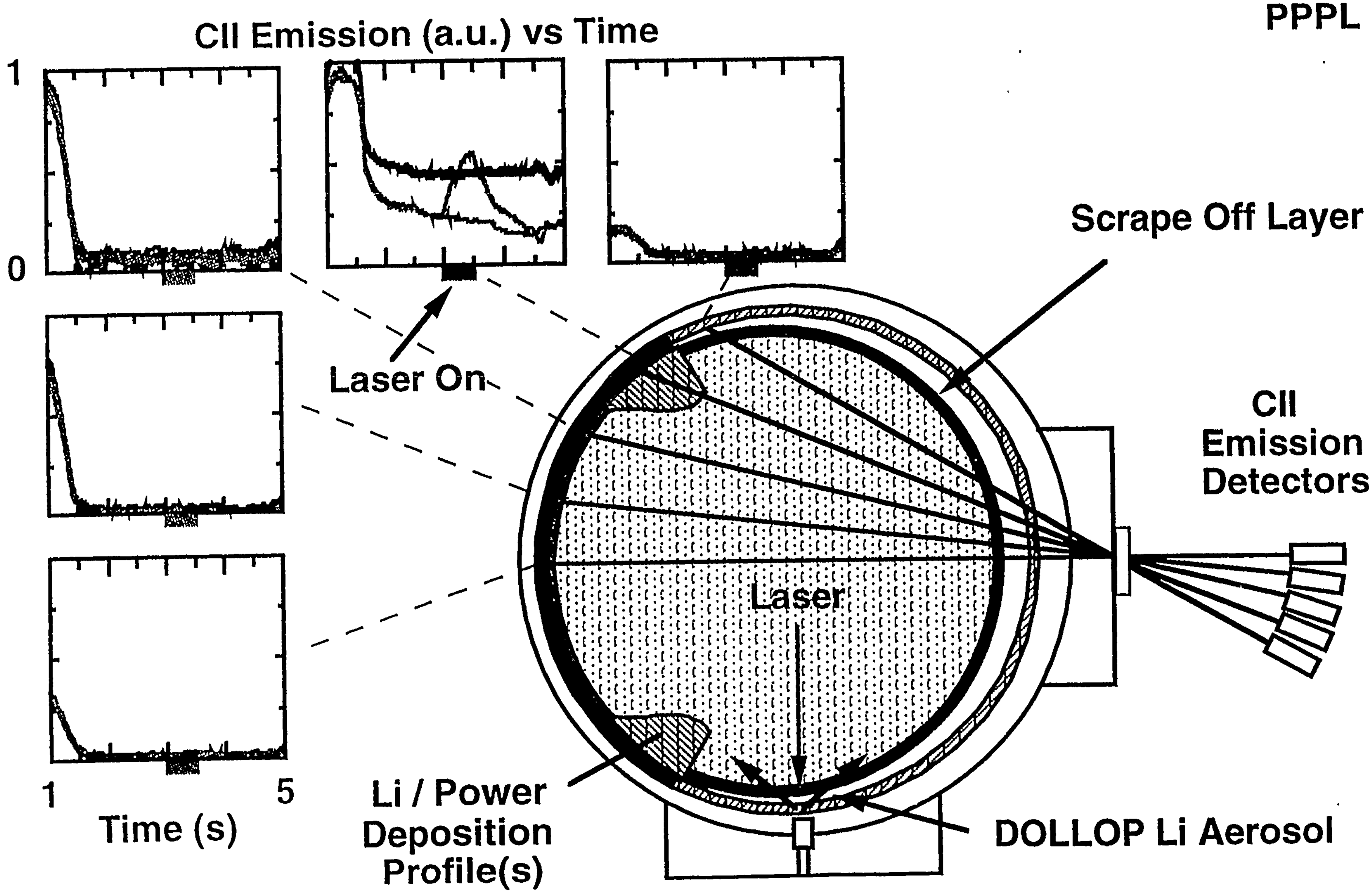

DOLLOP Has Led to Enhanced and Sustained Performance with No Harmful Effects

PPPL

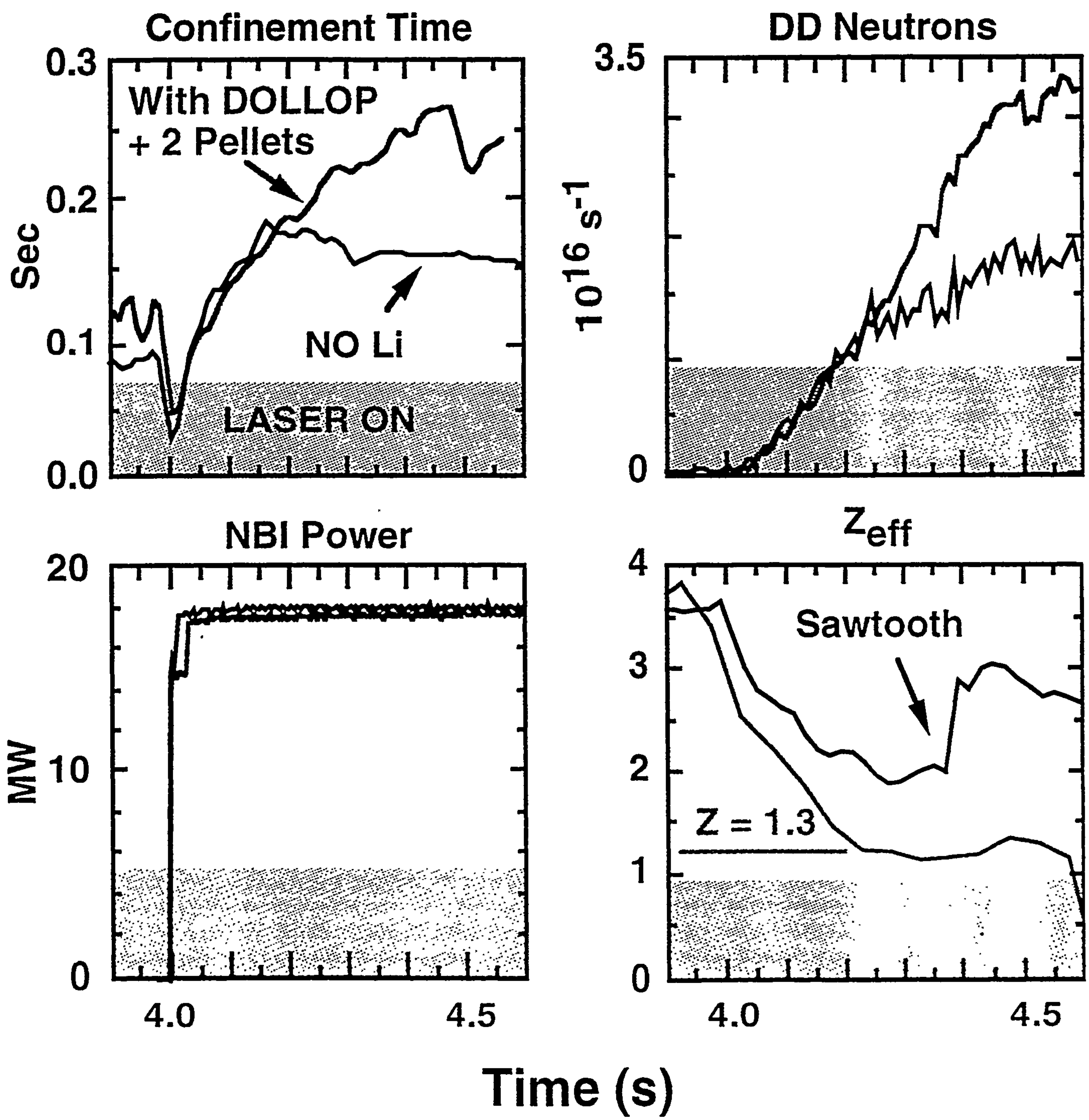

104017/104039

During its Initial Use, DOLLOP Has Raised the Plasma Internal Inductance

PPPL

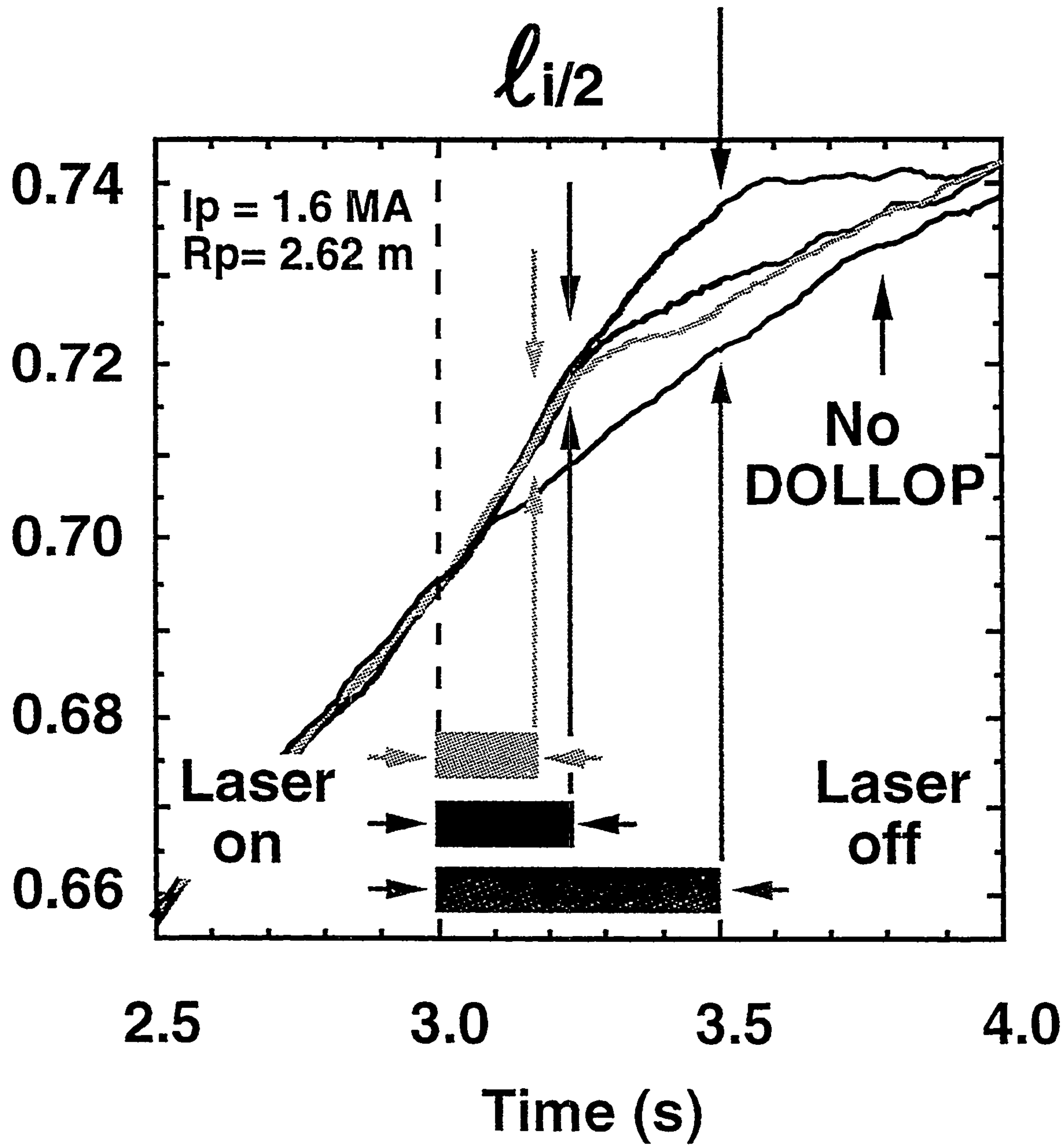

- Inductance Rises When the Laser is On
  - Optical Influence of Current Profile

103748/56/57/58

DOLLOP Causes a Prompt Improvement in Core Electron Energy Confinement

PPPL

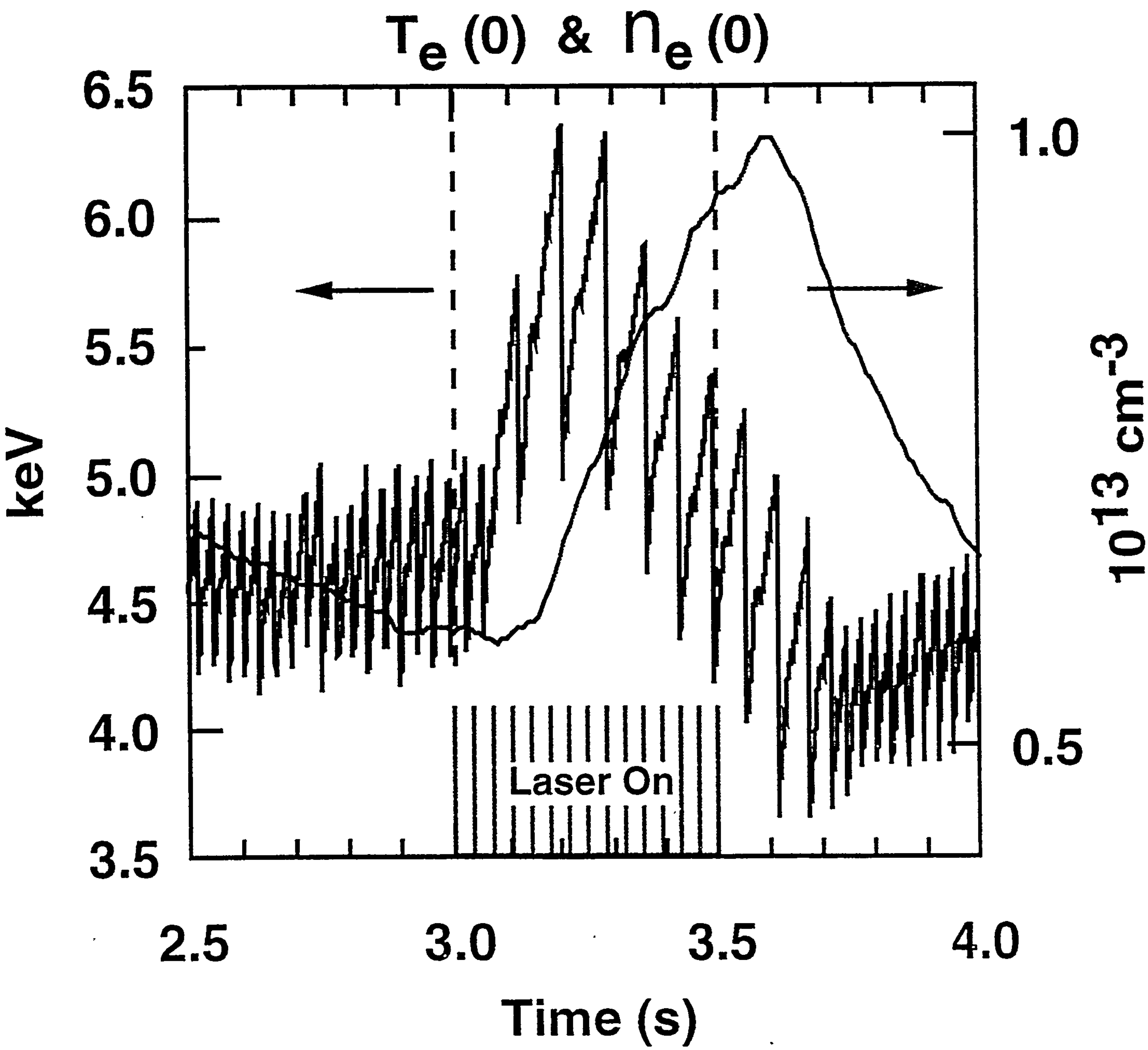

- Non-Local Paradigm for Electron Transport ?

V-28

HIGH SPEED IMAGES OF LI AEROSOL

R Maqueda, G Wurden; LANL.

shot 104023 @ 4.9070, 30μs, during Li injection (out of sight).

NB on @ 4.5 s, unidirectional once NB on. visible light (no filter)

videos on web: http://wsx.lanl.gov/ricky/disrupt.htm

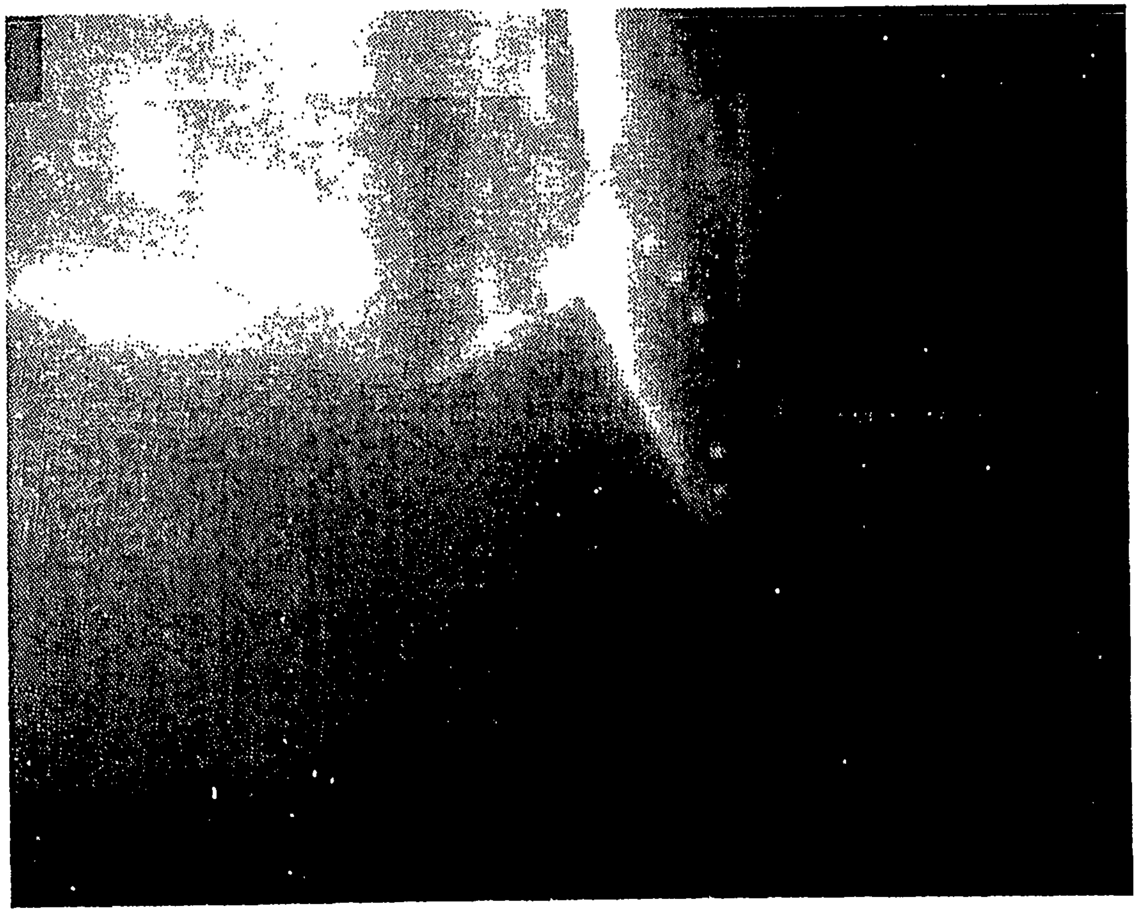

nnw1307.tif

PPPL

Emerging Theoretical Understanding of Li Effects

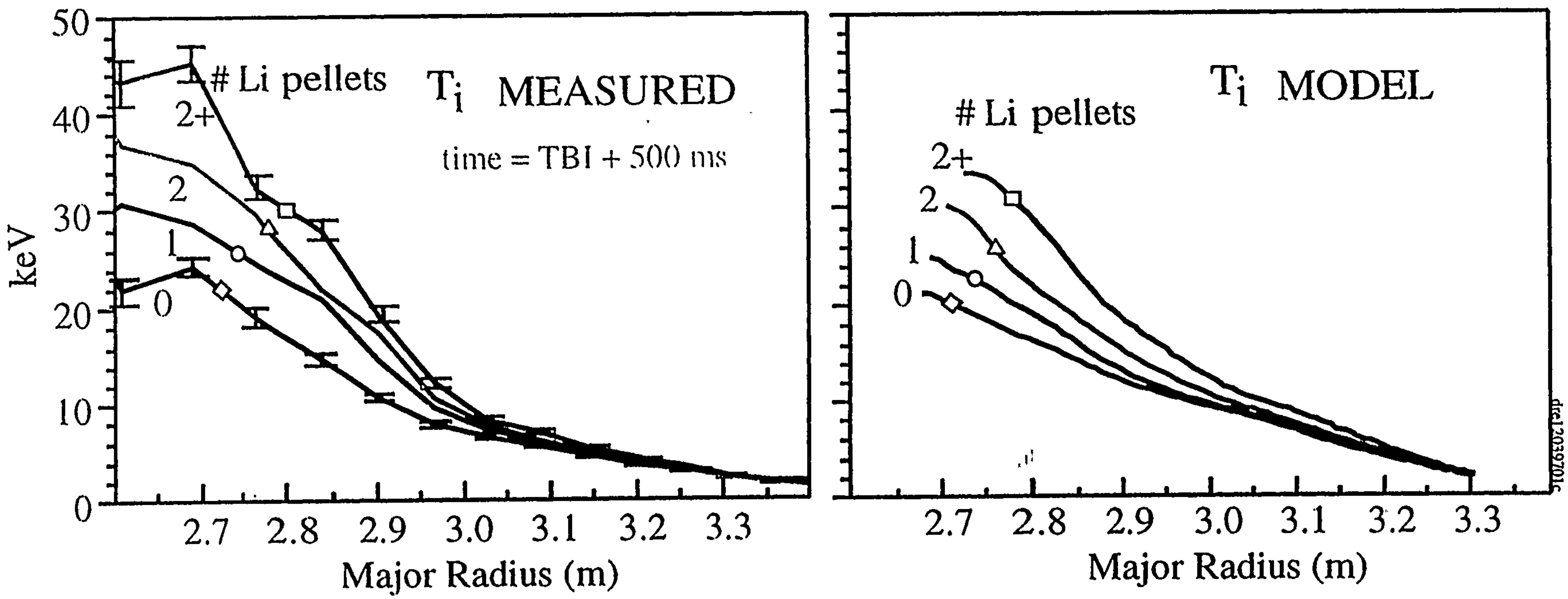

D. R. Ernst, PhD Thesis, MIT (1997): *Momentum Transport, Radial Electric Field, and Ion Thermal Energy Confinement in Very High Temperature Plasmas*

- Model of toroidal ITG modes with self-consistent neoclassical radial electric field
- "Lithium pellet conditioning diminishes the edge fueling source, which affects the thermal density profile in the outer half-radius, tending to increase its curvature near the radius where the beam fueling becomes dominant. The increased density profile curvature acts as the seed for stronger nonlinear increases in the stabilizing effect of radial electric field shear."

V-30

LABORATORY STUDIES ON LI EFFECTS

H Sugai, M Watanabe and H Toyoda; Nagoya University

Presented at PPPL October 1997

Basic Laboratory Studies reveal:

- abundant lithium chemistry on H,O (C?)
- very strong gettering reaction
- saturation occurs in bulk (large diffusion constant)
- Once saturated, no gettering effect
- LiH decomposed at T>400°C

Many Li effects explained by Li Chemistry:

- Low H recycling due to LiH formation

Necessary conditions to get Li Effects:

- Low O impurities - to keep Li surface clean
- Low H retention in graphite
- Need sufficient Li ($N_{Li}>N_D$) - free Li atoms on walls key.

A Few Possibilities ...

PPPL

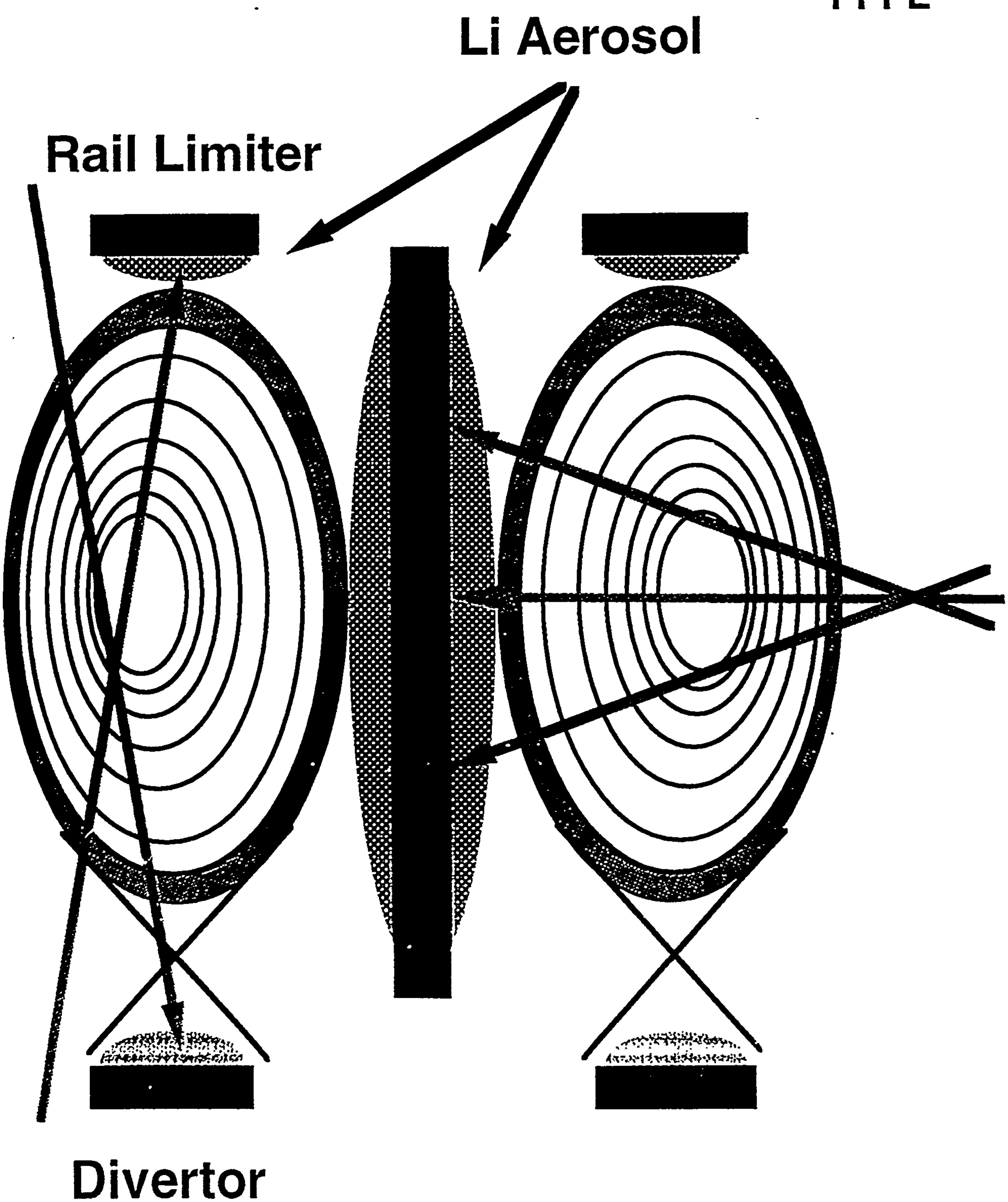

Deposition of Lithium onto an Edge Probe in TFTR

- Towards the understanding of lithium wall conditioning -

US-Japan Workshop
San Francisco, Dec. 8-11, 1997

Y. Hirooka [1], K. Ashida [2], H. Kugel [3], M. Bell [3],
M. Hara [2], S. Luckhardt [1], M. Matsuyama [2], D. Mueller [3],
C. Skinner [3], D. Walsh [4], W. Wampler [4], K. Watanabe [2]

1)University of California, San Diego
2)Toyama University
3)Princeton University
4)Sandia National Laboratories

FERP-UCSD

Acknowledgement

1. PPPL: TFTR Safety Staff

2. SNLs: EH&S Staff: Brad Elkin

3. Toyama Univ.: Hydrogen Isotope Res. Center Staff

4. UCSD: Radiation Safety Staff: Sandy O'brien
Ken Helm

5. PISCES-Lab. Staff: Leo Chousal
Alvin Viray
Daniel Sze

FERP-UCSD

Table of Contents

FERP-UCSD

How does Li-coated wall interact with DT-plasma ?

1. Li coatings can trap both energetic and thermal D, T, O, C, B.
2. If eroded by DT, Li can be auto-redeposited (2ndary ions).
3. If coated with C, Li can thermally diffuse out to the surface.
4. Li migration leads to compounds formation (hydride, oxide, carbide, etc.), perhaps differently in the two directions.
5. Surface analysis can provide the key information.

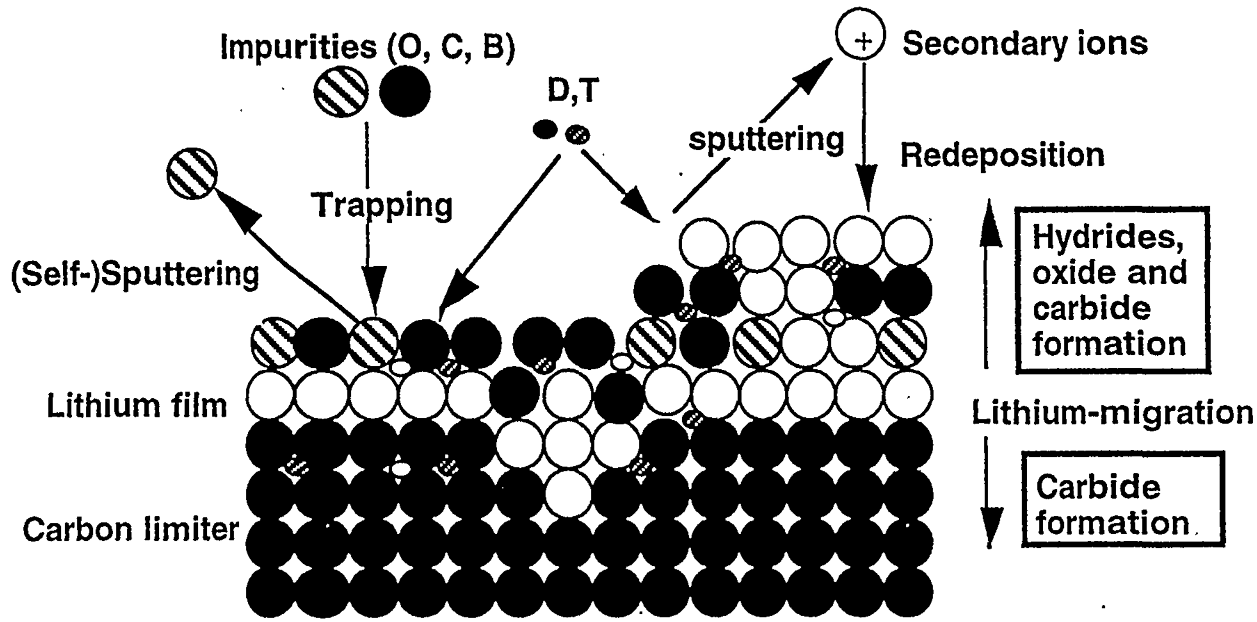

FERP-UCSD

Trapping coefficient data relevant to PMI in TFTR

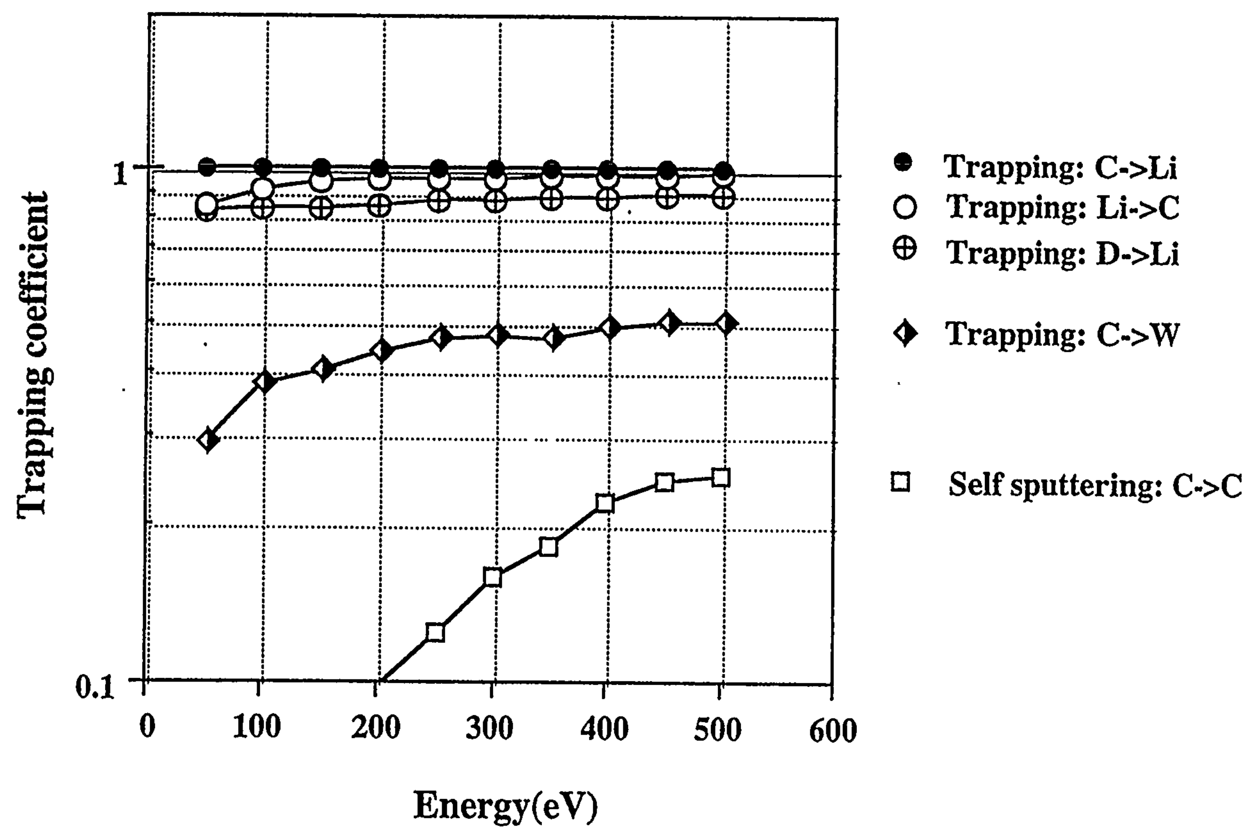

FERP-UCSD

TFTR deposition probe exposure conditions

*Jan. 31st, 1997
*Exposed to 3 x OH-DD-shots and one disrupted shot
*Plasma current: 1.6 MA
*Major radius: 2.6 m
*Probe position: 2.62 m (Bay-D)
*Probe material: 4D C-C composite (FMI)
*Li-pellet injection: 2,4,4 pellets (5x 10^{20}atoms/pellet)
*Li-6 enriched pellets to 95% (5%: Li-7)

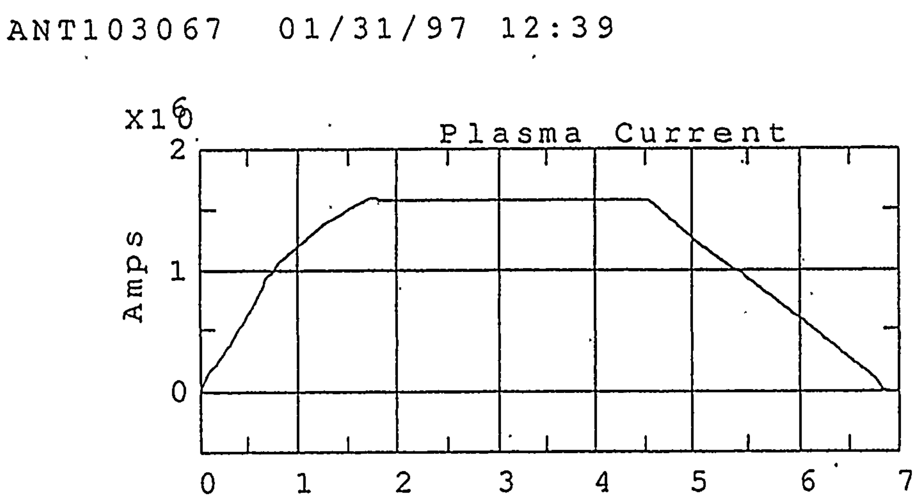

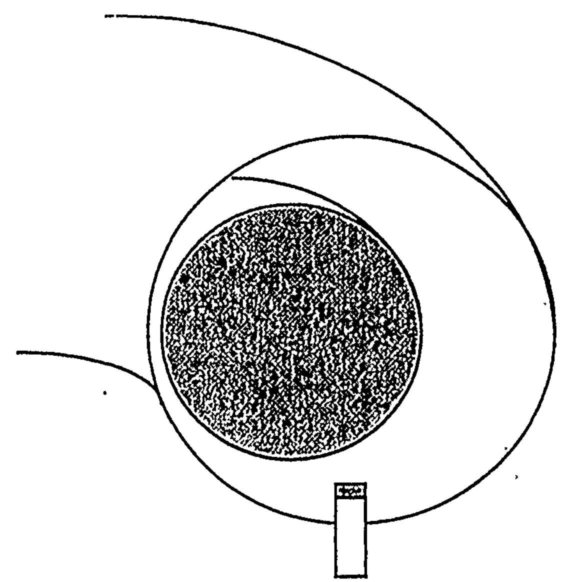

FERP-UCSD

CARBON PROBE HEAD
BY MICHAEL VOCATURO
11-27-96

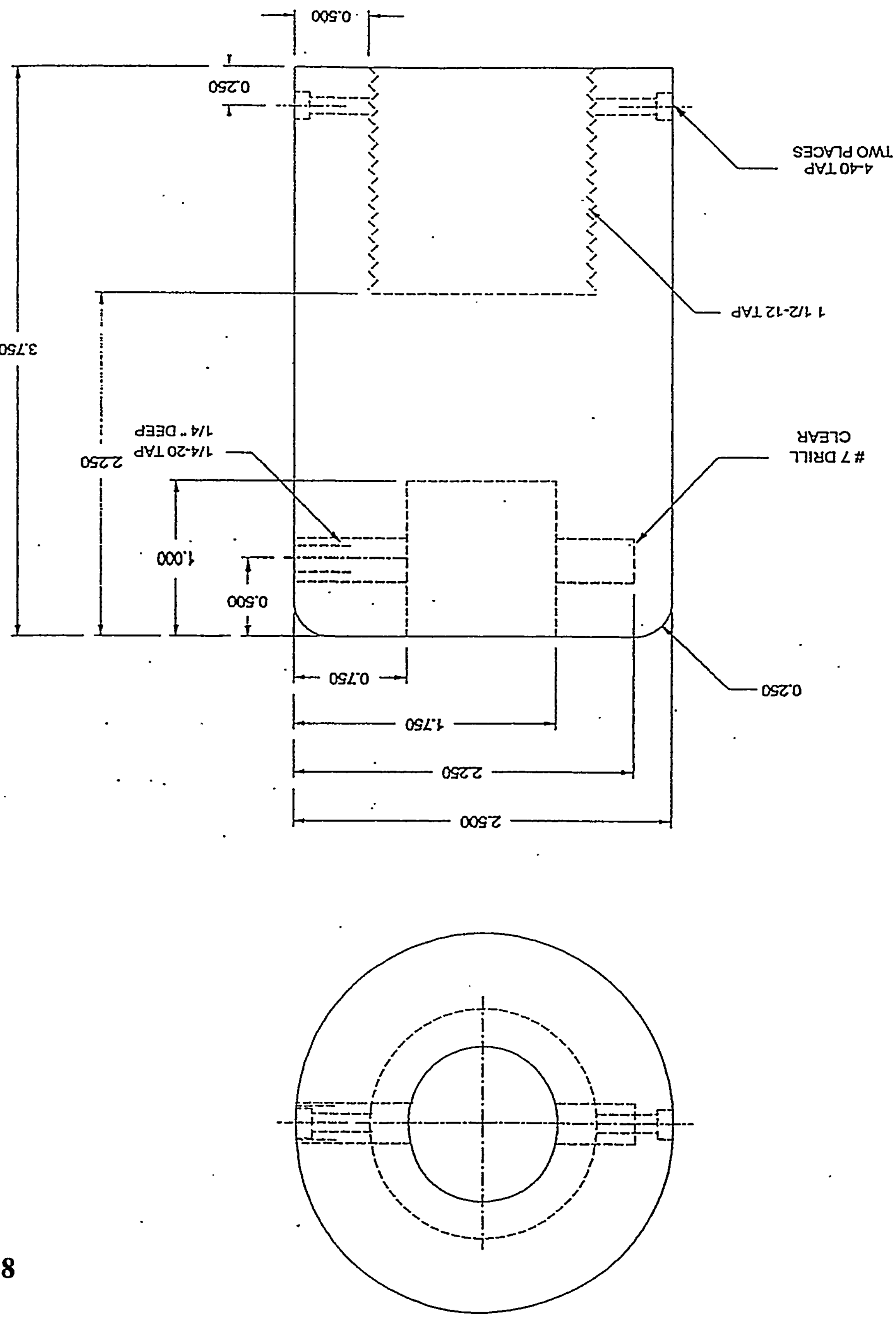

D-mapping with $^3He(d,p)\alpha$ over the probe surface

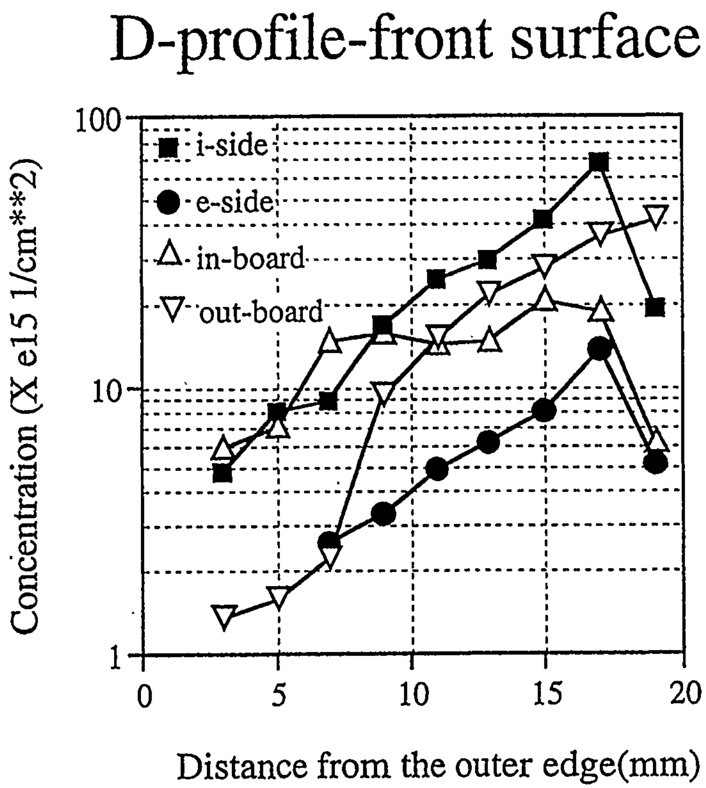

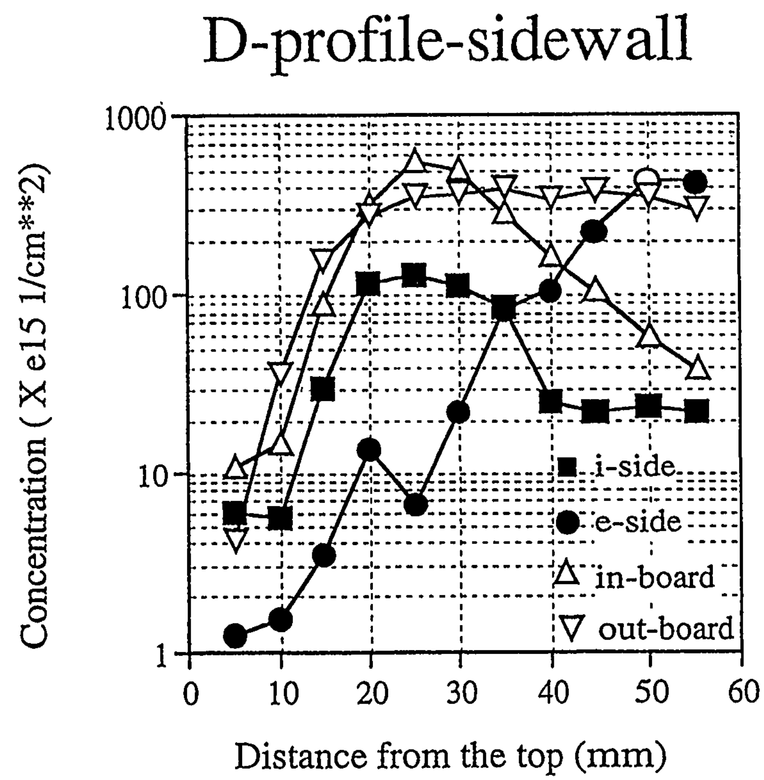

Li-7 mapping with $^7Li(p,\alpha)\alpha$ over the probe surface
- Recycling of Li-7 from previous shots -

Li-profile front surface

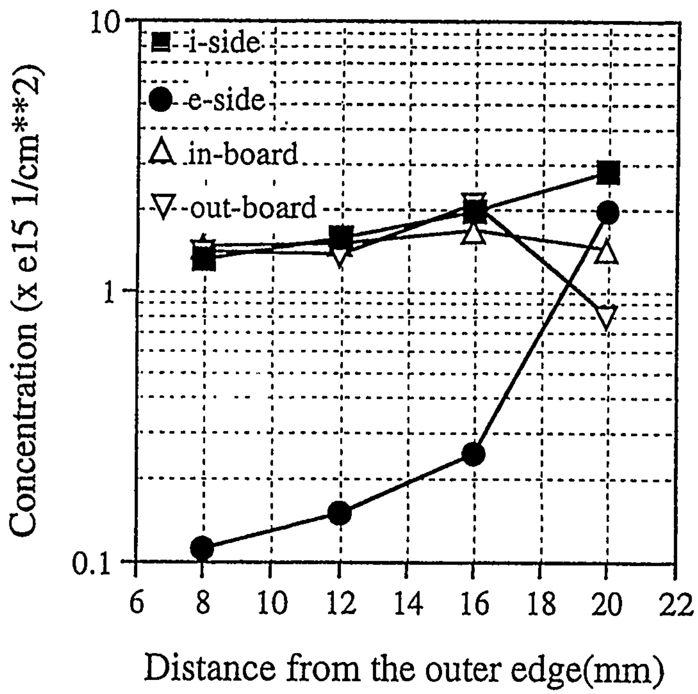

Li-profile sidewall

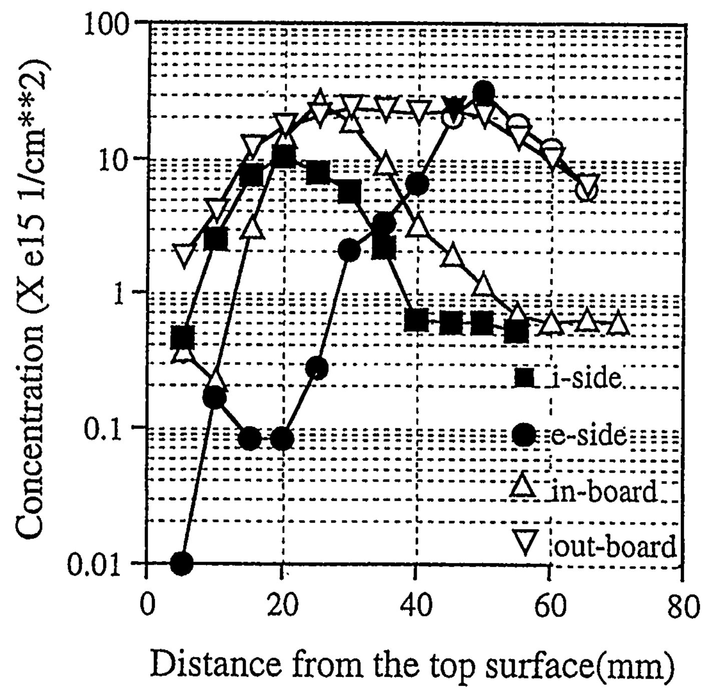

Li-6 depth profiling with SIMS for the TFTR probe samples (4 directions on front surface)

- Deposition of injected Li-6 -

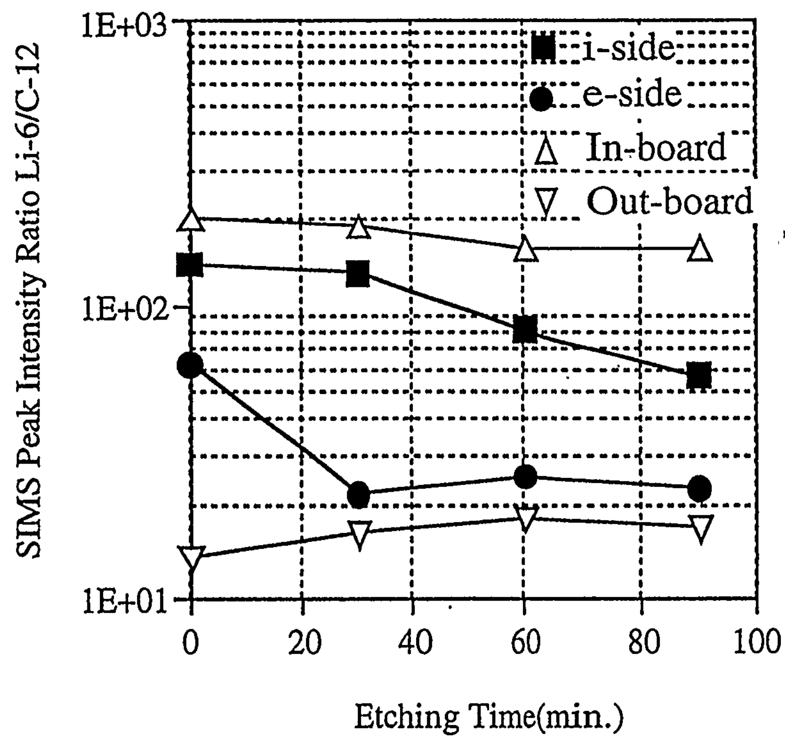

SIMS depth profiling for the TFTR probe-II (deeper etching on the e-side front-surface)

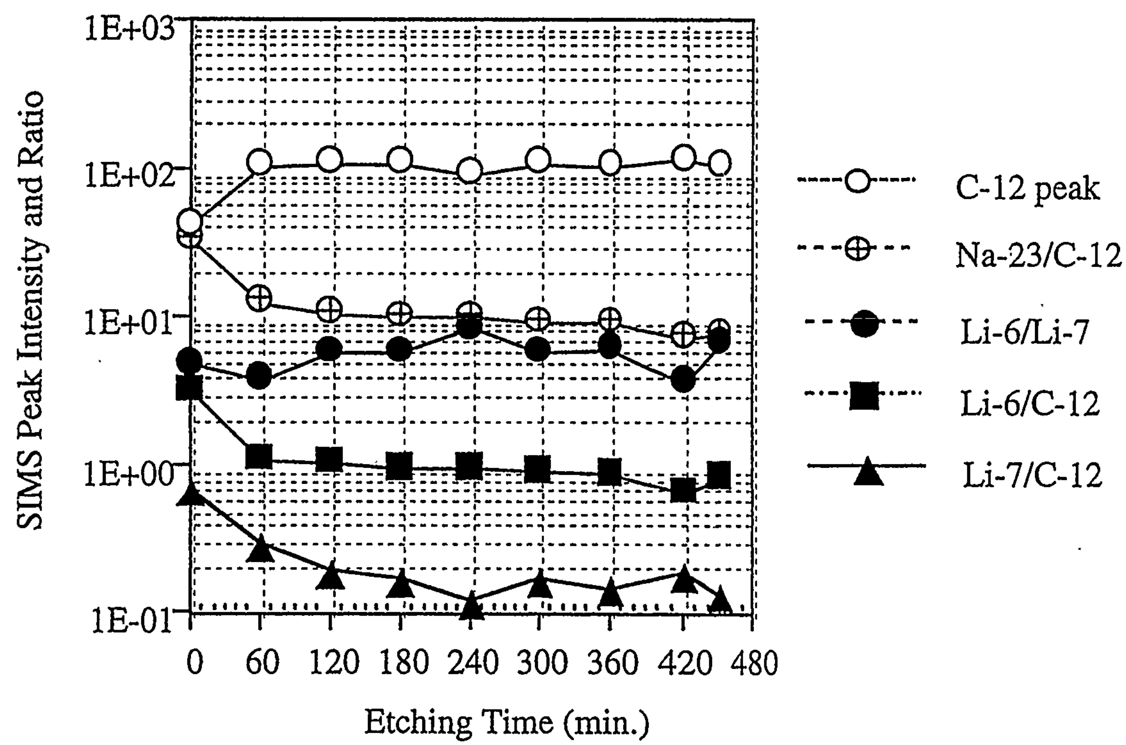

FERP-UCSD

Impurity contents in graphite materials

Impurity element	Contents(ppm) FMI-TFTR	Toyo Tanso IG-43	Toyo Tanso IG-430U
Li	2.9	<0.03	<0.001
B	17	3	0.1
Na	<10	<0.5	<0.002
Al	5-24	14	<0.001
Si	<50	2	<0.1
K	<50	2	<0.03
Ca	<10	6	<0.01
Ti	1.7	33	<0.001
V	10.9	40	<0.001
Cr	0.3	<0.3	<0.004
Fe	10	26	<0.02
Ni	<0.5	4	<0.001

Remarks:
(1) IG-43 is a general purpose graphite and IG-430U is a ultra-high purity graphite for special purposes (JT-60U and LHD).
(2) No significant difference as to other impurity elements.

Neg. SIMS data on D and O for the TFTR probe samples (4 directions front surface)

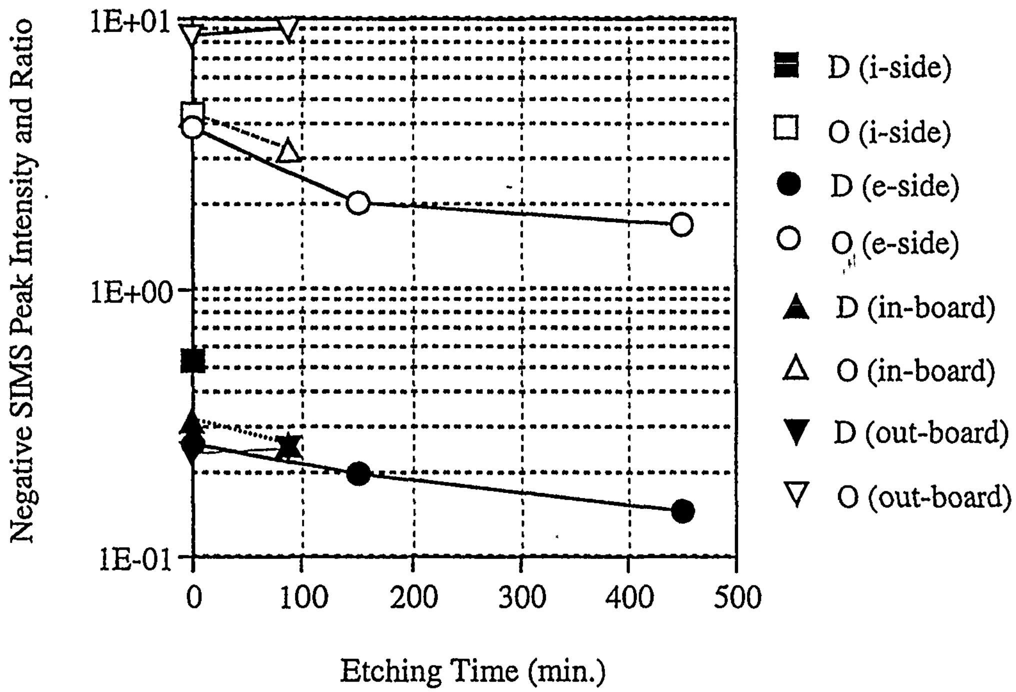

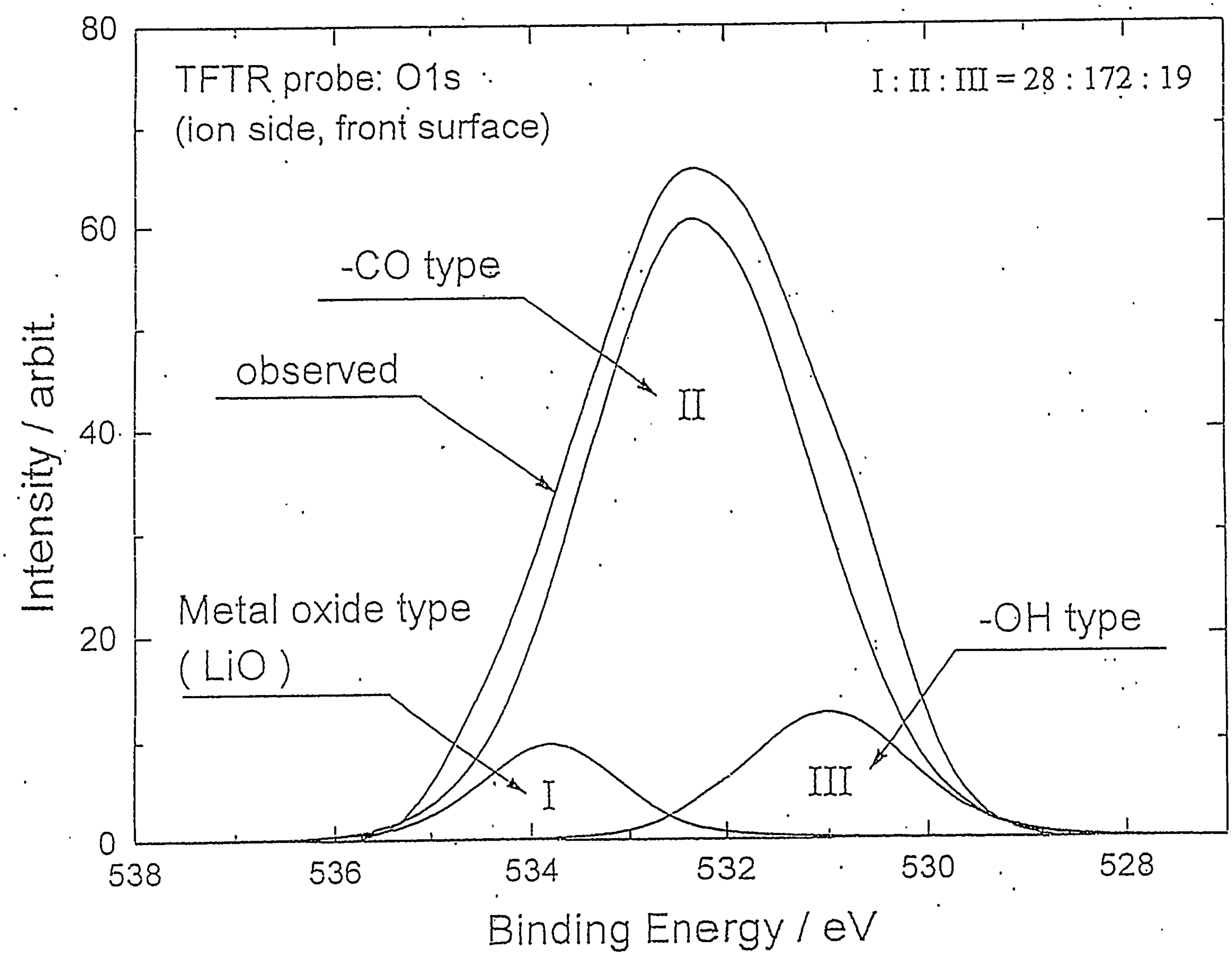
TFTR probe: O1s
(ion side, front surface)
I : II : III = 28 : 172 : 19
-CO type
observed
II
Metal oxide type
(LiO)
I
-OH type
III
Intensity / arbit.
Binding Energy / eV
0
20
40
60
80
538
536
534
532
530
528

Summary

1. TFTR edge probe has been found to be deposited with Li, D, T, O, etc. (The total tritium retention was about 30 μ Ci.)

2. NRA and SIMS data agree in that more Li and D are found in the i-side than e-side, presumably due to the heat flux effect (edge plasma data analysis under way).

3. SIMS depth profile data has shown a deep penetration of Li into C-C composite, indicative of some fast tranport path although details are unclear at present.

4. XPS data indicate that oxygen is partially bound to lithium. The estimated lithium concentration is a few atomic percent.

5. Drastically different surface morphologies have been observed for e-side and i-side, indicating the effects of high-flux plasma bombardment and resultant redeposition (e-side).

FERP-UCSD

Session VI: Development Issues for Near Term PFC's

{Verbal Sessions}

[page intentionally left blank]

~~coordinated~~ coordinated by Sapara & Wong

Issues for near term PFCs* KSTAR
(examples: LHD/W7X, NSTX, ITER)

Discussion topics:

1. Coupling with physics
2. Higher heat flux – longer pulse length
3. Use of W, Mo & C, Be (ITER)
4. S-C coil machine wall conditioning

~~5. Engineering tolerances is crucial for machine performance especially for~~
~~6. initial operation~~

5 PFC Engineering design

* · H_2O cooled
· Cu-heat sink – joints / interface
· Minimum or zero neutron radiation damage
· Low duty cycle
· Power conversion is not required

Topic 1: Coupling with physics

- Impacts on heat and particle flux spatial and temporal distributions
- Particles recycling, ash removal & pumping

	LHD/W7X	NSTX	ITER
• Radiative divertor	✓	✓	✓
• Mantle/core radiation	✓	✓	✓
• ELMs	?	?	✓
• Disruption	No	✓	✓
• Detached plasma	?	?	✓

- stellerator has H-mode. ELMs not observed yet
- Closely coupled with edge conditioning
- Question on momentum balance on radiation divertor?
- Active pumping brings in new observations on recycling
- Coupling with fueling options – puffing / pellet injection interaction with PSI
- Modeling efforts need to be continued and coupled between physics & PSI effects
- More efforts on bench marking between modeling and experiments, e.g. erosion, ELMs, disruptions, material damage
- Technology & PSI dedicated machine(s)?
- There is a trend of paying attention to higher Z material.

Topic 2.

Higher heat flux   5 – 25 MW/m²

Longer pulse length   5 – 20 s   ITER (1000 s)
passively cooled   Actively cooled

e.g. LHD 5 MW/m² — 10 s – ~~Active~~ from passive to active

- A potential disconnect between ~~near~~ the cooling of near term PFC & advanced designs that require active cooling — No clear path established. H_2O Vs Li Vs He
- Cooling > 5 MW/m² is not ~~obvious~~ necessarily simple. High heat flux component design must also be assessed for ~~future~~ reactor grade machines
- Stronger coupling required between physics & engineering communities
- Should we focused on ignition machine in the near term?

Topic 3

(4)

Use of W, Mo, C § Be (ITER)

- W may be suitable locally, e.g. high particle flux.
- mixed material issues need to be addressed
- Coating metallic wall ~~is~~ option is being utilized
- W-coated graphite being evaluated (0.5→1mm W)
- C-dust – Safety, Tritium concern for D-T operation – more concern for ITER.

Coating – Li, B, Si

Topic 4

S-C coil machine wall conditioning

- Vessel conditioning with B-on
- LHD wall limited to ≤ 100°C
- Concern of baking in ~~a~~ large machines – e.g. machine deformation (ITER, LHD)

Topic 5 PFC Engineering design

- Engineering tolerance is crucial for machine performance especially for initial operation

- For the next major device, we can run into the ~~major~~ serious problem of the inadequacy of engineering data in order to produce reliable components. (e.g. ITE divertor tiles.)

Section VII: PFM Issues and Development

[page intentionally left blank]

Design/R&D Activities of Target Structure

M.Shibui, M.Takahashi, K.Osemochi

Presented by M.Shibui

Toshiba Corporation
2-4, Suehiro, Tsurumi, Yokohama, 230 Japan

- W/Cu gradient material
  by <u>composite VPS</u> method

- Multi-layered cooling tube
  with tritium permeation resistant layer

  <u>SUS316L/Cu/W/Cu</u> trial structure

US/Japan Workshop, Warwick Regis Hotel, San Francisco,Dec.8-11,1997

M.Shibui, Toshiba Corporation

Design issues on PFCs

■ Material issues on W
- High DBTT
- Very low ductility near RT
- Expensive curved surface by brazing

⇒ Reduction of residual thermal strain
⇒ Film rather than bulk material

■ Safety issues
- (IA)SCC problem of coolant boundary
- Tritium permeation

⇒ Use of SUS316L as boundary
⇒ Use of W as permeation barrier

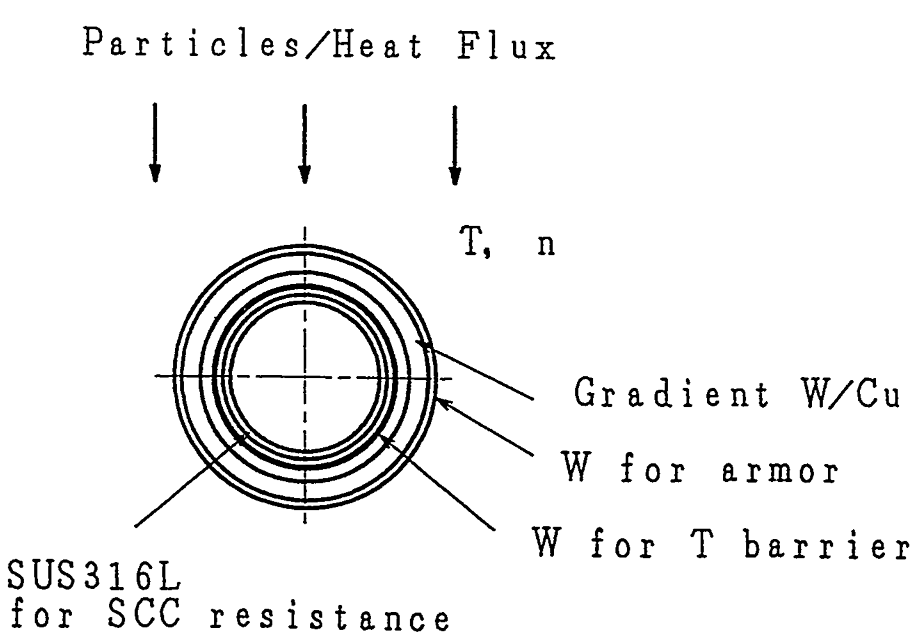

W/Cu material by composite VPS method

- Advantages

  - Composite gradient material
  - Low cost
  - Applicability to curved surface
  - Potential in-situ repairability

- Analytical prediction

- R&D of W/Cu composite VPS method

  - Deposition rate
  - Deposition efficiency of Cu powder
  - Reduction of porosity in pure W layer
  - Trial fabrication of W target

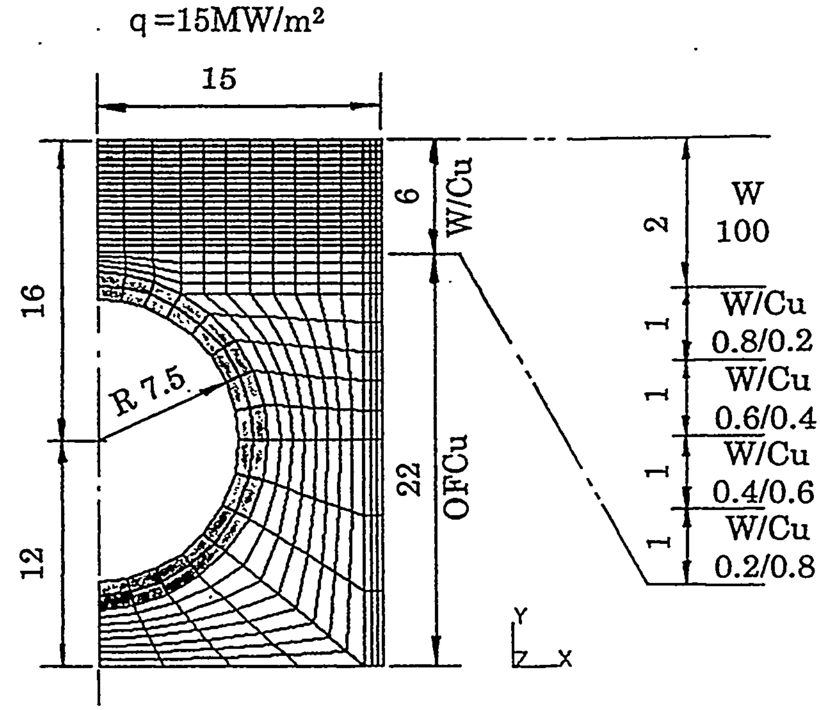

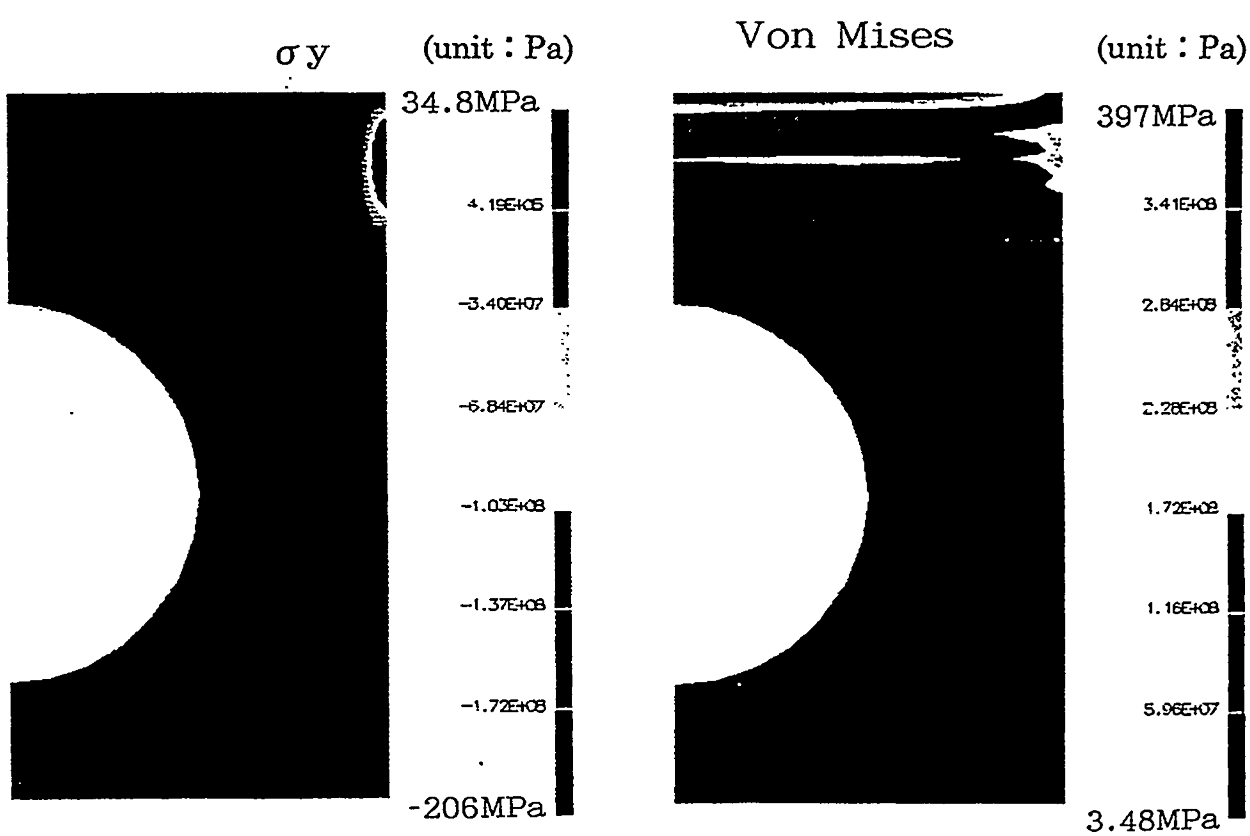

Stresses under q=15Mw/㎡

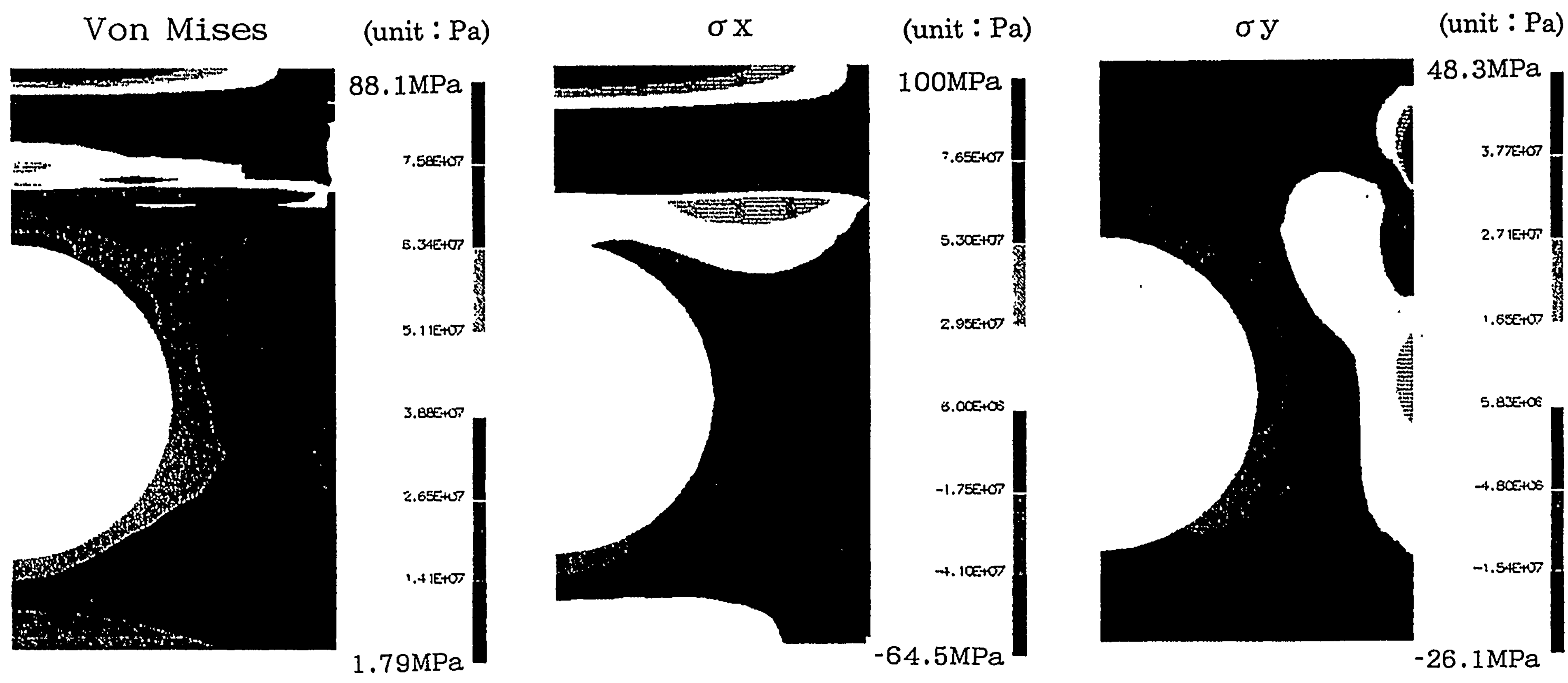

Stresses after cooldown to 150°C

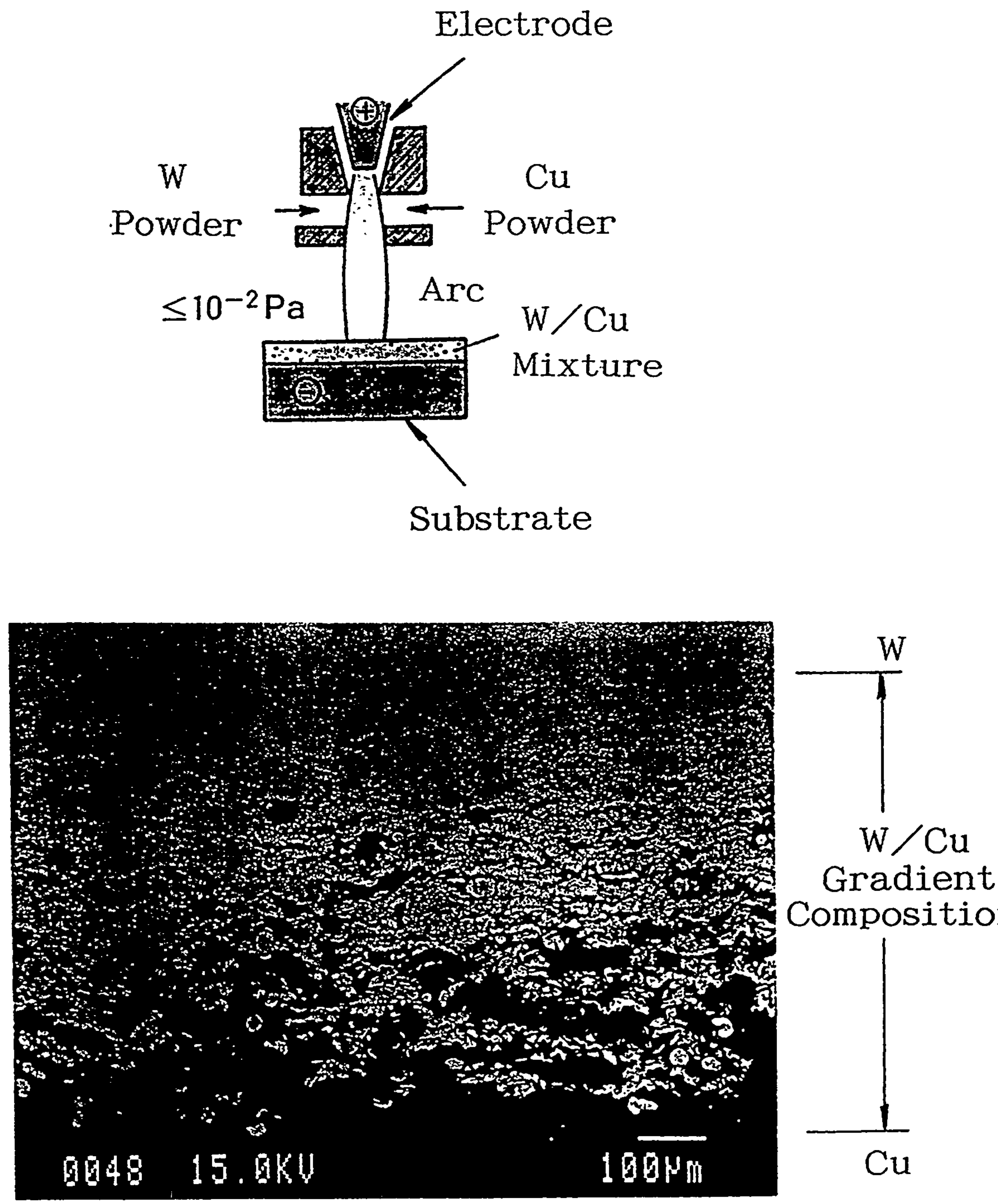

VII-8 Composition gradient W/Cu by VPS method

M.Shibui, Tishiba Corporation

VPS conditions for W/Cu composite

Atmosphere	Ar, 137 Torr
Power supply	700A - 65V
Spray distance	275 mm
Spray rate	400 mm/sec
Working gas	Ar : 25 L/min H_2 : 9 L/min
Surface preparation	Abrasive blasting

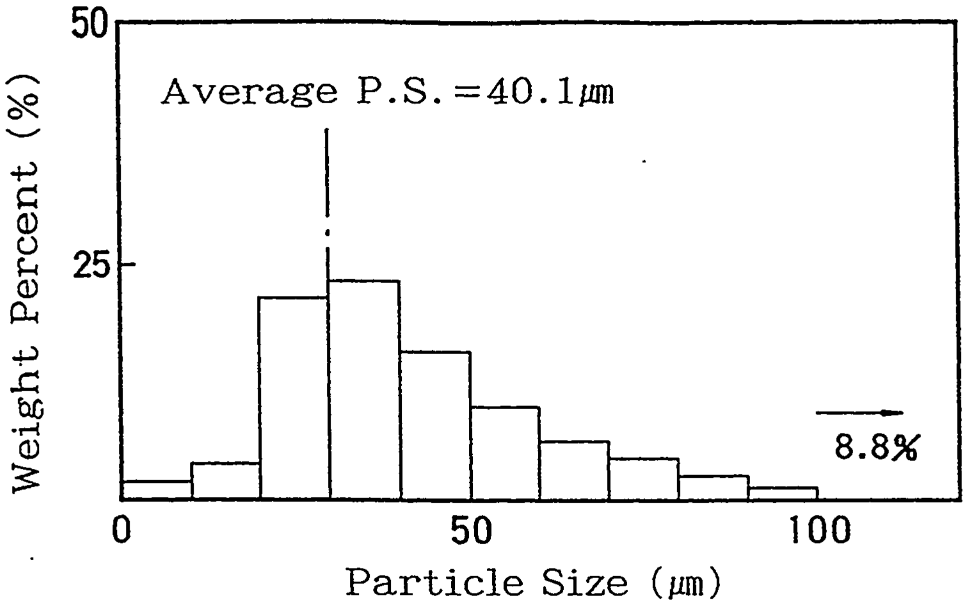

(a) W powder

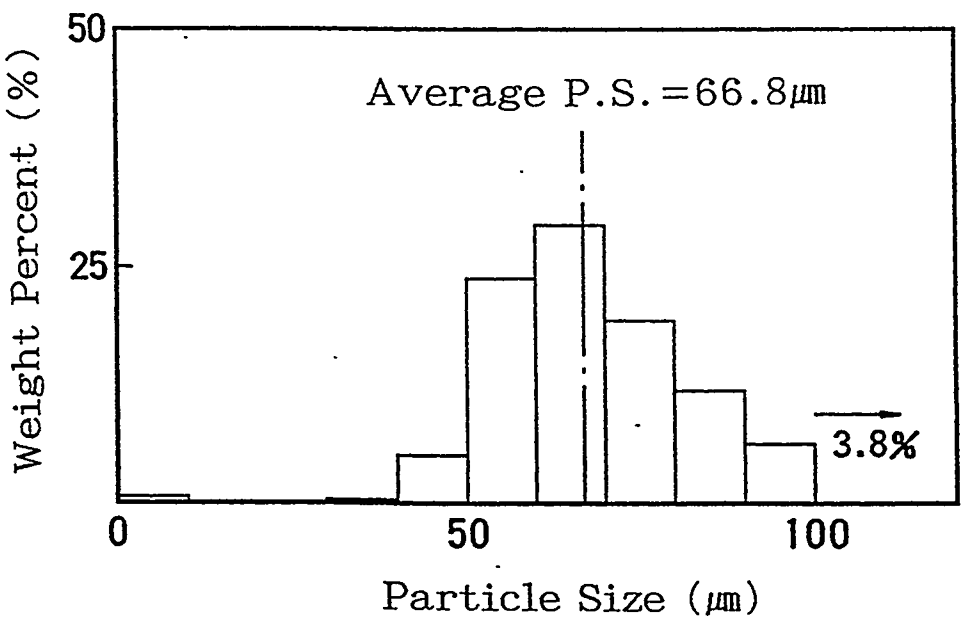

(b) Cu powder

Cu and W powder for composite spraying.

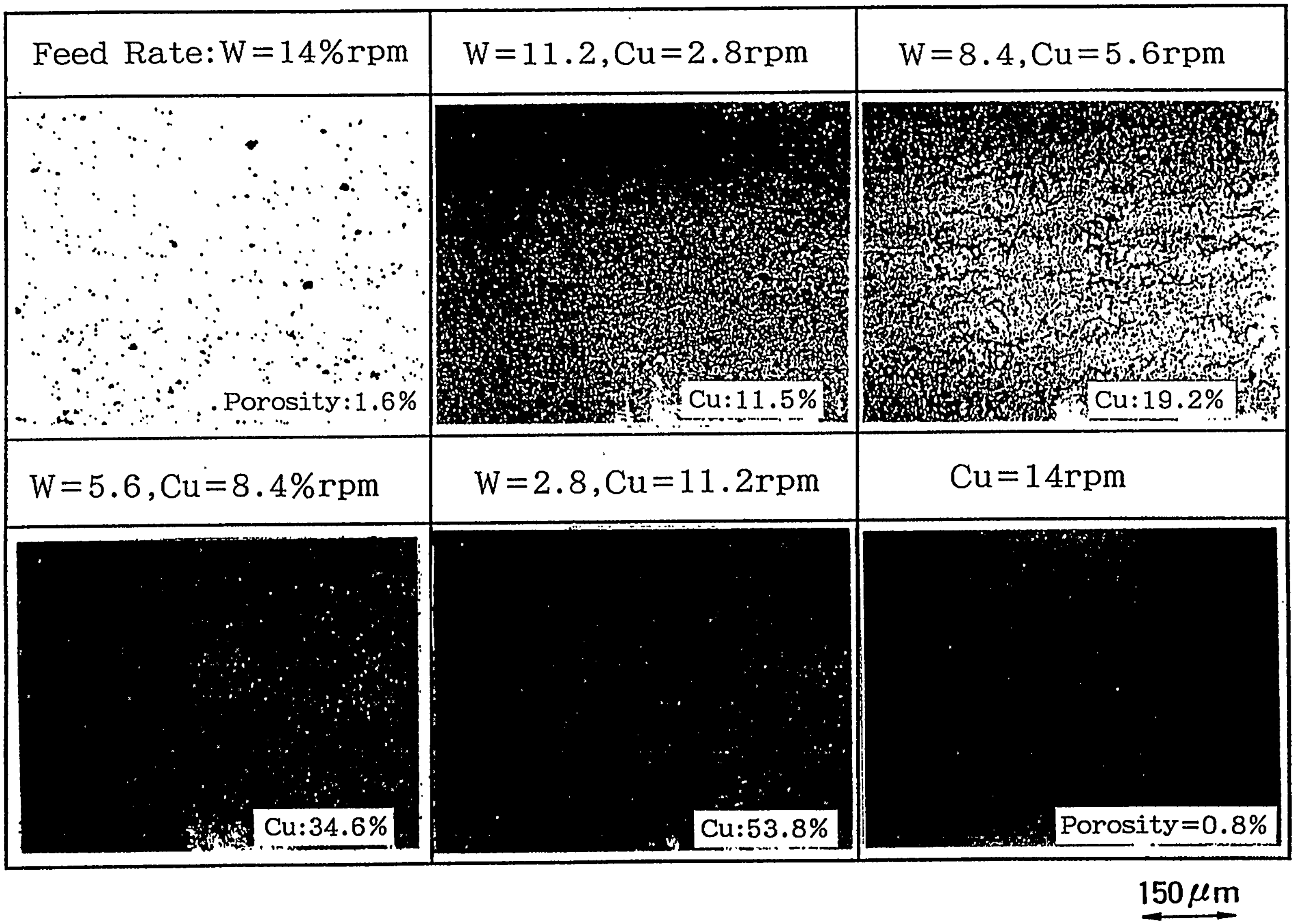

Composition gradient W/Cu material

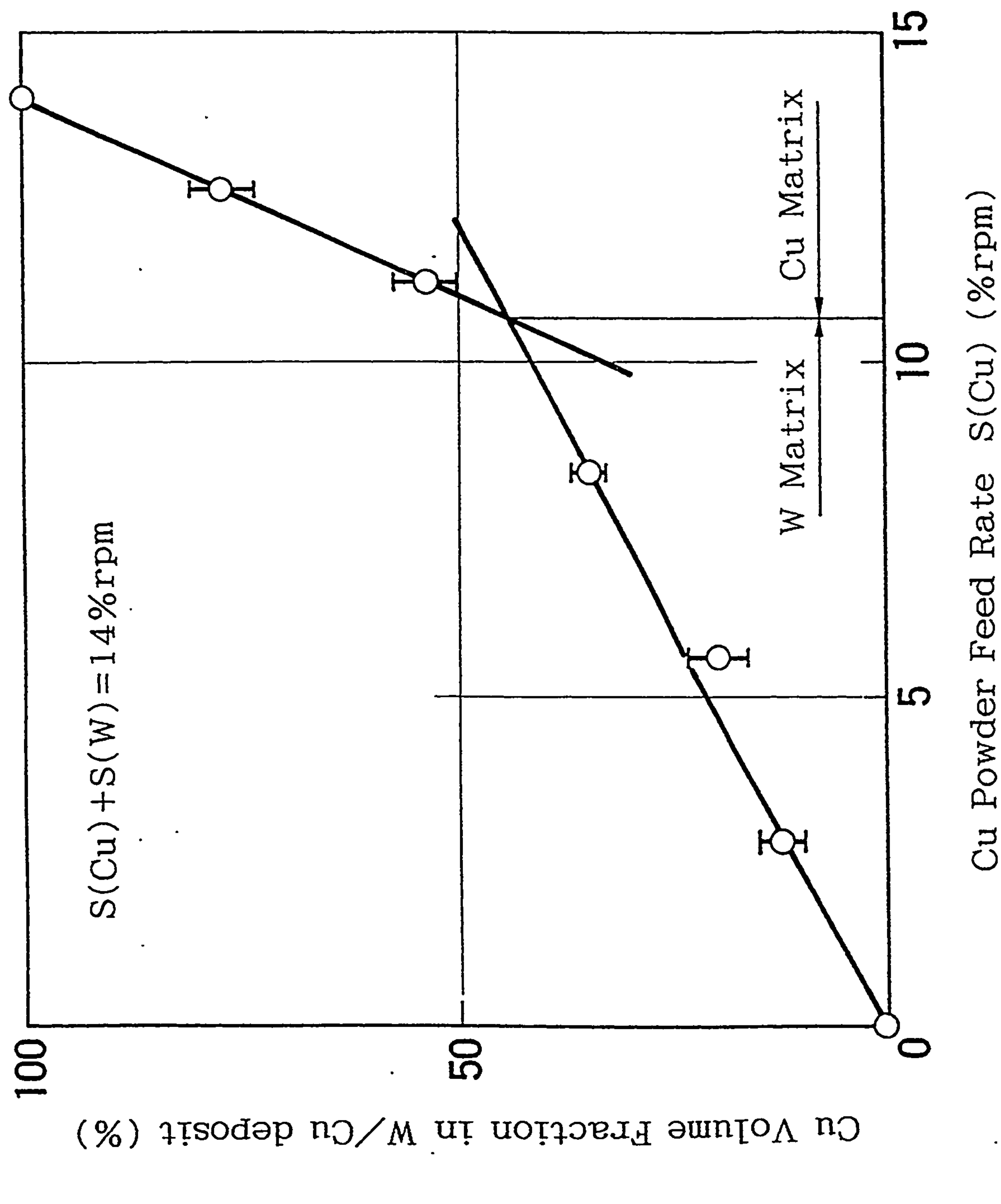

Cu deposition efficiency

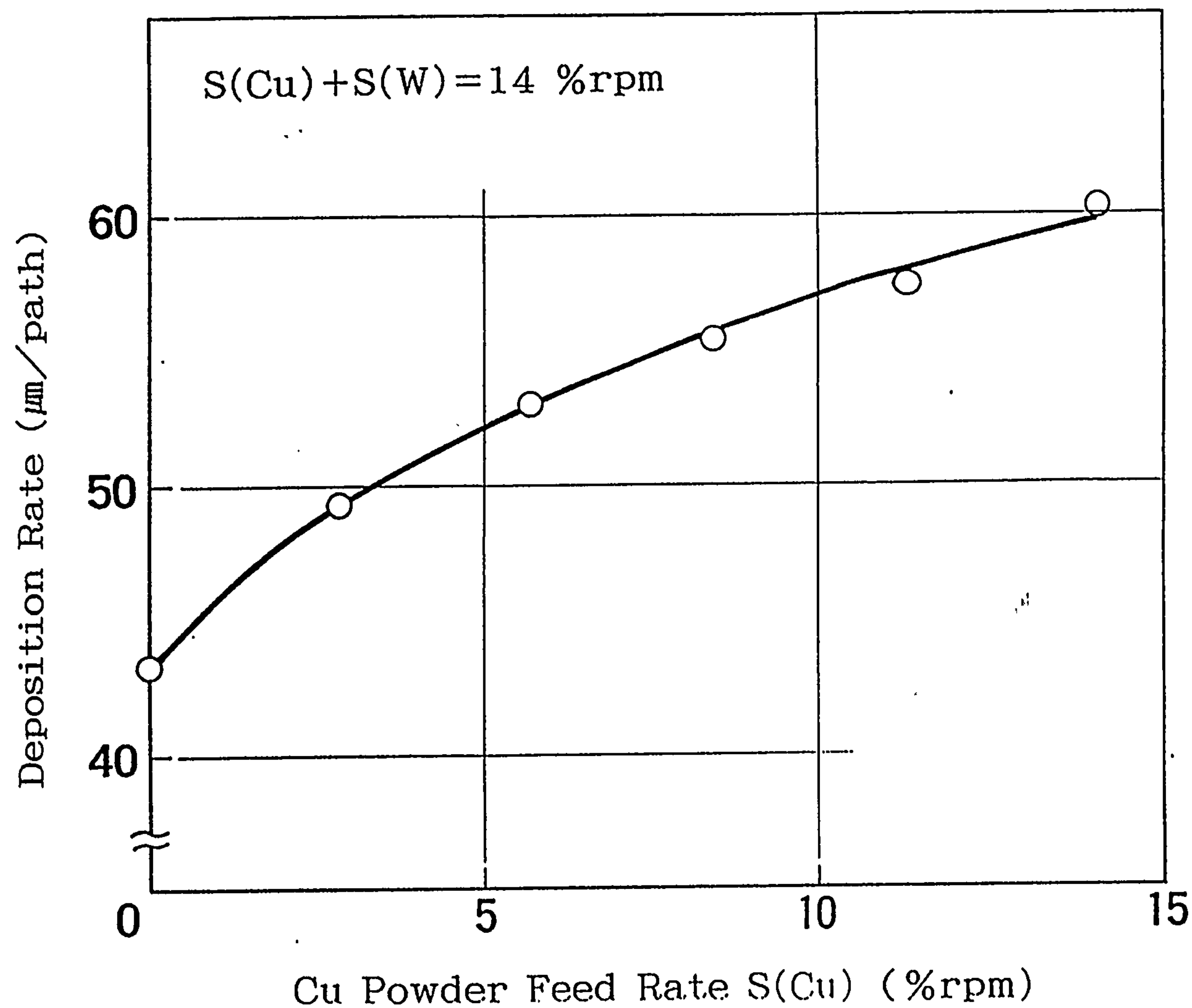

Deposition rate vs.Cu powder feed rate

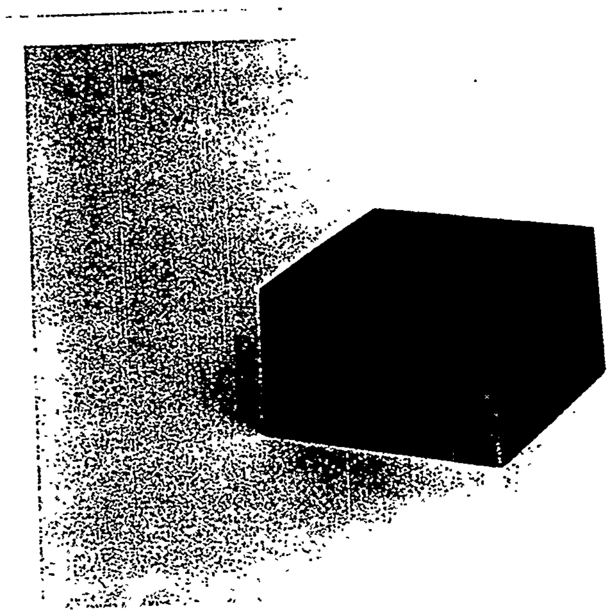

20mm

t(W)=2mm
t(W/Cu)~3mm

Trial fabrication of W target
by composite VPS method

M.Shibui, Toshiba Corporation

Development of multi-layered cooling tube

- Analytical prediction of T permeation

  - 1-D analysis without armor
  - Objective : Effective thickness of W layer

- Multi-layered structure

  - SUS316L layer for SCC resistance
  - Two W layers for T permeation resistance
  - Cu layer for heat conduction
  - 0.2tSUS316L/Cu/0.03tW/Cu/0.03tW/OFCu

Physical properties for T permeation analysis

Material	Diffusivity		Solubility	
	Do m^2/sec	Eo eV	So $mol/m^3atm^{1/2}$	Es eV
Cu	$1.1x10^{-6}$	0.4	$2.1x10^{2}$	0.37
SUS	$2.0x10^{-7}$	0.54	$1.2x10^{2}$	0.11
W	$4.1x10^{-7}$	0.39	$1.1x10^{3}$	0.98

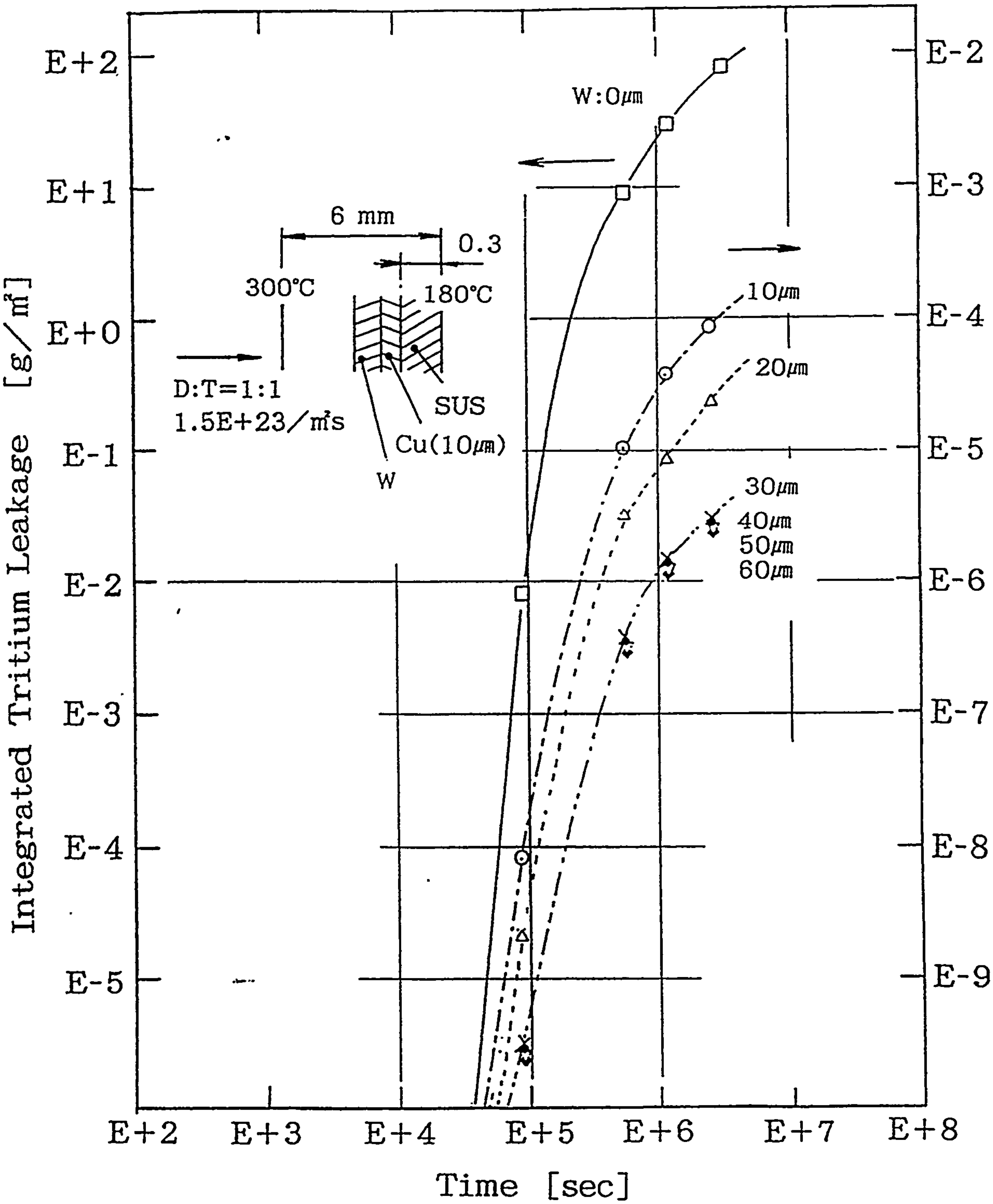

Intergated tritium leakage

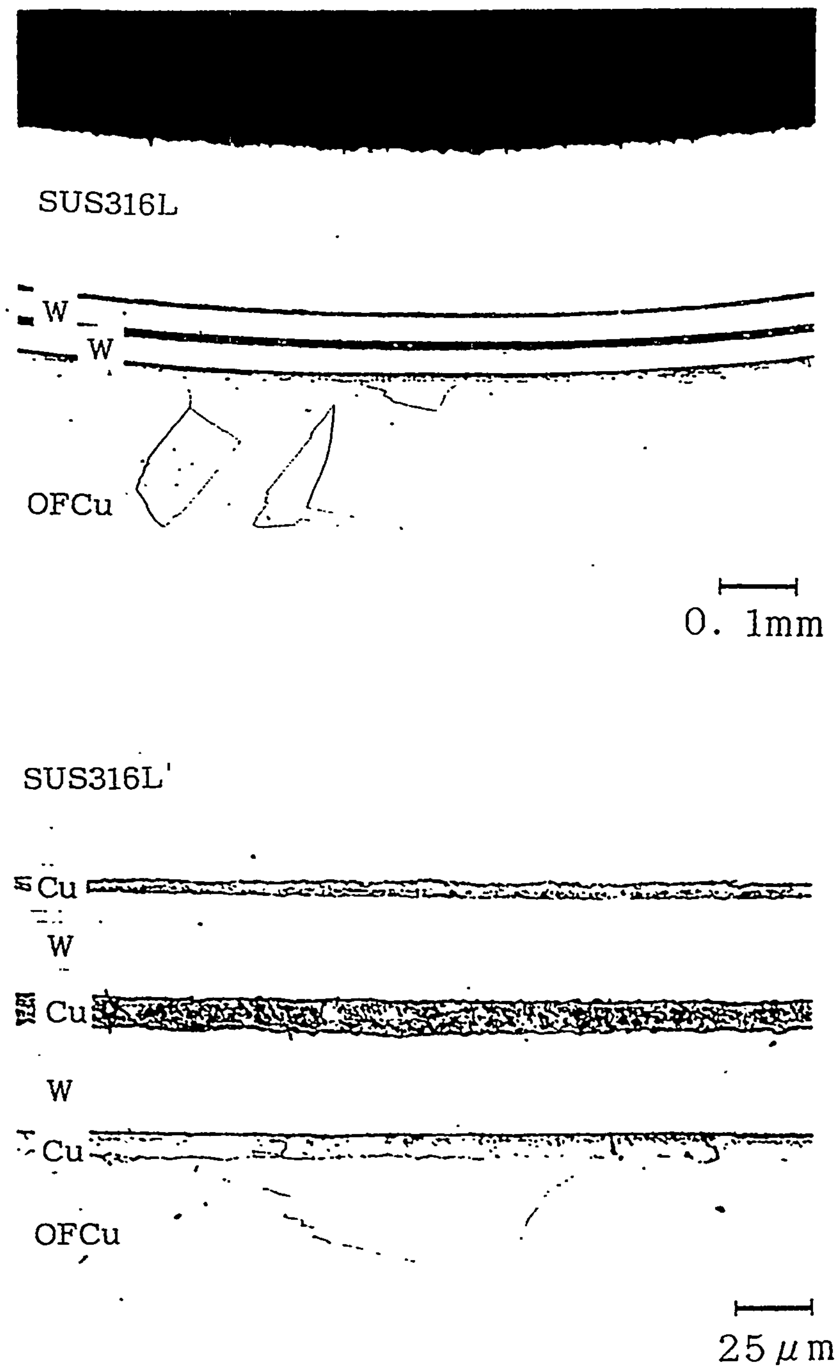

Optical micrographs of multi-layered cooling tube

Concluding remarks

1. Formation of W/Cu gradient material by the composite VPS method has been demonstrated :

   @ with sufficiently small amount of porosity in pure W layer,

   @ with easy controllability of Cu volume fraction in the deposit.

2. Multi-layered cooling tube has been proposed :

   @ with SUS316L as SCC resistant layer and

   @ W as T permeation resistant layer.

   Its fabricability has also been demonstrated by using HIP.

REVIEW OF RECENT WORK ON REMOVING TRITIUM FROM PFCs.

C H Skinner, D Mueller, A Haaz, D Cowgill, G Federici...

Princeton Plasma Physics Laboratory
Univ. Toronto
Sandia National Laboratory
ITER JCT

US-Japan Workshop, San Francisco December 8-11th, 1997

TRITIUM REMOVAL

Motivation:

- Tokamaks experience appreciable retention of tritium fuel.
- Tritium supply is limited
- In-vessel inventory is limited
- Tritium inventory control essential for fusion reactors. Steady state advantages of stellerators e.g. LHD would not result in practical fusion reactors without control of tritium inventory.
- Current retention levels are too high.
- Current removal methods are too slow and underdeveloped,

Development of highly efficient tritium removal techniques is essential for *any* DT fusion reactor.

TFTR Experience: how much tritium was retained and where?

Summary of 3 run periods over 3.5 years in TFTR:

Total tritium injected (NBI+puff)	5 g
Total tritium retained in torus during run periods	2.5 g
Total tritium removed from torus in clean up months	1.7 g

Deuterium Measurements:

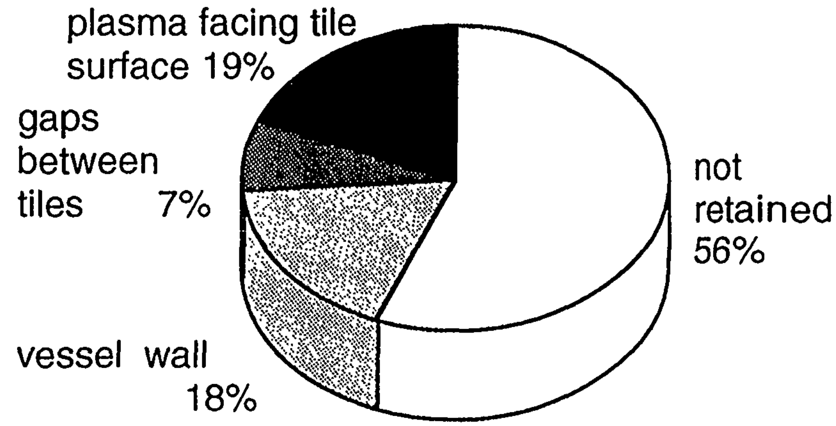

Tritium Analysis currently in progress:

- 10 Tritiated tiles, removed 9/97; to be shipped to Idaho State for nuclear elastic recoil analysis of H, D and T concentration vs. depth (range 15-40 μ) Experiments planned at PPPL for tritium release by air baking.
- Dust vacuumed into filter housings and removed from diagnostic windows. Presently at INEL for particle size and BET analysis.
- Samples scraped from limiter surface at LANL for thermal outgassing of the tritium for total content and temperature of release.

ITER FUEL CYCLE

Fuel per 1,000 s pulse (270 g) = 1/10th of annual supply !

Tritium Retention experienced by:

TFTR -	≈ 2.5 / 5 g
JET DTE1	≈ 4 g / 11 g
JT60 (exhaust)	70-90%
JT-60 (tiles)	10% wall,
"	40% divertor
DIII-D (tiles)	10-20%

CFTSIM - ITER dynamic fuel model

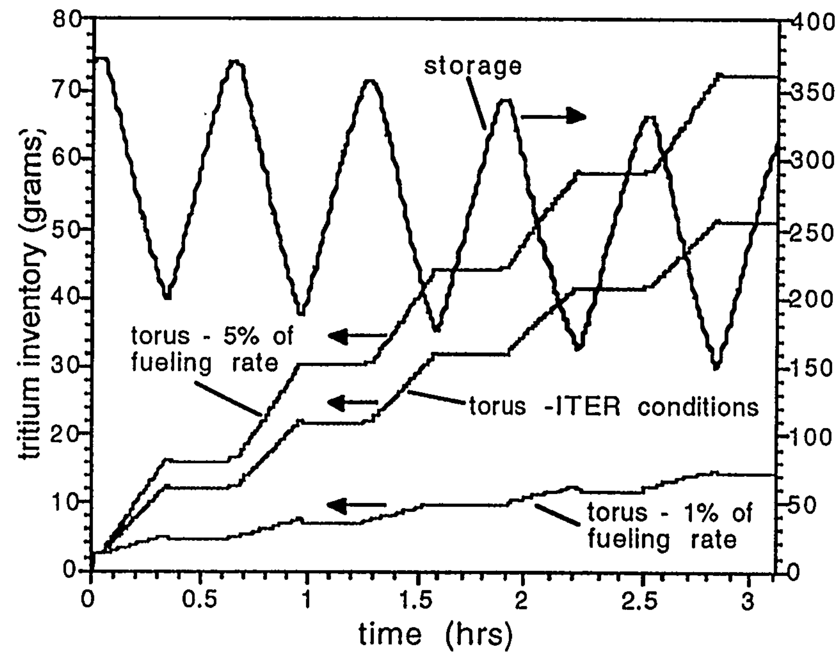

Fig. 3. ITER tritium inventories

Sugihara et al. EPS '97 Kuan et al. SOFE '97

<u>CFTSIM - ITER dynamic fuel model</u>

Assumes ITER retention 1-5% !

- lower % than present tokamaks

Consistent with co-deposition rates predicted by Brooks.

Urgent need to develop ways to reduce retention and remove tritium !

PPPL

Modeling ITER T Removal

CFTSIM - ITER model applied
to tritium removal.

Kuan et al. SOFE '97

Time available for removal:
≈ 1/1,000 of present tokamaks.

Desired removal rate in
nm/s range (or microns / hour)

Measured HeO glow removal rates:

Laboratory	0.064 nm/s
TFTR	0.004 nm/s

CFTSIM - ITER dynamic fuel model

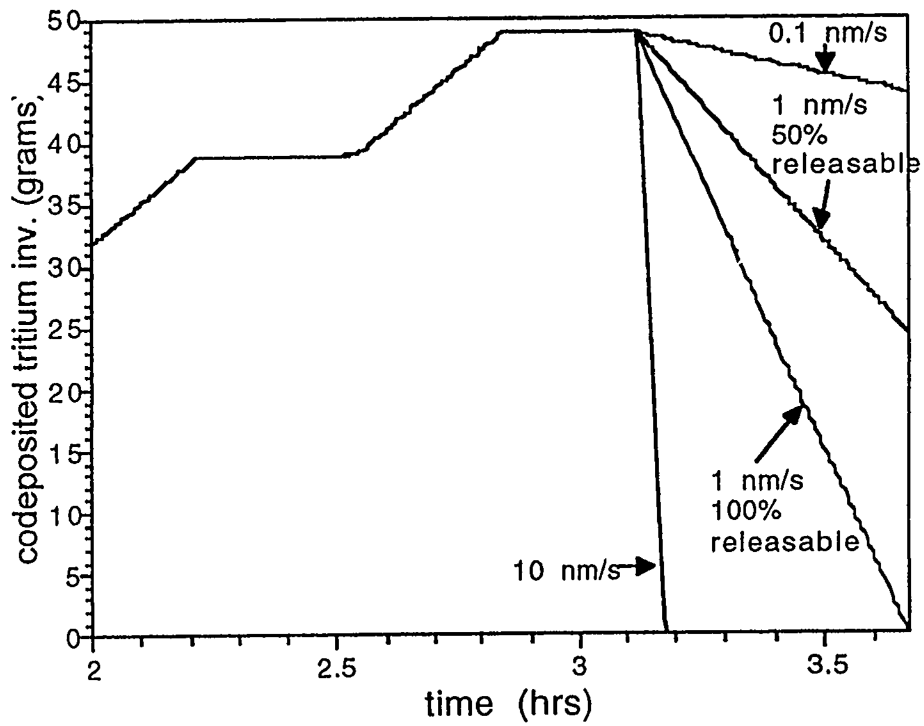

Fig. 4. Release of codeposited tritium

Comparison of tritium removal techniques, (1995)

TFTR

He-GDC, outgas, D soak	Ineffective
D-GDC	Initial removal rate high (>170 Ci/hour), declining to 10 Ci/hour. Accesses only tritium on surfaces exposed to discharge.
HeO-GDC	Rate ≈ 50Ci/hour - constant with time
room air	2,086 Ci removed, access to all surfaces
Disruptions	Flash heating of limiter surface near midplane. - Release of recently retained tritium.
Pulse discharge cleaning	Heats limiter to 250° C. 956 Ci removed over 23 hours.
Boronization	Little tritium released, most near surface tritium already removed.

Removal by D and HeO glow discharge (GDC)

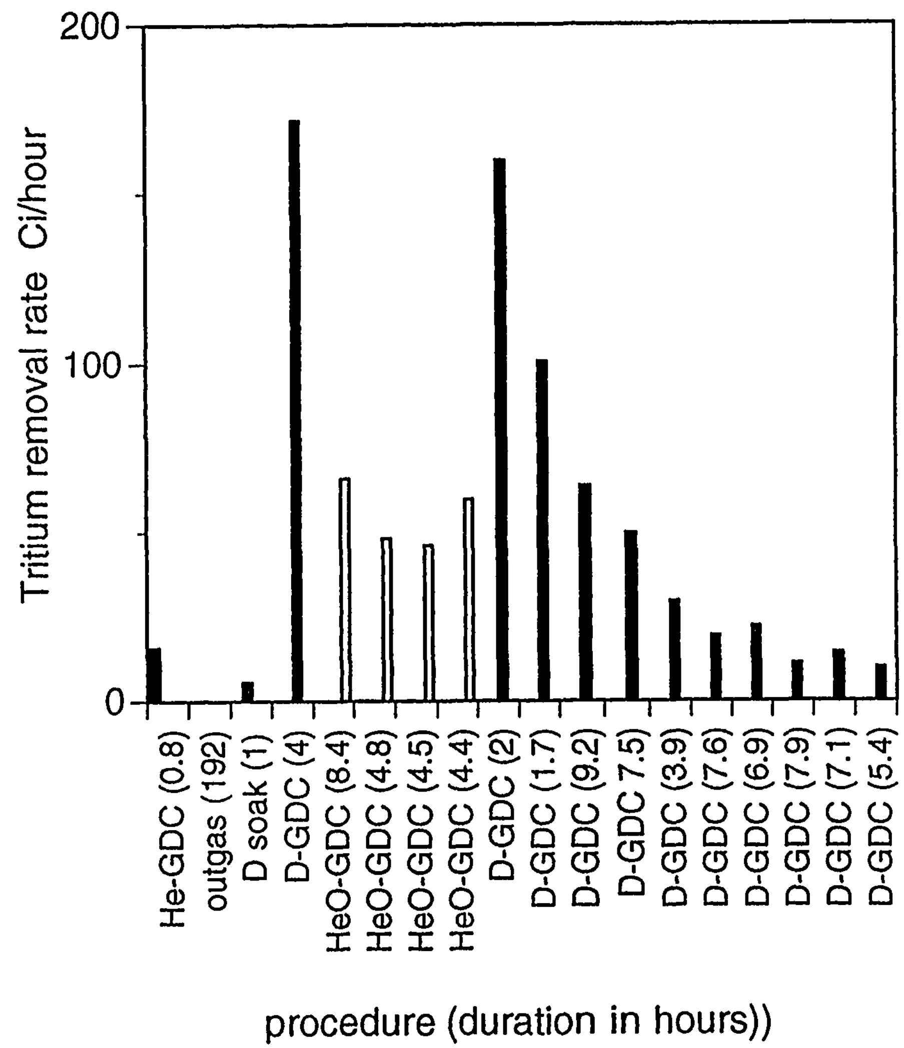

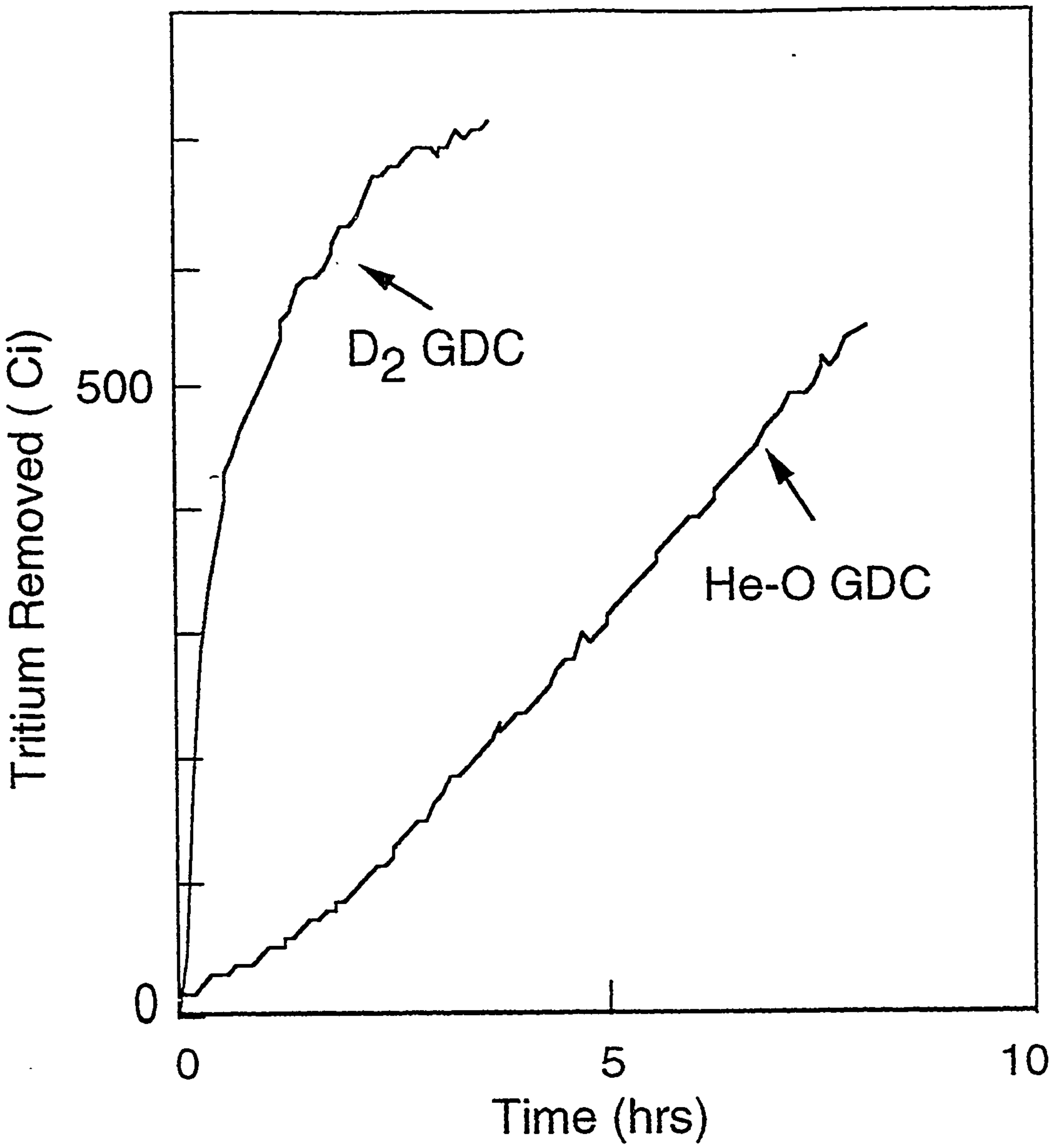

D2 GDC
He-O GDC
500
0
Tritium Removed (Ci)
0
5
10
Time (hrs)

Short term tritium retention high with strong tritium puffs

TFTR

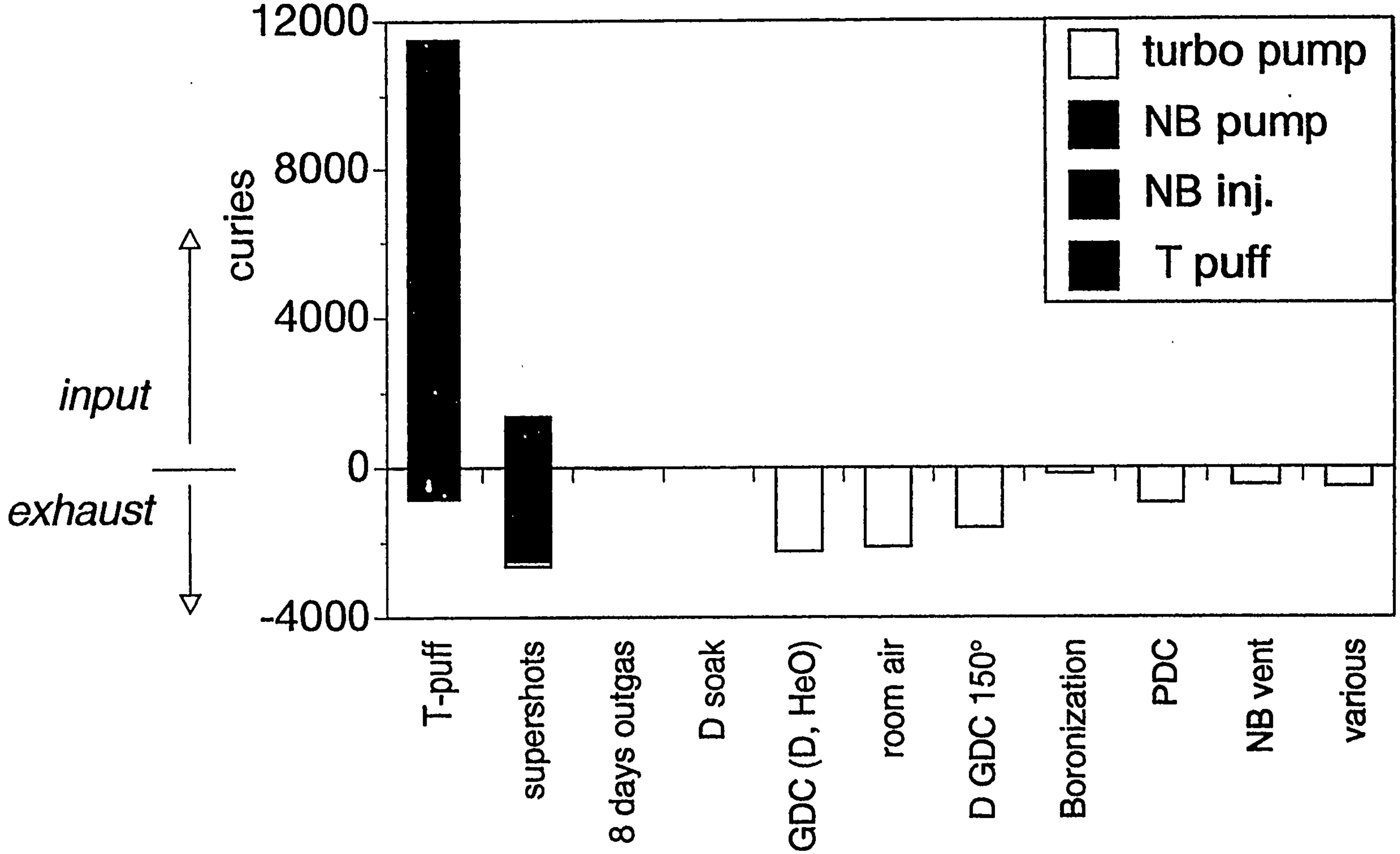

Tritium fraction maximized for L-mode study, (September 1995)
Short term retention >90%

Tritium successfully removed by combination of glow discharge (D and HeO), room air, and pulsed discharges.

Tritium removal for 1996 in-vessel maintenance.

TFTR

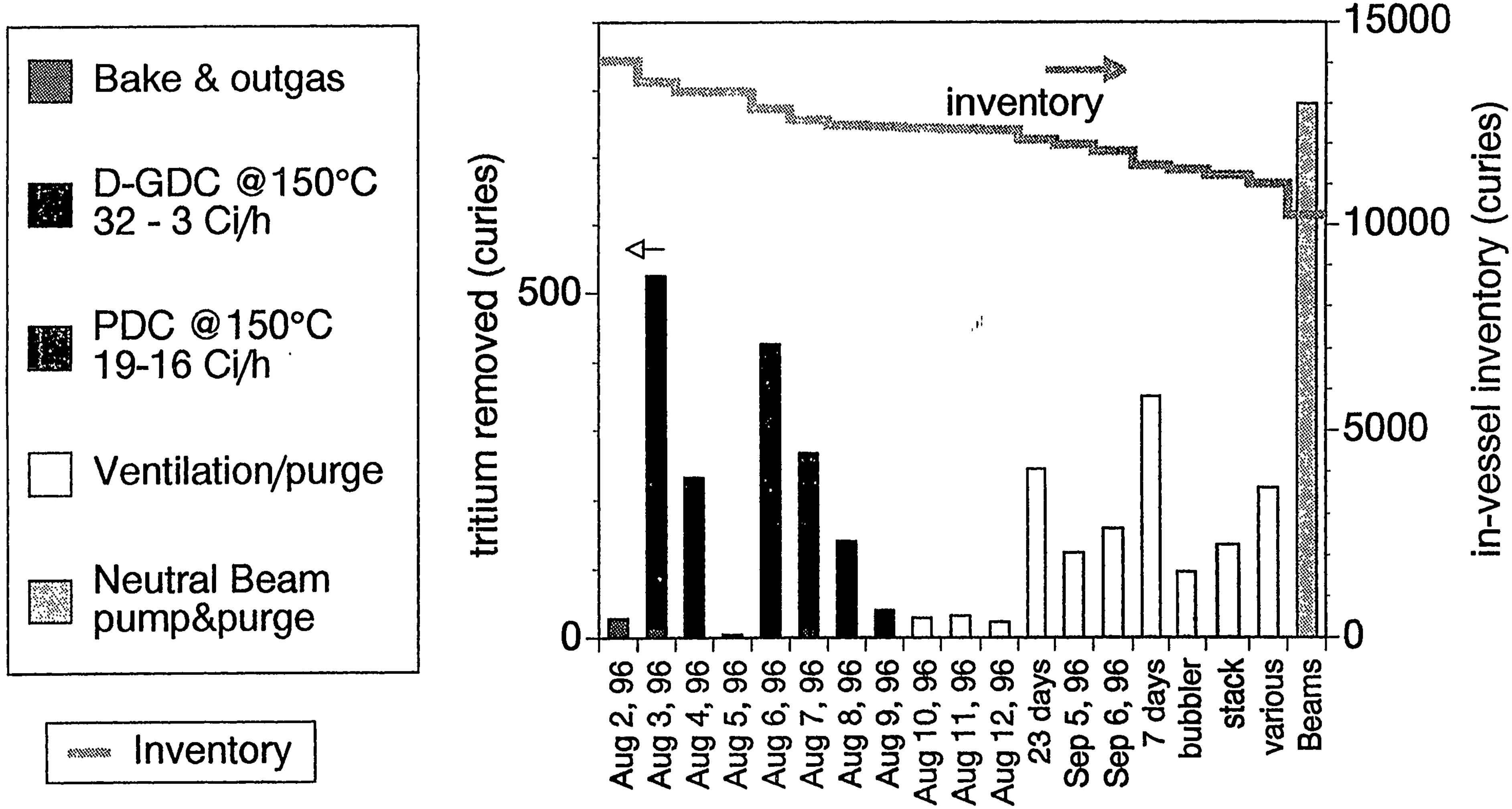

Personnel radiation exposure mostly from activation, not from tritium.

Vacuum Vessel Tritium Recovery April 4 through May 8, 1997

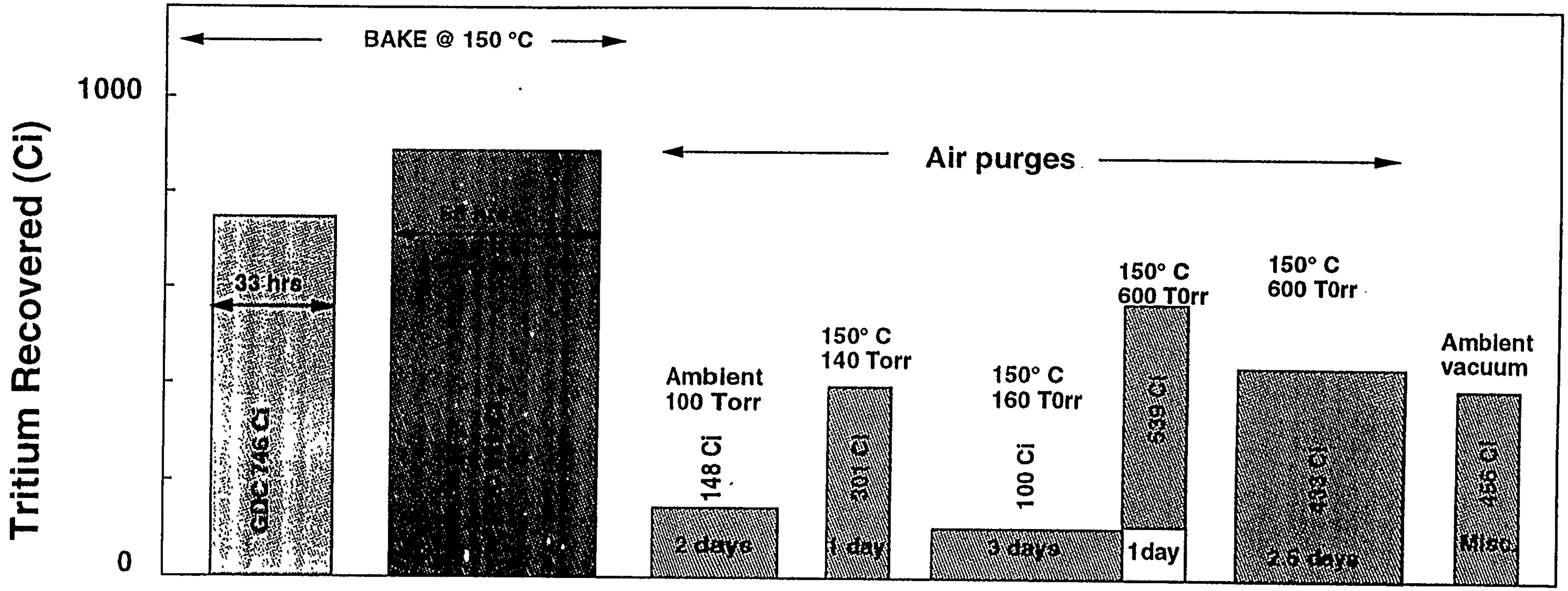

- During air purges, after about 1/2 day following temperatue or pressure change, no change was observed in the tritium content of the air in the vacuum vessel.
- Misc. refers to the sum of tritium removed between the various removal tactics. Mostly this is from outgassing of the vessel and various pumping appendages.
- In addition 331 Ci were recovered from the neutral beams during this period.
- In total 4279 Ci were removed from the neutral beams up until August 14 mainly by purging them with air.

SUMMARY OF TFTR EXPERIENCE

TFTR is the first tokamak with extensive tritium experience
(≈1,000 DT discharges over 3.5 years).

TFTR high power phase is ≈ 1 s, so total DT duration is ≈1,000 s
≈ 1 ITER 1,000s pulse

In TFTR: of 5 g tritium fuel, 2.5 g was retained, and 1.7 g removed
in 3 campaigns over ≈ 3 months.

ITER Physics and Technology program requires a duty cycle ≈ 1 - 10%
(compared to ≈ 10^{-4} for TFTR)
(future DT Reactor availability required is: ≈ 50%)

Much faster tritium removal required for ITER to fulfil its Physics and Technology goals.

TEN REMOVAL METHODS CONSIDERED FOR ITER.

Adapted from Figure 3 in "Tritium Inventory in ITER PFC's, Predictions, Uncertainties, R&D Status and Priority Needs"; International Symposium on Fusion Nuclear Technology, Tokyo April 6-11, 1997. Paper L164 G. Federici, et al.,

Identified Options	Merits	Shortcomings
Glow Discharge Cleaning	• well established tokamak practice • does not require vent or opening of the vacuum vessel	• TF off, long shut-down • limited access to shadowed areas • HeO glow discharge requires active conditioning to remove residual O. • low removal efficiency for ITER (even with O as a min. species)
D_2 soaking with heated walls	• some tokamak experience	• low removal efficiency
Air/ O_2 exposure with hot walls.	• expected good removal efficiency ≥50% and short cleaning time at wall temperature T'~250°C) • accessibility of non-line-of-sight and shadowed regions, gaps, etc. • mechanisms of removal are reasonably well understood. • may oxidise Be dust and may reduce its chemical reactivity with steam in case of an accident.	• need venting; • ratcheting effects could limit cleaning at 240°C (max temp. in ITER) • wall conditioning is required for decontamination of residual O and H_2O. • very limited tokamak practice and at too low wall temperature (TFTR) • removal of T from thick deposits and mixed materials requires R&D.

Recent Results......

EROSION OF CODEPOSITED FILMS VIA OXYGEN EXPOSURE

A.A. Haaz and J W Davis, University of Toronto; R Causey, Sandia; Jacob et al, Garching

Laboratory produced a-C:H and aC-D Films
20nm - 2 μm thick, at 200 - 350°C in low pressure O_2 or air.

Erosion rates: 2nm/hour - 50 nm / hour - *too low.*

Co-deposits from tokamaks:

- Causey et al [Sandia]
  TFTR tile: ~ 50 μm thick [H/C ~ 0.4] heated in air [760 Torr] at 350°C
  erosion ~ 50 μm/h [metals: < 0.2 at%; Mills et al]

- Jacob et al [Garching]
  ASDEX-U tile: ~ 750 nm film [D/C ~ 0.4] heated in air [760 Torr]
  at 380°C erosion ~ 0.3 μm/h [presence of B on the layer]

Erosion rates differ by two orders of magnitude !
The structure [and impurity type and content] of the codeposits from the two machines are different.

NEW RESULTS

[Haasz and Davis; US-HT/JCT Meeting on T inventory and Control in ITER PFCs [Pittsburgh, PA, 97 Nov16-17]

TFTR tile [POCO graphite] removed from machine in 1987, thickness:
~ 30 μm [D/C ~ 0.35], effective density: ~ 320 kg/m3
Exposure to oxygen, pressure: 16 Torr, temperature: 250°C, 300°C, and 350°C

J. Nucl. Mater. 343, 162 (1989)

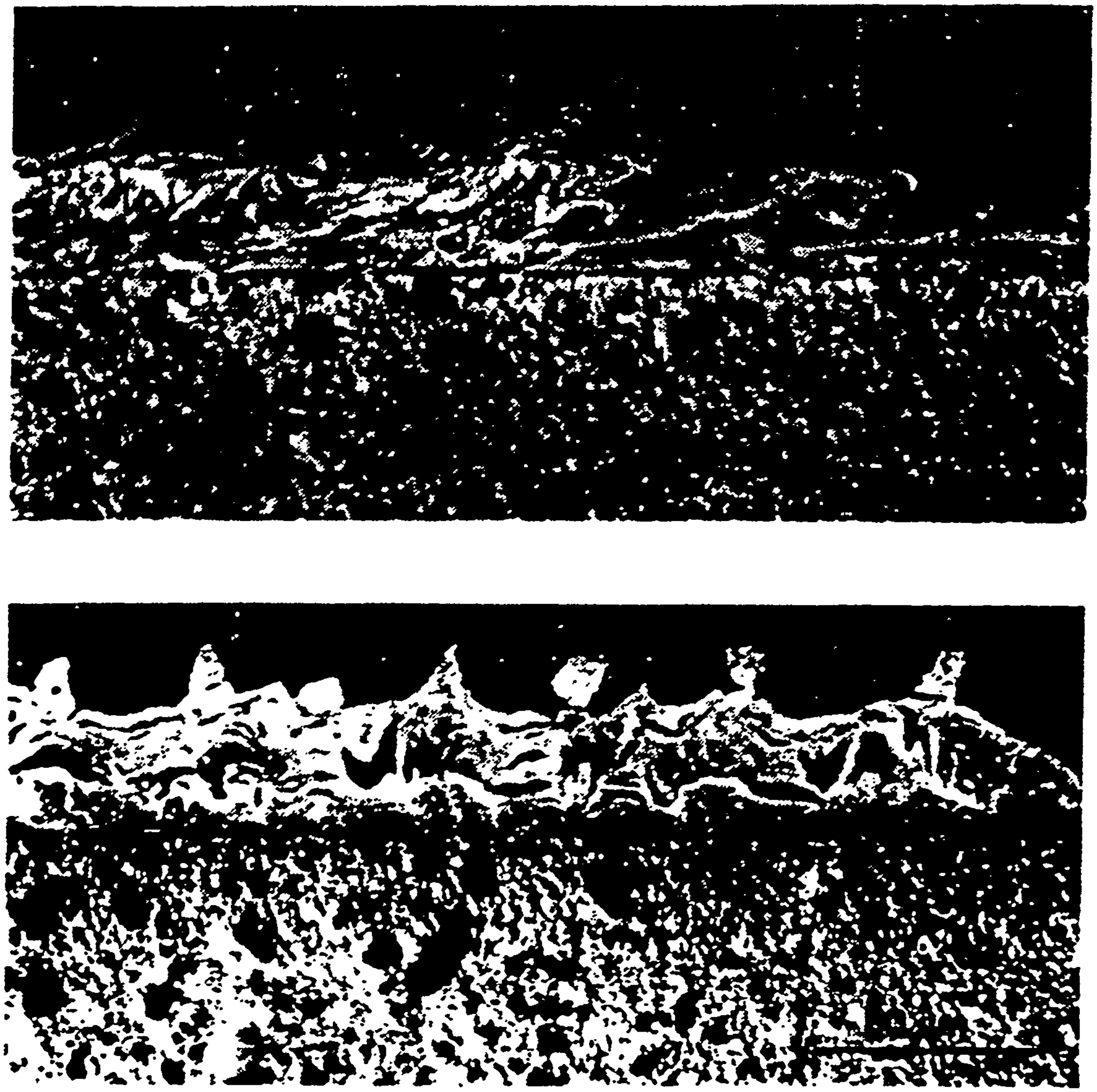

Fig. 5. Poloidal (top) and toroidal (bottom) cross-sections of the plasma-facing surface of a bumper limiter tile in the moderate deposition region, the surface of which is seen in figure 4C.

Counts (arbitrary units)

ncentration

Not off the shelf graphite but C layers codeposited & eroded
by plasma + radiated by neutron flux.
Bernice Mills Lab 80's
Hassanein ~~poster~~ talk on codeposition

QeddP_T Nov. 13,1997 9:00:21 AM

TFTR Codeposit (~30 μm)

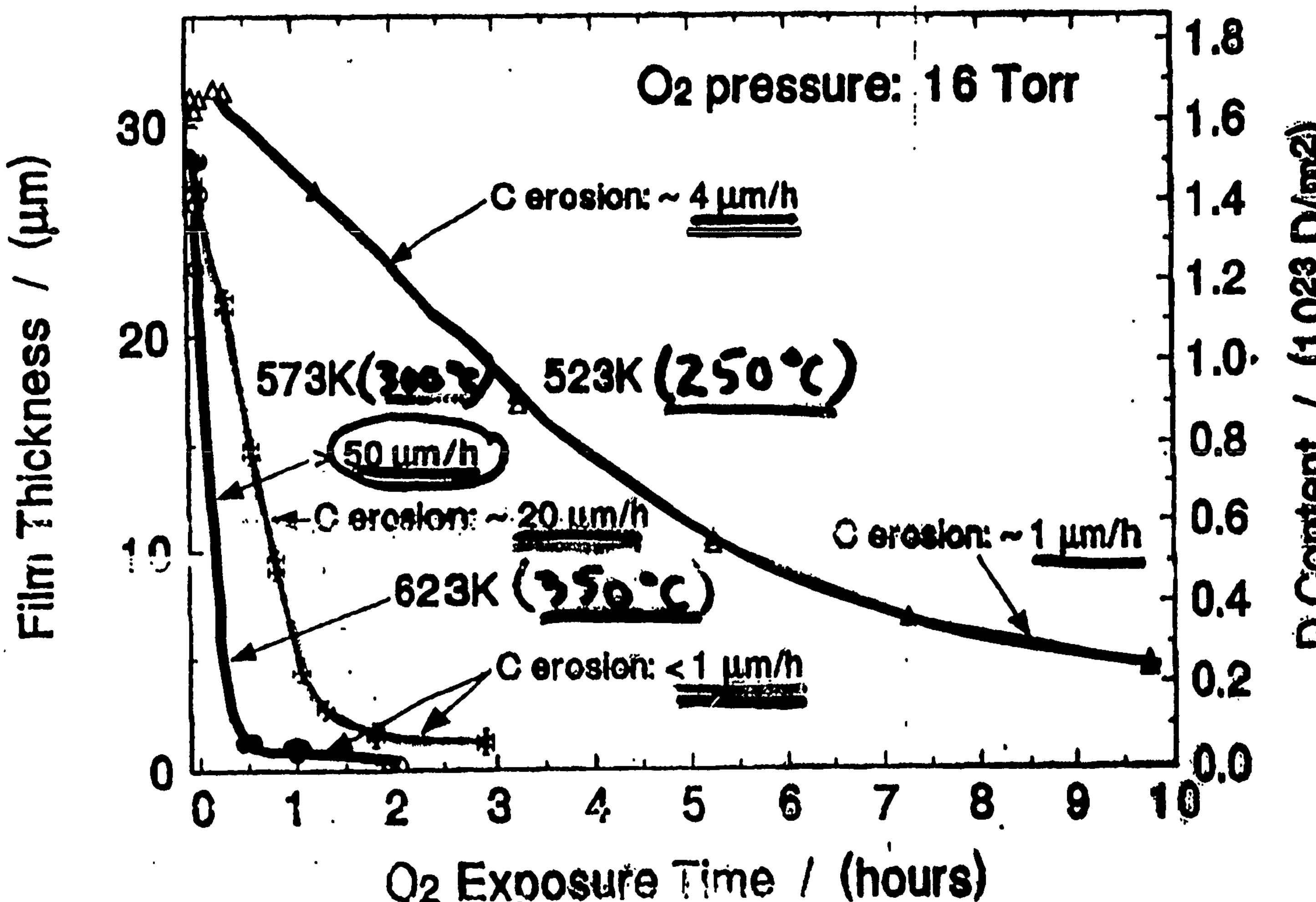

Haasz and Davis Figure 3

Rapid erosion of co-deposits - but not substr

Identified Options	Merits	Shortcomings
Hot Xe/ O_2 (or N_2O), with Xe >> O_2 (or N_2O to minimise O contamination	• enhanced impact-induced conditioning by using Xe to increase momentum transfer. • using N_2O, rather than O2, should increase surface oxidation of codeposited layers and reduce O-contamination.	• more study is needed.
Reaction with gaseous radicals (e.g., O_3)	• efficient. • works at ambient temperature and with TF on.	• short path length before decomposition • conditioning may be needed afterward to remove non-volatile products.
Isotope exchange with D plasmas.	• no change in magnetisation needed • no opening of the vacuum vessel • no solid waste • gaseous residue could be processed by the existing fuel cleanup system	• some conditioning may be needed to re-establish fuel recycling rates to the plasma • R&D needed to establish feasibility and quantify process.
Abrasive methods such as CO_2 blasting, LN_2 jets	• high expected removal efficiency (short cleaning time). • may induce flaking and ease collection at the bottom of the divertor through venting , pump-out of debris. • tokamak application: used for beryllium cleaning in JET • know-how available from other industrial applications (e.g., paint removal/ cleaning and decontamination of surfaces) • some limited R&D for ITER is in progress in the US.	• TF off, needs opening to allow access to equipment; long shut-down, RH intervention • production of debris or residual waste; ventilation required for debris removal, but no abrasives in waste stream • needs line-of-sight to surfaces to be cleaned. • no or limited access in gaps, limited access in remote areas • requires some R&D to extrapolate with confidence to ITER

Identified Options	Merits	Shortcomings
Collection of flakes spalled from the plenum into the bottom of the divertor cassette and outgassing by heating	• in situ method • tritium evolved can be simply handled by the existing gas recycling system • no interference with the pulse duty cycle • minimal ancillary equipment required • may be a major deposition site • JET is assessing technical feasibility	• some modification to the cassette design likely • experiments may suggest ways to maximise spallation rate
ICRC (direct ion resonance)	• does not require vent or opening of the vacuum vessel • no conditioning requirements • some limited R&D for ITER is in progress in the US • some tokamak conditioning experience (TEXTOR, TORE Supra)	• *erosion is line-of-sight. Shadowed areas are not eroded* • expected to be slow • requires active conditioning to remove residual O. • may be difficult to get long wavelength RF into the divertor. • requires significant R&D.
Surface heating to 2000°C with continuous wave CO_2 laser	• no solid waste • gaseous residue could be processed by the existing fuel cleanup system	• R&D needed to establish feasibility and quantify process.

TRITIUM REMOVAL BY LASER HEATING

- In vacuum, temp. > 1,000 K releases tritium over time scale of 30 minutes (Causey) but heating ITER vessel to 1000 K is impractical.
- Heating to >≈2,000 K by nanosecond laser pulse releases surface tritium (Terrault).
- Transient surface heating by a scanning CO_2 or Nd:Yag laser could release tritium in co-deposits without the severe engineering difficulties of bulk heating of the vessel.
- A ≈ 3 kw/cm^2 flux with a exposure time of order 10 ms will heat a 50 micron co-deposited layer to 1,000-2,000 K.
- Substantial amounts of co-deposited tritium may be potentially removed by laser surface heating in an overnight cleanup.
- Improved wall conditioning may be a significant side benefit.
- Experimental validation is required.

ref: Tritium Removal by CO_2 Laser Heating
C. H. Skinner, H. Kugel, D. Mueller, B. L. Doyle, and W. R. Wampler
Proceedings of the 17th IEEE/NPSS Symposium on Fusion Engineering
San Diego, October 6-10, 1997. PPPL Report # PPPL-3273 (Nov. 1997)

Temperature vs. time at different depths into pyrolitic perp. under 3,000 w/cm2 for 20 ms.

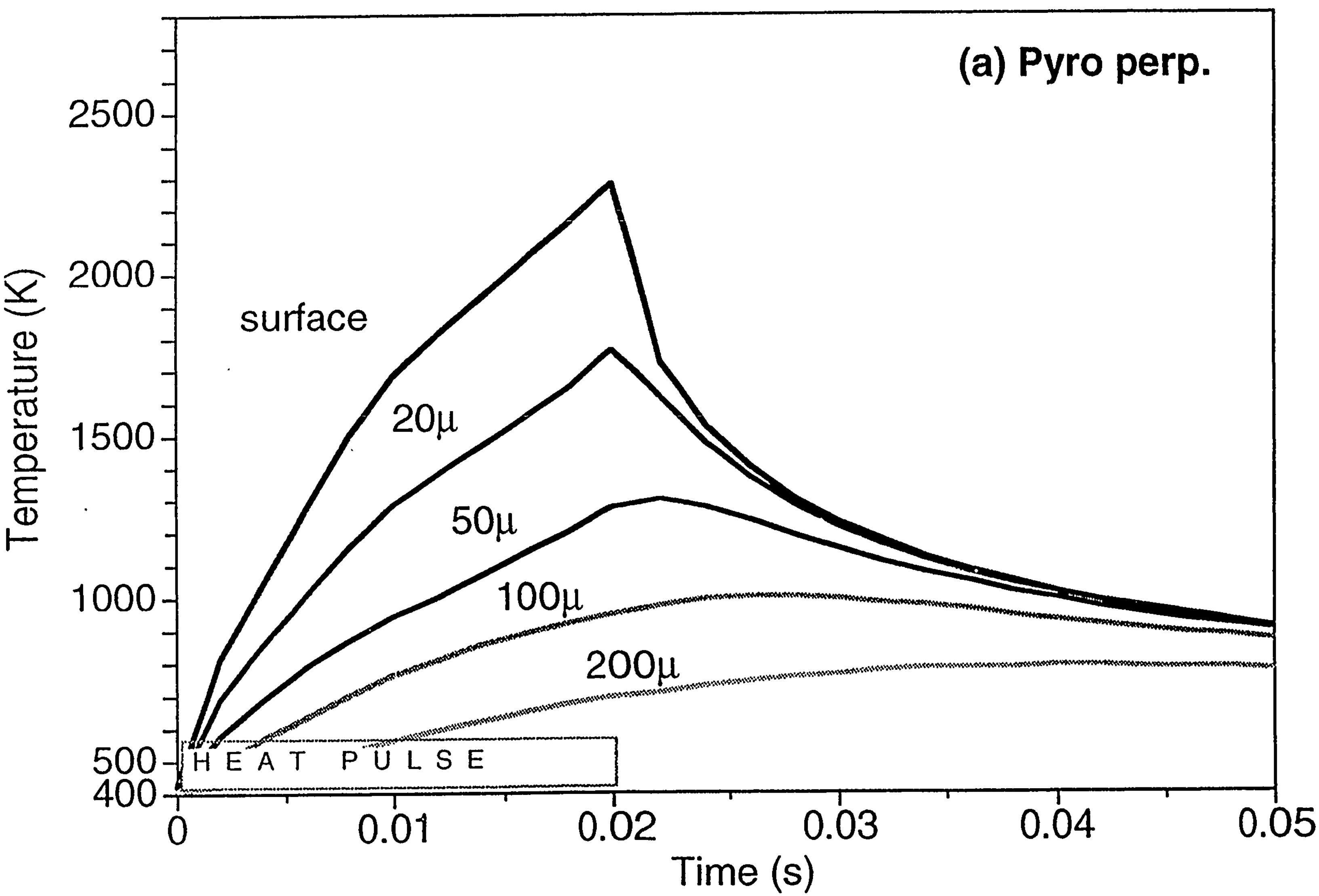

from numerical heat code HEAT1DS by M. Ulrickson

FUTURE ?

Need much lower retention than present tokamaks:

- More global physics understanding:
  Need more in-situ, time dependent measurements e.g. DiMES, QCO's...
  - relative contribution of startup, termination, long pulses, high power, attached/detached regimes, disruptions..... to compare to modeling.
- Need global models that combine PSI database, plasma codes, local co-deposition codes and tokamak geometry, *- benchmarked with tokamak measurements*.

Need much faster tritium removal than current techniques.

- Time available for removal is ~ 1/1,000 of present tokamaks.
- Global T removal from all surfaces would effectively double erosion rate and reduce divertor lifetime - need directed removal of co-deposits.
- Issues serious enough to warrant a dedicated tokamak program ?
  - can one confidently model co-deposition during disruptions ?
- Need to justify research on basis of 'dual use' with relevance to advanced tokamaks (ST) and alternates (stellarators).

PPPL

VII-40

Chemical Compatibility of Carbon with Beryllium

HRC
Toyama University

Kan ASHIDA and Kuniaki WATANABE

Hydrogen Isotope Res. Center
Toyama University
Gofuku 3190
Toyama 930
JAPAN

I. Background:

HRC
Toyama University

Use of two or more components as Plasma Facing Materials caused the Formation of Mixed Plasma Facing Materials (MPFM) due to...

1. Erosion (sublimation, etc.)
2. Chemical Sputtering
3. Physical Sputtering

II. Objectives:

HRC
Toyama University

To understand...

1. physical/chemical properties of MPFM
2. changes in the chemical states of MPFM due to solid state reactions
3. changes in the physical properties of MPFM due to the formation of new compound(s)
4. changes in the trap/release behavior of hydrogen isotopes in/from MPFM

III. Plausible Mixed Material systems:

HRC
Toyama University

1. (Li + C + Q)
2. (Be + C + Q)
3. (Mo + C + Q)
4. (W + C + Q)
5. Other by-reactions with oxygen containing molecule(s) as H_2O and CO

(Q=H, D, and T)

IV. Data needs:

HRC
Toyama University

1. Phenomenological:

1-1. plausible chemical reaction(s) under various temp. and energy

→ XPS, AES, SIMS, RS, XRD

1-2. changes in trap/release behavior and distributions of fuel particles before and after reactions

→ TDS, SIMS, RBS

Change in the Be1s spectrum of [C/Be] sample with elevated temperatures

HRC
Toyama University

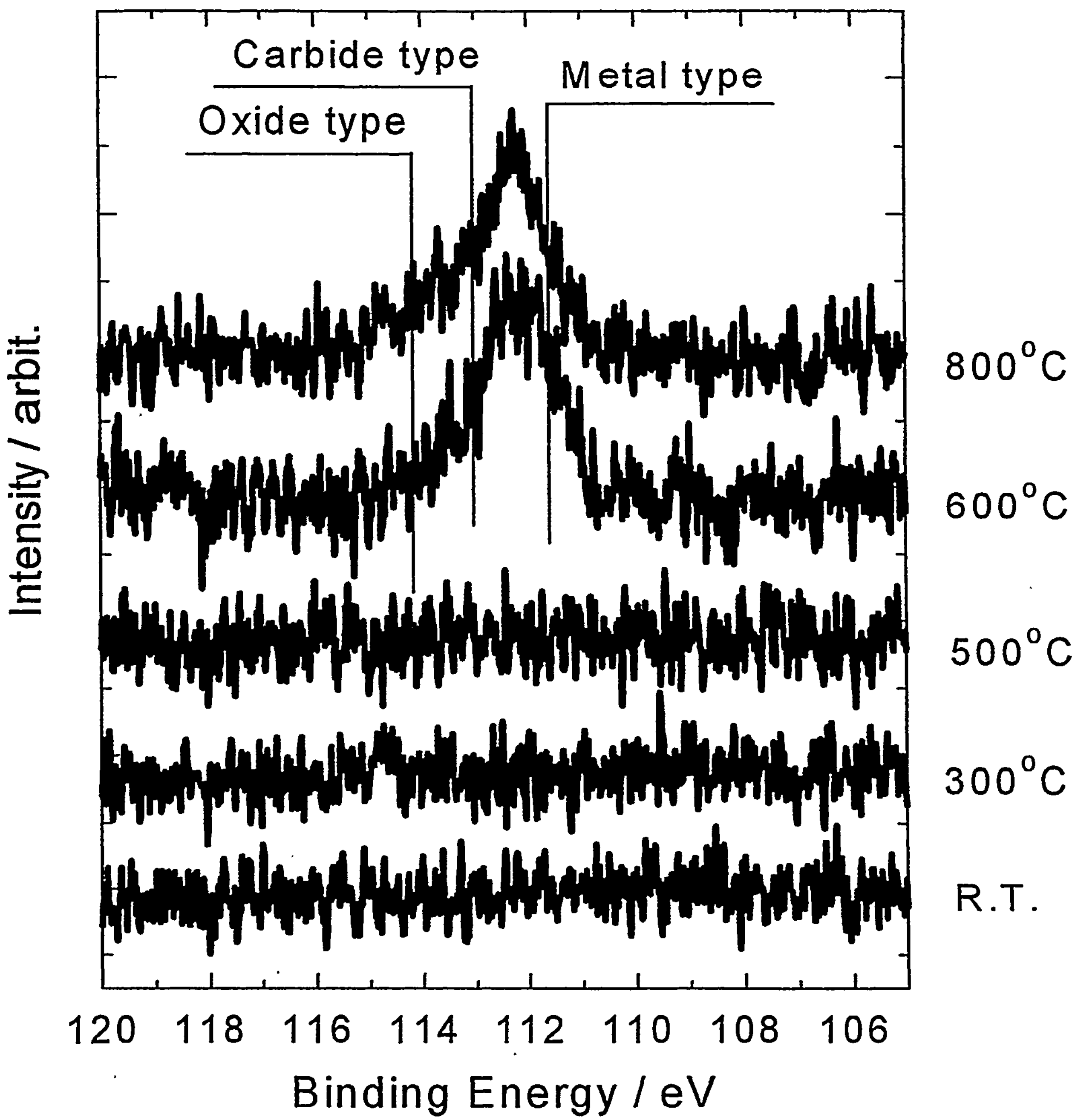

Change in the C1s spectrum of [C/Be] sample with elevated temperatures

HRC
Toyama University

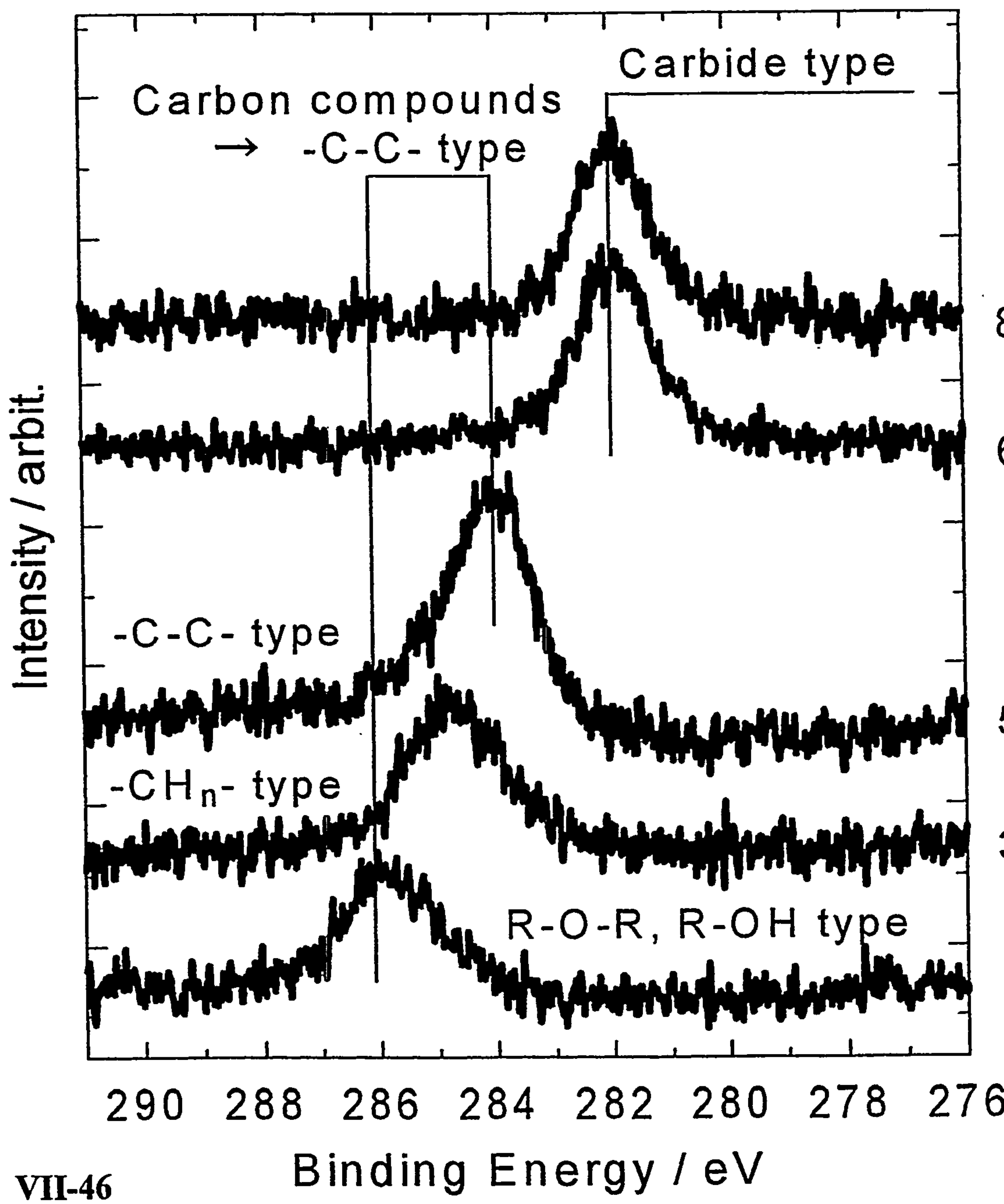

Change in the O1s spectrum of [C/Be] sample with elevated temperatures

HRC
Toyama University

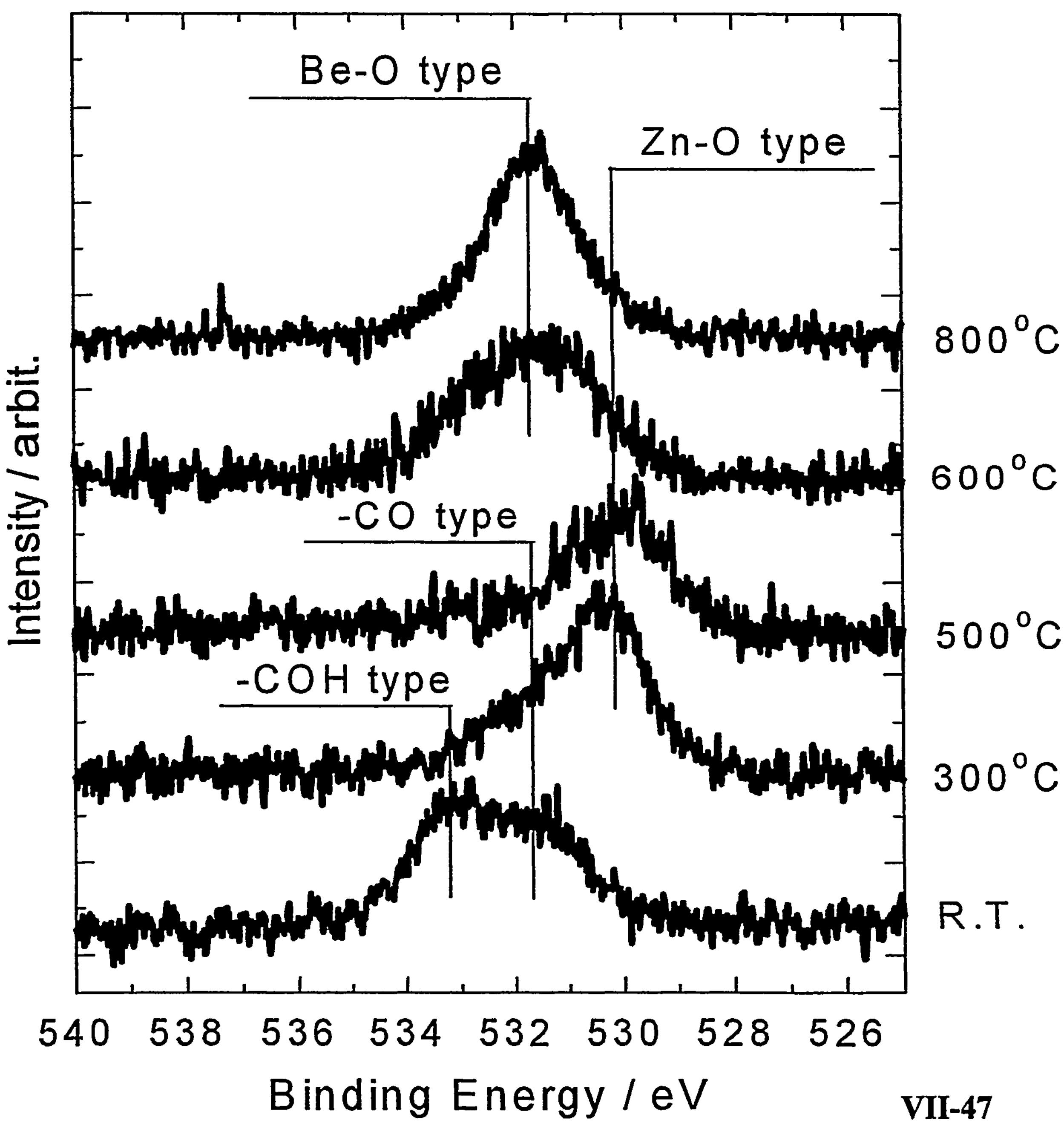

Observed Be1s spectrum (solid line) and its three component peaks (dotted lines) of [C/Be] sample

HRC
Toyama University

[oxide] : [carbide] : [metal] = 1 : 5 : 1 ([Be] : [C] : [O] = 65% : 23% : 10%)
[Be-oxide] = 65% x (1/7) = 9%, [Be-carbide] = 65% x (5/7) = 46%
[Be] : [O] = 1 : 1 (BeO), [Be] : [C] = 2 : 1 (Be_2C)

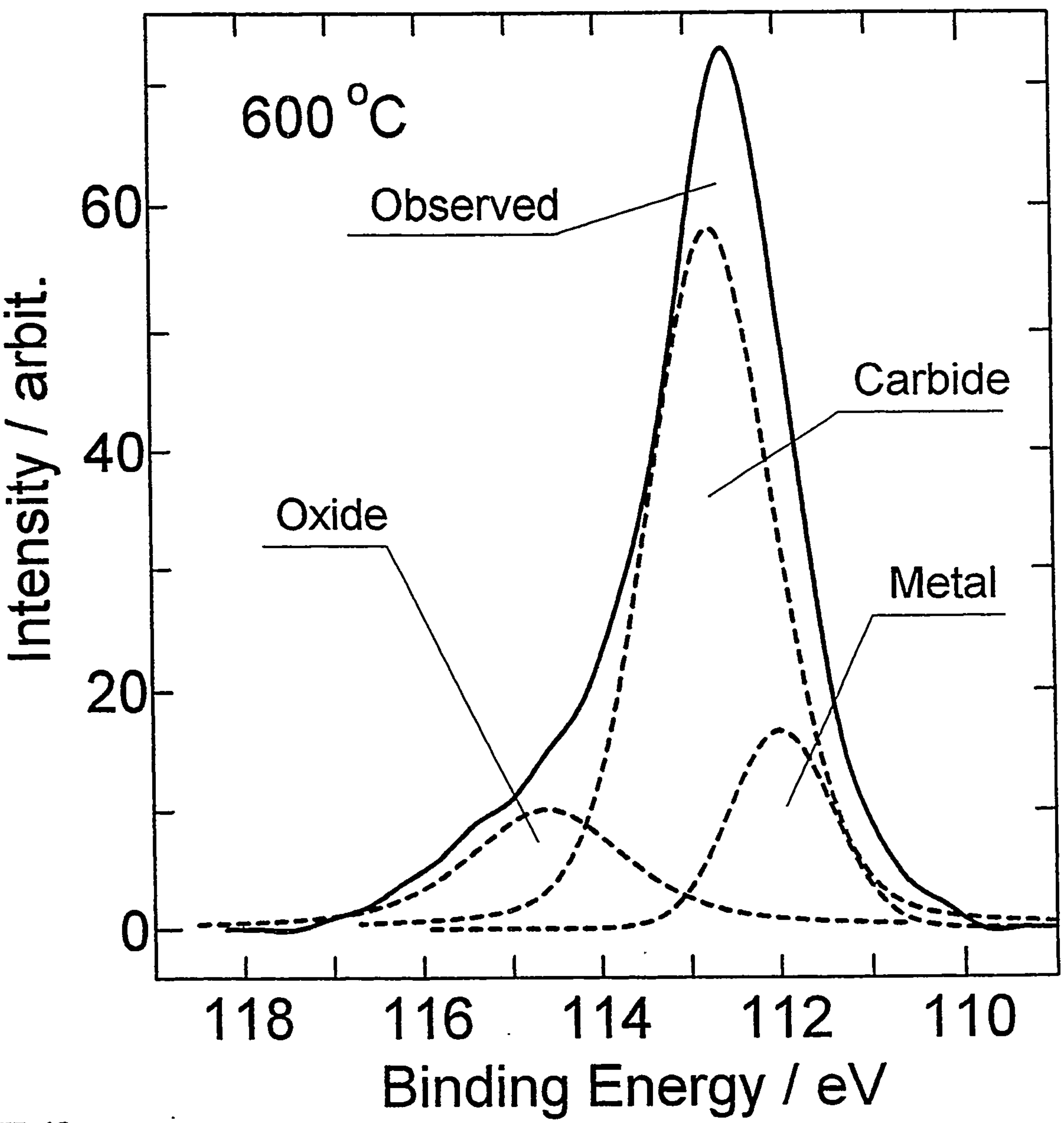

Positive SIMS spectrum of [C/Be] sample with ($Ar+D_2$) mixed gas as primary ion source

HRC
Toyama University

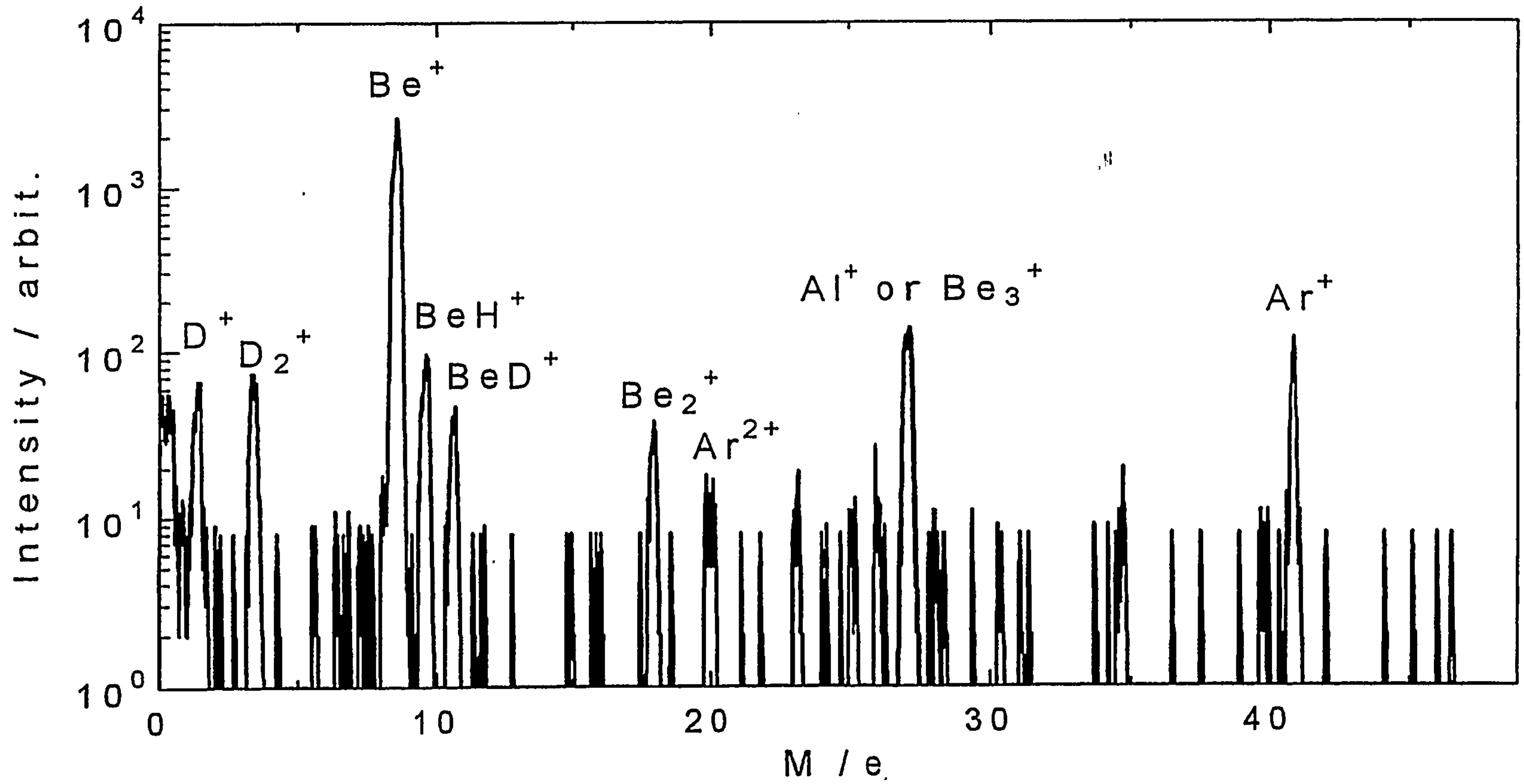

Negative SIMS spectrum of [C/Be] sample with (Ar+D_2) mixed gas as primary ion source

HRC
Toyama University

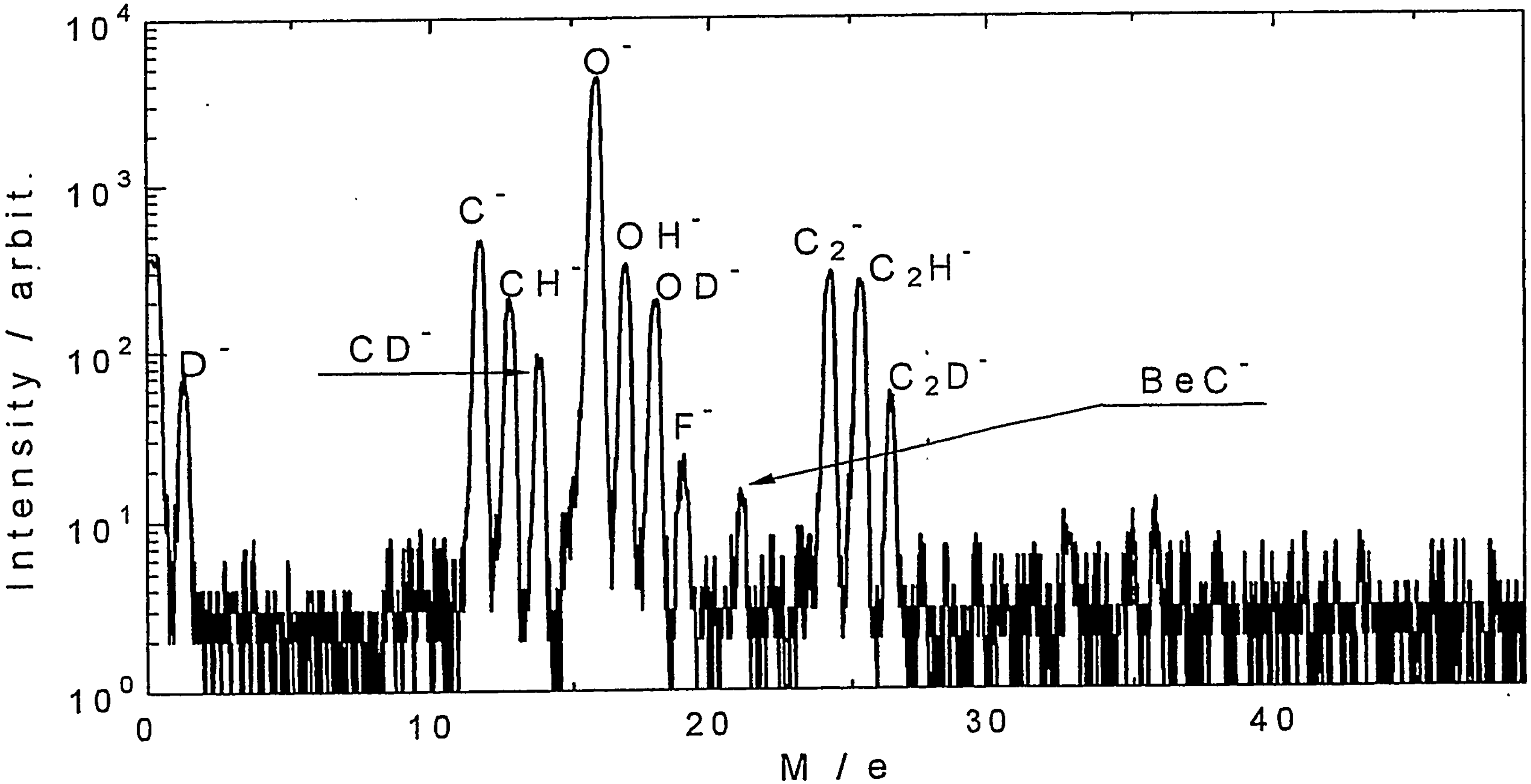

Raman spectra for a hydrogen containing carbon deposits before and after vacuum heating at 800°C for 10 min

HRC
Toyama University

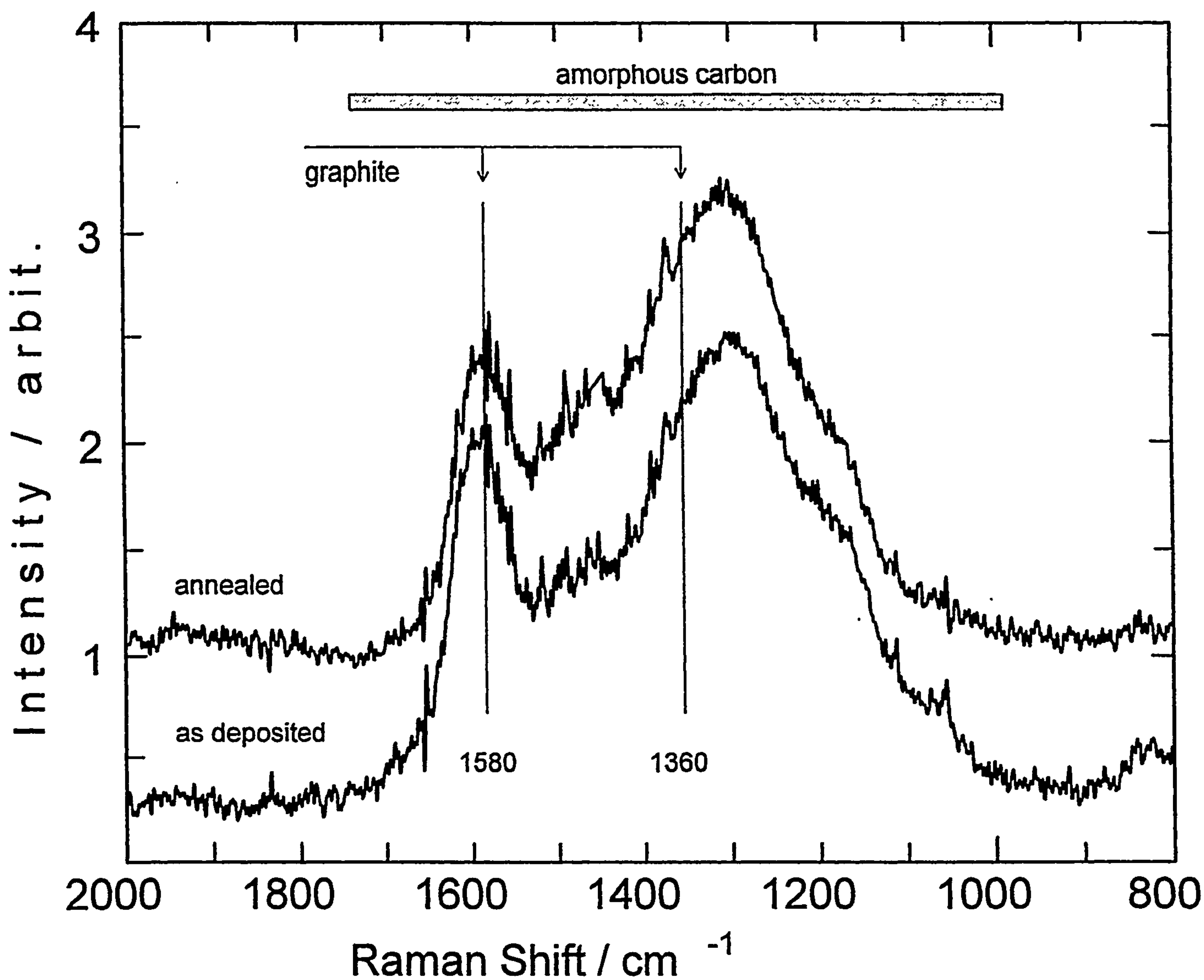

TDS spectra of main desorption gases from Quartz plate covered with hydrogen containing carbon film

HRC
Toyama University

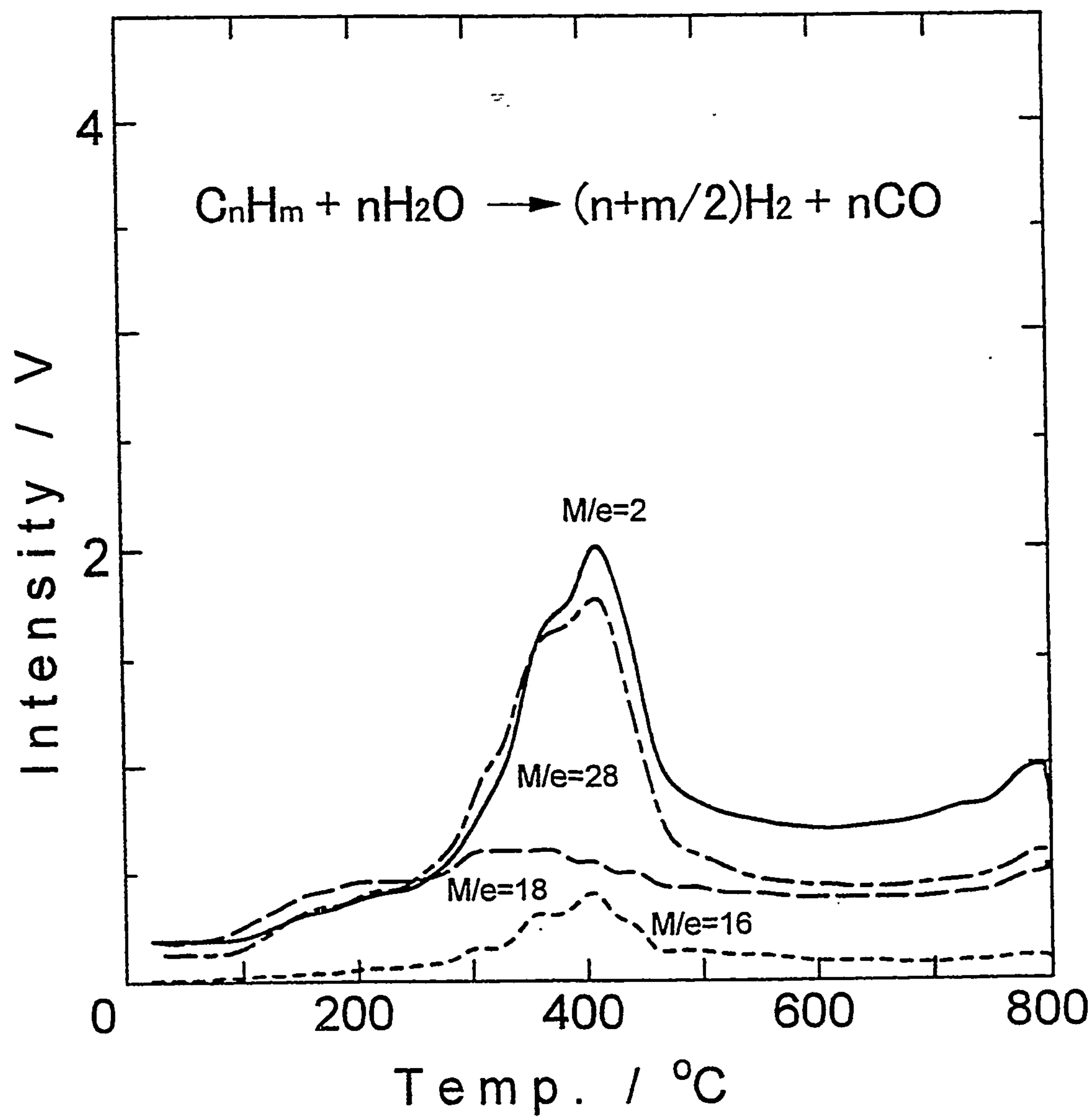

TDS spectra of main desorption gases from Be plate covered with hydrogen containing carbon film

HRC
Toyama University

$$C_nH_m + nH_2O \longrightarrow (n+m/2)H_2 + nCO$$
$$C_nH_m + 2nBe \longrightarrow nBe_2C + (m/2)H_2$$

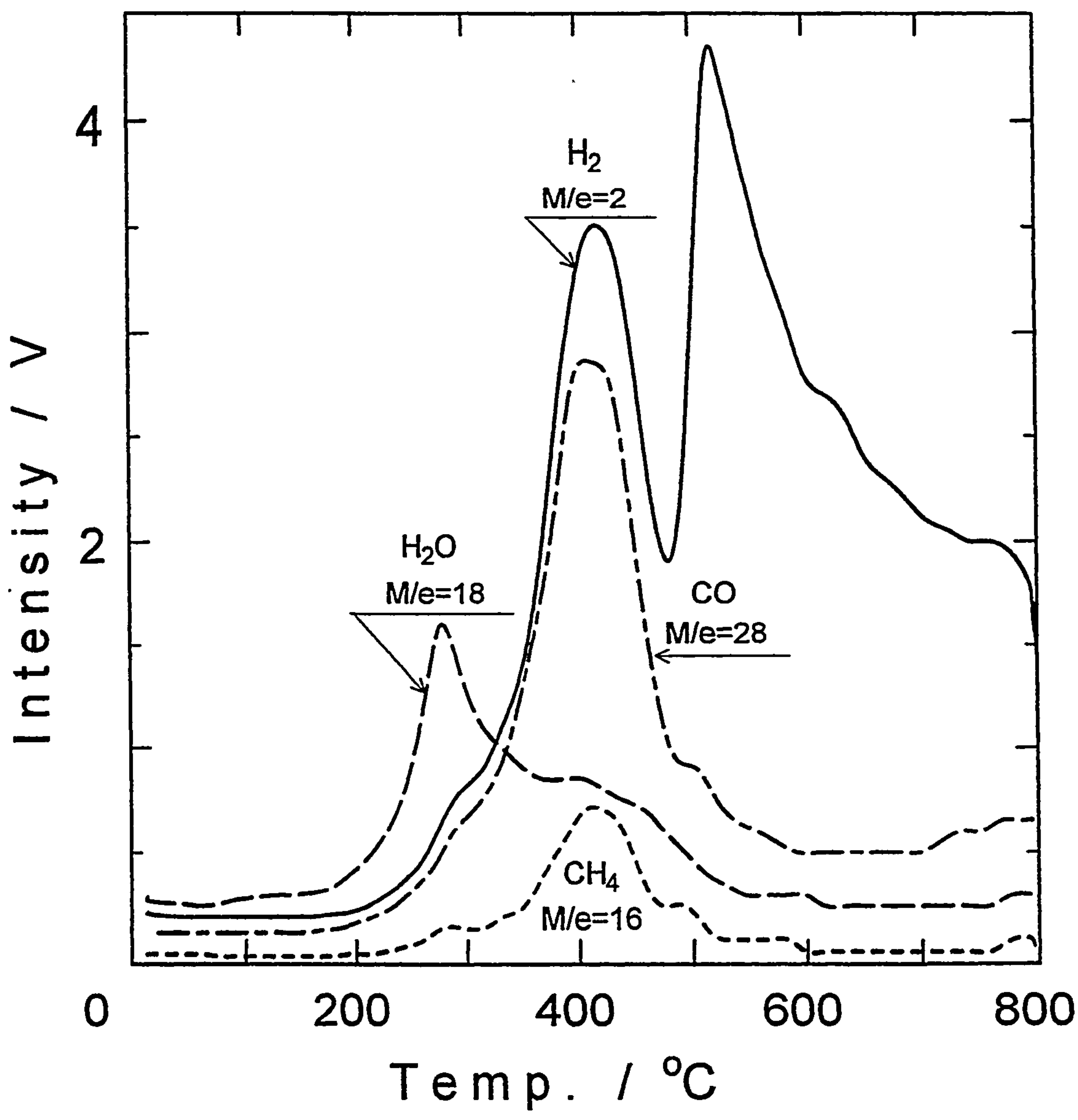

Variation of XRD patterns for the [C(H)/Be] sample with vacuum heating for 10 min at given temperatures

HRC
Toyama University

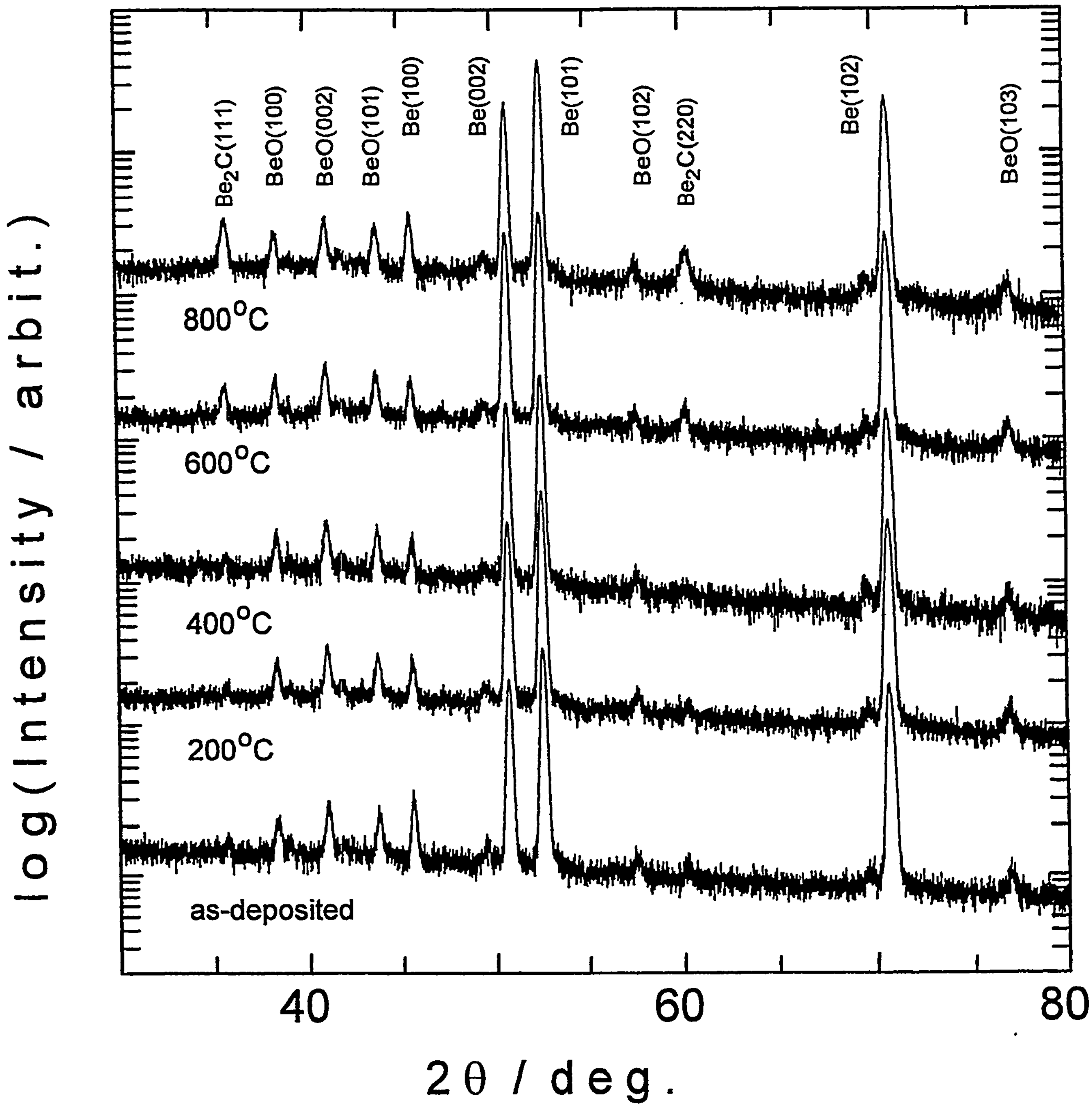

Change in the relative intensities of Be2C(111) peak with vacuum heating at given temperatures

HRC
Toyama University

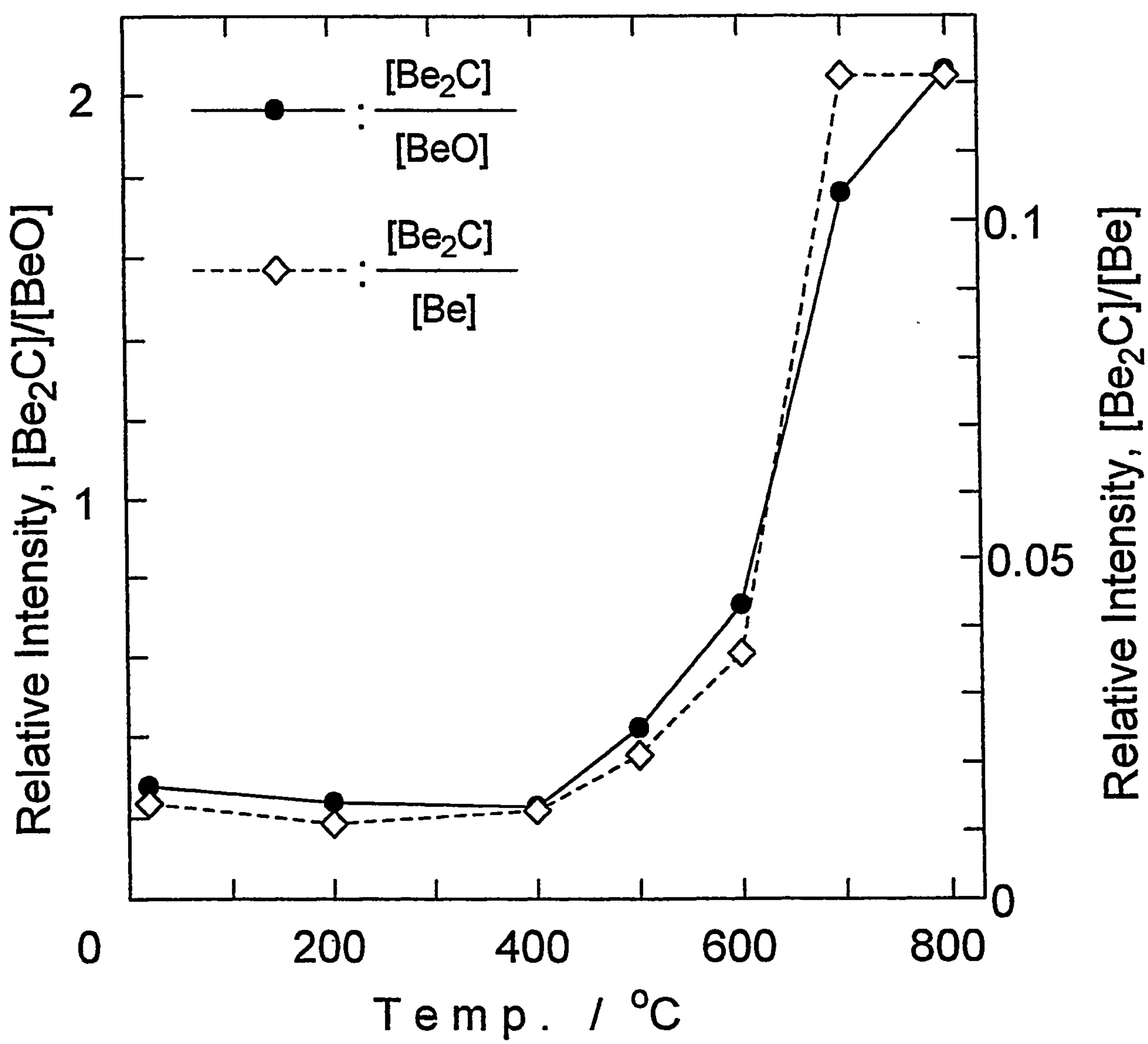

Change in the XRD patterns for the [C(H)/Be] sample with given heating time at 700°C

HRC
Toyama University

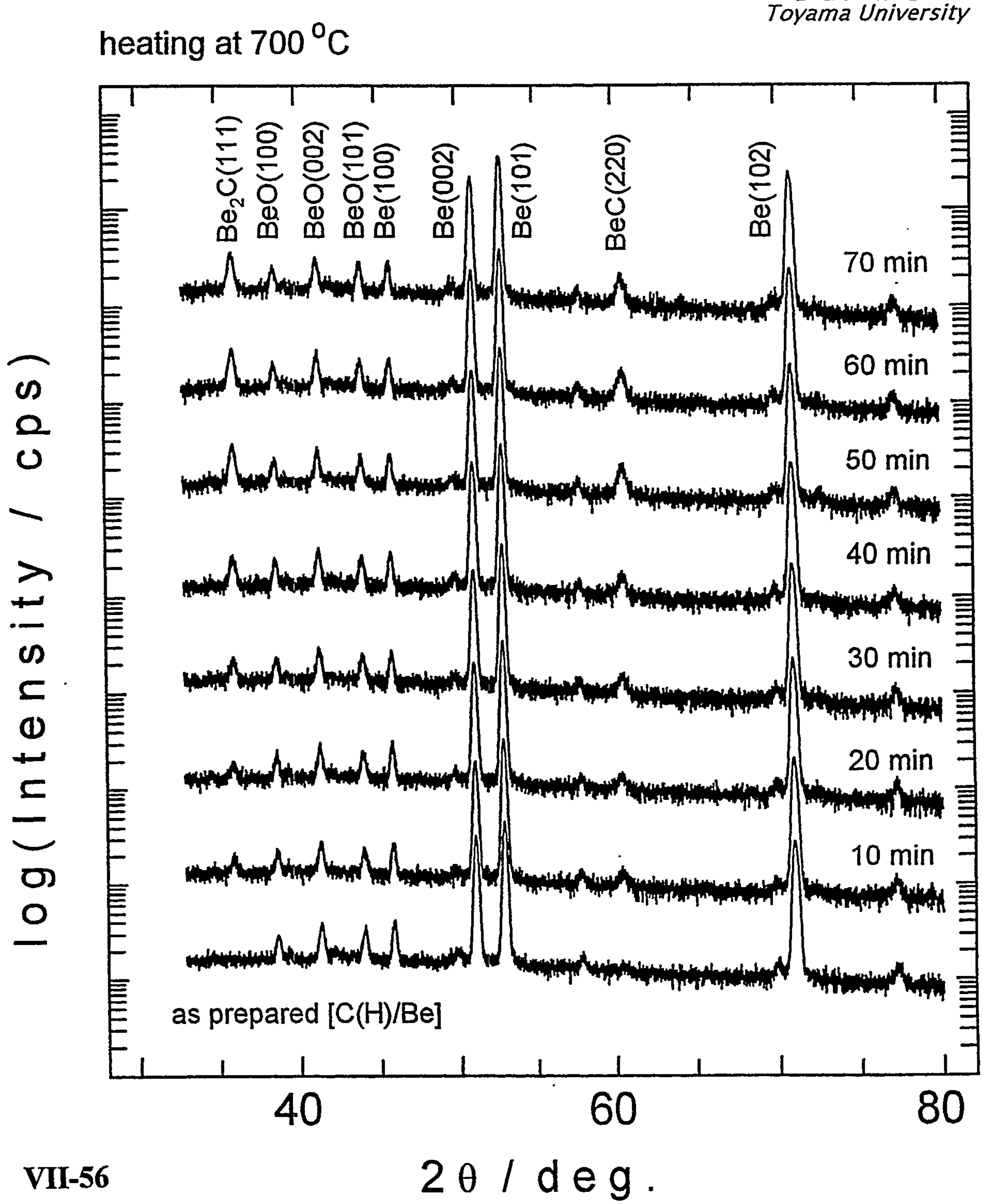

Change in the relative intensities of $Be_2C(111)$ peak normalized by Be(101) with time

HRC
Toyama University

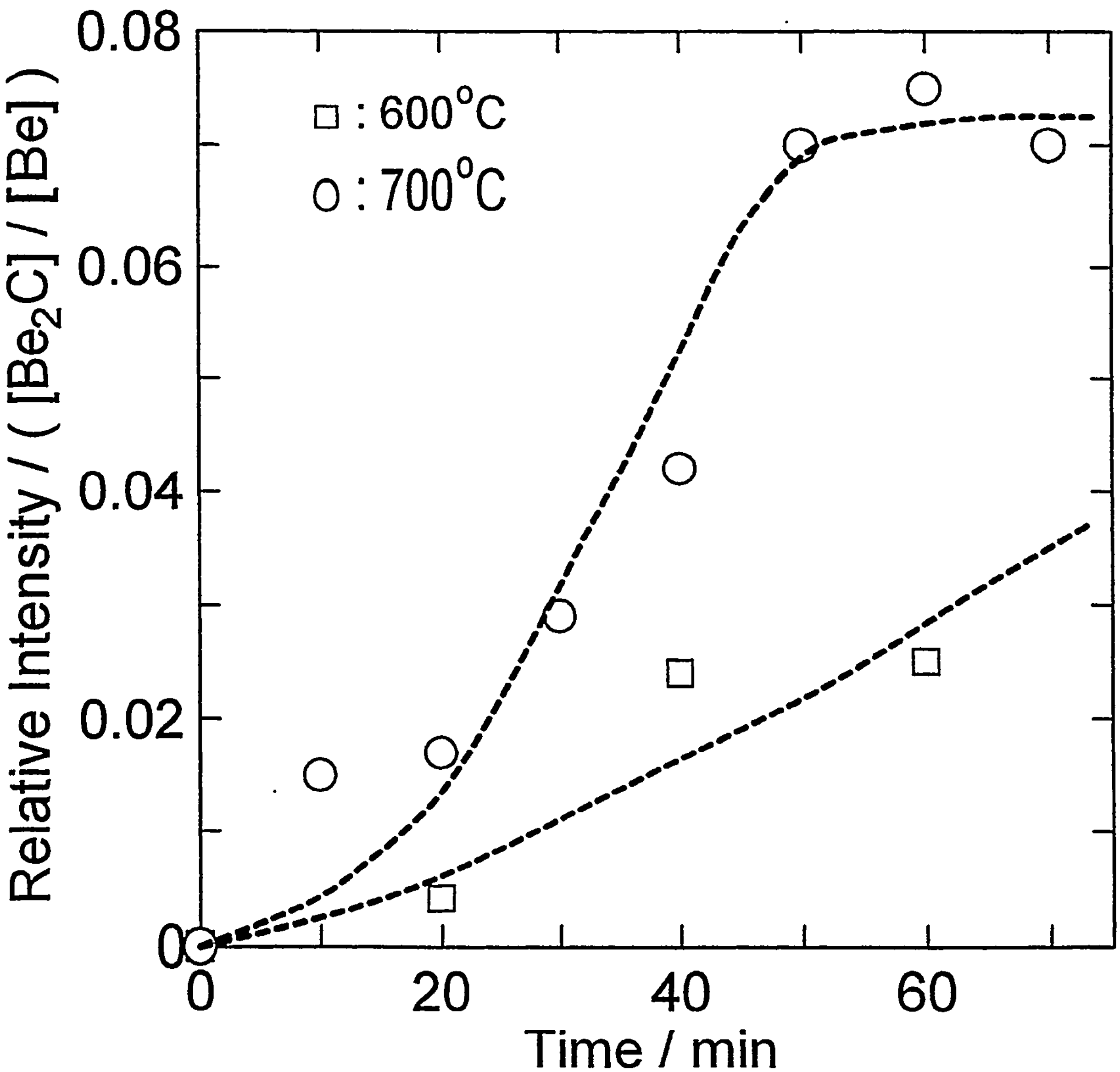

$$A3(\alpha) = \left(-ln\,(1-\alpha) \right)^{1/3} = kt$$
$$= 0.8850\,(t / t_{1/2}), \qquad \text{(nucleation controlled)}$$

$$R3(\alpha) = \left(1 - (1-\alpha)^{1/2} \right) = (u / r)\,t$$
$$= 0.2063\,(t / t_{1/2}), \qquad \text{(boundary controlled)}$$

$$D3(\alpha) = \left(1 - (1-\alpha)^{1/3} \right)^{2} = (k / r^{2})\,t$$
$$= 0.0426\,(t / t_{1/2}), \qquad \text{(diffusion controlled)}$$

$$F1(\alpha) = -ln\,(1-\alpha) = -\,kt$$
$$= -\,0.6931\,(t / t_{1/2}), \qquad \text{(first order reaction)}$$

$t_{1/2}$: the half-life period corresponding to $\alpha = 1/2$
k : the rate constant
u : the velocity of moving interface
r : the radius of a sphere

J.H.Sharp et al., J. Am. Ceram. Soc., 49 (1966) 379

Plots of various crystal growth model against relative time scale with observed data

HRC
Toyama University

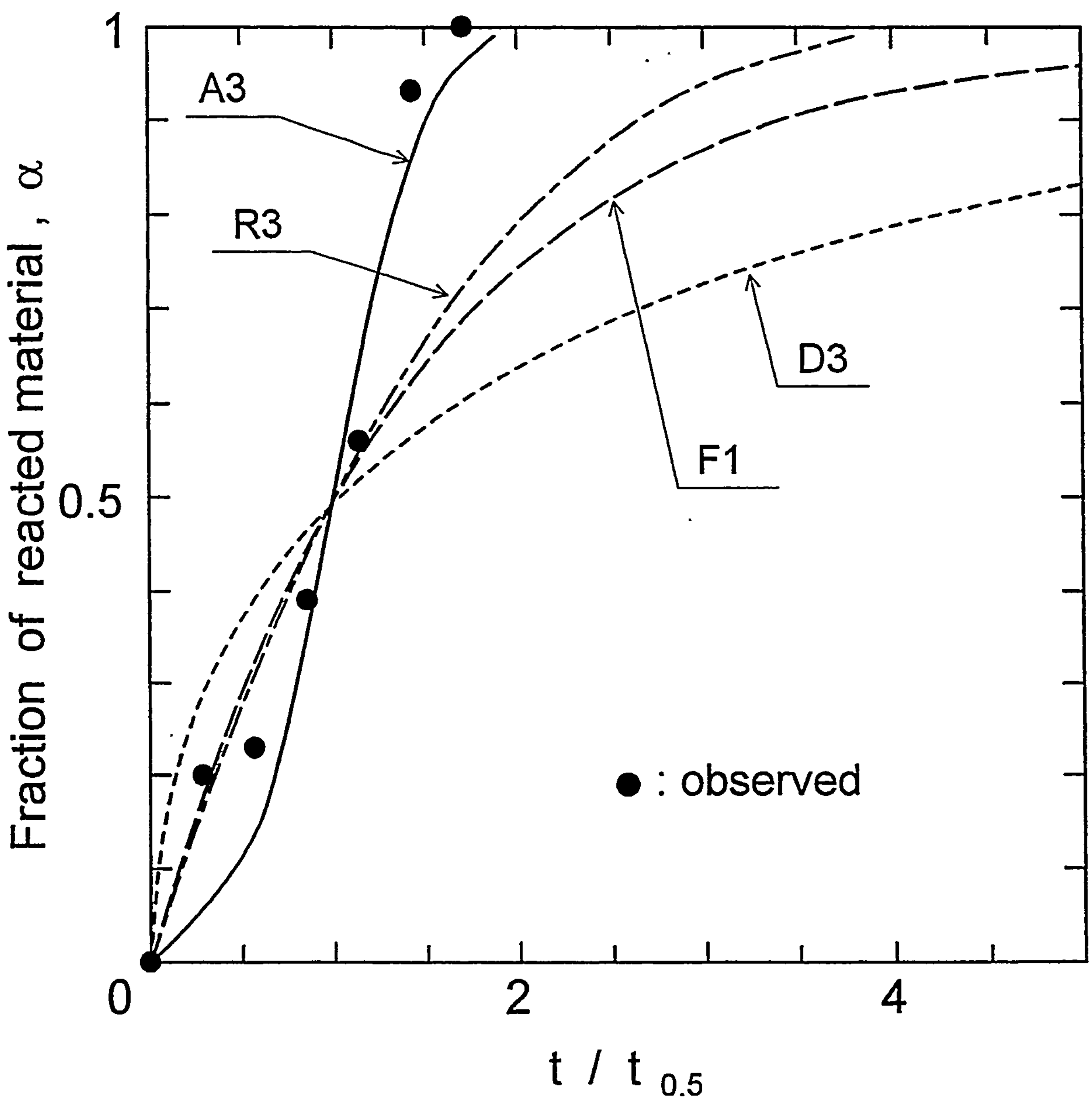

Formation of Be_2C in the C-Be binary system by elevated temperature

HRC
Toyama University

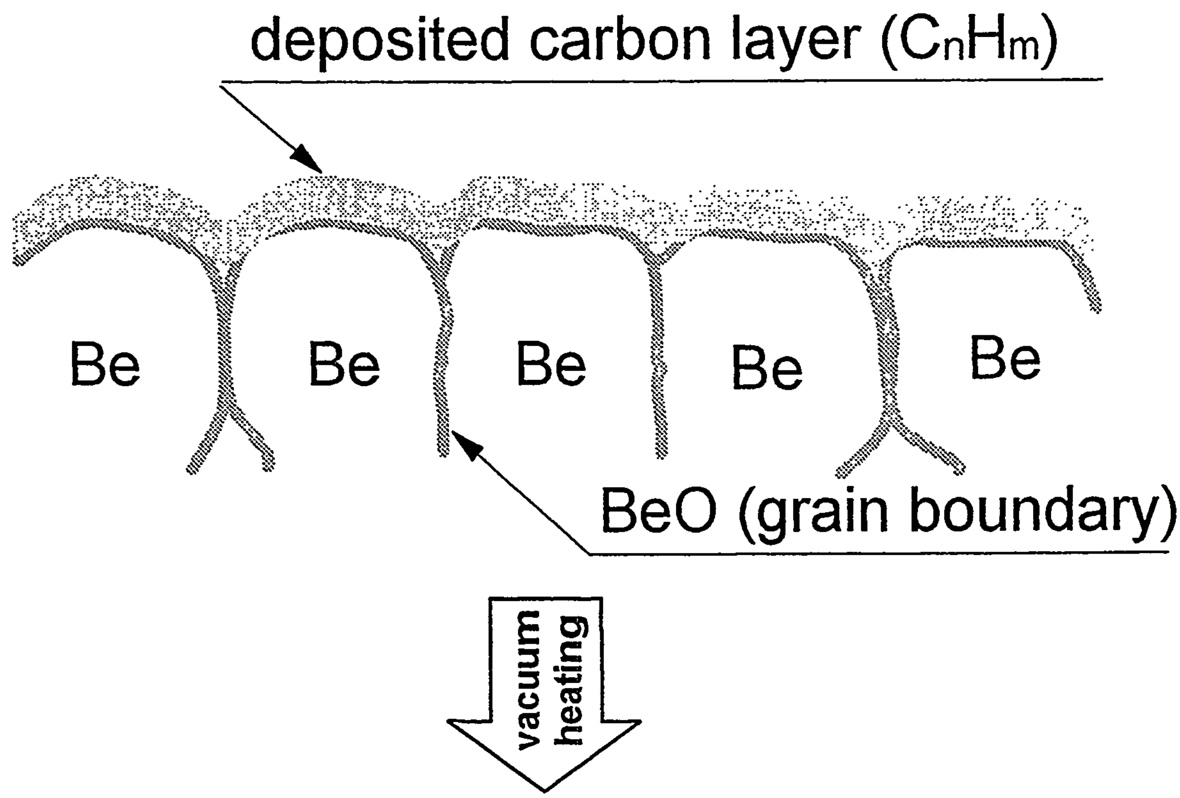

$$C_nH_m + nH_2O \longrightarrow (n+m/2)H_2 + nCO \quad : \sim 400^\circ C$$

$$C_nH_m + 2nBe \longrightarrow nBe_2C + (m/2)H_2 \quad : \text{ above } 500^\circ C$$

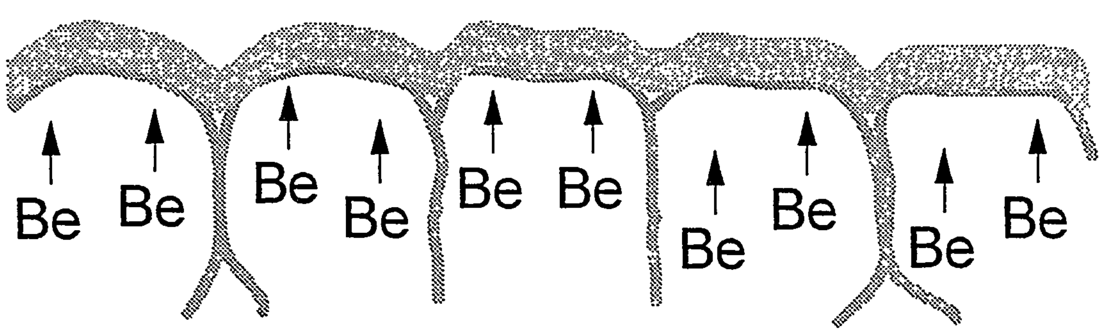

diffusion of Be to the surface

Summary:

1. Formation of Be-oxide, BeO, is unavoidable because Be has high affinity to oxygen and/or oxygen containing molecules such as H_2O.

2. Formation of Be-carbide, Be_2C, takes place above 600°C for Be-C binary system.

3. Rate of Be_2C formation reaction is limited by Random Nucleation mechanism.

4. Carbon atoms lose its ability to capture hydrogen (or deuterium) to release them to gas phase when it forms carbide.

5. Hydrogen isotope atoms are captured by Be, C and O in the form of Be-Q, C-Q and O-Q. (Q=H and D)

Tritium Retention in Beryllium

Rion A. Causey
Sandia National Laboratories
Livermore, Ca 94550

US/Japan Workshop
San Francisco, Ca

December 8-10, 1997

Outline

Beryllium Experiments

- High Flux Retention Measurements
- Low Flux Retention Measurements
- Codeposition Measurements

Tungsten Experiments

- Tungsten with 1% Lanthanum Oxide

The Tritium Plasma Experiment (TPE) is a Unique Facility Devoted to Plasma-Materials Interaction Studies for the US DOE Magnetic Fusion Energy Program

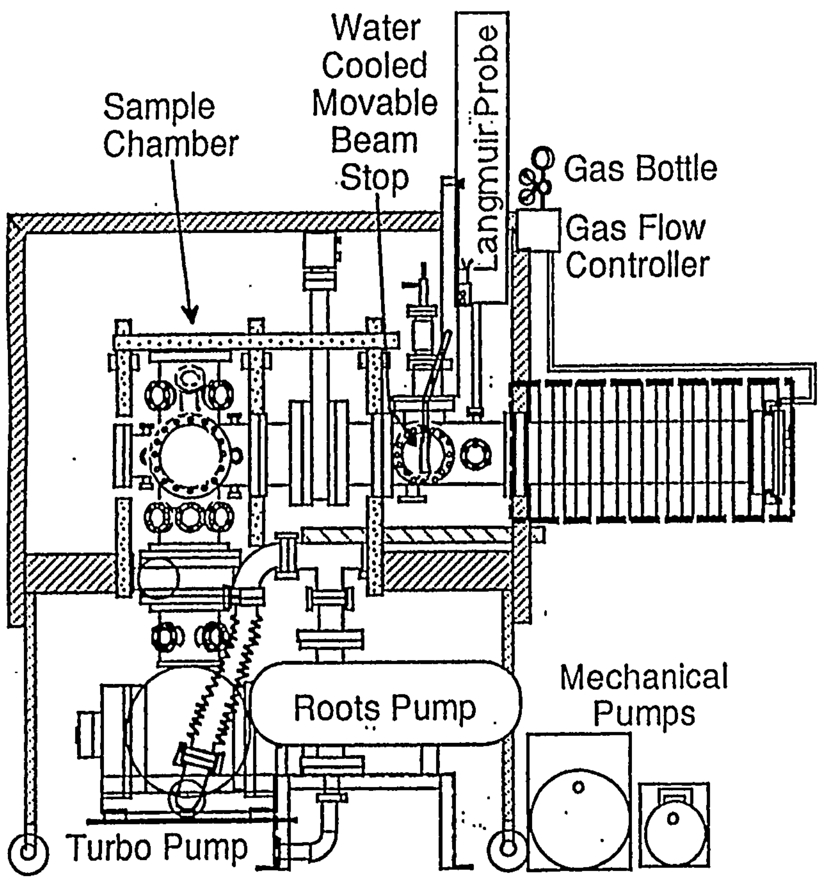

The Tritium Plasma Experiment is now located at the TSTA Facility in Los Alamos National Laboratory

This experimental facility is capable of delivering 1 A/sq.cm of 100 eV tritons uniformly over a 2 inch diameter sample. The tritium inventory of this experiment is greater than 6 grams.

TPE is being used in experiments to determine the tritium migration parameters for materials (Be, C, and W) to be used in the ITER fusion reactor.

Sandia National Laboratories

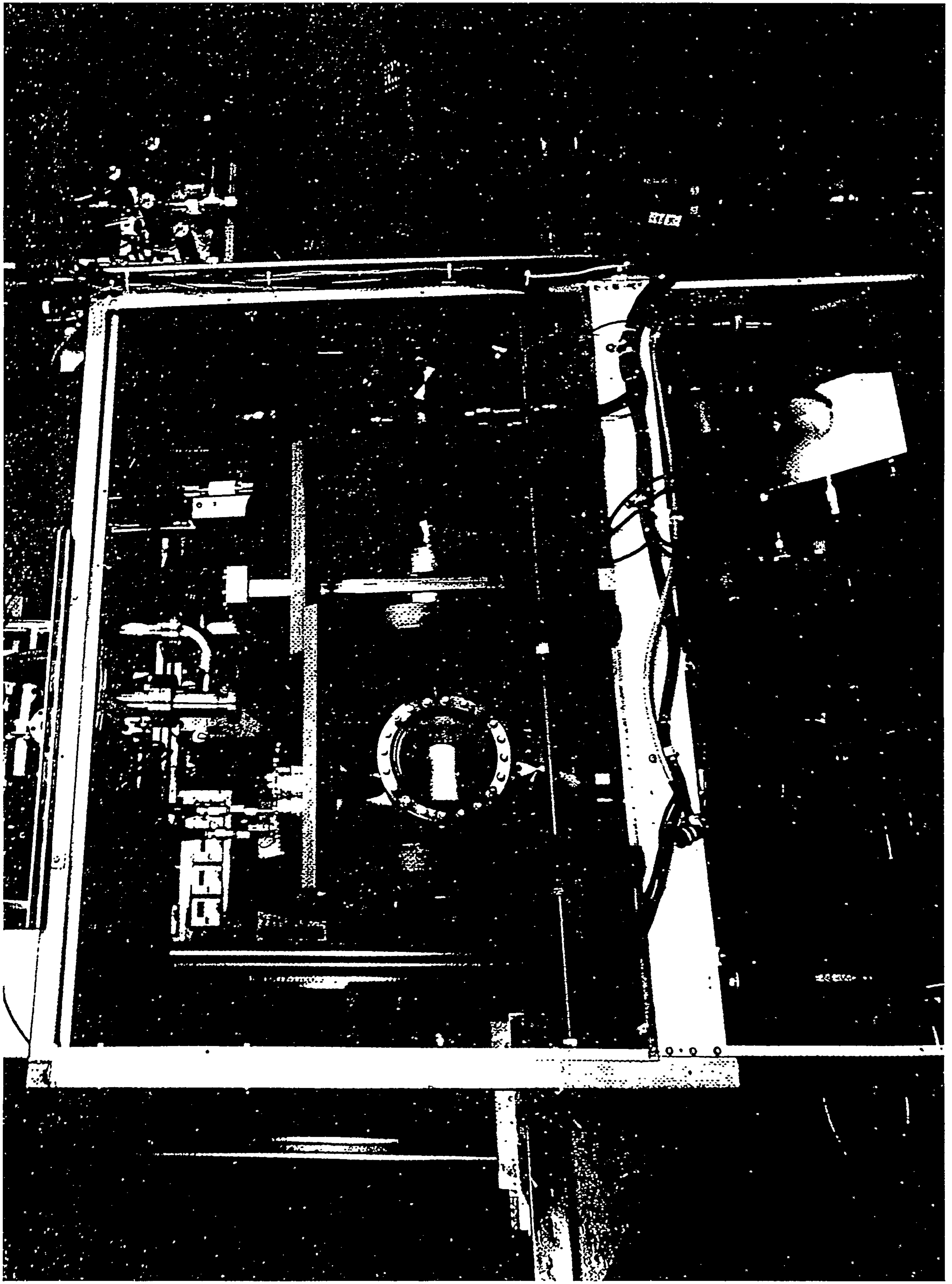

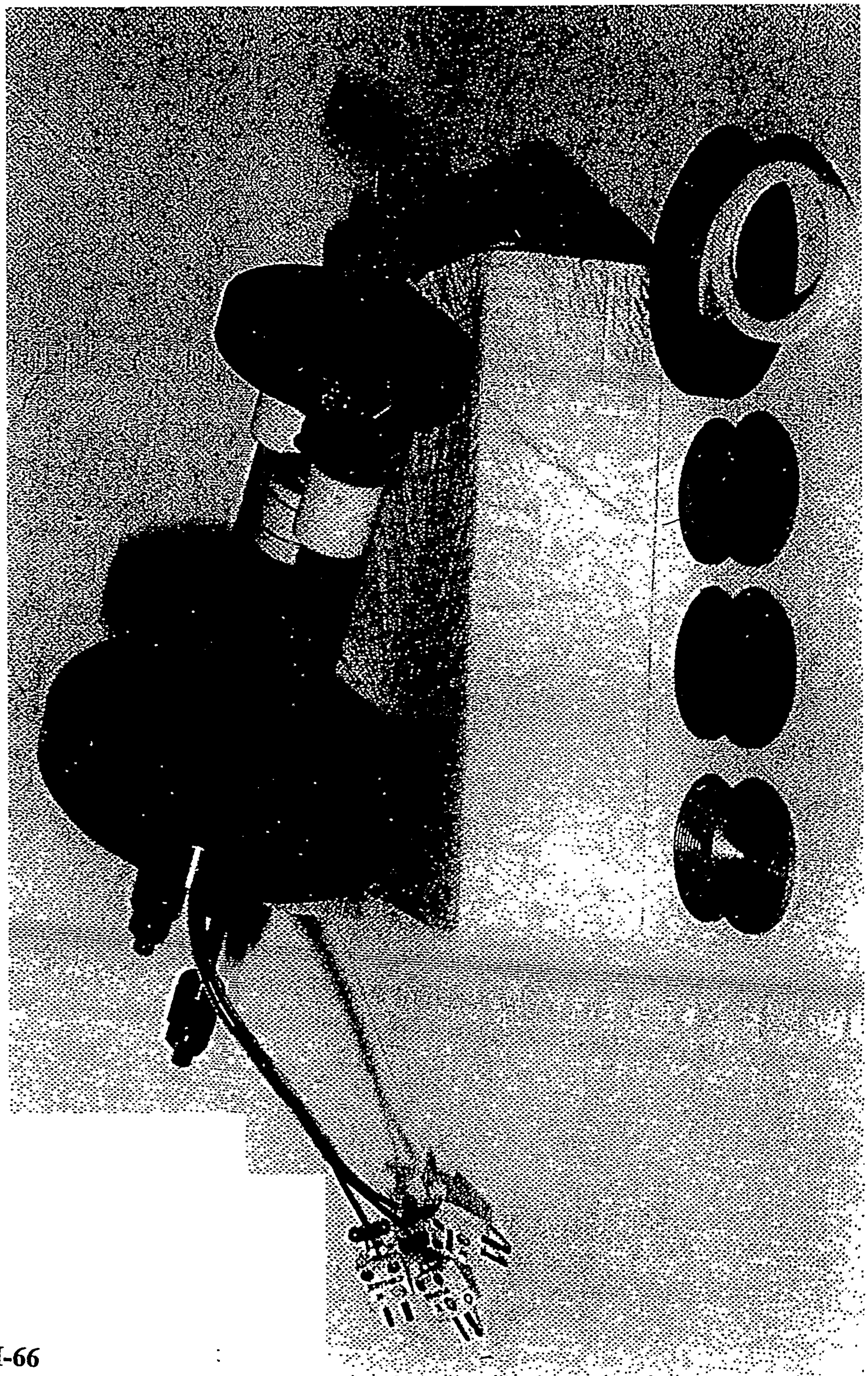

Experimental Procedures

Material

The beryllium used in this study was Brush Wellman S-65. It is 99.4% Be and 0.6% BeO. It is hot pressed, and has 99.8% of theoretical density.

Procedures

1. Sample was loaded into the TPE sample holder. Holder was installed and vacuum was established.

2. Plasma was started using pure deuterium. Once impurities generated by the initiation of the plasma were removed by the vacuum system, the bias was applied to the sample and the plasma intensity was increased until the desired sample temperature was obtained. Bias elevated the energy of the deuterons and tritons to 100 eV. Once the desired temperature was obtained, the tritium was added to the plasma gas. The plasma was maintained for one hour from the time the tritium was added.

3. After the plasma exposure, the sample was remove from TPE and transported to the outgassing system. Here the sample was linearly increased in temperature up to 800 C. During this time, gas consisting of 99% helium and 1% hydrogen was swept across the sample at a flow rate of 100 cc/min. This gas was first sent through and ionization chamber. After exiting the ionization chamber, 10% oxygen was added before the gas was sent through a copper oxide bed. This converted the hydrogen and tritium to water for collection in the subsequent glycol bubblers. Liquid scintillation counting of the tritium in the water/glycol was used as a check on the data obtained by the ionization chamber.

New Measurements of Tritium Retention in S-65 Beryllium at Divertor-Like Conditions Suggest Retention to be Controlled by Near-Surface Saturation Alone. Retention Values Lower Than Predicted.

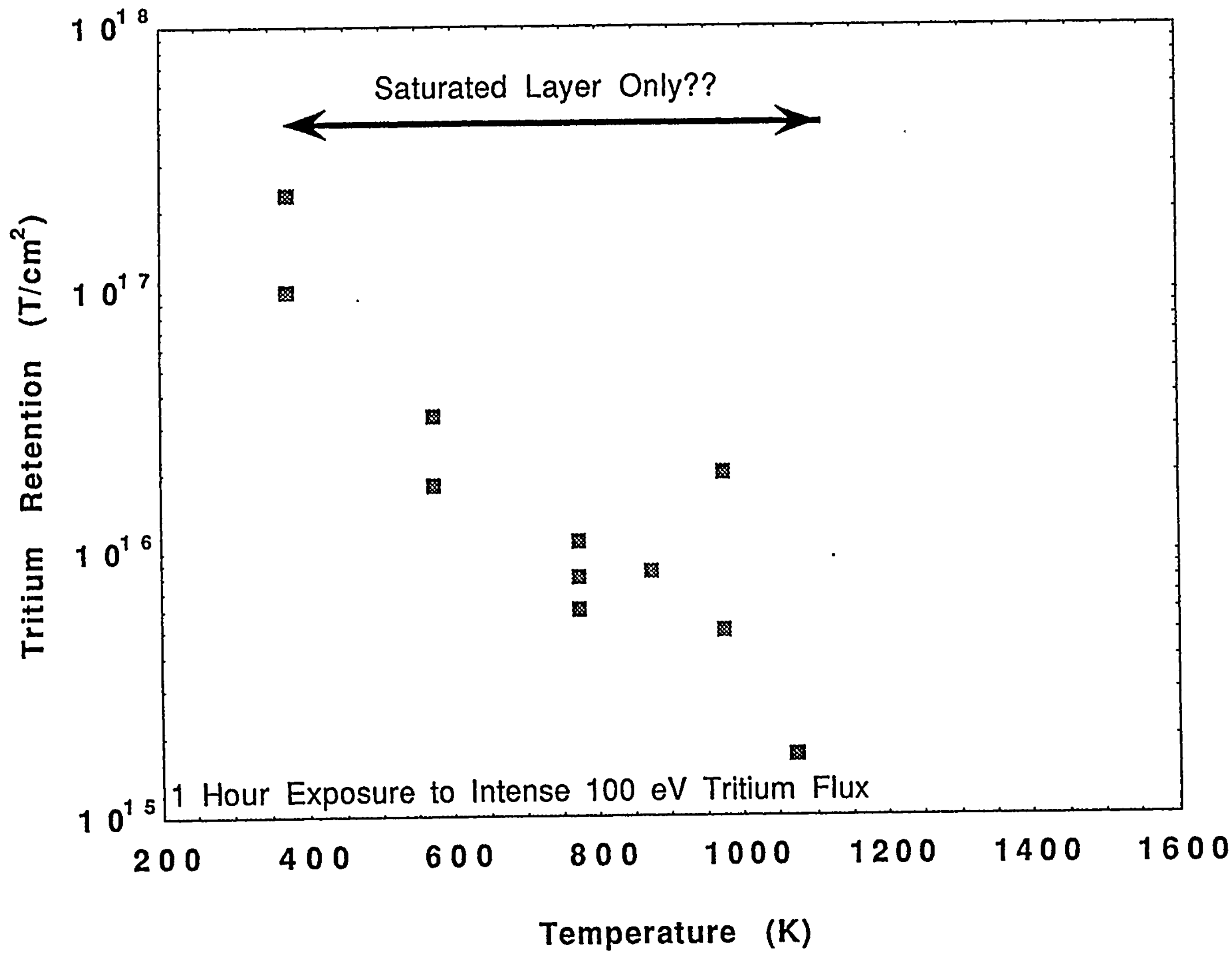

Comparison of TPE Beryllium Data to that Predicted by Assuming C=0 at Boundary

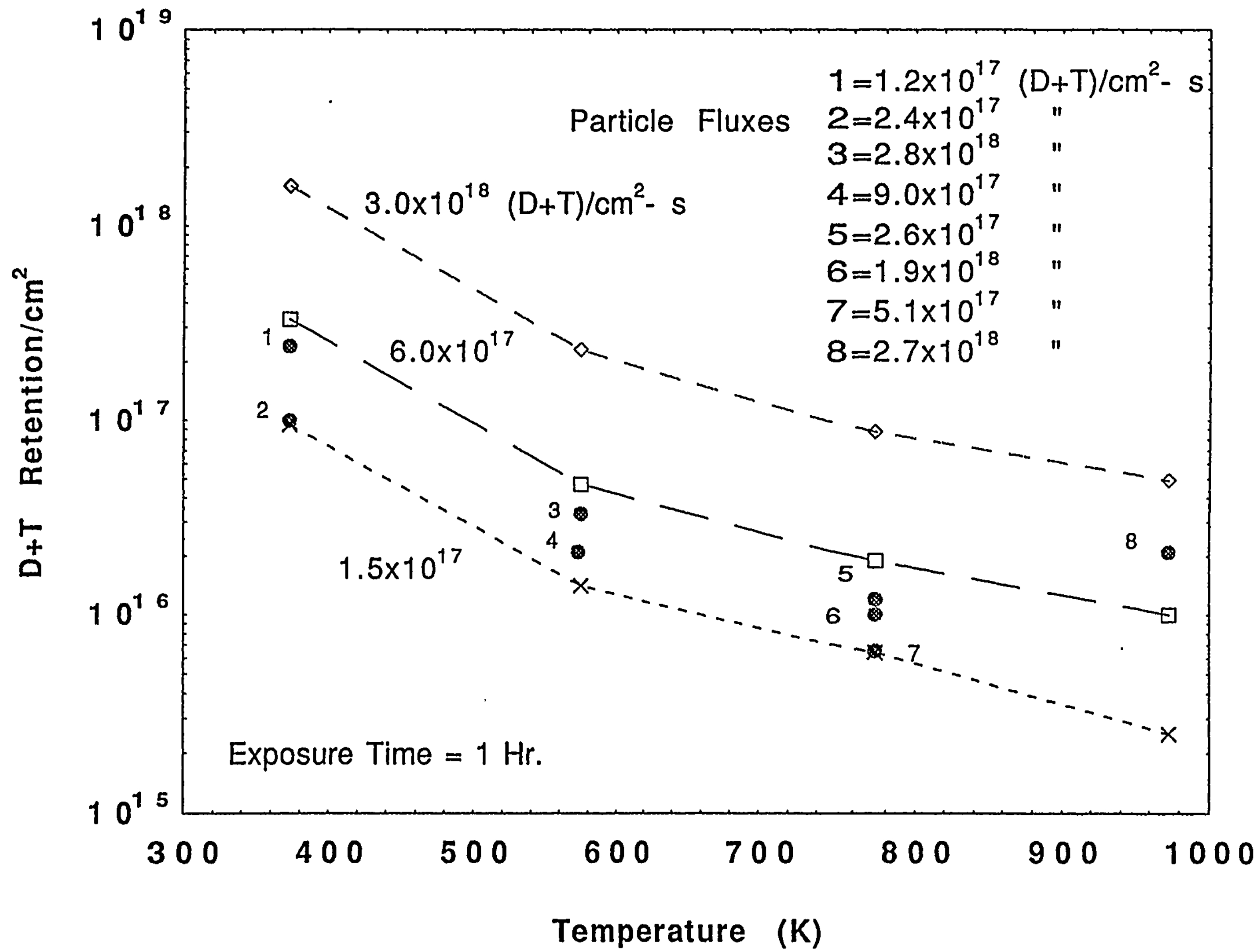

Earlier work by Chernikov et al. has shown hydrogen implantation into beryllium to open porosity in the implant zone. This would result in relatively rapid saturation in the hydrogen retention with longer or more intense exposure having no effect on the amount of hydrogen retained.

V.N. Chernikov, V.Kh. Alimov, A.V. Markin, and A.P. Zakharov, J. Nucl. Mater. 220-222 (1996) 47.

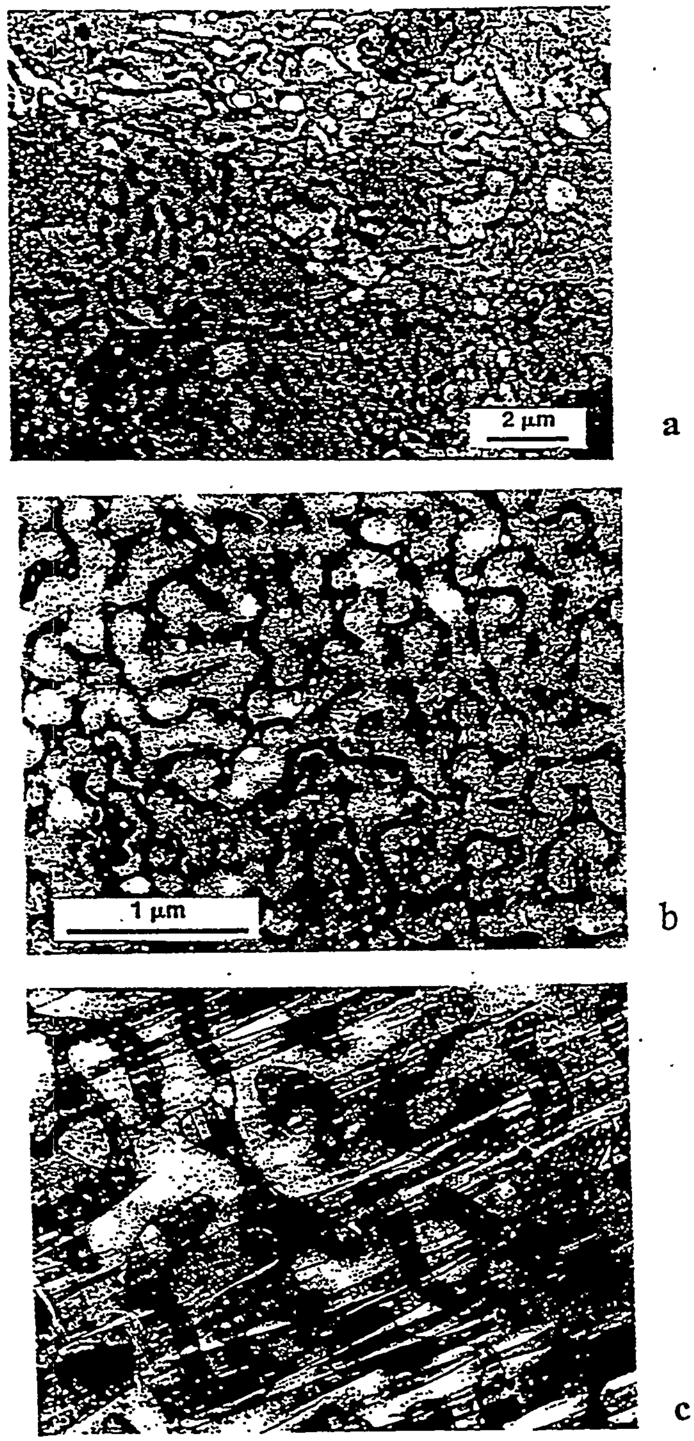

Figure 9. Deuterium bubbles and labyrinths of oblate interconnected channels after irradiation at 700 K with 10 keV D ions up to 2×10^{21} D/m^2: a) viewing field covers some grains, low magnification; b) surface plane of the grain is close to (0001); c) surface plane of the grain is nearly parallel to c axis ($t_r \approx 450$ nm).

Tritium Retention in Beryllium at ITER First Wall-Like Conditions

- At 250 C, increasing the plasma exposure time by two orders of magnitude increased the tritium retention only by a factor of 2.4
- The 40 hour exposure represents 144 one thousand second shots in ITER
- Extrapolation of this data to the ITER first wall predicts only a few grams of tritium retention

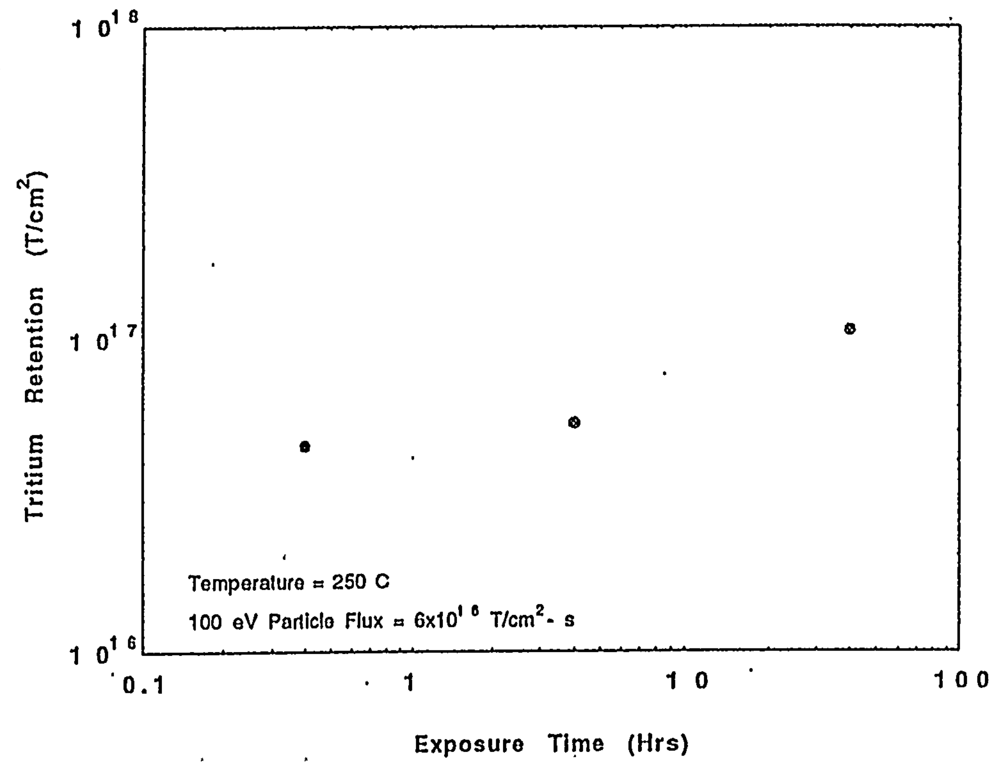

Causey (Sandia National Laboratories)

Beryllium Codeposition Experiment

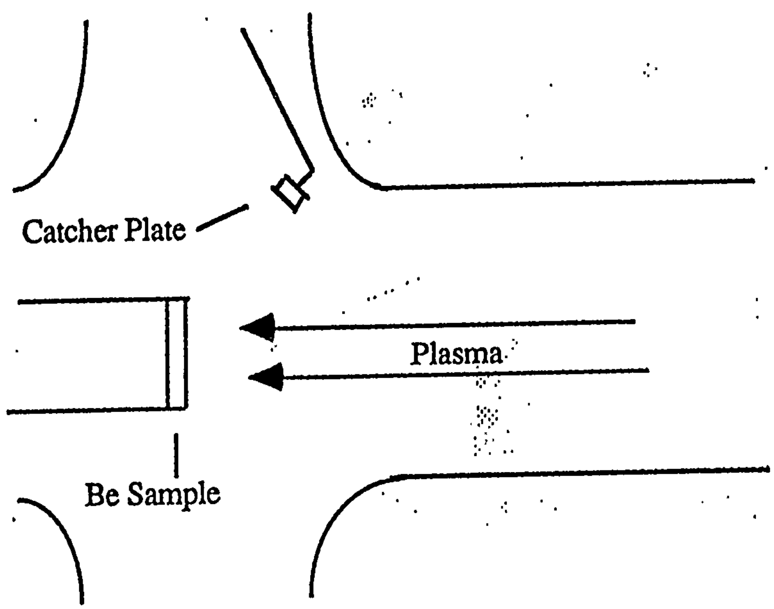

- A standard 5 cm diameter beryllium disk was loaded into the TPE sample holder.
- A small copper or aluminum catcher plate was located on a Varian™ heater 5 cm in front of the disk and 5 cm to the side of the center of the disk.
- The catcher plate was heated to 100, 200, or 300 C.
- A 100 eV D+T plasma was maintained for 1 hour with a particle flux of 3.3×10^{17} ions/cm^2-s.
- The catcher plate was removed from TPE after the exposure and outgassed to 800 C. The data was collected from an ionization chamber and from liquid scintillation counting.

Beryllium Codeposition Experiments

- The beryllium/deuterium codeposition experiments have been repeated in the Tritium Plasma Experiment

- In these recent experiments, the amount of oxygen in the plasma was significantly reduced from that existing in the earlier experiments

- The samples were analyzed by Dave Walsh (SNL/NM) using accelerator techniques

Sample Summary

Sample Temp	Thickness	O/Be	D/Be
100 C	1200 Å	0.125	0.15
200 C	1200 Å	0.125	0.07
300 C	1500 Å	0.06	0.02
150 C	3200 Å	0.03	0.10

The carbon content of all samples was below 1.5 %

Codeposition of Hydrogen Isotopes and Beryllium

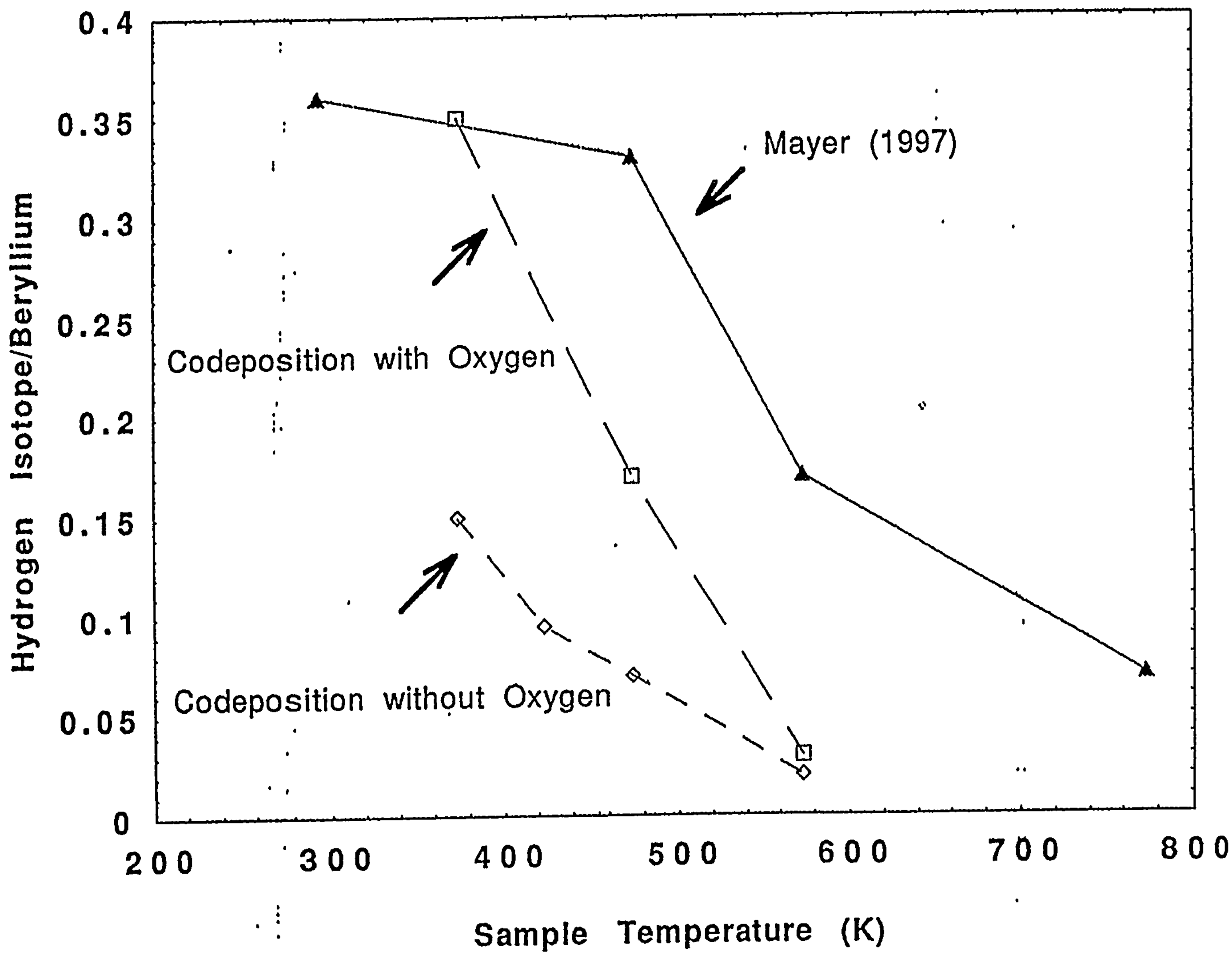

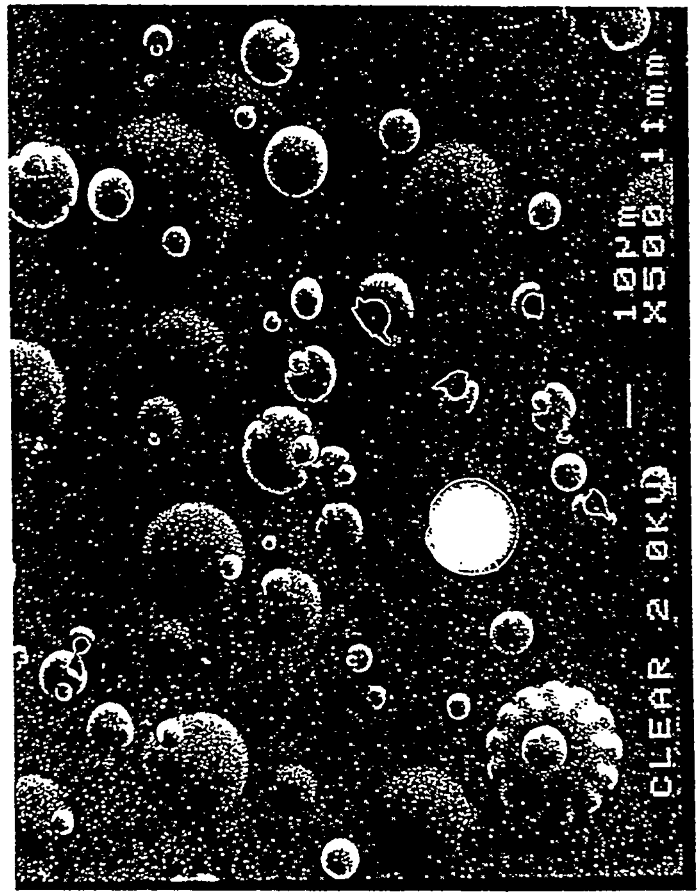

#4

Beryllium Results

Implications for ITER

- If used as either a divertor or first wall material, the tritium retention of S-65 beryllium due to implantation should be small. The effects of neutron damage on the retention are unknown, but suspected to be minimal [work planned for next year].

- The codeposition of beryllium with tritium has been found to depend on the availability of oxygen. Even with oxygen present, the tritium inventory in sputtered beryllium will be below that of carbon (lower sputtering coefficient and lower dissociation temperature).

Session VIII: First Wall Development

[page intentionally left blank]

HPD APPROACHES, CORE RADIATION AND HELIUM BLANKET, GA-LAR AS AN EXAMPLE

by

CLEMENT WONG

Presented at
U.S./Japan Workshop (97FT5-06) on High Heat Flux Components
and Plasma Surface Interactions for Next Generation Fusion Devices
San Francisco, California

DECEMBER 8–11, 1997

290–97

GENERAL ATOMICS

WHY HPD?
(DESIGN AND ECONOMIC IMPLICATIONS)

- A goal for economic fusion power is to compete with advanced energy sources*

- ARIES-RS† shows:

$$\frac{\text{Reactor plant equipment cost}}{\text{Plant direct cost}} = \frac{\$1.4\text{B}}{\$2.2\text{B}} = 0.64 \Rightarrow \text{COE} = 76 \text{ mill/kWhr}$$

- GA-LAR‡ shows:

$$\frac{\text{Reactor plant equipment cost}}{\text{Plant direct cost}} = \frac{\$1.1\text{B}}{\$2.8\text{B}} = 0.4 \Rightarrow \text{COE} = 53 \text{ mill/kWhr}$$

  ⇒ Smaller and/or cheaper fusion power core

  ⇒ High power density design (plasma q''' at >5 MW/m^3)

- High heat flux and Γn FW/blanket design (e.g., Ave Γn ~ 8 MW/m^2)

---

*Coal and APWR: 50–60 mill/kWhr beyond the year 2000.

†P_e at 1 GW.

‡P_e at 2 GW.

CORE RADIATION LOGIC

- Impurity in plasma core will radiate
- Minute fraction of impurity may be useful
- $f_z \Uparrow$, $Z_{eff} \Uparrow$, core radiation $\Uparrow$, $\varnothing_{fw} \Uparrow$, $\varnothing_{Div} \Downarrow$
- Approach applicable to tokamak and LAR concepts
- Lower ϕ_{Div} can also means lower erosion rate
- Penalty: $f_z \Uparrow$, $n_i \Downarrow$, $Q_{plant} \Downarrow$, $Z_{eff} \Uparrow$, CD – power $\Uparrow$

IMPURITY CORE RADIATION (GA-LAR DESIGN)
(TO TRADE OFF FW AND DIVERTOR HEAT FLUX)

V

Inputs

- n_e, He concentrations
- Other physics parameters
- Uniform impurity density
- Line radiation at coronal equilibrium
- Divertor flux expansion = 10
- Inclined divertor plate, radiation, geometry etc.

Design Criteria

- $\phi_{max\ divertor} < 10\ MW/m^2$
- $\phi_{ave\ FW} < 2\ MW/m^2$
- Favorable energy balance
- Rad. Temp Stability

Design

- Uniform distribution $n_{Kr} = 0.0019\ n_e$
- He fraction = 0.1
- Proton defect

$$\frac{n_D + n_T}{n_e} = 0.87$$

Results (R_o = 2.9 m, Kr)

- $\phi_{FW} = 1.95\ MW/m^2$
- $\phi_{DIV} = 9.3\ MW/m^2$
- $Z_{eff} = 3.59$
- $P^{*}_{Kr} = 796\ MW$
- $P^{\dagger}_{Brem} = 30\ MW$

$$n_i T_i = \frac{\beta_T B_T^2}{2\mu_o} (1 + Sn + S_T) \left[\frac{1 + f_z}{1 - f_z Z_z} + 1 \right]^{-1}$$

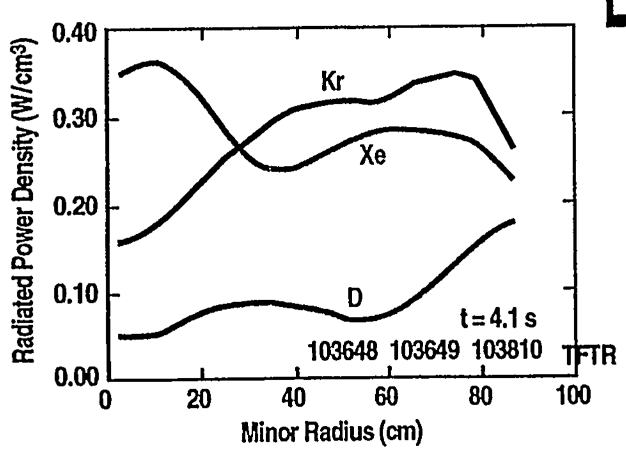

*Includes Kr line and Brem radiations.

†Includes only D, T, and He radiation.

GENERAL ATOMICS

OBSERVATIONS

- Kr and Xe could be effective core radiation impurities
- ϕ_{div} could be adjusted and made equal to ϕ_{fw}
- TFTR showed supportive results
- Acceptable power balance is shown for GA-LAR design
- Core radiation approach applicable to tokamak, LAR and other confinement concepts
- Effects on transport and confinement not clear
- Temperature instability can be a concern
- Verification experiments are being proposed to be performed in present tokamaks

289-97

GENERAL ATOMICS

FW/BLANKET DESIGN

- Functions
  - Tritium production
  - SC-coils and biological shielding
  - Power conversion
  - First wall heat flux removal

- Conventional approaches

Structural Material	Tritium Breeder	Coolant	Comment
Ferritic steel	Solid	H_2O	$\eta_{th} \sim 33\%$
Ferritic steel	Solid	He	$\eta_{th} \sim 33\%$
V-alloy	Li circulating	Li circulating	• MHD-insulator required for acceptable ΔP ($\eta_{th} = 45\%$) • Safety concern

- Concept being evolved

Structural Material	Tritium Breeder	Coolant	Comment
V-alloy + ferritic steel (bi-metallic design)	Li or LiPb (stagnant)	He	$\eta_{th} = 45\%$ • High He pressure • Safety concern • Possible for HPD design

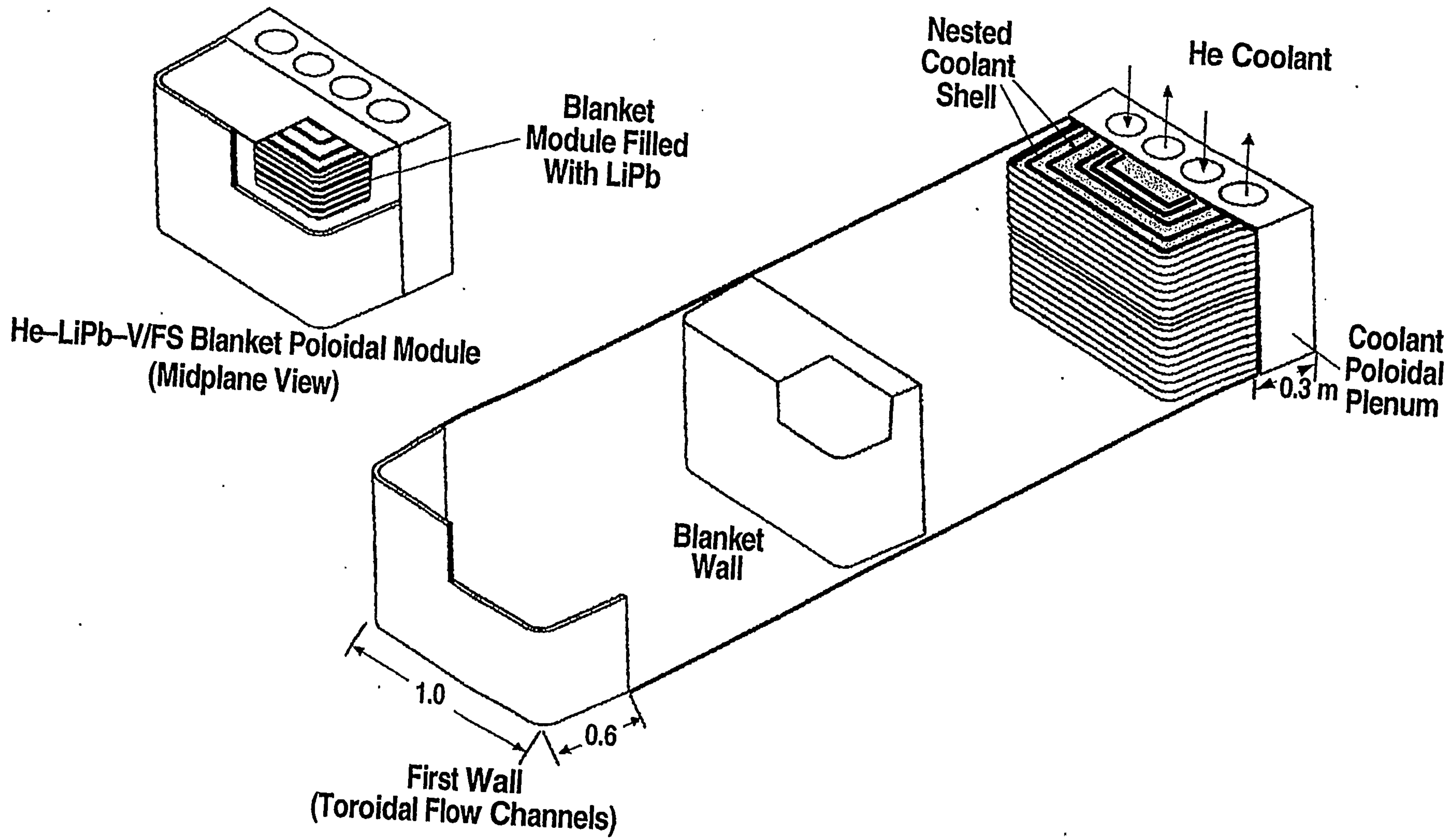

Blanket
Module Filled
With LiPb
He–LiPb–V/FS Blanket Poloidal Module
(Midplane View)
Nested
Coolant
Shell
He Coolant
Coolant
Poloidal
Plenum
0.3 m
Blanket
Wall
1.0
0.6
First Wall
(Toroidal Flow Channels)

290-97

FIRST-WALL BLANKET DESIGN (R_0 = 2.9 m)

"Applicable to any high power density fusion system"

Inputs

- Γ_n – Ave/max = 7.96/11.2 MW/m^2
- ϕ_{FW} – Ave/max = 1.95/2.69 MW/m^2
- Geometry
- Neutronics results
- He at 15 MPa
- T_{in} = 250°C
- T_{out} = 650°C
- He, Li Pb, V-alloy properties
- Nested shell geometry

Design Criteria

- V–T_{max} < 700°C
- LiPb–T_{max} < 1000°C
- $V_{He} < \frac{1}{3}$ sonic speed
- $V_{He} << V_{critical\ vibration}$
- Primary and secondary stresses (simple tube)

Design

(A nest shell poloidal module)

- He–cooled, V/FS-alloy, LiPb breeder
- First wall, blanket

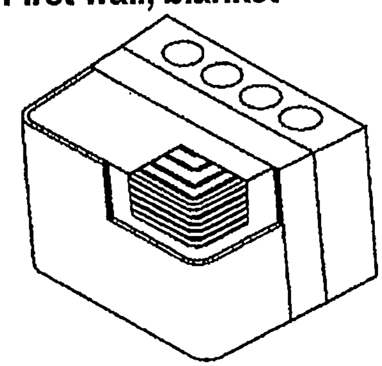

Results

- Design Criteria met.

Tube	Diameter	Wall Thickness
FW, mm	8	2
Blanket, mm	10	1.5

- Layer by layer volume fractions generated for neutronics iteration (Average volume fractions –V-alloy 15%, LiPb – 65%)
- η_{Th} – 45%
- 1-D TBR = 1.2 (90% ^{6}Li)

GENERAL ATOMICS

LOW ASPECT RATIO CONCEPT FOR A FUSION POWER PLANT

Inputs

GA–LAR physics formalism*

Key Parameters:

- A = 1.4
- β_T = 62%
- κ = 3
- BS fraction $\doteq$ 87%
- Ti = 25 keV

Design Approach

Optimized by:

- Approaching technology limits
- Minimizing physical size
- Minimizing recirculating power
- Eliminating inboard shield
- Spreading transport Power to first wall
- Using high power density blanket
- Maintaining low activation goal

Critical Elements Evaluated

- TF–coil central column
- Impurity core radiation
- First–wall blanket design
- COE

Design Code Results

- R_o = 2.9 m
- Pe–net: 1998 MW
- COE* = 52.8 mill/kWh†

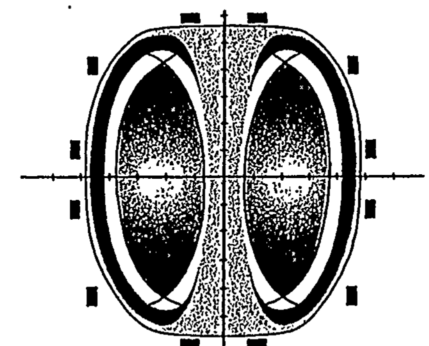

* Includes central column and blanket replacements

* R. Stambaugh et al, "The Spherical Tokamak Path To Fusion Power," submitted to Fusion Technology

†Coal and APWR: 50–60 mill/kwh beyond the year 2000

290-97

GENERAL ATOMICS

PHYSICS AND ENGINEERING PARAMETERS OF A LAR 1998 MW(e) DESIGN

Plasma aspect ratio, A	1.4
Plasma vertical elongation	3.0
Minor plasma radius, a (m)	2.08
Major toroidal radius, R_0 (m)	2.91
Plasma volume (m^3)	741
First-wall surface area (m^2)	493
Radial profile exponent for density, s_n	0.25
Radial profile exponent for temperature, s_T	0.25
Toroidal beta (%)	62
Poloidal beta (%)	1.43
On-axis toroidal field (T)	2.17
Plasma current, I (MA)	32.6
Plasma ion temperature (keV)	25
Plasma electron density, n_e ($10^{20}/m^3$)	2.4
Plasma ion density ($10^{20}/m^3$)	1.74
Kr fraction that of n_e (%)	0.19
Effective plasma charge, Z_{eff}	3.6
Fusion power density (MW/m^3)	6.6
Fusion power (MW)	4909
Toroidal field coil summary	
Number of TF coils	12
Mass of TF coil set (tonne)	1193
TF-coil current per coil,(MA)	2.6
Central column average current density (MA/m^2)	18.5
TF coil resistive power consumption [MW(e)]	271
Engineering summary	
Thermal conversion efficiency (%)	45
CD/heater [FWCD*] power (MW)	58
Total useful thermal power (MW)	5833
Gross electrical output power [MW(e)]	2625
Net electrical output power [MW(e)]	1998
Plant Q	4.2
14.06-MeV neutron load (MW/m^2)	7.96
Average LiPb blanket energy multiplication	1.4
First wall heat flux (MW/m^2)	1.95
Divertor max. heat flux (MW/m^2)	9.3

*Fast wave current drive

LAR FIRST WALL PARAMETERS

Plasma aspect ratio, A	1.4
Plasma vertical elongation	3.0
Minor plasma radius, a (m)	2.08
Major toroidal radius, R_0 (m)	2.9
Plasma volume (m^3)	741
First-wall surface area (m^2)	493
Number of TF coil	12
Module midplane width (m)	1.3
Module length (m)	14.6
Fusion power density (MW/m^3)	6.6
Fusion power (MW)	4909
Γn, ave/peak (MW/m^2)	7.96/11.2
φ_{fw}, ave/peak (MW/m^2)	1.95/2.69
Blanket energy multiplication	1.4
Helium pressure (MPa)	15
T_{in} (°C)	250
First wall circular tube:	
Inside diameter (mm)	8
Wall thickness (mm)	2

	Inlet	Middle	Outlet
$T_{coolant}$ (°C)	250	280	310
Coolant velocity (m/s)	138	146	154
Heat transfer coefficient (W/m^2K)	17780	17920	18060
T_{max} V-alloy (°C)	591	621	650
Pressure drop first wall (MPa)	0.5		
Allowable primary stress (MPa)	120		
Allowable secondary stress (MPa)	360		
Primary stress (MPa)	30		
Secondary stress (MPa)	203		

GA–LAR COE VERSUS PLANT SIZE AND TECHNOLOGY IMPROVEMENT

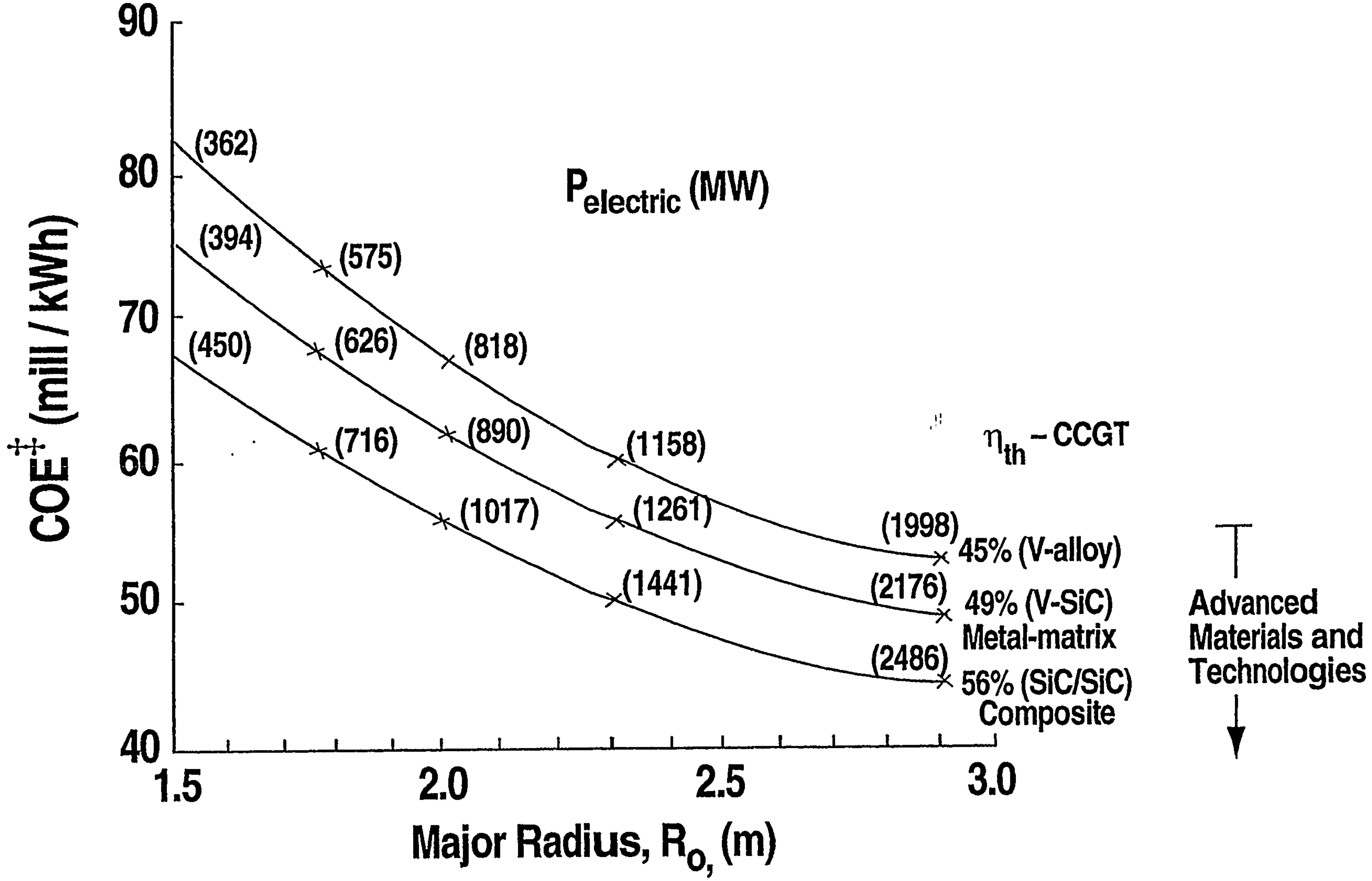

‡Including replacements

171-97/rs

GENERAL ATOMICS

CONCLUSIONS

- HPD design approach is a key to reduce magnetic fusion COE
- Core radiation has the possibility of distributing transport power between first wall and divertor — further experimental verification is essential
- He-cooled, V/FS, LM breeder FW/blanket design can possibly handle $\Gamma n \sim 8$ MW/m^2 — further technology developments are required
- GA-LAR shows the possibility of reaching a respectable and competitive COE of 53 mill/kWhr

SUMMARY OF ECONOMIC PARAMETERS

Account #	Account Title	$M (1992)
20.	Land and land rights	10.438
21.	Structures and site facilities	557.5
22.	Reactor plant equipment	1140
22.1	Reactor equipment	687.3
22.1.1.	FW/blanket/reflector	94.9
22.1.2.	Shield	36
22.1.3.	Magnets	85.3
22.1.4.	Supplemental-heating/CD systems	106.7
22.1.5.	Primary structure and support	119.1
22.1.6.	Reactor vacuum systems	90
22.1.7.	Power supply, switching and energy storage	134.3
22.1.8.	Impurity control	16.7
22.1.9.	Direct energy conversion system	0.000
22.1.10	ECRH breakdown system	4.3
22.2.	Main heat transfer and transport systems	452.5
23.	Turbine plant equipment	498.4
24.	Electric plant equipment	159.5
25.	Miscellaneous plant equipment	87.8
26.	Special materials	60.1
90.	Direct cost (not including contingency)	2503
91.	Construction services and equipment	330.4
92.	Home office engineering and services	137.7
93.	Field office engineering and services	165.2
94.	Owner's cost	508
96.	Project contingency	677.3
97.	Interest during construction (IDC)	755.3
99.	Total cost ($$10^6$)	5327

Key design parameters:

Unit overnight cost [$/kW(e)]	4572
Capital return [mill/kW(e)h]	39.4
Plant availability	0.75
O&M (1.68%) [mill/kW(e)h]	9.16
Replace.[mill/kW(e)h]	3.7
Decommissioning [mill/kW(e)h]	0.5
Fuel [mill/kW(e)h]	0.03
LSA*=2 total COE [mill/kW(e)h]	52.8 at η_{th}= 45%
	49.3 at η_{th}= 49%
	44.4 at η_{th}= 56%

*Level of safety assurance

GENERAL ATOMICS

Concept of Flibe blanket in FFHR

Akio Sagara

O. Motojima, O. Mitarai[1], S. Imagawa, K. Watanabe, H. Yamanishi, T. Uda, H. Chikaraishi, A. Kohyama[2], H. Matsui[3], T. Muroga, N. Noda, T. Noda[4], N. Ohyabu, T. Satow, A.A. Shishkin[5], Dai-Kai Sze[6], A. Suzuki[7], S. Tanaka[7], T. Terai[7], S. Toda[3], and FFHR Group

National Institute for Fusion Science, Toki 509-52, Japan

Collaboration works have made great progress in design studies for Force-Free Helical Reactor, FFHR, by standing on major advantages of current-less steady operation with no dangerous plasma disruptions. FFHR is a demo-relevant heliotron-type D-T fusion reactor (P_f=3GW, R=20m, a_p=2m, B_0=12T, B_{max}=16T, $<\beta>$=0.7%, enhancement factor h_H=1.5 for the energy confinement, and the neutron wall loading of 1.5 MW/m^2.) based on the great amount of R&D results obtained in the LHD project. Aiming at power generation from 2025 by introducing innovative concepts available in a coming few decades, the design parameters at the first stage for concept definition have been investigated to make clear key issues required for power-plant engineering including materials development. Cost estimation and design optimization are planned at the next stage after the current Phase-I studies.

The main feature of FFHR is force-free-like configuration of helical coils, which gives three attractive merits : simplification of coils supporting structures by opening areas for maintenance works, widening of the coil-to-plasma clearance needed for the blanket and shield space, use of high magnetic fields allowing operation with a fairly low plasma beta, $<\beta>$.

The other feature is the selection of molten-salt Flibe as a self-cooling tritium breeder from the main reason of safety : low tritium solubility, low reactivity with air and water, low pressure operation, and low MHD resistance which is compatible with our high magnetic field design.

- ♦ The 1-D blanket design with the forward layer of Be pebbles is optimized with the local TBR of 1.2, saving the Be amount, and increasing the surface of Be reacting with corrosive TF molecules, where the nuclear heating in Flibe is as high as 60% of the total fusion output.
- ♦ The self-cooling Flibe of 40mol % BeF_2 is operated at inlet/outlet temperatures of 450°C/550°C with the pressure drop lower than 1 MPa at the flow rate of $7m^3/s$, where the double walled tube is reliable to sweep out the permeated tritium using He gas.
- ♦ The vacuum disengager is promising to recover more than 90% of tritium with the T inventory less than 1g in 400ton of Flibe in the loop.
- ♦ Nuclear properties such as radioactivity and transmutation at 450dpa are investigated on JLF-1, V-alloy, SiC as well as materials compatibility with Flibe, aiming at replacement-free FFHR.
- ♦ Collaboration R&D programs on Flibe chemistry and engineering have been set off by making a materials test device and an active flow loop.

In the course of FFHR design studies, many subjects have been pointed out as future works under the present encouraging positive results.

Reference : A. Sagara, et al, ISFNT-4 (1997) in press in Fusion Engrg. Design.

Concept of Flibe blanket in FFHR

Akio Sagara

O. Motojima, O. Mitarai[1], S. Imagawa, K. Watanabe, H. Yamanishi, T. Uda,
H. Chikaraishi, A. Kohyama[2], H. Matsui[3], T. Muroga, N. Noda,
T. Noda[4], N. Ohyabu, T. Satow, A.A. Shishkin[5], Dai-Kai Sze[6],
A. Suzuki[7], S. Tanaka[7], T. Terai[7], S. Toda[3],
and FFHR Group

National Institute for Fusion Science, Japan

1) Kyushu Tokai University, Japan
2) Kyoto University, Japan
3) Tohoku Univ., Japan
4) National Research Institute for Metals, Japan
5) NSC"Kharkov Phys. and Tech. Institute", Ukraine
6) Argonne National Laboratory, USA
7) University of Tokyo, Japan

US-Japan Workshop on
High Heat Flux Components & Plasma Surface Interactions for Next Fusion Devices
Dec. 8 - 11, 1997
Warwick Regis Hotel, San Francisco

Design studies of FFHR have been performed from 1993

(1) as one of collaboration studies

(2) based on LHD under construction in NIFS

(3) to make clear key issues for D-T demo-plants

(4) to introduce innovative concepts

(5) by aiming at power generation from 2025.

Current-less steady operation is the major advantage of helical-type reactors.

FFHR has two main features

Reduction of the magnetic force between SC helical coils by giving three attractive merits:

- **simplification of coils supporting structures**
  which gives wide open areas for maintenance works,
- **widening of the coil-to-plasma clearance**
  needed for the blanket and shield space,
- **use of high magnetic fields**
  allowing operation with a fairly low beta, $<\beta>$,
  requiring less-sever enhancement for τ_E.

Practical designs realizing these merits are actually required.

Reduction of the magnetic force gives three attractive merits

(1) Simplification of coil supporting structures
(2) Use of high magnetic fields
(3) Wide coil-to-plasma clearance

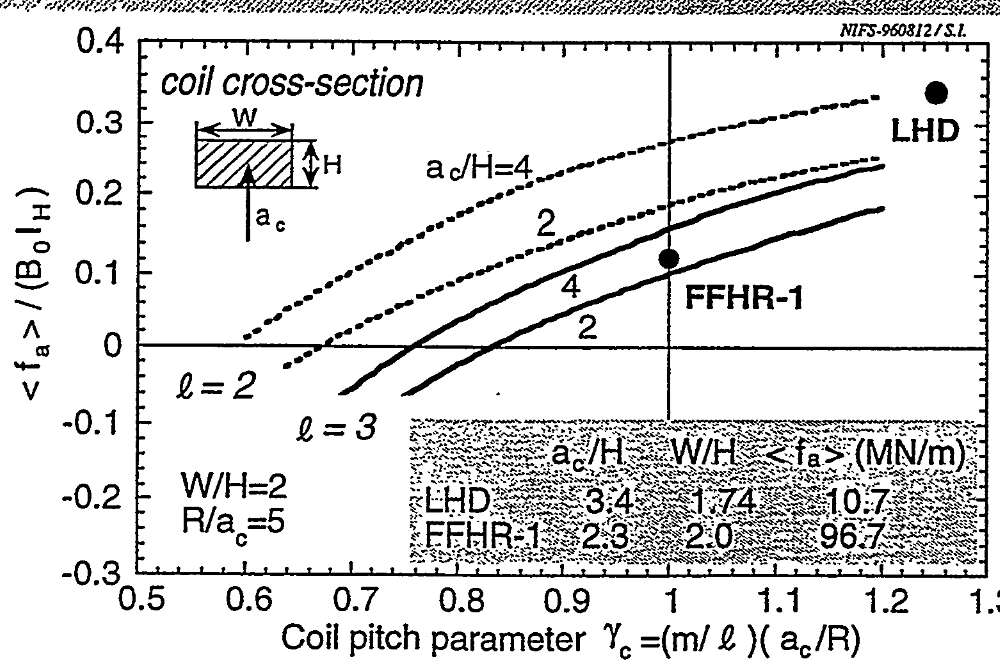

Collaboration & Publication Network

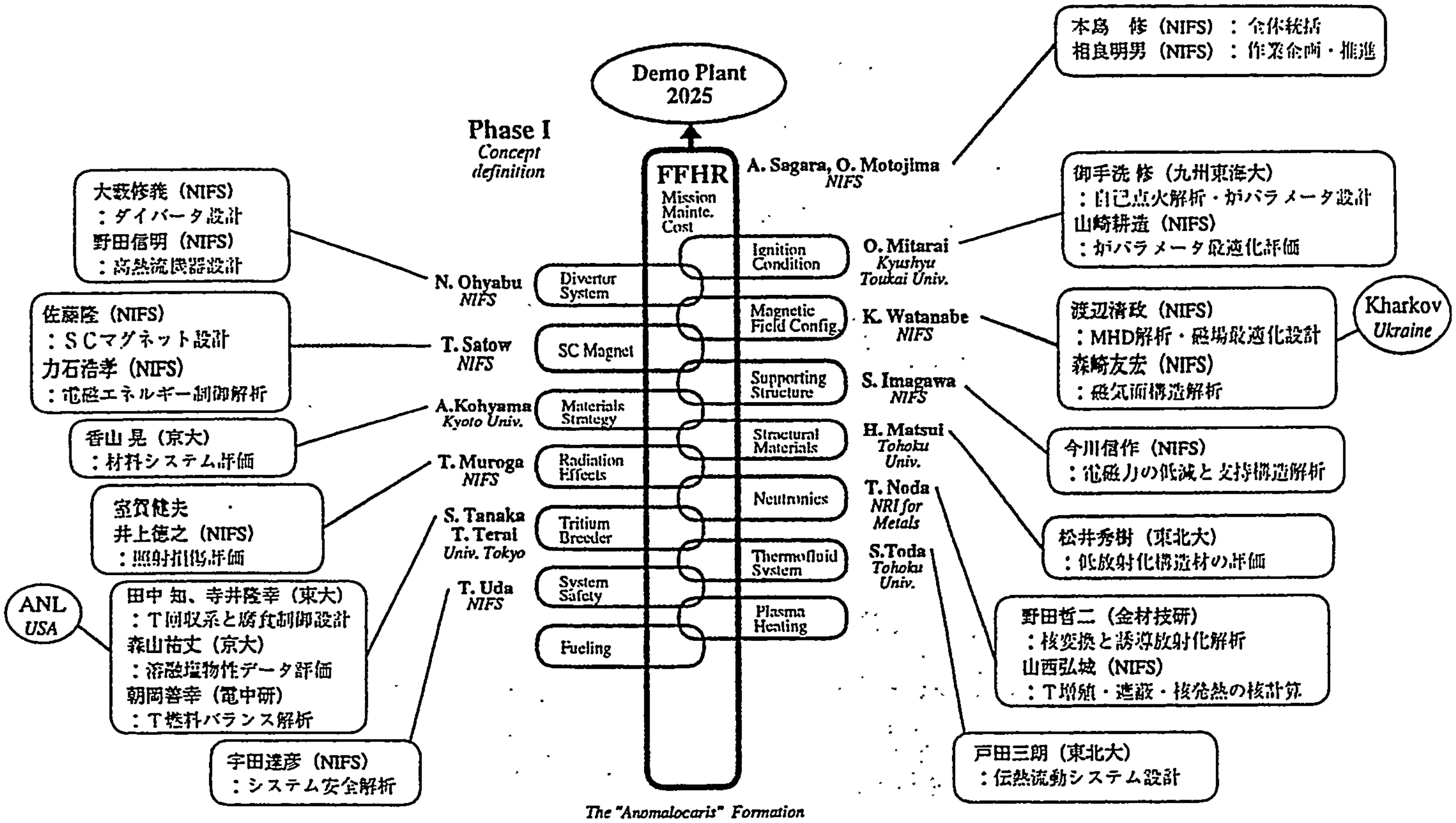

The "Anomalocaris" Formation

NIFS-970417-A.S.

LHD-type Reactor Design - - FFHR - -

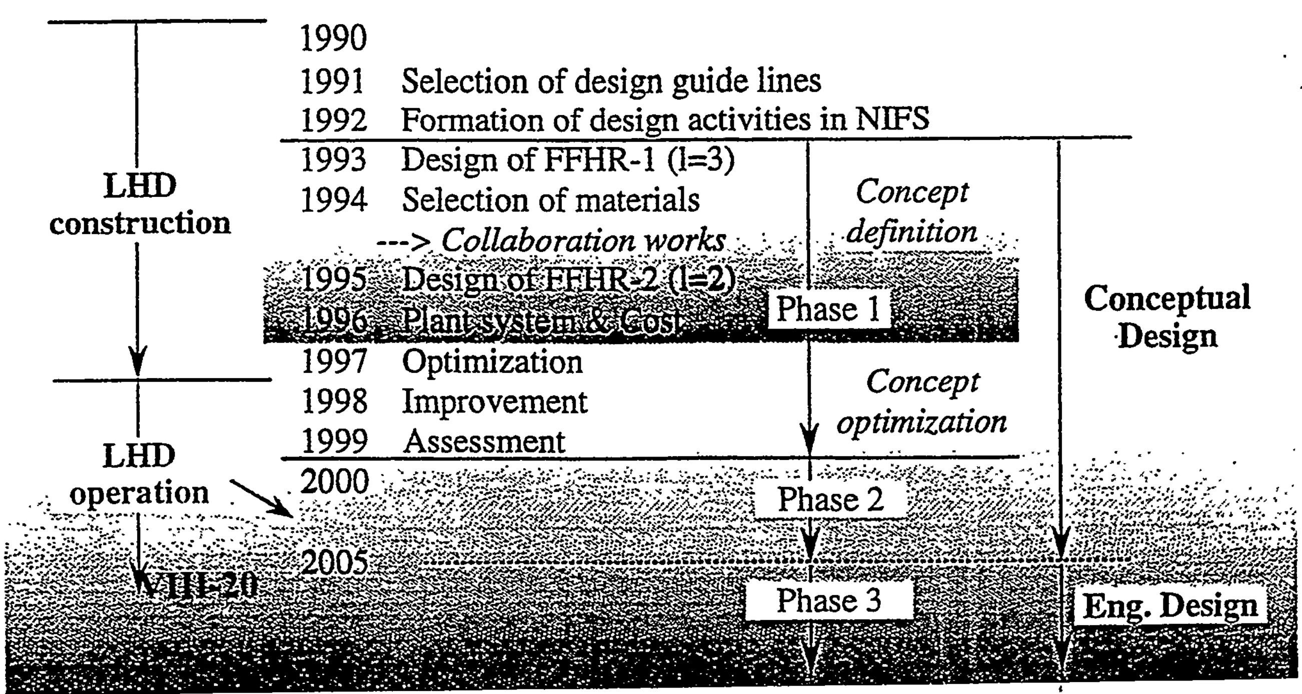

FEM analyses have been done on cylindrical coils supporting structures

- large maintenance holes
- under the merit of force-free-like coils.

The max. stress is below the yield stress of ss-316LN.

Structure designs of the SC itself is the next work.

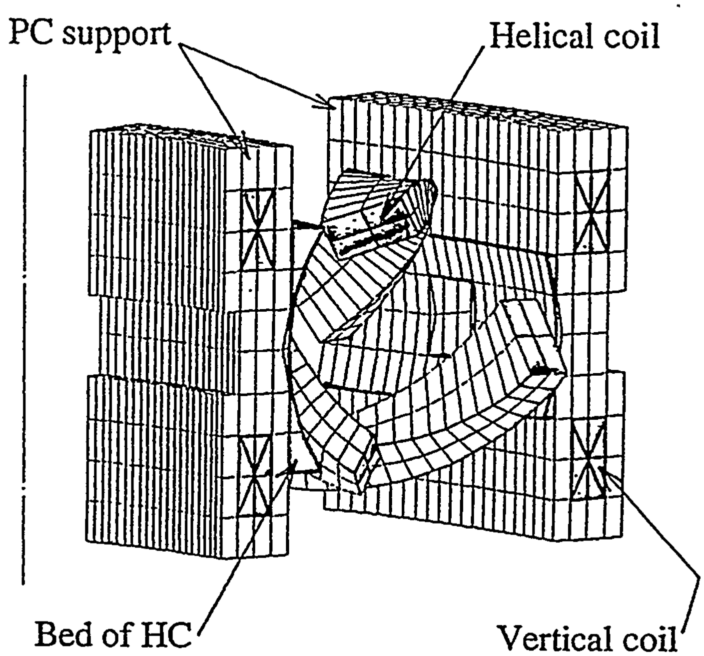

The case A is almost optimum for constraints; the $B_{\perp max} < 15$ T, the clearance $\Delta < 1$ m, and the enhancement factor $h_H < 2$ for τ_{LHD}

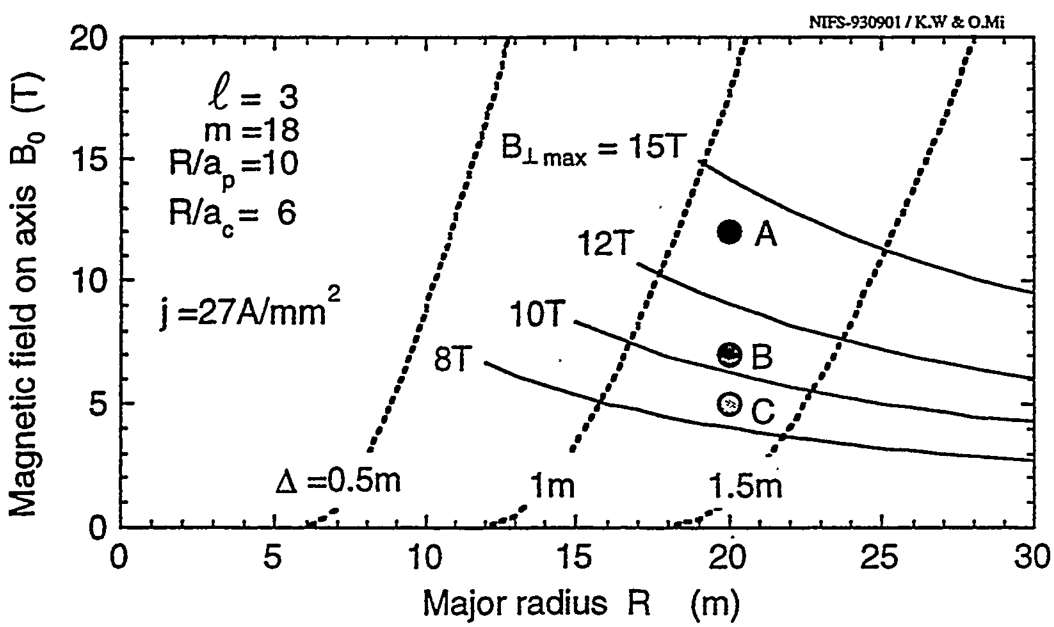

Ignition conditions for the 3GW fusion output

case A: $T_i(0)$=22keV, $n(0)=2.0\times10^{20} m^{-3}$, $<\beta>$ =0.7 %, h_H=1.5

case B: $T_i(0)$=24keV, $n(0)=1.9\times10^{20} m^{-3}$, $<\beta>$ =2.2 %, h_H=2.25

case C: $T_i(0)$=29keV, $n(0)=1.5\times10^{20} m^{-3}$, $<\beta>$ =4.5 %, h_H=3.5

LHD and FFHR-1 Design Parameters

	LHD	FFHR-1 case A	case B	cace C
Plasma parameters				
number of pole : ℓ	2	3		
toroidal pitch number : m	10	18		
major radius : R (m)	3.9	→ 20		
av. plasma radius : $<a_p>$ (m)	< 0.65	2		
fusion power : P_f (GW)	-	3		
external heating power : P_{ex} (MW)	< 20	100		
toroidal field on axis : B_0 (T)	4	→ 12	7	5
average beta : $<\beta>$ (%)	> 5	→ 0.7	2.2	4.5
enhancement factor of τ_{LHD}		→ 1.5	2.25	3.5
plasma density : $n_e(0)$ (m-3)	$1x10^{20}$	$2x10^{20}$	$1.9x10^{20}$	$1.5x10^{20}$
plasma temperature : $T_e(0)$ (keV)	> 10	22	24	29
effective ion charge : Z_{eff}		1.5		
alpha heating efficiency : η_α	-	0.7		
alpha density fraction : f_α	-	0.05		
Engineering parameters				
av. helical coil radius : $<a_c>$ (m)	0.975	3.33		
pitch parameter : $\gamma_c=m<a_c>/(\ell R)$	1.25	1		
coil modulation : α	+ 0.1	0		
coil to plasma clearance : Δ (m)	0.03	→ 1.1	1.25	1.3
coil current : I_H (MA/coil)	7.8	66.6	38.9	27.8
coil current density : J (A/mm^2)	(53)	27		
max. field on coils : B_{max} (T)	(9.2)	16	11.5	10
stored energy with poloidal coils (GJ)	1.64	1290		
neutron wall loading : P_n (MW/m^2)	-	→ 1.5		
av. heat load on divertor: P_d (MW/m^2)	< 10	1.6		
blanket material	-	Flibe(40vol.%)+Be(40vol.%)		
operation temperature	-	inlet 450°C / outlet 550°C		
T breeding ratio (TBR)	-	1.1		
SC material	NbTi	Nb$_3$Al or (NbTi)$_3$Sn		

Force-Free-like Helical Reactor **FFHR**
based on The LHD in National Institute for Fusion Science

a_c=3.3m
'=20m, a_p=2m
=3, m=18, γ=1
$_0$=12T, $<\beta>$=0.7%
$_f$=3GW, 1.5 τ_{LHD}
$_n$=1.5MW/m^2

ICC-SC coils of
b$_3$Al or (NbTi)$_3$Sn

'iBe blanket
'th ferritic-alloy
lt. V-alloy, ODS)

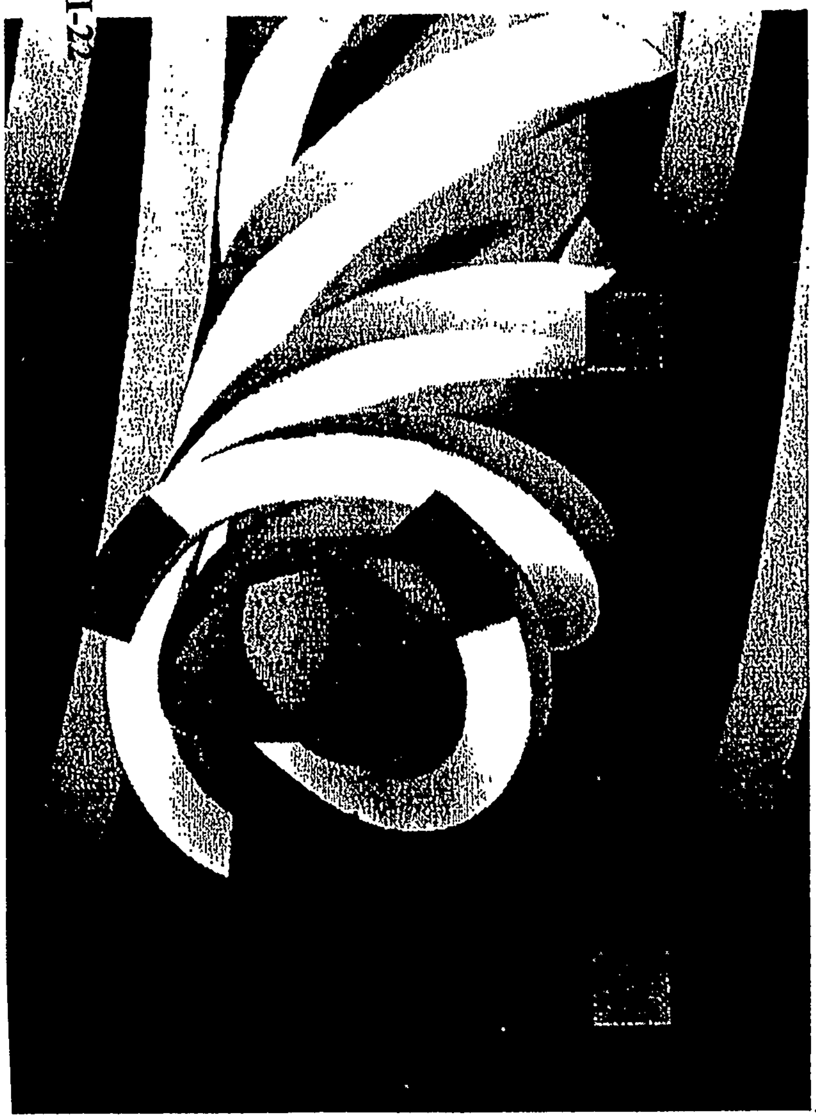

The Flibe of 40mol % BeF_2 is operated with $\Delta P < 1$ MPa,

where the total pump power is only 0.8% of the fusion output Pf.

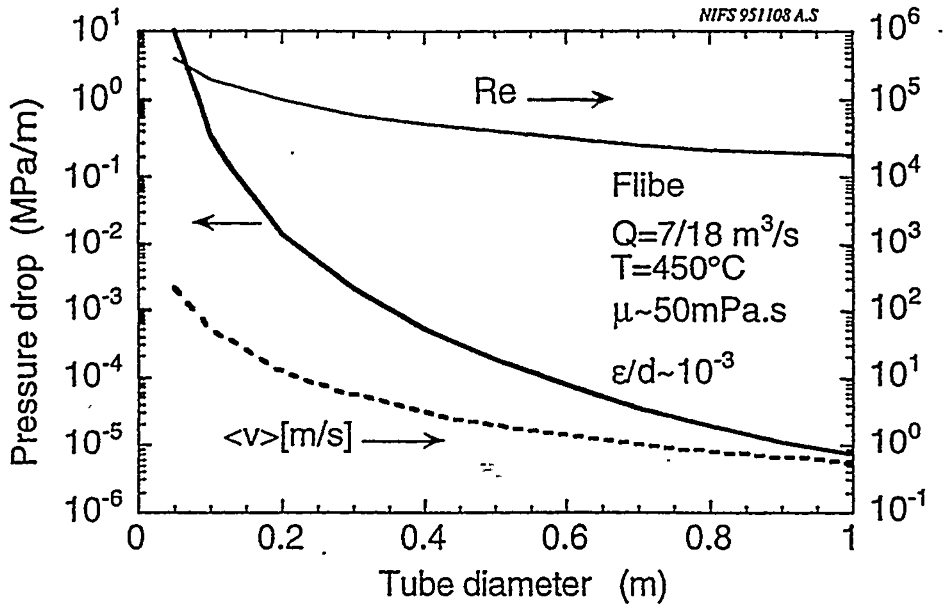

Flibe Blanket in FFHR

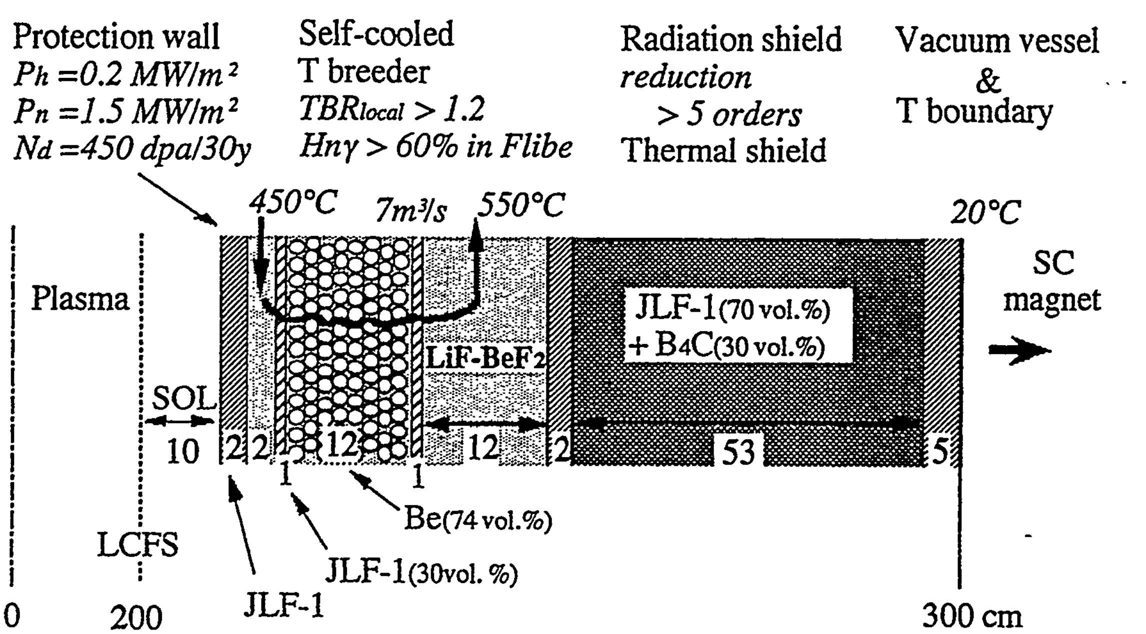

- **Ferritic steel JLF-1 (Fe9Cr2W)** was selected as the first candidate.
- **Vanadium alloy or ODS steel** are second options.
- **If SiC is available** in future, it gives high thermal efficiency with He gas turbine system.

Selection of molten-salt Flibe as a self-cooling T breeder from the main reason of safety :

- low tritium solubility
  (~ 8 orders lower than liq.Li)
- low reactivity with air and water,
- low pressure operation(< 1MPa),
- low MHD resistance (~ 1Ωcm)
  compatible with high B field.

In order to fully take advantage of inherent safety with Flibe, it is still now required to improve the Flibe blanket concept and to clarify safety related issues.

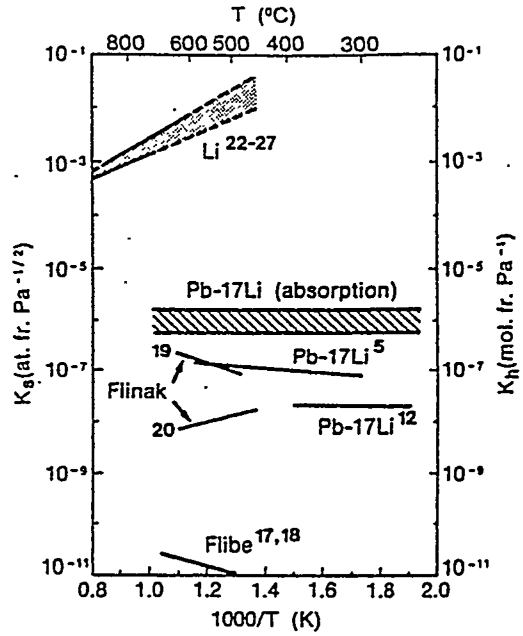

Fig. 1. Solubility constants for hydrogen isotopes in liquid breeders.

Caorlin et al. FUSION TECHNOLOGY VOL. 14 SEP. 1988

The low solubility of T in Flibe gives two advantages

(1) T_2 recovery system is probably quite simple.

The vacuum disengager is promising

to recover > 90% of T in Flibe,

where the double walled tube is reliable

to sweep out the permeated T with He,

(2) In this case the T inventory is less than 1g

in 400 ton of Flibe in the loop.

More specified data bases are desired on

- rate-determining steps of T_2 release,

Force-Free Helical Reactor FFHR

- ♦ D-T Demo Reactor (P_f=3GW, **R=20m**, a_p=2m, B_0=12T)
- ♦ Current-less plasma (**steady** operation, no disruption)
- ♦ Reduced wall loading (1.5MW/m^2 , 30 years = **450 dpa**)
- ♦ Liquid Flibe blanket (> **450°C** for T_m, < 550°C for JLF-1)

If there is no need to replace in-vessel materials, FFHR can be operated with not only the high safety but also a **high availability**, resulting in reducing not only COE but also the total amount of **radwaste**.

The materials integrity at 450 dpa and **compatibility with Flibe** are the key issues to realize **replacement-free FFHR**.

Induced Radioactivity

The surface dose rate after 45 MWa/m^2

- ♦ **JLF-1, V-alloy < 1μSv/h after 100 years cooling.**
  This level satisfies the shallow land disposal limits *such as Class C limits of US 10CFR61* or the allowable hands-on dose rate of 10μSv/h.
- ♦ **Pure SiC satisfies the shallow land disposal limits.**
- ♦ **Mo and Nb must be lower than 10 ppm.**

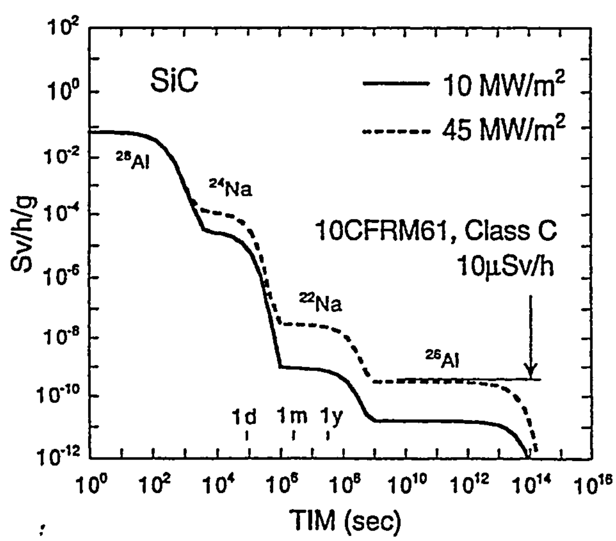

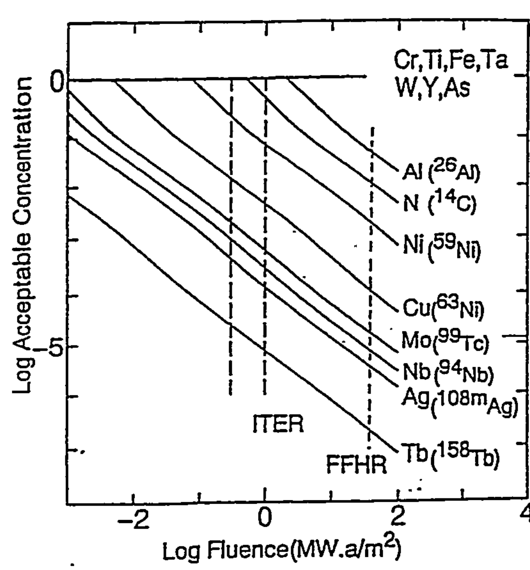

Flibeの運転温度

- ●入口温度　：融点と粘性の妥協点(40%BeF2)で450°C
- ●出口温度　：JLF-1の照射下クリープより550°、熱応力低減を検討
- ●Flibe流量　：熱出力3GW、ΔT=100°C に対して7m3/s,
- ●流動圧損　：1MPa 以下（18流路、φ20cm、50m、５エルボー）
- ●ポンプ動力：核融合出力の1%以下
- ●初期充填　：ヒーターと加熱ガス併用を検討、回収含む手順が課題

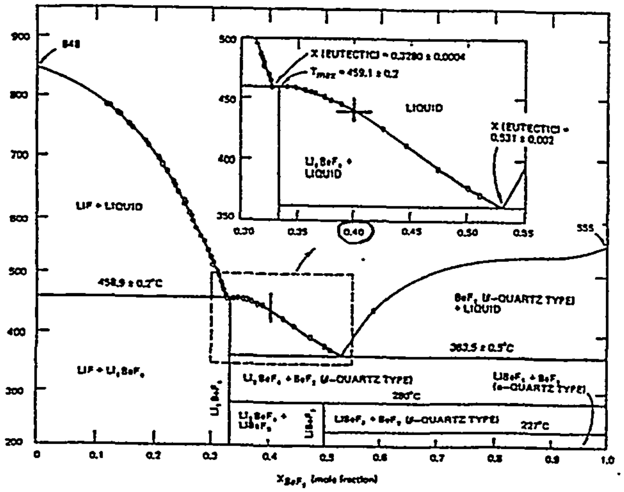

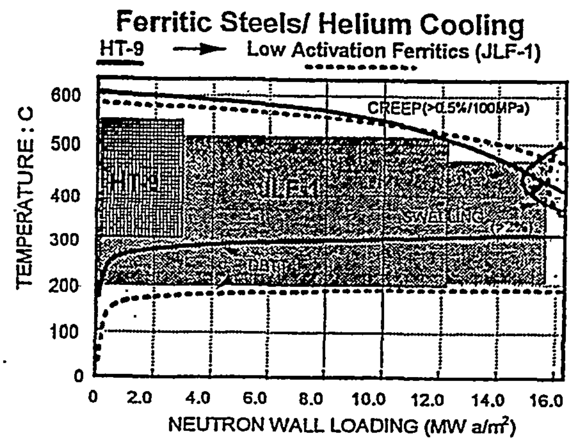

(after Kohyama)

FFHR has many inherent and passive safety features

- ♦ current-less plasma,
- ♦ steady state operation,
- ♦ use of Flibe,
- ♦ high-temp. &T devices inside the torus area.

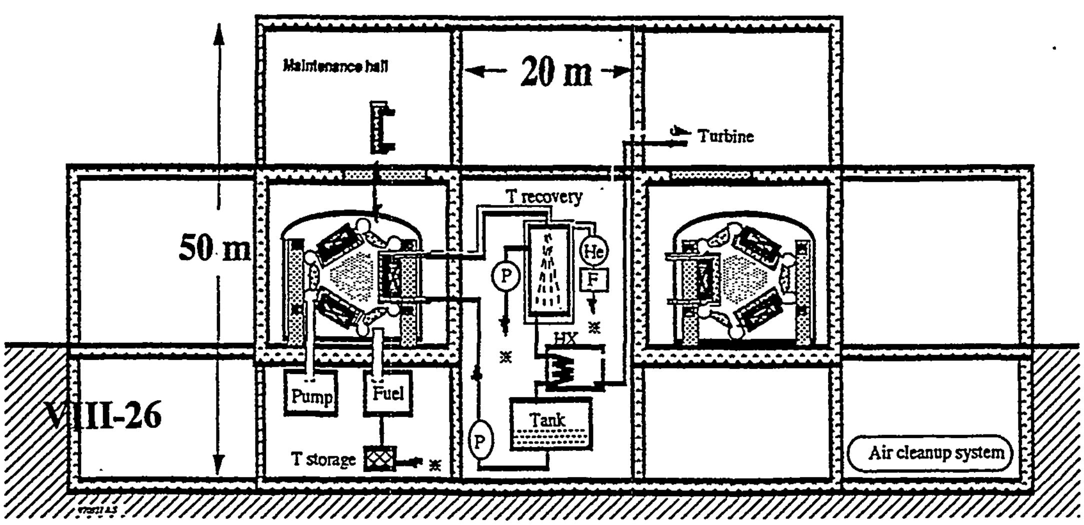

Solid Transmutation Products

after 45 MWa/m^2

- From W to almost 10% W, 20% Re and 70% Os.
- Investigation JLF-1 after transmutation of W are desired..
- From V to Cr is about 2wt.% under Flibe blanket.
- V4Cr4Ti has a sufficient margin to the DBTT shift.

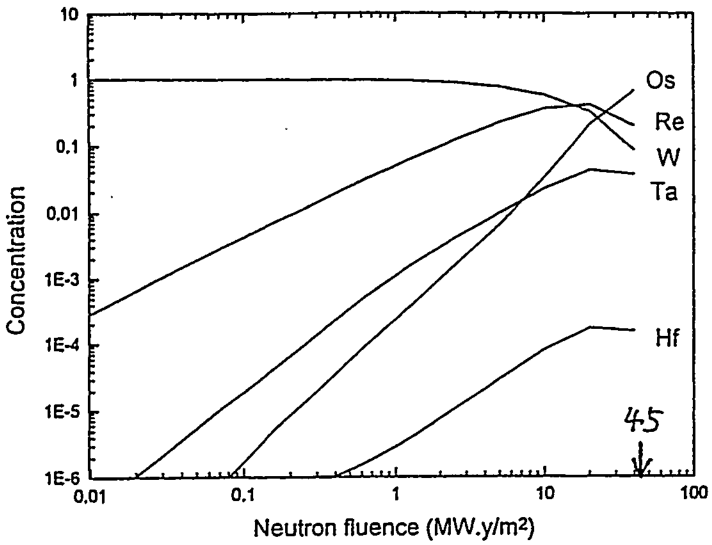

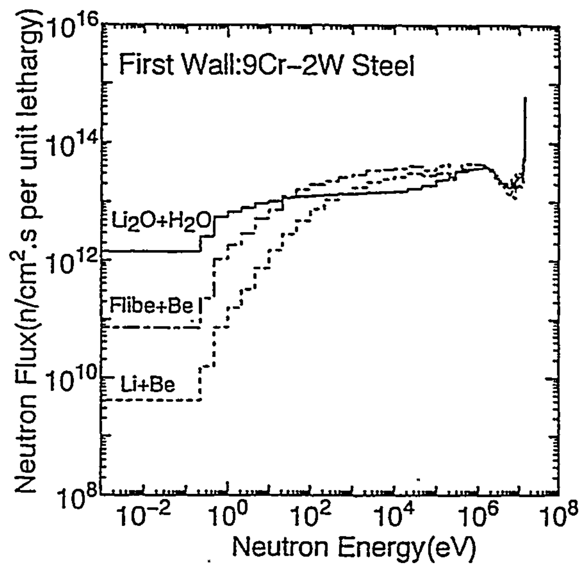

Decay Heat Qd

$dT/dt = Q_d/C_v$ under adiabatic condition

- On W, Mo and Nb, dT/dt < 0.5°C/s after 1 week cooling, this may be acceptable.
- On Ta, dT/dt=15°C/s for 100 days cooling is not acceptable.

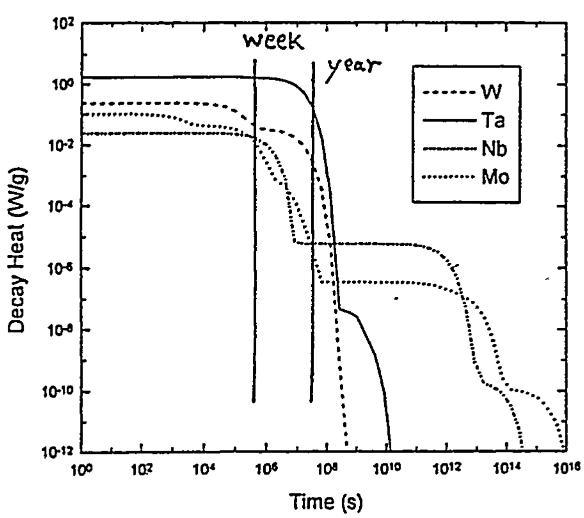

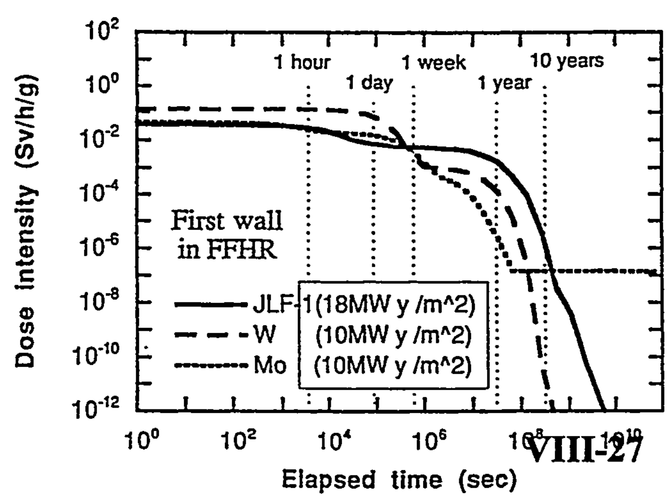

Compatibility with Flibe

- ♦ The neutron multiplier Be is used to reduce corrosive TF molecules.
  ($Be + 2TF \rightarrow BeF_2 + T_2$)
- ♦ MoF_6 can be often used to form Mo layers on the coolant tube.
  ($MoF_6 + 3T_2 \rightarrow 6TF + Mo$)
- ♦ **Data bases on chemical kinetics are strongly desired.**

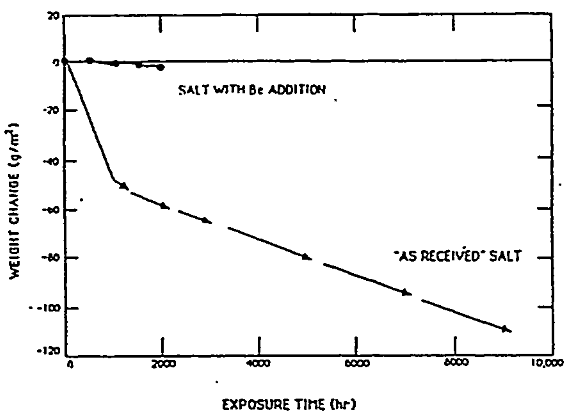

Fig. 2 Weight change versus exposure time for type 316 stainless steel in LiF-BeF_2 salt at the maximum loop temperature of 650°C.

by J.R. Keiser et al. (1979)

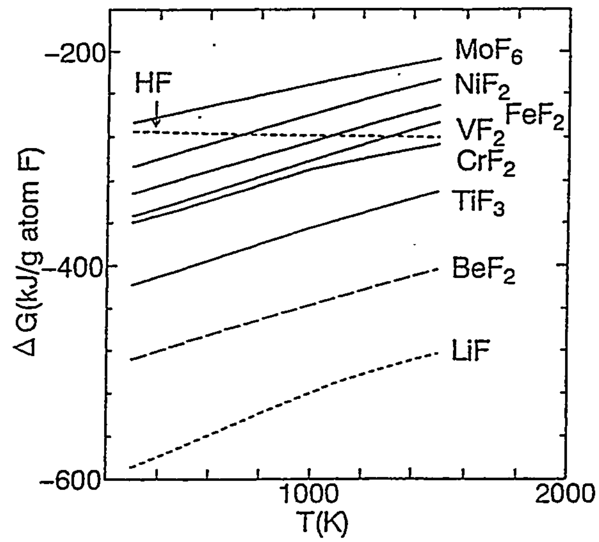

R&D's on Flibe chemistry and engineering have been set off

by making

a materials test device (Univ. of Tokyo), an active flow loop (Tohoku Univ.).

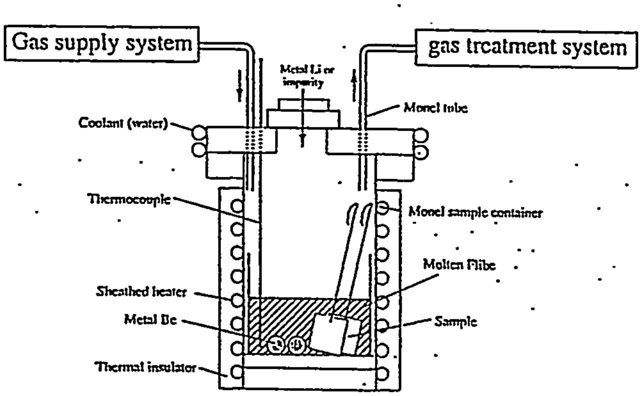

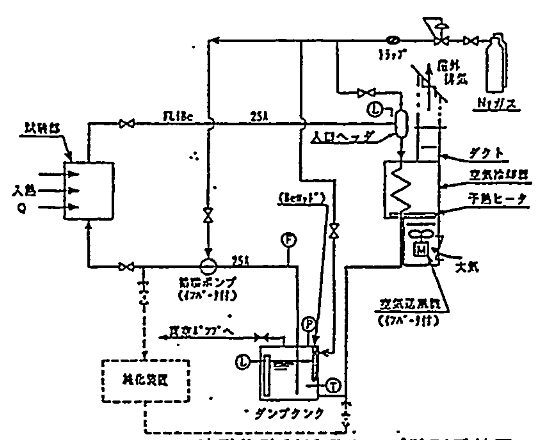

溶融塩強制循環ループ計画系統図

The blanket units are replaced through maintenance ports by sliding along the continuous helical coils.

(1) Since FLiBe is moved to a drain tank, each unit is below 5 ton.

(2) Radioactive wastes in each replacement are

- 800 ton of JLF-1
- ~~160 ton of Mo-TiC or 300 ton of W-TiC~~

  ~~which is only 16 m^3 in volume and can be managed~~
- ~~350~~ 200 ton of Be which is the mass of recycling use

  as well as 400 ton of FLiBe

Summary

(1) Molten-salt Flibe is selected as a self-cooling tritium breeder from the main reason of safety.

(2) The 1-D blanket design with the forward layer of Be pebbles is optimized with $TBR_{local} > 1.2$, saving Be amount, and increasing the surface of Be reacting with corrosive TF, where the nuclear heating in Flibe > 60% of Pf.

(3) The self-cooling Flibe(40mol % BeF_2) is operated at inlet/outlet of 450°C/550°C with the $\Delta P < 1$ MPa at 7m^3/s, where the double walled tube is reliable to sweep out the permeated T using He gas.

(4) The vacuum disengager is promising to recover more than 90% of tritium with the T inventory < 1g in 400ton of Flibe in the loop.

(5) Nuclear properties such as radioactivity and transmutation at 450dpa are investigated on JLF-1, V-alloy, SiC as well as materials compatibility with Flibe, aiming at replacement-free FFHR.

(6) Collaboration R&D programs on Flibe chemistry and engineering have been set off by making a materials test device and an active flow loop.

(7) In FFHR design studies, many subjects have been pointed out as future works under the present encouraging positive results.

VIII-30

Motivation, Scope, and Preliminary Approach for APEX

Neil B. Morley
Mohamed Abdou
Fusion Science and Technology, UCLA

US-Japan Workshop on High Heat Flux Components and Plasma Surface Interactions

San Francisco, USA
December 8-11, 1997

APEX

Ultimate Goal

Significant contributions to making the (long-term) fusion energy system more competitive through exploring and developing more attractive concepts for Fusion Power Technology (FPT)

FPT: Region from the edge of the plasma to the inner surface of the magnets

Near-Term Objective

Explore new (and possibly revolutionary) concepts that can provide the capability to efficiently extract heat from systems with high neutron and surface heat loads while satisfying all FPT functional requirements and maximizing reliability, maintainability, safety and environmental attractiveness

The Motivation for Conducting APEX Emerged from the New Vision for Fusion Restructured Program

New Vision

- Take the long term view
- Emphasize science (including engineering sciences) as basis for innovation
- Key is Improving Fusion
  - ➢ Make the ultimate product more attractive
  - ➢ Have more effective R&D pathways

How to Improve Fusion

1) Plasma Physics Innovation
2) Technology Innovation
   - can make product more competitive
   - can define the limits
     - ➢ provide boundary conditions to physics research
     - ➢ better evaluation of fusion's potential

A Conceptual FPT Design

1. Must satisfy functional requirements

2. Strive to be attractive

   - There are many attractiveness criteria. **It** is probably impossible to satisfy (or win) all of them

   - Ultimately, the best choice is based on trade-offs among the various criteria

Functional Requirements of Fusion Power Technology

1) provision of VACUUM environment

2) EXHAUST of plasma burn products

3) POWER EXTRACTION from plasma particles and radiation (surface heat loads)

4) POWER EXTRACTION from energy deposition of neutrons and secondary gamma rays

5) TRITIUM BREEDING at the rate required to satisfy tritium self sufficiency

6) TRITIUM EXTRACTION and processing

7) RADIATION PROTECTION

General Attractiveness Criteria for Fusion Energy System

1. ECONOMICS
    a) cost per unit thermal power
    b) thermal conversion efficiency
    c) mean time between failure (MTBF)
    d) mean time to repair (MTTR)
    e) lifetime
2. SAFETY
    a) chemical reactivity
    b) decay heat
    c) tritium inventory
    d) dose
    e) etc.
3. ENVIRONMENTAL
    a) waste disposal
    b) routine releases (e.g. tritium)
    c) material resources utilization
    d) etc.

APEX (initial) focus: Economics
APEX (initial) DRIVER: Capability for High Neutron Wall Load and Associated Surface Heat Flux

Most Challenging Issues for FPT

1. Heat removal at high temperature and high wall load

2. Failure rate

3. Time to recover from a failure

4. Tritium fuel self sufficiency

This provides critical framework for:

- understanding the motivation for APEX
- evolving the APEX approach

Current Design Concepts and Materials for First Wall / Blanket **Do NOT** Have the Capability to Meet the Fusion Challenge

Concept	Wall Load Capability MW/m^2	Other Observations
Ferritic / He / Breeder **Ferritic / H_20 / Li Pb**	2	Magnetic material Fracture toughness
Vanadium Alloy / Lithium	2.5	V works only with lithium Is lithium acceptable? Not feasible until a self healing coating is found
SiC / SiC / He / Breeder	1.5	Serious feasibility issues Do NOT know how to design Poor thermal conductivity

N. Morley, UCLA

Summary of FPT most challenging issues

1) Economic competitiveness requires **higher power density**. Current first wall/blanket concepts are limited to about 2 or 2.5 MW/m^2 P_{NL}. Comparison to fission reactors reveals that much more higher neutron wall loads should be the goal for fusion R & D.
2) Tritium self-sufficiency is highly uncertain with present concepts.
3) Failure rates as extrapolated from current technologies are too high with present first wall/blanket concepts.
4) Maintainability is a serious issue with current concepts. Specifically, MTTR (mean time to recover from failure) is very long. Such long MTTR (>2 months) seriously reduces reactor availability and make requirements on MTBF impractical.

Path to Improving Fusion

- All the above four issues need to be addressed (ultimately).
- We need concepts that:
  - (a) can handle a much higher wall load
  - (b) can provide better margins for insuring tritium self-sufficiency,
  - (c) have lower failure rate (longer MTBF), and
  - (d) faster maintenance (shorter MTTR)

APEX Focus

- APEX is only the first leg along the path toward improving fusion
- APEX will focus specifically on simulating new design concepts for in-vessel components that are capable of handling high neutron wall loads and the associated surface heat flux

- Of course, we should keep an eye on maintainability, failure rate, and tritium self sufficiency plus many other criteria (low decay heat, low activation, etc.)
- However, we should not over-constrain the problem from the beginning. If we succeed in finding high power density concepts, we can work later on making them better for other issues.

We invite comments on this

Proposed Goals for Neutron Wall Load and Surface Heat Flux at the First Wall

1) Average Neutron Wall Load $P_{NL,ave}$= 5 MW/m^2
   Peaking Factor = 1.4
   Peak Neutron Wall Load = 7.0 MW/m^2

Reasons
- High enough to improve economics
- Not overly ambitious: we probably can find a concept or two that meet the goal

2) Surface Heat Flux

Radiate most of the α-power to the first wall (reduce divertor problem)
- first wall surface area is more than ten times the divertor area
- this also allows useful (sensible) heat recovery for the $\propto$- power

Suggested Peak Surface Heat Flux ~ .85 x 0.25 x 7 ~ 1.5 MW/m^2

Design goals that must be met in a concept to be considered suitable for APEX **Neutron Wall Load = 7** **Surface Heat Flux = 1.5**

Participating Organizations

University of California, Los Angeles (UCLA)

Professor Mohamed Abdou, Lead Investigator
Dr. Mahmoud Youssef, APEX Secretary (youssef@fusion.ucla.edu)

Argonne National Labs (ANL)
General Atomics (GA)
Idaho National Engineering & Environmental Labs (INEEL)
Lawrence Livermore National Labs (LLNL)
Oak Ridge National Labs (ORNL)
Princeton Plasma Physics Lab (PPPL)
Rocketdyne
Sandia National Labs (SNL)
UC San Diego (UCSD)
University of Wisconsin (UWM)

APEX Project Groups

(1) Design Conceptualization and Analysis
Chair: Mohamed Abdou, UCLA. Core of APEX project

(2) Mechanical Design and Availability Group
Chair: Brad Nelson, ORNL. This group will be responsible for assisting all design conceptualization groups in developing mechanical design and integration.

(3) Materials Group
Chair: Steve Zinkle, ORNL. Suggest materials for high power density applications and provide basic material properties for design.

(4) Power Conversion
Chair: D. Sze, ANL. Delineate operating temperature, materials, and technology requirements and issues. Also estimate efficiency as a function of blanket/first wall outlet coolant temperature.

(5) Physics Interface Group
Chair: Dale Meade, PPPL. Provide physics boundary conditions for FPT design (some issues may require interface with the physics community to get the best input.

(6) Safety Group
Chair: Kathy McCarthy, INEL

(7) Alternate Confinement Concepts
Chair: Dale Meade. Summarize the main configuration features and general range of parameters (wall load, surface heat flux, etc.) for alternate confinement concepts and contrast them to tokamaks.

(8) Expert Judgment and Selection Panel (TBD)

APEX Tasks

Task 1: Delineate function requirements and develop evaluation Approach (criteria)

A. Special driver criteria (high wall load)
B. General Criteria (economics, safety, environmental)
C. R & D and potential success criteria

Task 2: Determine the key limiting factors on high power density
- understand the limits to learn how to extend them

Task 3: Explore concepts with high power density capability
- A primary task
- Primary sources of new concepts:
  A) concepts previously proposed in literature
  B) "Innovation through analogy" to other technologies (e.g. rocket engine)
  C) "Innovation through pursuit of engineering science logic" (building on what we learn from Task 2)

Task 4: Preliminary conceptual designs for new concepts

- Approach:
  - Concepts identified in Task 3 will be carefully analyzed and evaluated
  - Initially, examine the scientific foundation of the concept
  - If a concept has sound scientific basis, a preliminary conceptual design will be attempted to satisfy all functional requirements of FPT
  - Only if such effort is successful for a concept, will we attempt to improve and optimize it using the evaluation criteria as a guide

- Please note that some concepts require new models and methods of analysis to predict behavior. This can be a major effort

- Initially, we will not constrain conceptualization too much. For example, low activation will not be an initial requirement.

- Output of this task

  a) a set of preliminary conceptual designs for a number of promising concepts

  b) preliminary evaluation of each concept

  c) a set of key issues for each concept

Task 5: Comparative evaluation and selection of most promising concepts

- The magnitude of this effort will strongly depend on the outcome of Task 4, i.e. how many concepts (There may be none, or only one, or many)
- If there are several concepts, then the evaluation criteria developed in Task 1 will be utilized to select the most promising concepts that are worthy of further detailed studies

Task 6: Detailed analysis and evaluation of most promising concepts

- The most promising new concepts selected in Task 5 will be subjected to more comprehensive analysis and detailed evaluation
- Key issues will be identified and key R & D items will be recommended

Task 7: Study conclusions and report

APEX: Relationships between Tasks and Groups

	Task 1 Functional Requirements, Scientific feasibility, Evaluation Approach	Task 2 Key Limiting Factors in current concepts	Task 3 EXPLORE concepts with High Power Density Capabilities	Task 4 Preliminary Conceptual Designs for new concepts	Task 5 Comparative Evaluation and Selection of most promising concepts	Task 6 Detailed Analysis & Evaluation of most promising concepts
Group 1: Design Conceptualization & Analysis		(essentially complete, no further work required)	***	***	X X	X X X
Group 2: Mechanical Design and Availability	X		X X X	X X X	X X	X X
Group 3: Materials	X		Material properties and limits	Material properties and limits	X X	X X
Group 4: Power Conversion System			provide outlet coolant temp. requirements and $\eta(T_{in},T_{out})$			
Group 5: Physics Interface	X		Physics boundary conditions			
Group 6: Safety Environment	X X					
Group 7: Alternate Confinement Concepts	X		Requirements for alternate concepts			
Group 8: Judgement and Selection Panel	***					

Current Work (Next Meeting, Jan. 1998)

- Material database (FS, V, SiC, Nb-Zr, Ti-SiC, etc.)

- Continue creative evolution of new concepts (prize for best concept, any suggestions??)

- Solidify physics issues
  1. Peaking factors
  2. Physics radiation scenarios
  3. Spectrum of radiated alpha power
  4. Alternative confinement concept definition

- Concept Analysis
  1. Convective liquid layers
  2. Thick liquid walls
  3. Porous walls
  4. Flowing solid particulates

Porous FW Concepts

- Porous material infiltrated with high thermal conductivity liquid
  1. Reduce the elastic modulus
  2. Retain or increase effective thermal conductivity
  3. Add renewable liquid surface layer
  4. Possibly enhance heat transfer to bulk coolant (reduce film temperature drop)
  5. Change nature of failure and stress response in wall

- Different incarnations considered
  1. controlled surface porosity (no flow)
  2. Sealed surface (no plasma contact)

- Analysis focusing on characterizing porous materials and thermalhydraulic calculations

Liquid Film/Porous FW

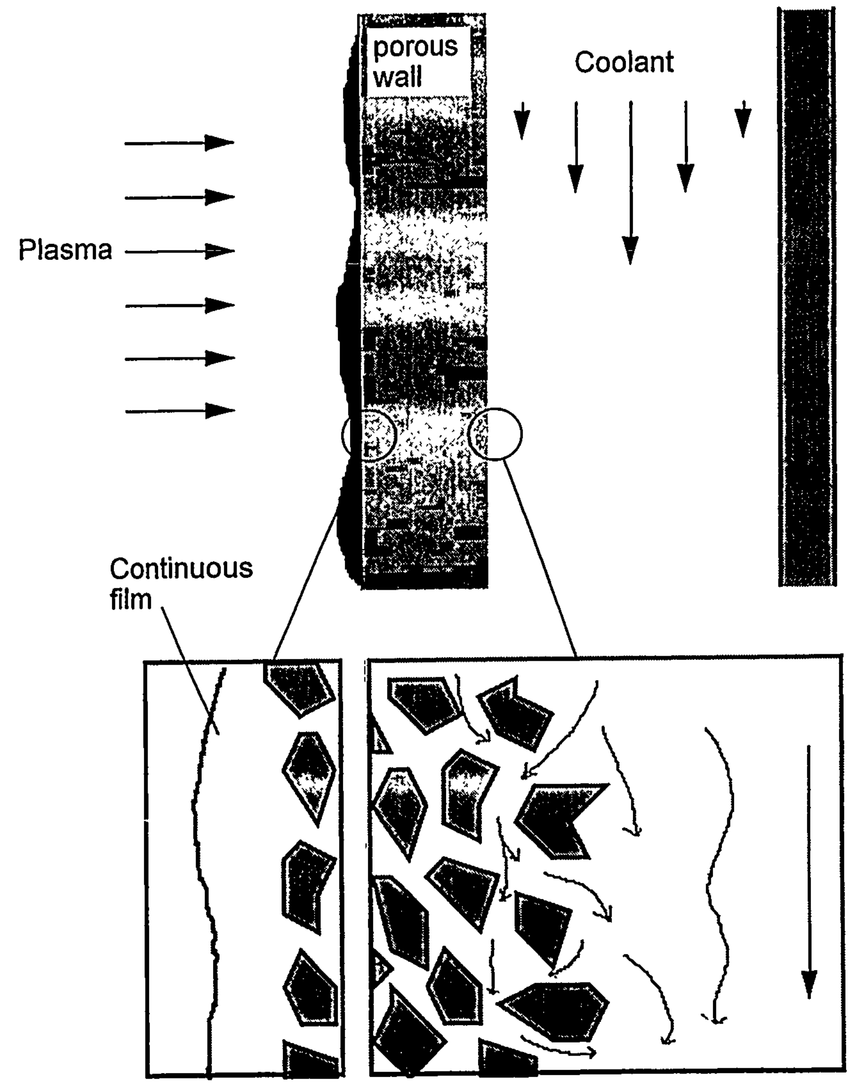

Convective Liquid Layers

- Fast flowing liquid layer:
  1. Removes surface heat flux
  2. Removes initial peak in neutron deposition
  3. Contributes to breeder and/or neutron multiplication Change nature of failure and stress response in wall
  4. Provides renewable surface

- Different incarnations considered
  1. Recycle liquid to LM blanket
  2. Thick layer (serves as FW/Blanket)
  3. Multiple layers
  4. EM adhesion

- Analysis focusing on photon penetration depth and thermalhydraulic and fluid mechanical calculations

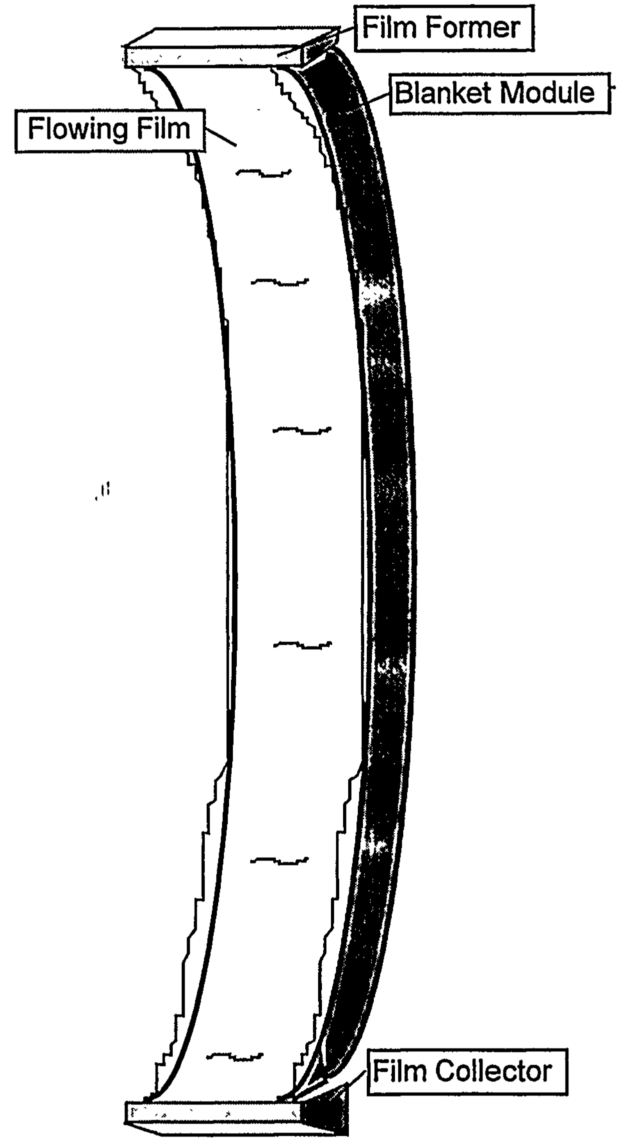

Damage in the Plasma Facing Part of the First Wall

Naoaki YOSHIDA

RIAM Kyushu University

US-Japan Workshop(97FT5-06) on High Heat Flux Components & Plasma Surface Interactions for Next Fusion Devices

(December 8-11, 1997, San Francisco)

Introduction

What will happen in PFM by the bombardment of plasma particles, especially energetic particles?

surface damage, effect on bulk properties, etc.

- **Damage by Tokamak Plasma**
  Results from the long pulse TRIAM-1M experiments
- **In situ TEM Observation Experiments under Hydrogen Ion Irradiation**
- **In situ TEM Observation Experiments under Helium Ion Irradiation**
- **Temperature Variation Effects**

Damage by Long Pulse Plasma in TRIAM-1M

T. Hirai et al. (P-1A-063)

$\langle n_e \rangle \approx 2\mathrm{x}10^{18}/\mathrm{m}^3$, $T_i \approx 500\mathrm{eV}$, t_j=78.4min.(P1, 5 shots), t_j=72.1min.(P2, 1 shot)

Tungsten

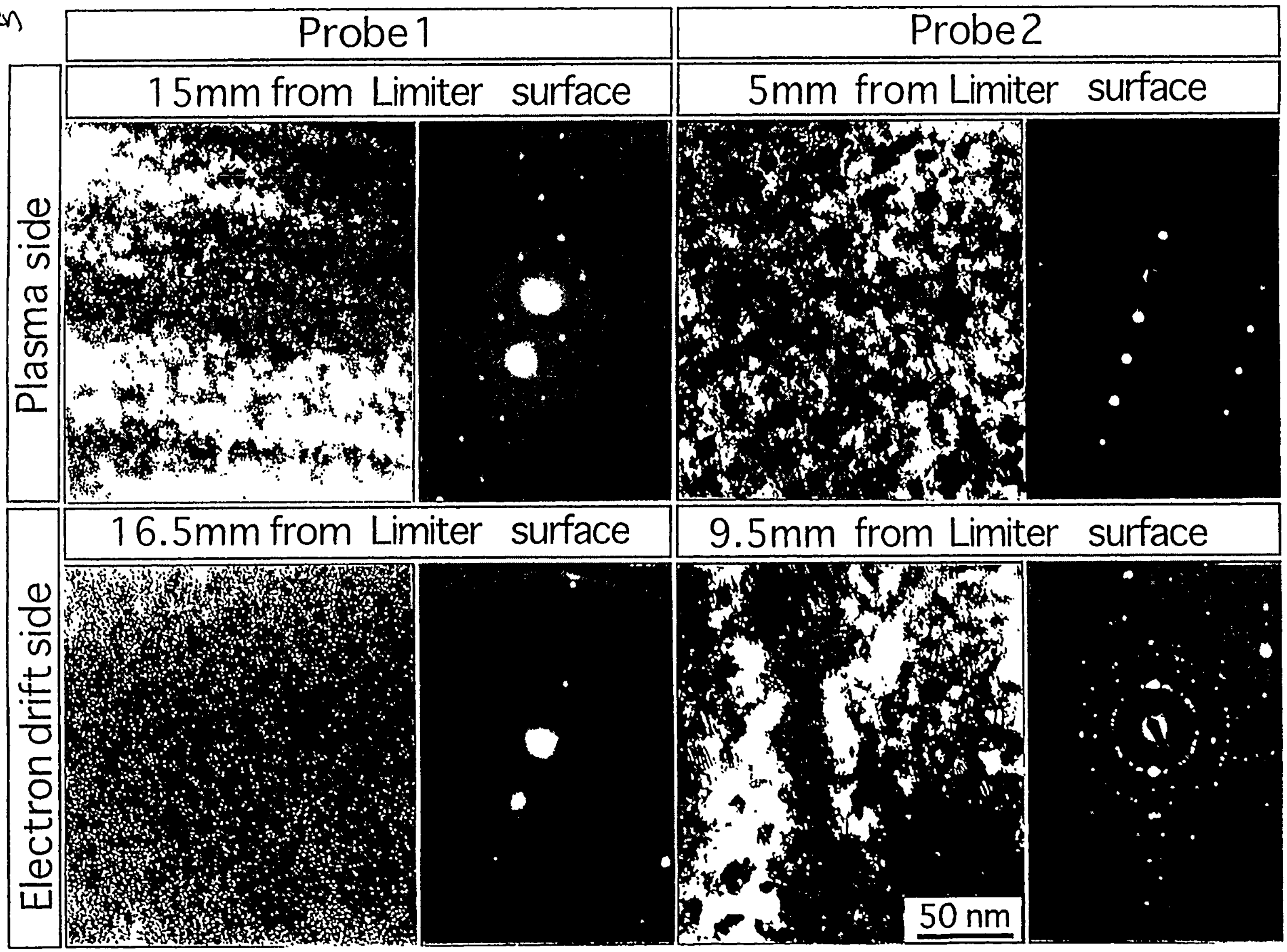

Depth Distribution of Dislocation Loops in W

T. Hirai (P-1A-063)

TRIAM-1M, $<n_e> \approx 2x10^{18}/m^3$, $T_i \approx 500eV$, t_j=72.1min.(1 shot)

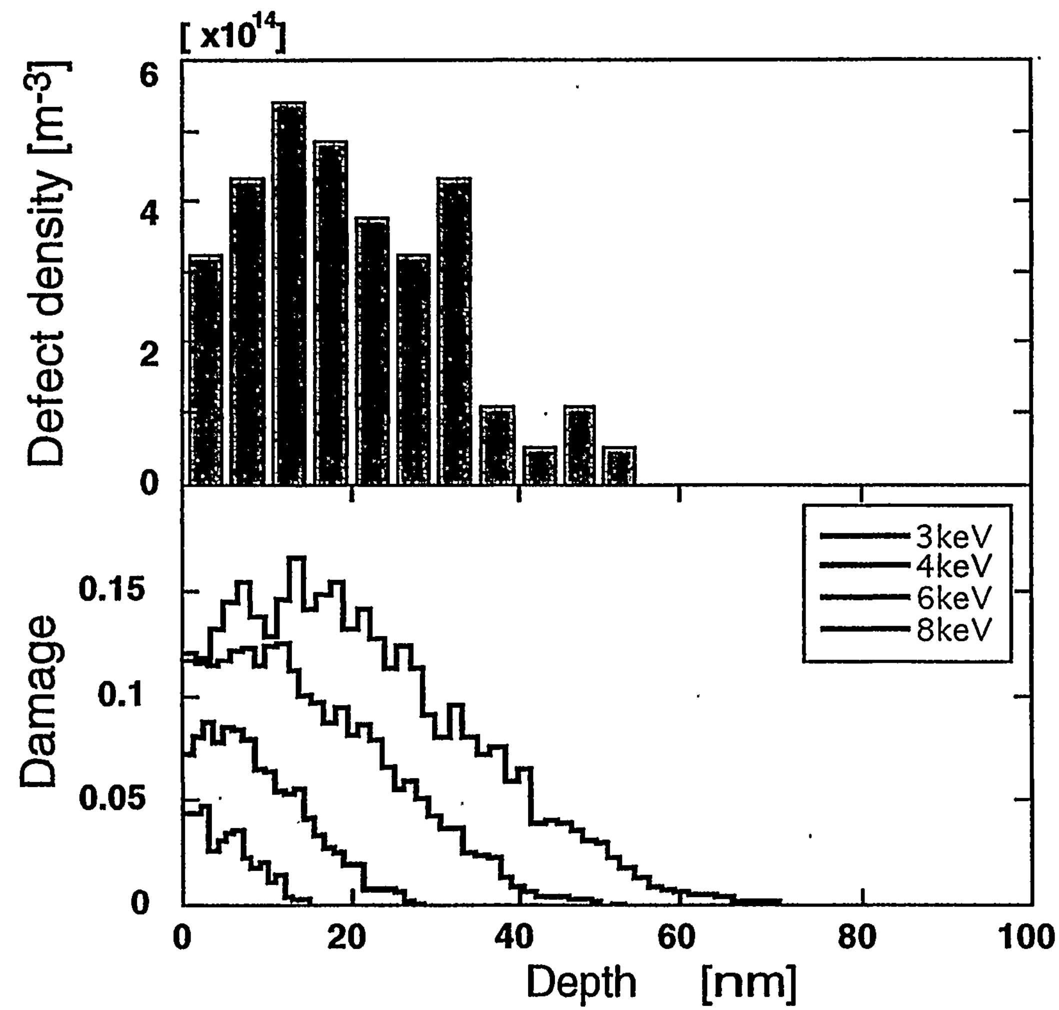

Damage of Long Term W Specimen

T. Hirai et al. (1997)

Pre-thinned TEM specimen: Exposed to TRIAM-1M LHCD discharges for a half year on the vacuum vessel wall

⇨ Embrittlement of bulk specimen···common phenomena of H irradiated W

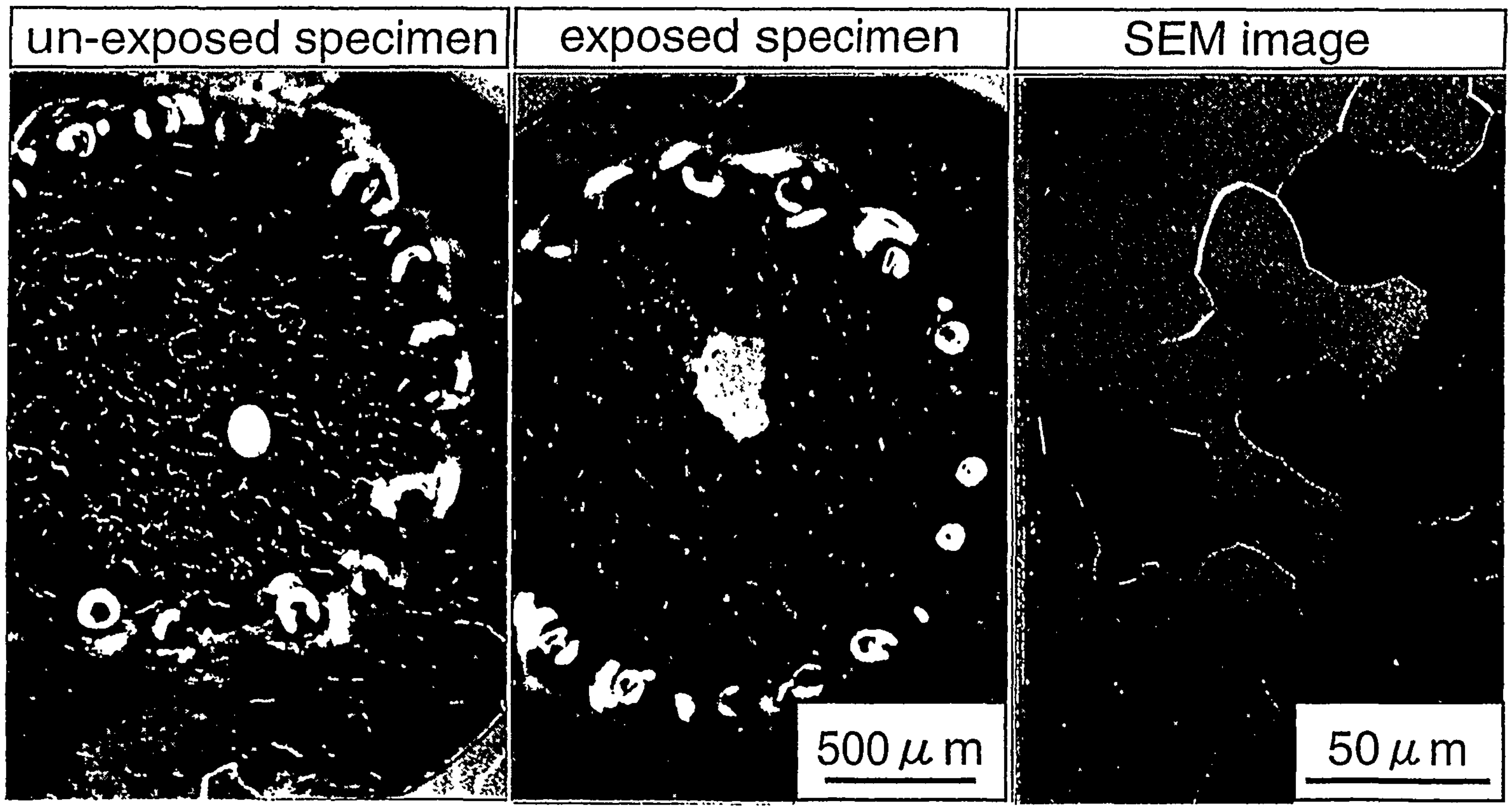

Simulation Irradiation with H(D) Ions

MATERIALS
Mo, W, Be, etc.

EXPERIMENTS
In-situ observation of microstructural evolution under irradiation

Link of Duoplasmatoron Ion Gun and TEM

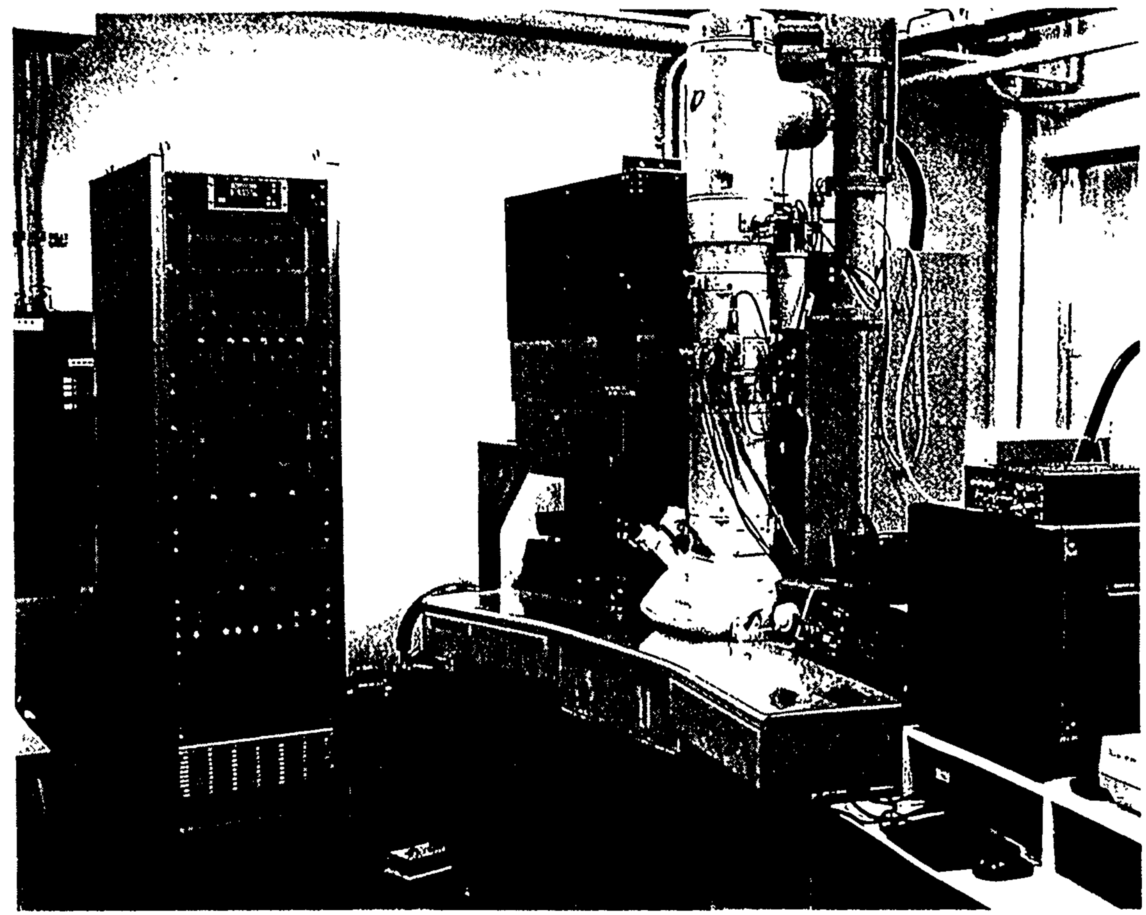

Ion Energy Dependence of Damage in W and Mo by H^+ Irradiation at 300K

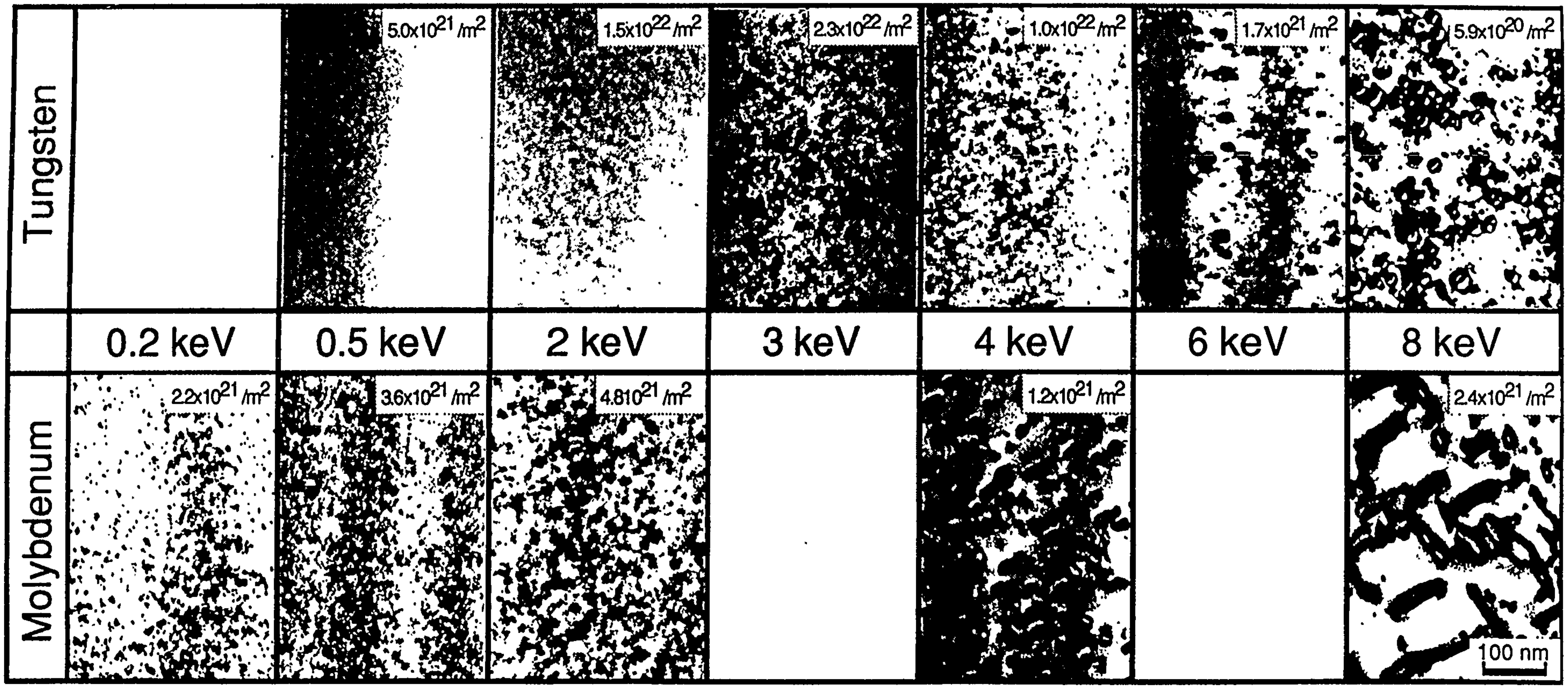

Temp. Dependence of Damage of W by H^+ Irrad.

8keV H^+, HP-W(99.995%), PM-W(99.95%)

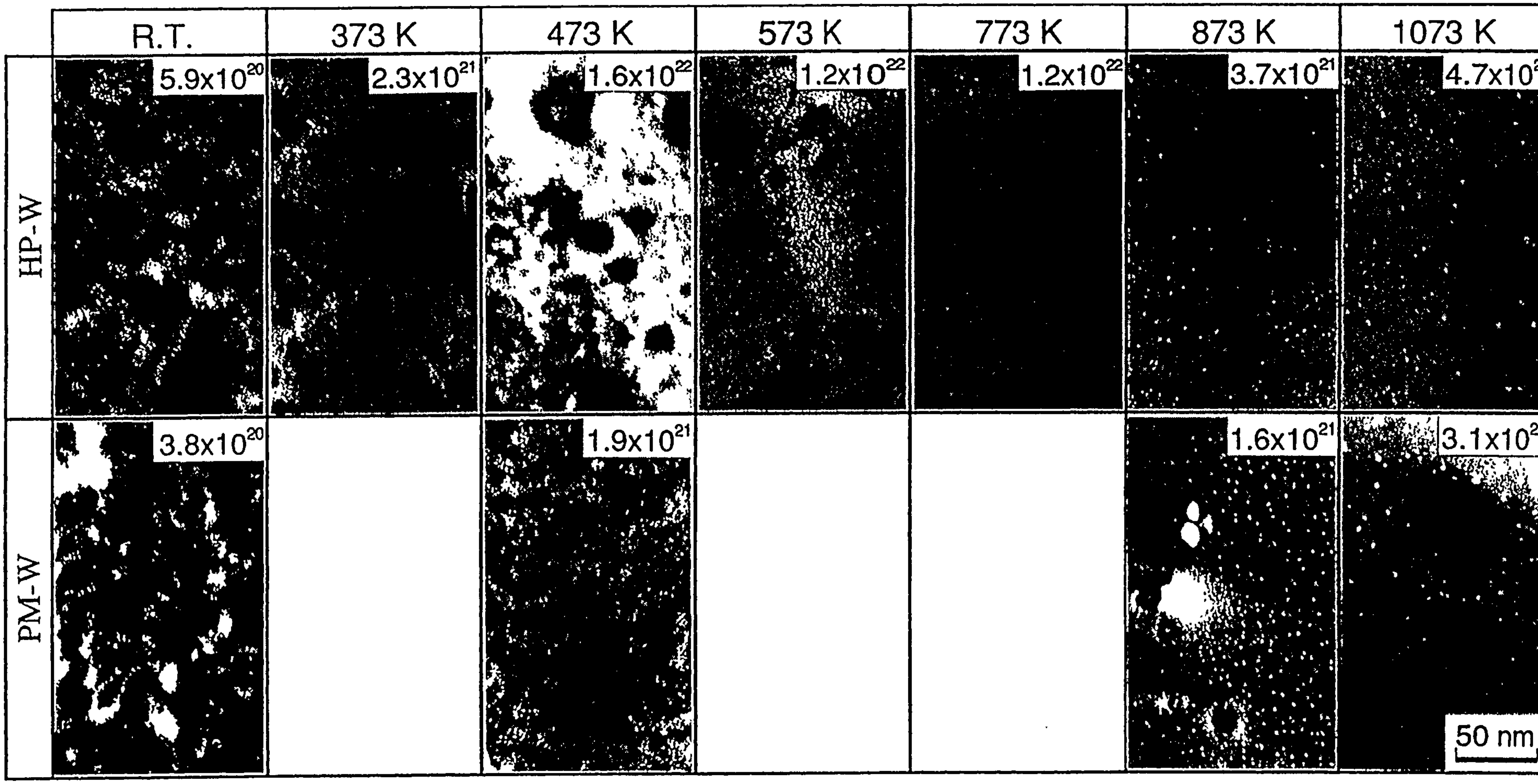

Thermal Stability of Loops Formed by H^+ Irrad.

Irrad.: 300K, 8keV H^+, 4.7×10^{20} ions/m^2(HP-W), 6.1×10^{20}(PM-W), 2.4×10^{21}(Mo)

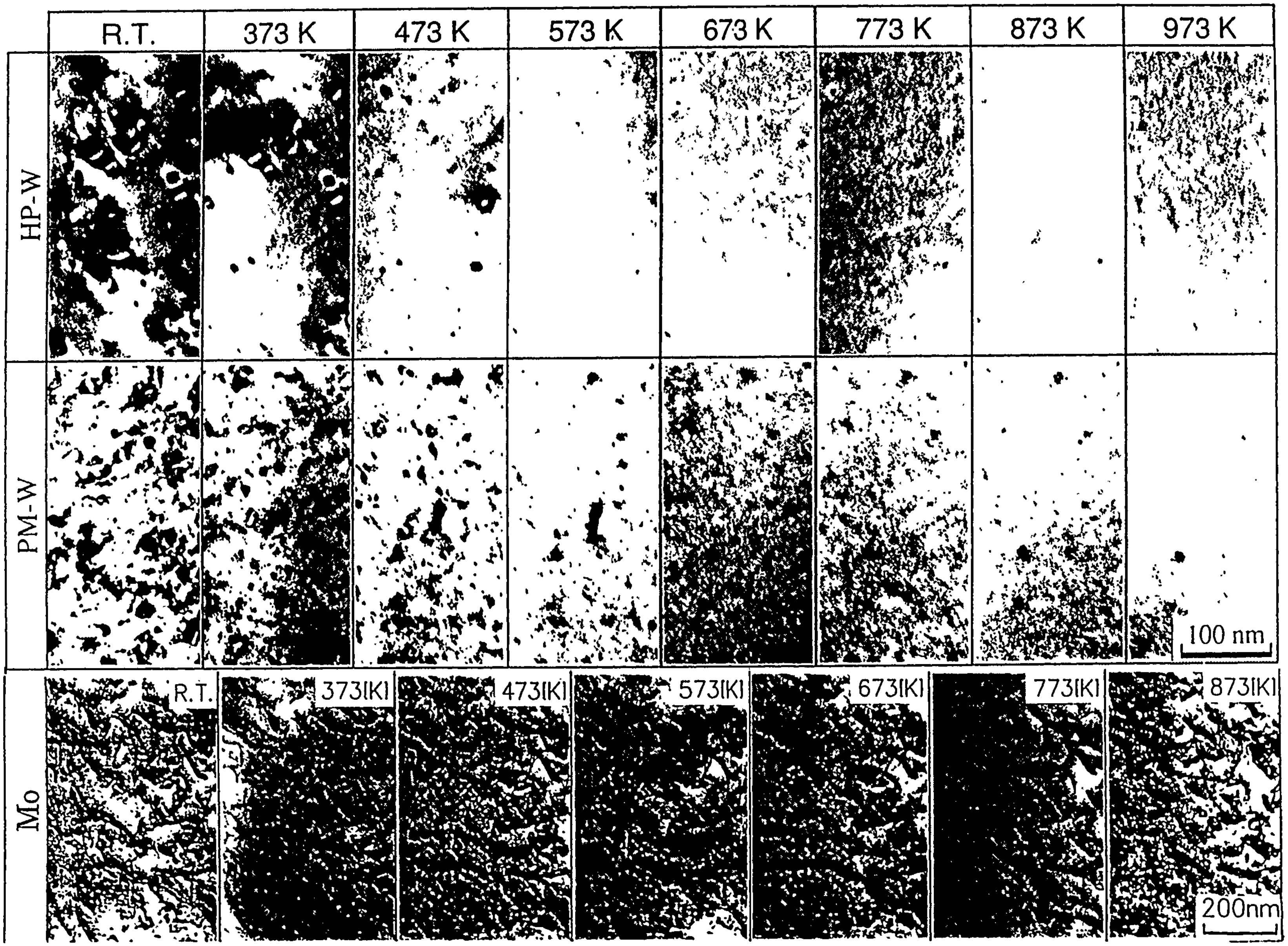

Microstructure of D Ion Irradiated Be

N. Yoshida et al.(1996)

8 keV-D_2^+, 5x10^{18} ions/m^{2}s

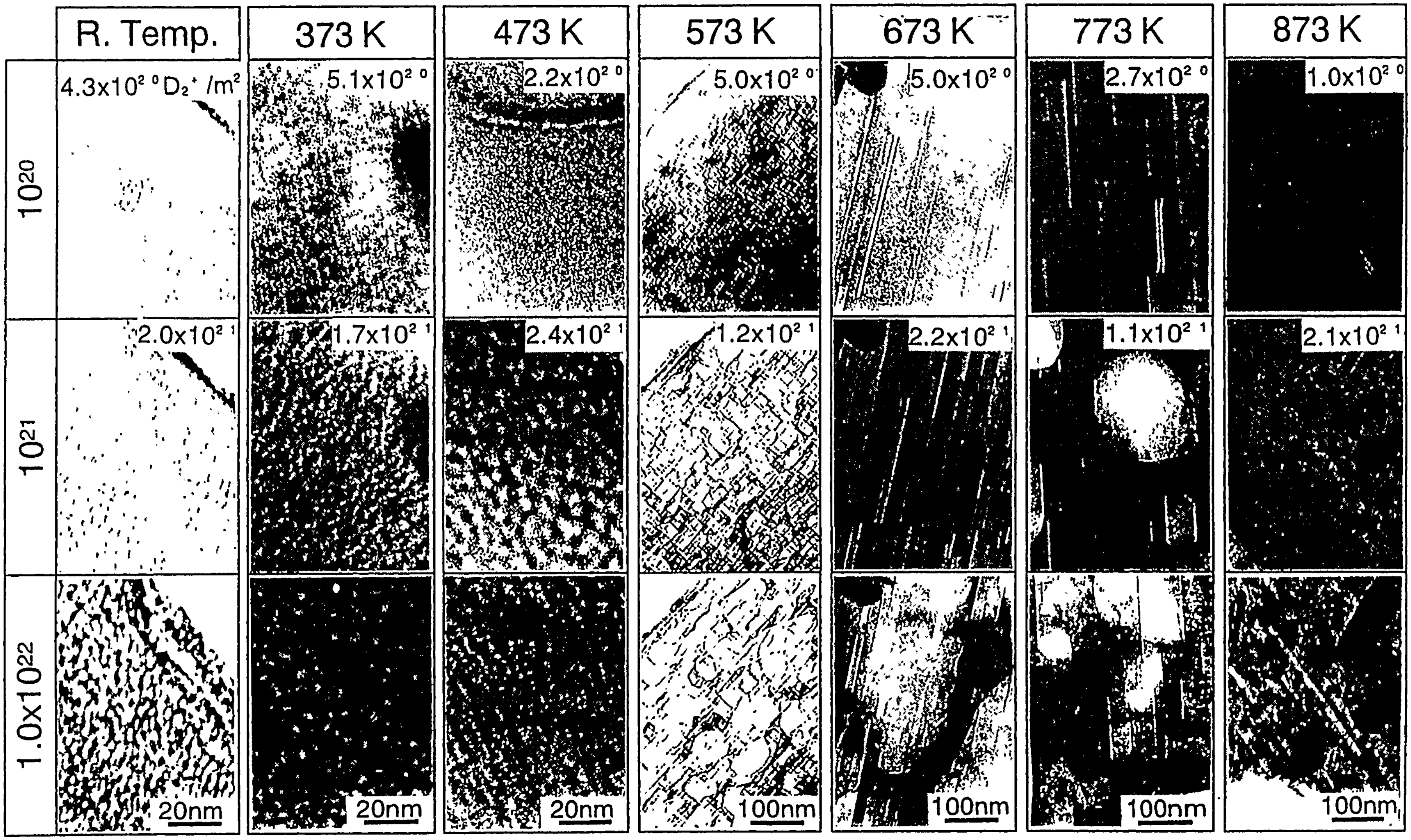

Irradiation Temp. Dependence of TDS

Be, 8keV-D_2^+, $1x10^{21}$ions/m^2, Ramp. rate; 1K/s

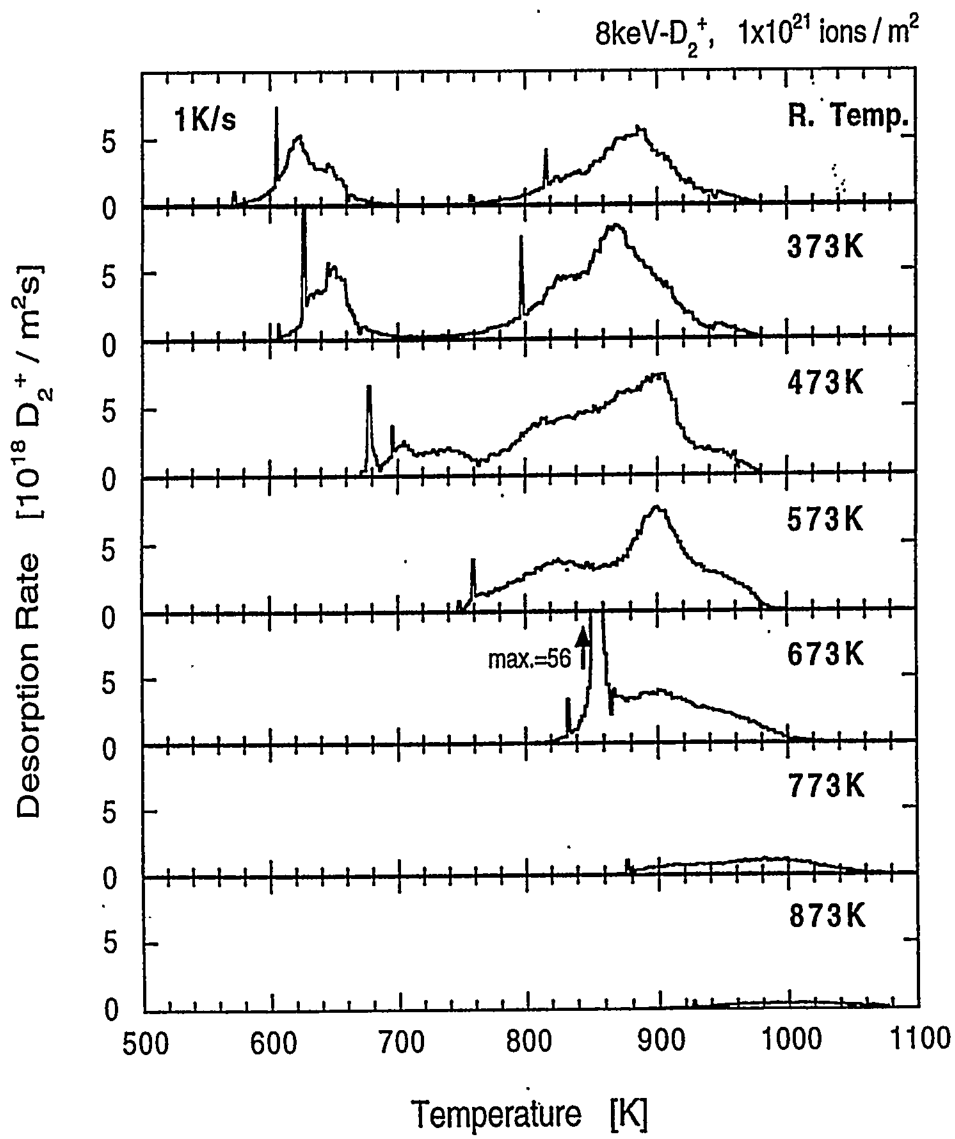

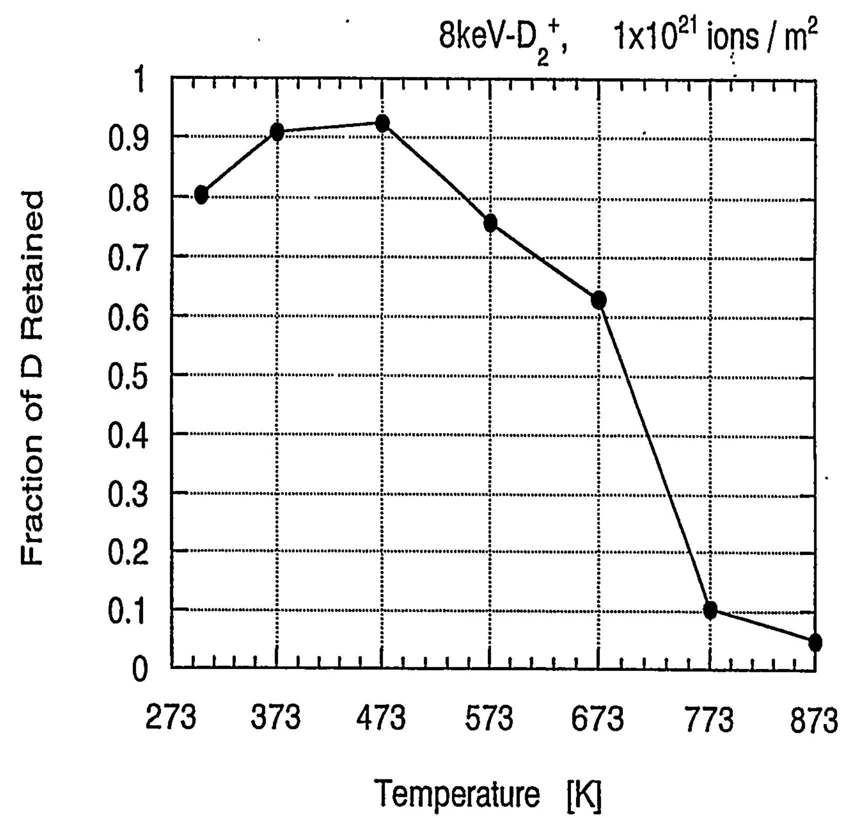

Degradation Mechanism of PFM by Hydrogen

(1) ELEMENTARY PHENOMENA

Direct knock-on damage of sub-surface region

⇩

Dislocation network, bubbles···hydrogen retention, hardening, etc.

W: weak effects at high temperature

Be: strong effects even up to 673K

(2) SECONDARY PHENOMENA

Bulk damage due to long range diffusion of H and free defects

⇩

Strong degradation of bulk materials (embrittlement, etc.)

The effects of hydrogen particle bombardments are not limited in the subsurface regions but spread into bulk.

Recovery of Damage in W formed by D^+ and He^+ Irradiation

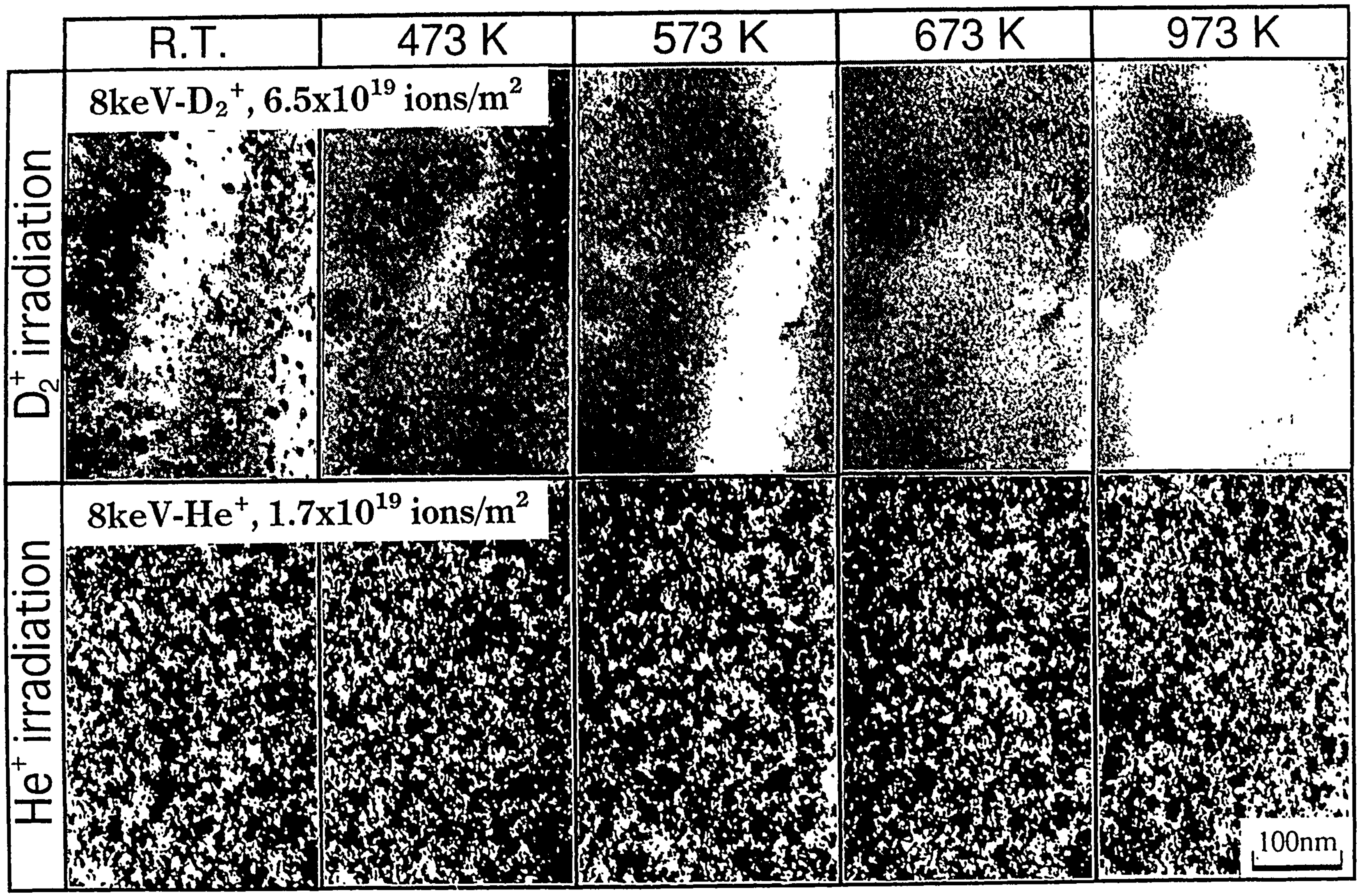

Microstructure of He Ion Irradiated Mo

N. Yoshida et al.(P1A-043)

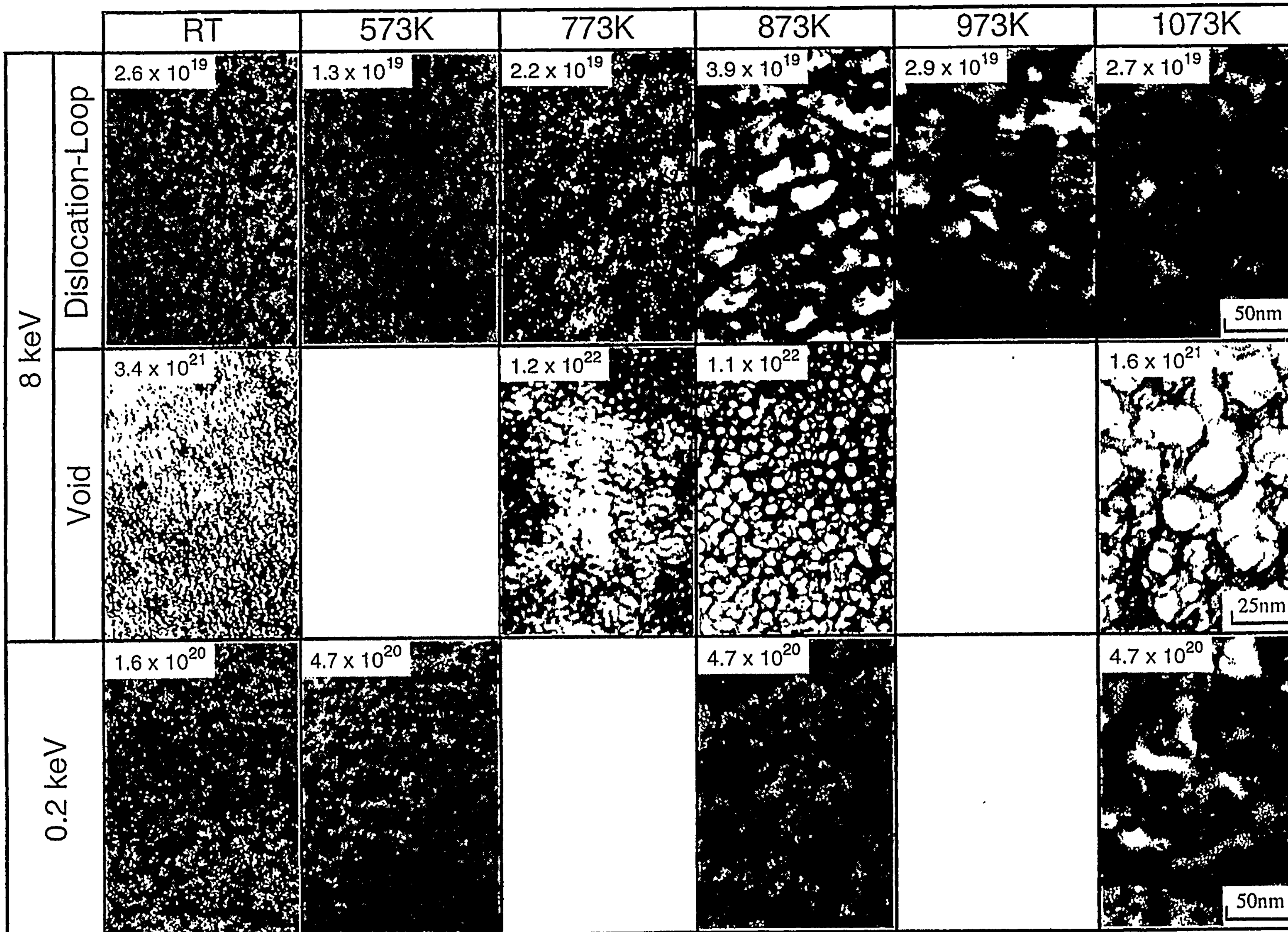

Hardening of Sub-Surface Layer by He (D) Irra.

H. Iwakiri et a. (P-1A-048)

300K-He Ion Irra.
- low dose:
  - dislocation & I-loop
- high dose:
  - He bubbles

873K-He Ion Irra.
- dislocation & I-loop

300K-D Ion Irra.
- dislocation & I-loop

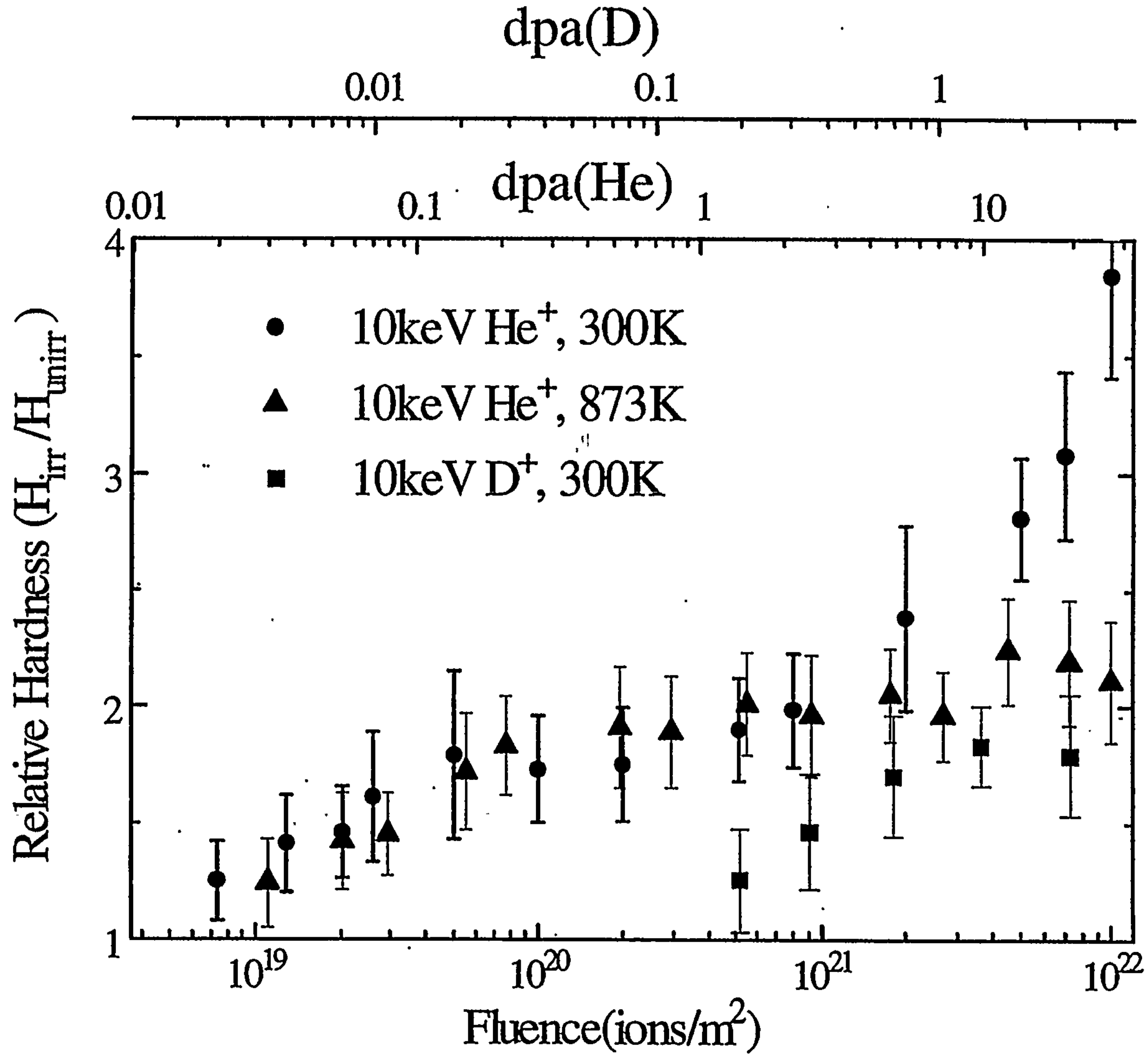

Effects of He Irra. on Heat Loading Properties

K. Makise et al.(1997)

Specimen:
Powder Metallurgy W
He Ion Irradiation:
8keV-He Ions, $5x10^{21}$ions/m^2
Room Temp.
Heat Loading (Electron Beam):
20MW/m^2

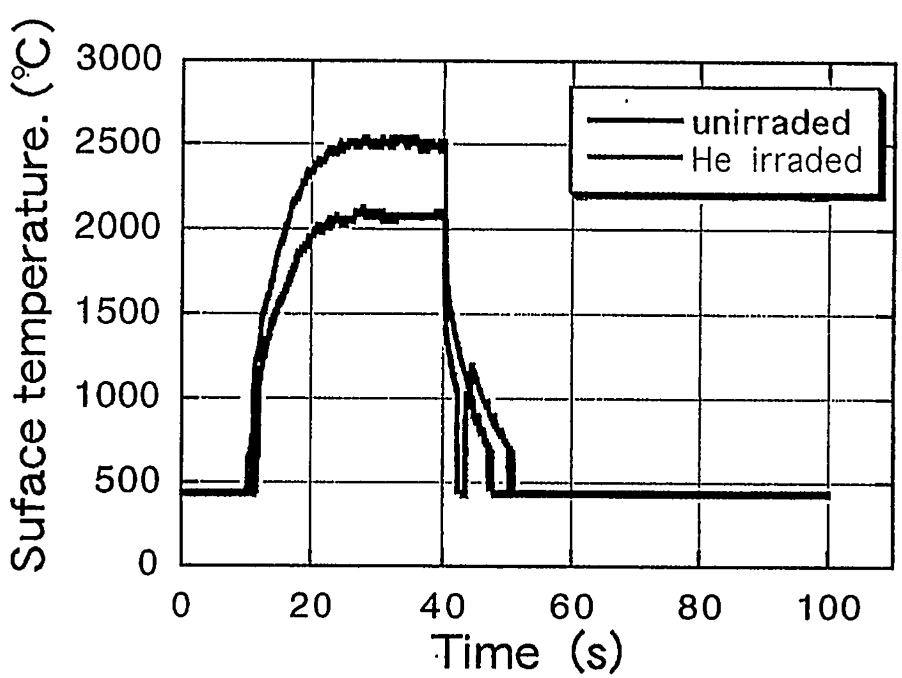

Unirradiated

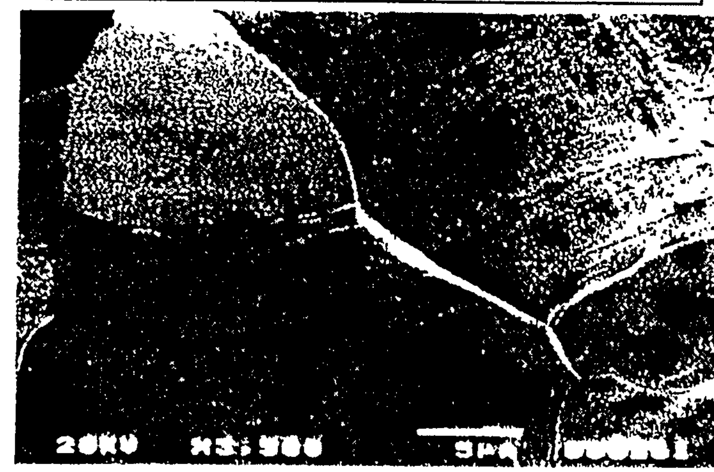

He Ion Irradiated

Microstructure of He Ion Irradiated Be

T. Inoue et al.(1997)

8 keV-He^+, $2x10^{18}$ ions/m^2s

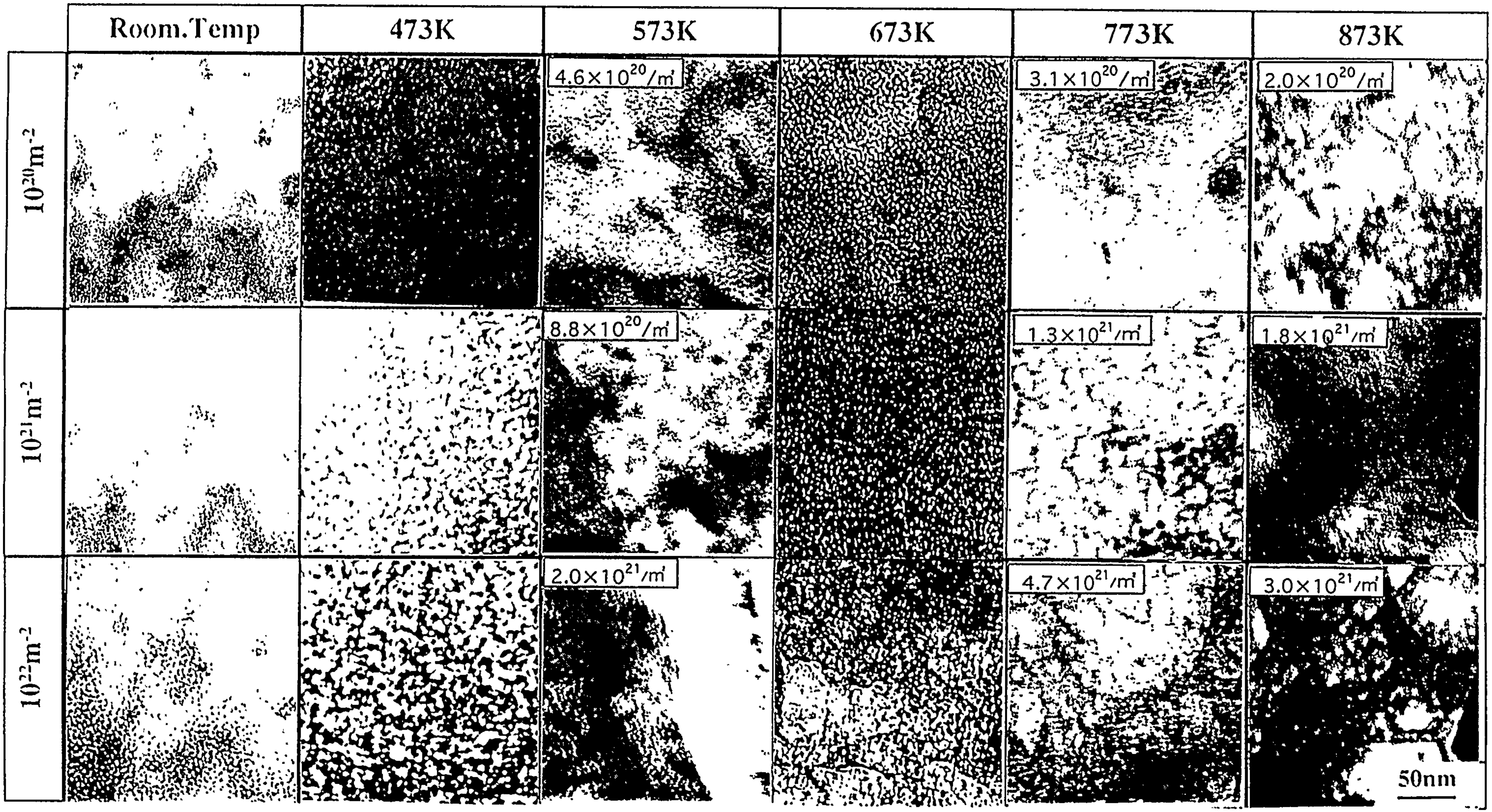

Impacts of He Irra. on Material Properties

Accumulation of defects is extremely high due to strong He-defect interaction.

- **Accumulation of dislocation loop up to very high temp. (>1073K)**
  (high nucleation rate, strong stability ···)
- **Active formation of He bubbles from low to high temp.**
- **Hardening, embrittlement of subsurface layer**
- **Embrittlement of grain boundary and matrix of bulk materials**
- **Reduction of thermal conductivity at subsurface layer**

⇩

- **Radiation embrittlement , Reduction of fatigue lifetime**
- **Increasing of tritium retention**
- **Reduction of heat load resistance**

Variation of Irradiation Environment
-----Temperature Variation Effects-----

Formation of Defects

thermally activated process

(mobility of defects, binding force of defects, etc.)

⇩

temperature is very essential for defect formation and damage accumulation

Irradiation Effect

constant temp.irra. vs varying temperature irra.

Heating Effects

slow heating vs fast heating

Effects of Steady Heating on He Implanted Ni

- Room Temp., 5keV He Ions, 3×10^{21} ions/m^2
- Heating 1 hour at each temperature

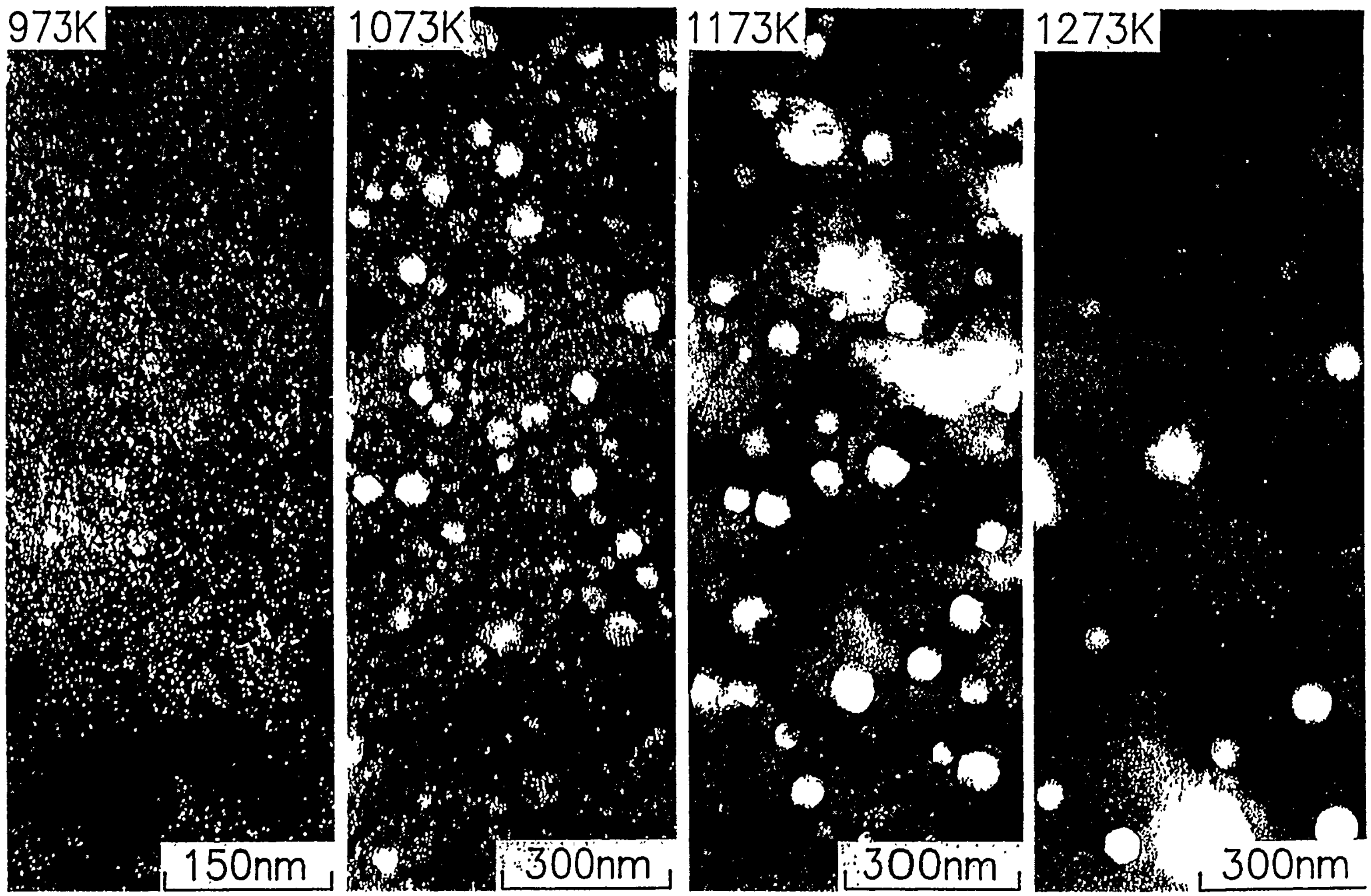

Effects of Pulse Heating on He Implanted Ni

- Room Temp., 5keV He Ions, $3x10^{21}$ions/m^2
- Ruby laser heating (1ms pulse, heating rate ~1000℃/ms)

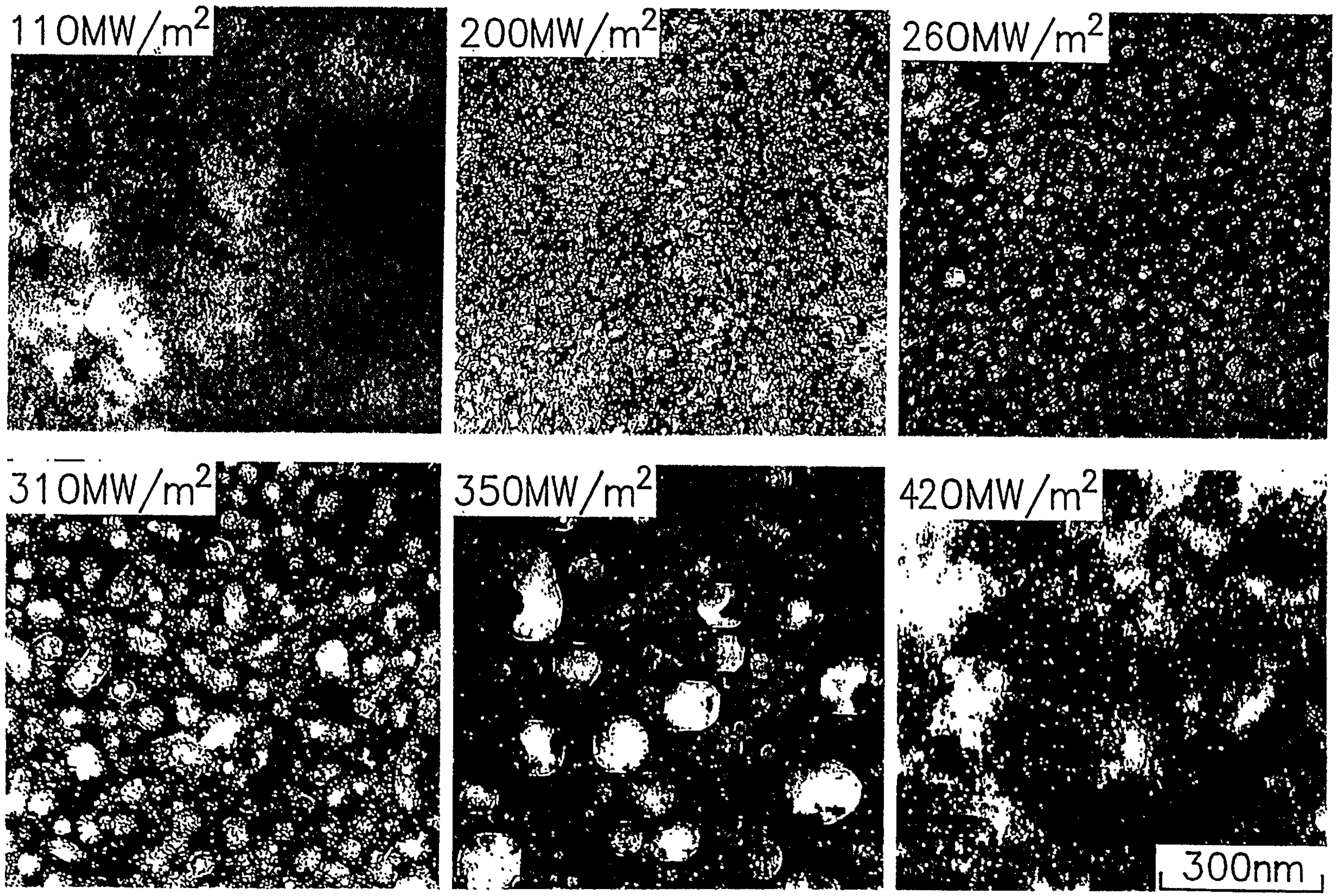

Effects of Pulse Heat Load on He Implanted Ni

Total Bubble Volume

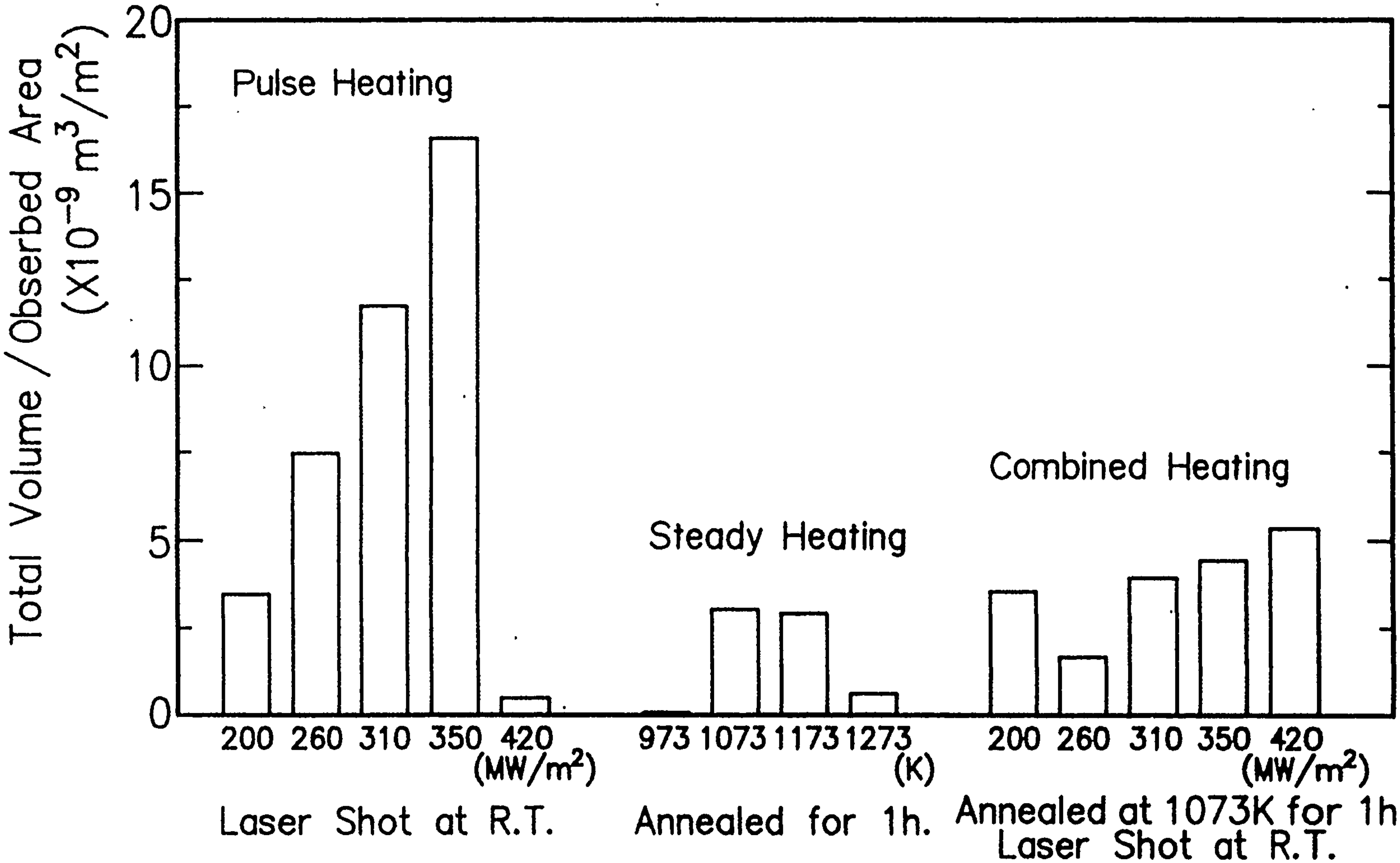

Summary

- Change exchanged neutrals cause heavy damage at first wall surface.
- Effect of implanted H on bulk properties of PFM was demonstrated. This should be a next important issue.
- Energetic H and He form sponge-like microstructure in Be at wide temperatures range.

  ⟹ Tritium inventory, degradation of thermal and mechanical properties
- Helium irradiation enhances formation of defects such as I-loops and bubbles in Mo and W at wide temperature range but rather weak effect of H.
- Pulse heating changes microstructure very much; enhance bubble formation
- Irradiation effects under varying temperature condition and synergistic effects of plasma-neutron-heat is the next issue.

Protective Coating at the Plasma Facing Part of First Wall

N. Noda (NIFS)

Contents

NIFS

Boron Film as a Protecting Layer for Tritium, and Energetic Particles (D^0, T^0, He^0)

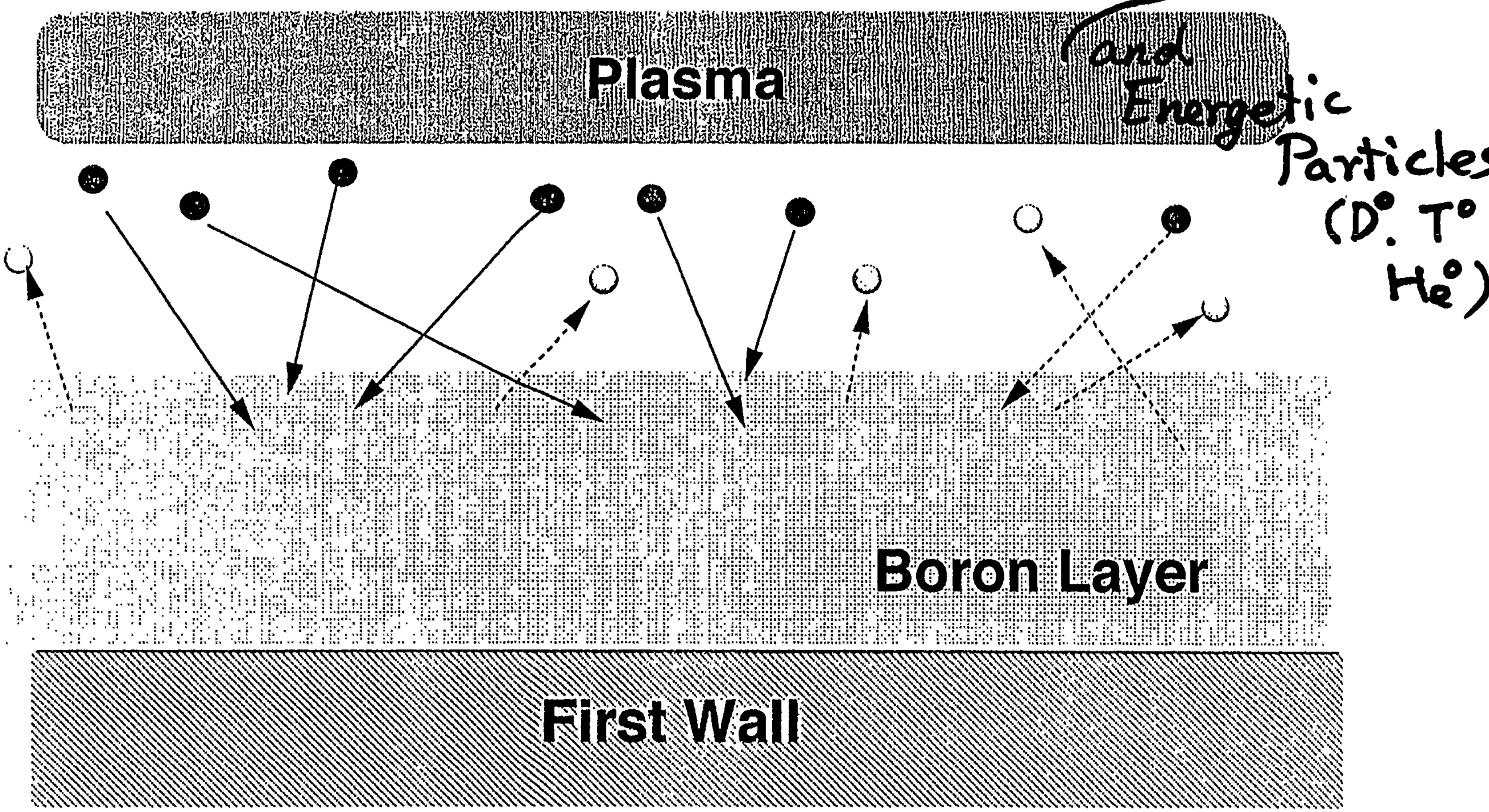

- Energetic (CX) T, D atoms
- Slow Molecules

What is the role of B-film ?

Present Roles of reduction in

(1) oxygen? (2) hydrogen? (3) wall materials?
↑relative to C walls

Future

Roles of (1), (2) must be taken over by divertor pumping

(3) will be effective
(4) T-free wall
(5) protection from energetic particle

N. Noda

Thermal Desorption Experiment in SUT

Hydrogen is removed from B-film below 400 ℃

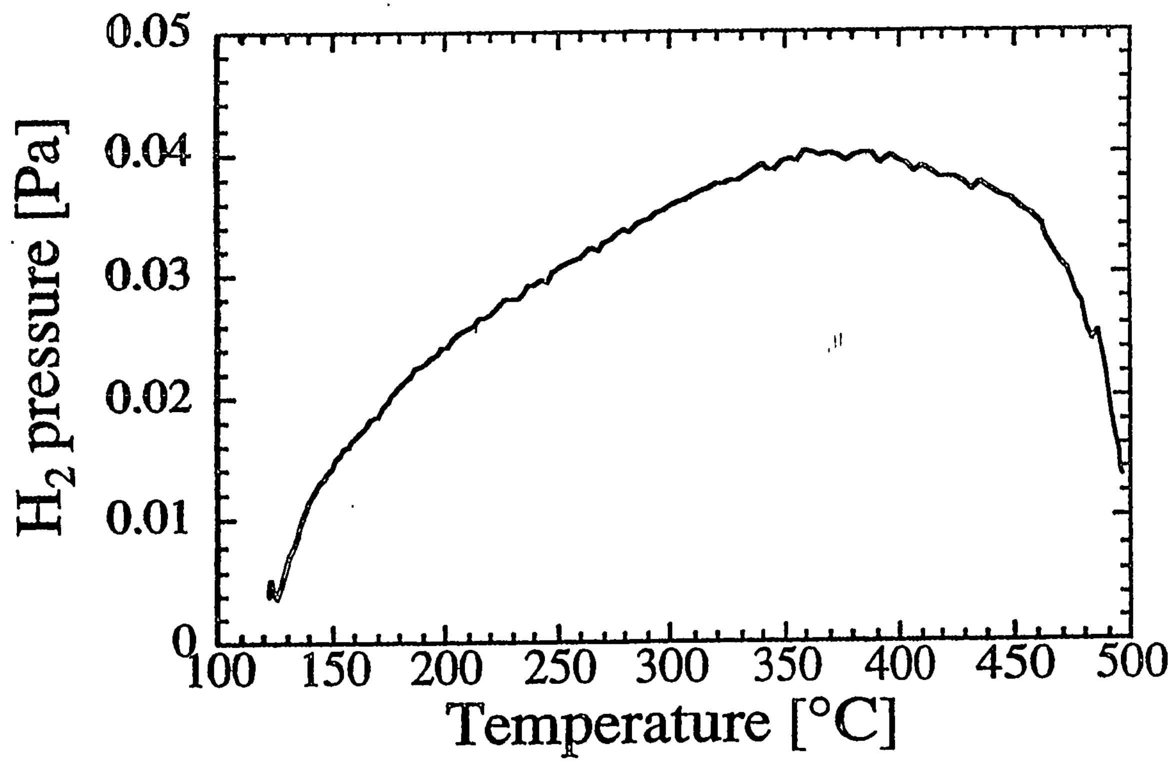

It gives us T-free first wall in future machines !!

Questions and problems

(1) What role is really important in future?
(2) Detail behavior, quantitative information and mechanisms on hydrogen isotopes.
(3) Impact of impurity contamination (O,C,W,...)
(4) What is the best material combination?
(5) What is equilibrium distribution?

(6) How the thin films can be maintained
Is it possible to avoid gross immigration?
Is it necessary to add boron during operation?
If it is, is the dust formation tolerable?

N. Noda

Possible answers

(1) A carbon film is lost due to methane formation
because methane molecules reach pumping
ducts and pumped away.

(2) It is not the case in a boron film.
B–H compound is fragile, easily broken by
plasma impact, cannot reach pumping ducts.
B atoms are redeposit on the first wall.
A boron films is expected to be kept long enough.

(3) Gross immigration is left as the major problem.
If B–addition is necessary, dust problem, too.

p

CR MARKER ...

6L-IIIA APRIL/MAY 96 AFTER 95/96 CAMPAIGN (1090) SHOTS

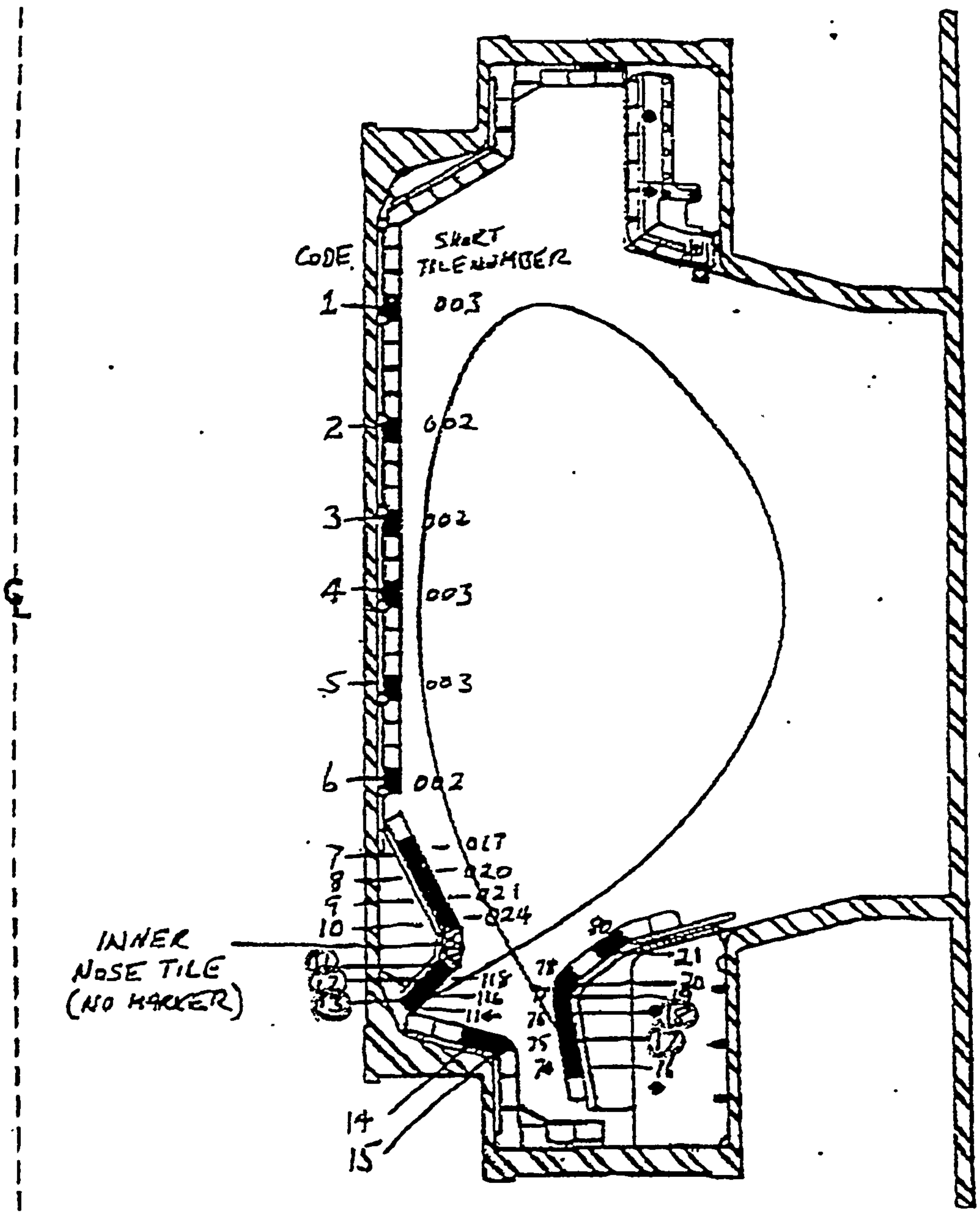

W. Wampler & S. Pitcher

Fig 3

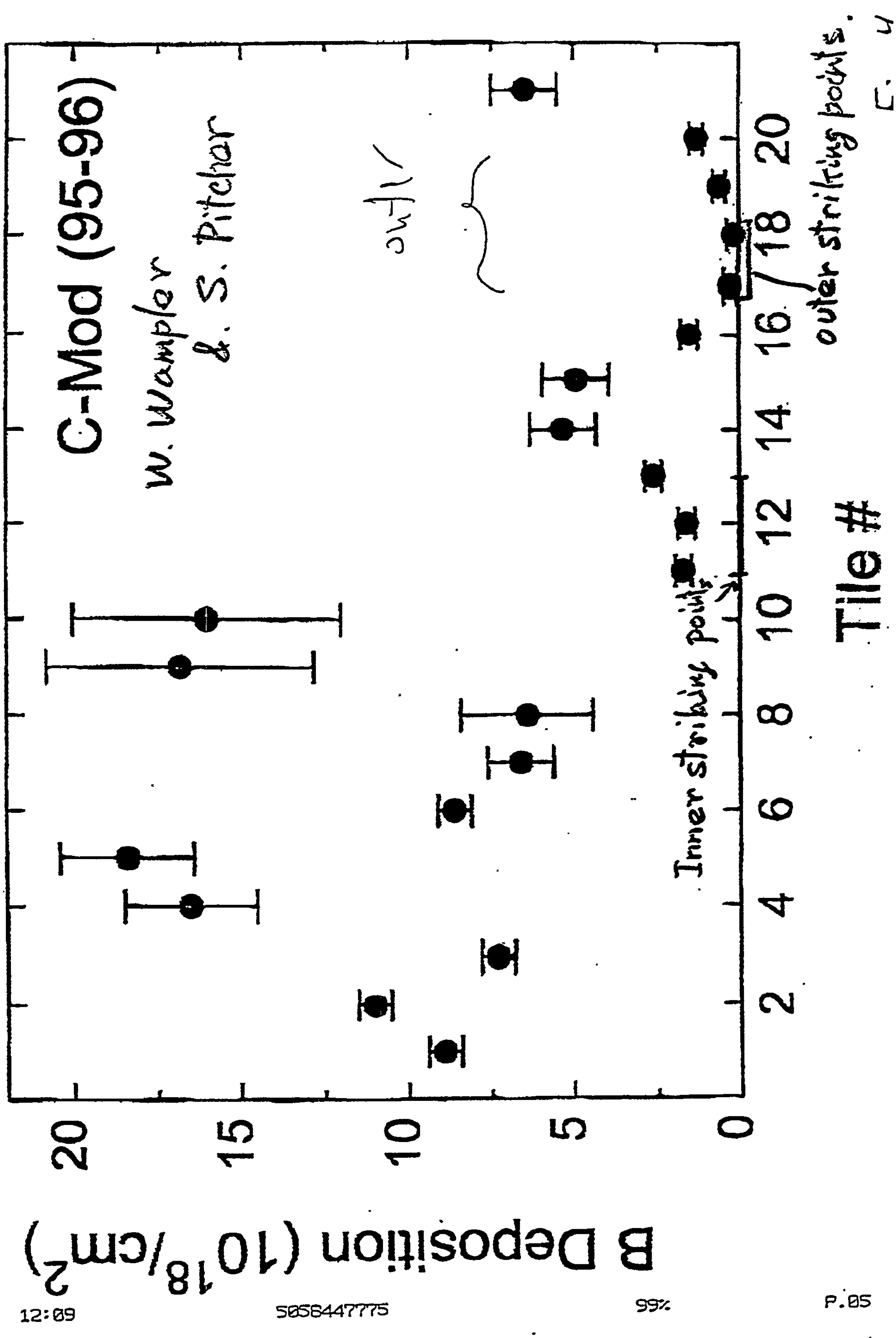

APR-28-1997 12:09 5058447775 99% P.05

Summary

- A thin boron film is attractive as the protecting layer of the first wall
- It protects the surface against energetic particles such as CX neutrals of He, D, T
- Boron layer could be stable and resistant to erosion because of redeposition of B-H compound during operation
- Gross immigration of boron atoms is one of the big problems to be investigated

N. Noda

MST-6/Sep 97/RCc-269a

VIII-82

Fabrication and High Heat Flux Testing of Plasma Sprayed Beryllium ITER First Wall Mock-Ups

R. G. Castro and K. E. Elliott
Los Alamos National Laboratory
Materials Science and Technology Division
Los Alamos, New Mexico 87545, USA

R. D. Watson and D. L. Youchison
Sandia National Laboratory
Fusion Technology Department
Albuquerque, New Mexico 87185, USA

K. T. Slattery
High Energy Systems
The Boeing Company
St. Louis, Missouri 63166, USA

U.S. Material and Joining Option Selections for ITER First-Wall/Shield Modules

Limiter Modules	*Heat Flux (MW/m^2)*	*Structural Alloy (primary, backup)*	*Armor/ Segment Joint*	*Comment*
First Wall	5.0	P: SS-DS Cu (Al-25, IG0) (950°C HIP, slow cool will degrade PH properties).	Be: EP Cu-Cu DB at 450°C	Initial 950°C HIP to form SS-Cu structure. Then attach armor. Could use EP to pre-join tiles into matrix prior to canning.
		B: CuNiBe (Hycon-3HP, AT) (May consider Alloy-3 due to lower heat flux.)	Be: Al-Si HIP-Braze at 600°C	Al-Si process adequate for FW heat flux. Plasma spray Ti diffusion barrier and Al-Si after 950°C HIP cycle.
			Be: Low Press Plasma Spray (LANL process)	See below. Properties need to be verified for limiter heat fluxes.
Shield Body		Cast/HIP (SS316L-IG)	Module size consistent with single cast/HIP piece.	Need mechanical properties, vacuum, ferrite, irrad data. Also need to verify core length limits.

Primary FW Modules	*Heat Flux (MW/m^2)*		*Armor/ Segment Joint*	*Comment*
First Wall	0.5	P: SS-DS Cu (Al-25, IG0) B: CuNiBe (Hycon-3HP, AT)	Be: Low Press Plasma Spray (LANL process)	Plasma spray process has achieved properties sufficient for primary first wall. Low-cost way to coat large areas. Demonstrated 80% deposition rate coats 5 mm over 1 m^2 area in 1 hour.
			Be: EP Cu-Cu DB at 450°C	See above.
			Be: Al-Si HIP-Braze at 600°C	See above.
Shield Body		Cast/HIP (SS316L-IG)	Module size consistent with single cast/HIP piece.	Same as for limiter module.

Note: DS Cu selected where manufacturing cycle requires temperatures exceeding 600°C for extended periods. PH alloys preferred elsewhere due to weldability and cost advantages. Armor joining options are listed in order of priority.

Background

Received from K. Slattery (6) EBTS Mockups

- (2) explosive bonded 1100 Al with Ti to CuCrZr (Elbrodur-G)
- (2) CuNiBe (Hycon)
- (2) GlidCop Al-25

Delivered (4) Be Plasma Sprayed EBTS Mockups for Machining

Sample ID	*Heat Sink Material*	*Surface Condition*
96-29*	CuNiBe (Hycon)	Knurled surface - no interlayer
96-30	CuCrZr (Elbrodur-G)	Flat surface - Ti/Al interlayer
96-31	GlidCop Al-25	Flat surface - vanadium interlayer
96-33*	CuCrZr (Elbrodur-G)	Knurled surface - Ti/Al interlayer

Knurled Surfaces - EDM Machined

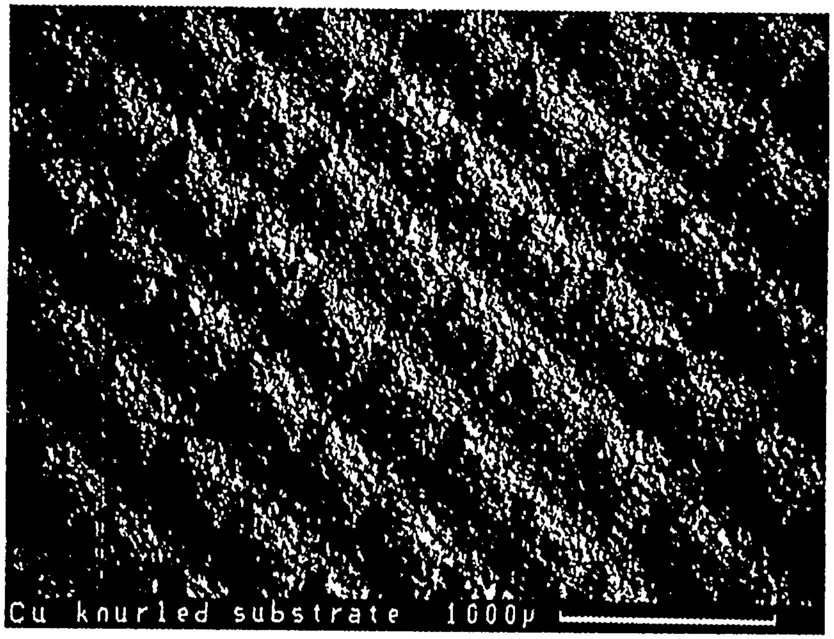

Copper

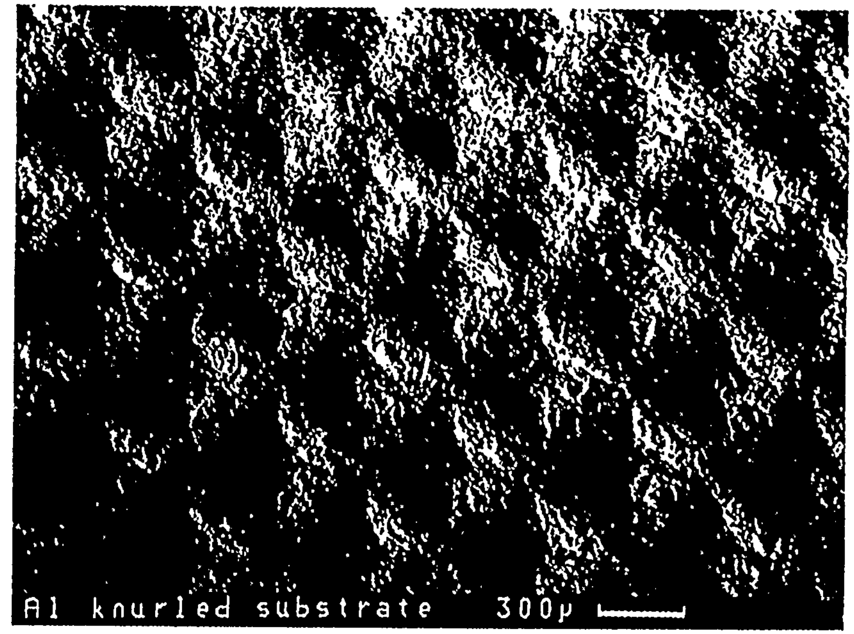

Aluminum

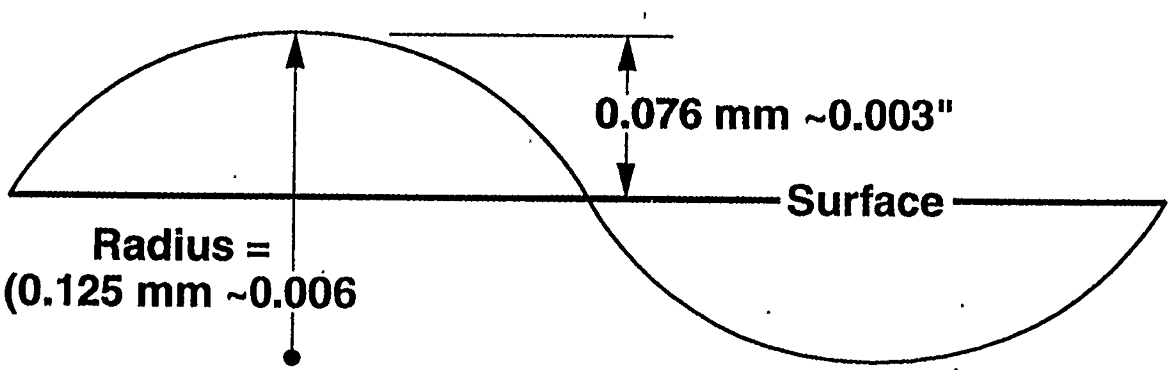

Fabrication of EBTS Divertor Mock-Ups

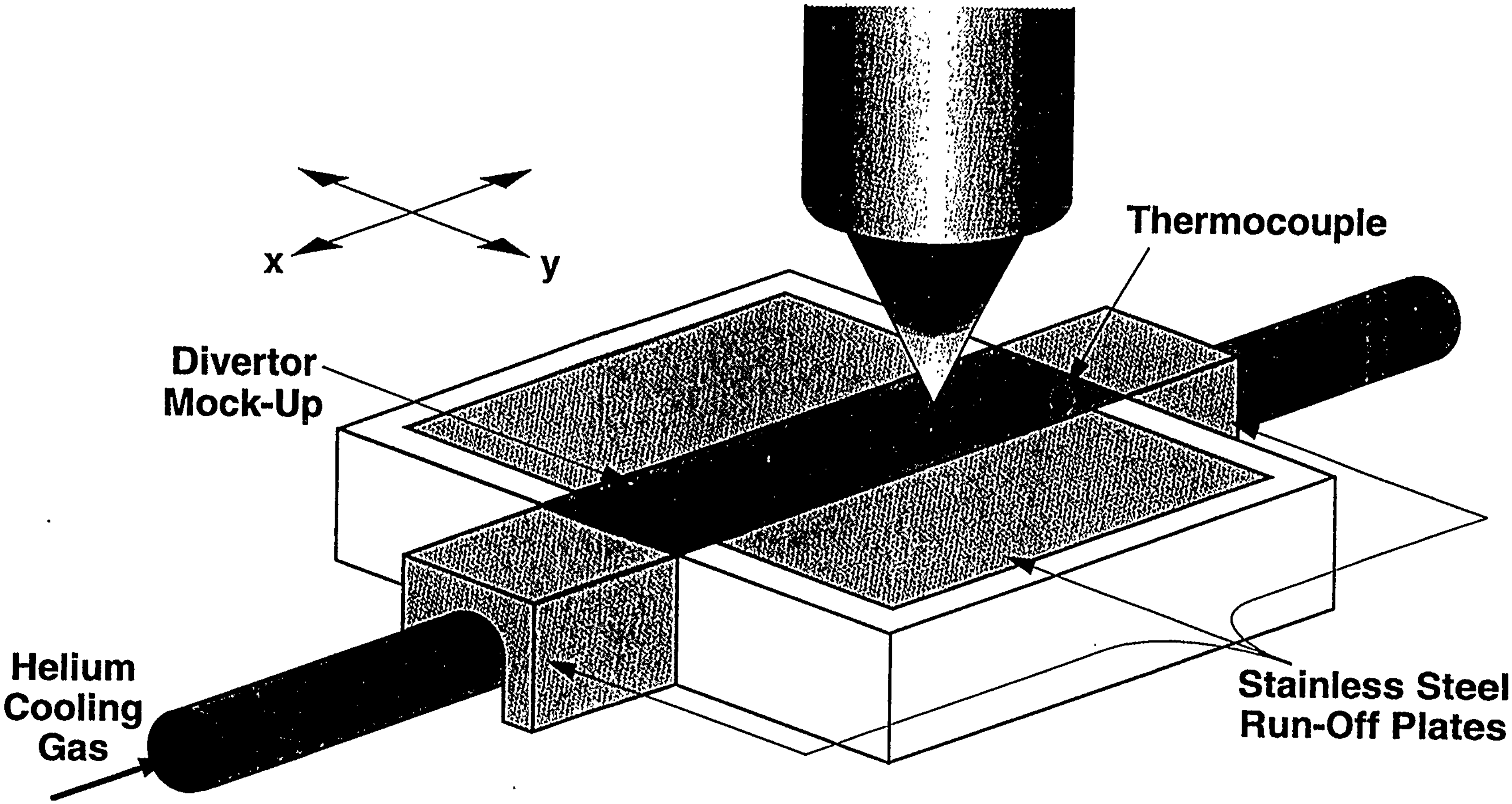

Processing Conditions for Fabricating EBTS Mock-Ups

T/A Parameters	Settings	Torch Parameters	Settings
Peak Amps (A)	40	Arc Gas (Ar)	40 slm
Background Amps	40	Secondary Gas (H_2)	1 slm
Pulser (on/off)	(off)	Powder Gas (Ar)	1 slm
Chamber Pressure	40 torr	Feed Rate (lb/h)	~1
Plasma Torch Current (A)	400	Current (A)	400
Substrate Preheat Temp	550-600°C	Volts	35
Distance (cm)	10 cm	Chamber Pressure	400-450 torr
		Substrate Temp	550-600°C

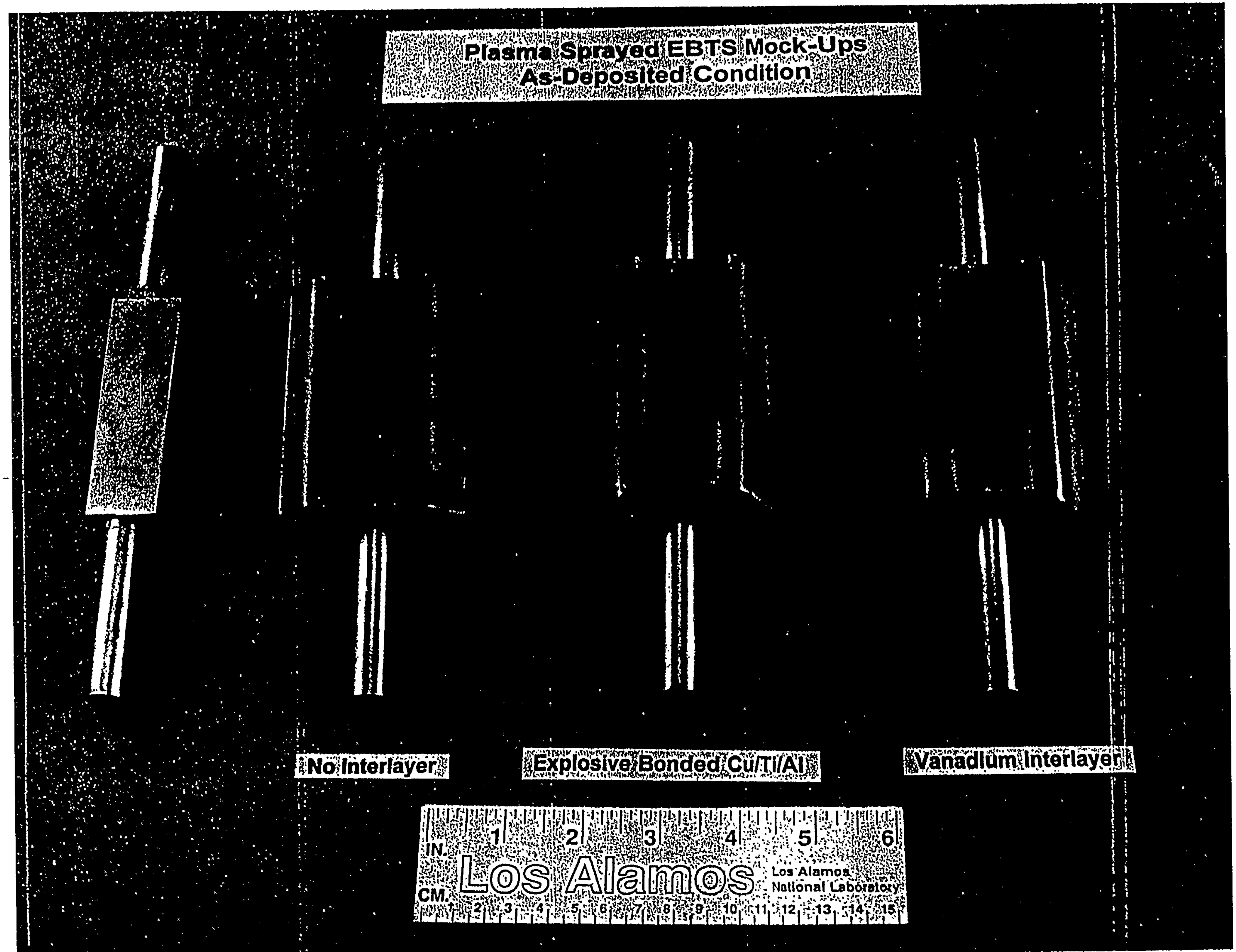
Plasma Sprayed EBTS Mock-Ups
As-Deposited Condition
No Interlayer
Explosive Bonded Cu/Ti/Al
Vanadium Interlayer
IN.
CM.
Los Alamos
Los Alamos
National Laboratory

Machining Beryllium Plasma Sprayed EBTS Mockups

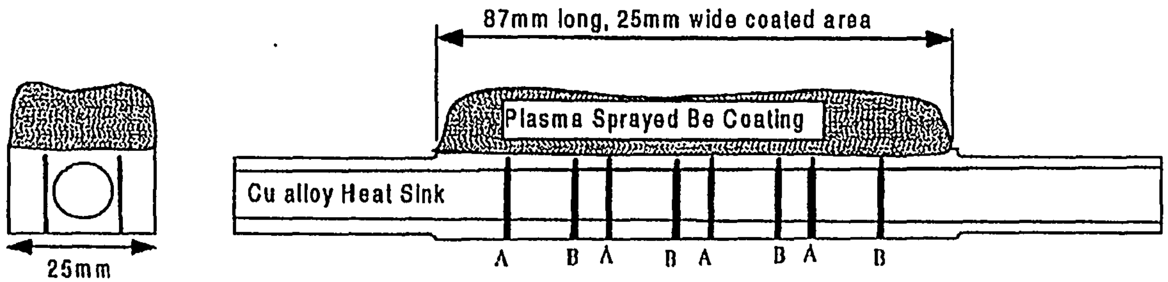

Armor and Heat Sink Diagram:

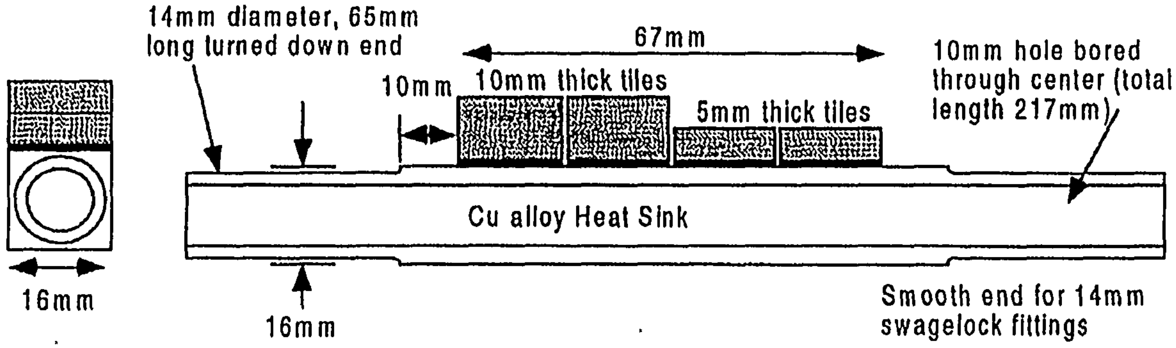

Armor Thermocouple Hole Diagram:

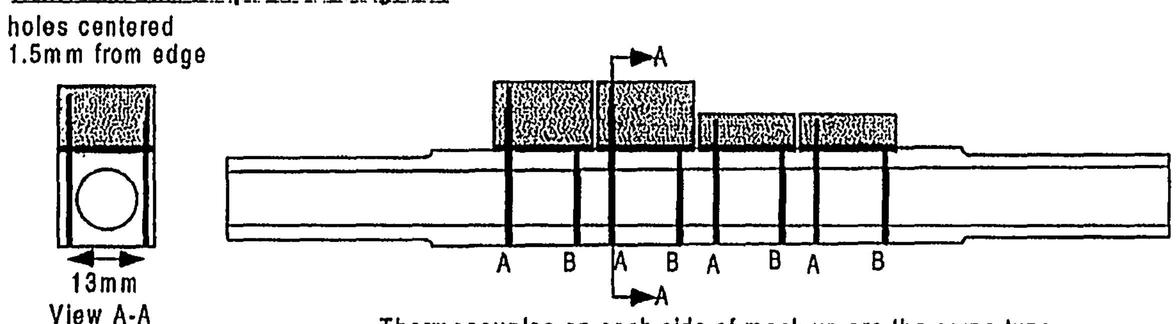

Thermocouples on each side of mock-up are the same type

Machining of Subcastellations

Sub-Castellation Diagram:

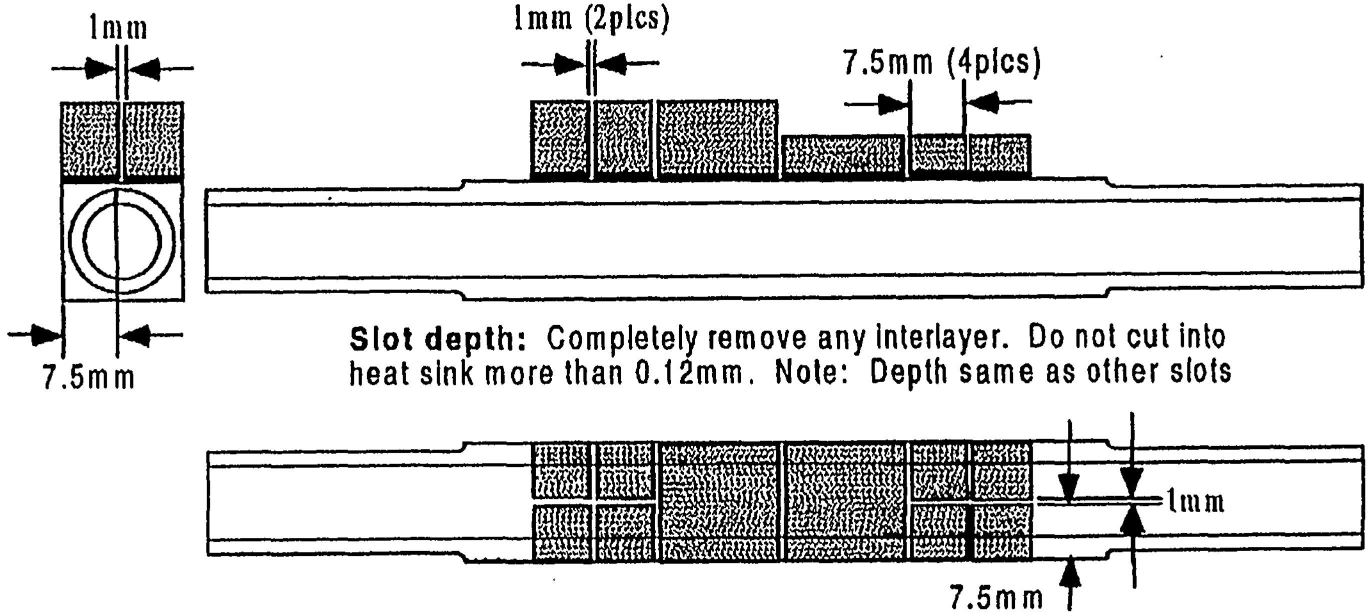

Slot depth: Completely remove any interlayer. Do not cut into heat sink more than 0.12mm. Note: Depth same as other slots

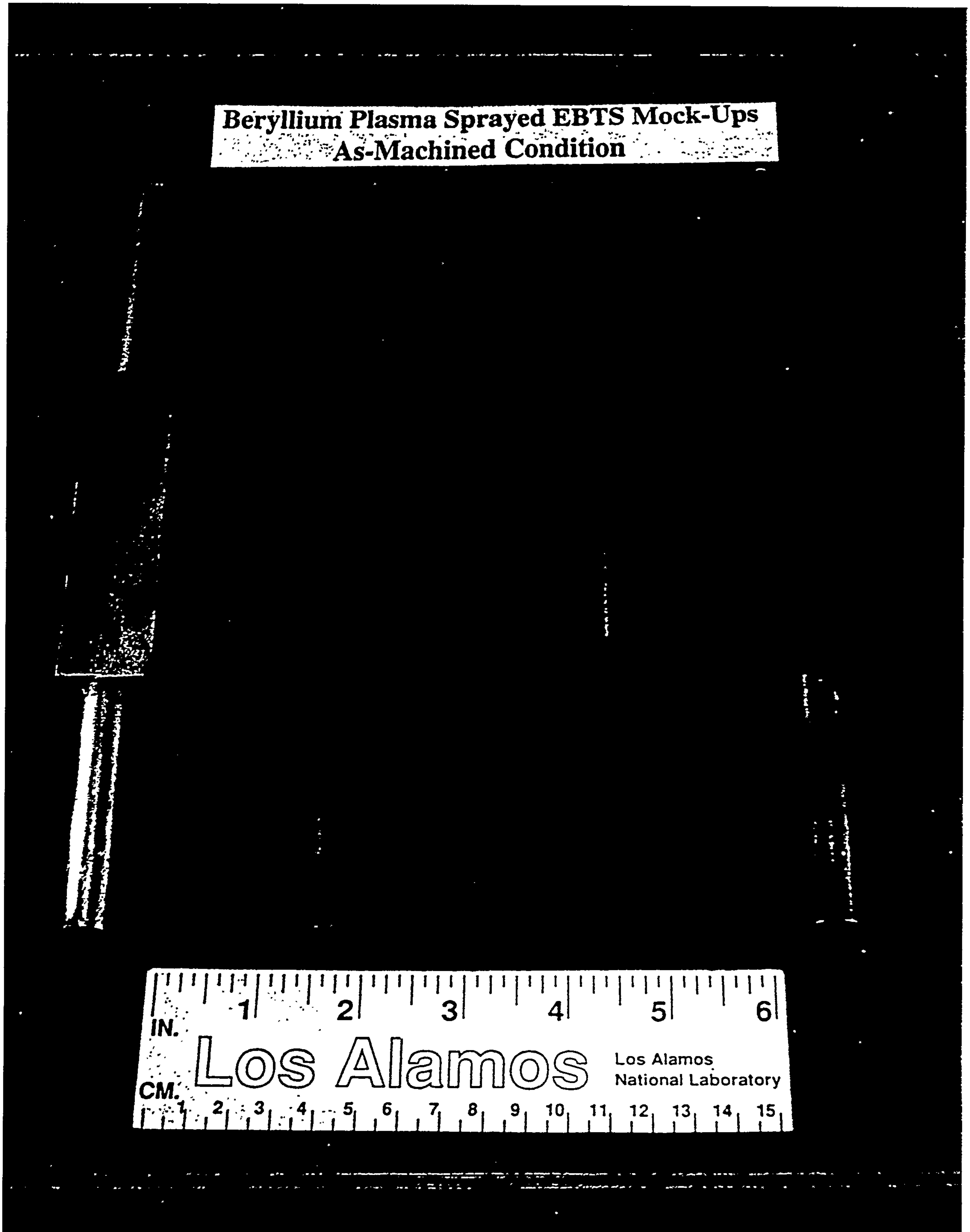
Beryllium Plasma Sprayed EBTS Mock-Ups
As-Machined Condition
IN. 1 2 3 4 5 6
Los Alamos
Los Alamos
National Laboratory
CM. 1 2 3 4 5 6 7 8 9 10 11 12 13 14 15

77606-1-5

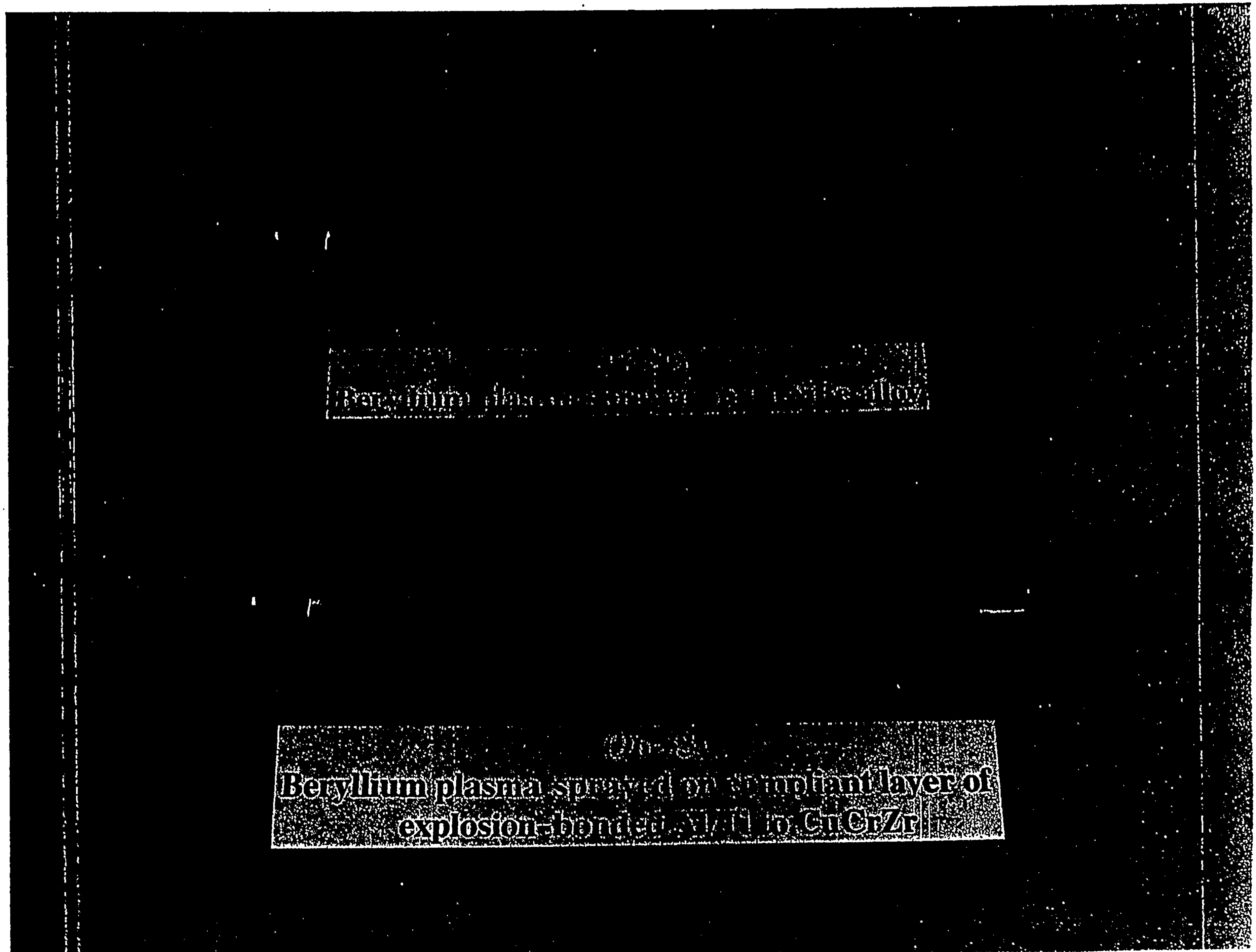

Summary: High Heat Flux Test - Mockup 96-29

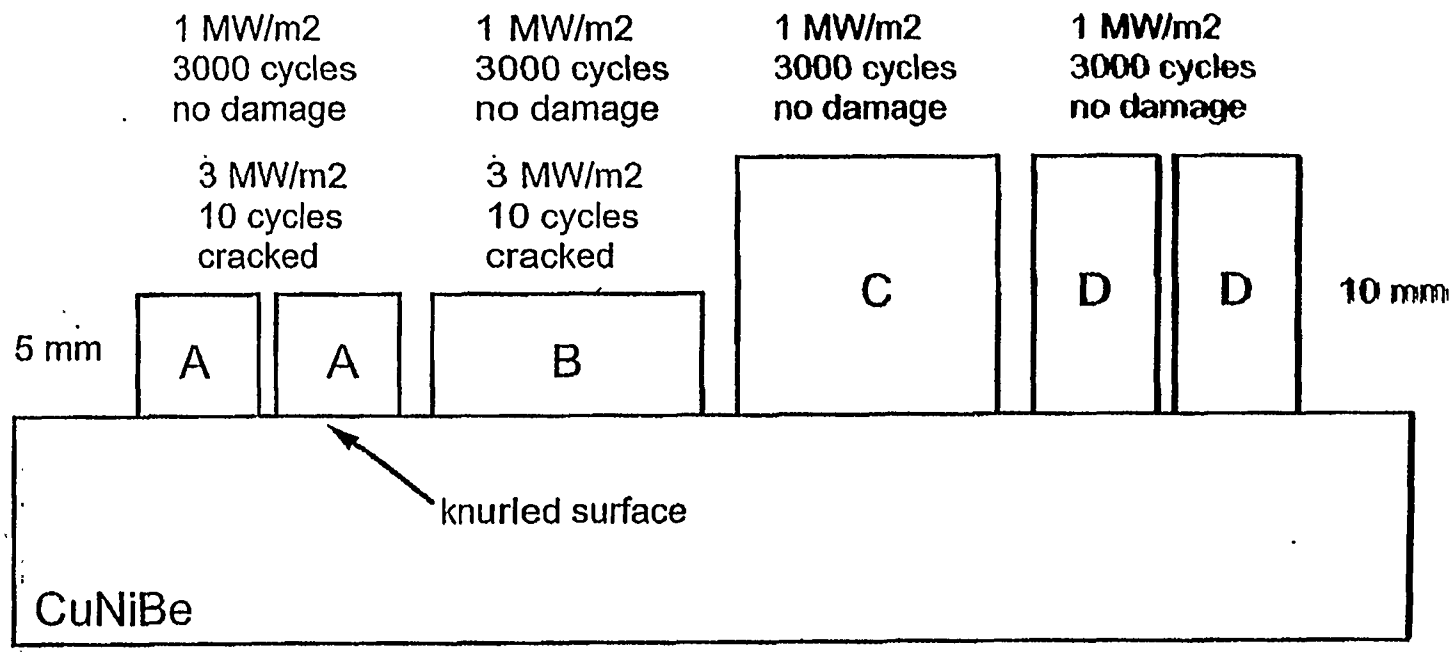

Summary: High Heat Flux Test - Mockup 96-33

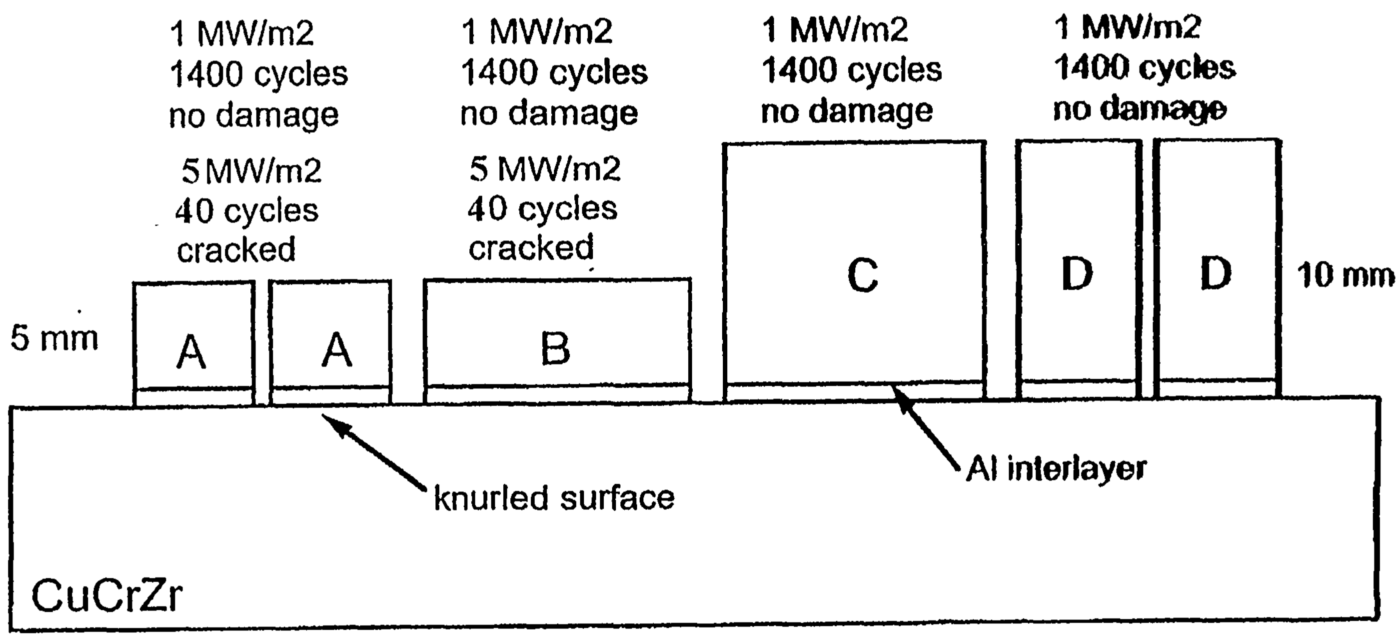

EBTS Mockup 96-29 Be/Cu

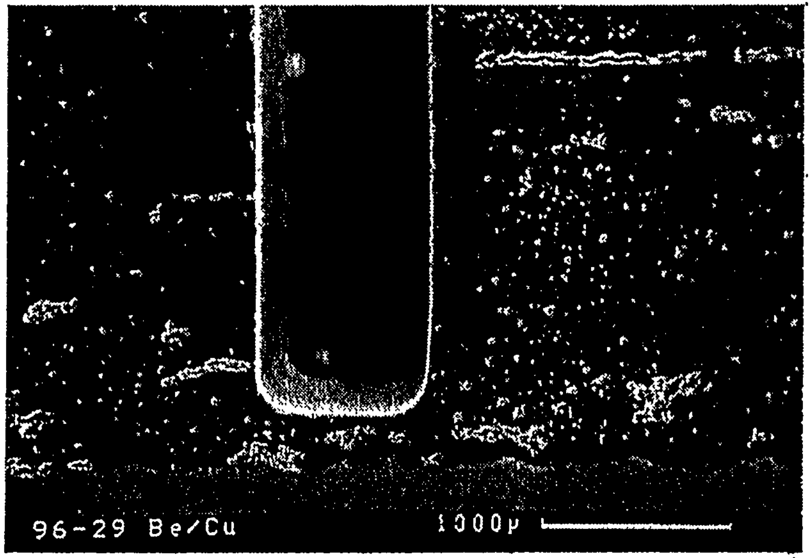

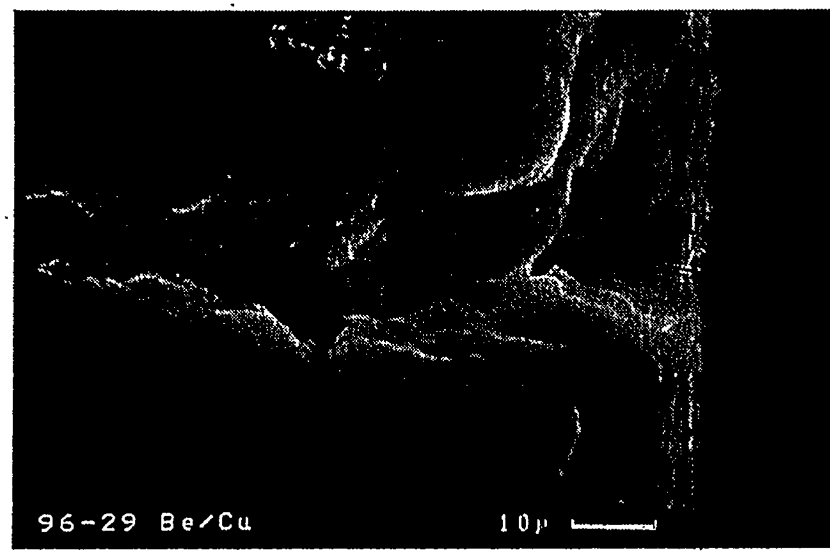

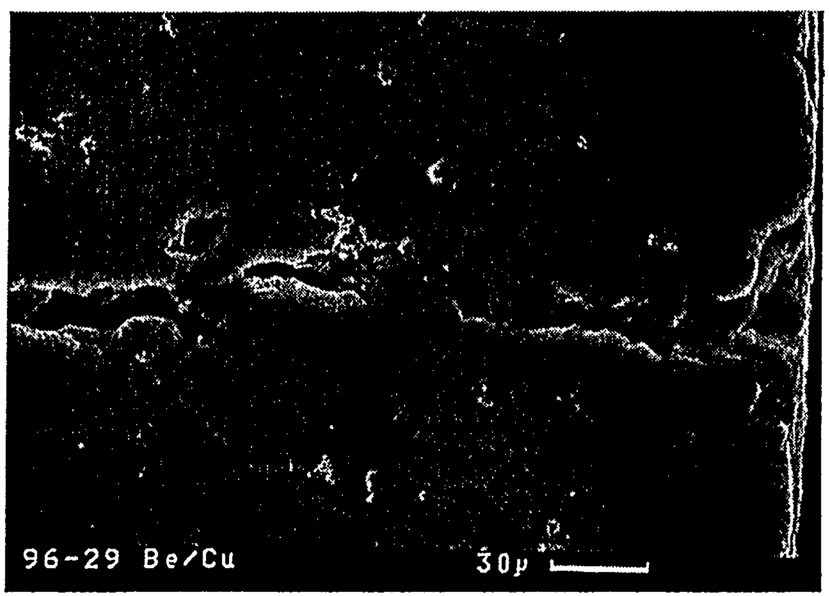

- Cracks may initiate at unmelted particles
- No evidence of cracking at root of castellation
- Cracks extend parallel to the Be/Cu interface
- Cracks may be extending along unmelted particles

EBTS Mockup 96-33 Be/Al/Ti/Cu

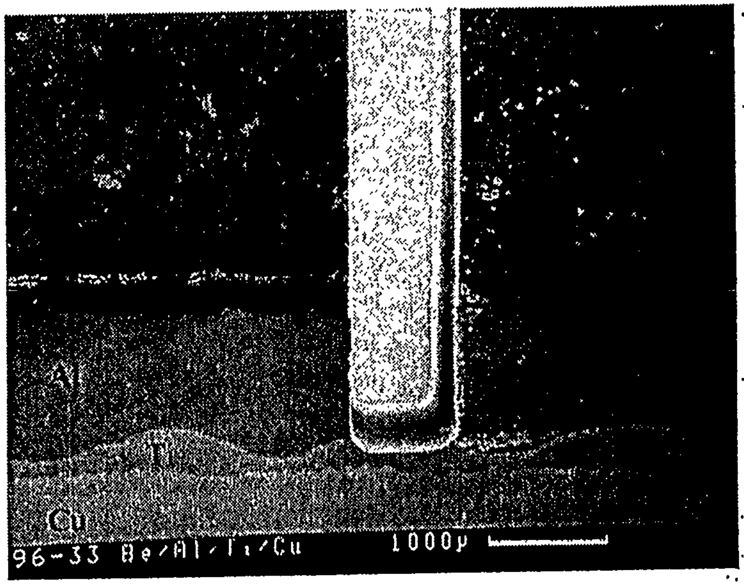

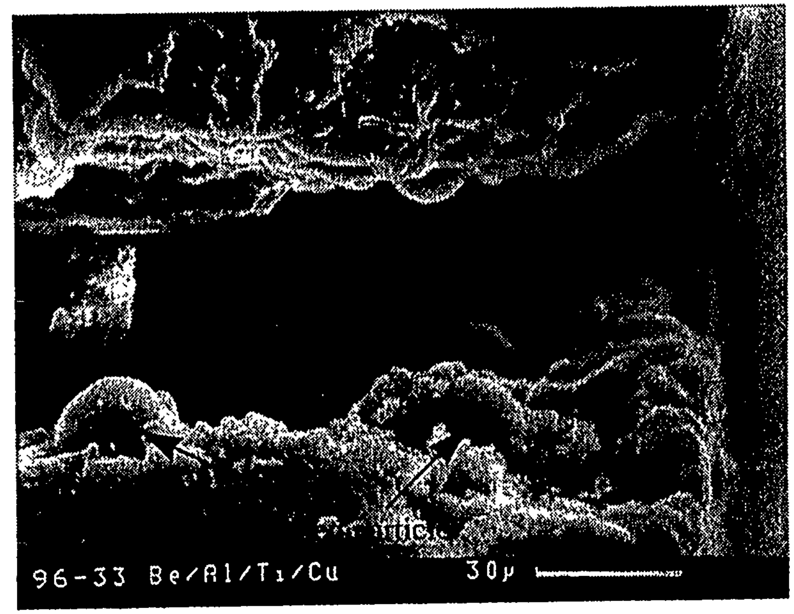

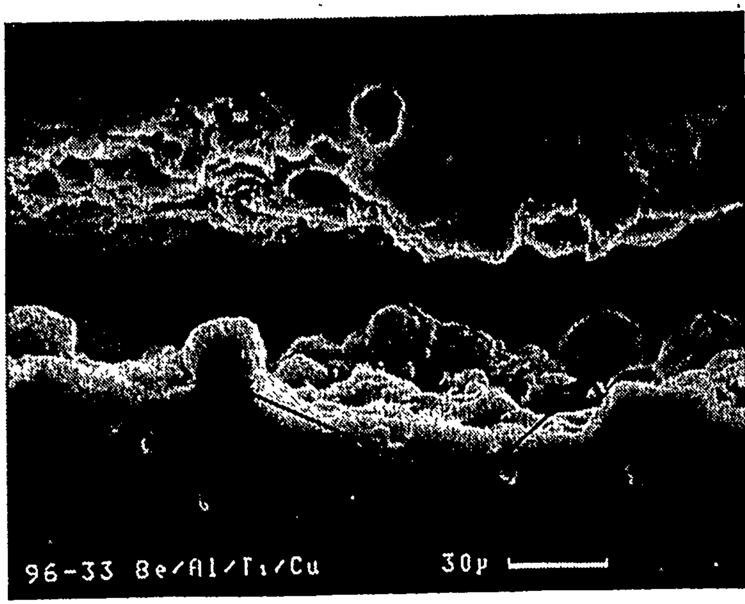

- Presence of unmelted particles in crack wake
- Crack initiates at approx 250 um from Be/Al interface
- No evidence of cracking at Be/Al interface
- No evidence of cracking along other interfaces

DOE Newsnote 1/10/97

Plasma Sprayed beryllium First Wall Mockup Survives 3000 HHF Cycles

A plasma-sprayed beryllium ITER first wall mockup fabricated by LANL has survived 3000 thermal fatigue cycles at 1 MW/m^2 without damage during testing at the Plasma Materials Test Facility at Sandia National Laboratories. This heat flux is four times the expected average heat flux for ITER primary first wall modules (0.25 MW/m^2), and is twice the peak design heat flux (0.5 MW/m^2). These successful results demonstrate the potential for using plasma-sprayed beryllium as a method for both initial fabrication and for *in-situ* repair of eroded beryllium armor-tiles in ITER.

Development of PFC Armor Utilizing Vacuum Plasma Spray Processes

Scott O'Dell

and

Timothy McKechnie

Plasma Processes Inc.

Fabrication Technique for SBIR Phase I Mockup PW-3

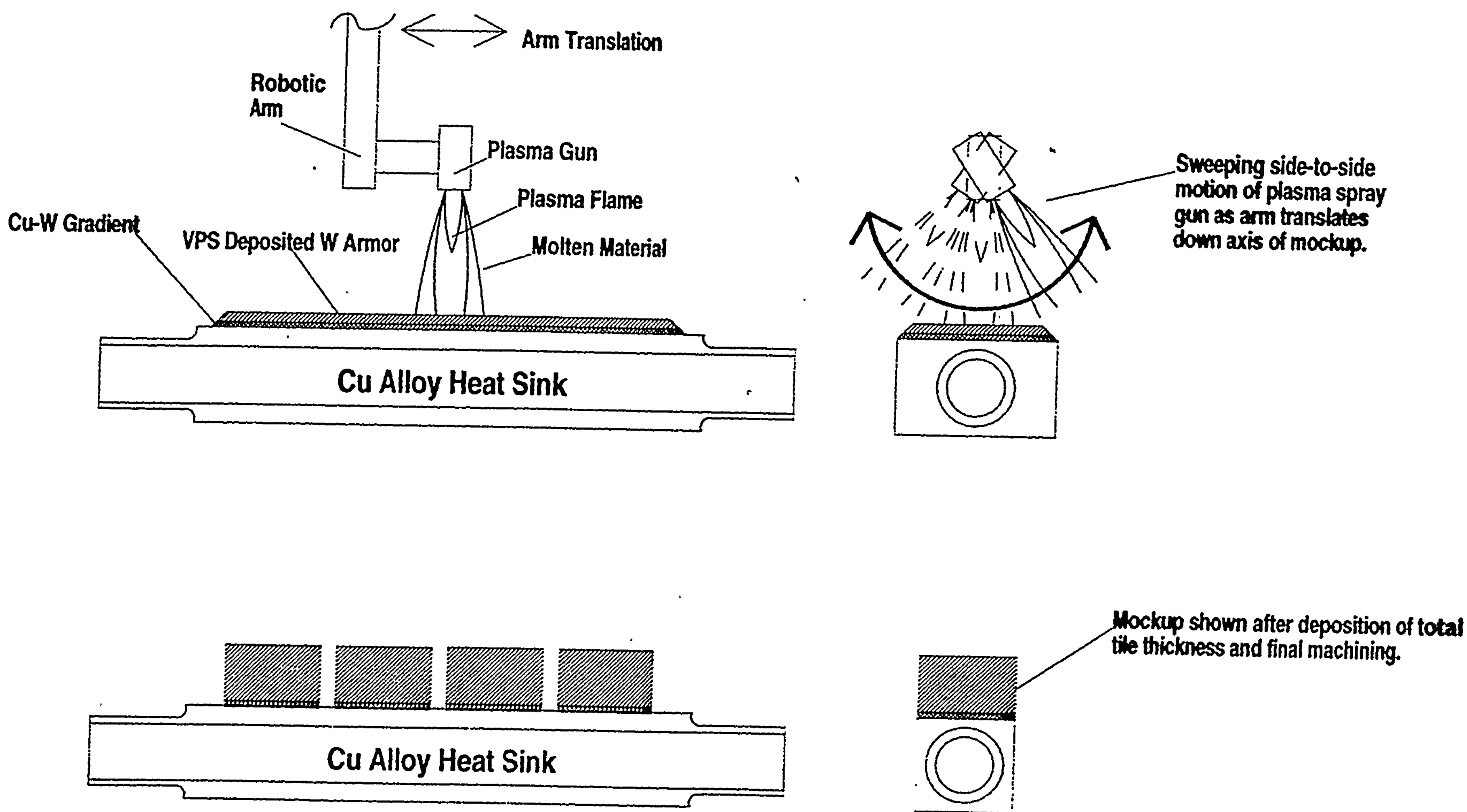

VPS Beryllium Using R18 Nozzle

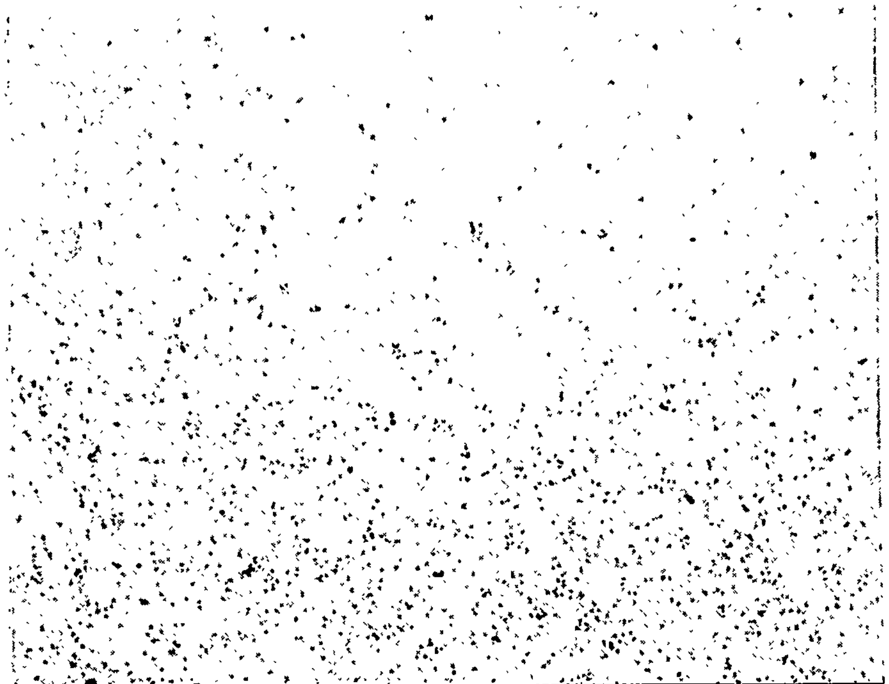

Substrate side

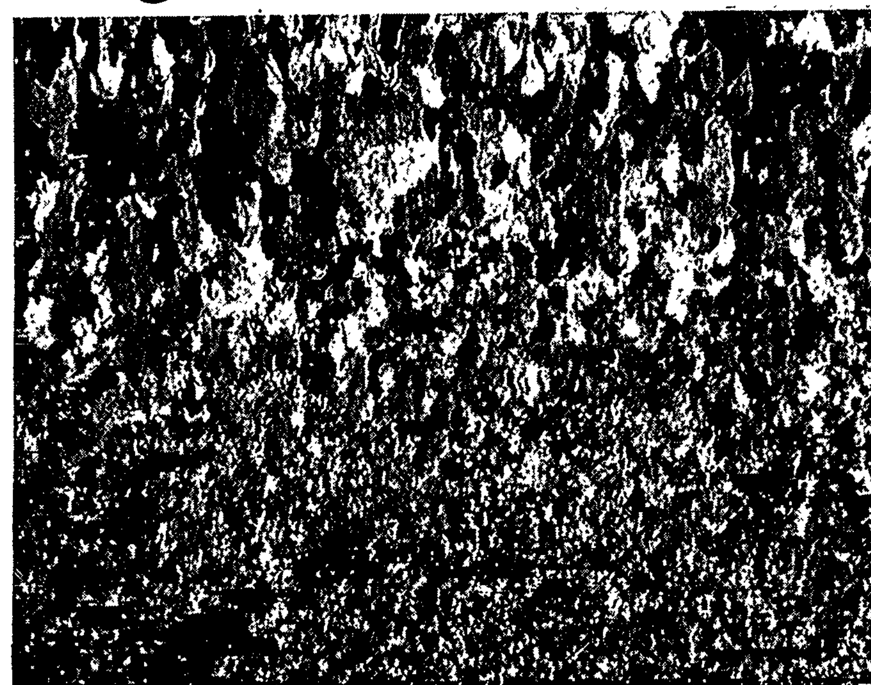

Substrate side

- BF image (50x)
- PL image (50x)
- Recrystallized grain structure; large, columnar grains due to grain growth near top of the deposit
- Increase in density of 92% of theoretical at the substrate side to 98% near the top of the deposit due to grain growth

R/N 9424-2 LANL

Plasma Processes Inc.

Thermal Conductivity of VPS Be and VHP Be as a Function of Temperature

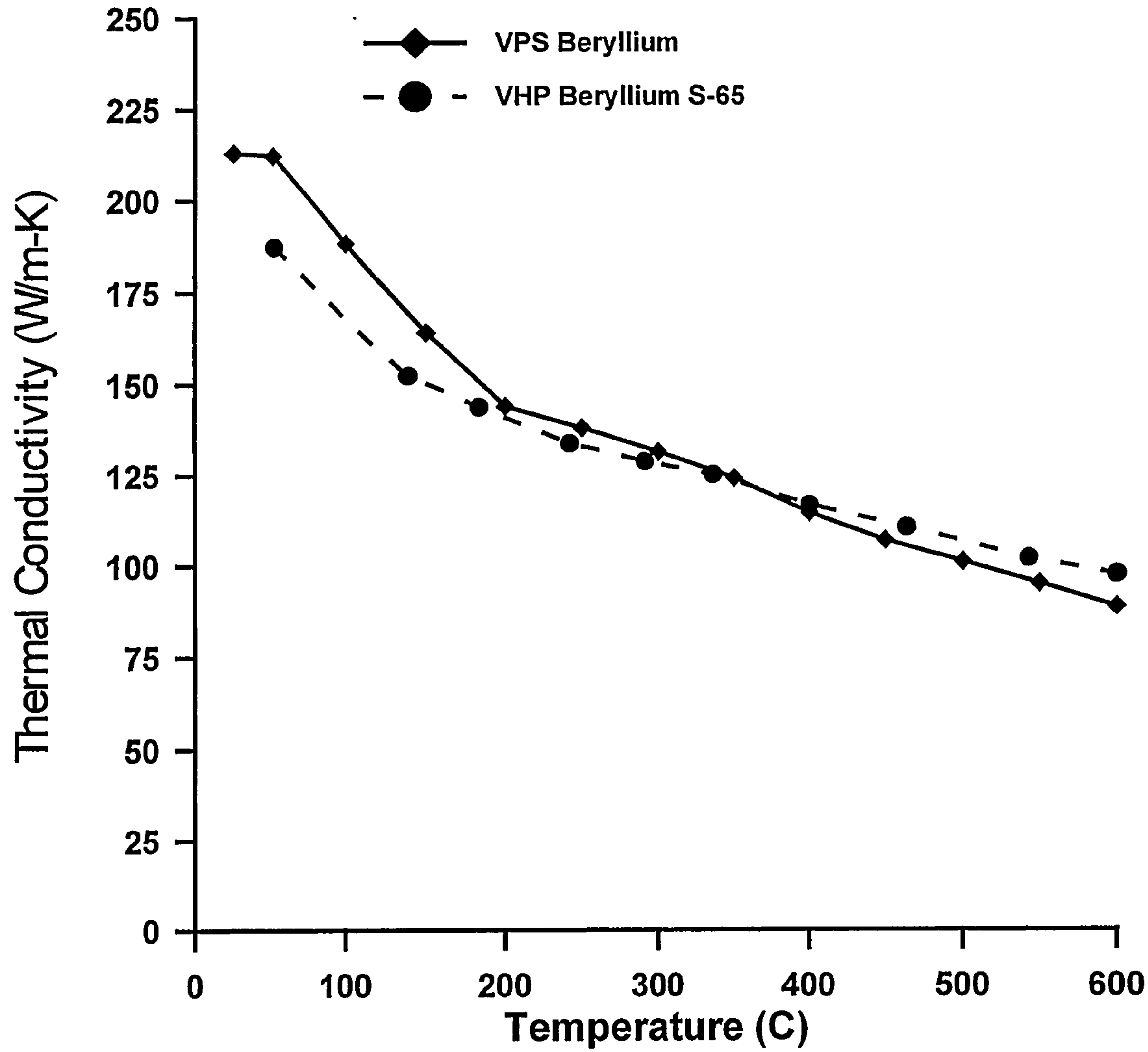

Plasma Processes Inc.

Ultimate Tensile Strength and 0.2% Offset Yield Strength for VHP S-65 Be and VPS Be

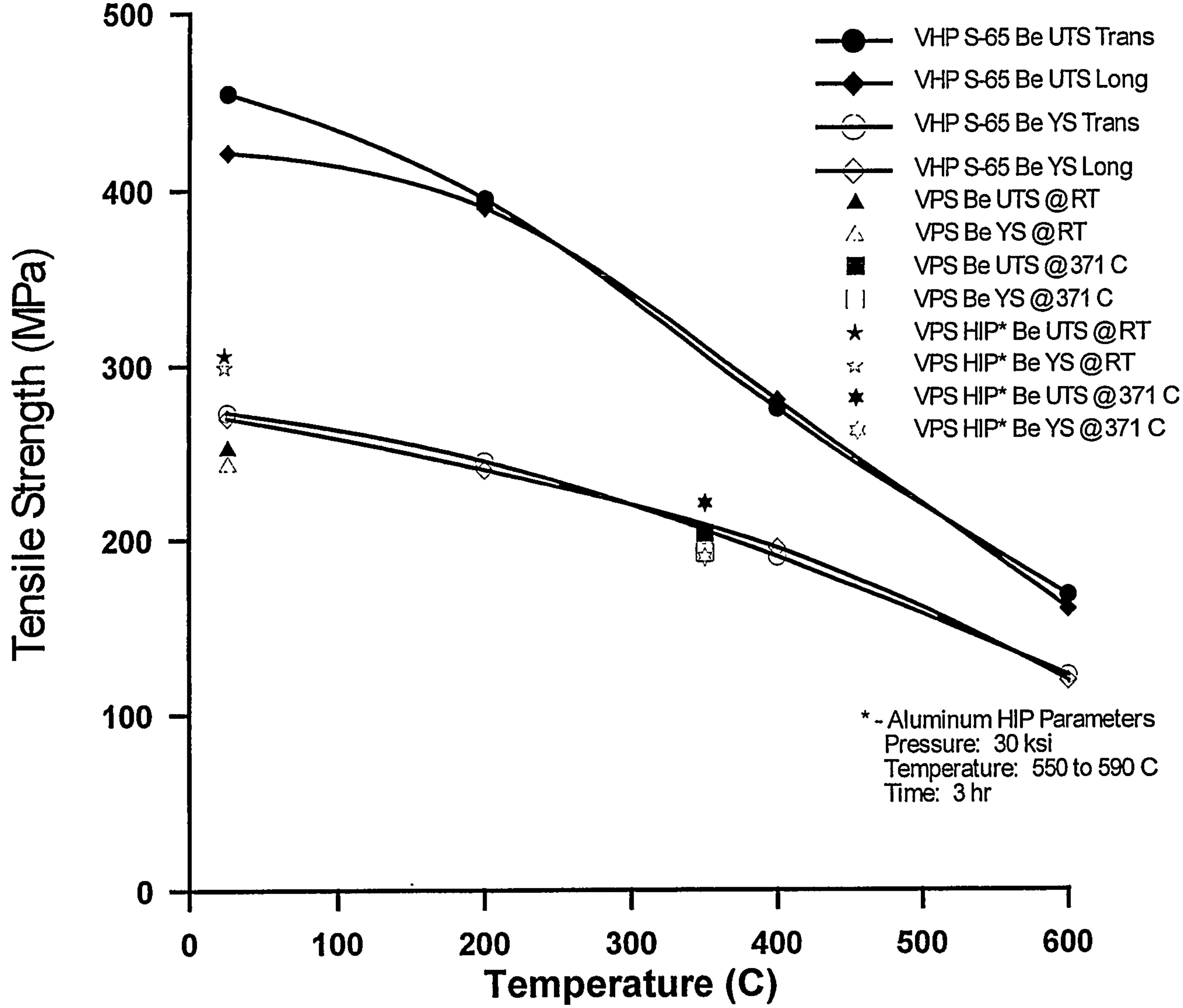

Plasma Processes Inc.

Stress Analysis of Armor Joint

- ABAQUS Finite Element Model (SNL)
- 2-D plane stress
- Elastic behavior
- Temp. dependent props.
- 2000 elements (8-node quad)

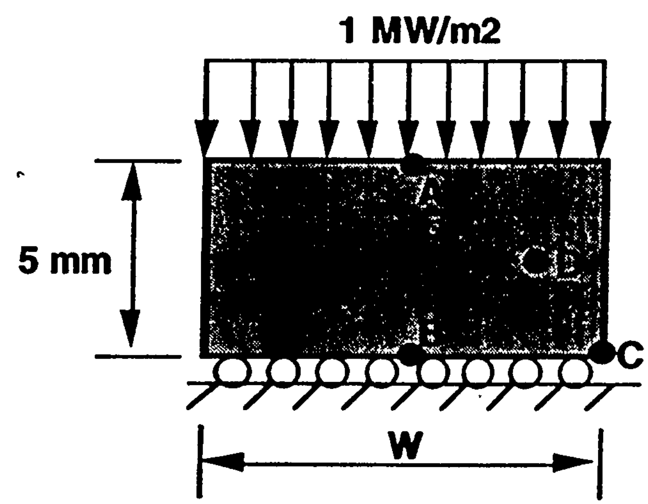

Stress Analysis of Cu/W Joint

Tungsten, 5 mm thick, 1 MW/m2, Elastic

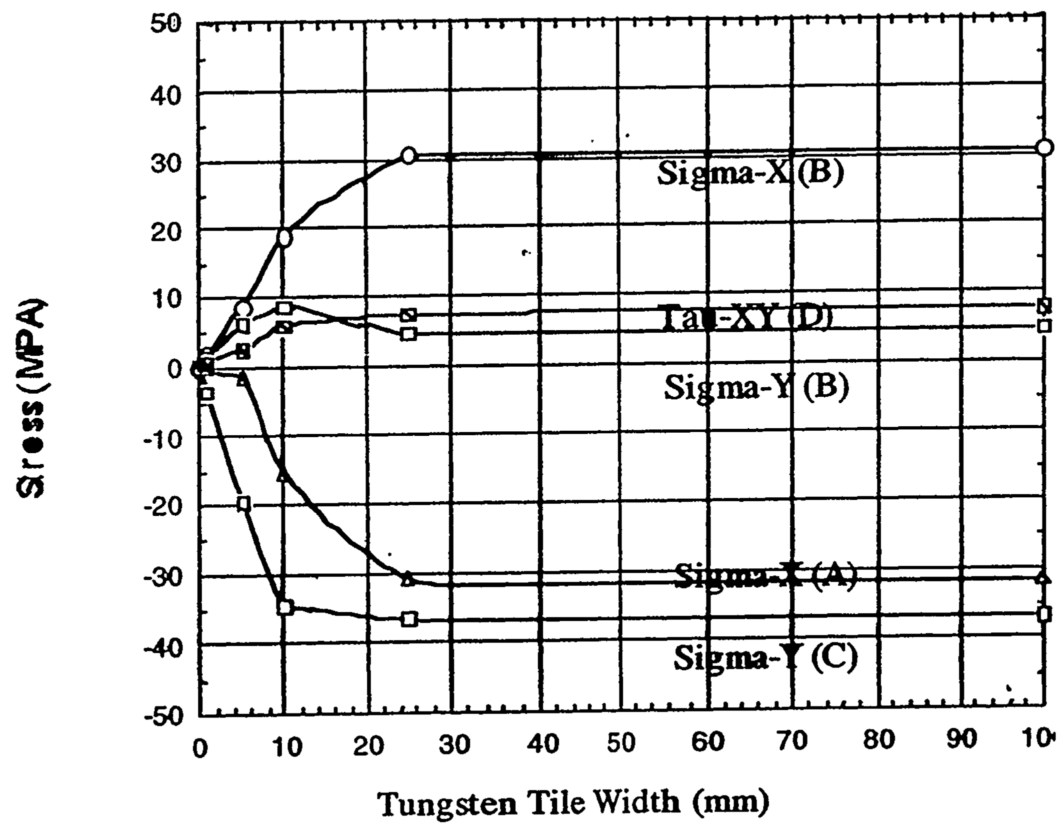

Evolution of Plasma Facing Component Armor

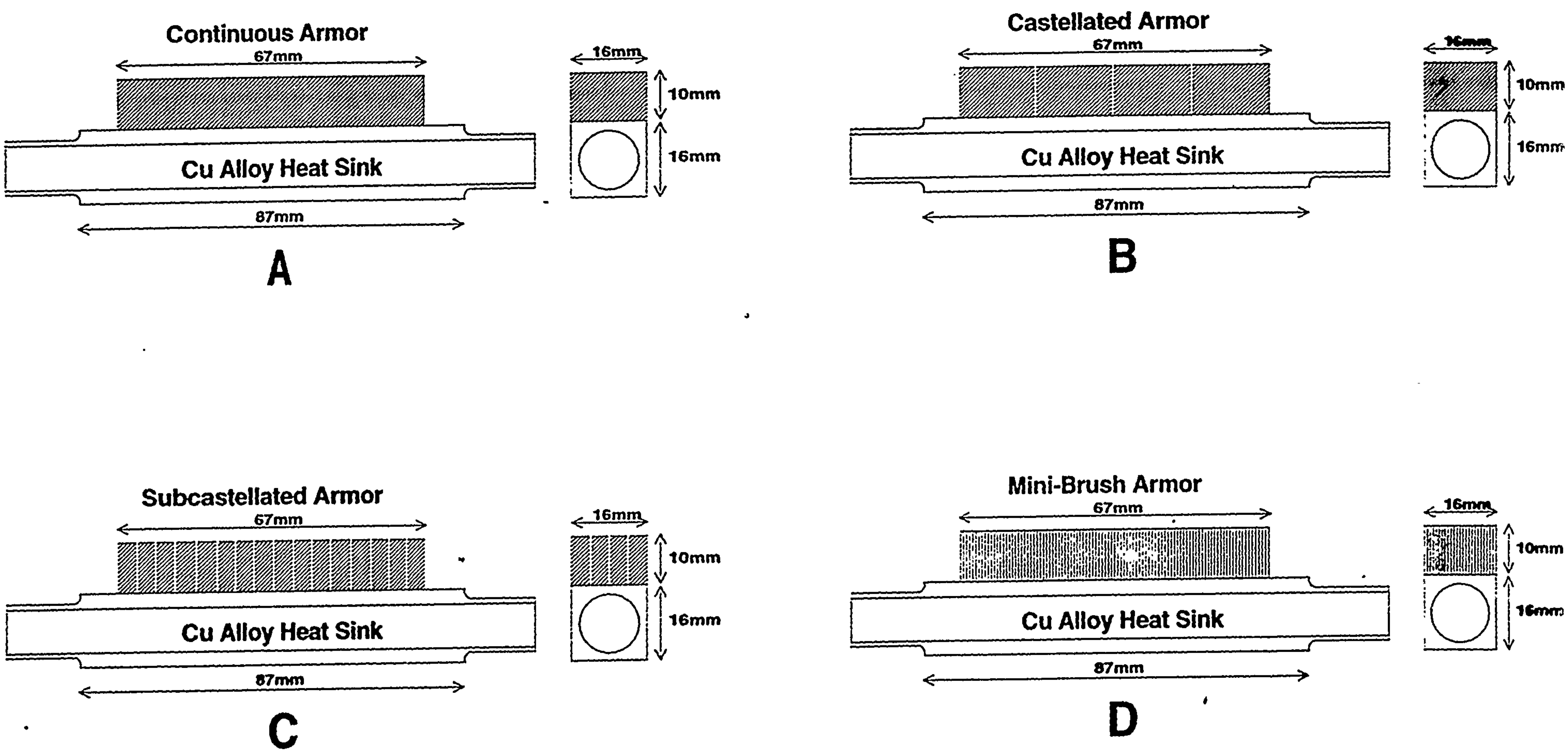

Figure 7 - The evolution of plasma facing component armor from the continuous covering to the mini-brush structure.

VIII-105

Vacuum Plasma Spray Brush Armor for Plasma Facing Components

- Process is applicable to many different materials, i.e., W, Be, Carbon Composites
- Structure minimizes stress singularity of a flat bond line
- Grain orientation of the brush maximizes heat transfer to the copper alloy heat sink
- Small cross-sectional area reduces stress at interface (FEM)

Brush Armor with End Points

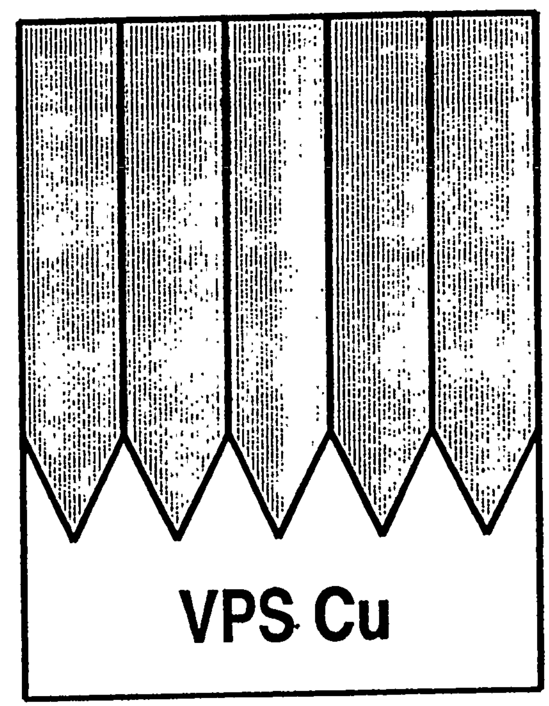

Fabrication Technique for SBIR Phase I Mockups PW-4 & PW-7

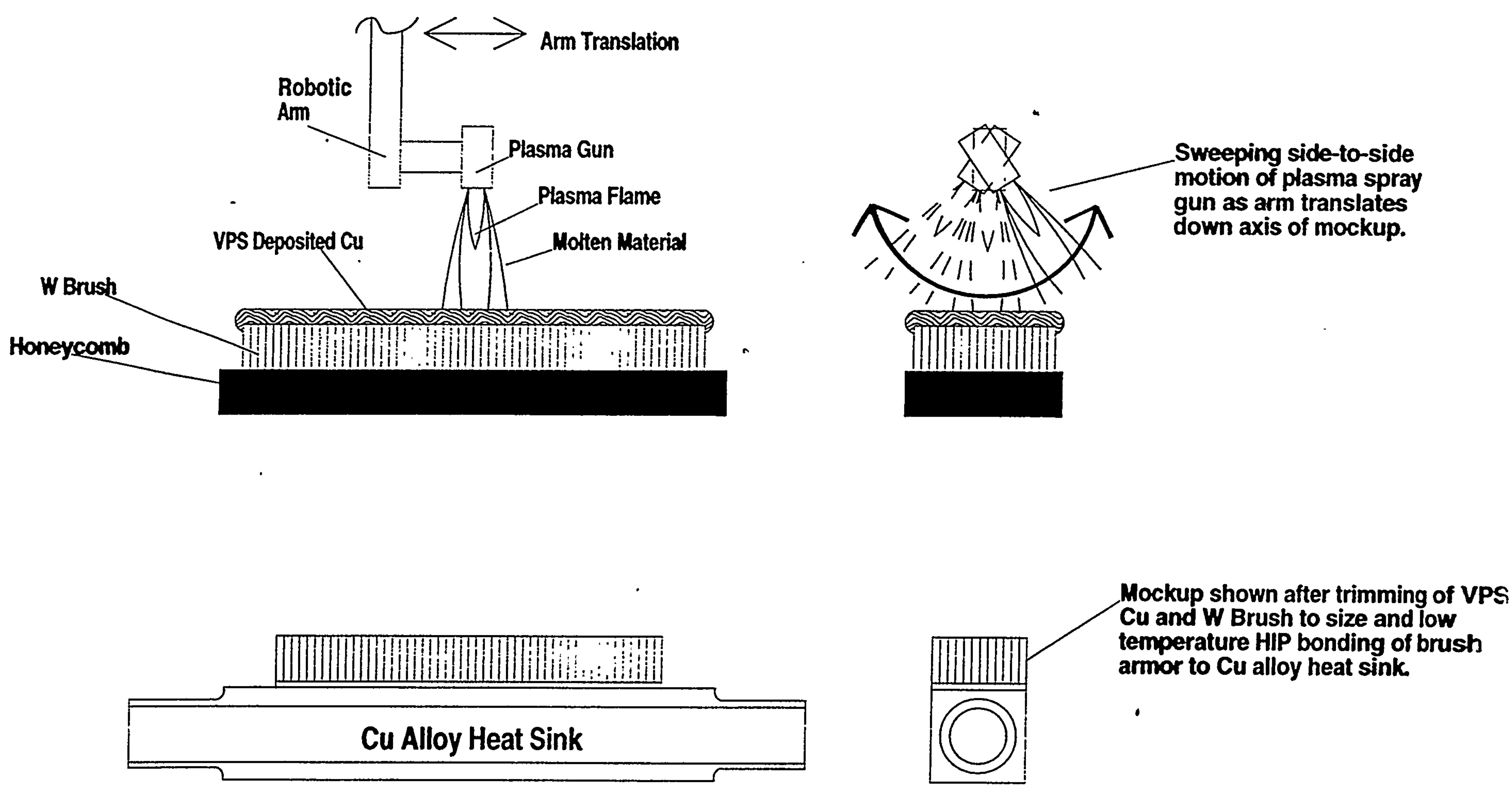

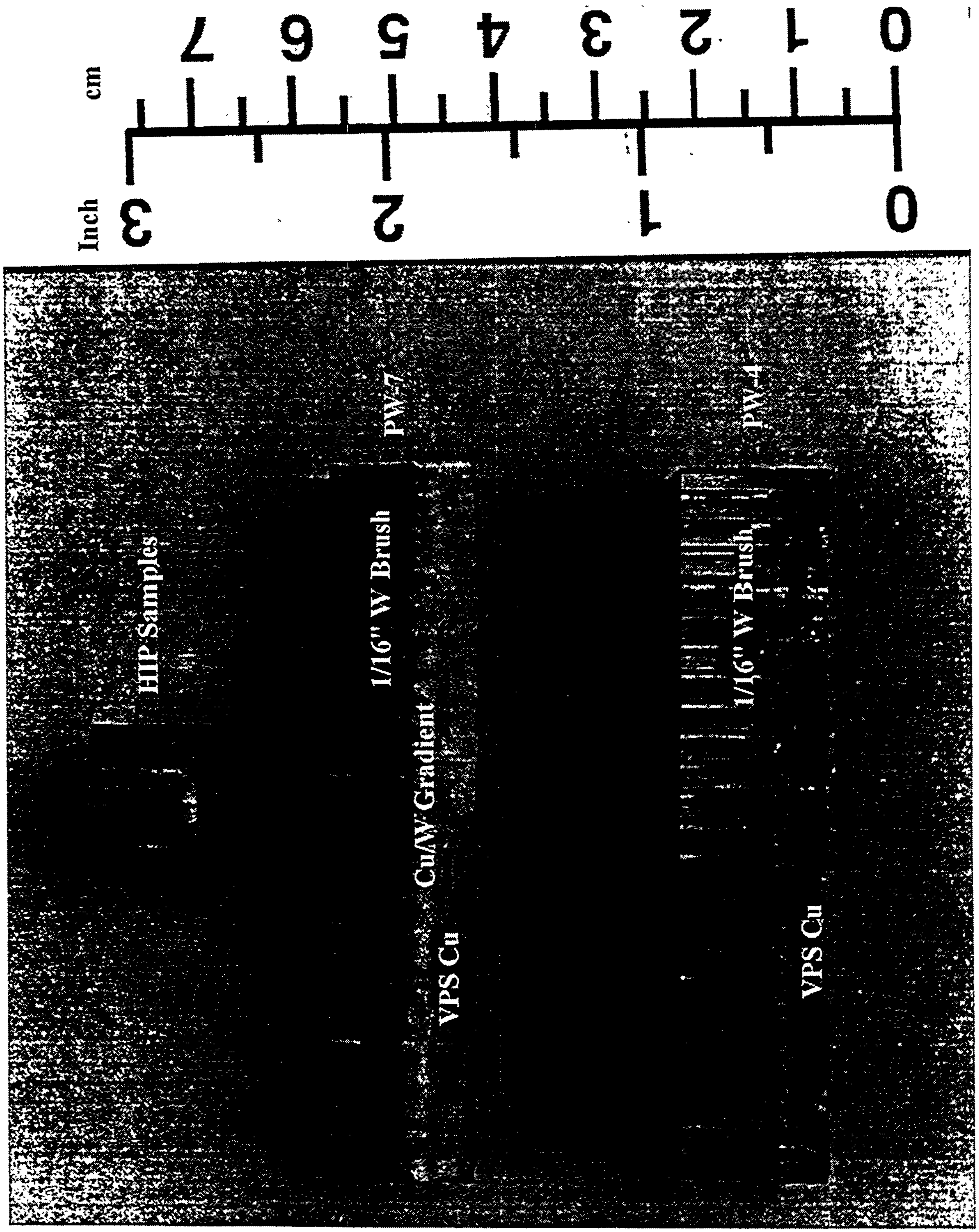
Inch
cm
0
1
2
3
0
1
2
3
4
5
6
7
HIP Samples
PW-7
1/16" W Brush
Cu/W Gradient
VPS Cu
PW-4
1/16" W Brush
VPS Cu

Bonding Brush to Cu Alloy Heat Sink

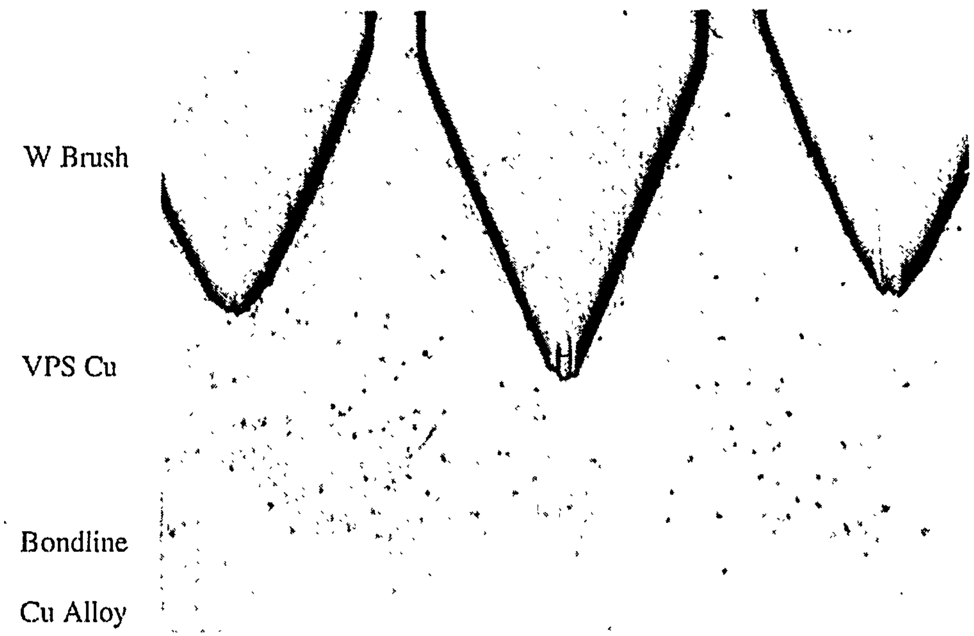

As-HIP, 25x

- VPS Cu and heat sink material cleaned and coated with PVD Ni
- Components placed in intimate contact in HIP can
- Joining accomplished through 450°C HIP diffusion bonding process
- Note penetration of W brush into VPS Cu (~1mm) for can #107 (R/N V97-83A)

Plasma Processes Inc.

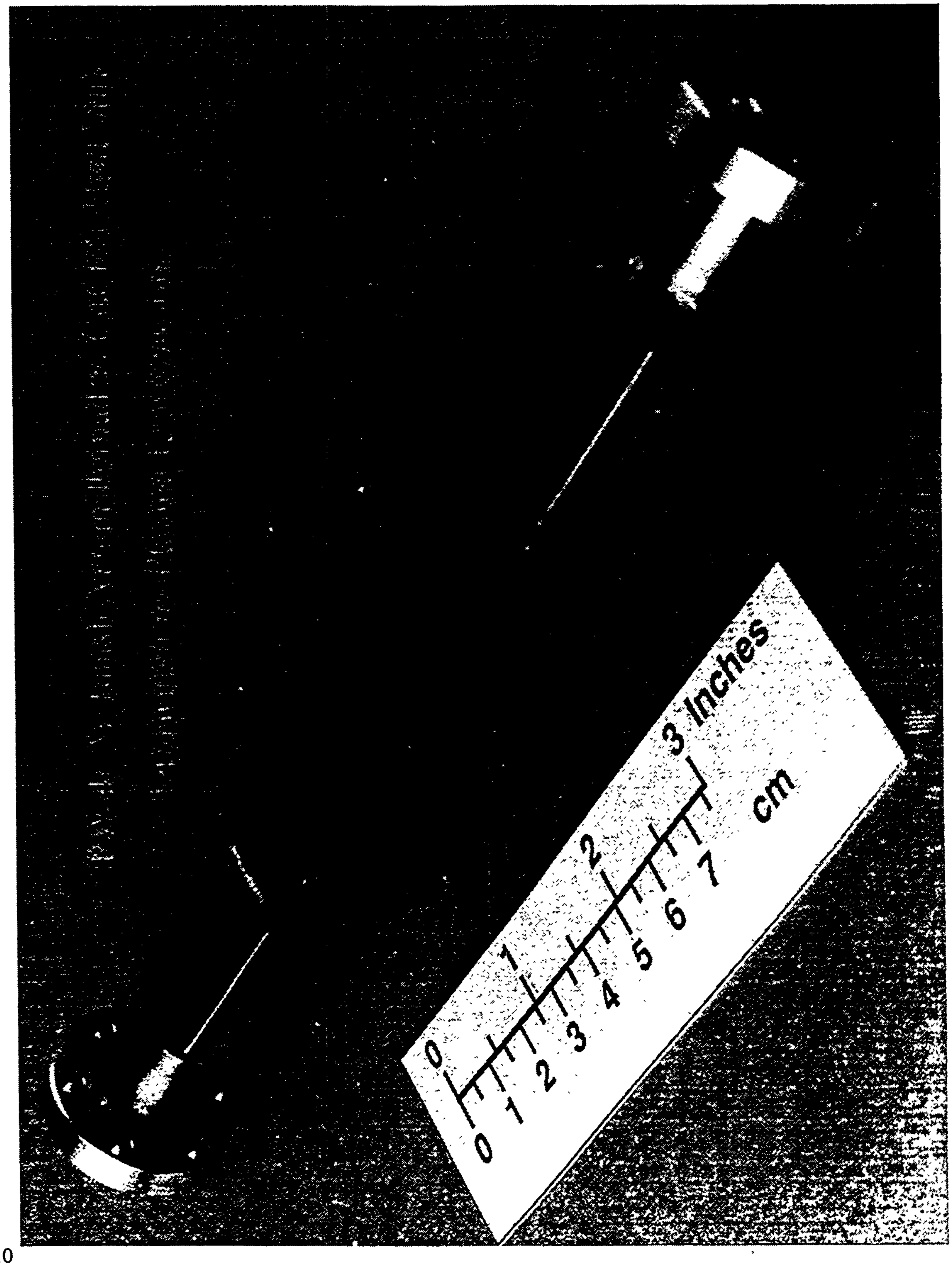
0 1 2 3 Inches
0 1 2 3 4 5 6 7 cm

Optimization of Tip Design

- Surface condition
- Coatings on tips (25-50 micron)
- Copper alloys
- Tip angles and depth of penetration in VPS Cu

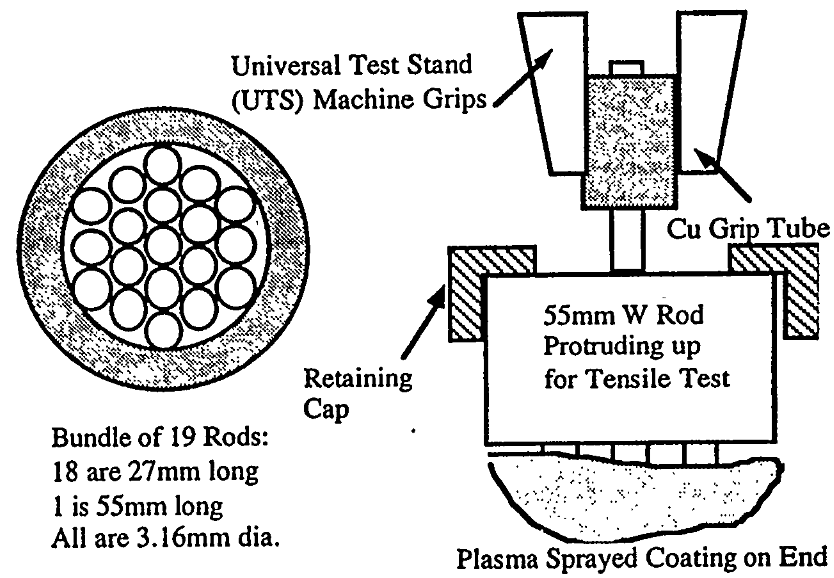

Plasma Processes Inc.

Initial Results of Pull-out Tests

VPS Coating	Thermal Treatment	Failure Stress (MPa)
Cu	VA 900C + HIP	139
Cu	HIP	136
Fine Ni	VA 900C	110
Fine Ni	VA 600C + HIP	118
Fine Ni	VA 900C + HIP	108
Fine Ni	HIP	101
Coarse Ni	VA 600C	119
Coarse Ni	VA 900C + HIP	109
Coarse Ni	HIP	107
PPI-1	VA 600C	141
PPI-1	HIP	97

Plasma Processes Inc.

Summary of Armor Development by Plasma Processes Inc.

- PW-8: small scale divertor mockup armored with 3.2 mm diameter W rods
- Medium scale mockup (33 mm wide x 1 m long) armored with 3.2 mm diameter W rods
- Beryllium brush (1.6 mm diameter rods) for a small scale mockup
- Electron beam welding of brush armor to copper alloy heat sinks
- Laser consolidation of plasma sprayed material

Plasma Processes Inc.

Section IX: PSI/PFM Issues of Collaboration

[page intentionally left blank]

Subjects of collaborations

near term, US - JPN frame work

1. PSI studies, edge plasma physics in LHD

SNL. UCSD, GA
proposing several programs

- heat load distribution
- wall conditioning with mag. field
- boronization
- net erosion with long pulse ope.
- edge diagnostics
- identification of surface situation

2. Long term issues of PFC

- high Z target plates
- protecting layers on 1st walls
- net erosion studies
- high heat flux components

  brazing, thermal hydrolics,
  materiels, He gas cooling.

  .....

3. Series of WS on HHFC & PSI

4. UNIV. in Japan Kyushu U.
   Nagoya U.
   Osaka U. Hokkaido U.
   Toyama U
   U. Tokyo

5. JAERI

PMI-HHF Collaborations

JFY 98:

preliminary proposals from US

Workshop in Japan (NIFS)

Plasma edge studies	UCSD → NIFS	
Te boundary physics	UCSD → NU	Nagoya U
advanced div. simulator	UCSD → NU	
Ponderomotive force limiter	UCSD ← NIFS	
innovative divertor concept	UCSD → NIFS	
ICR wall conditioning	SNL → KU/NIFS	
Particle energy analyzer	SNL → NIFS	
HHF testing (ion beam)	SNL → JAERI	
advanced PFCs	SNL → NIFS	

wall conditioning test in DIIID

JFY 99:

? items related to:

completion/installation of LID

experiments in LHD

PMI/HHF development

progress on NSTX

JT-60U, DIIID, C-MOD TRIAM

APEX/ALPS programs

advanced divertor simulator

Material testing in NSTX Modeling.

in-situ observation/characteriz.

US-J Joint Project. ← 99

Session X: Panel on Future PFC Concepts

[page intentionally left blank]

ALPS Summary

ALPS Working Group

Presented by Dai-Kai Sze
Argonne National Laboratory
Argonne, IL.

US-Japan Workshop on
High Heat Flux Components & Plasma Surface Interactions for next Fusion Devices, San Francisco
December 8-11, 1997

Objectives of Meeting

- Review capabilities in individual areas
- Identify near term focus for plasma confinement
- Identify information and database needs
- Identify key questions/issues to be addressed in next ~3 months
- Specify tasks to be performed over next ~3 months

Introduction of New PFC Concepts

- A mechanism is needed for review of new concepts that could be introduced in the future
  - Free-surface liquid systems
  - Solid surface systems (moving)

- APEX is to review all new concepts for blankets

- ALPS is the most approporate way for reviewing PFC concepts

- Formal guidelines for review are yet to be established

Potential Advantages of Liquid Free-surface Systems

- Unlimited Erosion Lifetime
- No Neutron Damage Concerns for Liquids
- High Power Density Capability
- Active Pumping of Liquid Surface
- High Temperature Operation
- High Power Conversion Efficiency
- Low Pressure Operation

Participating US Institutions

- Argonne National Laboratory
- General Atomic
- Idaho National Environmental Engineering Laboratory
- Lawrence Livermore National Laboratory
- Oak Ridge National Laboratory
- Princeton Plasma Physics Laboratory
- Sandia Natioanal Laboratory
- University of California - Los Angeles
- University of California - San Diego
- University of Illinois
- University of Wisconsin

Operating Target

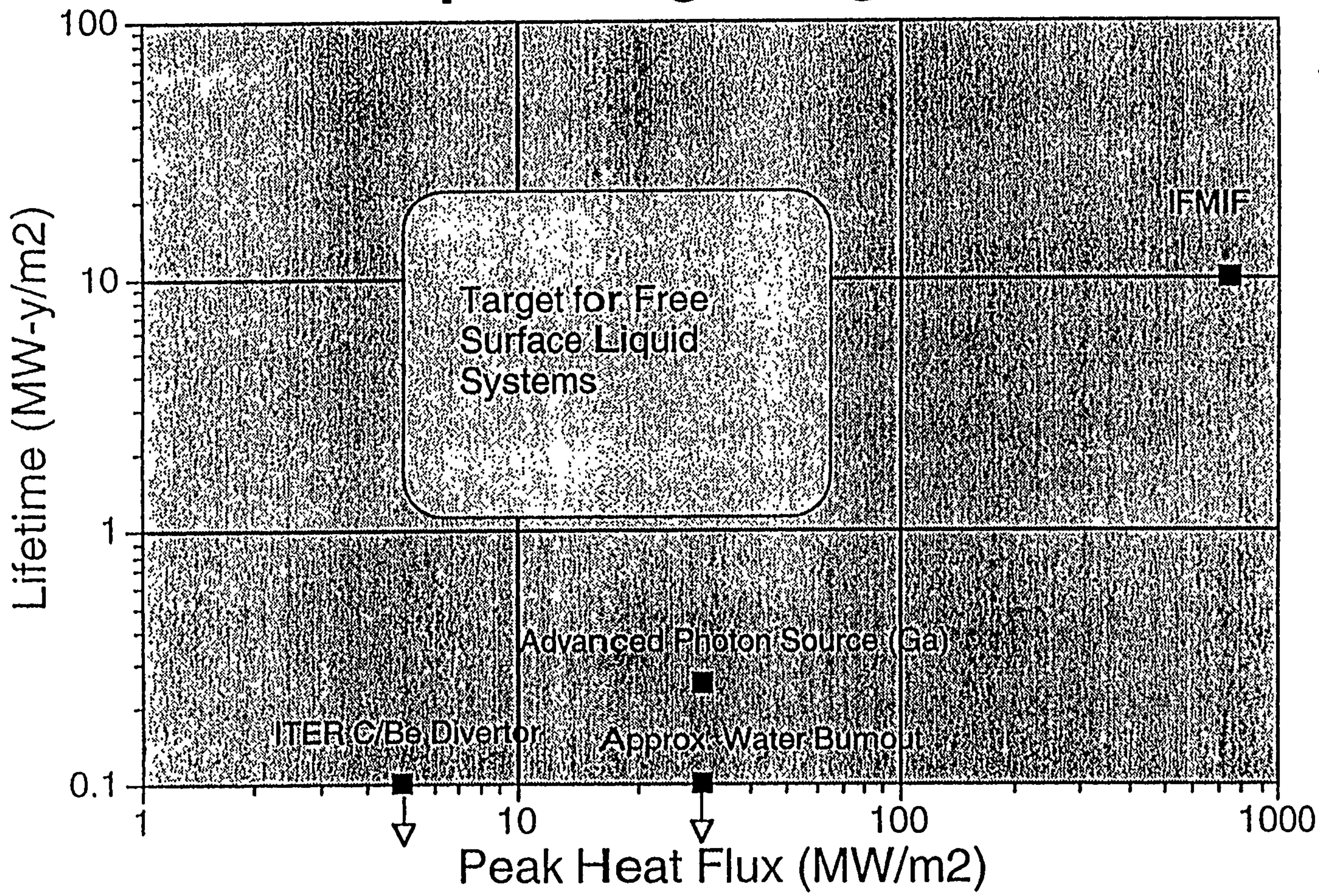

Assumes 1MW-y/m2 = 10dpa

Key Questions

- What are the heat flux and power density limits for liquid free-surface systems?
- What are the maximum allowable evaporation rates for liquids that still insure stable plasma operation?
- How stable is the liquid surface during normal and off-normal conditions?
- How will the liquid free-surface systems alter the plasma edge conditions?
- How will the liquid free-surface systems affect other fusion systems?

Initial Assessment of Issues and R&D for Liquid Plasma-Facing Components

Issue	R&D Needs
Sputtering and redeposition	Assess sputtering yields along with sheath and near-surface transport at liquid surfaces by hydrogen, helium, and self-sputtering. Validate models with plasma experiments.
Species transport to plasma	Measure H, He and self-sputtering rate vs. energy for Li, Ga, LiPb, Sn and Flibe and other canditate liquids. Model/measure edge plasma transport from liquid surface.
Plasma-liquid interface stability	Modeling and data on plasma momentum flux effects. Modeling and data on electric field and current effects.
Tritium (and He) removal	Measure tritium and deuterium uptake in TPE and DiMES for candidate liquids, respectively. Determine basic thermophysical properties. Benchmark DIFFUSE with TPE, and DiMES data. Define tritium extraction system, estimate size and cost. Determine tritium inventory using DIFFUSE
Integrated plasma tests	Multiple effect liquid surface / plasma interaction tests in PISCES, DiMES, DIIID tests.
Power density limits and heat removal	Calculate MHD external pressure drop. Define maximum allowable temperature. Evaluate thermal response to establish maximum q. Produce benchmark heat transfer data
MHD Behavior of Liquid Metal Free Surfaces	Develop models of flows of free surfaces including internal recirculation and turbulent fluctuations. Provide benchmark data for internal flows.
Insulator Coating Development	Develop insulator coatings and test in-situ resistivity. Determine irradiation effects on coating resistivity.
Radioactivity	Define existing and goal impurity levels. Identify chemical processes needed for impurity removal. Identify missing cross section data data and dose conversion factors.Investigate waste management and safety characteristics of liquid candidates and associated structure materials and insulator coatings.
Tritium Fuel Cycle	Develop models for overall fuel cycle
Material transport to vacuum pump	Plasma tests with liquid at high temperature. Model the transport of liquid to the vacuum pumping system

Examples of liquid surface divertor systems

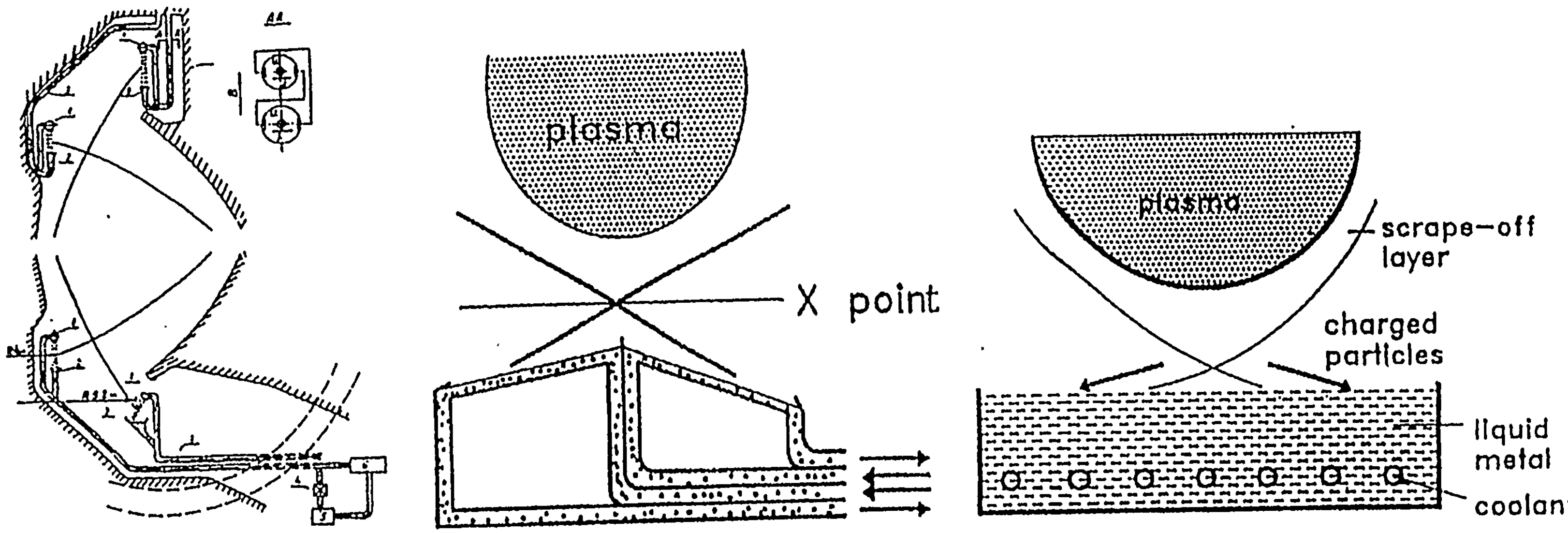

(a) (b) (c)

(a) Droplet double-null option, (b) Liquid flow over divertor plate option and (c) Stagnant pool with separate cooling

Possible Materials, Configuration, and Confinement Options

- **Liquid species**
  Li, Pb-17Li, Ga, Flibe, Sn, Flibe, Al, Al-Si

- **Flow configuration**
  Fast film, droplets, water fall, stagnant film, pool, backside impinging jet

- **Confinement**
  Tokamak, Advanced Tokamak, SphericalTorus, Field Reversed Configuration, Stellerator

- **Near term objective is to reduce the number of options under consideration**

Primary Objectives of the Evaluation Phase

- Demonstrate that the advantages of free-surface liquid systems are real

  One or more concepts are feasible and could operate as planned

- Provide sufficient confidence in their operation such that a significant follow-on activity can proceed

  Installation of prototypes into plasma confinement devices.

There are Three, Closely Integrated Activities

- Concept Evaluation
- PMI/Transport
- Engineering
- PMI/Transport and Engineering support the Evaluation
  - Review and summary of the existing database
  - Application of state-of-the-art models
  - Providing key experimental data
  - Developing improved codes.

Fig. 2-1 Evaluation Phase Schedule
Free Surface Liquid Plasma Facing Systems

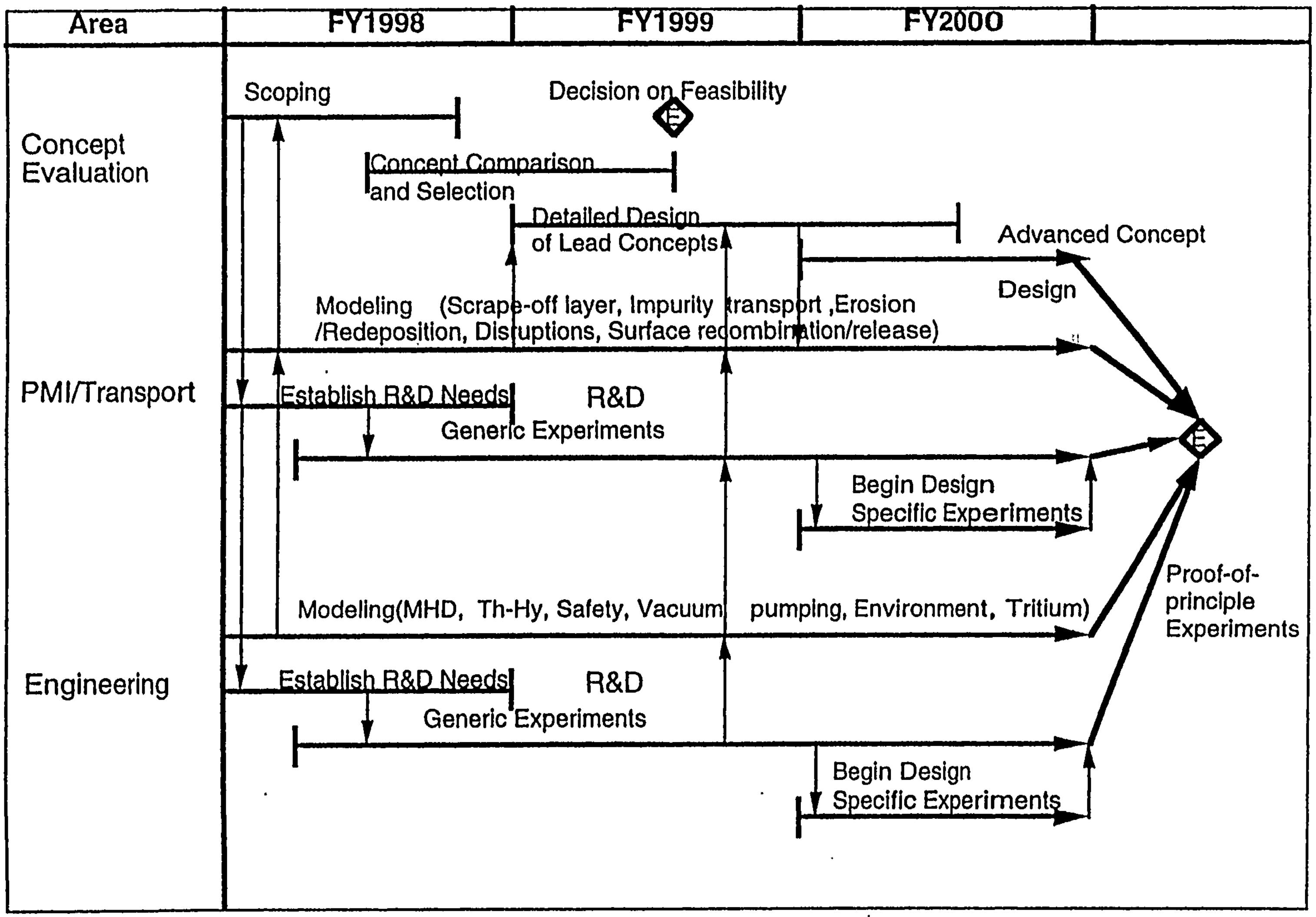

Phases of Evaluation

- Scoping Phase
- Comparison and Selection Phase
  - Pre-conceptual design
  - Identification of key issues
  - Perform analyses to resolve issues
  - Design modification
  - Comparison and selection
- Detailed Design Phase
  - 1-2 concepts to be examined in more detail.
  - Free-surface liquid system that is fully integrated with other reactor
  - Investigate the overall system response and address system interface issues.
- Advanced Concept Phase

Scoping Phase Tasks

- Definition of design criteria
- Selection of different concepts
- Selection of materials
- Identification of the level of detail that is required to perform a meaningful evaluation
- Definition of the plasma parameters to be used in the evaluation
- Definition of generic R&D needs.

Scoping Phase Tasks

- Near Term Tasks for PMI/Transport
  - Chamber surface configuration of conventional and alternate concepts
  - Reference design physics parameters
  - Allowable impurity fraction
  - Impurity operation fraction
    Distribution of first wall and divertor heat flux

- Near Term Tasks for Engineering
  - Preliminary liquid flow calculations
  - Preliminary heat transfer calculations
  - Preliminary estimates on liquid temperature limits

Performance Goals for Attractive Fusion Energy Systems

Attribute	Minimum Goal	Grand Challenge
Coolant Inlet/Outlet Temperature (°C) (goal of 45% conversion efficiency)	250/500	250/1000
Peak / Average Neutron Wall Load (MW/m^2)	6 / 3	20 / 10
Peak / Average Heat Flux (MW/m^2)	5 / 2	50 / 20
First Wall Fluence Lifetime ($MW\text{-}y/m^2$)	10	20
First Wall Erosion Lifetime (y)	2	∞
Time to Repair/Replace	< 1 month	< 1 week
Average Cost of Core Materials ($/kg)	100	<50
Waste Disposal Limit	Class C Major Components	Class C All Components
Worst-Case Accident Dose at Site Boundary	1 rem	0.1 rem

Set of Device Parameters for ARIES-RS

Plasma major radius	5.5 m
Plasma minor radius	1.4 m
Divertor plate toroidal width	1.5–2 m
Divertor plate length	~1 m
Magnetic field on axis	8.0 T
Plasma current	11.32 MA
Neutron wall load normal to divertor	~1 MW/m^2
Total transport power	431 MW
Divertor surface heating	348 MW
Average divertor surface heat flux	2 MW/m^2
Peak divertor surface heat flux	6 MW/m^2
Heat exchanger outlet/inlet temperature	610 / 330 °C
Plasma Z_{eff}	1.7
Mid-plane SOL thickness	1 cm
He exhaust rate	7.7 x 10^{20}/s
H exhaust rate	1000 Torr-l/s
$n_e(a)$	0.6x10^{20} /m^3

PMI/Transport Proposed Tasks

- Priority 1: (Needed in the first 3 to 6 months of the study)
  - Chamber surface configuration of conventional and alternate concepts
  - Reference design physics parameters
  - Allowable impurity fraction
  - Impurity operation fraction
    (Defined as: The First wall and divertor having the same heat flux)

PMI/Transport Proposed Tasks (Cont.)

- Priority 2: (Some results can be generated in the first year of the study and beyond)

Reference solid surface design:

- **Definition of a solid surface reference divertor design**
- **PMI, basic and integrated data, for modeling and experiments:**
- **Sputtering yield of relevant liquid materials from hydrogen, He and self-sputtering**
- **Basic data on trapping and up-take of hydrogen and He**
- **Design limits modeling**
- **Erosion and redeposition integrated data**
- **Disruption simulations**
- **Review of TFTR results**
- **PMI integrated transient effects modeling**
- **Heated DiMES**

Transport, basic and integrated, data for analysis, modeling and experiments:

- **Transport of impurities at divertor, SOL, core...modeling**
- **Transport of impurities at divertor, SOL, core...experiments**

PMI/Transport Proposed Tasks (Cont.)

- Priority 3: Possibly be done in the second or third year of the study

  Addition to existing experiments:
  - PISCES vertical target experiments
  - Mid-plane DiMES station

  Tokamak and other experiments:
  - Transport experiment and modeling in DIII-D
  - Impurity core and mantle radiation in DIII-D
  - Liquid surface experiment in CDX-U
  - Laser blow-off experiment
  - Separatrix and liquid surface contact experiment
  - Experiments in Russia

Engineering Proposed Tasks

Priority 1: Initial Assessement of Candidate Heat Removal Surfaces (Results needed in the first 6 months of the study)

- Preliminary liquid flow calculations
- Preliminary heat transfer calculations
- Preliminary estimates on liquid temperature limits

Priority 2: General System Analysis of Candidate Heat Removal Surfaces (Some results can be generated in the first year of the study and beyond)

Modeling

- Limits on material transport (plasma/pumps) (to refine the temperature limit on the liquid surface)
- Effect of transients and disruptions
- Waste management evaluation
- Continued heat transfer / liquid flow calculations

Engineering Proposed Tasks (Cont.)

- Priority 2 (Cont.)

  Experiment

  - Properties of tritium in candidate liquids
  - Activation cross sections and corresponding dose conversion factors (including impurities)
  - Insulator coating development for liquid metals

- Priority 3: Detailed Engineering Performance Analysis of Promising Concepts (Possibly be done in the second or third year of the study)

  Modeling

  - MHD flow behavior of free-surface liquid metals
  - Heat transfer
  - System response under off-normal conditions (scoping calculations)

  Experiment

  - MHD flow characteristics of free-surface liquid metals
  - Thermalhydraulic/High Heat Flux tests in a high magnetic field

Interface with APEX

- ALPS will generate baseline physics parameters
  - Relative level of heat flux to first wall affects choices for blanket
- ALPS will include first wall PMI considerations
- ALPS will set limits on free-surface liquid evaporation and temperatures
- Common Materials Database
  - ALPS will be resposible for PMI data
  - ALPS will be reponsible for liquid bulk properties
  - APEX will be reposible for solid materials properties
  - APEX will be reponsible for irradiation effects
- APEX will be responsible for overall system integration with in-vessel components

Task Priorities Strawman

Physics/Engineering Parameters
    Focus on advanced tokamak (ARIES - RS)

Materials Database
    Lists of needed data
    Review of existing database
    Needed R&D

Establish the limitations of Li and Ga (Selection of materials)
    Allowable evaporation
    Core impurity limits
    Edge transport and recycling

Design Selection Criteria (Selection of engineering concepts)

ALPS Web Page

- ANL will establish a web page for ALPS
- The web page will be similar to the ARIES web page
- Information to be included
  - Reports
  - Materials database
  - Physics parameters
  - Project overview
- Access will be limited

Comments on Heat Transfer in Liquid Surface Plasma Facing Components

Richard Nygren (Sandia)

This work represents preliminary ideas being discussed in two recently formed US programs, APS and APEX.

- basics concerns about what limits heat transfer
- specific issues regarding "waterfalls" and "droplet screens"
- general questions about how we measure heat transfer
- comment about global power loads on liquid surface PFCs

Sandia National Laboratories

US-Japan Workshop on High Heat Flux Components & Plasma Surface Interactions for Next Fusion Devices
San Francisco December 8-11, 1997

Liquid Surface High Heat Flux Technology

ALPS basic issue: What limits heat removal in liquid surface PFCs?

heat transfer

- near surface heat transfer limits heat removal capability
- MHD effects dominate (for liquid metals)
- appropriate experiments (B + HHF) may be challenging

surface stability

- sputtering erosion from liquid surfaces
- plasma wind effects
- transients (e.g., disruptions)
- problem of collection of "free flow" systems

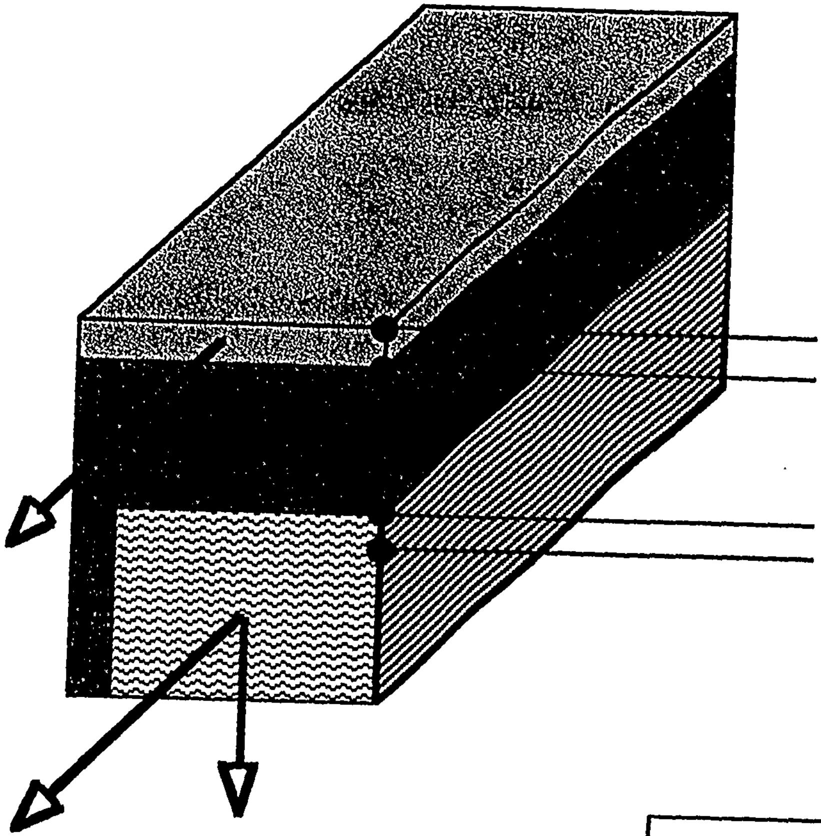

Basic HHF Limits on Cell Size

50 MW/m^2

ΔT=105°C, 0.1mm Li

ΔT=285°C , 2mm CuCrZr

ΔT=500°C (too much), water,

h=.1 MW/m^2-K,
need h~1
heat pipes (q>100 MW/m^2)

distance for flowing Li to reach 500°C from 220°
2.5 mm (t=0.0025) at 1 m/s with 50 MW/m^2 24.5 mm at 10 m/s with 50 MW/m^2

Sandia National Laboratories

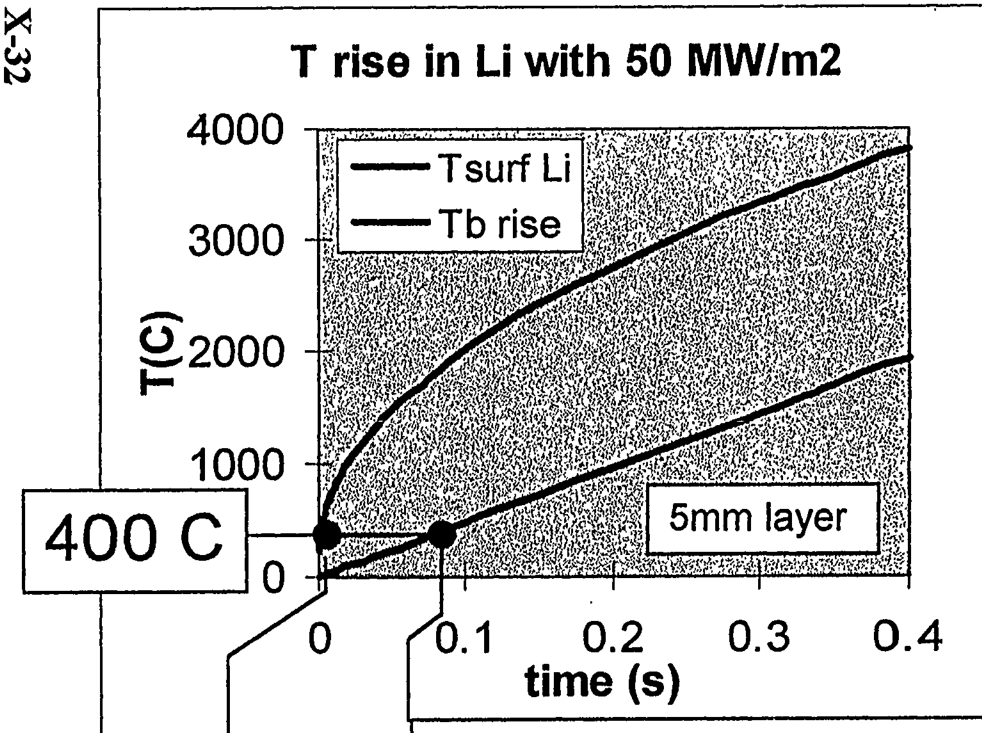

0.084s bulk reaches 620 C

$z(1m/s) = 84mm$
$z(10m/s) = 0.84m$

0.005s surface reaches 620 C

$z(1m/s) = 5mm$
$z(10m/s) = 50mm$

High <u>k</u> and enhanced heat transfer (turbulence) decrease the temperature gradient.

The surface temperature always exceeds the bulk temperature.

Sandia National Laboratories

Heat Acceptance Limit

- laminar (MHD slug) flow has high temperature gradient
- limit is probably evaporation rate at the maximum surface temperature
- total power is more important than heat flux profile
- mixing is necessary for long flow paths

liquid metal flowing film

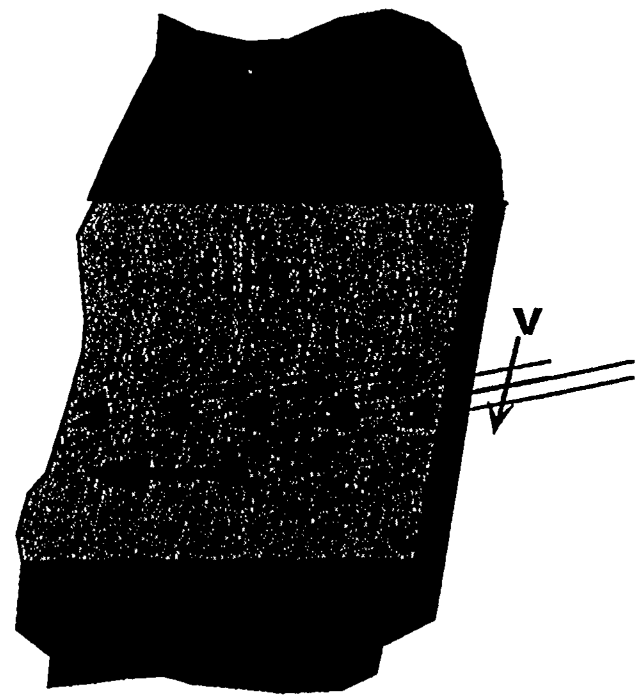

Sandia National Laboratories

Heat Source?

- e-beam: 40keV e^- R_{Larmor}<1mm in 1T field , not feasible in B field.
- laser: High power steady state laser needed, feasible, $$.
- neutral beam: Feasible, $$.
- <u>sun</u>: Feasible, SNLsolar facility (concentrator, ~20 MW/m^2).

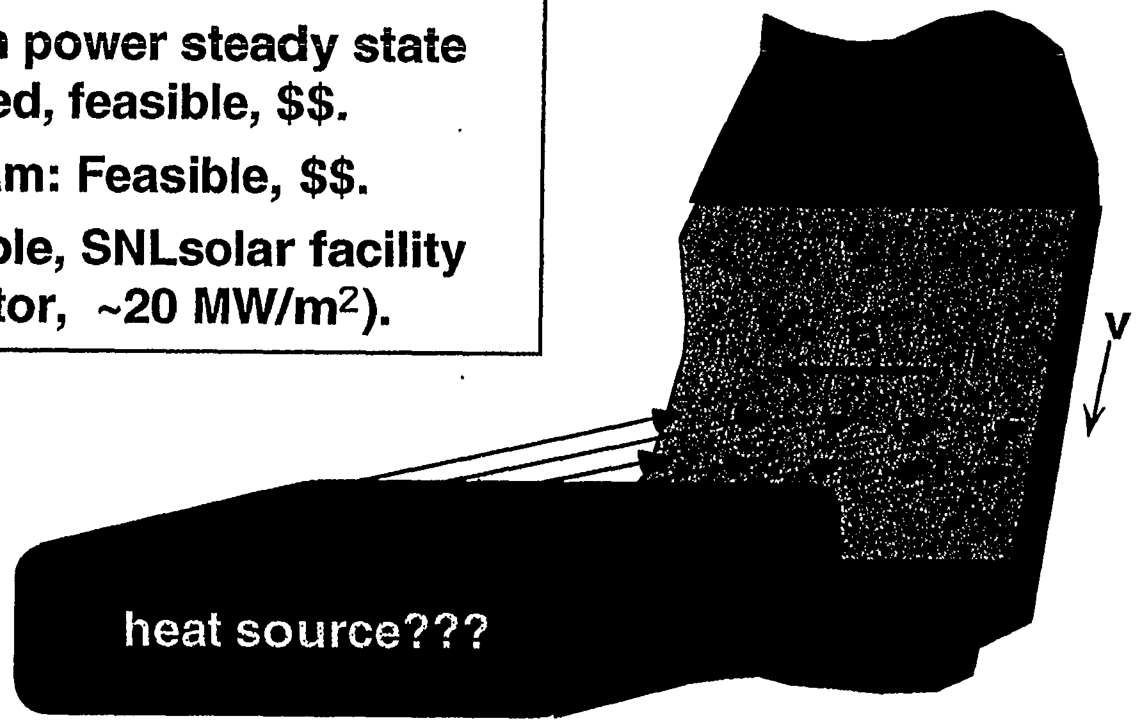

Sandia National Laboratories

liquid metal droplet curtain

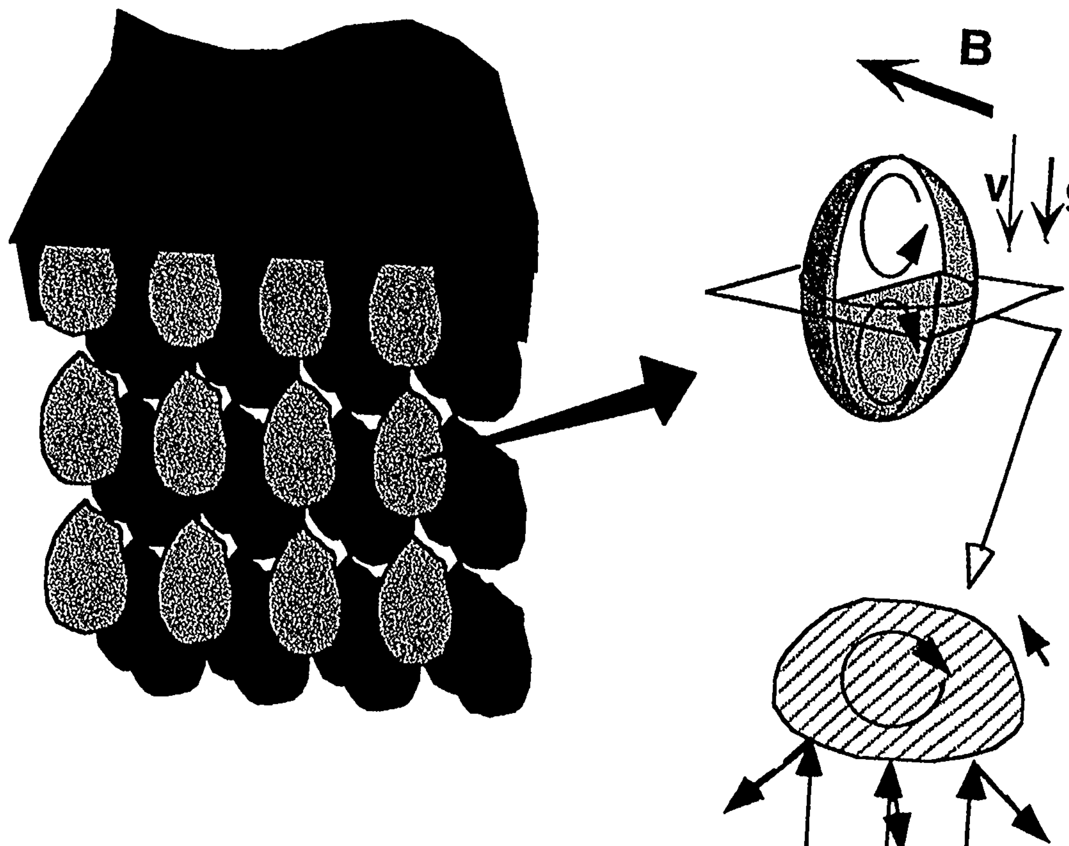

Resolution?

Drop moves 33mm in 1/30s (IR frame) at 10m/s.

Emmisivity?

Pixel size?

rotation, shape, internal circulation

heat flux
absorbed/reflected

HELIUM COOLING EXPERIMENTS AND PROSPECTS

C. B. Baxi

General Atomics

US/Japan Workshop on HHF Components, San Francisco

December 8-11, 1997

ADVANTAGES OF HELIUM COOLING

- Safety leaks not serious
- Helium characteristics
  - Chemically inert
  - Neutronically inert
  - No phase changes
- Developed technology
  - Heat transfer
  - Purification (including tritium recovery)
- Maintenance advantages
  - No activation
  - No trace heating

115-94

SNLA HELIUM LOOP

- Pressure = 4 MPa
- Flow = 23 g/sec
- Pressure drop = 0.5 bar
- Helium inlet temperature 20° to 45°C
- Heat flux source electron beam
  - Beam Power 30 kW
  - 57 cm diameter and 96 cm long vacuum chamber
  - Maximum sample size = 25 cm long

FLOW AND PUMPING POWER

Volumetric flow,

$$V = \frac{Q}{\rho_o Cp\left[T_{max} - \theta_i - q''_{max}/(\kappa/\delta) - q''_{max}/\alpha\right]}$$

and the ratio of pumping power, W, to power removed, Q, is:

$$\frac{W}{Q} = \frac{q_a''^2}{8\varepsilon(T_a - \theta_i)^3 \rho_i \rho_a Cp^3}\left(\frac{f}{St^3}\right)$$

CONCEPTS TESTED

1) Porous Metal Heat Exchanger

2) Normal Flow Heat Exchanger

3) Extended Surfaces

4) Roughness/ Swirl Flow /---

FINS:
PITCH = 1mm
THICKNESS = 0.4 mm

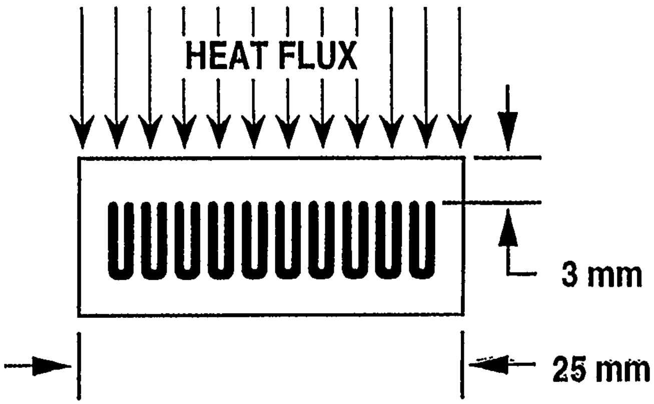

MATERIAL: Dispersion strengthened copper
(GLIDCOP by SCM)

RESULTS OF TESTS AT SNLA

AT INLET PRESSURE = 4 MPa

Flow Rate (kg/s)	Heat Flux (MW/m^2)	Peak Surface Temperature (°C)	Pumping Power [W (% of power removed)]
0.022	10	380	157 (0.8)
0.011	6	422	21 (0.2)
0.0064	3	242	3.4 (0.06)

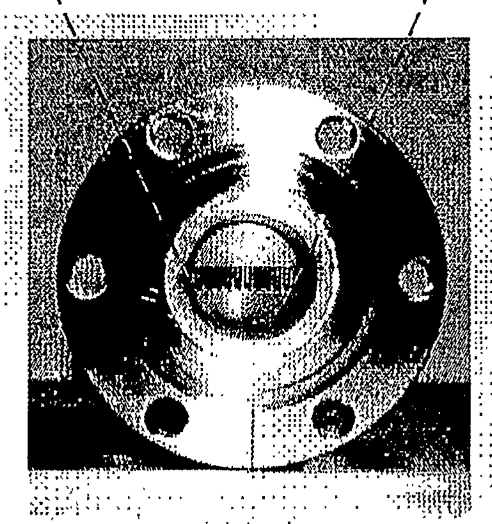

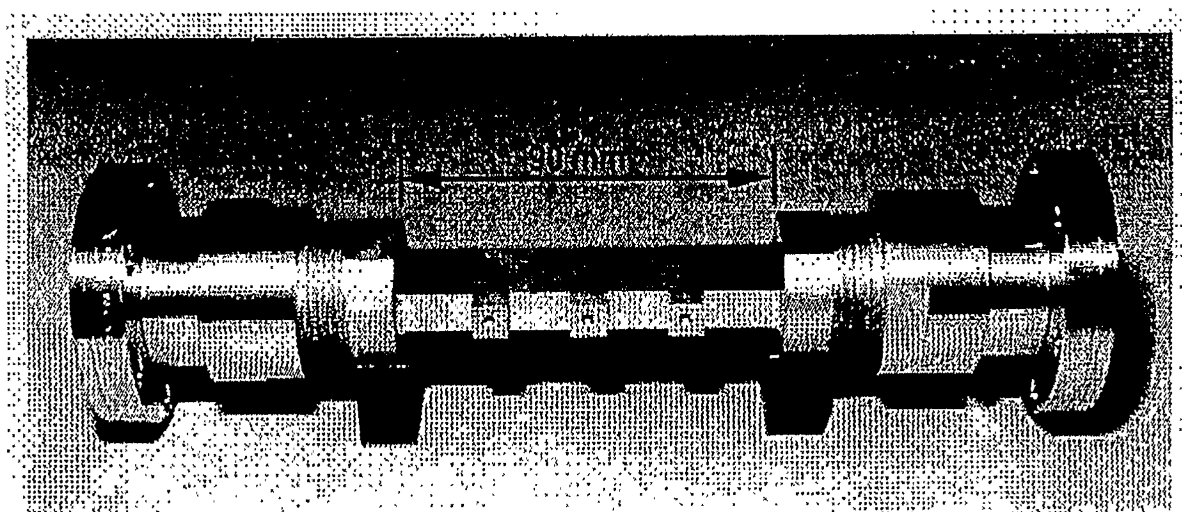

GENERAL ATOMICS

104-94

Creare

NORMAL FLOW HX CONCEPT

- High heat flux
- High effectiveness
- Low pressure drop
- Uniform wall temperature
- Fins 150 microns thick
- Spacing 50 microns

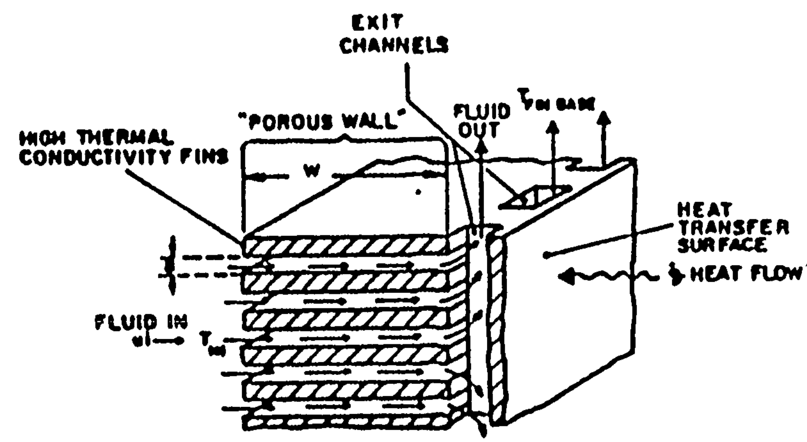

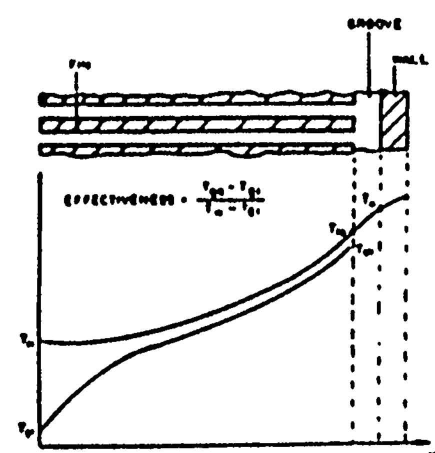

POROUS METAL HEAT EXCHANGER

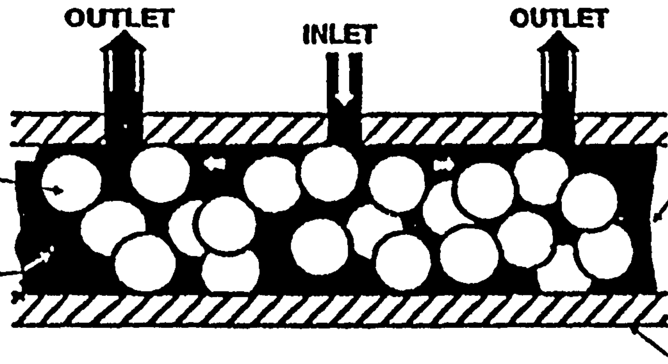

$$\frac{Q}{A} = \left[\epsilon h + \sqrt{h k_w S_p}\right]\Delta T \qquad (1)$$

where

- Q/A is the heat flux, W/m^2
- ϵ is the porosity
- k_w is thermal conductivity of the wick, $W/m/°C$
- S_p is the surface area of the porous medium, m^2/m^3
- ΔT is the wall-to-fluid temperature drop °C, and
- h is the local particle to fluid convective heat transfer coefficient, $W/m^2/°C$

SECTION

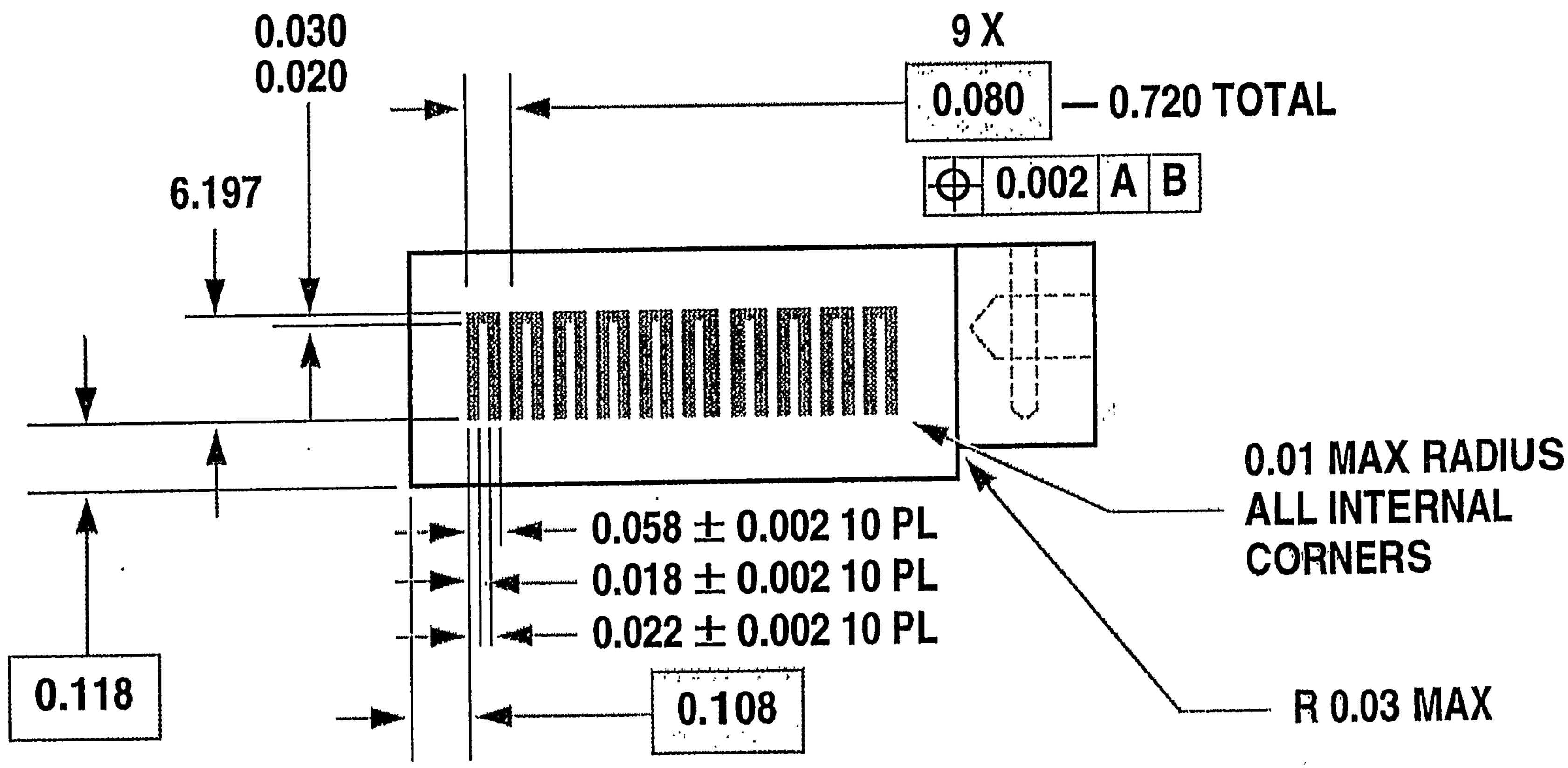

SCALE 3:1

115-94

HELIUM-COOLED VANADIUM MODULE

- Heat transfer enhancements provide a 3MW/m2 capability

Internal surface modification

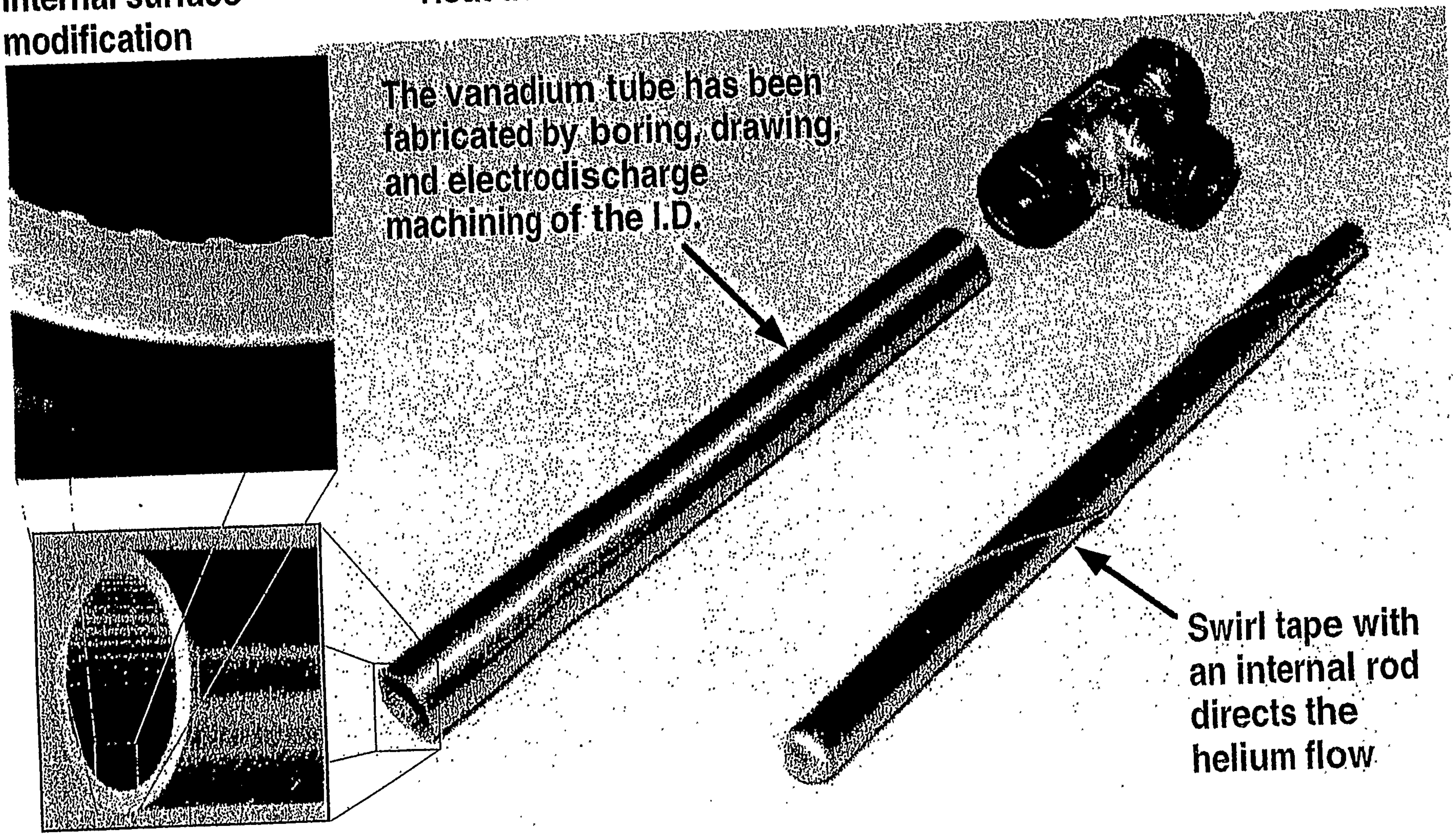

GENERAL ATOMICS

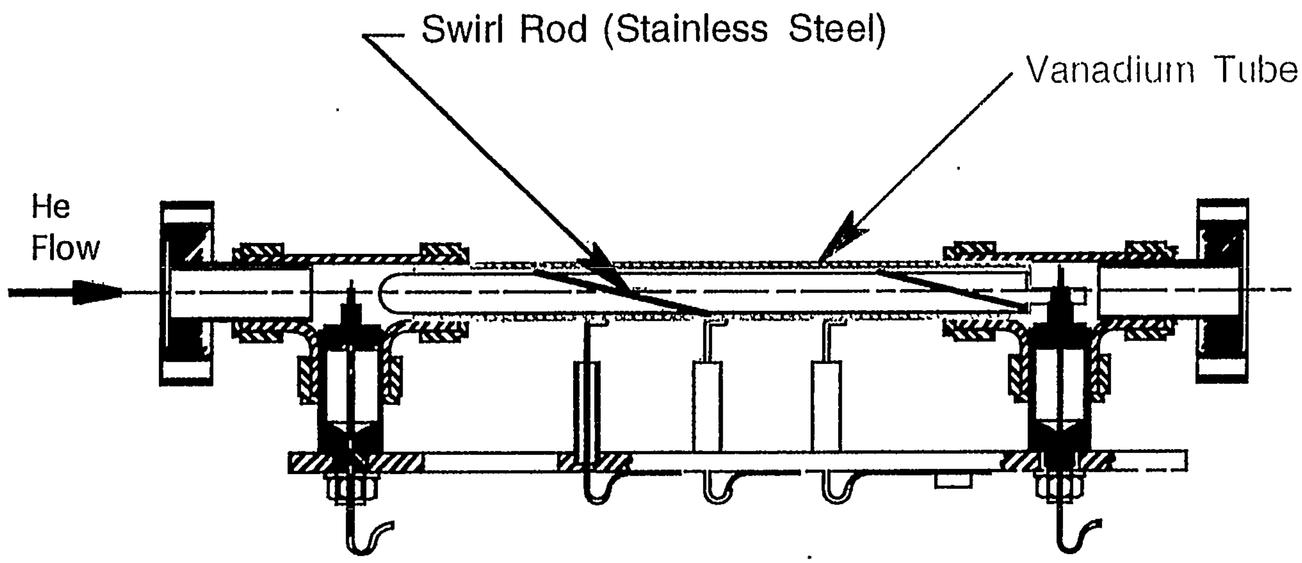
Swirl Rod (Stainless Steel)
Vanadium Tube
He
Flow

GA DIVERTOR MODULE

RESULTS OF DECEMBER 7, 1994 TESTING AT SANDIA NATIONAL LABORATORY, ALBUQUERQUE

Heat Flux	Area (Cm^2)	Limited By
9 MW/m^2	20.0	Facility Limit
18 MW/m^2	5.8	Surface Temperature (700 ^oC)
34 MW/m^2	2.0	All Objectives Achieved

Diverse helium HX designs were tested under different conditions.

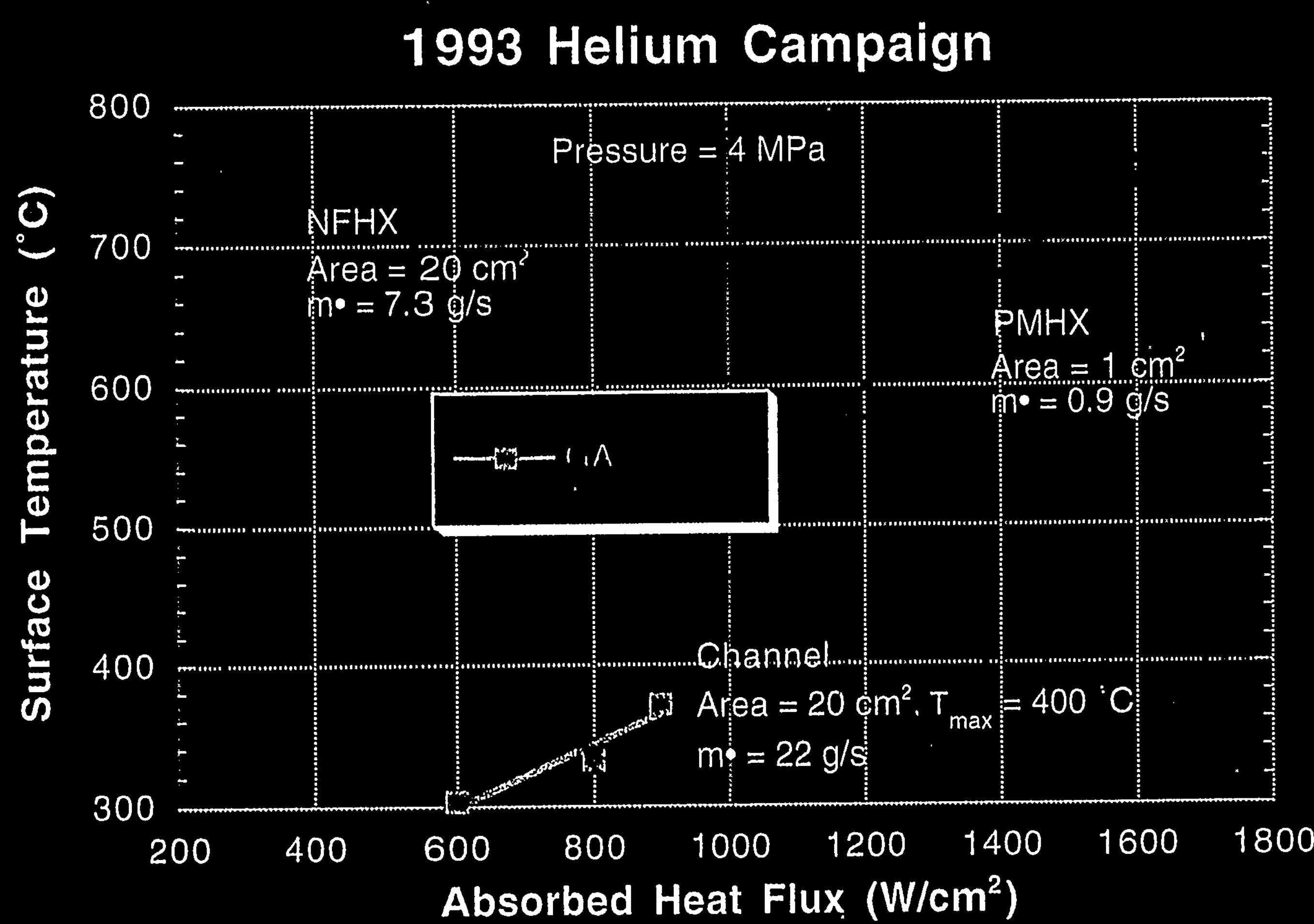

Sandia National Laboratories

5932 140 1291 (?) dly:USA/apan 0182

Attainable heat fluxes with helium also dependent on heated area.

Thermacore phase II

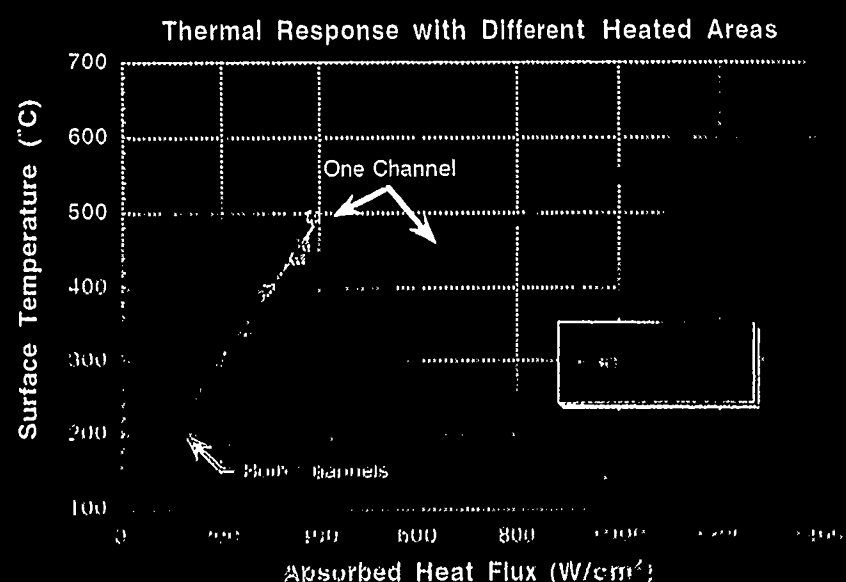

GA Helium Module test 2

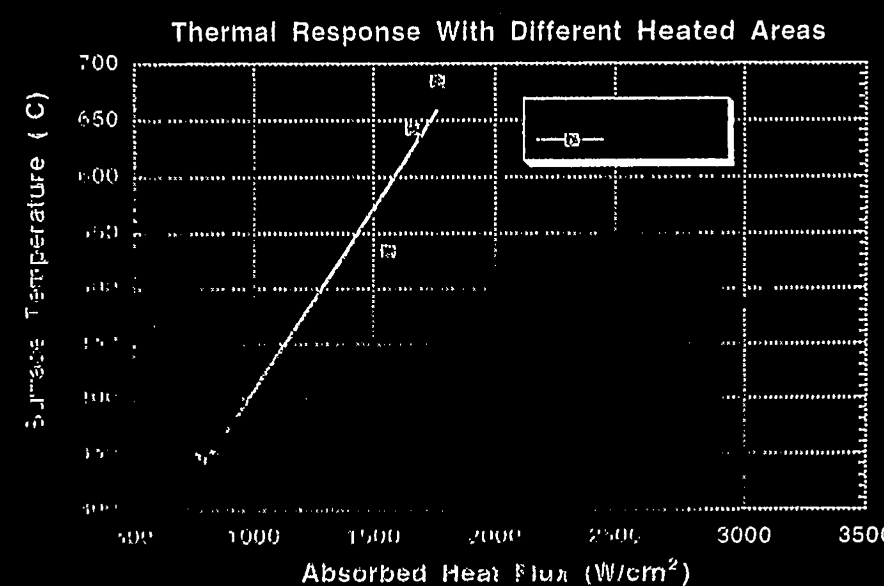

5932.140 12/13/94
dly.US/Japan 0182

Sandia National Laboratories

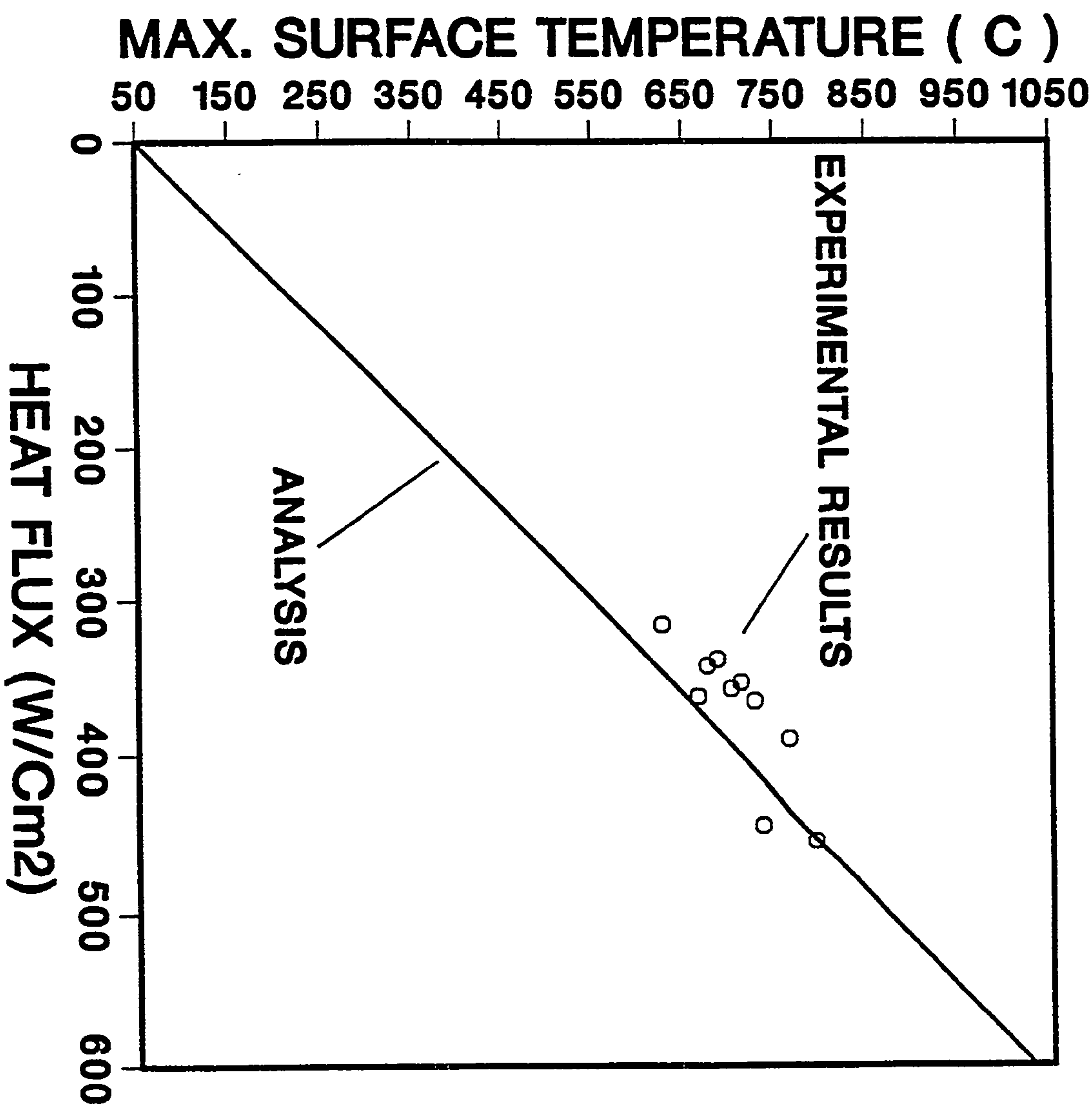
MAX. SURFACE TEMPERATURE (C)
50 150 250 350 450 550 650 750 850 950 1050
0 100 200 300 400 500 600
HEAT FLUX (W/Cm2)
EXPERIMENTAL RESULTS
ANALYSIS

FUTURE PLANS

Helium cooled Faraday Shield Antenna to be tested on DIII-D within next few months

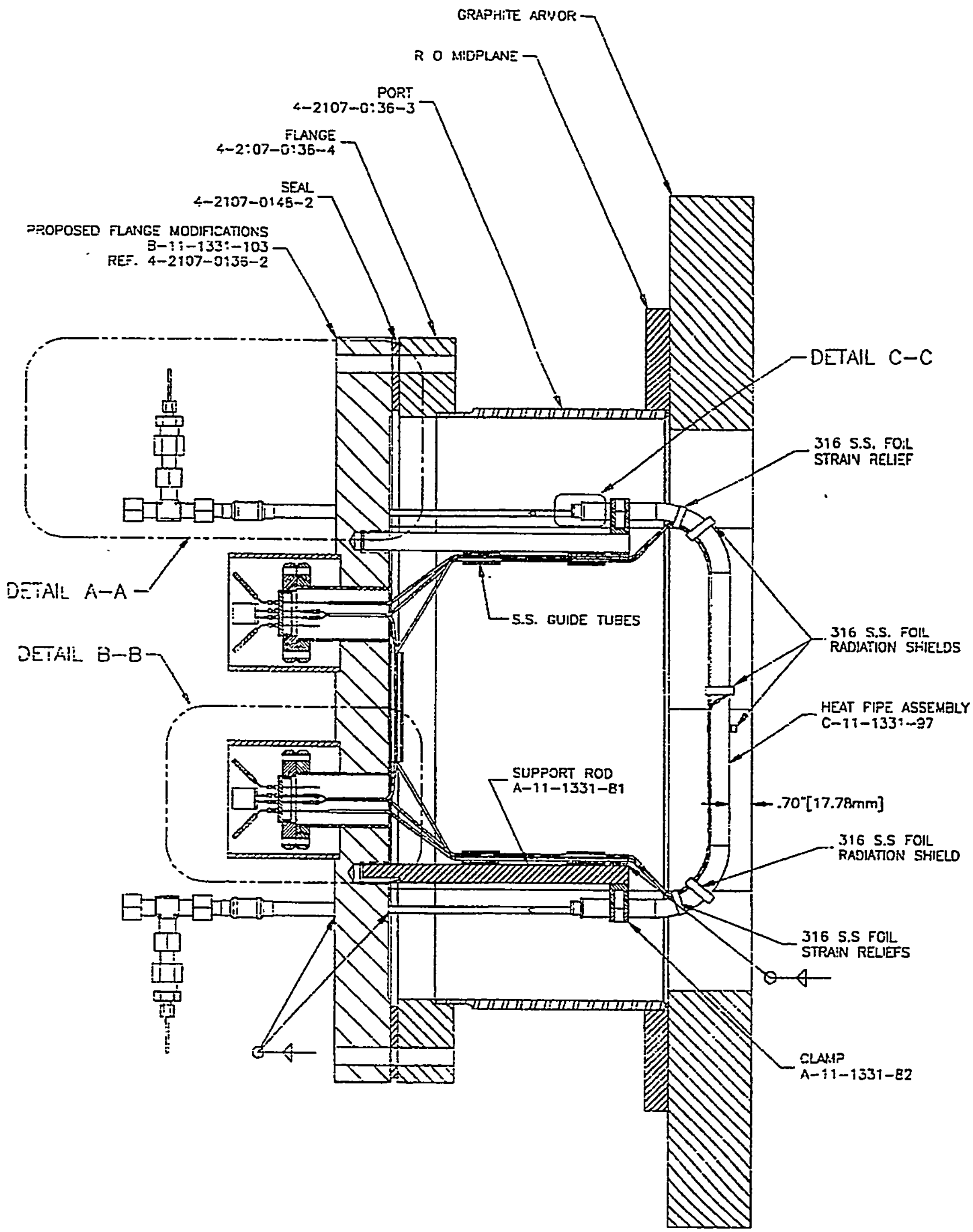

DIII-D FARADAY SHIELD TEST ASSEMBLY - SIDE VIEW.

CONCLUSION

IT is feasible to remove a steady state heat flux in excess of 5 MW/m^2 with helium cooling at a moderate pressure (4 MPa) and modest pumping power (5 %).

Advanced Plasma Facing Component by using Multi-layer Coated Pebbles (Comments on liquid/pebble divertor)

M. Isobe, M. Nishikawa
Graduate School of Engineering,
Osaka University
(presented by Y. Ueda)

Outline

1. Basic concept of pebble drop divertor
2. Divertor pebble and performance of pebble drop divertor
   A. Maximum heat load
   B. Fuel pumping function
3. Conclusions

Basic concept of pebble drop divertor using multi-layer coated pebbles

Small (about diameter of 1 - 2 mm) special coated pebbles are used as divertor surface. This pebbles consists of <u>ceramic microspherical kernel</u>, <u>coating layer for tritium permeation barrier</u> and <u>plasma-facing layer</u>.

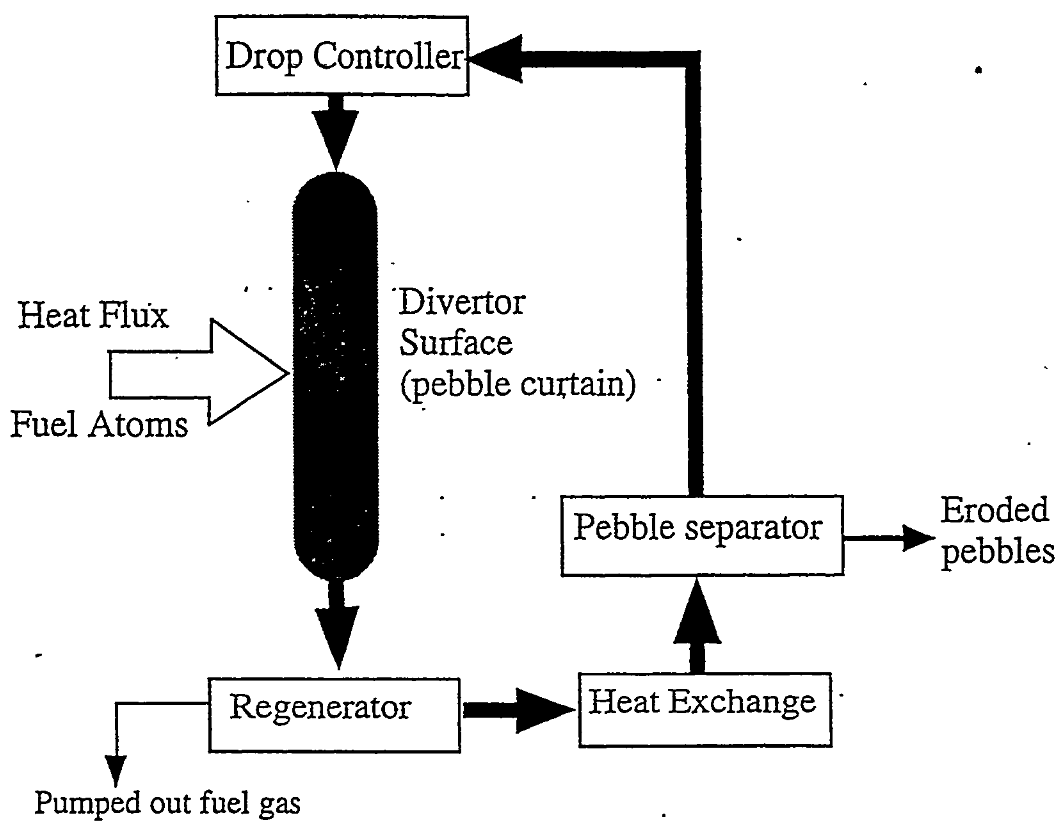

<u>Functional Scheme of pebble drop divertor</u>

Multi-layer coated pebble

Tritium Permeation Barrier (TBL)

Tritium permeation barrier layer prevents the diffusion of tritium from the PFL to the kernel and reduces the tritium retention in the bulk of pebble.

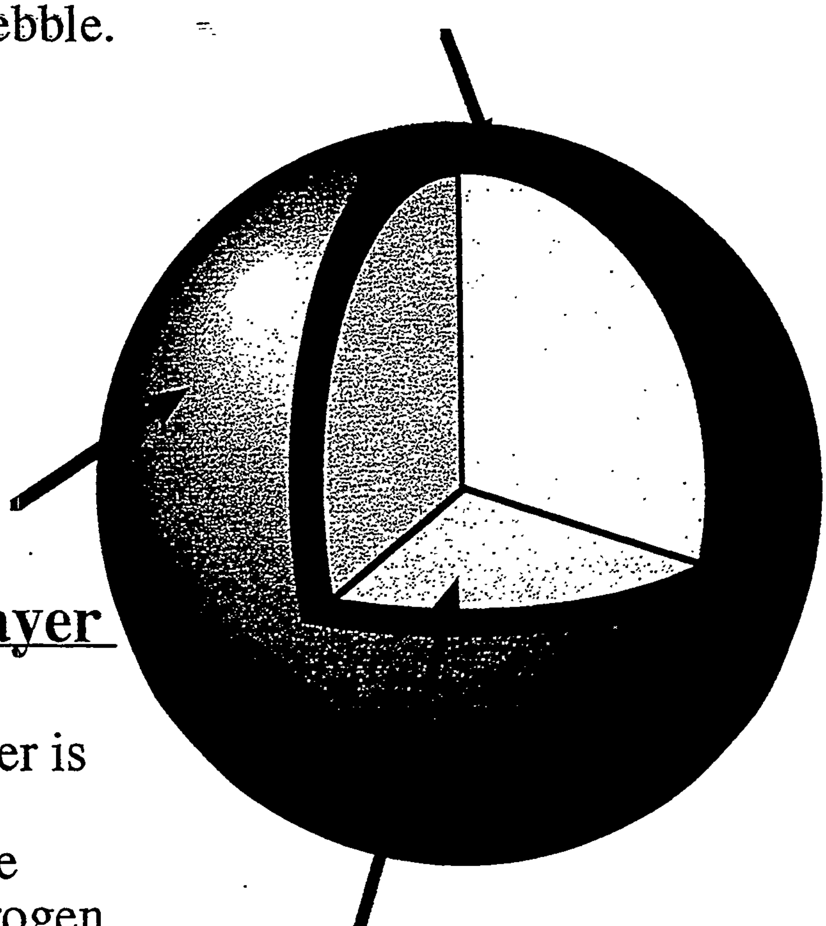

Plasma Facing Layer (PFL)

Plasma facing layer is optimized for the compatibility with core plasma. By using hydrogen gettering material, the pebbles have a function of fuel gas pumping.

Kernel

A kernel sustains mechanical force and thermal stress. It also determines the heat capacity of a pebble.

Advantages of pebble divertor

- Using insulator kernels, pebble circulation is not subject to MHD effects.

- Heat removal and fuel gas pumping can be realized simultaneously.

- Using tritium permeation barrier, the tritium retention of divertor pebbles can be significantly reduced.

- Continuous replacement of eroded surface is possible.

- The fabrication technology of multi-layer coated pebble has been developed for High Temperature Gas-Cooled Fission Reactor's fuel particle.

Typical Stress Distribution in the Divertor Pebble

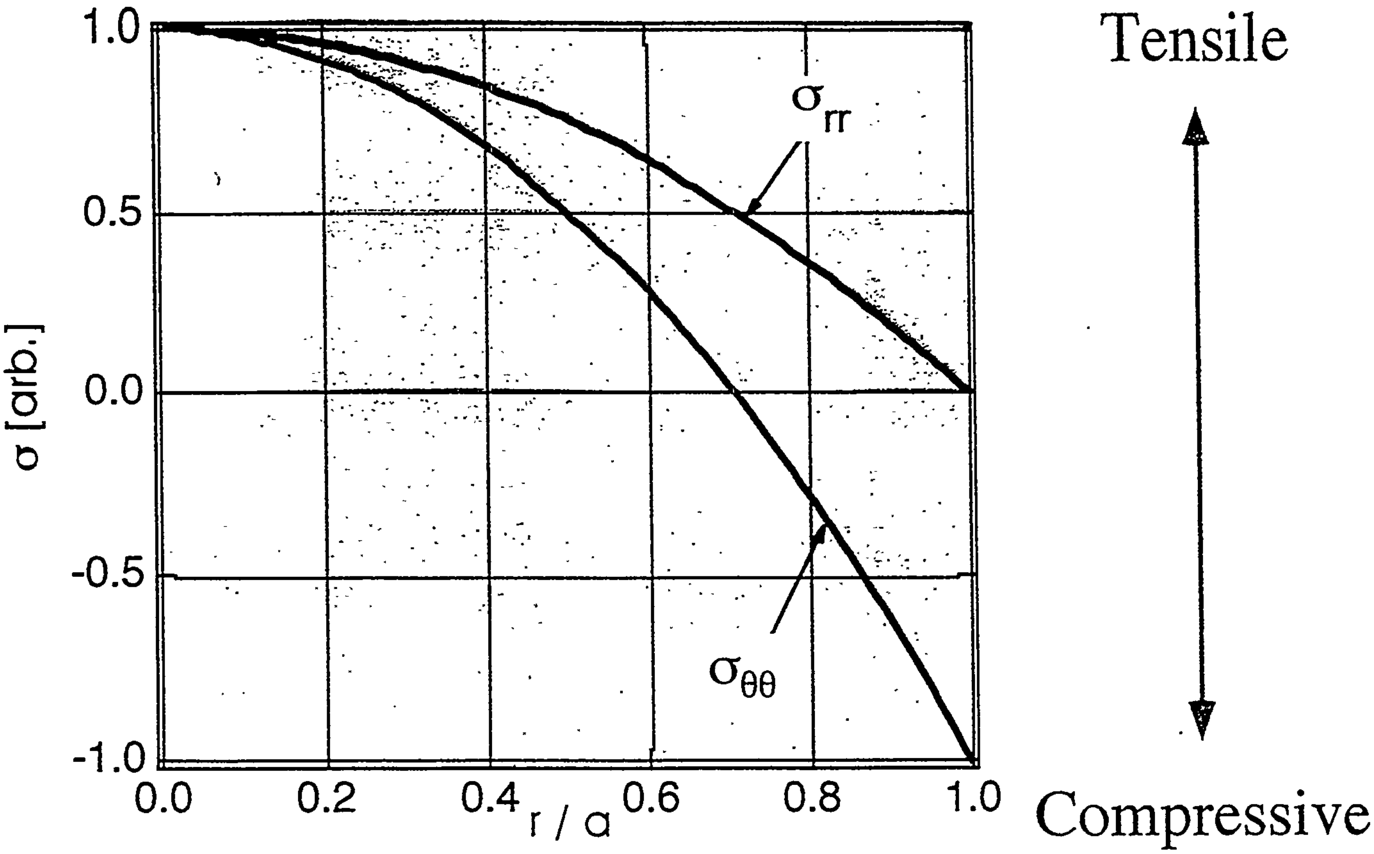

- Radial stress shows maximum tensile force at the center of the pebble

- Angular stress shows maximum tensile force at the center of the pebble and maximum compressive force at the surface.

➡ A pebble will be safe if surface compressive stress does not exceed the compressive strength of the kernel material.

Maximum Heat Load of Various Kernel Materials

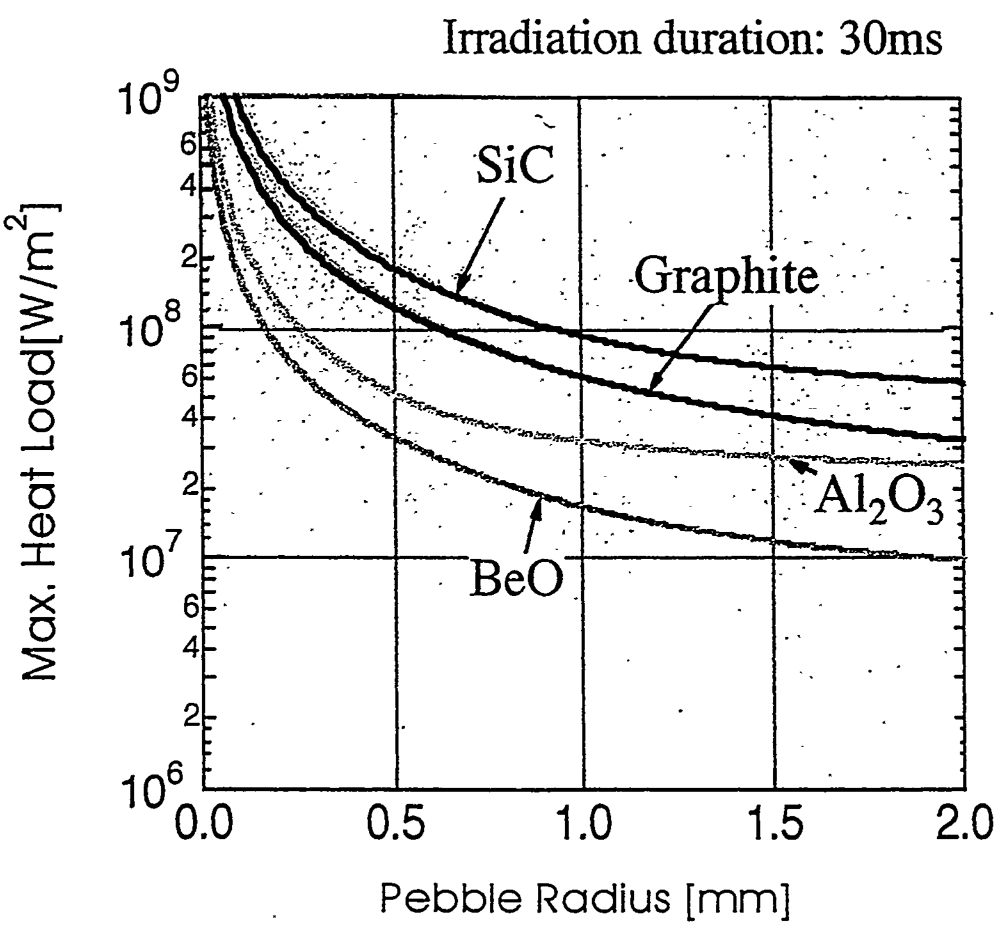

When the divertor pebble of 0.5 - 1 mm in radius is used, all candidate materials can be used in 15 MW/m^2 of surface heat flux.

Surface Temperature of pebbles

Heat flux : $30 MW/m^2$
Irradiation duration : 30 ms.

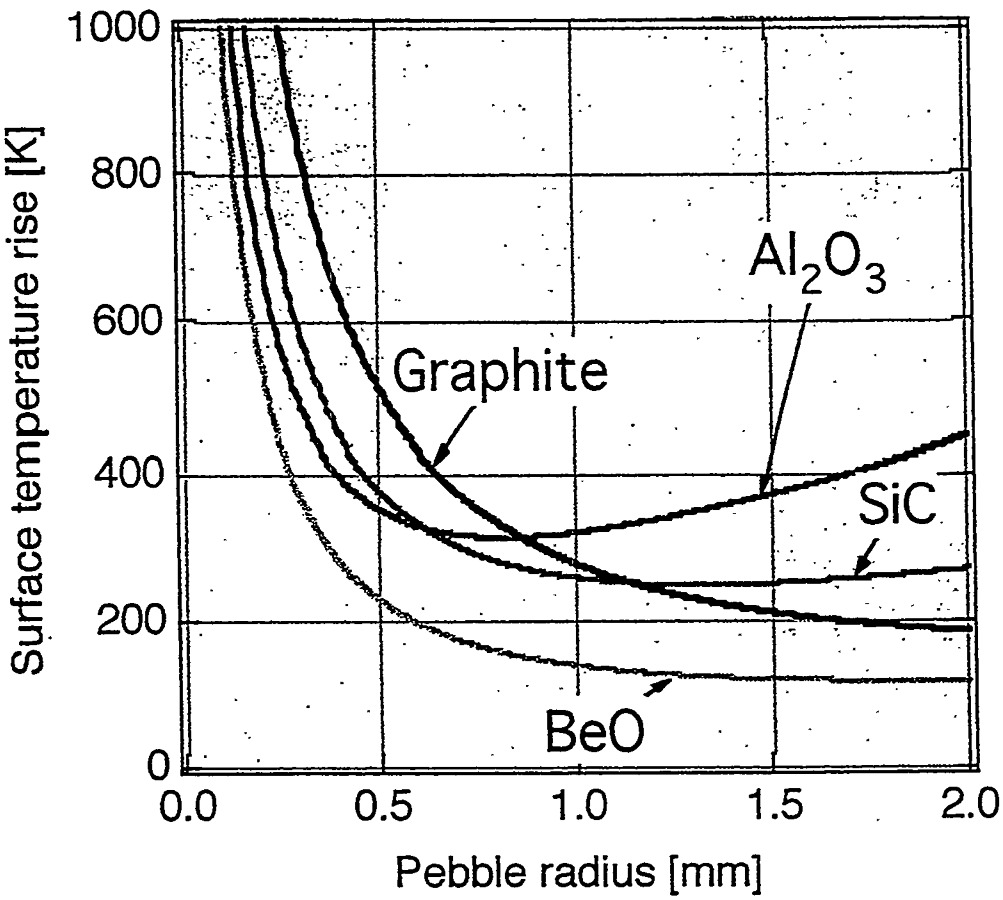

Fuel gas pumping performance

Basic application of wall pumping

Temperature rise 200K ~ 300K (dropping height ~ 1m)

Ref. A. Sagara, et.al
"Design of Carbon Sheet Pump for LHD and Demonstration of Hydrogen Pumping"

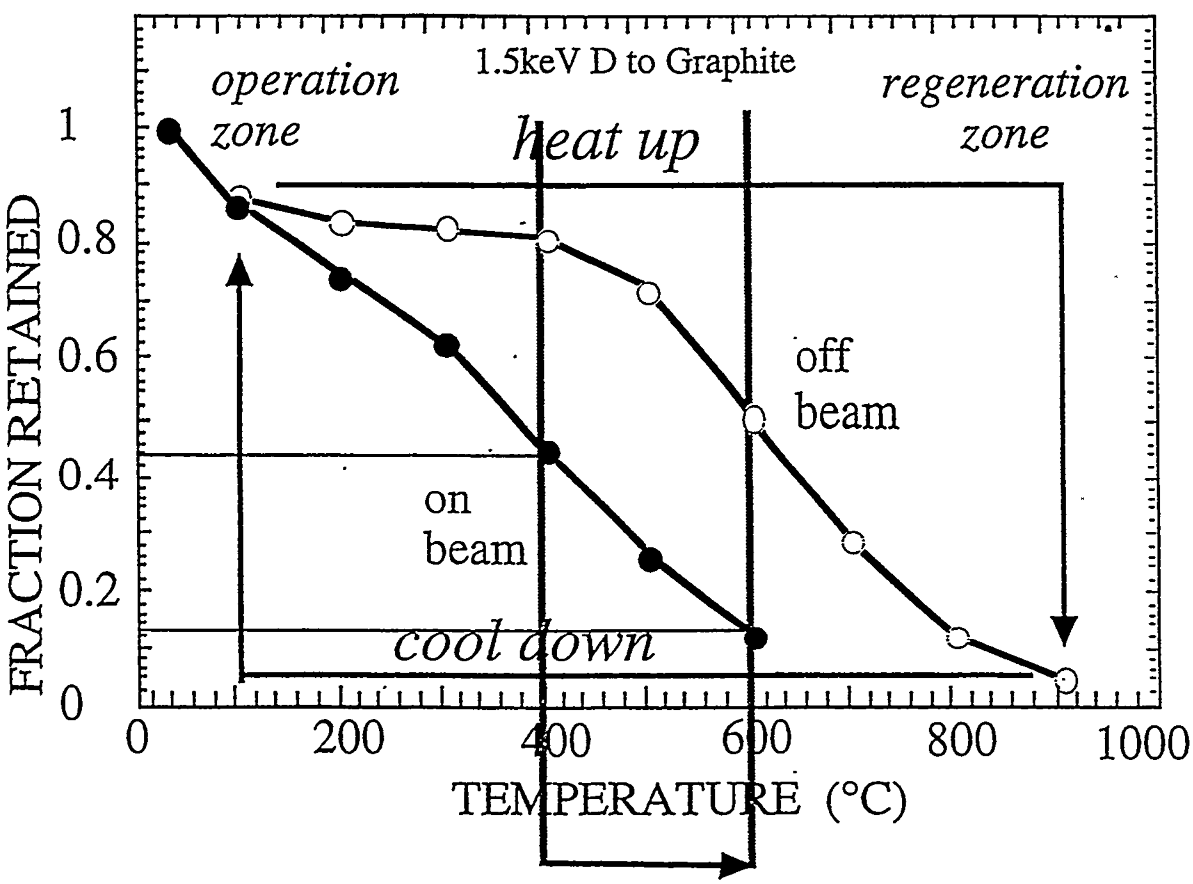

Calculated saturated concentration of hydrogen during irradiation

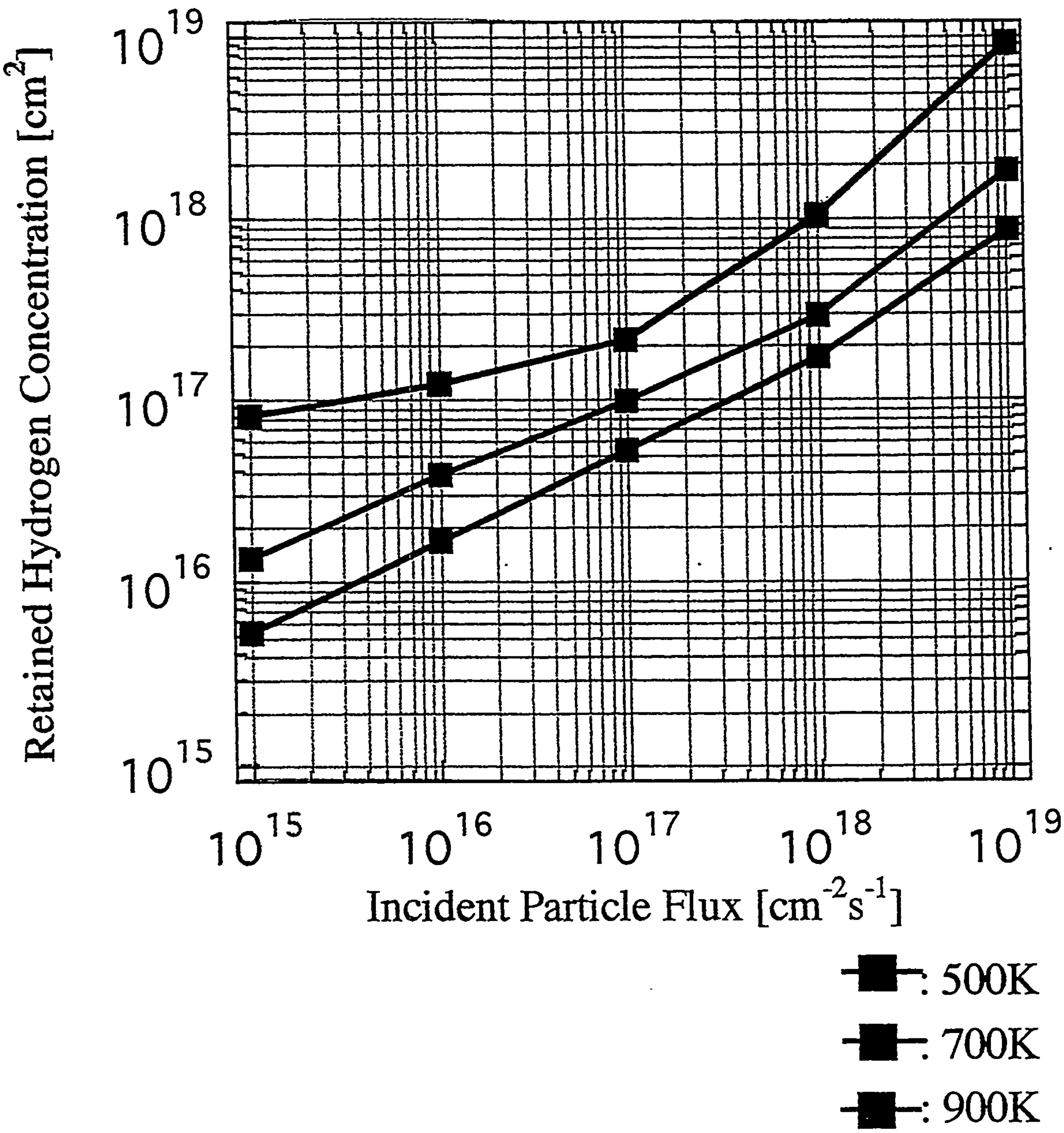

Transient behavior of retained hydrogen

Particle Flux: $5 \times 10^{22}\ m^{-2}s^{-1}$
Heat Flux: $17.5\ MW/m^2$

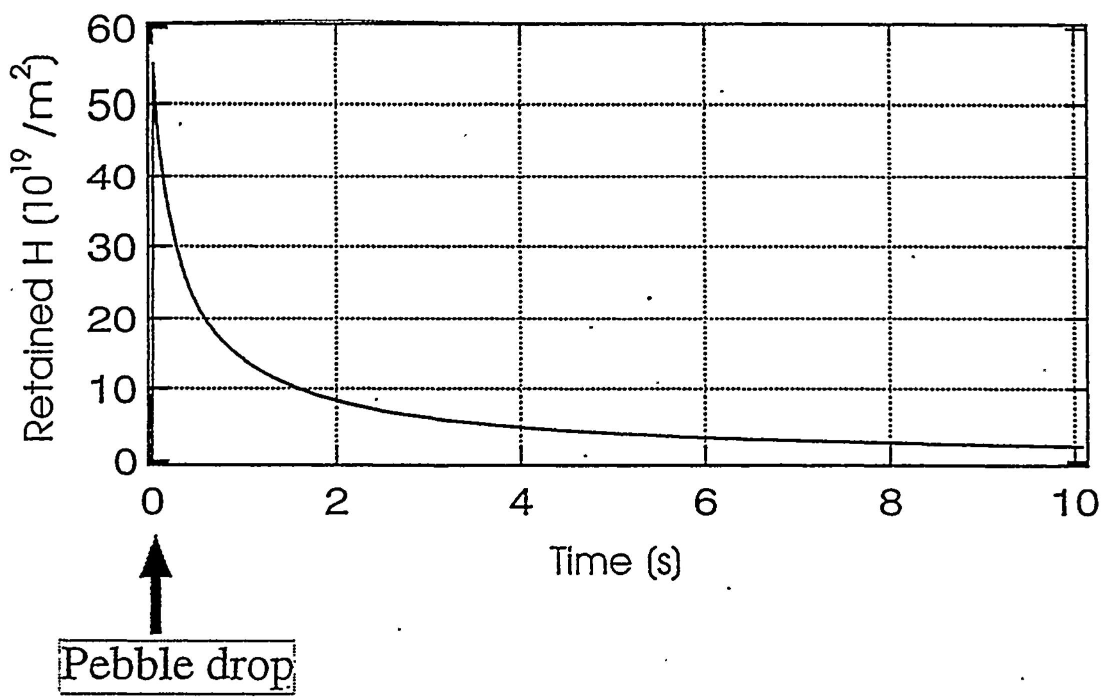

Spontaneous release of retained hydrogen at high temperature operation

Estimation of pumping performance of the pebble drop divertor

- The divertor surface area

  Major radius of torus : 7 m

  Width of strike zone : 50 mm about 4.4m^2
- Retained hydrogen: 5.5×10^{23} /m^2
- Pebble flow rate: 4.4m/s (drop from 1m in height)

→ **<u>2.1×10^{23}</u>** hydrogen atoms/s

Conclusions

- The maximum heat load was determined by the induced thermal stress in the pebble. The divertor pebble 1-2 mm in diameter can be used in $15 MW/m^2$ heat load.

- The pumping performance of pebble drop divertor was numerically studied by calculating mass balance equations. It was found that dynamic retained hydrogen in the pebble increased with heat load (particle flux), and sufficient pumping could be achieved.

Steady-State Impurity Control by Moving-Belt PFCs

US-Japan Workshop
San Francisco, Dec. 8-11, 1997

Y. Hirooka, M. S. Tillack and A. Grossman

University of California, San Diego
Fusion Energy Research Program
Dept. of Applied Mechanics and Engineering Sciences

FERP-UCSD

Acknowledgement

Productive discussions with:

UCSD	Dr. R. W. Conn
	Dr. S. Luckhardt
	Dr. J. Boedo
ANL	Dr. D.K. Sze
	Dr. J. Brooks

have been highly appreciated.

Table of Contents

1. Motivation of the present work

   Technical issues on impurity control technologies

2. Review of innovative PFC concepts

   Liquid lithium waterfall divertor
   Rotating shell divertor, etc.

3. MB-PFC with ex-situ inline belt processing systems

   Possible applications

4. Case study resutls

5. Summary

Issues on the impurity control by PFC technolgies

1. Wall conditioning-boronization, lithium injection, etc.:

   Effective but saturable, necessitating re-conditioning.
   Not desirable to steady-state reactors.

2. Tritium recovery necessary to meet the site regulation:

   Codeposition leading to a continuous build-up of tritium.
   Periodic removal of codeposited materials

3. Core plasma contamination by eroded PFC materials:

   Low-Z materials preferred but limited lifetime.
   Can we have a long-lifetime low-Z PFC ??

4. Heat removal:

   Thermal conductivity being the key, quality control for
   thousands of brazed tiles on heat sink becomes an issue.

FERP-UCSD

Comparison between conventional and moving-belt PFCs

ISSUE	Stationary PFC	Moving-belt PFC
Lifetime	Limited (low-Z)	Unlimited (w/gettering)
Impurity	Periodic wall cond.	Continuous gettering
Heat removal	Conduction	Radiation or contact
Tritium	Periodic removal	Continuous removal
MHD-effects	None	Minimal (for SiC)
PMI-damages	Periodic repair	Continuous repair
Neutron effects	Radioactivity (Mo, W) Bubble formation (Be)	Reduced radioactivity (for SiC)

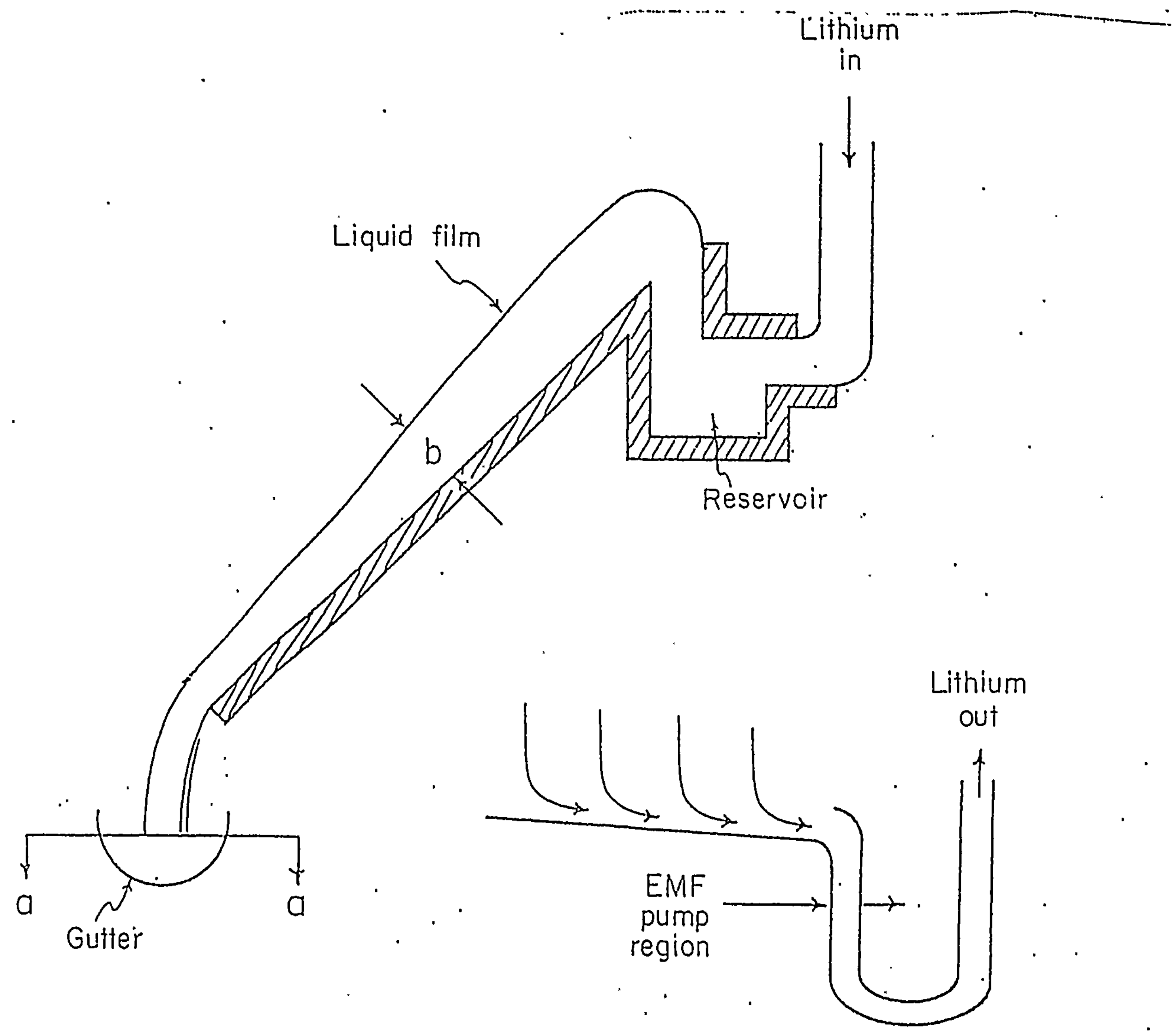

Lithium Trough Collector
(a-a cross-section)

FERP-UCSD

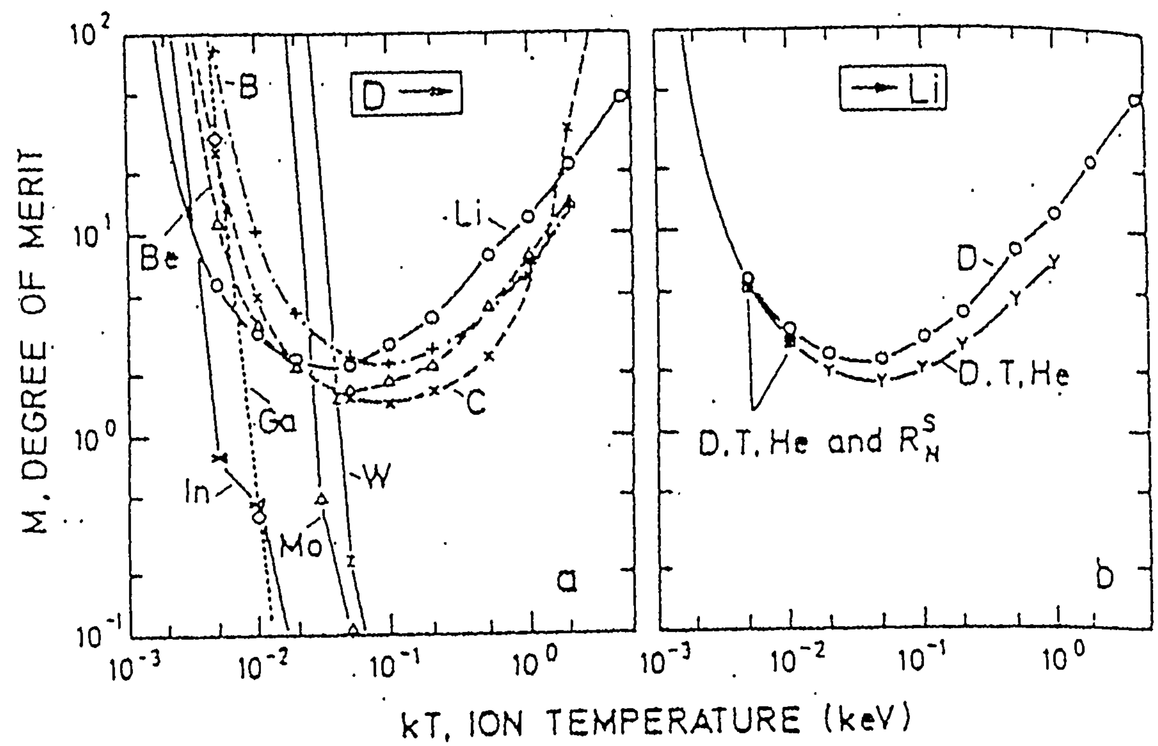

Fig. 9. The degree of merit of elements as a function of plasma temperature. The degree of merit is described by

$$M = \frac{c}{Y_D/(1 - Y_S)}, \qquad c = \begin{cases} 3.1/(2Z)^{1.5} & \text{if} \quad Z \le 14 \\ 295/(2Z)^{2.87} & \text{if} \quad Z \ge 14 \end{cases}$$

FERP-UCSD

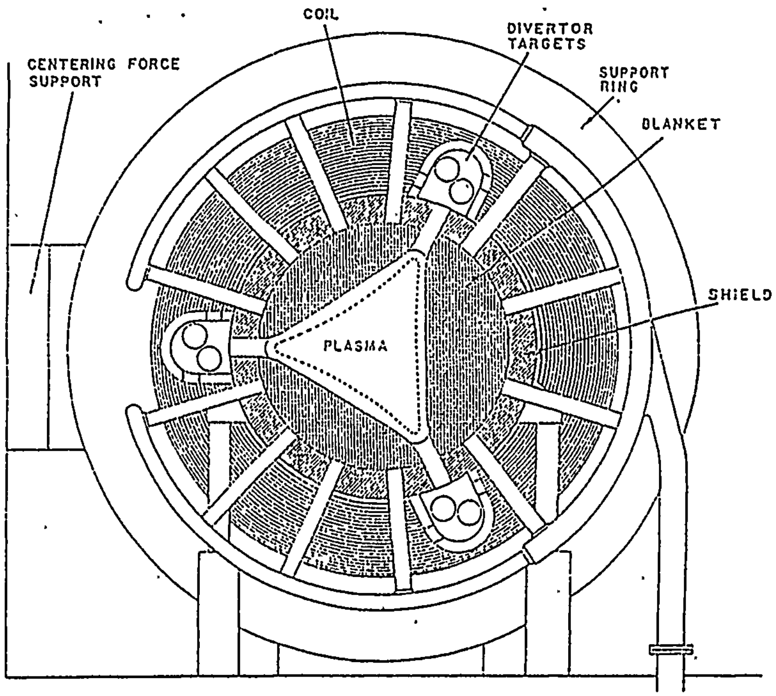

Figure VIII.2-1 Cross section of reactor showing location of divertor targets.

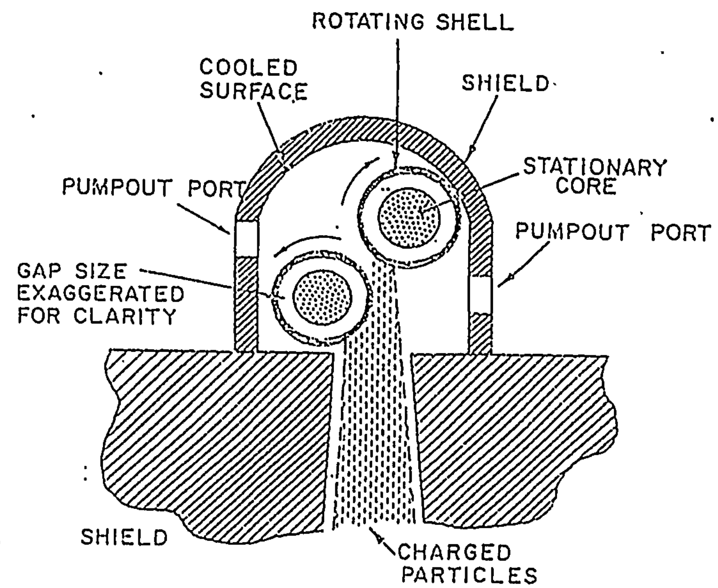

CROSS SECTION OF DIVERTOR TARGETS

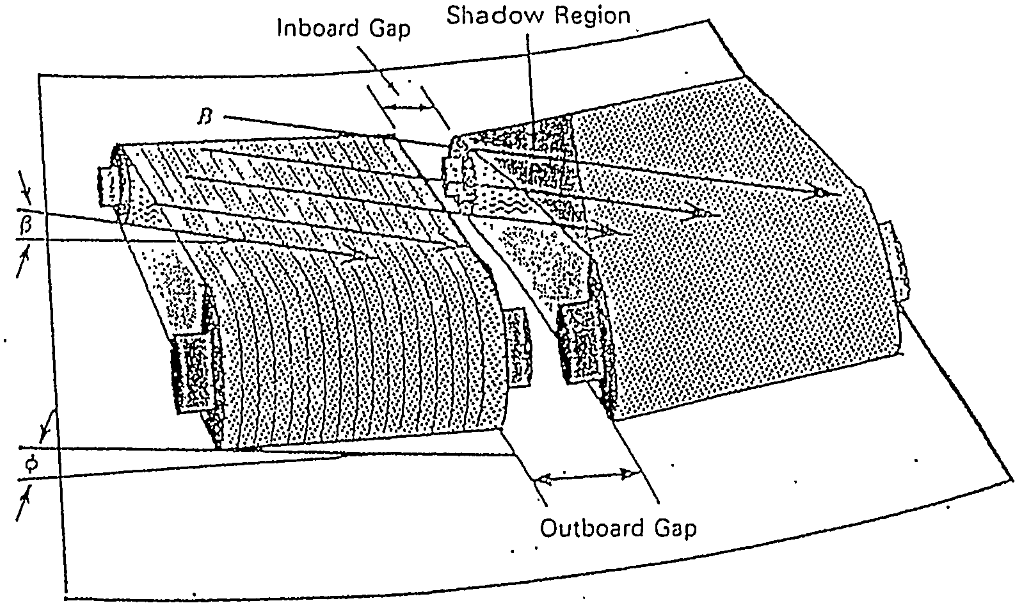

Fig. 8. Side-by-side view of a divertor belt showing tilt geometry.

Moving-belt plasma-facing components with ex-situ belt processing systems

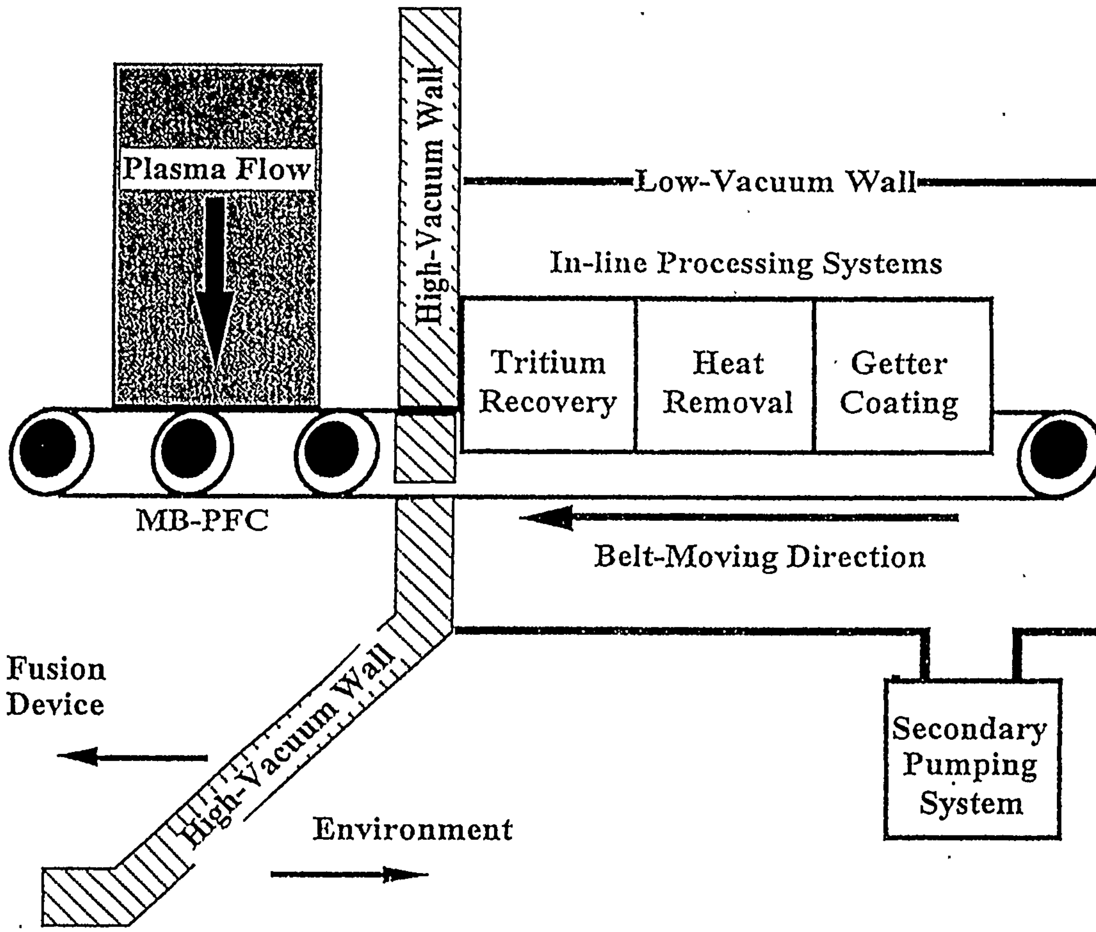

X-75

FERP-UCSD

Applications of MB-PFCs in a fusion device

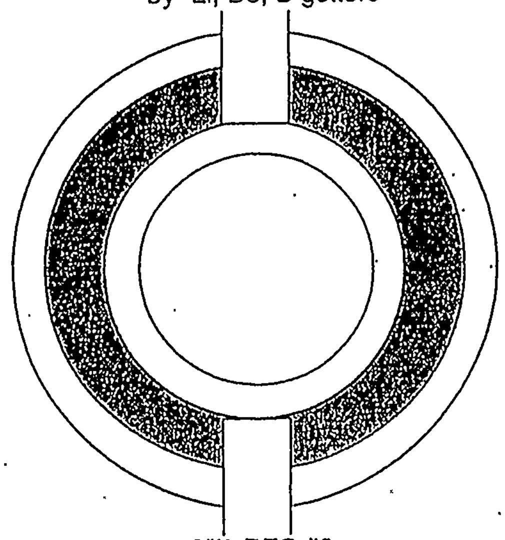

Multi-spot toroidal application
(for poloidal divertors)

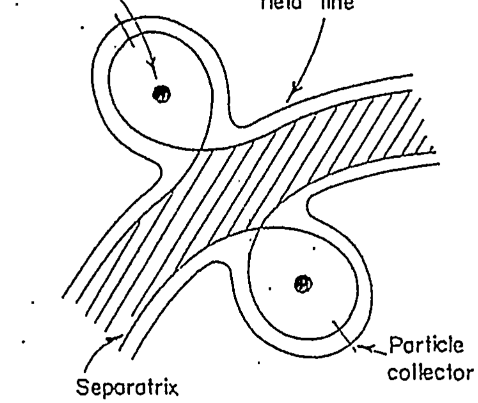

TOROIDAL DIVERTOR

(Top view of torus)

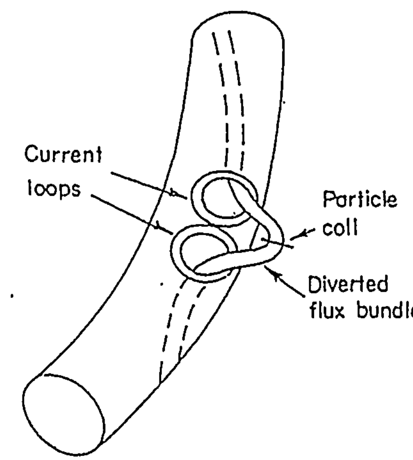

BUNDLE DIVERTOR

X-76

FERP-UCSD

Table 1 MB-PFC system operating conditions and belt properties*.

Belt length, L	20 m
Belt width, W	1m
Belt thickness, t_b	1 mm
Belt density, ρ	2.2 g/cm^3
Belt speed, v_b	2 m/s
Plasma interaction length, l_1	1 m
Tritium recovery section length, l_T	2 m
Getter-coating section length, l_2	2 m
Fuel plasma fluxes, $\Gamma_D + \Gamma_T$	each 0.995A/cm^2
Oxygen impurity flux, Γ_O	0.01A/cm^2
Particle bombarding energy, E	100 eV
Redeposition probability, P_{redep}	50%
Belt surface temperature	1000 ^oC
Surface emissivity, ε	0.8
Getter deposition efficiency, $v\phi(\vartheta)$	50 %
Thermal conductivity, k	5 W/m-K
Heat capacity, C_p	0.710 J/g-K
Thermal diffusivity, α	0.032 cm^2/s
Stefan-Boltzman constant	5.7×10^{-12}/sW/cm^2-K^4

*Property data for carbon materials are listed here.

Impurity control scenario

(1) Erosion rate of a moving belt (Independent of moving speed)

$$\Gamma_{MB\text{-}net} = \Gamma_{net}\,(l_1/L)$$: "Diluted" erosion over the belt length

(2) Deposition rate of low-Z getter material (evaporation source*)

$$\Gamma_{MB\text{-}depo.} = \Gamma_{evap.}\,(l_2/L)\,\nu\,\phi(\vartheta)$$

*Plasma spray is possible but coverage uniformity over a moving-belt is a potential issue.

(3) Is "zero-erosion" condition possible at a practical evaporation source temperature ? -------"Yes !"

Getter coating deposition rates for Li, Be, B

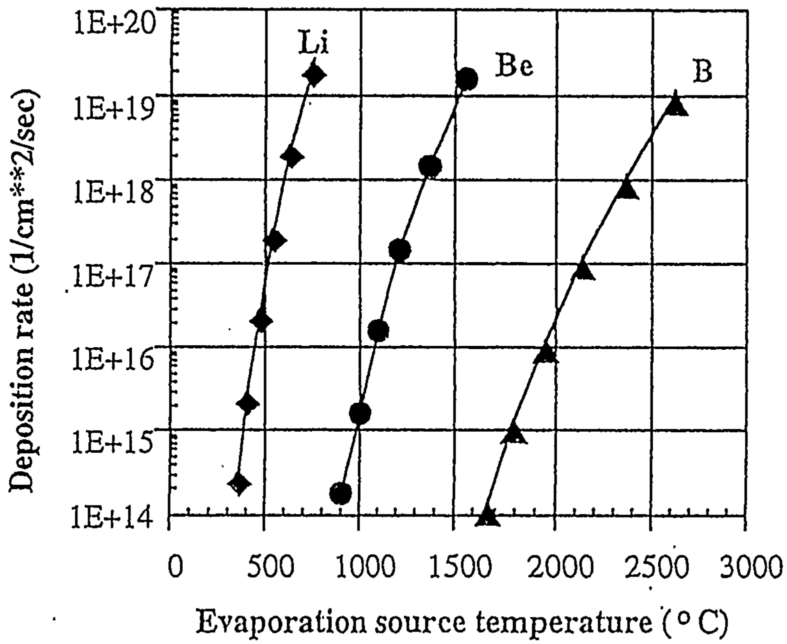

$$\Gamma_{evap.} = \frac{P_{eq.}}{\sqrt{2\pi mkT_s}}$$

$$\Gamma_{MB\text{-}depo.} = \Gamma_{evap.}\,(l_2/L)\ \nu\ \phi(\vartheta)$$

Tritium recovery and in-belt inventory

(1) TMAP + TRIM.SP code calculation

Numerical solution of diffusion equation with boundary conditions related to particle implantation in carbon.

(2) High-recovery efficiency: 99%

High surface temperature after plasma exposure (1000°C)

(3) Tritium inventory: not an issue for MB-PFCs

Slow (parabolic) increase due to bulk diffusion
Saturation not occur until 1.8×10^9 rotations (each 10 sec), i.e., 570 years !

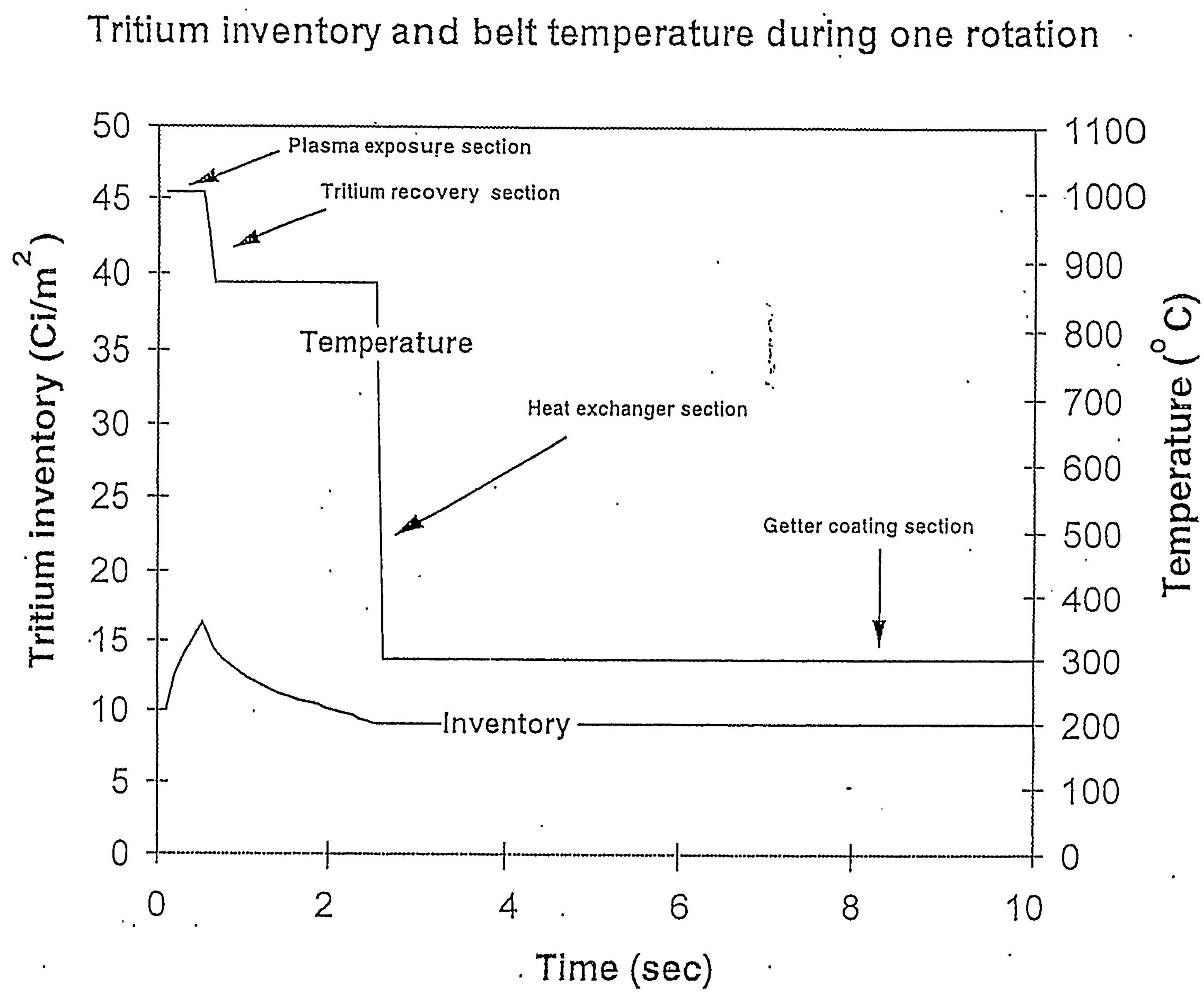

Tritium inventory and belt temperature during one rotation
Plasma exposure section
Tritium recovery section
Temperature
Heat exchanger section
Getter coating section
Inventory
Tritium inventory (Ci/m^2)
Temperature (°C)
Time (sec)
0
5
10
15
20
25
30
35
40
45
50
0
100
200
300
400
500
600
700
800
900
1000
1100
0
2
4
6
8
10

FERP-UCSD

Tritium recovery and inventory

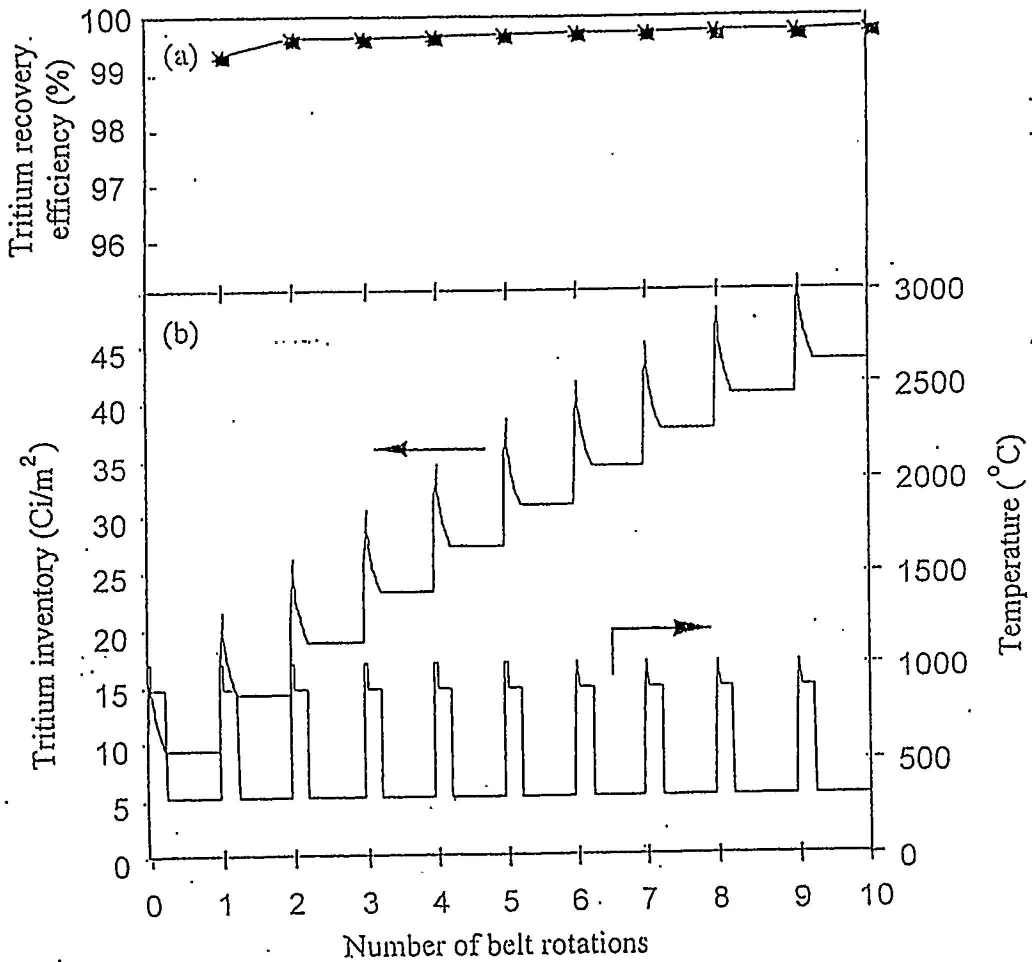

$$I_T(n) = \int_0^{t_b} C_T(x,\ t = t_r)\,dx$$

$$\eta(n) = \frac{\Gamma_T l_l/v_b - \{I_T(n) - I_T(n-1)\}}{\Gamma_T l_l/v_b}$$

Transverse Conduction in the Belt is Sufficient to Ensure Full Penetration of Heat

$$\rho c_p v \frac{\partial T}{\partial x} = k \frac{\partial^2 T}{\partial y^2}$$

$$Nu = \frac{2ht}{k} \qquad = \frac{2qt/k}{T_w - T_b}$$

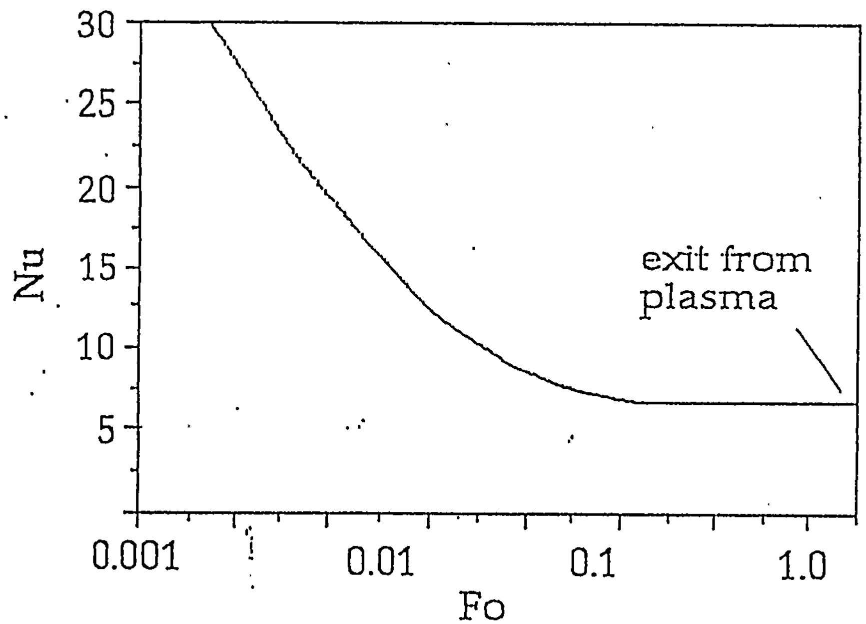

$$Fo = \frac{\tau}{t^2/\alpha}$$

τ is the exposure time,
t is the thickness of the belt
α is the thermal diffusivity ($\alpha = k/\rho C_p$)

$$\rho\, C_p\, v \frac{dT_b}{dx} = \frac{q}{t}$$

FERP-UCSD

Temperature profiles on a C-C moving belt

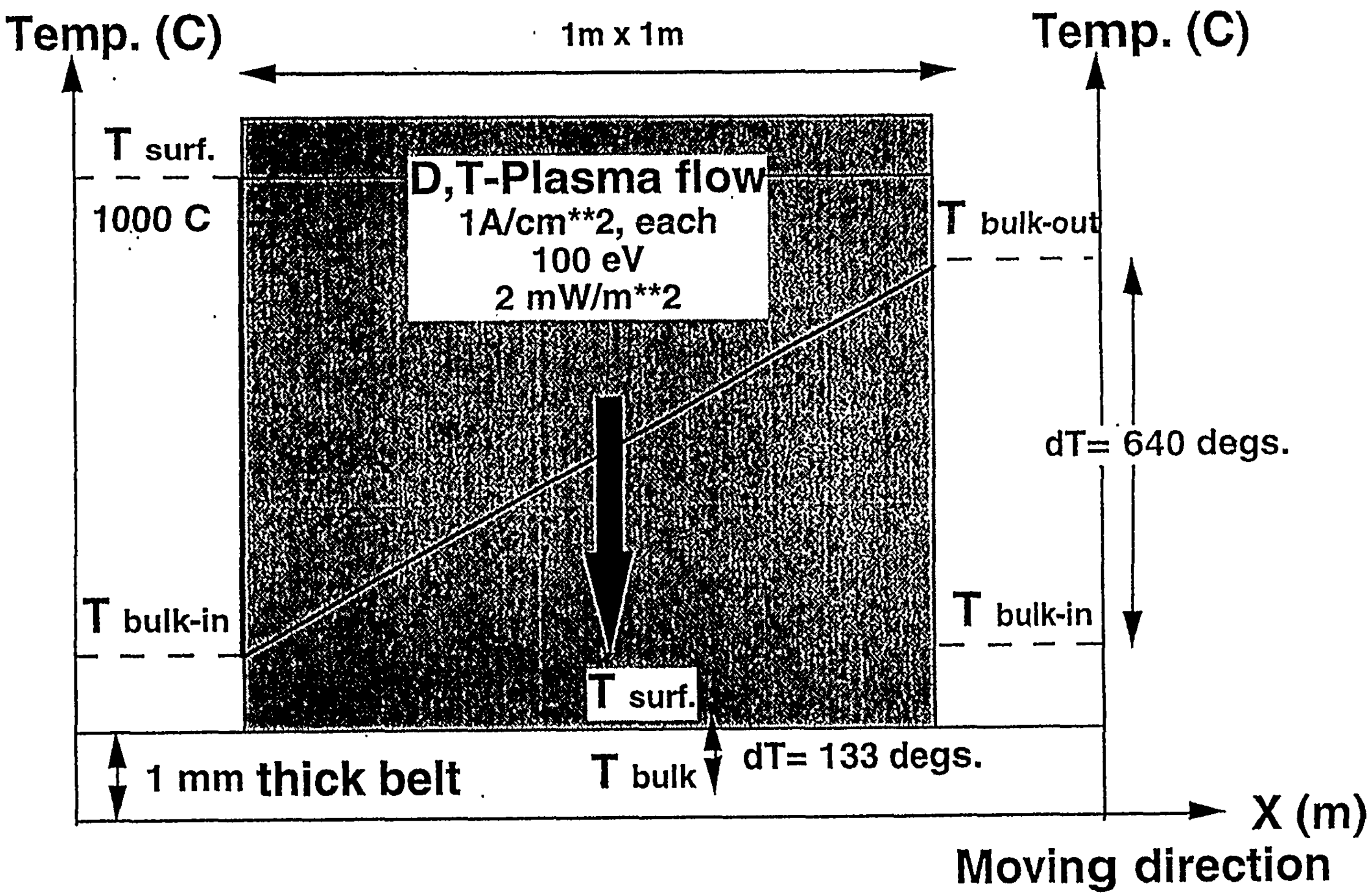

FERP-UCSD

Summary

1. Moving-belt PFC with ex-situ belt-processing systems have been proposed for steady-state impurity control, heat removal, and tritium recovery.

2. To minimize the MHD effects and induced radioactivity, semi-metallic and semi-conductor materials such as C-C and SiC-SiC fabrics are proposed as the belt materials.

3. In the case study assuming DT fluxes of 20kA/m^2(at 100eV), heat flux of 2MW/m^2, belt temp. of 1000^{o}C, belt-speed 2m/s, a MB-PFC system has demonstrated the following possible:
(1) Unlimited lifetime with non-saturable impurity gettering,
(2) Effective heat removal by radiation or contact heat transfer
(3) Efficient tritium recovery for long-term operation.

4. Optimization and limitations of MB-PFCs will be investigated.

5. Currently, the application for LHD is under discussion.

FERP-UCSD

X-86

Review of He Self-Pumping Concept

work by Jeff Brooks (ANL) and Richard Nygren (Sandia)
in collaboration with:

- Sandia surface physics lab (Doyle, Wampler, Walsh)
- ANL chemistry lab (Krauss)
- IPP Garching surface physics lab
- PISCES group
- TEXTOR group
- MIT Alcator C-MOD group

Papers by Nygren et al and Brooks et al. (He implantation and TEXTOR experiments)
10th PSI (Monterey, 1992, JNM 196-198), 9th PSI (Bournemouth, 1990 JNM 176-177)

Sandia
National
Laboratories

Summary of work on He self pumping

- concept proposed in 1980s by ANL and Sandia
- He implantation work at low energies (<100 eV)
- TEXTOR He self pumping experiment
- experimental plan for Alcator C-MOD
- preliminary concepts for fusion reactors

Goal for He self pumping effort

- reestablish program
- perform follow on test (C-MOD?)
- further develop concepts for fusion reactors
- develop larger concept demonstration test

Sandia National Laboratories

implantation process + selective detrapping of D

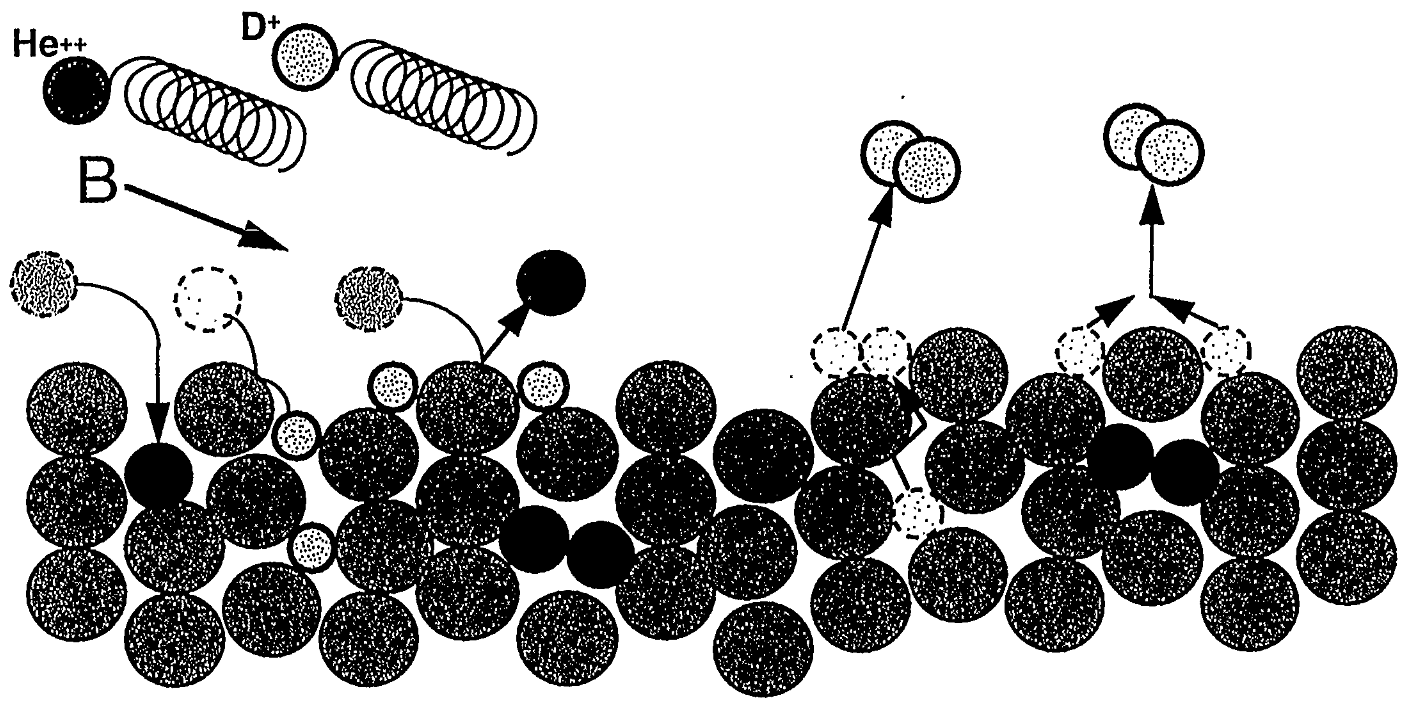

result: selective trapping of He
and eventual saturation of sites

Sandia National Laboratories

Key requirements for materials

- high probability of He trapping
- high He saturation level
- high D solubility, diffusivity
- no hydride formation
- temperature window: $T_{He\ release} < T_{D\ release} < T_{max\ operation}$

- adequate heat removal (good k)
- adequate neutronics
- self sputtering coefficient less than unity

Candidates: Ni, V, Fe, Nb, Mo, Ta

We have used Ni in our experiments.

Sandia National Laboratories

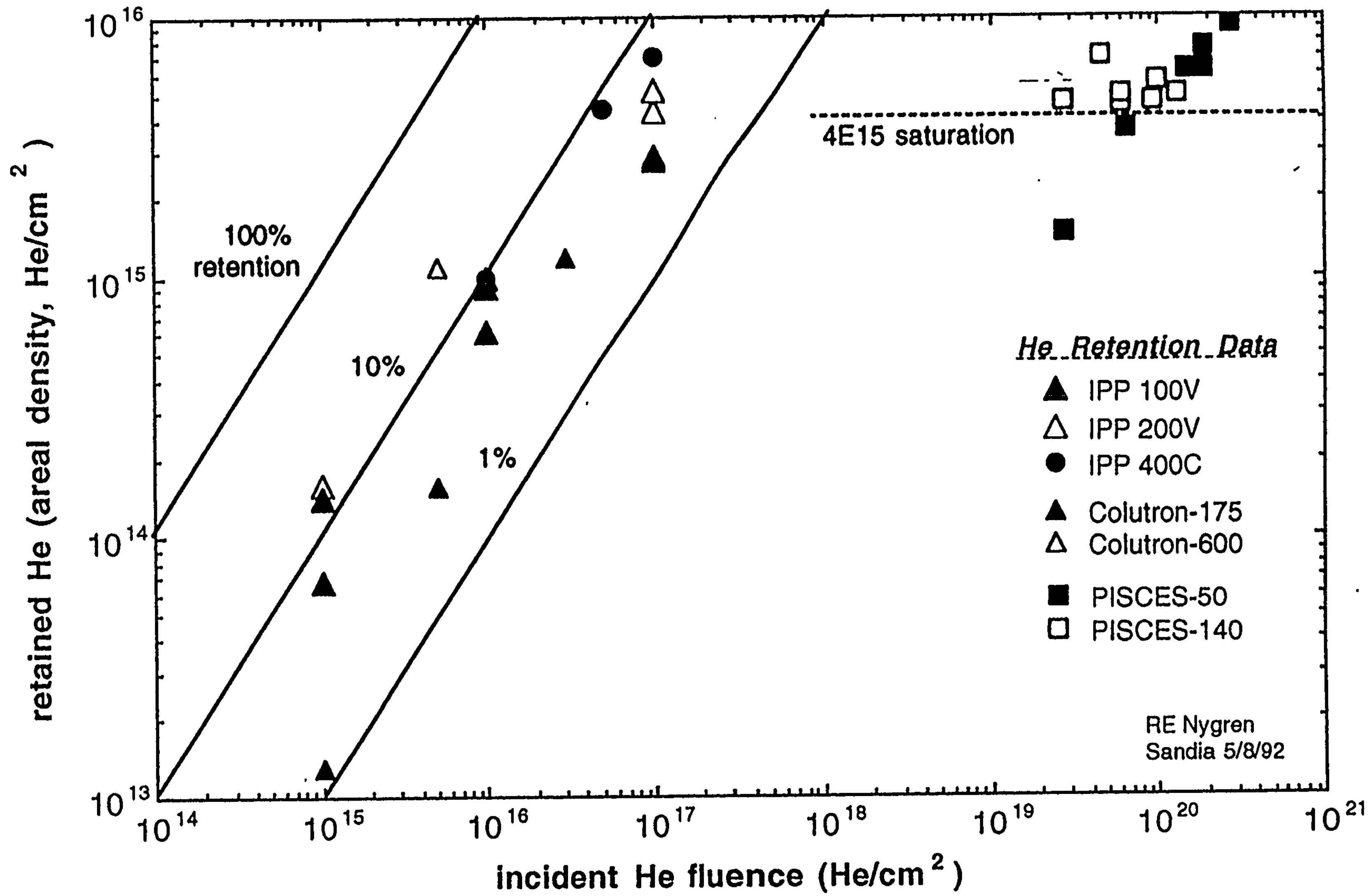
100%
retention
10%
1%
4E15 saturation
He Retention Data
IPP 100V
IPP 200V
IPP 400C
Colutron-175
Colutron-600
PISCES-50
PISCES-140
RE Nygren
Sandia 5/8/92
retained He (areal density, He/cm 2)
incident He fluence (He/cm 2)
10 13
10 14
10 15
10 16
10 17
10 18
10 19
10 20
10 21

TEXTOR experiment with ALT-I modular limiter

Two Ni plates with embedded heaters, a Ni deposition system

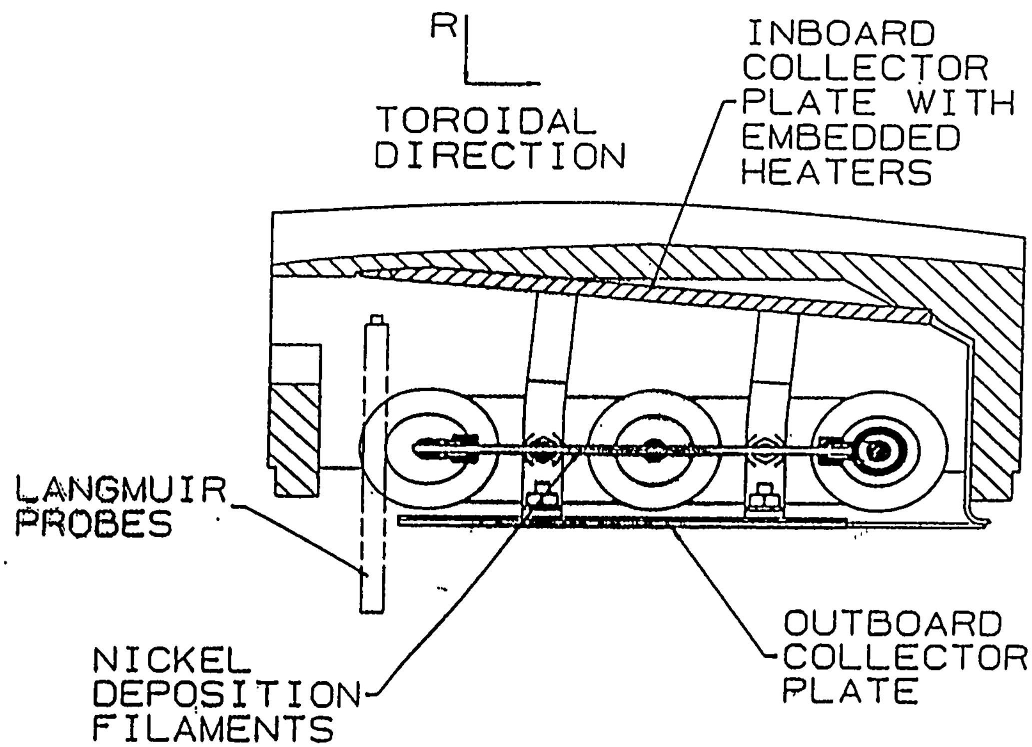

We operated the plate at ~450°C and did observe He self pumping by comparing He in the plasma in shots with saturated Ni to He in shots with fresh Ni.

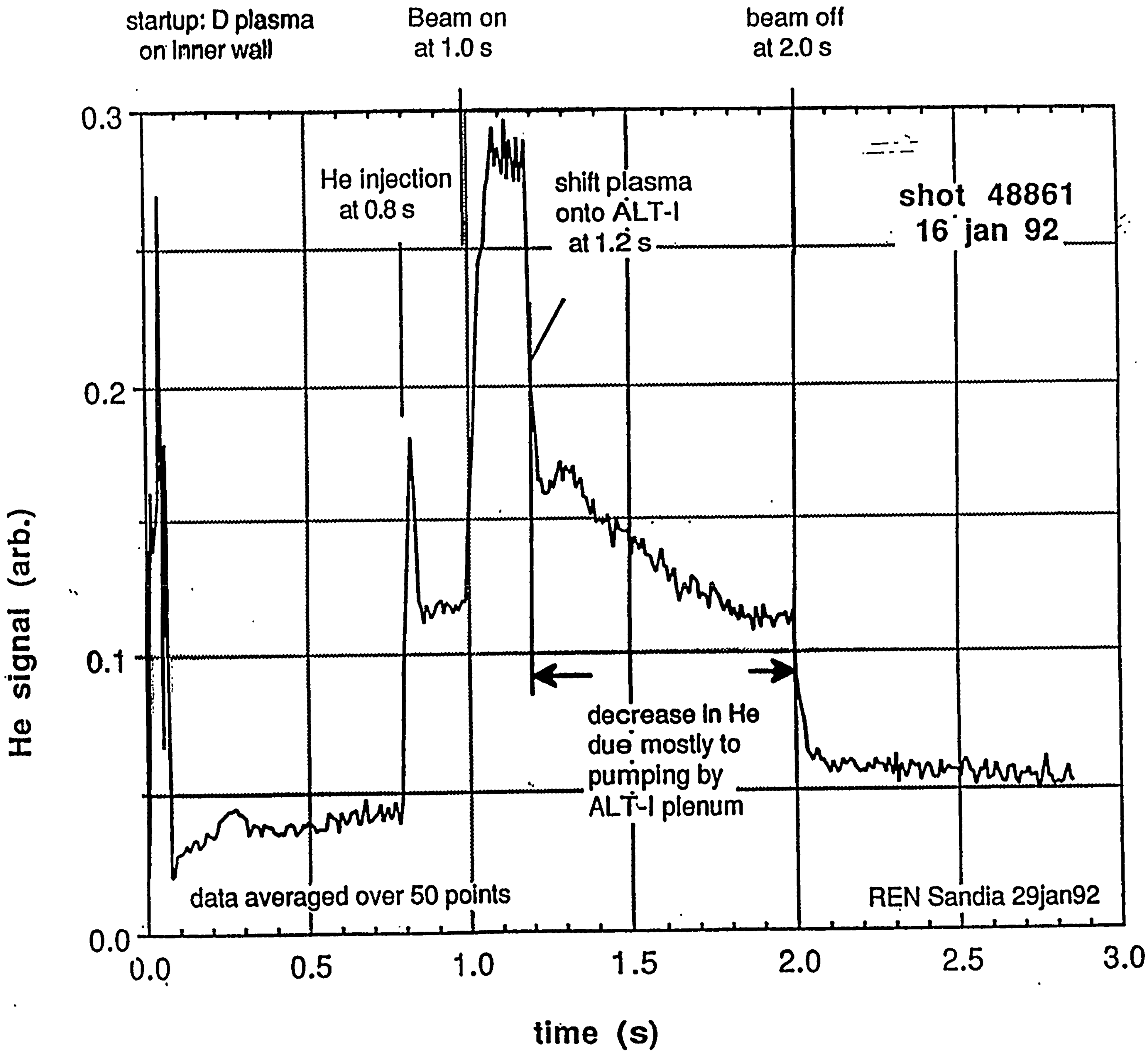

startup: D plasma on inner wall
Beam on at 1.0 s
beam off at 2.0 s
He injection at 0.8 s
shift plasma onto ALT-I at 1.2 s
shot 48861
16 jan 92
decrease in He due mostly to pumping by ALT-I plenum
data averaged over 50 points
REN Sandia 29jan92
He signal (arb.)
time (s)
0.0
0.1
0.2
0.3
0.0
0.5
1.0
1.5
2.0
2.5
3.0

Comparison of He Self Pumping Shot 48861, "Standard" Shots 48860 &4[illegible], and Simulation (48865) of Conditions in 48861 but Without Ni Deposition

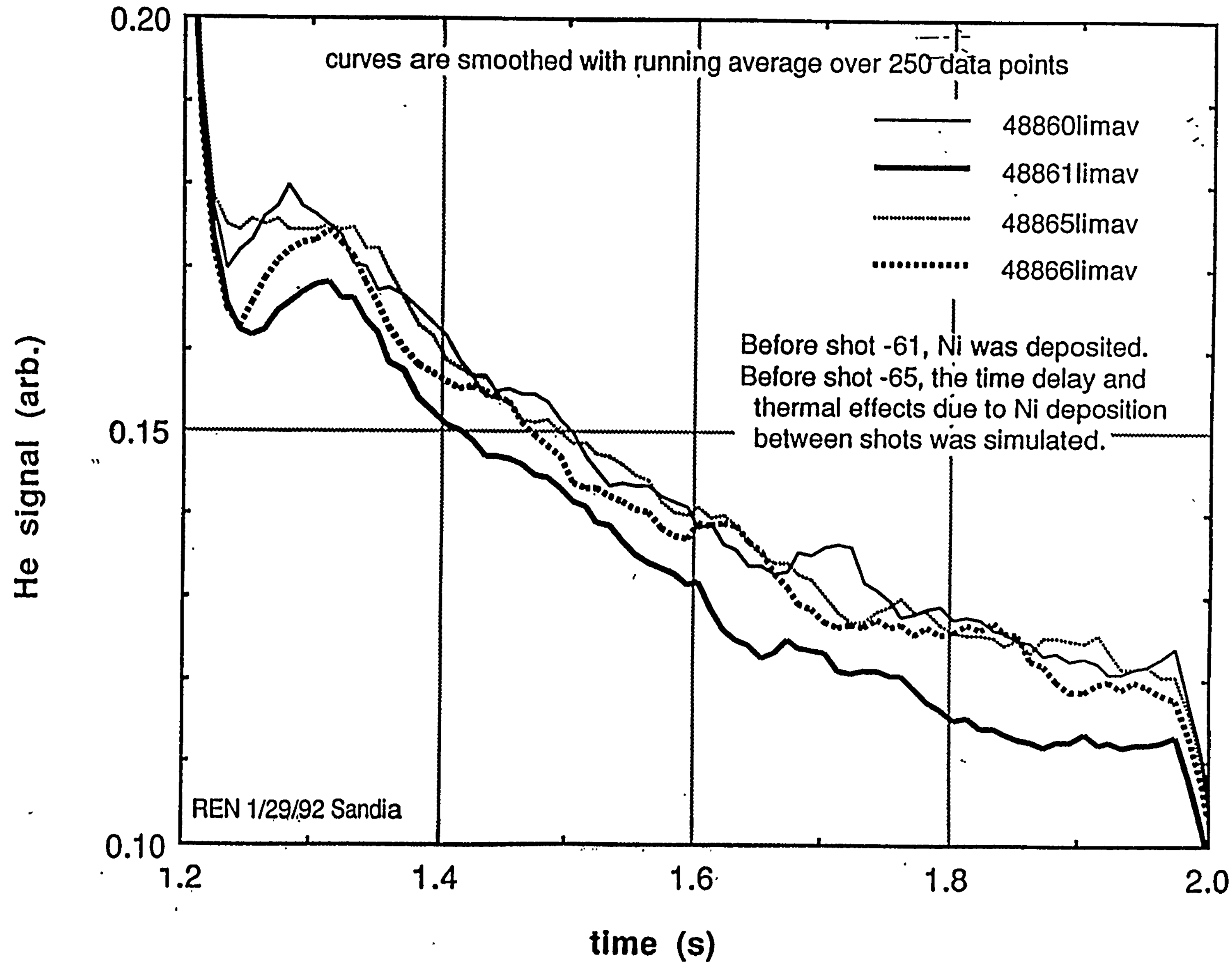

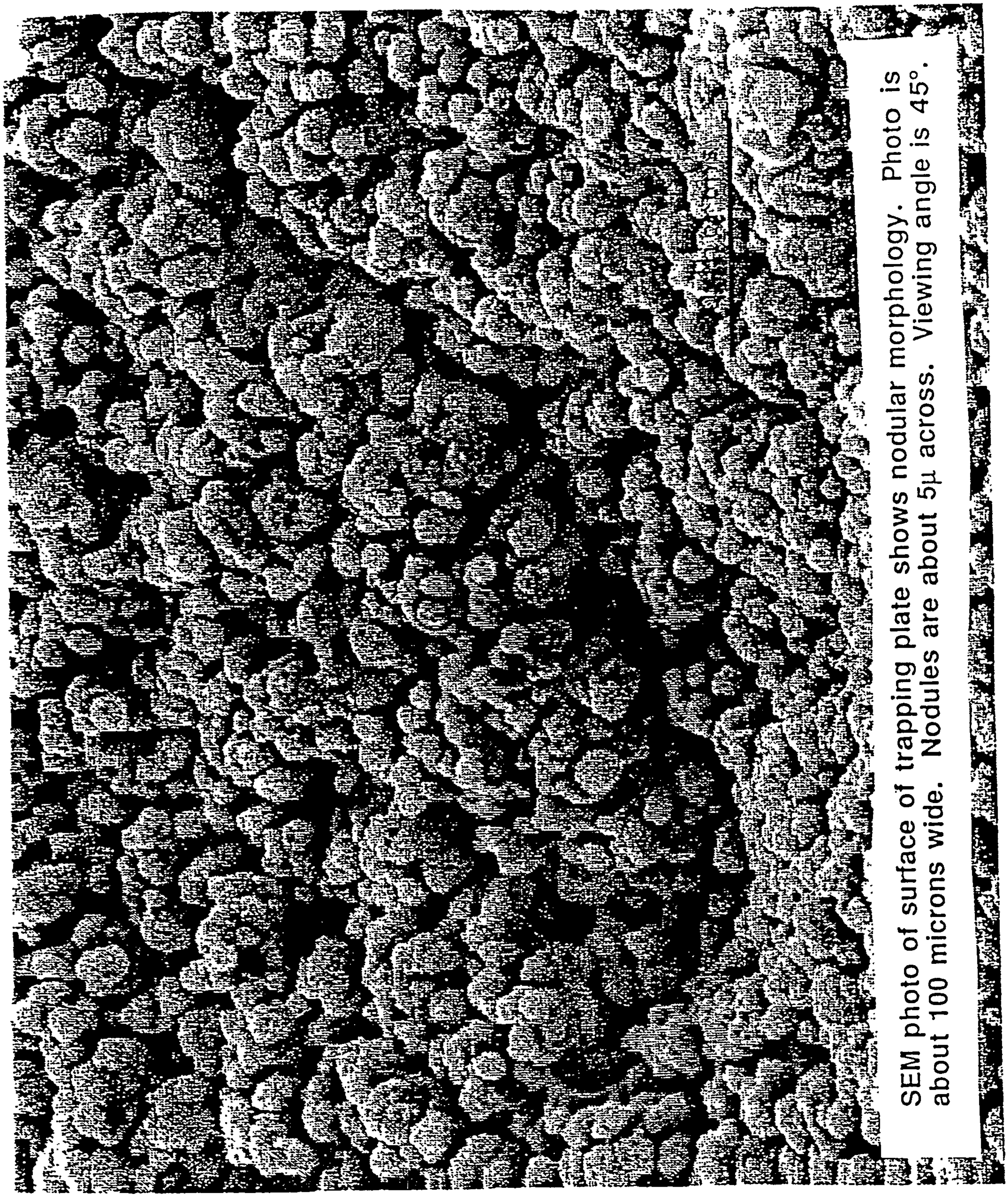

SEM photo of surface of trapping plate shows nodular morphology. Photo is about 100 microns wide. Nodules are about 5μ across. Viewing angle is 45°.

TEXTOR experiment: post test analysis

The two Ni plates were analyzed:

- Rutherford backscattering (W, Ni, O, C, B)
- elastic recoil detection (He)
- nuclear reaction analysis (D)

Both the inner plate (exposed to plasma) and the outer plate had significant ($1\text{-}2 \times 10^{16}$ He/cm^2) and roughly amounts of He. *The trapping by the outer plate implies that trapping of reflected neutral He occurred and was important.*

The inner plate had very little D, but did have significant carbon deposition. (This might trap D but not He.)

Sandia National Laboratories

Concept development should explore:

- erosion as source of host material
- auxiliary deposition system
- biasing to increase implantation depths
- trapping located in a deposition region
- trapping located to exploit reflected neutral He
- realistic edge conditionsm including impurities
- assessment of D/T recycling along with He pumping

Materials development should include:

- samples that simulate a mix of impurities and host material
- materials directed toward specific designs,
  e.g., system A for W walls, system B for Be walls

A Strategy for Development of Helium Self Pumping

Richard Nygren, Sandia National Laboratories
Jeff Brooks, Argonne National Laboratory

from June 1992 plan

A novel concept for helium (He) self pumping offers the potential to reduce and simplify vacuum pumping and tritium processing in fusion reactors. This year an ANL-Sandia-KFA team completed a successful proof-of-principle experiment of He self pumping on TEXTOR. After a brief explanation of the He self pumping concept, a proposed strategy for further development is outlined here.

To avoid diluting the plasma in a magnetic fusion reactor, He "ash" formed when deuerium (D) and tritium (T) combine, must be continually removed. Conventional vacuum pumping poses the problem that the D and T (fuel) would be pumped along with the He; this pumped fuel must then be recovered from the exhaust stream. With He "self pumping", there is no exhaust. He ions from the plasma are implanted and trapped in a host material at the plasma edge. Simultaneously implanted D and T are mobile in the host material and diffuse out and recycle.

The TEXTOR experiment verified two important features of He self pumping. First, the host material, nickel at about 450°C trapped He and no D from a D-20%He plasma. Second, even with a relatively low edge temperature of 25 eV (at the throat of ALT-I) and only 0.08 m^2 of host material, a significant fraction (5-10%) of the He in the plasma was trapped. The amount of He pumped would have even been larger but carbon contamination of the nickel decreased its capacity to trap He.

The next step in developing this concept is to confirm He self pumping in a diverted plasma. In these experiments, the host material must be specifically chosen for the plasma conditions present. For example, different host materials would be chosen for a carbon machine than for a metal machine. Work in design and in materials development is also necessary to support the development of a well founded experiment.

Diverted Plasma: He self pumping involves ions accelerated through the sheath at surfaces where magnetic flux lines are incident at an oblique angle and important neutral interactions, including reflection and trapping of energetic neutral He. These features cannot now be well simulated outside a tokamak and an experiment with an ITER-like (diverted) plasma is needed.

Here are some guidelines specific to the configuration of a tokamak experiment. (1) A prerequisite for tokamak experiments is a good understanding of the possible options for the applications of He self pumping in ITER. (2) The trapping surface must be in a deposition region at the plasma edge rather than a region of erosion. (3) The placement must permit adequate He pumping. (4) The configuration should exploit the trapping of reflected energetic neutral He. (5) Plasma impurities should be representative of the end application. For example, if impurity seeding in the ITER divertor is anticipated, then it would be desirable to simulate this in the experiment. (6) The experiment will require sufficient edge diagnostics to measure the He and H or D content, n_e and T_e at the plasma edge at a minimum. (8) There will be limitations on how tokamak experiments represent ITER applications. The aim of the experiment should be to maximize the He pumping and deal effectively with the plasma conditions (e.g., impurities) that will exist in the tokamak experiment itself. It can then be argued by analogy that effective solutions specific to ITER can be obtained. The placement of the trapping surface in a tokamak experiment will be a compromise based on the configurations of components, locations of diagnostics, etc. In principle, compromises in placement that decrease He pumping can be compensated by increasing the He in a H-He plasma. However, the basic objective should be to develop an experiment in which particle fluxes, heat loads, impurities, etc. are as representative as possible of ITER applications. This may mean that several experiments, each specific to a certain application and range of conditions should be proposed and developed.

Materials: The primary application of interest is for the ITER Technology Phase, i.e., most probably for an all metal machine (Be or W). He self pumping might also be considered for a carbon machine, either for the Physics Phase or as the alternate for the Technology Phase. Metal versus carbon is an important distinction because the primary issue for carbon contaminated systems is probably degradation of the He trapping capacity due to carbon poisoning; whereas for all metal systems, the primary issue is probably adequate recycling of hydrogen. It is not necessary to argue for one instead of the other but simply to recognize that there may be differing sets of issues for these applications.

Here are some guidelines related to materials. (1) Applications for the Technology Phase of ITER should be tested in an all metal tokamak. (2) The impurity levels in the plasma should be representative of the end application in ITER. (3) The product of the area, integrated flux and the trapping rate (equal to the arrival rate of He times the pumping efficiency) must exceed the rate of He production. (4) The net rate of deposition of the host material must exceed the He trapping rate divided by the atomic fraction of He at saturation (f_{He}). (5) In materials development supporting tokamak experiments (e.g., He trapping and H recycling studies), simulations of plasma surface interactions should be representative of the surface impurities anticipated in the tokamak experiments.

Design : Several options for depositing the host material should be pursued. Criteria should be developed that are specific to each option for each ITER application.

Here are some guidelines related to design. (1) The trapping surface must be replenished at a rate that keeps up with the He production in the plasma. (2) If sputtering from an adjacent region is the source then the sputtering rate will have to be great enough to supply the desired deposition rate.

$$\sum \{A_{12}(1-\delta_i)\,\Gamma_{i-1}\,Y_{i-1}(E_1) - \Gamma_{i-2}\,Y_{i-2}(E_2)\} > \frac{\Gamma_{He-2}\,r_{He}}{f_{He}}$$

A_{12} is a ratio of area-1 (erosion) to area-2 (deposition) and δ_i is the loss of sputtered particles between the source and the region of deposition. Γ's are the fluxes of various plasma constituents in area-1 and area-2. Y's are the sputtering yields which depend on energy E. At area-2, Γ_{He-2}, r_{He}, and f_{He} are respectively the He flux, He trapping efficiency and atomic fraction of trapped He at saturation. (3) For a host material different from the chamber and deposited from a filament, a batch process would probably be necessary in which the surface would be isolated during the deposition process. It is conceivable that this could be done mechanically and the outage for deposition would be rotated among several pumping stations to provide sufficient pumping. (4) If a "heat and dump" process were used to release trapped He from the host material, then some type of isolation from the plasma would be needed. Again it is conceivable that either the surface itself could be moved mechanically or an interceding gate could be moved and rotation of active trapping stations would provide continuous pumping.

US–Japan Workshop on HHF Components and PSI for Next Fusion Devices
December 8–11, 1997, San Francisco

Characterization of Liquid Metal Surfaces

R. Bastasz*, R. Causey, and K. Wilson
Sandia National Laboratories
Livermore, California
*(tel: 510 294–2013 email: bastasz@sandia.gov)

topics

- Use of liquid metals as plasma-facing surfaces
- PMI effects at liquid metal surfaces
- Research needs

RB:SNL:8716:97121001

Potential advantages of liquid systems for plasma facing components:

1. Unlimited erosion lifetime.
2. No neutron damage concerns.
3. High power density capability.
4. Active pumping of DT and/or He.
5. High temperature operation at high efficiency.
6. Low pressure operation.

RB:SNL:8716:97121002

PMI research for liquid metal systems

Issue: How will a liquid divertor surface behave when bombarded by energetic particles?

Need: Fundamental data on ion-liquid interactions needed to properly model conditions that will be found in a fusion reactor.

Tasks:
- Measure H and D sputtering of liquid metals
- Measure liquid metal self-sputtering
- Examine surface composition and impurity effects
- Measure T uptake and release

RB:SNL:8716:97121003

Sandia National Laboratories

Lithium Self-Sputtering Yields:

TRIM Calculation Results (for solid Li)						
Energy (eV)	0°	15°	30°	45°	60°	75°
10	≈0	≈0	≈0	0.01	≈0	0
20	0.01	0.02	0.04	0.14	0.16	≈0
50	0.07	0.10	0.18	0.44	0.72	0.10
100	0.14	0.17	0.29	0.55	1.1	0.59
200	0.20	0.21	0.36	0.65	1.4	1.6
500	0.21	0.24	0.39	0.68	1.4	2.4

preliminary calculations (1997 August)

RB:SNL:8716:97121004

Sandia National Laboratories

Liquid metal surfaces appear to be *stratified.*

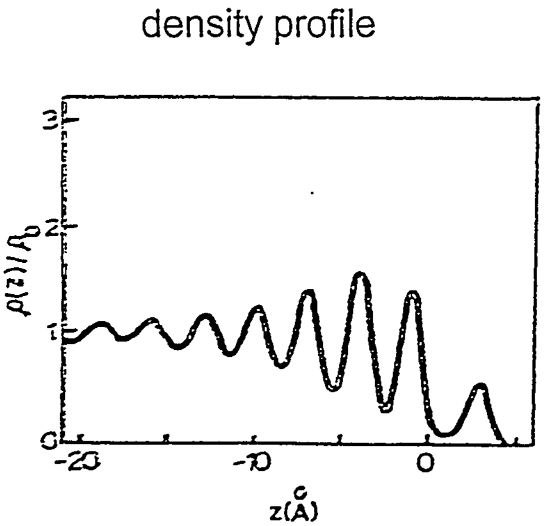

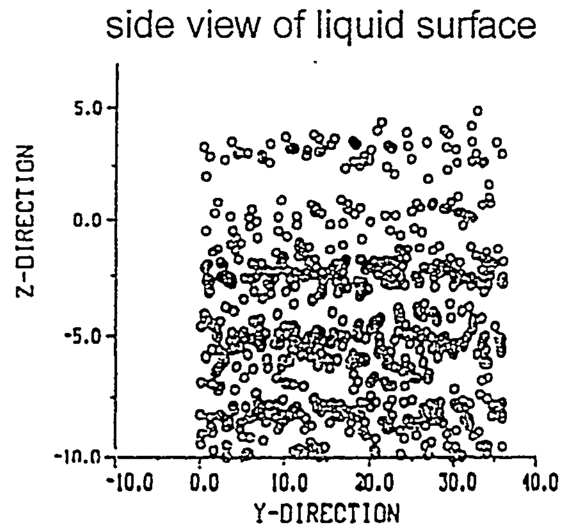

References: P. D'Evelyn and S. A. Rice,
J. Chem. Phys. 78 (1983) 5081.
W. L. Morgan, J. Appl. Phys. 65 (1989) 1265.

RB·SNL 5716.971110nn

Sandia National Laboratories

Self-sputtering simulations using a stratified liquid-metal model show an *enhanced* low-energy sputter yield.

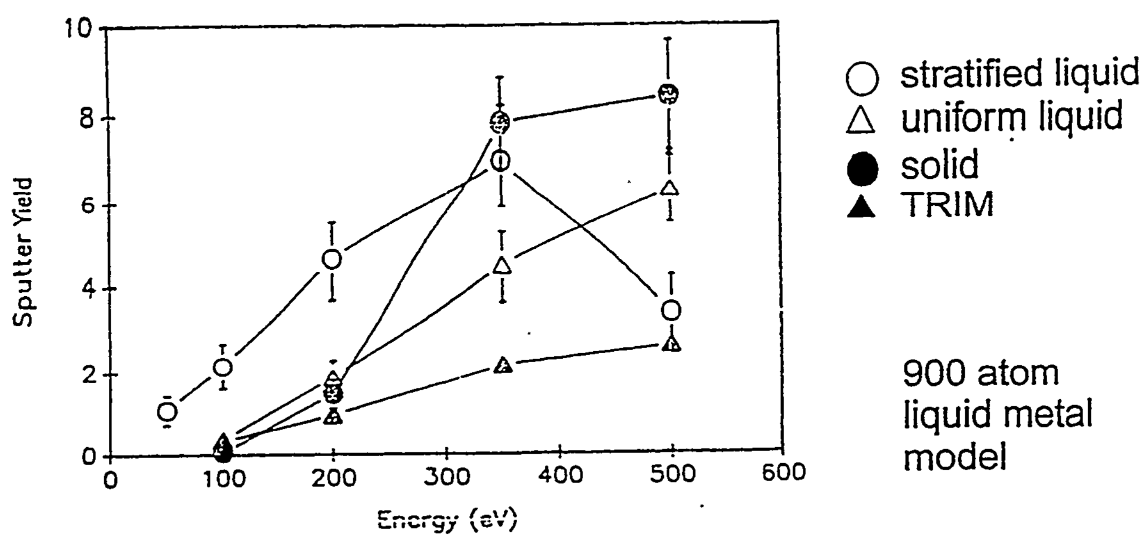

Reference: W. L. Morgan, J. Appl. Phys. 65 (1989) 1265.

RB·SNL 5716.971110nn

Sandia National Laboratories

The composition of a liquid surface can much different than the composition of the bulk liquid.

- The component with the lowest surface tension tends to segregate to the surface.
- For binary liquids, the Gibbsian segregation rule is

$$\gamma_A + \frac{RT}{\sigma_A}\ln\left(\frac{1-x_s}{1-x_b}\right) = \gamma_B + \frac{RT}{\sigma_B}\ln\left(\frac{x_s}{x_b}\right)$$

- Example: the surface of the Ga-In eutectic alloy.
  surface composition: $\geq$94 % In
  bulk composition: 16.5% In

Reference: M. J. Regan, et al., Phys. Rev. B 55 (1997) 15874.

RB:SNL:8716:97121007

Surface tension of the elements as liquids

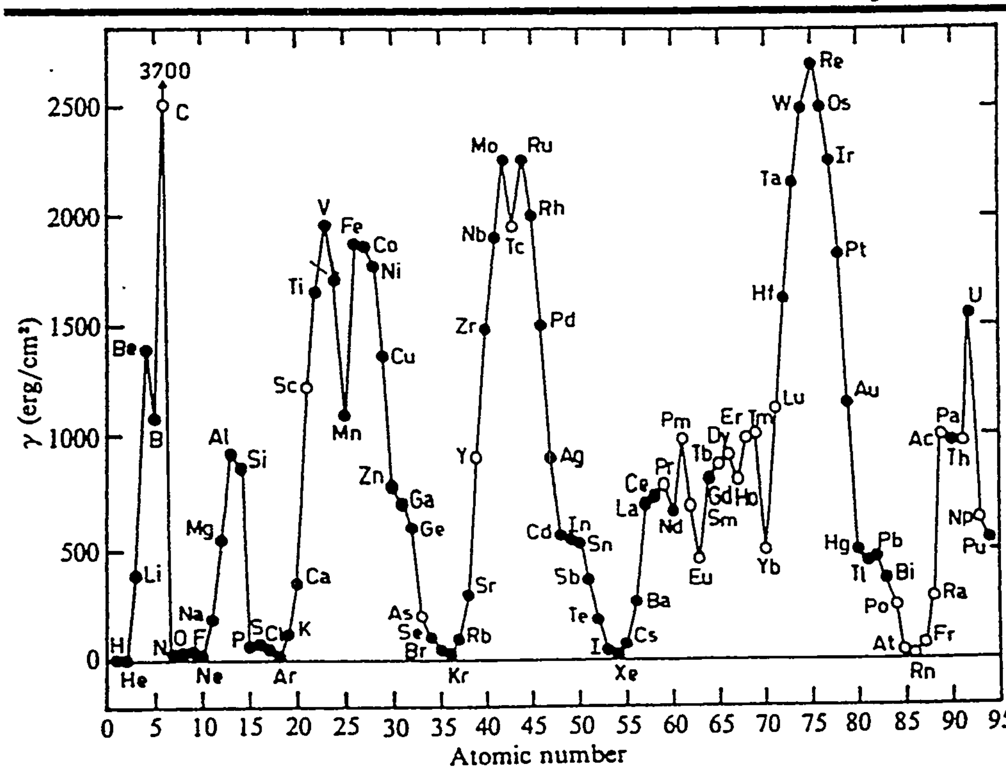

Reference: A. Zangwill, ***Physics at Surfaces*** (Cambridge University Press, 1988) p. 11.

RB:SNL:8716.971110nn

Low-Energy Ion Beam Laboratory: The primary research tools are ARIES & SIMS.

- ARIES: Angle–Resolved Ion Energy Spectrometer
  - → extremely surface-sensitive method for studying ion-surface interactions.
  - → measures energy and intensity of reflected and ejected ions from surfaces.
  - → provides fundamental data on sputtering, reflection, composition, and structure.
- SIMS: Secondary-Ion Mass Spectrometer
  - → sensitive detector of atoms and molecules on surfaces.
  - → mass analyzes ions sputtered from the surface (including H,D,T) and can measure depth profiles.
  - → useful for characterizing the distribution of impurities in the near-surface region.

RB:SNL:8716:97121009

The ARIES instrument measures the energy and intensity of low-energy ions scattered or recoiled in the forward direction.

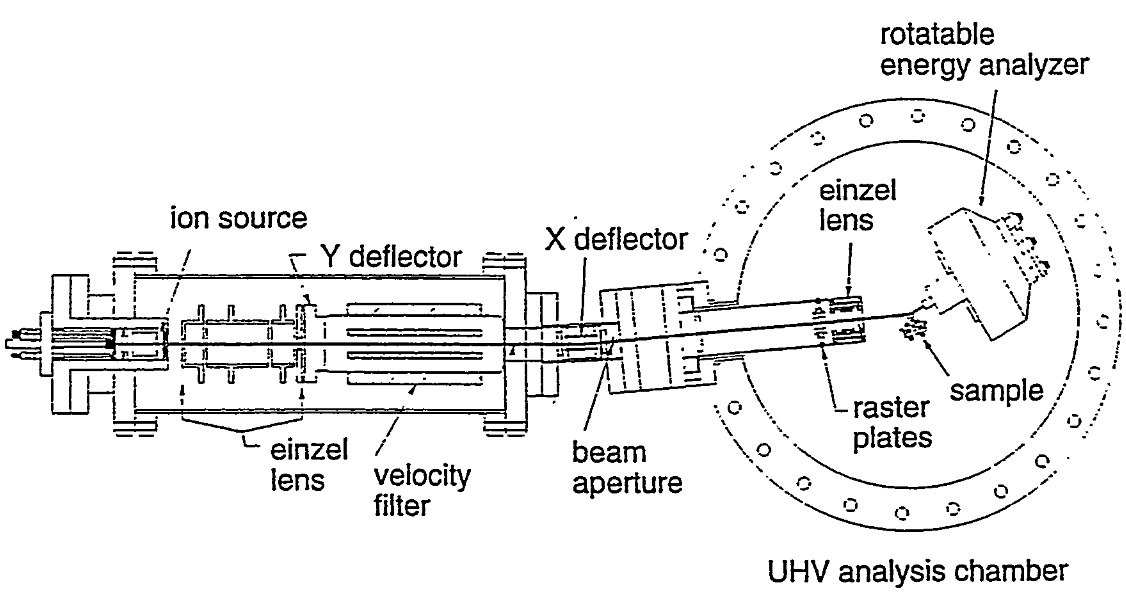

RB:SNL:8716:97121010

The SIMS instrument contains a low-energy ion source, a quadrupole analyzer, and a heated sample stage (4 exchangable samples).

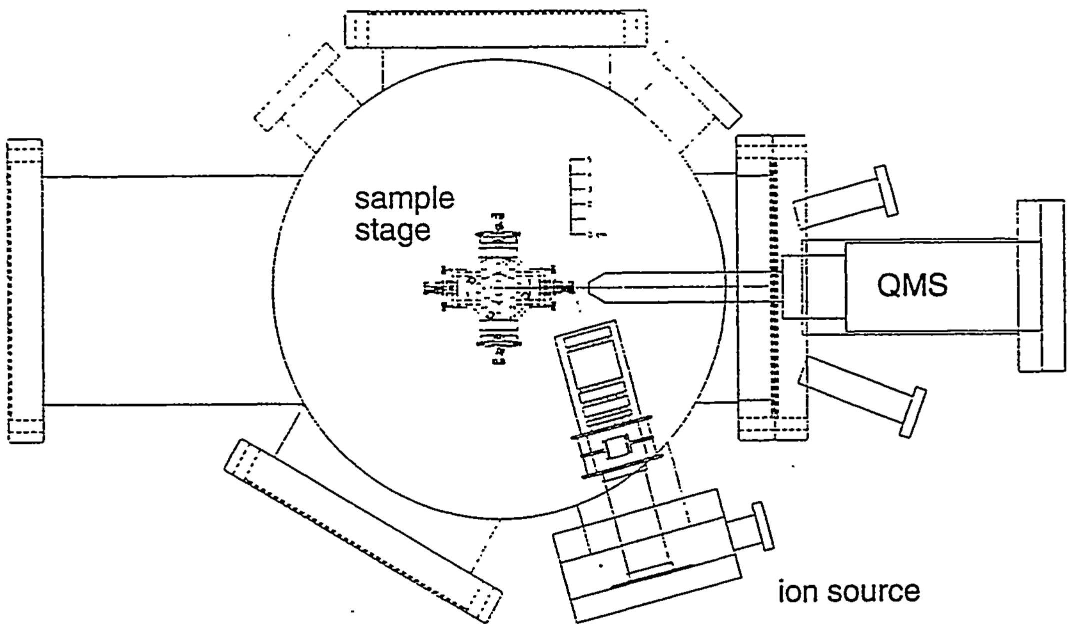

RB:SNL:8716:97121011

Low-energy SIMS geometry is arranged to maximize depth resolution and sensitivity.

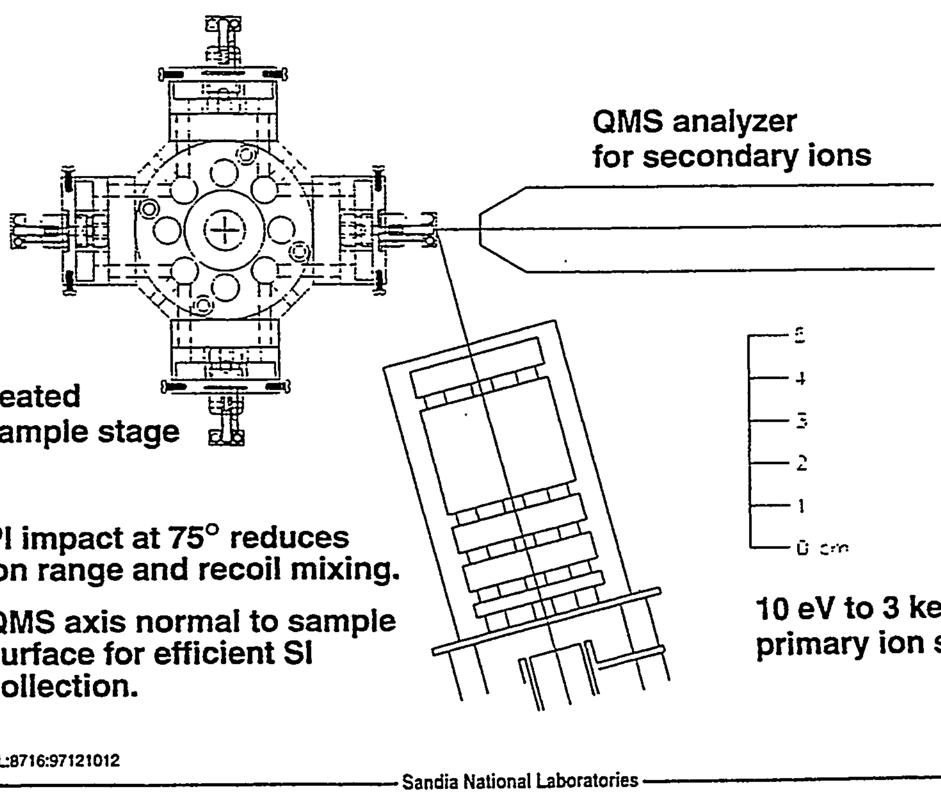

- PI impact at 75° reduces ion range and recoil mixing.
- QMS axis normal to sample surface for efficient SI collection.

RB:SNL:8716:97121012

The Tritium Plasma Experiment (TPE) will play an important role in the ALPS experiments. Several of the experiments can only be completed with the use of Tritium

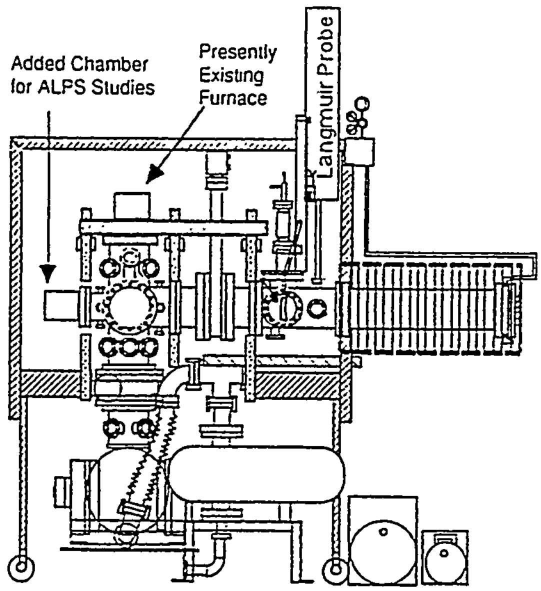

A high temperature furnace already exists on the TPE experiment. It can be used in studies of tritium solubility and diffusivity.

A new chamber can be bolted directly onto the end of TPE. This chamber can be used to house several different types of ALPS prototypes. The liquid metal can be directly measured for tritium uptake after plasma exposure. Heated catcher plates located in this special chamber can also be used to determine the codeposition rate of tritium with the sputtered liquid metal.

Sandia National Laboratories

DiMES can be used to test ALPS concept.

Concept of DiMES sample for ALPS test

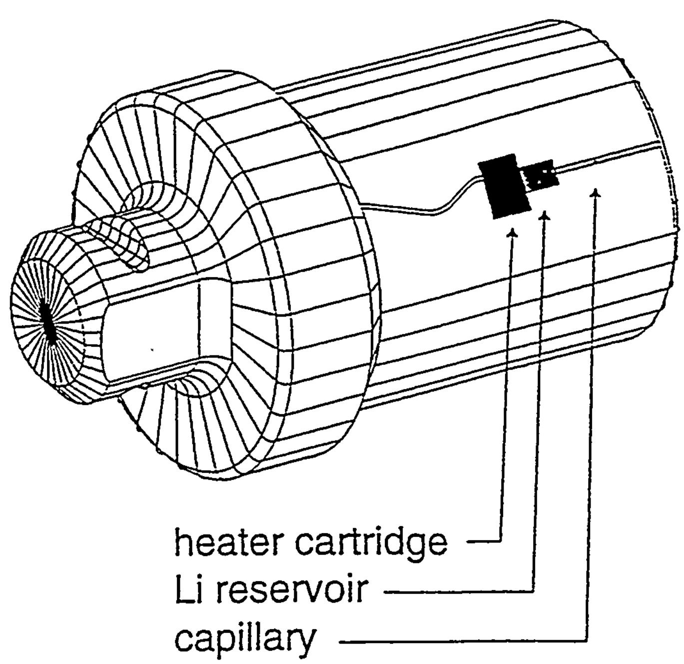

Study:

- stability
- erosion
- transport

RB:SNL:8716:97121013

Sandia National Laboratories

Summary:

- Liquid metal surfaces can be:
  - stratified
  - compositionally altered
  - transiently structured.
- Plasma-surface interactions at liquid metal surfaces may be fundamentally different than at solid surfaces.
- Accurate data are needed for:
  - D, T, and He pumping, retention, and release
  - D, T, and He sputtering yields
  - Liquid metal self-sputtering yields
  - Surface composition of liquid alloys and mixtures.
- A realistic model of plasma-surface interactions needs to be developed for liquids.

RB:SNL:8716:97121014

Sandia National Laboratories

Section XI: Long Range PFC Development and Collaborations

[page intentionally left blank]

LONG RANGE PFC / PFS (systems) + PMI + Collaborations

goals

1. • X10 Increase of heatflux, part. flux
2. • Self healing continuously renewable wall / off normal event handling.
3. • Optimization Tools for boundary / core interaction and control

Approachs

3 Develop integrated physics models that couple PFS — EDGE - CORE
— (Nuclear) —

and

Use to optimize system as a whole

1, 2 Novel PFS ideas -

in-situ coatings, Li, B, etc coatings
gas boundary
pebble beds - flows e.g. Osaka Univ.
belts
RF boundary
biasing, currents

LONG RANGE NEEDS

SCIENCE FOCUS

→ Integrated plasma materials models

→ optimized boundary PMI/PFC syst

CORE - EDGE - MATERIALS

→ IN-SITU MATERIALS DIAGNOSTICS

→ Handling of off-normal events

FACILITIES

DIVERTOR / BOUNDARY SIMULATORS

- Flux tube
- Pisces-Upgrade etc.
- Flux sheet

long connection length

island, chain, magnetics effe

Dedicated Tokamak or Stellarator?

High Power density ~50 MW/m² for ALPS.

Advanced / Novel / PFS / PMI concepts

convection systems $V_{CONV.} >> V_{COND.}$

pebblebeds, flows e.g. Osaka Univ.

liquid metals

belts - M. B. Diverter Y. Hirooka et al.

boundary control systems

in-situ coatings Li, B etc.

gas mantle, RI like

RF boundary

biasing, currents from edge, walls.

interaction with new magnetic configs -

ST, QA stellarator, FRC, ... etc.

Session XII: Supplement Session

[page intentionally left blank]

More Activities/Results in Japan

Presented by N. Noda (NIFS)

Contents

- Li Conditioning Studies
- Boronization Studies
- CFC-OFHC Joining
- Evaluation of High Z Metals
  (Thermomechanical Characteristics)

Simulation Experiments on Screening of Lithium by boundary plasma

— LIF measurement of Li atom density profile —

H. Sugai and H. Toyoda
Nagoya University, Nagoya, Japan

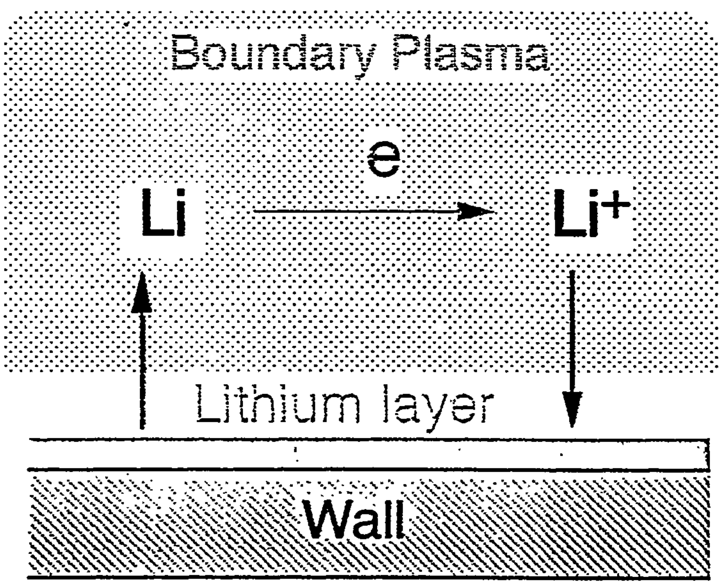

Ionization threshold of Li
5.4 eV
↓
Easily screened by plasma
↓
Redeposition of Li

Laboratory Simulation Experiment

- Lithium effusion from a small orifice
- RF helium plasma without magnetic field
  $n_e=10^{11}cm^{-3}$, $T_e=3eV$, 35 mTorr He
- ~~LIF~~ LIF detection of lithium atom

Schematic of experimental set up

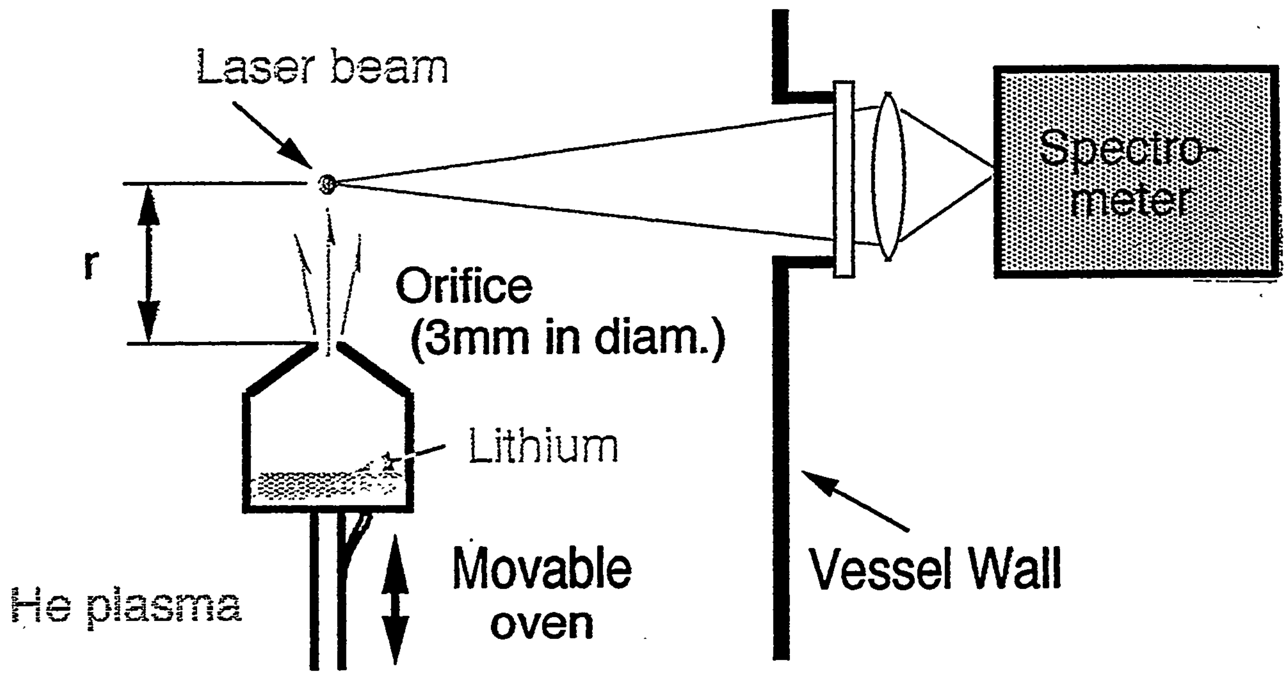

Li atom density profile

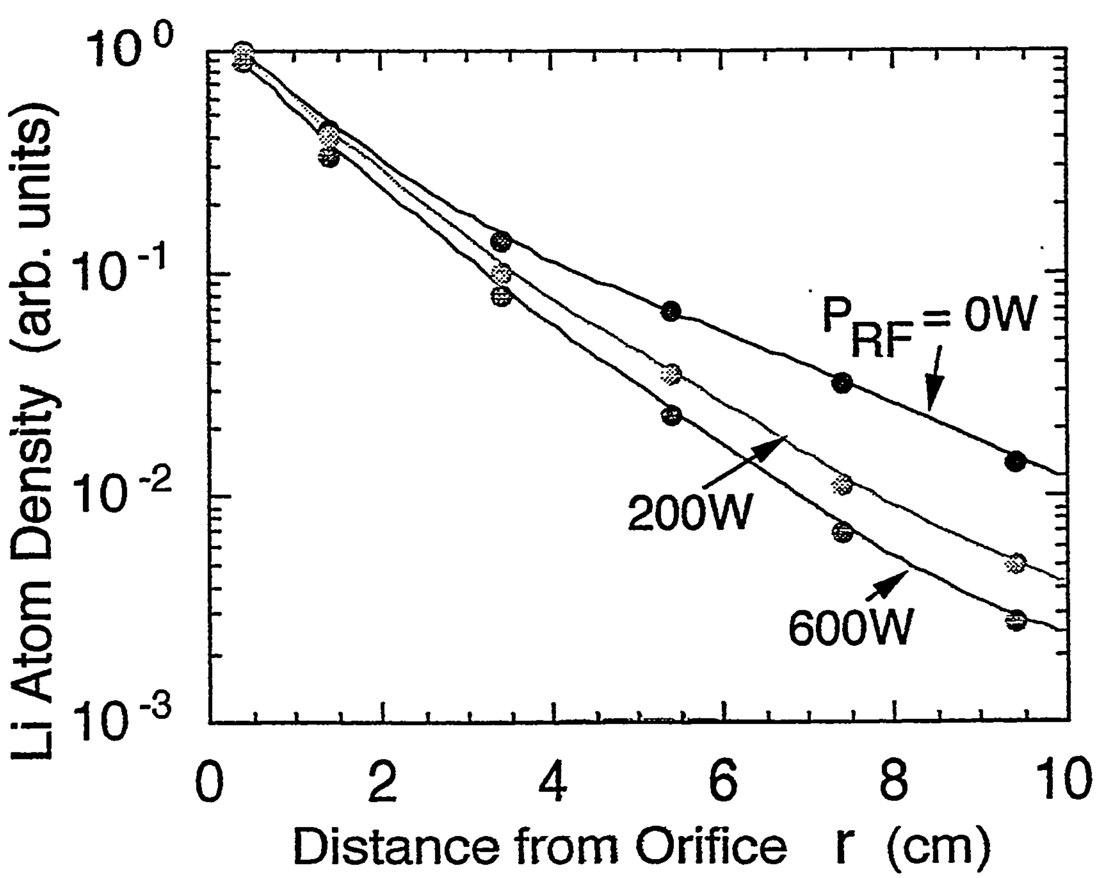

Strong decrease in high density plasma

Diffusion equation for lithium density

$$\frac{\partial N}{\partial t} - D\nabla^2 N = -\nu_I N$$

N ; Lithium density

ν_I ; Ionization frequency

Solution for a point source

$$\boxed{N = \frac{A}{r}\exp\left(-\sqrt{\frac{\nu_I}{D}}\,r\right)}$$

Decay length : $\lambda = \sqrt{\frac{D}{\nu_I}}$

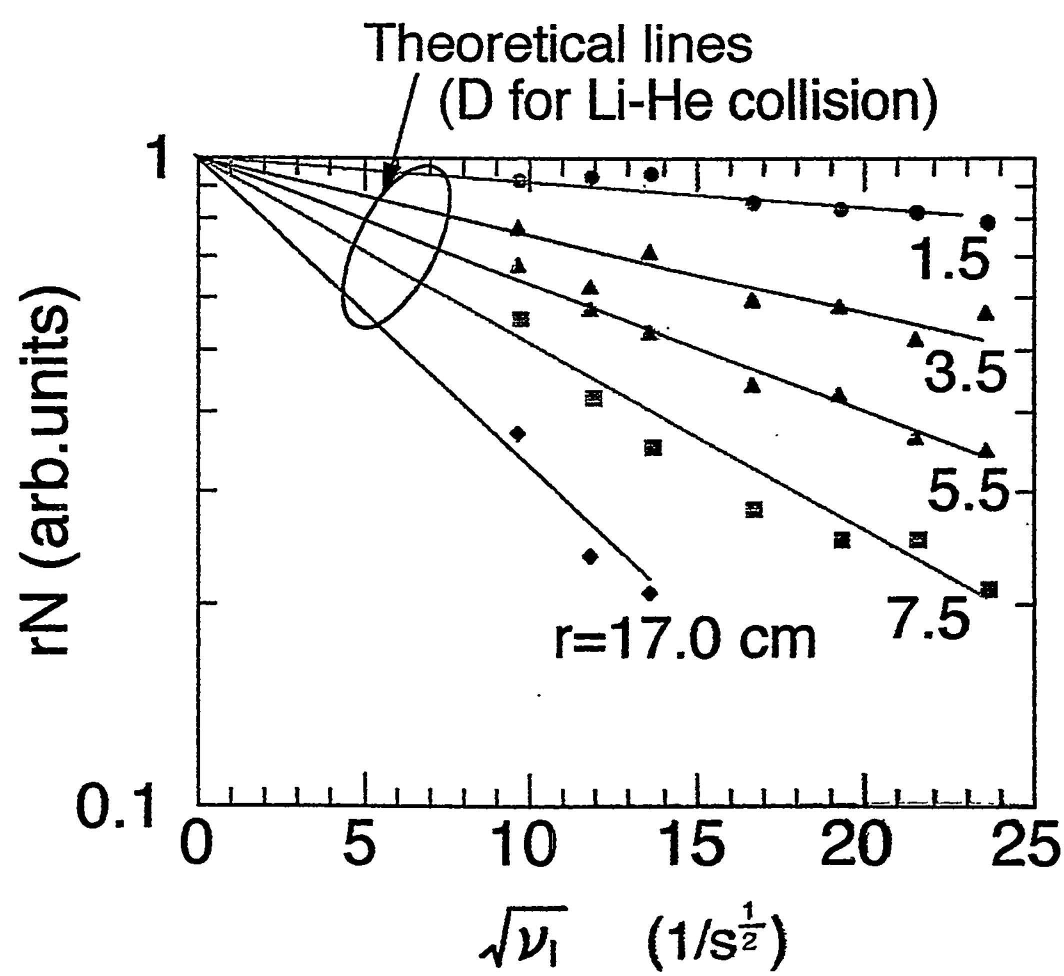

Experimental results are well explained by the equiation

Hydrogen Absorption/Desorption by Oxygen Contaminated Boron film

H. Eiki (Hokkaido University)
K. Tsuzuki (National Inst. Fusion Science)

- Hydrogen absorption is reduced by O contamination
- Temperature for Max. desorption is not changed

Impact of Oxygen on H-Behavior in B-film

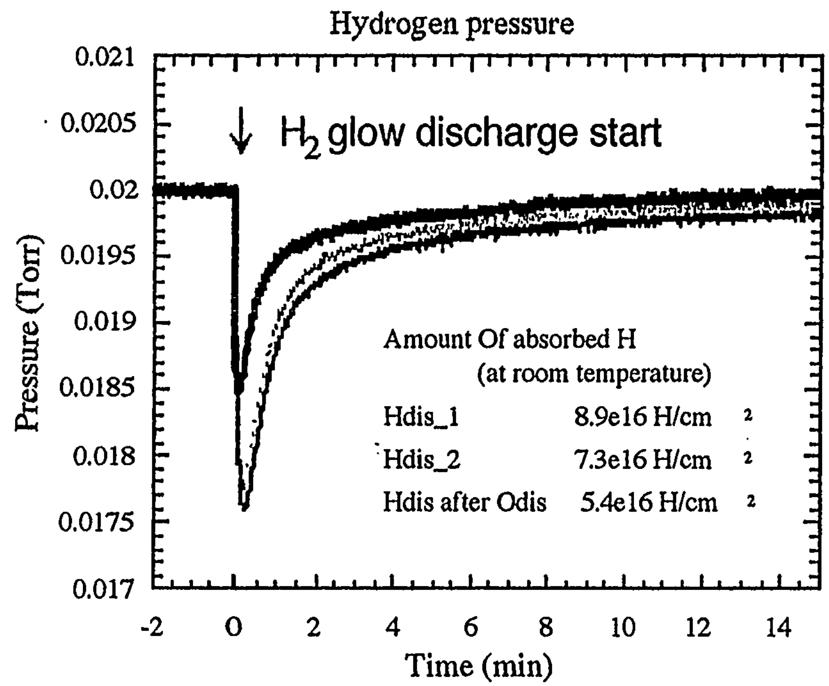

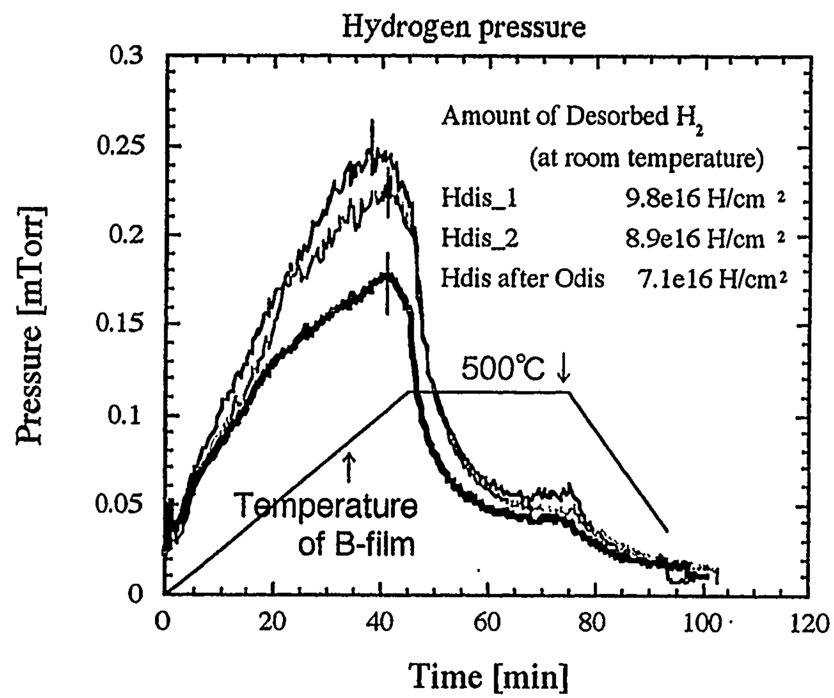

[Pure B film]

[Pure B film]

[B film fully implanted by oxygen (B/O=3/2)]

→ H absorption is reduced

→ peak temperature becomes higher ??

More precise investigation needed for O-contaminated B-films !!!

N. Noda

Joining of C/C Composite with Oxygen-Free Copper by Titanium Foil

Tatsuo OKU*, Yoshio IMAMURA*, Akira KURUMADA*, Kiyohiro KAWAMATA*, Nobuaki NODA**, Yusuke KUBOTA** and Osamu MOTOJIMA**

* Faculty of Engineering, Ibaraki University
(4-12-1, Nakanarusawa, Hitachi, Ibaraki, 316, Japan)
** National Institute for Fusion Science
(322-6, Oroshi, Toki, Gifu, 509-52, Japan)

Purpose

- Development of a joining material for LHD divertor
- Joining by titanium foil only

Joining material : ($10 \times 10 \times 40 mm^3$)
- CX-2002U (Rayon carbon fiber felt C/C composite)
- Oxygen-free copper
- Titanium foil (thickness : 50 μ m, purity : 99.6%)

Joining condition :
- Argon gas, no-pressure
- 10 minutes folding at 900~1000℃
  (heating rate : 40℃/min., cooling rate : 4℃/min.)

Tests :
- 4-point bending strength ($3 \times 4 \times 40 mm^3$, 10mm and 30mm spans)
- Continuous indentation test (Berkovich diamond indenter,
  load : 49mN, loading speed : 2.2mN/s, holding time : 5s)

  Parameter B : the slope at the maximum load point in load/depth versus depth curve for loading tests (proportional to hardness and strength)

  Parameter D : the slope at the maximum load point in load/depth versus depth curve for unloading tests (proportional to Young's modulus)
- Observation of the microstructure by SEM

Results :

- Success of joining above 900℃
  (eutectic alloy of Ti and Cu, formation of TiC)
- Bending strength was almost equal to that of C/C composite.
  (fractured in C/C composite)
- Joining area became widely with increase in joining temperature.
  (diffusion of Ti)
- Peaks of parameter B and D decreased with increase in joining temperature.
  (diffusion of Ti)
- Parameter B and D changed gradually at joining point.
  (good joining)
- Cracks were not observed in the joining area.
  (good joining)

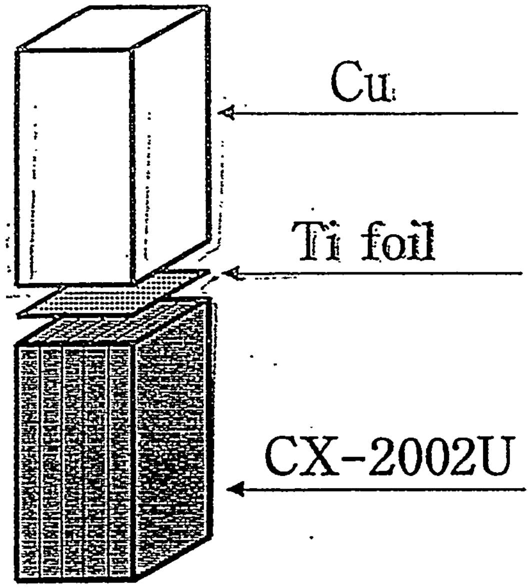

Fig. Test piece.

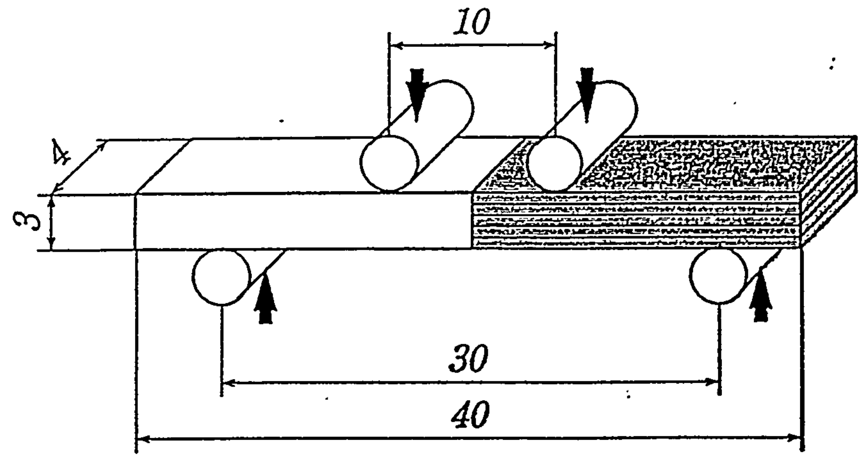

Fig. Bending test.

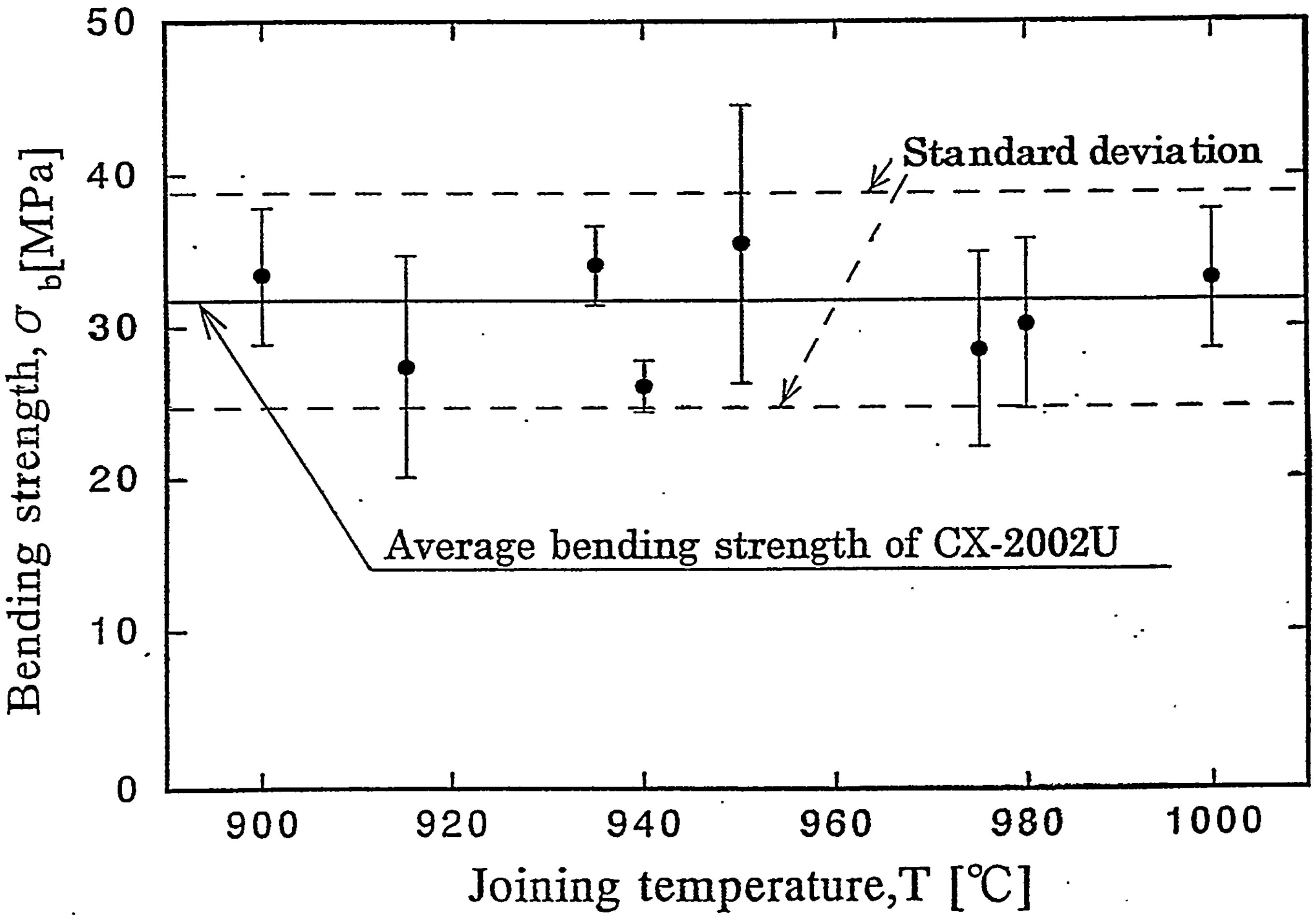

Fig. Relation between bending strength, σ_b and joining temperature,T.

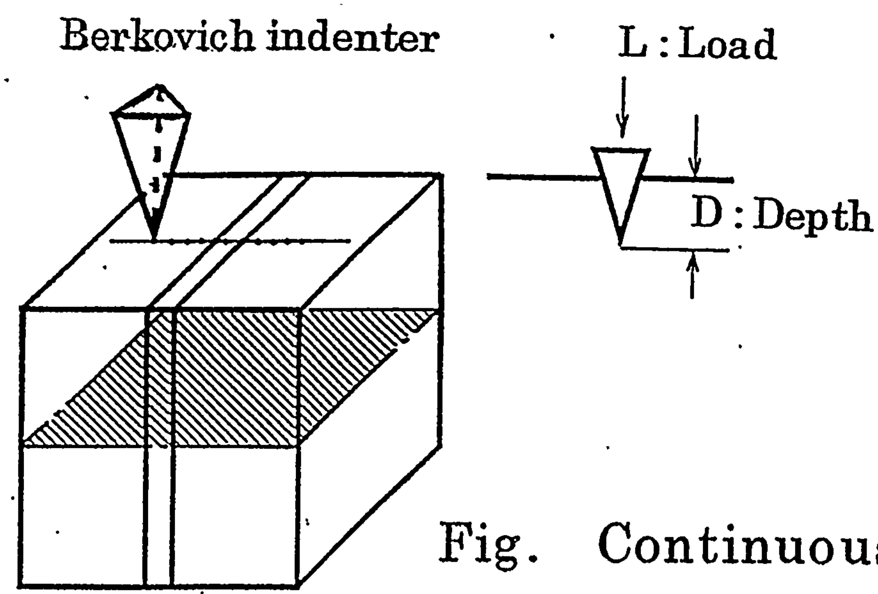

Fig. Continuous indentation test.

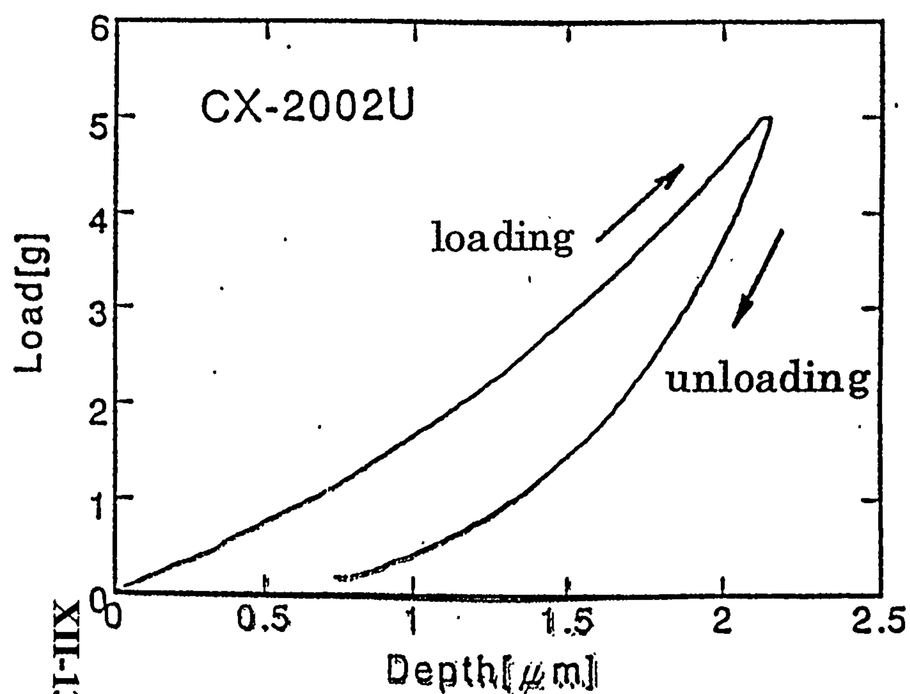

Fig. Load-Depth curve.

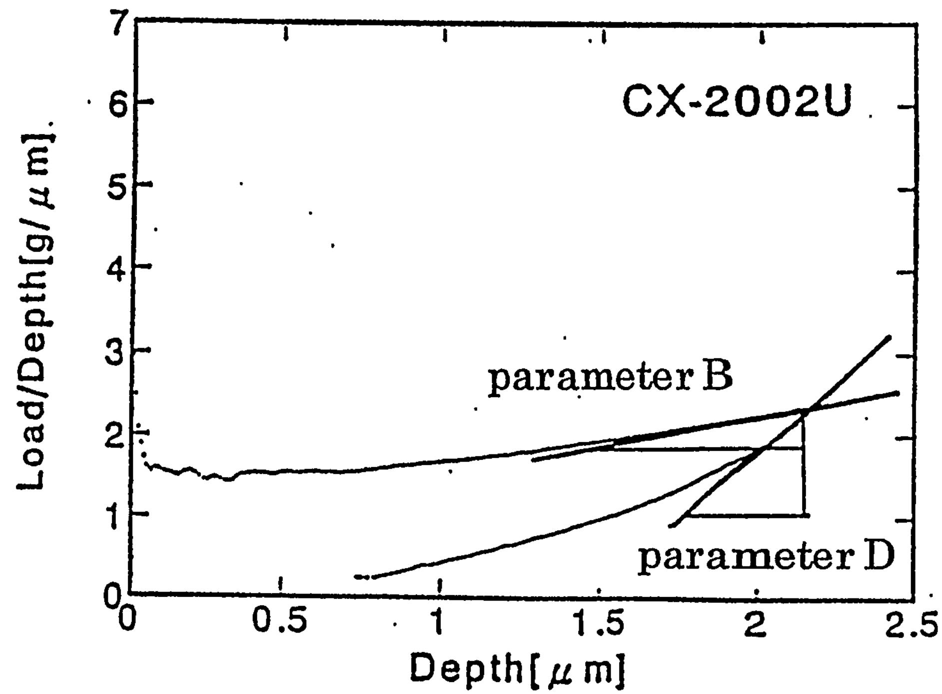

Fig. (Load/Depth)-Depth curve.

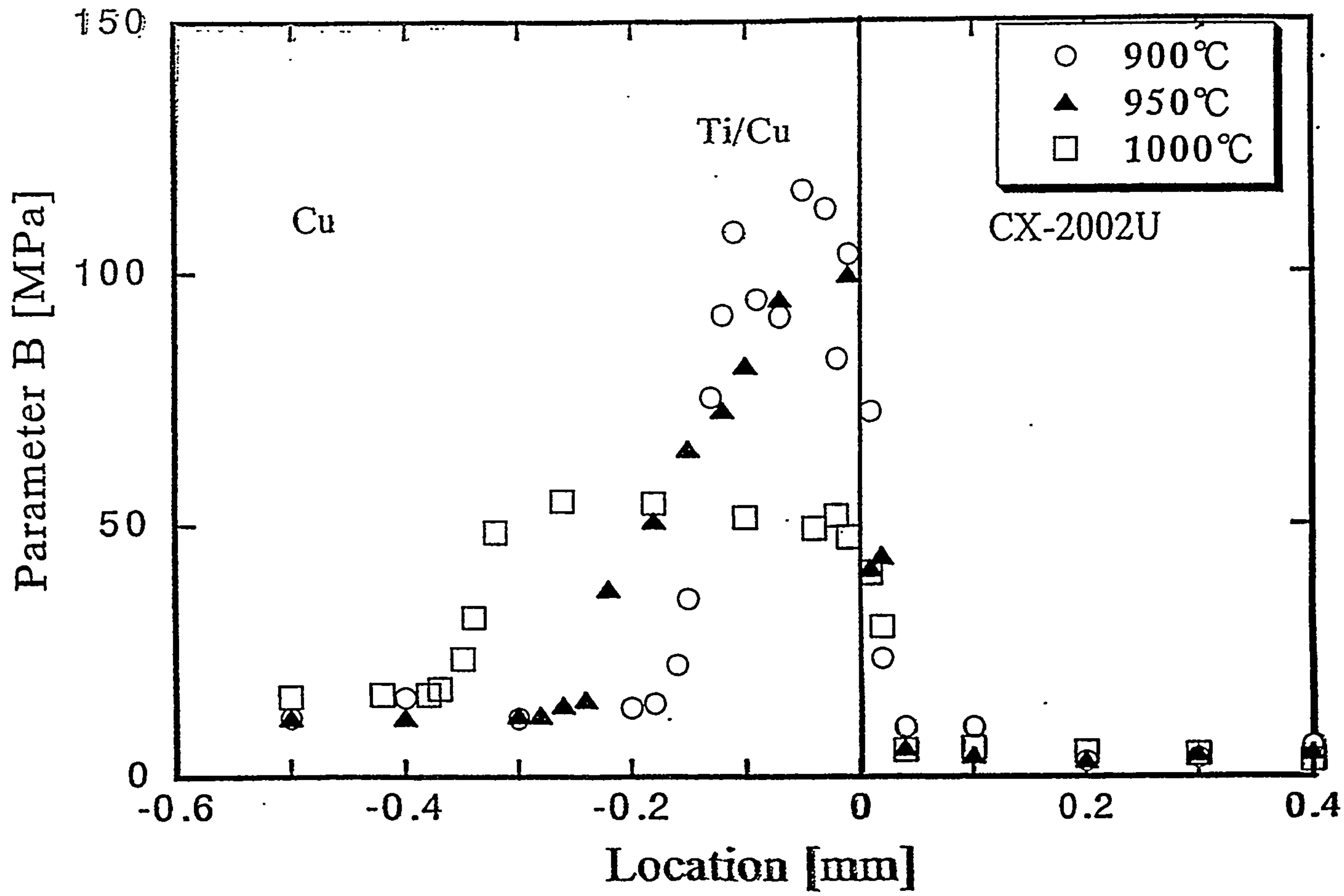

Fig. Distribution of parameter B.

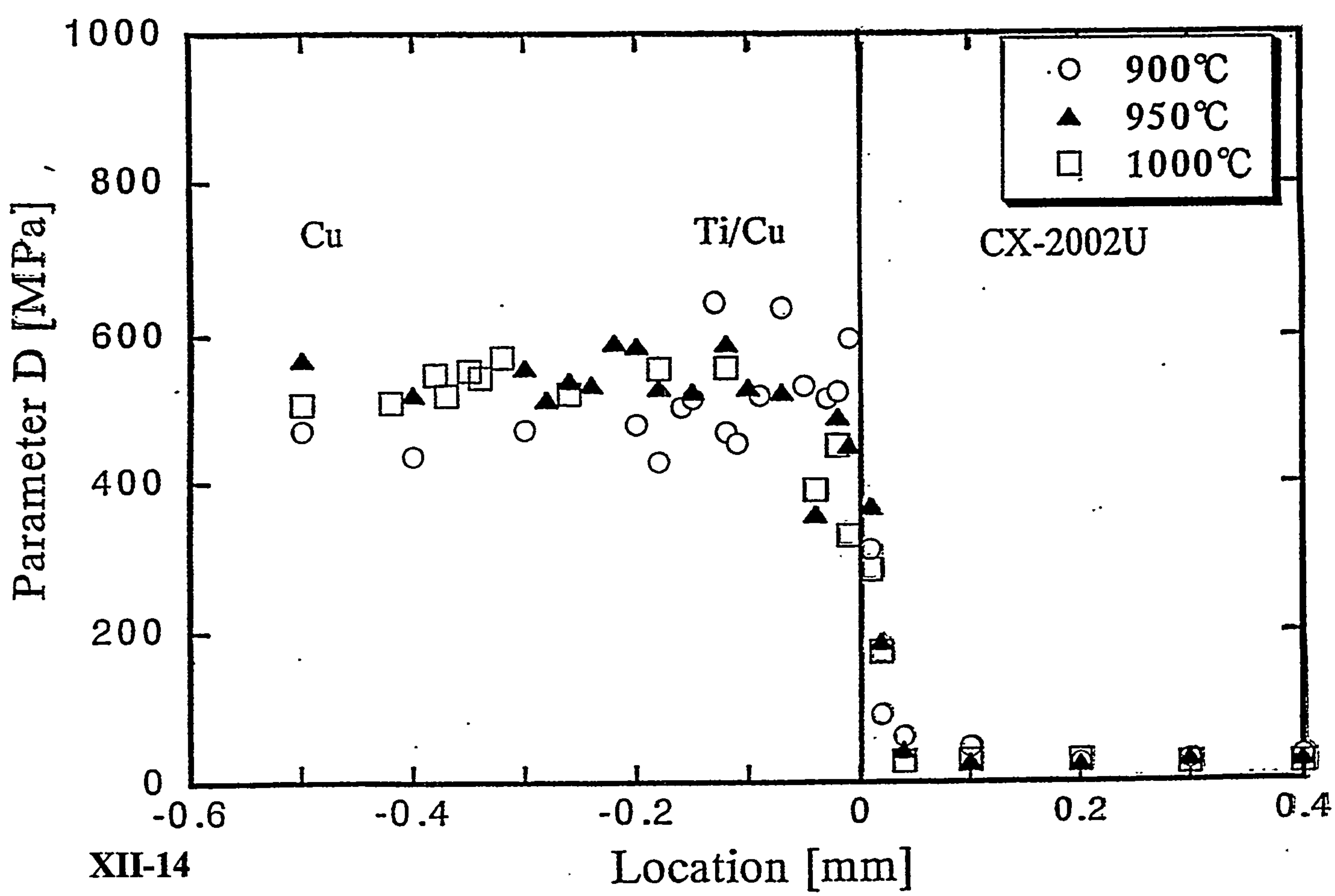

Fig. Distribution of parameter D.

joined at 900 ℃

CX-2002U

Ti+Cu

Cu

joined at 950 ℃

CX-2002U

Ti+Cu

Cu

joined at 1000 ℃

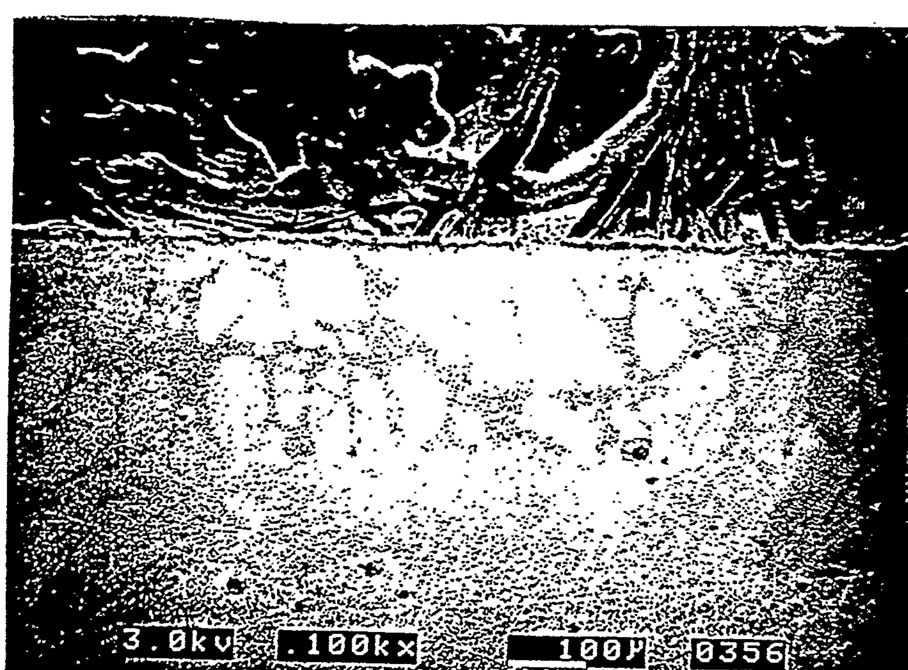

CX-2002U

Ti+Cu

Cu

Fig. Observations of microstructures of carbon/copper materials

Evaluation of High Z Metals

S. Yamazaki *(Kawasaki Heavy Industry Co.)*

Design Windows based on thermomechanical analyses are given.

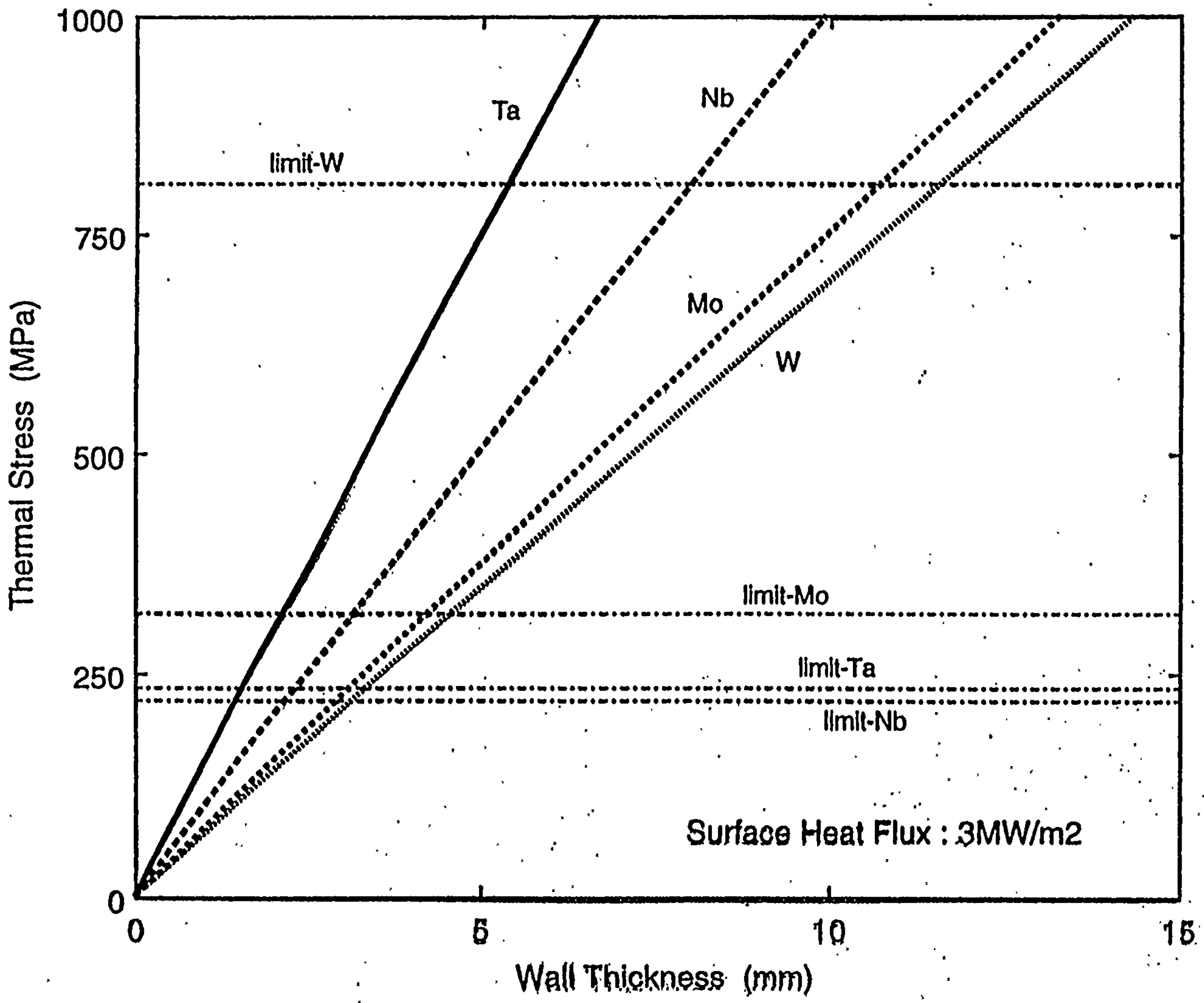

Fig. 3 Thermal Stresses of the Plasma Facing Wall of Various High-Z Materials Loaded to the Heat Flux of 3MW/m2.

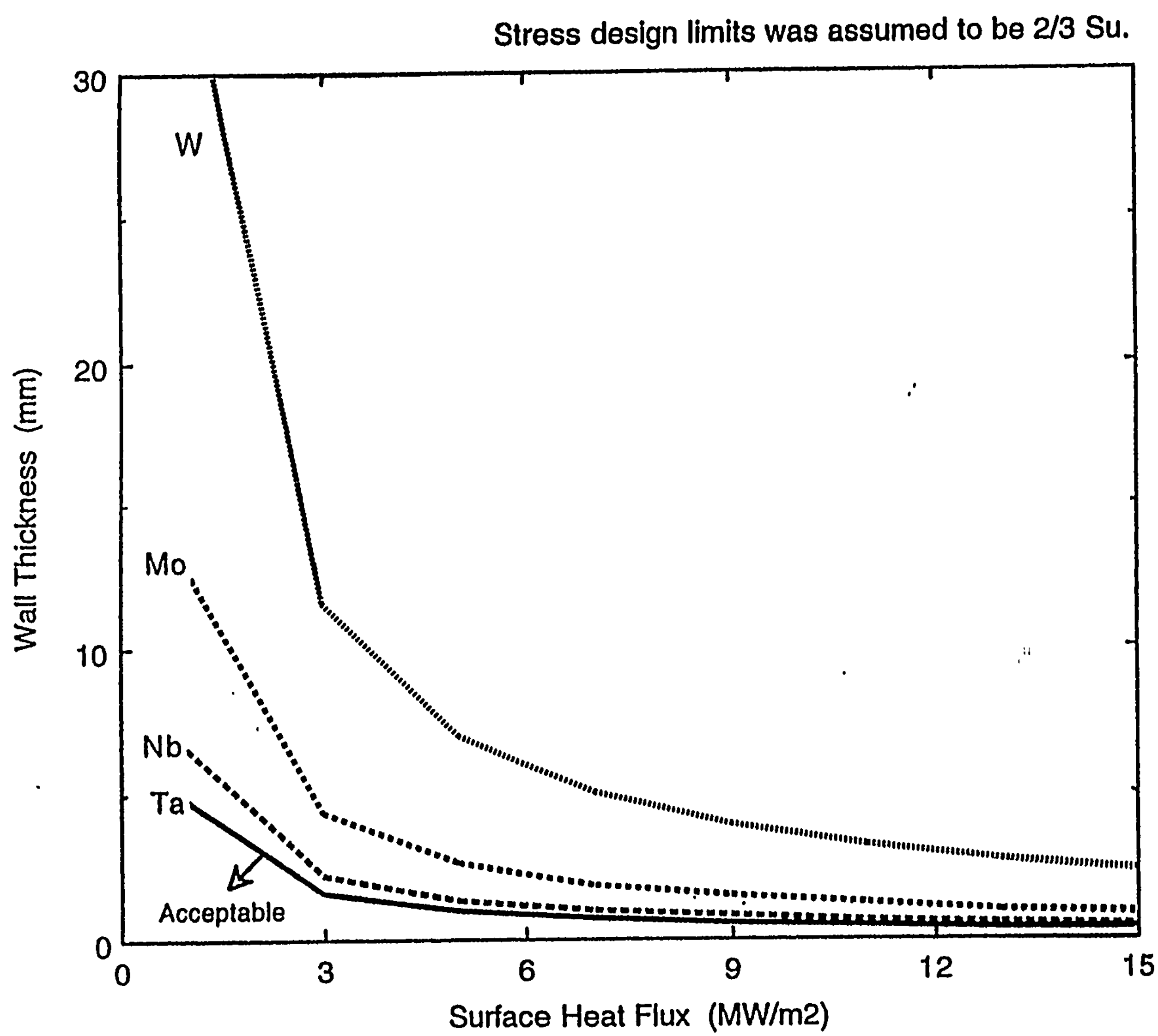

Fig. 5 Design Windows of the Plasma Facing Wall of Various High-Z Materials.

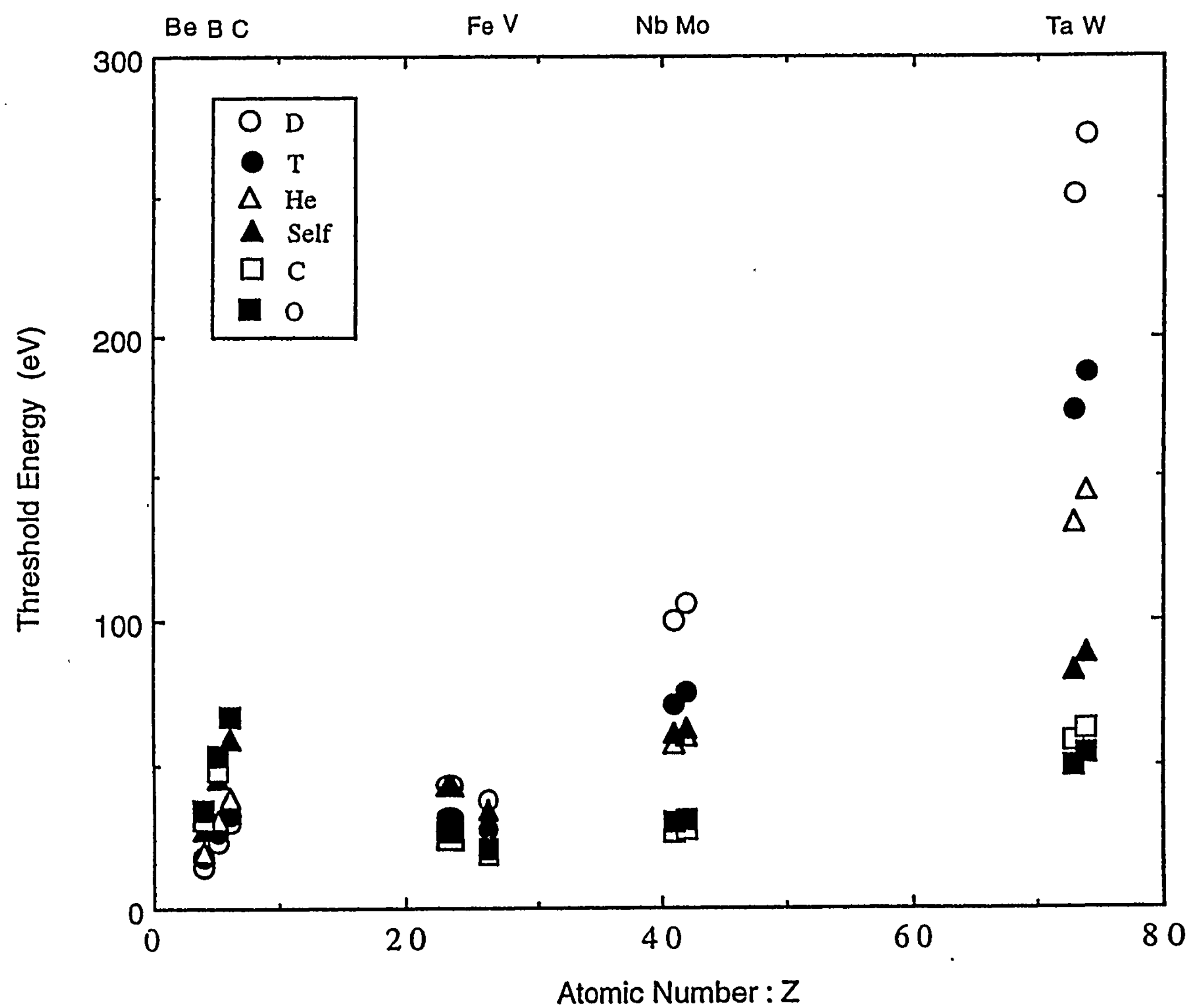

Fig. Threshold Energies of Physical Sputtering for Various Plasma Facing Materials.

SF 2712-SSC# (7-97)
Supersedes (3-97) issue

CERTIFICATION OF SYSTEM SANITIZATION/CLEARING

It is the responsibility of the person sending a computer system or component to Property Reapplication to ensure that all information is removed. In most cases, this consists of removing all information from the hard drive, if any, and any other disks being sent with the system.

If the computer (or disk) was ever used to process classified information, the discs must be degaussed. This is a process where a certified device uses an intense magnetic field to remove all information from the disk. Degaussing at SNL/NM can be performed in the Central Computing Facility in Building 880. Call Computer Operations at 844-5976 to schedule an appointment for degaussing..

If the computer (or disk) was used to process sensitive unclassified information (PRIVATE, UCAI, UCNI, OUO, etc.) the disk must be overwritten. A utility, such as Norton Utilities can be used to overwrite every location on the disk with a single character. Using delete, erase, and format commands does NOT meet the requirement, as these commands often leave the file data on disk where it can be "undeleted". If the disk is inoperable and cannot be overwritten it must be degaussed.

Even for those computers that have processed only non-sensitive unclassified information, the information must be overwritten. Therefore, these systems are cleared in the same way as sensitive unclassified systems.

Property Reapplication will not pick-up the system or disk until the required sanitization has been performed and this form has been certified. Users at SNL/NM who require assistance in sanitizing a system can contact a CSR/CSU via CCHD @ 845-2243. A case number is required.
At SNL/CA, users should call Albert James at 294-2508.

For additional questions, contact the Computer Security Department.

Control Number (from Pick-Up Request Form): ____________________

Property Number: ____________________

Vendor: ____________________ Model No.: ______________ Serial No.: ______________

Check the highest sensitivity level for which this system (or disk) has been used. Then check the box indicating how the information has been removed.

☐ Classified
- ☐ System contains no fixed drive.
- ☐ All disk drives have been degaussed.

☐ Sensitive Unclassified
- ☐ System contains no fixed drive.
- ☐ All disk drives have been degaussed.
- ☐ All disk drives have been wiped by Norton Utilities or equivalent.

☐ Non-Sensitive Unclassified
- ☐ System contains no fixed drive.
- ☐ All disk drives have been degaussed.
- ☐ All disk drives have been wiped by Norton Utilities or equivalent.

I certify that all information has been removed from this system (or disk) as described above.

____________________	____________________	__________
User (or System Administrator)	Signature	Date
____________________	____________________	__________
Computer Security Officer (CSR, CSSO, NSO, or CSU Rep.)	Signature	Date

Forschungszentrum Jülich

High heat flux testing of neutron irradiated divertor modules

R. Duwe, J. Linke, M. Rödig

Forschungszentrum Jülich, EURATOM Association, D-52425 Jülich, Germany

R. Nygren

Sandia National Laboratories Albuquerque, New Mexico 87185-1129, USA

US-Japan PMI / HHF Workshop
San Francisco, December 08 – 11, 1997

Conclusions

- Unirradiated CFC monoblock mock-ups have been tested at power densities up to 25 MWm^{-2}
- Neutron irradiation has been performed in the HFR Petten up to fluences of 0.3 dpa at 320 and 770°C.
- Irradiated CFC modules show a significant increase in surface temperature during electron beam loading. This effect is less distintive for samples irradiated at 770°C.

thermal cycling (see transparency)

- Similar tests with neutron irradiated beryllium mock-ups are in progess.

⇒ **Draft**

Testing of Actively Cooled High Heat Flux Mock-Ups

M. Rödig, R. Duwe, W. Kühnlein, J. Linke, M. Scheerer, I. Smid[a], B. Wiechers

Forschungszentrum Jülich, EURATOM Association, D-52425 Jülich, Germany
a) Forschungszentrum Seibersdorf, A-2444 Seibersdorf, Austria

Abstract

Several un-irradiated CFC monoblock mock-ups have been loaded in thermal fatigue tests up to 1000 cycles at power densities < 25 MW/m^2. No indication of failure was observed for these loading conditions. Two of the mock-ups were inspected by ultrasonic methods before thermal cycling. It could be proved that the voids found in the post-mortem metallography existed before and had no effect on the integrity of the mock-up.

For the first time, neutron-irradiated CFC monoblock mock-ups have been tested in the electron beam facility JUDITH. These mock-ups had been irradiated before in the High Flux Reactor at Petten up to 0.3 dpa at 320 and 770 °C. All samples showed a significant increase of surface temperature, due to the irradiation induced decrease in thermal conductivity of the CFC materials.

Keywords

carbon and carbon materials (C01), divertor materials (D06), electron irradiation (E02), high heat flux materials (H03), joining (J01), neutron irradiation (N01)

1. Introduction

High heat flux components of ITER will be exposed to heat loads of up to 5 MW/m^2 under normal and 20 MW/m^2 under transient conditions. In order to remove these high heat loads, tiles of a plasma compatible armour material must be attached to a water-cooled heat sink. Candidates for plasma facing materials are beryllium, tungsten and carbon reinforced carbon materials (CFCs). Heat sink materials are copper alloys and, as a back-up, molybdenum alloys. Several joining processes have been developed for the attachment of the plasma facing materials to the heat sinks. In order to assess these bonds, high heat flux tests with actively cooled mock-ups have been carried out in the electron beam facility JUDITH. The results for beryllium – copper modules have been reported elsewhere [1, 2]; this paper deals with the high heat flux performance of CFC monoblock modules.

In former experiments, only un-irradiated mock-ups have been tested. But during the operation of ITER, the first wall and divertor components will be affected by 14 MeV-neutrons. In order to study the degradation of material properties under neutron irradiation, the irradiation experiment PARIDE has been performed in the High Flux Reactor (HFR) at Petten, The Netherlands. First mock-ups from this irradiation experiment have been tested under screening and thermal fatigue conditions in JUDITH.

2. Experimental Details

2.1 Samples

Fig. 1 shows the drawing of the CFC monoblocks. Three different CFC armour materials were used: Dunlop Concept 1, SEPcarb N31 and SEPcarb N112. Heat sink tubes were made from Glidcop Al25, CuCrZr and Mo5Re. All samples were produced by Plansee AG by active metal casting (AMC®). After drilling, the CFC tiles were coated with liquid copper at 1250°C; Ti additives were used as carbide formers. Then the tubes made from the two copper alloys were brazed in by means of pure titanium [3]. The Mo5Re tubes were joint in one step with the the AMC.

2.2 Test Facility

The electron beam facility JUDITH in general was described in [4]. It consists of an electron gun of 60 kW electric power and a number of powerful diagnostic devices. The heating of the mock-ups is performed by sweeping of a focussed electron beam (≈ 1 mm ∅) over the sample surface at high frequencies up to 100 kHz. During the thermal heating tests, the heat sink tubes are water-cooled (water pressure: 40 bars, flow rate: 50 l/min). A swirl is mounted inside the tube to avoid burn-out. The following diagnostics have been used in the tests reported in this paper:

- infra-red camera system (RT ... 3000°C),
- one-color pyrometer (200 ... 1100°C),
- two-color pyrometers (550 ... 1600°C and 1000 ... 3500 °C),
- video camera,
- thermo-couples,
- instrumented cooling loop (flow rate, in/outlet temperature).

For the investigation of neutron-irradiated samples, some modification to former testing procedures were required. These modifications concerned on one hand the samples and on the other hand the testing facility.

Due to the limited space in the neutron irradiation rig, the samples had to be miniaturized. Therefore the length of the cooling tubes exceeded the length of the CFC tiles only by 5 mm on each side of the module. This was not sufficient for commercial squeezing or flange connectors, and a special clamping mechanism was developed. For installing, the radioactive samples are placed on a small tray which is transported to the clamping mechanism by manipulator. When the sample is in the correct position, the water connectors are clamped to the sample. This is performed by a motor while the force is controlled by a load cell. Sealing is achieved by special sealing adapters machined from soft copper in combination with O-ring sealings and springs. The whole clamping system is attached to the door of the vacuum chamber of JUDITH. Once the sample has been installed, the door is closed and the sample is in the correct shooting position.

For better comparison, the samples in the pre-irradiation reference tests were designed identically to those of the post-irradiation experiments.

2.3 Evaluation of Data

The power absorbed by the mock-up during high heat flux loading P_{abs} can be calculated directly from the increase of cooling water temperature. If the absorbed power is compared to the incident electrical power, an absorption coefficient of 80 to 85% is found for CFC monoblock modules.

Therefore the absorbed power can be measured rather exactly, but the definition of power density is more complicated. During the heat loading, the area covered by the electron beam is a little smaller than the total surface. If the power density is calculated, the value depends strongly on the assumed loading area (heated area or total surface area). For the assessment of the joints, a power density which refers to the total surface area D_t is thought to be more suitable and the corresponding numbers are used in the following.

2.4 Neutron Irradiation Experiment PARIDE

The neutron irradiation experiment was performed in the High Flux Reactor in Petten. More than 600 samples of beryllium, CFC and tungsten alloys have been irradiated in this campaign. Nominal loading conditions were 0.5 dpa at 350°C and 700°C respectively. The actual irradiation condition differed more or less from these nominal values according to the position of samples in the reactor. For the CFC monoblock mock-ups which are discussed in this paper, the following irradiation conditions must be assumed:

- 320°C, 0.34 dpa (according to = 0.33 x 10^{25} m^{-2}, E>0.1 MeV), 49.6 full power days,

- 770°C, 0.35 dpa (according to = 0.37 x 10^{25} m^{-2}, E>0.1 MeV), 23.7 full power days.

3. Results

3.1 Testing of Un-Irradiated Mock-Ups

Three CFC monoblock mock-ups several times have been exposed to 1000 heating cycles (10 s heating, 10 s cooling) at different power densities. Aim of these tests was on one hand to study the heat removal efficiency of the different variants and on the other hand their performance under thermal cycling conditions as they are expected in the operation of ITER. The tested materials combinations and power densities D_t were:

- SEPcarb N31/ Glidcop: 7, 18 MW/m^2
- Dunlop Concept 1/ Glidcop: 7, 15, 19 MW/m^2
- Dunlop Concept 1/ CuCrZr: 7, 15, 24 MW/m^2

A more detailed description of the loading conditions is given in [5].

The surface temperature measured by means of the infra-red camera showed strong fluctuations. Normally (e.g. in the case of Be/ Cu mock-ups) this is an indication of a bad braze connection. But here strong fluctuations in the thermal conductivity of the CFC materials are responsible for this behaviour [6]. Such fluctuations lead to differences of the surface temperature of up to 200° C. In spite of this non-uniformity, the thermal fatigue behaviour of the three mock-ups was excellent. Each of the modules was loaded several times up to 1000 heating cycles at different power densities, but no failure or degradation was observed. The distribution of surface temperatures measured by the infra-red camera stayed stable during all tests, this is an indication that no failure occurred during the tests.

In the post-mortem metallography of the first mock-up (SEPcarb N31/ Glidcop), small voids up to 1 mm approx. were observed in the braze layer. It was assumed that these voids were generated during the production process. In order to clarify this topic, the two other mock-ups were inspected by ultra-sonic methods before they were loaded with the last 1000 heating cycles at the highest power densities. Fig. 2 compares the result of this ultra-sonic inspection with the post-mortem metallography (mock-up Dunlop Concept 1/ Glidcop). This ultrasonic inspection is performed with a transducer inside the copper tube. The left picture shows the two dimensional map of the intensity of reflection. Areas with a high reflectance (red) are a sign for pores, voids or detachments. By comparison of these areas with the post-mortem metallography (right picture) it becomes clear that the voids in the braze at angular positions of 210° and 310° existed before the fatigue loadings. Nevertheless, they were stable during the thermal fatigue loading.

3.2 Post-Irradiation Testing

After neutron-irradiation, most of the mock-ups were optically in a good condition. In the screening tests, one mock-up showed over-heating during loading by the electron beam (SEPcarb N31/ Glidcop T_{irr} = 350°C. But it cannot be proven that this fault was due to the neutron irradiation.

Only a limited number of mock-ups was pre-tested in screening experiments before they were irradiated in the fission reactor (mock-ups with Mo5Re heat sink tubes). The other irradiated mock-ups have to be compared with identical reference samples of the same materials combination (modules with Cu tubes).

Mock-ups with Mo5Re tubes

Identical monoblock mock-ups with Mo5Re heat sink tubes were compared in the electron beam facility at constant power densities before and after neutron-irradiation (T_{irr} = 770°C). Fig. 3 gives an example for such a comparison for a mock-up made from Dunlop Concept 1. The distribution of surface temperatures measured by the infra-red camera did not change after neutron irradiation, but the surface temperature increased significantly. In fig. 4 for three mock-ups with different CFC armor the surface temperatures (measured by pyrometer) are plotted versus the absorbed power density. In all cases a significant increase of temperature after exposure to neutrons is observed. This is due to a decrease in thermal conductivity which was reported before for the CFC material SEPcarb N112 [7], and which is expected for the other CFC materials too [8]. The exact values of thermal conductivity will be available later from samples which had been included in the irradiation experiment PARIDE.

Dunlop Concept 1 which before irradiation had the best thermal conductivity of all three CFCs, was more influenced by the neutron irradiation than SEPcarb N31 and shows a higher increase of surface temperature than the latter. SEPcarb N112 shows the lowest thermal conductivity of the three CFCs before and after neutron irradiation.

Mock-ups with copper tubes

In a second test series, CFC monoblock mock-ups with copper heat sink tubes were loaded under screening conditions (steady state) from the top (12 mm CFC) and from the bottom (6 mm CFC) side. The tests were limited to surface temperatures below 2200°C, according to power densities of 10 and 15 MW/m^2 approximately. After screening, all samples were loaded by 100 heating cycles at power densities between 8 and 15 MW/m^2 and one sample (Dunlop Concept 1/ Glidcop) up to 1000 cycles at 15 MW/m^2. None of these samples showed failure or any instabilities.

Due to the better annealing effects of irradiation damages with increasing temperature, the decrease of thermal conductivity for the samples irradiated at 770 °C was found to be less distinctive. This is shown in fig. 5 for the materials combination Dunlop Concept 1/ Glidcop.

Summary

No indication of failure was observed for CFC monoblock mock-ups loaded under thermal fatigue condition up to 1000 cycles at power densities ≤ 25 MW/m². Two of the mock-ups were inspected by ultra-sonic methods before the last campaign of thermal cycling. It could be proved that the voids found in the post-mortem metallography existed before and had no effect on the integrity of the mock-up.

First neutron-irradiated CFC monoblocks have been tested in the electron beam facility JUDITH. These mock-ups had been irradiated in the High Flux Reactor in Petten up to 0.3 dpa at 320 and 770 °C. All samples showed a significant increase of surface temperature, due to the decrease in thermal conductivity of the CFC materials. This effect is less distinctive for those samples irradiated at the higher temperature of 770°C. During short thermal fatigue tests (100 cycles at 8 to 15 MW/m²) no failure or instability occurred at any of the mock-ups.

Acknowledgements

The authors would like to acknowledge the help of F. Meuser in the preparation of the neutron-irradiation experiment. H. Klöcker and H. Münstermann assisted in the electron beam experiments. In addition V. Gutzeit and H. Hoven assisted in the metallographic examination.

References

[1] M. Rödig, R. Duwe, J. Linke, A. Schuster, B. Wiechers, 3rd IEA International Workshop on Beryllium Technology for Fusion, Mito City (Japan), Oct. 22-24, 1997

[2] M. Rödig, R. Duwe, J. Linke, A. Schuster, Fusion Engineering and Design, 37(1997), p. 317-334

[3] G. Vieider et al., 19th Symposium on Fusion Technology (SOFT), Lisbon (Portugal), Sept. 16-20, 1996

[4] R. Duwe, W. Kühnlein, H. Münstermann, 18th Symposium on Fusion Technology (SOFT), Karlsruhe (Germany), Oct. 22.-26, 1994

[5] M. Rödig et al, 4th International Symposium on Nuclear Fusion Technology (ISFNT-4), Tokyo, April 06-11, 1997

[6] M. Rödig, R. Duwe, A. Gervash, J. Linke, A. Schuster, Physica Scripta Vol. T64, 60 – 66, 1996

[7] D. Moulinier: "Evolution des proprietes thermiques des materiaux composites carbone-carbone sous irradiation neutronique", Ph.D. thesis Conservatoire National des Arts et Metiers, Paris 1996

[8] V. Barabash et al., this conference

Figure captions

Fig. 1: Drawing of CFC monoblock mock-up

Fig. 2: Comparison of ultrasonic inspection (left) and post mortem metallography (right)

Fig. 3: Infra-red image of a monoblock mock-up made from Dunlop Concept 1 and Mo5Re, power density D_t = 2 MW/m^2

Fig. 4: Surface temperature during electron beam loading before and after neutron irradiation for three CFC materials brazed to Mo5Re tubes.

Fig. 5: Surface temperature during electron beam loading for three CFC mockups (unirradiated, T_{irr} = 350 °C and T_{irr} = 700°C)

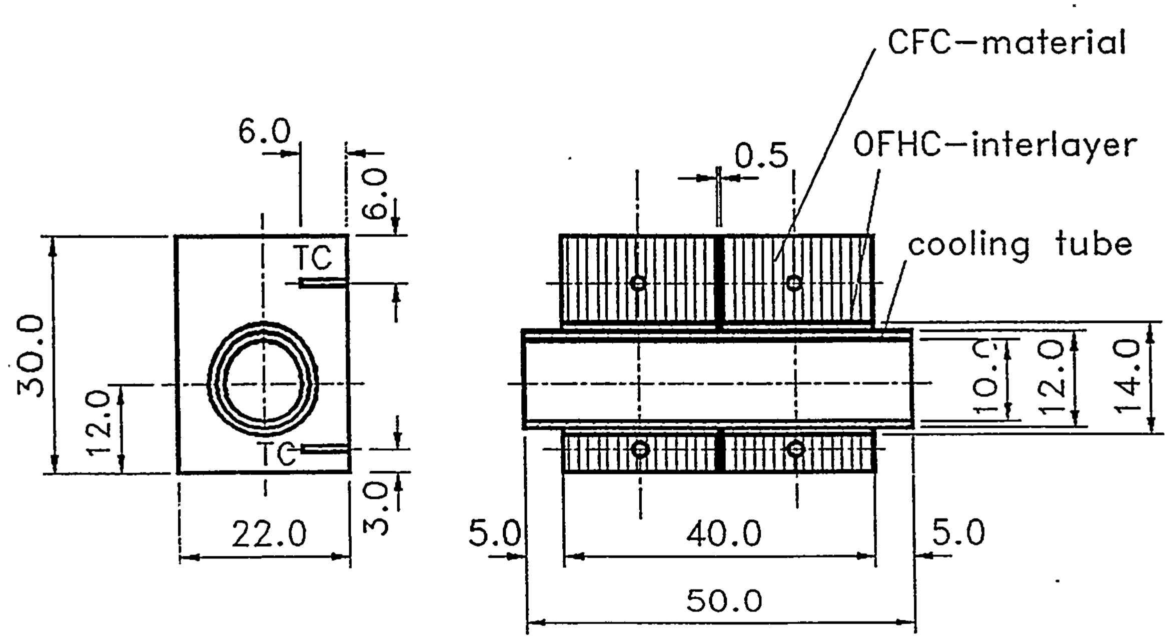

Fig. 1

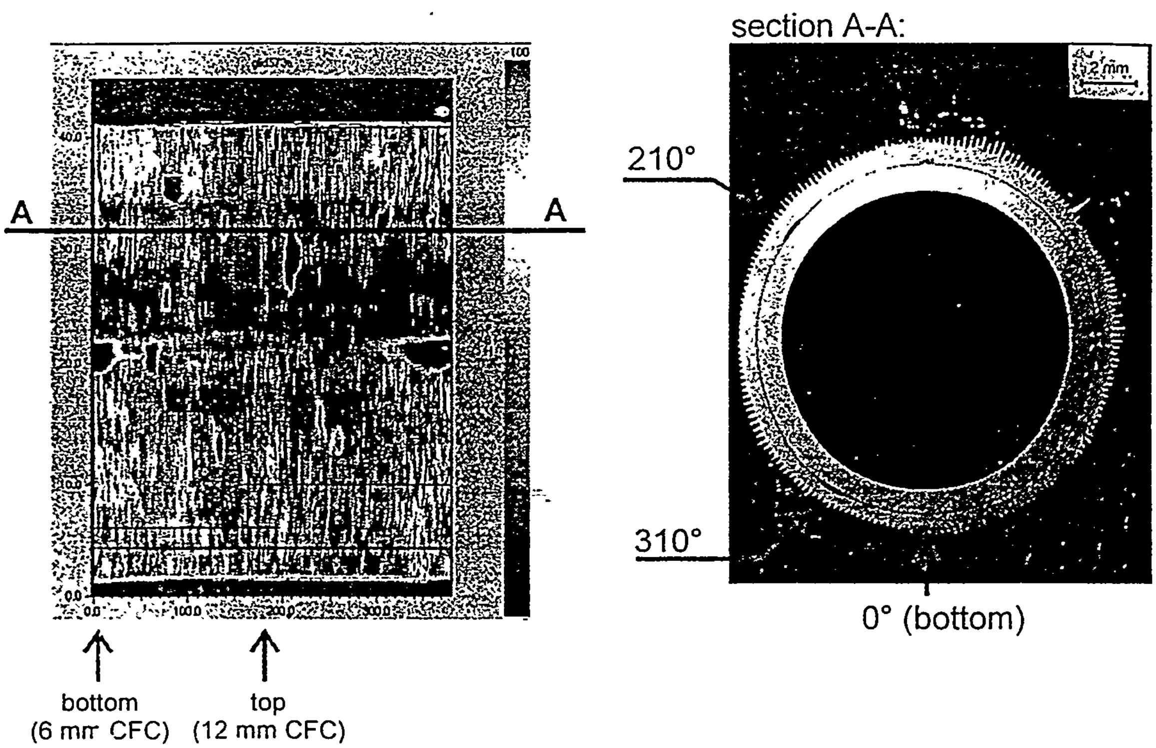
A
A
section A-A:
2 mm
210°
310°
0° (bottom)
bottom
(6 mm CFC)
top
(12 mm CFC)

Fig. 2

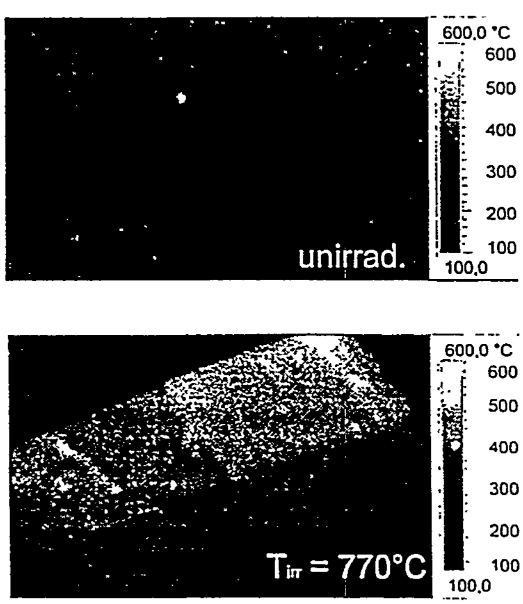
600,0 °C
600
500
400
300
200
100
100,0
unirrad.
600,0 °C
600
500
400
300
200
100
100,0
T_{irr} = 770°C

Fig. 3

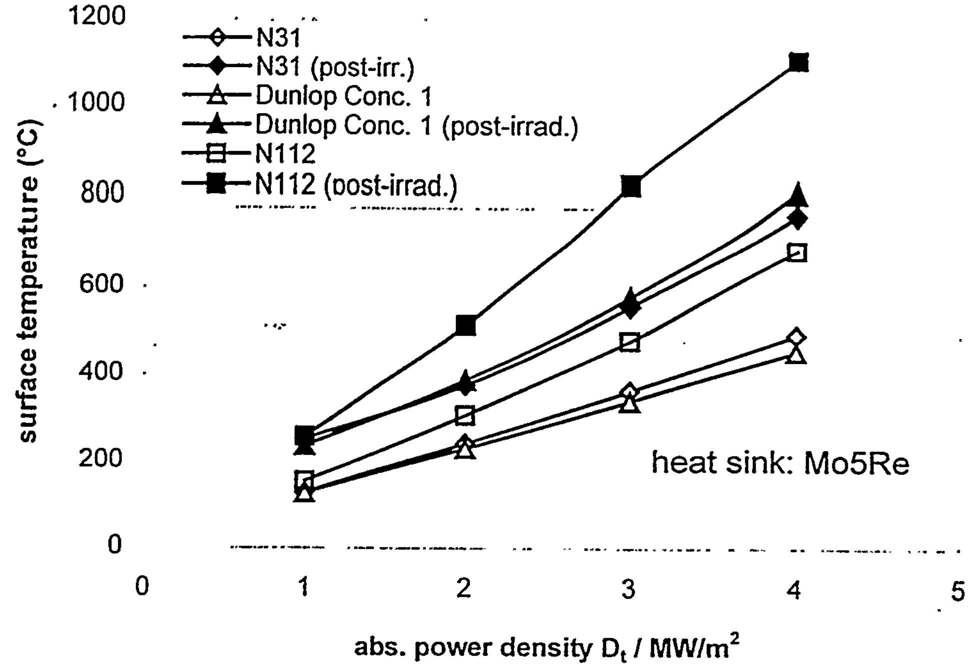

1200
1000
800
600
400
200
0
0
1
2
3
4
5
surface temperature (°C)
abs. power density D_t / MW/m^2
N31
N31 (post-irr.)
Dunlop Conc. 1
Dunlop Conc. 1 (post-irrad.)
N112
N112 (post-irrad.)
heat sink: Mo5Re

Fig. 4

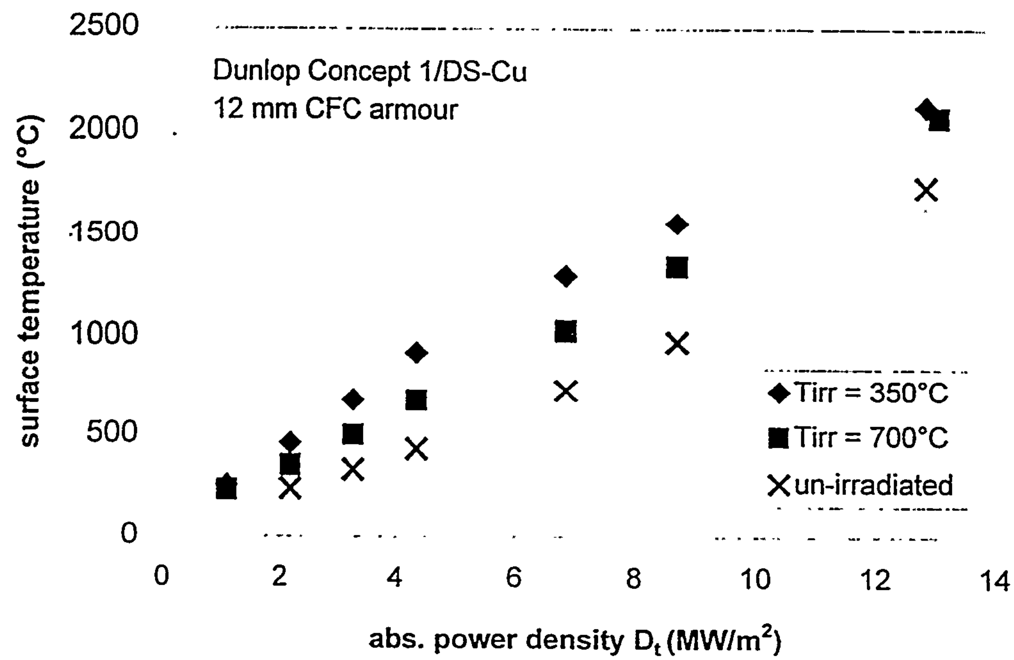

2500
2000
1500
1000
500
0
0
2
4
6
8
10
12
14
surface temperature (°C)
abs. power density D_t (MW/m^2)
Dunlop Concept 1/DS-Cu
12 mm CFC armour
Tirr = 350°C
Tirr = 700°C
un-irradiated

Fig. 5

Summary Session

{Verbal Discussions}

[page intentionally left blank]

Appendix A

Workshop Agenda

Agenda: US-Japan Workshop (97FT5-06) on
High Heat Flux Components & Plasma Surface Interactions for Next Fusion Devices
December 8-11, 1997 12/1/1997

Warwick Regis Hotel
490 Geary St., San Francisco
800-827-3447, 415-928-7900, fax 415-441-8788

December 8 (Mon.)

9:00	Opening Remarks (20)	R. Nygren (Sandia), S. Berk (DOE), N. Noda (NIFS), K. Wilson (Sandia)
Session I : activities in present and near term devices		*O. Motojima & S. Berk*
9:20	Present status of LHD (30)	O. Motojima (NIFS)
9:50	Divertor, first wall and PSI issues in LHD (30)	N. Noda (NIFS)
10:20	Status of NSTX and PSI issues (25)	M. Peng (PPPL)
10:45	*coffee break*	
11:00	Design & initial operation of W-shaped divertor in JT-60U (30)	K. Masaki (JAERI)
11:30	Progress in DIII-D (25)	C. Wong (GA)
11:55	Highlights and plans for C-MOD (20)	MIT/Nygren (Sandia)
12:15	*announcements and lunch*	
Session II : PFC Development for near term devices		*K. Nakamura & C. Wong*
14:00	Utilization of high Z materials as PFCs (30)	T. Tanabe (Nagoya U.)
14:30	Develoment of W brush armor (20)	G. Wille (Boeing)
14:50	Development of high heat flux components at JAERI (30)	K. Nakamura (JAERI)
15:20	*coffee break*	
15:40	Be-Cu Joining (20)	C. Cadden (Sandia)
16:00	Problems and evaluation of plasma facing materials (30)	N. Yoshida (Kyushu U.)
Special Session III : Historical Progress in PSI Studies		*N. Noda & K. Wilson*
16:30	Small personal history on plasma surface interactions	T. Yamashina (Hokkaido U.)
17:00	*adjourn until reception*	
19:00	*Reception*	

The reception, hosted by Sandia National Laboratories and the US Department of Energy, will be held in the reception area at one end of the main dining room adjacent to the restaurant on the first floor of the Warwick Regis Hotel.

US-Japan Workshop Agenda continued

December 9 (Tue.)

Session IV: wall conditioning, sputtering, erosion		*T. Tanabe & Y. Hirooka*
8:30	Wall conditioning at the start up phase of LHD (30)	A. Sagara (NIFS)
9:00	RF wall contioning (20)	D. Cowgill (Sandia)
9:20	Erosion/redeposition of high-Z materials in a linear divertor simulator (30)	N. Ohno (Nagoya U.)
9:50	Erosion and impurity effects on PFC materials in PISCES-B (20)	R. Doerner (UCSD)
10:10	Recent erosion/redeposition analysis (15)	Sze/Brooks (ANL)
10:25	*coffee break*	
10:45	Dependence of graphite erosion yield on irradiation flux close to actual edge plasma condition (30)	Y. Ueda (Osaka U.)
11:15	DiMES experiments (20)	D. Whyte (GA)
11:35	Reflected neutral particle spectra on MAP (30)	S. Ohtsu, K. Kobayashi, S. Tanaka (U. Tokyo)
12:05	*lunch*	
Session V: Plasma Studies		*S. Luckhardt*
13:40	Effects of turbulent fluctuations on boundary ion temperatures in PISCES (20)	S. Luckhardt (UCSD)
14:00	TFTR Experiments with Li (15)	C. Skinner (PPPL)
14:15	Deposition of Li on a probe in TFTR (15)	Y. Hirooka (UCSD)
Session VI: Development Issues for Near Term PFCs		*A. Sagara & C. Wong*
14:30	Discussion, development issues for near term PFCs	A. Sagara & C. Wong
15:30	*coffee break*	
Session VII: PFM issues and development		*N. Yoshida & R. Causey*
15:45	W/Cu layers resistant to erosion and tritium permeation (30)	M. Shibui (Toshiba)
16:15	Review of recent work on removing tritium from PFCs (25)	C. Skinner (PPPL)
16:40	Chemical compatibility of C with Be (30)	:. Ashida & K. Watanabe (Toyama U.)
17:10	Tritium retention in Be (20)	R. Causey (Sandia)
17:30	Modeling of H isotope retention/release in PFC materials (15)	A. Grossman (UCSD)
17:45	*adjourn*	

Dinner arrangements on Tuesday and Wednesday evenings can be made during the day at the workshop if participants wish to dine together in groups for work or pleasure. San Francisco has many fine restaurants and a list of nearby restaurants is included with the workshop materials.

December 10 (Wed.)

Session VIII: First Wall Development		*M. Tillack & N. Noda*
8:30	HPD approaches, core radiation and He blanket, ST example (25)	C. Wong (GA)
8:55	Concept of FliBe blanket in FFHR (30)	A. Sagara (NIFS)
9:25	APEX high fusion power density evaluation (20)	N. Morley (UCLA)
9:45	Damage in the plasma facing part of the first wall (20)	N. Yoshida (Kyushu U.)
10:05	Protective coating at the plasma facing part of first wall (20)	N. Noda (NIFS)
10:25	*coffee break*	
10:35	Plasma spray coating development (20)	Castro/Nygren (LANL)
10:55	Recent progress at PTI in plasma spraying (15)	S. Odell (Plasma Processes)
Session IX: PSI/PFM Issues and Collaboration		*N. Noda & R. Nygren*
11:10	Discussion on PSI/PFM issues and collaborations	N. Noda & R. Nygren
12:10	lunch	
Session X : Panel on Future PFC Concepts		*M. Tillack & Y. Ueda*
13:40	ALPS summary (20)	D. K. Sze (ANL)
14:00	Heat removal issues with liquid metal PFCs (15)	R. Nygren (Sandia)
14:15	Helium cooling experiments and prospect (15)	C. Baxi (GA)
14:30	Comments on liquid/pebble divertor (15)	Y. Ueda (Osaka U.)
14:45	Novel concept for a moving belt PFC (15)	Y. Hirooka (UCSD)
15:00	He self pumping summary (15)	R. Nygren (Sandia)
15:15	Characterization of liquid metal surfaces (15)	R. Bastasz (Sandia)
15:30	coffee break	
Session XI: Long Range PFC Development and Collaborations		
15:45	Group A Discussion: Liquid surface PFCs & collaborations	R. Nygren & A. Sagara
15:45	Group B Discussion: Other PFCs & collaborations	N. Noda & S. Luckhardt
17:15	adjourn	
18:00	dinner groups per request of participants	

December 11 (Thur.)

Session XII : Supplement Session		*K. Masaki & D. K. Sze*
9:00	more activities / results in Japan (20)	N. Noda
9:20	Recent highlights from Judith (15)	KFA/R. Nygren
9:35	Contributions from U. Toronto (15)	UT/R. Nygren
Summary Session		*K. Wilson & N. Yamashina*
9:50	Remarks on the outlook for collaborations (20)	Motojima/Noda, S. Berk
10:10	Summary/discussion: Liquid surface PFCs & collab. (20)	R. Nygren & A. Sagara
10:30	*coffee break*	
10:40	Summary/discussion: other PFCs & collaborations (20)	N. Noda & S. Luckhardt
11:00	Summary/discussion: Dev. issues for near term PFCs (20)	A. Sagara & C. Wong
11:20	Summary/discussion: PSI/PFM issues & collaborations	N. Noda & R. Nygren

(20)

11:40 Closing remarks — N. Noda & R. Nygren

11:50 adjourn

Appendix B

List of Participants And Addresses

List of Participants

Dr. Kan ASHIDA
Phone: 81-764-45-6927
Fax: 81-764-45-6931

Toyama University
Hydrogen Isotope Research Center
Gofuku 3190, Toyama 930-8555
JAPAN
e-mail: ashida@hrc.toyama-u.ac.jp

Bob BASTASZ
Phone: 510-294-2013
Fax: 510-294-3231

Sandia National Laboratories, MS9162
P.O. Box 969
Livermore, CA 94551, USA
e-mail: bastasz@ca.sandia.gov

Chandu BAXI
Phone: 619-455-3150
Fax: 619-455-2266

General Atomics
P.O. Box 85608
San Diego, CA 92186-5608
e-mail: Baxi@gav.gat.com

Sam Berk
Phone: 301-903-4171
Fax: 301-903-1233

US Department of Energy
Office of Energy Research
ER-52, Germantown
Washington, DC 20585, USA
e-mail: sam.berk@mailgw.er.doe.gov

Chuck CADDEN
Phone: 510-294-3650
Fax: 510-294-3410

Sandia National Laboratories, MS9403
P.O. Box 969
Livermore, CA 94551, USA
e-mail: chcadde@sandia.gov

Rion CAUSEY
Phone: 510-294-3326
Fax: 510-294-3231

Sandia National Laboratories, MS9161
P.O. Box 969
Livermore, CA 94551, USA
e-mail: CAUSEY@sandia.gov

Don COWGILL
Phone: 510-294-2146
Fax: 510-294-3231

Sandia National Laboratories, MS9161
P.O. Box 969
Livermore, CA 94551, USA
e-mail: DFCOWGI@sandia.gov

Russ DOERNER
Phone: 619-534-7830
Fax: 619-534-7716

University of California at San Diego
9500 Gilman Drive, Building 302
La Jolla, CA 92093-0035, USA
e-mail: rdoerner@fusion.ucsd.edu

Arthur GROSSMAN
Phone: 619-534-9712
Fax: 619-534-7716

University of California at San Diego
9500 Gilman Drive
La Jolla, CA 92093-0035, USA
e-mail: grossman@fusion.ucsd.edu

Yoshi HIROOKA
Phone: 619-534-9720
Fax: 619-534-7716

University of California at San Diego
9500 Gilman Drive, Building 302
La Jolla, CA 92093-0035, USA
e-mail: yhirooka@fusion.ucsd.edu

Stan LUCKHARDT
Phone: 619-534-9725
Fax: 619-534-7716

University of California, San Diego
9500 Gilman Drive
La Jolla, CA 92093, USA
e-mail: sluckhardt@fusion.ucsd.edu

Dr. Kei MASAKI

Japan Atomic Energy Research Institute
801-1 Mukouyama
Naka-machi, Naka gun
Ibaraki-ken, JAPAN 311-01
e-mail: masakik@fusion.naka.jaeri.go.jp

Teruo MATSUDA

Toyo Tanso America

Neil MORLEY
Phone: 310-206-1228
Fax: 310-825-2599

University of California, Los Angeles
43-133 Engineering IV
405 Hilgard Avenue
Los Angeles, CA 90024-1597 USA
e-mail: morley@fusion.ucla.edu

Prof. Osamu MOTOJIMA
Phone: 81-572-58-2140
Fax: 81-572-58-2617

National Institute for Fusion Science
322-6 Oroshi-cho, Toki 509-52, JAPAN
e-mail: motojima@LHD.nifs.ac.jp

Hiroo NAKAMURA

Japan Atomic Energy Research Institute/ITER
801-1 Mukouyama
Naka-machi, Naka gun
Ibaraki-ken, JAPAN 311-01
e-mail: nakamuh@ipp..mpg.de

Dr. Kazuyuki NAKAMURA

Japan Atomic Energy Research Institute
801-1 Mukouyama
Naka-machi, Naka gun
Ibaraki-ken, JAPAN 311-01
e-mail: nakamuk@naka.jaeri.go.jp

Prof. Noda NOBUAKI
Phone: 81-572-58-2152
Fax: 81-572-58-2618

National Institute for Fusion Science
322-6 Oroshi-cho, Toki-shi 509-5292
JAPAN
e-mail: noda@LHD.nifs.ac.jp

Richard NYGREN
Phone: 505-845-3135
Fax: 505-845-3130

Sandia National Laboratories, MS1129
Fusion Technology Department, 6428
Albuquerque, NM, 87185-1129, USA
e-mail: renygre@sandia.gov

Scott O'DELL
Phone: 205-851-7653
Fax: 205-859-4134

Plasma Processes, Inc.
4914 D Moores Mill Road
Huntsville, AL 35811, USA

Dr. Noriyasu OHNO
Phone: 81-52-789-3145
Fax: 81-52-789-3944

Nagoya University
Department of Energy Engineering and Science
Graduate School of Engineering
Nagoya, 464-8603, JAPAN
e-mail: ohno@nuee.nagoya-u.ac.jp

Shigeki OHTSU
Phone: 81-3-3812-2111
Ext 7010
Fax: 81-3-3818-3455

University of Tokyo
Dept. of Quantum Eng. & Systems Science
7-3-1 Hongo Bunkyo-ku Tokyo, 113 JAPAN
e-mail: ohtsu@q.t.u-tokyo.ac.jp

Martin PENG
Phone: 609-243-2305
Fax: 609-243-3315

Princeton Plasma Physics Laboratory
P. O. Box 451
Princeton, NJ 08543-0451

Dr. Akio SAGARA
Phone: 81-0572-58-2155
Fax: 81-0572-58-2618

National Institute for Fusion Science
Research Operations Division, LHD Project
Shimoishi-cho-322-6, Toki-shi, 509-52
JAPAN
e-mail: sagara@LHD.nifs.ac.jp

Dr. Masanoa SHIBUI
Phone: 045-510-5879
Fax: 045-500-1412

Toshiba Corporation
Advanced Engineering Gr.
2-4, Suehiro, Tsurumi, Yokohama, 230-0045
JAPAN
e-mail: masanao.shibui@toshiba.co.jp

Charles SKINNER
Phone: 609-243-2214
Fax: 609-243-2418

Princeton Plasma Physics Laboratory
Princeton University, P. O. Box 451
Princeton, NJ 08543, USA
e-mail: cskinner@rax.pppl.gov

Dai Kai SZE
Phone: 630-252-5180
Fax: 630-252-5287

Argonne National Laboratory
9700 South Cass Avenue, Bldg. 207
Argonne, IL 60439
e-mail: u1747@f.nersc.gov

Prof. Tetsuo TANABE

Nagoya University
Department of Energy Engineering and Science
Nagoya, 464-8603, JAPAN
tanabe@cirse.magoya-u.ac.jp

Mark TILLACK

University of California at San Diego
9500 Gilman Drive
La Jolla, CA 92093 USA

Yoshio UEDA
Phone: 81-6-879-7236
Fax: 81-6-879-7867

Osaka University
Department of Electronic, Information Systems, and Energy Engineering
Graduate School of Engineering
2-1 Yamada-Oka, Suita, Osaka 565-0871
JAPAN
e-mail: yueda@ppl.eng.osaka-u.ac.jp

Gerry WILLE

Boeing Company
MS 106 7211
P.O. Box 516
St. Louis, MO 63166 USA

Ken WILSON
Phone: 510-294-2497
Fax: 510-294-3057

Sandia National Laboratories, MS9161
P.O. Box 969
Livermore, CA 94551-0969 USA
e-mail: klwilso@sandia.gov

Clement WONG
Phone: 619-454-4258
Fax: 619-454-2266

General Atomics
P.O. Box 85608
San Diego, CA 92186-5608 USA
e-mail: won@gav.gat.com

Prof. Toshiro YAMASHINA
Phone: 81-11-706-6659
Fax: 81-11-747-9366

Hokkaido University
Division of Quantum Energy Engineering
Sapporo, JAPAN 060
e-mail: yamasina@hune.hokudai.ac.jp

Prof. Naoaki YOSHIDA
Phone: 81-92-583-7716
Fax: 81-92-583-7690

Research Institute for Applied Mechanics
Kyushu University
6-1 Kasugakoen, Kasuga, Fukuoka 816-8580
JAPAN
e-mail: yoshida@riam.kyushu-u.ac.jp

DISTRIBUTION

DISTRIBUTION

1 Mohamed ABDOU
University of California, Los Angeles
Mechanical & Aerospace Engineering
Department
44-114 Engineering IV
Box 951597
Los Angeles, CA 90095-1597, USA

1 Dr. Masato AKIBA
NBI Heating Laboratory, JAERI,
Naka-machi, Naka-gun, Kbaraki-ken, 311-0193, JAPAN

1 Dr. Kan ASHIDA
Toyama University
Hydrogen Isotope Research Center
Gofuku 3190, Toyama 930-8555, JAPAN

1 Charles BAKER
University of California, San Diego
9500 Gilman Drive
La Jolla, CA 92093, USA

1 Chandu BAXI
General Atomics
P.O. Box 85608
San Diego, CA 92186-5608, USA

1 Sam BERK
US Department of Energy
Office of Energy Research
ER-52, Germantown
Washington, DC 20585, USA

1 Jeffrey BROOKS
Argonne National Laboratory
Fusion Power Program
9700 S. Cass Avenue
Argonne, IL 60439, USA

1 Robert CONN
University of California at San Diego
9500 Gilman Drive, Building 302
La Jolla, CA 92093-0035, USA

1 James DAVIS
University of Toronto
21 King's College Circle
Toronto, Ontario M5S 3J3, CANADA

1 Russ DOERNER
University of California at San Diego
9500 Gilman Drive, Building 302
La Jolla, CA 92093-0035, USA

1 Gianfranco FEDERICI
ITER Garching Joint Work Site
Max-Planck-Institut fur Plasmaphysik
Boltzmannstrasse 2
D-85748 Garching bei Munchen, GERMANY

1 Arthur GROSSMAN
University of California at San Diego
9500 Gilman Drive
La Jolla, CA 92093-0035, USA

1 Anthony HAAS
University of Toronto
21 King's College Circle
Toronto, Ontario M5S 3J3, CANADA

2 Ahmed HASSANEIN
Argonne National Laboratory
Fusion Power Program
9700 S. Cass Avenue
Argonne, IL 60439, USA

1 Yoshi HIROOKA
National Institute for Fusion Science
322-6 Oroshi-cho, Toki 509-52, JAPAN

1 Prof. Satoshi ITOH
Advanced Fusion Research Center
Research Institute for Applied Mechanics
Kyushu University
87, Kasuga 816, JAPAN

1 Dr. Y. KUBOTA
National Institute for Fusion Science
322-6 Oroshi-cho, Toki-shi 509-5292, JAPAN

1 Bruce LIPSCHULTZ
Massachusetts Institute of Technology
Plasma Science and Fusion Center
Room No. 17-103
77 Massachusetts Avenue
Cambridge, MA 02139, USA

1 Stan LUCKHARDT
University of California, San Diego
9500 Gilman Drive
La Jolla, CA 92093, USA

1 Dr. Kei MASAKI
Japan Atomic Energy Research Institute
801-1 Mukouyama
Naka-machi, Naka gun
Ibaraki-ken, 311-01 JAPAN

1 Dr. S. MASUZAKI
National Institute for Fusion Science
322-6 Oroshi-cho, Toki-shi 509-5292, JAPAN

1 Richard MATTAS
Argonne National Laboratory
Fusion Power Program
9700 S. Cass Avenue
Argonne, IL 60439, USA

1 Dale MEADE
Princeton Plasma Physics Laboratory
P.O. Box 451
Princeton, NJ 08543-0451, USA

1 Peter K. MIODUSZEWSKI
Fusion Energy Division
Oak Ridge National Laboratory
P. O. Box 2009
Oak Ridge, TN 37831-8070, USA

1 Dr. T. MORISAKI
National Institute for Fusion Science
322-6 Oroshi-cho, Toki-shi 509-5292, JAPAN

1 Neil MORLEY
University of California, Los Angeles
43-133 Engineering IV
405 Hilgard Avenue
Los Angeles, CA 90024-1597, USA

1 Prof. Osamu MOTOJIMA
National Institute for Fusion Science
322-6 Oroshi-cho, Toki 509-52, JAPAN

1 Farouk NAJMABADI
University of California at San Diego
9500 Gilman Drive, Building 302
La Jolla, CA 92093-0035, USA

1 Hiroo NAKAMURA
Japan Atomic Energy Research Institute/ITER
801-1 Mukouyama
Naka-machi, Naka gun
Ibaraki-ken, 311-01, JAPAN

1 Dr. Kazuyuki NAKAMURA
Japan Atomic Energy Research Institute
801-1 Mukouyama
Naka-machi, Naka gun
Ibaraki-ken, 311-01, JAPAN

1 Prof. M. NISHIKAWA
Osaka University
Department of Electronic, Information Systems, and
Energy Engineering
Graduate School of Engineering
2-1 Yamada-Oka, Suita, Osaka 565-0871, JAPAN

1 Prof. Nokuaki NODA
National Institute for Fusion Science
322-6 Oroshi-cho, Toki-shi 509-5292, JAPAN

1 Scott O'DELL
Plasma Processes, Inc.
4914 D Moores Mill Road
Huntsville, AL 35811, USA

1 Dr. Noriyasu OHNO
Nagoya University
Department of Energy Engineering and Science
Graduate School of Engineering
Nagoya, 464-8603, JAPAN

1 Shigeki OHTSU
University of Tokyo
Dept. of Quantum Eng. & Systems Science
7-3-1 Hongo Bunkyo-ku Tokyo, 113, JAPAN

1 Dr. N. OHYABU
National Institute for Fusion Science
322-6 Oroshi-cho, Toki-shi 509-5292, JAPAN

1 Martin PENG
Princeton Plasma Physics Laboratory
P.O. Box 451
Princeton, NJ 08543-0451, USA

1 Dave RUZIC
University of Illinois
Fusion Studies Laboratory
100 Nuclear Engineering Laboratory
103 South Goodwin Avenue
Urbana, IL 61801-2984, USA

1 Dr. Akio SAGARA
National Institute for Fusion Science
Research Operations Division, LHD Project
Shimoishi-cho-322-6, Toki-shi, 509-52, JAPAN

1 Michael J. SALTMARSH
Fusion Energy Division
Oak Ridge National Laboratory
P. O. Box 2009
Oak Ridge, TN 37831-8070, USA

1 Dr. Masanoa SHIBUI
Toshiba Corporation
Advanced Engineering Gr.
2-4, Suehiro, Tsurumi, Yokohama, 230-0045, JAPAN

1 A. SHIMIZU
Research Institute for Applied Mechanics
Kyushu University
6-1 Kasugakoen, Kasuga, Fukuoka 816-8580, JAPAN

1 Charles SKINNER
Princeton Plasma Physics Laboratory
Princeton University
P. O. Box 451
Princeton, NJ 08543, USA

1 Ron STAMBAUGH
General Atomics
Fusion Group
P.O. Box 85608
San Diego, CA 92186-5608, USA

1 Dai Kai SZE
Argonne National Laboratory
9700 South Cass Avenue, Bldg. 207
Argonne, IL 60439, USA

1 Prof. S. TAKAMURA
Nagoya University
Department of Energy Engineering and Science
Graduate School of Engineering
Nagoya, 464-8603, JAPAN

1 Prof. Tetsuo TANABE
Nagoya University
Department of Energy Engineering and Science
Nagoya, 464-8603, JAPAN

1 Mark TILLACK
University of California at San Diego
9500 Gilman Drive
La Jolla, CA 92093, USA

1 Prof. K. TOKUNAGA
Research Institute for Applied Mechanics
Kyushu University
6-1 Kasugakoen, Kasuga, Fukuoka 816-8580, JAPAN

1 Yoshio UEDA
Osaka University
Department of Electronic, Information Systems, and
Energy Engineering
Graduate School of Engineering
2-1 Yamada-Oka, Suita, Osaka 565-0871, JAPAN

1 Gerry WILLE
Boeing Company
MS 106 7211
P.O. Box 516
St. Louis, MO 63166, USA

1 Clement WONG
General Atomics
P.O. Box 85608
San Diego, CA 92186-5608, USA

1 Prof. Toshiro YAMASHINA
Hokkaido University
Division of Quantum Energy Engineering
Sapporo, 060, JAPAN

1 Prof. Naoaki YOSHIDA
Research Institute for Applied Mechanics
Kyushu University
6-1 Kasugakoen, Kasuga, Fukuoka 816-8580, JAPAN

1	MS0736	N. R. Ortiz, 6400
2	MS1056	B. L. Doyle, 1111 W. R. Wampler, 1111
7	MS1129	M. A. Ulrickson, 6428 (1) R. E. Nygren, 6428 (2) D. L. Youchison, 6428 (1) 6428 File (3)

5	MS9161	Ken Wilson, 8716 Rion Causey, 8716 Don Cowgill. 8716 Bob Bastasz, 8716 Dean Buchenauer, 8716
1	MS9403	Chuck Cadden, 8240
1	MS9018	Central Technical Files, 8940-2
2	MS0899	Technical Library, 4916
1	MS0619	Review & Approval Desk, 12690